

Lecture Notes in Civil Engineering

Bashar S. Mohammed · Teh Hee Min ·
Muslich Hartadi Sutanto ·
Tri Basuki Joewono ·
Sholihin As'ad *Editors*

Proceedings of the International Conference on Emerging Smart Cities (ICESC2022)

 Springer

Lecture Notes in Civil Engineering

Volume 324

Series Editors

Marco di Prisco, Politecnico di Milano, Milano, Italy

Sheng-Hong Chen, School of Water Resources and Hydropower Engineering,
Wuhan University, Wuhan, China

Ioannis Vayas, Institute of Steel Structures, National Technical University of
Athens, Athens, Greece

Sanjay Kumar Shukla, School of Engineering, Edith Cowan University, Joondalup,
WA, Australia

Anuj Sharma, Iowa State University, Ames, IA, USA

Nagesh Kumar, Department of Civil Engineering, Indian Institute of Science
Bangalore, Bengaluru, Karnataka, India

Chien Ming Wang, School of Civil Engineering, The University of Queensland,
Brisbane, QLD, Australia

Lecture Notes in Civil Engineering (LNCE) publishes the latest developments in Civil Engineering—quickly, informally and in top quality. Though original research reported in proceedings and post-proceedings represents the core of LNCE, edited volumes of exceptionally high quality and interest may also be considered for publication. Volumes published in LNCE embrace all aspects and subfields of, as well as new challenges in, Civil Engineering. Topics in the series include:

- Construction and Structural Mechanics
- Building Materials
- Concrete, Steel and Timber Structures
- Geotechnical Engineering
- Earthquake Engineering
- Coastal Engineering
- Ocean and Offshore Engineering; Ships and Floating Structures
- Hydraulics, Hydrology and Water Resources Engineering
- Environmental Engineering and Sustainability
- Structural Health and Monitoring
- Surveying and Geographical Information Systems
- Indoor Environments
- Transportation and Traffic
- Risk Analysis
- Safety and Security

To submit a proposal or request further information, please contact the appropriate Springer Editor:

- Pierpaolo Riva at pierpaolo.riva@springer.com (Europe and Americas);
- Swati Meherishi at swati.meherishi@springer.com (Asia—except China, Australia, and New Zealand);
- Wayne Hu at wayne.hu@springer.com (China).

All books in the series now indexed by Scopus and EI Compendex database!

Bashar S. Mohammed · Teh Hee Min ·
Muslich Hartadi Sutanto · Tri Basuki Joewono ·
Sholihin As'ad
Editors

Proceedings
of the International
Conference on Emerging
Smart Cities (ICESC2022)

 Springer

Editors

Bashar S. Mohammed
Civil and Environmental Engineering
Department
Universiti Teknologi PETRONAS
Seri Iskandar, Perak, Malaysia

Teh Hee Min
Civil and Environmental Engineering
Department
Universiti Teknologi PETRONAS
Seri Iskandar, Malaysia

Muslich Hartadi Sutanto
Civil and Environmental Engineering
Department
Universiti Teknologi PETRONAS
Seri Iskandar, Malaysia

Tri Basuki Joewono
Sekolah Pascasarjana
Universitas Katolik Parahyangan
Bandung, Indonesia

Sholihin As'ad
Civil Engineering, Faculty of Engineering
Universitas Sebelas Maret
Surakarta, Indonesia

ISSN 2366-2557 ISSN 2366-2565 (electronic)
Lecture Notes in Civil Engineering
ISBN 978-981-99-1110-3 ISBN 978-981-99-1111-0 (eBook)
<https://doi.org/10.1007/978-981-99-1111-0>

© Institute of Technology PETRONAS Sdn Bhd 2024

This work is subject to copyright. All rights are solely and exclusively licensed by the Publisher, whether the whole or part of the material is concerned, specifically the rights of translation, reprinting, reuse of illustrations, recitation, broadcasting, reproduction on microfilms or in any other physical way, and transmission or information storage and retrieval, electronic adaptation, computer software, or by similar or dissimilar methodology now known or hereafter developed.

The use of general descriptive names, registered names, trademarks, service marks, etc. in this publication does not imply, even in the absence of a specific statement, that such names are exempt from the relevant protective laws and regulations and therefore free for general use.

The publisher, the authors, and the editors are safe to assume that the advice and information in this book are believed to be true and accurate at the date of publication. Neither the publisher nor the authors or the editors give a warranty, expressed or implied, with respect to the material contained herein or for any errors or omissions that may have been made. The publisher remains neutral with regard to jurisdictional claims in published maps and institutional affiliations.

This Springer imprint is published by the registered company Springer Nature Singapore Pte Ltd. The registered company address is: 152 Beach Road, #21-01/04 Gateway East, Singapore 189721, Singapore

Paper in this product is recyclable.

Preface

This book contains papers presented at the 1st International Conference on Emerging Smart Cities (ICESC2022) under the banner of World Engineering, Science and Technology Congress (ESTCON2022) held on 1–2 December 2022 at Borneo Convention Centre, Kuching, Malaysia.

ICESC aims to provide a platform for academia and industry practitioners to showcase their novel and worthwhile research findings for the advancement of civil engineering disciplines, with an emphasis on emerging smart cities for the ultimate shape of urban living in the near future. The conference has provided tremendous opportunities to exchange existing ideas and share experiences to build new alliances between academia and industry practitioners around the world.

The articles in this book were accepted after a rigorous review process. All accepted papers are categorized based on the following themes:

- Climate adaptive materials.
- Environmental sustainability.
- Infrastructure efficiency.

We would like to express our gratitude to the technical programme committee and advisory committee who undertook the biggest responsibility in the paper reviewing process. We are also grateful to the additional reviewers who helped the authors deliver better papers by providing them with constructive comments. We hope that this process contributed to a consistently good level of the papers that are included in the book.

Bashar S. Mohammed
Teh Hee Min
Muslich Hartadi Sutanto
Tri Basuki Joewono
Sholihin As'ad

Organization

Organizing Committee

Conference Chair

Bashar S. Mohammed

Universiti Teknologi PETRONAS,
Malaysia

Conference Co-chair

Dimas Bayu Endrayana

Universiti Teknologi PETRONAS,
Malaysia

Secretary

Ng Cheng Yee

Universiti Teknologi PETRONAS,
Malaysia

Treasurer

Niraku Rosmawati Ahmad

Universiti Teknologi PETRONAS,
Malaysia

Technical Committee

Teh Hee Min

Universiti Teknologi PETRONAS,
Malaysia

Publication Committee

Muslich Hartadi Sutanto

Universiti Teknologi PETRONAS,
Malaysia

IT and Media

Mohamed Latheef

Universiti Teknologi PETRONAS,
Malaysia

Event Management Committee

Lavana Baloo

Universiti Teknologi PETRONAS,
Malaysia

Co-organizer Division

Dimas Bayu Endrayana

Universiti Teknologi PETRONAS,
Malaysia

Sponsorship

Hisham B. Mohamad

Universiti Teknologi PETRONAS,
Malaysia

Contents

Climate Adaptive Materials

Application of Pervious Concrete Principles on U-Ditch Covers in Overcoming Puddles	3
M. A. P. Handana, Syahrizal, R. Karolina, M. W. A. Srg, and B. Banjai	
Study on Compressive Strength of Geopolymer Mortar Based on Fly Ash and GGBFS with Various Molar Variations	13
Rahmi Karolina, Johannes Tarigan, Harianto Hardjasaputra, and Kenrick Hermanto	
Influence of Fly Ash, Volcanic Ash and Rice Husk Ash as Filler Asphalt Concrete Wearing Course Based on Marshall Characteristics	29
Alfia Magfirona, Riza Syaiful Billad, Gurawan Djati Wibowo, and Tsulis Iq'bal Khairul Amar	
Mechanical Performance Improvement by Carbon Dioxide Curing of Cement Concrete Incorporating Oil Shale Residue	41
Syahidus Syuhada, Marsail Al Salaheen, Wesam Salah Alaloul, and Khalid Mhmoud Alzubi	
Flood Susceptibility Mapping Using GIS-AHP of Kuala Krai	51
Zafarullah Nizamani, Riaz Ahmed Soomro, Akihiko Nakayama, and Montasir Osman Ahmed Ali	
Utilization of Zeolite Material with Chemical and Physical Activation as SCC Concrete (Self Compacting Concrete)	63
Ahmad Yudi, Axcel Joshua, Yeremi Alexander, Syahidus Syuhada, and W Rindu Trisna	

Comparative Study of Vacuum Bagging and Hand Lay Up Methods for Coconut Coir Fiber Composite Materials as an Alternative to Wood Boards 77
 Juriah Mulyanti, Sukamto, Bayu Megaprasatio, Muhammad Arief Saputro, and Andi Prayoga

Improved Resistance of Reinforced Concrete Columns in Fire Exposure by Strengthening Stirrup Reinforcement 85
 Prasetya Adi, Arusmalem Ginting, and Bing Santosa

Environmental Sustainability

Reducing Bod and TSS Levels in Batik Wastewater Using Moringa Seeds Coagulant (Moringa Oleifera) 97
 Gustiana Zaskya Sinaga, Andika Munandar, and Rahma Yanda

Characterization of Fly Ash: Effect on Compressive Strength and Thickening Time of Alkaline-Activated Fly Ash Cement at Downhole Condition 107
 Nurul Nazmin Zulkarnain, Yon Azwa Sazali, Afif Izwan A. Hamid, Noraini Kamizan, Siti Humairah A. Rahman, Ahmad Amirhilmi A. Razak, and MFirdaus Habarudin

Lithium and Boron Recovery From Oil Field Produced Water: A Mini Review 119
 Rabia Khatoun, Yeek-Chia Ho, Shamsul Rahman B. Mohamed Kutty, Khairulazhar Jumbri, Maung Maung Myo Thant, and Dong Suk Han

Pyrolysis Behavior of Polyethylene Terephthalate (PET) Plastic Waste Under the Presence of Activated Montmorillonite Catalyst: TGA and EGA-MS Studies 133
 Tarmizi Taher, Andika Munandar, Nurul Mawaddah, Raden Putra, Neza Rahayu Palapa, and Aldes Lesbani

Evaluation of Land Subsidence Prevention to Minimize the Flood Risk in a Port City 145
 Nurul Fajar Januriyadi, So Kazama, Idham R. Moe, and Shuichi Kure

Removal of Naphthalene from Produced Water Using Oil Palm Leaves Waste Activated Carbon 155
 Muhammad Raza Ul Mustafa, Hifsa Khurshid, Yeek-Chia Ho, and Mohamed Hasnain Isa

Characterization and Potential Analysis of Paper Waste as Raw Material for Refuse Derived Fuel (RDF) Pellet Substitution 165
 Nurulbaiti Listyendah Zahra, Intan Rahmalia, Fatimah Dinan Qonitan, I Wayan Koko Suryawan, and Ariyanti Sarwono

The Perception of Vertical Holiness in Development of Multilevel Infrastructure As an Effort for Environmental Conservation and Preventing Transfer of Land Conversion 181
 I Made Sastra Wibawa, Shinta Enggar Maharani, Krisna Kurniari, and I. Kadek Ardi Putra

The Effects of Changes in Socializing Trips, Discretionary Trips & Activities, During COVID-19 Pandemic on Affective Well-Being 193
 M. Ridwan, Anas Zahkiah Hanum Azmera, Dimas B. E. Dharmowijoyo, and Liza Evianti Tanjung

Design of E-Waste Management System for Flood- Prone Area (Case Study: Jakarta, Indonesia) 217
 Nova Ulhasanah, Sinthia Apriani, and Mega Mutiara Sari

Review of Rubber-Based Waste in Compressed Bricks 233
 Ai Shyn Tan, Jee Cheat Tan, Lee Woen Ean, Cheng Yee Ng, Bashar S. Mohammed, and Shuhairy Norhisham

Zero Runoff Drainage System for Bintaro Jaya Xchange Mall Project in South Tangerang, Indonesia 243
 Luhur Budi Nanda and Teddy W. Sudinda

Development of Rainfall-Runoff Model Using Mock Formula with the Calibration of Stream Discharge in Cisadane Watershed - Indonesia 253
 Dina P. A. Hidayat, W. D. Sri Legowo, and Mohammad Farid

Performance Analysis of Green Company in State Electricity Company Indonesia 263
 Arinda Soraya Putri, Hafidh Munawir, Dyah Widayanti, and Nadiea Aurealnisa Syazili

Case-Based Reasoning Method Implementation for Well Water Feasibility Recommendation System with Nearest Neighbor Algorithm 275
 Jemmy Edwin Bororing, Yumarlin MZ, Sri Rahayu, Agustin Setyorini, Fatsyahrina Fitriastuti, and Jeffry Andhika Saputra

Most Prioritised Points in GREENSHIP New Building Certification 287
 Muhammad Rizky Waskito Aribowo and Bambang E. Yuwono

The Impacts of Revitalization on the Saribu Rumah Gadang Cultural Area Sustainability 297
 Dhani Mutiari, Marwah Dwi Ramadhanti, and Fadilla Tri Nugraheni

Effect of Polypropylene Fibre on High Volume Fly Ash Self-compacting Concrete in Terms of Compressive Strength, Tensile Strength, and Concrete Abrasion 309
Mochamad Solikin and Fauzi Mubarak

The Effectiveness of COD Removal from Industrial Effluent Using Treatment Train System 321
Muhammad Faris Mohd Ramli, Husna Takaijudin, Manal Osman Mohamed Ali, Wafaa Ali Nsaif Alhamzah, and Nor Amirah Ahmad Zubairi

Life Cycle Assessment of Utilization of Shredded Tire for Sustainable Road Embankment 329
Vera H. Loo, Wahidul K. Biswas, and Nicholas Z. S. Chin

Effect of Fire on High-Strength Fly-Ash-Based Geopolymer Concrete 339
Siti Nooriza Abd Razak, Nasir Shafiq, Laurent Guillaumat, Vicky Kumar Lohana, Syed Ahmad Farhan, and Farah Amira Ahmad Shafee

Study on Correlation Among Roof Area, Reservoir Volume and Domestic Water Availability from Rainwater Harvesting in East Part of Surabaya 351
Umboro Lasminto, Satria Damarnegara, Bernadeta Elie, Rayhan Airlangga, Dina Permatasari, and Javier Aqilla

Criteria of Low Embodied Energy Material Selection for Sustainable Building Design 365
Yani Rahmawati, Rissa Syafutri, Ariessa K. Pratami, Jatmika Adi Suryabrata, Christiono Utomo, and Aqsha

Improving the Quality of Agricultural Wastes for Solid Fuels Employing Torrefaction: A Case Study in Indonesia 375
Untoro Budi Suro, Mochamad Syamsiro, and Nugroho Agung Pambudi

Forecasting Longshore Sediment Transport on a Wave-Dominated Coast Using Various Wave Data Sources 389
Tania Edna Bhakty, Khusnul Setia Wardani, Nizar Achmad, Titiek Widayarsi, and Gregorius Ranggawuni

Literature Review on Covid-19 Pandemic Emergency Response 399
Afiqoh Akmalia Fahmi, Gustisia Rahmi Nastiti, Eko Setiawan, and Arinda Soraya Putri

Investigation on the Properties of Reclaimed Asphalt Pavement Rejuvenated with Rubber Seed Oil	411
Nur Izzah Batrisyia Binti Mohd Yusof, Abdul Muhaimin Memon, and Muslich Hartadi Sutanto	
Environmental Impact Analysis on Dyes in Handwritten Batik	421
Etika Muslimah, Maharani Reynara, and Ratnanto Fitriadi	
Effects of Change of Discretionary Trips & Activities, During COVID-19 Pandemic Towards Social & Mental Health	429
Rahayu Sulistyorini, Nur Shalin Abdi, Dimas B. E. Dharmowijoyo, and Liza EviantiTanjung	
Performance Border Gateway Protocol (BGP) on VLAN Network for Development Smart Hospitals	449
Ryan Ari Setyawan, Fatsyahrina Fitriastuti, and Agus Wari Yulianto	
Optimum Content of Matos as an Additive in the Application of Cement Soil Stabilization as a Cement Composite Soil Base Layer ...	461
Teguh Widodo, Nur Ayu Diana, and Arusmalem Ginting	
IoT Implementation to Minimize the Vehicle Queue at the Traffic Lights Intersection	469
Fatsyahrina Fitriastuti, Ryan Ari Setyawan, Muhammad Arif Ma'ruf Setiawan, and Jemmy Edwin Bororing	
Organic Matter Removal from Sanitary Landfill Leachate Through Chemical Oxidation	479
Nurfarizah Didi Binti Abdullah, Mohamed Hasnain Isa, Rozeana Hj Md Juani, Asmaal Muizz Sallehhin Bin Hj Mohammad Sultan, Zuliana Binti Hj Nayan, and Muhammad Raza Ul Mustafa	
Infrastructure Efficiency	
Construction Players' Awareness on the Use of Building Information Modelling (BIM) and Industrialized Building System (IBS) in Malaysian Construction Industry	491
Mohamad Zain Hashim, Idris Othman, Nur Syahirah M. Khalid, Siti Hafizan Hassan, and Muriatul Khusmah Musa	
Experimental, Numerical and Field Investigations on the Hydraulics Performance of Stormwater Curb-Opening Inlets	505
Zahiraniza Mustafa, Ebrahim Hamid Hussein Al-Qadami, Aifaa Balqis Kamarul Zaman, and Syed Muzzamil Hussain Shah	

Nonlinear Modeling and Analysis of Cold-Formed Steel Beam-Column Connection 521
 Data Iranata, Djoko Irawan, and Muhammad Fauzan Akbari

Instrumented Pile Load Test Using Distributed Fibre Optic Sensor: Automation in Data Processing 537
 Aizat Akmal A. Mohamad Beddelee, Hisham Mohamad, Bun Pin Tee, and Rini Asnida Abdullah

Diagonal Shear Test on Indonesian Masonry Walls 549
 Farisal Akbar Rofussan, Ahmad Basshofi Habieb, Djoko Irawan, and Budi Suswanto

Analysis of the Effect of Asbuton on Porous Asphalt Mixtures for Heavy Load Traffic 555
 Sutoyo, Mochtar, and Prastyanto

Assessment of an Eight-Story Hospital Building with Nonlinear Static Analysis 571
 Fahmy Hermawan and Nicolas Kanisius Sianturi

Consolidation Analysis Using Prefabricated Vertical Drain (PVD) and Preloading in the Phase I Belawan Reclamation Project with PLAXIS 2D and 3D 583
 Gina Cynthia Raphita Hasibuan, Yunike Wulandari Br Tarigan, Roesyanto, and Rudianto Surbakti

Numerical Modeling of One-Way Reinforced Concrete Wall Panels with Openings Strengthened with Carbon Fiber Reinforced Polymer (CFRP) 599
 M. J. Qaddura, L. W. Ean, B. S. Mohammed, and Cheng Yee Ng

The Effect of Transfer Function on Fatigue Life Determination in Spectral Fatigue Analysis 611
 Arianta, Frengki Pardede, and Muhammad Sholeh

The Impact of Way Sekampung Dam Development on the Economy of the Community in Bumi Ratu, Indonesia 621
 Ragil Arswindo, I. B. Ilham Malik, and Yudha Rahman

Gas Pipeline Stress Analysis Affected by Landslide Induced Soil Deformation 627
 Kadek W. Ghaneswari, Ranga A. Sudisman, and Andri Mulia

Testing Using Bi-directional Method for Bored Pile on Clay Soil in Indonesia 637
 Aksan Kawanda

Traditional Practices and Potential of Industrial Revolution 4.0 in the Construction Projects 647
 I Gusti Agung Ayu Istri Lestari, I Gede Angga Diputera, Abdullah O. Baarimah, Wesam Salah Alaloul, Muhammad Ali Musarat, Aawag Mohsen Alawag, and Khalid Mhmoud Alzubi

Image Processing Applications in Construction Projects: Challenges and Opportunities 661
 Tjokorda Istri Praganingrum, Ni Luh Made Ayu Mirayani Pradnyadari, Khalid Mhmoud Alzubi, Wesam Salah Alaloul, Marsail Al Salaheen, Muhammad Ali Musarat, and Aawag Mohsen Alawag

Comparative Analysis of Vehicle Operating Cost Methods: (Cases Study: Medan-Binjai Toll Road) 673
 Ridwan Anas, David Barry Hariganta, and Derry W. Nasution

Underwater Sill Layout for Efficient Sediment Deflection 683
 Tania Edna Bhakty, Nur Yuwono, Bambang Triatmodjo, and Ahmad Faramarz Ghalizhan

Efficiency of Infrastructure Planning of Retaining Wall as Flood Control in Bangin River Pecatu Badung Bali 693
 Anak Agung Ratu Ritaka Wangsa, IMade Nada, and Ida Bagus Suryatmaja

Impact of Changes in SNI 1726 and SNI 2847 on Reinforcing Steel Weight of High-Rise Reinforced Concrete Buildings in Jakarta 707
 Suradjin Sutjipto, Indrawati Sumeru, and Sherrica Augustin Sucipto

Effective Mixing Lag Time of Two Phase Lime-Cement Stabilization on High Plasticity Clay 719
 Teguh Widodo and Nur Ayu Diana

The Thermal Comfort of Sangkring Art Space Yogyakarta 727
 Rini Hidayati, Martha Karerinna Anugerah, and Fadhillia Tri Nugrahaini

Challenges and Recommendations for Offshore Monopod Platform Installation 739
 Khairan Syuhada Binti Kassim

Infill-Walls Interaction on Steel Moment Resisting Frame Due to Lateral Forces 747
 I Ketut Diartama Kubon Tubuh, I Gede Gegiranang Wiryadi, I Putu Agus Putra Wirawan, I Kadek Aditya Setyawan, and I Made Laksana Wira Saputra

**Making the Strategic Disaster Mitigation in Building Foundations:
A Case Study Pandak II Public Health Center 757**
Widya Kartika, Buddewi Sukindrawati, and Sarju

**Analysis of Runoff Discharge on Kaliurang Road Drainage
Channels KM 6.5 – 7 Using SWMM 5.2 Model 765**
Titiek Widyasari, Nizar Achmad, Tania Edna Bhakty,
and Ardha Candra Perdana

**The Comparison of the Effect of Activity Space on Health
Performance (Physical and Mental Health) Between Malaysia City
and Indonesia City 775**
Tjokorda, Joan Rona Justin, Dimas B. E. Dharmowijoyo,
Nindy Cahyo Kresnanto, and Liza Evianti Tanjung

Climate Adaptive Materials

Application of Pervious Concrete Principles on U-Ditch Covers in Overcoming Puddles



M. A. P. Handana, Syahrizal, R. Karolina, M. W. A. Srg, and B. Banjai

Abstract Based on data released by the Badan Metereologi dan Geofisika (BMKG), the average rainfall rate for Medan City in 2020 reached 9,907 mm in accumulation. The use of asphalt or concrete on most roads results in puddles and even floods often occur because concrete or asphalt has a smooth surface so that it is not able to infiltrate into the ground properly and results in larger surface runoff. For this reason, a research has been carried out on the application of Pervious Concrete principles on U-ditch covers with an experimental method that utilizes sidewalk's paving block waste. This research was conducted by varying the addition of sidewalk's paving block waste as much as 3 variations in composition, i.e.; 10, 20 and 30%. The results obtained that the optimum composition in the application of pervious concrete on u-ditch covers which was effective and capable of draining water was variation I (10% addition of paving block waste.). With a compressive strength of 8.862 MPa; split tensile strength of 1,556 MPa; flexure strength of 2.453 Mpa and infiltration rate of 1.93×10^{-4} mm/h. And u-ditch covers in this research had a good infiltration value so that rainwater runoff could be passed to the drainage.

1 Introduction

The word concrete comes from Dutch or in Latin called *concretus* which means to grow together or combine into one [1]. Pervious concrete is a simple form of lightweight concrete made by reducing the use of fine aggregate (sand) which aims to create voids between coarse aggregates [2]. While a u-ditch cover is a concrete trench cover product which is a component of the precast u-ditch channel support. As

M. A. P. Handana (✉) · Syahrizal · R. Karolina · M. W. A. Srg · B. Banjai
Departemen Teknik Sipil, Fakultas Teknik, Universitas Sumatera Utara, Jl. Perpustakaan Kampus
USU, Medan, Indonesia
e-mail: agung.putra@usu.ac.id

R. Karolina
Integrated Research Laboratory, Universitas Sumatera Utara, Medan 20155, Sumatera Utara,
Indonesia

for the constituent materials of pervious concrete, i.e.: portland cement, a hydraulic cement consisting of calcium silicate that ground together with additional materials of one or more crystals of calcium sulfate compounds, as well as other materials [3]; Furthermore, Aggregate is a collection of natural mineral grains which have a function as a filler in mortar or concrete mixture; and finally, water [4].

In this research, pervious concrete and u-ditch covers were formed from Type I portland cement while the aggregate material used was sidewalk's paving block waste. And to determine the quality of the two, several tests were carried out, i.e. the compressive strength test in accordance with SNI 1974-2011 [5]; Split tensile strength according to SNI 2491-2014 [6]; Flexure strength in accordance with SNI-03-4431-2011 [7]; infiltration rate referring to ASTM C 1701/C 1701 M-09 [8]; visible properties and size test.

2 Research Background

Infrastructure development in transportation sector continues to be promoted in line with improving the quality of concrete or asphalt pavement construction which is considered the most economical, a longer service time and is safe for road users. Therefore, concrete or asphalt pavement becomes an option [9]. However, the rigid characteristics of concrete with a smoother surface than asphalt actually cause problems for the environment. Very fine pores in normal concrete reduce the rate of water infiltration during rain, as a result, surface runoff is retained longer before it reaches the drainage channel. Meanwhile, a u-ditch cover is also made of normal concrete which is impermeable to water, rainwater that falls on a u-ditch cover actually flows back to the road surface because the u-ditch cover which is also a sidewalk has a higher elevation than the road surface so that a high puddle of water is formed on the body of the road due to rainwater falling on the road surface or u-ditch covers. The problem of puddles can cause various negative impacts, for example, the impact of puddles on city infrastructures, while from a health perspective, it is clear that puddles can have a very large negative impact, such as: itching, or mosquito breeding places that can cause malaria or dengue hemorrhagic fever (DHF) [2].

Based on the problems above, an alternative is proposed to overcome these problems, i.e., applying the principles of pervious concrete to u-ditch covers so that u-ditch covers that used to drain water can pass water without reducing its use as a sidewalk for pedestrians. So that through its application, it is hoped that the infiltration rate of surface water flow can be increased and be able to overcome floods and puddles.

3 Materials and Method

The method used in this research was the experimental method. The factor studied was the use of sidewalk’s paving block waste as a substitute for coarse aggregate on the strength of pervious concrete. In determining the mixture proportion in this research, it refers to the ACI-522R-10, Report on Pervious Concrete Reapproved. After performing calculations using ACI 522-R-10, the design mix proportion composition of pervious concrete in 1 m³ was obtained with the innovation of recycled coarse aggregate as much as 10% in the volume of coarse aggregate in Table 1 below.

In this research, cylinder samples with 15 cm diameter and 30 cm height was used for the compressive strength and split tensile strength test of pervious concrete. While concrete beams with a size of 60 × 15 × 15 cm for flexure strength and infiltration rate test of pervious concrete. This research was conducted with addition variations of sidewalk’s paving block waste by 10, 20, 30% of coarse aggregate usage. The number of samples that would be made for this research were 30 pieces, with details shown in Table 2.

At the analysis stage, it would be examining the use of sidewalk’s paving block waste as a substitute for coarse aggregate percentage in pervious concrete which was reviewed based on the compressive strength, split tensile strength, flexure strength and infiltration rate that were tested when the pervious concrete was 28 days old. In addition, the optimum variation composition of sidewalk’s paving block waste addition would also be researched which can provide the most optimum values for compressive strength, split tensile strength, flexure strength and infiltration rate and

Table 1 Proportion of concrete mixture for each variation per m³

Composition in 1 m ³	
Cement	307,692 kg
Water	93,189 kg
Coarse Aggregate	1289,562 kg
Recycled Coarse Aggregate	121,478 kg

Table 2 Number of samples for mixture variations

No	Addition variation of sidewalk’s paving block waste (%)	Number of samples for each variation (pieces)				Total (pieces)
		Compressive strength	Split tensile strength	Flexure strength	Infiltration rate	
1	10	3	3	3	1	10
2	20	3	3	3	1	10
3	30	3	3	3	1	10
Total						30

Table 3 Results of visible properties test

Description	U-ditch cover		
	I	II	III
1. Planes			
a. Flatness	Yes	Yes	Yes
b. Crackness	No	No	No
c. Smoothness	Yes	Yes	Yes
2. Ribs			
a. Elbows	Yes	Yes	Yes
b. Sharpness	Yes	Yes	Yes
c. Strength	Yes	Yes	Yes

Table 4 Results of U-ditch cover thickness test

Sample	Right side thickness (cm)	Left side thickness (cm)	Mid side thickness (cm)	Average thickness (cm)
1	9,775	9,880	9,718	9,791
2	9,770	9,974	9,710	9,818
3	9,970	9,982	9,958	9,970
Average	9,838	9,945	9,795	9,860

Table 5 Calculation results of U-ditch cover infiltration rate

<i>U-Ditch Cover</i>				
Sample	Water mass (kg)	Infiltration time (s)	Infiltration rate (mm/s)	Infiltration rate (mm/h)
1	4.000	128	7.31E-01	2.03E-04
2	4.000	126	7.42E-01	2.06E-04
3	4.000	123	7.61E-01	2.11E-04
Average	4.000	125.667	7.45E-01	2.07E-04

would then be used for the process of making u-ditch covers with a size of $74 \times 60 \times 10$ cm and elbows of 3.53 cm.

4 Result and Discussion

A. Samples Testing

Table 6 Medan city average rainfall data in January–December 2020 per m²

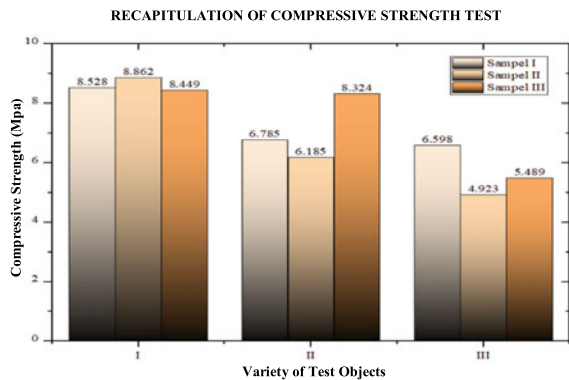
Year 2020	Average rainfall (mm)
January	2.803
February	2.759
March	3.352
April	10.967
May	15.671
June	20.500
July	9.687
August	6.537
September	7.637
October	15.023
November	11.220
December	12.729
Average	9.907

4.1 Compressive Strength of Pervious Concrete

In Fig. 1, it could be seen that the maximum stress that could be carried by pervious concrete was in variation I (10% addition of sidewalk’s paving block waste) with an average compressive strength of 8.613 MPa. And the minimum stress that could be carried by the pervious concrete was in variation III (30% addition of sidewalk’s paving block waste) with an average compressive strength of 5,670 MPa.

From the research results, it could be concluded that the use of sidewalk’s paving block waste addition as coarse aggregate affected the compressive strength of pervious concrete with an inverse relationship. Due to the greater use of sidewalk’s paving block waste as coarse aggregate in the composition, the lower the compressive strength value of pervious concrete. However, the results achieved from

Fig. 1 Recapitulation of Compressive Strength Test of 28 Days Concrete Cylinders



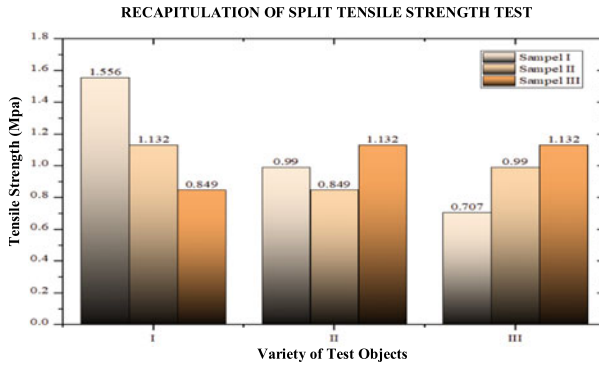


Fig. 2 Recapitulation of split tensile strength test of 28 days concrete cylinders

pervious concrete in this research have met the standard compressive strength of pervious concrete in ACI 522R-10 chapter 5.

4.2 Split Tensile Strength of Pervious Concrete

Based on Fig. 1, it could be seen that the optimum value of the split tensile strength of pervious concrete that can be carried was in variation I (10% addition of sidewalk's paving block waste) with an average split tensile strength value of 1.179 MPa. And the minimum split tensile strength value was in variation III (30% addition of sidewalk's paving block waste) with an average split tensile strength value of 0.943 MPa (Fig. 2).

From the research results, it could be concluded that the use of sidewalk's paving block waste addition as coarse aggregate affected the compressive strength of pervious concrete with an inverse relationship. Due to the greater use of the sidewalk's paving block waste as coarse aggregate in the composition, the lower the value of the split tensile strength of pervious concrete.

4.3 Flexure Strength of Pervious Concrete

Based on Fig. 3, it could be seen that the optimum value of the average flexure strength of pervious concrete was in variation I (10% addition of sidewalk's paving block waste) with an average flexure strength value of 2.196 MPa. And the average minimum flexure strength value was in variation III (30% addition of sidewalk's paving block waste) with an average flexure strength value of 2,071 MPa.

From the research results, it could be concluded that the use of sidewalk's paving block waste addition as coarse aggregate affected the flexure strength of pervious concrete with an inverse relationship. Due to the greater use of sidewalk's paving

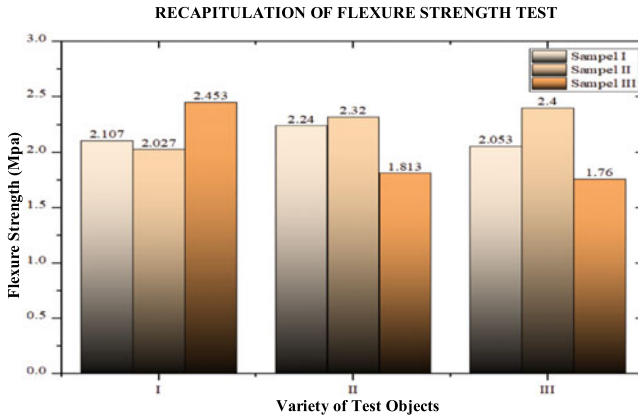


Fig. 3 Recapitulation of flexure strength test of 28 days concrete beams

block waste as coarse aggregate in the composition, the lower the compressive strength value of pervious concrete. The pervious concrete in this research have met the flexure strength standard of pervious concrete in ACI 522R-10 chapter 5.

4.4 Infiltration Rate

Based on Fig. 4, it could be seen that the optimum value of the average infiltration rate of pervious concrete was in variation III (30% addition of sidewalk’s paving block waste) with an average infiltration rate value of 1.95×10^{-4} mm/h. And the average minimum infiltration rate value was in variation I (10% addition of sidewalk’s paving block waste) with an average infiltration rate value of 1.93×10^{-4} mm/h.

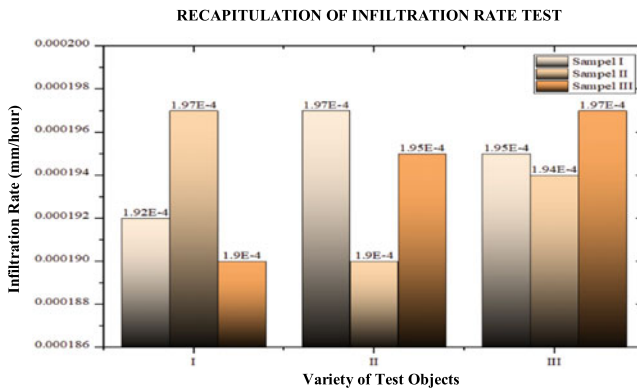


Fig. 4 Recapitulation of Infiltration Rate Test

Visible Properties Test

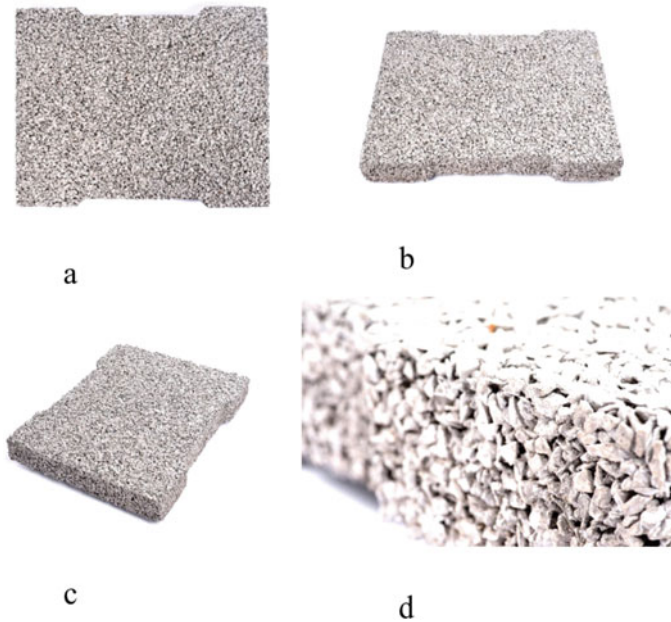


Fig. 5 Visible properties test of *U-Ditch* cover, a. Top View, b. Front View, c. Side View, d. Elbow Details

B. U-Ditch Cover Testing

From the examination results, it showed that this research produced a u-ditch cover that had a flat, uncracked, and smooth surface. From the examination results of visible properties of the u-ditch cover, the following data were obtained (Fig. 5, Table 3):

4.5 Size Test

After examining the visible properties, the dimensions and cross-section and dimensions could be checked as anticipated, using a u-ditch cover, on average, 3 intact samples were used. As a measuring tool, a ruler with an accuracy of 0.1 mm was used and thickness measurements were carried out at least 3 (three) times in different places and the average value was taken (Table 4).

Judging from the test results data above, the condition of u-ditch covers showed a difference in thickness caused by the way of making u-ditch covers manually so that u-ditch covers with non-uniform density were obtained. Because the density of the pores contained in u-ditch covers would greatly affected the density of u-ditch covers composition. On thickness examination, there were u-ditch covers which had

a thickness of more and less than 10 cm (100 mm), but still met the requirements, i.e. an 8% tolerance.

4.6 Infiltration Rate Test

From the u-ditch cover infiltration rate test using variation I (10% addition of sidewalk's paving block waste) at age of 7×24 h which was carried out at the Civil Engineering Field, Universitas Sumatera Utara, the following data were obtained (Table 5):

From the test results of field infiltration rate testing for u-ditch covers, the optimum infiltration rate value was 2.11×10^{-4} mm/h, and the minimum infiltration rate value was 2.03×10^{-4} mm/h (Table 6).

Based on the table above, it could be seen that the value of Medan City Average Rainfall Data in January 2020 to December 2020 which had been recorded by the Balai Besar Meteorologi, Klimatologi, dan Geofisika Wilayah I Medan (BBMKG Wil. I Medan), the maximum occurred in May 11, 2020 with an intensity of 130.9 mm. If it was assumed that this rain was a heavy rain for 2 h, then the intensity of rain per hour was 65.45 mm. From these data, it could be seen that the rate that occurs is 0.01818 mm/second. Based on the results of field infiltration rate test for u-ditch covers, the optimum infiltration rate value was 2.11×10^{-4} mm/h or 0.761 mm/s.

5 Conclusion

Based on the research that had been done, it could be concluded that:

1. The optimum composition for the application of pervious concrete principles on u-ditch covers which was effective for draining water and had enough strength out of the 3 composition variations tested was variation I (10% addition of sidewalk's paving block waste) with a compressive strength value of 8.613 MPa, split tensile strength of 1.179 MPa, flexure strength of 2.196 MPa, infiltration rate of 1.93×10^{-4} mm/h.
2. From the research results, it could be concluded that the use of sidewalk's paving block waste addition as coarse aggregate affected the compressive strength, split tensile strength and flexure strength of pervious concrete with an inverse relationship. Due to the greater use of sidewalk's paving block waste as coarse aggregate in the composition, the lower the compressive strength, split tensile strength, and flexure strength of pervious concrete. And referring to ACI 522-R-10 chapter 1, the pervious concrete in this research have met the compressive strength standard of permeable concrete which ranged from 2.8 MPa to 28 MPa.

3. Based on the test results, the optimum field infiltration rate of u-ditch covers obtained was 0.761 mm/s, and the rate of rainfall that occurred was 0.01818 mm/s. Based on these data, it was known that the rain rate was smaller than the rate that u-ditch covers could escape. Therefore, u-ditch covers had a good infiltration value so that rainwater runoff could be passed to the drainage which gave a good impact in overcoming puddles.

Acknowledgements TALENTA fund of USU 2021

References

1. Nugraha P (2007) *Antoni: Teknologi Beton*, Yogyakarta, p. 2007
2. Trisnoyuwono D (2014) *Beton Non-Pasir*. Graha Ilmu, Yogyakarta
3. SNI 15-2049-2004 (2004) SNI 15-2049-2004 Semen Portland, Badan Standar Nas Indones pp. 1–128
4. S. 2847:2013 (2013) *Persyaratan Beton Struktural untuk Bangunan Gedung*, Bandung Badan Stand Indones pp. 1–265
5. Badan Standardisasi Nasional (2011) SNI 03-1974-2011 Cara Uji Kuat Tekan Beton dengan Benda Uji Silinder, Badan Stand Nas Indones p. 20
6. SNI 2491 (2014) *Metode uji kekuatan tarik belah spesimen beton silinder Standard Test Method for Splitting Tensile Strength of Badan Stand Nas* pp. 1–17
7. SNI 4431:2011 (2011) *Cara uji kuat lentur beton normal dengan dua titik pembebanan*, Standar Nas Indones p. 16
8. ASTM C 1701 (2009) *Standard Test Method For Infiltration Rate Of In Place Pervious Concrete*. ASTM Int
9. Nasrullah A (2019) 2021, Bupati Serang Bakal Pasang Jalan Beton Sepanjang 601,13 Km. [www.detik.com. https://news.detik.com/berita/d-4474606/2021-bupati-serang-bakal-pasang-jalan-beton-sepanjang-60113-km](https://news.detik.com/berita/d-4474606/2021-bupati-serang-bakal-pasang-jalan-beton-sepanjang-60113-km) . Accessed 3 June 2020

Study on Compressive Strength of Geopolymer Mortar Based on Fly Ash and GGBFS with Various Molar Variations



Rahmi Karolina, Johannes Tarigan, Harianto Hardjasaputra,
and Kenrick Hermanto

Abstract The high production and demand for portland cement in the world can trigger even greater emissions produced by the cement industry which are expected to continue to increase. This can happen because the cement production process produces CO₂ gas emissions into the air which are equivalent to the amount of portland cement produced, thus triggering the greenhouse effect. Therefore, the application of geopolymers into cement and concrete contributes greatly to reducing CO₂ emissions and the greenhouse effect. This research examines the mechanical properties and morphological characteristics of geopolymer mortar based on fly ash and GGBFS with various variations of NaOH molarity which was cured at room temperature (25 °C) for 28 days. In addition to mortar, the fly ash used was also tested for microstructural characteristics. In this research, 165 samples were made in the form of geopolymer mortar with composition variations between fly ash and GGBFS at various NaOH molarity. Mechanical test that carried out was in the form of mortar compressive strength test. In addition, microstructural characteristics was also tested on fly ash and mortar with the highest compressive strength. The results of the mechanical mortar test showed that the highest compressive strength was 92 MPa that was obtained from FG19 mortar (fly ash 10%, GGBFS 90%) with NaOH molarity of 10 and 12 M. The results of the characteristic research of fly ash showed that fly ash was classified as class C and had a crystalline structure. The microstructural characteristics test results of the FG19 mortar with 12 M variation showed that the

R. Karolina (✉)

Doctoral Student Civil Engineering, Universitas Sumatera Utara, Medan 20155, Sumatera Utara, Indonesia

e-mail: rahmi.karolina@usu.ac.id

Integrated Research Laboratory, Universitas Sumatera Utara, Medan 20155, Sumatera Utara, Indonesia

J. Tarigan · K. Hermanto

Civil Engineering, Universitas Sumatera Utara, Medan 20155, Sumatera Utara, Indonesia

H. Hardjasaputra

Civil Engineering Department, Faculty of Engineering, Universitas Pembangunan, Jakarta, Indonesia

© Institute of Technology PETRONAS Sdn Bhd 2024

B. S. Mohammed et al. (eds.), *Proceedings of the International Conference on Emerging Smart Cities (ICESC2022)*, Lecture Notes in Civil Engineering 324,

https://doi.org/10.1007/978-981-99-1111-0_2

mortar had cracks and voids. However, the Al, Si, Na, and K elements were evenly distributed so that the mortar mixed homogeneously.

1 Introduction

Concrete is part of a structure that can be found in a construction process, for example, buildings, roads, and bridges [14]. The use of concrete as a building material provides various advantages. As stated by Sumajouw 2014: 215 that “The advantages of using concrete as a building material include: this material can be shaped according to the planner’s desire at the job site, the forming materials are relatively available and the concrete can be made by the workers.” Because of these factors, planning consultants still choose concrete as a building material that is applied in the design and planning of civil engineering buildings [13]. The use of concrete as a building construction cannot be separated from the availability of concrete materials, one of which is cement [6].

According to Purnawan and Prabowo (2017) [12], cement is the main basic material in building construction, making cement a strategic commodity. Bentur (2002) in [2] states that portland cement is a binding material that has been used in the construction field for nine millennia. Portland cement has the characteristics and form of a powder that is simple, easy to obtain and easy to work with. In addition, when mixed with water, filler material, and aggregate, it will form a dense mixture that is easy to form. In addition, if left at room temperature it will harden by itself. However, nowadays, the impact of various environmental sustainability considerations has influenced the use of cement in the construction industry.

The high production and demand for cement worldwide have resulted in the number of emissions released by the cement industry which is expected to continue to increase (Hasanbeigi et al. 2012 in [4]). Based on [16], experts who work in observation of global warming state that 7% of the production of CO₂ gas emissions in nature comes from cement production. This is because the cement production process can produce CO₂ emissions into the air which are equivalent to the amount of cement produced so if the cement produced is 1 ton, the CO₂ produced is also 1 tonne [15]. In addition, the United Nation Environment Program (2019) in Uda (2021) explains that the construction industry produces 39% of carbon dioxide (CO₂) gas emissions, of which 11% comes from the material production process, one of which is cement. The emission of CO₂ gas produced in excess can increase greenhouse gases in the atmosphere which have an effect on increasing global warming. This is contrary to the Paris agreement, which is an international agreement on climate change that seeks to limit the increase in global average temperature to less than 2 °C above pre-industrial levels and to continue efforts to suppress temperature increases to 1.5 °C in the world above the pre-industrial level (United Nations Framework 58 Convention on Climate Change 2015 in USA 2021).

In Indonesia itself, the portland cement industry has increased due to the increasing use of portland cement every year [7]. In a report made by the World Bank (2012)

in [1], it is stated that Indonesia as a producer of greenhouse gas emissions is in the top 10, producing 780 million metrics. Furthermore, in 2014 the Global Carbon Project stated that Indonesia was behind Germany and Japan by CO₂ emission results of 641 million metrics. Since CO₂ gas emissions from OPC (Ordinary Portland Cement) play an important role in global greenhouse gas concentrations, it can be a major contributing factor in the incorporation of geopolymers into cement and concrete applications (Mustafa Al [10]. Geopolymer concrete is concrete with natural materials that function as a binder [15].

According to [7], fly ash is one of the materials that can be used as a substitute for portland cement, but studies still need to be carried out in detail, itemized, and consistent. [7] further explained that basically fly ash does not have the ability to bind like portland cement. However, with the addition of water and an activator in the form of NaOH and Na₂SiO₃, it will produce a chemical reaction between the silicate oxide contained in fly ash with NaOH and Na₂SiO₃. Thus, fly ash which is synthesized into an inorganic alumino silicate compound (geopolymer) with the addition of NaOH and Na₂SiO₃ activator will have the ability to bind like portland cement in general. Based on Government Regulation Number 22 of 2021 of Indonesia concerning Guidelines for Environmental Protection and Management, the use of non-B3 waste, one of which is fly ash as a substitute for raw materials as referred to in Article 459 paragraph (3) letter a, can be carried out in the activities of making concrete, paving blocks, lightweight concrete, and other similar construction materials. The fly ash used in this research comes from the PLTU Pangkalan Susu which is one of the electricity industries in Indonesia and is estimated to be able to produce large amounts of fly ash as a result of its coal-burning activity [9].

In addition to fly ash, GGBFS (Ground Granulated Blast Furnace Slag) is also used as a substitute for portland cement so that it can help reduce construction costs due to the decreasing use of cement and from the aspect of structural strength that concrete with GGBFS produces concrete with better quality than concrete without GGBFS (Siddique and Kaur 2011 in Nursyafri and Taufan 2020 [11]). On the other hand, the use of GGBFS which is a waste material will provide benefits for environmental aspects. In this research, the GGBFS used came from PT. Krakatau Cement Indonesia.

2 Materials and Methods

2.1 Types and Locations of Research

The research method used was an experimental method with the studied was Fly Ash as the main component of geopolymer mortar formation with GGBFS variation substitution of 0%–100%. The samples were casted in the form of a 5 × 5 × 5 cm cube and 3 samples were made for each variation. The tests carried out in this research were setting time, mortar consistency, compressive strength, and morphological characteristics. This research was conducted at the Integrated Laboratory, Diponegoro

University and Integrated Research Laboratory, USU, Medan City, Medan Baru, North Sumatra 20,155.

2.2 *Research Materials and Tools*

The materials used for the making of geopolymer mortar include the following:

- Fly Ash, from the Pangkalan Susu PLTU located in Tanjung Pasir Village, Kec. Pangkalan Susu, Kab. Langkat.
- GGBFS (Ground Granulated Blast Furnace Slag), from PT. Semen Indonesia in collaboration with PT. Krakatau Steel Tbk.
- Sodium Hydroxide (NaOH), in the form of crystals obtained from chemical stores.
- Sodium Silicate (Na_2SiO_3), in the form of a solution obtained from a chemical store that has high purity of BE52 specifications for the making of geopolymer paste/concrete.
- Fine Aggregate, using *mesh 30up* silica sand.
- Water (H_2O)

The tools used in this research include the following::

- Pan.
- Sample Plastic
- Vessel
- Cement Spoon
- Scrap
- Sieve
- Scales
- Measuring cup
- Mixer
- Trigang
- Hammer
- Vibrating Table
- Mold
- Flow Table
- Vicat Apparatus Set
- Compression Machine

2.3 *Planning Phase of Samples*

In the material design, planning was carried out to make a mix design with variations in the air binder factor as planned. After the mortar mix design was obtained, then a trial was carried out on the design (trial mix design) to determined the feasibility

of the samples and the water factor value of the geopolymer mortar by using a flow table and Vicat apparatus. The calculation of the flow value using Eq. (1) as follows:

$$Nilai\ Flow = \frac{D_1 - D_0}{D_0} \times 100\% \tag{1}$$

where:

D_0 = Diameter of mortar when molding

D_1 = Diameter of mortar after knocking, measured at four positions and calculated the average value

The following is a planning table for the number of samples made for each composition variation between fly ash and GGBFS on variations in NaOH molarity (Table 1).

2.4 Curing of Samples

At this phase, the geopolymer mortar samples were treated with air curing at room temperature (25 °C) for 28 days.

2.5 Compressive Strength Test of Samples

The mortar compressive strength test aims to find out how much the compressive strength value of the samples at 28 days using a Compression Machine is. The compressive strength of mortar can be calculated using the following formula

$$\sigma_m = \frac{P}{A} \tag{2}$$

where:



Fig. 1 Samples of geopolymer mortar

σ_m = compressive strength of mortar (MPa)
P = maximum load (N)
A = cross-sectional area loaded (mm^2)

3 Results and Discussion

3.1 Samples of Geopolymer Mortar

The geopolymer mortar produced in this research was mortar with variations of fly ash and GGBFS and variations of molarity with air curing at room temperature for 28 days. The resulting geopolymer mortar samples can be seen in Fig. 1.

Fig. 2 Graph of initial setting time results

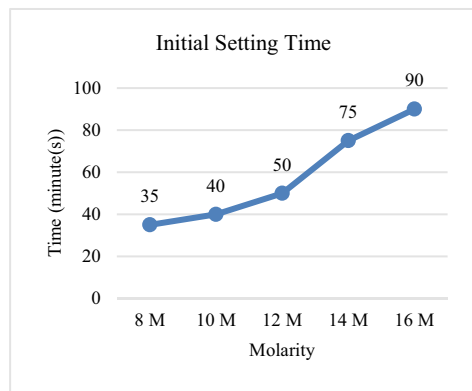


Fig. 3 Graph of final setting time results

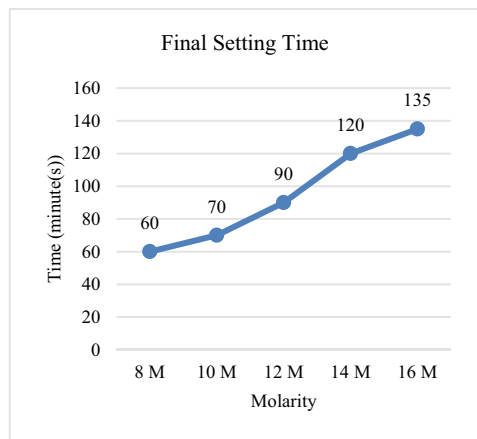
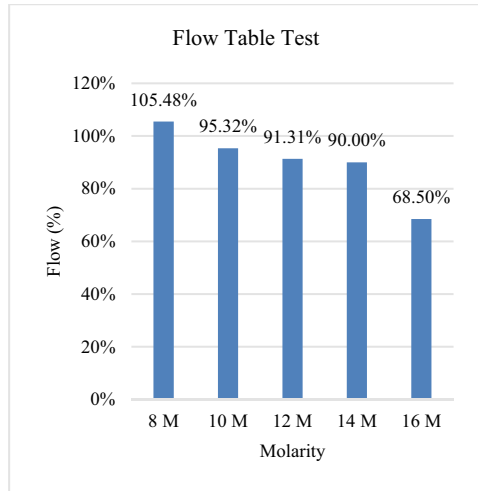


Fig. 4 Graph of mortar consistency test results



From the workability of the geopolymer mortar mixture in different variations of fly ash and GGBFS, there were differences, where the more fly ash content in the geopolymer mortar mixture, the easier the working process, while the more GGBFS content in the geopolymer mortar mixture, the more difficult the process was.

From the visual appearance of the geopolymer mortar product in different variations of fly ash and GGBFS, it produced different colors. The more fly ash content in the geopolymer mortar, the lighter the color of the geopolymer mortar, while the more GGBFS content in the geopolymer mortar, the darker the color of the geopolymer mortar.

3.2 Results of Setting Time Test

The following were the setting time test results of the FG55 binder where 50% fly ash and 50% GGBFS with various molarities (Figs. 2, 3 and Table 2):

The initial setting time of the binder for variations of FG55 8, 10, 12, 14, and 16 M, respectively, were 35, 40, 50, 75, and 90 min. The final setting time of the binder for variations of FG55 8, 10, 12, 14, and 16 M were 60, 70, 90, 120, and 135 min, respectively. From the test results, we can conclude that the higher the molarity of NaOH, the longer the initial and final setting time of the binder.

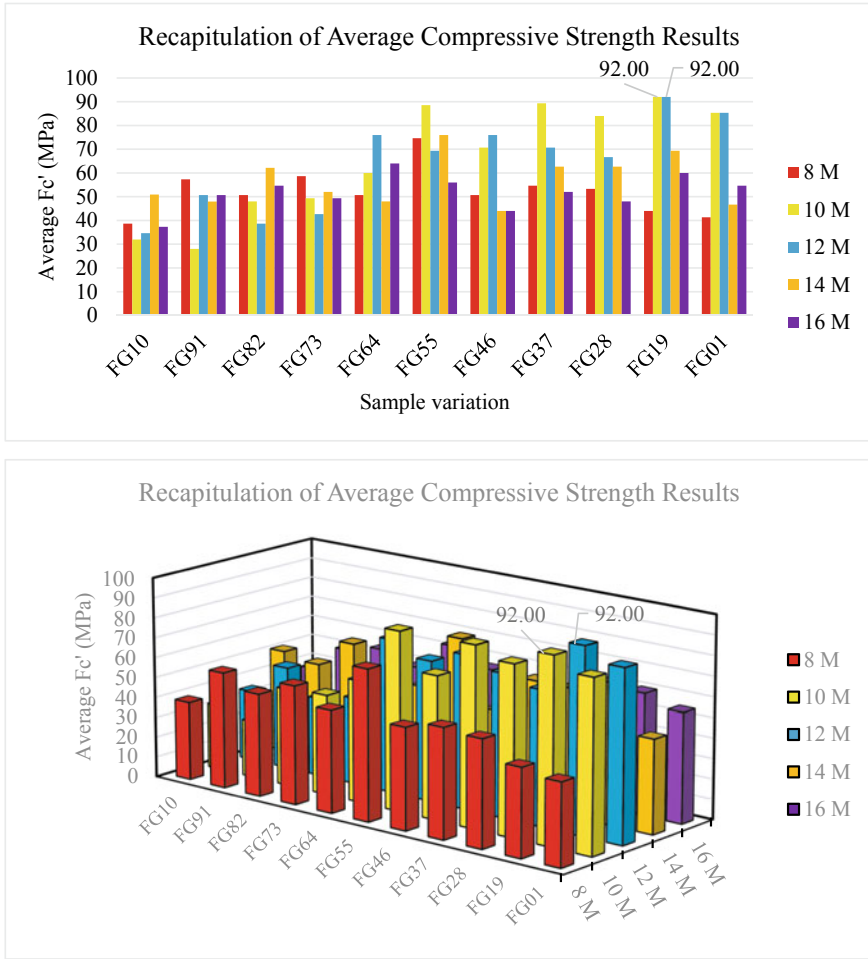


Fig. 5 Graph of 8–16 M average compressive strength results

3.3 Results of Mortar Consistency Test

The following were the results of the FG55 mortar consistency test where 50% fly ash and 50% GGBFS with various molarities (Fig. 4 and Table 3).

From the graph above, it can be seen that from the 8–16 M NaOH molarity variation, the consistency value decreased from 105.48 to 68.50%. Thus, it can be concluded that the best workability was found in the 8 M NaOH molarity variation, which was 105.48%.

3.4 Results of Samples Compressive Strength Test

The following was the results recapitulation of the compressive strength test of geopolymer mortar samples cured at room temperature for 28 days for each geopolymer mortar variation (Fig. 5):

From the graph above, it can be seen that the maximum compressive strength of geopolymer mortar occurred in the variation of FG19 with NaOH molarity of 10 and 12 M, which was 92.00 MPa, while the minimum compressive strength of geopolymer mortar occurred in the variation of FG91 with NaOH of molarity 10 M of 28.00 MPa. Thus, the most optimum geopolymer mortar based on the recapitulation of the average compressive strength was found in the FG19 sample with NaOH molarity of 10 and 12 M.

3.5 Results of Microstructural Characteristics Test

The following was the results recapitulation of the compressive strength test of geopolymer mortar samples cured at room temperature for 28 days for each geopolymer mortar variation.

3.5.1 Results of Fly Ash Microstructural Characteristics Test

Fly ash used in this research was fly ash from PLTU Pangkalan Susu located in Tanjung Pasir Village, Kec. Pangkalan Susu, Kab. Langkat. The tests carried out on the fly ash material were testing the composition of chemical compounds, i.e. XRF (X-Ray Fluorescence), SEM-EDX (Scanning Electron Microscope-Energy Dispersive X-Ray), and XRD (X-Ray Diffraction). These tests were carried out to determine the compounds contained in the fly ash material.

Results of X-Ray Fluorescence (XRF) Test

This test was carried out to obtain the chemical elements contained in fly ash so that the type of fly ash used in geopolymer mortar can be found. XRF fly ash test results can be seen in Table 4.

From the table, it can be seen that fly ash was classified as class C fly ash based on the ACI Manual of Concrete Practice 1993 Part 1 226.3R-3 in Eunike et al. (2014) [3]. This was because the amount of SiO_2 , Al_2O_3 , and Fe_2O_3 in fly ash were greater than 50%, i.e.54.51%. In addition, the content of CaO compounds in fly ash was greater than 10%, i.e.10.8879%.

Table 1 Planning the number of samples

Code	<i>Fly Ash</i>	<i>GGBFS</i>	8 M	10 M	12 M	14 M	16 M
FG10	100%	0%	3	3	3	3	3
FG91	90%	10%	3	3	3	3	3
FG82	80%	20%	3	3	3	3	3
FG73	70%	30%	3	3	3	3	3
FG64	60%	40%	3	3	3	3	3
FG55	50%	50%	3	3	3	3	3
FG46	40%	60%	3	3	3	3	3
FG37	30%	70%	3	3	3	3	3
FG28	20%	80%	3	3	3	3	3
FG19	10%	90%	3	3	3	3	3
FG01	0%	100%	3	3	3	3	3
Total of samples			165 pieces				

Table 2 Results of binder setting time

Code	Molarity	Initial setting time (menit)	Final setting time (menit)
FG55	8 M	35	60
FG55	10 M	40	70
FG55	12 M	50	90
FG55	14 M	75	120
FG55	16 M	90	135

Table 3 Results of mortar consistency test

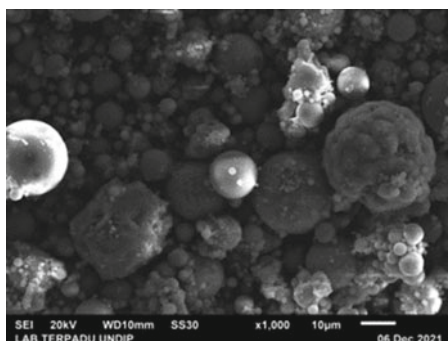
Molarity	Average	Flow (%)
8 M	205,48	105,48
10 M	195,32	95,32
12 M	191,31	91,31
14 M	190,00	90,00
16 M	168,50	68,50

Results of Scanning Electron Microscope (SEM) and Energy Dispersive X-Ray (EDX) Test

The SEM–EDX test aims to analyze the shape and surface morphology, as well as the composition of the fly ash. Tests were carried out with magnifications of 1,000×, 5,000×, 10,000×, and 20,000×. The results of the SEM-EDX test can be seen in Figs. 6, 7, and Table 5.

Table 4 Percentage of fly ash contents oxide using XRF

No.	Component	Value of analysis results (%)
1	MgO	1,14
2	Al ₂ O ₃	10,9634
3	SiO ₂	25,2197
4	P ₂ O ₅	0,0894
5	SO ₃	0,6432
6	Cl	0,0127
7	K ₂ O	0,9121
8	CaO	10,8879
9	TiO ₂	0,9332
10	MnO	0,4173
11	Fe ₂ O ₃	18,3237
12	NiO	0,0216
13	ZnO	0,019
14	SrO	0,1159
15	ZrO ₂	0,0269
16	BaO	0,2124
17	Balance	30,0617

Fig. 6 Results of SEM Fly Ash observation

From the table, it can be seen that fly ash was classified as class C fly ash based on the ACI Manual of Concrete Practice 1993 Part 1 226.3R-3 in Eunike et al. (2014) [3]. This was because the amount of SiO₂, Al₂O₃, and Fe₂O₃ in fly ash were greater than 50%, i.e. 66.95%. In addition, the content of CaO compounds in fly ash was greater than 10%, i.e. 10.09%.

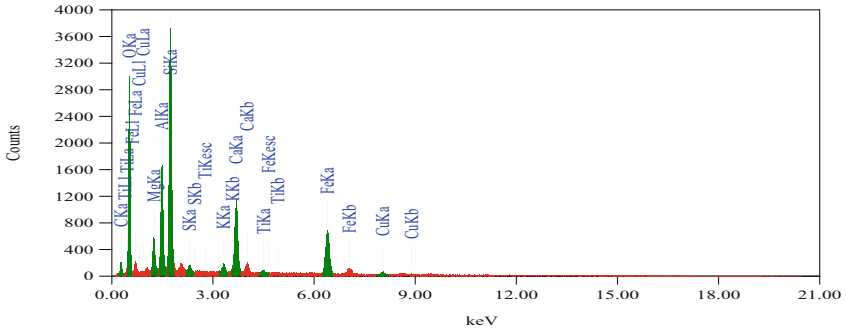


Fig. 7 Results of *Fly Ash* characterization using *SEM-EDX*

Table 5 Percentage of fly ash oxide contents using SEM-EDX

No.	Component	Value of analysis results (%)
1	C (balance)	14,60
2	MgO	4,08
3	Al ₂ O ₃	13,54
4	SiO ₂	35,87
5	SO ₃	1,35
6	K ₂ O	0,92
7	CaO	10,09
8	TiO ₂	0,61
9	FeO	17,54
10	CuO	1,40

Results of X-Ray Diffraction Test (XRD) Test

XRD test aims to identify the crystalline material of a material, its crystallite structure (qualitative), and phase (quantitative), by utilizing X-ray electromagnetic radiation. Through this test, a diffraction pattern was obtained, where the diffraction angle is 2θ , which is between an angle of 10° to 90° with an interval distance of 1,000 (deg). The results of the XRD diffraction pattern can be seen in Fig. 8.

Based on this figure, fly ash had a peak at a diffraction angle of $2\theta = 20-40^\circ$ with an intensity of 400 to 800. The intensity of fly ash belongs to the high-intensity category. The pattern formed also had peaks and in order so that the fly ash structure had a crystalline element. From this test, the scattering angle of 2θ identified the three highest peaks, i.e. at an angle of 26.9989° with an intensity of 1412, 36.1532° with an intensity of 451, and 21.2195° with an intensity of 308.

Fig. 8 Results of *Fly Ash* XRD test

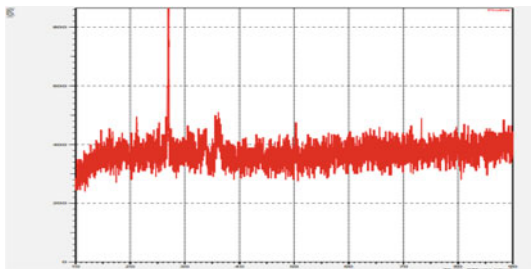
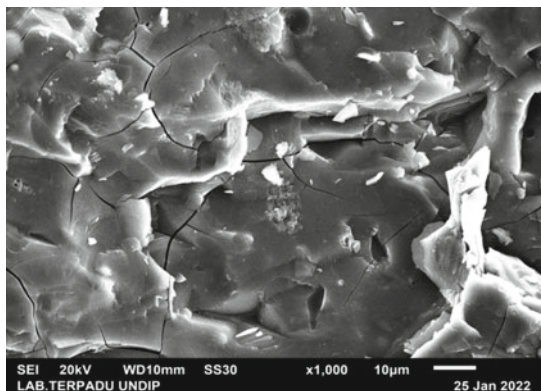


Fig. 9 Results of SEM observations on mortar



3.5.2 Results of Mortar Microstructural Characteristics Test

The geopolymer mortar that has been tested for compressive strength was taken from the flakes to then be tested for morphological characteristics. The geopolymer mortar used as the sample was the mortar that had the highest compressive strength, i.e. the mortar with the code FG19 with 12 M variation. The test that carried out on the geopolymer mortar was the composition of chemical compounds test, i.e. SEM–EDX (Scanning Electron Microscope–Energy Dispersive X-Ray). This test was carried out to determined the compounds contained in the mortar.

Results of X-Ray Diffraction (XRD) Test

SEM test aims to determine the morphological characterization of the geopolymer mortar formed due to the geopolymerization process between fly ash and GGBFS with NaOH molarity. SEM test results included top view geopolymer morphology with magnifications of 500×, 1,000×, 5,000× and 10,000× (Fig. 9).

Based on the figure above, it can be seen that in the geopolymer mortar flakes, voids were found. [8] explains that the formation of voids is caused by trapped air during the mortar-making process so that it can affect the mechanical properties

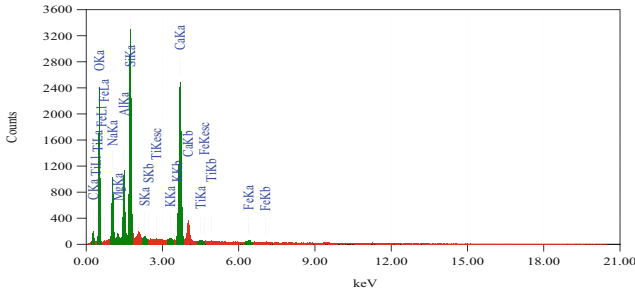


Fig. 10 Results of mortar characterization using SEM-EDX

Table 6 Percentage of mortar oxide content using SEM-EDX

No.	Component	Value of analysis results (%)
1	C	15,13
2	Na ₂ O	9,67
3	MgO	0,89
4	Al ₂ O ₃	9,28
5	SiO ₂	35,19
6	SO ₃	0,83
7	K ₂ O	0,27
8	CaO	26,99
9	TiO ₂	0,60
10	FeO	1,14

of the mortar. In addition to voids, cracks can also be seen which indicates that the polymerization or polycondensation process is not perfect. This area will later become an area that is prone to failure when the mortar compressive strength test is carried out which will indirectly reduce the compressive strength of the geopolymer mortar (Maragkos et al. 2008 in [8]). In addition, it can be seen that the constituent materials of the mortar, in the form of fly ash, GGBFS, silica sand, and alkali activator have been mixed so that it is difficult to distinguish each grain. Thus, it can be said that the location of the mortar that tested has been mixed homogeneously.

From Fig. 10. and Table 6, it can be seen that the component with the largest percentage value was SiO₂, which was 35.19%. This was because the composition of GGBFS used was 90% where one of the main compounds of GGBFS was silicate (SiO₂) (Nursyafri and Taufan, 2020 [11]). Judging from the fine aggregate used was silica sand which of course contained high silica elements. In addition, fly ash used was class C fly ash which contained high silicate components based on XRF and SEM-EDX tests.

Figure 11. showed the distribution of colors on the surface of the samples. In figure c, the Al element were indicated by green, dark green, and black colors. In figure d, the Na element were indicated by blue, dark blue, and black colors. In figure e,

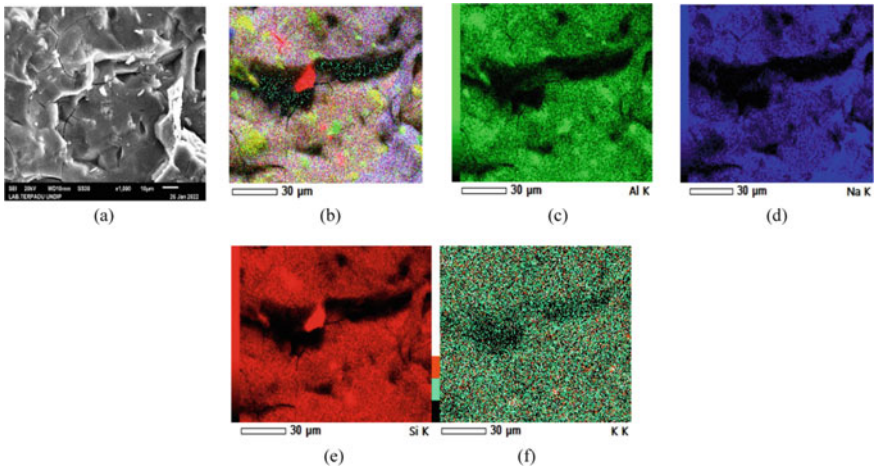


Fig. 11 Distribution of mortar elements

the Si element were marked by red, dark red, and black colors. In the figure f, the K element were marked by red, light green, and black colors. From the results of the mapping in Figure b, it can be concluded that the elements of Al, Si, Na, and K were evenly distributed at the location of the mortar being tested, which means that the mortar can be said to had mixed homogeneously.

4 Conclusions

- The length of time for setting the binder was influenced by the molarity of NaOH. The higher the molarity of NaOH, the longer the initial and final setting times.
- The value of mortar consistency (workability) was influenced by the molarity of NaOH. The lower the molarity of NaOH, the better the workability of the mortar
- The maximum compressive strength results occurred in FG19 samples (10% fly ash and 90% GGBFS) with 10 M and 12 M NaOH molarities of 92 MPa. Thus, the most optimum geopolymer mortar based on the recapitulation of the average compressive strength was found in the FG19 sample with NaOH molarity of 10 M and 12 M.
- Based on the analysis of the microstructural characteristics of the fly ash of PLTU Pangkalan Susu, the XRF and SEM-EDX results showed that fly ash was classified as class C fly ash. From the XRD results, fly ash was a material that had a crystalline structure.
- Based on the analysis of the microstructure characteristics of the FG19 geopolymer mortar with 12 M variation, the SEM results showed that the mortar had cracks and voids. From the EDX results, the highest compound content in mortar was SiO_2 . From the mapping results, the elements of Al, Si, Na, and K were evenly distributed so that the mortar had been mixed homogeneously

References

1. Anggraeni DY (2016) pengungkapan emisi gas rumah kaca, kinerja lingkungan, dan nilai perusahaan. *Jurnal Akuntansi Dan Auditing* 13(2):155 (2016). <https://doi.org/10.14710/jaa.v13i2.13870>
2. Bentur A (2002) Cementitious materials-nine millennia and a new century: past, present, and future. *J Mater Civ Eng* 14(1), ASCE, /1-2-22
3. Eunike et al (2014) Kuat Tarik Lentur Beton Geopolymer Berbasis Abu Terbang (Fly Ash). *Jurnal Sipil Statik* 2(1)
4. Hasanbeigi A, Lu H, Williams C, Price L (2012) International Best Practice for Pre-Processing and Orlando Co-Processing Municipal Solid Waste and Sewage Sludge in Cement Industry. Ernest Lawrence Berkeley National Laboratory, California
5. Indonesia R (2021) Peraturan Pemerintah Nomor 22 Tahun 2021 tentang Pedoman Perlindungan dan Pengelolaan Lingkungan Hidup. Sekretariat Negara Republik Indonesia, 1(078487A), p 483. <http://www.jdih.setjen.kemendagri.go.id/>
6. Kandi YS, Ramang R, Cornelis RK, Silas Y, Ramang R, Cornelis R (2012) Substitusi Agregat Halus Beton Menggunakan Kapur Alam dan Menggunakan Pasir Laut Sebagai Campuran Beton (Studi Analisis Bahan Kapur Alam dan Pasir Laut Dari Kabupaten Sumba Barat Daya Provinsi Nusa Tenggara Timur). *Jurnal Teknik Sipil* 1(4):74-86
7. Kasyanto H (2012) Tinjauan Kuat Tekan Geopolimer Berbahan Dasar Fly Ash Dengan Aktivator Sodium Hidroksida Dan Sodium Silikat. *Ind. Res. Workshop Natl. Sem.* 3:254-259
8. Malik Y (2016) Studi Pengaruh Temperatur Dan Waktu Curing Terhadap Sifat Fisik-Mekanik Semen Geopolimer Berbasis Slag Ferronickel. <http://repository.its.ac.id/71279/>
9. Muhammad Fakhru Rozi JT, dan AP (2020) Analisis Sifat Mekanik Beton Geopolymer Berbahan Dasar Fly Ash Pltu Pangkalan Susu 1(5):567-579 (2020)
10. Mustafa Al Bakri AM, Kamarudin H, Khairul Nizar I, Bnhussain M, Zarina Y, Rafiza AR (2012) Correlation between Na₂SiO₃/NaOH ratio and fly ash/alkaline activator ratio to the strength of geopolymer. *Adv Mater Res* 341-342:189-193. <https://doi.org/10.4028/www.scientific.net/AMR.341-342.189>
11. Nursyafril, Taufan M (2020) Pemanfaatan GGBFS sebagai Bahan Tambah Aduk Mortar. *POTENSI* 2(1)
12. Purnawan, Prabowo (2017) Pengaruh Penambahan Limestone terhadap Kuat Tekan Semen Portland Komposit. *Jurnal Rekayasa Proses* 11(2). <http://journal.ugm.ac.id/jrekpro>
13. Sumajouw MDJ, Dapas SO, Windah RS (2014) Pengujian Kuat Tekan Beton Mutu Tinggi. *Jurnal Ilmiah Media Eng.* 4(4):97267
14. Syarif A, Setyawan C, Farida I (2016) Analisa Uji Kuat Tekan Beton Dengan Bahan Tambahan Batu Bata Merah. *STT-Garut* 14(1):46-56
15. Triwulan, Ekaputri JJ, Adiningtyas T (2007) Analisa Sifat Mekanik Beton Geopolimer Berbahan Dasar Fly Ash dan Lumpur Porong Kering sebagai Pengisi. *Jurnal Teknologi dan Rekayasa Sipil* 33(3):33-45
16. Waani JE, Elisabeth L, Teoretis J, Bidang T, Sipil R, Terapan D, Rekayasa B, Abstrak S (2017) Substitusi Material Pozolan Terhadap Semen pada Kinerja Campuran Semen 24:31. <https://doi.org/10.5614/jts.2017.24.3.7>
17. Zaky Nugraha A, Wiloso EI, Yani M (2018) Pemanfaatan Serbuk Gergaji Sebagai Substitusi Bahan Bakar Pada Proses Pembakaran-Kiln Di Pabrik Semen Dengan Pendekatan Life Cycle Assesment (LCA) Utilization of Saw Dust as Substitution Fuel at Combustion Process-Kiln at Cement Plant Using Life Cycle Assesment (LCA) Approach. *Jurnal Pengelolaan Sumberdaya Alam dan Lingkungan* 8(2):188-198. <https://doi.org/10.29244/jpsl.8.2.188-198>

Influence of Fly Ash, Volcanic Ash and Rice Husk Ash as Filler Asphalt Concrete Wearing Course Based on Marshall Characteristics



Alfia Magfirona, Riza Syaiful Billad, Gurawan Djati Wibowo,
and Tsulis Iq'bal Khairul Amar

Abstract Filler serves as a filling for the voids between coarse aggregate and fine aggregate in the AC-WC mixture. The filler has a significant effect on the marshall characteristics of the AC-WC mixture even though it is only as a filler. This study aims to investigate the effect of fly ash, volcanic ash, rice husk ash on marshall characteristics. The research data obtained from secondary data based on previous researchers, (Pratama 2021) for fly ash filler, (Rezi 2021) for volcanic ash filler, (Malacca 2021) for rice husk ash filler. The data is in the form of variations in the percentage of filler (fly ash, rice husk and volcano ash) with the same asphalt content. The sample was processed for statistical testing using SPSS version 26 software to determine the effect of asphalt content and filler percentage on marshall characteristics. Optimum Asphalt Content (OAC) test results obtained 6.1% fly ash, 6.2% volcanic ash, 6.7% rice husk ash. The test results on Marshall showed the most influential filler in the 2% rice husk ash filler with density, stability, Marshall Quotient (MQ) and VMA values, while the Flow value obtained the highest value in 1% volcanic ash filler. For the VFB of fly ash and rice husk ash, there was a decrease in the value of the filler content of 2% and 2.5% and an increase in the filler content of 3%. The results of statistical tests using SPSS show that those that have a significant positive linear influence on the asphalt content and filler percentage are Stability and Marshall Quotient (MQ). Research has contributed to research in the field of materials for AC-WC mixtures.

Keywords Filler · Marshall · Asphalt

A. Magfirona (✉)

Centre for Transport Studies, Universitas Muhammadiyah Surakarta, Surakarta, Indonesia
e-mail: am389@ums.ac.id

R. S. Billad · G. D. Wibowo · T. I. K. Amar

Civil Engineering Study Program, Engineering Faculty, Universitas Muhammadiyah Surakarta,
Surakarta, Indonesia

© Institute of Technology PETRONAS Sdn Bhd 2024

B. S. Mohammed et al. (eds.), *Proceedings of the International Conference on Emerging Smart Cities (ICESC2022)*, Lecture Notes in Civil Engineering 324,
https://doi.org/10.1007/978-981-99-1111-0_3

1 Introduction

Road pavement is the main thing to support the development of an area, by improving the quality and feasibility of an area's roads, it can increase safety and comfort in driving, therefore adequate and proper pavement is needed to be used. There are many types of road pavement used in Indonesia, one of which is asphalt concrete. Asphalt is a binder for road pavement mixtures which is the main factor and affects the performance of asphalt mixtures, especially on flexible pavements [1]. The pavement layer using asphalt concrete is one of the widely used pavements, because apart from being easy to obtain, asphalt is more efficient and can extend the life of the road itself [2]. The surface layer on asphalt concrete tends to be damaged quickly because the surface layer directly withstands the load of vehicles that pass through the road, plus Indonesia has very extreme weather changes [3]. To prevent damage to the surface of the road pavement caused by the influence of overload and the influence of water and weather, overcoming these problems can use aggregate replacement materials in the form of materials that meet specifications aimed at improving the quality of the asphalt [4, 5]. Asphalt Concrete (Asphalt Concrete) in Indonesia is known as Laston (asphalt concrete layer) which is a structural surface layer or top foundation layer on highways. Asphalt concrete consists of three layers, namely Asphalt Concrete-Wearing Course AC-WC, Asphalt Concrete-Binder Course AC-BC, and AC-Base Asphalt Concrete-Base [6]. Asphalt Concrete-Wearing Course is the topmost pavement layer and functions as a wear layer. Even though it is non-structural, AC-WC can increase pavement resistance against deterioration of pavement construction [7–9]. The function of asphalt in road construction is to bind the stone grains, fill the voids between the aggregate grains so as to protect them against the entry of water into the rock and provide a kind of cushion to the rock. The asphalt used in this study is hard asphalt with a uniform penetration of 60/70, does not contain water, when heated to a temperature of 175 C, does not foam and meets the requirements according to the provisions. 60/70 penetration asphalt is used because if you use asphalt with lower penetration it will cause the mixture not constrict together maximally [10]. There are seven mixed characteristics that must be possessed by asphalt concrete, namely stability, durability, flexibility or flexibility, fatigue resistance, surface roughness or skid resistance, water resistance and workability [11]. The relationship between resistance (stability) and plasticity yield (flow) is directly proportional, the greater the stability, the greater the flow, and vice versa. So the greater the stability, the more asphalt will be able to withstand the load, and vice versa. And if the flow is higher, the asphalt is more able to withstand the load. From the observations on the Marshall test, a graph of the relationship between the percentage of asphalt content and the percentage of voids filled with asphalt (VFA), the percentage of voids in the mixture (VIM), melt (flow), stability, and the comparison between stability and fatigue was made to obtain the Marshall Quotient (MQ) [12, 13].

Based on its function, SPSS is used in the processing and analysis of quantitative data, because it is interconnected and also included in the scope of statistics. SPSS

can read various types of data by entering data directly into the SPSS Data Editor. Regardless of the structure of the initial data file, the data in the SPSS Data Editor must be in the form of rows (cases) and columns (variables) [14]. This study examines the use of filler on the effect of Marshall characteristic values. The data in this study used secondary data sourced from Pratama, 2021, Rezi, 2021, Malacca, 2021 [8, 15, 16]. With each researcher using a filler substitute in the form of fly ash, volcanic ash and rice husk ash [17]. The filler used in this study is a space filler between coarse aggregate and fine aggregate, fine grained which passes the sieve no. 200 as much as 75%. The composition of the filler used in the asphalt mixture is relatively small, but the filler can have a significant effect on the asphalt concrete mixture. This is due to the presence of filler so that the air voids in an asphalt mixture become smaller, have higher friction resistance and high intergranular locking, and increase the stability of the asphalt-concrete mixture. Another advantage with the presence of a filler is because a lot of it is absorbed in the bitumen material, it will increase its volume [18–20]. Therefore, this study aims to determine the optimum asphalt content value (OAC) obtained by Fly Ash, Volcanic Ash and Rice Husk Ash, investigate the effect of Fly Ash, Volcanic Ash and Rice Husk Ash as filler for AC-WC mixture based on Marshall characteristics, statistical testing using SPSS software to determine the significant value between variables on Marshall characteristic values.

2 Methods

The data used in this study is secondary data sourced from [8] for filler fly ash, [15] for filler volcanic ash, and [16] for filler rice husk ash. Next, compare the three types of fillers to find out which filler is more efficient in terms of filler material acquisition and strength. For fly ash, it can be obtained from PLTU or companies that use coal as fuel which later results from burning coal to produce solid waste, namely fly ash. Volcanic ash obtained from the volcanic ash of Mount Rinjani and rice husk ash from rice burning residue. Marshall properties testing was carried out to obtain optimum asphalt content (OAC). Parameters tested in Marshall Properties are flow, stability, marshall quotient (MQ), density, VIM (Void in the Mix), VFB (Void Filled with Bitumen), VMA (Void in Minerals). aggregate). After the process, statistical testing was carried out using a total sample of 81 samples with 27 samples from filler testing with the design asphalt content and 9 samples from filler testing with optimum asphalt content (OAC) using SPSS software. Tests carried out in statistical tests are data normality test, Pearson correlation, multiple linear regression analysis, hypothesis t test. After testing the characteristics of the marshall, statistical tests were carried out to determine the effect of the value of the marshall characteristics on the asphalt content and the percentage of filler.

Table 1 Comparison of marshall filler results

Indicator	Variation filler fly ash [8]		Variation filler volcanic ash [15]		Variation filler rice husk ash [16]		Unit	Specifications
	6,1%		6,2%		6,7%			
	2%	3%	2%	3%	2%	3%		
Mixed Density	2.538	2.541	2.500	2.498	2.685	2.654	gr/m3	
Stability	821	833	942	1107	1286	1215	kg	Min. 800
Flow	3.35	3.45	3.50	3.37	3.52	3.39	mm	2.0 - 4.0
Marshall Quotient	245	242	269	329	366	358	kg/mm	Min. 200
VMA	16.68	15.61	16.65	16.44	17.61	17.59	%	Min, 15
VIM	4.81	3.71	3.71	3.57	4.23	4.80	%	3.0 - 5.0
VFB	71.18	76.24	77.74	78.3	75.99	72.73	%	Min. 65

Source: [8, 15, 16]

3 Results and Discussion

3.1 Analysis Results of Marshall Filler Fly Ash, Volcanic Ash and Rice Husk Ash at Optimum Asphalt Content

The results of the analysis of 81 samples with 27 samples each obtained the optimum asphalt content for fly ash filler of 6.1%, volcanic ash filler 6.2%, rice husk ash filler 6.7% on all variations of asphalt content. Furthermore, 9 specimens were made with 3 variations in the percentage of filler for fly ash and volcanic ash fillers of 1–3%, while rice husk ash of 2–3% using Optimum Asphalt Content 6.1% fly ash filler, 6.2% filler volcanic ash, 6.7% filler rice husk ash. To compare the results of the characteristics of Marshall Filler Fly Ash, Filler Volcanic Ash and Filler Rice Husk Ash, it can be seen in Table 1.

3.2 Analysis Using SPSS

3.2.1 Data Normality Test

The following are the results of the normality test using SPSS version 26 which are presented in Table 2. Based on the data, it is known that the significant value (Sig F) for the value of Stability, Flow, MQ, VMA, VFB is 0.200 which means it is greater than 0.05 and if the probability is > than 0.05 then H0 will be accepted. While the VIM value is 0 then H0 is rejected. So it can be concluded that the value of Stability, Flow, MQ, VMA, VFB to asphalt content and filler percentage is normally distributed and has an effect.

Table 2 Data normality test results using SPSS

Type	Sig. F	α	Information
Stability	0.200	0,05	Valid
Flow	0.200	0,05	Valid
MQ	0.200	0,05	Valid
VIM	0	0,05	Invalid
VMA	0.200	0,05	Valid
VFB	0,200	0,05	Valid

3.2.2 Pearson Correlation

Tests that have been carried out on the data normality test, it is known that the VIM value is not valid, then the VIM value is not recalculated in the Pearson correlation test. The purpose of data analysis on the Pearson correlation test is to provide an explanation of the research results so that the research becomes easier to understand or understand and conclusions can be drawn so that suggestions or recommendations can then be formulated. The following are the results of the Pearson Correlation test using software SPSS 26 shown in Table 3.

The results listed in the Table 3, it is known that the Marshall characteristic value which has a positive linear relationship marked with valid information is the stability value with the Marshall quotient on asphalt content and percentage of filler and VFB on asphalt content. In addition, the relationship between the two variables is significant. This can be seen from the significance number at the stability value of 0.006 to the asphalt content and 0.021 to the filler percentage, the marshall quotient value is 0.006 to the asphalt content and 0.007 to the filler percentage, then the VFB value is 0 to the asphalt content which means that it is significant only to the asphalt content value, not with filler percentage. Of all the values of the Marshall characteristics, if it is less than 0.05 then the relationship between the two variables is significant. The calculation is done to find out how much influence the variables X1 (Asphalt Content) and X2 (Percentage Filler) have on the variables Y1 (Stability) and Y2 (Marshall Quotient), it is necessary to calculate the coefficient of determination

Table 3 Pearson correlation results using SPSS

Type	Asphalt content		% Filler		α	Information	
	<i>r</i>	<i>p - value</i>	<i>r</i>	<i>p - value</i>		Asphalt content	% Filler
Stability	0.446	0.006	0.383	0.021	0.05	Valid	Valid
Flow	0.061	0.724	-0.16	0.35	0.05	Invalid	Invalid
MQ	0.447	0.006	0.445	0.007	0.05	Valid	Valid
VMA	0.062	0.72	-0.144	0.403	0.05	Invalid	Invalid
VFB	0.66	0	-0.088	0.609	0.05	Valid	Invalid

Table 4 Calculation of the coefficient of determination on stability

Model summary ^b				
Model	R	R square	Adjusted R square	Std. error of the estimate
1	0.574 ^a	0.329	0.289	120.885

^a Predictors: (Constant), Percentage Filler, Asphalt Content

^b Dependent Variable: Stability

Table 5 Results of calculation of the coefficient of determination on the marshall quotient (MQ)

Model summary ^b				
Model	R	R square	Adjusted R square	Std. error of the estimate
1	0.615 ^a	0.379	0.341	32.944

^a Predictors: (Constant), Percentage Filler, Asphalt Content

^b Dependent Variable: MQ

using the help of a computer program, namely SPSS version 26 which is presented in Tables 4 and 5.

The results of testing the coefficient of determination using SPSS version 26 in Table 4 we can see that the result is 0.574 for the R value which indicates that the variable is moderately correlated. For the value of R square (the correlation number squared) obtained a value of 0.329 or equal to 32.9%, meaning that the influence of asphalt content and filler percentage on the Stability Value is 32.9% while 67.1% is influenced by other factors.

The results of testing the coefficient of determination using SPSS version 26 in Table 5 we can see that the result is 0.615 for the R value which indicates that the variables are strongly correlated. For the value of R square (the correlation number squared) obtained a value of 0.379 or equal to 37.9%, meaning that the influence of asphalt content and filler percentage on the Marshall Quotient (MQ) value is 37.9% while 62.1% is influenced by factors other.

3.2.3 Multiple Linear Regression Analysis

The results of the tests carried out on the Pearson correlation obtained the dominant factors for the variable asphalt content and filler percentage indicated by valid information, namely stability and marshall quotient, so that a regression analysis was carried out on the relationship between stability and marshall quotient on the variable asphalt content and filler percentage. The relationship that occurs forms a linear regression relationship indicating that there is a positive linear relationship to asphalt content and filler percentage. Based on these results, further analysis was carried out, namely multiple linear regression. With the independent variable (X1) is the asphalt content, the independent variable (X2) is the percentage of filler while the

dependent variable (Y1) is stability and (Y2) marshall quotient. Using SPSS version 26 software is presented in Tables 6 and 7.

The results of the analysis test in Table 6 are known to have a significant value stability to asphalt content of 0.005 less than 0.05 indicating that asphalt content affects the stability value while a significant value to the percentage of filler 0.016 is smaller than 0.05, this indicates that the percentage of filler has a significant effect on the value of stability. In column B the value of constant (a) is 0.078, while the value of asphalt content (b) is 149.781, and the percentage value of filler (c) is 68.489 so that the regression can be written.

$$Y_1 = 0.078 + 149.78X_1 + 68.48X_2$$

The regression equation above shows the relationship between the independent variables, namely asphalt content and percentage of filler with the dependent variable, namely partial stability. It shows that the regression coefficient of asphalt content and percentage of filler contributes positively to the value of stability. So that the higher the asphalt content and filler percentage, the higher the stability value.

Table 6 Results of multiple linear regression analysis on stability values

Coefficients ^a						
Model		Unstandardized coefficients		Standardized coefficients	t	Sig.
		B	Std. error	Beta		
1	(Constant)	0.078	307.248		0.000	1.000
	Asphalt Content	149.781	49.959	0.428	2.998	0.005
	Percentage Filler	68.489	27.066	0.361	2.530	0.016

^a Dependent Variable: Stability

Table 7 Results of multiple linear regression analysis on marshall quotient (MQ) value

Coefficients ^a						
Model		Unstandardized coefficients		Standardized coefficients	t	Sig.
		B	Std. error	Beta		
1	(Constant)	4.806	83.731		0.057	0.955
	Asphalt Content	42.216	13.615	0.426	3.101	0.004
	Percentage Filler	22.714	7.376	0.423	3.079	0.004

^a Dependent Variable: MQ

The results of the analytical test in Table 7 are known that the marshall quotient (MQ) significant value to asphalt content of 0.004 is less than 0.05 indicating that asphalt content has an effect on stability value while a significant value to the percentage of filler 0.004 is smaller than 0.05, this indicates that the percentage of filler significant effect on the value of stability. In column B the value of constant (a) is 4,806, while the value of asphalt content (b) is 42,216, and the percentage value of filler (c) is 22,714 so that the regression can be written.

$$Y_2 = 4.806 + 42.218X_1 + 22.71X_2$$

The regression equation above shows the relationship between the independent variables, namely asphalt content and percentage of filler with the dependent variable, namely partial stability. It shows that the regression coefficient of asphalt content and percentage of filler contributes positively to the Marshall Quotient (MQ) value. So that the higher the asphalt content and filler percentage, the higher the Marshall Quotient (MQ) value.

3.2.4 Hypothesis Test (t)

The hypothesis that will be used in this study relates to the presence or absence of the influence of the variable (X) on the variable (Y) and how big the influence is. The results of the Hypothesis Research with T-Test are presented in Tables 8 and 9.

The result above shows that the calculated t values for asphalt content and filler percentage are 2,998 and 2,530, respectively, while the t table is 2,035 with a significant value of 0.005 for asphalt content and 0.016 for filler percentage. From these two values, it is known that it has a value less than 0.05. It turns out that the result of t count is greater than t table (2,998 and 2,530 > 2,035) which means that H0 is rejected and H1 and H2 are accepted. So it can be concluded that Asphalt Content and Filler Percentage have a positive and significant effect on the Stability value.

Table 8 Hypothesis research results with T-Test for stability values

Coefficients ^a						
Model		Unstandardized coefficients		Standardized coefficients	t	Sig.
		B	Std. error	Beta		
1	(Constant)	0.078	307.248		0.000	1.000
	Asphalt Content	149.781	49.959	0.428	2.998	0.005
	Percentage Filler	68.489	27.066	0.361	2.530	0.016

^a Dependent Variable: Stability

Table 9 Hypothesis research results with T-Test for Marshall Quotient (MQ) values

Coefficients ^a						
Model		Unstandardized coefficients		Standardized coefficients	t	Sig.
		B	Std. Error	Beta		
1	(Constant)	4.806	83.731		0.057	0.955
	Asphalt Content	42.216	13.615	0.426	3.101	0.004
	Percentage Filler	22.714	7.376	0.423	3.079	0.004

^a Dependent Variable: MQ

Based on the data above, it is known that the calculated t values for asphalt content and filler percentage are 3.101 and 3.079, respectively, while the t table is 2.035 with a significant equal value of $0.004 < 0.05$. It turns out that the result of t arithmetic is greater than t table (3.101 and $3.079 > 2.035$) which means that H_0 is rejected and H_1 and H_2 are accepted. So it can be concluded that Asphalt Content and Filler Percentage have a positive and significant effect on the Marshall Quotient (MQ) value.

4 Conclusions

The results of testing the effect of using fly ash, volcanic ash, and rice husk ash as a substitute for filler in the AC-WC mixture on the characteristics of the Marshall test can be concluded as follows:

1. The results of the Marshall test on the Planned Asphalt Content obtained that the optimum asphalt content value for fly ash filler is 6.1%, volcanic ash filler is 6.2% and rice husk ash is 6.7%.
2. Marshall test results obtained values for density, stability, Marshall Quotient (MQ), VIM and VMA on fly ash, volcanic ash, and rice husk ash, the highest value was obtained at the filler content of 2% rice husk. As for the Flow value, the highest value is obtained at 1% volcanic ash filler. For pores filled with asphalt (VFB) for fly ash and rice husk ash, there was a decrease in the value of the filler content of 2% and 2.5% and an increase in the filler content of 3%.
3. The test results can be concluded that fly ash, volcanic ash, and rice husk ash can be used as fillers and have met the General Specifications of Highways 2018. For stability min 800 kg, flow 2.0–4.0 mm, Marshall Quotient min 200 kg/mm, VMA min 15%, VIM 3.0 – 5.0%, VFB min 65%.
4. The results of the analysis using SPSS version 26 concluded that the Stability and Marshall Quotient (MQ) values for the Pearson Correlation had a positive linear correlation with the asphalt content value and the filler percentage value.

As for the VFB only on the value of asphalt content only. In Multiple Linear Regression Analysis and t-test using SPSS version 26 software, it was concluded that the asphalt content and filler percentage had a positive contribution to the Stability and Marshall Quotient (MQ) values.

References

1. Saodang H (2005) Konstruksi jalan raya. Bandung Nov
2. Riyanto A, Pramesti Y (2022) Pemanfaatan Limbah Plastik Dengan Teknologi Daur Ulang Pada Hot Rolled Asphalt Ditinjau Dari Aspek Properties Marshall, Nilai Ketidakrataan, Dan Durabilitas. *Din Tek Sipil* 15(1):18–27
3. Pomantow SY, Jansen F, Waani JE (2019) Kinerja Campuran AC-WC dengan Menggunakan Agregat dari Batu Kapur. *J Sipil Statik* 7(2)
4. Anugrah DI (2022) Pengaruh Zeolit Sebagai Filler Terhadap Campuran Lapisan Aspal Beton AC-WC (Asphalt Concrete Wearing Course). *Abstr. Undergrad. Res Fac Civ Plan Eng Bung Hatta Univ* 1(1):1–2 (2022)
5. Pratiwi AA (2020) Pemanfaatan Recycle Asphalt Pavement dengan Peremaja Aspal Berupa Endapan Crude Palm Oil untuk Struktur Perkerasan Jalan AC-WC
6. Harnaeni SR, Pramesti FP, Budiarto A, Setyawan A, Khan MI, Sutanto MH (2020) Study on structural performance of asphalt concrete and hot rolled sheet through viscoelastic characterization. *Materials* 13(5):1133. <https://doi.org/10.3390/ma13051133>
7. Matheus A, Akhmadali A, Mukti ET: Pengaruh Penggunaan Abu Kelapa Sawit Sebagai Filler Pada Lapisan Perkerasan Aspal AC-WC (Asphalt Concrete-Wearing Course). *JeLAST J PWK Laut Sipil Tambang* vol 9, no 1
8. Syahrul HP (2021) Studi Penggunaan Limbah Abu Batu bara (fly ash) Sebagai Pengganti Filler Pada Campuran AC-WC Terhadap Karakteristik Uji Marshall. *Universitas_Muhammadiyah_Mataram*
9. Tandiabang S (2022) Pengaruh Styrofoam Sebagai Bahan Tambah Campuran AC-WC Batu Sungai Tetean Kabupaten Mamasa. *Paulus Civ Eng J* 4(1):80–87
10. Ali H (2011) Karakteristik Campuran Asphalt Concrete-Wearing Course (Ac-Wc) Dengan Penggunaan Abu Vulkanik Dan Abu Batu Sebagai Filler. *J.Rekayasa J Ilm Fak Tek. Univ Lampung* 15(1):21–32
11. Al-Sabaei AM, Mustofa BA, Sutanto MH, Sunarjono S, Bala N (2020) Aging and rheological properties of latex and crumb rubber modified bitumen using dynamic shear rheometer. *J Eng Technol Sci* 52(3):385–398. <https://doi.org/10.5614/j.eng.technol.sci.2020.52.3.6>
12. Sukirman S (2003) Perkerasan Jalan Raya. Penerbit NOVA, Bandung
13. Wahjoedi W (2009) KARAKTERISTIK MARSHALL DAN INDEKS KEKUATAN SISA (IKS) PADA CAMPURAN BUTONITE MASTIC ASPHALT (BMA). *J Tek Sipil dan Perenc* 11(2):121–130
14. McCormick K, Salcedo J (2017) SPSS Statistics for Data Analysis and Visualization. Wiley
15. Lalu SFR (2021) Pengaruh Penggunaan Abu Vulkanik Gunung Rinjani Sebagai Pengganti Filler Untuk Campuran Laston (AC-WC) Dalam Karakteristik Uji Marshall. *Universitas_Muhammadiyah_Mataram*
16. Prillia EDM (2021) Pemanfaatan Limbah Abu Sekam Padi (Rice Husk Ash) Sebagai Substitusi Material Pengisi Campuran AC-WC Terhadap Karakteristik Marshall. *Universitas_Muhammadiyah_Mataram*
17. Triyanto J, Subroto S, Effendy M (2019) Karakteristik Pembakaran Biobriket Campuran Ampas Aren, Sekam Padi, Dan Batubara Sebagai Bahan Bakar Alternatif. *Media Mesin Maj Tek Mesin* 19(2):66–73. <https://doi.org/10.23917/mesin.v19i2.7497>

18. Leo Ramadona L, Khadavi ST, MT K, Eko Prayitno ST (2022) Pengaruh Penambahan Cangkang Kelapa Sawit Sebagai Substitusi Agregat Halus Pada Campuran Aspal (AC-WC). Universitas Bung Hatta
19. Deyan AS (2022) Pengaruh Penambahan Limbah Genteng Tanah Sebagai Pengganti Sebagian Filler Terhadap Nilai Stabilitas Marshall Laston (AC-WC). Universitas_Muhammadiyah_Mataram
20. Suhardi S, Pratomo P, Ali H (2016) Studi Karakteristik Marshall Pada Campuran Aspal Dengan Penambahan Limbah Botol Plastik. J Rekayasa Sipil dan Desain 4(2):284–293

Mechanical Performance Improvement by Carbon Dioxide Curing of Cement Concrete Incorporating Oil Shale Residue



Syahidus Syuhada, Marsail Al Salaheen, Wesam Salah Alaloul, and Khalid Mhmoud Alzubi

Abstract The influence of carbon dioxide (CO₂) curing on the compressive strength of oil shale ash (OSA) concrete as partial cement replacement was investigated. 15 cm cubes with a 30% replacement percentage were tested after seven days of conventional curing and carbonation curing at 4 bar CO₂ pressure. Research results demonstrate that CO₂ curing influences the compressive strength of concrete significantly. There is a linear relationship between CO₂ pressure and the duration of curing, as well as the compressive strength of OSA-based concrete. A sample of ordinary Portland cement was used as the control sample. The replacement of 30% cement by OSA increased the 7-day compressive strength from 48.5 to 55.5 MPa for plain cement samples and from 36.5 to 42.3 MPa for ash-based samples. From a technical standpoint, OSA-based concrete carbonation curing is still too immature for widespread application. Nonetheless, it is continuously developing in response to greenhouse gas reduction and paving the path for a more sustainable construction materials business.

Keywords Carbonation · Oil shale ash · CO₂ curing · Compressive strength · XRD

S. Syuhada

Civil Engineering Study Program, Department of Infrastructure Technology and Planning, Institut Teknologi Sumatera, Sumatera, Indonesia
e-mail: syahidus.syuhada@si.itera.ac.id

M. Al Salaheen · W. S. Alaloul (✉) · K. M. Alzubi

Department of Civil and Environmental Engineering, Universiti Teknologi PETRONAS, Seri Iskandar, Malaysia
e-mail: wesam.alaloul@utp.edu.my

M. Al Salaheen

e-mail: marsail_20001253@utp.edu.my; marsail.salaheen@bau.edu.jo

K. M. Alzubi

e-mail: khalid_20001254@utp.edu.my; alzoubi_khalid@bau.edu.jo

M. Al Salaheen · K. M. Alzubi

Department of Civil and Environmental Engineering, Al-Husun University College, Irbid, Jordan

© Institute of Technology PETRONAS Sdn Bhd 2024

B. S. Mohammed et al. (eds.), *Proceedings of the International Conference on Emerging Smart Cities (ICESC2022)*, Lecture Notes in Civil Engineering 324,
https://doi.org/10.1007/978-981-99-1111-0_4

1 Introduction

Global warming is prompted by the emission of greenhouse gases; consequently, efficient strategies for lowering their production, as well as installing capture and storage systems, are required. Carbon dioxide (CO₂) and methane (CH₄) are the most abundantly released greenhouse gases, accounting for 56% and 18% of total emissions, respectively [1]. Global warming surpassed its limits recently, owing mostly to high levels of CO₂ in the atmosphere [2]. In terms of CO₂ emissions; fossil fuel power plants account for 40% of total CO₂ emissions, the Portland cement sector accounts for 15%, and other percentages come from transportation and general industries [3].

This made the introduction of green practises an essential idea, not a luxury. There are several materials (natural and byproducts) that can be used as partial replacements for cement and/or aggregates in the manufacture of construction materials, including fly ashes, bottom ashes, steel slag, metakaolin, granulated blast-furnace slag, and silica fume. Also, increasing the amount of solid waste raises the immediate requirement to eliminate unregulated garbage disposal methods and achieve sustainable development goals while reducing the massive negative environmental and health repercussions [4, 5]. Various waste treatment processes, such as bio-drying, dumping, land farming, compost supplements, pyrolysis, incineration, sewage treatment, and reutilization, are now in use; however, some result in environmental degradation [6].

The combustion waste of oil shale is a byproduct with 80% of the ash entrained in the flue gas and collected as fly ash (OSA). The particle fraction size varies from (30 to 150) μm and is suitable for concrete manufacture [7]. According to statistics, retorting oil shale yields up to 30 times more than crude oil [7]. In other words, there will be a large quantity of OSA that will need to be disposed of in the future, and if it is not managed appropriately, the expansion of the oil shale sector may be inhibited [8]. Furthermore, the sustainable building sector emphasized the use of sustainable materials at every stage of construction [9]. Thus, engineering supplementary materials can play a significant role in the creation of successful sustainable construction.

A list of the most relevant papers for further detailed review and analysis is given below in Table 1. In the concrete technology field, as mentioned, a lot of parameters were investigated, and inequality results were observed. So, adding a new valuable material or new treatment technology to the ash-based concrete can improve the properties in such a way that it can be used as a partial replacement for cement or aggregates in concrete mixtures.

Carbonation of waste residues for CO₂ sequestration benefits both because the waste material's behavior is typically enhanced following carbonation mechanism. Carbonation curing concept is that clinker and its products react with CO₂ [14]. CO₂ combines with tricalcium silicate (C₃S) and dicalcium silicate (C₂S) and the hydration products to produce CaCO₃ and C-S-H, as demonstrated in Eqs. (1), (2), (3), and (4) [15]. In contrast to natural weathering carbonation, specimens suffer fast carbonation at an early age.

Table 1 List of related research papers

Ref.	Researchers Work and Aims	Methodology	Remarks		
			Ash Origin	Ash Quantity	Ash Shape
[10]	The possibilities of utilizing the OSAs in building materials with different OSAs with	*Determination of total carbon, inorganic carbon, and free CaO content by XRF analysis.	Estonia	Water to ash was 0.7 and ash to sand was 0.33.	Coarse fraction was used as fine aggregate replacement.
	three binder systems were considered: -self-cementation of ashes -accelerated carbonation -ceramic in clay brick.	*(40×40×160) mm paste prisms cured, compacted and, after 28 days, flexural and compressive strength were tested.			
			Comments		
			- Ash specimens broke during the curing as cohesion is lost after water evaporation. - The behavior of carbonates influences the brick microstructures and reduces the shrinkage degree.		
[11]	Detect the characteristic of concretes made up with pozzolanic OSA added Portland cement	freezing-thawing experiments were casted on cement paste samples (40×40×160 mm) that have 0, 10, 20, and 30% of OSA additions.	Turkey	content of ashes was 0, 10, 20, and 30%.	Fine Ash
			Comments		
			-It was determined that freezing-thawing cycles caused greater fractures and weight loss in air-entrained samples.		

(continued)

Table 1 (continued)

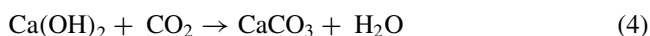
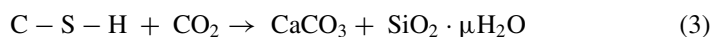
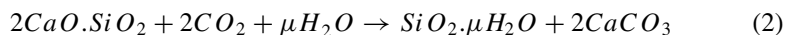
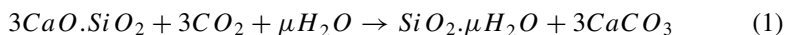
[12]	Study the effect of three input variables, namely oil ash, pressing pressure, and heat treatment temperature on the characteristics of ceramics.	Two (100 g each) mixtures were prepared by mixing the waste glass powder with the OSA at different proportions, then pressed under different loads into a cylindrical shape of 30 mm in diameter and 8 mm in length and subjected to heat treatment for four hours to ensure the formation of a crystalline phase in the glass ceramic.	Jordan	content of oil ash (30 and 50 %).	The size of fraction (70–125) µm.
Comments					
<p>-Increasing the ash content from 30 to 50 wt% increased slightly water absorption.</p> <p>-Increasing the heat treatment temperature from 900 to 1050 °C reduced water absorption.</p>					
[13]	Maximize the benefits of oil shale from quarries by backfilling them with OSA-based concrete.	- OS ash-based hardened concretes strength was tested for 7, 28 and 91 days.	Estonia	50 %wt OSA - based binder and about 50 %wt limestone	Fine Ash
Comments					
-To use OSA on a large scale, the composite might be changed by adding ground high-calcium fly ashes and Portland cement.					

Table 2 Materials chemical compositions

Oxide (Wt.%)	Raw sample	Cement
SiO ₂	25.50	17.60
Al ₂ O ₃	2.66	4.02
Fe ₂ O ₃	1.13	3.19
CaO	41.40	66.41
MgO	1.08	1.35
Na ₂ O	0.43	0.02
K ₂ O	0.44	0.40
SO ₃	2.49	4.17
P ₂ O ₅	4.49	0.08
MnO	0.01	0.19
LOI	19.33	3.10

Table 3 Mixtures details

Mix number	W:C	Cement content (kg/m ³)	OSA content (kg/m ³)	Fine aggregate (kg/m ³)	Coarse aggregate content (kg/m ³)
1	0.45	456	0	522	1097
2	0.45	319.2	93.9	522	1097



Carbonation treatment is a sufficient processing procedure due to the high content of CaO in supplementary materials. Free CaO would be consumed clearly throughout carbonate testing process, enhancing the volume stability of the cementitious matrix and solving the issue for these materials [16]. When compared to the same qualities obtained after pure hydration curing, samples exposed to carbonation have significantly higher and considerably more favourable hydrophysical and mechanical parameters [17]. Furthermore, carbonation processes generate chemicals that have opposing impacts on pore structure, adding complexity to prediction models [15]. Therefore, the aim of the current research was to develop a proposal for industrial-scale guidelines for CO₂ sequestration and accelerate natural weathering processes using OSA from Jordanian power plants. As well as to evaluate and characterize the carbonation behaviour of OSA based on the obtained values of compressive strength.

2 Materials and Methodology

A characterised OSA sample obtained from the Jordanian National Recourse Authorities (NRA) was studied. To remove moisture, OSA was dried in an oven at (105 ±5) °C for 24 h. The dried OSA was sieved through a 150 µm sieve to eliminate coarser particles. The chemical compositions of OSA and cement obtained by XRF using a Bruker AXS: S4 PIONEER X-ray spectrometer are provided in Table 1. The phases were identified by comparing the resulting pattern to the international centre of diffraction data (ICDD) reference database patterns using the DIFFRAC plus program. Using the ORIGIN PRO program (Table 2).

Proportioning of concrete mixtures was done following the ACI 211 procedures. Two concrete mixtures including the control were prepared with 0% and 30% replacement by OSA. For each mix design, six (150 mm) cubes were prepared, casted and

tested for the compressive strength test after applying water and CO₂ curing, respectively. Graded aggregates were used in their dry conditions with a 2.57 specific gravity and a 2.04 water absorption. Specific gravity of OSA used is 2.15 with particle size range of (60–100 μm) (Table 3).

The samples were stored for 24 h in standard laboratory conditions (25 °C) before being removed from the moulds and divided into two groups. One group was cured in water, while the other was cured via an accelerated carbonation test with a chamber attached to a CO₂ pipe. The chamber has been equipped with the available equipment to regulate the environmental parameters, such as humidity, temperature, and CO₂ levels. The CO₂ pressure in the carbonation test was 4 bar, the relative humidity was 60%, and the temperature was 25 °C. Before being placed in the chamber, the samples were thoroughly dried and then cured for 7 days. After curing was completed, samples were removed and kept in the lab conditions until testing.

3 Discussion and Findings

3.1 X-ray Diffraction Analysis

XRD has been identified as one of the most widely used methods for determining the mineralogical composition of materials. XRD analysis is often used to determine the degree of crystallinity and amorphousness of a material. Similar to earlier research [18, 19], the primary minerals contained in the original sample include calcite, quartz, anhydrite, fluorapatite, and traces of clay minerals as shown in the figure (Fig. 1).

3.2 Compressive Strength

The compressive strength of samples after 7 days of curing is compared in Fig. 2. The strength of concrete after CO₂ curing increased noticeably when compared to the water-cured reference; CO₂-cured concrete had a strength of 16.5% higher for cement and 29.3% higher for OSA samples. This might be because calcium hydroxide and C-S-H are synthesised after demolding when the composites are ready for carbonation. Extended traditional curing after casting may lower CO₂ absorption capacity, whereas too short conventional curing improves composite strength growth.

The impact of CO₂ curing was evident until 28 days, when the compressive strength of water and CO₂-cured concrete seemed equivalent. The cement concrete had a 28-day strength of 55.5 MPa and the OSA concrete had a strength of 42.3 MPa after CO₂ curing, but the water cured counterpart had a strength of 48.5 MPa and the OSA concrete had a strength of 36.5 MPa, as shown in Fig. 3. Fine calcite particles formed during the carbonation procedure are responsible for the favourable effect of CO₂-cured OSA-based concrete on cement strength increase. Causing fills the pores,

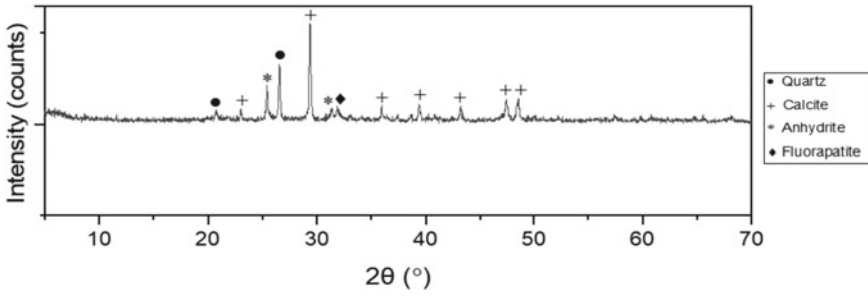


Fig. 1 XRD pattern for the OSA material

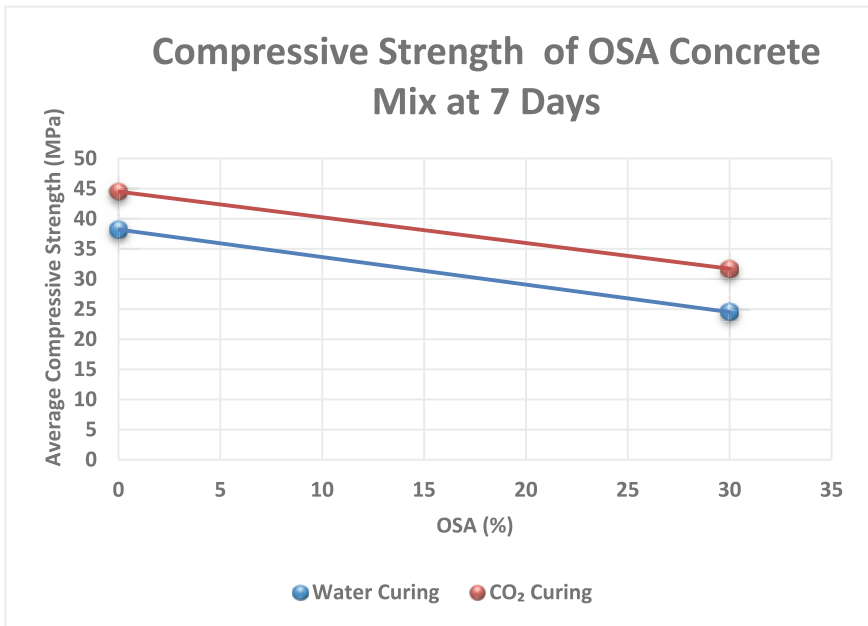


Fig. 2 Compressive Strength of OSA at 7 Days after water and CO₂ curing

lowering pore size, and the calcite formed reacts with aluminate (C₃A), leading to the development of calcium carboaluminate phases.

Figure 4 Displays the study’s conceptual structure. The use of CO₂ curing in the concrete industry has a number of advantages, including lower global greenhouse gas emissions, overcoming industrial and technological limitations to waste utilization, and improving waste-based material performance.

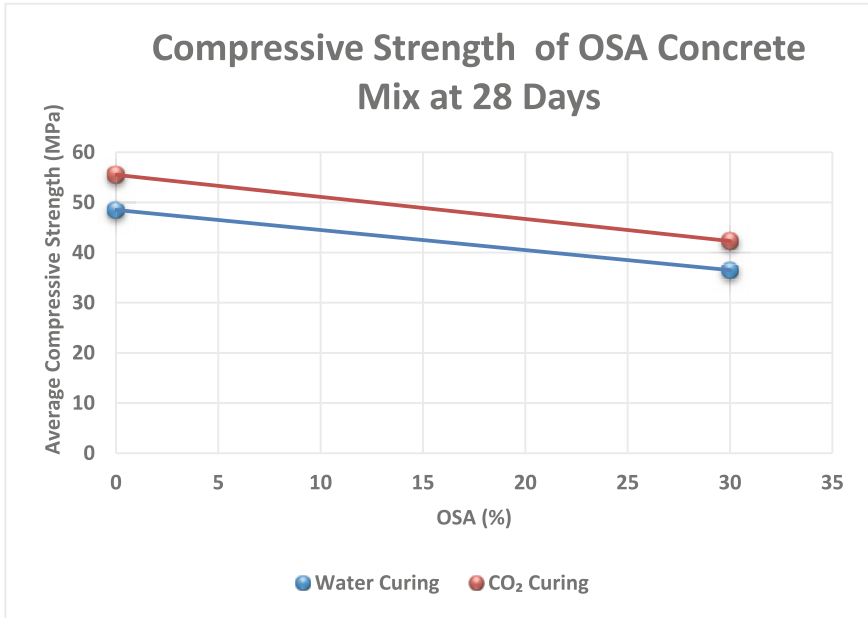


Fig. 3 Compressive Strength of OSA at 28 Days after water and CO2 curing

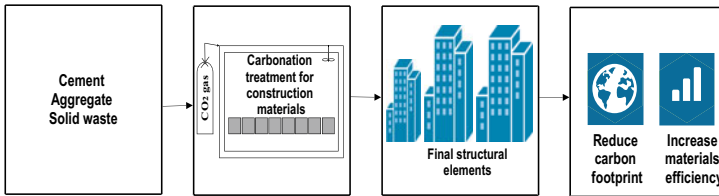


Fig. 4 Research conceptual framework

4 Conclusions

Over the last few decades, there has been a growing amount of research focused on the utilisation of CO₂ curing for concrete composites. However, due to the complexities of carbonation details in diverse building materials and the lack of consistency in previous studies, the practical application of carbonation treatment in the concrete industry is currently limited. The current research is primarily focused on the influence of carbonation curing on the mechanical characteristics of OSA-based concrete, particularly compressive strength. OSA was employed in the combinations as a 30% cement substitution.

The evaluated compressive strength following carbonation increases significantly, especially at early ages, where it exceeds 15% when compared to water-cured

instances. Furthermore, the 28-day strength improved to 45 MPa compared to less than 40 MPa for water curing. Even for plain cement samples, the strength after carbonation exceeds 55.5 MPa, whereas water curing achieves 48.5 MPa. Further research needs to be conducted on the chemical effect and danger of carbonation-induced corrosion in OSA-based CO₂-cured concrete.

Acknowledgement The authors would like to thank Universiti Teknologi PETRONAS and Institut Teknologi Sumatera for the support provided in this research.

References

1. Zoundi Z (2017) CO₂ emissions, renewable energy and the Environmental Kuznets Curve, a panel cointegration approach. *Renew Sustain Energy Rev* 72:1067–1075. <https://doi.org/10.1016/j.rser.2016.10.018>
2. Szulejko JE, Kumar P, Deep A, Kim K-H (2017) Global warming projections to 2100 using simple CO₂ greenhouse gas modeling and comments on CO₂ climate sensitivity factor. *Atmos Pollut Res* 8(1):136–140. <https://doi.org/10.1016/j.apr.2016.08.002>
3. Huang L, Krigsvoll G, Johansen F, Liu Y, Zhang X (2018) Carbon emission of global construction sector. *Renew Sustain Energy Rev* 81:1906–1916. <https://doi.org/10.1016/j.rser.2017.06.001>
4. Viswanathan R, Telukdarie A (2022) The role of 4IR technologies in waste management practices-a bibliographic analysis. *Procedia Comput Sci* 200:247–256. <https://doi.org/10.1016/j.procs.2022.01.223>
5. Alaloul W, Musarat MA, Rabbani M, Altaf M, Alzubi K, Al-Salaheen M (2022) Assessment of economic sustainability in the construction sector: evidence from three developed countries (the USA, China, and the UK). *Sustainability* 14:6326. <https://doi.org/10.3390/su14106326>
6. Bányai T, Tamás P, Illés B, Stankevičiūtė Ž, Bányai Á (2019) Optimization of municipal waste collection routing: impact of Industry 4.0 technologies on environmental awareness and sustainability. *Int J Environ Res Public Health* 16(4):634. <https://doi.org/10.3390/ijerph16040634>
7. Alaloul WS, Salaheen MA, Malkawi AB, Alzubi K, Al-Sabaei AM, Musarat MA (2021) Utilizing of oil shale ash as a construction material: a systematic review. *Construct Build Mater* 299:123844. <https://doi.org/10.1016/j.conbuildmat.2021.123844>
8. Liu J, Qiu J, Wu P, Sun X, Zhang S, Guo Z (2021) Calcined oil shale residue as a supplementary cementitious material for ordinary Portland cement. *Constr Build Mater* 306:124849. <https://doi.org/10.1016/j.conbuildmat.2021.124849>
9. Altuma MI, Ghasemlounia R (2021) Effects of construction materials to achieve sustainable buildings. *Int J Eng Manage Res* 11(1):25–30. <https://doi.org/10.31033/ijemr.11.1.4>
10. Usta MS et al (2020) Evaluation of new applications of oil shale ashes in building materials. *Minerals* 10(9), Art. no. 9. <https://doi.org/10.3390/min10090765>.
11. Oymael S, Bideci A, Bideci ÖS (2019) Oil shale ash addition effect in concrete to freezing-thawing. In: Hemeda S (ed) *Sustainable Construction and Building Materials*. IntechOpen. <https://doi.org/10.5772/intechopen.79285>
12. Aljbour SH (2016) Production of ceramics from waste glass and jordanian oil shale ash. *Oil Shale* 33(3), Art. no. 3. <https://doi.org/10.3176/oil.2016.3.05>
13. Uibu M et al (2016) Oil shale ash based backfilling concrete – strength development, mineral transformations and leachability. *Constr Build Mater* 102:620–630. <https://doi.org/10.1016/j.conbuildmat.2015.10.197>

14. Liu Z, Meng W (2021) Fundamental understanding of carbonation curing and durability of carbonation-cured cement-based composites: a review. *J CO₂ Utilization* 44:101428. <https://doi.org/10.1016/j.jcou.2020.101428>
15. Zhang D, Ghouleh Z, Shao Y (2017) Review on carbonation curing of cement-based materials. *J CO₂ Utilization* 21:119–131. <https://doi.org/10.1016/j.jcou.2017.07.003>
16. Chen T, Bai M, Gao X (2021) Carbonation curing of cement mortars incorporating carbonated fly ash for performance improvement and CO₂ sequestration. *J CO₂ Utilization* 51:101633. <https://doi.org/10.1016/j.jcou.2021.101633>
17. El-Hassan H (2020) Accelerated carbonation curing as a means of reducing carbon dioxide emissions. *IntechOpen*. <https://doi.org/10.5772/intechopen.93929>
18. Nabih K, Kada MK, Hmiri M, Hamsi N (2014) Effects of the addition of oil shale ash and coal ash on physic-chemical properties of CPJ45 cement, vol 11. <https://doi.org/10.1051/mat/econconf/20141101012>
19. Wang D, Yuan K, Liu B, Qu Z (2020) Effect of Activator on Alkali-Slag-Oil Shale Ash Cement under Thermal Excitation, vol 1578, no 1. <https://doi.org/10.1088/1742-6596/1578/1/012236>.

Flood Susceptibility Mapping Using GIS-AHP of Kuala Krai



Zafarullah Nizamani, Riaz Ahmed Soomro, Akihiko Nakayama,
and Montasir Osman Ahmed Ali

Abstract Flood is frequently occurring natural disaster and is among the most expensive in terms of individual lives and environmental impact. Identifying flood-prone locations is critical for formulating good flood control policies. The current study aims to provide an integrated framework for assessing flood susceptibility utilizing the GIS-AHP method for the Kuala Krai district in Kelantan state, Malaysia. Ten flood causative factors are considered for this study, such as (a) rainfall, (b) slope, (c) aspect, (d) curvature, (e) drainage density, (f) distance from the river, (g) land used and land covered (LULC), (h) soil map, (i) topographical wetness index (TWI), and (j) stream power index (SPI). A pairwise comparison matrix is built by Saaty's scale. In the Kuala Krai region, the rainfall and the slope cause more floods than others. The natural break Jackson method is used to classify the flood susceptible map into five classes: very high, high, moderate, low, and very low. The northern and southern regions of Kuala Krai are very high and highly susceptible to flooding.

Keywords Flood · Geographic information system (GIS) and remote sensing (RS) · AHP · Causative factors · Flood susceptibility

1 Introduction

The frequency of flood events is increasing due to climate change and extreme weather [1]. Floods are among the world's most dangerous natural disasters [2]. They appear to have a profound negative impact on human lives. For instance, it negatively influences the economy; hence, the quality-of-life results in poor health

Z. Nizamani (✉) · R. A. Soomro · A. Nakayama
Faculty of Engineering and Green Technology, UTAR, 31900 Kampar, Malaysia
e-mail: zafarullah@utar.edu.my

M. O. A. Ali
Civil and Environmental Engineering Department, Universiti Teknologi PETRONAS, 32610
Bandar Seri Iskandar, Perak, Malaysia

© Institute of Technology PETRONAS Sdn Bhd 2024
B. S. Mohammed et al. (eds.), *Proceedings of the International Conference on Emerging Smart Cities (ICESC2022)*, Lecture Notes in Civil Engineering 324,
https://doi.org/10.1007/978-981-99-1111-0_5

conditions after its occurrence, psychological impact, and social impact. The effects of floods can undermine sustainable development goals such as 9, 11, and 13 [3].

Therefore, the research into spatial flood modelling at the basin scale at the regional level is critical to apply adaptation and mitigation strategies against the disastrous flood repercussions [4]. Flood susceptibility is crucial for flood exposure, damage, and risk management [5]. Flood susceptibility mapping (FSM) significantly contributes to the early warning system, which provides policymakers with the essential data for managing flood risk [6].

Natural disaster management has been considered to be effective by GIS and remote sensing (RS) technologies. Various researchers have used GIS and RS to assess flood susceptibility, generate flood risk maps, and handle post-disaster scenarios [7–11]. However, GIS alone cannot assign the relative flood causative factors' accurate weight, which limits the susceptibility mapping's accuracy [12]. Several studies have merged GIS, and AHP approaches for FSM, monitoring, and mapping to overcome this limitation [8, 13–15].

The AHP is an essential and straightforward method for mapping flood susceptibility. AHP solves complex problems in a simple elementary hierarchy, from the high ranking to the lowest one [13]. The main goals of this project are to create a framework for investigating and predicting the flood-prone area of Kuala Krai, as well as to construct a flood-susceptible map of Kuala Krai utilizing the GIS-AHP method.

2 Literature Review

2.1 Flood Causative Factors Selection and Their Importance

Flood causative factors are essential to generate the flood susceptible map. The process choosing the relevant causative factors is crucial for constructing an accurate flood susceptibility model, with environmental aspects of the research area that can affect flood model performance taken into account [16]. Since no appropriate number of flood causative factors were specified [9], we selected the study's factors from the literature. The morphometric setting of the study region is represented by the ten flood causative factors listed below, which are comparable to the ones identified in earlier studies [6, 17, 18], were identified: (a) slope, (b) rainfall, (c) curvature t (d) Aspect (e) drainage density (f) distance from the river (g) LULC (h) soil map (i) TWI and (j) SPI.

The most influential factor in flood susceptibility mapping is rainfall [19]. An area with a low slope is usually prone to flooding [20]. The direction or orientation of the highest slope of the terrain surface influences hydrologic conditions because different aspects experience varying effects of solar radiation and precipitation [21]. It affects evapotranspiration, soil moisture, solar radiation, local climate change, and infiltration [22]. The curvature considerably affects the infiltration and surface

runoff [8]. There is contrary to the role of curvature on runoff production. In some studies, the concave slope curvature has more potential to generate runoff than the convex slope curvature. Some studies show that the convex slope curvature has more potential for runoff generation [23]. The flood risk is higher where multiple rivers join as they add the precipitation runoff from multiple unit areas [24]. The high drainage density catchment areas are more flood-prone than the lower ones [25].

The distance from the river influences the extent of flood risk and flood velocity [26]. It critically controls the expansion of a riverine flood event [5]. LULC is considered a serious flood causative factor. The built-up or settlement region has triggered more flooding than the vegetation and the forest land [27]. The soil types have a more significant impact on floods occurring. The clay and loamy soil cause more floods than the sandy soil [21].

The topographic wetness index (TWI) is the effect of topography on runoff generation and flow accumulation at any site in the river catchment area. It is the proportion of a specific basin area to the slope. It is calculated by Eq. (1).

$$TRI = \sqrt{Abs(max^2 - minum^2)} \quad (1)$$

whereas

the maximum and minimum values are the cell size of the slope and flow accumulation [8].

Stream Power Index (SPI) is the erosive power of the discharge and basin relative to a specific area within the watershed. It is measured by using Eq. (2).

$$SPI = As \times \tan\beta \quad (2)$$

whereas

As is the specific catchment area (m^2/m), β is the slope gradient in degrees. It is indicated that the erosive power of water flows [8].

2.2 Analytical Hierarchy Process

The AHP is the structural-based method used to solve a complex problem by breaking it into simple elementary hierarchies, from the high hierarchy to the lowest one. It combined experts' opinions to determine relative evaluation weights for several competing elements. The relevance and relative influence of eleven flood-causative elements were assessed using Saaty's importance scale. The AHP method in flood modelling is documented in [14]. A single expert judgment is sufficient in such a survey [12].

The consistency ratio (CR) is the ratio of a random matrix's consistency to the ratio of a specified evaluation matrix. If the consistency ratio reaches 0.1, the judgment may be too erratic to be trusted. Nonetheless, if CR equals 0, the decision appears

Fig. 1 Study area map

consistent [14]. The consistency ratio was calculated using Eqs. (3) and (4).

$$CR = \frac{CI}{RI} \quad (3)$$

$$CI = (\lambda_{\max} - n)/(n - 1) \quad (4)$$

3 Methodology

3.1 Study Area

The Kuala Krai district is selected for the flood susceptibility mapping. The latitude and the longitude of the Kuala Krai are 6.245647 and 102.663516, as shown in Fig. 1. The total area of 2,329 km² is considered for the flood susceptibility mapping. It is covered with forest and has hilly regions. The Kuala Krai has the highest elevation of 440 m. It is hot and humid all year, with a mean low temperature of 21 °C and a high temperature of 32 °C [28].

3.2 Data Collection

The collected data from different sources are explained in Table 1. The DEM is derived from the ASTER, GDEM at 30 m. The LULC map of the study is obtained from the Esri website ([www.esri.com/landcovermap.com](http://www.esri.com/landcovermap)). The soil map of the study

Table 1 Data sources used in flood susceptibility mapping

Data	Descriptions	Sources
Digital elevation model (DEM)	ASTER, GDEM of 30 m	US Geological Survey
Land cover and land used (LULC)	Land cover map of 10 m updated by 2021	Esri website
Soil	Global soil map of FAO	Food Agriculture Organization
Rainfall	Rainfall collected between 1985–2021	NASA satellite

region is derived from the global soil map of FAO. Rainfall statistics from 1985 to 2021 are obtained from the National Aeronautics and Space Administration (NASA).

3.3 Preparation of Flood Causative Factors Maps

The flood causative factors map such as (a) rainfall, (b) slope, (c) aspect, (d) curvature, (e) drainage density, (f) distance from the river, (g) LULC, (h) soil map, (i) TWI, and (j) SPI were selected. The interpolation distribution weightage (IDW) method constructs the average annual rainfall thematic layer. The aspect, slope, and curvature maps are derived from DEM. The lineament density and Euclidean distance were used to generate drainage density and distance from the river map. The soil and LULC maps were extracted from the global maps. The TWI and SPI maps are generated using Eqs. (1) and (2) in the raster calculator.

4 Results and Discussion

4.1 Flood Causative Factors

Ten flood causative factors are selected for flood susceptibility mapping, shown in Fig. 2.

The rainfall map of Kuala Krai is shown in Fig. 2a. The rainfall map of Kuala Krai is divided into five classes. The rainfall of the Kuala Krai ranges from 1184.42 to 2575.9 mm. The northwest regions of Kuala Krai experience more rain than the other regions. The slope thematic layer of the Kuala Krai is shown in Fig. 2b. The slope of the Kuala Krai ranges from 0.000001 to 69.2669 degrees. Kuala Krai has more slope areas in the northeast and southwest. The aspect map of the Kuala Krai is shown in Fig. 2c. The Kuala Krai aspect value ranges from -1 to 360 degrees. The Kuala Krai has more slopy aspects in the north and the northwest regions. The Kuala Krai curvature map is shown in Fig. 2d. The curvature value of Kuala Krai ranges

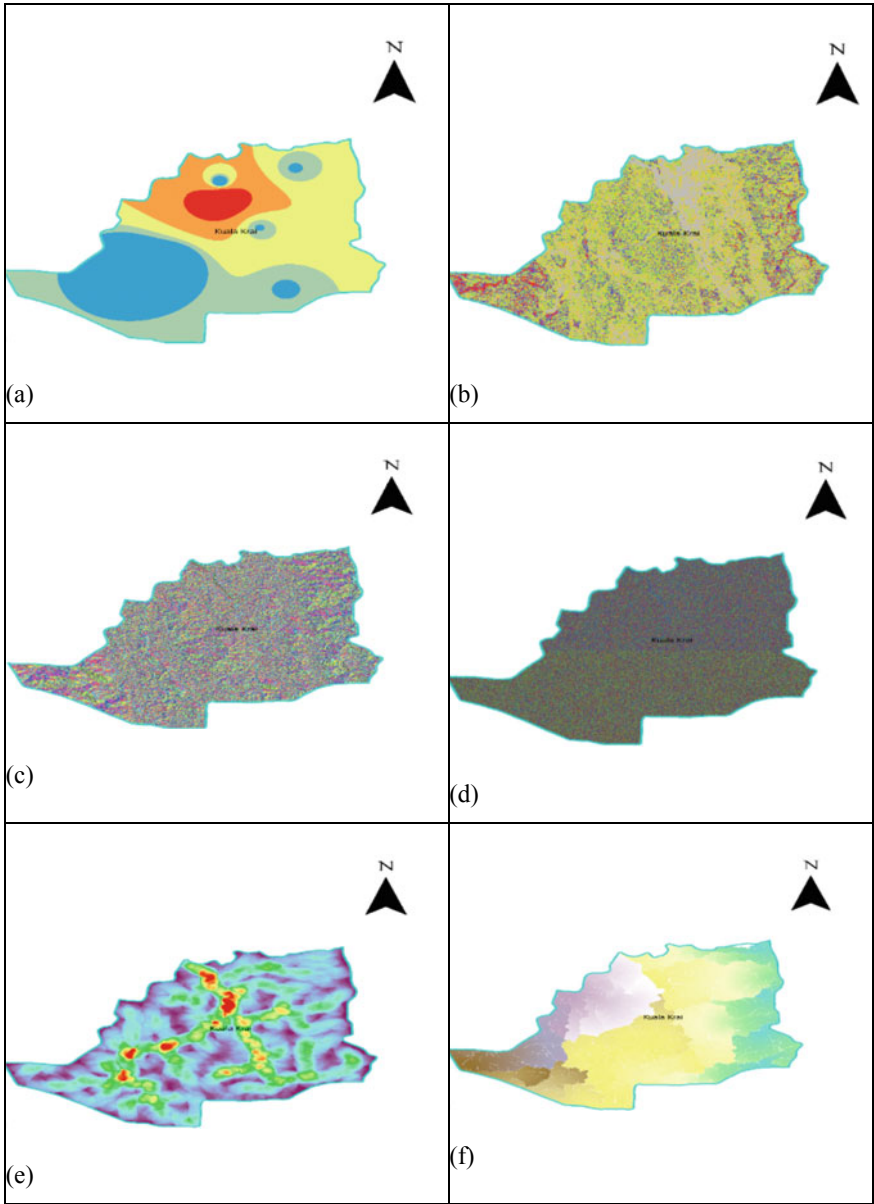


Fig. 2 Flood influential factors thematic maps (a) rainfall (b) slope (c) Aspect (d) curvature (e) drainage density (f) distance from the river (g) LULC (h) soil map (i) TWI and (j) SPI

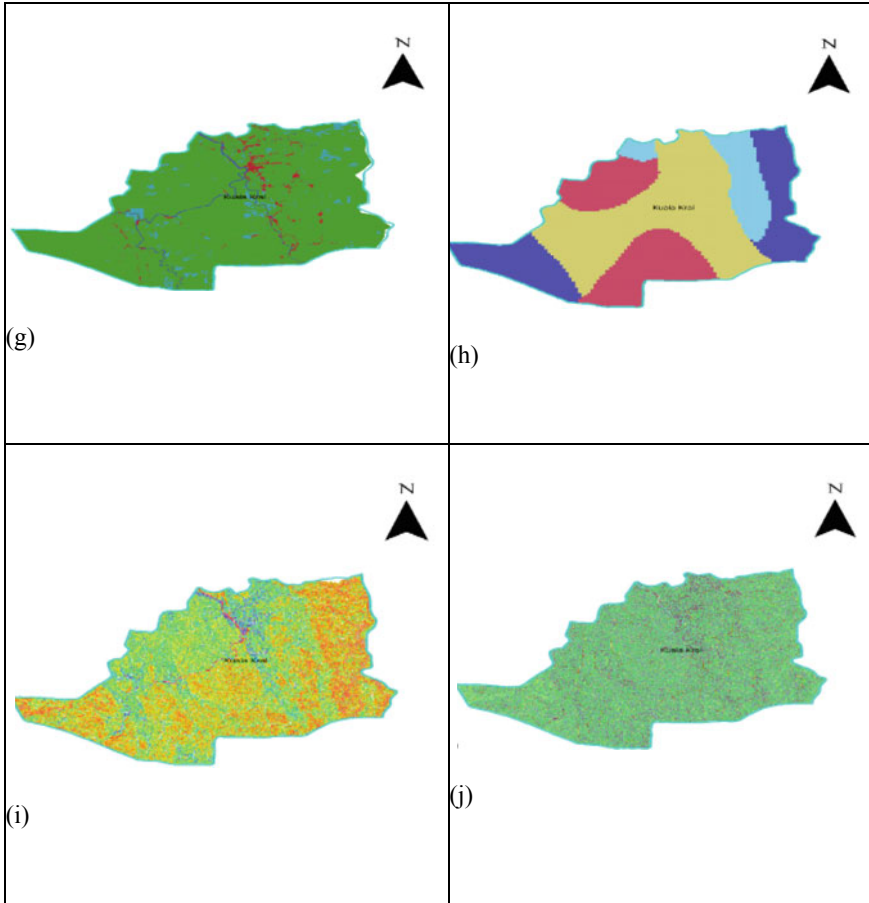


Fig. 2 (continued)

from -6.03936 to 7.20576 m^{-1} . The curvature value of the Kuala Krai is higher in the northwest regions due to the downstream. The drainage density of Kuala Krai is shown in Fig. 2e. The Kuala Krai drainage density values range from 0 to 547.614 m/km . The Kuala Krai has more drainage density in the northern region. In Fig. 2f, the distance from the river map of Kuala Krai is shown. The distance from the river of Kuala Krai ranges from 0 to 1.15229 m . The northeast region of Kuala Krai has a lower distance from the river, so there will be more chances of a flood occurring.

The LULC map of the Kuala Krai is shown in Fig. 2g. The map is divided into five classes: water, trees, build area, bare ground, and rangeland. Most of the land of the Kuala kraï was covered with forest and trees, which were highlighted in green. The water portions are highlighted in blue. The built areas are nearer the water bodies—the less bare or rangeland available in the study area. The soil map of the study is shown in Fig. 2h. The soil of the Kula kraï district is mostly clay and loam. The

Table 3 Pairwise comparison matrix of ten criteria for AHP process

Factors	1	2	3	4	5	6	7	8	9	10
Rainfall (1)	1	2	2	5	7	5	7	3	3	9
Slope (2)	0.5	1	1	3	5	5	2	3	2	9
Aspect (3)	0.5	1.00	1	3	5	5	5	2	3	6
Curvature (4)	0.2	0.33	0.33	1	0.5	0.2	0.14	0.14	1	1
Drainage density (5)	0.14	0.20	0.2	2	1	1.0	0.2	0.2	3	3
Distance from the river (6)	0.20	0.20	0.2	5	1	1	0.33	0.33	2	5
LULC (7)	0.14	0.5	0.2	7	5	3	1	1	3	5
Soil map (8)	0.33	0.33	0.5	7	5	3	1	1		5
TWI (9)	0.33	0.5	0.33	1	0.33	0.5	0.33	0.2	1	2
SPI (10)	0.11	0.17	0.11	1	0.33	0.2	0.2	0.2	0.5	1

clay soil is a more influenced soil with less permeability, which is dangerous and causes more floods. The TWI map of the Kuala Krai is shown in Fig. 2i. The TWI value of Kuala Krai ranges from -8.89149 to -0.514403 level. The north region of Kuala Krai has more TWI value than other regions. The SPI map of the Kuala Krai is shown in Fig. 2j. The SPI value of the Kuala kraai ranges from -13.8155 to 12.7263 . More erosion may be caused in the northern region of the Kuala Krai due to more SPI values.

4.2 AHP Weight of the Flood Causative Factors

The criteria are arranged hierarchically, as shown in Table 3. The importance of the two factors is shown in each row of the matrix. The first row described the significance of rainfall in comparison to the other parameters provided in the columns. For example, rain is more important than other factors such as aspect, curvature, TWI, SPI, and other factors assigned the values 3, 5, 7, and 9. These weights were normalized according to the methods of the AHP. The model was integrated into the GIS environment to create a flood-susceptible model [13].

4.3 Flood Susceptible Map

The Kuala Krai flood susceptible map using AHP is presented in Fig. 3. The map is classified into five classes using the natural break algorithm. The AHP susceptibility map identified the northern and southern portions of the research area as highly vulnerable to flooding. The AHP model also categorizes the western as extremely low to low and moderately sensitive zones.

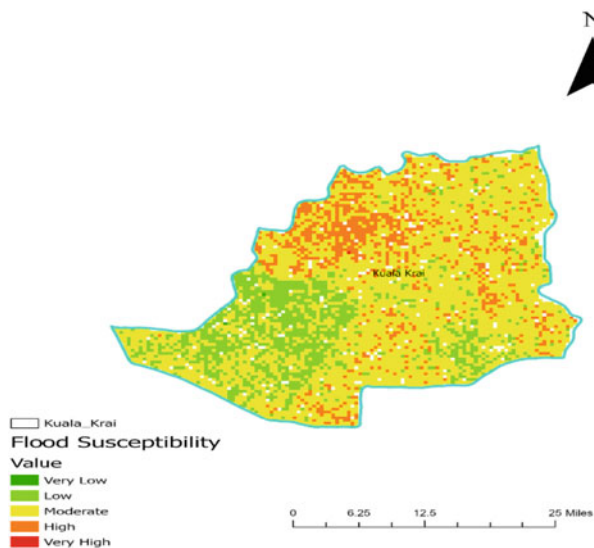


Fig. 3 Flood susceptible map of Kuala Krai

5 Conclusion

The GIS-AHP approach was used to create the Kuala Krai flood susceptibility map. This study chose ten flood-causing factors. In the Saaty scale, A matrix of pairwise comparisons is created. Rainfall and slope have higher weightage values, such as 9 and 7, than the other flood causes. The flood susceptible map is divided into five classes: very high, high, moderate, low, and very low by the natural break Jackson method. The southern and northern regions of Kuala Krai are more flood-prone areas due to the high rainfall and slope.

Acknowledgements This work was supported by Universiti Tunku Abdul Rahman through the research fund UTAR-RF IPSR/RMC/UTARRF/2021-C1/Z01.

References

1. Tsakiris G (2014) Flood risk assessment: concepts, modelling, applications. *Nat Hazard* 14:1361–1369. <https://doi.org/10.5194/nhess-14-1361-2014>
2. Choubin B, Moradi E, Golshan M, Adamowski J, Sajedi-Hosseini F, Mosavi A (2019) An ensemble prediction of flood susceptibility using multivariate discriminant analysis, classification and regression trees, and support vector machines. *Sci Total Environ* 651:2087–2096. <https://doi.org/10.1016/j.scitotenv.2018.10.064>
3. Ekmekcioğlu Ö, Koc K (2022) Explainable step-wise binary classification for the susceptibility assessment of geo-hydrological hazards. *Catena (Amst)*. 216:106379. <https://doi.org/10.1016/j.catena.2022.106379>.

4. Balogun A, Quan S, Pradhan B, Dano U, Yekeen S (2021) An improved flood susceptibility model for assessing the correlation of flood hazard and property prices using geospatial technology and Fuzzy-ANP. *J Environ Inf* 37:107–121. <https://doi.org/10.3808/jei.202000442>
5. Das S (2019) Geospatial mapping of flood susceptibility and hydro-geomorphic response to the floods in Ulhas basin, India. *Remote Sens Appl.* 14:60–74. <https://doi.org/10.1016/j.rsase.2019.02.006>
6. Tehrany MS, Pradhan B, Jebur MN (2014) Flood susceptibility mapping using a novel ensemble weights-of-evidence and support vector machine models in GIS. *J Hydrol (Amst)*. 512:332–343. <https://doi.org/10.1016/j.jhydrol.2014.03.008>
7. Costache R, Țincu R, Elkhrachy I, Pham QB, Popa MC, Diaconu DC, Avand M, Costache I, Arabameri A, Bui DT (2020) New neural fuzzy-based machine learning ensemble for enhancing the prediction accuracy of flood susceptibility mapping. *Hydrol Sci J* 65:2816–2837. <https://doi.org/10.1080/02626667.2020.1842412>
8. Mojaddadi H, Pradhan B, Nampak H, Ahmad N, Ghazali AH (2017) Bin: ensemble machine-learning-based geospatial approach for flood risk assessment using multi-sensor remote-sensing data and GIS. *Geomat Nat Haz Risk* 8:1080–1102. <https://doi.org/10.1080/19475705.2017.1294113>
9. Tehrany MS, Lee MJ, Pradhan B, Jebur MN, Lee S (2014) Flood susceptibility mapping using integrated bivariate and multivariate statistical models. *Environ Earth Sci* 72:4001–4015. <https://doi.org/10.1007/s12665-014-3289-3>
10. Kia MB, Pirasteh S, Pradhan B, Mahmud AR, Sulaiman WNA, Moradi A (2012) An artificial neural network model for flood simulation using GIS: Johor River Basin, Malaysia. *Environ Earth Sci*. 67:251–264. <https://doi.org/10.1007/s12665-011-1504-z>
11. Youssef AM, Hegab MA (2019) Flood-hazard assessment modeling using multicriteria analysis and GIS. In: *Spatial MODELING in GIS and R for earth and environmental sciences*, pp. 229–257. Elsevier. <https://doi.org/10.1016/b978-0-12-815226-3.00010-7>.
12. Balogun A-L et al (2022) Assessment of data mining, multi-criteria decision making and fuzzy-computing techniques for spatial flood susceptibility mapping: a comparative study Assessment of data mining, multi-criteria decision making and fuzzy-computing techniques for spatial flood susceptibility mapping: a comparative study DEMATEL-ANP: Decision Making Trial and Evaluation Laboratory. *Geocarto Int* 1–25. <https://doi.org/10.1080/10106049.2022.2076910>.
13. Swain KC, Singha C, Nayak L (2020) Flood susceptibility mapping through the GIS-AHP technique using the cloud. *ISPRS Int J Geoinf* 9. <https://doi.org/10.3390/ijgi9120720>.
14. Ramkar P, Yadav SM (2021) Flood risk index in data-scarce river basins using the AHP and GIS approach. *Nat Hazards* 109:1119–1140. <https://doi.org/10.1007/s11069-021-04871-x>
15. Shafapour Tehrany M, Kumar L, Neamah Jebur M, Shabani F (2019) Evaluating the application of the statistical index method in flood susceptibility mapping and its comparison with frequency ratio and logistic regression methods. *Geomat Nat Haz Risk* 10:79–101. <https://doi.org/10.1080/19475705.2018.1506509>
16. Khosravi K et al (2019) A comparative assessment of flood susceptibility modeling using Multi-Criteria Decision-Making Analysis and Machine Learning Methods. *J Hydrol (Amst)*. 573:311–323. <https://doi.org/10.1016/j.jhydrol.2019.03.073>
17. Balogun AL, Matori AN, Hamid-Mosaku AI, Umar Lawal D, Ahmed Chandio I (2017) Fuzzy MCDM-based GIS model for subsea oil pipeline route optimization: an integrated approach. *Mar Georesour Geotechnol* 35:961–969. <https://doi.org/10.1080/1064119X.2016.1269247>
18. Youssef AM, Pradhan B, Sefry SA (2016) Flash flood susceptibility assessment in Jeddah city (Kingdom of Saudi Arabia) using bivariate and multivariate statistical models. *Environ Earth Sci* 75:1–16. <https://doi.org/10.1007/s12665-015-4830-8>
19. Fang Z, Wang Y, Peng L, Hong H (2021) Predicting flood susceptibility using LSTM neural networks. *J Hydrol (Amst)* 594. <https://doi.org/10.1016/j.jhydrol.2020.125734>.
20. Abu El-Magd SA, Amer RA, Embaby A (2020) Multi-criteria decision-making for the analysis of flash floods: a case study of Awlad Toq-Sherq, Southeast Sohag, Egypt. *J African Earth Sci* 162. <https://doi.org/10.1016/j.jafrearsci.2019.103709>.

21. Wang Y, Fang Z, Hong H, Peng L (2020) Flood susceptibility mapping using convolutional neural network frameworks. *J Hydrol (Amst)* 582. <https://doi.org/10.1016/j.jhydrol.2019.124482>.
22. Pham BT et al (2021) Flood risk assessment using hybrid artificial intelligence models integrated with multi-criteria decision analysis in Quang Nam Province, Vietnam. *J Hydrol (Amst)* 592. <https://doi.org/10.1016/j.jhydrol.2020.125815>.
23. Chapi K, Singh VP, Shirzadi A, Shahabi H, Bui DT, Pham BT, Khosravi K (2017) A novel hybrid artificial intelligence approach for flood susceptibility assessment. *Environ Model Softw* 95:229–245. <https://doi.org/10.1016/j.envsoft.2017.06.012>
24. Ziyilan A, Dogan S, Agopcan S, Kidak R, Aviyente V, Ince NH (2014) Sonochemical degradation of diclofenac: byproduct assessment, reaction mechanisms and environmental considerations. *Environ Sci Pollut Res* 21:5929–5939. <https://doi.org/10.1007/s11356-014-2514-7>
25. Ali SA et al (2020) GIS-based comparative assessment of flood susceptibility mapping using hybrid multi-criteria decision-making approach, naïve Bayes tree, bivariate statistics and logistic regression: a case of Topľa basin, Slovakia. *Ecol Indic* 117. <https://doi.org/10.1016/j.ecolind.2020.106620>.
26. Dou X, Song J, Wang L, Tang B, Xu S, Kong F, Jiang X (2018) Flood risk assessment and mapping based on a modified multi-parameter flood hazard index model in the Guanzhong Urban Area, China. *Stoch Env Res Risk Assess* 32:1131–1146. <https://doi.org/10.1007/s00477-017-1429-5>
27. Mind'je R et al (2019) Flood susceptibility modeling and hazard perception in Rwanda. *Int J Disaster Risk Reduct* 38. <https://doi.org/10.1016/j.ijdr.2019.101211>.
28. Udin WS, Malek NA (2018) Flood risk analysis in Sg. Sam, Kuala Krai, Kelantan using remote sensing and GIS technique. In: *IOP conference series: earth and environmental science*. Institute of Physics Publishing. <https://doi.org/10.1088/1755-1315/169/1/012060>.

Utilization of Zeolite Material with Chemical and Physical Activation as SCC Concrete (Self Compacting Concrete)



Ahmad Yudi, Axcel Joshua, Yeremi Alexander, Syahidus Syuhada, and W Rindu Trisna

Abstract Concrete is a combination of coarse aggregate, sand, cement, and water. In construction technology that is increasingly developing, it is required to make the answer to the problem of providing constructive materials one of the innovations is that SCC concrete has a fairly high workability value. In previous studies that used zeolite as a substitute for cement for SCC concrete, what was different in this study was that the zeolite material was moderated first by chemical and physical activation. This study aims to determine the effect of zeolite activation on the compressive strength and workability of SCC fresh concrete. In chemical activation using 1 M NaOH and physical activation using a temperature of 250 °C. Activated zeolite was used as a substitute for cement with variations of 0%, 10%, 20% and 30% for each variation of 3 samples. The use of SP is 1.2% by weight of cement. This research provides knowledge about the use of zeolite by being activated first. In the manufacture of SCC concrete using 55% fine aggregate and 45% coarse aggregate and the design quality in this study is 40 MPa with reference to the procedure for making concrete SNI 03-2843-2000 with a sample of 12 cylinders with a diameter of 150 mm and a height of 300 mm. The compressive strength test of concrete was carried out at the age of 28 days of concrete. The results and research indicate that the optimum compressive strength with the use of zeolite in chemical activation is found in the 10% compressive strength variation and on physical activation there is a 20% compressive strength variation.

Keywords zeolite · SCC concrete · chemical activation · physical activation

A. Yudi (✉) · A. Joshua · Y. Alexander · S. Syuhada
Civil Engineering, Institut Teknologi Sumatera, South Lampung, Indonesia
e-mail: ahmad.yudi@si.itera.ac.id

A. Yudi
Civil Engineering, Universitas Indonesia, Jakarta, West Java, Indonesia

W. Rindu Trisna
Balai Besar Wilayah Sungai Mesuji, Kementerian Pekerjaan Umum Dan Perumahan Rakyat, Kota Bandar Lampung, Lampung, Indonesia

1 Introduction

The distribution of natural zeolite in Indonesia is quite high, one of which is in Lampung Province. Based on Zeolite Production and Consumption Data, 2002 “Central Agency for Statistics” the distribution of zeolite minerals in Lampung Province is the second largest in Indonesia. If tested, the chemical content of zeolite contains the chemical compound silica (SiO_2) and will act chemically with calcium hydroxide and result from the hydration reaction in cement so as to make a substance that can be like cement [1]. In this experiment, the use of zeolite minerals which directly came from the southern Lampung area of CV products Minatama.

To improve the performance of the use of zeolite minerals, it is necessary to undergo activation first in order to function optimally. With the process of activating zeolite expanding the pore surface as well as the loss of impurity elements in zeolite, through the activation of zeolite can change the ratio of Si / Al. So, zeolite is the same as the material to be adsorbed. This process is carried out using two chemical and physical methods. In chemical assets, you can use NaOH 1 M [2].

Physical activation of zeolite through the stages of physical activation will affect the properties of the resulting concrete. With zeolite is given physical treatment with a temperature of 250 °C zeolite. The variation in the size of the zeolite at the activation stage will affect the compressive strength, the larger the particle size of the zeolite feeding the greater the compressive quartz produced.

This research was carried out to determine the effect of chemical and physical activation on zeolite which will be used as a substitute for cement as SCC (Self Compacting Concrete) Concrete. With a variability of 0%, 10%, 20%, and 30% against cement used in concrete mixtures. The use of SP in concrete mixtures is 1.2% against the weight of cement.

2 Literature Review and Theoretical Foundations

2.1 Literature Review

Construction and the sector in building materials in Indonesia have soared significantly, helped by the rapid advancement of property in Indonesia, the development of private investment and state spending. This has resulted in the increasing competition and advancement of businessmen in the construction industry and the material sector in domestic buildings, this is required to create an innovation by maintaining balance, namely by utilizing such as examples in construction materials, namely concrete [3]

2.2 *Theoretical Foundations*

2.2.1 SCC Concrete

Self Compacting Concrete (SCC) is the development of findings on the composition of concrete that is able to fill the space/ shape of the formwork thoroughly and tighten by itself using the weight of the concrete itself without mechanical compaction such as a vibrator with a result that remains homogeneous. Basically, the composition of self compacting concrete is similar to conventional concrete, but it is given additional chemical admixture and makes adjustments to the use of coarse aggregates. Some literature says to obtain self compatibility with aggregate adjustment, low w/c ratio, and using admixture additives such as superplastiziers. Characteristics of Self Compacting Concrete (SCC) Based on concrete can be claimed as self compacting concrete if the workability of fresh concrete properties meets the characteristics of fresh concrete such as:

a. Filling Ability.

In fresh concrete mixtures should have the character to fill the room or formwork mold with its flowability throughout the area with its own weight.

b. Passing ability.

The character in fresh concrete has the ability to flow fresh concrete in the space between the reinforcement or the room of a tight structure.

iii. Segregation resistance.

The ability of fresh concrete mixtures to be maintained in homogeneous conditions during jetting/transportation during casting in order to avoid the effects of segregation.

2.2.2 Zeolite

This mineral is very widely spread in the world, especially in Indonesia. Is a material that is often used in sharing bidang such as water treatment, agriculture, and industrial waste [4]. Materials that enter the zeolite group are formed from the sedimentation of volcanic dust that undergoes an acteration stage. Geologically, zeolite deposits are formed due to alkaline stages of volcanic dust sedimentation, diagenetic processes, and hydrothermal processes in the lake environment.

Zeolite is calcified as a pozzolan material as in cement this is because the mineral zeolite contains quite a lot of silica (72.51%) which can be replaced as cement substitution material. When used as a filler material or substitute for cement, it usually ranges from 10–35% of the weight of cement. Cement has the main components, namely calcium oxide (CaO) of 60–65%, silica oxide (SiO₂) of 20–24%. According to the similarity of the elements possessed by cement and zeolite, the use of zeolite

Table 1 Chemical Composition of Natural Zeolite

Sample Code: ZEOLITE			
Omnian ED- XRF PANalytical Epsilon 3 XLE			
<i>Element Oxides</i>			
<i>Compound Conc Unit</i>	<i>Compound Conc Unit</i>		
Al 9.632%	Al ₂ O ₃	11.569%	
Si 61.243%	SiO ₂	72.751%	
P 0.829%	P ₂ O ₅	0.843%	
K 10.057%	K ₂ O	5.147	%
Ca 8.537%	CaO	4.724	%
Ti 0.516%	TiO ₂	0.322	%
Mn 0.141%	MnO	661.2	Ppm
Fe 8.304%	Fe ₂ O ₃	4.275	%
Zn 277.4 ppm	ZnO	116.4	Ppm
Ga 102.5 ppm	Ga ₂ O ₃	46.4	Ppm
Rb 811.2 ppm	Rb ₂ O	295.0	Ppm
Sr 0.235%	SrO	920.8	Ppm
Y 117.0 ppm	Y ₂ O ₃	49.2	Ppm
Te 183.7 Ppm	TeO ₂	80.3	Ppm
Ba 0.130%	BaO	518.0	Ppm
Ce 210.0 Ppm	CeO ₂	91.7	Ppm
Eu 426.9 Ppm	Eu ₂ O ₃	180.9	Ppm
Pb 98.6 Ppm	PbO	35.5	Ppm
Th 138.5 Ppm	ThO ₂	52.3	Ppm
Sn 484.4 Ppm	SnO ₂	212.1	Ppm
Zr 929.2 Ppm	ZrO ₂	416.0	Ppm

as a substitute for cement such as the example of paving block construction materials can be a new reference to produce a low budget with high quality [5] Table 1.

2.2.3 Zeolite Activation

This natural zeolite is still very much mixed with impurity materials other than zeolite, because this natural zeolite has a hollow or porous surface, which is approximately above 30% of it is total volume, therefore it is necessary to activate zeolite with the aim of removing impurities. At this stage of activation we can do with the heating method that is physical activation or by adding acids or bases, namely the chemical activation of zeolite can be increased by activation. In addition to being able to reduce from impurities and in this activation process can increase and reduce the Si/Al ratio so that the properties of this mineral are like the material to be adsorbed [2].

Natural zeolite measuring 100 mesh is mixed as much as 20 g into 100 mL of NaOH solution with variations in concentrations of 2, 4 and 6 M. Zeolite is activated using an ultrasonic tool for 1 h at a temperature of 60 °C then the zeolite is filtered and rinsed using aqueous until the pH is neutral. Then it is dried in the oven for 4 h at a temperature of 110 °C. The results of the XRF analysis showed that the composition of SiO₂ decreased significantly as the concentration of NaOH increased. The results of the XRD analysis showed that NaOH-activated natural zeolite using ultrasonic waves obtained the main component / basic skeleton in the form of mordenite mineral type [6].

3 Research Methodology

3.1 Zeolite Activation Method

Before zeolite was used in concrete mixtures as a substitute for cement against concrete first zeolite was activated which was divided into two chemical and physical activations. In activating zeolite chemically by using a 1 M NaOH at the ITERA Chemistry Laboratory. With the asset process carried out, among others:

a. Preparation of Natural Zeolite.

The zeolite used was dioven dive 5 h with a temperature of 130 °C. The dried zeolite is then sifted mesh 200.

b. Mixing 1 M NaOH with zeolite

Zeolite is introduced into the NaOH solution at a ratio of 2 ml of 1M NaOH solution to 1 g of zeolite. The mixture is then heated to a temperature of 110 °C and stirred for 1 hour.

iii. Neutralization of pH.

Zeolite that has been heated is allowed to stand to room temperature and then rinsed with aquades to a neutral pH and zeolite is filtered using a cloth.

iv. Zeolite Drying.

Filtered zeolite and then oven to dry with a temperature of 130 °C.

In physical practice, first enter the preparation period with zeolite sifted with mesh 200. Entering into the process of activation of physics, zeolite is equipped with a temperature of 250 °C for 3 h. And zeolite, which has been activated physically and chemically, is then used in concrete mixtures as a mixture to replace cement or SCC concrete.

Table 2 Composition of Concrete Mix Material 1 m³

No	Description	Value (Kg)
1.	Cement Weight	548.26
2.	Water Weight	230.04
3.	Fine Aggregate Weight	1017.20
4.	Aggregate Weight Grade	832.25

3.2 Concrete Mix Composition Planning

In planning the composition of the concrete mixture, it is aimed at obtaining the proportion of the mixture of cement and other materials in order to optimize the proportion of the mixture. In this mixing, the compressive strength is hinted at $f'c = 40$ Mpa at the age of 28 days. Planning of fresh concrete mixture self compacting concrete (SCC) refers to the procedure for planning concrete mixtures with the foundation of SNI 03-2843-2000. In the manufacture of this test object is set using a composition of fine aggregate and coarse aggregate 55%: 45%. The addition of SP of 1.2% to the weight of the cement used in this presentation was obtained from the trial and error that had been carried out Table 2.

3.3 SCC Fresh Concrete Test

a. Slump Flow.

This experiment was carried out so that we can see the results of the characteristics of the filling ability in fresh concrete SCC Slump flow test this SCC concrete first wets the surface of the slab and cone equipment without causing increased water, then places the base plate on a flat ground surface and slump cone in the middle of the baseplate and holds it firmly. Then fill the cones with a spoon, then when they are completely filled, clean the remaining spilled fresh concrete. Then, Vertical and stably lift the cone and let the concrete flow and at the same time turn on the stopwatch, record the time if the diameter of the concrete reaches a diameter width of 500 mm. after which measure and record the diameter in two directions perpendicular.

b. L-Shaped Box.

This experiment was carried out so that we could see the results of the characteristics of the passing ability in fresh concrete SCC. By pouring fresh concrete with a spoon, and not compacting, by hitting the upper concrete surface and allowing (10 ± 2) s then lift the vertical door and let the concrete flow into the horizontal part. The movement stops measuring the height of the concrete in the horizontal direction of the tool in three positions wide of the horizontal box (H2). Further doing the same at the height of the concrete in the vertical direction of the tool, it is used as (H1).

iii. V-Funnel Test.

Testing this tool we will know the evaluation results of the resistance of fresh concrete to segregation. By pouring fresh concrete with a spoon, do not carry out compaction, by hitting the upper concrete surface and leave (10 ± 2) s. Next, place the container under the funnel opening to accommodate the descent of fresh concrete. Then, open the vertical door and let the concrete flow into the container. At the same time calculate the time with the stopwatch and record until fresh concrete passes through the funnel.

In the process of this research, it can be seen the process from beginning to end on the flow chart below (Fig. 1)

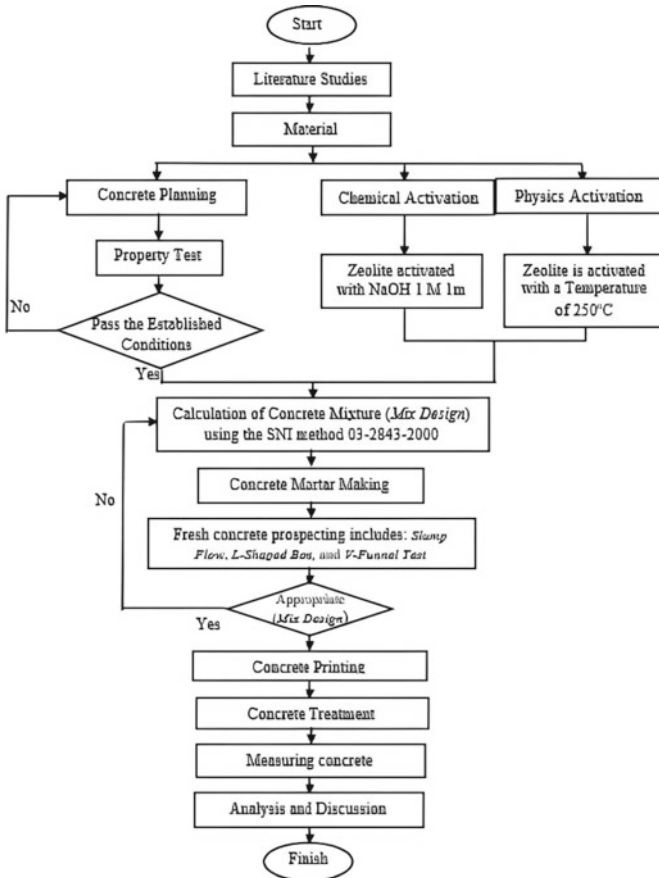


Fig. 1 Flowchart

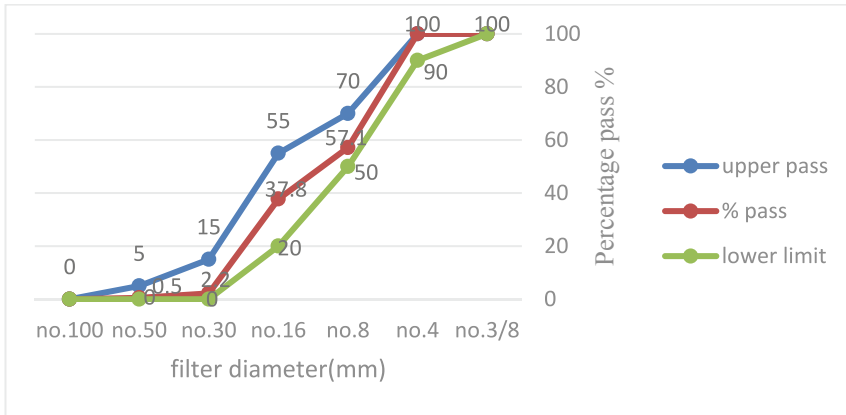


Fig. 2 The Relationship Between The Size Of The Sieve And The Percentage Of Passed The Aggregate Sieve Halus

4 Results and Discussion

4.1 Pre-implementation of Concrete Mixture

Testing of the materials that will be used in the concrete mixture to find out the composition of the materials used in the concrete mixture.

4.1.1 Fine Aggregate Test

- Sludge Content Examination on fine aggregates, the result obtained was 4%.
- Water Content Check obtained a moisture content of 1.42%.
- Weight testing was obtained for fine aggregates of 1387.273 kg/m³.
- Specific Gravity and Water Absorption Check. From the results of the examination of specific gravity and water absorption in the fine aggregate, a dry specific gravity of the oven (bulk specific gravity) of 2.57 g was obtained, the dry specific gravity of the saturated surface (bulk specific SSD) was 2.59 g and the pseudo-specific gravity (apparent) was 2.62 g and absorption was 0.8%.
- The modulus of fineness of the fine aggregate is 2.306. The value has met the requirements required according to SE Number: 07/SE/M/2016 the fine aggregate is in Zone 2 (Fig. 2)

4.1.2 Rough Aggregate Test

- Water Content Testing Water content check on coarse aggregates of 2.01%.

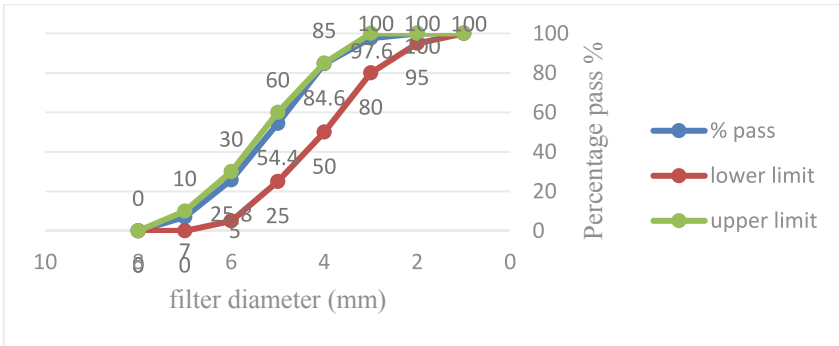


Fig. 3 The Relationship Between The Size Of The Sieve And The Percentage Of Coarse Aggregate Sieve Pass

- b. Examination of the specific gravity and water absorption in the coarse aggregate obtained a dry specific gravity of the oven (bulk specific gravity) of 2.35 g, the dry specific gravity of the saturated surface (bulk specific SSD) of 2.412 g and the pseudo-specific gravity (apparent) of 2.491 g and absorption of 2.25%.
- c. Weight testing of the volume, from this test was obtained for coarse aggregates of 1199.192 kg/m³.
- d. Sieve Analysis Testing Obtained the modulus of fineness of the coarse aggregate was 7.024 (Fig. 3).

4.1.3 Cement Test

The test of this cement material is carried out by two examinations. First, testing the specific gravity of cement obtained by 3150 kg/m³. Furthermore, the initial visual inspection has good conditions. However, the mixing process is carried out with a fairly long time distance so that the condition of the cement becomes clogged. The cement that clogs will affect the strong result of the concrete at the time of testing.

4.1.4 Zeolite Test

The zeolite used in this study came from CV Minatama and was packaged with 50 kg. Which is used as a variation of concrete mixture material. This material is carried out specific gravity testing obtained by this test is obtained by obtaining a zeolite specific gravity of 2100 Kg /m³.

4.2 Test Results of SCC Fresh Concrete Mixture

At the time of making the fresh concrete mixture, fresh concrete workability testing was carried out with the three parameters, but it has not been achieved. Then there is an addition of water in order to reach the parameters of the workability test. With the addition of water automatically the e.q. FAS value; FAS Percentage will change with each variation. On the addition of water to the concrete mixture both using zeolite chemical activation and physical activation are the same. Here is the correction of the cement water factor on the Table 3.

4.2.1 Slump Flow Test

Based on Fig. 4. In zeolite the highest activation of physics and chemistry is obtained at a variation of 10%. In Physical activation by 62 cm while chemical activation is higher by 72 cm. This slump flow value describes the flowable properties of fresh concrete itself. If an analysis of the form of the graph obtained, it is illustrated that along with the addition of zeolite variations after a variation of 10% there is a decrease in the flowability of fresh concrete itself with the lowest slump value attributed to variations in zeolite levels by 30%.

Table 3 FAS Correction Results

No	Variation Water (kg)	Addition of Water (Kg)	Weight of Cement	FAS
1	10%	1,219	0	2,905
2	10%		0,25	
3	20%		0,75	
4	30%		1	
				0,420
				0,506
				0,678
				0,764

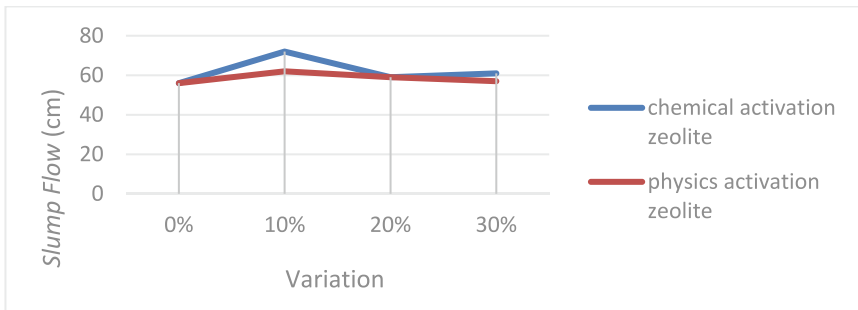


Fig. 4 The Relationship of Slump Flow to Variation

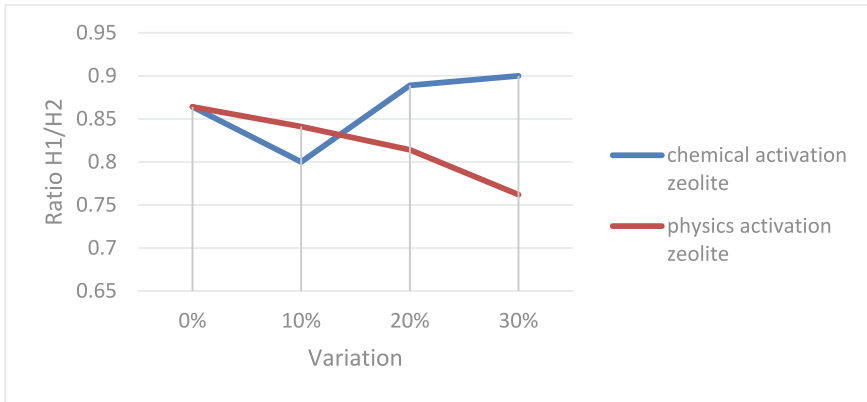


Fig. 5 Relationship of H1/H2 Ratio to Variation

4.2.2 L-Shaped Box Test

It can be seen in Fig. 5. In zeolite activation physics is presented an overview of the ratio obtained in each variation, where there is a decrease in workability along with the increase in the number of zeolite. However, the chemical activation zeolite describes the increase in the ratio in the L-Box seassy has been the addition of chemically activated zeolite from a variation of 10%. Based on the 2005 EFNARC parameters for L-Box exposure the recommended ratio is between 0.8–1. In this test, it was categorized as PA2 because it used a 3-reinforcement tool.

4.2.3 V-Funnel Test

The results of this test are shown in the graph in Fig. 6. In zeolite chemical activation occurs a decrease after the addition of zeolite of a variation of 10%. While the physics activation zeolite in the V-Funnel test of the 30% zeolite variation was found to be 27 s, so this variation did not meet the requirements recommended by the 2005 EFNARC, this also illustrated in an experiment conducted by Ahmad Shofiul Iqbal in 2018 where the author explained that there was also a reduction in *workability* in SCC concrete along with the addition of *zeolite* variations.

4.3 Weight Effect of Concrete Volume

From the chart in Fig. 7. From zeolite that has been activated chemically and physically it can be seen that every addition of zeolite variations, there is a decrease in the weight of concrete volume. The largest volume weight is found at a variation of 0% and the smallest is found at a variation of 30%. Referring to SNI 7657:2012

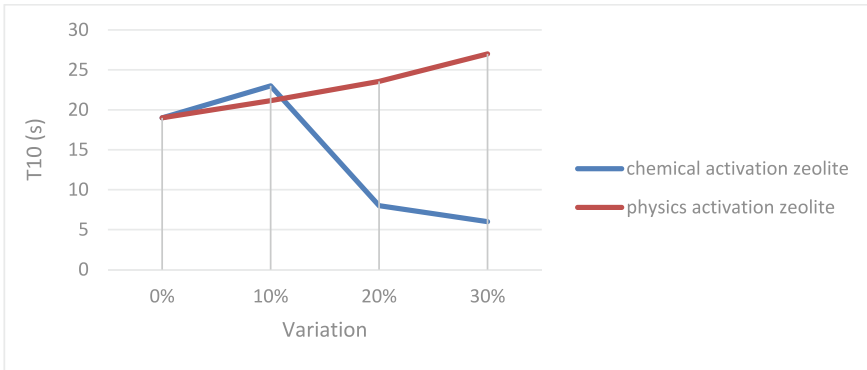


Fig. 6 The Relationship of T₁₀ to Variation

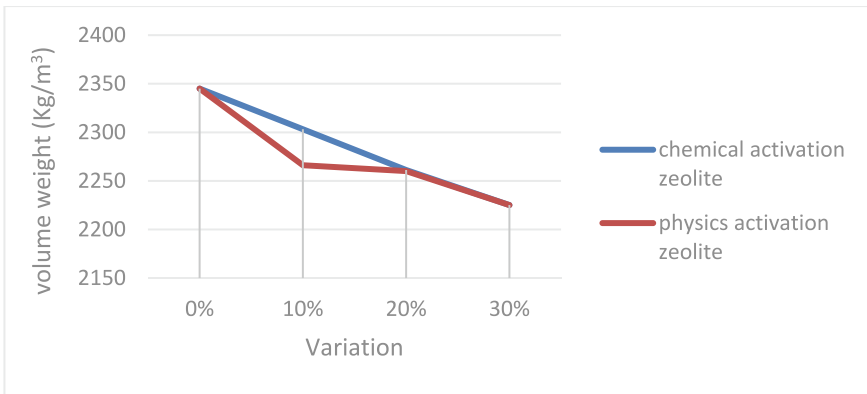


Fig. 7 Relationship of Zeolite Variation to Concrete Volume Weight

in Sect. 3.1, the weight of concrete volumes between 2200 kg/m³ to 2500 kg/m³ is included in the normal concrete category, so that all samples in each experiment are still categorized as normal concrete.

4.4 Concrete Compressive Strength Results

Based on Fig. 8. In the use of zeolite, the highest compressive strength physical activation using a zeolite variation of 20% with an average compressive strength of 37,367 MPa, this compressive strength is not far from the magnitude of the 10% variation. Meanwhile, in chemical activation, the highest compressive strength using zeolite variations is 10% with an average compressive strength of 47.12 MPa. At a 10% variation the difference from zeolite chemical and physical activation was

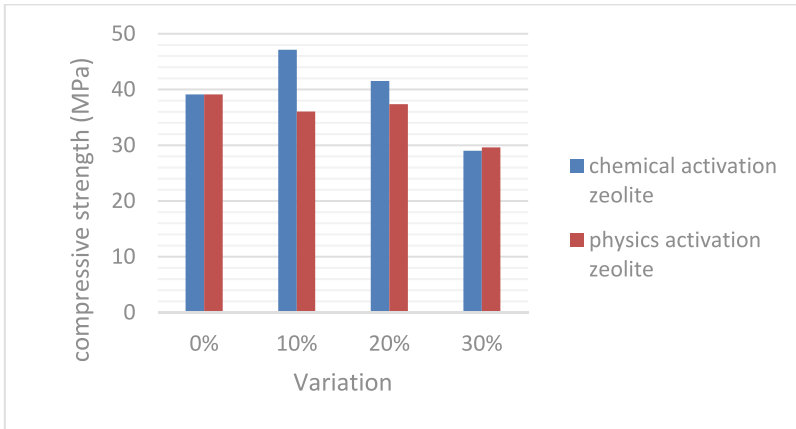


Fig. 8 The Relationship of Compressive Strength with Variation

11,074 MPa. This compressive strength is taken at the age of 28 days according to the life of the compressive strength plan there is a mix design made, the compressive strength of the plan on the mix design is 40%. It can be seen that zeolite by means of chemical activation of compressive strength is produced much higher than physical activation at optimal variations at 10%.

5 Conclusion

After material testing, linking of test objects, compressive strength testing, and data analysis, several conclusions can be drawn from this study. First, the results of fresh self compacting concrete (SCC) testing, namely slump flow testing, L-Box testing, and V-Funnel testing, all variations of zeolite substitution that have been chemically activated meet the requirements for the manufacture of self compacting concrete (SCC). However, zeolite that had been activated by the parameter physics of L-Box and V Funnel testing was not achieved with the result of the L-Box ratio of 0.762 and the test result of the V Funnel of 27 s.

The results of the compressive strength test of concrete produced with variations of zeolite 0%, 10%, 20%, and 30% that have been chemically activated as suggestion cement substitutes are 39.12, 47.12, 41.54, and 29.03 Mpa, respectively. Meanwhile, those that have been activated by physics are obtained in a series of 39.12, 36,046, 37,367, 29.63 MPa. In the use of zeolite chemical and physical activation The weight of concrete volumes of all variations is categorized as normal structure or concrete. With the addition of zeolite, both physical and chemical activation, the lower the volume weight will be due to the increasing number of zeolite so that the shape of the concrete is increasingly hollow.

In this study, the manufacture of optimal Self-Compacting Concrete (SCC) using zeolite that has been chemically activated at a variation of 10% compressive strength is produced the highest of 47.12 MPa with a composition for 3 cylinders of water 3,657 kg, cement 8,715 kg, coarse aggregate 13,230 kg, fine aggregate 15,170 kg, zeolite 0.574 kg and SP 1.2% of the weight of the cement. Although in the practice of zeolite through a long process, it produces a high compressive strength compared to the physical activation.

As for suggestions to perfect the results of this study. First, every planning using added materials must pay attention to the function and type of use of the added material because the use of added materials in the concrete mixture can affect the concrete itself. Furthermore, there is chemical activation is very much in attention to the use and condition of the materials and tools used. Finally, there is an XRF test on zeolite which is after being activated chemically and physically.

Acknowledgements I would like to thank the Sumatera Institute of Technology and the Ministry of Education, Culture, Research, and Technology Indonesia.

References

1. Poerwadi MR, Zacoeb A, Syamsudin R, Haryono JMT (2005) The effect of local mineral use of natural zeolite on the characteristics of self-compacting concrete (SCC) found in Indonesia is natural zeolite. Another addition is the homogeneous concrete Magnesium Oxide. Is the granules used for SCC are for, pp 1–10
2. Ngapa YD (2017) Study of the influence of acid-base on zeolite activation and its characterization as an adsorbent of blue metilena dye, JKPK. *J Kim Educ Kim* 2(2):90–96. <https://doi.org/10.20961/jkpk.v2i2.11904>
3. Santoso VY, Sugiyarto, Sunarmasto (2020) Application of value engineering to building structures (case study: surakarta city fire service office building project). *Matrix Tek. Civil*, pp 236–245. <https://matriks.sipil.ft.uns.ac.id/index.php/MaTekSi/article/view/1104>
4. Al Muttaqii M et al (2019) Effect of chemical activation using acid and base solutions on natural zeolite characteristics. *J Ris Teknol Ind* 13(2):266. <https://doi.org/10.26578/jrti.v13i2.5577>.
5. Agung Rizki Pratomo AG, Supriani F (2018) The effect of the use of zeolite as a substitute for part of cement on the compressive strength of conventional paving blocks, pp 35–40
6. Sumarni, Hindryawati N, Alimuddin (2018) Activation and characterization of natural zeolite using NaOH. *J At* 3(2):106–110

Comparative Study of Vacuum Bagging and Hand Lay Up Methods for Coconut Coir Fiber Composite Materials as an Alternative to Wood Boards



Juriah Mulyanti, Sukamto, Bayu Megaprastio, Muhammad Arief Saputro, and Andi Prayoga

Abstract The concept of green material has begun to be developed to make environmentally eco-engineering materials. The abundant availability of coco fiber can be used as reinforcement in composite materials. This experimental research was conducted to see the effect of making coconut fiber composite material using the vacuum bagging method and the hand lay-up method on the occurrence of voids in it. Then it will be used as an alternative material to replace wooden boards. From the tensile test, the vacuum bagging method obtained a tensile strength value of 53.16 Mpa, an increase of 47.17% compared to the other method. From this value, this material cannot be used as a substitute for wooden boards, but can be used for waterproof and termite-resistant board materials. The use of the vacuum bagging method is also good enough to reduce the possibility of hole defects that arise in the other method.

Keywords Coconut coir fiber · Vacuum bagging · Voids · Alternative materials

J. Mulyanti (✉) · Sukamto · B. Megaprastio · M. A. Saputro · A. Prayoga
Departement of Mechanical Engineering, Universitas Janabadra, Jl. Tentara Rakyat Mataram 57,
Yogyakarta, Indonesia
e-mail: jm.yanti@janabadra.ac.id

Sukamto
e-mail: kamto@janabadra.ac.id

B. Megaprastio
e-mail: bayumegaprastio@janabadra.ac.id

M. A. Saputro
e-mail: ariefsaputro@janabadra.ac.id

A. Prayoga
e-mail: prayogjhaandy@gmail.com

1 Introduction

Wood as the material for building construction and furniture has begun to switch to other materials. The need for wood has become increasingly difficult since 1980, so there is a need for alternative substitutes [1]. Mild steel has begun to be widely used with considerations, among others, that it is light, only requires a cutting and installation process, and is not weathered or eaten by termites. However, there are still other needs in the building, namely boards used as ceilings, furniture, and wall panels [2].

The latest developments are many businesses run by the community, especially the culinary, beverage, credit, and other businesses that require small-sized buildings. The building is of course outside which will be exposed to rain, heat, and wind loads. Therefore, the use of wood as wall panels have a weakness in that is easily damaged due to temperature changes, and absorbs water so that it is easily weathered, easily burned, and eaten by termites. The advantages are high tensile strength and ease to form.

The use of natural fibers in the manufacture of composites is increasingly being used, because natural fibers themselves have several advantages including being strong, lightweight and environmentally friendly. Natural fibers have also begun to be applied as composite materials in the manufacture of bumpers, dashboards and other interior panels.

One of the natural fibers that has been widely developed is coconut fiber (coconut fiber). Coir fiber is the outermost part of the coconut fruit that wraps around the coconut shell with a thickness of 5–6 cm, which consists of an outermost layer (exocarpium) and an inner layer (endocarpium) [3]. The use of this coconut coir fiber is gaining interest because in addition to being easy to obtain, cheap, it can reduce environmental pollution (biodegradability) so that this composite is able to overcome environmental problems that may arise from the large amount of coconut fiber that is not utilized. The development of coconut fiber as a composite material is in great demand because the availability of natural fiber raw materials, especially coconut fiber in Indonesia is quite abundant. This underlies the need for research that can increase the use value and also utilize coconut fiber so that it can increase its economic value. From several studies that have been carried out, the advantages of composites that are reinforced with coconut fiber are that they are non-abrasive and have minimal negative impacts on nature and health. Composites made from coir-reinforced polyester resins with coconut fiber has a rough, stiff, but light surface, and is clear in color [4]. Fiber addition coconut fiber can increase tensile and flexural stress composite [5] (Fig. 1).

The process of making composites generally still uses the hand lay-up method. However, the product results obtained surface smoothness only on one side, uneven product thickness, and the emergence of voids (air bubbles) in the composite material [7]. The emergence of air bubbles (voids) in the product using the hand lay up method will cause the mechanical properties of the material to decrease, especially its tensile

strength. To remove trapped voids, the vacuum bagging method is carried out, namely inserting the composite into a plastic bag and then a vacuum process is carried out.

From the description above, research on the manufacture of coconut fiber composites becomes necessary as an alternative to wood materials. The manufacture of this composite material is carried out using the Hands lay-up method and the vacuum bagging method. The test is a tensile test to see if the vacuum bagging method can increase the tensile strength of the coconut fiber reinforced composite, compared to the hands lay-up method. In addition, microscopic testing/observations were also carried out to see the voids that occurred in each of these manufacturing methods. Then from the results of the tensile test, it will be seen whether this coconut fiber composite material can be an alternative to wood board material (Fig. 2).

2 Method

This research produces a new materials by utilizing natural materials in the fiber section as reinforcement for composite materials mixed with polyester resin as a binder and a catalyst as a hardener. Coconut coir fiber has good compatibility with polyester resin [8]. The composition used in the manufacture of this composite using weight of coconut coir used is 40%, and the rest is polyester resin with 1% catalyst. The polyester resin possessed by this type of resin is in addition to a relatively cheap price, it also has excellent adhesion, high heat resistance, good mechanical properties and good electrical insulation ability [9]. The natural fiber used is coconut coir fiber which was previously carried out with water ratting treatment to obtain biodegradable coco fiber. Before being used as a reinforcement of the composite, an alkaline process was carried out using a 5% NaOH solution and the processing time was 30 minutes. Composite manufacture uses unsaturated polyester resin as the matrix. The specimen mold uses glass material with a thickness of 5 mm, dimensions of length 180 mm, width of 100 mm and height of the mold is 4 mm.

2.1 Composite Making Process

Vacuum Bagging Method. The previously treated coconut coir fibers are then arranged in a mold with a one-way fiber orientation. Then the mixed catalyst and resin mixture is poured according to the percentage of each fiber weight. Pouring is done evenly until the resin covers the entire surface of the fiber. Then the mold is put into a vacuum bag. The next step is to perform a vacuum process using a pressure of -30 Psig for 30 min. After the composite material hardens, the composite is removed from the mold using a scraper or cutter. The formation of the test object is carried out using the help of a cutting grinder, file and sandpaper. Cutting is carried out according to ASTM D 638-03 standard.

Hand Lay-Up Method. The process of pouring resin in the hand lay-up method is the same as using the vacuum bagging method. Close the mold using the glass slowly so that no voids appear, then overlap the glass with a ballast. If the composite has hardened then the composite can be taken from the mold. The specimen formation process is the same as in the vacuum bagging method.

2.2 Specimen Testing

Tensile Strength Test. The tensile test of composite specimens is used to determine the magnitude of the tensile strength of the composite material that has been made. In this study, the tests were carried out at the Materials Laboratory of Janabadra University using the Hung Ta HT-9591 Series universal testing machine.

Void Observation. This study uses a microscope to see whether the vacuum process can reduce or eliminate voids trapped in the composite and also to see the surface topography of each composite with variations in fiber weight. Specimens were cut according to the dimensions specified in the microstructural test, namely $40 \times 40 \times 4$ mm

Specimen Test Results. The coconut fiber composite was then compared with the tensile strength data of natural wood planks to determine the potential application of the coconut coir fiber composite.

3 Results and Discussion

3.1 Tensile Strength Test

One way to determine the strength of this composite is to know the value of its tensile strength. In order to know which method is better used for the manufacture of this composite. The higher the value of the tensile strength, the better it will receive the stress (Figs. 3 and 4).

The results of the composite tensile test using the vacuum bagging method showed a higher average tensile strength value than the hand lay-up method. The vacuum process can minimize the occurrence of voids and production defects, so that the density of the composite structure is better to withstand the load. The denser of the composite, is better it will accept the load. The results of the calculation of the average strain value between the two methods also shows that the strain with the vacuum bagging method has a higher yield, so the initial conclusion that the vacuum bagging method will obtain better composite results has been proven. The presence of voids in the specimen will cause the tensile strength of the composite to decrease because the density of the composite decreases.

3.2 Void Observation

Observations using a microscope can be seen the number of voids that occur in each specimen. In the specimen with the hand lay-up method, it appears that the number of voids is more for the same area than the specimen with the vacuum bagging method (Figs. 5 and 6).

3.3 Analysis of Physical and Mechanical Properties

When viewed from the physical properties of this coconut fiber composite, it consists of a polyester resin matrix so that it can be resistant to water. In contrast to wood, which absorbs water, it can cause damage to wood materials such as rotting or porous. This is because the surface structure of the resin is denser than wood so that water cannot be absorbed into the resin. So that this composite will not quickly weathered or porous. In addition, wood is also potentially attacked by termites, while the basic material of this composite is polyester resin so that termites will not attack. So this composite will last longer than wood. It also takes a long time to get the wood used as boards. it takes a long time to wait for a tree to grow large enough to be used as a board. As for this composite, the basic material is easy to obtain and can be processed immediately. If viewed from the mechanical properties through the tensile test of the coconut fiber composite material, it can be seen from the graph in Fig. 7 the comparison with the tensile strength values of several types of wood planks [10]. The data obtained that the coconut fiber composite material has a much lower tensile strength value, so it cannot be used as an alternative material as a substitute for wood board material.

Judging from the tensile strength of the coconut coir fiber composite with the vacuum bagging method compared to various types of wood, the value is smaller. That is because the composite is a combination of several materials, which are very different from the properties of each of the original materials. In contrast to wood which only has 1 material so that it will be in direct contact with the weather and pests that result in a decrease wood quality. Coconut fiber composites use polyester



Fig. 1 Coconut coir fiber [6]

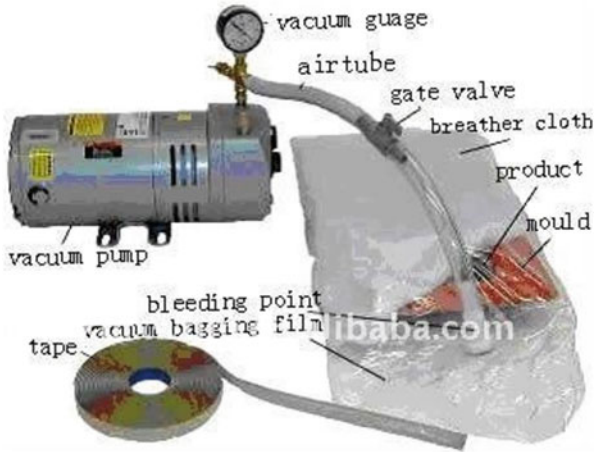


Fig. 2 Process of vacuum bagging method

Fig. 3 Tensile strength test result

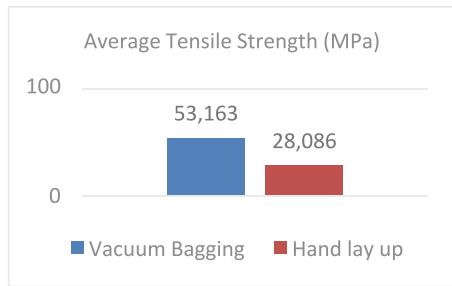
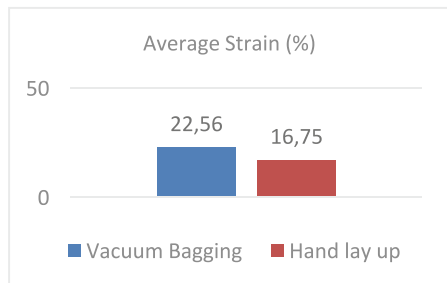


Fig. 4 Composite strain



resin as a matrix which is a liquid thermoset polymer with a relatively low viscosity and can harden at room temperature using a catalyst. The mixture will be easy to wet the fiber, also obtain a good bond between the fiber and the matrix, the resin will protect the coco fiber from external contact such as the influence of weather or pests that will damage the quality of the fiber.

Fig. 5 Hand lay-up method specimen

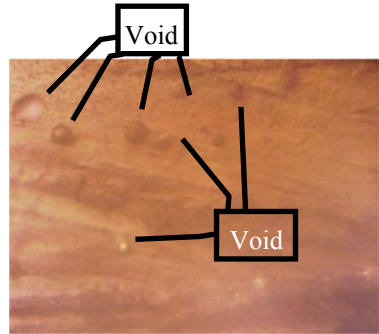


Fig. 6 Vacuum bagging method specimen

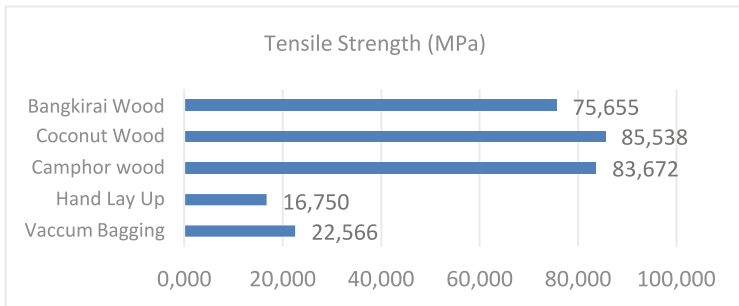
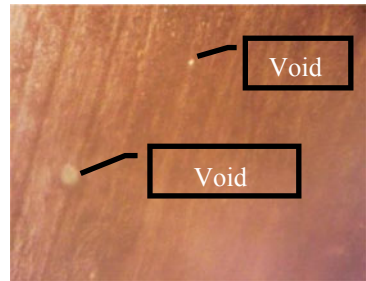


Fig. 7 Comparison of tensile strength values between woods and composites [10]

The use of vacuum bagging will suck air trapped (voids) between the fibers and the matrix when the composite manufacturing process occurs. The process is stated to be effective in the manufacture of composites because it reduces the voids trapped in the composite material before the freezing or hardening process occurs which will result in an increase in the density between the resin and the coco fiber, the increased density will increase the tensile strength value that occurs, this is evident in the comparison of the tensile strength of the composite by vacuum bagging method and hand lay-up method.

4 Conclusion

1. The use of the vacuum bagging method in the manufacture of coconut coir fiber composite materials increases the tensile strength by 47.17%, and can also reduce voids in the composite material compared to the hand lay-up method.
2. When viewed from the tensile strength of several types of wood planks, the coconut fiber composite material cannot replace the use of wooden boards. However, it can be used as an alternative to water-resistant and termite-resistant materials.

References

1. Badri AM, dan Yohanes (2016) Analisis Sifat Mekanis Komposit Serat Sabut Kelapa Sebagai Material Alternatif Pengganti Kayu Untuk Pembuatan Kapal Tradisional, Jom FTEKNIK, vol 3, no 2
2. Purkuncoro AE (2017) Pengaruh Anyam Serat Ijuk (Arenga Pinata) Sebagai Filler dan Bermatrik Tepung Garut (Marantha Erundacea) Dengan Perlakuan Alkali Terhadap Kekuatan Impak. J. Ilm. Cendekia Eksakta, hal. 23–28 [Daring]. Tersedia pada: <https://www.publikasiilmiah.unwahas.ac.id/index.php/CE/article/view/1720/1> 91
3. Daud J, Abanat J, Purnowidodo A, dan Irawan YS (2012) Pengaruh Fraksi Volume Serat Pelepah Gebang (Corypha Utan Lamarck) Terhadap Sifat Mekanik Pada Komposit Bermatrik Epoksi. Rekayasa Mesin vol 3, no 2, hal. 352–361
4. Titani FR, Imalia, CL, dan Haryanto (2018) Pemanfaatan Serat Sabut Kelapa sebagai Material Penguat Pengganti Fiberglass pada Komposit Resin Polyester untuk Aplikasi Bahan Konstruksi Pesawat Terbang. Techno (Jurnal Fak. Tek. Univ. Muhammadiyah Purwokerto), vol. 19, no. 1, hal. 23–28. <https://doi.org/10.30595/techno.v19i1.2397>.
5. Sudiarsa IG, Gde T, Nindhia T, dan Surata IW (2018) Pengaruh Fraksi Berat Serat Daun Nanas Terhadap Kekuatan Tarik Dan Lentur Komposit Polyester, vol 7, no 1, hal. 103–108
6. Surya dan Suhendar I (2016) Sifat Mekanis Komposit Serat Acak Limbah Sabut Kelapa Bermatriks Polyester Resin. J Tek Mesin Univ Bandar Lampung 2(1):37–48 [Daring]. Tersedia pada: <http://jurnal.ubl.ac.id/index.php/JTM/article/view/741/735%0A%0A>
7. Ridlwan M, dan Bahadjai MB (2017) Pembuatan Produk Rekayasa Komposit Serat Bulu Ayam Menggunakan Metode Vacuum Bagging dan Metode Vacuum Infusion Process, hal. 17–20. <https://doi.org/10.21063/pimimd4.2017.17-20>.
8. Prasajo S, Respati, SMB, dan Purwanto H (2018) Pengaruh Alakalisasi Terhadap Kompatibilitas Serat Sabut Kelapa (Cocos nucifera) Dengan Matriks Polyester J Ilm Cendekia Eksakta 2.(2):25–34
9. Amarudin A, dan Respati SMB (2017) KOMPATIBILITAS SERAT PELEPAH POHON PISANG KEPOK (Musaceae) PADA PERLAKUAN PEREBUSAN AIR JAHE (Zingiber Officinale) DAN PERLAKUAN RESIN POLYESTER. Momentum 13:84–89 [Daring]. Tersedia pada: <https://publikasiilmiah.unwahas.ac.id/index.php/MOMENTUM/article/view/2042/2072>
10. Baroto GA, dan Wijanarko S (1996) Analisis Tegangan Kayu Pada Beberapa Jenis Kayu Di Pasaran Berdasarkan Uji Laboratorium

Improved Resistance of Reinforced Concrete Columns in Fire Exposure by Strengthening Stirrup Reinforcement



Prasetya Adi, Arusmalem Ginting, and Bing Santosa

Abstract Fire exposure is very dangerous to the column. The strength of the column will be reduced due to exposure to fire. Stirrups can be used to confine concrete from spalling and minimize buckling of reinforcing steel. Based on these reasons, it is necessary to conduct research on the improved resistance of reinforced concrete columns in fire exposure by strengthening stirrup reinforcement. Six concrete columns with a cross section of $150 \times 150 \text{ mm}^2$ with a length of 1000 mm were used in this study. Four reinforcement bars with a diameter of 10 mm and stirrups with a diameter of 6 mm were used with stirrup spacing variations of 60, 90, and 120 mm. Three specimens were exposed to fire and the other three were not. From the results of the study, it was found that the variation of stirrup spacing below the maximum space based on the code did not significantly affect the strength of the column. Maximum stirrup spacing in code was enough for fire exposure.

Keywords Column · fire exposure · stirrup

1 Introduction

Columns play an important role in keeping the building standing because the collapse of the column means the collapse of the structure above it or the collapse of the entire building.

When exposed to fire the physical and mechanical qualities of concrete have a negative impact. The fire significantly damaged a high quality concrete structure built for great strength with low permeability and caused the structure to collapse [1].

The strength of the concrete column after a fire (temperature has become normal/ room temperature) is more influenced by the remaining strength of the concrete

P. Adi (✉) · A. Ginting · B. Santosa
Civil Engineering Department, Faculty of Engineering, Janabadra University, Yogyakarta,
Indonesia
e-mail: prasetya@janabadra.ac.id

© Institute of Technology PETRONAS Sdn Bhd 2024
B. S. Mohammed et al. (eds.), *Proceedings of the International Conference on Emerging Smart Cities (ICESC2022)*, Lecture Notes in Civil Engineering 324,
https://doi.org/10.1007/978-981-99-1111-0_8

because at normal temperatures the yield stress of the steel returns to its original state [2].

The mineral composition of aggregates and the evolution of the concrete microstructure during heating are related to the evolution of thermal properties [3].

The residual compressive strength of concrete exposed to fire will decrease. There are two methods for measuring the residual compressive strength of concrete. The first method is to look at the discoloration of the concrete surface and the color path to distinguish the temperature zones. The second method is increasing the porosity by observing the increase in the weight of the concrete core after being immersed in water [4].

The bond strength of reinforcement with concrete decreases when the concrete structure is exposed to fire at a temperature of 200 °C or higher [5].

The load on the first crack of a column that is not exposed to fire is different from that of a column that is exposed to fire. The first crack in the column that is not exposed to fire occurs at 80% of the column failure load, while the first crack in the column exposed to fire occurs at 50% of the column failure load [6].

Remarkable strain rates occur in the dynamic stress–strain curve of normal concrete at high temperatures. The failure of normal concrete due to high temperature loading and high strain is different from the failure of concrete at ambient temperature [7].

The bearing capacity of the column has decreased and the lateral deflection has increased due to high temperatures. The ultimate column load was reduced by about 14% at 400 °C, 29% at 500 °C, and 43% at 650 °C [8].

Reinforced concrete columns exposed to a fire of 300 °C for 3 h will lose an ultimate strength of about 15% to 25%, 600 °C for 6 h of about 40%. The increased surface area to volume ratio will decrease the ultimate strength of reinforced concrete columns exposed to fire. The best fire-exposed reinforced concrete column shapes are circular, then square, and finally rectangular [9].

Reinforced concrete columns lose their bearing capacity about 47.60% to 51.4% after being exposed to fire at 500 °C for 1 h. An increase in the applied load level during fire exposure results in a significant decrease in residual bearing capacity [10].

The main factor that causes damage such as spalling in concrete is thermally induced stress, while pore pressure is a secondary factor [11].

Spalling on the compression face of reinforced concrete columns is affected by the eccentricity of the axial load. This effect is more dominant in high strength concrete. Low spacing of transverse tie reinforcement helps reduce concrete spalling [12].

The ultimate fire resistance of columns can be reduced by up to 70% due to spalling of the concrete [13].

Increasing the amount of stirrups significantly increases the axial bearing capacity of reinforced concrete columns at high temperature conditions. The volume of stirrup reinforcement is one of the parameters that significantly affects the axial compressive strength of reinforced concrete columns at high temperature conditions [14].

Columns using stirrup spacing as recommended in the code may experience premature failure due to inelastic buckling of the main reinforcement between adjacent stirrups [15].

The limiting factor for determining the fire resistance of reinforced concrete columns is spalling. Spalling depends on permeability, load eccentricity and fire scenario. Factors that play a positive and negative role in increasing the fire resistance of reinforced concrete columns are transverse reinforcement. It is necessary to investigate the effect of transverse reinforcement spacing on spalling because predictions of theoretical methods based on reduced cross-sectional area are not accurate [16].

2 The Research Method

In general, structural models are grouped into 3 types, namely true models, adequate models, and distorted models. True model has complete similarity, adequate model is only the first order similarity, while the distorted model is if one or more variables that are included in the first order are not fulfilled the similitude requirements. The column model used in this study includes an adequate model. Table 1 shows the relationship between the model and the prototype for the thermal test [17].

The concrete material consists of crushed stone from Clereng Kulon Progo, sand from the Krasak River, and Holcim Portland cement. The reinforcing steel is checked before being assembled. The inspections carried out include diameter checks and tensile tests. Table 2 shows the test object and the treatment given. Figure 1 is the specimen mold and Fig. 2 is the placement of the measuring instrument.

Table 1 Scale factor for thermal modelling

Quantity	Dimension	The material and temperature of the model are the same as the prototype
Stress, σ	FL^{-2}	1
Strain, ϵ	-	1
Modulus of elasticity, E	FL^{-2}	1
Poisson ratio, ν	-	1
Coefficient of linear expansion,	θ^{-1}	1
Thermal diffusivity, D	L^2T^{-2}	1
Dimension, l	L	Sl
Displacement, δ	L	Sl
Temperature, θ	θ	L
Time, t	T	Sl^2
Load, q	FL^{-2}	1
Moment, M	FL	Sl^3

Table 2 Test objects and treatments given

Number	Identification	Stirrup distance	Treatments	Eccentricity
1	S12T	120 mm	Unburned	5 mm
2	S9T	90 mm	Unburned	5 mm
3	S6T	60 mm	Unburned	5 mm
4	S12B	120 mm	Burned	5 mm
5	S9B	90 mm	Burned	5 mm
6	S6B	60 mm	Burned	5 mm

Fig. 1 Mold of specimen

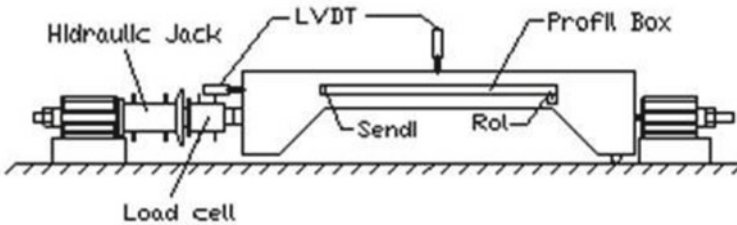


Fig. 2 Placement of measurement instruments

The spacing of the column stirrups shall not exceed 16 times the diameter of the longitudinal bars, 48 times the diameter of the stirrups, or the smallest size of the column cross-section [18]. In this case, the maximum stirrup column spacing is 150 mm. In this study, stirrup spacing variations used were 120 mm, 90 mm, and 60 mm.

The load measuring device (load cell) and its reader (data logger) are calibrated using a concrete compression tester. The deformation measuring instrument (LVDT) is calibrated and the factor value is found that must be entered in the data logger. Burners are prepared and tested in advance to ensure they are all functioning properly.

Figure 3 shows the burner test, Fig. 4 shows the placement of the specimen into the burning room, Fig. 5 shows the burning process, and Fig. 6 shows the temperature measurement in the burning room.

The post-combustion test includes a hammer test to determine the quality of post combustion concrete and a column strength test to determine the strength of the

Fig. 3 Burner test



Fig. 4 Speciment placement into burning room



Fig. 5 Burning process



Fig. 6 Temperature measurement in the burning room



Fig. 7 Column strength test



column. Column strength test is carried out by giving the load gradually until it is destroyed. The load worked in the form of an axial load with an eccentricity of 5 mm. The eccentricity is under the condition of balance to ensure the condition of the column at compression failure. Figure 7 shows the column strength test.

3 Results and Discussions

All test specimens fail in concrete (compression failure), meaning that the eccentricity taken is in accordance with the type of failure of the planned column. All test specimens experienced concrete destruction in the compression section, starting with crushing followed by concrete spalling. The difficulty experienced is measuring the lateral deflection of the column, especially at the final deflection before column failure. This happens because the value of the deflection is relatively small and the speed of the failure process. Figure 8 shows the failure of the compression section, and Fig. 9 shows the load and lateral deflection of all test specimens.

Fig. 8 Failure in compression section (below)

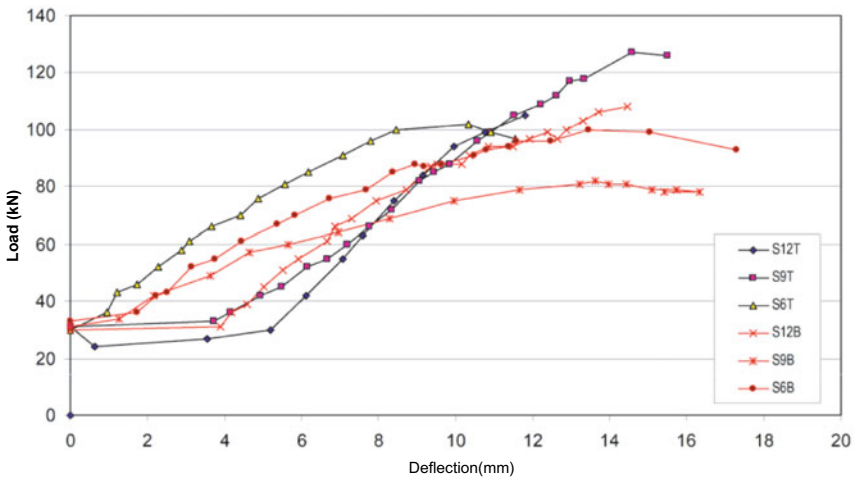


Fig. 9 Load and lateral deflection of all specimen

Theoretical column capacity is calculated based on the strength of steel and concrete. The strength of the concrete is obtained by hammer test while the reinforcement is not tested considering the eccentricity of the column is made to fail in compression, so the quality of the concrete is decisive. The hammer test was chosen because it can test the strength of concrete without damaging it so that it can be carried out on concrete before it is burned and after it is burned.

The hammer test showed a decrease in the quality of the concrete on all test objects. The S6B test object showed a significant decrease compared to the other test objects. Visually, the test object shows that it has experienced the highest temperature compared to the others. This happens because the test object is located on top of another test object (2 test objects are located at the bottom, one test object is stacked on top). The temperature in the combustion chamber tends to be higher at the top. The location of the burner is at the bottom, the front of the burner is given a refractory

brick deck to prevent direct spraying on the test object, this results in the flow of hot air to the top so that high temperatures occur in the upper chamber of the furnace (the thermocouple recorded temperature is the temperature in the upper chamber). The effect of post-burning reinforcing steel does not exist because the steel will return to its original strength after returning to room temperature, besides that the temperature that occurs in the steel is not too high because it is located in the concrete. The theoretical column interaction diagrams before and after exposure to fire for a stirrup space of 120 mm are shown in Fig. 10, for a stirrup space of 90 mm in Fig. 11, and for a stirrup space of 60 mm in Fig. 12.

Fig. 10 Theoretical column interaction diagram with 120 mm stirrups before and after fire exposure

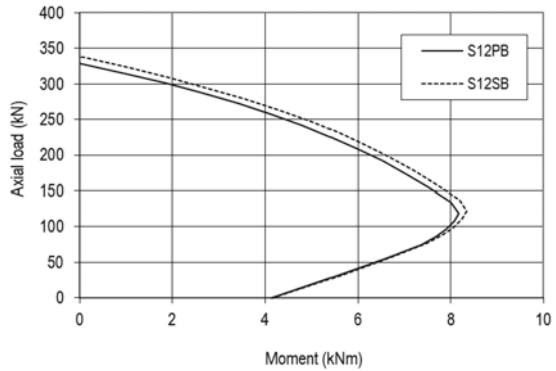


Fig. 11 Theoretical column interaction diagram with 90 mm stirrups before and after fire exposure

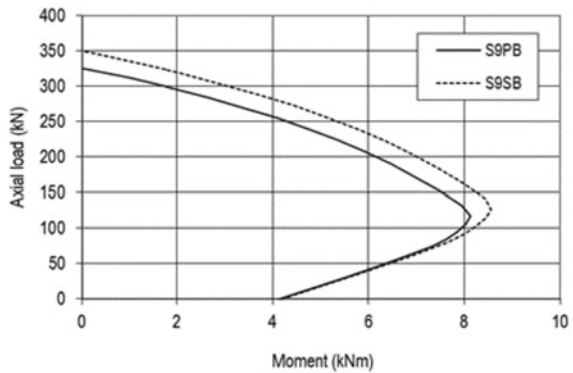
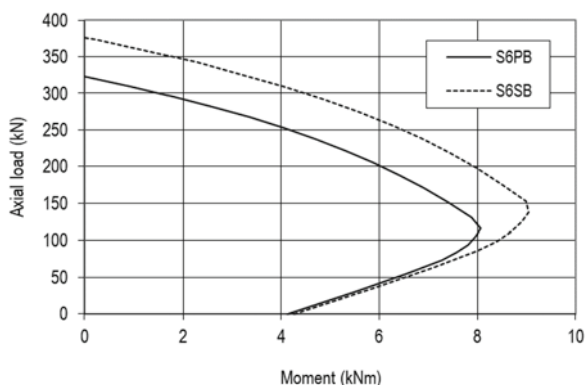


Fig. 12 Theoretical column interaction diagram with 60 mm stirrups before and after fire exposure



4 Conclusion

The variation of stirrup spacing below the maximum spacing based on the code does not show a significant change in the column compressive strength capacity. The spacing of the stirrups below the maximum spacing according to the code is sufficient to ensure that there is no buckling of the compression reinforcement in both the unburned and post-burned columns.

References

1. Sanket R, Aniruddha T, Bahurudeen A, Appari S (2015) Performance of concrete during fire exposure-a review. *Int J Eng Res Technol* 4(03):1–8
2. Adi P (2005) Pengaruh Ketebalan Selimut Beton Terhadap Penurunan Kapasitas Lentur Kolom Pendek Akibat Kebakaran. *J Tek Sipil*, 5 (2005). (In Indonesian).
3. Xing Z, Beaucour AL, Hebert R, Noumowe A, Ledesert B (2015) Aggregate's influence on thermophysical concrete properties at elevated temperature. *Constr Build Mater* 95:18–28. <https://doi.org/10.1016/j.conbuildmat.2015.07.060>
4. Annerel EVR, Taerwe LR (2010) Basic approach for the diagnosis of concrete after fire exposure. *J Struct Fire Eng* 1(3):135–144. <https://doi.org/10.1260/2040-2317.1.3.135>
5. Chiang C-H, Tsai C-L (2003) Time–temperature analysis of bond strength of a rebar after fire exposure. *Cem Concr Res* 33(10):1651–1654. [https://doi.org/10.1016/S0008-8846\(03\)00139-X](https://doi.org/10.1016/S0008-8846(03)00139-X)
6. Bikhiet MM, El-Shafey NF, El-Hashimy HM (2014) Behavior of reinforced concrete short columns exposed to fire. *Alexandria Eng J* 53(3):643–653. <https://doi.org/10.1016/j.aej.2014.03.011>
7. Chen L, Fang Q, Jiang X, Ruan Z, Hong J (2015) Combined effects of high temperature and high strain rate on normal weight concrete. *Int J Impact Eng* 86:40–56. <https://doi.org/10.1016/j.ijimpeng.2015.07.002>
8. Al-Naqeeb F, Al-Thairy H (2021) The behavior of reinforced concrete columns exposure to eccentric loads at high temperature. *J Phys Conf Ser* 1895(1):012055. <https://doi.org/10.1088/1742-6596/1895/1/012055>
9. Awad YAE, Khalaf MA, Ali YA (2018) Effect of fire temperature & duration on ultimate strength of R. C. columns with different cross sectional shapes. *Int J Sci Eng Res* 9(4):66–71

10. Jawad SA, Ali AY (2020) Structural response of post-fire exposed reinforced concrete column with pre-load. *IOP Conf Ser Mater Sci Eng* 928(2):022151 <https://doi.org/10.1088/1757-899X/928/2/022151>
11. Zhang HL, Davie CT (2013) A numerical investigation of the influence of pore pressures and thermally induced stresses for spalling of concrete exposed to elevated temperatures. *Fire Saf J* 59:102–110. <https://doi.org/10.1016/j.firesaf.2013.03.019>
12. Buch S, Sharma UK (2017) Fire resistance and spalling performance of eccentrically loaded reinforced concrete columns (2017). <https://doi.org/10.1007/s10694-019-00823-x>
13. Bajc U, Kolsek JC, Planinc I, Bratina S (2022) Fire resistance of RC columns with regard to spalling of concrete. *Fire Saf J* **130** (2022). <https://doi.org/10.1016/j.firesaf.2022.103568>
14. Chinthapalli HK, Agarwal A (2020) Effect of confining reinforcement on fire behavior of reinforced concrete columns: experimental and numerical study. *J Struct Eng* 146(6):1–12. [https://doi.org/10.1061/\(asce\)st.1943-541x.0002617](https://doi.org/10.1061/(asce)st.1943-541x.0002617)
15. Seręga S (2015) Effect of transverse reinforcement spacing on fire resistance of high strength concrete columns. *Fire Saf J* 71:150–161. <https://doi.org/10.1016/j.firesaf.2014.11.017>
16. Buch SH, Sharma U (2017) Fire resistance of reinforced concrete columns: a systematic review. In: *Proceedings of the international conference of applications of structural fire engineering (ASFE 2017)*, pp 141–150 <https://doi.org/10.1201/9781315107202-17>
17. Suhendro B (2000) *Teori Model Struktur dan Teknik Eksperimental*. Yogyakarta: Beta Offset (In Indonesian)
18. SNI 2847:2013, *Persyaratan Beton Struktural untuk Bangunan Gedung*. Jakarta, Indonesia: Badan Standardisasi Nasional (2013) (In Indonesian)

Environmental Sustainability

Reducing Bod and TSS Levels in Batik Wastewater Using Moringa Seeds Coagulant (Moringa Oleifera)



Gustiana Zaskya Sinaga, Andika Munandar, and Rahma Yanda

Abstract Batik wastewater contains suspended particles and high organic matter originating from the process of pelodorant and cloth washing, so that batik wastewater has BOD and TSS characteristics that exceed the quality standards of Per Men LHK No. 16 of 2019 concerning Textile Industry Wastewater Quality Standards. To overcome this problem, there is a need for wastewater treatment, such as coagulation. Moringa seeds powder is one of natural coagulant that has potential to be used in coagulation. This study was conducted to analyze the characteristics of Moringa seeds as a natural coagulant and its optimum dose in reducing TSS and BOD concentration in batik wastewater. FTIR was carried out to determine the Moringa seeds substances characteristics. Variations of dose natural coagulant Moringa seeds used were 2, 6, 10, 14, 18, dan 22 gr/L. The test was carried out using jar test with a stirring speed of coagulation and flocculation were 100 rpm for 3 min and 40 rpm for 12 min, respectively settling time was set for 45 min. Based on the results, TSS concentration was decreased significantly for about 84.47% at 18 gr/L. While for BOD, the concentration was reduced about 37.84% at 22 gr/L. From correlation analysis through the SPSS software program, it was found that decrease in TSS concentration has weak correlation with BOD.

Keywords Batik wastewater · Moringa seeds · BOD · TSS · FTIR · Jar test

G. Z. Sinaga · A. Munandar (✉)

Environmental Engineering, Institute Technology of Sumatera, South of Sumatera,
Sumatera 35365, Indonesia
e-mail: andika.munandar@tl.itera.ac.id

R. Yanda

Integrated Water Management Engineering, Institute Technology of Sumatera, South of Sumatera,
Sumatera 35365, Indonesia

© Institute of Technology PETRONAS Sdn Bhd 2024

B. S. Mohammed et al. (eds.), *Proceedings of the International Conference on Emerging Smart Cities (ICESC2022)*, Lecture Notes in Civil Engineering 324,
https://doi.org/10.1007/978-981-99-1111-0_9

1 Introduction

Batik home industry produces liquid waste that can be less than factory. However, its discharge often flow into the river directly without appropriate treatment. Batik wastewater comes from fabric processing, dyeing, and polishing activities [1]. From the research conducted by [2], that batik wastewater contains 1470,036 mg/L TSS and 386,810 mg/L BOD which is based on the Regulation of the Minister of the Environment and the Forestry Republic of Indonesia No. 16/2019 concerning Wastewater Quality Standards, these concentrations exceed wastewater quality standard. Therefore, apply wastewater treatment for batik home industry is needed in order to prevent negative impacts for river and its surrounding ecosystem.

Currently, we are faced with challenges in choosing wastewater treatment so that the results from the treatment process do not cause other problems. Coagulation and flocculation are wastewater treatment units that can be applied to small-scale industries or home industry because of the easy processing and affordable maintenance costs. In supporting the coagulation and flocculation processes, a coagulant is needed to bind suspended particles and produce a stable precipitate, which one is implementation of biocoagulant which has advantages such as biodegradable, economical, and easy to find [3].

Moringa seeds powder coagulant is the one type of coagulant that contains 78,9% positive polyelectrolyte protein and antimicrobial compounds that make moringa seeds as a great coagulant [4, 5]. Previous study found that [6], Moringa powder coagulant is polar solution so that it can bind to suspensions that generally negative charged that is difficult to dissolve in water. With this potential, this study aims to identify the potential of Moringa seed powder coagulant in reducing the concentration of excess TSS and BOD in batik wastewater. Samples was taken from the batik home industry "X" which is located in Kemiling sub-district, Bandar Lampung. The purpose of this study was to identify the coagulant characteristics of Moringa seed powder by using FTIR, analyze the optimum dose of Moringa seed powder coagulant on TSS and BOD parameters, and analyze the correlation between TSS and BOD reduction in batik wastewater as Moringa seed powder is added.

2 Materials and Methods

2.1 Sampling

Sampling was done by grab sampling method based on SNI 5989.59:2008 pertaining to wastewater sampling method. The equipment needed is a 1L sample bottle as much as 19 bottles, a funnel, and a coolbox.

2.2 Coagulant Preparation

The process of making Moringa seed powder coagulant in this study refers to research conducted by [7]. Moringa seeds selected for use are ripe and then peeled from the skin and dried in an oven at 105°C for 30 minutes. Then, sieve with a sieve measuring 100 mesh. Scales the Moringa seed powder with a dose of 1, 3, 5, 7, 9, and 11 gr. Moringa seed powder coagulant is also taken about 3 gr to be tested for characteristics using FTIR method by using third-party services LTSIT, Lampung University.

2.3 Jar Test Process

Coagulation and flocculation was conducted by using jar test method based on SNI 19-6449:2000. 500 mL of wastewater was used to be mixed with the following coagulant dosage variations: 2, 6, 10, 14, 18, and 22 gr/L. Coagulation process was carried out with rapid mixing for 3 min. Then, flocculation was carried out with slow mixing 12 min. Later, settling time was given for above 45 min. The test for each dose was done triplo.

2.4 Parameter Test

There are two water quality parameters tested in this study, namely TSS and BOD. For the TSS test, it is carried out with reference to SNI 6989.3:2019 pertaining to Total Suspended Solids (TSS) testing by using the gravimetric method. TSS testing was carried out by filtering 100 mL of untreated wastewater using Whatman 42 10 mm filter paper. Before filtering, scale the empty filter paper which is recorded as the first weight. After filtering 100 ml of filter paper, it was dried in the oven for 1 h at a temperature of 103–105 °C, then cooled in a desiccator for 15 min. Next, scale the filter paper again and record it as the final weight. Finally, calculate the concentration of TSS using the following formula (1). The process of measuring TSS in wastewater after treatment is carried out in the same steps.

$$TSS = \frac{(\text{firstweight} - \text{finalweight}) \times 1000}{\text{Volume of water}} \quad (1)$$

Next, the BOD parameter testing is carried out by a third-party service, namely UPTD DLH Lampung Province based on SNI 6989.72:2009 pertaining to how to test Biochemical Oxygen Demand (BOD). In principle, this test calculates the dissolved oxygen concentration required by microorganisms to decompose organic compounds. Observations were made on day 0 and after 5 days.

After getting the first and final concentrations, the percentage decrease in concentration can be calculated using the formula below:

$$\begin{aligned} & \text{Percentage decrease in concentration} \\ &= \frac{\text{first concentration} - \text{last concentration}}{\text{first concentration}} \times 100\% \end{aligned} \quad (2)$$

2.5 Data Analyze

The variables in this study are divided into three, namely:

1. Independent variables, is the dose of coagulant were 2, 6, 10, 14, 18, and 22 g/l.
2. The dependent variables, are BOD and TSS concentration.
3. Control variables, is stirring speed which is 100 rpm and 40 rpm.

Furthermore, the research data is presented in the form of graphs and images to show the changes in concentration from before to after processing. The research data will also be processed using the statistical software program IBM SPSS Statistics 25.0 for Windows computer software and tested for normality, homogeneity, significance, linearity, and correlation.

3 Result and Discussion

3.1 First Batik Wastewater Characteristic

Based on Table 1 batik wastewater characteristic, BOD and TSS concentration are exceed the quality standard. The high concentration of TSS is caused by the use of detergents, textile dyes, and wax residues which cause the presence of particles or solids that are difficult to dissolve in water and cause high TSS [8, 9]. While high BOD is caused by the high content of organic compounds in batik wastewater which generally comes from oil or fat from residual wax and detergent also [10].

TABLE 1. First TSS and BOD Concentration Batik Wastewater

Parameter	Unit	Concentration	Quality Standard
TSS	mg/L	3446	50
BOD	mg/L	9577	60

3.2 Coagulant Moringa Seeds Powder Characteristic

In order to know characteristics of Moringa seeds powder through its functional group. Fourier Transform Infrared (FTIR) was used [11]. Figure 1 show the results of infrared spectra that describe the peak at the wavelength of the detection of a group of compounds.

Based on the infrared spectra result in Fig. 1. There are several functional groups detected. Amine (N-H) and O-H groups were detected at almost the same wavelength. At wavelengths 2974 and 2855 m^{-1} there are two sharp valleys that detect the presence of a strong single C-H group. At a wavelength of 1640 m^{-1} C=O groups were detected. At a wavelength of 1647 m^{-1} detected N-H bend [12].

Regarding to [13] statement, the absorption of vibrations of the hydroxyl group (O-H) which overlaps at the same wavelength as the N-H group occurs. With wavelength values that coincide with each other, the O-H group causes a graph that tends to widen, while the presence of the N-H group forms a sharp and narrow valley. Because the valley produced by the O-H group is wider than the N-H, it covers the stretching of the N-H functional group. With the discovery of amide, carboxyl, and hydroxyl functional groups, explained that infrared spectra detect amino acid compounds where these compounds are the main active constituents in Moringa seeds.

The formation of proteins is composed by 10-1000 functional groups of amino acids that bind to each other and form a number of peptides. When a protein is dissolved in water, the O-H active site on the amino acid will create a zwitterion condition, in which one type of compound has two opposite ionic poles. Therefore, the

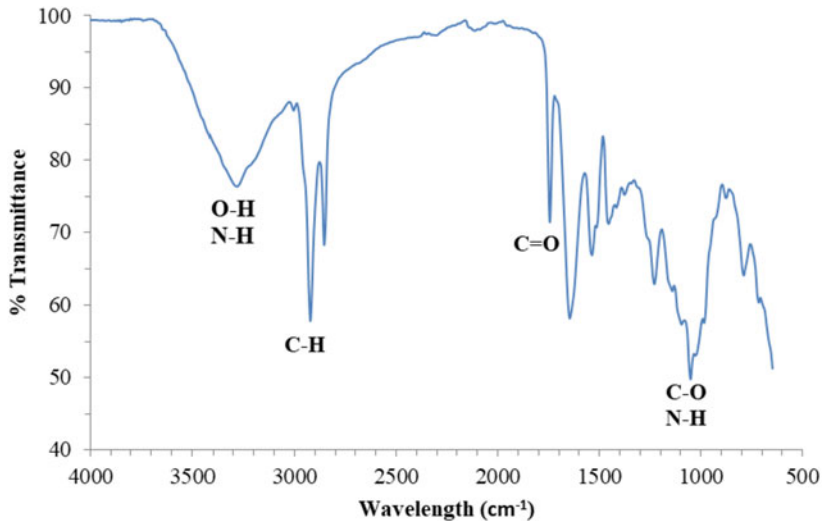
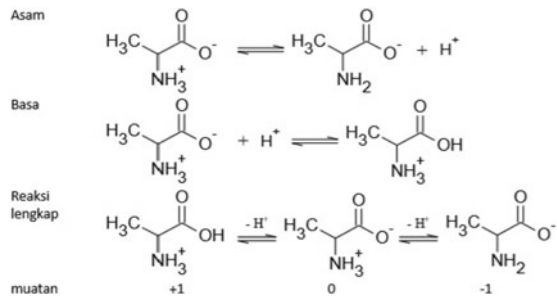


Fig. 1 Infrared Spectra Results of Moringa Seeds Powder

Fig. 2 Zwitterion Amino Acid Process [51]



nature of amino acids that act as coagulants can function as acids and bases together, often referred to as amphoteric [14]. With its amphoteric advantage, coagulants will work to bind colloidal particles which are generally negatively charged and other positively charged amino acids at the same time. The zwitterion reaction of amino acids can be seen in Fig. 2.

3.3 *The Effect of Variations in the Coagulant Dose of Moringa Seed Powder to Decrease TSS Level*

Based on the graph shown in Fig 3. The coagulation-flocculation process with Moringa seed powder as a coagulant has an effect on decreasing the concentration. The highest reduction efficiency was given at a dose of 18 g/L with a percentage decrease of 84,47% (535 mg/L). The dose of 18 g/L being the optimum dose, it is strongly suspected that the addition of coagulant followed by rapid mixing makes the positively charged protein distributed throughout the wastewater and then interacts with the negatively charged suspended particles which are dispersed. This interaction will cause van der Waals forces to form flocs which have been neutralized and precipitated [15]. Overall, the decrease in TSS concentration using Moringa seed powder as a coagulant has not met the quality standard based on the Regulation of the Minister of Environment and Forestry Number 16 of 2019 which is 50 mg/L. R^2

3.4 *The Effect of Variations in the Coagulant Dose of Moringa Seed Powder to Decrease BOD Level*

Based on the results of the BOD measurement shown in Fig. 4. The decrease in BOD concentration continued to occur, but decreased slowly. The decrease continued until the maximum variation was 22 g/L with a percentage of 37.84% (5953 mg/L). Previous study found that [16], when the optimum reduction has been obtained, the BOD content will increase with the addition of an excessive dose. However, in this

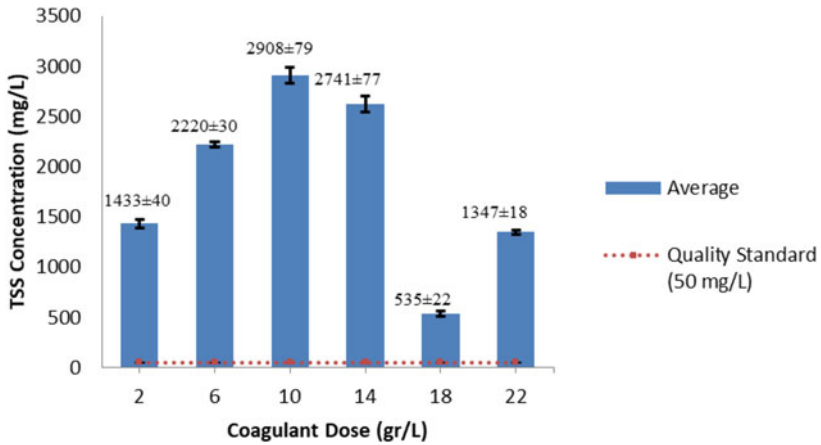


Fig. 3 The Result of TSS Concentration Measurement

study with a given dose variation, the optimum reduction could not be determined. However, according to research conducted by [17] the administration of doses >30 g/L caused an increase in the concentration of BOD in batik wastewater. Therefore, a dose of 22 g/L is assumed to be the optimum dose.

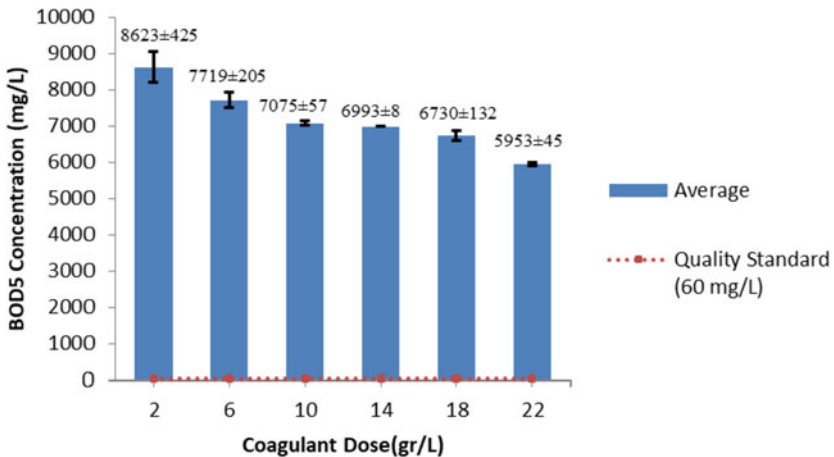


Fig. 4 The result of BOD₅ Concentration Measurement

3.5 Statistical Analysis of the Relation Between a Decrease in TSS and BOD

The relation between decreased TSS and BOD concentration can be demonstrated through the Pearson correlation test. Before performing the Pearson correlation test necessary to carry out preliminary tests such as normality, homogeneity, significance, and linearity tests using IBM SPSS Statistics 25.0 for Windows computer software.

Based on the results of the normality test of two parameters, showed that the concentration data of TSS and BOD were normally distributed with the evidence of the Asymp. Sig. (2-tailed) $0.200 > 0.05$. Furthermore, based on the results of the homogeneity test using the Levene's method, it shows that the research data measuring the concentration of TSS and BOD of batik wastewater is homogeneous data or the data has the same variances [18]. As evidenced by the value of Sig. Based on the mean of $0.871 > 0.05$. With data that is normally distributed and homogeneous, the test can be continued to the significance test. The significance test showed that adding coagulant dose had a significant impact on decreasing the levels of TSS and BOD. This is evidenced by the P TSS value is 0.008 and the P BOD value is 0.006 which is smaller than the Sig. level is 0.05 then statistical testing can be continued to linearity test. Based on the results of the linearity test, the SPSS output table does not appear. Therefore, further tests are needed, namely the linear regression test. The results of the linear regression test can be seen in Fig. 5. With a linear regression value of 0.325, it shows that the data on the decrease in TSS and BOD does not have a linear relationship, which means that the decrease in the two parameters is influenced by different factors. Based on the linear regression result that do not meet the requirements, then the linear relationship and

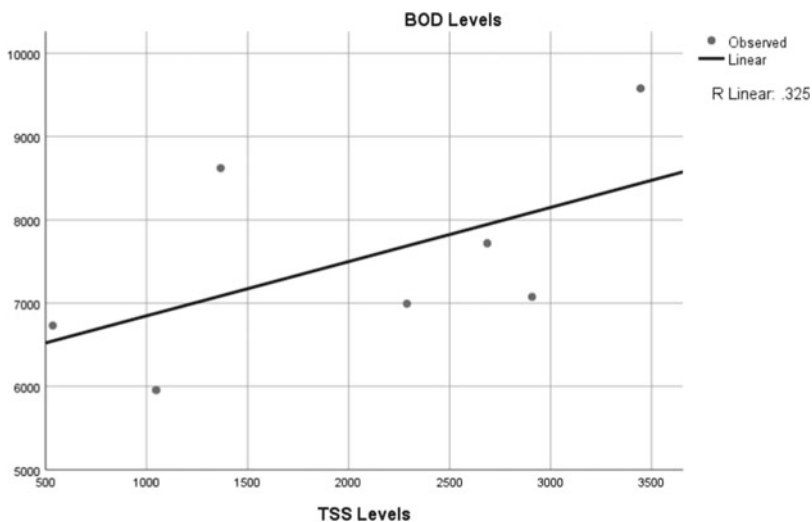


Fig. 5 The Result of Regression Linear Test

correlation of the two parameters can be concluded that the decrease in the concentration of TSS and BOD does not have a linear and correlated relationship.

4 Conclusion

Based on the results of the observations and the results of the discussion of this study, the following conclusions can be drawn:

- 1 Characteristics of Moringa seed powder as a coagulant found groups such as C- H, O-H, N-H, and C = O where the groups are positively charged protein constituent groups to bind negatively charged suspended particles.
- 2 Coagulant dosage has a significant effect on decreasing BOD and TSS concentrations. The maximum decrease in TSS occurred at a dose of 18 g/L as much as 84.47% and the highest decrease in BOD at a dose of 22 g/L as much as 37.84%.
- 3 Based on a series of statistical tests, it shows that there is no correlation between the parameters because the parameters do not have a linear relationship with the R result of 0.325.

Acknowledgements Tons of thanks to my parents who have been supportive in the ups and downs. Thank you to the lecturers who have helped me in understanding the material so that this research is carried out and published.

References

1. Dewanti BSD, Prastiwi TF, Sutan Haji AT (2019) Pengolahan limbah cair batik menggunakan kombinasi metode netralisasi dan elektrokoagulasi. *J Rekayasa Dan Manaj Agroindustri* 7(3):358 <https://doi.org/10.24843/jrma.2019.v07.i03.p03>
2. Indrayani L (2018) Pengolahan limbah cair industri batik sebagai salah satu percontohan ipal batik di Yogyakarta. *ECOTROPHIC J. Ilmu Lingkungan*. *Journal Environ Sci* 12(2):173 <https://doi.org/10.24843/ejes.2018.v12.i02.p07>
3. Hardiyanti IM (2021) Pemanfaatan serbuk kulit pisang kepok sebagai koagulan alami untuk menurunkan tss dan cod pada limbah cair rumah makan, Institut Teknologi Sumatera
4. Tiew J, Jianga M, Lia H, Zhanga S, Zhangb X (2015) A comparison between moringa oleifera seed presscake extract and polyaluminum chloride in the removal of direct black 19 from synthetic wastewater. *J Ind Crop Prod* 01(74):530–534
5. Aminah S et al (2015) Kandungan nutrisi dan sifat fungsional tanaman kelor (moringa oleifera). *Bul Pertan Perkota* 5(30):35–44
6. Putra RS, Iqbal AM, Rahman IA, Kimia J, Islam U (2019) Dengan Koagulan Alami Dalam proses laboratorium, *Khazanah J. Mhs.* 11(01):1–4. <https://journal.uii.ac.id/khazanah/article/view/16687>.
7. Irmayana I, Hadisantoso EP, Isnaini, S (2017) Pemanfaatan Biji Kelor (Moringa oleifera) sebagai koagulan alternatif dalam proses penjernihan limbah cair industri tekstil kulit. *J. Istek* 10(2):48–61 (2017). <http://journal.uinsgd.ac.id/index.php/istek/article/view/1477/1039>.

8. Metcalf L, Eddy HP (1991) *Wastewater engineering: treatment, disposal, and reuse*. Singapore: McGraw-Hill Book
9. Amal N (2006) *Info teknik*, vol 7, no 1, pp. 29–36
10. Nilasari NI, Wulandari SN, Susilowati (2020) Penurunan COD, TDS, TSS, Warna Pada Limbah Batik Dengan Berbagai Jenis Koagulan. *Semin. Nas. Tek. Kim. Soeardjo Brotohardjono Xvi*. 3:1–8
11. Sari NW, Fajri M, Terpadu L, Unggul UE, Barat J, Jeruk K (2018) Analisis fitokimia dan gugus fungsi dari ekstrak etanol pisang. *IJOB* Vol. 2, Nomor 1, no. L
12. Tyagustin NS (2021) Pengolahan Air Gambut Menggunakan Proses Elektroflotasi- Biokoagulasi Dengan Kacang Koagulan Alami. Yogyakarta
13. Kurniasih M, Kartika D (2011) Sintesis dan karakterisasi fisika-kimia kitosan (synthesis and physicochemical characterization of chitosan). *J Inov* 5(1):42–48
14. Kurniawati P, Banowati R (2018) Modul Asam Amino, Peptida dan Protein. Diploma Chem. Uii, pp 15–35
15. Bramantyo AE, Mustofa A (2014) Pembuatan Bio Koagulan Dari Biji Kelor (*Moringa Oleifera*) Sebagai Pengganti Koagulan Sintetis (Tawas), Institut Teknologi Sepuluh Nopember
16. Haslinah A (2019) Optimalisasi serbuk biji kelor (*moringa oleifera*) sebagai koagulan untuk menurunkan turbiditas dalam limbah cair industri tahu. *ILTEK J. Teknol.* 11(02):1629–1633. <https://doi.org/10.47398/iltek.v11i02.80>
17. Effendi H, Sari RD, Hasibuan S (2015) *Moringa oleifera* as coagulant for batik effluent treatment. *Int. Assoc. Impact Assess. Conf.*, no. April, pp 1–6. [http://conferences.iaia.org/2015/Final-Papers/IAIAManuscript-Hefni\(15May2015\).pdf](http://conferences.iaia.org/2015/Final-Papers/IAIAManuscript-Hefni(15May2015).pdf)
18. Jackson SL (2003) *Research methods and statistics: a critical thinking approach*, third edit. Wadsworth, Belmont

Characterization of Fly Ash: Effect on Compressive Strength and Thickening Time of Alkaline-Activated Fly Ash Cement at Downhole Condition



Nurul Nazmin Zulkarnain, Yon Azwa Sazali, Afif Izwan A. Hamid, Noraini Kamizan, Siti Humairah A. Rahman, Ahmad Amirhilmi A. Razak, and MFirdaus Habarudin

Abstract The construction industry is currently switching to geopolymer cement, a greener product from power plant waste. While the utilization of geopolymer cement in the construction industry is well-known, its application as well cement is still being researched. Current study analyzes fly ash composition from two power plants, Tanjung Bin and Manjung Power Plant, on compressive strength and thickening time under downhole conditions per API RP 10B-2. Findings on compressive strength reveal that silica to alumina ratios of 2.0 to 2.5 resulted in higher compressive strength than ratios of less than 2.0. In addition, compressive strength increases as iron oxide and calcium oxide concentrations increase from 7.79% to 15.9% and 6.73% to 22.2%, respectively. Fly ash composition had almost no effect on geopolymer cement thickening time at 60 °C and 2000psi. The thickening time is more likely to

N. N. Zulkarnain (✉) · Y. A. Sazali · S. H. A. Rahman · A. A. A. Razak · M. Habarudin
PETRONAS Research Sdn Bhd, Kajang, Malaysia
e-mail: nurul_20001289@utp.edu.my

Y. A. Sazali
e-mail: yonazwa.sazali@petronas.com.my

S. H. A. Rahman
e-mail: humairah.rahman@petronas.com.my

A. A. A. Razak
e-mail: amirhilmi.razak@petronas.com.my

M. Habarudin
e-mail: mfirdaus.habarudin@petronas.com.my

N. N. Zulkarnain · A. I. A. Hamid · N. Kamizan
Department of Civil and Environmental Engineering, Universiti Teknologi PETRONAS, Seri
Iskandar, Malaysia
e-mail: afif.hamid@utp.edu.my

N. Kamizan
e-mail: norainikamizan@utp.edu.my

be influenced by extrinsic factors, including temperature, pressure, and the presence of a retarder or accelerator.

Keywords Geopolymer well cement · Fly ash composition · Compressive strength · Thickening time

1 Introduction

Approximately one tonne of carbon dioxide is released into the atmosphere while producing one tonne of ordinary Portland cement (OPC). Since the cement is the primary material in construction, the construction industry is currently switching to geopolymer cement, which is manufactured from more environmentally friendly raw materials. While the use of geopolymer cement in the construction industry is well recognized, research is still being done on its application as well cement. At the same time, the challenging downhole environment, such as high pressure, high temperature, and the presence of carbon dioxide and hydrogen sulfide, could affect the cement's integrity. Hence, compared to the use of geopolymer in the construction industry, the application of geopolymer cement in well cementing requires substantial research and testing. Geopolymerization is a chemical reaction between aluminosilicate and an alkaline activator solution, resulting in three (3) structures: polysialate, polysialate-siloxo, and polysialate-disiloxo with silica-alumina ratios of 1, 2, and 3 [1]. Alkaline activators such as Na^+ , K^+ , Ca^{++} , Ba^{++} , NH_4^+ , and H_3O^+ dissolve and activate aluminosilicate sources such as metakaolin, slag, or fly ash [2]. The degree of dissolution of the aluminosilicate source in the alkaline activator solution will effects the formation of the structure [3].

Fly ash is a byproduct of coal-fired power plants where coal is pulverized and burned in pulverized coal-fired boilers. The mechanical collector will filter out fly ash larger than 10 mm as the flue gas from the boiler passes through it. The fly ash smaller than 10 m is removed using an electrostatic precipitator or wet scrubber and can then be collected at the disposal area [4]. Fly ash is divided into classes C and F; both have pozzolanic qualities, but only Class C possesses cementitious capabilities [5]. The difference between Class C and Class F, according to ASTM C618-19, is in the calcium oxide maximum concentration, which is over 18% for Class C and 18% as the maximum volume for Class F [5]. Both classes are required to meet the same other chemical standards, including the weight composition of silica oxide (SiO_2), aluminium oxide (Al_2O_3), iron oxide (Fe_2O_3), sulphur oxide (SO_3), loss of ignition, and moisture content.

Malaysia has six (6) power plants, with four (4) in Peninsular Malaysia and the remaining three (3) in West Malaysia. Current study aims to characterize seven different types of fly ash received from two different power plants in Malaysia; Tanjung Bin and Manjung and analyze the compressive strength and thickening time for each fly ash to observe the performance of the fly ash as raw material for well cement.

2 Materials and Methods

2.1 Materials

The raw materials for the study comprised of four (4) fly ash sample from Tanjung Bin power plant located in Johor and three (3) fly ash samples from Manjung power plant located in Perak. Sodium hydroxide (NaOH) and sodium silicate (Na₂SiO₃) both at 50 wt.% concentration were used as an alkaline activator. NaOH and Na₂SiO₃ were obtained from Merck KGaA and R&M Chemical, respectively. No additive involves in the current formulation.

2.2 Compositional Testing

Four (4) and three (3) fly ash samples from Tanjung Bin, and Manjung Power Plant are prepared, respectively. The sample characterization test is done using X-ray Fluorescence (XRF) to obtain the composition of the fly ash sample in accordance with ASTM C 618-19 [5].

2.3 Compressive Strength

Geopolymer cement will be mixed in accordance with API RP 10B-2 Clause 5 and cured in a water bath at 60 °C [6]. The API compressive strength tester is used to perform the compressive strength testing in accordance with API RP 10B-2 Clause 7 [6].

2.4 Thickening Time

The thickening time is conducted using pressurised consistometer with simulated condition 2000psi and 60 °C in accordance with API RP 10B-2 Clause 9 [6]. The reported result presented the thickening time at 70 Bearden Consistency (BC).

Table 1 The composition of seven (7) fly ash samples from two (2) different power plants

Samples	SiO ₂	Al ₂ O ₃	Fe ₂ O ₃	SiO ₂ + Al ₂ O ₃ + Fe ₂ O ₃	CaO	Class	Power plant
TB-01	38.80	19.40	13.60	71.80	16.50	F	Tg. Bin
TB-02	35.39	15.93	15.90	67.22	20.18	C	Tg. Bin
TB-03	34.00	14.70	14.50	63.20	22.70	C	Tg. Bin
MJ-01	40.70	16.60	12.90	70.20	15.50	F	Manjung
MJ-02	46.30	21.60	7.79	75.69	6.73	F	Manjung
MJ-03	42.05	20.45	11.30	73.80	10.50	F	Manjung
MJ-04	43.65	20.30	11.15	75.10	10.10	F	Manjung

3 Results and Discussions

3.1 Compositional Analysis

The composition analysis demonstrates that two (2) of the fly ash samples fall into Class C fly ash, while the remaining five (5) samples fall into Class F fly ash. Table 1 provides a breakdown of the compound's constituents, which include SiO₂, Al₂O₃, Fe₂O₃ and CaO. Tg. Bin represents Tanjung Bin power plant.

The findings indicated that the same type of power plant could produce different classes of fly ash due to various reasons such as the amount of thermal energy used during coal combustion, thus it is advisable to conduct compositional analysis on fly ash sample prior to use the sample for geopolymer mix.

3.2 Relationship Between Silica to Alumina Ratio and Compressive Strength

Silica is an essential component in the development of geopolymer structures due to its capacity to bind to other silica atoms or by cross-linking, such as Si-O-Si, which contributes to the compressive strength of the geopolymer. The current finding shows that the compressive strength of geopolymer cement cured at 60 °C is more significant when the silica-to-alumina ratio is between 2 to 2.5. In contrast, geopolymer cement with silica to alumina ratio lower than 2 demonstrates lower compressive strength than the former. The distribution of compressive strength data against the ratio of silica to alumina is presented in Fig. 1.

The compressive strength of geopolymer cement ranged from 331 to 507 psi when the ratio of silica to alumina is between 1.85 and 2.0. On the other hand, the compressive strength went from 751 to 1434 psi when the ratio is between 2.0 and 2.5. The finding also reveals that all the fly ash samples from Tanjung Bin resulted in a compressive strength higher than 500psi, whereas just one fly ash sample from

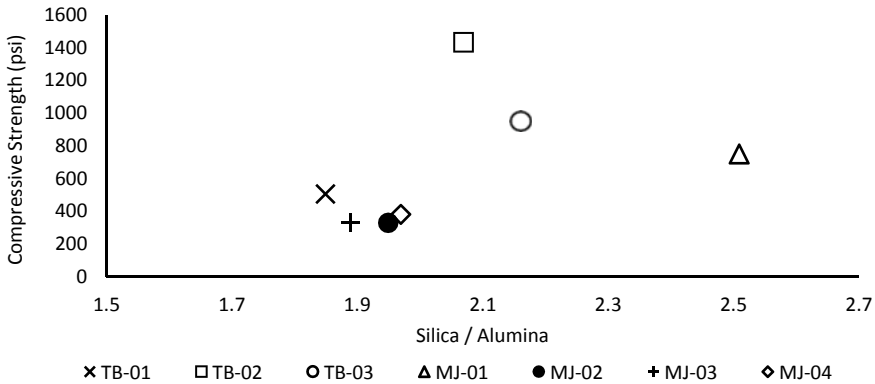


Fig. 1 Silica to alumina ratio versus compressive strength of geopolymer cement

Manjung resulted in a compressive strength higher than 500 psi. Analysis from previous researchers is presented in Table 2; which demonstrates that none of the researchers fixes to one ratio of silica to alumina to give high or low compressive strength.

For example, Timakul et al. discovered that when the ratio of SiO₂:Al₂O₃ goes from 2.6 to 2.65, the compressive strength increases by 25% [7]. The compressive strength is reduced by 40% when SiO₂:Al₂O₃ ratios increase from 2.65 to 3.00. According to Rahman and Ekaputri, a ratio of 1.49 demonstrates the highest compressive strength of geopolymer cement [8].

They also noticed that changing the aluminium portion to lower the ratio of silicate to aluminium did not result in a substantial change in compressive strength compared to changing the silicate portion. Wijaya et al. found the highest compressive strength is between the ratio of silica to alumina, 1.875 to 2.078, while the lowest is between 2.5 to 3.0 [11]. The compressive strength is at its peak when the ratio of SiO₂:Al₂O₃ is 4.00; however, ratios between 4.00 and 4.79 significantly diminish the compressive strength value [9]. Szabo and Mucsi similarly find a dramatic decrease in compressive strength as the ratio increases from 3.67 to 6.77 [10]. The compressive strength results were also affected by the molarity of the hydroxide and ratio

Table 2 Previous findings by other researchers on the silica to alumina ratio that resulted in high and low compressive strength

Previous Research	High Compressive Strength	Low Compressive Strength
Timakul et. al [7]	2.60 to 2.65	2.65 to 3.00
Rahman and Ekaputri [8]	1.49	–
Chindaprasirt et. al [9]	4.0	4.0 to 4.79
Szabo and Mucsi [10]	3.67	3.67 to 6.77
Wijaya et al. [11]	1.875 to 2.078	2.5 to 3.0

of alkaline activator to activate the geopolymerization process. This may be why previous researchers observed various ratios of silica to alumina that could lead to high and low compressive strength.

3.3 Relationship of Iron Oxide and Calcium Oxide with Compressive Strength

Current research reveals, as illustrated in Fig. 2 that the compressive strength of geopolymer cement increases approximately from 331 psi to 1434 psi as iron oxide composition rises from 7.79 to 15.9 wt.%. The compressive strength of Tanjung Bin fly ash exhibits a sharply rising trend, while Manjung fly ash gradually increases in compressive strength as the iron oxide concentration increases. However, the impact of iron oxide on geopolymer cement has yet to be extensively studied. According to Joseph Davidovits, iron oxide can boost the compressive strength of geopolymer paste by up to 33 % and 20% for seven (7) and 28 days, respectively [12].

Previous findings from Gomes et al., S. Wang et al. and Bai et al. supported the present results. Gomes et al. observed that the synthesis of iron-rich alkaline activated product show compressive strength of 20 to 80 Mpa [13] while S. Wang et al. found that the compressive strength of geopolymer paste increase with the concentration of steel slag [14].

The steel slag comprises high iron oxide compared to fly ash and metakaolin. Adding steel slag into metakaolin geopolymer cement increases the compressive strength of geopolymer by 8 %, as discovered by Bai et al. [15]. Nevertheless, the opposite finding was observed by Lemouagna et al., as they found that adding volcanic ash containing high iron oxide reduces the compressive strength of geopolymer [16].

On the other hand, calcium oxide (CaO) is an element that reacts with water through the hydration process. The reaction contributes to the compressive strength

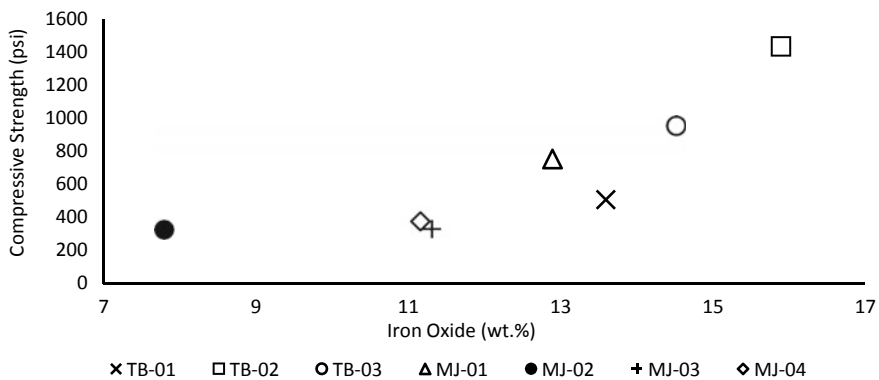


Fig. 2 Iron oxide versus compressive strength of geopolymer cement

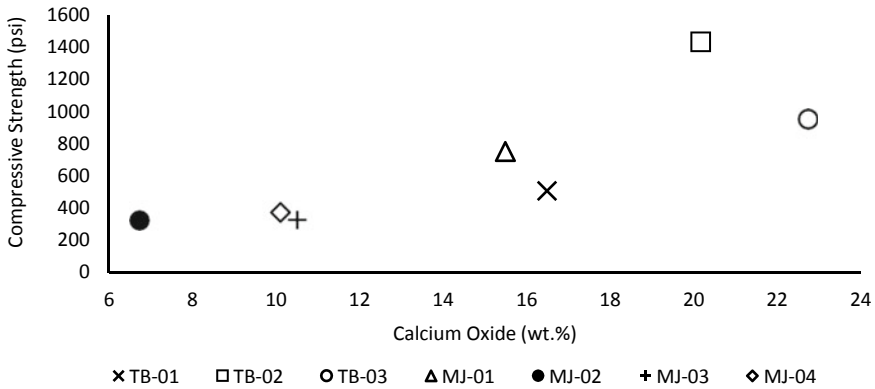


Fig. 3 Calcium oxide weight percentage versus compressive strength of geopolymmer cement

development of Portland cement. However, an excessive amount of CaO will deteriorate the adhesive through a carbonation reaction with carbon dioxide. Fig. 3 reveals that an increase in calcium oxide composition from 6.73 to 22.7 wt.% will increase geopolymmer cement’s compressive strength from approximately 331 psi to 1434 psi. Matalkah et al. reported that adding five (5) wt.% of CaO enhanced the compressive strength by 68%, and adding 10 wt.% of CaO increased the compressive strength to roughly 105%, which supported the present study’s findings [17]. Another research found that adding three (3) wt.% CaO to geopolymmer cement increases the 7- day compressive strength by 93% [18].

Adhitya et al. found that CaO has a direct relationship with the strength of fly ash paste; as the concentration increase, the strength of fly ash paste for both 3-days and 28-days strength [11]. A study by Diab found that increasing lime content from 0 to 2% raises the compressive strength; further, increasing lime content by more than 2% decreases the compressive strength [19]. The compressive strength of alkali-activated fly ash/slag increases as the slag concentration increase, except when the amount of slag is 25 % and 30 % [20]. Slag contains higher CaO compared to fly ash.

The strength reduction at 30 % is low due to crack evolution within alkali-activated fly ash/slag paste. Chindraprasirt, on the other hand, observed that the compressive strength of seven (7) and 28 days decreased when the calcium oxide replacement ratio increased [21]. It was most likely owing to the rapid setting, which caused an inadequate initial matrix framework.

3.4 Relationship of Silica:Alumina with Thickening Time

The variation in the ratio of silica to alumina and the amount of iron oxide and calcium oxide does not produce a noticeable trend in the thickening time at 70

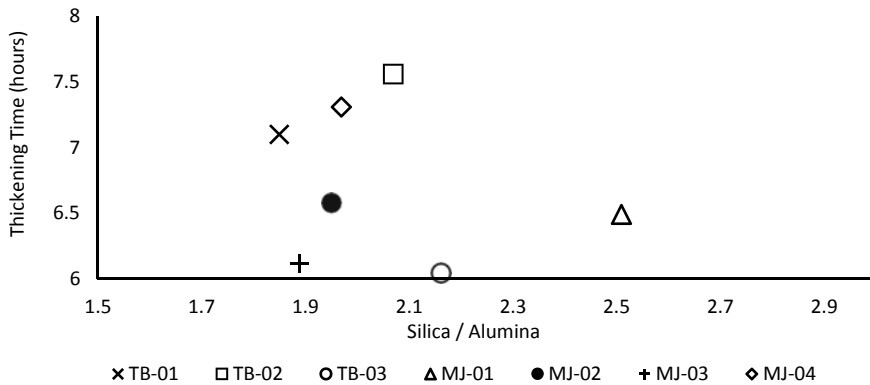


Fig. 4 Silica to alumina ratio versus thickening time of geopolymer cement

Bearden Consistency (BC), contrary to what was shown in the compressive strength. 70 Bc thickening time is a standard measurement to consider in well cementing, which, at this point, the slurry will be gelled up and cannot be pumped. The standard slurry will take a longer time from 40 Bc to 70 Bc; however shorter period to reach 100 Bc, which is known as the right angle set of the cement. Fig. 4 illustrates thickening time results for the ratio of silica to alumina between 1.85 to 2.51, which shows a comparable value between 6.05 to 7:56 h.

The fly ash, with a ratio of silica to alumina between 2.0 to 2.5, corresponding to the top three (3) high compressive strength, has a thickening time value of 6.05 to 7.56; which concludes that no significant correlation can be created between thickening time and compressive strength of the present research. The findings from Antoni et al. were similar to the current discovery as they observed no correlation between silica and alumina ratio with setting time [22]. The lowest setting time is shown by a ratio of silica to alumina of 2.2, followed by a ratio of 1.7, while the highest setting time is demonstrated by a ratio of 2.7.

Siyal et al. observed that the ratio of silica to alumina from 1.8 to 2.2 increased the setting time due to the high amount of soluble silica [23]. However, as the ratio drop below 1.8, less setting time is observed due to low amount of silica available for geopolymerization process. However, as the ratio drop below 1.8, less setting time is observed due to the low amount of silica available for the geopolymerization process. However, as the ratio goes beyond 2.2 to 2.6, the geopolymerization process has been expedited due to a high number of silica, causing compaction of the paste, thus requiring less setting time. In addition, Tajunnisa et al. observe a significant relationship between the ratio of silica to alumina with the final setting time of low calcium fly ash; as the ratio increase from 1.5, 2.0 to 2.5, the final setting time increase from 1.5, 1 and 2 days, respectively [24]. They found that the ratio of 2 resulted in a quick setting time for silica to form oligomers, while the surplus can obstruct the dissolution by silica concentration.

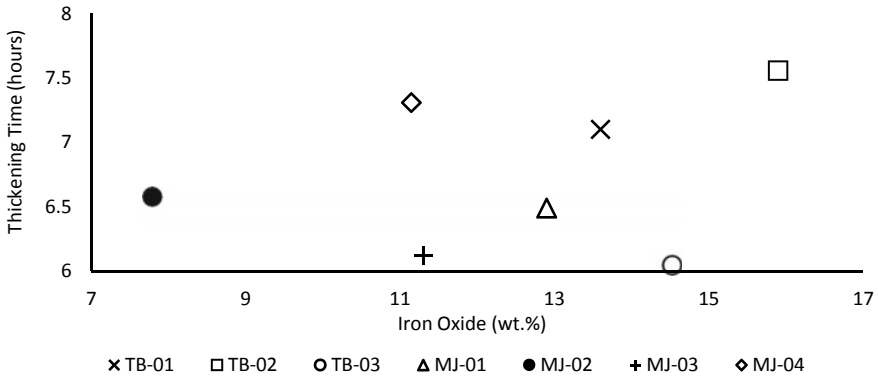


Fig. 5 Iron oxide versus thickening time of geopolymer cement

3.5 Relationship of Iron Oxide and Calcium Oxide with Thickening Time

The effect of iron oxide on the thickening time of geopolymer cement is demonstrated in Fig. 5, in which the variation of iron oxide from 7.79 to 15.9 wt.% did not show a noticeable trend in the thickening time. The fly ash sample with a high concentration of iron oxide of 15.9 % resulted in the longest thickening time of 7.55 hours; however, the lowest thickening time is shown by fly ash samples with 14.5 %. Both samples are from Tanjung Bin power plant. Meanwhile, the fly ash sample with the least iron oxide of 7.79 % has a thickening time of 6.58 h, which is average.

The substitution of Al atoms by Fe in the ferro-sialate molecules substantially changes the composition of geopolymeric compound; however, the effect cannot be observed from the thickening time of the present study [25]. Compared with previous research, geopolymer composition comprised of volcanic ash shows that the initial and final settings reduce as the volcanic ash concentration increases [16]. Volcanic ash has higher iron oxide content than the slag used in the study. The finding from Lemouagna et al. is opposite to the result by Zailani et al. as they discovered that due to high atomic mass and large atomic diameter of iron oxide, the component would take time to react with geopolymer to form iron silicate binder gel compared to silica and alumina [26].

Similar to iron oxide, the variation of calcium oxide from 6.73 to 22.7 wt.% did not show a significant trend in the thickening time, as shown in Fig. 6. Fly ash sample with the highest CaO of 22.7% resulted in the lowest thickening time of 6.05 h, while the sample with lowest CaO of 10.1% resulted in thickening time of 7.31. The fly ash sample with a CaO value of 20.18% represents the highest thickening time value. No correlation can be formed from CaO with 70 Bc thickening time. Only sample TB-03 correspond to the finding of previous research.

A finding from Wijaya et al. stated that a high concentration of CaO has a faster initial setting time [22]. Wijaya et al. found that the concentration of CaO has a

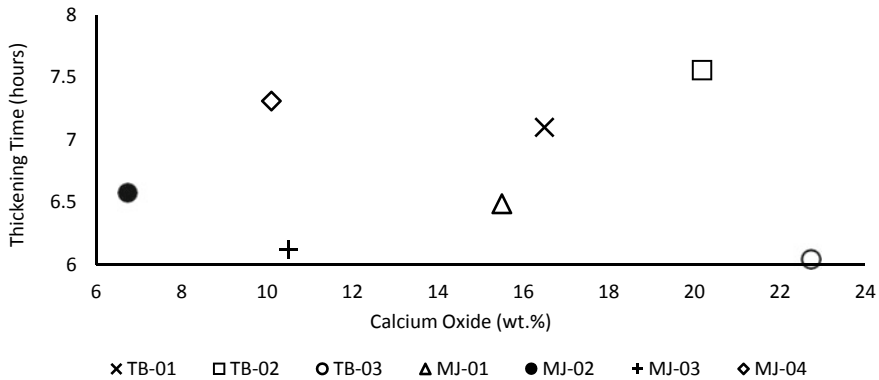


Fig. 6 Calcium oxide versus thickening time of geopolymer cement

negative exponential trend with the setting time of fly ash paste; as the concentration of CaO increase, the setting time decrease [11]. A study from Diab mentioned that increasing the concentration of lime content from 0 % to 1 %, 2% and 3 % reduced final setting time from 36 hours to 24, 7 and 4.25 h, respectively [19]. Slag has higher CaO content than fly ash, thus, increasing the slag concentration from 10 to 30 wt.% reduced the initial and final setting time of alkaline-activated concrete [20]. N.K and H.K suggested slag replacement to fly ash are between 15–20 % to obtain optimum setting time, workability and development of compressive strength [20].

Present findings conclude that the ratio of silica to alumina, iron oxide and calcium oxide does not significantly impact the thickening time and are not the best elements to predict the thickening time of geopolymer cement under downhole well conditions. Other internal components such as magnesium oxide or sodium oxide, or external components such as temperature, can be further studied to observe the correlation between these components with thickening time.

4 Conclusion

The compressive strength of geopolymer cement with a silica-to-alumina ratio between and 2.5 is higher than that of less than 2.0. Compressive strength also increases concurrently with calcium oxide and iron oxide increases. On the other hand, the thickening time shows comparable values on the variation of the silica to alumina ratio, iron oxide, and calcium oxide. The thickening is likely influenced more by other internal factors such as magnesium oxide and sodium oxide content and the pH of fly ash. At the same time, factors outside of the fly ash itself, such as the pressure, temperature, and presence of accelerator and retarder, also play a significant role in determining the thickening time of the geopolymer cement. It was also revealed that fly ash from the same power plant could lead to two (2) different fly

ash classes; hence, compositional analysis is required before using it for functional testing. Finally, the current study examines the sustainability of geopolymer cement in well environments, which will help to accelerate the use of greener materials for well cement.

References

1. Davidovits J (2002) 30 Years of successes and failures in geopolymer applications. Market trends and potential breakthroughs. In: Geopolymer 2002 conference, Melbourne
2. Davidovits J (1979) Synthesis of new high-temperature of geo-polymers for reinforced plastics/composites. In: Pacific technical conference and technical displays, Costa Mesa
3. Davidovits J (1991) Geopolymers inorganic polymeric new materials. *J Therm Anal* 37:1633–1656
4. Roy WR, Thiery RG, Schuller RM, Suloway JJ (1981) Coal fly ash: a review of the literature and proposed classification system with emphasis on environmental impacts. Illinois State Geological Survey. Illinois
5. ASTM International: ASTM C618-19 Standard specification for coal fly ash and raw or calcined natural pozzolan for use in concrete, West Conshohocken
6. A. P. Institute (2010) ANSI/API recommended practice 10B-2. API Publishing Services, Washington
7. Timakul P, Thanaphatwetphisit K, Aungkavattana P (2015) Effect of silica to alumina ratio on the compressive strength of class C fly ash-base geopolymers. *Key Eng Mater* 659:80–84
8. Rahman A, Ekaputri JJ (2018) The effect of additional aluminum to the strength of geopolymer paste. In: MATEC Web of conferences
9. Chindaprasirt P, Silva PD, Sagoe-Crentsil K, Hanjitsuwan S (2012) Effect of SiO₂ and Al₂O₃ on the setting and hardening of high calcium fly-ash based geopolymer systems. *J Mater Sci* 47:4876–4883
10. Szabo R, Mucsi G (2019) Effect of SiO₂, Al₂O₃ and Na₂O content and fly ash fineness on the structure and mechanical properties of fly ash based geopolymer. *Recycl Sustain Dev* 12:61–68
11. Wijaya AL, Ekaputri JJ, Triwulan (2017) Factors influencing strength and setting time of fly ash based-geopolymer paste. In: MATEC web conferences EACEF 2017, Seoul
12. Davidovits J, Davidovits R (2020) Ferro-sialate geopolymers, Technical papers #27, Geopolymer Institute Library
13. Gomes KC, Torres SM, De Barros S, Vasconcelos IF, Barbosa NP (2011) Mechanical properties of geopolymers with iron rich precursors. In: XIII international congress on the chemistry of cement, Madri
14. Wang S, Yu L, Huang L, Wu K, Yang Z (2021) Incorporating steel slag in the production of high heat resistant FA based geopolymer paste via pressure molding. *J Clean Prod* 325:129265
15. Bai T, Song Z-G, Wu Y-G, Hu X-D, Bai H (2018) Influence of steel slag on the mechanical properties and curing time of metakaolin geopolymer. *Ceram Int* 44(13):15706–15713
16. Lemougna PN, Nzeukou A, Aziwo B, Tchamba A, Wang K.-t., Melo UC, Cui X-m (2020) Effect of slag on the improvement of setting time and compressive strength of low reactive volcanic ash geopolymers synthesized at room temperature. *Mater Chem Phys* 239:122077
17. Matakah F, Aqel R, Ababneh A (2020) Enhancement of the mechanical properties of kaolin geopolymer using sodium hydroxide and calcium oxide. *Procedia Manuf* 44:164–171
18. Temujin J, Riessen A, Williams R (2009) Influence of calcium compounds on the mechanical properties of fly ash geopolymer pastes. *J Hazard Mater* 167(1–3):82–88
19. Diab MA (2022) Enhancing class F fly ash geopolymer concrete performance using lime and steam curing. *J Eng Appl Sci* 69(59):1–19
20. Lee N, Lee H (2013) Setting and mechanical properties of alkali-activated fly ash/slag concrete manufactured at room temperature. In: Construction and building materials 47:1201–1209

21. Chindapasirt P, Phoo-ngernkham T, Hanjitsuwan S, Horpibulsuk S, Poowancum A, Injorhor B (2018) Effect of calcium-rich compounds on setting time and strength development of alkali-activated fly ash cured at ambient temperature. *Case Stud Constr Mater* 9(e00198):1–8
22. Antoni, Wijaya SW, Hardjito D (2016) Factors affecting the setting time of fly ash-based geopolymer. *Mater Sci Forum* 841:90–97
23. Siyal AA, Azizli KA, Man Z, Ullah H (2016) Effects of parameters on the setting time of fly ash based geopolymers using Taguchi method. In: 4th International conference on process engineering and advanced materials. Elsevier Ltd.
24. Tajunnisa Y, Sugimoto M, Sayo T, Shigeishi M (2017) A study on factors affecting geopolymerization of low calcium fly ash. *Int J GEOMATE* 13(36), 100–107
25. Davidovits J, Davidovits R (2020) Ferro-sialate geopolymers, technical papers # 27, geopolymer institute library. <https://www.geopolymer.org>. <https://doi.org/10.13140/RG.2.2.25792.89608/2>. Accessed 31 Oct 2022
26. Zailani WWA, Abdullah MMA, Arshad MF, Burduhos-Nergis DD, Tahir MFM (2020) Effect of iron oxide (Fe₂O₃) on the properties of fly ash based geopolymer. In: International conference on innovative research - ICIR EUROINVENT 2020, Iasi

Lithium and Boron Recovery From Oil Field Produced Water: A Mini Review



Rabia Khatoon, Yeek-Chia Ho, Shamsul Rahman B. Mohamed Kutty, Khairulazhar Jumbri, Maung Maung Myo Thant, and Dong Suk Han

Abstract Produced water (PW) from oil and gas industries contains strategically important elements such as Lithium (Li) and Boron (B). The multiple application of Li and B apart from the production of heavy-duty batteries and ceramic industry give boom to the economic growth worldwide. Various effort have been poured in to investigate the cost-effective, sustainable and high recovery of Li and B. In this review paper, technologies for Li and B recovery from brine and PW is discussed emphasizing on the utilization of the PW for the recovery of these elements. Future outlook should tap into the need for the characterization of produced water to extract valuable elements and the use of hybrid technologies would be beneficial for the treatment and extraction of rare metals from the oil field produced water.

R. Khatoon · Y.-C. Ho (✉) · S. R. B. M. Kutty

Centre for Urban Resource Sustainability, Institute of Self-Sustainable Building, Civil and Environmental Engineering Department, Universiti Teknologi PETRONAS, 32610 Seri Iskandar, Perak Darul Ridzuan, Malaysia
e-mail: yeekchia.ho@utp.edu.my

R. Khatoon

e-mail: rabia_22000906@utp.edu.my

S. R. B. M. Kutty

e-mail: shamsulrahman@utp.edu.my

K. Jumbri

Centre for Research in Ionic Liquids, Institute of Contaminant Management, Department of Fundamental and Applied Sciences, Universiti Teknologi PETRONAS, 32610 Seri Iskandar, Perak Darul Ridzuan, Malaysia
e-mail: khairulazhar.jumbri@utp.edu.my

M. M. Myo Thant

Advanced Expertise Common Centre, Group Research and Technology, Project Delivery and Technology Division, Petroliaam Nasional Berhad (PETRONAS), 50088 Kuala Lumpur, Malaysia
e-mail: maungmyothant@petronas.com

D. S. Han

Center for Advanced Materials and Department of Chemical Engineering, Qatar University, Doha, Qatar
e-mail: dhan@qu.edu.qa

© Institute of Technology PETRONAS Sdn Bhd 2024

B. S. Mohammed et al. (eds.), *Proceedings of the International Conference on Emerging Smart Cities (ICESC2022)*, Lecture Notes in Civil Engineering 324,
https://doi.org/10.1007/978-981-99-1111-0_11

Keywords Produced water · Lithium · Boron · Recovery · Technology

1 Introduction

1.1 *The Implication of Brine Mineral Recovery*

There is an urgent need to investigate and employ alternative methods of producing energy and materials due to the growing global population, rising resource demand, and declining environmental quality. Despite significant research and development efforts to produce energy from renewable sources in a more sustainable manner, the majority of materials production still relies on the traditional mining process, which uses energy-intensive methods to extract minerals from the available underground geological reserves.

The development of sustainable methods for brine mineral recovery is mainly influenced by two key factors. First, to keep up with production demands, the fast industrial expansion and increased demand for raw materials necessitate expedited mineral exploration and extraction. Several international organizations have conducted thorough analyses that foresee an exponential rise in demand for several essential materials and a corresponding rise in price in the future decades. For instance, according to the International Energy Agency (IEA), by 2040, the renewable energy industry alone would need four times as much lithium, nickel, and graphite [1]. Likewise, according to a recent worldwide study, the demand for copper (Cu) is likely to rise by over 3 million tons globally over the next five years [2]. The only way to meet this much increased demand satisfactorily and sustainably is to investigate alternate methods of resource recovery. The environmental risk presented to people and other animals as a result of traditional mining operations is the second main factor driving a rise in interest in extracting minerals from brine. For instance, a 2017 study found that mining corporations discharged roughly 2 billion pounds of hazardous waste into the rivers, putting both people and aquatic life at considerable risk [3].

Thus, conventional land-based mining needs to be reduced over time in order to preserve a cleaner environment in the long term. As noted earlier, the vast quantities of brine deposits present themselves as an appealing resource for the recovery of important minerals that may be able to meet the growing industrial demand while minimizing environmental degradation.

1.2 *Prospects for Lithium*

Among the various elements that may be commercially recovered from brine, Li is by far the most important for a multitude of applications. To begin with, the amount

of Li in naturally occurring brine is predicted to be 230 Gt, roughly 104 times that of land-based reserves [4]. The quantity of Li in saltwater brine is relatively low (0.17% ppm). Subsurface and geothermal brines, on the other hand, contain Li in quantities as high as 102–103 ppm, making them an appealing resource for Li recovery. Second, by 2100, commercial demand for Li is predicted to skyrocket, reaching 4.5 million tons per year [5]. In addition to the car sector, where the focus has turned to mass manufacturing of electric vehicles, it is certain that the electronic industry will continue to be the major user of Li (Electric Vehicle). The amount of Li required to make heavy-duty batteries for electric vehicles is several orders of magnitude more than the amount used to make batteries for portable gadgets. The price of Li metal has soared by around tenfold in the previous 20 years due to this fast demand [6]. At the present, lithium carbonate and lithium hydroxide are the two most common minerals employed in industrial Li extraction. During the year 2020–2021, demand for these items increased by around 30%, while prices went up by nearly 300% [3]. As a result, both demand and price for Li will continue to rise, necessitating a larger focus on extracting Li from current brine supplies effectively. The brine concentration process is being optimized at various scales, and numerous technologies have been researched and used in this respect at the laboratory, pilot, and commercial sizes. Noteworthy, traditional evaporative techniques for brine concentration for Li recovery are no longer economically viable due to time and demand constraints. Precipitation, ion-exchange, solvent-extraction, membranes, and electrochemistry are all examples of brine concentration technologies that have advanced. With their distinct benefits and limitations, these technologies have a good prospect for brine concentration and subsequent Li-based mineral recovery that is both cost-effective and long-term.

1.3 The Significance of Boron Recovery

Global boron consumption is increasing due to the discovery of novel uses for boron compounds. Several nations have advanced the use of boron chemicals to boost economic growth. Along with its existing uses in the making of glass, which accounts for 56% of the world's need for borate, cosmetics, wire drawing, fireproofing textiles, and the production of leather and carpets, boron is also used in a number of other new applications on a regular basis. To improve boron-deficient soils, boron-containing composites are frequently employed in fertilizers. Due to its adequate fungicidal and bactericidal effects, boric acid is used to preserve food and clean surfaces. The material borax, which is sometimes known as boron, is frequently used in metal brazing and welding. For hand washing, detergents (17% of the world's usage of borate), catalysts, high-energy fuels, and cutting fluids, borate compounds have proven to be suitable [7].

In terms of B_2O_3 , the yearly worldwide consumption of boron from presently accessible boron deposits [8]. Boron waste may be utilized to produce a variety of borax compounds, with a typical yield of 90%. Nevertheless, to reduce the danger

of water and land contamination, boron must be extracted from wastewater. For instance, the amount of boron in the effluents of power plants in Pauzhetka, Russia, and Kizildere, Turkey, is about 40 mg/L. This causes ecological disasters in these places and irrevocably damages the distinctive rivers of Kamchatka [9]. Borax waste discharged into the environment has been linked to an increase in ecotoxicological effects, agricultural risks, and requirement for more sanitary landfill sites, all of which need principal expenses and demand substantial expense to settle [10].

1.4 Lithium and Boron in Produced Water

Produced water (PW) is a complex mixture whose volume, content, and features are influenced by the geological location of the field, geological circumstances, reservoir life duration, and hydrocarbon chemical makeup [11–13]. Table 1 may be used to classify the major components of PW.

Despite having a lower concentration, oil and gas field wastewater has the potential to be used as a Li and B resource since it eliminates the need for drilling new wells and allows oil companies to profit from the income stream. In general, Li oil field deposits typically have much higher Li concentrations. For instance, the Canadian deposits Fox Creek and Valleyview have 362 000 and 385 000 metric tons of Li metal equivalent, respectively, while the American Smackover Formation has 750 000 metric tons of Li metal equivalent [15]. The produced water from Marcellus shale gas has a comparatively high lithium content compared to seawater (0.17 mg/L), with median values of 95 mg/L after 14 days of flowback [16]. Recent studies have attempted to extract Lithium from shale gas produced water containing high concentrations of organic compounds for example the recovery of lithium from simulated shale gas produced water was examined. Solvent extraction was used in this investigation to recover lithium from generated water that had two phases of varying alkane types and quantities. In the first and second stages, the produced water's divalent ions were taken out as well as Li ions, respectively. Organic compounds had an inhibiting effect on the extraction process, with their effects on the Li recovery efficiency being more noticeable in the first stage than the second stage. With longer alkane chains and higher n-hexane concentrations, the final lithium recovery efficiency after two extraction steps declined [17].

Due to the numerous chemical additives it contains, produced water (PW) from hydraulic fracturing poses major environmental risks in large quantities [18]. There is an issue that has to be solved regarding how to handle this harmful generated water [19]. Presently, the process of using recycled PW as consequent fracturing water, is an environment friendly and economically feasible approach to fulfill the shortage of oilfield water by re-preparing fracturing gels in hydraulic fracturing stimulation. Typically, crosslinked hydroxypropyl guar is the major ingredient in fracturing gels (HPG). Nevertheless, PW with residual boron crosslinker will cause an early cross-linking phenomenon. This alters the pH levels, which negatively affects how fracturing gels are prepared afterwards [20]. In the course of hydraulic fracturing, these

Table 1 The most common components found in the PW, together with their usual concentrations [14]

Components	Concentration range (mg/L)
Total dissolved solids (TDS)	100–400,000
Total suspended solids (TSS)	1.2–1000
Chemical oxygen demand (COD)	1220–2600
Total organic carbon (TOC)	0–1500
Total oil & grease	2–560
Total organic acids	0.001–10,000
Salinity	5,000–300,000,000
Aliphatic hydrocarbons	17–30
Phenols (primarily C0-C5-phenols)	0.4–23
Ketones	1–2
Polycyclic aromatic hydrocarbons (PAH)	0.04–3
Total BTEX	0.73–24.1
Benzene	0.032–14.97
Toluene	0.058–5.86
Ethylbenzene	0.086–0.57
Naphthalene	0.194–0.841
Na	0–150,000
Cl	0–250,000
Ba	0–850
Sr	0–6250
SO ₄ ²⁻	0–15,000
HCO ₃ ³⁻	0–15,000
Ca	0–74,000
K	24–4300
SO ₃ ²⁻	10
Mg	8–6000
Fe	0.1–100
Al	310–410
B	5–95
Cr	0.02–1.1
Li	3–50
Mn	0.004–175
Ti	0.01–0.7
Zn	0.01–35
As	0.005–0.3
Pb	0.008–0.88

early crosslinking systems with high base fluid viscosities will produce excessive friction pressure [21] that lowers the pumping rate and alters fracture geometry. The solution to recycling PW is to prevent this unfavorable effect of residual boron from harming subsequent fracturing applications. In this regard, few studies have been conducted by using ion transfer and electrocoagulation technique for the removal of boron from produced water [22, 23].

2 Lithium and Boron Recovery from the Produced Water

In a traditional procedure, Li-containing brine collected from the source is initially concentrated to an adequate concentration (about 6000 ppm Li) for practical recovery [24, 25]. This is frequently accomplished by the wind and sun radiation from extensive open shallow ponds evaporating raw brine. The typical evaporation process is schematically depicted in Fig. 1.

Due to large climatic variations, the evaporative process is time-consuming and not suitable for all geographical regions. Additionally, as brine composition varies widely from one region to another, this method's effectiveness is highly dependent on geographical location. The co-precipitation of other ions in the presence of Li might lead to the Li recovery procedure become even more challenging. For instance, Mg^{2+} ions can coprecipitate as Mg carbonate and Li carbonate because their chemistry is extremely similar to that of Li ions, which makes it difficult to recover the necessary Li salts further [26]. More significantly, in Chile, water shortage in the surrounding areas may result from evaporative technology coupled with significant water loss [27]. In light of these drawbacks of evaporative techniques, researchers have been concentrating on “non-evaporative” technologies for brine concentration, Table 1 and 2 shows the technologies of treating brine and recover Li and B from recent studies respectively (Table 3).

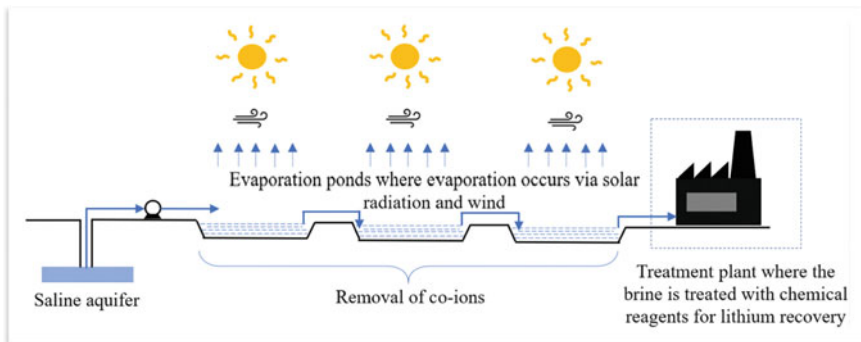


Fig. 1 Schematics of the brine evaporation process for Li recovery (Adapted from reference [25])

Table 2 Recent studies on Lithium extraction

Year	Sources	Extraction technology	Reagents	Li recovery (%)	Adsorption capacity(mg/g)	Ref
2019	Natural brine	Adsorption	$\text{Li}_{1.33}\text{Mn}_{1.67}\text{O}_4$	—	>50	[28]
2019	Simulated brine	Solvent extraction	TBP [Bmim] ₃ PW ₁₂ O ₄₀ , Dimethyl phthalate	99.23	—	[29]
2019	Simulated brine	Precipitation	Sodium Metasilicate Nonahydrate	86.73	—	[30]
2020	Salt Lake brine	Adsorption	Granular H4Mn5O12	—	17.2	[31]
2020	Salt Lake brine	Solvent extraction	TBP, FeCl ₃ and Diethyl succinate	65	—	[32]
2020	Refined Salt Lake brine	Precipitation	Na ₂ HPO ₄ solution	93.2	—	[33]
2021	Simulated brine	Solvent extraction	TBPOHEMIM][NTf ₂]	94.2	—	[34]
2022	Simulated Geothermal brine	Precipitation & solvent extraction	Ca (OH) ₂ , Na ₂ CO ₃ , (Di-(2-ethylhexyl) phosphoric acid, C ₁₆ H ₃₅ O ₄ P), BP,C ₁₂ H ₂₇ O ₄ P	87.7	—	[35]

Table 3 Recent studies on Boron extraction

Year	Sources	Extraction technology	Reagents	B Recovery (%)	References
2019	Industrial wastewater	Chemical precipitation/ Chemical coagulation	Ca (OH) ₂ , B ₂ O ₃ , Al ₂ (SO ₄) ₃ , 18 H ₂ O	94.88	[36]
2021	Boron containing solution	Solvent extraction method	Methanol, Thymol, 2,2,4-Trimethyl-1,3-entanediol, Lithium chloride, Calcium Chloride and Boric acid	~98	[37]
2021	Salt Lake brine	Floatation method	N-methyl-D-glucamine 1-bromooctadecane	89.12	[38]
2021	Boron containing water	Co-precipitation method	Calcinated oyster shell, H ₃ BO ₃ , NH ₄ H ₂ PO ₄ , NaOH and HCl	>90	[39]

2.1 Advance Treatment Technologies of Produced Water (PW)

Petroleum is significant in today's economy and is now essential to the continued economic success of nations that produce oil. Ecosystems, especially those close to the petroleum sectors, have seen environmental degradation as a result of operating operations[40]. In this section, advance treatment technologies are briefly discussed.

2.1.1 Membrane-Based Ions Removal

In PW, several ions exist, some of which are beneficial and others of which are harmful. Crops are harmed by the presence of boron in PW, even at low amounts [41]. Targeted removal or augmentation would not be practical using conventional methods like evaporation and precipitation [42]. The creation of anti-fouling membranes has received a lot of interest from researchers, but the selective separation of certain solutes has received less attention [43, 44]. The primary disadvantage of employing the membrane separation method to separate a single ion is the membrane's ion-specific selectivity[45].

2.1.2 Membrane Distillation

Membrane distillation (MD), particularly from saltwater and brackish water, is an emerging technique that shows promise for desalination. Water vapor molecules move through a porous hydrophobic membrane in this thermally driven mechanism. MD offers several benefits, including a high rejection of inorganic ions, macromolecules, and other non-volatile chemicals, the ability to operate at low temperatures, and the need for less demanding membrane material [46]. In comparison to other membrane processes, MD has a low permeate flow and is more susceptible to concentration, heat losses, fouling, air entrapment, and feed temperature [47].

2.1.3 Electrocoagulation

By adding direct current through a metal electrode, electrocoagulation (EC) encourages the precipitation of metals as hydroxides. This has been found to be inexpensive and effective for wastewater [48].

Through the production and commercialization of Cu^{2+} , Mn^{2+} , Zn^{2+} , Al^{3+} , Fe^{3+} , Ni^{2+} , Mg^{2+} , Ca^{2+} , Na^{+} , and several other metal hydroxides, the precipitation of metal cations in the form of hydroxides may be further utilized to make the treatment of PW more economically viable for the industrial sector. Additionally, the chlorine gas that is created throughout the operation might be hydrolyzed to form HCl [49].

2.1.4 Adsorption

Adsorption is used to sequester pollutants like metals and organics. However, rather than serving as a stand-alone separation approach, it serves more as a finishing step for other earlier therapy techniques. It is essential to note that salinity mediates how well different mediums adsorb substances. Organic pollutants can be removed using activated carbon medium, whereas scaling ions like Ca^{2+} and Mg^{2+} [50] that are often present in high quantities in PW may be removed with active zeolite.

3 Conclusion and Future Outlook

Produced water (PW) could be a source of different valuable elements like lithium and boron. To build a stronger basis for experimenting in this area, more research on the characterization of PW is required. It is unlikely that a single separating method will meet all the PW's treatment goals. However, the economic viability of PW treatment would significantly increase by integrating several separation techniques in recovering elements like Li and B. Li and B producers can reduce capital expenditures related with Li and B recovery by using existing oil and gas wells. Oil and gas firms might also boost their earnings by selling Li and B derived from their effluent. Thus, serious consideration should be given to the exploitation of oil and gas production wastewater given its considerable potential as a Li and B resources, especially in areas that often import Li and B from other regions which provide prospective advantage for both Li and B's final consumers and oil and gas producers.

References

1. (2021) Global mineral demand for clean energy technologies 2010–2040. IEA. <https://scholar.google.com/scholar?q=Global>. Mineral demand for clean energy technologies 2010–2040
2. (2021) Global copper market: insights & forecast with potential impact of COVID-19 (2021–2025)
3. Khalil A, Mohammed S, Hashaikeh R Hilal N (2022) Lithium recovery from brine: recent developments and challenges. *Desalination* 528. <https://doi.org/10.1016/j.desal.2022.1156111>
4. Meshram P, Pandey B, Mankhand TR (2014) Extraction of lithium from primary and secondary sources by pre-treatment, leaching and separation. *Hydrometallurgy* 150:192–208. <https://doi.org/10.1016/j.hydromet.2014.10.012>
5. Ambrose H, Kendall A (2020) Understanding the future of lithium: Part 1, resource model. *J Ind Ecol* 24:80–89. <https://doi.org/10.1111/jiec.12949>
6. (2022) <https://www.metalary.com/lithium-price>
7. Neal C, et al (2010) Decreasing boron concentrations in UK rivers: insights into reductions in detergent formulations since the 1990s and within-catchment storage issues. *Sci Total Environ* 408:1374–1385. <https://doi.org/10.1016/j.scitotenv.2009.10.074>
8. Korkut T, Karabulut A, Budak G, Aygün B, Gencil O, Hançerlioğulları A (2012) Investigation of neutron shielding properties depending on number of boron atoms for colemanite, ulexite and

- tincal ores by experiments and FLUKA Monte Carlo simulations. *Appl Radiat Isot* 70:341–345. <https://doi.org/10.1016/j.apradiso.2011.09.006>
9. Belova T, Ershova L, Ratchina T (2019) Boron recovery from separate of Pauzhetskaya geothermal station based on modified zeolites of Yagodninsky deposit of Kamchatka. *IOP Conf Ser Earth Environ Sci* 249. <https://doi.org/10.1088/1755-1315/249/1/012031>
 10. Ezechi E, Isa M, Kutty S, Sapari N (2011) Boron recovery, application and economic significance: a review. In: 2011 national postgraduate conference - energy and sustainability: exploring the innovative minds
 11. Jiménez S, Micó M, Arnaldos M, Medina F, Contreras S (2018) State of the art of produced water treatment. *Chemosphere* 192:186–208. <https://doi.org/10.1016/j.chemosphere.2017.10.139>
 12. Wang X, Goual L, Colberg P (2012) Characterization and treatment of dissolved organic matter from oilfield produced waters. *J Hazard Mater* 217–218:164–170. <https://doi.org/10.1016/j.jhazmat.2012.03.006>
 13. Alley B, Beebe A, Rodgers J, Castle J (2011) Chemical and physical characterization of produced waters from conventional and unconventional fossil fuel resources. *Chemosphere* 85:74–82. <https://doi.org/10.1016/j.chemosphere.2011.05.043>
 14. Ghafoori S, et al (2022) New advancements, challenges, and future needs on treatment of oilfield produced water. *Sep Purif Technol* 289. <https://doi.org/10.1016/j.seppur.2022.120652>
 15. Ekberg C, Petranikova M (2015) Lithium batteries recycling. In: *Lithium process chemistry: resources, extraction, batteries, and recycling extraction, batteries, and recycling*. Elsevier Inc, pp 233–267
 16. Haluszczak L, Rose A, Kump L (2013) Geochemical evaluation of flowback brine from Marcellus gas wells in Pennsylvania, USA. *Appl Geochem* 28:55–61
 17. Lee J, Chung E (2020) Lithium recovery by solvent extraction from simulated shale gas produced water – impact of organic compounds. *Appl Geochem*
 18. Lester Y, Ferrer I, Thurman E, Sitterley K, Korak J, Aiken G, Linden, K (2015) Characterization of hydraulic fracturing flowback water in Colorado: implications for water treatment. *Sci Total Environ* 512–513:637–644. <https://doi.org/10.1016/j.scitotenv.2015.01.043>
 19. Dong X, Tremblay J, Bayless D (2017) Techno-economic analysis of hydraulic fracturing flowback and produced water treatment in supercritical water reactor. *Energy* 133:777–783. <https://doi.org/10.1016/j.energy.2017.05.078>
 20. Ezechi E, Isa M, Kutty SRBM (2012) Boron in produced water: challenges and improvements: a comprehensive review. *J Appl Sci* 12, 402–415. <https://doi.org/10.3923/jas.2012.402.415>
 21. Willingham J, Tan H, Norman L (1993) Perforation friction pressure of fracturing fluid slurries. *Vacuum* 16:383–384. <https://doi.org/10.2523/25891-ms>
 22. Pieruz G, Grassia P, Dryfe R (2004) Boron removal from produced water by facilitated ion transfer. *Desalination* 167:417. <https://doi.org/10.1016/j.desal.2004.06.156>
 23. Ezechi E, Isa M, Kutty S, Yaqub, A (2014) Boron removal from produced water using electrocoagulation. *Process Saf Environ Prot* 92:509–514
 24. Xu P, et al (2020) Materials for lithium recovery from salt lake brine. *J Mater Sci* 16–63. <https://doi.org/10.1007/s10853-020-05019-1>
 25. Flexer V, Baspineiro C, Galli C (2018) Lithium recovery from brines: a vital raw material for green energies with a potential environmental impact in its mining and processing. *Sci Total Environ* 639:1188–1204. <https://doi.org/10.1016/j.scitotenv.2018.05.223>
 26. Vikström H, Davidsson S, Höök M (2013) Lithium availability and future production outlooks. *Appl Energy* 110:252–266. <https://doi.org/10.1016/j.apenergy.2013.04.005>
 27. (2020) <https://undark.org/2020/12/21/chile-debate-over-lithium-brine/>. <https://undark.org/2020/12/21/chile-debate-over-lithium-brine/>. Accessed 26 Jun 2022
 28. Ohashi F, Tai Y (2019) Lithium adsorption from natural brine using surface-modified manganese oxide adsorbents. *Mater Lett* 251:214–217. <https://doi.org/10.1016/j.matlet.2019.05.064>
 29. Wang Y, Liu H, Fan J, et al (2019) Recovery of lithium ions from salt Lake brine with a high magnesium/lithium ratio using heteropolyacid ionic liquid in tributyl phosphate. *ACS Sustain Chem Eng* 7:3062–3072. <https://doi.org/10.1021/acssuschemeng.8b04694>

30. Zhang Y, Hu Y, Sun N, Khoso S, Wang L, Sun W (2019) A novel precipitant for separating lithium from magnesium in high Mg/Li ratio brine. *Hydrometallurgy* 187:125–133. <https://doi.org/10.1016/j.hydromet.2019.05.019>
31. Lai X, Yuan Y, Chen Z, Peng J, Sun H, Zhong H (2020) Adsorption–desorption properties of granular EP/HMO composite and its application in lithium recovery from brine. *Ind Eng Chem Res* 59:7913–7925. <https://doi.org/10.1021/acs.iecr.0c00668>
32. Zhou Z, Fan J, Liu X, et al (2020) Recovery of lithium from salt-lake brines using solvent extraction with TBP as extractant and FeCl₃ as co-extraction agent. *Hydrometallurgy* 191. <https://doi.org/10.1016/j.hydromet.2019.105244>
33. Lai X, Xiong P, Zhong H (2020) Extraction of lithium from brines with high Mg/Li ratio by the crystallization-precipitation method. *Hydrometallurgy* 192. <https://doi.org/10.1016/j.hydromet.2020.105252>
34. Zhou W, Xu S, Li Z (2021) Recovery of lithium from brine with a high Mg/Li ratio using hydroxyl-functionalized ionic liquid and tri-n-butyl phosphate. *J Sustain Metall* 7:256–265. <https://doi.org/10.1007/s40831-020-00331-1>
35. Lee J, Chung E (2022) Lithium recovery from a simulated geothermal fluid by a combined selective precipitation and solvent extraction method. *Geothermics* 102. <https://doi.org/10.1016/j.geothermics.2022.102388>
36. Özyurt B, Camcıoğlu Ş, Firtın M, Ateş Ç, Hapoglu H (2019) Boron removal from industrial wastewaters by means of optimized sequential chemical precipitation and coagulation processes. *Desalin Water Treat* 172:292–300. <https://doi.org/10.5004/dwt.2019.24932>
37. Alm Mustafa G, et al.: Liquefaction of 2,2,4-trimethyl-1,3-pentanediol into hydrophobic eutectic mixtures: a multi-criteria design for eco-efficient boron recovery. *Chem Eng J* 426 (2021). <https://doi.org/10.1016/j.cej.2021.131342>
38. Bai C, et al (2021) Efficient separation of boron from salt lake brine using a novel flotation agent synthesized from NMDG and 1-bromooctadecane. *Colloids Surfaces A Physicochem Eng Asp* 627. <https://doi.org/10.1016/j.colsurfa.2021.127178>
39. Yang-Zhou C, Cao J, Dong S, Chen S, Michael, R (2022) Phosphorus co-existing in water: a new mechanism to boost boron removal by calcined oyster shell powder. *Molecules* 27. <https://doi.org/10.3390/molecules27010054>
40. Liu Y, et al (2021) A review of treatment technologies for produced water in offshore oil and gas fields. *Sci Total Environ* 775. <https://doi.org/10.1016/j.scitotenv.2021.145485>
41. Brdar-Jokanović M (2020) Boron toxicity and deficiency in agricultural plants. *Int J Mol Sci*. <https://doi.org/10.3390/ijms21041424>
42. Li X, Mo Y, Qing W, Shao S, Tang C, Li J (2019) Membrane-based technologies for lithium recovery from water lithium resources: a review. *J Memb Sci* 591. <https://doi.org/10.1016/j.memsci.2019.117317>
43. Tong T, Wallace A, Zhao S, Wang Z (2019) Mineral scaling in membrane desalination: mechanisms, mitigation strategies, and feasibility of scaling-resistant membranes. *J Memb Sci* 579:52–69. <https://doi.org/10.1016/j.memsci.2019.02.049>
44. Goh P, Lau W, Othman M, Ismail A (2018) Membrane fouling in desalination and its mitigation strategies. *Desalination* 425:130–155. <https://doi.org/10.1016/j.desal.2017.10.018>
45. Epsztein R, DuChanois R, Ritt C, Noy A, Elimelech M (2020) Towards single-species selectivity of membranes with subnanometre pores. *Nat Nanotechnol* 15:426–436. <https://doi.org/10.1038/s41565-020-0713-6>
46. Lawson K, Lloyd D (1997) Membrane distillation. *J Memb Sci* 124:1–25. [https://doi.org/10.1016/S0376-7388\(96\)00236-0](https://doi.org/10.1016/S0376-7388(96)00236-0)
47. Alkudhiri A, Darwish N, Hilal, N (2012) Membrane distillation: a comprehensive review. *Desalination* 287:2–18. <https://doi.org/10.1016/j.desal.2011.08.027>
48. Khor C, et al (2020) Performance, energy and cost of produced water treatment by chemical and electrochemical coagulation. *Water* 12. <https://doi.org/10.3390/w12123426>

49. Moradi M, Vasseghian Y, Arabzade H, Khaneghah, AM (2021) Various wastewaters treatment by sono-electrocoagulation process: a comprehensive review of operational parameters and future outlook. *Chemosphere* 263. <https://doi.org/10.1016/j.chemosphere.2020.128314>
50. Chang H, Liu T, He Q, Li D, Crittenden J, Liu B (2017) Removal of calcium and magnesium ions from shale gas flowback water by chemically activated zeolite. *Water Sci Technol* 76:575–583. <https://doi.org/10.2166/wst.2017.237>

Pyrolysis Behavior of Polyethylene Terephthalate (PET) Plastic Waste Under the Presence of Activated Montmorillonite Catalyst: TGA and EGA-MS Studies



Tarmizi Taher, Andika Munandar, Nurul Mawaddah, Raden Putra, Neza Rahayu Palapa, and Aldes Lesbani

Abstract Production of PET-based plastics, which are mainly used for food and beverage packaging, continuously increases in amount annually, which has been widely reported to cause various severe environmental issues. Pyrolysis is one of the possible methods to convert PET plastic wastes into valuable products such as benzene-rich oil. Unfortunately, its larger-scale development is still hindered and challenging to pursue since it produces acidic compounds as the main product, such as terephthalic acid, which is undesirable because it can cause blockage of the reactor pipeline and corrosion. In this work, catalytic pyrolysis of PET has been investigated over a thermally activated montmorillonite (AMMT) catalyst to increase the feasibility of PET recycling for energy production. The thermal and catalytic pyrolysis behavior of PET under AMMT was comprehensively investigated by TGA and EGA-MS analyses. TGA analysis results indicated that the presence of AMMT reduced the onset and maximum decomposition temperature of PET pyrolysis. Moreover, the isothermal TGA result exhibited that the presence of AMMT could significantly reduce the amount of the produced carbonaceous residue. From EGA-MS analysis, it can be obtained that the presence of AMMT indeed changed the amount and distribution of evolved gaseous products, as indicated by the difference in the extracted ion thermogram intensities.

T. Taher (✉) · A. Munandar · N. Mawaddah · R. Putra
Department of Environmental Engineering, Institut Teknologi Sumatera, Jalan Terusan Ryacudu, Way Hui, Kecamatan Jati Agung, Lampung Selatan 35365, Indonesia
e-mail: tarmizi.taher@tl.itera.ac.id

N. R. Palapa
Department of Chemistry, Faculty of Mathematic and Natural Science, Sriwijaya University, Jl. Palembang-Prabumulih, Km. 32, Indralaya, Ogan Ilir, South Sumatera, Indonesia

A. Lesbani
Magister of Materials Science, Graduate School of Sriwijaya University, Jl. Padang Selasa No. 524 Bukit Besar, Palembang, Indonesia

Keywords PET waste · Pyrolysis · Feedstock recycling · Montmorillonite

1 Introduction

Global plastic production has increased 1.5 times in the last 10 years, during which the packaging sector used around 36% of all plastic produced [1]. Polyethylene terephthalate (PET) is the third most-produced plastic polymer, along with polyethylene and polypropylene, which are widely used in food and beverage containers and the packaging [2]. Unfortunately, most plastic-based packaging is single-use and is disposed of directly after its first use [3]. Consequently, the amount of PET plastic waste that enters the environment increases every year. Therefore, reducing the amount of PET plastic in the environment is highly necessary, especially by means of the 3Rs (reduce, reuse, and recycle).

Currently, mechanical recycling, feedstock recycling, and energy recovery recycling methods are widely used for treating PET waste [4]. Mechanical recycling, the most adopted method, processes PET waste into a secondary raw material without significantly changing its chemical structure. However, this method weakens the recycled product quality, limiting its subsequent use. For instance, food and beverage containers cannot contain mechanically recycled PET because they can contain hazardous substances that could leech into the food [5].

Feedstock recycling, which includes monomerization, liquefaction, and gasification, is one of the most sustainable but challenging methods of plastic waste recycling since it can transform plastic waste into high-value chemicals. Pyrolysis is a feedstock recycling method that converts plastics into three main products—gases, liquids, and solids—using high temperatures in nonoxygen environments [6]. Pyrolysis is highly advantageous for treating low-quality and low-purity plastic wastes that conventional mechanical recycling cannot treat. This process cleaves plastic polymer bonds into their respective monomers or other valuable chemicals, depending on the temperature used [7].

Much research has focused on PET waste pyrolysis that reported significant results. For example, the previous researcher reported that they could recover 27–32 wt% of benzoic acid from PET plastic pyrolysis at operating temperatures of 450–600 °C [8]. Unfortunately, they also reported that PET pyrolysis produces complex products that limit further, large-scale PET pyrolysis development. PET pyrolysis produces significant amounts of high-boiling terephthalic acid (TPA) and benzoic acid, which cause pipe clogging and corrosion. Furthermore, under ordinary conditions, pyrolysis cannot completely decompose PET, leaving around 20 wt% as a carbonaceous residue [6]. Therefore, investigations introducing particular catalysts into PET pyrolysis to facilitate the PET reaction and enhance pyrolysis products have been widely conducted.

Catalytic pyrolysis appears to be a practical approach for converting the main product of PET thermal decomposition into smaller and more valuable products, such as benzene and other mono aromatic hydrocarbons [9]. For instance, Park et al. [10]

used 5 wt% of palladium metal catalyst loaded on activated carbon and reduced polycyclic hydrocarbon production by 44%. Furthermore, this catalyst reduced biphenyl derivative products by 74%. In PET catalytic pyrolysis in the presence of ZSM-5, the aromatic hydrocarbon product yield increased by 21.82% with a zeolite-to-PET mass ratio of 2:1; ZSM-5 also reportedly facilitated the decomposition of carboxyl and the aliphatic group produced from the primary product of PET thermal decomposition. Based on Du et al., PET carpet waste pyrolysis using ZSM-5 resulted in a high yield of benzene, benzene derivatives, and indene/naphthalene [4].

Clays and clay minerals have long been used as effective catalysts for facilitating many organic reactions due to their abundance, low cost, and high acidity [11]. Montmorillonite (MMT) is a 2:1 type of clay with high hydrothermal stability and a high surface area, and it contains both Lewis and Bronsted acid site [12]. Moreover, it is a low-cost, non-corrosive, easy to handle, environmentally friendly, and regenerable solid catalyst. MMT consists of an octahedral aluminate layer located between two tetrahedral silicate layers. Motokura et al. [13] reported that MMT exhibited outstanding catalytic activity for nucleophilic substitution of alcohol compounds over aniline due to its unique acidity. MMT is also an effective catalyst for biomass pyrolysis in which the addition of the catalyst to the fast pyrolysis of cellulose promotes high-value product formation, for example, furfural, furan derivatives, and levoglucosenone.

According to Du et al., [4] solid acid catalysts such as ZSM-5 are excellent at enhancing the carboxylation reaction in the pyrolysis of PET and some other plastic polymers. Therefore, investigating the effect of MMT addition during PET pyrolysis is worthwhile. To the best of the author's knowledge, this is the first report on the catalytic pyrolysis of PET over an MMT catalyst. The effect of the addition of MMT in PET pyrolysis was investigated based on the following three analytical techniques: thermogravimetry (TGA), evolved-gas analysis coupled with mass spectrometry (EGA-MS). Furthermore, the catalyst's effect on the formation of the carbonaceous residue was directly investigated during the TGA analysis.

2 Experimental Section

2.1 Materials

PET plastic used in this work was pure PET pellet. Before being used in the pyrolysis experiment, the PET pellet was first crushed and sieved to obtain a PET powder with a particle size less than 150 μm . The elemental analysis of PET powder indicated that it consisted of 62% carbon, 34% oxygen, and 4% hydrogen, which is consistent with the theoretical composition of PET polymer. MMT sample used as the catalyst was purchased from Sigma Aldrich, USA, and used as received without further purification. The surface area of the used montmorillonite is 250 m^2/g with a pH of 3–4.

2.2 *Catalyst Activation*

MMT was activated by a thermal activation procedure. MMT powder was subjected to calcination under an air atmosphere at 500 °C for 2 h. To confirm that the activation process was not changed the MMT structure, the calcined MMT was characterized by XRD and FTIR.

2.3 *TGA Pyrolysis*

The effect of temperature on the PET thermal and catalytic pyrolysis was first investigated by thermal gravimetry analysis (TGA) under an inert N₂ atmosphere using Shimadzu DTG-60H TG-DTA apparatus, Shimadzu Corp, Japan. For thermal pyrolysis, 10 mg of PET powder was placed in an alumina crucible and then transferred into the TG machine to be heated up to 800 °C with a heating rate of 10 °C/min. The catalytic pyrolysis experiment was conducted by mixing the calcined MMT catalyst and PET powder with different ratios before introducing them to the TG machine. The catalytic pyrolysis was conducted under the same heating condition as the thermal pyrolysis.

2.4 *EGA-MS Analysis*

The evolved gases from thermal and catalytic pyrolysis of PET under the presence of thermal activated MMT were investigated by evolved gas analysis coupled with mass spectroscopy (EGA-MS) apparatus. The thermal and catalytic pyrolysis was conducted in a multi-shot micro pyrolizer (EGA/PY 3030D, Frontier Lab, Japan) directly connected to a GC-MS instrument (QP-2010 Ultra, Shimadzu Corp, Japan). The schematic appearance of the EGA-MS instrument can be seen in Fig. 1.

The EGA analysis was conducted by transferring 0.5 mg of PET or a mix of PET and MMT into the deactivated stainless-steel cup. The filled cup was then moved to the micro pyrolizer that was heated at 100 °C. Just after being introduced, the micro pyrolizer temperature gradually increased under the heating rate of 5 °C/min until reaching the final heating temperature of 600 °C under a helium atmosphere. The evolved gases during the pyrolysis process were swept to pass through a deactivated metal tube (UA-DTM-2.5 N, Frontier Laboratories, Ltd) and then directly introduced to the MS detector without separation process (after being splatted with a splitting ratio of 1:200).

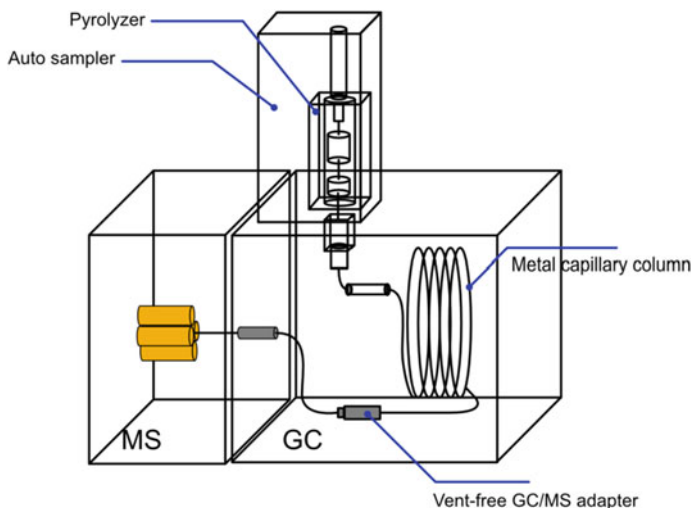


Fig. 1 The schematic appearance of the EGA and Py-GCMS apparatus

2.5 Carbonaceous Residue Analysis

The investigation of carbonaceous residue formation during the thermal and catalytic pyrolysis of PET over AMMT was investigated in a TG instrument. In brief, 10 mg of PET or mixed PET and AMMT was heated to the targeted temperature and held in an N_2 atmosphere for a predetermined period. Then, the N_2 gas flow was stopped and directly switched to compressed air to facilitate the combustion of the remaining carbonaceous residue in the presence of air atmosphere.

3 Results and Discussion

3.1 Catalyst Characterization

The effect of the thermal treatment on the structure and crystallinity of MMT after the thermal activation process has been investigated. The XRD patterns of MMT and AMMT are shown in Fig. 2. The main diffraction feature of MMT showed the typical diffraction pattern of montmorillonite minerals (JCPDS 13-0135) as observed at 2θ of 17.6, 19.7, 23.5, 29.5, 34.7, 34.8, 61.7, and 62.1°. Furthermore, sharp peaks corresponding to the diffraction pattern of quartz minerals (JPDS 45-1045) appeared at 2θ of 20.8, 26.6, and 50.1°.

Following thermal activation, the resulting diffraction pattern did not differ from the MMT diffraction pattern, indicating that the structure and crystallinity of the

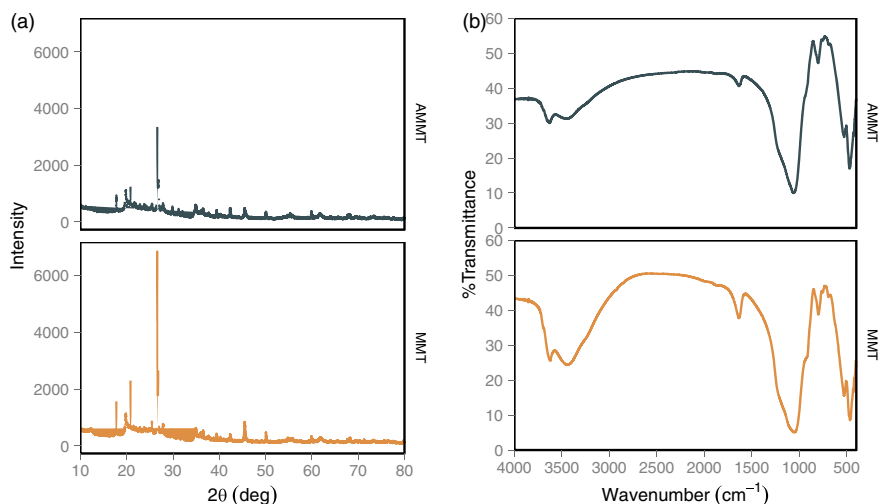


Fig. 2 XRD pattern (a) and FTIR spectra (b) of the pristine and activated montmorillonite

AMMT did not change. By contrast, the peak intensity decreased after thermal activation. The intensity of the sharpest diffraction peak belonging to the quartz minerals was significantly reduced. This finding is in agreement with that reported by Feddal et al., who found that thermal treatment of montmorillonite could significantly reduce the number of impurities, such as calcite, quartz, and cristobalite [14].

The FTIR spectra of the MMT and AMMT are shown in Fig. 2(b). The spectra of MMT exhibited eight main peaks at around 3623, 3447, 1634, 1056, 801, 531, and 471 cm^{-1} . The peak at 3623 cm^{-1} corresponds to the stretching vibration of the $-\text{OH}$ group belonging to the $\text{Si}-\text{OH}-\text{Al}$ structure [12]. The strong vibration peak at 3448 cm^{-1} and the sharp vibration band at 1634 cm^{-1} are related to the stretching and bending vibration bands, respectively, of the $-\text{OH}$ bond of water found in the interlayer space. The sharp, strong peak at 1056 cm^{-1} is related to the stretching vibration of $\text{Si}-\text{O}-\text{Si}$. After thermal activation, the FTIR spectra of the AMMT showed a significantly reduced intensity for the $-\text{OH}$ group (3448 and 1634 cm^{-1}), indicating that the interlayer water molecules had been removed [12]. Furthermore, most of the typical absorption bands of the layered double hydroxide structure could be preserved and did not display any significant changes.

3.2 TGA Pyrolysis

Figure 3 shows the TGA and DTG curves of the PET pyrolyzed under catalytic and non-catalytic conditions at a heating rate of 10 $^{\circ}\text{C}/\text{min}$ under N_2 atmosphere. The distinct differences in final residual mass between the catalytic and non-catalytic processes were due to the mass of the catalyst, which remained the same at the

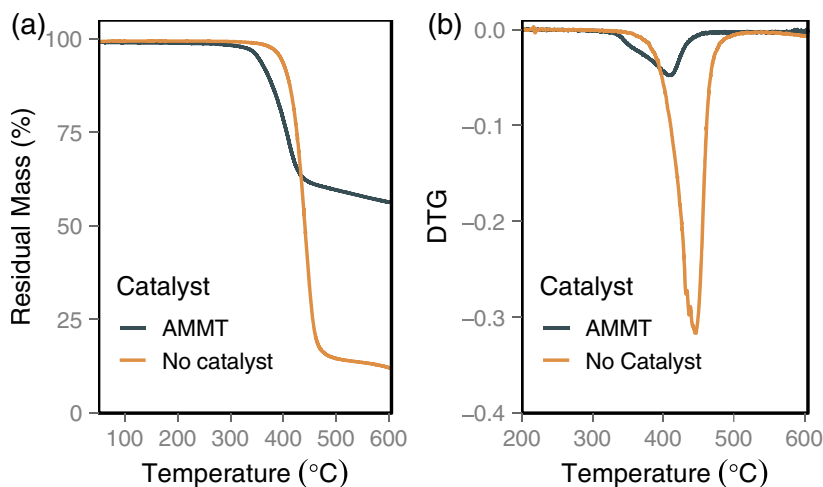


Fig. 3 TGA (a) and DTG (b) profile of PET decomposition under the presence of AMMT

end of the catalytic pyrolysis. In addition to the final residual mass difference, a difference in the initial starting temperature was observed. It has been widely reported that temperature plays an essential role in controlling cracking reactions in plastic polymers, including PET. Studies have indicated that PET decomposition starts at temperatures above 300 °C [15]. In the present work, the PET started to decompose at 350 °C and reached the maximum decomposition rate at 450 °C during the non-catalytic pyrolysis. After the final temperature was reached, about 14% of the sample remained, which is the carbonaceous residue. This result is in line with a previous finding showing that PET pyrolysis produces 10–20% carbon residue.

In catalytic pyrolysis, the presence of AMMT is expected to affect the PET decomposition mechanism. Therefore, it might alter the thermal decomposition behavior of the sample. The presence of a catalyst might decrease or increase the onset and maximum decomposition temperatures during a pyrolysis process. For instance, Park et al. [16] have reported that acid and base solid catalysts could increase the onset decomposition temperature during biomass (yellow poplar wood) pyrolysis. By contrast, most studies on plastic polymer pyrolysis have indicated that catalysts could significantly reduce the onset and maximum decomposition temperatures [8]. In the present work, as shown in Fig. 3(a), the onset temperature for PET pyrolysis in the presence of AMMT was 300°C, which was lower compared to that for non-catalytic pyrolysis. Moreover, based on the obtained DTG curve, the maximum decomposition temperature was reduced by about 50 °C in the presence of AMMT. This finding is in agreement with that obtained by Xue et al., who found that the presence of ZSM-5 decreased the maximum decomposition of PET from 436 to 420 °C during pyrolysis [17].

3.3 Isothermal TG Pyrolysis

To further investigate the effect of AMMT on the PET pyrolysis behavior, isothermal pyrolysis was carried out at 400, 500, and 550 °C. For this purpose, the TG technique was used to calculate the mass change of the sample as a function of contact time. The isothermal pyrolysis was conducted for 60 min after the targeted temperature was achieved under N₂ atmosphere. After the isothermal period was completed, the internal atmosphere was changed to air, and the furnace temperature was increased to 600°C to completely decompose the remaining carbonaceous residue through oxidative combustion.

Figure 4 shows the TGA profile of the PET subjected to isothermal pyrolysis in the presence of AMMT. From Fig. 4(a), it can be inferred that the holding temperature significantly affected the pyrolysis performance. The higher the holding temperature, the lesser the residual mass that remained at the end of the isothermal pyrolysis. At the end of the isothermal pyrolysis at 400 °C, the total sample mass (PET + catalyst) was reduced by approximately 23%. At 500 °C and 550 °C, the amount of decomposed sample reached 30% and 33%, respectively. This is because at 400 °C, the maximum PET decomposition has not yet been reached, as shown in Figure X. Grause et al. have reported similar results obtained from an actual pyrolysis experiment [18]. They conducted an isothermal pyrolysis experiment at 450, 500, and 550°C and found that production of benzene as the main product was accelerated by increasing temperature.

As previously stated, the amount of carbonaceous residue remaining at the end of the isotherm decomposition reaction was analyzed by air combustion. Figure X(b) exhibits a decrease in the sample mass due to the combustion reaction under the air atmosphere. The amount of sample mass lost due to combustion reaction is considered as the amount of carbonaceous residue formed during the pyrolysis reaction under the nitrogen atmosphere. Calculations indicated that mass lost in

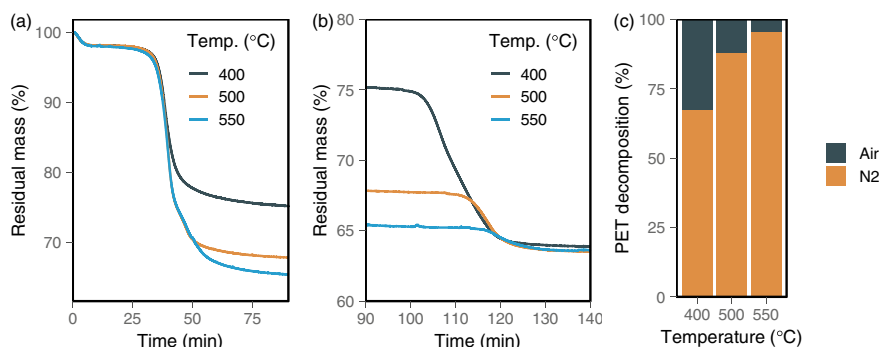


Fig. 4 TG isotherm profile of PET catalytic pyrolysis under N₂ atmosphere (a), TG isotherm profile of the residue in an air atmosphere (b), and the calculated fraction of the PET decomposed under N₂ and air atmosphere

the combustion reaction decreased with increasing decomposition temperature. At decomposition temperatures of 400, 500, and 550 °C, the recorded mass lost in the combustion reaction was 11%, 4%, and 1.5%, respectively. Therefore, it can be concluded that the higher the pyrolysis temperature, the smaller the amount of produced carbonaceous residue.

The total amount of PET decomposed, calculated from the total mass lost in both pyrolysis reaction (under nitrogen atmosphere) and combustion reaction (under air atmosphere), is summarized in Fig. 4(c). Clearly, the amount of PET decomposed due to the pyrolysis increased significantly along with increasing holding temperature. In detail, as much as 67%, 87%, and 95% of PET could be decomposed under the holding temperatures of 400, 500, and 550 °C, respectively. Consistently the amount of carbonaceous residue produced decreased as holding temperature increased. Interestingly, the use of AMMT as a catalyst in PET pyrolysis could significantly reduce the amount of generated carbonaceous residue. In the non-catalytic pyrolysis of PET, as previously described, the amount of the produced carbonaceous residue is in the 10–25% range.

3.4 EGA-MS Analysis

EGA-MS analysis was performed under temperature-programmed pyrolysis from 100 to 600 °C under a heating rate of 10 °C/min. During the pyrolysis process, the resulting gases were directly transferred to the MS detector without going through a separation column to monitor the formed pyrolysis products online. Figure 5(a) shows the EGA thermogram of PET pyrolysis under the presence and absence of AMMT as the catalyst. The thermogram was recorded at temperature intervals of 100–600 °C, in which the curve is obtained from the total ion current (TIC). It can be observed that only one peak intensity resulted from the pyrolysis of PET with and without the presence of an AMMT catalyst. This finding is in line with the result obtained from the thermogravimetric analysis, which indicated that PET pyrolysis occurred through one major decomposition step.

The obtained EGA thermogram displayed in Fig. 5(a) indicated that the maximum peak intensity of PET was recorded at 460 °C. Meanwhile, the maximum peak intensity of PET pyrolysis with the AMMT catalyst slightly shifted to the lower temperature (400 °C), similar to the TGA analysis mentioned earlier. This finding further indicated that the presence of AMMT in PET pyrolysis indeed changes the route of PET thermal degradation. It certainly brings advantages to PET pyrolysis since AMMT can decrease the maximum pyrolysis temperature.

The extracted ion chromatogram (EIC) related to the total ion thermogram displayed in Fig. 5(b, c) can further explain the effect of AMMT in PET pyrolysis and the possible reaction mechanism involved. Based on the EIC of the evolved products, both samples exhibited mass fragments (m/z) of 51, 65, 77, 105, and 121/122 corresponding to benzoic acid and vinyl benzoate, which are the typical m/z from PET thermal pyrolysis [19]. However, the intensity of each mass fragment was

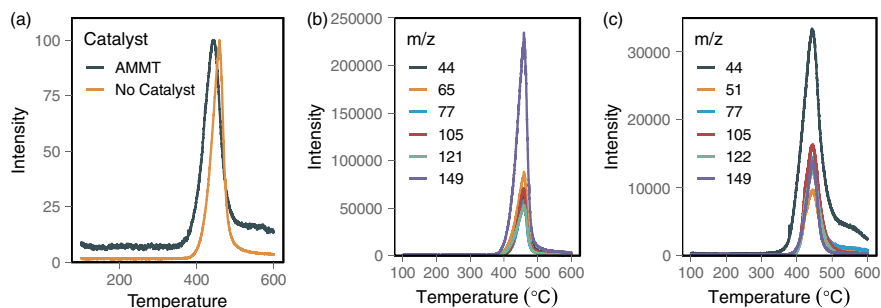


Fig. 5 Total ion chromatogram (TIC) (a) and extracted ion chromatogram (EIC) of PET pyrolysis without catalyst (b) and under the presence of AMMT catalyst (c)

significantly different. These differences indicated the effect of the AMMT catalyst in changing the amount of product distribution. As widely reported, the thermal pyrolysis of PET yields a mixture of terephthalic acid, vinyloxycarbonyl, and divinyl terephthalate via random-chain scission of the ester linkage that detected the mass fragments (m/z) of 65, 121, and 149 [19]. These statements are in accordance with the EIC resulting from the thermal pyrolysis of PET without catalyst as displayed in Fig. 5(b), in which the main mass fragment was m/z 149.

As aforementioned, the mass fragment intensities obtained from PET pyrolysis under the presence of AMMT were significantly different compared to those obtained from thermal pyrolysis only. As illustrated in Fig. 5(c), m/z 149 no longer has the most prominent intensity. Rather, m/z 44 emerged as the most intense mass fragment produced from PET pyrolysis under the presence of AMMT. m/z 44 is identified as the characteristic mass fragment of condensable gases such as CO_2 . This finding might be attributed to the further decomposition of the products resulting from the thermal pyrolysis of PET, such as terephthalic acid and benzoic acid, into smaller molecules that have been facilitated by the catalyst active site.

In an earlier report, Kumagai et al. described that terephthalic acid and benzoic acid vinyl ester, as the most abundant compound in the products of PET pyrolysis, could be further decomposed into benzene and CO_2 under the presence of CaO as the catalyst [20]. Furthermore, it has been reported that the use of ZSM-5 as an acid catalyst in PET pyrolysis enhances the decarboxylation reaction of the produced acid from PET thermal pyrolysis, thereby yielding more valuable aromatic products [4]. Although it is too early to determine the role of AMMT in changing the product formation route of PET pyrolysis based on the EGA-MS results, it is possible to indicate that it is affected by the presence of both Bronsted and Lewis acid sites of the catalyst. This was also reported by Solak et al., who investigated the effect of clay catalysts, including montmorillonite K10, on the co-pyrolysis of cellulose and polyethylene [21]. They reported that the use of montmorillonite K10 is shown to promote the effective and deeper degradation of polyethylene into liquid hydrocarbon and gas formation owing to their Lewis acidity.

4 Conclusions

Since PET will produce harmful substance when treated by thermal pyrolysis, the use of catalysts during the pyrolysis treatment is the best choice to overcome these drawbacks. During the catalytic pyrolysis process, the less valuable products can be converted into safer and more profitable products with the help of the used catalyst. The results of this study indicate that the use of a catalyst in the form of natural montmorillonite clay can help reduce the amount of terephthalic acid product and reduce the amount of carbon residue produced during the pyrolysis process. Thus, it becomes possible to utilize these catalysts as an alternative catalyst in the pyrolysis of PET plastic waste to produce high-value products.

Acknowledgements The author thanks the Institute of Regional innovation (IRI), Hirosaki University, for fully supporting this research work. A big thank you also to Prof. Akihiro Yoshida, who has provided advice and guidance to the author.

References

1. Kumagai S, Yoshioka T (2016) Feedstock recycling via waste plastic pyrolysis. *J Jpn Petrol Inst* 59:243–253
2. Kumagai S, Nakatani J, Saito Y, Fukushima Y, Yoshioka T (2020) Latest trends and challenges in feedstock recycling of polyolefinic plastics. *J Jpn Petrol Inst* 63:345–364
3. De Souza Machado AA, et al (2019) Microplastics can change soil properties and affect plant performance. *Environ Sci Technol* 53:6044–6052
4. Du S, Valla JA, Parnas RS, Bollas GM (2016) Conversion of polyethylene terephthalate based waste carpet to benzene-rich oils through thermal, catalytic, and catalytic steam pyrolysis. *ACS Sustain Chem Eng* 4:2852–2860
5. Hopewell J, Dvorak R, Kosior E (2009) Plastics recycling: challenges and opportunities. *Philos. Trans. R. Soc. B Biol. Sci.* 364:2115–2126
6. Yoshioka T, Grause G, Eger C, Kaminsky W, Okuwaki A (2004) Pyrolysis of poly(ethylene terephthalate) in a fluidised bed plant. *Polym Degrad Stab* 86:499–504
7. Brems A, Baeyens J, Vandecasteele C, Dewil R (2011) Polymeric cracking of waste polyethylene terephthalate to chemicals and energy. *J Air Waste Manag Assoc* 61:721–731
8. Diaz-Silvarrey LS, McMahon A, Phan AN (2018) Benzoic acid recovery via waste poly(ethylene terephthalate) (PET) catalytic pyrolysis using sulphated zirconia catalyst. *J Anal Appl Pyrol* 134:621–631
9. Jia H, Ben H, Luo Y, Wang R (2020) Catalytic fast pyrolysis of poly (ethylene terephthalate) (PET) with zeolite and nickel chloride. *Polymers* 12:705
10. Park C, et al. (2020) Pyrolysis of polyethylene terephthalate over carbon-supported Pd catalyst. *Catalysts* 10:496
11. Tong DS, et al (2013) Catalytic hydrolysis of cellulose to reducing sugar over acid-activated montmorillonite catalysts. *Appl Clay Sci* 74:147–153
12. Zuo Q, et al (2017) Investigation on the thermal activation of montmorillonite and its application for the removal of U(VI) in aqueous solution. *J Taiwan Inst Chem Eng* 80:754–760
13. Motokura K, Nakagiri N, Mizugaki T, Ebitani K, Kaneda K (2007) Nucleophilic substitution reactions of alcohols with use of montmorillonite catalysts as solid Brønsted acids. *J Org Chem* 72:6006–6015

14. Feddal I, Ramdani A, Taleb S, Gaigneaux EM, Batis N, Ghaffour N (2013) Adsorption capacity of methylene blue, an organic pollutant, by montmorillonite clay. *Desalin Water Treat* 52:2654–2661
15. Brems A, Baeyens J, Beerlandt J, Dewil R (2011) Thermogravimetric pyrolysis of waste polyethylene-terephthalate and polystyrene: a critical assessment of kinetics modelling. *Resour Conserv Recycl* 55:772–781
16. Park Y-K, et al (2019) Catalytic co-pyrolysis of yellow poplar wood and polyethylene terephthalate over two stage calcium oxide-ZSM-5. *Appl Energy* 250:1706–1718
17. Xue Y, Johnston P, Bai X (2017) Effect of catalyst contact mode and gas atmosphere during catalytic pyrolysis of waste plastics. *Energy Convers Manag* 142:441–451
18. Grause G, Handa T, Kameda T, Mizoguchi T, Yoshioka T (2011) Effect of temperature management on the hydrolytic degradation of PET in a calcium oxide filled tube reactor. *Chem Eng J* 166:523–528
19. Dimitrov N, Kratofil Krehula L, Ptiček Siročić A, Hrnjak-Murgić Z (2013) Analysis of recycled PET bottles products by pyrolysis-gas chromatography. *Polym Degrad Stab* 98:972–979
20. Kumagai S, et al (2017) Tandem μ -reactor-GC/MS for online monitoring of aromatic hydrocarbon production via CaO-catalysed PET pyrolysis. *React. Chem. Eng.* 2:776–784
21. Solak A, Rutkowski P (2014) The effect of clay catalyst on the chemical composition of bio-oil obtained by co-pyrolysis of cellulose and polyethylene. *Waste Manag* 34:504–512

Evaluation of Land Subsidence Prevention to Minimize the Flood Risk in a Port City



Nurul Fajar Januriyadi, So Kazama, Idham R. Moe, and Shuichi Kure

Abstract The study aims to evaluate the indirect benefit of artificial groundwater recharge in reducing the flood risk in a port city. A flood inundation model and flood damage costs model are conducted to obtain the spatial hazard map and flood damage costs. The study used three scenarios of groundwater recharge, which are indicated by the groundwater table increase. They are groundwater table increase by 0.1, 0.5, and 1.0 m. Based on the results, each scenario produces a distinct reduction in flood risk. Increasing the groundwater level by 1-m could avoid the severer future flood risk by 24.2%. In comparison, the increasing 0.1-m groundwater could decrease the future flood risk by 3.8%. Our findings could give insight to the policymakers about the importance of slowing down the land subsidence rate.

Keywords Land subsidence · Flood risk · Port city

1 Introduction

Many world civilization developments began in the port cities because the oceans and rivers facilities to move people and goods inside the worlds. Water transportation facilitates the consumption of goods and energy in the contemporary global

N. F. Januriyadi (✉)

Department of Civil Engineering, Universitas Pertamina, Jakarta, Indonesia
e-mail: nurul.fj@universitaspertamina.ac.id

S. Kazama

Department of Civil Engineering, Tohoku University, Sendai, Japan
e-mail: so.kazama.d3@tohoku.ac.jp

I. R. Moe

Ministry of Public Works and Housing, Jakarta, Indonesia
e-mail: idham.moe@pu.go.id

S. Kure

Environment and Civil Engineering, Toyama Prefectural University, Imizu, Japan
e-mail: kure@pu-toyama.ac.jp

© Institute of Technology PETRONAS Sdn Bhd 2024

B. S. Mohammed et al. (eds.), *Proceedings of the International Conference on Emerging Smart Cities (ICESC2022)*, Lecture Notes in Civil Engineering 324,
https://doi.org/10.1007/978-981-99-1111-0_13

world, even through fast transportation modes. The development of port cities not only has a positive impact but also harms the environment. Land subsidence is one of the impacts of the rapid development of the cities. Land subsidence is a problematic hydrogeological and geological phenomenon caused by various factors such as drawdown of groundwater tables, the load of upper buildings, and natural consolidation of alluvial soil [1]–[3]. Among those factors, over-extraction of groundwater is thought as the main factor of land subsidence phenomenon [4]–[8].

Multiple damages may be caused through land subsidence. The impact of land subsidence in Jakarta could be seen in several forms, such as cracking infrastructure and increasing flood inundation areas. Land subsidence in low-lying coastal zones is expected to lower part of the land under sea level [9, 10]. Some studies found that land subsidence is expected to increase the flood risk [11]–[14]. Moe et al. [12] found that uncontrolled land subsidence is expected to increase the flood inundation area by 10.3% within four decades. The finding portrays the strong correlation between the increase in land subsidence to the flood risk. Therefore, the reduction in land subsidence rate is equivalent to the flood risk reduction.

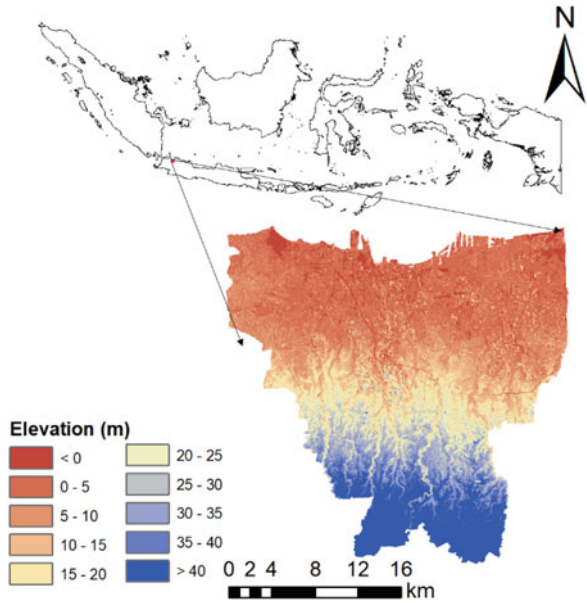
Artificial recharges are engineered systems where surface water is put into the ground for infiltration into aquifers to increase groundwater resources [15]. It can be one solution for preventing land subsidence and reducing the severe flood risks in the future. Some studies show that artificial recharge could increase the groundwater level [16]–[19], which means could alleviate the land subsidence rate. The lower land subsidence rate is expected to decrease the severe future flood risk.

Based on the above explanation, the flood risk condition corresponds to the land subsidence rate, which influences groundwater tables. This study aims to evaluate the benefit of land subsidence rate prevention to minimize future flood risk. Using several scenarios of groundwater recharges, we evaluate the flood inundation area using a numerical flood model. The various amount of groundwater recharge leads to different land subsidence rates. The study focuses on the impact of land subsidence rate reduction on the flood inundation area.

2 Area of Study

The study was conducted in Jakarta city, which is the largest and capital city of Indonesia. Jakarta is located on Java Island with approximately 660 km², as shown in Fig. 1. Figure 1 shows that most of the Jakarta area is located in the lowland area, which is one factor of Jakarta's flood problem. Jakarta experienced several huge flood events, namely in 2002, 2007, and 2013 [20]. Those floods affected many people with high economic losses. The flood problem in Jakarta is associated with land subsidence phenomena, and the high land subsidence rate corresponds to the high inundation area [9, 12]. Based on Abidin et al. [9], the land subsidence rate in the Jakarta range of vary 1 to 28 cm/year. They observed the land subsidence from 1982 to 2010 using several methods (i.e., GPS survey, Leveling survey, and InSAR). They found that the land subsidence rate is proportional to the groundwater table

Fig. 1 Location of study area



change, as shown in Fig. 2. The figure shows the correlation of groundwater table change in the middle aquifer and land subsidence rate on survey points. The figure indicates that groundwater extraction is the primary factor in the land subsidence problem.

3 Methodology

3.1 Flood Inundation Model

This study modified the previous flood model of Jakarta [21]. The flood inundation model consists of three modules (i.e., the rainfall-runoff module, the 1-D module, and the 2-D module). The model was calibrated using the radar rainfall dataset. They found that the correlation coefficient between observations and simulated averages is 0.8. The modification of the previous model is by adding the unfixed boundary condition in the 2-D module, which allows the model to simulate flood from coastal or ocean.

3.2 *Flood Damage Costs*

The study used the flood damage costs to represent the change in the flood risk. The study used the flood damage costs model applied in the previous study [22]. The flood damage costs are calculated based on the flood inundation and exposure asset value. The two input data are then linked by the damage-rate function provided by MLIT [23]. In contrast to the previous model, the study uses different asset value values, which are lower than the previous study. The previous study used total asset; this study assumes that not all asset is affected by flooding. For example, the high buildings are only affected to the lower floor.

3.3 *Artificial Recharge Scenarios*

Evaluation of the impact of land subsidence prevention conducted using several scenarios. The scenarios are based on the assumption of groundwater recharge, which is indicated by the groundwater table's increase. The average annual rainfall in the Jakarta region is approximately 2600 mm. This study assumes that groundwater recharge is based on the height of infiltrated rainfall into the ground. There are three groundwater recharge assumptions: the groundwater table increase by 0.1, 0.5, and 1 m. Based on these assumptions, we can obtain the spatial land subsidence rate for each scenario, as shown in Fig. 2. Figure 2(a) is the average spatial land subsidence rate from 2001 to 2010, adopted from Abidin et al. [9]. Figures 2(b), 2(c) 2(d) are the land subsidence rate that calculates based on the correlation of groundwater extraction and land subsidence. All these land subsidence rates linearly project to obtain the future bathymetry map by 2050. The flood simulations are based on the different bathymetry; therefore, we can evaluate land subsidence prevention's impact to minimize the severer future flood risks.

4 Results

Based on the simulation, a significant increase in flood inundation due to uncontrolled land subsidence, as shown in Fig. 3. The inundation area of the 50-years returns period increase by 39.8% in 2050. The results also show that the groundwater recharge could alleviate the severer future flood. The groundwater table increase by 0.1 m is expected to increase in flood inundation by 37.4%, or the flood inundation decrease by 1.8% compare to without intervention. The amount of groundwater recharge has a different impact on the flood inundation reduction. The groundwater table increase by 0.5 and 1.0 m are expected to decrease the future flood respectively by 6.8 and 13.8%. It indicates that the increase in groundwater table corresponds to the increase

Fig. 2 Comparison land subsidence rate each scenario

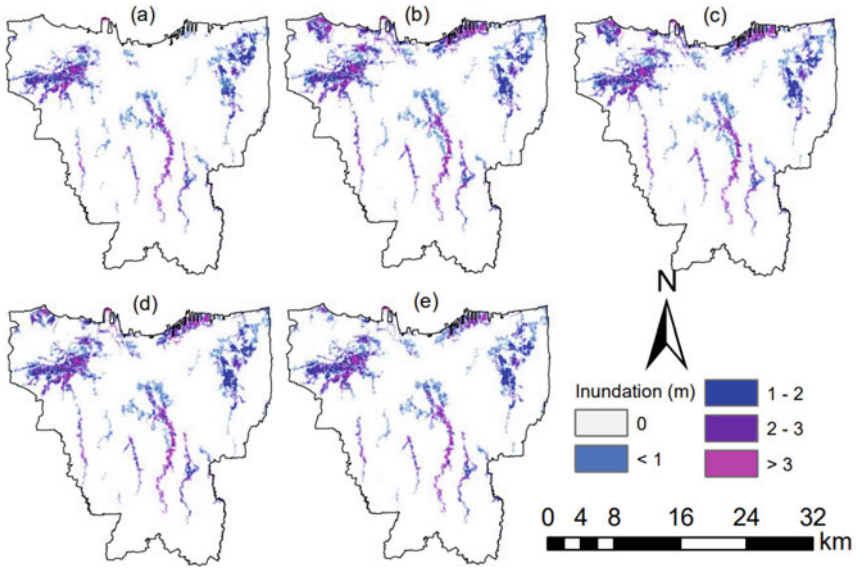
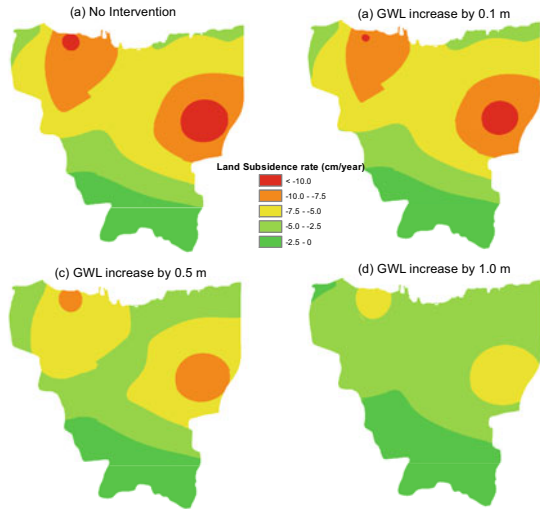


Fig. 3 Comparison spatial flood inundation of 50-years return period (a) represent the 50 year return period for current scenario, (b) represent the 50 year return period for 2050 projection scenario without land subsidence prevention, (c) represent the 50 year return period for 2050 projection scenario with 0.1-m water table increase (d) represent the 50 year return period for 2050 projection scenario with 0.5-m water table increase (e) represent the 50 year return period for 2050 projection scenario with 1-m water table increase

in flood inundation reduction, or each 0.1-m groundwater increase could decrease the inundation area of the 50-year return period by an average of 1.1 km².

Moreover, the evaluation of flood inundation was also conducted to compare the inundation depth. The results show that inundation areas with a depth of more than 2 m decrease significantly by 25.4% for a 1-m groundwater level increase. In comparison, the 0.5-m groundwater level increase could alleviate the flood inundation by 15.5%. It indicates that land subsidence prevention could alleviate the flood hazard in the area and the depth.

Furthermore, the flood damage costs are calculated to represent the flood risk in monetary terms. Figure 4 shows the comparison of flood damage costs in each scenario. The results portray that the percentage increase of flood damage costs is higher than the flood inundation. The flood damage costs of the 50-year return period increase by 54.6%, whereas the inundation increases by 39.8%. The results also show that the flood damage costs significantly increase for the higher probability (i.e., 2-year return period). The flood damage costs of the 2-year return period increase by 250% in 2050 due to uncontrolled land subsidence, whereas the flood damage costs of the 100-year return period increase by 51.0%. The flood damage costs reduction of high probability is higher compare to the lower probability. The 1.0-m groundwater level increase could decrease the 2-years flood damage by 35.9% while the reduction for the 100-year return period of 13.6%. It indicates that land subsidence prevention is more effective in reducing the high probable flood events.

In addition, expected annual damage costs (EADC) were calculated to evaluate each scenario's annual impact of flood hazard. The EADC value of Jakarta's present flood condition is approximately 168.5 million USD, whereas significantly

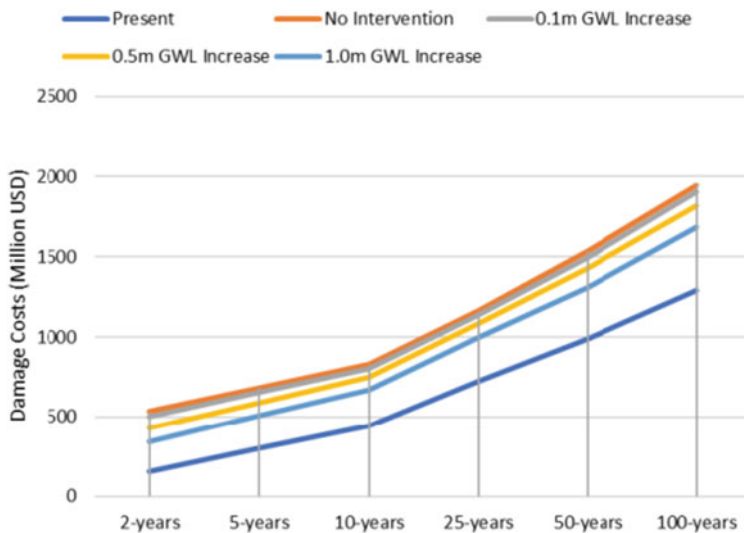


Fig. 4 Comparison flood damage costs each scenario

increased by 115.2% due to the uncontrolled land subsidence in 2050. The groundwater recharge scenarios could alleviate the future flood's annual impact by 24.2% for the 1-m groundwater level increase scenario. In comparison, the 0.1-m and 0.5-m groundwater increase could reduce the future flood risk by respectively 3.8% and 12.9%. The results show the land subsidence prevention succeeds in avoiding severer flood risk in the future.

5 Discussion

Januriyadi et al. (2020) evaluated the effectiveness of artificial recharge (i.e., Recharge Ponds and Recharge Wells) in reducing the flood risk. They found that recharge wells and recharge ponds could reduce the future flood risk by 5.6% and 33.2%, respectively. If we combine the direct and indirect benefits of artificial recharge, it can reduce flood risks.

Several scenarios of groundwater recharge were applied to evaluate the reduction of future flood risk in Jakarta. The results show that land subsidence prevention by slowing down land subsidence could decrease the severer future flood risk. The rate of land subsidence is associated with the groundwater table condition. Abidin et al. [1, 9] pointed out that groundwater over-extraction is one of the major factors of land subsidence in Jakarta. The land subsidence rate could be slowing down by increase the groundwater recharge. Shi et al. [24] show evidence that artificial groundwater recharge could reduce the land subsidence rate. The artificial recharge allows recharging more water into groundwater. The artificial recharge not only reduces flood risk by slowing land subsidence but also directly reducing flood risk by itself. Januriyadi et al. [25] evaluated the effectiveness of artificial recharge (i.e., Recharge Ponds and Recharge Wells) in reducing the flood risk. They found that recharge wells and recharge ponds could reduce the future flood risk by 5.6% and 33.2%, respectively. If we combine the direct and indirect benefits of artificial recharge, it can reduce flood risks.

Even though the artificial recharge, directly and indirectly, could reduce the flood risks. It also has some caveats that should be considered. The clogging and water quality problems are always found in the artificial recharge infrastructure. The clogging could reduce the infiltration rate, which also reduces the amount of groundwater recharging. The routine maintenance of artificial recharge infrastructure could be one of the solutions to solve the clogging problem. Another problem, the recharged water still bring some pollutant, which can contaminant the groundwater. The surface water should be treated before it is recharged into groundwater.

6 Summaries

This study evaluated the indirect benefit of artificial groundwater recharge to reduce the future flood risk in a port city. The flood inundation and damage costs models are conducted to obtain the spatial hazard map and flood damage costs. The study used three scenarios of groundwater recharge, which are indicated by the groundwater table increase. They are groundwater table increase by 0.1 m, 0.5 m, and 1.0 m. Based on the results, each scenario produces a distinct reduction in flood risk. Increasing the groundwater level by 1-m could avoid the severer future flood risk by 24.2%. In comparison, the increasing 0.1-m groundwater could decrease the future flood risk by 3.8%.

Our findings show that the land subsidence could amplify the future flood risk in a port, and we can reduce the future flood risk by slowing the land subsidence. Several options should be considered in reducing the land subsidence rate. The policymakers should consider not only reducing groundwater extraction but also increase the amount of groundwater. Besides, good maintenance and water treatment should include in one package in artificial recharge.

References

1. Abidin HZ et al (2001) Land subsidence of Jakarta (Indonesia) and its geodetic monitoring system. *Nat Hazards* 23(2):365–387. <https://doi.org/10.1023/A:1011144602064>
2. Aghai AK (2015) Survey of land subsidence – case study: the land subsidence formation in artificial recharge ponds at South hamadan power plant, Northwest of Iran. *J Earth Syst Sci* 124(1):261–268. <https://doi.org/10.1007/s12040-014-0532-y>
3. Aly MH, Klein AG, Zebker HA, Giardino JR (2012) Land subsidence in the Nile Delta of Egypt observed by persistent scatterer interferometry. *Remote Sens Lett* 3(7):621–630. <https://doi.org/10.1080/01431161.2011.652311>
4. Erban LE, Gorelick SM, Zebker HA (2014) Groundwater extraction, land subsidence, and sea-level rise in the Mekong Delta, Vietnam. *Environ Res Lett* 9(8):084010. <https://doi.org/10.1088/1748-9326/9/8/084010>
5. Feng Q, Liu G, Meng L, Fu E, Zhang H, Zhang K (2008) Land subsidence induced by groundwater extraction and building damage level assessment — a case study of Datun, China. *J China Univ Min Technol* 18(4):556–560. [https://doi.org/10.1016/S1006-1266\(08\)60293-X](https://doi.org/10.1016/S1006-1266(08)60293-X)
6. Gong H et al (2018) Long-term groundwater storage changes and land subsidence development in the North China Plain (1971–2015). *Hydrogeol J* 26(5):1417–1427. <https://doi.org/10.1007/s10040-018-1768-4>
7. Zhang Y et al (2015) Land subsidence and uplift due to long-term groundwater extraction and artificial recharge in Shanghai, China. *Hydrogeol J* 23(8):1851–1866. <https://doi.org/10.1007/s10040-015-1302-x>
8. Zhu L et al (2015) Land subsidence due to groundwater withdrawal in the Northern Beijing plain, China. *Eng Geol* 193:243–255. <https://doi.org/10.1016/j.enggeo.2015.04.020>
9. Abidin HZ, Andreas H, Gumilar I, Fukuda Y, Pohan YE, Deguchi T (2011) Land subsidence of Jakarta (Indonesia) and its relation with urban development. *Nat Hazards* 59(3):1753–1771. <https://doi.org/10.1007/s11069-011-9866-9>
10. Bakr M (2015) Influence of groundwater management on land subsidence in deltas: a Case study of Jakarta (Indonesia). *Water Resour Manag* 29(5):1541–1555. <https://doi.org/10.1007/s11269-014-0893-7>

11. Carisi F, Domeneghetti A, Gaeta MG, Castellarin A (2017) Is anthropogenic land subsidence a possible driver of riverine flood-hazard dynamics? A case study in Ravenna, Italy. *Hydrol Sci J* 62(15):2440–2455. <https://doi.org/10.1080/02626667.2017.1390315>
12. Moe I.R. et al. (2016) Effect of land subsidence on flood inundation in Jakarta, Indonesia. *J Jpn Soc Civ Eng Ser G Environ Res* 72(5):I_283-I_289. https://doi.org/10.2208/jscej.72.I_283.
13. Moe I.R. et al. (2017) Future projection of flood inundation considering land-use changes and land subsidence in Jakarta, Indonesia. *Hydrol Res Lett* 11(2):99–105. <https://doi.org/10.3178/hrl.11.99>
14. Rodolfo KS, Siringan FP (2006) Global sea-level rise is recognised, but flooding from anthropogenic land subsidence is ignored around northern Manila Bay, Philippines: global sea-level rise is recognised. *Disasters* 30(1):118–139. <https://doi.org/10.1111/j.1467-9523.2006.00310.x>
15. Bouwer H (2002) Artificial recharge of groundwater: hydrogeology and engineering. *Hydrogeol J* 10(1):121–142. <https://doi.org/10.1007/s10040-001-0182-4>
16. Eusuff MM, Lansey KE (2004) Optimal operation of artificial groundwater recharge systems considering water quality transformations. *Water Resour Manag* 18(4):379–405. <https://doi.org/10.1023/B:WARM.0000048486.46046.ee>
17. Hao Q, Shao J, Cui Y, Zhang Q, Huang L (2018) Optimization of groundwater artificial recharge systems using a genetic algorithm: a case study in Beijing, China. *Hydrogeol J* 26(5):1749–1761. <https://doi.org/10.1007/s10040-018-1781-7>
18. Kumar S, Bhadra BK, Paliwal R (2017) Evaluating the impact of artificial groundwater recharge structures using geo-spatial techniques in the hard-rock terrain of Rajasthan, India. *Environ Earth Sci* 76(17):613. <https://doi.org/10.1007/s12665-017-6953-6>
19. Pliakas F, Petalas C, Diamantis I, Kallioras A (2005) Modeling of groundwater artificial recharge by reactivating an old stream bed. *Water Resour Manag* 19(3):279–294. <https://doi.org/10.1007/s11269-005-3472-0>
20. Kure S, et al (2014) Several social factors contributing to floods and characteristics of the January 2013 flood in Jakarta, Indonesia. *J Jpn Soc Civ Eng Ser G Environ Res* 70(5):I_211-I_217 (2014). https://doi.org/10.2208/jscej.70.I_211
21. Moe IR, Kure S, Farid M, Udo K, Kazama S, Koshimura S (2016) Evaluation of flood inundation in Jakarta using flood inundation model calibrated by radar rainfall. *J Jpn Soc Civ Eng Ser B1 Hydraul Eng* 72(4):I_1243–I_1248. https://doi.org/10.2208/jscejhe.72.I_1243
22. Fajar Januriyadi N, Kazama S, Riyando Moe I, Kure S (2018) Evaluation of future flood risk in Asian megacities: a case study of Jakarta. *Hydrol Res Lett* 12(3):14–22. <https://doi.org/10.3178/hrl.12.14>.
23. MLIT (2018) The flood control economy investigation manual (proposed). Ministry of land, infrastructure, transport and tourism, 2005. Accessed 12 Jun 2018. http://www.mlit.go.jp/riss/ver/basic_info/seisa-ku_hyouka/gaiyou/hyouka/h1704/chisui.pdf
24. Shi X, Jiang S, Xu H, Jiang F, He Z, Wu J (2016) The effects of artificial recharge of groundwater on controlling land subsidence and its influence on groundwater quality and aquifer energy storage in Shanghai, China. *Environ Earth Sci* 75(3):195. <https://doi.org/10.1007/s12665-015-5019-x>
25. Januriyadi NF, Kazama S, Moe IR, Kure S (2020) Effectiveness of structural and nonstructural measures on the magnitude and uncertainty of future flood risks. *J Water Resour Prot* 12(5):5 (2020) <https://doi.org/10.4236/jwarp.2020.125024>

Removal of Naphthalene from Produced Water Using Oil Palm Leaves Waste Activated Carbon



Muhammad Raza Ul Mustafa, Hifsa Khurshid, Yeek-Chia Ho,
and Mohamed Hasnain Isa

Abstract The dissolved fractions of polycyclic aromatic hydrocarbons (PAHs) in wastewater have many adverse effects on humans, animals, and water species. The objective of this study is to study the removal of PAHs in produced water (PW) using oil palm leaves activated carbon (OPLAC). The OPLAC was applied for the degradation of naphthalene (NAP), one of the commonly found PAH, in aquatic solution and PW at various pH (3–9), dosage (100–3000 mg/L) and contact time (5–90 min). The parameters were optimized using response surface methodology (RSM). The optimum parameters were as follows: pH of 3, dosage of 2197 mg/L and contact time of 72 min giving removal efficiency of 92.48% in aquatic solution. The results were verified in the laboratory. The removal efficiency of NAP from PW sample was 70.5% at optimized parameters. It was closer to the experimental results with 19% difference.

Keywords Polycyclic aromatic hydrocarbons · Naphthalene · Produced water · Adsorption · RSM

M. R. Ul Mustafa · H. Khurshid (✉) · Y.-C. Ho
Department of Civil and Environmental Engineering, Universiti Teknologi PETRONAS, 32610
Seri Iskandar, Perak Darul Ridzuan, Malaysia
e-mail: hifsa_18002187@utp.edu.my

M. R. Ul Mustafa
e-mail: raza.mustafa@utp.edu.my

Y.-C. Ho
e-mail: yeekchia.ho@utp.edu.my

M. R. Ul Mustafa
Centre for Urban Resource Sustainability, Institute of Self-Sustainable Building, Universiti
Teknologi PETRONAS, 32610 Seri Iskandar, Malaysia

M. H. Isa
Civil Engineering Programme, Faculty of Engineering, Universiti Teknologi Brunei, Tungku
Highway, Gadong 1410, Brunei Darussalam
e-mail: Mohamed.isa@utb.edu.bn

1 Introduction

Oil is one of the world's primary energy sources, and its production is a critical issue. While oil is being produced, some negative environmental effects occur. One of the most significant sources of negative effects is produced water (PW), which is produced as wastewater during the oil production process [1]. The water is highly contaminated by polycyclic aromatic hydrocarbons (PAHs), salinity, heavy metals, radionuclides, and oilfield chemicals [2]. Numerous investigations have established that PAHs are the primary cause of PW's acute and chronic toxicity [3]. The PAHs include two or more fused aromatic rings of carbon and hydrogen atoms and have been classified as priority pollutants by the U.S. Environmental Protection Agency (USEPA) because of their prevalence and cancer-causing potential [4]. Therefore, it is essential to investigate economical and ecotechnological options for reducing PAHs from PW.

Adsorption is a widely used and efficient method for treating wastewater [5]. However, adsorption is quite material-dependent in terms of its effectiveness and cost. For the process of wastewater treatment, activated carbon (AC) is a renowned adsorbent [6]. Nowadays, attempts are made to replace commercially available AC with AC produced from biomass waste due to the necessity for inexpensive adsorbents [7]. The current study focused on the removal of PAHs in PW by using an AC synthesized by locally available oil palm leaves waste.

Malaysia is the leading exporter of palm oil on the global market, and the country alone produces almost 53 million tonnes of oil palm waste per year, with that quantity rising at a rate of 5% each year [8]. The utilization of oil palm waste as a precursor material for AC has been researched over the years. In wastewater, it has been utilized to adsorb a variety of organic and inorganic contaminants [9, 10]. However, very few research have documented the synthesis of AC utilizing waste oil palm leaves, which are widely accessible, and their use for PAHs adsorption in wastewater is also unexplored, particularly in PW.

This study focused on the application of AC using oil palm leaves waste in Malaysia for the treatment of PAHs in PW. Naphthalene (NAP) was chosen as representative PAH compound. It is one of the commonly found (USEPA priority) PAHs. The response surface methodology (RSM) was used to model the adsorption processes and optimize the parameters [11]. The removal of NAP, as the current study's target pollutants cannot only offer helpful information for NAP treatment but also be viewed as the main research approach for handling complex PAHs. To meet the objectives of sustainable development through waste management and water purification, this study will contribute to extending the application of largely available oil palm leaves waste, developing green materials, and treating abundantly found PAHs.

2 Materials and Methods

2.1 Materials

The zinc chloride (ZnCl_2) and Sigma-Aldrich Supelco analytical solid standard of NAP (C_{10}H_8 , mol. weight = 128.17 g/mol) was purchased from Avantis Laboratory Supply. The oil palm leaves waste was taken from FELCRA Berhad, Perak in Malaysia. The PW sample was collected from an oil and gas company operating in Southeast Asia

2.2 Characterization of PW

The NAP in PW was quantified using high performance liquid chromatography (HPLC). An inertsil ODS-P HPLC column ($5\ \mu\text{m}$, $250 \times 4.6\ \text{mm}$) and an ultraviolet (UV, 254 nm) detector were used. The injection volume was $20\ \mu\text{L}$ and column temperature was $40\ ^\circ\text{C}$. The quantified concentration of NAP in PW was $195 \pm 5\ \mu\text{g/L}$. The finding was consistent with past studies, in which a number of studies observed PAHs of PW in the range of $100\text{--}1000\ \mu\text{g/L}$ [3].

2.3 Oil Palm Leaves AC

The oil palm leaves AC was synthesized as our previous reported method [12]. Briefly, the leaves waste was chemically activated by ZnCl_2 (1:1) and pyrolyzed at $800\ ^\circ\text{C}$ using tube furnace. The obtained AC was named oil palm leaves AC (OPLAC) and stored for further use.

2.4 Adsorption Batch Experiments

The impact of initial pH of wastewater (3–9), dosage of OPLAC (100–3000 mg/L) and contact time (5–90 min) was analyzed through batch testing. The batch experiments were conducted on a hot plate with magnetic stirrer in a beaker. The aqueous solution was prepared at initial concentration of NAP as $200\ \mu\text{g/L}$, similar as obtained by the analysis of PW. The samples were placed for stirring (220 rpm at $25 \pm 5\ ^\circ\text{C}$). Following the completion of the stirring period, samples were removed, filtered using a 0.45 m syringe filter, and then analyzed using HPLC to determine the final amount of NAP.

2.5 Design of Experiments Using RSM and Application of OPLAC in PW

The RSM-based polynomial central composite design (CCD) in design expert (DE) software was used for the design of adsorption batch experiments. Adsorptive removal efficiency of NAP was taken as outputs. Initial pH of wastewater (3–9), dosage of OPLAC (100–3000 mg/L) and contact time (5–90 min) were taken as inputs. The design gave a total of 25 experimental runs (Table 1).

The experimental data collected through batch tests is represented in Table 1. Analysis of variance (ANOVA) was used to assess the suitability of the developed model. ANOVA also helps to assess the statistical significance of the constant regression coefficients. The obtained optimized parameters were confirmed in the lab. The optimized parameters were used to evaluate the removal efficiency of NAP in PW.

3 Results and Discussion

3.1 Batch Experiments Results

Figure 1 (a) shows the results of the percentage removal of NAP in wastewater using OPLAC, with a change in the initial pH value (3–9). The results showed that percentage removal of NAP in wastewater reduced from 72% to 65% ($\pm 2\%$) with an increase in pH from 3 to 6. A further increase in pH, from 7 to 9, slightly increased the NAP ($68 \pm 2\%$) removal. Hence, pH 3 was considered as optimum value for the removal of NAP using OPLAC. Similar results have been observed for removal of PAHs in wastewater, where pH of 2–3 was found as suitable pH for the adsorption of NAP using AC [13, 14]. Figure 1 (b) shows the plot between the removal efficiency of NAP and OPLAC dosage. The removal efficiency of PAHs increased with increasing dosage of OPLAC from 100 mg/L to 3000 mg/L due to increased amounts of available binding sites. The maximum adsorptive removal of NAP was $70.62 \pm 2\%$ around dosage of 3000 mg/L. The change in NAP removal efficiency at various contact times (5–90 min) is represented in Figure 1 (c). The removal of NAP considerably increased when the contact time increased from 0 to 5 min followed by a slower adsorption rate. Increasing the contact time further did not improve the removal capacity considerably. Hence, a contact time of 45 min was the optimal time for the removal of NAP. The maximum removal efficiency of NAP was $65.17 \pm 2\%$ at this contact time. Similar adsorption trend has been reported in other studies for PAHs removal [15].

Table 1 Experimental runs and outputs

Sr. No.	pH	Dosage (mg/L)	Contact time (min)	NAP Removal efficiency (%)
1	6	100	47.5	61.8
2	6	3000	47.5	70.6
3	3	3000	90.0	89.5
4	9	3000	5	85.6
5	6	1550	5	57.0
6	9	1550	47.5	68.6
7	9	100	5	84.7
8	6	1550	47.5	65.2
9	9	3000	5	44.8
10	9	100	90	25.7
11	6	1550	90	61.0
12	9	3000	90	48.3
13	3	100	5	36.3
14	3	3000	5	52.1
15	3	3000	90	50.4
16	3	3000	5	87.0
17	3	1550	47.5	72.5
18	3	100	90	89.0
19	6	1550	47.5	86.2
20	3	100	5	85.4
21	9	100	5	38.5
22	6	1550	47.5	59.7
23	3	100	90	35.3
24	9	3000	90	94.1
25	9	100	90	84.0

3.2 Modelling of RSM

A total 25 experimental runs were conducted as obtained by RSM in DOE software. Table 1 lists the performed runs and their experimental results. The findings of ANOVA show the validity of the used design as well as the relationships and relevance of variables. Table 2 shows that all parameters pH, dosage, and contact time significantly influenced the adsorption process. The Model F-value of 27.59 implied that the model was significant for adsorption of NAP onto OPLAC. There was only a 0.01% chance that an F-value this large could occur due to noise. A p-values less than 0.05 indicated that model terms were significant. The Predicted R2 of 0.8514

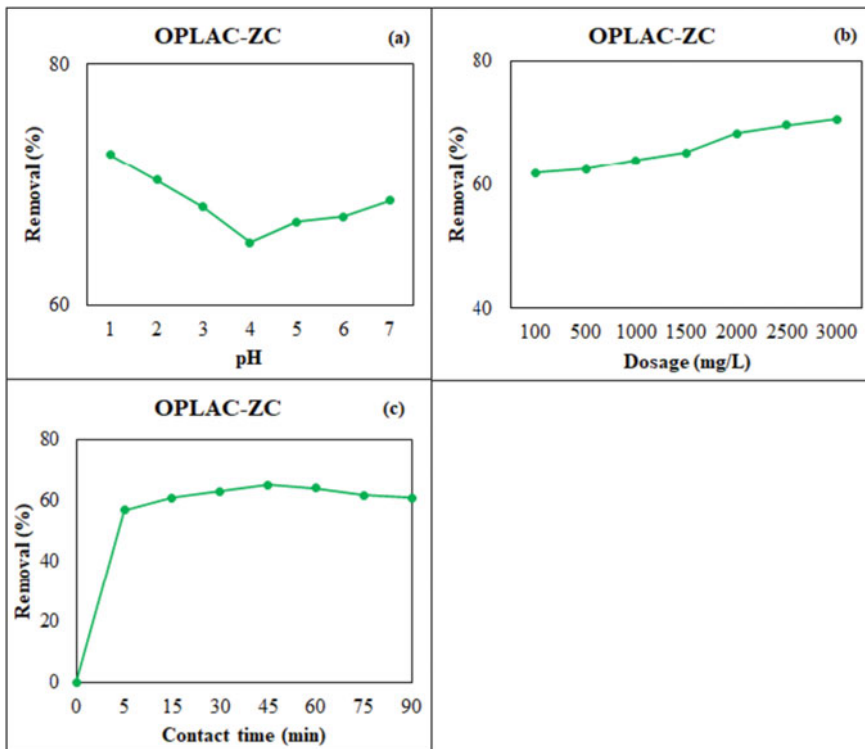


Fig. 1 Impact of pH, OPLAC dosage and contact time on adsorptive removal percentage of NAP

was in closer agreement with the Adjusted R2 of 0.9394. Adeq. Precision (AP) ratio should be greater than 4. Here ratio of 16.915 indicated an adequate signal for NAP.

3.3 3D Plots Describing Impact of Operating Variables on NAP Adsorptions

3D plots with various peak values and curves show how independent variables and their interactions affect the removal of NAP. In 3D plots, two independent variables were deliberately changed while the other independent variable was kept constant. Fig. 2 (a–c) indicate the 3-D plots on effects of pH, dosage and contact on NAP removal efficiency (%). Higher removal efficiency of NAP was observed at pH of 3 and 9 showing that increase in H⁺ and OH⁻ ions increased the electrostatic interactions between OPLAC and NAP. Increasing the dosage of OPLAC and increasing contact time until 45 min increased the removal efficiencies due to abundant available adsorption sites on OPLAC. Further increase in contact time did not increase the removal efficiencies due to saturation of OPLAC. It can be seen that the wastewater

Table 2 Statistical analysis using ANOVA for model validation

Source	SS	DF	MS	F-value	P-value
ANOVA for NAP					
Model	9529.46	14	680.68	27.59	<0.0001
A-pH	29.79	1	29.79	1.21	0.02975
B-Dosage	369.12	1	369.12	14.96	0.0031
C-Contact time	1.98	1	1.98	0.0801	0.0001
AB	2.94	1	2.94	0.1191	0.007371
AC	1.36	1	1.36	0.0551	0.008192
BC	35.54	1	35.54	1.44	0.02577
A ²	17.12	1	17.12	0.6938	0.04243
B ²	7.85	1	7.85	0.3184	0.05850
C ²	204.97	1	204.97	8.31	0.0163
Residual	246.68	10	24.67		
Model summary	R ² 0.9748	R ² _{adj} 0.939	R ² _{pred} 0.8514	AP 16.9149	CV 7.60%

pH did not significantly affect the removal efficiencies of NAP. Whereas dosage and contact time greatly affect the removal efficiencies.

To assess the adequacy of the selected models, two types of plots were chosen: predicted vs experimental values plot and normal plot of residual. Figures 2 (d) shows that model's anticipated and experimental responses were related. The plots revealed a good match between actual and experimental values. Furthermore, as shown in Figure 2 (e), the distribution of all data points was near to the 45° straight line.

3.4 Optimization and Application of OPLAC in PW

After ANOVA model validation, the RSM-based method of numerical optimization is frequently employed to identify the optimal values for each independent variable. The NAP removal efficiencies predicted by numerical optimization was 92.48%, using OPLAC. This removal efficiency was estimated at the wastewater pH of 3, dosage of OPLAC 2197 mg/L and contact time of 72 min. Additional tests were carried out utilizing the suggested optimal values of independent parameters to validate the optimal conditions and the complete model. The model's validity was confirmed by a small divergence between experimental and predicted outcomes under optimal conditions (Table 3).

The OPLAC was utilized to extract NAP from PW sample to confirm the applicability of the OPLAC. The PW sample was mixed with OPLAC at optimized parameters viz., pH (3), dosage (2197 mg/L) and contact time (72 min). Table 3 shows

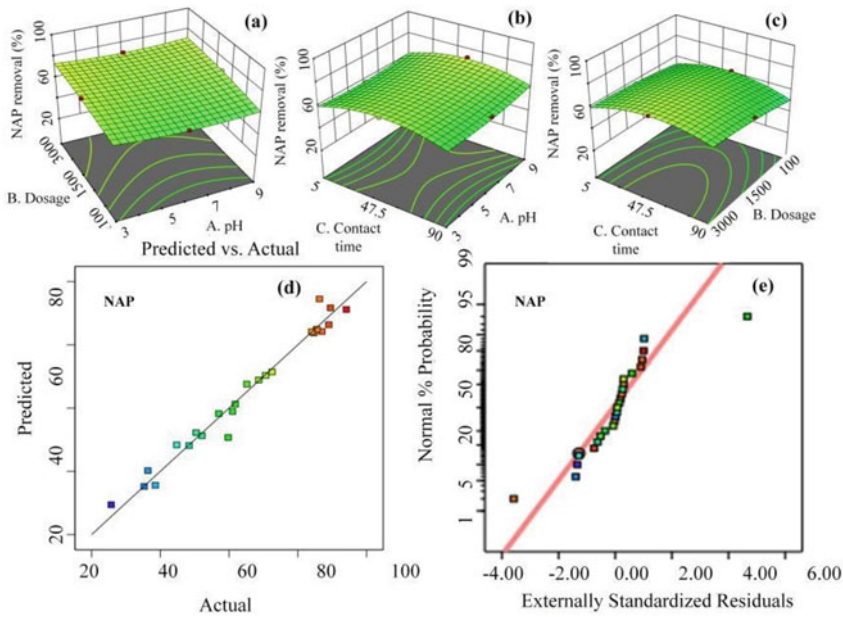


Fig. 2 Plot of (a) impact of pH, (b) impact of OPLAC dosage, (c) impact of contact time, (d) predicted vs actual removal (%) and (e) normal plots of residuals for removal of NAP

Table 3 Validation of optimized results

Material	Pollutant	Predicted Removal (%)	Experimental removal (%)	Removal in PW (%)
OPLAC	NAP	92.48	89.5	70.5

the effectiveness of NAP removal from PW sample. The removal efficiency of NAP from PW sample was closer to the experimental result with a 19% difference. It is evident that OPLAC was able to remove 70.5% NAP in PW. The lower removal of PAHs from PW compared to aqueous solution may be correlated to the presence of numerous other pollutants in PW [16].

4 Conclusion

The oil palm leaves AC (OPLAC) was efficiently applied for the removal of NAP in wastewater. The removal process was optimized by RSM, and the model was validated by ANOVA analysis. The model was significant (p -value < 0.05) to predict the adsorption process. The NAP removal efficiency predicted by numerical optimization was 92.48% at pH of 3, dosage of OPLAC 2197 mg/L and contact time of 72

min. The results were verified in the laboratory experiments. The removal efficiency of NAP from PW sample was closer to the experimental results (70.5%) with a 19% difference at optimized parameters.

Acknowledgements The authors acknowledge the financial support provided under FRGS grant with cost center 0153AB-L71 and YUTP grant with cost center 015LCO-190. The oil palm leaves waste provided for this study by FELCRA Berhad, Perak, Malaysia, is also acknowledged by the authors.

References

1. Al-Ghouti MA, Al-Kaabi MA, Ashfaq MY, Da'na DA (2019) Produced water characteristics, treatment and reuse: a review. *J Water Process Eng* 28:222–239. <https://doi.org/10.1016/j.jwpe.2019.02.001>
2. Lu J, Wang X, Shan B, Li X, Wang W (2006) Analysis of chemical compositions contributable to chemical oxygen demand (COD) of oilfield produced water. *Chemosphere* 62:322–331. <https://doi.org/10.1016/j.chemosphere.2005.04.033>
3. Haneef T, et al (2020) Removal of polycyclic aromatic hydrocarbons (PAHs) from produced water by Ferrate (VI) oxidation. *Water* 12:1–17. <https://doi.org/10.3390/w12113132>
4. Malakahmad A, Law MX, Ng KW, Manan TSA (2016) The fate and toxicity assessment of polycyclic aromatic hydrocarbons (PAHs) in water streams of Malaysia. *Procedia Eng* 148:806–811. <https://doi.org/10.1016/j.proeng.2016.06.572>
5. Khurshid H, Mustafa MRU, Isa MH (2022) A comprehensive insight on adsorption of polyaromatic hydrocarbons, chemical oxygen demand, pharmaceuticals, and chemical dyes in wastewaters using biowaste carbonaceous adsorbents. *Adsorpt Sci Technol* (2022). <https://doi.org/10.1155/2022/9410266>
6. Khurshid H, Mustafa MRU, Isa MH (2022) Adsorption of chromium, copper, lead and mercury ions from aqueous solution using bio and nano adsorbents: a review of recent trends in the application of AC, BC, nZVI and MXene. *Environ Res* 212:113138. <https://doi.org/10.1016/j.envres.2022.113138>
7. Zhou Y, Zhang L, Cheng Z (2015) Removal of organic pollutants from aqueous solution using agricultural wastes: a review. *J Mol Liq* 212:739–762. <https://doi.org/10.1016/j.molliq.2015.10.023>
8. Mohammed MAA, et al (2011) Hydrogen rich gas from oil palm biomass as a potential source of renewable energy in Malaysia. *Renew Sustain Energy Rev* 15:1258–1270. <https://doi.org/10.1016/j.rser.2010.10.003>
9. Sahu JN, Karri RR, Jayakumar NS (2021) Improvement in phenol adsorption capacity on eco-friendly biosorbent derived from waste palm-oil shells using optimized parametric modelling of isotherms and kinetics by differential evolution. *Ind Crops Prod* 164:113333. <https://doi.org/10.1016/j.indcrop.2021.113333>
10. Chew TL, Husni H (2019) Oil palm frond for the adsorption of Janus Green dye. *Mater Today Proc* 16:1766–1771. <https://doi.org/10.1016/j.matpr.2019.06.047>
11. Alhothali A, Khurshid H, Mustafa MRU, Moria KM, Rashid U, Bamasag OO (2022) Evaluation of contemporary computational techniques to optimize adsorption process for simultaneous removal of COD and TOC in wastewater. *Adsorpt Sci Technol* (2022). <https://doi.org/10.1155/2022/7874826>
12. Khurshid H, Mustafa MRU, Isa MH (2022) Modified activated carbon synthesized from oil palm leaves waste as a novel green adsorbent for chemical oxygen demand in produced water. *Sustainability* 14. <https://doi.org/10.3390/su14041986>

13. Balati A, Shahbazi A, Amini MM, Hashemi SH (2015) Adsorption of polycyclic aromatic hydrocarbons from wastewater by using silica-based organic–inorganic nano hybrid material. *J Water Reuse Desalin* 5:50–63. <https://doi.org/10.2166/wrd.2014.013>
14. Gupta H (2015) Removal of phenanthrene from water using activated carbon developed from orange rind. *Int J Sci Res Environ Sci* 3:248–255. <https://doi.org/10.12983/ijres-2015-p0248-0255>
15. Dai Y, Niu J, Yin L, Xu J, Xi Y (2011) Sorption of polycyclic aromatic hydrocarbons on electrospun nanofibrous membranes: sorption kinetics and mechanism. *J Hazard Mater* 192:1409–1417. <https://doi.org/10.1016/j.jhazmat.2011.06.055>
16. Godlewska P, Siatecka A, Kończak M, Oleszczuk P (2019) Adsorption capacity of phenanthrene and pyrene to engineered carbon-based adsorbents produced from sewage sludge or sewage sludge-biomass mixture in various gaseous conditions. *Bioresour Technol* 280:421–429. <https://doi.org/10.1016/j.biortech.2019.02.021>

Characterization and Potential Analysis of Paper Waste as Raw Material for Refuse Derived Fuel (RDF) Pellet Substitution



Nurulbaiti Listyendah Zahra, Intan Rahmalia, Fatimah Dinan Qonitan, I Wayan Koko Suryawan, and Ariyanti Sarwono

Abstract The city of West Jakarta, in the capital of Indonesia, produces paper waste in large quantities per year, approximately 60.74 tons of paper waste per day. Paper waste may have a high potential for energy recovery based on its characteristics and quantity. This study aims to compare the potential utilization of various types of paper waste as raw material for refuse-derived fuel (RDF) based on proximate analysis and their calorific value. Samples of paper waste of different types, including HVS paper, calendars, paperboard, baking paper, and newsprint, were collected from a temporary waste disposal site in West Jakarta. Samples were analyzed in a laboratory for proximate analysis, including the determination of water content, ash content, volatile matter content, fixed carbon content, and calorific value. Multiple linear regression is performed to determine variables that have a statistically significant correlation with the calorific value, then Technique for Order Preference by Similarity to Ideal Solution (TOPSIS) Method was used to determine the best type of paper waste. Results showed a regression model for determining the calorific value of paper waste based on its proximate variables with an F-test result of Sig. <0.05. Based on TOPSIS, newsprint waste was selected as highest potential among other types of paper waste, with a calorific value of 4,366.942 kcal/kg, water content of 7.87%, volatile content of 73.66%, fixed carbon of 16.85, and ash content of 2.75%.

Keywords Calorific value · Paper waste · Proximate analysis · Newsprint · Refusederived fuel

N. L. Zahra (✉) · I. Rahmalia · F. D. Qonitan · I. W. K. Suryawan · A. Sarwono
Environmental Engineering, Universitas Pertamina, DKI, Jakarta, Indonesia
e-mail: nurulbaiti.lz@universitaspertamina.ac.id

© Institute of Technology PETRONAS Sdn Bhd 2024
B. S. Mohammed et al. (eds.), *Proceedings of the International Conference on Emerging Smart Cities (ICESC2022)*, Lecture Notes in Civil Engineering 324,
https://doi.org/10.1007/978-981-99-1111-0_15

1 Introduction

Indonesia still needs a lot of waste treatment facilities, especially in urban areas [1–4]. Technological solutions to this waste problem have been widely applied, but no one has answered this problem definitively. This is because the improvement of the waste problem is not only from the technological aspect but also involves the socio-cultural aspects of the community. The public's willingness to sort waste would increase if they get financial incentives. The community who practiced waste sorting agrees that the unavailability of sufficient incentives or benefits makes it difficult for them to sort waste [5]. One interesting option is the conversion of waste into energy through thermal technology. The main principle is that the mass of waste is reduced, while the energy produced is a bonus. Public awareness related to environmental issues, especially those related to waste, and the perceived benefits positively impact public perception of waste to energy [6]. In addition, converting waste into energy can be a milestone that leads to the implementation of a circular economy [7]. Various technology offerings with promising claims, ranging from higher energy efficiency, more environmentally friendly installations, and so on, are not accompanied by sufficient comparative data on the scale of their implementation [8].

Indonesia's domestic waste has a low calorific value because of its high biodegradable organic composition [9]. If waste is to be converted into alternative energy, it is necessary to pre-treat the waste such as sorting it according to certain types of waste. Refuse-derived fuel (RDF) is an alternative fuel formed from a mixture of domestic waste separated between the flammable fraction and the non-combustible fraction from its generation [8]. RDF comprises flammable materials, namely household waste, paper, plastic, sewage sludge, and others [10].

The cement industry is one of the manufacturing industries in Indonesia that requires high energy consumption in its large-scale combustion system, which is 3,000–3,300 MJ per tonne of clinker [11]. According to Holcim Group Support Ltd & Deutsche GTZ (2006), much of this energy is obtained from heating coal as the main fuel [12]. Energy recovery efforts are needed through co-processing to reduce the use of coal. Co-processing is the use of waste as AFR (alternative fuel and raw material) in the form of Refused Derived Fuel (RDF) to replace some of the main fuel fuels used by the cement industry [9].

Based on the National Waste Management Information System (SIPSN) by the Ministry of Environment and Forestry of Indonesia (2020), the waste generation per person per day in the city of West Jakarta (0.81 kg/person/day) is the second largest in DKI Jakarta, after South Jakarta region (0.86 kg/person/day). With a population of 2,434,511, West Jakarta will produce 1,971.97 tons of waste/day [13]. It was the second largest, after the East Jakarta (Jakarta Timur) region (2,265.64 tons of waste/day) [13]. In West Jakarta, paper (3.08%) is the second largest amount of combustible materials waste after wood (5.78%) [13]. This means that around 60.74 tons of paper waste are produced per day in that region. With calorific values ranging from 2,598.95 kcal/kg to 4,129.48 kcal/kg [14–17], this large amount of paper waste

has the potential to be used as raw material for RDF, mainly to be implemented in the cement industry which has RDF calorific value standard around $\geq 3,000$ kcal/kg [9].

One of the temporary waste disposal sites (TPS) that accommodates domestic waste from the West Jakarta area is TPS RW 02 Duri Kosambi. The waste generated at TPS RW 02 Duri Kosambi includes inorganic waste of 300–350 kg/day, one of which is paper [18]. Paper waste in TPS RW 02 Duri Kosambi has been categorized according to its type from source and does not mix with other domestic waste. The categories of paper waste include white paper (HVS paper, calendars, paperboard, baking paper, and newsprint), packaging paper (duplex), magazine paper, and cardboard paper [18]. The calorific value test of various papers has been carried out in various studies, such as art cartons, art paper, kraft paper, baking paper, and cardboard [14–17]. However, there has been no research that has carried out a more complete characteristic test, including the proximate test and calorific value on more types of paper.

This study aims to analyze the potential utilization of 8 types of paper waste, which are HVS paper, calendars, paperboard, baking paper, newsprint, packaging paper (duplex), magazine paper, and cardboard paper, as raw material for RDF; analyze the correlation between variables that affect the calorific value of paper waste; and determine the type of paper that has the highest potential to be the raw material for RDF used in cement industry.

2 Methodology

This study analyzes the selection of paper waste as raw material for RDF based on the results of proximate testing and the calorific value of eight types of paper. The eight types of paper are HVS paper, newsprint, duplex paper, art paper, art carton paper, kraft paper, baking paper, and cardboard. In this study, paper waste was sourced from TPS RW 02 Duri Kosambi, West Jakarta, Indonesia. The proximate analysis explains the physical characteristics of paper as fuel, including moisture, ash, volatile, and fixed carbon content. Then, the paper is selected using the Technique for Order Preference by Similarity to Ideal Solution (TOPSIS).

2.1 Proximate and Calorific Value Test

The proximate test includes the measurement of water content, ash content, volatile matter content, and fixed carbon content [12].

Water Content. Water content is the large fraction of water in the material that evaporates when heated at temperatures up to 107 °C whose amount is expressed in the following Eq. 1.

$$\text{Water Content (\%)} = \frac{W - D}{W} \times 100\% \quad (1)$$

W = Sample weight (gr)

D = Weight of sample after heating (gr)

Ash Content. Ash content is the content of solid residue in the material left after heating at a temperature of up to 750 °C whose amount is expressed in Eq. 2.

$$\text{Ash Content (\%)} = \frac{R - C}{S} \times 100\% \quad (2)$$

R = Weight of the cup and solid residue left after combustion (gr)

C = Weight of empty cup (gr)

S = Sample weight (gr)

Volatile Matter Content. The volatile matter content is the fraction of waste material that disappears after heating at a temperature of 950 °C whose amount is stated in Eq. 3.

$$\text{Volatile Content (\%)} = \left[\frac{L - D}{D} \times 100\% \right] - R \quad (3)$$

L = Sample weight (gr)

D = Weight of sample after heating (gr)

Fixed Carbon Content. Fixed carbon content is the content of the RDF pellet material fraction in addition to water content, volatile matter content, and ash content, the amount of which is stated in the following Eq. 4.

$$\begin{aligned} \text{Fixed carbon content (\%)} = & 100\% - (\% \text{ moisture content} \\ & + \% \text{ volatile content} + \% \text{ ash content}) \end{aligned} \quad (4)$$

Calorific Value. The calorific value for RDF is tested using a bomb calorimeter based on the ASTM D-5865-04 standard and the dried basis (DB) test basis.

2.2 Statistical Analysis

Kolmogorov Smirnov Test. The Kolmogorov-Smirnov test is a statistical tool used to determine whether a sample comes from a population with a certain data distribution or follows a normal or tidal distribution. Then the interpretation is that if the value is above 0.05, then the data distribution is declared to meet the normality assumption. If the value is below 0.05, then it is interpreted as abnormal.

Durbin Watson Value. Where a good regression model is a regression that is free from autocorrelation, the basis for decision-making is if the Durbin Watson value is in the interval $1 < DW < 3$, it can be concluded that there is no autocorrelation [20].

Pearson Correlation. Pearson correlation is one of the correlation measures used to measure the strength and direction of the linear relationship between two variables [27, 28].

Multiple Linear Regression Analysis. The statistical technique for relating a set of two or more variables that is most commonly used is Multiple Linear Regression [21].

Analysis of Variance (ANOVA). Analysis of Variance (ANOVA) is one of the foremost applied statistical techniques to decide whether there are any statistically significant contrasts between the means of three or more independent (unrelated) groups. The necessity for ANOVA emerges from the error of alpha-level inflation. This increases the change of type 1 (false positive) errors, caused by multiple comparisons. ANOVA employs the measurement F, which is the proportion of the between-groups and the within-group variances. The main attentiveness of the analysis is focused on the differences in group means; nevertheless, ANOVA focuses on the difference in variances [34].

Decision Analysis. The method used to determine the best paper type as the raw material of RDF is the Technique for Order Preference by Similarity to Ideal Solution (TOPSIS). The TOPSIS method is an alternative selection method using weighting on the selection criteria to obtain a preference value for each choice [22]. This method was chosen because it can provide a systematic calculation model in building a multi-criteria decision support system. The chosen optimal alternative is the alternative that has the closest positive ideal solution and the farthest negative ideal solution [23]. The following are the calculation stages and the equations used in the TOPSIS analysis [9].

Decision Matrix

$$ij = \begin{bmatrix} X_{11} & \cdots & X_{1q} \\ \vdots & \ddots & \vdots \\ X_{p1} & \cdots & X_{pq} \end{bmatrix} \tag{5}$$

i = available alternative options (alternative 1, 2, 3, ..., p)
 j = criteria that become the reference for measuring each alternative (criteria 1, 2, 3, ... q)

Normalized Decision Matrix

$$R_{ij} = \frac{x_{ij}}{\sqrt{\sum_{i=1}^m x_{ij}^2}} \tag{6}$$

R_{ij} = Normalized Decision Matrix

X_{ij} = Decision Matrix

Weighted Normalized Decision Matrix

$$V_{ij} = W_j \times R_{ij} \tag{7}$$

V_{ij} = Weighted Normalized Decision Matrix

R_{ij} = Normalized Decision Matrix

W_j = Weight of each criterion 1 to q

Matrix of Positive Ideal Solution (S+) and Negative Ideal Solution (S-)

$$\begin{aligned} S^+ &= \{(\max V_{ij}) (\min V_{ij} | j \in J), i = 1, 2, 3, \dots p\} \\ &= V_{j^+} ; \{V_{1^+}, V_{2^+}, V_{3^+}, \dots V_{q^+}\} \end{aligned} \tag{8}$$

$$\begin{aligned} S^- &= \{(\max V_{ij}) (\min V_{ij} | j \in J), i = 1, 2, 3, \dots p\} \\ &= V_{j^-} ; \{V_{1^-}, V_{2^-}, V_{3^-}, \dots V_{q^-}\} \end{aligned} \tag{9}$$

Thus, the preference value is obtained through the following equation.

$$C_i = \frac{N_i^-}{N_i^- + N_i^+} \tag{10}$$

where $0 < C_i < 1$ = dan $i = 1, 2, 3, \dots p$

3 Results and Discussion

3.1 Proximate Analysis and Calorific Value Results

Paper waste is the second largest composition of municipal waste in major Indonesian cities, based on recent studies. In 2018, major cities in Indonesia including DKI Jakarta, Tangerang, Bekasi, Bandung, Semarang, Surakarta, Surabaya, Makassar, Denpasar, and Palembang, generated 0.69 kg/capita-day municipal solid waste consisting of 43.78% of food waste, 16.05% of paper, and 14.08% of plastics [6]. In this study, the raw material is paper waste from the West Jakarta administrative area. Based on data from the DKI Jakarta Environmental Agency (2020), the West Jakarta administrative area has a composition of 2.97% paper waste. One of the temporary waste disposal sites (TPS) that accommodates domestic waste from the West Jakarta area is TPS RW 02 Duri Kosambi. Daily, the waste disposal site collected 8–10 tons of domestic waste, which includes organic waste of 10 kg/day, inorganic waste of 300–350 kg/day, B3 waste of 3 kg/day, electronic waste of 1 kg/day and residue for

Table 1 Proximate test results and calorific value of 8 types of paper waste

Type of paper waste	Water content (%)	Volatile content (%)	Fixed carbon (%)	Ash content (%)	Calorific Value (kcal/kg)
HVS	5.66%	58.13%	24.34%	11.88%	3,219.802
Newsprint	7.87%	73.66%	16.85%	2.75%	4,366.942
Duplex	6.02%	61.51%	19.99%	12.47%	3,439.897
Art paper	3.81%	45.65%	25.98%	24.08%	2,551.544
Art carton	4.29%	50.53%	22.83%	22.84%	3,037.245
Kraft	6.96%	62.08%	20.53%	10.45%	3,645.106
Baking paper	6.74%	63.00%	19.80%	9.74%	3,705.25
Cardboard	7.47%	68.74%	18.65%	4.75%	3,789.285

final disposal. Paper-type waste in TPS RW 02 Duri Kosambi has been categorized according to its type from the source and does not mix with other domestic waste. The categories of paper waste include white paper (HVS paper, calendars, paper-board, baking paper, and newsprint), packaging paper (duplex), magazine paper, and cardboard paper.

Proximate analysis and calorific value of paper waste were carried out to identify the characteristics of eight types of paper and select one paper as raw material for RDF. Based on Table 1, newsprint has the highest calorific value, which is 4,366.942 kcal/kg. Meanwhile, art paper has the lowest calorific value, 2,551.544 kcal/kg. The high calorific value of newsprint is caused by the presence of carbon content from cellulose fibers with levels of 38.707–58.653% [24].

3.2 Correlation Between the Proximate Values with Calorific Value

Multiple Linear Regression analysis was conducted between variables to determine which variable affects the calorific value of paper waste and whether they can be used for estimation of the calorific value. Multiple regression analysis was conducted between the calorific value (kcal/kg) as response variable (Y) and the predictor variables: water content (X1), volatile content (X2), fixed carbon (X3), and ash content (X4).

Linearity Test. One of the most important assumptions for linear regression analysis is the linearity assumption. Scatterplots in Fig. 2 are used to visually determine whether there is any linear relationship between the variables. Based on Fig. 2, it was concluded that all proximate variables have a linear relationship with the calorific value, where it shows a positive linear relationship for water content (%) and volatile content (%), and a negative linear relationship for fixed carbon (%) and ash content



Fig. 1 Location of TPS RW 02 Duri Kosambi, West Jakarta, Indonesia [19]

(%). This linear relationship was further investigated using the Pearson Correlation test (Fig. 1).

Kolmogorov-Smirnov Test for Normality. One of the assumptions necessary for the linear regression analysis is the normality assumption. The Kolmogorov-Smirnov test for normality is a statistical tool used to determine whether a sample comes from a population with a certain data distribution or follows a normal distribution. The Kolmogorov-Smirnov Test is based on the largest discrepancy between a cumulative distribution that is empirical and one that is hypothetical [25]. For $\alpha = 0.05$, the interpretation is that if the value is above 0.05, then the data distribution is declared to meet the normality assumption. If the value is below 0.05, then the data failed to meet the normality assumption. The result of each variable is presented in Table 2. Overall, the *p-value* or *Asymp. Sig. (2-tailed) value* >0.05 for all variables, therefore all variables have successfully met the normality assumption.

Durbin-Watson Test for Autocorrelation. To determine whether a regression model's errors have autocorrelation, the Durbin-Watson statistic is used. The term autocorrelation refers to the correlation between neighboring observations' mistakes. Least-squares regression may overestimate the standard error of the coefficients if the errors are correlated. Autocorrelation can cause the predictors may appear to be significant when they are not due to under-estimated standard errors [26]. Table 3 shows the comparison table in the autocorrelation test. The value obtained from the calculation is 2.871. Where a good regression model is a regression that is free from autocorrelation, the basis for decision-making is if the Durbin Watson value is in the interval $1 < DW < 3$, it can be concluded that there is no autocorrelation. The *p-value* of the test also shows consistent results, with *Sig. F Change* value <0.05 .

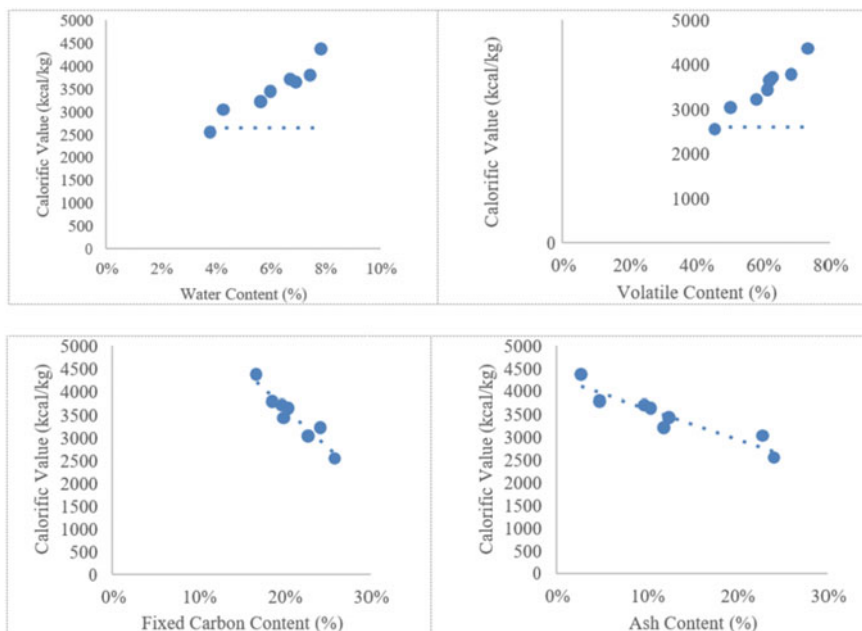


Fig. 2 Scatterplots showing linearity between all variables and the calorific value

Table 2 Results of Kolmogorov–Smirnov test for normality

Parameters		Calorific value	Water content	Volatile content	Fixed carbon	Ash content
Normal parameters ^{a,b}	Mean	0.061	0.604	0.211	0.124	3,469.384
	Std. deviation	0.015	0.091	0.030	0.076	545.998
Most extreme differences	Absolute	0.169	0.173	0.202	0.245	0.154
	Positive	0.143	0.138	0.202	0.245	0.154
	Negative	-0.169	-0.173	-0.105	-0.165	-0.126
Test statistic		0.169	0.173	0.202	0.245	0.154
Asymp. sig. (2-tailed)		0.200^{c,d}	0.200^{c,d}	0.200^{c,d}	0.174^c	0.200^{c,d}

Table 3 Results of the Durbin-Watson test for autocorrelation

R square	Adjusted R square	Std. the error in the estimate	Change statistics				Sig. F change	Durbin-Watson
			R square change	F change	df1	df2		
0.983	0.96	109.22	0.983	42.985	4	3	0.006	2.871

^aPredictors: (Constant), Water Content, Volatile Content, Fixed Carbon, and Ash Content; ^b Dependent Variable: calorific value

Pearson Correlation Analysis. Pearson correlation is one of the correlation measures used to measure the strength and direction of the linear relationship between two variables [27, 28]. The results are presented in Table 4. This case shows a positive relationship between water content and volatile content, while a negative relationship exists between fixed carbon content and ash content on calorific value. In addition, each proximate variable has a strong relationship with the other (Table 5).

Multiple Linear Regression Analysis. Multiple Linear Regression was employed to model the linear relationship between the calorific value (response variable) and proximate variables (water content, ash content, fixed carbon, and volatile content) as continuous predictors. The results of the regression analysis are presented in Table 5. Upon analyzing each variable, it was found that the regression model, represented by Equation 11, included all four variables (water content, ash content, fixed carbon, and volatile content) with p-values greater than 0.05. This indicates that none of these variables are statistically significant in influencing the calorific value. Consequently, the equation derived from the analysis cannot be applied to estimate the calorific value of paper waste in this study.

$$Y = -12988.38 + 359.39X_1 + 166.24X_2 + 107.12X_3 + 158.37X_4 \quad (11)$$

where Y = calorific value (kcal/kg); X₁ = Water Content (%); X₂ = Volatile Content (%); X₃ = Fixed Carbon (%); and X₄ = Ash Content (%).

A simultaneous test using ANOVA was performed to assess the impact of multiple independent variables on a single dependent variable. The decision criterion for the p-value is based on a significance level < 0.05. If the value is below this threshold, it indicates that the independent variables collectively have a simultaneous impact on the dependent variable (Table 6). This result implies that the set of independent variables, as formulated in the equation, has a simultaneous effect on determining the

Table 4 Pearson correlation analysis

Correlations		Calorific value	Water content	Volatile content	Fixed carbon	Ash content
Pearson correlation	Calorific value	1	0.956	0.975	-0.948	-0.931
	Water content	0.956	1	0.978	-0.898	-0.98
	Volatile content	0.975	0.978	1	-0.926	-0.981
	Fixed carbon	-0.948	-0.898	-0.926	1	0.847
	Ash content	-0.931	-0.98	-0.981	0.847	1
	calorific value		0	0	0	0
Sig (1-tailed)	Water content	0		0	0.001	0
	Volatile content	0	0		0	0
	Fixed carbon	0	0.001	0		0.004
	Ash content	0	0	0	0.004	

Table 5 Multiple regression analysis

Term	Coef	SE coef	95% CI	T-Value	P-Value	VIF
Constant	-12,988.38	8911	(-41,346, 15,369)	-1.46	0.241	
Water content	359.39	228	(-365, 1084)	1.58	0.212	64.63
Volatile content	166.24	79.5	(-86.7, 419.2)	2.09	0.128	305.28
Fixed carbon	107.12	101	(-214, 428)	1.06	0.366	55.14
Ash content	158.37	90.5	(-129.6, 446.3)	1.75	0.178	280.15

Table 6 Analysis of variance of the regression model

ANOVA	Sum of squares	df	Mean square	F	Sig.
Regression	2,051,007.094	4	512,751.773	42.985	0.006
Residual	35,785.95	3	11,928.65		
Total	2,086,793.043	7			

calorific value. However, it's important to note that despite the statistical significance, this equation lacks support from the predictive power of the variable model. In other words, while the independent variables jointly influence the dependent variable, the model may not adequately predict or explain the variations in the calorific value."

Besides, normal probability plots in this study were performed to identify substantive departures from normality, and partial plots are used to generate scatter diagrams of the residuals for the response variables. The results are shown in Fig. 3. The residual plot showed good consistency with the analysis of variance results.

3.3 Decision Analysis of Best Type of Paper Waste

In general, each type of paper has a similar pattern for water content, volatiles, fixed carbon, and ash [29–32]. The material with the highest calorific value is characterized by proximate characteristics with the lowest ash and moisture content and the highest volatile and fixed carbon content (Table 7).

The test results show that art paper has the highest ash content and low volatile content but the lowest water content and the highest fixed carbon content. Meanwhile, newsprint has the lowest ash content and the highest volatile content but has the highest moisture content and the lowest carbon remains. In this case, the paper's moisture content and fixed carbon content varied based on the theoretical review. The

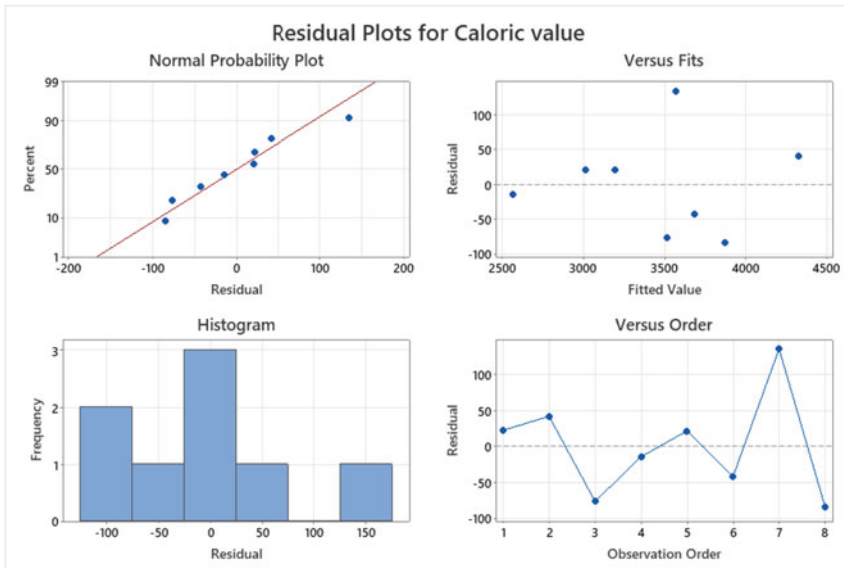


Fig. 3 Residual plots for the response variable

selection of one of eight types of paper was carried out through TOPSIS analysis. The choice of paper type is based on the results of the calorific value and paper proximate test results. The selection of alternatives is based on the criteria, the range of criteria, the weight of the criteria, and the score of each criterion.

The range of proximate values on paper selection criteria is based on SNI 8021-2014 [33], namely the standard for wood pellets. In addition, the division of 5 groups of values in the standard range of proximate value criteria is based on quartile calculations. The calorific value criteria for paper selection are based on SNI 8021-2014, EURITS, PT Semen Indonesia, and PT Indocement. The higher the score, the better the combustion ability and the best chance to be used as an RDF mixture. Meanwhile, the determination of the weight is based on the explanation in Table 7.

Co-processing uses waste as AFR (alternative fuel and raw material) in industrial processes that use large-scale combustion systems to replace some of the main fuels used. In this case, the industry that uses a large-scale combustion system is the cement industry. Based on the European Cement Research Academy (2017), calorific value, moisture content, and ash content are mandatory criteria needed to analyze RDF fuel before entering co-processing in cement kilns. The results of the heat analysis on the paper follow the literature, so the criterion weights 3 (Table 8).

In the analysis of the physical characteristics of the paper, it is found that the ash content of the paper is following the results of the calorific value so it is following the theory. However, the water content value on the paper does not support the calorific value produced, so the criteria vary based on the theoretical review. Therefore, the ash content criterion weights 3, and the water content criterion weights 2. A weight

Table 7 Paper selection criteria with TOPSIS method

Weight	Criteria	Criteria range	Score	Quality interval
3	Calorific value	>4000 kcal/kg	5	SNI 8021-2014 [33]
		4000–3600 kcal/kg	4	EURITS
		3600–3000 kcal/kg	3	PT Semen Indonesia
		3000–2500 kcal/kg	2	PT indocement
		<2500 kcal/kg	1	–
2	Water content (SNI <12%)	0%–2,5%	5	High
		2,5%–6%	4	
		6%–9,5%	3	
		9,5%–12%	2	
		>12%	1	Low
3	Ash content (SNI <8%)	0%–1,5%	5	High
		1,5%–4%	4	
		4%–6,5%	3	
		6,5%–8%	2	
		>8%	1	Low
2	Volatile content (SNI <80%)	0%–19,5%	1	Low
		19,5%–40%	2	
		40%–60,5%	3	
		60,5%–80%	4	
		>80%	5	High
1	Fixed carbon (SNI >14%)	<14%	1	Low
		14%–36%	2	
		36%–58%	3	
		58%–80%	4	
		80%–100%	5	High

of 2 is also applied to the opposite condition, namely the non-mandatory criteria in the RDF fuel analysis before entering co-processing in the cement kiln.

Furthermore, a weight of 1 is given a non-mandatory criterion in the analysis of RDF fuel before entering co-processing in the cement kiln and has the results of the analysis of criteria experiencing variations based on the theoretical review, namely the fixed carbon criteria. Furthermore, the TOPSIS matrix analysis method uses Eqs. 5–10. Thus, one type of paper is selected based on its preference value (Table 9).

Based on the analysis of paper selection using the TOPSIS method, newsprint is the paper with the largest preference value is 0.9. Therefore, the preference value is generated from a largely negative and a small positive separation value. This means that newsprints can produce solutions that are far from the ideal solution that

Table 8 Weighting criteria for TOPSIS method

Weight	Priority level	Information
1	Low	Not a mandatory criterion in the analysis of RDF fuel before entering co-processing in a cement kiln, and the results of the criteria analysis vary based on the theoretical review
2	Moderate	Mandatory criteria in the analysis of RDF fuel before entering co-processing in a cement kiln and the results of the analysis of criteria vary based on the theoretical review or Not a mandatory criterion in the analysis of RDF fuel before entering co-processing in a cement kiln and the results of the analysis of the criteria are following the theory
3	Important	The mandatory criteria in the analysis of RDF fuel before entering the co-processing of the cement kiln and the results of the analysis of the criteria are following the theory

Table 9 Weight of paper selection criteria with TOPSIS method

Type of Paper Waste	C
HVS	0.17
Newsprint	0.90
Duplex	0.17
Art Paper	0.10
Art Carton	0.17
Kraft	0.27
Baking Paper	0.66
Cardboard	0.27

is negative and close to the positive ideal solution. The positive ideal solution is meant as a good combustion capability. Meanwhile, the negative ideal solution is the opposite condition.

4 Conclusion

There are 8 (eight) categories of paper waste examined in this study, including HVS paper, newsprint, duplex paper, art paper, art carton paper, kraft paper, baking paper, and cardboard. The material with the highest calorific value is characterized by proximate characteristics with the lowest ash and moisture content and the highest volatile and fixed carbon content. Based on all categories, newsprint waste has the highest calorific value, which is 4,366.942 kcal/kg. Meanwhile, art paper has the lowest calorific value, which is 2,551.544 kcal/kg.

Multiple linear regression analysis resulted a linear model with an F-test of Sig. < 0.05 between the proximate variables and calorific value. The equation concluded that all proximate variables affected the calorific value of paper waste, and their values can be used for estimation of the calorific value. The regression model for determining the calorific value of paper waste is as follows:

$$Y = -12988.38 + 359.39X_1 + 166.24X_2 + 107.12X_3 + 158.37X_4$$

where Y = calorific value (kcal/kg); X_1 = Water Content (%); X_2 = Volatile Content (%); X_3 = Fixed Carbon (%); and X_4 = Ash Content (%).

Decision analysis was conducted to determine the best type of paper waste for utilization as raw material for refuse-derived fuel in cement industries using the Technique for Order Preference by Similarity to Ideal Solution (TOPSIS) method. The decision analysis concluded that newsprint waste has the highest potential for refuse-derived fuel utilization. Newsprint waste has a calorific value of 4,366.942 kcal/kg, water content of 7.87%, volatile content of 73.66%, fixed carbon of 16.85, and ash content of 2.75%.

Acknowledgements This work is supported by the UPer-UTP (Universitas Pertamina – Universiti Teknologi Petronas) Research Grant. We gratefully thank both institutions for their financial support during the research and publication of this paper.

References

1. Amir M, Anto RP (2018) A study policy implementation of waste management in Konawe regency-Indonesia. *J Sustain Dev* 11(1): 90
2. Bao PN, Abfertiawan MS, Kumar P, Hakim MF (2020) Challenges and opportunities for septage management in the urban areas of Indonesia – a case study in Bandung City. *J Eng Technol Sci* 52(4):481–500
3. Yuniastuti E, Hasibuan HS (2019) Green open space, towards a child-friendly city (a case study in Lembah Gurame Park, Depok City, Jakarta Greater Area, Indonesia). *IOP Conf Ser Earth Environ Sci* 328
4. Wijaya IMW, Sari NK, Yenis I (2021) Potential of energy municipal solid waste (MSW) to become refuse derived fuel (RDF) in Bali Province, Indonesia. *J Bahan Alam Terbarukan* 10(200):9–15
5. Sarwono A, et al (2021) Refuse derived fuel for energy recovery by thermal processes. A case study in Depok City, Indonesia. *J Adv Res Fluid Mech Therm Sci* 88(1):12–23
6. Qonitan FD, Suryawan IWK, Rahman A (2021) Overview of municipal solid waste generation and energy utilization potential in major cities of Indonesia. *J Phys Conf Ser* 1858(1)
7. Porshnov D, Ozols V, Ansone-Bertina L, Burlakovs J, Klavins M (2018) Thermal decomposition study of major refuse derived fuel components. *Energy Procedia* 147:48–53. <https://doi.org/10.1016/j.egypro.2018.07.032>
8. Pranolo SH, Muzayanha SU, Yudha CS (2017) Kajian Konsumsi Energi Spesifik Sektor Industri Kimia Di Indonesia Sebagai Acuan Efisiensi Energi 48–55

9. Mardiana G, Mahardika R (2010) Pemanfaatan limbah biomass sebagai bahan bakar alternatif dalam kegiatan co-processing di semen gresik. *Semin Rekayasa Kim dan Proses* 3:1–6
10. Gulyurtlu I, Pinto F, Abelha P, Lopes H, Crujeira AT (2013) 9 - Pollutant emissions and their control in fluidised bed combustion and gasification. In: Scala G. (ed.) *Woodhead publishing series in energy*. Woodhead Publishing, pp 435–480
11. Axegård P (2019) The effect of the transition from elemental chlorine bleaching to chlorinedioxide bleaching in the pulp industry on the formation of PCDD/Fs. *Chemosphere* 236:124386
12. Tchobanoglous G, Vigil SA (1993) *Integrated solid waste management engineering principles and management*. McGraw-Hill, New York
13. Kementerian Lingkungan Hidup dan Kehutanan. <http://sipsn.menlhk.go.id>. Accessed 2021
14. Tchobanoglous G, Theisen H, Samuel V (1993) *Integrated solid waste management: engineering principles and management issues*. McGraw-Hill B. Co, pp 83–91
15. Erdinciler AU (1993) Energy recovery from mixed paper waste. *Waste Manag Res*
16. Novita DM, Damanhuri E (2009) Perhitungan Nilai Kalor Berdasarkan Komposisi dan Karakteristik Sampah Perkotaan di Indonesia dalam Konsep Waste To Energy. *J Tek Lingkungan* 16(2):103–114
17. Pasek AD, Gultom KW, Suwono A (2013) Feasibility of recovering energy from municipal solid waste to generate electricity. *J Eng Technol Sci* 45(3):241–256
18. Dinas Lingkungan Hidup Provinsi DKI Jakarta (2017) *Timbulan, Komposisi, dan Karakteristik Sampah di TPS dan TPST Bantar Gebang*. In: D. L. Jakarta, Keputusan Kepala Dinas Lingkungan Hidup Provinsi Daerah Khusus Ibukota Jakarta. Dinas Lingkungan Hidup Provinsi DKI Jakarta, DKI Jakarta, pp 1–4
19. Google Map. <https://www.google.com/maps/place/>. Accessed 2021
20. Natanael Y, Sufren (2014) *Belajar otodidak SPSS pasti bisa*. PT. Elex Media Komputindo, Jakarta
21. Jobson JD (1991) *Multiple linear regression BT - applied multivariate data analysis: regression and experimental design*. Springer, New York, pp 219–398
22. Susanto F, Informatika PT, Utara L, Sherly A, Sari N, Salim A (2018) *Sistem Pendukung Keputusan Dalam Menentukan Kualitas Jambu Biji Unggulan Menggunakan Metode Weighted Product*, vol 01
23. Sari RE (2015) *Pemilihan Alternatif Kualitas Terbaik Kayu untuk Kerajinan Meubel dengan Metode TOPSIS*. *Semin Nas Inform* 1:211–216
24. Hidayati S, Zuidar AS, Widyastuti R (2018) *Pemutihan Kertas Koran Bekas dengan Menggunakan Asam Peroksida dalam Media Asam Asetat*. *Agrointek* 12(1):29
25. Massey FJ (1951) The Kolmogorov-Smirnov test for goodness of fit. *J Am Stat Assoc* 46(253):68–78
26. Alonso MJ, et al (2022) Evaluation of low-cost formaldehyde sensors calibration. *Build Environ* 109–380
27. KokoIW, et al (2022) Effect of sludge sewage quality on heating value: a case study in Jakarta, Indonesia. *Desalin Water Treat* 28071:1–8
28. Akoglu H (2018) User's guide to correlation coefficients. *Turk J Emerg Med* 18(3), 91–93
29. Suryawan IWK et al (2022) Pelletizing of various municipal solid waste: effect of hardness and density into calorific value. *Ecol Eng Environ Technol* 23(2):122–128
30. Sari MM, et al (2022) Identification of face mask waste generation and processing in tourist areas with thermo-chemical process. *Arch Environ Prot* 48(2)
31. Zahra NL et al (2022) Substitution garden and polyethylene terephthalate (PET) plastic waste as refused derived fuel (RDF). *Int J Renew Energy Dev* 11(2):523–532
32. Suryawan IWK et al (2022) Municipal solid waste to energy: palletization of paper and garden waste into refuse derived fuel. *J Ecol Eng* 23(4):64–74
33. Badan Standarisasi Nasional (2014) SNI 8021:2014. *Standar, Pelet Kayu*. Badan Standarisasi Nasional, Jakarta
34. Kim (2017) Understanding one-way ANOVA using conceptual figures. *Korean J Anesthesiol* 70(1):22–26

The Perception of Vertical Holiness in Development of Multilevel Infrastructure As an Effort for Environmental Conservation and Preventing Transfer of Land Conversion



I Made Sastra Wibawa, Shinta Enggar Maharani, Krisna Kurniari, and I. Kadek Ardi Putra

Abstract The increase in population requires the availability of residential locations that are increasing as well. Horizontal development results in land- use change, while the concept of Bali vertical development has been rejected by some due to discomfort when passing through the lower floors of high- rise infrastructure. This feeling arises because there are activities of people on the top floor so that they feel stepped on. The cause of feeling *cemer/leleh* is because the vertical limit of purity has not been understood as a limit that causes you to no longer feel *cemer/leleh*. This study aims to demonstrate the link between vertical sanctity and multilevel infrastructure design to curb land conversion and protect the environment. The method used is interviews and filling out questionnaires by stakeholders in order to obtain a relationship between vertical sanctity and multilevel infrastructure design. The results of this study are interrelated and indicate that communities embrace the sacred vertical distance of sanctity that must be applied when designing multilevel infrastructure. This concept is expected to be accepted by the global and in- ternational community.

Keywords multilevel infrastructure · vertical sanctity · environmental preservation · land conversion

I. M. S. Wibawa (✉) · K. Kurniari
Prodi Teknik Sipil, Fakultas Teknik, Universitas Mahasaraswati Denpasar, Bali, Indonesia
e-mail: sastrawibawa@unmas.ac.id

K. Kurniari
e-mail: krisnakurniari@unmas.ac.id

S. E. Maharani · I. K. A. Putra
Fakultas Teknik, Prodi Teknik Lingkungan, Universitas Mahasaraswati Denpasar, Bali, Indonesia
e-mail: shintamaharani@unmas.ac.id

I. K. A. Putra
e-mail: ikadekardiputra@unmas.ac.id

1 Introduction

The people of the island of Bali have always rejected the existence of flyovers and flats. The permitted building height is 15 m high, equivalent to a four-level building. The rapid development of the number of local residents as well as the existence of urbanization and the arrival of residents from other areas requires the provision of housing which is also increasing. Developments in other fields, especially in the economic sector, also require infrastructure that is capable of serving and has good quality. The construction of new settlements requires the support of public facilities, especially transportation infrastructure and other activities that will require new land. This new land use often takes land that was previously designated for reforestation or agricultural or plantation land. This new land use is often referred to as land conversion.

If the new land use can follow the rules that have been set, then the conversion of land use does not create new problems. The new problem in question is using dry land that is less productive. Due to the compulsion to use agricultural or plantation land, the condition of land conversion causes environmental problems that can threaten the sustainability of nature. In this case, consistency in complying with spatial planning regulations will be very much needed, so that development that adheres to legality and maintains environmental sustainability is achieved. The serious problem faced is the unbalanced distribution of economic activity, causing an imbalance in the distribution of the population. When the economic sector is concentrated in an area, residential areas will also be focused around that area. This happens because of efficiency in various ways and often leads to violations of existing spatial arrangements, for example: an area that has been designated by regulations as a green open area is often violated as a residential area or industrial area. This condition can be said to be a land use change that does not pay attention to environmental sustainability.

Efforts to preserve the environment often fail due to activities that violate the legality of spatial planning or the intentional change of an open green area into a residential location. Agricultural areas and green open areas are part of the lungs of the world which are proven to be able to produce oxygen for the needs of living things on Earth. As long as the infrastructure development policy only relies on the horizontal direction, there will forever be an effort to change the function of this land, so that efforts to preserve the environment will fail.

A serious effort to prevent land use change is to minimize development efforts in a horizontal direction and infrastructure development should be more in a vertical direction. If it is constrained by the legality that limits the construction of a building to a maximum height of 15 m [1], it may be possible to conduct a more in-depth study. Doubts about entering under multilevel buildings are often an obstacle because some people feel un-sanctity when passing in lower-floor buildings. To implement something new, we will definitely face considerable challenges, especially regarding the complexity of the problems that must be studied. But if it is for the good, especially in an effort to prevent land conversion and the desire to preserve the environment, it is very necessary to propose. In accordance with this description, a more in-depth

and specific study of infrastructure development efforts in a vertical direction is very necessary.

Based on the description of the background, which is the main subject of the discussion above, the problem statement can be formulated as follows. What are the challenges in implementing multilevel infrastructure development? and 2). What is the community's view on multilevel infrastructure development to maintain environmental sustainability and minimize land use change?

To answer the problems that become problematic from this topic, in general the objectives of infrastructure development are not in the same plane, namely: 1). To find out the things that are obstacles in multilevel infrastructure development efforts. 2). Knowing people's opinions about multilevel infrastructure development in an effort to preserve the environment and reduce land conversion.

2 Multilevel Infrastructure

Developments in various sectors require adequate infrastructure support, because all activities will run smoothly if the infrastructure is able to support all activities carried out. Building infrastructure and transportation infrastructure have a very important role to support the smooth running of all activities. If the building is not able to accommodate workers who carry out activities, this condition will cause disruption of business productivity. Inadequate transportation infrastructure can cause congestion and can interfere with performance which in turn causes delays in production and delivery of products. Infrastructure development which is always carried out in a horizontal direction causes the land supply to be depleted and the price to be higher, in addition to opening up opportunities for land conversion and the risk of environmental damage. With these problems, a solution is needed as a solution and does not cause new problems. According to [2], conducting a study in Malaysia focused on providing affordable housing throughout the country, as an effort to overcome the problem of increasing ownership costs due to the economic crisis and limited land.

The occurrence of the transfer of land functions from agriculture to settlements, can also cause a lack of oxygen (O₂) supply. Plants as carbon dioxide (CO₂) absorbers and produce oxygen are now starting to decrease in existence. This situation causes metabolic needs to be disrupted. In the European Union it is reported that building efficiency can reduce CO₂ emissions significantly [3]. Therefore, it is very appropriate to have a program to reduce the conversion of green land into settlements and offices.

2.1 Vertical Sanctity in a Space

The existence of an un-sanctity to pass through to the lower floor in Bali, can be answered by the existence of a vertical sanctity that has limits. Vertical sanctity is the

distance or height from the lower floor to the lowest elevation of the building above it (ceiling). An understanding of the existence of this vertical sanctity can answer so that we no longer feel un-sanctity if enter the lower floor of a multilevel building. The limit of vertical sanctity as stated in the *Lontar* as a highly sacred library in Bali is *dua dasa Guli* [4], *Lontar Purwaka weda*, and [5], *Lontar Surya Sewana*. *Dua dasa Guli* comes from the word *dua dasa* which means twelve, and *Guli* is a unit of the *Balinese Hindu Gegulak* tradition which is the length of the middle segment of the index finger (about 2,5 cm). Thus *dua dasa Guli* is equal to 2,5 times twelve equals 30 cm, this is measured from the top of the head (the crown). Thus, the distance of 30 cm from the top of our heads should not be disturbed, or if the height of the building above the head is more than 30 cm, then there is no violation of vertical sanctity. Another *Lontar* which contains vertical sanctity is the *Lontar Swamandala* which contains the limit of vertical sanctity as high as one *Hasta* [6]. The length of the arm from the elbow to the tip of the finger is called one *Hasta*, or an average of 40 cm. Likewise *Lontar Asta Kosala-Kosali* contains the limit of sanctity from the bottom floor is *Adepe Ngadeg* [7]. *Adepe Ngadeg* is the size of a human standing with his arms stretched up, so if we look above the head it is the same as one arm, so that vertical holiness on this *Lontar* is equal to 40 cm. Four *Lontars* that regulate the height of vertical sanctity, all of them are close to 30 cm to 40 cm, so we take the longest distance, i.e. 40 cm.

2.2 Vertical Sanctity According to Balinese Cultural Values

Vertical sanctity in Balinese culture is a local wisdom that must be maintained and preserved because it comes from the religious philosophy of the cosmos which is inspired by Hinduism. The Hindu community believes that this cosmic religion is able to harmonize the relationship between the psyche and the mortal world through symbols as a form of relationship between the macro and micro cosmos. The two are considered to be always different but still related to influence each other to form a unity of *Rwa Bhineda* (dualistic). The human body as a whole is described as a micro cosmos which is distinguished from the universe as a macro cosmos [8].

Humans as micro cosmos are also in Bali called *Bhuana Alit* in their various activities in the macro cosmos or also called *Bhuana Agung* [9]. These two forms must establish harmony in order for harmony to occur. Infrastructure development that is not on a plot should also create a sense of security, comfort for residents and users. The harmony of the multilevel infrastructure that is built must meet the requirements for the height of vertical sanctity so that residents and users do not have any doubts.

2.3 *The Dynamics of Multilevel Infrastructure*

Civil infrastructure is a basic physical need for organizing a structural system to ensure that the economy can function properly [10]. Civil is meant in this case is a branch of engineering that studies how to design, build, renovate, not only buildings and infrastructure, but also includes environmental sustainability.

The dynamics or development of multilevel infrastructure in Bali can be said to be very slow, caused by the existence of local wisdom that limits the existence of vertical sanctity. According to [11], who conducted a study on the intersection area that aims to overcome major conflicts such as collisions, vehicle maneuvers, and others, called the Rotary Method. The result is that a large area of land is required for design planning in the intersection area. For Bali this is contrary to land use that can threaten environmental sustainability. Therefore, the suggestion that can be done is to make a multilevel intersection.

The obstacle faced in building infrastructure is not on the same level as thermal comfort. To achieve thermal comfort in urban areas, a vertical greening system is implemented that is affixed to the walls of the building, so as to reduce heat stress because the walls are green and save land use [12].

The operation of the Trans Sarbagita Bus (Transport Denpasar, Badung, Gianyar, and Tabanan) being constrained by the lack of existing facilities, especially on feeder vehicles, this also cannot solve the problem because when there is traffic jams, this vehicles is also stuck in congestion [13]. Likewise, the Trans Metro Dewata Bus which is currently operating has not received a response from the public due to inadequate feeder vehicles. A study conducted by [14], who conducted a study under the flyover in Kuala Lumpur, Malaysia, where at two different locations that were used as a place of study according to his observations that there was a very large chance and possibility that the space under the flyover which they call the remaining space can be given to the surrounding community. Its purpose is to develop its activities such as: opening cafes, food stalls, and recreational activities, as well as business and weekly activities or activities that are not permanent in nature.

Another studied by [15], who conducted a study at the intersection of road traffic modeling which is a very interesting field for interdisciplinary study. The modeling carried out is based on the cellular automat approach and observations of vehicle movement. From the results presented according to the model's observations that one can only observe quantitative, not qualitative differences, and light-controlled junctions start to be the most efficient. Research [16], conducted a study on driver behavior, a study with the theme of traffic conflict was carried out by adopting statistical methods to determine the weight of driver behavior. This study shows that driving behavior incorporating intersection characteristics is helpful in explaining traffic performance at intersections.

The views of the Balinese people in general in building infrastructure are sacred - un-sanctity, *hulu - teben*, up - down, and the direction of the wind that is guided by the mountains and the sea. Something that is categorized as un-sanctity will occupy a location at the bottom, south, and leads to the sea. This is for example: the location

of the cemetery, the location of animal cages, the location of garbage disposal sites, and so on [17].

2.4 *Environmental Sustainability and Land Conversion*

In the context of multilevel infrastructure, if development in a horizontal direction can be reduced, it means reducing the use of new land which has an impact on preserving nature and reducing land conversion. Non-level infrastructure or non-rise buildings are buildings that have a minimum of two floors with different elevations. According to [10], non-level infrastructure is classified as civil infrastructure whose physical arrangement of the structural system is well guaranteed. Because it is under the organization of Civil Engineering, it is certain that the infrastructure created also regulates ensuring environmental sustainability. With the existence of local geniuses such as: vertical sanctity, *Tri Angga, Hulu – Teben*, and others, the development of infrastructure that is not on a plot in Bali is rather slow, in addition to the limitation of building height, which is a maximum of four floors, as stated in the Bali Provincial Regulation No. 16 of 2009, [1]. The limited land available compared to the rapid development of the population, of course, requires the right solution so that land conversion does not often occur that threatens environmental sustainability. Efforts to develop non-universal infrastructure are a very bright idea to develop, especially in densely populated areas. In Bali, Denpasar and Mangupura City, especially the Kuta area, need serious attention, so that agricultural areas and mangrove forests are not converted into settlements or other infrastructure. A further problem that often arises in non-level infrastructure, especially high-rise buildings, is the occurrence of disturbed thermal comfort, this problem can be overcome by making vertical greenery, potted plants attached to the wall so that the heat that occurs is absorbed by the leaves and then the environmental temperature can be controlled [12]. Sometimes settlement problems become quite difficult for the community to solve, therefore the role of the government is needed to be able to provide adequate housing infrastructure and affordable prices, [2].

3 Research Methods

The southern part of Bali Island was chosen in this study, namely Badung Regency as the research location because there are many high-rise buildings and there are two underpasses which are multilevel infrastructure for infrastructure classification in the transportation sector. Data were obtained through direct observation of the object of research, conducting interviews with stakeholders who were considered to understand and master the material being studied, and data were collected through questionnaires which contained several questions which were directly filled out by respondents.

The research procedure can be described as follows: 1). Approaching stakeholders who are considered to understand the problem of vertical sanctity and absorb information through interviews. Obtaining related literature on vertical sanctity and multi-level infrastructure, especially in relevant previous research. 2). Determine the variables used in research and make research instruments, as well as the preparation of questionnaires. 3). Collecting necessary secondary data and completing primary data as needed. 4). Data analysis so that complete and accurate conclusions can be drawn.

The data were analyzed qualitatively for the identification of vertical sanctity and then a theoretical framework was developed as a guide for the preparation of interviews and questionnaires. Furthermore, the data obtained from the questionnaire was categorized in a Likert Scale and analyzed with a descriptive approach to be able to make conclusions from the results of the study.

4 Results and Discussion

Infrastructure development that involves many people should be studied with a broader perspective, especially regarding local wisdom because there are social, cultural, and religious touches in it. The fact that local wisdom is supported by religious beliefs with cultural values has been integrated with people's lives, so it is very difficult to separate because it is also used as a basis for everyday life.

The questionnaire that was circulated was to obtain data on the relationship and acceptance of the community towards vertical sanctity in the design of non-uniform infrastructure. The questions and statements contained in the questionnaire are: a). By building infrastructure that is not on a plot, it can overcome the problems of land conversion and environmental sustainability, b). Residents have or often pass through / enter infrastructure that is not on the same level so that they understand its relation to vertical sanctity, c). The vertical purity limit above the crown is 12 Guli according to what is stated in the lontar, d). When crossing/entering infrastructure that is not on a plot, there is a feeling of doubt, awkwardness, *leteh/cemer*, because someone above us has stepped over it, e). In my opinion, infrastructure development is not on a plot that will prevent land conversion and protect the environment.

An analysis of the data obtained from filling out questionnaires was carried out, especially those related to the vertical sanctity of the height of each floor of the multilevel infrastructure and the variable of public acceptance. The analysis begins by calculating the average value (mean) of the answers to questions about the relevance and acceptance of society to the concept of vertical sanctity. Next, the Standard Deviation (SD) is calculated and all scores obtained are converted from the five Likert Scale values, so that the percentage of linkage and public acceptance of the value of vertical sanctity is obtained. Likert Scale categories are grouped into: strongly agree, agree, undecided, disagree, and strongly disagree. Of the 100 respondents in the research sample, with educational qualifications deemed relevant to be able to provide information, namely Doctoral Degree = 6%; Master Degree = 14%; Bachelor = 47%; Diploma = 4%, and high school level = 29%.

In accordance with the questionnaire that was entered and analyzed further, then if viewed from the education of the respondents who filled out the questionnaire, it can be said to be of very high quality. Their education is at least high school, and 71% of those belonging to diplomas and bachelors are. Based on the educational data from those who provided information as respondents, it can be said to be very good and it is believed that the information provided is equivalent to their educational qualifications. The following graph shows the educational qualifications of the research respondents (Graph 1).

Of the 105 copies of the questionnaires that were circulated, 103 were collected again, of those collected there was 1 blank copy, and 2 copies of incomplete answers (not all questions were answered). So 100 copies were then analyzed as stated in the following table (Table 1):

Based on data collection, it can be shown: 24 people strongly agree, 44 people agree, 29 people are unsure, 2 people disagree, and 1 person strongly disagrees. The data shows that 68% of the sample stated that there was a relationship between vertical sanctity and the height of the multilevel and thought that they accepted the concept of vertical sanctity being applied in the design of multilevel infrastructure.

Graph. 1. Research Respondents based on Educational Qualifications

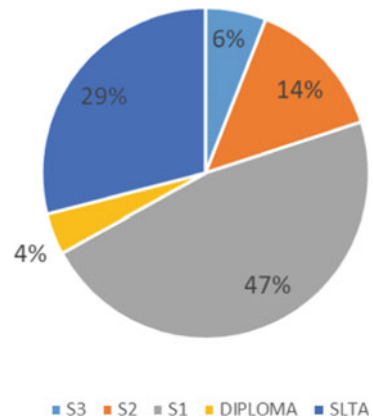


Table 1. Results of Questionnaire Circulation

NO	ANSWER					
	QUESTION	STRONGLY DISAGREE	DON'T AGREE	DOUBTFUL	AGREE	STRONGLY AGREE
1	a)	–	–	35	42	22
2	b)	–	–	24	43	25
3	c)	–	1	21	42	25
4	d)	1	1	19	44	21
5	e)	–	–	46	49	27
	AVERAGE	–	–	29	44	24

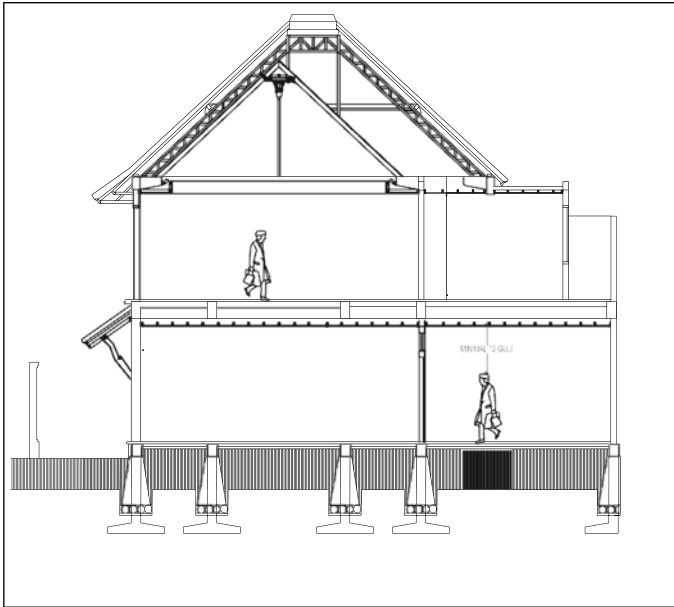


Fig. 1 The vertical sanctity of holiness above the crown

As many as 29% were hesitant, because they did not understand what the vertical sanctity meant, even though in interviews they stated that they often went in and out of the lower floors of multilevel buildings and did not feel anything strange. The remaining 2% said they did not agree and 1% strongly disagreed, this is because they are used to not wanting to go to the lower floor and if they forced it, they often experience headaches after that (Fig. 1).

At first the vertical sanctity limit was carried out as a reference in determining the distance between upakara facilities in Hindu religious ceremonies, then continued in setting the layout and dimensions, especially the height of the residents' houses. The design of the space height of each floor of a high-rise building should be guided by the minimum height of vertical purity [18, 19]. Public understanding of the existence and function of vertical sanctity is needed so that in the future socialization or focus group discussion is needed to accept development in a vertical direction, not only relying on a horizontal direction with the aim of minimizing land conversion and preserving the environment.

Based on the opinion of respondents as representatives of the community who were presented during interviews as well as from the results of filling out questionnaires, for those who accept or reject the concept of vertical sanctity in infrastructure development, it is very necessary to make definite legalities regulated in legislation such as regional regulations. If the community still refuses to enter the lower floor of multilevel infrastructure because of their uncomfortable feelings and as long as an alternative that is acceptable to their feelings has not been found, then during that

time they will not be able to enter the lower floor of the multilevel infrastructure. Likewise, if development in a horizontal direction cannot be carried out while the needs and development of the population continue to grow, then development in a vertical direction cannot be dammed anymore. In this phase it can be said that time will be the final determinant of this condition.

5 Conclusions and Suggestions

Based on the results of data analysis and discussion conducted, it can be concluded that: 1). In general, the community can accept the concept of vertical sanctity to be applied in the design of non-level infrastructure, according to the problem it is a challenge to develop non-level infrastructure and it is proven in the results of studies which state that vertical sanctity is the answer to doubts about entering/*mesulub* in non-level infrastructure. namely with the hope of minimizing land conversion and preserving the environment. 2). The minimum height of each floor of non-level infrastructure should be adjusted to the minimum height of vertical purity. In accordance with the formulation of the problem, objectives, and results of the study, 68% stated that the relationship between vertical sanctity and the height of infrastructure was not on the same level. 3). Because it involves local wisdom, the community's understanding of vertical sanctity must be more mature so that it is not outdated.

Suggestions that can be conveyed are that every building infrastructure is not on a plot of paying attention to the minimum limit of vertical sanctity. The community's understanding of local wisdom should be sharpened, especially on vertical sanctity, because this concept can be applied continuously to non-universal infrastructure, and allows it to be applied internationally and accepted by the general public.

Acknowledgements The author would like to thank the PETRONAS University of Technology (UTP), which has supported the output of this research.

References

1. Pemda Prov. Bali: Perda Provinsi bali No. 16 Tahun 2009 tentang : Rencana Tata Ruang Wilayah Provinsi bali Tahun 2009 – 2029, Ka. Biro Hukum & Ham Provinsi bali, Denpasar (2009)
2. Kamaruzzaman SN, et al (2018) Residents' satisfaction towards the indoor environmental quality of re-engineered affordable housing scheme in Malaysia. *International J. Technol.* **9**(3):501-512
3. Bevilacqua P, et al (2017) Thermal inertia assessment of an experimental extensive green roof in summer conditions. *Building and Environment* **131**:264–276
4. Budayoga-A, Lontar Purwaka Weda, Milik dari Drs. I.B. Gede Budayoga, M.Si ; Grya Basang Tamiang, Kapal, Mengwi, Badung, Bali
5. Budayoga-B, Lontar Surya Sewana, Milik dari Drs. I.B. Gede Budayoga, M.Si ; Grya Basang Tamiang, Kapal, Mengwi, Badung, Bali.

6. Tinglis K Lontar Swamandala, Milik dari Jro mangku Ketut Tinglis ; Pemangku Gede Pura Desa, Desa Adat Abianbase, Mengwi, Badung.
7. Geni IPMNM Lontar asta Kosala-Kosali, Milik Ida Pandita Mpu Nabe Manik Geni ;Grya Manuaba Banjar sengguan, Abianbase, Mengwi, Badung
8. Puja Pelaksanaan P4 Bagi Umat Hindu Dharma, Jakarta, Dirjen Bimas Hindu dan Budha, Departemen Agama (1978)
9. Ardana, Agama Hindu dan Lingkungan Hidup, Denpasar, Proyek Seminar Kesatuan Tafsir Terhadap Aspek-aspek Agama Hindu (1982)
10. Dan Arthur S (2003) Economics: Principles in Action, Upper Saddle River, New Jersey 07458: Pearson Prentice Hall. (474), ISBN 0-13-063085-3
11. Mahajan SK, et al (2013) New concept of traffic rotary design at road intersections. *Procedia - Social and Behavioral Sciences* **96**:2791-2799
12. Medl A, et al (2017) Vertical Greening System – A Review on Recent Technologies and Research Advancement, *Building and Environment* **125**:227239
13. Sukarelawan E (2018) Kemacetan Lalu-lintas Acuan Pariwisata Bali, *kabar24.bisnis.com* diakses 11 Pebruari 2018
14. Zaman NQ et al (2012) Opportunity in leftover spaces: activities under the flyovers of Kuala Lumpur. *Procedia-Social and Behavioral Sciences* **68**(2012):451-463
15. Gwizdala TM, dan Grzebielucha S (2010) The traffic flow through different form of intersections. *International Conference on Computer Information System and Industrial Management Applications (CISIM)*
16. Xiaoqiu F, et al (2011) Intact of driving behavior on the traffic safety of highway intersection. *Third International Conference on measuring Technology and Mechatronics Automation*
17. Parimin AP (1986) Fundamental Study On Spasial Formation of Island Village : Environmental Hierarchy of Sacred-Profane Concept in Bali. Unpublished Ph.D, Dissertation, Osaka University, Japan
18. Wibawa IMS, et al (2020) The role of vertical holiness in the multi story infra- structure design. *Paduraksa* **9**(1), P.ISSN: 2303-2693 ; E.ISSN: 2581-2939
19. Wibawa IMS, dan Maharani SE (2022) The concept of vertical sanctity in environmentally friendly store building design. *International Journal of Applied Science and Sustainable Development* **4**(1), P. ISSN: 2656-9051; E. ISSN: 2775-6874 24-30

The Effects of Changes in Socializing Trips, Discretionary Trips & Activities, During COVID-19 Pandemic on Affective Well-Being



M. Ridwan, Anas Zahkiah Hanum Azmera, Dimas B. E. Dharmowijoyo, and Liza Evianti Tanjung

Abstract The outbreak of COVID-19 in 2019 affected various countries worldwide, forcing national, provincial, and local governments to impose widespread travel restrictions in the interest of public health. Men, women, and children have been mostly confined to their homes for several months due to the imposed travel restrictions. As a result, people had to adapt to alternative living/working in restricted situations. A prolonged period of confinement to one's home seemed to impact people's behaviour and affective well-being. Hence, this study is particularly interested in analysing changes in socialising trips and discretionary trips during the COVID-19 pandemic on affective well-being. An online survey was conducted in Malaysia (N = 438) to seek the effects of the COVID-19 pandemic on travel behaviour activity and as well as to affective well-being. By using the Malaysia 2021 dataset, this study analyses the effects of changes in socialising, discretionary trips, and activities on

M. Ridwan (✉)

Department of Civil Engineering, Universitas Sumatera Utara, Medan, Indonesia
e-mail: ridwan.anas@usu.ac.id

A. Z. H. Azmera · D. B. E. Dharmowijoyo · L. E. Tanjung

Department of Civil and Environmental Engineering, Universiti Teknologi PETRONAS, Perak, Malaysia
e-mail: zakiah_17001817@utp.edu.my

D. B. E. Dharmowijoyo

e-mail: dimas.bayu@utp.edu.my

L. E. Tanjung

e-mail: liza_19001673@utp.edu.my

D. B. E. Dharmowijoyo

Institute of Transport and Infrastructure, Universiti Teknologi PETRONAS, Perak, Malaysia

Civil Engineering, Universitas Janabadra, Medan, Indonesia

School of Planning and Policy Development, Institut Teknologi, Bandung, Indonesia

L. E. Tanjung

Department of Civil Engineering, Universitas Muhammadiyah Sumatera Utara, Medan, Indonesia

© Institute of Technology PETRONAS Sdn Bhd 2024

B. S. Mohammed et al. (eds.), *Proceedings of the International Conference on Emerging Smart Cities (ICESC2022)*, Lecture Notes in Civil Engineering 324,
https://doi.org/10.1007/978-981-99-1111-0_17

affective well-being. The bivariate and multivariate analysis has been used to determine the relationship between variables. From the findings, the trip that has the most significant impact on affective well-being is the trip to dining on the weekdays during the PKPP phase while for other trips the result is varied. It is crucial to understand the relationship between these variables as it could help with predicting future human travel behaviour.

Keywords Travel behaviour during COVID-19 pandemic · socializing trips · discretionary trips · online activities · trips comparison · affective wellbeing · Malaysia

1 Introduction

The World Health Organization (WHO) has declared the Coronavirus Disease 2019 (COVID-19) a global pandemic, with the first case being recorded in late December 2019 in Wuhan, Hubei Province, China. As of November 7, 2021, more than 250 million cases had been documented worldwide, resulting in more than 5.05 million fatalities. Beginning March 18, 2021, the Malaysian Federal Government's Movement Control Order (Malay: Perintah Kawalan Pergerakan Kerajaan Malaysia), often known as the MCO or **PKP**, is a set of nationwide quarantine and cordon sanitaire measures implemented in response to the COVID-19 pandemic. Local and foreign media outlets have referred to the directives as "lockdowns". To combat the spread of the COVID-19 virus, MCO measures included restrictions on mobility, assembly, international travel, as well as the shutdown of businesses, industries, government agencies, and educational institutions. On 7 June 2020, Prime Minister Muhyiddin Yassin announced that the Conditional Movement Control Order (CMCO) (Malay: Perintah Kawalan Pergerakan Bersyarat (**PKPB**)) ended on 9 June, with the country entering the Recovery Movement Control Order (RMCO) (Malay: Perintah Kawalan Pergerakan Pemulihan (**PKPP**)) phase between 10 June and 31 August (Table 1).

Before the pandemic, most people travelled every day for various reasons such as going to work, school, shopping, sports, hobbies, socialising, etc. Some of the activities are out-of-home activities, hence travelling is one of the necessities in life for people to fulfil their needs and desires. During the pandemic, studies revealed that office work is being replaced by teleworking, while in-store shopping is being replaced by teleshopping (Irawan et al. 2021). Thus, these mobility restrictions during the pandemic had a significant impact on people's participation in out-of-home activities.

During the pandemic, people are less likely to socialise and take discretionary trips because of the mobility restrictions enforced by the government. Discretionary travel is defined as all trips other than home-based work and home-based school (Dalton, 1999). While socialising trips are the trips that are taken in order to participate in social activities. Social activities include spending time with family members or friends, going out to eat, playing board games, etc. Some examples of discretionary

Table 1 Timeline of MCO, CMCO and RMCO

Phase	Date
Movement Control Order (MCO, 18 March 2020 - 3 May 2020)	
Phase 1	18 March 2020 - 31 March 2020
Phase 2	1 April 2020 - 14 April 2020
Phase 3	15 April 2020 - 28 April 2020
Phase 4	29 April 2020 - 3 May 2020
Conditional Movement Control Order (CMCO, 4 May 2020 - 9 June 2020)	
Phase 1	4 May 2020 - 12 May 2020
Phase 2	13 May 2020 - 9 June 2020
Recovery Movement Control Order (RMCO, 10 June 2020 - 31 March 2021)	
Phase 1	10 June 2020 - 31 August 2020
Phase 2	1 September 2020 - 31 December 2020
Phase 3	1 January 2021 - 31 March 2021

trips are family visits, vacations, the birth of a family member such as a grandchild, nieces, nephews, and attending family members' funerals. Travel for discretionary purposes is associated with higher levels of positive emotions and lower levels of negative emotion than travel for work or household maintenance (Jing and Fan, 2018).

These sudden changes with having out-of-home activity restrictions in their daily lives have been seen to influence individuals' affective well-being and mental health as some of the activities are essential to maintain or enhance people's affective well-being. Individuals with high levels of emotional well-being (i.e., those who experience more positive mood and less negative feelings) are often successful in a variety of life domains, including marital relationship, friendship, earnings, work, and health (Achat, 2000; Lyubomirsky et al. 2005).

According to studies, mental health issues increase in direct proportion to the amount of lockdown days (McKimm, 2020, as cited in Irawan et al. 2021). It is well known that a new routine involving continuous repetitive use of places for an extended length of time has an effect on one's mental health; (Campbell, 2020, as cited in Irawan et al. 2021). Certain negative emotions (e.g., unpleasant experiences, demotivation) tend to increase, which may link with people's emotional or affective well-being in particular and with overall subjective well-being (Rizki et al. 2020).

Brooks et al. (2020), as cited in Rizki et al. (2020), conducted an analysis of 24 papers from the SARS pandemic and the various citywide quarantines and discovered that, during the quarantine/lockdown, people were extremely likely to experience a variety of psychological stress and disorder symptoms, as well as negative emotions. Additionally, the study revealed that post-traumatic stress symptoms occurred in correlation with post-pandemic behaviour, including activity participation. Thus, once current restrictions are relaxed, it is expected that out-of-home leisure activities

(e.g., socialising, and discretionary) will be conducted more frequently in order to improve overall well-being and mental health.

Thus, this study aims to investigate the effects of changes in socialising trips, discretionary trips, and activities during COVID-19 pandemics on affective wellbeing because understanding the individual's affective well-being state during the pandemic is crucial for predicting future travel-activity patterns after the lockdown is lifted. At the end of this study, new information on how individuals having less discretionary and socialising trips during the pandemic would impact individuals' affective well-being and future travel activity patterns. This information will be very beneficial in future traffic planning analysis.

Every person has their constraints, desires, and needs in their everyday lives. Thus, each person will have their daily activity-travel pattern because of the decision-making process that shapes their activity-travel pattern. For instance, a student and a worker will have distinct tasks. They will be assigned different daily activities and travel schedules based on their physical characteristics, such as gender or age.

According to Dharmowijoyo and Joewono (2020), individuals' activity-travel behaviour is complex. Treating individuals' activity-travel behaviour as a self-contained entity that varies simply in socio-demographic and built environment terms undervalues the complex mechanism behind individuals' decision-making processes. The conventional method, or what is commonly referred to as trip-based analysis, may fail to account for the interdependence of trips and activities, the temporal limitations on activity scheduling, and the activities of persons within a home or social network (Flyvberg et al. 2005, as cited in Dharmowijoyo and Joewono, 2020). The conventional approach assumes that the individual engages in similar travel and activities every day and, therefore, such approach encompasses only inter-personal variability (Senbil and Kitamura, 2009, as cited in Dharmowijoyo and Joewono, 2020).

Knowing how individuals shape their activity-travel behaviour as a result of their individual and interpersonal characteristics within a multidimensional and multi-hierarchical time and space perception, as well as its correlation with health factors, may be able to suggest a policy that can ensure improvement of individuals' health, particularly social and mental health (Dharmowijoyo and Joewono, 2020).

Life is composed of various domains, including work and family (T., 1998), and contentment in each domain can affect overall quality of life (Diener, 2009). Several researchers have studied the leisure domain—the domain of life linked to the discretionary use of time—and its major impact on life satisfaction or subjective wellbeing (Neal et al. 1995). With an increased level of stress in other realms of life, such as work stress (Barling et al. 2004), financial stress (Kim and Gordon, 2014), or family stress (Boss et al. 2016), individuals strive to improve their experiences in regions where they can recharge their energy (as cited in Yu and Kim, 2021).

Subjectively perceived well-being has recently gained prominence in transportation and mobility research. However, this research is still in their early stages, and many of the complex relationships between travel behaviour and wellbeing remain unexplored; most studies only investigate at one component of this link (i.e., travel satisfaction) (Vos et al. 2013). Some academics claim that leisure activities frequently

involve contact with others and thus meet basic social needs (Hills et al. 2000). Others have argued for the benefits of the activities themselves, claiming that participating in them can make people feel alive and active (Rodriguez et al. 2008). (As cited in Yu and Kim, 2021).

Since taking socialising and discretionary trips and activities tend to correlate on better well-being and social and mental health (Dharmowijoyo, 2020), this study will provide an insight into the effects of changes in socialising trips, discretionary trips, and activities on affective well-being during the COVID-19 pandemic while considering the complexities of travel behaviour that are overlooked in trip-based analyses, which includes household and individual sociodemographic characteristics, daily different individuals' activity-travel pattern (including multi-tasking) and well-being related questions.

Hence, the objectives of this study are to correlate the effects of changes in socialising trips and discretionary trips during COVID-19 pandemics on affective well-being using the bivariate analysis method and to correlate the effects of changes in socialising trips and discretionary trips during COVID-19 pandemics on affective well-being using the multivariate analysis method. Once the objectives are achieved, this research could be a valuable resource for future urban transportation planning, promoting desirable human travelling pattern activities.

2 Literature Review

2.1 Time Geography

Miller in 2017, characterises temporal geography as a constraint-based framework for studying human behaviour in place and time. Time geography acknowledges that humans have fundamental geographical and temporal limitations: people may only be physically present in one area at a time, and activities take place in a limited number of locations for limited durations. Participating in an activity entail devoting limited available time to access and complete the activity. Time geography is concerned with determining one's freedom of action in the face of multiple spatial and temporal restrictions, rather than with directly forecasting travel behaviour (Neutens et al. 2011 as cited in Rizki et al. 2020).

Furthermore, temporal geography categorises activities depending on their suitability to a certain individual. Work and meetings are examples of fixed activities that cannot be readily rescheduled or relocated, whereas shopping and amusement are examples of flexible activities that may be postponed or conducted in numerous places (Miller, 2017).

2.2 *Types of Constraints*

Time geography recognises three fundamental limits on human activities: capability, coupling, and authority constraints. Individuals' activities are constrained by their physical capabilities and/or available resources (Miller, 2017). For instance, people need to do their daily maintenance routines such as eating and sleeping, which necessitate time and location. Another example is that individuals with extra resources such as private cars can generally travel faster than those who use public transportation.

Coupling constraints define where, when, and how long an individual must collaborate with others on shared activities such as work, meetings, and classes. Fiat imposes authority constraints on specific space-time domains. For example, a retail mall or gated community may make entry difficult and illegal during certain hours (Miller, 2017). These interactions between needs and constraints must be considered to better understand an individual's daily activity-travel pattern. Each person has different time-prisms based on their lifestyle, influenced by the interaction of needs and constraints.

2.3 *Space–Time Path*

Personal and household upkeep, employment, shopping, health care, education, and recreation are all spread out in time and space; they are only available in a few places for a limited period. Taking part in activities requires exchanging time for space in order to have access to these places during operational hours (Miller, 2017).

Figure 1 depicts a space-time path between activity stations. Stations are locations for activities; in classical time geography, these are referred to as tubes due to their spatial proximity and temporal availability (e.g., work hours, store working hours, appointments, and scheduled lectures). Anchor points—Cullen and Godson (1975), as cited in Neutens et al. (2011), are referred to as "pegs" because they signal the beginning and finish of defined activities; the time budget restricts the amount of time available for discretionary travel and activity participation.

2.4 *Space–Time Prism*

Figure 2 illustrates a space-time prism representing a person's travel and activity choices within the limits of a time budget given by two vertices. A spacetime prism aggregates all conceivable space-time pathways that a person can travel within a certain time budget. Its outer boundaries are determined by the greatest attainable travel speed, the duration of the time budget, the minimum time necessary for activity participation, and the physical distance between the anchor points.

Fig. 1 Space–Time Path
Among Activity Stations

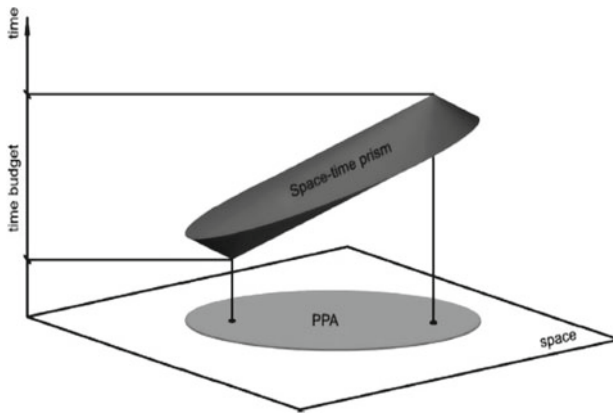
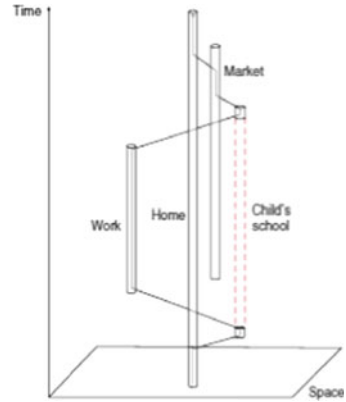


Fig. 2 Time Geographical Concepts

2.5 Affective Well-Being

Two measures of affective or emotional well-being are valence and activations (Dharmowijoyo et al. 2020; Russell 2003; Västfjäll et al. 2002, as cited in Rizki et al. 2020). Valence is a pure hedonic measure of well-being that quantifies how someone feels about an event, a service, or a choice, whereas activation refers to energy activation or mobilisation. Two more dimensions, termed as unpleasant activation and unpleasant deactivation, are added from combinations of valence and activation (Russell, 2003, as cited in Schwanen and Wang, 2014).

The well-being protagonist is thought to be multifaceted, encompassing both cognitive and affective well-being (Schwanen and Wang, 2014). The phrase “cognitive well-being” refers to the appraisal of one’s life satisfaction over a longer period of time. (e.g., work satisfaction, marriage satisfaction), but life satisfaction is an

appraisal of how nice one's life is over a (much) shorter period of time for emotional well-being (e.g., the past two weeks or right now).

2.6 Measuring Well-Being (Core Affects)

Core affects are attributes of a current mood, an emotional reaction, or an anticipated emotional reaction that are cognitively accessible. They are present all the time, even at a neutral level. (Västfjäll et al. 1998). The core affect is simply how we feel at any given moment. Thus, at any particular point in time, we may feel calm (low activation and pleasant), tense (high activation and unpleasant), or happy (pleasant, high activation).

It was proposed early on that core affects can be described by a set of underlying dimensions, according to Västfjäll et al. (2000). The two main affect dimensions or axes, according to Russell (1980), as cited in Västfjäll et al. (2000), represent degrees of pleasantness-unpleasantness and arousal. Participants in the study tended to arrange the eight affect categories of excitement, pleasure, contentment, sleepiness, depression, misery, distress, and arousal in a circular pattern, with axes corresponding to pleasure-misery and aroused-sleepy at right angles and secondary axes corresponding to excitement-depression and contentment-distress at 45 degrees.

To summarise, valence and activation appear to be equally important in defining core affect structure. Västfjäll et al. (2000) proposed that the intermediate dimensions of positive affect, energetic arousal, or activated pleasant affect-deactivated unpleasant affect be referred to as pleasant activation-unpleasant deactivation, whereas the intermediate dimensions of negative affect, tense arousal, or activated unpleasant affect-deactivated pleasant affect be referred to unpleasant activation-pleasant deactivation. The valence dimension, which expresses the strength of emotion and gives information about one's current state of well-being, is an obviously crucial part of the human experience (Fig. 3).

2.7 Time Geography of Well-Being

Time-geography notions are widely accepted among transportation experts, who contend that effective policy levers to impact travel behaviour can only be employed if daily activity patterns and time usage are recognised (Timmermans, Arentze, and Joh, 2002, as cited in Schwanen and Wang 2014). As a result, these researchers looked at daily activity and travel events, as well as individual activity episodes. An activity episode is a sequence of actions that occur in a single location in space and are continuous in time. It is characterised by a variety of interconnected factors, the most widely discussed of which are the type of activity, the beginning time, the period, the geographical location, and the individual engaging (Schwanen and Wang, 2014).

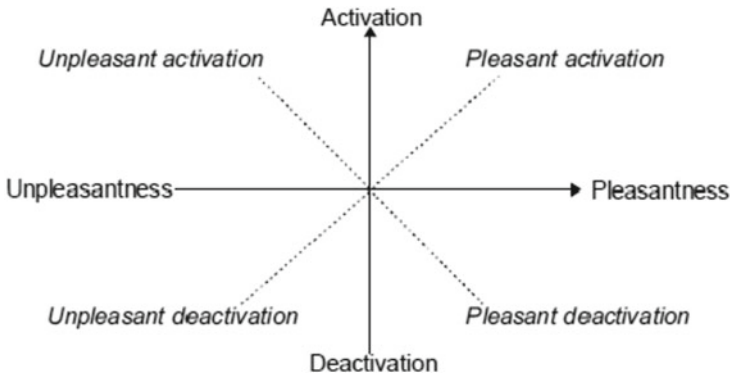


Fig. 3 The Circumplex Model of Affect

Time–geographical analysis enables precise judgements about whether and how time spent with certain people or groups of social interactions (for example, family and friends) influences well-being (Schwanen and Wang, 2014). Furthermore, temporal geography aids in understanding how longer-term processes, such as life satisfaction ratings, influence and are influenced by daily activities (Pred, 1983, as cited in Schwanen and Wang, 2014).

2.8 COVID-19 as a Contextual Moderator

Satisfaction with an individual’s leisure life domain, one of several subdomains of their existence, has a beneficial influence on their subjective well-being through a bottom-up spill over process (Kuykendall et al. 2015). After completing one’s required tasks and chores, one spends the remainder of one’s time to leisure pursuits. Individuals choose non-obligatory, voluntary activities that result in intrinsic good sentiments of satisfaction, autonomy, and motivation (Neulinger, 1982). Aside from the inherent benefits of leisure, scientists have postulated a need-satisfaction process via which leisure life enjoyment might favourably contribute to one’s subjective health. Individuals’ social needs (Hills et al. 2000), efficacy needs (Argyle, 1987), and sensation seeking needs are met during leisure, and this state of fulfilment may contribute to happiness.

According to the American Psychological Association, during the COVID-19 pandemic in 2021, people would feel heightened stress and unanticipated limitations in their everyday responsibilities (Heid et al. 2021). Individuals are barred from engaging in their usual interpersonal interactions and gatherings; access to public spaces is restricted, limiting the range of opportunities and settings that people can use in their daily lives; and a higher level of perceived uncertainty in life reduces people’s sense of control or autonomy. COVID-19 creates a social environment that

decreases people's life satisfaction when compared to prepandemic levels (Wanberg et. al, 2020).

According to the hierarchical leisure constraints model (Jackson et al. 1993), constraints in leisure engagement and activities can reduce subjective wellbeing because people are less confident in their ability to pursue interests, have fewer people with whom to engage in leisure activities, and lack local opportunities or financial resources to pursue leisure. Individuals in the COVID-19 condition have a limited pool of leisure activities and leisure companions, resulting in numerous leisure limitations (Du et al. 2020). (As cited in Yu and Kim, 2021).

It is also stated that in recent decades, the capacity and flexibility to properly control emotional reactions has been connected to well-being (Hu et al. 2014). However, this has mostly been studied in a stable environment with a long-term perspective, rather than in severe or rapidly changing circumstances like pandemics (Diener et al. 2003). People use emotions to interpret and handle situations in their everyday lives, and it has been claimed that the individual's judgement of the situation is more important than the event itself for the emotional reaction (Troy and Mauss, 2011). People are more prone to have stronger and more negative emotions during a crisis like the COVID-19 epidemic because it places them in new demanding and stressful situations like managing new family routines or swiftly shifting to work or study from home (Restubog et al. 2020). Aside from their physical impacts, emotional reactions to the COVID-19 epidemic appear to have a role in people's motivation to take preventative measures (Capraro and Barcelo, 2020).

The emotional well-being characteristics of respondents during the outbreak are described in Table 2. It shows that the average response of emotional well-being of respondents tended to be higher than the neutral (3 represents neutral) or approving that they are in the negative state of emotional well-being. Most respondents felt irritated (4.19), dull (3.94), worried (3.81), tired (3.25) and annoyed (3.23) during the outbreak. The frustration and depression feelings were found to be the lowest of emotional well-being states during outbreak indicating that the respondents are able to cope up with the situation. However, whether someone is displeased with the experiences during the pandemic showed neutral value (3.06) indicating their indifference (Rizki et al. 2020).

Table 2 indicates how the outbreak impacted people's travel frequency for various reasons. Mandatory out-of-home journeys (e.g., to work/school) are the most common out-of-home trips and appear to be the most sensitive to disruption. Surprisingly, the number of flexible or reschedulable visits, such as electronics/fashion trips, has only marginally decreased. There is a possibility that respondents frequented electronics/fashion stores even when travel limits were in place to alleviate boredom and to meet their travel and out-of-home needs within their travel/out-of-home time budget. During the outbreak, as expected, offline activities were substituted by online activities (Table 3)

In comparison to the period prior to the pandemic, the frequency of various sorts of online in-home activities, such as work from home (WFH) or schooling from home

Table 2 Respondents Attitude Towards Covid-19 and Their Subjective Well-Being

Variables		N	Proportion	Mean	SD
Pandemic towards COVID-19 risk	No dangerous at all	1	0.1		
	Less dangerous	15	1.8		
	Don't Know	14	1.7		
	Dangerous	375	45.0		
	Extremely dangerous	429	51.4		
Number of days at home from 3 rd March 2020	< 10 days	43	5.2		
	10–20 days	61	7.3		
	21–30 days	57	6.8		
	31–40 days	85	10.2		
	41–50 days	105	12.6		
	51–60 days	197	23.6		
	61–70 days	167	20.0		
	> 70 days	119	14.3		
Emotional/Affective subjective well-being					
<i>Negative volence</i>					
Displeased experiences					
<i>Deactivation</i>		3.06			1.136
Passive		2.98			1.239
Dull		3.94			1.059
<i>Unpleasant activation</i>					
Frustrated		2.79			1.060
Annoyed		3.23			1.081
Irritated		4.19			0.966
Worried		3.81			0.915
<i>Unpleasant deactivation</i>					
Depressed		2.64			1.026
Tired		3.25			1.072

(SFH), entertainment activities, and so on, increased. Surprisingly, online entertainment activities were the most often conducted activities throughout the outbreak, with the second highest difference after work/school activities (Rizki et al. 2020)

Table 3 Travel Activity Changes During the Pandemic

Type of trips	Frequency of travel before COVID-19 (trips/week)		Frequency of travel during COVID-19 (Trips/week)		Difference in frequency of travel during and before COVID-19		
	Mean	SD	Mean	SD	Mean	SD	t-stat
Work/school trips	6.7	3.309	2.77	2.84	-3.93	3.688	-26.024**
Grocery/shopping	3.78	2.405	2.58	1.686	-1.2	2.121	-11.791**
trips Electronic/fashion shopping trips	2.12	1.726	1.41	1.085	-0.71	1.59	-10.074**
Out-of-home during trips	3.4	2.385	1.45	1.33	-1.95	2.372	-20.631**
Recreation trip	2.76	1.99	1.36	1.17	-1.4	1.976	-17.462**
Social trips	3.59	2.458	1.89	1.63	-1.7	2.245	-16.624**
Type of online Inhome Activity	Frequency of online in-home activities before COVID-19 (trips/week)		Frequency of online in-home activities during COVID-19 (Trips/week)		Difference in frequency of online in-home activities during and before COVID- 19		
	Mean	SD	Mean	SD	Mean	SD	t-stat
E-meeting/elearning	2.28	2.351	5.49	3.782	3.21	3.743	20.786**
Grocery e- shopping	2.16	1.729	2.89	2.166	0.73	1.842	7.583**
Electronic/fashion e-shopping	1.8	1.433	2.07	1.769	0.27	1.418	3.377**
Online delivery food/drinks	3.67	2.577	3.8	2.8	0.13	2.652	1.019
Entertainment activities	4.51	3.544	6.4	3.597	1.89	2.931	10.799**

**Significant at 5%, *Significant at 10%

3 The Malaysia 2021 Dataset

During May 2021, a cross-sectional, online-based survey titled “Kajian tinjauan kesan pandemik COVID-19 terhadap tingkahlaku aktiviti-perjalanan di Malaysia” was conducted in Malaysia. To ensure a large-scale distribution and recruitment of participants, consenting adults aged 20 and above were recruited electronically using the convenience and snowball sampling methods. In this study, the samples were drawn from states in Malaysia: Johor, Kedah, Kelantan, Kuala Lumpur, Labuan, Melaka, Negeri Sembilan, Pahang, Perak, Perlis, Pulau Pinang, Putrajaya, Sabah, Sarawak, Selangor, and Terengganu. A total of 438 participants have completed the questionnaire, and their responses were recorded in the analysis.

The goal of the data collection was to identify changes in activity and travel participation in response to the outbreak. The questionnaire consisted of five sections—section A, B, C, D, and E. In the first section, information on the socio-demographic characteristics of the respondents was collected, including age, gender, country of residence, education level, employment status, marital status, work, or study setting, number of cars or motorcycles owned, household income, etc. The second section collected data on the travel activity behaviour, such as comparing the frequency of travel on working days during the lockdown vs before the lockdown started for various purposes. The third section asked about the vehicles' mode of choices during the lockdowns and before the lockdown, such as cars, motorcycles, busses, LRT, etc to travel.

Social activities and subjective well-being questions were asked in the fourth section of the survey. The subjective well-being questions consist of nine emotional well-being states ranging from negative valence (unpleasant experiences), deactivation (passive and dull), combination between negative valence and activation (frustrated, annoyed, irritated, and worried), and combination between negative valence and deactivation (depressed and tired). In the last section of the survey, health-related questions were asked. Questions such as how much body pain the participants experience, how do they feel about their health, mental health, and other health issues during the pandemic. In most sections, Likert scales of seven points were used to record the participants' responses (Tables 4, 5, 6 and 7).

Table 4 Socio-demographic and Spatial Characteristics

Type of Data	Category
Individual sociodemographic information	Gender, Age, Highest level of education, Occupation, Occupation sector, Marital status
Household sociodemographic information	Household size, Household income, Number of cars owned by household, Number of motorcycles owned by household, State of residence, Postcode of residence
Journey to nearest amenity	Perceived time taken for journey to nearest city, nearest school, nearest grocery shop, nearest health clinic, nearest hospital, nearest mall

Table 5 Activity Travel Behaviour Comparison Before and After COVID-19 Pandemic

Comparison of travel frequency	Weekdays	Time period	Type of trips
		Before and after the COVID-19 pandemic (PKP and PKPB)	
Comparison of total number of daily trips	Weekends	Before and after the COVID-19 pandemic (PKPP)	

Table 6 Online Activities Comparison Before and After COVID-19 Pandemic

Comparison of weekly activity frequency	Activity	Time period	Purpose of Travelling
	Work/study from home Grocery e-shopping	Before and after the COVID- 19 pandemic (PKP and PKPB)	Work/school trips, Grocery shopping trips, Dining trips,
	E-shopping E-meeting Online delivery food/ drinks Streaming movies	Before and after the COVID- 19 pandemic (PKPP)	Socialising trips, Sport/recreational trips, Healthcare trips, Others

Table 7 Health Before and After COVID-19 Pandemic

Health-related Quality of Life (QOL) Questions	Weekdays	Time period
	Weekends	Before PKP
		During PKP and PKPB
		During PKPP

3.1 Summary of the Dataset

Table 8 displays the respondents’ socio-demographic and spatial characteristics. Females account for the vast majority of respondents (66.4%). The majority of respondents (84.5%) are between the ages of 23 and 45, and the majority have a bachelor’s degree as their highest level of education (48.6%). In terms of employment, most respondents (59.3 %) work full-time, with 69.1% not working in essential services. Respondents with monthly incomes ranging from 3001 to 7000 Ringgit Malaysia dominate the monthly income distribution (32.6%). In terms of marital status, most respondents (61.4%) were either single or married (38.1%). The respondents are mostly from families with four to six persons (57.3%), and they own one to two automobiles and motorcycles (83% and 56.4%, respectively).

4 Descriptive Analysis

4.1 Overall Affective Well-Being During COVID-19 Pandemic

The affective well-being index was obtained from factor scores analysis with a varimax rotation of all questions in the survey related to the research using a fundamental principle component analysis with a single-factor solution. Factor scores analysis is commonly used to reduce a large number of variables into fewer factors. The SPSS software creates the factor scores with the least square method.

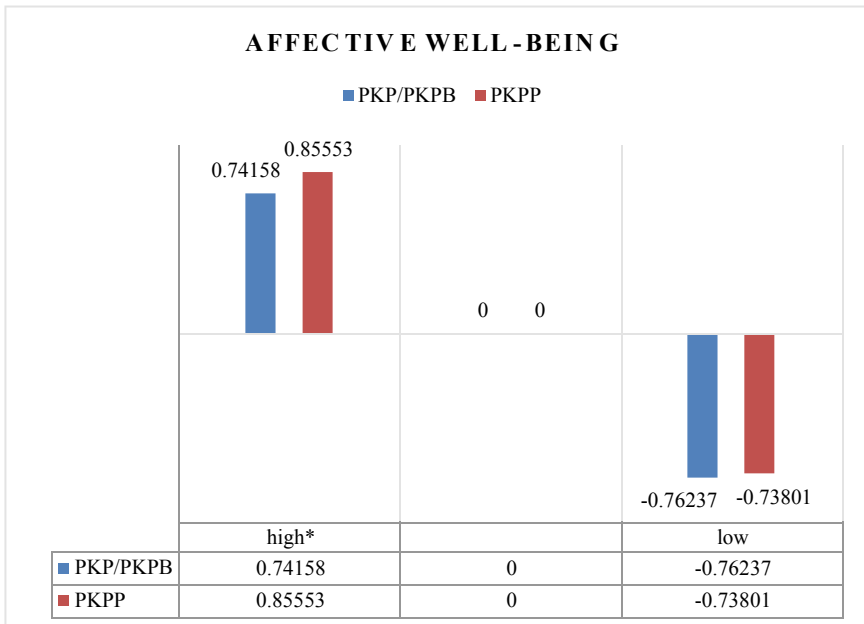
Table 8 Respondents' socio-demographic and spatial characteristics, N = 438

Variables	Percentage	Variables	Percentage
Gender		Working in essential services	
Male	33.50	Not working in essential services	69.10
Female	66.40	Health services	5.70
Age		Banking and finance	4.10
< 22 years old	10.90	Food Supply and Services	3.70
23–45 years old	84.50	Internet and Communications	3.00
46–55 years old	3.90	Electricity	2.70
> 56 years old	0.70	Hospitality	1.80
Education		Retail	1.60
High School	6.60	Safety	1.40
Diploma	15.30	Fuels	1.10
Degree	48.60	Logistics	1.10
Master	21.20	Waste Management	1.10
Doctorate	8.20	Online Shop	0.90
Employment		Broadcaster	0.90
Full time	59.30	Transportation	0.70
Part time	3.40	Courier	0.70
Student	30.60	Water services	0.20
Housewife	2.50		
Not working	4.10		
Marital status		Household number	
Married	38.10	< 3	24.90
Single	61.40	4–6	57.30
Single Parents	0.50	8–9	11.90
Car numbers		> 10	5.70
0.00	6.90	Income (RM)	
1–2	83.00	< 3000	28.30
> 2	35.60	3001–7000	32.60
Motorcycle numbers		7001–10,000	17.30
0.00	32.00	> 10,000	21.70
1–2	56.40		
> 2	11.60		

The factor scores also produce factor loadings of the multidimensional information, which shows the interrelationships among variances of multidimensional information to the discretionary and socialising trips taken during the pandemic and to the overall affective well-being. These scores are then classified as high affective well-being or low affective well-being. Positive scores indicate a high level of affective well-being, whilst negative scores indicate a low level of affective wellbeing.

The factor score analysis results are then analysed by plotting a graph of the average of individuals who had high and low affective well-being during PKP/PKPB and PKPP. The overall affective well-being during PKP/PKPB and PKPP is depicted in Figure 4. Figure 4 shows that the average of individuals with high affective well-being during PKP/PKPB and PKPP is 0.74 and 0.86, respectively. For low affective well-being, the average of individuals' affective well-being during PKP/PKPB and PKPP are -0.76 and -0.73, respectively. When PKPP is compared to PKP/PKPB, there is a rise in the overall affective well-being of the respondents. More people have high affective well-being during the PKPP, while fewer have low affective well-being.

This is due to the fact that during PKPP, some movement restrictions are eased in comparison to PKP/PKPB, where mobility limits are stricter. Most industries are allowed to reopen as long as they follow the government's SOPs. During PKPP, people are allowed to fulfil their needs and desires by undertaking more discretionary and socialising trips, such as travelling to work (working in the office), dining out,



*p-value < .1; significantly different

Fig. 4 Overall Affective Well-being during PKP/PKPB and PKPP

shopping at malls, sporting activities, visiting family members, vacations, and so on. As a result, the individuals' affective well-being is influenced.

4.2 Bivariate Analysis of Individuals' Travel Behaviour and the Effect to the Affective Well-Being

During PKP/PKPB

The survey results have demonstrated that the COVID-19 pandemic has changed individuals' activity-travel behaviour. The data has captured five types of discretionary and socialising trips (trips to groceries, dining, socialising trips, trips to sport, and healthcare) taken during the pandemic.

Figures 5 and 6 show the relationship between the frequency of taking discretionary and socialising trips during PKP/PKPB on weekdays and weekends and the affective well-being of the respondents during the phase. The Likert scale was employed in the survey questions to record the responses of the respondents. Those who select 1 to 3 are classified as taking more trips before PKP, those who select 4 to 5 are classified as taking similar trips before and during PKP, and those who select 6 to 7 are classified as taking more trips during PKP/PKPB. The study employs one-way ANOVA analysis methods to assess whether there are any statistically significant differences between the means of the groups.

Referring to Figure 5 and 6 for both weekdays and weekends, it can be seen that the mean of the people who took higher trips to the groceries during the PKP/PKPB have higher affective well-being compared to those who took higher trips before PKP. Those who took similar trips before and during PKP have the lowest affective well-being. For trips to dining, the highest mean of affective wellbeing was contributed by the people who took higher trips during the PKP/PKPB— comparing between the other two categories, people who are taking higher trips before PKP has better affective well-being compared to people who took similar trips before and during PKP.

People who took more trips to socialising during the PKP/PKPB has the highest affective well-being of all other kinds of trips. It seems that taking trips to socialising has the greatest impact on affective well-being. Spending quality time with friends or loved ones is good for the soul as it helps to lighten up the mood and make them feel happier. The cases are just as similar to the previously mentioned trips for trips to sports and healthcare. People who took higher trips during the PKP/PKPB generally have higher affective well-being than those who took a similar number of trips and higher trips during the PKP for both trips.

During PKPP

During the PKPP, as observed in Figure 7, for trips to groceries, trips to dining, trips to sport and trips to healthcare, people who took higher trips before PKPP has higher affective well-being compared to those who took higher trips during PKPP and to those who took a similar number of trips during PKPP. For trips to socialising, those

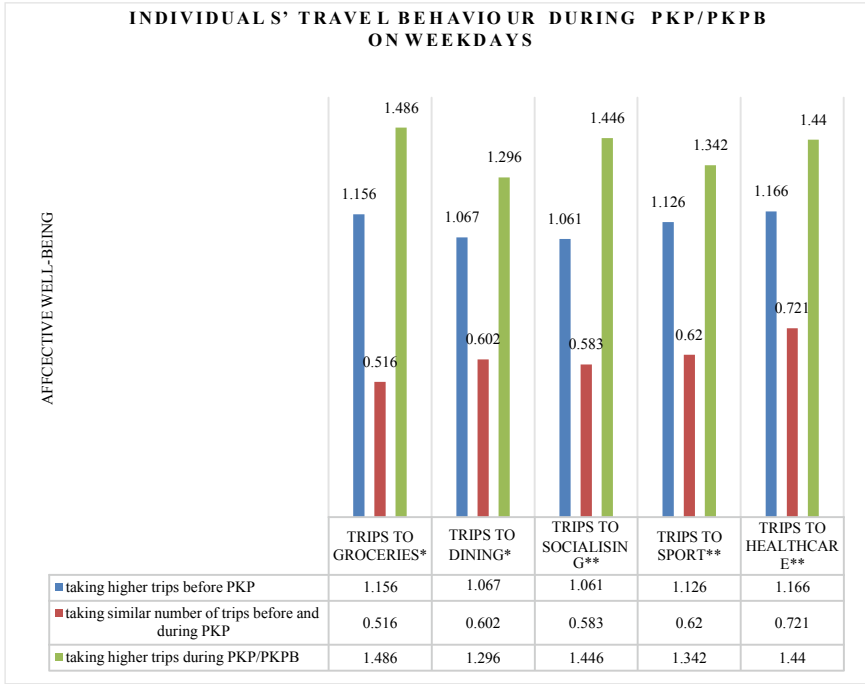


Fig. 5 Individuals' Travel Behaviour and The Affective Well-Being During PKP/PKPB On Weekdays

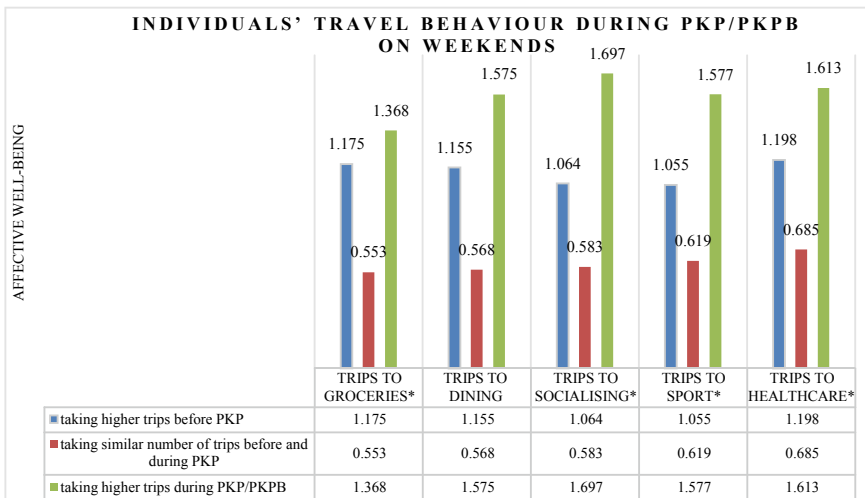


Fig. 6 Individuals' Travel Behaviour and The Affective Well-Being During PKP/PKPB On Weekends

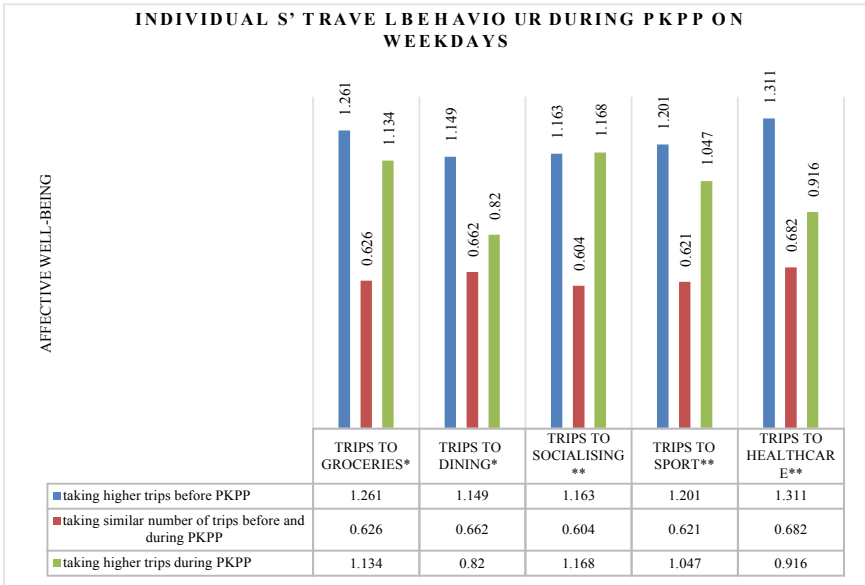


Fig. 7 Individuals’ travel behaviour during and the affective well-being PKPP on weekdays

who took higher trips during PKPP had higher affective well-being (0.168) than those who took higher trips before PKPP (1.163) and those who took a similar number of trips before and during PKPP (0.604).

As seen in Figure 8, the result is the opposite of weekdays for the weekends. In most categories (trips to groceries, trips socialising, trips to sport), the highest affective well-being was found in the people who took higher trips during the PKPP. Second higher affective well-being came from the people who took higher trips before PKPP, and the lowest affective well-being was from the people who took a similar number of trips before and during the PKPP. However, for trips to dining and trips to healthcare, the highest affective well-being is from the people who took higher trips before PKPP compared to those who took higher trips during the PKPP. The lowest affective well-being still comes from the people who took similar trips before and during the PKPP.

According to the findings, it seems people have more free time during the weekends to perform discretionary and socialising trips. Since some of the mobility restrictions has been relaxed during PKPP, some people have to travel to perform fixed activities such as going to work in the office, causing them to have less activity participation due to their time budget, which delimits the time available for other discretionary activities during the weekdays. As defined by Miller in 2017, humans have fundamental geographical and temporal limitations: people can physically be in only one place at a time, and activities take place in a limited number of locations for restricted durations. As a result, their limited time budget has influenced

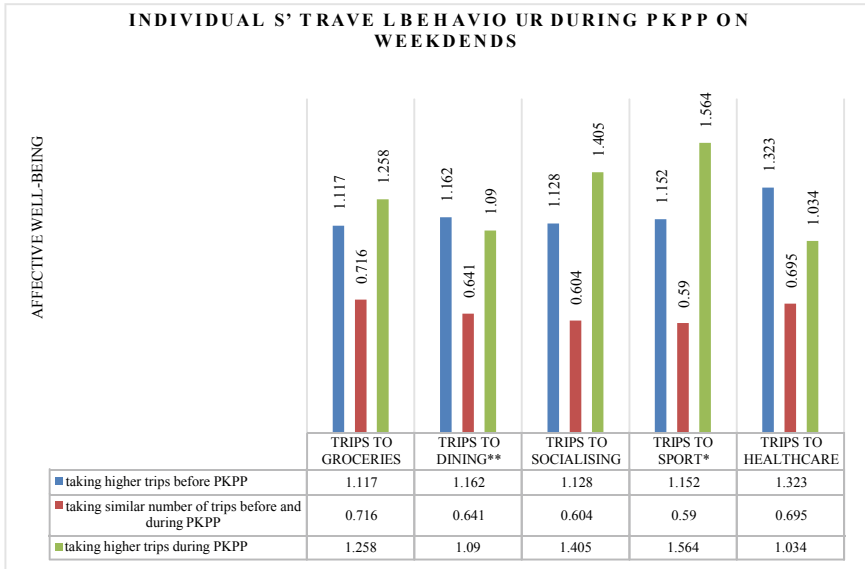


Fig. 8 Individuals’ Travel Behaviour and the Affective Well-Being During PKPP On Weekends

the frequency with which they take trips during the PKPP, effecting their affective wellbeing.

5 Model Estimation Result

Regression is a statistical approach for building models and analysing the relationship between dependent and independent variables. Its goal is to determine the degree of relationship between two or more variables. The dependent variables in this study, as shown in Tables 9,10,11 and 12 are trips to grocery, dining, socialising, sports, and healthcare, work & school from home, e-groceries, e- shopping, e-meeting, food delivery and streaming movies. The independent variables are affective well-being during PKP/PKPB and PKPP. The coefficients table below illustrates the strength of the relationship between the dependent and independent variables, i.e., the variables’ significance.

The beta of the standardised coefficients indicates the amount of variation in the dependent variable caused by the independent variable, whereas the significance shows the degree of error in the regression model. The value should be less than the study’s tolerated level of significance, i.e., less than 0.1 for a 95 percent confidence interval in this study. The *p*-value denotes the statistical significance of the data. Trips with a probability of less than 0.1 suggest statistically significant data that may affect the dependent variable, which in this case is affective well-being.

Table 9 Coefficients Table for Trips During the PKP/PKPB

PKP/PKPB				
Types of Trips	Standardised Coefficients beta		Significance	
	Weekdays	Weekends	Weekdays	Weekends
Groceries	0.10	-0.07	0.13	0.34
Dining	0.11	0.03	0.14	0.68
Socialising	-0.23	0.08	0.01*	0.44
Sport	0.15	-0.04	0.08*	0.62
Healthcare	0.10	0.05	0.10*	0.51

* p -value < 0.1**Table 10** Coefficients Table for Trips During the PKPP

PKPP				
Types of Trips	Standardised Coefficients		Significance	
	Weekdays	Weekends	Weekdays	Weekends
Groceries	-0.08	0.15	0.24	0.07*
Dining	0.25	-0.08	0.00*	0.35
Socialising	0.03	-0.09	0.74	0.37
Sport	-0.08	0.11	0.39	0.28
Healthcare	0.03	0.04	0.76	0.61

* p -value < 0.1**Table 11** Coefficients Table for Activity Performed During PKP/PKPB

PKP/PKPB		
Activity Performed	Standardised Coefficients Beta	Significance
WFSH	-0.10	0.16
E-grocery	0.16	0.04*
E-shopping	-0.11	0.17
E-meeting	0.01	0.90
Food Delivery	0.03	0.68
Streaming Movies	-0.04	0.56

* p -value < 0.1

Table 9 shows that trips to socialising (0.01), sports (0.08), and healthcare (0.10) have p -values < .1 during the weekdays, indicating that the data is statistically significant, and the null hypothesis is rejected. Taking trips to socialising, sports and healthcare have the most significant impact on the affective well-being during the COVID-19 pandemic. During PKP/PKPB most people have less engagement with other people due to confinement to their homes, thus taking more trips from those

Table 12 Coefficients Table for Activity Performed During PKPP

PKPP		
Activity Performed	Standardised Coefficients Beta	Significance
WFSH	-0.12	0.09*
E-grocery	0.02	0.80
E-shopping	-0.03	0.75
E-meeting	0.15	0.07*
Food Delivery	0.02	0.75
Streaming Movies	0.04	0.60

* *p-value < 0.1*

categories has been seen to influence their affective well-being. In a study it was found higher level of social engagement was consistently associated with less perceived depression, better self-rated health, and higher quality of life (Luo et. Al, 2020). Other trips, such as grocery and dining, have insignificant values, indicating that the null hypothesis is not rejected and has no effect on emotional well-being.

During the PKPP, Table 10 revealed trips to groceries on weekends (0.07) and trips to dining on weekdays (0.00) have a *p-value* <.1, signifying that the data is significant which has an impact on the dependent variable whereas trips to socialising, sports, and healthcare both on weekdays and weekends are not statistically different. During the PKPP, some people have to limit their discretionary trips because of they have to make more time available for fixed activities and lesser time available for flexible activities. Thus, it explains why affective well-being seems to be impacted. People also have fewer restrictions during PKPP making them have enough social engagement thus leaving having no impact on affective well-being.

For activities performed during PKP/PKPB in Table 11, the type of activity that is statistically significant is e-grocery due to the *p-value* being less than 0.1. This evidence suggests that e-groceries activity does impact the affective well-being during the COVID-19 pandemic. For WFSH, e-shopping, e-meeting, food delivery, and streaming movies are not statistically significant, and the null hypotheses are not rejected due to the *p-values* being more than 0.1. In PKPP (according to Table 12), the WFSH and e-meeting activities are statistically significant, with the *p-value* being .09 and 0.07, respectively. However, for the other activities, the *p-value* is not statistically significant indicating that the independent variables have no effect on affective well-being.

6 Conclusion

To conclude, discretionary and socialising trips and activities are necessary to maintain or improve an individual’s affective well-being. Because of mobility restrictions enforced by the government during the pandemic, people took less discretionary,

socialising trips and activities such as vacations and spending time with family members. Aside from that, this study successfully correlated a bivariate and multivariate analysis between changes in socialising and discretionary trips and affective well-being. The findings show that changes in socialising and discretionary trips and activities may have a significant effect on affective wellbeing, however it only applies to certain types of trips. It can be concluded that the survey does not fully capture all of the possible factors affecting the affective wellbeing such as the environmental factors, the time-space prism of each individual, and others type of factors. Hence, explaining the insignificance results of some of the trips.

In terms of future work, several steps can be taken to improve the research and increase its prominence, including emphasising the study's main point, collecting additional articles on the research topic, and reviewing case studies on the effects of changes in discretionary and socialising trips on affective well-being.

References

- Achat H, Kawachi I, Spiro A, Demolles DA, Sparrow D (2000) Optimism and depression as predictors of physical and mental health functioning: The normative aging study. *Annals of Behavioral Medicine*
- Boss P, Bryant CM, Mancini JA (2016) *Family Stress Management: A Contextual Approach*; Sage Publications: Southend Oaks, CA, USA
- Capraro V, Barcelo H (2020) The effect of messaging and gender on intentions to wear a face covering to slow down COVID-19 transmission. *J Behavioral Economics for Policy* 4(2):45–55
- Dalton P (1999) Discretionary Travel. 1996 Transportation Tomorrow Survey
- Dharmowijoyo DB, Joewono TB (2020) Mobility and health: the interaction of activity-travel patterns, overall well-being, transport-related social exclusion on health parameters. In S. A. Sulaiman, *Energy Efficiency in Mobility Systems*. Springer Nature Singapore Pte Ltd.
- Hu T, Zhang D, Wang J, Mistry R, Ran G, Wang X. Relation between emotion regulation and mental health: a meta-analysis review. *Psychol Rep.* 2014 A pr;114(2):341–62. pmid:24897894
- Irawan MZ, Belgiawan PF, Joewono TB, Bastarianto FF, Rizki M, Ilahi A (2021) Exploring Activity-Travel Behavior Changes during the Beginning of COVID-19 Pandemic in Indonesia
- Jing Z, Fan Y (2018) Daily travel behaviour and emotional well-being: Effects of trip mode, duration, purpose, and companionship. *Transportation Research Part A: Policy and Practice*
- Miller HJ (2017) Time Geography and Space-Time Prism. *The International Encyclopedia of Geography*
- Neutens T, Schwanen T, Witlox F (2011) The prism of everyday life: towards a new research agenda for time. *Transp Rev* 31(1):25–47. <https://doi.org/10.1080/01441647.2010.484153>
- Restubog SLD, Ocampo ACG, Wang L (2020) Taking Control Amidst the Chaos: Emotion Regulation During the COVID-19 Pandemic
- Rizki M, Dharmowijoyo DB, Balijepalli C, Joewono TB, Farda M, Maulana A (2020). Travel-Activity Changes During New Normal Period: Learning from the COVID-19
- Schwanen, T., & Wang, D. (2014). Well-Being, Context, and Everyday Activities in Space.
- Västfjäll D, Friman M, Gärling T, Kleiner M (1998) The Measurement of Core Affects: A Swedish Self-Report Measure Derived from the Affect Circumplex
- Vos JD, Schwanen T, Acker VV, Witlox F (2013) Travel and Subjective Well-Being. A Focus on Findings, Methods and Future Research Needs, *Transport Reviews*
- Yu GB, Kim N (2021) The effects of leisure life satisfaction on subjective wellbeing under the covid-19 pandemic: the mediating role of stress relief. *Sustainability* 13:13225

Design of E-Waste Management System for Flood- Prone Area (Case Study: Jakarta, Indonesia)



Nova Ulhasanah, Sinthia Apriani, and Mega Mutiara Sari

Abstract Pesanggrahan District is one of the flooded areas which results in high generation of electronic waste (e-waste). electronic equipment that was exposed to floodwaters becomes damaged and becomes e-waste. Pesanggrahan Subdistrict has a pick-up system of at least 5 kg of e- waste using an application from the DKI Jakarta Provincial Environmental Service. Residents were reluctant to dispose of their e-waste and choose to store it because they do not understand how to use the application and the minimum pick-up is 5 kg. If e-waste is stored for too long and is not disposed of immediately it can endanger health and the environment. Pesanggrahan District has an e-waste temporary storage building (TSB). However, the TSB has not met the design criteria according to government role No. 101 of 2014. Design of e-waste management system was carried out so that the e-waste generated in the Pesanggrahan sub-district was managed appropriately based on regulations and easier for citizens to dispose of their e-waste. There are two alternative solutions, namely scenario 1 using an indirect communal collection pattern and scenario 2 using an indirect individual pattern. Based on the analysis of economic and environmental aspects, scenario 1 is the selected scenario because it has a lower potential environmental impact than scenario 2. This project can make a significant contribution to the filed of e- waste management in Indonesia in particular and the world community in general because of limited data of e-waste research.

Keywords Flood · Electronic Waste · Pick-up · Temporary Storage Building

1 Introduction

The use of technology in the current era of globalization raises the demand for electronic equipment. The more a country's economic growth increases, the more people's purchasing power for electronic devices increases. This is exacerbated by

N. Ulhasanah (✉) · S. Apriani · M. M. Sari
Faculty of Infrastructure Planning, Universitas Pertamina, Jakarta, Indonesia
e-mail: nova.u@universitaspertamina.ac.id

© Institute of Technology PETRONAS Sdn Bhd 2024
B. S. Mohammed et al. (eds.), *Proceedings of the International Conference on Emerging Smart Cities (ICESC2022)*, Lecture Notes in Civil Engineering 324,
https://doi.org/10.1007/978-981-99-1111-0_18

the increasing population growth of Indonesia from year to year [1]. The value of gross domestic product (GDP) is directly proportional to the number of computers in each country. The greater the value of GDP, the greater the number of computers used [1]. Technological advances cause the life of electronic devices to not last long. Today's society tends to want to use more sophisticated technological features rather than stick with old technology that is still in good condition [2]. Examples that are often encountered are the use of fans that have been replaced by air conditioners. This phenomenon causes the duration of the use of an electronic device to become shorter and leads to an increase in electronic waste due to its disuse by the owner. Using e-waste with a short lifetime generates e-waste [2]. Electronic waste is included in hazardous waste, so it needs serious handling in processing. This is due to the presence of carcinogenic content in the waste so that it can endanger human health [3, 4]. Data released by the United Nations University states that every person in Indonesia disposes of around three kilograms of electronic waste on average, making it the largest supplier of electronic waste in Southeast Asia [5]. In general, the management of electronic waste in Indonesia is regulated by three regulations, including Law No. 32 of 2009 concerning Environmental Protection and Management; Government Law No. 101 of 2014 concerning Hazardous Waste Management; and Law No. 18 of 2008 on waste management. However, the aforementioned regulations only explain in general terms (not specifically), so that the detailed e-waste management policies cannot be known [6]. Indonesia only has a few management facilities for the separation of electronic components. Based on data released by the Ministry of the Environment, there are four areas for separating electronic components, namely in Batam, Central Java, West Java, and Tangerang [7].

One of the consequences of mismanagement of the e-waste management system is the dissolution of hazardous and toxic substances from electronic devices into flood water, making it easier for people living around floods to be exposed to their hazardous and toxic characteristics [3]. One of the sub-districts in Jakarta that is prone to flooding and has been a subscriber to the flood since 2013 is Pesanggrahan sub-district. The sub-district is included in the administrative city of South Jakarta with an increase in population of 15.97% (340 thousand people) since the last 11 years [8]. The increase in the distribution of the percentage of the population affects the growth of activity so that it raises several problems, such as the volume of waste that increases every day. According to the Head of the Disaster Data Center and Disaster Information (Pusdatin) of Jakarta, the Pesanggrahan sub-district is a flood-prone area, and the sub-district has been a frequent flood client since 2013 [9].

The Pesanggrahan sub-district is a flood-prone area because it is crossed by the Pesanggrahan River. The Pesanggrahan River broke down three times in 2010 due to rushing water and old embankment walls [10]. From these problems, there has been an increase in electronic waste because of the submergence of electronic devices due to flood waters, which leads to damage. According to data from the Head of the Implementation Unit (KASATPEL) of the Pesanggrahan sub-district, the average electronic waste generation in 2018 was around 8.8 kg. However, specifically in February, it generated 50.1 kg. E-waste generation in February was much higher

than in other months of the same year. This is caused by the peak of the rainy season every year in February, which results in flooding.

E-waste in Pesanggrahan sub-district has not become a concern for the community due to a lack of knowledge about the dangers of the waste. The Environmental Service (Dinas Lingkungan Hidup (DLH)) of DKI Jakarta Provincial has made efforts to overcome the problem, such as making e-waste collection programs, e-waste pick-up, as well as socialization activities [11]. In addition, the Head of the Hazardous Waste Management Section of DLH DKI Jakarta Province said the Pesanggrahan sub-district has a warehouse for storing hazardous materials to facilitate public awareness of electronic waste [12]. However, the application in the field, there are several things that are not in accordance with the requirements of electronic waste management in PP No. 101 of 2014. Among them, there is no lighting or roof on the building for temporary storage of the waste, and the area of the building where the waste is stored is smaller than the generation, and e-waste collection systems have not been structured systematically, resulting in the accumulation of e-waste in people's houses. If e-waste is not handled properly, the hazardous components contained in e-waste will be released and pollute the environment and health [13].

This research aims to get the actual e-waste generation in Pesanggrahan sub-district by field sampling and design a better system of e-waste management as well as building for temporary storage of the waste based on PP No. 101 of 2014. The results of this study can greatly contribute to the development of regulations related to electronic waste management in flood-prone areas in Indonesia and in developing countries in general.

2 Methodology

This study used direct observation in the Pesanggrahan sub-district to collect field data on the current state of the e-waste management system. A direct interview was conducted with the head of the implementation unit in Pesanggrahan sub-district to inquire about the pick-up system and e-waste storage at the Pesanggrahan sub-district office. Secondary data used in this paper included the generation of e-waste generated by residents' homes for one year (2018), the operational costs for picking up e-waste for one year, the construction cost of e-waste temporary storage in the Pesanggrahan sub-district, and previous research on components made from e-waste. Duration of data collection is 3 months from May to July 2020. The data were then used to evaluate the e-waste management system in the Pesanggrahan sub-district. The evaluation aims to see whether the management system is in accordance with applicable regulations. The design of a better e-waste management system is carried out by comparing the 2 scenarios with the existing condition. The aspects compared are economic, environmental, and social, so that a sustainable e-waste management system can be selected.

Some things that are taken into consideration in the design of the e-waste management system in this study are:

1. The condition that the Pesanggrahan sub-district is a flood-prone area until it reaches a pool of water as high as 4 m.
2. The design of the e-waste management system refers to Government Regulation No. 101 of 2014 concerning Hazardous and Toxic Waste Management.
3. The design of electronic waste storage facilities refers to SNI 03–6572-2001 concerning Procedures for Designing Ventilation and Air Conditioning Systems in Buildings and Government Regulation Number 101 of 2014 concerning the Management of Hazardous and Toxic Waste.
4. The SNI 19–2454-2002 (Indonesia Nasional Standard) method on Operational Technical Procedures for Urban Waste Management was used in the design of e-waste collection and collection facilities in Pesanggrahan sub-district.
5. The design of electronic waste containers in Pesanggrahan sub-district was based on SNI 3242:2008 concerning Waste Management in Settlements and Public Works Ministerial Decree Number 3 of 2013 concerning the Implementation of Waste Infrastructure & Facilities in Handling Household Waste and Types of Household Waste.
6. Evaluation of the environmental impact of the scenario was carried out by Life Cycle Assessment (LCA), and economic evaluation by considering the budget plan.

Life Cycle Assessment is an overall impact analysis method starting from the production stage to processing in determining the energy or environmental impact produced [14]. In determining the steps, LCA refers to ISO 14040 and ISO 14041. In this paper, open LCA software version 1.9 was employed. There are 13 impact categories which can be interpreted by LCA version 1.9. They are acidification, ecotoxicity, eutrophication, global warming, habitat alteration, HH cancer, criteria air pollutants, HH noncancer, indoor air quality, natural resource depletion, ozone depletion, smog, and water intake.

3 Results

3.1 E-Waste Generation

In 2018, Pesanggrahan sub-district produced 13 kg of e-waste in January, 50.1 kg in February, 15 kg in March, 1.3 kg in April, 0 kg in May, 6 kg in June, 13 kg in July, 0 kg in August, 0 kg in September, 0 kg in October, 0 kg in November, and 7.3 kg in December. It is very clear from the data that floods greatly affect the amount of e-waste generation because floods usually occur in February every year. The types of e-waste produced include one refrigerator, two washing machines, one mobile phone, two DVD players, two TVs, and two PCs.

3.2 Existing Condition

In existing conditions, e-waste collection activities are carried out by pick-up by the environmental implementing unit officer of the Pesanggrahan sub-district to each resident's house. The pick-up fee becomes free if the garbage picked up has a minimum mass of 5 kg with prior registration on the website <https://lingkunganhidup.jakarta.go.id>. E-waste that is picked up will be taken to hazardous waste temporary storage at the Pesanggrahan sub-district office before being sent to a third party. The e-waste collection pattern uses an indirect individual pattern, where waste is collected door to door. Officers from the Pesanggrahan sub-district will knock on the door of each resident's house and transport the electronic waste to a storage building in the Pesanggrahan sub-district. The transportation used was a pick-up car with a special cover for hazardous waste.

Evaluation of Existing Condition from Economic Aspect

The total cost for e-waste management in Pesanggrahan sub-district is 198,793,750 IDR/year. These expenses include the cost of e-waste collection (35,182,500 IDR), the purchase of transportation (140,000,000 IDR), and the operational and maintenance costs of the transportation equipment (23,611,250 IDR). Meanwhile, the construction cost of hazardous temporary storage is 7,744,717 IDR. The component details of the budget plan can be seen in Table 1.

Evaluation of Existing Condition from Environmental Aspect

Based on the composition of e-waste generation in Pesanggrahan sub-district, which consists of refrigerators, washing machines, mobile phones, DVD players, TVs, and PCs, it can be determined that the electronic components contained in them are copper, aluminum, iron, plastic, and brass. Based on Chui & Zhang (2008), the percentage of these components in each waste composition of the Pesanggrahan sub-district can be seen in Table 2.

The pick-up of e-waste in Pesanggrahan sub-district uses a pick-up car, which has the potential to produce CO₂ emissions of 3180 g/kg fuel, NO_x of 2 g/km, and CO of 40 g/km. To find out the emission load, the formula determined by the regulation of the state minister of the environment Number 10, 2012 can be used.

$$E = C \times TD \times EF \quad (1)$$

Note:

E : Emission Load (g/year)

C : Amount of Conveyance (amount)

TD : Total Distance (km)

EF : Emission Factor (g/km or g/kg fuel)

With a total pickup distance of 500 km, the number of transport vehicles of 1 unit, and a gasoline density of 0.76 kg/liter, the CO₂ emission load is 600,420,200

Tabel 1 Component Detail of Economic Aspect

Operational Cost for Pick-up Collection of E-Waste			
No.	Component	Quantity	Unit
Data Related to Operational Cost			
1	Population	25097	Household
2	E-Waste Generation every year	105.7	Kg/year
	Amount of Conveyance (pick-up car)	1	unit
3	Conveyance Capacity	800	Kg
	Number of trips served	10	Ritation/year
4	Number of Employee	1	Driver
		1	Co-Driver
Pick-up Fee			
5	Salary of Driver	1920000	IDR/year
	Salary of Co-Driver	1560000	IDR/year
6	Petrol Price	7650	IDR/liter
7	Distance from source to Temporary Storage	25	Km
8	Distance for Each Ritation (round trip)	50	Km
9	Total Distance for 1 year per unit Conveyance	500	Km
10	Total Distance	500	Km
11	Amount of Fuel Needed	50	Liter/year
Total Cost of Operational Cost for E-Waste Pick-up		35182500	IDR/year
Budget Plan for Construction of E-Waste Temporary Storage			
No.	Job Description	Quantity	Unit
1	Preparatory Work	940252	Lump sum
2	Wall work	3143363	Lump sum
3	Roofing work	2839986	Lump sum
4	Floor Work	821116	Lump sum
Total Cost for Construction		7744717	IDR
Maintenance Cost			
No.	Component	Quantity	Unit
1	Salary of Employee	15600000	person/year
2	Maintenance Fee of Temporary Storage	5000000	IDR/year
Maintenance of Conveyance			
3	Lubricant	730000	IDR/year
	Machine Service	2281250	IDR/year
Total Cost for Maintenance		23611250	IDR/year

Table 2 E-Waste Components of Pesanggrahan Sub-District

			Machine	Phone	Player		
1	Copper	0.75%	1.48%	-	5%	3%	0.03%
2	Aluminum	3.50%	0.88%	2%	5%	-	4.92%
3	Iron	39.75%	50.64%	8%	62%	12%	75.06%
4	Plastic	18.50%	40.60%	44%	-	23%	5.60%
5	Brass	-	0.04%	-	-	-	0.02%

Source: Cui & Zhang, 2008

g/year, NO_x is 1000 g/year, and CO is 20,000 g/year. The emission data is then interpreted using open source LCA software to determine the potential impacts. With LCA analysis, it is known that the e-waste collection system in Pesanggrahan sub-district has the potential to cause acidification of 2594,45920 H⁺ moles, ecotoxicity of 27.89640 g 2,4-D, eutrophication of 2.86999 g N, global warming of 3.89072x10⁷ g CO₂, and smog of 101.86560 g NO_x eq.

Meanwhile, for e-waste temporary storage, the buildings are made of concrete, which is not yet in accordance with government regulatory standards regarding hazardous waste management. These discrepancies include no ventilation, lighting, and doors, as well as roofs and floors that are not waterproof. These conditions allow e-waste to come into contact with rainwater and animals to enter the temporary storage building. By the interpretation of the LCA software, it is known that the temporary storage building has a potential impact on ecotoxicity of 7.67555x10⁴ g 2,4-D eq and an impact in the form of noncancerous HH of 8.30905x10⁷ g C7H7. The material flow in Fig. 1 can describe in detail the existing management system of the Pesanggrahan sub-district.

3.3 Alternative Design of E-Waste Management System

Based on the evaluation of the existing condition of the e-waste management system in the Pesanggrahan sub-district, it was found that there were many things that needed to be improved from the economic and environmental aspects. For this reason, a new, better design is needed to improve the existing system. There are two alternative systems proposed in this study, and they will be compared with the existing system from an economic and environmental perspective. The comparison between the three systems can be seen in Fig. 2.

3.3.1 Scenario 1

Electronic waste collection in scenario 1 uses an indirect communal pattern. E-waste originating from each resident's house in the Pesanggrahan sub-district will be

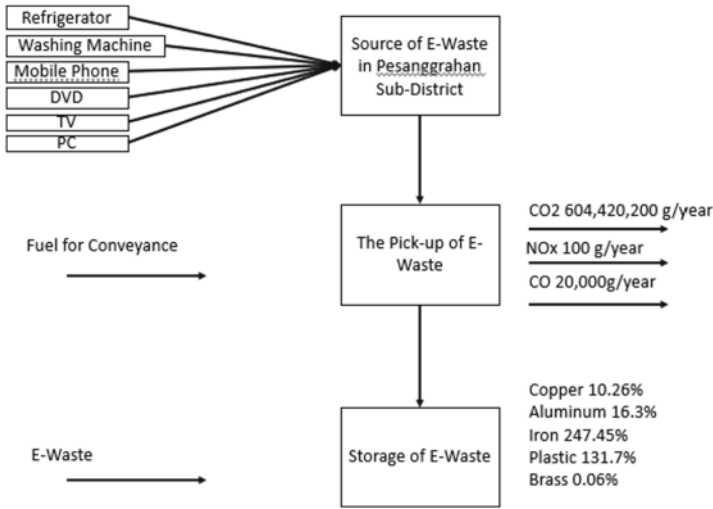


Fig. 1 Mass Balance of E-Waste Management System in Pesanggrahan Sub-District

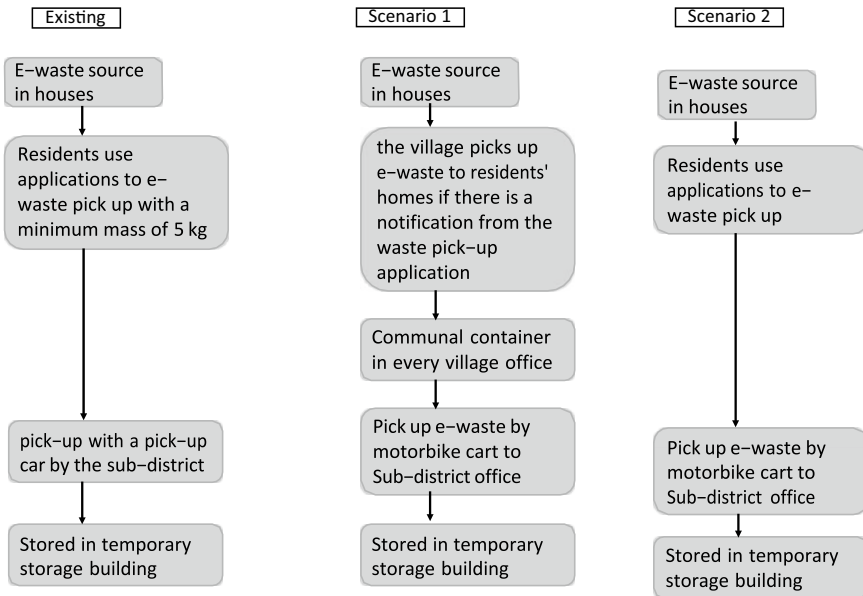


Fig.2 Comparison between Three Alternative Systems

discarded by residents through communal containers that have been prepared in each village office in the Pesanggrahan sub-district. Each e-waste that has been disposed of on the communal container will be picked up once a month by the Pesanggrahan sub-district via the application using the hazardous waste special motorcycle cart. E-waste that has been picked up will be taken to the TSB Pesanggrahan sub-district.

Evaluation of Scenario 1 from Economic Aspect

The determination of the volume of communal containers was based on the largest amount of e-waste generated in Pesanggrahan District. Container design is based on SNI 3242:2008 regarding Waste Management in Settlements; Minister of Public Works Regulation No. 3 of 2013 concerning the Implementation of Infrastructure & Facilities for Waste in the Handling of Household Waste & Types of Household Waste; and SNI No. 19-2454-2002 concerning Procedures for Operational Techniques for Urban Waste Management. The communal container used is made of plastic because it is not easily damaged or impermeable to water, is economical, and easily available on the market. For container height, the Indonesian Ministry of Health standard is used regarding the average height of Indonesians, which is 170 cm (Ministry of Health of the Republic of Indonesia). The length and width are taken from the dimensions of e-waste with the largest volume, namely washing machines and refrigerators. The dimensions of the refrigerator are length 48 cm, width 55 cm, and height 120 cm, and the dimensions of the washing machine are length 85 cm, width 53 cm, and height 55 cm. The length of the container refers to the length of the washing machine (longer than the length of the refrigerator), and the width of the container refers to the total width of the washing machine and refrigerator, which is 108 cm.

The cost of procurement of waste containers consists of wages for workers; making frames; container wheels; screws; locking slots; and painting. The total cost is around 6,390,000 IDR. Containers will be built in 5 urban villages, so the total cost for container procurement in all urban villages is 31,950,000 IDR. Electronic waste pick-up is carried out at each sub-district office in Pesanggrahan sub-district. The distance from TPS in Pesanggrahan sub-district to every TPS in 5 kelurahan and ending at Pesanggrahan sub-district again is 24.8 km, with a total travel time of about 54 minutes. The means of transportation used is a motorized tricycle with a capacity of 451 kg (125 cm x 150 cm x 125 cm). The total cost incurred for scenario 1 is 193,603,359 IDR, which consists of the cost of purchasing communal containers in each kelurahan, purchasing a motorbike cart, pick-up operational costs, and investment costs.

Evaluation of Scenario 1 from Environmental Aspect

The communal container used is made of iron. Iron is one of the biggest elements on earth. Iron is one of the elements that are environmentally friendly because iron can be reused after usage. Iron has a high resistance to hot weather or corrosion, so it can save costs by not frequently replacing trash containers made of iron. Motorized carts used for pickup emit 493.877.9 g of CO₂, 28,768 g of NO_x, and 1,388.8 g of CO₂. Furthermore, using LCA, it is interpreted that scenario 1 has a potential impact on

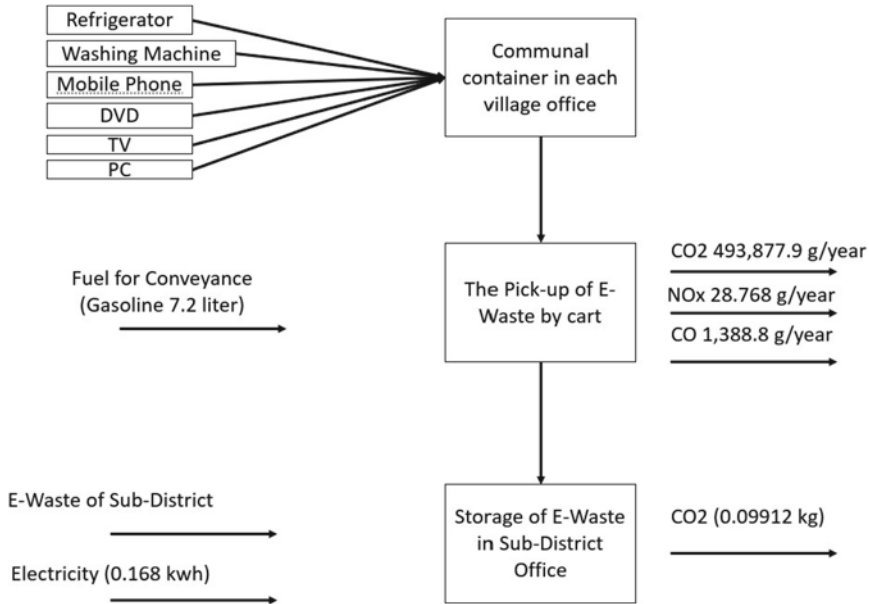


Fig. 3 Mass Balance of Scenario 1

acidification of 76,64122 H+ moles, ecotoxicity of 1.88310 g 2.4-D, eutrophication of 0.08256 g N, global warming of 3.230033x104 g CO2, and smog of 3.80547 g NOx eq. Figure 3 depicts the material flow into and out of scenario 1.

3.3.2 Scenario 2

Scenario 2 uses an indirect individual collection pattern using a door-to-door method. The e-waste generated in each resident’s house will be picked up by the Pesanggrahan sub-district waste service, and then the e-waste will be taken to the Pesanggrahan sub-district temporary storage at the Pesanggrahan sub-district office. E-waste pick-up in scenario 2 uses a pick-up route based on flood-prone areas in the Pesanggrahan sub-district. The conveyance for pick-up is using a special hazardous motorized cart. E-waste collection is carried out in the Pesanggrahan sub- district, which includes five sub-districts, namely Ulujami village, North Petukangan village, South Petukangan village, Bintaro village, and Pesanggrahan village.

Evaluation of Scenario 2 from Economic Aspect

The highest volume of e-waste generation in the sub-district of Pesanggrahan is 108 cm x 85 cm x 120 cm. Thus, the motorized cart used has a load capacity of 451 kg with a tub volume of 125 cm x 150 cm x 125 cm at a price of IDR 32,800,000. Fig. 4 shows an illustration of an e-waste motorcycle cart in scenario 2.

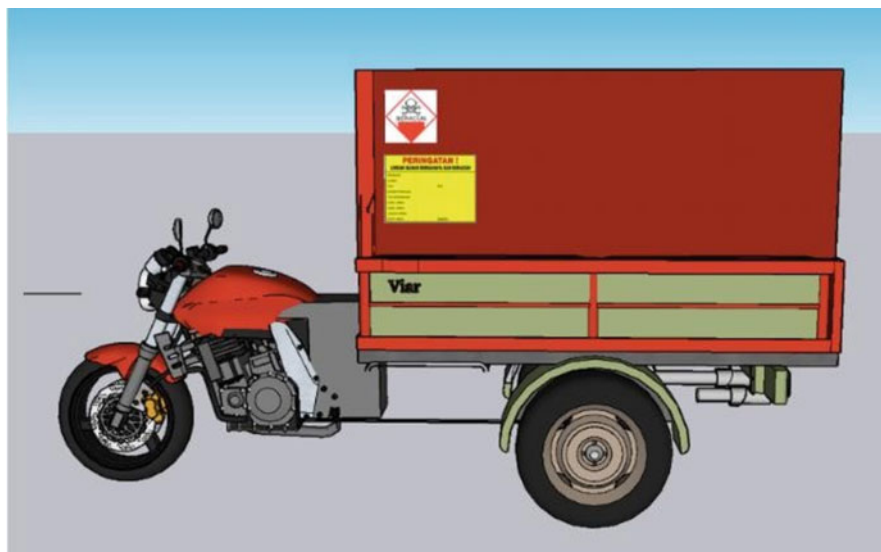


Fig. 4 E-waste Motor Cart Scenario 2

The travel route for e-waste transportation is different for each village, including the southern Petukangan village about 50.2 minutes, the Bintaro village about 57 minutes, the Ulujami village about 54 minutes, the northern Petukangan village about 41 minutes, and the Pesanggrahan village about 36 minutes. The total cost required for scenario 2 is 99,580,653 IDR, which consists of the cost of purchasing a pick-up cart (32,800,000 IDR), operational costs for picking up e-waste (19,353,153 IDR), and maintenance costs for temporary storage, transportation equipment, and staff salaries (47,427,500 IDR).

Evaluation of Scenario 2 from Environmental Aspect

The total generation was 105.7 kg/year for e-waste stored in each kelurahan. The resulting e-wastes include refrigerators, washing machines, cell phones, DVDs, TVs, and PCs. Electronic waste can be harmful to the environment if not managed properly. As with e-waste, if affected by flooding, it will result in environmental impacts such as ecotoxicity of 1.3025×10^5 g 2.4-D eq and noncancerous HH of 1.22382×10^8 g C7H7.

For pick-up of e-waste in each village, it emitted NO_x emissions of 278.8 g/year, CO emissions of 13,456 g/year, and CO₂ emissions of 46,490,360 g/year. Potential environmental impacts that occur from the results of LCA in the form of acidification produce 723.37225 H⁺ moles, ecotoxicity of 18.24531 g 2.4-D, eutrophication of 0.80015 g N, global warming of 3.01258×10^6 g CO₂, and smog of 36.87649 g NO_x eq.

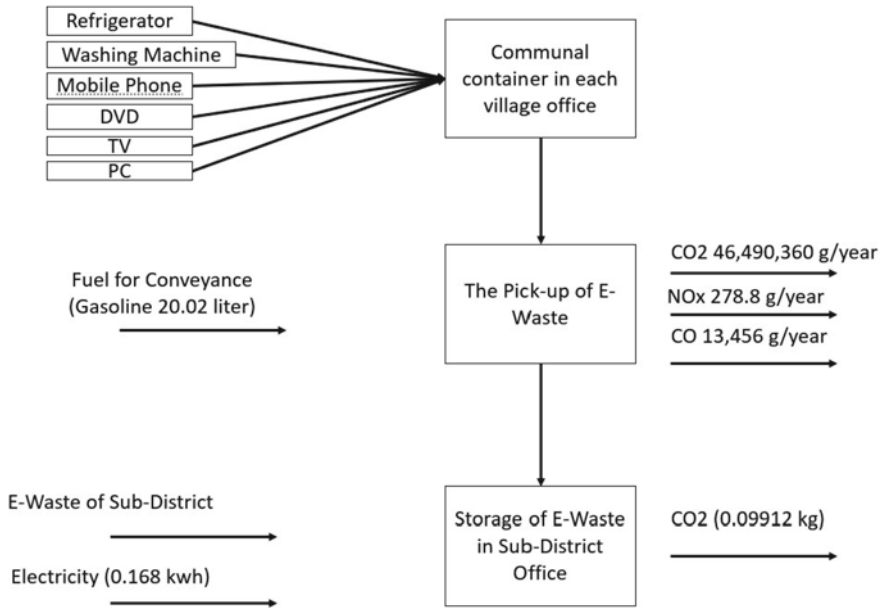


Fig. 5 Mass Balance of Scenario 2

For TSB in the sub-district, using electrical energy of 0.168 kwh produces CO2 emissions of 0.09912 kg with a potential global warming impact of 99.12 g CO2 eq.-Details of material flow from environmental aspects can be seen in Fig. 5.

3.3.3 Alternative Solution Selection

Based on the economic and environmental analysis, the alternative solution chosen is scenario 1. This is because scenario 1 produces a lower environmental impact than scenario 2. Even though scenario 1 costs more than scenario 2 (scenario 1 is 193,603,359 IDR, and scenario 2 is 99,580,653 IDR), this is not a problem because the e-waste management fund has indeed been allocated by the sub-district of 200 million rupiah, so the costs for scenario 1 are still in the budget plan.

3.4 Design of Temporary Storage Building of E-Waste in Pesangrahan Sub-District

The temporary storage building in the Pesangrahan sub-district has not been in accordance with the technical regulations that have been set, namely Government Regulation No. 101 of 2014, Regulation of the Minister of the Environment No. 30

of 2009, and the Decree of the Environmental Impact Management Agency No. 01 of 1995. The following is an explanation of the management contained in the technical regulations for storing e-waste:

1. E-waste Storage Locations

The location of the e-waste storage warehouse is designed in a flood-free area, away from hazardous materials, and has a hazardous waste symbol in front of the storage room. The location of the sub-district office is indeed a flood-free area.

2. Storage Capability

The capacity of the existing TPS in Pesanggrahan sub-district has an area of 15 m². Based on Ministerial Regulation of the State of the Environment Number 18 of 2009 concerning Procedures for Licensing Waste Management Hazardous and toxic materials Proper e-waste storage space can accommodate the waste according to the rate of its generation. The highest generation of e-waste in 2018 was 50.1 kg. To determine the storage capacity, it is necessary to know the volume produced for each e-waste stream. The largest volume of e-waste is refrigerators and washing machines. so that the storage height is designed with the highest value of a refrigerator or washing machine, which is a refrigerator height of 120 cm. For the length, the largest length was chosen, namely the length of the washing machine, 85 cm, and the width was the sum of the widths of the refrigerator and washing machine (55 cm for the refrigerator and 53 cm for the washing machine), which was 108 cm. The volume of the existing storage has been able to accommodate the highest generation of e-waste in the Pesanggrahan sub-district.

3. Storage Room Lighting

E-waste in temporary storage in Pesanggrahan sub-district does not have lights for lighting. A good e-waste storage place must have adequate lighting from lights and sunlight. Based on the Decree of the Head of the Environmental Impact Management Agency Number 01 of 1995, the distance between the lamp and the closest waste is at least 1 meter. Each block will be given an LED light for lighting at a distance of 2 meters.

4. Storage Room Ventilation

E-waste in temporary storage in Pesanggrahan sub-district does not have ventilation. Based on SNI 036572-2001, it is stated that a good storage room has good ventilation and has a ventilation area of at least 5% of the floor area.

5. Storage Building Physical Condition

According to Government Regulation No. 101 of 2014, the building of e-waste storage rooms must be protected from leaks with a roof or wall, and the floor of the room must be waterproof, not corrugated, strong, and not cracked. The storage room building uses bricks because the material properties of the bricks can withstand water seepage (waterproofing), and the walls are made of bricks that are not easy to crack. The brick wall thickness is 23 cm following the Decree of the Environmental Impact Management Agency No. 01 of 1995.

6. Label and Symbol

The label used is for e-waste storage activities, which contains information about the waste generated. The definition of the label is specific information for the storage of hazardous waste. According to Ministry of Environment Regulation No. 14 of 2013, the size has a minimum size of 15 cm x 20 cm. The label contains information related to the producer, address, producer number, date of packaging, type of waste, waste code, amount of waste, and characteristics of waste. The label must be affixed to an easily visible point. The symbol used is a toxic substance. This symbol is used because e-waste in the Pesanggrahan sub-district has the potential to cause serious illness if it enters the human body through breathing, skin, or mouth. The e-waste generated from the Pesanggrahan sub-district contains hazardous materials such as used refrigerants classified as category 1 and wire rubber classified as category 2. Therefore, e-waste in Pesanggrahan sub-district has the characteristics of toxic materials. Fig. 6 shows the label and the symbol used in the temporary storage building.

7. Emergency Response Tools

Emergency response tools are not yet available at the temporary storage building in Pesanggrahan sub-district, according to government regulation No. 101 of 2014 emergency response tools must be available at the hazardous waste storage area. The tools that must be provided at a minimum are fire extinguishers and other tools as needed.



Fig. 6 The Label and The Symbol used in The Temporary Storage Building in Pesanggrahan Sub-District

4 Conclusion

The volume of e-waste in the Pesanggrahan sub-district obtained from secondary data in 2018 was 85 cm x 108 cm x 120 cm. There are 2 scenarios of the management system compared with the existing conditions from the economic (operational and investment cost) and environmental (using LCA software) aspects.

Scenario 1 was chosen because it has been proven to have a lower potential environmental impact than scenario 2, although it requires a higher cost. The redesign of the temporary storage building was carried out based on the design criteria of government regulation No. 101 of 2014 which required it to have ventilation, doors, hazardous waste symbols and labels, fire extinguishers, and lighting.

References

1. Gaidajis Gaidajis G, Angelakoglou K (2010) A: e-waste: environmental problems and current management. *J Eng Sci Tech Review* 3(1):193–199
2. Nindyapuspa A. (2018) Kajian tentang Pengelolaan Limbah Elektronik di Negara Maju dan Berkembang. *J Info Manaj Tek* 20 [in Indonesian Language]
3. Sudaryanto S, Yusriyah K, Andesta ET (2009) Studi Komparatif Kebijakan Pengelolaan Sampah Elektronik di Negara Berkembang. *Univ. Gunadharma Doc.* 1–10 [in Indonesian Language]
4. Indonesia PR Undang-Undang Republik Indonesia Nomor 18 Tahun 2008 Tentang Pengelolaan Sampah.: <https://pelayanan.jakarta.go.id/download/regulasi/undangundang-nomor-18-tahun-2008-tentang-pengelolaan-sampah.pdf>. [In Indonesian Language]
5. Balde CP, Wang F, Kuehr R, Husmain J (2015) *The Global E-Waste Monitor 2014*. United Nations Univ, Germany [In Indonesian Language]
6. Ayuni T, Nurrochmat DR, Indrasti NS (2016) Strategi Pengelolaan Limbah Elektronik Melalui Pengembangan Infrastruktur Ramah Lingkungan. *Risalah Kebijakan Pertanian dan Lingkungan* 3:78–86 [In Indonesian Language]
7. Firman T Gunung Sampah Elektronik Menanti Penanganan. *Tirto.id*: <https://tirto.id/gunungan-sampah-elektronik-menantipenanganan-bGif>. [In Indonesian Language]
8. BPS (2010) Jumlah Penduduk Menurut Kecamatan (ribu). <https://jakselkota.bps.go.id/indicator/12/135/2/jumlah-penduduk-menurut-kecamatan.html>. [In Indonesian Language]
9. Bima DA BPBD DKI Ungkap Daftar 86 RW di Jakarta Rawan Banjir. <https://jakarta.tribunnews.com/2019/10/10/bpbd-dki-ungkap-daftar-86-rw-dijakarta-rawan-banjir>. [In Indonesian Language]
10. Encyclopedia Jakarta: Kali Pesanggrahan, Kali Besar. <http://encyclopedia.jakarta-tourism.go.id/post/kali-pesanggrahan--kalibesar?lang=id>. [In Indonesian Language]
11. Jakarta Smart City: Pengelolaan E-Waste Melalui Pengumpulan dan Penjemputan Sampah Elektronik. <https://smartcity.jakarta.go.id/blog/349/pengelolaan-e-waste-melalui-pengumpulan-dan-penjemputan-sampah-elektronik>. [In Indonesian Language]
12. Suwanti: Jakarta Siapkan Enam Gudang Limbah B3. <https://bengkulu.antaranews.com/nasional/berita/991022/jakarta-siapkan-enam-gudang-limbah-b3>. [In Indonesian Language]
13. Damanhuri, Purwanto, Astuti: Studi Persepsi dan Perilaku Jasa Servis dalam Memperpanjang Aliran Limbah Elektronik (E-Waste) di Kota Semarang. *Prosiding Seminar Nasional Pengelolaan Sumber Daya Alam dan Lingkungan* (2012). [In Indonesian Language]
14. Harjanto TR, Fahrurrozi M, Bendiyasa I (2012) Lice Cycle Assessment Pabrik Semen PT. Holcim Indonesia Tbk. Pabrik Cilacap: Komparasi antara Bahan Bakar Batubara dengan Biomassa. *Jurnal Rekayasa Proses*, 6. [In Indonesian Language]

Review of Rubber-Based Waste in Compressed Bricks



Ai Shyn Tan, Jee Cheat Tan, Lee Woen Ean, Cheng Yee Ng, Bashar S. Mohammed, and Shuhairy Norhisham

Abstract The management of the production and post-use waste disposal from rubber-based materials production or rubber waste has been a concern as it might negatively impact the environment, e.g. water and soil pollution. Henceforth, this study investigates the feasibility of utilizing rubber waste in compressed rubberized bricks. This study discusses the source of rubber waste and the design parameters for the mix ratio of compressed bricks and rubber waste. Compressive strength and water absorption were observed to examine the behaviour of the compressed bricks.

Keywords Rubber waste · interlocking bricks · rubberized bricks · mechanical and physical properties

A. S. Tan · J. C. Tan · L. W. Ean (✉) · S. Norhisham
Institute of Sustainable Energy, Universiti Tenaga Nasional, Jalan IKRAM-UNITEN, 43000 Kajang, Selangor, Malaysia
e-mail: leewoen@uniten.edu.my

J. C. Tan
e-mail: tjcheat@uniten.edu.my

S. Norhisham
e-mail: shuhairy@uniten.edu.my

C. Y. Ng · B. S. Mohammed
Department of Civil and Environmental Engineering, Universiti Teknologi PETRONAS, Perak, Malaysia
e-mail: chengyee.ng@utp.edu.my

B. S. Mohammed
e-mail: bashar.mohammed@utp.edu.my

1 Introduction

Malaysia is the world's fourth-largest rubber producer. In Malaysia, the processing techniques of raw natural rubber are the manufacture of natural rubber latex (NRL) concentrates and Standard Malaysian Rubber (SMR). The rubber industry's manufacturing process always generates a considerable volume of polluted effluent due to the large amount of water required during processing. Untreated effluent from the rubber industry is commonly connected with a severe odour issue and includes a significant number of toxins and pollutants [1].

Recently, the production and usage of disposable nitrile gloves have shown a significant increment due to the Covid-19 pandemic. This has also been reflected in the production of nitrile gloves and rubber waste. Rubber nitrile gloves are classified as non-biodegradable waste. With that, the waste produced from the production is also considered hazardous. On top of that, multiple waste processes are needed to reduce the environmental impact of disposal [2]. Researchers have proposed to recycle the rubber waste in the construction field as it replaces and reduces the use of natural aggregates, reduces the harm to the environment, and also reduces the burden of polluting the environment [2].

This purpose of the study is to discuss the use of rubber waste in compressed brick production. There are different types of rubber waste that had been used in the construction sector. The mix design of rubber waste in brick production observed from the article of other researchers and study the behaviour of rubber particles that had been used in the brick mixture.

2 Sources of Rubber Waste

Waste production is considered an outcome of the growth of human populations and economic development. The main components of municipal solid waste are including food waste, rubber and leather waste. An estimated 2.01 billion tonnes of municipal solid waste were produced in 2016 and are anticipated to reach at an amount of 3.4 billion tonnes in the upcoming 34 years. Asia was believed to be the biggest waste contributor, accounting for a total of 60%. East Asia, the Pacific and Europe generated 23% and central Asia produced 20% of waste. Meanwhile, South Asia contributed 17% of global solid waste [3].

Rubber is widely used in the medical and home appliances. Due to the Covid-19 pandemic occurred, there are roughly 65 billion rubber gloves waste was recorded in the past year alone. As a result, there are many used rubber gloves and PPE equipment was consumed and discarded. The increasing demand for these products during the pandemic period is not helping the amount of rubber waste produced. The quantity of rubber waste is increasing and leading to a huge amount of waste management [3]. In addition, another major source of rubber waste tyres is the waste tyre and it is widely categorized as automotive and truck tyres. Taiwan generates around 100,000

tonnes of tyre trash per year, and in year 2002 alone, more than 37 million tonnes of tyres were used in UK. In addition, in Europe of 90 facilities, account for about a quarter of global output where 355 million tyres are produced annually [3]. Every year, the world generates more than 6.5 billion tonnes of discarded plastic and rubber waste, and their disposal poses a significant environmental danger due to requiring a longer time for deterioration.

Thence, recycling and repurposing of wastes products waste products consisting of rubber and plastic as green building materials has the potential to lessen environmental impact. The synthetic polymer materials rubber and plastic share the identical fundamental constituents but different topologies. The workability of concrete is decreased by the presence of plastic, but the size and replacement amount of rubber aggregate determine the effect. In addition, as compared to the natural aggregate, the smooth surface and low specific gravity of plastic or rubber aggregate increased pore structure, lowering matrix density and mechanical strength [4]. Rubber waste from tyres can used as a replacement in concrete components due to their high strength, ductility, and strain control qualities. Rubber can be used to replace fine aggregates (FA) and coarse aggregates (CA) in concrete and mortar, or as a binder. The physical qualities and compositions of tyres from diverse sources vary widely. As a result, they have distinct effects on concrete strength when in use. Natural and synthetic rubbers, carbon black, metal, textile fabric, and additives are all popular tyre constituents [5]. Other than concrete, several researchers were conducted for waste tyres rubber in brick production and found that it can be used as fine aggregate replacement or as a filler [6, 7].

Rubber waste contains many used items such as rubber gloves, rubber condoms, and other rubber products that essential to household, commercial and industrial. Regardless, waste tyres account for the majority of the total amount of rubber waste. Figure 1 shows the rubber wastes in the various types of sectors [3]. Waste tyre recycling has a significant market potential in highway building construction. Mechanical shredding of rubber automobile sector waste provided the rubber particles. Waste tyre-modified Portland cement concrete has been the subject of several investigations. The advantages of rubberized concrete composition are lower density, higher impact resistance, ductility and sound insulation [8]. Waste tyre rubber is disposed of in a variety of methods, including burning and landfilling, as well as being utilized as mulch on sports fields and as a binder modifier in asphalt. Possible uses for used tyre rubber are their incorporation into concrete as a replacement for cement and natural aggregates. It is an ecological approach to repurpose the discarded tyre rubber particles as raw materials in concrete production [9].

3 Mix Design of Rubber Waste in Brick Production

There are various types of bricks. The first type of brick is burnt clay brick or also known as fire clay brick. This type of brick was formed by pressing the wet clay into mould form, being dried, and being fired in the kiln. Burnt clay brick was sold in

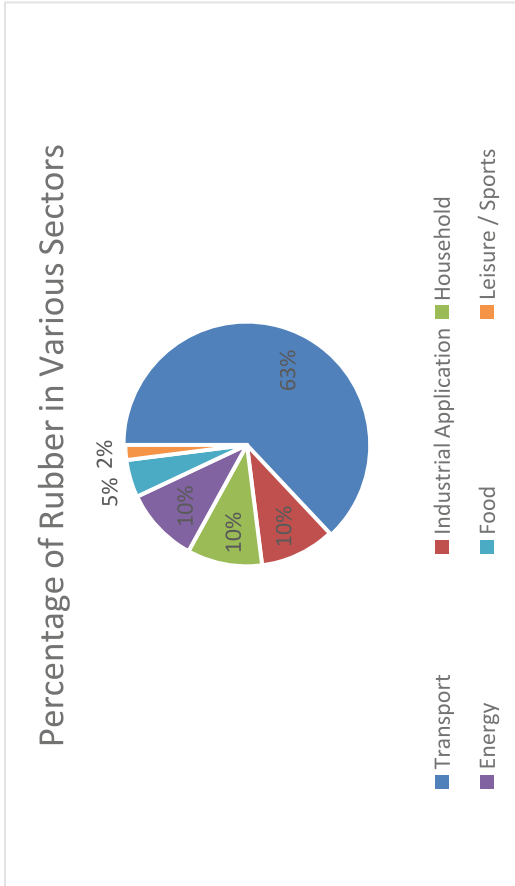


Fig. 1 Percentage of rubber in various sectors [3]

four type of classes and it is not only based on its appearance but also categorised according to its porosity and strength [10]. The next type of brick is fly ash bricks, it was produced from a combination with fly ash and clay that was fired under extremely high temperature. The use of fly ash in brick manufacturing leads to a greater content of calcium oxide with less porosity and show a lower level of water penetration [11]. The last type of brick is concrete bricks, which was used as a building material in the construction of walls with a mixture of powdered cement, water, sand, and gravel [12].

Bricks are a common building and construction material all throughout the world. Zhang [13] state that the conventional bricks are made by using high- temperature kiln fires or from Ordinary Portland cement (OPC), which has a high embodied energy and a huge carbon footprint. The rubberized waste in the past research paper act as raw materials of the construction sector, especially in brick production.

Benazzouk et al. [8] studied on the thermal properties of lightweight construction products with rubber waste. The study was conducted under dry conditions by using a transient plane source (TPS) technique. Mechanical shredding of rubber automobile sector waste provided the rubber particles employed in this investigation. These rubber waste particles are made up of less than 1 mm in diameter and contain around 20% by volume of synthetic fibres. According to Standard NF P 15–301, the cement used was CPJ CEM II 32.5. In a laboratory mixer, the dry mixing is involved with rubber particles and cement. Rubber was used as a replacement for cement in combinations at a volume ratio ranging from 0 to 50%. Before and after demolding, two cubic samples of $10 \times 10 \times 10$ cm were made for each combination. It is moisture cured 98% humidity for 28 days. The inclusion of rubber particles in the composite resulted in a significant decrease in heat conductivity. the performance of 50% of rubber particles used has obtained 0.47W/mK of thermal conductivity, 10.50 MPa of compressive strength, 3.25 MPa of flexural weight and 1150 kg/m³ of unit weight. As a result, the development potential appears to be rather high. The inclusion of the material might have a variety of uses, including preventing heat transmission and conserving energy in structures with a poor load-bearing capacity.

Bashar S. Mohammed et al. [14] developed crumb rubber hollow concrete block (CRHCB). To achieve the purpose of this work, 64 trial mixes were prepared to produce hollow concrete blocks with 0%, 10%, 25% and 50% crumb rubber (CR) as a substitute for fine aggregate. The materials used in this research is OPC Type I followed specification of ASTM C150, class F fly ash according to the requirement ASTM C618, silica fume followed specification ASTM C1240, the processed crumb rubber mesh size 600 μ m, river sand and 10 mm nominal size gravel were selected as aggregate in the mixtures. This study included fifteen experimental mixes with three degrees of crumb rubber substitution (10%, 25%, and 50%) by volume, as well as a control mix. Fly ash (5%, 15%, and 30%) and silica fume (5%, 10%, and 20%) were used to replace by volume to cement content. For the effort to meet the BS EN 771 and ASTM C90 concrete block requirements, the best substitute for crumb rubber is 50%. The appropriate quantity of fly ash replacement to cement, which was 15%, may have beneficial impacts on the interfacial connection between the cement paste and the aggregate. Furthermore, fly ash in concrete can decreases the

quantity of lime (calcium hydroxide) used and convert to calcium silicate hydrate, providing additional cementitious material and increasing the strength of the concrete block mix. As the CR % grows, the adhesion between the cement pastes and coarse aggregate diminishes, lowering the compressive strength as well as splitting tensile strength.

Ankush Thakur et al. [7] studied waste crumb rubber tyres used to partially substitute fine aggregates for developing bricks which have the parameters of using 5%, 10%, 15%, and 20% of crumb rubber by volume of fine aggregates, while keeping a constant water/cement ratio of 0.43 for all specified mixtures. The size range of ground tyre powder is between 45 μm and 1.2 mm. The flow ability was measured using fresh characteristics such as slump and density. The mechanical parameters of hardened concrete bricks, such as compressive strength, tensile strength, and impact resistance, were investigated, and tensile strength was estimated using regression analysis. After curing for 28 days, the maximum value of compressive strength is 7.5 MPa (5% CR) and minimum value is 5.67 MPa (20% CR). It was discovered that when the percentage of crumb rubber grew, the slump and water absorption increased linearly.

Sodupe-Ortega et al. [15] examined the use of crumb rubber (CR) as an aggregate in dry-mix mortars to make rubberized long hollow blocks and bricks with automated brick machines. The first material is rubberized mortar mixes were made with ASTM Type II Portland cement (A-L 42.5 R) with a density of 3150 kg/m^3 . Fine aggregate with a size range of 0 to 4 mm was used in this study. Crumb rubber was introduced in the range of from 10 to 40% with the water/cement ratio of 0.7, 0.8 and 0.9. The particle size which is ranging from 1 to 4 mm in diameter is used as an alternative for fine aggregate. The mixing water was used to dissolve a semi-dry and prefabricated concrete superplasticizer which was then applied to the mortar mixtures. For the three batches of w/c ratios generated, totally of 64 slump tests were performed and saturated weight content was measured. Compressive strength tests were performed on laboratory and commercial samples in accordance with EN 12,390-3 and EN 772-1, respectively. SEM was used to examine the microstructure of rubberized mortar samples following a 28-day curing period. The compressive strength of mortar specimens with a w/c ratio of 0.9 was marginally lower than that of specimens with w/c ratios of 0.7 and 0.8. The increased use of CR resulted in a reduction in compressive strength.

Paki Turgut et al. [16] make research about the properties of rubber-added bricks in terms of physico-mechanical and thermal insulation. By adding varied amounts of crumb rubber to regular cementitious mixtures, it will improve the thermal insulation efficacy. The quantity of crumb rubber utilized is affecting the percentage gains in thermal insulation performance ranging from 5 to 11 percent. The main material, crumb rubber employed in this study is made from steel-free scrap tyre sections. It is made up of particles with sizes ranging from 4.75 mm to 0.075 mm. The sand used was taken from the Goksu River in Adiaman, Turkey, and the largest particle size was 4.75 mm. the water used in this studied was test the sulphate concentration pH value and hardness. The tap water used in this study tested sulfate concentration, pH value and hardness of 5.6 mg/l, 6.2 and 3.7, respectively. Also, the Portland cement

utilized is manufactured in Sanliurfa, Turkey. The cement amount and water ratios in the mixtures are maintained constant to assess the effects of different sand and crumb rubber combinations. Then, replacement of 10% crumb rubber indicates that crumb rubber replaces 10% of the volume of equivalent sand. The bricks are left to cure for 28 days in curing tank after demoulding process. Highest result of water absorption and porosity test shown on sample R-70 with 7.41% and 11.4% respectively. The sample R-70 contains highest value of crumb rubber (705 g) and lowest content of sand (786 g). Highest result of compressive strength, flexural strength and splitting strength shown on sample R-10 with lowest rubber content (101 g) and highest sand content (2357 g). The result is 25.1%, 4.94% and 2.46% respectively.

Table 1 shows the summary of the papers discussed in the paragraph. Based on the paper from the researchers, the size and percentage of rubber waste in mixture affects the results of mechanical and physical properties. 20% of crumb rubber provided approximately 6.8% of water absorption after curing. Meanwhile, 70% of crumb rubber replacement shows approximately 7.41% of water absorption result. These results indicate the presence of microcracks in concrete masonry bricks is caused by rubber expansion, and the bonding force between rubber and cement is weak [7]. However, shredded rubber waste with a size of less than 1 mm replaced 10% of the cement and achieved a compressive strength of 49.5 MPa [7].

Table 1 Summary of rubber mix design and behaviour

Ref	Type of rubber	Size of rubber	Mix design	Compressive strength (MPa)	Water absorption (%)
[8]	Shredded rubber	Less than 1 mm	10% rubber replacement of cement	49.5 MPa	-
[14]	Mesh size crumb rubber	600 µm	Replacement of silica fume, fly ash or both	13.5 MPa (10% CR)	< 288 kg/m ³
[7]	Crumb rubber		Range of 5%-20% of rubber	7.5 MPa (5% CR)	6.8% (20% CR)
[15]	Mechanical shredding crumb rubber	1-4 mm	10%-40%	22 MPa (10% CR with w/c 0.8, 28 days curing)	-
[16]	Crumb rubber	0.075 mm-4.75 mm	Range of 10%-70% rubber replacement	28.7 MPa (10% CR)	7.41% (70% CR)
[17]	Rubber glove manufacturing residue (RGMR), crumb rubber	< 500 µm (RGMR), 600 µm - 2.36 mm (crumb rubber)	10% rubber replacement of sand	13.94 MPa (10% RGMR, < 500 µm)	10.46% (10% RGMR, < 500 µm)

Moreover, the comparison between the utilization of rubber glove manufacturing residue (RGMR) results by Soo et al. [17] showed that the finer particle size of RGMR has slightly increased the compressive strength of compressed brick, and enhanced the performance of water absorption. Based on the observation through Scanning Electron Microscope (SEM), the interlocking brick that using finer particles (less than 500 μm) are filled the interstitial areas between the sand particles and resulting in a denser volume distribution. It also can be proved that the compressed brick is hydrophobic by using of rubber-based material as the fine aggregate substitute and decreasing the strength significantly. However, all the compressed brick that using rubber-based material have satisfied the non-load-bearing concrete masonry in accordance with ASTM C129 which stated must at least obtained 4.14 MPa.

4 Conclusion

The main source of rubber waste is tyre rubber. Waste tyre rubber is disposed by incineration or landfill which has possibility to pollute the environment. Therefore, waste tyre rubber is utilized in construction field is an eco-friendly option to reduce the waste. The general conclusion for waste rubber tyres as building materials is as follows:

- The proportion of rubber powder is mostly between 0 and 20%, and the size range of rubber particles is varying, ranging from 500 μm to 4 mm. The shape and size of the rubber particles and their low specific gravity have an impact on the strength.
- The results of compressive strength gradually reduced with increasing rubber content in the construction material. A poor connection is formed between the rubber particles and the grout, resulting in micro-cracks and poor bonding in the mixture. The water absorption increases linearly with the amount of rubber in the compound, but the compressive strength decreases.

In short, for the application of rubber waste in bricks, it is recommended that the proportion of rubber particles should not exceed 20% of the replacement amount, and the size of the rubber should be less than 4 mm to achieve higher compressive strength. A recommendation for future research is to determine the performance of building materials by utilizing other sources of rubber waste, especially the high volumes of waste produced in the manufacturing line.

Acknowledgements The authors would like to acknowledge the financial support from Ministry of Higher Education Malaysia, for funding this study under the Fundamental Research Grant Scheme (FRGS): FRGS/1/2021/TK01/UNITEN/02/1.

References

1. Mokhtar NM, Lau WJ, Ismail AF, Veerasamy D: Membrane distillation technology for treatment of wastewater from rubber industry in Malaysia. In: *Procedia CIRP* **26**, pp. 792–796 (2015)
2. Steyn ZC, Babafemi AJ, Fataar H, Combrinck R (2021) Concrete containing waste recycled glass, plastic and rubber as sand replacement. In: *Constr. Build. Mater.* **269**, p. 121242
3. Chittella H, Yoon LW, Ramarad S, Lai Z-W (2021) Rubber waste management: a review on methods, mechanism, and prospects. In: *Polym. Degrad. Stab.* **194**:109761
4. Li X, Ling TC, Mo KH (2020) Functions and impacts of plastic/rubber wastes as eco-friendly aggregate in concrete – a review. In: *Constr. Build Mater* **240**, 117869
5. Siddika A, Al-Mamun MA, Alyousef R, Amran YHM, Aslani F, Alabduljabbar H (2019) Properties and utilizations of waste tire rubber in concrete: a review. In: *Constr Build Mater* **224**:711–731
6. Ganjian E, Khorami M, Maghsoudi AA (2009) Scrap-tyre-rubber replacement for aggregate and filler in concrete. In: *Constr Build Mater* **23**(5):1828–1836
7. Thakur A, Senthil K, Sharma R, Singh AP (2020) Employment of crumb rubber tyre in concrete masonry bricks. In: *Mater Today Proc* **32**:553–559
8. Benazzouk A, Douzane O, Mezreb K, Laidoudi B, Quéneudec M (2008) Thermal conductivity of cement composites containing rubber waste particles: Experimental study and modelling. In: *Constr Build Mater* **22**(4):573–579
9. Li Y, Zhang S, Wang R, Dang F (2019) Potential use of waste tire rubber as aggregate in cement concrete – a comprehensive review. In: *Constr Build Mater* **225**:1183–1201
10. Kadir AA, Sarani NA (2012) An overview of wastes recycling in fired clay bricks. In: *Int J Integr Eng* **4**(2):53–69
11. Priyadarshini M, Giri JP, Patnaik M (2021) Variability in the compressive strength of non-conventional bricks containing agro and industrial waste. In: *Case Stud Constr Mater* **14**:e00506
12. Javan AR, Seifi H, Lin X, Xie YM (2020) Mechanical behaviour of composite structures made of topologically interlocking concrete bricks with soft interfaces. In: *Mater Des* **186**:108347
13. Zhang L (2013) Production of bricks from waste materials – a review. In: *Constr Build Mater* **47**:643–655
14. Mohammed BS, Hossain KMA, Ting JES, Wong G, Abdullahi M (2012) Properties of crumb rubber hollow concrete block. In: *J Clean Prod* **23**(1):57–67
15. Sodupe-Ortega E, Fraile-Garcia E, Ferreiro-Cabello J, Sanz-Garcia A (2016) Evaluation of crumb rubber as aggregate for automated manufacturing of rubberized long hollow blocks and bricks. In: *Constr Build Mater* **106**:305–316
16. Turgut P, Yesilata B (2001) Physico-mechanical and thermal performances of newly developed rubber-added bricks. In: *Energy Build* **40**(5):679–688
17. Soo S-Q, Ean L-W, Ng C-Y, Tan J-C (2022) Feasibility study of compressed bricks utilizing rubber glove manufacturing residue. *E3S Web Conf* **347**: 02005

Zero Runoff Drainage System for Bintaro Jaya Xchange Mall Project in South Tangerang, Indonesia



Luhur Budi Nanda and Teddy W. Sudinda

Abstract Population growth in Indonesia is increasing day by day, especially in South Tangerang. Infrastructure development in the housing and recreation sector has begun to be intensified. One of the areas being developed is Bintaro Xchange Mall Phase II, South Tangerang. In its development, special attention is needed to hydrological problems that can occur such as puddles and even floods. In this study, a drainage system will be planned using the zero runoff concept so as not to provide water runoff into city drains using infiltration wells and rainwater harvesting (RWH). Based on the result of drainage calculations the peak discharge was 0.116 m³/s, therefor to fulfill the zero runoff concept, 106 infiltration wells were built in the area, and used 3 rainwater harvesting to collect water that falls from the roof of the building.

Keywords drainage · eco drainage · infiltration wells · water harvesting · zero runoff

1 Introduction

As a tropical nation, Indonesia experiences a lot of rain. Flooding may occur as a result of heavy rain (Elokpere et al. 2022). Rain that falls on the roof and asphalt cannot be absorbed by the ground, resulting in runoff that flows into the city channel (Lestari 2016). Therefore, it is necessary to plan a good drainage system so that it does not add to the burden of drainage into the city canals. Planning a drainage system with the concept of zero runoff is very suitable to overcome the problem of runoff in an area. Where the zero runoff concept itself is a concept of managing

L. B. Nanda (✉)
Civil Engineering, Universitas Trisakti, Jakarta, Indonesia
e-mail: luhur99945@gmail.com

T. W. Sudinda
Civil Engineering, Universitas Trisakti and Research Center for Environmental and Clean Technology - BRIN, Jakarta, Indonesia

© Institute of Technology PETRONAS Sdn Bhd 2024
B. S. Mohammed et al. (eds.), *Proceedings of the International Conference on Emerging Smart Cities (ICESC2022)*, Lecture Notes in Civil Engineering 324,
https://doi.org/10.1007/978-981-99-1111-0_20

rainwater by accommodating or holding runoff on the surface, so as not to increase runoff discharge into city drains. This concept can also maintain the availability of water in the soil (Onainor 2019)

Infiltration wells and water harvesting are two drainage technologies that have been developed. Several studies have been conducted in the context of implementing infiltration wells in various locations (Belladonna et al. 2018)(Handayani 2020)(Kusumastuti and Jokowinarno, 2014) as well as the implementation of water harvesting (Aly et al. 2022, Demeke et al. 2021, Eun et al. 2022, Kubiku et al. 2022)

The purpose of this study is to plan a drainage system so that there is no runoff into city drains. It is hoped that this research can be useful for sustainable development stack holders.

2 Research Methodology

2.1 Location Study

The research location is in the Pondok Aren sub-district, South Tangerang City, which is included in the Banten Province, with an area of 147.19 Km². The Bintaro Xchange Mall Phase-2 project stands on an area of 220000 m². Geographically, the land slope of South Tangerang City has a relatively flat topography with an average land slope ranging from 3-8% and an area of 0-25 m above sea level. Meanwhile, the average air temperature in the area is between 23.74-32.68°C, with air humidity and sun intensity on average around 79% and 53.8%, respectively. And has a water table depth ranging from 2.70 - 8.00 meters below ground level.

2.2 Methodology

Rainfall Plan. The BMKG Climatology, South Tangerang, Pondok Betung rain station will be used to calculate the maximum rainfall for this study. Data spanning a 10-year return period, starting from 2012 - 2021, will be used. mm units are used (Table 1).

Data Consistency Test. RAPS is used by paying attention to the value of the calculated Q must be smaller than the Q table and the R count must be smaller than the R table.

Distribution Frequency Analysis. Four different distribution methods are used to calculate the time and return period for the frequency analysis, including Normal Distribution, Gumbel distribution, Log-Normal Distribution, and Log Pearson III Distribution. The Chi-Square test and the Smirnov-Kolmogorov test are two methods for completing the distribution test.

Table 1 Data of Maximum Rainfall from 2012–2021

No	Year	Climatology Station, Pondok <u>Betung</u>
1	2012	80
2	2013	96
3	2014	120
4	2015	117
5	2016	97
6	2017	80
7	2018	86
8	2019	77
9	2020	209
10	2021	323

1. Chi-Square Distribution Test

The calculated chi-square value will be appropriate if it is less than the critical chi-square value obtained from the 5% or 0.05 degree of confidence table by looking at the degrees of freedom. The degrees of freedom and Chi-Square calculation formulas are as follows.

$$Dk = k - (m - 1) \quad (1)$$

$$K = 1 + 3,3 \text{ Log } n \quad (2)$$

$$X^2 = \sum_{i=1}^n \frac{(Of - Ef)^2}{Ef} \quad (3)$$

where DK = degree of freedom, K = number of classes, X^2 = chi-squared count.

2. Smirnov-kolmogorov Distribution Test

If the Δp max value is less than the critical Δp obtained from the 5% or 0.05 degree of confidence table by looking at the number of years of the return period used, the Smirnov- Kolmogorov distribution test value will be appropriate. The calculation formula is as follows.

$$\Delta p = P(X_i) - P'(X_i) \quad (4)$$

$$P(X_i) = \frac{m}{n + 1} \quad (5)$$

$$P'(X_i) = 1 - P(X_i) \quad (6)$$

where, $P(X_i)$ = empirical opportunity, $P'(X_i)$ = theoretical opportunity

Rainfall intensity. Concentration time is the time it takes for raindrops to fall to the ground and become runoff. In this study using the time of concentration with the Federal Aviation Administration (FAA) method. With the following formula.

$$t_c = t_i + t_d \quad (7)$$

where, t_c = concentration time, t_i = inlet time, t_d = drain time

The monobe formula is used to calculate rainfall intensity to know the value of rainfall at each time unit based on daily, monthly, and annual data.

$$I = \frac{R}{24} \frac{(24)^{2/3}}{t} \quad (8)$$

where, I = rain intensity, R = rainfall on return

Peak Flood Discharge. The planned flood discharge calculation aims to find the maximum value of drainage using a return period of 2-5 years. The following formula (Rational formula) is used to calculate the design flood discharge.

$$Q = 0.00278 \times I \times C_s \times A \quad (9)$$

where, Q = Peak Flood Discharge (m^3/second), I = rain intensity (mm/jam), C_s = deviation coefficient, A = area of flow (Ha)

Channel Dimensions. Planning for affordable channel dimensions is necessary for hydraulic analysis. A rectangular cross-sectional channel with the Manning equation was employed in this study.

$$Q = \frac{1}{n} \times R^{2/3} \times S^{1/2} \times A \quad (10)$$

where, Q = channel discharge (m^3/second), n = manning coefficient, R = hydraulic radius, S = channel slope, A = cross-sectional area.

3 Results and Discussions

3.1 Distribution Frequency Analysis Test

From the results obtained in this study, the intensity of rain will be used with the Log Pearson III method. Because the results of the calculations on the Chi-Square Test and the Smirnov-Kolmogorov Test are appropriate (Table 2, 3, 4).

Table 2 Chi-Square Test Calculation Result

		Chi-Square Test	
Method	Count	Critical	Description
Gumbel	9.00	5.991	not suitable
Normal	12.00	5.991	not suitable
Log-Normal	12.00	5.991	not suitable
Log Pearson III	1.00	5.991	suitable

Table 3. Smirnov Kolmogorov Test Calculation Result Smirnov Kolmogorov Test

		Smirnov Kolmogorov Test	
Method	Count	Critical	Description
Gumbel	0.23	0.41	suitable
Normal	0.27	0.41	suitable
Log-Normal	0.19	0.41	suitable
Log Pearson III	0.18	0.41	suitable

Table 4 Calculation Result of Planned Rainfall

Return Period (years)	Gumbel	Normal	Log-Normal	Log Person III
2	117.877	128.510	114.147	101.601
5	211.750	194.564	169.407	157.207

3.2 Peak Flood Discharge

Drainage Plan. The planning for the drainage scheme above uses infiltration wells and rainwater reservoirs that collect water that falls from the roof and then goes down to the rainwater reservoir and will be accommodated with a calculated capacity. If it rains continuously and the rainwater reservoir can no longer hold water, the water will be run off to the nearest infiltration well to prevent runoff from flowing out of the channel. As for the area of the area, square channels are used to accommodate water that falls around the area, then the water will be channeled to infiltration wells, if the infiltration well can no longer hold water, the water will automatically flow into the drainage channel and go to the next infiltration well so as not to give runoff to city drains (Fig. 1 and 2).

The results of the rainfall intensity (I) and the planned flood discharge (Q) calculations will be obtained in each planned channel during the calculation of the planned flood discharge (Table 5).

Channel dimensions. Based on the results of the dimension calculation, the channel that will be used as dimensions $b = 0.3$ m and $h = 0.3$ m.

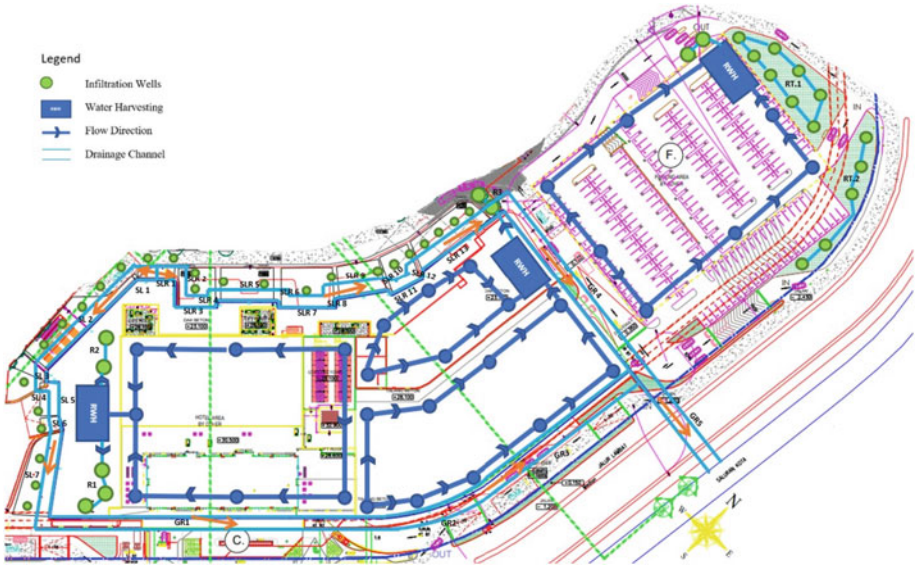


Fig. 1 Drainage Plan



Fig. 2 Detail Drainage Plan

Table 5 Calculation of the Result of rainfall intensity (I) and the planned flood discharge (Q)

Channel Name	$\Sigma(C X A)$	Cs	I (mm/jam) (5 years)	Q Area (m ³ /sec) (5 years)	Q Design
S.L.1	0.003	0.99	234.11	0.0024	0.0024
S.L.2	0.061	0.98	229.04	0.0382	0.0382
S.L.3	0.068	0.98	228.65	0.0428	0.0428
S.L.4	0.068	0.97	228.19	0.0427	0.0427
S.L.5	0.071	0.97	226.85	0.0442	0.0442
S.L.6	0.079	0.97	226.29	0.0487	0.0487
S.L.7	0.132	0.96	222.96	0.0792	0.0792
G.R.1	0.132	0.96	211.38	0.0750	0.0750
G.R.2	0.132	0.95	208.74	0.0735	0.0735
G.R.3	0.132	0.93	202.41	0.0699	0.0699
S.L.R.1	0.137	0.92	234.74	0.0823	0.0823
S.L.R.2	0.137	0.91	233.70	0.0818	0.0818
S.L.R.3	0.152	0.91	231.96	0.0899	0.0899
S.L.R.4	0.0006	0.99	238.49	0.0004	0.0004
S.L.R.5	0.010	0.99	236.15	0.0070	0.0070
S.L.R.6	0.010	0.99	235.96	0.0070	0.0070
S.L.R.7	0.021	0.98	233.44	0.0139	0.0139
S.L.R.8	0.021	0.98	233.17	0.0138	0.0138
S.L.R.9	0.037	0.97	231.17	0.0238	0.0238
S.L.R.10	0.037	0.97	230.99	0.0238	0.0238
S.L.R.11	0.013	0.99	218.73	0.0083	0.0083
S.L.R.12	0.013	0.99	218.55	0.0083	0.0083
S.L.R.13	0.038	0.98	215.00	0.0224	0.0224
G.R.4	0.038	0.96	208.30	0.0212	0.0212
G.R.5	0.038	0.95	204.34	0.0205	0.1116

Calculation of Rainwater Harvesting Storage. For the calculation of the rainwater reservoir, the volume of water that can be stored for one hour of rain will be determined (Fig. 3 and Table 6, 7).

Infiltration wells. The groundwater level must be higher than 2 meters to use infiltration wells. As a result, the groundwater level at the Bintaro Jaya Xchange Mall Phase 2 project ranges from -2.7 to -8 m. Infiltration wells will be designed with a diameter of 2m and a depth of 3m for all infiltration wells in the area (Fig. 4 and Table 8).

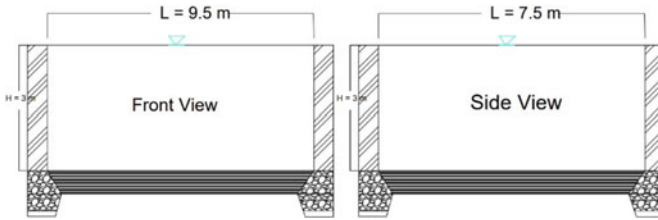


Fig. 3 Front and Side View of Rainwater Harvesting Tank

Table 6 Calculation of Rainwater Storage

Water Harvesting Location	A	Rainfall intensity	C	Rain duration		Volume
	(m ²)	(m/hour)		(hour)	(m ³)	Liter
Hotel	4475,457	0,05	0,85	1	207,328	207.328,010
Mall	3363,372	0,05	0,85	1	155,810	155.810,064
Mall and Field	1516,062	0,05	0,85	1	70,232	70.232,434
Parking Area	4517,997	0,05	0,85	1	209,299	209.298,720

Table 7 Dimensions of Rainwater Storage

Water Harvesting Location	Depth	Long	Wide	Results
	(m)	(m)	(m)	(m ³)
Hotel	3	9.5	7.5	213.75
Mall and Field	3	9.5	8	228
Parking Area	3	9.5	7.5	213.75

Fig. 4 Side and Top View of Infiltration Wells

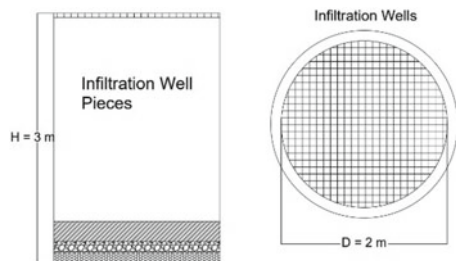


Table 8. infiltration well calculation results

Infiltration Well Location	Diameter (m)	Hsr (m)	Qsr (m ³ /hour)
Hotel	2	3	7.91
Mall and Field	2	3	7.91
Parking Area	2	3	7.91

Conclusion The conclusion of this study is to use rainwater harvesting (RWH) with dimensions of (RWH) in the hotel and parking area is $3 \text{ m} \times 9.5 \text{ m} \times 7.5 \text{ m}$ which can accommodate as much as 213750 liters of water, for the mall area and not concrete the dimensions of the RWH are $3 \text{ m} \times 9.5 \text{ m} \times 8 \text{ m}$ which can accommodate 228000 Liters of water and required 106 infiltration wells, 43 for runoff from water harvesting, 57 for collecting from regional drains and 6 for garden areas. The 5-year planned flood discharge is $0.1116 \text{ m}^3/\text{s}$ and the planned flood discharge for the 5 years after eco drainage is $0.0911 \text{ m}^3/\text{s}$.

Acknowledgements The author would like to thank PT. Jaya Real Property has provided the data for this research. Also, the Department of Civil Engineering, Trisakti University, has provided support.

References

- Aly MM, Sakr SA, Zayed MSM (2022) Selection of the optimum locations for rainwater harvesting in arid regions using WMS and remote sensing. case study: Wadi Hodein Basin, Red Sea, Egypt. *Alexandria Engineering J* **61**(12):9795–9810. <https://doi.org/10.1016/j.aej.2022.02.046>
- Belladonna M, Nasir N, Agustomi E (2018) Design of Infiltration Well to Reduce Inundation in Rawa Makmur Village , Bengkulu City. *Design of Infiltration Well To Reduce Inundation in Rawa Makmur Village, Bengkulu City*, pp. 53–58
- Demeke GG, Andualem TG, Kassa M (2021) Evaluation of the sustainability of existing rainwater harvesting ponds: a case study of Lay Gayint District, South Gondar zone. Ethiopia. *Heliyon* **7**(7):e07647. <https://doi.org/10.1016/j.heliyon.2021.e07647>
- Elokpere IN, Waspodo RSB, Setiawan BI (2022) Analisis Konsep Zero Runoff pada Kawasan RT02, Desa Babakan, Kecamatan Dramaga, Bogor. *Jurnal Teknik Sipil Dan Lingkungan* **7**(1):65–76. <https://doi.org/10.29244/jsil.7.1.65-76>
- Eun J, Humphrey D, Hofman J (2022) Evaluation of harvesting urban water resources for sustainable water management : case study in Filton Airfield. UK. *Journal of Environmental Manage* **322**(January):116049. <https://doi.org/10.1016/j.jenvman.2022.116049>
- Handayani P (2020) *Al Ulum Seri Sainstek , Volume VIII Nomor 1 , Tahun 2020 ISSN 2338- 5391 (Media Cetak) | ISSN 2655–9862 (Media Online) Al Ulum Seri Sainstek , Volume VIII Nomor 1 , Tahun 2020 ISSN 2338–5391 (Media Cetak) | ISSN 2655–9862 (Media Online) . VIII*, 1–11.
- Kubiku FNM, Mandumbu R, Nyamadzawo G, Nyamangara J (2022) Field edge rainwater harvesting and inorganic fertilizers for improved sorghum (*Sorghum bicolor* L.) yields in semi-arid farming regions of Marange, Zimbabwe. *Heliyon* **8**(2):e08859. <https://doi.org/10.1016/j.heliyon.2022.e08859>
- Kusumastuti DI, Jokowiarno D (2014) Infiltration well to reduce the impact of land use changes on flood peaks: a case study of Way Kuala Garuntang catchment, Bandar Lampung, Indonesia. *Hydrology and Earth System Sciences Discussions* **11**(5):5487–5513. <https://doi.org/10.5194/hessd-11-5487-2014>
- Lestari E (2016) Penerapan Konsep Zero Runoff Dalam Mengurangi Volume Limpasan Permukaan (Perumahan Puri Bali, Depok). *Jurnal Forum Mekanika* **5**(1):27–34. <https://stt-pln.e-journal.id/forummekanika/article/download/638/389>
- Onainor ER (2019) Bab Ii Tinjauan Pustaka **1**:105–112

Development of Rainfall-Runoff Model Using Mock Formula with the Calibration of Stream Discharge in Cisadane Watershed - Indonesia



Dina P. A. Hidayat, W. D. Sri Legowo, and Mohammad Farid

Abstract Rainfall-runoff model is one way to model the amount of rainfall that will become runoff and baseflow. Many models have been developed such as the Mock model which is quite simple but has a fairly good level of accuracy. This study aims to model rainfall runoff with the Mock formula and calibrate the model with measured discharge at one discharge station. This study uses the Cisadane watershed in West Java Indonesia for the location study and Serpong station as the discharge station. The modeling will be carried out with 2 scenarios, a monthly rainfall-runoff model in 1 year and the average monthly rainfall-runoff model for several years. The calibration parameter used is Nash Sutcliffe Efficiency (NSE) and coefficient of determination (R^2). From the model results, it is obtained that the model calibration results with a fairly good measured discharge with a satisfactory NSE value and R^2 is close to 1.

Keywords Calibration · Mock · Model · Rainfall · Runoff

1 Introduction

In the lengthy history of hydrological sciences, rainfall-runoff modeling has attracted a great deal of attention [1]. Without a doubt, one of the most important hydrological study areas when interacting with catchments is runoff prediction. Hydrologists frequently struggle with forecasting and estimating runoff using rainfall data.

D. P. A. Hidayat (✉)

Doctoral Program of Civil Engineering Institut Teknologi Bandung, Bandung, Indonesia
e-mail: Dinaparamitha06@students.itb.ac.id; dina.hidayat@trisakti.ac.id

W. D. S. Legowo

Water Resources Engineering Research Group, Faculty of Civil and Environmental Engineering, Institut Teknologi Bandung, Bandung, Indonesia

M. Farid

Civil Engineering Department, Universitas Trisakti, Jakarta, Indonesia
e-mail: mfarid@ftsl.itb.ac.id

© Institute of Technology PETRONAS Sdn Bhd 2024

B. S. Mohammed et al. (eds.), *Proceedings of the International Conference on Emerging Smart Cities (ICESC2022)*, Lecture Notes in Civil Engineering 324,
https://doi.org/10.1007/978-981-99-1111-0_21

The rainfall-runoff process is incredibly difficult to understand and very complex [2]. Nowadays, the expertise in rainfall-runoff modeling in watersheds with a high percentage of urban cover remains limited. It is important to note that fast land use change in watersheds caused by urbanization highly modifies runoff formation, and many common rainfall-runoff models are frequently inapplicable in such conditions [3]. Environmental change related to hydrology and water resources has gotten a lot of attention in recent years (Zheng, Wang, and Liu, 2022). Urbanization can increase the area of impervious surfaces, reduce the time it takes for runoff to confluence, and raise flood peak discharge, while deforestation can affect the process of runoff yield and affect soil infiltration.

Over the past 20 years, numerous rainfall-runoff models have been developed. One rainfall-runoff model that was created in 1973 by F.J. Mock is called the Mock Model [5]. Continuous stream discharge data is commonly used to calibrate rainfall-runoff models (Jian, Ryu and Wang, 2021). Accurate discharge time series are required for calibrating model parameters in rainfall-runoff modeling. Continuous discharge data are typically derived from observed water-level data at each monitoring station using established rating curves [7]. This research is aim to develop rainfall-runoff model using Mock model with the calibration of stream discharge data and further can analyze watershed conditions based on runoff dan baseflow. To evaluate the performance of the models, this research use the following performance metrics: the Nash–Sutcliffe efficiency (NSE) [8–10]. The location study is in the Cisadane watershed in West Java-Banten Province Indonesia. Cisadane watershed is one of priority watersheds in Indonesia.

2 Research Methodology

2.1 Study Location

One of Indonesia's larger watersheds, the Cisadane has a catchment area of 154,547 ha and is mainly located in West Java and Banten Province, both of which are close to the country's capital, DKI Jakarta. For the past five years, the population of the Cisadane watershed has increased by 1.17 to 2.41% as it supports the capital city and the surrounding economic growth. the selection of the research site is based on the various upstream to downstream hydrological conditions and watershed characteristics. The topography of the Cisadane watershed varies; in the upstream, a mountainous region with a steep slope (10–30%) predominates, while in the middle and downstream, a field and residential area with a flat slope (0–5%) predominates. According to hydrology conditions, the upstream side receives more yearly rainfall (3200 mm) than the downstream side (2700 mm). Table 1 shows the monthly rainfall of Cisadane watershed (2011–2017), varying between 22–674 mm. Stream discharge at the Serpong point is shown at Table 2.

Table 1 Monthly rainfall of Cisadane watershed

Year of	Jan	Feb	Mar	Apr	May	Jun	Jul	Aug	Sep	Oct	Nov	Dec
2011	232	161	110	259	263	221	177	61	138	185	225	192
2012	422	393	176	379	147	41	45	157	103	248	443	331
2013	567	264	459	296	553	134	342	255	254	266	258	330
2014	674	495	250	535	516	143	118	454	22	224	458	534
2015	365	93	451	251	296	105	44	27	129	177	757	362
2016	438	566	362	570	475	464	753	330	784	729	833	106
2017	261	496	362	382	282	384	147	251	179	470	281	167
Average	423	352	310	382	362	213	232	219	230	328	465	289

Table 2 Stream discharge data of Serpong Station

Year of	Jan	Feb	Mar	Apr	May	Jun	Jul	Aug	Sep	Oct	Nov	Dec
2011	55	32	30	65	77	61	62	21	19	35	117	62
2012	106	132	46	111	67	32	31	10	23	67	188	136
2013	196	97	81	108	122	62	109	49	59	65	89	83
2014	280	236	101	104	89	50	59	83	31	27	81	83
2015	61	184	70	63	75	45	13	10	10	13	110	98
2016	67	98	107	144	82	82	101	98	162	116	125	53
2017	48	194	117	117	112	135	92	56	65	112	100	81
Average (m ³ /s)	116.3	139.0	78.7	101.8	89.0	66.5	66.7	46.6	52.8	62.1	115.6	85.2

3 Methodology

Rainfall-Runoff Model. FJ Mock model was first developed by FJ Mock [5] and adopted the principle of water balance. This model divided runoff as direct runoff (DF) and baseflow (BSF) with less input data [11]. Baseflow is dependent on infiltration (Ii) and groundwater from the saturated zone, whereas direct runoff depends on water surplus (WSi) and infiltration (Ii) (GWSi). The quantity of effective rain (total rain minus evaporation) that the soil retains is known as soil storage. The amount of soil storage depends on the amount of rainfall and evaporation, following the following equation:

$$if P_i > E_i \text{ and } P_{i-1} > E_{i-1}, SS_i = 0 \tag{1}$$

$$if P_i > E_i \text{ and } P_{i-1} < E_{i-1}, SS_i = (P_i - E_i) \tag{2}$$

$$if P_i < E_i, SS_i = (P_i - E_i) \tag{3}$$

P_i = Monthly rainfall (mm).

E_i = Evapotranspiration (mm).

SS_i = Soil storage (mm).

Soil moisture is the amount of water needed to moisten the soil. The calculation of the amount of soil moisture follows the following equation:

$$SM_i = SM_{i-1} + SS_i \quad (4)$$

SM_i = Soil moisture (mm).

Water surplus is the volume of water that will enter the soil surface. Water surplus with the FJ Mock method, is calculated through the following equation:

$$WS_i = (P_i - E_i) - SS_i \quad (5)$$

$$DF_i = WS_i - I_i \quad (6)$$

$$BSF_i = I_i - (GWS_i - GWS_{i-1}) \quad (7)$$

$$Q = (DF_i + BSF_i)A \quad (8)$$

WS_i = Water surplus (mm).

Df_i = Direct flow or direct runoff (mm) BSF = Baseflow (mm).

Q = Runoff discharge (m^3/s).

Calibration Parameter. The Efficiency Parameter of Nash and Sutcliffe was used to assess the effectiveness of the various calibration models (NSE) (Eq. 9) [12]. The effectiveness of hydrological model predictions is measured using the Nash–Sutcliffe model efficiency (NSE) coefficient [9, 13]. This statistical parameter statistical parameters are used as the objective function to optimize both the Nash–Sutcliffe efficiency (NSE) and the match between the observed and modeled discharge [14]. The present study use validation point on 1 observed discharge station in the downstream (Serpong station).

$$NSE = 1 - \frac{\sum_{n=1}^N (Q_{model} - Q_{obs})^2}{\sum_{n=1}^N (Q_{obs} - \overline{Q_{obs}})^2} \quad (9)$$

4 Result and Discussion

4.1 Average Rainfall Runoff Model (2011–2017)

Monthly average rainfall varies between 213–465 mm/month with relatively high rainfall occurring in October–May (8 months of wet season) and relatively low rainfall in June–September (4 months of dry season), The highest rainfall is in November and the lowest is in June. Calculation of monthly evapotranspiration using the Penmann method ranges from 126–166 mm/month with daily values ranging from 4–5 mm/day. The results of the rainfall runoff model in the Cisadane watershed using the FJ Mock method are shown in Table 3. The water surplus is always positive for 12 months which indicates that the monthly rainfall is higher than the evapotranspiration value so that the soil moisture is met by 200 mm and there is an excess of water (water surplus). From the optimization results, the coefficient i value is 0.4 for the NSE optimization parameter of 0.81 (meet) as shown in Table 3. When viewed from the correlation coefficient between the measured discharge and the discharge model results, the R^2 value is obtained at 0.989 which shows a fairly high linearity and correlation between the measured discharge and RO discharge from the FJ Mock model.

Table 3 Mock rainfall runoff model

Parameter	Jan	Feb	Ma r	Apr	Ma y	Jun	Jul	Aug	Sep	Oct	Nov	Dec
											12	
Infiltration (i)	107	98	60	94	87	35	39	31	32	63	2	49
$1/2(1 + K)I$	77	71	43	68	63	25	28	22	23	45	88	35
		50										
$KV_n - 1$	38	40	53	42	48	49	32	27	21	20	29	51
											11	
Storage Vol	115	121	96	110	111	74	61	49	45	65	7	86
$\Delta V_n = -V_n - 1 + V_n$	29	6	-25	14	1	-37	-13	-12	-4	20	51	-30
Baseflow = $i - \Delta V_n$	78	92	85	80	86	72	52	43	37	43	71	79
Direct Runoff											18	
(DRO)	161	147	90	142	131	52	59	47	49	95	3	74
Run Off							11			13	25	15
(mm/month)	239	239	175	222	217	124	1	89	85	7	4	3
QB (m ³ /s)	34	45	37	36	38	33	23	19	17	19	32	35
QDRO (m ³ /s)	70	72	39	64	57	24	26	20	22	41	83	32
											11	
QRO (m ³ /s)	105	116	77	101	95	56	49	39	39	60	5	67

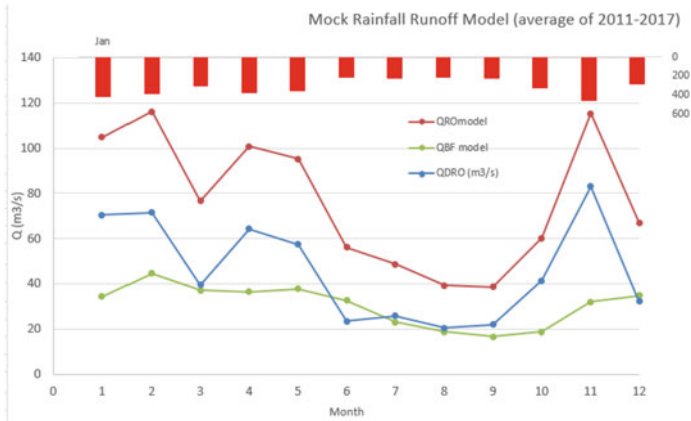


Fig. 1 Mock rainfall runoff model (average of 2011–2017)

The results of the RO discharge model show that the discharge variation is between 39–115 m³/s with a relatively high Q value in October–May (>=60 m³/s) and a relatively low Q value in June–September (<60 m³/s). If analyzed, this corresponds to the wet and dry seasons that occur (rainfall in the Cisadane watershed). If further analyzed the results of the Baseflow baseflow model have variations between 19–45 m³/s. Although in the dry season (relatively small rainfall) in June–September there is still water discharge in the Cisadane River, the trend of the size of the base flow is quite in accordance with the value of the size of the rainfall, but there are differences in the month of transition of the season, namely June (wet season) to dry season where baseflow is still large and October (dry season to wet season) where baseflow is still relatively small (Fig. 1). This is probably because the base flow which takes time to flow into the river (slower passing through the soil grains) is not spontaneous and fast like surface runoff (direct runoff).

4.2 Rainfall Runoff Model for Each Year (2013, 2014, 2015)

The runoff discharge model results for 2013 and 2014 were relatively higher than the 2015 discharge. Year of 2015 was drier than 2013 and 2014 in the cisadane watershed, except in March and November. This affects the resulting baseflow model value. Baseflow in 2013 and 2014 tended to be larger than 2015. The smallest runoff discharge from the model occurred in October 2015 at 3 m³/s, while the largest runoff discharge from the model occurred in January 2014 at 192 m³/s. The lowest baseflow occurred in October 2015 at 3 m³/s (Fig. 2). This is a very small discharge for a fairly large area of das cisadane. If analyzed further, the ratio between the maximum and minimum discharges is very large, this indicates that the cisadane watershed is classified as a critical watershed, with very large discharge indicators

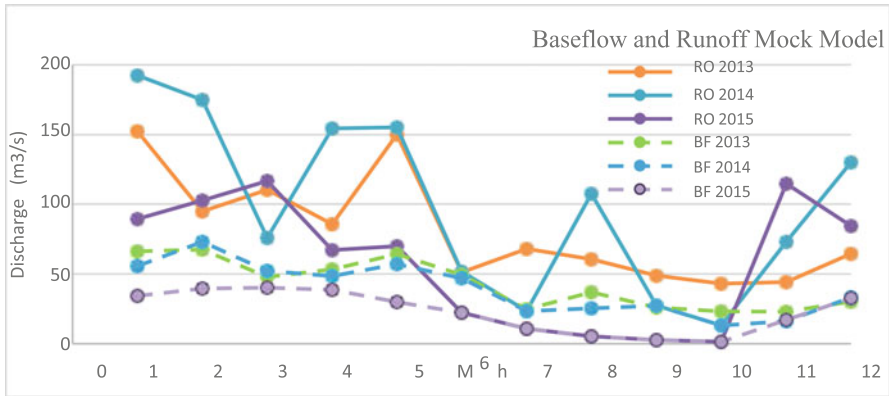


Fig. 2 Comparison of rainfall runoff model for each year

when rainfall is high and very small discharges when almost no rain occurs. This indicates that the catchment condition in the cisadane watershed has been greatly reduced, one of which is due to changes in land use that continue to occur in the cisadane watershed.

4.3 Calibration Parameter

From the calibration results of the Mock runoff discharge model compared to the measured discharge, the NSE parameter value is quite satisfactory, with a variation of the NSE value from 0.48 to 0.81 (Table 4), qualified-good category. This indicates that the Mock model is quite good in modeling the rainfall runoff process for the Cisadane watershed. When viewed from the linearity between the flow of the Mock model and the flow measurements also obtained very good results with the smallest R^2 value = 0.8625 and the largest R^2 = 0.9889 (Fig. 3).

Table 4 Nash and Sutcliffe (NSE) calibration parameter

Years	NSE value	Description
2013	0.48	Qualified
2014	0.65	Qualified
2015	0.64	Qualified
2013–2015	0.81	Good

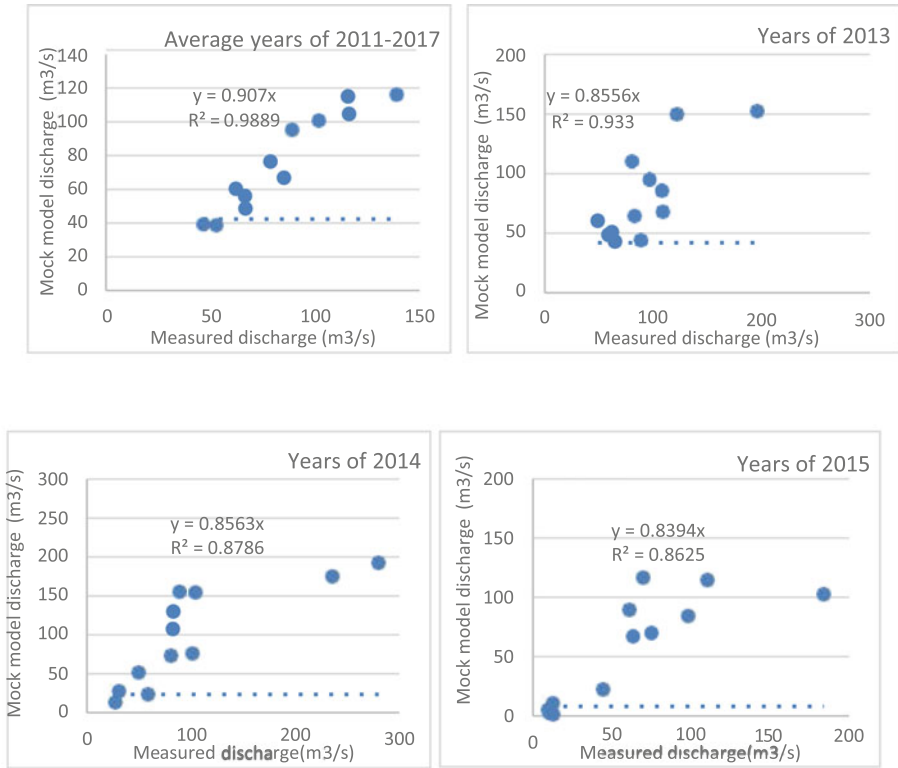


Fig. 3 Linearity of Mock model discharge

5 Conclusion

According to the model results, the ratio of maximum to minimum discharges is very large, indicating that the Cisadane watershed is classified as a critical watershed. This indicates that the catchment condition in the Cisadane watershed has deteriorated significantly, owing in part to changes in land use that continue to occur in the Cisadane watershed. The NSE parameter value is quite satisfactory, with a variation of the NSE value from 0.48 to 0.81, qualified-good category, based on the calibration results of the Mock runoff discharge model compared to the measured discharge. When the linearity between the flow of the Mock model and the flow measurements was considered, the results were very good, with the smallest R² value = 0.8625 and the largest R² value = 0.9889. This indicates that the Mock model does a good enough job of simulating the Cisadane watershed’s rainfall runoff process.

Acknowledgements We gratefully acknowledge the Ministry of Public Works and Housing of the Republic of Indonesia, as well as the Meteorological, Climatological, and Geophysical Agency, for their assistance in gathering data. We would also like to thank the Institut Teknologi Bandung and Universitas Trisakti teams for their support.

References

1. Yin H et al (2022) Rainfall-runoff modeling using long short-term memory based step-sequence framework. *J Hydrol* 610:127901. <https://doi.org/10.1016/j.jhydrol.2022.127901>.
2. Negi A, Rawat KS, Nainwal A, Shah MC, Kumar V (2021) Quality analysis of statistical and data-driven rainfall-runoff models for a mountainous catchment. *Mater Today Proc* 46:10376–10383. <https://doi.org/10.1016/j.matpr.2020.12.544>
3. Petroselli A, Wałęga A, Młyński D, Radecki-Pawlik A, Cupak A, Hathaway J (2021) Rainfall-runoff modeling: a modification of the EBA4SUB framework for ungauged and highly impervious urban catchments. *J Hydrol* 606:2022. <https://doi.org/10.1016/j.jhydrol.2021.127371>
4. Zheng J, Wang H, Liu B (2022) Impact of the long-term precipitation and land use changes on runoff variations in a humid subtropical river basin of China. *J Hydrol Reg Stud* 42:101136. <https://doi.org/10.1016/j.ejrh.2022.101136>
5. Mock FJ (1973) Land Capability Appraisal, Indonesia. Water Availability Appraisal - Basic Study
6. Jian J, Ryu D, Wang QJ (2021) A water-level based calibration of rainfall-runoff models constrained by regionalized discharge indices. *J Hydrol* 603:126937. <https://doi.org/10.1016/j.jhydrol.2021.126937>
7. McMillan H, Krueger T, Freer J (2012) Benchmarking observational uncertainties for hydrology: rainfall, river discharge and water quality. *Hydrol Process*. <https://doi.org/10.1002/hyp>
8. Nyatuame M, Amekudzi LK, Agodzo SK (2020) Assessing the land use/land cover and climate change impact on water balance on Tordzie watershed. *Remote Sens Appl Soc Environ* 20:100381. <https://doi.org/10.1016/j.rsase.2020.100381>
9. Amponsah TY, Danuor SK, Wemegah DD, Forson ED (2021) Groundwater potential characterisation over the voltaian basin using geophysical, geological, hydrological and topographical datasets. *J African Earth Sci* 192:104558. <https://doi.org/10.1016/j.jafrearsci.2022.104558>
10. Jha MK, Mahapatra S, Mohan C, Pohshna C (2019) Infiltration characteristics of lateritic vadose zones: field experiments and modeling. *Soil Tillage Res* 187:219–234. <https://doi.org/10.1016/j.still.2018.12.007>
11. Reichl F, Hack J (2017) Derivation of flow duration curves to estimate hydropower generation potential in data-scarce regions. *Water (Switzerland)* 9(8). <https://doi.org/10.3390/w9080572>
12. Galván L, Olías M, Izquierdo T, Cerón JC, Fernández de Villarán R (2014) Rainfall estimation in SWAT: an alternative method to simulate orographic precipitation. *J Hydrol* 509:257–265. <https://doi.org/10.1016/j.jhydrol.2013.11.044>
13. Zeng X, Kiviat KL, Sakaguchi K, Mahmoud AMA (2012) A toy model for monthly river flow forecasting. *J Hydrol* 452–453:226–231. <https://doi.org/10.1016/j.jhydrol.2012.05.053>
14. Paquet E, Garavaglia F, Garçon R, Gailhard J (2013) The SCHADEX method: a semi-continuous rainfall-runoff simulation for extreme flood estimation. *J Hydrol* 495:23–37. <https://doi.org/10.1016/j.jhydrol.2013.04.045>

Performance Analysis of Green Company in State Electricity Company Indonesia



Arinda Soraya Putri, Hafidh Munawir, Dyah Widayanti,
and Nadiea Aurealnisa Syazili

Abstract A green firm is a notion where businesses minimize or eliminate harmful effects on the environment while achieving their objectives. This study evaluates the effectiveness of State Electricity Company as a green business. The research employs the green company analysis method, which is carried out by compiling KPIs and then looking for the weights on each KPI with a questionnaire of the AHP. The performance of the green company, State Electricity Company, improved by 60% as a result of this study, putting it in the marginal or average range. However, there is still room for improvement, including more research on reasonably priced renewable energy sources, providing transportation to the company from a specific location, enhancing the system from waste accumulation, and optimizing efforts to reduce waste. The findings of this study can be used to assess how well green businesses are performing and to suggest ways to make improvements.

Keywords Green company · analytical hierarchy process · performance measurement · key performance indicators

1 Introduction

There have been many advancements in technology and human life worldwide. Additional variables that may increase the consumption of energy and natural resources utilized to meet human requirements include growing populations and globalization. Natural resources including wood, nickel, copper, and steel are among those whose demand is rising globally. Additionally, it leads to an increase in the industrial sector's energy consumption, where in the past 50 years the required energy consumption has reached half of the global energy supply [1]. Environmental harm is also caused by the production process and the trash that is produced to suit human

A. S. Putri (✉) · H. Munawir · D. Widayanti · N. A. Syazili
Department of Industrial Engineering, Faculty of Engineering, Universitas Muhammadiyah
Surakarta, Surakarta, Indonesia
e-mail: asp835@ums.ac.id

© Institute of Technology PETRONAS Sdn Bhd 2024
B. S. Mohammed et al. (eds.), *Proceedings of the International Conference on Emerging
Smart Cities (ICESC2022)*, Lecture Notes in Civil Engineering 324,
https://doi.org/10.1007/978-981-99-1111-0_22

needs. These industrial, production, and business processes may result in air, soil, and water pollution, as well as a major or appreciable rise in environmental pollution [2].

Reducing trash is a solution to the environmental problems mentioned above because increased waste output will worsen the situation. Applying the idea of a green firm is one of the efforts a business may do.

The business will achieve or be guided toward the sustainability of natural life in the future while still serving the needs of the current society thanks to the green idea, which has taken into account numerous business operations factors [3]. Growing emphasis is being paid to how human activities affect the environment, particularly how industrial activities begin with design activities and end with produced goods [4]. This is a significant concern for the global economy and industry. Because of the emphasis on consumers and the environment, as well as the fact that customers like green products, it is also known as one of the requirements of both government and non-government organizations [5].

One remedy offered by modernizing the industrial process while still paying attention to environmental balance is the “Green” idea [6]. A green firm is essentially a concept that concentrates on the process in an effort to reduce negative environmental impacts or even does not produce any negative environmental consequences. In order to lessen adverse effects on the environment, the green company also engages in a number of actions like pollution prevention and limiting the usage of poisonous substances. Utilizing waste more effectively, enhancing workplace health and safety, paying attention to ongoing business processes by using environmentally friendly raw materials, and using raw materials that are included in the category of renewable energy in a variety of industries are just a few ways to implement a company with the green company concept.

Fortunately, people are beginning to notice and are highly aware of this problem, which is increasing the focus on this idea [7]. To be more competitive, several businesses have adopted a green concept [8]. Although many businesses are having some trouble swiftly adopting the green concept, this is because the current goals, targets, and indicators are so complex [9].

Performance can be understood as motivation and aptitude since one needs a particular level of aptitude and willingness to finish a task or work. In order to increase their [10] competitiveness and transform into businesses with a green philosophy, many businesses are introducing new business models and strategies [8]. The KPI is one that can be used to assess how well a green business is performing. KPIs are a number of metrics that concentrate on certain organizational performance [11]. KPI may also be characterized as a quantitative scale indicator that can be used to assess how well a company is doing in terms of attaining its goals up until the predetermined target is reached [12]. The findings of KPIs can also be employed as a company strategy to reach targets by offering ideas for low KPI values. Performance calculations such as KPIs describe the facilities and levels that have been objectively attained by the organization [13].

State Electricity Company (Perusahaan Listrik Negara or PLN) in Indonesia is a business that provides services, specifically distribution of electricity. In addition to

the limited K3 training available within the purview of State Electricity Company South Banten, the primary energy source still involves the use of materials that are not environmentally friendly and fall under the category of non-renewable materials. Additionally, the waste produced by State Electricity Company South Banten includes hazardous waste as well as waste in the form of transformers and cables from a variety of products that, if not properly managed, could have a negative impact on the environment. The idea of a green business and its execution phase of recycling waste can both lower the amount of waste produced and benefit the business. Because recycling waste that is not used might lessen the need to buy new things while also reducing the volume of waste. In this study, it will be described how State Electricity Company South Banten goes about adopting a green company, as well as how State Electricity Company South Banten evaluates the effectiveness of green companies in their organizations and what areas still require development. In order to measure the performance of green companies at State Electricity Company South Banten and to offer suggestions for improvements to KPIs that are still categorized in the less category, it is expected that the research objectives, namely the identification of KPIs that will be used to measure the performance of green companies, be achieved.

2 Method

This green idea aims to lessen the adverse effects on the environment caused by the business processes used, based on the Indonesian Green Company Assessment Indicators and the Green Industry Assessment from the Ministry of Industry in 2018 [14]. Six indicators can be examined to ascertain if a corporation has embraced the green concept or not, according to Dreher et al. (2009) [15].

a. Analysis of green company identification

The key performance indicators for green firm performance in this study are compiled from three sources: scientific publications, evaluations of green company awards, and the green industry of the Ministry of Industry in 2018. Given the restriction of the problem, which only examines one unit, namely State Electricity Company South Banten, where the unit does not have a production process, the three sources are combined and chosen in accordance with the business processes that run at that location. We do not use all of the KPIs that are available.

The following are the steps in determining KPIs to gauge Green Company's performance:

1. List the company's business procedures.
2. Knowledge of scientific journals about eco-friendly businesses
3. Creating a map of the criteria based on the business procedures of the firm and knowledge of scientific journals, which is then validated through an interview with the HR manager to assess the performance of the organization as a green company.

Creating a set of key performance indicators to assess the success of a green business (Table 1).

At this time, the Ministry of Industry laws and scientific publications are being used to establish metrics for each KPI on the performance of green enterprises.

Gathering data

In this study, two methods—observation or observation and interviewing—were utilized to gather data from two different events.

Population and sampling strategy

All 57 employees of State Electricity Company South Banten, which is located in State Electricity Company South Banten, made up the population of this study. Purposive sampling, however, was employed during the sample procedure. Because this research uses AHP to determine the relative importance of various existing categories, the criteria for respondents in this study were employees whose fields were related to the analysis of the Green Company's performance in accordance with interviews with related sources, namely the supervisor of the HR department at State Electricity Company South Banten. An incorrect level of importance will come from a less accurate choice of the respondent. These factors led to the identification of a population of 5, consisting of supervisors in the disciplines of TE, network, logistics, HR, and K3L.

Snorm de Boer normalization for the normality test.

This phase is carried out to ensure that all KPI values are consistent or same. One method for normalization is the Snorm de Boer formula 16 s.

Calculation

The normality test using Snorm de Boer is calculated using Microsoft Excel as a computation tool and straightforward formulas. The next step is to calculate the weights based on the AHP questionnaire findings using Expert Choice software to assess the significance of each KPI in light of the responses provided by the five respondents.

Traffic signalization

A traffic light system will be employed to make determining KPI improvements easier (Table 2).

3 Result and Conversation

The importance of each category, element, and key performance indicator in the success of this green company is weighted according to the results of this weighting algorithm. The outcomes of State Electricity Company South Banten's calculation of the green company performance weights are shown below (Table 3).

The Snorm de Boer normalization calculation, which seeks to balance or equalize the value of each KPI that has been acquired, comes next. The performance of the green company State Electricity Company South Banten was normalized using the Snorm de Boer method, and the results are shown below (Table 4).

Table 1 KPI Determination

Criteria	Key Performance Indicators	Category	Scientific Journals	Green Company Award Winner	Ministry of Industry's green industry 2018
Environmental Impact	% Energy from renewable resources	en	v	v	v
	% Employees who take public or eco-friendly transportation	en, so, ec	v	v	v
Waste Management	Waste removal efficiency/unit	en,so,ec	v	v	v
Energy Consumption	Hazardous waste	en,so	v	v	v
Occupation Safety	Recycling waste	en, so, co	v	v	v
	Energy efficiency	en, so, co	v	v	v
	Total energy	en, so, co	v	v	v
	Diffusion of work	so	v	v	v
	Number of lines stop due to safety concern	so	v	v	v
	Number of workdays missed due to illness	so	v	v	v
Personal Health	Number of medical LOA	so	v	v	v
	Sick/Work days ratio	so	v	v	v
	Participation in health education / wellness program	so	v	v	v
CSR	Number of CSR Programs	so		v	v
	Amount of CSR Assistance	so		v	v
New PLN	Number of Features on	so	v		
Mobile	PLN Mobile				
	% Customers who use	so	v		
	% Customers who use	so	v		

(continued)

Table 1 (continued)

Criteria	Key Performance Indicators	Category	Scientific Journals	Green Company Award Winner	Ministry of Industry's green industry 2018
	PLN				
Future Healthy	Use of plants both inside and outside	so, en	v		
	Use of stairs	so,en,ec	v		

Table 2 Traffic Light System

Color	Performance Score	Description
	≤ 60	Not Satisfactory
	$60 < \text{performance score} < 80$	Marginal
	≥ 80	Satisfying

Table 3 Results of Weighing Green Company Performance

Criteria	Weight	Key Performance Indicator	Weight
Environmental Impact		% Energy from renewable resources	0.779
	0.071	% Employees who take public or eco- friendly transportation	0.221
waste management	0.058	Waste removal efficiency/unit	0.484
		Hazardous waste	0.34
		Recycling waste	0.176
energy consumption	0.078	Energy efficiency	0.69
		Recycling waste	0.31
occupation safety	0.37	Diffusion of work	0.133
		Number of lines stop due to safety concern	0.191
Personal Health	0.202	Number of workdays missed due to illness	0.191
		Number of medical LOA	0.488
		Sick/Work days ratio	0.301
		Participation in health education / wellness program	0.211

The following is the result of the final calculation of the green company's performance at State Electricity Company South Banten after obtaining the weights and normalization results for each KPI. The category for each performance indicator will be decided by this final outcome. The final estimate of the green company's

Table 4 Results of Normalization

Code	Category	Skor KPI			SNORM
		Actual	Min	Max	
A1	Larger is Better	5%	4%	6%	51%
A2	Larger is Better	22%	21%	22%	17%
B1	Larger is Better	85%	68%	118%	33%
B2	Lower is Better	1905.5	1030	3502	65%
B3	Lower is Better	373.833	0	901	59%
C1	Larger is Better	90%	89%	91%	36%
C2	Lower is Better	118962086.4	113432176.9	125499022.3	54%
D1	Lower is Better	60.667	2	347	83%
D2	Larger is Better	87.333	74	94	67%
D3	Lower is Better	8	1	18	61%
E1	Larger is Better	47	46	47	67%
E2	Lower is Better	11%	4%	30%	73%
E3	Larger is Better	4.833	0	22	22%
F1	Larger is Better	0.833	0	2	42%
F2	Larger is Better	50000000	0	125000000	40%

performance at State Electricity Company South Banten is shown in the table below (Table 5).

At State Electricity Company South Banten, the green company performance value is 60%. This value illustrates the green firm performance at State Electricity Company South Banten, comprising the average work indicator and the end outcome, where it is included in the marginal category. The performance is still in the middle of the good and bad categories on average. Thus, in order to improve the performance of the green firm at State Electricity Company South Banten, it is required to assess a number of KPIs that are still at low levels (Table 6).

For KPIs with a value of 60, suggestions for improvement will be made by looking at the value of each KPI indicator. The following are some recommendations for enhancements that could assist State Electricity Company South Banten function better as a green business.

1. State Electricity Company South Banten uses PLTMH or micro-hydro power plants to generate 1% of the energy it uses, which is subsequently made available to the general public. When compared to the overall amount of energy used, it can be seen that the utilization of renewable energy is rather minimal. distributed around the locality. The public's lack of knowledge about solar energy and the high initial expenses of production or investment both contribute to the low adoption of renewable energy. Additionally, there are barriers related to company plans that may change as a result of legislation and EBT facilities, which are often currently modest in scale with limited storage with sporadic locations Optimising

Table 5 Calculation Results of The Green Company’s Final Performance

Criteria	Key Performance Indicator	Snorm	Final Weight	Snorm X Final Weight	Total Work Value	%
Environmental Impact	% Energy from renewable resources	51%	0.055	0.028	0.597	60%
	% Employees who take public or eco-friendly transportation	17%	0.016	0.002		
Waste Management	Waste removal efficiency/unit	33%	0.028	0.009		
	Hazardous waste	65%	0.019	0.012		
	Recycling waste	59%	0.010	0.005		
Energy Consumption	Energy efficiency	36%	0.053	0.019		
		54%	0.024	0.013		
	Total energy					
Occupation Safety	Diffusion of work	83%	0.049	0.040		
	Number of lines stop due to safety concern	67%	0.070	0.047		
Personal Health	Number of workdays missed due to illness	61%	0.250	0.152		
	Number of medical LOA	67%	0.098	0.065		
	Sick/Work days ratio	73%	0.060	0.044		
	Participation in health education / wellness program	22%	0.042	0.009		
CSR	Number of CSR programs	42%	0.040	0.017		
	Amount of CSR Assistance	40%	0.015	0.006		
New PLN Mobile	Number of features on PLN Mobile	67%	0.058	0.039		
	% Customers using PLN Mobile	70%	0.022	0.012		
Future Healthy	Use of plants both inside and outside	83%	0.070	0.058		
	Use of stairs	100%	0.013	0.013		

the use of renewable energy can be accomplished by conducting in-depth research and research in the State Electricity Company South Banten region regarding the processing of various renewable resources in order to increase the use of renewable energy by increasing the percentage of energy distributed to the community. Optimize the utilization of other renewable energy sources as well.

2. The percentage of employees who utilize public or environmentally friendly modes of transportation shows how many people use these modes of transportation. This is due to the fact that many employees like using private vehicles due to the office’s accessibility. To increase the usage of ecologically friendly automobiles, namely electric cars, which don’t create any emissions, the option that can be offered is to provide a vehicle that travels from one point to the office site.
3. Waste removal is an endeavour to reuse waste that can be used, hence reducing waste. In this instance, transformer waste is reused by State Electricity Company South Banten. Due to the fact that not all damaged transformers may be reused and that each damaged transformer has a different level of damage, waste removal is poor. The recommendation that can be made is that the reuse of transformer

Table 6 Traffic Light System on Every KPI

Criteria	Key Performance Indicator	Category	Actual	Score KPI Min	Max	Normalized Score
Environmental Impact	% Energy from renewable resources	Larger is Better	5%	4%	6%	51%
	% Employees who take public or eco-friendly transportation	Larger is Better	22%	21%	22%	17%
Waste Management	Waste removal efficiency/unit	Larger is Better	85%	68%	100%	33%
	Hazardous waste	Lower is Better	1905.5	1030	3502	65%
	Recycling waste	Lower is Better	373.8	0	901	59%
Energy Consumption	Energy efficiency	Larger is Better	90%	89%	91%	36%
	Total energy	Lower is Better	118962086.4	113432176.9	125499022.3	54%
Occupation Safety	Diffusion of work	Lower is Better	60.67	2	347	83%
	Number of lines stop due to safety concern	Larger is Better	87.33	74	94	67%
	Number of workdays missed due to illness	Lower is Better	8	1	18	61%
Personal Health	Number of medical LOA	Larger is Better	47	46	47	67%
	Sick/Work days ratio	Lower is Better	11%	4%	30%	73%
	Participation in health education / wellness program	Larger is Better	4.83	0	22	22%
CSR	Number of CSR programs	Larger is Better	0.83	0	2	42%
	Amount of CSR Assistance	Larger is Better	50.000.000	0	125.000.000	40%
New Pln Mobile	Number of features on PLN Mobile	Larger is Better	12.67	8	15	67%
	% Customers using PLN Mobile	Larger is Better	93%	37%	100%	70%
Future Healthy	Use of plants both inside and outside	Larger is Better	24	23	24	83%
	Use of stairs	Larger is Better	2	0	2	100%

waste be further optimized, and for transformers that are not suitable for reuse, extensive research can be done on transformer parts that can be utilized because transformers that cannot be reused have to wait years for an auction to be carried out with State Electricity Company central in order to reduce this waste removal effort.

- Waste that can be recycled is waste that is recycled. Even though the outcome is a return, the waste is A3CS cable, whose use can still be transported to a location where it is needed. Reusing the A3CS cable and lowering procurement can also be used to raise the KPI.

5. Energy efficiency, which measures how effectively State Electricity Company South Banten sold energy compared to the amount of energy that was successfully produced, received a relatively low rating of 36%. This figure was determined because, in comparison to the energy that was successfully sold, more energy is still required for production. This can happen for a number of reasons, including losses incurred, which can be both technical and non-technical. In order to increase the value of this KPI, it is suggested that efforts be made to reduce losses by periodically checking on the losses that take place and evaluating each result obtained so that there will always be improvements regarding this loss.
6. Total energy is the total amount of energy production that will be directed to the community, which is still largely dominated by plants that have not used renewable sources. As a result, total energy is included in the lower, better category so that the solutions that can be given are with energy production that is in accordance with the capacity and needs of the community.
7. The number of employees taking part in occupational health and safety training is referred to as participation in health education/wellness programs. Because there are restrictions on how many employees can participate in this occupational health and safety training and because the center typically hosts events related to occupational health and safety, the best solution is to regularly hold both online and offline training sessions on occupational safety and health. Offline with internal State Electricity Company South Banten so that staff members are more knowledgeable of OH&S policies in the office
8. One of the regular activities carried out by State Electricity Company South Banten by giving to those who truly need it is the number of CSR programs. A solution that can be offered is to spread the regularly held events so that more and more people in need are assisted by the criteria provided by the company. Since five programs were implemented in a period of six months, this criterion is included in the section the larger, the better or the more, the better.
9. The nominal used in CSR events is the amount of CSR support. It is anticipated that the quantity of help offered will increase with the addition of CSR programs. By doing so, the issue can be resolved by offering the appropriate level of support in line with the issues that the community is experiencing and by defining various sorts of criteria for various issues.

4 Conclusion

Based on data analysis and conversations about the green company's performance at State Electricity Company South Banten, it can be said that: the value is generated by assessing the green company's performance at State Electricity Company South Banten using 19 KPIs. The ultimate performance of 60% indicates that State Electricity Company South Banten's performance is in the middle of the good and bad categories, or in the average performance indication range. Using the AHP questionnaire findings, which are processed using expert choice software, performance

processing is carried out by computing the weights for each criterion and KPI. This is followed by completing a data normalization test to ensure that each KPI roughly has an equivalent value. Obtaining the ultimate performance figures for the green business is the next phase. It can be seen that the weights for the significant criteria, such as environmental impact, waste management, and energy consumption, which are the main focus of this research, have a low weight at the stage of taking importance weights with AHP, which is processed with expert choice software. This can have an impact on the outcomes. The outcome can alternatively be taken to mean that the three criteria are not significant enough. The occupational health and safety-related criteria, on the other hand, are given enough weight to warrant attention from the company.

Nine out of the 19 KPIs have low performance levels because their values are less than 60. There are various recommendations for the nine poor KPIs, including: conducting studies on renewable energy sources, such as wind or energy from trash, while taking into account production costs for beginning or investment expenses that are within the capabilities of the organization. supplying amenities like public transportation from a single pickup location to the business area or multiple eco-friendly vehicles. employing recyclable garbage to improve the system's waste utilization and build up. increasing the amount of used cable waste. optimizing production and loss-reduction efforts in accordance with the estimated energy requirements of the community. generating energy in accordance with local requirements and maximizing the usage of renewable sources. introducing occupational health and safety and conducting training. extend the geographic or demographic reach of CSR recipients. Set parameters for the CSR programs' level of help.

References

1. Sangwan KS, Mittal VK (2015) A bibliometric analysis of green manufacturing and similar frameworks. *Manag Environ Qual Int J* 26:566–587
2. Ying L, Li M, Yang J (2021) Agglomeration and driving factors of regional innovation space based on intelligent manufacturing and green economy. *Environ Technol Innov* 22. <https://doi.org/10.1016/j.eti.2021.101398>
3. Vătămănescu EM, Dabija DC, Gazzola P, Cegarro-Navarro JG, Buzzi T (2021) Before and after the outbreak of Covid-19: linking fashion companies' corporate social responsibility approach to consumers' demand for sustainable products. *J Clean Prod* 321. <https://doi.org/10.1016/j.jclepro.2021.128945>
4. Trujillo-Gallego M, Sarache W, Sellitto MA (2021) Identification of practices that facilitate manufacturing companies' environmental collaboration and their influence on sustainable production. *Sustain Prod Consum* 27:1372–1391
5. Swarnakar V, Singh AR, Tiwari AK (2021) Evaluation of key performance indicators for sustainability assessment in automotive component manufacturing organization. *Mater Today Proc* 47:5755–5759
6. Shukla GP, Adil GK (2021) A four-stage maturity model of green manufacturing orientation with an illustrative case study. *Sustain Prod Consum* 26:971–987
7. Ghazilla RAR et al (2015) Drivers and barriers analysis for green manufacturing practices in Malaysian SMEs: a preliminary findings. *Procedia CIRP* 26:658–663

8. Tanco M, Kalemkerian F, Santos J (2021) Main challenges involved in the adoption of sustainable manufacturing in Uruguayan small and medium sized companies. *J Clean Prod* 293. <https://doi.org/10.1016/j.jclepro.2021.126139>
9. Calabrese A, Costa R, Gastaldi M, Levialdi Ghiron N, Villazon Montalvan RA (2021) Implications for sustainable development goals: a framework to assess company disclosure in sustainability reporting. *J Clean Prod* 319. <https://doi.org/10.1016/j.jclepro.2021.128624>
10. Hersey P, Blanchard K (1988) *Management of organizational behaviour: utilizing human resources*. 5th Edn. Leadership Studies, Inc.
11. Parmenter D (2015) Key performance indicators-developing, implementing and using winning KPIs
12. Banerjee J, Buoti C (2012) General specifications and key performance indicators
13. Fotovatfard A, Heravi G (2021) Identifying key performance indicators for healthcare facilities maintenance. *J Build Eng* 42
14. Gani A, Asjad M, Talib F (2020) Prioritization and Ranking of indicators of sustainable manufacturing in Indian MSMEs using fuzzy AHP approach. *Mater Today Proc* 46:6631–6637
15. Dreher J, Lawler M, Stewart J, Straszorier G, Thorne M (2009) General motors metrics for sustainable manufacturing Laboratory for Sustainable Business
16. Sumiati M (2006) Pengukuran Performansi Supply Chain Perusahaan dengan Pendekatan Supply Chain Operation Reference (SCOR) DI PT MADURA GUANO INDUSTRI (KAMAL-MADURA)

Case-Based Reasoning Method Implementation for Well Water Feasibility Recommendation System with Nearest Neighbor Algorithm



Jemmy Edwin Bororing, Yumarlin MZ, Sri Rahayu, Agustin Setyorini,
Fatsyahrina Fitriastuti, and Jeffry Andhika Saputra

Abstract Water is the most important natural resource used by humans to meet the needs of life. And water is one of the media that can be used by pathogenic microorganisms as a place to breed and also as a temporary residence before moving to humans so polluted water can cause health problems. The community must be able to know the requirements for drinking water, especially the use of well water that will be used suitable for consumption by the body. In addition, the quality of water in clean water supply facilities, namely well water that does not meet the requirements is also a problem that needs attention and is often found in the community. The aim of this research is to apply the case based reasoning method in the recommendation system for the feasibility of well water using the nearest neighbor algorithm. Measurement of the feasibility of well water uses physical parameters consisting of 6 attributes, namely (1) turbidity, (2) color, (3) dissolved solids, (4) temperature, (5) taste and (6) smell. In testing the system on 5 aspects of usability testing based on the results of questionnaires to 20 respondents, namely the auxiliary aspect gave a value of 71%, the interface aspect gave a value of 80%, the navigation aspect was 84%, the pedagogical aspect was 78% and the robustness aspect was 78%. With a total

J. E. Bororing (✉) · MZ. Yumarlin · S. Rahayu · A. Setyorini · F. Fitriastuti · J. A. Saputra
Informatics Engineering, Faculty of Engineering, Janabadra University, Daerah Istimewa
Yogyakarta Yogyakarta, Indonesia
e-mail: jemmy@janabadra.ac.id

MZ. Yumarlin
e-mail: yumarlin@janabadra.ac.id

S. Rahayu
e-mail: ayu.dj@janabadra.ac.id

A. Setyorini
e-mail: agustin@janabadra.ac.id

F. Fitriastuti
e-mail: fatsyahrina@janabadra.ac.id

J. A. Saputra
e-mail: jeffry@janabadra.ac.id

average of 78% overall test results which identify the well water recommendation system suitable for use by users.

Keywords Well Water · Case Base Reasoning · Nearest Neighbor

1 Introduction

Water is the most important natural resource for the survival of humans and living creatures for daily needs such as drinking, cooking, washing, bathing and others. In meeting water for survival, clean water is needed. Basically clean water has an impact on good health for the user and unclean water will have a bad impact on health [1]. Water is one of the media that can be used by pathogenic microorganisms as a breeding ground and also as a temporary residence (intermediary) before moving to humans, so that polluted water can cause health problems, and to prevent this, the water used must be clean water [2]. Clean that meets health requirements. The need for clean water is arranged in one of the government programs, namely the provision of clean water, that water quality in clean water supply facilities that do not meet the requirements is also a problem that needs attention and is often found in the community.

In [3], The assumption is that the majority of Yogyakarta residents still use shallow aquifers to meet their daily needs. One in ten households experience a shortage of clean water, especially during the dry season. As the population increases, the need for water will also increase. In Yogyakarta City, Bantul Regency and Sleman Regency there will be a water deficit in 2010, 2015 and 2030 which will reach 1,288, 1,330 and 1,750 L/s respectively. To meet the need for clean water, efforts must be made to find alternative sources of raw water for clean water [4]. Then the research conducted by the Amrita Institute [5] found that PDAMs in Yogyakarta still rely on groundwater as a source of water. Since 2010, the use of groundwater by PDAMs in Yogyakarta has been around 80%. Even in 2015, PDAM used groundwater sources reaching 86.76. Excessive use of water can be a serious problem for the sustainability of the area.

The aim of this research is to apply the case based reasoning method in the well water feasibility recommendation system so that it can help the community in general in identifying well water, especially from the physical parameters of water that can be felt and seen before using the nearest neighbor algorithm. With the limitations of the problem in this study, namely: 1. The parameters used as input are physical parameters of water, namely turbidity, color, dissolved solids, water temperature, taste and smell. 2. The recommendation for well water given are Worthy, Decent Enough, Not Worth it, and Not Feasible.

Clean water used must be of good quality for consumption in accordance with sanitation hygiene standards in Indonesia, namely Regulation of the Minister of Health of the Republic of Indonesia No. 32 of 2017 concerning environmental health quality standards and water health requirements for sanitation for hygiene purposes. In sanitation hygiene there are three parameters used, namely physical, biological and

chemical in meeting water quality standards. Regulation of the Minister of Health No. 492/Menkes/Per/IV/2010 concerning Requirements for Consumable Drinking Water. Explaining the quality of drinking water that is safe for consumption, must meet two standard parameters. The mandatory parameters consist of Microbiology which means it does not contain E-Coli, and Colfrom Bacteria, free of toxic chemicals, PH 6.5 to 8.5. Additional parameters, must pay attention to two things, namely Physical and Chemical Parameters [6].

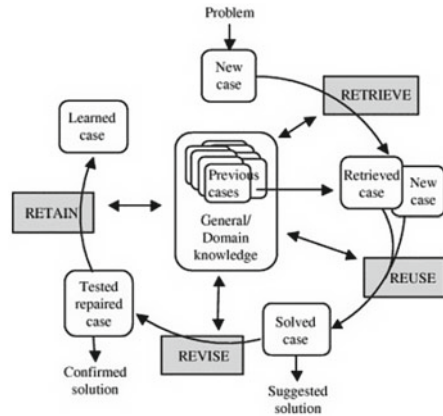
[7], Spatial Patterns of Water Availability and Needs in Sleman Regency and Yogyakarta City in the Context of Readiness to Enter the Habitat Era. Research objectives To explain the spatial pattern of availability and demand for clean water resources in Sleman Regency and Yogyakarta City. The analysis was carried out using a statistical approach with spatial analysis for each district. The sub-district areas in Sleman Regency and Yogyakarta City have a high percentage rate predicted in 2036. The percentage level of water balance has a high trend. Several sub-districts have percentages below 80%. In several districts, the water used in these areas is more than 40% of the available water. Further research from [8], Study of Winongo River Border Urban Clean Water, Kricak Village, Tegalrejo District. This research uses descriptive analysis method with quantitative and qualitative approaches. The data used are primary and secondary data. The objectives include (1) identifying the need for clean water, (2) assessing the supply of clean water, and (3) identifying problems and ways of managing water for each house in residential areas along the river. The results show that the demand for clean water is still 49% of these settlements consuming standard volumes of water, and tend to use well water as a source of clean water.

In this study, physical parameters are used to measure the feasibility of well water with 6 attributes, namely turbidity, color, dissolved substances, temperature, taste and odor which will provide recommendations to system users based on the physical water that can be seen and felt by users whether it is feasible or not used along with the solutions given to the results of the feasibility of the given well water.

Case Based Reasoning is an approach to solving a problem based on the solution of the previous problem. This method is related to the Nearest Neighbor Algorithm. The case base contains cases with solutions that have been reached. To find a solution for a given new case, the system will search for a case in the case base that has the highest degree of closeness [9]. In general, this method has 4 steps [10], namely: 1. Retrieve Finds the previous cases in the case memory that are most similar to the new case problem. 2. Reuse Reusing the previous case as a diagnostic reference in the case memory. 3. Revise In this process information about the solutions provided will be calculated, evaluated, and corrected again to minimize errors that occur in new problems. 4. Retain This process solutions will be indexed, integrated, and extract new solutions and then stored in the knowledge base to solve the next problem [11]. The flow of this method can be seen in Fig. 1.

The nearest neighbor algorithm is an algorithm for classifying objects based on learning data and the data closest to the object [12]. K-NN is a way to calculate the level of similarity (distance) of a case to a new case based on several attributes that are defined with a certain weight and then the level of similarity of all attributes

Fig. 1 Case Base Reasoning



will be added up [12]. The similarity calculation can be seen in the equation in the following formula:

$$Sim(T, S_i) = \frac{\sum_{i=1}^n f(T, S_i) \times w_i}{\sum_{i=1}^n w_i} \tag{1}$$

Which is: T = new case.

S = cases in storage.

n = number of attributes in each case.

f = similarity function attribute I between case T and case S w_i = weight similar to absolute.

2 Methodology

2.1 Framework of Thinking

This frame of mind is an argument in formulating hypotheses. In formulating a hypothesis, argumentation frame of mind using deductive logic by using scientific knowledge as the basic premise [13]. Can be seen in Fig. 2.

Determinants of data and solutions in the intent is the data provided by experts in this case the Sleman Regency Environment Agency for the parameters of the feasibility of well water can be used. Recommendation system approach is a stage to recommend the feasibility of well water using case based reasoning method and nearest neighbor algorithm method. The results of well water recommendations given are feasible to use, quite feasible, less feasible and not feasible. Storage of new cases this process is done if there are new symptoms or determinations that have not been included or do not exist on the system that has been running.

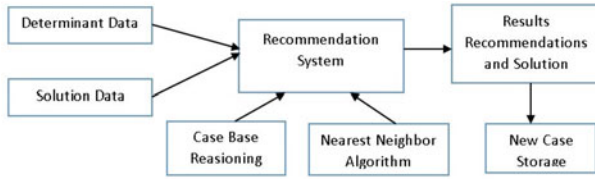


Fig. 2 Framework of Thinking

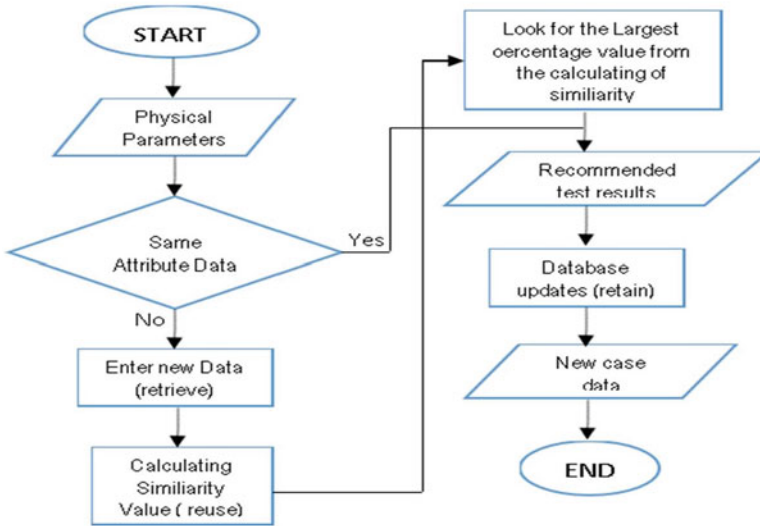


Fig. 3 Well water Recommendation Test Flowchart

2.2 Case Base Reasoning Flowchart

The flowchart for the well water recommendation test is shown in Fig. 3.

2.3 Nearest Neighbor Algorithms for Well Water Feasibility Test

The nearest neighbor algorithm in the recommendation system for the feasibility test of well water is used to find the closeness of physical parameter attributes by calculating the closeness between the attributes of the new well water and the old well water attributes, which is based on matching the weights of the existing physical parameters. The attribute of the new well water uses the solution from the old well

Table 1 Attributes and Weights of Physical Parameters

Code	Attribute	Weight
C1	Turbidity	3
C2	Color	3
C3	Dissolved solid	5
C4	Temperature	1
C5	Flavor	3
C6	Smell	5

water attribute by calculating the proximity of the new well water to all the old well water attributes.

2.4 Weight Value Proximity Factor

This in-depth interview used an instrument in the form of a research checklist to informants from the Health and Environment Office of Sleman Regency. Observations and in-depth interviews help in obtaining determinant data and solution data used. Then obtained attribute values for physical parameter measurements. In Table 1 below.

In Table 2, Table 3, Table 4, Table 5, Table 6, and Table 7, proximity values between sub-attributes have been determined based on the order of observation and interview results.

Table 2 Turbidity Attribute Value Proximity

Turbidity	Clear	Clear Enough	Slightly Clear	Cloudy	Very Cloudy
Clear	1	0.75	0.5	0.25	0
Clear Enough	0.75	1	0.75	0.5	0.25
Slightly Clear	0.5	0.75	1	0.25	0
Cloudy	0.25	0.5	0.75	1	0
Very Cloudy	0	0.25	0.5	0.75	1

Table 3 Color Attribute Value Proximity

Color	Clear	Dull white	Yellow	Green
Clear	0.75	0.5	0.25	0
Dull white	0.5	0.75	0.5	0.25
Yellow	0.25	0.5	0.75	0
Green	0	0.25	0.5	0.75

Table 4 Flavor Value Proximity

Flavor	Have Taste	Tasteless
havetaste	0	0.75
tasteless	0.75	0

Table 5 Smell Value Proximity

Smell	No Smell	Smells	Very Smelly
No Smell	1	0.25	0
Smells	0.25	1	0.25
Very Smelly	0	0.25	1

Table 6 Case Data According to Well Water

Physical Parameters	Turbidity	Color	Dissolved Solids	Temperature	Flavor	Smell	Eligibility
A001	Clear	Dull white	There Is't any	3	tasteless	No Smell	Worthy
A002	Clear Enough	Clear	There Is't any	<3	tasteless	No Smell	Decent Enough
A003	Clear	Dull white	A Little Bit	<3	tasteless	No Smell	Not Worth it
A004	Clear Enough	Dull white	There Is't any	<3	tasteless	Smells	Not Feasible
A005	Clear	Clear	A Little Bit	3	havetaste	No Smell	Not Worth it
A006	Clear	Clear	There Is't any	<3	havetaste	No Smell	Decent Enough
A007	Clear Enough	Clear	There Is't any	<3	It is tasteless	No Smell	Decent Enough
A008	Clear	Clear	There Is't any	3	havetaste	No Smell	Worthy
A009	Clear Enough	Dull white	There Is't any	3	tasteless	No Smell	Decent Enough

Calculation of nearest neighbor algorithm in steps of Case Based Reasoning method feasibility test of well water.

a. Retrieve Process

There is a new case which is AF001 data which will be entered by the user. By using well water feasibility data from old cases in Table 6, the first step is Retrieve.

b. Process Reuse

The second step is Reuse by performing proximity calculations using attribute data from Table 2, proximity data values from each attribute in Table 3, Table 4, Table 5 and the nearest neighbor algorithm to determine whether well water is feasible or not suitable for use.

Table 7 Results of Questionnaire Against Respondents

Respondent	Aux	Int	Nav	Pen	Rob	Average	Description
A	80%	75%	70%	70%	90%	77%	W
B	60%	85%	90%	100%	80%	83%	VW
C	93%	85%	100%	90%	80%	90%	VW
D	80%	95%	90%	70%	80%	83%	VW
E	67%	75%	80%	90%	90%	80%	W
F	67%	90%	90%	80%	80%	81%	VW
G	73%	75%	80%	90%	50%	74%	W
H	47%	75%	80%	90%	70%	72%	W
I	93%	55%	70%	70%	80%	74%	W
J	67%	85%	50%	90%	80%	74%	W
SUM	71%	80%	80%	84%	78%	78%	W
Average	78%						W

Using the general formula of the Nearest Neighbor algorithm and using the data in Table 2, Table 3, Table 4, Table 5 and Table 6, calculations were made to find the closeness between the attributes of the new water well AF001 and the data on the case of Old Well Water that had been previously entered.

$$Sim(AF001, A001) = \frac{\sum_{i=1}^n f(T, S_i) \times wi}{\sum_{i=1}^n wi} \tag{2}$$

Proximity of case A001 to AF001|

$$= \frac{(0.75 \times 3) + (0.5 \times 3) + (1 \times 5) + (0.25 \times 1) + (0 \times 3) + (1 \times 5)}{(3 + 3 + 5 + 1 + 3 + 5)} = \frac{17,67}{20} = 0.70$$

Proximity of case A002 to AF001

$$= \frac{(1 \times 3) + (0.75 \times 3) + (1 \times 5) + (0 \times 1) + (0 \times 3) + (1 \times 5)}{(3 + 3 + 5 + 1 + 3 + 5)} = \frac{15,25}{20} = 0.7625$$

Proximity of case A003 to AF001

$$= \frac{(0.75 \times 3) + (0.5 \times 3) + (1 \times 5) + (0.25 \times 1) + (0 \times 3) + (1 \times 5)}{(3 + 3 + 5 + 1 + 3 + 5)} = \frac{10}{20} = 0.50$$

Proximity of case A004 to AF001

$$= \frac{(1 \times 3) + (0.5 \times 3) + (1 \times 5) + (0 \times 1) + (0 \times 3) + (0.25 \times 5)}{(3 + 3 + 5 + 1 + 3 + 5)} = \frac{10,75}{20} = 0.54$$

Proximity of case A005 to AF001

$$= \frac{(0.75 \times 3) + (0.75 \times 3) + (0.25 \times 5) + (0.25 \times 1) + (0.75 \times 3) + (1 \times 5)}{(3 + 3 + 5 + 1 + 3 + 5)} = \frac{13,25}{20} = 0.66$$

Proximity of case A006 to AF001

$$= \frac{(0.75 \times 3) + (0.75 \times 3) + (1 \times 5) + (0 \times 1) + (0.75 \times 3) + (1 \times 5)}{(3 + 3 + 5 + 1 + 3 + 5)} = \frac{16,75}{20} = 0.84$$

$$\begin{aligned} &\text{Proximity of case A007 to AF001} \\ &= \frac{(1 \times 3) + (0.75 \times 3) + (1 \times 5) + (0.25 \times 1) + (0 \times 3) + (1 \times 5)}{(3 + 3 + 5 + 1 + 3 + 5)} = \frac{15,50}{20} = 0.77 \end{aligned}$$

$$\begin{aligned} &\text{Proximity of case A008 to AF001} \\ &= \frac{(0.75 \times 3) + (0.75 \times 3) + (1 \times 5) + (0.25 \times 1) + (0.75 \times 3) + (1 \times 5)}{(3 + 3 + 5 + 1 + 3 + 5)} = \frac{17}{20} = 0.85 \end{aligned}$$

$$\begin{aligned} &\text{Proximity of case A009 to AF001} \\ &= \frac{(1 \times 3) + (0.5 \times 3) + (1 \times 5) + (0.25 \times 1) + (0 \times 3) + (1 \times 5)}{(3 + 3 + 5 + 1 + 3 + 5)} = \frac{14,75}{20} = 0.74 \end{aligned}$$

From the calculation of the proximity between the weight value of the new case AF001 with the old case data in Table 6 obtained that the largest proximity value obtained in the case data A008 by 85% of the data in the case of A008 to be used by the new data AF001 based on physical parameters shows can be recommended as well water feasible for use.

a. Reuse Process

After the results of the calculation of the closeness of the new AF001 data are obtained, then in this case-based reasoning method new data will be entered on the physical parameters of the AF001 cases that were resolved with the status “fit for use” into the database then the user will take the third step, namely revising the data changes if necessary.

b. Retain Process

After the physical parameter data for AF001 well water is entered, it will undergo the last step, namely retain, the process of converting the results of the new AF001 physical parameter data into a database which will be reviewed for further input of new well water attributes.

3 Results and Discussion

The testing of the drinking water feasibility recommendation system was carried out on 10 respondents with different professional backgrounds. In the assessment of respondents according to [14] the assessment carried out includes aspects, namely auxiliary information, interface, navigation, pedagogy and robustness. The following table of questionnaire results in percent value given to 10 respondents with different backgrounds can be seen in table 10 with the following information: Very Worth it (VW); Worthy (W); Decent Enough (DE); Not Feasible (NF); Very Inappropriate (TI).

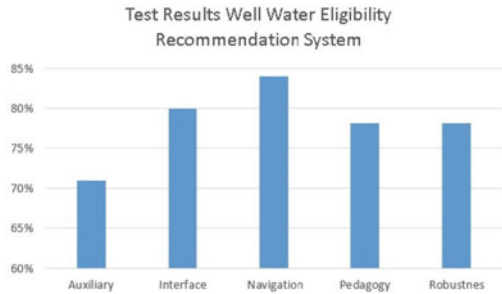
The Following is Table 8. To determine the value of the feasibility level of the system according [14]

The calculation of the feasibility of the well water recommendation system used to determine the percentage value uses the following formula:

Table 8 System Eligibility Category

Score In Percentage	Eligibility Category
81–100%	Very Worth it
61–80%	Worthy
41–60%	Decent Enough
21–40%	Not Feasible
<21%	Very Inappropriate

Fig. 4 Test Result Well Water Eligibility Recommendation System



$$Result = \frac{Total\ Score\ Obtained}{Maximum\ Score} \times 100\% \tag{3}$$

Which is: $P = \frac{F}{N} * 100$

P = Percentage.

F = Frequency of each answer N = Total score of the question.

The following are the results of the feasibility test of the recommendation system based on the respondents input, which can be seen in Fig. 4.

The picture above shows that the percentage of feasibility in terms of the auxiliary aspect gets an average value of 71% based on, the interface aspect gets an average of 80%, the navigation aspect gets an average of 80%, the pedagogy aspect is 84%, the robustness aspect gets an average of 78%. The total percentage of all aspects obtained from the respondents’ assessment is 78%, so it can be concluded that the recommendation system for the feasibility of well water is categorized as suitable for use by users with a percentage value of 78%.

4 Conclusion

The results of the study based on the main priority of well water using physical parameters with 6 attributes, namely turbidity, color, dissolved substances, temperature, flavor and smell with weight for dissolved substances, and smell attributes based on the test results giving a great influence on the proper consideration of water for the test results. In testing the system on 5 aspects of usability testing based on the results

of a questionnaire to 20 respondents, namely the additional aspect gave a value of 71%, the interface aspect gave a value of 80%, the navigation aspect was 84%, the pedagogical aspect was 78% and the resilience aspect was 78%. With a total average total test results of 78% which determines the well water recommendation system is suitable for user use.

References

1. Andini NF (2017) Uji Kualitas Fisik Air Bersih Pada Sarana Air Bersih Program Penyediaan Air Minum dan Sanitasi Berbasis Masyarakat (Pamsimas) di Nagari Cupak Kecamatan Gunung Talang Kabupaten Solok. *J Kepemimp Dan Pengur Sekol* 2(1):7–16
2. Heluth OM (2013) Kualitas Air Sumur Gali Masyarakat Desa Tifu Kecamatan Waeapo Kabupaten Buru Propinsi Maluku, p 7
3. Manny L, Atmaja RRS, Eka Putra DP (2017) Groundwater level changes in shallow aquifer of Yogyakarta City, Indonesia: distribution and causes. *J Appl Geol* 1(2):89. <https://doi.org/10.22146/jag.27584>
4. Triyono J, Yulistiyanto B (2014) Studi Ketersediaan Sumberdaya Air Untuk Memenuhi Kebutuhan Air Bersih di Propinsi Daerah Istimewa Yogyakarta, Universitas Gadjah Mada, Yogyakarta. <http://etd.repository.ugm.ac.id/penelitian/detail/68704>
5. TIFA Foundation: Darurat Air Bersih. Laporan Hari Air Sedunia, March 2017. <https://www.tifafoundation.id/artikel/darurat-air-bersih/>
6. Maman: Standar Kemenkes RI Tentang Syarat Air Minum Layak Konsumsi, August 2019. <https://hulondalo.id/standar-kemenkes-ri-tentang-syarat-air-minum-layak-konsumsi/>. Accessed 19 Aug 2022
7. Putra BR, Taquuddin T, Kuswanto K (2019) Pola Spasial Ketersediaan Dan Kebutuhan Air di Kabupaten Sleman Dan Kota Yogyakarta dalam Rangka Kesiapan Memasuki Era Habitat 3. *Semin Nas Geomatika* 3:315. <https://doi.org/10.24895/SNG.2018.3-0.971>
8. Siregar AH, Mei ETW (2017) Kajian Air Bersih Perkotaan Sempadan Sungai Winongo Kelurahan Kricak, Kecamatan Tegalrejo, 10
9. Prakoso IM, Anggraeni W, Mukhlason A (2013) Penerapan Case-Based Reasoning pada Sistem Cerdas untuk Pendeteksian dan Penanganan Dini Penyakit Sapi. *Sisfo* 4(5):360–368. <https://doi.org/10.24089/j.sisfo.2013.09.007>
10. Sulistiani H, Darwanto I, Ahmad I (2020) Penerapan Metode Case Based Reasoning dan K-Nearest Neighbor untuk Diagnosa Penyakit dan Hama pada Tanaman Karet. *J Edukasi Dan Penelit Inform JEPIN* 6(1):23. <https://doi.org/10.26418/jp.v6i1.37256>
11. Pal SK, Shiu SCK (2004) *Foundations of soft case-based reasoning: pal/soft case-based reasoning*. Wiley, Hoboken. <https://doi.org/10.1002/0471644676>
12. Nugraha I., Siddik M (2019) Penerapan metode case based reasoning (CBR) dalam sistem pakar untuk menentukan diagnosa penyakit pada tanaman hidroponik 2(2):91–96
13. Harsani P, Qur'ania A (2018) Penerapan K-Nearest Neighbor (KNN) untuk Klasifikasi Anggrek Berdasarkan Karakter Morfologi Daun dan Bunga. *KOMPUTASI* 15(1):118–125
14. Setiyowati P, Maharani ET, Astuti AP (2018) Analisis Tingkat Kelayakan Aplikasi Android 'Chemical Lab Work Guide' Sebagai Media Pembelajaran, 9

Most Prioritised Points in GREENSHIP New Building Certification



Muhammad Rizky Waskito Aribowo and Bambang E. Yuwono

Abstract The GREENSHIP New Building issued by the Green Building Council Indonesia (GBCI) is currently the most widely used assessment tool by buildings to assess performance in terms of environmental friendliness, where the goal is to gain recognition as a green building through the GREENSHIP certification system. This research was conducted to identify points from the criteria in the GREENSHIP New Building, which are priority points for building owners to take in achieving a rank in the GREENSHIP certification system. Based on the data in the GBCI, it can be sorted, selected and then statistically to identify and illustrate the priorities of the building owner in achieving the GREENSHIP certification rating. The results of this study is to identify the behavior of building owners in achieving GREENSHIP certification ratings so that obstacles in the implementation of green building certification can be identified.

Keywords Certification · GREENSHIP · new building · point

1 Introduction

The Paris Agreement is a legally binding international treaty on climate change with a goal to limit global warming below 1.5°C, compared to pre-industrial levels [1]. Currently, the building sector is responsible for almost 40% of global energy-related carbon emission and 50% of all extracted materials [2]. There is an urgent need to decarbonized and greening the building sector around the world.

With this raising issue, green building certification system is growing around the world. Green building certification is needed as benchmark whether a building is

M. R. W. Aribowo (✉)
Green Building Council Indonesia, South Jakarta, Indonesia
e-mail: titoaribowo@gbcindonesia.org

B. E. Yuwono
Department of Civil Engineering, Universitas Trisakti, West Jakarta, Indonesia
e-mail: bambang.endro@trisakti.ac.id

© Institute of Technology PETRONAS Sdn Bhd 2024
B. S. Mohammed et al. (eds.), *Proceedings of the International Conference on Emerging Smart Cities (ICESC2022)*, Lecture Notes in Civil Engineering 324,
https://doi.org/10.1007/978-981-99-1111-0_24

considered as green building or not. Green building certification is also needed as the recognition from the third-party rather than self-claim from the building itself.

GREENSHIP is a rating tools developed by the Green Building Council Indonesia as a standard for green building implementation in Indonesia. Currently, GREENSHIP has 6 different kind of rating tools to facilitate the standardization of different type of building which are: GREENSHIP New Building (NB), GREENSHIP Existing Building (EB), GREENSHIP Interior Space (IS), GREENSHIP Homes, GREENSHIP Neighborhood (NH), and GREENSHIP Net Zero. As the standard, each of this rating tools has a different benchmark to maximize the building performance.

For the rating tools intended to buildings such as GREENSHIP NB, EB, IS, and Homes, there are 6 categories which are: Appropriate Site Development (ASD), Energy Efficiency and Conservation (EEC), Water Conservation (WAC), Material Resources and Cycle (MRC), Indoor Health and Comfort (IHC), and Building Environment Management (BEM). Below it, there are several different criteria and benchmark for each type of rating tools with different point structure.

A building owner needs to have strategy in order to get certain desired achievement. This strategy will include efforts, technologies availability, expertise presence, and also financial power. All of this strategy will later translated into what points are most feasible to be achieved by a building from the available points in GREENSHIP certification scheme.

Currently there are more than 40 buildings that has been certified under GREENSHIP New Building certification scheme. The purpose of this study was to analyze what points that the building owners most prorititize to get in order to achieve their certification, thus we can see the behavior of the building owners in achieving GREENSHIP certification rating so that the obstacles in the green building certification implementation can be identified.

2 Literature Review

GREENSHIP New Building certification had been studied from many different angles. Mostly of this study are focusing on how to implement the rating tools into a designated building. There is a study that examine implementation of GREENSHIP New Building by using fuzzy logic method [4]. However, some of the prerequisite criteria are not met the standards so the certification can be said as invalid. Another case is implementation of GREENSHIP New Building until design recognition (DR) stage [5]. Design recognition is a milestone phase where a building design is recognized by GBC Indonesia as a green building design. It has fewer points compared to final assessment (FA) stage because some of the measurement needs to be conducted at the completion of the building construction. Other study aims to obtain an assessment index and evaluate the green building concept in that building design [8]. It was conducted at the Design Recognition (DR) stage, which is the assessment stage carried out when the project is in design and planning finalization. The results generate ratings of GREENSHIP level at gold predicate. The

category which generates the most point is the Energy Efficiency Conservation and Appropriate Site Development with the improvement in building material used.

GREENSHIP as a rating tool can also be compared to another rating tool such as LEED. There is a comparative study between the implementation of GREENSHIP and LEED in a building in Indonesia [6]. In this study, by using LEED, although only achieved a lower points compared than GREENSHIP, but the building can still achieved a LEED platinum level with some innovation on zero-runoff design concept, water recycles, and efficient water fixtures.

Some of the studies are only targeting some category in GREENSHIP. There is a study to identify the suitability of the requirement of the green building system standard tool for the GREENSHIP New Building version 1.2 with the building object being reviewed [7]. From this study, it can be concluded that the category of material resources and cycle (MRC) aspects of the object of the building being reviewed is in accordance with the standard requirements of the GREENSHIP New Building version 1.2.

These studies, while they covers the implementation of GREENSHIP rating tools, but cannot express the whole picture and actuality of GREENSHIP new building certification.

3 Research Methodology

This research is conducted by using descriptive statistical analysis to analyse building certification achievement using GREENSHIP New Building version 1.2 in Indonesia from 2012–2021 towards six GREENSHIP categories which are Appropriate Site Development (ASD), Energy Efficiency and Conservation (EEC), Water Conservation (WAC), Material Resources and Cycle (MRC), Indoor Health and Comfort (IHC), and Building Environment Management (BEM).

4 GREENSHIP New Building (NB)

GREENSHIP New Building is a rating tool released by the Green Building Council Indonesia (GBC Indonesia) specifically to assess a new building construction to become a green building. The newest GREENSHIP NB is version 1.2 which is a development from GREENSHIP NB 1.0 and summary of benchmark of GREENSHIP NB 1.1 [2].

As stated before, GREENSHIP NB 1.2 has seven category which are Appropriate Site Development (ASD), Energy Efficiency and Conservation (EEC), Water Conservation (WAC), Material Resources and Cycle (MRC), Indoor Health and Comfort (IHC), and Building Environment Management (BEM). Below these categories there are various type of criteria, which are:

- Prerequisite criteria, is a type of criteria that needs to be fulfilled. This criteria is a representation of minimum standard for a building to be called as a green building. If there is a prerequisite criteria that don't meet the requirement needed, then the certification of that particular building can be dismissed.
- Credit criteria, is a type of criteria that consists points that can determine the certification level of particular building. These criteria doesn't have to be all fulfilled and every building can choose which points to get according to their ability.
- Bonus criteria, is a type of criteria that can give added points beside the main points from credit criterion. Points from bonus criteria will not affect the maximum points of the rating tools, but will be counted as an achievement. Usually this bonus criteria has a relatively difficult requirement and rarely implemented in the project.

To summarize how many criteria under a category, we can refer to the Table 1 below:

After this, the prerequisite criteria will be stated as P (ASD P, EEC P1, EEC P2, and so on), credit and bonus criteria will be stated with numbers (ASD 1, ASD 2, EEC 1, EEC 2, and so on). The only bonus criterion is on EEC 5.

Under this criteria, there are several benchmark that contains points to be acquire by the building to be certified as the GREENSHIP certified building. There are 101 points available to acquire that spread across 6 categories with 5 bonus points. The points structure for the GREENSHIP New Building ver. 1.2 is (Table 2):

Table 1 Criteria in GREENSHIP NB 1.2

Category	Criteria		
	Prerequisite	Credit	Bonus
ASD	1	7	
EEC	2	4	1
WAC	2	6	
MRC	1	6	
IHC	1	7	
BEM	1	7	

Source: GREENSHIP for New Building Version 1.2, Criteria and Benchmark Summary

Table 2 Point Structure in GREENSHIP NB 1.2

Category	Points	Bonus
Appropriate Site Development	17	
Energy Efficiency and Conservation	26	5
Water Conservation	21	
Material Resources and Cycle	14	
Indoor Health and Comfort	10	
Building Environment Management	13	

Source: GREENSHIP for New Building Version 1.2, Criteria and Benchmark

5 Points Achievement of GREENSHIP New Building Project

The points achievement in the certified GREENSHIP New Building projects are depend on the project capability to achieve it. While all the prerequisite criteria are all achieved since it is mandatory, the credit criteria is varies across the projects. This paper will analyze 40 certified GREENSHIP New Building projects, regardless building type and location.

5.1 Appropriate Site Development (ASD)

Appropriate site development category has seven credit criteria under it, which are:

- ASD 1 – Site Selection
- ASD 2 – Community Accessibility
- ASD 3 – Public Transportation
- ASD 4 – Bicycle Facility
- ASD 5 – Site Landscaping
- ASD 6 – Micro Climate
- ASD 7 – Stormwater Management

From 40 projects, here is the result of the most prioritised credit criteria achieved by these projects (Fig. 1).

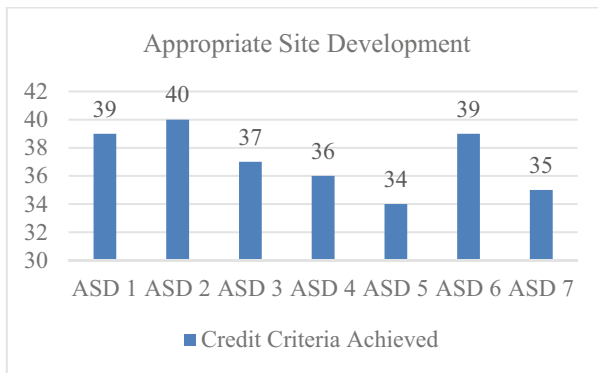


Fig. 1 ASD Criteria Achieved. *Source:* Derived from Rating Development and Certification GBC Indonesia data

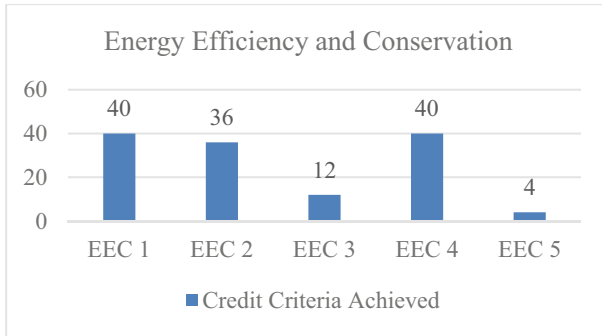


Fig. 2 EEC Criteria Achieved. *Source:* Derived from Rating Development and Certification GBC Indonesia data

5.2 Energy Efficiency and Conservation

Energy Efficiency and Conservation category has 5 criteria under it, which are:

- EEC 1 – Energy Efficiency Measures
- EEC 2 – Natural Lighting
- EEC 3 – Ventilation
- EEC 4 – Climate Change Impact
- EEC 5 – On Site Renewable Energy

From 40 projects, here is the result of the most prioritised credit criteria achieved by these projects (Fig. 2).

5.3 Water Conservation

Water Conservation category has 6 criteria under it, which are:

- WAC 1 – Water Use Reduction
- WAC 2 – Water Fixtures
- WAC 3 – Water Recycling
- WAC 4 – Alternative Water Resources
- WAC 5 – Rainwater Harvesting
- WAC 6 – Water Efficiency Landscaping

From 40 projects, here is the result of the most prioritised credit criteria achieved by these projects (Fig. 3).

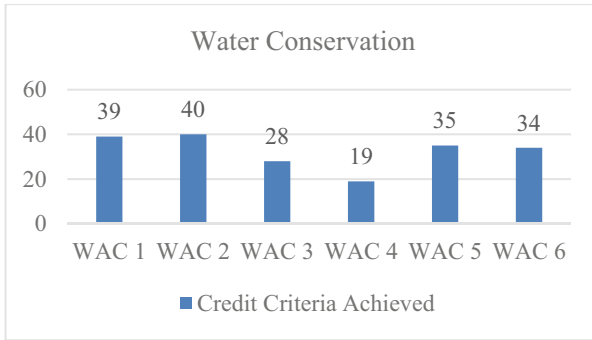
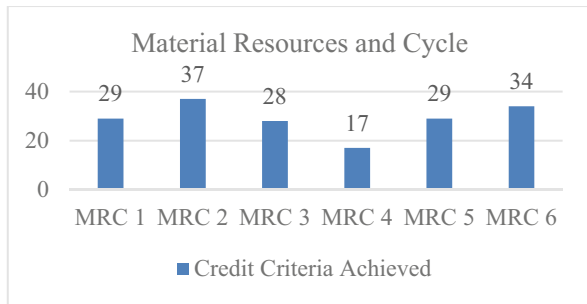


Fig. 3 WAC Criteria Achieved. *Source:* Derived from Rating Development and Certification GBC Indonesia data

Fig. 4 MRC Criteria Achieved. *Source:* Derived from Rating Development and Certification GBC Indonesia data



5.4 Material Resource and Cycle

Material Resources and Cycle category has 6 criteria under it, which are:

- MRC 1 – Building and Material Reuse
- MRC 2 – Environmentally Friendly Material
- MRC 3 – Non ODS Usage
- MRC 4 – Certified Wood
- MRC 5 – Prefab Material
- MRC 6 – Regional Material

From 40 projects, here is the result of the most prioritised credit criteria achieved by these projects (Fig. 4).

5.5 Indoor Health and Comfort

Indoor Health and Comfort category has 7 criteria under it, which are:

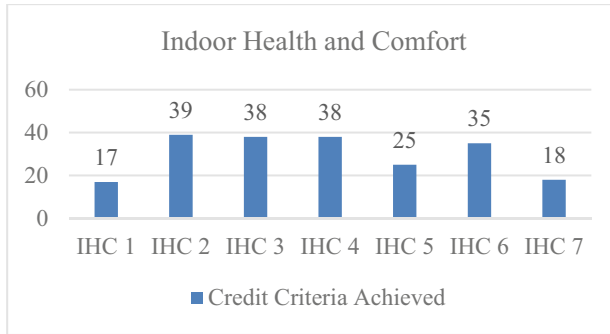


Fig. 5 IHC Criteria Achieved. *Source:* Derived from Rating Development and Certification GBC Indonesia data

- IHC 1 – CO2 Monitoring
- IHC 2 – Environmental Tobacco Smoke Control
- IHC 3 – Chemical Pollutant
- IHC 4 – Outside View
- IHC 5 – Visual Comfort
- IHC 6 – Thermal Comfort
- IHC 7 – Acoustic Level

From 40 projects, here is the result of the most prioritised credit criteria achieved by these projects (Fig. 5).

5.6 Building Environment Management

Building Environment Management category has 7 criteria under it, which are:

- BEM 1 – GP as a Member of Project Team
- BEM 2 – Pollution of Construction Activity
- BEM 3 – Advanced Waste Management
- BEM 4 – Proper Commissioning
- BEM 5 – Green Building Submission Data
- BEM 6 – Fit Out Agreement
- BEM 7 – Occupant Survey

From 40 projects, here is the result of the most prioritised credit criteria achieved by these projects (Fig. 6).

From the graphics above, there are several criteria that become the most prioritised to take by the building owner:

- 40 buildings took ASD 2, EEC 1, EEC 4, WAC 2, BEM 1, BEM 5, BEM 7
- 39 buildings took ASD 1, ASD 6, WAC 1, IHC 2

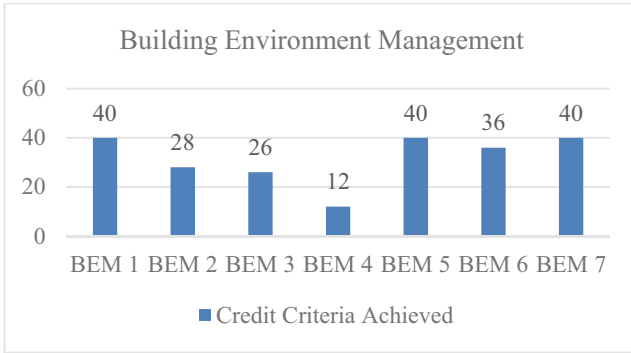


Fig. 6 BEM Criteria Achieved. *Source:* Derived from Rating Development and Certification GBC Indonesia data

- 38 buildings took IHC 3, IHC 4
- 37 buildings took ASD 3, MRC 2
- 36 buildings took ASD 4, EEC 2, BEM 6
- 35 buildings took ASD 7, WAC 5, IHC 6
- 34 buildings took ASD 5, WAC 6, MRC 6
- 29 buildings took MRC 1, MRC 5
- 28 buildings took WAC 3, MRC 3, BEM 2
- 26 buildings took BEM 3
- 25 buildings took IHC 5
- 19 buildings took WAC 4
- 18 buildings took IHC 7
- 17 buildings took MRC 4, IHC 1
- 12 buildings took BEM 4, EEC 3
- 4 buildings took EEC 5

6 Findings and Conclusions

From the data above it can be concluded that the building owners are targeting the criteria with the most points which is EEC 1 with maximum of 20 points and WAC 1 with 8 points. Meanwhile ASD 2 is relatively easy since the location of these buildings mostly in a city which already equipped with public facilities.

WAC 2 is also relatively easy since the water fixtures technology that has an water efficient performance is widely available. While the EEC 4, BEM 5, and BEM 7 are the low-hanging fruit criteria because it only require easy calculation and document submittance.

In contrary, only few buildings took EEC 5. We can assume that the implementation of renewable energy is still difficult in Indonesia, whether it is from the

technology availability or the existing regulation. This should be solved soon since decarbonization from building industry is needed.

These findings can be the base when the GREENSHIP New Building will be improved in the future to make it more reliable to ensure the building performance improved.

References

1. World Green Building Council (2021) Annual Report 2021. <https://worldgbc.org/sites/default/files/WorldGBC%202021%20Annual%20Report.pdf>. Accessed 15 Aug 2022
2. United Nations (2022) The Paris Agreement. <https://unfccc.int/process-and-meetings/the-paris-agreement/the-paris-agreement>. Accessed 15 Aug 2022
3. Rating and Technology Division Green Building Council Indonesia (2013) GREENSHIP untuk Bangunan Baru Versi 1.2, Ringkasan Kriteria dan Tolok Ukur. <https://gbcindonesia.org/files/resource/9b552832-b500-4b73-8c0e-acfaa1434731/Summary%20GREENSHIP%20New%20Building%20V1.2.pdf>. Accessed 7 Aug 2022
4. Fajrin NA, Sri S, Anita T (2020) Penilaian Green Building berdasarkan Perangkat Greenship untuk Bangunan Baru Versi 1.2 Menggunakan Logika Fuzzy (Studi Kasus: Gedung Pascasarjana Fakultas Hukum Universitas Jember). ISSN Media Elektronik 2723-5378
5. Apiff MH, Dian A (2018) Towards the greenship assessment and certificate of new building Design Recognition (DR) for the design of IDB-funded integrated classroom building Universitas Negeri Malang, Indonesia. <https://doi.org/10.1051/mateconf/201820403015>. Accessed 15 Aug 2022
6. Hanif H (2022) Towards achieving Platinium standards for Green Building Certification: a case study using Jakarta Internation Stadium (JIS) design. IOP Conf Ser Earth Environ Sci 997:012006
7. Fahnurlisa Q (2019) Evaluasi penerapan aspek material resources and cycle sesuai standar green building rating tool for new building version 1.2 pada proyek bangunan gedung. Jurnal Konstruksia
8. Busono T et al (2021) Impelementation of the greenship rating tools in the centre of excellent (CoE) building at Universitas Pendidikan Indonesia. IOP Conf Ser Earth Environ Sci 738

The Impacts of Revitalization on the *Saribu Rumah Gadang* Cultural Area Sustainability



Dhani Mutiari, Marwah Dwi Ramadhanti, and Fadilla Tri Nugraheni

Abstract The *Saribu Rumah Gadang* (SRG) area in South Solok Regency has been around for hundreds of years. In its development, *Rumah Gadang* which is located in this area has decreased in quality due to unfriendly weather. Between 2019–2020 the Ministry of PUPR (*Dinas Pekerjaan Umum dan Tata Ruang*/Department of Public Works and Spatial Planning) carried out revitalization efforts for the cultural area. The revitalization process causes changes to the *Saribu Rumah Gadang* area. The purpose of this study was to determine the diversity of changes after the revitalization process in the SRG area and the impacts they caused. This study uses a survey method, with the process of searching for direct observation data and interviews from traditional advice, homestay managers and local communities. The results showed that the revitalization activities in the SRG area had a positive impact in the form of an increase in the fields of tourism, economy, social and culture and proved to increase the value of regional cultural tourism in the area. Besides the positive influence of conservation activities, there are also negative effects, namely the local community feels disturbed by the arrival of tourists to the SRG area, but overall that this revitalization program has a major impact on the sustainability of the *Saribu Rumah Gadang* cultural area.

Keywords Impacts · Revitalization · *Rumah gadang*

1 Introduction

Historic preservation and heritage conservation are currently two basic podiums for promoting the sustainability of historic houses from the perspective of cultural memory. Historic preservation emphasizes “repairing the old as the old” and guarantees the preservation only of the original appearances of historic houses [1].

D. Mutiari (✉) · M. D. Ramadhanti · F. T. Nugraheni
Department of Architecture, Engineering Faculty, Muhammadiyah University of Surakarta,
Surakarta, Indonesia
e-mail: dhani.mutiari@ums.ac.id

© Institute of Technology PETRONAS Sdn Bhd 2024
B. S. Mohammed et al. (eds.), *Proceedings of the International Conference on Emerging Smart Cities (ICESC2022)*, Lecture Notes in Civil Engineering 324,
https://doi.org/10.1007/978-981-99-1111-0_25

Conservation of cultural heritage areas is a process of maintaining their existence so that they are able to adapt to new conditions. This conservation process can bring social benefits to an area or city, because it can also indirectly promote the local community's economy [2]. This activity was also carried out as a step to attract tourists, as stated by Jiemei Luo, Izzy Yi Jian, Edwin H.W. Chan, Weizhen Chen [3], that at the present time cultural regeneration not only focuses on adding more cultural facilities or spaces, but also emphasizes the transformation of the image of a city or place to attract tourists, the creative class, and investment.

One of the conservation processes is the revitalization program in the *Saribu Rumah Gadang* culture area. The Saribu Rumah Gadang (SRG) area is one of the cultural tourism destinations in Nagari Koto Baru, Sungai Pagu District, Regency, South Solok, and West Sumatra Province in Indonesia. In this area there are 142 vernaculars house namely *Rumah Gadang*, but there are 40 houses whose condition is damaged (Fig. 1). Since 2019, several vernacular houses have been renovated by the local government and the addition of public facilities for tourism purposes, because heritage, including vernacular traditional models, has been constantly reused, adapted to local environments, and revered as cultural evidences which deliver a straightforward connection to the past [4]. This restoration was carried out on the *Rumah Gadang* which was originally a residential house. This change is intended to revive the *Rumah Gadang* for homestay to tourism purposes. The restoration process was carried out with slight changes to the layout without reducing the value and nature of *Rumah Gadang*.

The process of revitalizing the SRG Area includes the restoration of 38 Gadang Houses, structuring the area's landscape, the construction of the Songket Tower and facilities that make it easier for tourists. The revitalization process is not easy because restoration of cultural heritage like vernacular houses (*rumah gadang*) is a complex process, involving a variety of methods and many different professions [5]. This activity was completed in December 2020. This research was carried out at the end of 2021 two years after the completion of the revitalization program in this area. In the past two years there have been some differences that can be felt by the people in the region. Looking at the differences before and after the revitalization program in this area, the purpose of this research is: to find out what is the diversity of changes

Fig. 1. The Saribu Rumah Gadang Area. Source: [6]



that occur after the revitalization process in the SRG Area and the impact of the revitalization process.

Conservation is the process of managing a building or city space so that its cultural meaning can be preserved. Conservation can be expanded in terms of the preservation of the morphology and functions in it [7]. There are several strategies in conservation, including restoration and revitalization. Restoration is an effort made to restore the original shape of the building and the cultural heritage environment from damage by cleaning, repairing, replacing, and reassembling the parts of the building that are loose, damaged, after being repaired with the same materials and methods, similar, in accordance with the original [8]. Changes or transformations in the use of space in the dwelling that need to be carried out are identification into several categories, namely: 1) Fixed feature space, space that is limited to elements and is not easy to change. 2) The room features semi fixed, there are room furniture and wall partitions that are easy to move as needed. 3) Informal space, there is a change in the features of fixed and semi-fixed spaces, involving more people in a predetermined function of space. As a result, the supervision of the function of the room will not be maximized [9].

Revitalization is an effort to revitalize an area or part of a city that was once vital (living) which then experienced degradation. The area revitalization process includes improving the physical, economic and social aspects by recognizing and utilizing the potential of the environment (history, meaning, uniqueness of the location and image of the place) [10]. In the revitalization of the area in this SRG, which needs to be considered is the circulation path for pedestrians, natural potential, geological elements including archaeological, ecological and cultural values, and buildings [11]. The change in the function of residential to commercial in Chinatown in Semarang has an impact on land prices in the area studies are increasing every year. This condition makes the area a potential area for good investment. Commercial space is directly proportional to land prices. The increase in commercial activity has an impact on higher land prices [9].

Rumah Gadang is the name for the traditional Minangkabau traditional house in south Sumatra [12]. *Rumah Gadang* is one of the traditional houses in the Minangkabau natural area. Minangkabau is one of the tribes on the island of Sumatra, precisely in the province of West Sumatra. *Rumah Gadang* is a material culture and a Minang cultural heritage that has a function and meaning in the life of the Minangkabau tribe. Apart from being a form of culture, the *rumah gadang* is an identity or an identity for the Minangkabau people [13]. The local people call it the Bagonjong House. It is called Bagonjong because the shape of the roof resembles buffalo horn or bamboo shoots (young bamboo). Dt. Rajo Panghulu explained that what was included in the light of the nagari were the *Gadang House*, the *Beranjuang Traditional House*, *Lumbuang Berpereng*, carved *Rubuang*, silver gold, rice fields, artificial *banda*, live-stock and plants. Symbolically, *Rumah Gadang* is one of the elements called *cahayo Nagari*. The variety of types of *Gadang Houses* in the SRG Area based on data from the 2016 South Solok Regency can be seen in Table 1.

Table 1. 10 types of *rumah gadang* in the *Saribu Rumah Gadang* area

House Name	Space Plan	Facade	House Name	Space Plan	Facade
1. Dt. Rajo Indo Suku Kutianyir (1387 M)			6. Dt. Rangkayo Majo Lelo Suku Durian (1878 M)		
2. Dt. Bando Panjang Suku Bariang (Abad ke-19 M)			7. Dt. Rajo Bagindo Suku Kampai (1920 M)		
3. Dt. Lelo Panjang Suku Melayu Buah Anau (1794 M)			8. Dt. Sutan Nangkodo Kaum Bariang (1827 M)		
4. Dt. Bando Labiah Suku Sikumbang (1852 M)			9. Dt. Sati Kaum Panai Tanjung (1900-an M)		
5. Dt. Bando Labiah Suku Sikumbang (1852 M)			10. Dt. Kando Sutan Kaum Dt. Kando Sutan (1900-an M)		

Source: [14]

2 Research Method

2.1 Variable and Data Collecting

This study uses a survey method with data collection by observation and interviews. Research variables, data sources and data search methods can be seen in Table 2.

The method used in data analysis is to compare the condition of the SRG area before and after revitalization program. The research steps were carried out in 4 stages, namely: 1) Problem seeking and determine boundaries and objectives for the area as a whole, 2) Conduct a data collecting process by observation, interviews and study literature. The data is accompanied by field documentation and statements of

Table 2. Variables and Data Collection Methods

No	Variable	Data Collection	Methods
1.	Addition and function changes of space in public Facility	Existing of area and <i>Petua Adat</i>	Observation and questioner
2.	Function change of spacial in <i>rumah gadang</i> (dwellings/houses)	Spacial Lay-out of <i>Gadang</i> houses and their occupants	Observation and questioner
3.	The impact of the revitalization program	Existing of area and <i>Gadang</i> house	Observation, questioner, literature study

Table 3. Public Facilities Built during Revitalization Program

<p>1. <i>Songket</i> Tower</p>		<p>The Songket Tower is a viewing post tower which is the highest peak in the WRS area. With a height of 32 m, the shape of the roof resembles a <i>gonjong</i> and is filled with typical Minang decorations.</p>
<p>2. Pedestrian Access</p>		<p>This SRG area is based on ecotourism and geoparks, there are pedestrian facilities equipped with street lights, road markings, traffic signs, and chairs in the shape of a <i>gonjong</i> roof to rest and information boards scattered throughout the area.</p>
<p>3. Information Center and souvenir shop</p>		<p>The building has 2 spaces that function as an information and souvenir center, but can be rented for exhibitions. Gable-shaped roof</p>
<p>4. <i>Songket</i> Tower Stage</p>		<p>This stage adapts the shape of the <i>gonjong</i> which is equipped with a toilet and changing room at the back of the stage. This stage is a gathering place for local people</p>

Sources: Observation, 2021

The discussion started with the building of public facilities, and then continued with the restoration of houses in the *Saribu Rumah Gadang* area before and after the revitalization program.

3.2 Development of Public Facilities in the Saribu Rumah Gadang Area









There are 4 public facilities that were built during the revitalization in the *Saribu Rumah Gadang* area, namely Songket Tower, Pedestrian Access, Information Center and souvenir shop, and *Songket* Tower stage (Table 3). This public facility was built as an effort to improve the tourism function in this area.

3.3 The Condition of the Gadang House Before and After Restoration

Based on Table 2, only 6 out of 10 types of houses underwent restoration. Prior to the revitalization, a feasibility survey was conducted to review the condition of the *Rumah Gadang* which was damaged and could not support the daily activities of the local community optimally. The following table shows the condition of several Gadang Houses before and after undergoing restoration can be seen in Table 4.

The purpose of the restoration of 6 out of 10 types of Gadang Houses in the *Saribu Rumah Gadang* area is to restore function and repair damaged parts of the house without changing the shape and layout. The size of the land and buildings as well as the construction technique did not change. Changes only occur in the function

Table 4. Condition of Gadang Houses

Rumah Gadang	Before Restoration	After Restoration
Dt. Bando Labiah (Kaum Sikumbang)		
Dt. Bando Panjang (Suku Bariang)		
Dt. Sati (Kaum Panai Tanjung)		
Dt. Rangkayo Majo Lelo (Suku Durian)		
Dt. Kando Sutan (Kaum Dt. Kando Sutan)		
Dt. Rajo Bagindo (Suku Kampai)		

Sources : Documentation, 2021

of Rumah Gadang, which was originally a place for Rajo and Datuk’s appointment, but now it has turned into a residence. As well as updating old and weathered zinc and wood roofing materials.

3.4 Positive Impact of Revitalization in the Saribu Rumah Gadang Area

Since the revitalization program in the *Saribu Rumah Gadang* area has provided opportunities for local communities to start MSMEs, such as the emergence of souvenir centers, culinary centers, *Songket* Weaving Houses and dance houses (Fig. 5). On the banks of the *Batang Bangko* River it is also a hawker center filled

Fig. 4. Souvenir Shop in Saribu Rumah Gadang Area. Sources: Documentation, 2021



Fig. 5. Songket Tower of Snack Area. Sources: Documentation, 2021



with local people in the afternoon. In addition, 3 souvenir shops (Fig. 4), 1 restaurants, 14 daily shops, 12 homestays and 7 street vendors began to appear from the conversion of *Rumah Gadang* which previously had not been restored by PUPR and a small number of new buildings.

From Table 5 there are 12 Homestays that are officially registered in the SRG Area. 11 of the 12 homestays were original house buildings without restoration by PUPR, but only changed their function from residential houses to homestays. Another homestay or 1 of the 12 homestays, namely homestay 012 (Fig. 6) is the result of restoration from PUPR. According to Indah Nilam Sari (2021), the 007 homestay manager in 2019 at least 1–2 visits a week with ± 140 guests in a year or after the revitalization program the number of guests increased by 20%. Another homestay, namely *Rumah Gadang Gajah Maram* (Fig. 7) has not undergone any restoration considering its function and building is still solid. On the page of this house is a stone signed by President Joko Widodo at the inauguration of the SRG area.

In addition to the increase in the number of visitors to the homestay, it turned out that after the area revitalization program, South *Solok* tourism was aggressively promoting cultural tourism in the SRG Area, so that cultural activities in the area began to be visited by tourists. Cultural activities also began to be displayed, one of which was the *Datuk's* Inauguration and a banquet for homestay guests with the tradition of eating *bajamba* or eating together with a long stretch of side dishes. Indirectly, these cultural activities introduce the daily lives of residents and local culture to tourists (Fig. 8).

Table 5. Number of Economic Facilities in *Saribu Rumah Gadang Area*

Sarana Ekonomi	Jumlah
Toko Souvenir	3
Rumah Makan	1
Toko Harian	14
Homestay	12
PKL	7

Sources : Observation,
2021

Fig. 6. Homestay 012.
Sources: Documentation,
2021



Fig. 7. The Gadang Gajah Maram House of the Malays Buah Anau Dt. Lelo Lengh.
Source: Documentation,
2021



Fig. 8. The tradition of eating *Bajamba* & Inaugurating *Datuak* Tribe.
Source: Indah Nilam Sari,
2021



3.5 *Negative Impact of Revitalization Program*

In addition to the positive impacts, it turns out that there are also negative impacts from revitalization activities in the SRG Area. This can be seen in the reactions of some local people who live in the area. People with daily activities of farming and using environmental roads as a place to dry rice, coffee and cinnamon feel a little disturbed by tourists when entering the area using four-wheeled vehicles. The

Table 6. Positive and Negative Impacts of the Revitalization Program in the Saribu Rumah Gadang Area

	Revitalisation Program	Positive Impacts	Negative Impacts
Development of public facilities supporting tourism	Songket Tower	Appearance 1. Souvenir and culinary center, 2. <i>Songket</i> Weaving House 3. Dance house 4. Souvenir shop (3), 5. Restaurant (1), 6. Daily shop (14), 7. Homestay (12) 8. Street vendors (7). 9. Attractions of cultural activities 10. 20% increase for previously established homestays	Disruption of the activities of farmers who use environmental roads to dry rice, coffee and cinnamon, because many tourists use four-wheeled vehicles/ car
	Pedestrian acces		
	Information center and souvenir shop		
	Songket Tower Stage		
Restoration of <i>Rumah Gadang</i>	<i>Dt. Bando Labiah (Sikumbang ethnic group)</i>		
	<i>Dt. Bando Panjang (Bariang ethnic group)</i>		
	<i>Dt. Sati (Panai Tanjung ethnic group)</i>		
	<i>Dt. Rangkayo Majo Lelo (Durian ethnic group)</i>		
	<i>Dt. Kando Sutan (Dt. Kando Sutan ethnic group/family)</i>		
	<i>Dt. Rajo Bagindo (Kampai ethnic group)</i>		

positive and negative impacts after the revitalization program in the *Saribu Rumah Gadang* area were found can be seen in Table 6.

4 Conclusion

The Revitalization Program in the Saribu Rumah Gadang Area in the form of adding public facilities to support tourism and the restoration of several gadang houses to improve the quality of the area as a cultural tourism area. With this revitalization program, the community in this area has begun to clean up by developing businesses that can improve the local economy and cultural activities, either with new developments or the transfer of functions from the remaining *Gadang* houses. Although there is a negative impact on the comfort of the local community with the presence of tourists, this area now feels alive again and is widely known by people outside the area. The *Saribu Rumah Gadang area* is located in Nagari Koto Baru in the form of a dense residential area with 3 m wide road access. One of the best ways to get around the area is on foot or by bicycle. This method is also in accordance with the concept of ecotourism in the area. Local people also dry rice, coffee and cinnamon on the road due to limited land. The South *Solok* Regency Government should be more active and optimal in managing the area such as providing parking spaces outside the area so that tourists do not bring private vehicles into narrow areas and many children. This is to maintain comfort and safety between tourists and the local community. That way the community is not disturbed and tourists can see the daily life and culture of the local community as a whole.

References

1. Feng K, Song S, Zhou W (2022) The sustainability cycle of historic houses and cultural memory: controversy between historic preservation and heritage conservation. *Front Archit Res* 11:1030–1046. <https://doi.org/10.1016/j.foar.2022.04.006>
2. Wu J, Lu Y, Gao H, Wang M (2021) Cultivating historical heritage area vitality using urban morphology approach based on big data and machine learning. *J Comput Environ Urban Syst* 91:101716
3. Luo J, Jian IY, Chan EHW, Chen W (2022) Cultural regeneration and neighborhood image from the aesthetic perspective: case of heritage conservation areas in Shanghai. *J Habitat Int* 129:102689
4. Salameh MM, Touqan BA, Awad J, Salameh MM (2022) Heritage conservation as a bridge to sustainability assessing thermal performance and the preservation of identity through heritage conservation in the Mediterranean city of Nablus. *Ain Shams Eng J* 13:101553
5. Rebec KM, Deanovic B, Oostwegel L (2022) Old buildings need new ideas: holistic integration of conservation-restoration process data using heritage building information modelling. *J Cult Heritage* 55:30–42
6. Putra, Y.M.P.: Kawasan Saribu Rumah Gadang Menuju Warisan Dunia (2018). <http://nasional.republika.co.id/berita/nasional/daerah/18/01/17/p2p0iv284-kawasan-saribu-rumah-gadang-menuju-warisan-dunia>
7. Rukayah S, Respati PD, Susilo SES (2016) Morphology of traditional city center in Semarang: towards adaptive re-use in urban heritage. *Environ Behav Proc J* 1(4):109. <https://doi.org/10.21834/e-bpj.v1i4.91>
8. Truscott MC (2014) Burra Charter: the Australia ICOMOS charter for places of cultural significance (1999). In: Smith C (ed) *Encyclopedia of Global Archaeology*. Springer, New York, pp 1078–1082. https://doi.org/10.1007/978-1-4419-0465-2_1046
9. Kurniati R, Erlambang FR (2014) Changes the pattern of residential space into commercial space in Chinatown Semarang. In: 2014 International Conference on Tropical and Coastal Region Eco-Development, ICTCRED 2014
10. Bintang R, Putera S, Widodo RP (2020) Revitalisasi Sumber Daya Air Sungai Kalimalang Sebagai Strategi Pemanfaatan Lahan Di Kota Bekasi (Studi Kasus Kawasan Sungai Kalimalang, Kota Bekasi, Jawa Barat) Jurusan Administrasi Negara, Fakultas Ilmu Administrasi, Universitas Islam Malang, *J. Jurnal Respon Publik* 14(4):89–96
11. MacKeith MA (1993) “Rubenstein, Harvey M., ‘Pedestrian Malls, Streetscapes, and Urban Spaces’ (Book Review).” *Town Plan Rev.* <https://doi.org/10.3828/tpv.64.4.pl2276734285j2n2>.
12. Mutiari D (2018) *Sejarah Arsitektur di Indonesia*. Muhammadiyah University Press, Surakarta, pp 29–33
13. Noviantti Y (2020) Transformasi Nilai Budaya Di Kawasan Seribu Rumah Gadang Pada Etnis Minangkabau Di Kabupaten Solok Selatan. *JBS (Jurnal Berbasis Sosial)* 1:43–49. e-ISSN. 2723-0449 Pendidikan IPS STKIP Al Maksum. <https://jurnal.stkipalmaksum.ac.id/index.php/jbs>
14. Dinas Kebudayaan Pariwisata Pemuda dan Olahraga Kab. Solok Selatan (2016) Laporan Studi Kelayakan Cagar Budaya Kawasan Saribu Rumah Gadang. Solok Selatan: CV. Merpati

Effect of Polypropylene Fibre on High Volume Fly Ash Self-compacting Concrete in Terms of Compressive Strength, Tensile Strength, and Concrete Abrasion



Mochamad Solikin and Fauzi Mubarak

Abstract Concrete is the most widely used material in building construction because of its various advantages. Although it has many advantages, concrete in water faces problems of abrasion due to water flow. Therefore, the use of High volume fly ash (HVFA) in conjunction with polypropylene fibres is expected to be an alternative solution to the problem of concrete abrasion. This paper presents the study on the effect of high-volume fly ash concrete reinforced with polypropylene fibres in increasing the resistance of concrete to water flow abrasion. The testing program includes testing of fresh concrete (slump flow and T50 tests) and testing of hardened concrete (compressive strength of concrete, tensile strength of concrete and concrete abrasion). The Concrete abrasion test was conducted based on the standard of concrete abrasion in water. This study reveals that the use of polypropylene fibre had a positive impact in reducing the percentage of weight loss up to 24% for the abrasion test of HVFA. Furthermore, 0.6 kg/m³ of polypropylene fibre utilization can increase the tensile strength and compressive strength in comparison to High-volume fly ash concrete without fibre.

1 Introduction

Concrete is widely used as a construction material both for land construction and water construction as it has many advantages in comparison to other construction materials. However, concrete in water tends to have mechanical damage problems caused by water abrasion on concrete surfaces due to water flow. The main cause of concrete abrasion is the impact of solid specimens on the concrete surface carried by the flow of water such as sand, mud, gravel, wood debris or others [1]. Water structures that often experience severe abrasion occur at bends or basins of water

M. Solikin (✉) · F. Mubarak
Civil Engineering, Universitas Muhammadiyah Surakarta, Surakarta 57169, Indonesia
e-mail: msolikin@ums.ac.id

© Institute of Technology PETRONAS Sdn Bhd 2024
B. S. Mohammed et al. (eds.), *Proceedings of the International Conference on Emerging Smart Cities (ICESC2022)*, Lecture Notes in Civil Engineering 324,
https://doi.org/10.1007/978-981-99-1111-0_26

flow. The characteristics of concrete undergoing abrasion are the formation of cavities or cracks on the surface of the concrete, therefore continuous abrasion process in concrete will reduce the strength of the concrete [1].

Previous studies have shown that the abrasion resistance of concrete largely affects by the compressive strength of concrete [2]. Besides the strength, the parameters that give influence to the abrasion resistance include concrete strength design, aggregate properties, type and amount of additional cement, fibre addition, concrete hardening process, and concrete surface treatment [2, 3]. Therefore, high-strength concrete is chosen as good abrasion resistance of concrete as a consequence of the high cement content in the mix proportion of concrete.

The higher content of cement in mix proportion leads to the increase of heat of hydration and shrinkage of the concrete. This situation potentially generates cracks on the surface of the concrete. Therefore, it is necessary to adjust the cement content by utilizing cement substitute materials as one alternative. Fly ash as pozzolan is possible to be used as partial cement substitution to produce concrete.

Publications regarding the use of fly ash as concrete binders increased from year to year [4]. Fly ash is a by-product of a coal-fired steam power plant (PLTU) which has spherical fine particles with a diameter between 1–150 μm [5]. Fly ash is used as an additive in concrete mixtures which are considered to have the ability to improve the quality of the concrete, especially on the strength of concrete, reduce the heat of hydration, and high sulphate resistance, increase the workability of concrete and reduce the permeability of concrete [6]. This capability is expected to prevent fine cracks on the concrete surface by reducing the heat of hydration and producing a denser final concrete product.

The improvement in fly ash content utilization is possible to be used more than 50% as a substitute of cement in concrete mixtures. This utilization is known as High Volume Fly Ash (HVFA) in which this term HVFA is associated to the researchers working at the CANMET research centre located in Canada in the 1980s [7]. However, the use of fly ash produces a lower early-age compressive strength when compared to conventional concrete [8]. Efforts to accelerate the process of concrete hardening at an early age is possible by using a superplasticizer, a chemical admixture to produce Self-Compacting Concrete (SCC).

SCC was first developed by researchers from Japan in the 1980s caused by the reduction of labour during the concrete compaction process. The reduce causes the quality of the concrete made to decrease. To overcome this problem, the researcher developed self-compacting concrete (SCC). SCC is concrete with the ability to pass through gaps, fill, and flow by itself, can maintain the homogeneity of the concrete without segregation and does not require compaction to fill the formwork and achieve its own highest density [9].

The characteristics of SCC make the concrete very dense so that the compressive strength of the concrete increases. However, it is found that the higher the compressive strength the more brittle concrete is [10]. Therefore, it is necessary to add fibre to the concrete mixture to overcome the problem of brittle concrete. Fibres that are often used in concrete mixtures are steel fibres. However, the use of steel fibres causes other problems such as corrosion and high volumetric density [11].

Based on these considerations, the use of polymer fibre (polypropylene fibre) is an alternative solution. Polypropylene fibre is a fibre that has characteristics that do not absorb water and are resistant to corrosion [12]. Because of these characteristics, the use of fibre does not affect the amount of water used in the concrete mix. The addition of this fibre also is expected to have a positive impact on the concrete mix which can resist abrasion. According to Product Data Sheet Sika Fiber 12, the utilization of these product is 0.6 kg/m^3 of concrete [13].

Based on the background, concrete quality parameters have a significant influence on the ability of concrete to withstand abrasion. Previous researchers have said that high-strength concrete produces good abrasion resistance values. However, this paper tries to provide another alternative for making concrete with normal quality combined with the use of high volume fly ash self-compacting concrete with the addition of polypropylene fibres in the concrete mixture. Thus, this paper aims to obtain a concrete mix composition using high volume fly ash self-compacting concrete and the use of polypropylene fibres that meets the criteria for good concrete abrasion.

2 Method

The research method was carried out using an experimental laboratory conducted at the Civil Engineering Laboratory of the Universitas Muhammadiyah Surakarta. Implementation begins with the preparation of research materials and continues with an examination of the quality of the materials used in the research. Materials include fine aggregate, coarse aggregate, cement, fly ash, polypropylene fibre, and superplasticizer. The materials used such as fine aggregate, cement, and fly ash from PT Solusi Bangun Beton, while the coarse aggregate from PT Pancadarma Beton Readymix. The properties of fly ash and polypropylene fibre are described in Table 1 and Table 2. Moreover Fig. 1 shows the fly ash and the fibre which were used in this research.

The mixture consists of 3 types of mixtures including a mixture of HVFA-SCC (FA50) with the addition of polypropylene fibre (SP), and a mixture of NS-SCC and HS-SCC without the addition of fly ash or fibre as control concrete. The mixture of HVFA-SCC and NS-SCC is normal strength concrete ($f'c$ 25 MPa) while the HS-SCC mixture is high strength concrete ($f'c$ 45 MPa). The HVFA mixture uses 50% fly ash as a substitute for cement with the use of polypropylene fibre with variations in the content of 0 kg/m^3 , 0.4 kg/m^3 , and 0.6 kg/m^3 .

Table 1 Chemical content of fly ash

Chemical content	Percentage (%)
SiO ₂	43,22
Al ₂ O ₃	19,56
Fe ₂ O ₃	14,57
CaO	8,31

Table 2 Polypropylene fibre specifications

Base	<i>Polypropylene Fibre</i>
Colour	Natural
Specific Gravity	0,91 gr/cm ³
Fibre Length	12 mm
Fibre Diameter	18 μ -nominal
Tensile Strength	300–440 MPa
Water Absorption	-
Softening Point	160 °C

**Fig. 1.** Fly ash and Polypropylene fibre

The concrete mix design method uses the [14] method with some adjustments through the trial mix to determine the proportion of the SCC mixture to be made. The test specimen consisted of a cylinder with a diameter of 150 mm and a height of 300 mm for testing the compressive strength and tensile strength, and a beam with a size of 300 mm \times 150 mm \times 60 mm for testing concrete abrasion. Fresh concrete testing was also carried out including slump flow testing and T_{50} .

The next step is casting of concrete based on mix design preparation in Table 3. In addition, fresh concrete was tested in for slump flow and T_{50} test. After one day in the mould, the specimens were taken out from the mould for curing stage. However, for the concrete abrasion test specimen the specimen was not removed from the mould as the mould is needed for testing stage in abrasion test apparatus as stated in Indonesian standard for abrasion test [16]. The curing stage is important to ensure complete hydration process of concrete. The duration of curing stage is 28 days before compressive strength, tensile strength, and abrasion test.

The last step in this research is data analysis and discussion. Data analysis is carried out based on the results of tests that have been carried out and then a discussion is carried out regarding the results of the data which will conclude.

Table 3. Mix proportion

No	Specimen	f'c	Proportion per m ³						
			Cement	Fly Ash	Sand	Gravel	PF	SP	Water
			kg	kg	kg	kg	kg	lt	lt
1	FA50-PF0	25	198,86	198,86	1020,65	696,45	0	5,97	175
2	FA50-PF0.4	25	198,86	198,86	1020,65	696,45	0,4	5,97	175
3	FA50-PF0.6	25	198,86	198,86	1020,65	696,45	0,6	5,97	175
4	NS-SCC	25	397,72	-	1020,65	696,45	-	5,97	175
5	HS-SCC	45	606,67	-	928,03	644,25	-	9,1	182

Note: SP = Superplasticizer; PF = Polypropylene Fibre

3 Result and Discussion

3.1 Slump Flow and T₅₀ Test

Slump flow and T₅₀ tests were carried out to determine one of the characteristics of SCC concrete, namely flowability. This test is carried out by measuring the final diameter and the time it takes to reach a diameter of 500 mm during the testing process. This test uses Slump cone tool according to the EFNARC method and test standards [9]. The results of the slump flow and T₅₀ tests are described in Fig. 2 and 3.

The test results in Fig. 3 and Fig. 4 show that in the research concrete there was a decrease in the slump flow value and an increase in time on the T50 test along with the addition of fibre content in the concrete mixture. In addition, the mixture with the use of fly ash 50% without the addition of fibre (FA50-PF0) has the highest slump flow test and fastest flow time in the T₅₀ test, when compared to the mixture of NS-SCC and HS-SCC. This is possible due to the use of fly ash material with a

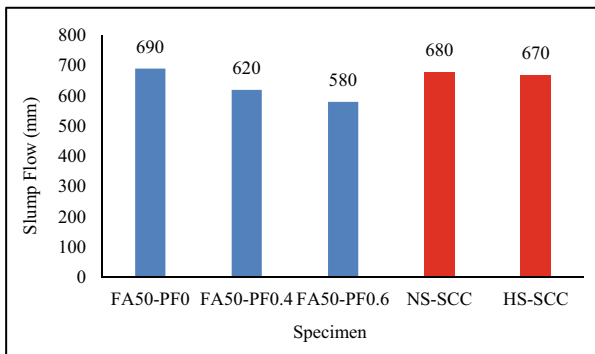


Fig. 2. Slump flow test

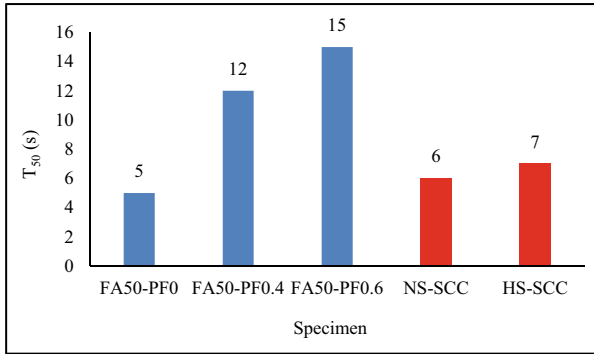


Fig. 3. T₅₀ test

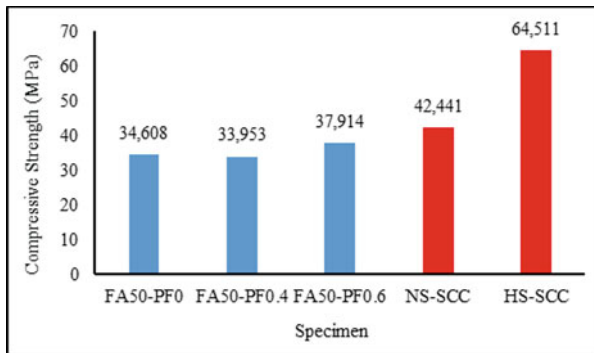


Fig. 4. Compressive strength

content of >50% which has a spherical particle shape to increase the flowability of the mixture.

However, when polypropylene fibre is added to the mixture, the flowability of the concrete decreases and the flow time increases. This is due to the increased friction between the ingredient of concrete [11]. Similar results were also obtained by Abed et al. [11] who found that the use of polypropylene fibres could reduce the flowability of SCC concrete. The slump flow distribution decreased from 730 mm for the control concrete without fibres to 700 mm and 670 mm with the addition of polypropylene fibres in the concrete mix.

3.2 Compressive Strength

The compressive strength test was carried out at the age of 28 days with a cylindrical test specimen having a diameter of 150 mm and a height of 300 mm. The test was

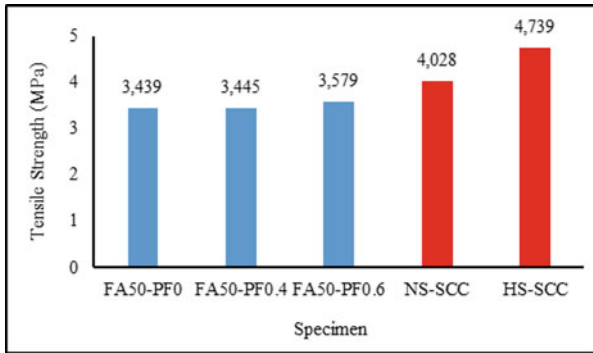


Fig. 5. Tensile strength

carried out using a Compression Testing Machine (CTM) which was carried out at the Civil Engineering Laboratory, Universitas Muhammadiyah Surakarta. Before testing the compressive strength, the specimens that have been prepared have gone through the concrete curing process. The test method was carried out according to compressive strength test standard [15]. The data from the test results are then calculated using the following formula:

$$f'_c = P/A \quad (1)$$

where:

f'_c = compressive strength (N/mm²)

P = maximum load (N)

A = section area (mm²)

The results of the compressive strength test can be seen in Fig. 5.

The test results in Fig. 4 show that there is an increase in the compressive strength of the research concrete along with the increase in the fibre content in the concrete mixture. The maximum increase was 9.55% for FA50-PF0.6 specimen. The mixture of HVFA without the addition of fibre (FA50-PF0) when compared to the mixture of NS-SCC and HS-SCC has lower compressive strength. This result is possibly caused by fly ash is an unreactive binder lin comparison to cement and only small particle size of fly ash contribute in binder hydration reaction. When the mixture is added with polypropylene fibre, there is an increase in compressive strength due to contribution of fibre to prevent early cracking [16]. The positive effect of early cracking prevented by the fibre has an impact on increasing the yield of compressive strength.

In addition, the compressive strength of HVFA concrete is lower in comparison to NS-SCC and HS-SCC. It is noted in here that mix proportion of HVFA concrete was prepared to produce normal strength concrete. The lower strength of HVFA concrete is possible because slow reaction of fly ash in comparison to cement as

binder. Moreover, the addition of polypropylene fibres gives small improvement on the compressive strength about 8.7%. This is also in line with the research conducted by Grdic et al. [2] which found that the use of polypropylene fibres increased the compressive strength of concrete. The average increase that occurred ranged between 7 and 8%.

3.3 Tensile Strength

The tensile strength test of concrete was carried out at the age of 28 days by using similar specimen as compressive strength test. The test was conducted on the Universal Testing Machine (UTM) in Civil Engineering Laboratory, Universitas Muhammadiyah Surakarta. The test method was carried out according to tensile strength test of concrete standard [17]. The data from the test results are then calculated using the following formula:

$$T = \frac{2P}{\pi ld} \quad (2)$$

where:

T = tensile strength (MPa)

P = maximum load (N)

$\pi = 3.14$

l = length (mm)

d = diameter (mm)

The results of the tensile strength test is shown in Fig. 6.

The test results in Fig. 5 show that there was an increase in the tensile strength of the concrete specimen along with the increase of fibre content in the mixture. The highest improvement was 4.07% which is obtained in FA50-PF0.6 mixture. Moreover, HVFA concrete without fibre (FA50-PF0) has lower tensile strength when compared to NS-SCC and HS-SCC. This result is possible because the use of high-volume fly ash tends to lower concrete strength test results when compared to concrete without fly ash. However, the presence of fibre is beneficial to increase the tensile strength due to the initial working load is taken by the fibres which then continue to the concrete [18]. Previous study conducted by Abed et al. [11] found that the use of polypropylene fibre can increase the tensile strength of concrete. The increase that occurred was 34.8%.

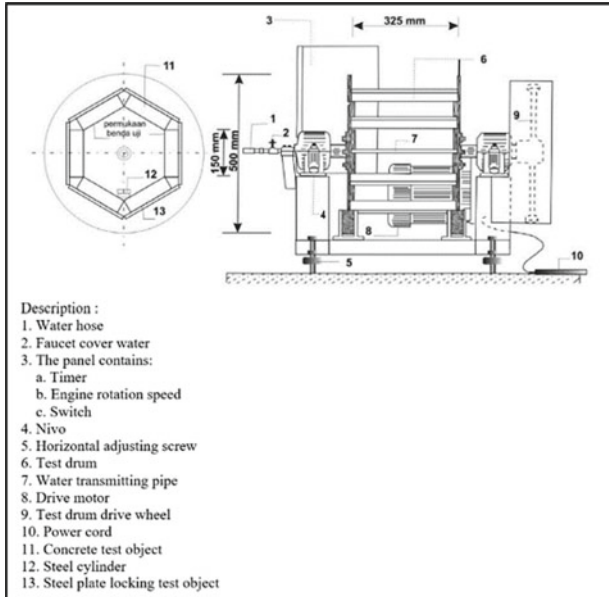


Fig. 6. Schematic of concrete abrasion test equipment

3.4 Abrasion Test

The concrete abrasion test was carried out after curing stage for 28 days on small beam specimen with a dimension of 300 mm × 150 mm × 60 mm. The test was carried out using a concrete abrasion apparatus at the Laboratory of the Sabo Engineering Centre, Yogyakarta. The test was carried out according to concrete abrasion test in water [19] by measuring the reduction of the dimensions and the weight of each specimen. For each stage of test six specimens per variation were prepared. After that, the test specimen is inserted into holder that has been provided in the abrasion test equipment and 22 small steel ball (2000 g) are added which are then supplied with sufficient water during the testing process.

The testing process lasts for 3 h in which for every 1 h of testing, the test equipment is stopped and all test specimens are removed to measure the weight. These steps were repeated until they were completed (test duration of 3 h). After 3 h of testing scheme test specimen is removed from the abrasion formwork. The test results data obtained were in the form of the percentage of weight loss during the test duration of 3 h of testing. The data is then calculated using the following formula:

$$\%KB = \frac{W_o - W_n}{W_n} \times 100\% \tag{3}$$

where:

$\%KB = \text{loss of weight (\%)}$

$W_o = \text{total weight of the mould and test specimen before testing (gram)}$

$W_n = \text{the total weight of the mould and test specimen after the first hour, the second hour and the third hour (gram)}$

The following is a schematic drawing of the abrasion test equipment which can be seen in Fig. 6.

The test results in Fig. 7 show that the percentage loss of weight increases following the duration of the test. The research specimen tends have significant increase in loss of weight at each additional test duration. For NS-SCC specimen is compared with HS-SCC, the loss of weight of both specimens is only in small amount. Moreover, for all the test specimens, the highest abrasion value is shown by the FA50-PF0 specimen, in which the specimen did not use fibre. A high abrasion value indicates that the concrete is less able to withstand the abrasion that occurs the concrete. When the research concrete was added with polypropylene fibre, the percentage loss of weight decreased along with the addition of fibre content in the research concrete mixture. This is possible due to an increase in the bonding between the concrete constituent materials due to the use of fibres so that the concrete pores become smaller and reduce porous concrete [2].

Although the presence of polypropylene fibre reduces the abrasion of HVFA concrete, the reduction still above the loss weight of NS-SCC and HS-SCC. It is indicated that the use of fly ash in HVFA concrete tends to reduce abrasion resistance of concrete. In addition, the HS-SCC concrete in this research is denser that lead to the higher abrasion resistance of concrete. Based on these results, the addition of polypropylene fibres can have a positive effect on reducing the percentage loss of weight in concrete abrasion tests. This is also in line with the research conducted by

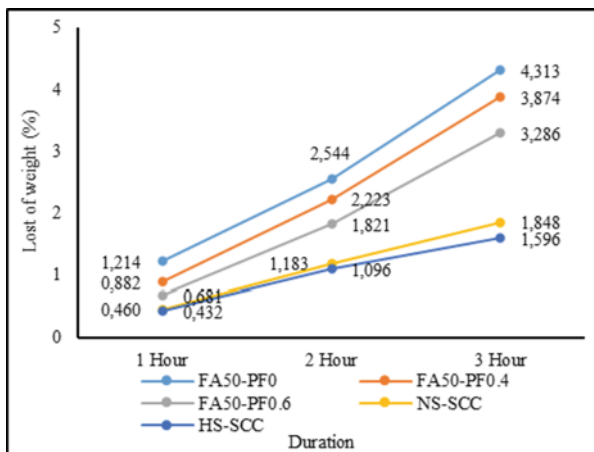


Fig. 7. Abrasion test

Grdic et al. [2] which found that the use of polypropylene fibres can reduce the level of concrete abrasion.

4 Conclusion

The use of polypropylene fibre in High-Volume Fly ash concrete has a positive effect on improving the abrasion resistance of concrete. In addition, the fibre gives improvement in compressive strength and tensile strength, up to the utilization fibre content of 0.6 kg/m^3 .

Acknowledgements This research made possible with the help of Allah The Most Merciful. An appreciation is also addressed to PT. Holcim Bangun/Concrete Batching Plant Solution Yogyakarta which provided sponsors material for this research. Correspondingly, a sincere appreciation gives to the Laboratory of Universitas Muhammadiyah Surakarta and Laboratory of the Sabo Engineering Centre for facilities to conduct this study.

References

1. Abid SR, Hilo AN, Ayoob NS, Daek YH (2019) Underwater abrasion of steel fiber-reinforced self-compacting concrete.pdf. *Case Stud Constr Mater* 11:e00299
2. Grdic ZJ, Curcic GAT, Ristic NS, Despotovic IM (2012) Abrasion resistance of concrete micro-reinforced with polypropylene fibers. *Constr Build Mater* 27(1):305–312. <https://doi.org/10.1016/j.conbuildmat.2011.07.044>
3. Kabay N (2014) Abrasion resistance and fracture energy of concretes with basalt fiber. *Constr Build Mater* 50:95–101. <https://doi.org/10.1016/j.conbuildmat.2013.09.040>
4. Alterary SS, Marei NH (2021) Fly ash properties, characterization, and applications: a review. *J King Saud Univ Sci* 33(6):101536. <https://doi.org/10.1016/j.jksus.2021.101536>
5. Siddique R (2004) Performance characteristics of high-volume Class F fly ash concrete. *Cem Concr Res* 34:487–493
6. Solikin M (2016) Compressive strength development of high strength high volume fly ash concrete by using local material. *Mater Sci Forum* 872:271–275. <https://doi.org/10.4028/www.scientific.net/MSF.872.271>
7. Marthinus AP, Sumajouw MDJ, Windah RS (2015) Pengaruh Penambahan Abu Terbang (Fly Ash) terhadap Kuat Tarik Belah Beton. *J Sipil Statik* 3(11):729–736
8. Karthik D, Nirmalkumar K, Priyadarshini R (2021) Characteristic assessment of self-compacting concrete with supplementary cementitious materials. *Constr Build Mater* 297:123845. <https://doi.org/10.1016/j.conbuildmat.2021.123845>
9. EFNARC (2002) Specification and Guidelines for Self-Compacting Concrete. Surrey, UK
10. Sulthan F (2019) Pengaruh Tipe Bentuk Serat Baja Terhadap Sifat Fisik Dan Mekanik Beton Berserat Baja Memadat Sendiri. *Cantilever* 8(1):29. <https://doi.org/10.35139/cantilever.v8i1.71>
11. Abed MA, Fořt J, Naoulo A, Essa A (2021) Influence of polypropylene and steel fibers on the performance and crack repair of self-compacting concrete. *Materials (Basel)* 14(19):5506. <https://doi.org/10.3390/ma14195506>
12. Lussy CL, Sugiharto H (2020) Pengaruh Penggunaan Polypropylene Fibre Terhadap Karakteristik self compacting concrete. *Dimens. Pratama Tek. Sipil* 9(1)
13. Admin (2017) PRODUCT DATA SHEET SikaFiber-12. Bahrain

14. ACI Committee 211 (2006) Standard Practice for Selecting Proportions for Normal, Heavy-weight, and Mass Concrete (ACI 211.1-91), no 9, pp 120–121
15. SNI 1974-2011 (2011) Cara Uji Kuat Tekan Beton dengan Benda Uji Silinder. Badan Standar Nasional Indonesia, p 20
16. Wu C, Liu Y, Huang C, Yen T, Hsu T (2010) Research on the abrasion erosion and impact resistance of fiber concrete. In: *Collected Papers on Building Technology: 18th CIB World Building Congress*, May 2010 Salford, United Kingdom, vol i, no May, pp 333–344
17. SNI 2491-2014 (2014) Metode Uji Kekuatan Tarik Belah Spesimen Beton Silinder. Badan Standarisasi Nasional Indonesia, pp 1–17
18. Ojha PN, Trivedi A, Singh B, Kumar NSA, Patel V, Gupta RK (2021) High performance fiber reinforced concrete for repair in spillways of concrete dams. *Res Eng Struct Mater* 7:505–522. <https://doi.org/10.17515/resm2021.252ma0128>
19. SNI 3419-2008 (2008) Cara Uji Abrasi Beton di Laboratorium. Badan Standar *Nasional Indonesia*

The Effectiveness of COD Removal from Industrial Effluent Using Treatment Train System



Muhammad Faris Mohd Ramli, Husna Takaijudin,
Manal Osman Mohamed Ali, Wafaa Ali Nsaif Alhamzah,
and Nor Amirah Ahmad Zubairi

Abstract In some cases, the steel industrial effluents may be treated and not be treated before it discharged into water bodies. The purposes of conducting this study are to characterize the steel industrial effluent from past research as a pollutant source benchmark and evaluate the effectiveness of COD removal for industrial effluent in a treatment train system. Three (3) sets of treatment trains (Set A, Set B & Set C) were set up as cascaded (stepped) system with various plant species planted in the engineered soil media. The best performance between the three (3) different configurations was Set C (Soil with *Cordyline Fruiticosa* plant). Set C obtained the highest removal rate than the other two (2) sets which was 98.9%. To conclude, the bioretention treatment train was very effective to treat steel industrial effluent and it is suggested that further study involve monitoring the performance of the treatment train system for a longer period of time to observe if the quality of effluent degrades over time.

Keywords Chemical oxygen demand · bioretention · configuration · steel industrial wastewater · pollution · plant · removal rate · concentration · contaminants

M. F. M. Ramli · H. Takaijudin (✉) · M. O. M. Ali · W. A. N. Alhamzah · N. A. A. Zubairi
Department of Civil and Environmental Engineering, Faculty of Engineering, Universiti
Teknologi PETRONAS, 32610 Seri Iskandar, Perak, Malaysia
e-mail: husna_takaijudin@utp.edu.my

M. O. M. Ali
e-mail: manal_17005662@utp.edu.my

W. A. N. Alhamzah
e-mail: wafaa_19001087@utp.edu.my

N. A. A. Zubairi
e-mail: nor_19001668@utp.edu.my

© Institute of Technology PETRONAS Sdn Bhd 2024
B. S. Mohammed et al. (eds.), *Proceedings of the International Conference on Emerging
Smart Cities (ICESC2022)*, Lecture Notes in Civil Engineering 324,
https://doi.org/10.1007/978-981-99-1111-0_27

1 Introduction

1.1 Background of Study

The steel industry is one of nine industries that use a lot of energy and produce a lot of wastewaters. Steel is made by chemically reducing iron ore through an integrated steel manufacturing process or a direct reduction method. According to [2], total suspended particles, lead, chromium, cadmium, zinc, fluoride, and oil and grease are all major contaminants found in steel manufacturing wastewaters. Industrial wastewater treatment is necessary because it pollutes the atmosphere, produces discoloration and turbidity, depletes dissolved oxygen, promotes algal and fungal growth, and results in sludge deposits, among other things. The steel industry is one of nine industries that use a lot of energy and produce a lot of waste. The toxicity to marine life, a decrease of DO, silting due to suspended solids, taste and odour problems, temperature rise affecting dissolved oxygen and marine life, and formation of oil slicks due to floating oil are the significant pollution effects of untreated steel industry wastewaters if discharged into the receiving water bodies. A case studies in Nigeria found that the discharge of industrial effluents into receiving water bodies invariably result in the presence of high concentrations of pollutant in the water and sediment (Kanu et al., 2011). Hence, the best indicator that can be used to characterize pollutants for steel industrial effluent is Chemical Oxygen Demand (COD).

The chemical oxygen demand (COD) is a measurement of the quantity of oxygen necessary to oxidize the part of organic matter in wastewater and the quantity of oxygen used by organic matter in a boiling acid potassium dichromate solution. COD is a monitoring test that counts all the oxidizable materials in a runoff sample and determines how much of it depletes dissolved oxygen in receiving waters.

Bioretention systems' primary purpose is to filter out unwanted pollutants and nutrients. A bioretention system is made of a soil bed that has been planted with non-invasive (ideally native) vegetation. In this case, bioretention systems are used to extract a variety of contaminants from steel industrial effluent, including suspended particles, fertilizers, metals, COD, hydrocarbons, and bacteria. A typical bioretention system can be referred to in Fig. 1. The goal of connecting several bioretention systems should be to synchronize diverse treatment methods in order to improve water quality and reduce pollutant export [1].

The degradation of organic matter was promoted with the increase of oxygen content and the microbial population of the systems, leading to the rapid increase of the COD removal in the three bioretention units [5]. Similar to [3] found that the accumulation of bacteria with COD degradation functions decreased in soil, whereas it increased in fillers. Pb promoted and inhibited COD removal in the soil and filler layer, respectively.

Hence, the aim of this paper is to assess the performance treatment train system in treating COD mainly from industrial effluent.

Fig. 1. Bioretention Layers and Hydrologic Function of Bioretention System [4]

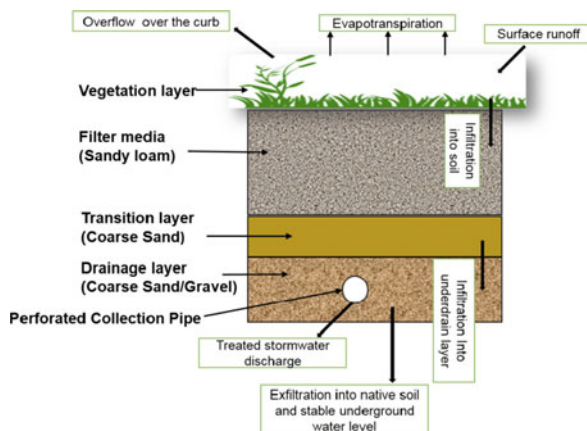


Table 1. Composition of Synthetic Water

Synthetic Agricultural Runoff Constituents	Chemical	Amount (g)
TSS	Silicon Dioxide (SiO ₂)	39.16
COD	Glucose (C ₆ H ₁₂ O ₆)	40.97

2 Methodology

2.1 Preparation of Steel Industrial Effluent

To get the steel industrial effluent, preparation of synthetic effluent needs to be done. The way to prepare the synthetic effluent was by using the previous studies information to determine what concentration of steel industrial effluent the author used in the article. The key parameters that should be provided from the research studies are pH, Total Suspended Solids (TSS), Biochemical Oxygen Demand (BOD), Oil & Grease (O&G), and Chemical Oxygen Demand (COD). Due to constraints of chemicals, out of four contaminants (TSS, BOD, COD, and O&G), only two contaminants were used to produce the synthetic water. The two contaminants were TSS and COD. To mimic the real steel industrial effluent, all of the pollutants from Table 1 should be employed.

2.2 Treatment Train System Setup

Each set of bioretention column represents different configuration. The following were the configuration of each set:

- A. No vegetation + soil (control)

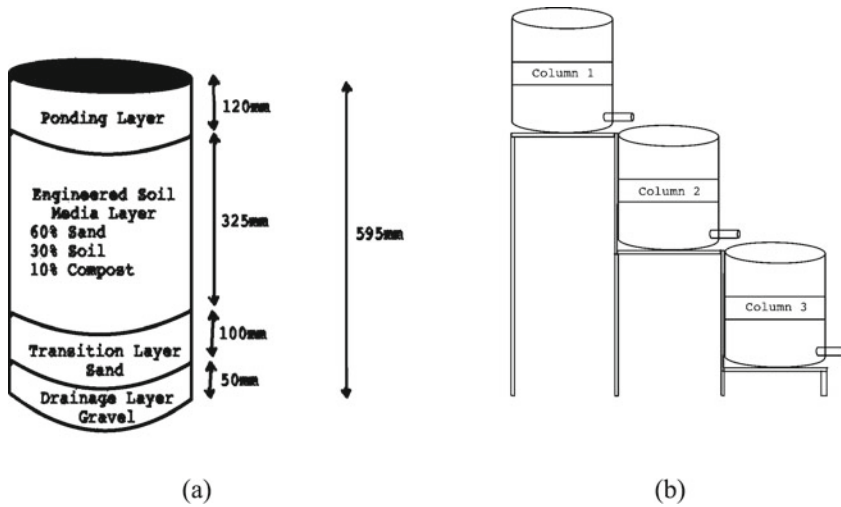


Fig. 2. (a) soil layer in bioretention column (b) cascaded column setup

B. Single Vegetation A (*Cyperus Alternifolius* plant) + soil

C. Single Vegetation B (*Cordyline Fruticosa* plant) + soil

Each set has 3 cascaded columns. Set A consists of columns namely A1, A2 and A3, respectively. Set B with vegetation A namely B1, B2 and B3 while Set C with Vegetation C namely C1, C2 and C3, respectively. According to MSMA, for each column, four (4) layers of required specification soil media was inserted. The layers were: Ponding layer; Engineered Soil Media layer (60% of Sand, 30% of Soil, and 10% of Compost); Transition layer; and Drainage layer. The details of these layers are shown in Fig. 2(a) and the setup in Fig. 2(b) below.

Soil Preparation. According to MSMA, some of the components of a bioretention system consist of a soil bed and sand bed. Hence, a considerable amount of soil was used to fill up the columns. A soil classification was conducted to identify the type of soil. Four types of tests were performed: the sieve analysis test, specific gravity test, hydrometer test, and permeability test using the falling head.

2.3 Water Sampling and Analysis

After all the preparation were done, it was time to run the synthetic water into the treatment train. For this project, five runs were executed. The water samples were taken at each column's effluent for the first, third, and fifth run. Whereas, for the second and fourth run, the water samples were collected only at the end of the treatment train (the last column only). After all the runs were executed, the samples

were ready for COD testing. COD test required around three hours to complete according to USEPA Reaction Digestion Method (Standard Method 8000) (USEPA, 1999). There were two types of COD range: Low Range (LR) and High Range (HR). LR COD could read the amount of COD concentration ranging from 3 to 150 mg/L, while HR COD could read the amount of COD ranging from 3 to 1500 mg/L. For this project, both LR and HR would be used to determine the COD value, and the method was similar.

3 Results and Discussion

3.1 Chemical Oxygen Demand (COD) Analysis

For each sample, the COD test was done two times, and the average value was taken. Figure 3 shows the bar graph of average COD readings of all runs for each column. It was found the significant reduction of COD in Set A and Set C. According to Industrial Effluent Treatment System (IETS) regulations, the acceptable conditions for discharge of industrial effluent containing COD for steel industry are Standard A, 80 mg/L, and Standard B, 200 mg/L. Hence, the final discharge effluent for all sets: Set A: 26.8 mg/L; Set B: 34.5 mg/L; and Set C: 5.4 mg/L, were fall under Standard A. Standard A means the effluent can be discharged into any water within any catchment area. Other than that, from the figure, a decrease trend COD can be seen from the first column to the last column. This indicates that the treatment train can reduce the amount of steel industrial effluent COD.

Figure 4 below shows the COD removal rate of column configurations. As the steel industrial effluent travels through each bioretention column, the COD is reduced. Every column configuration shows an initial reduction of more than 52%. When

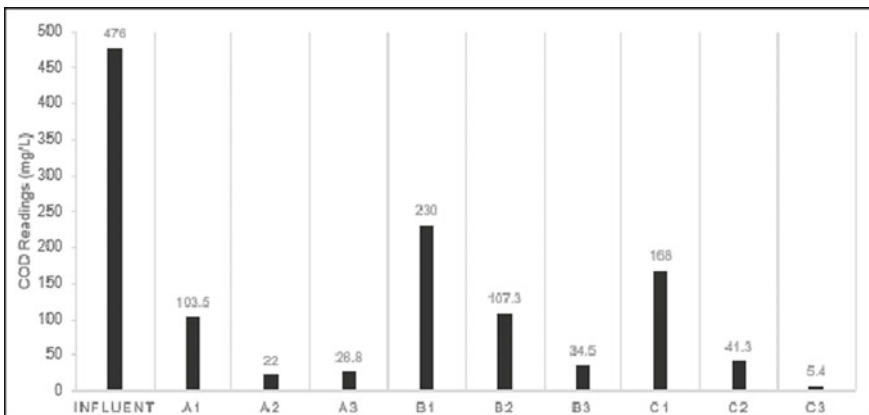


Fig. 3. Average COD Concentration of steel industrial effluent passing through treatment train

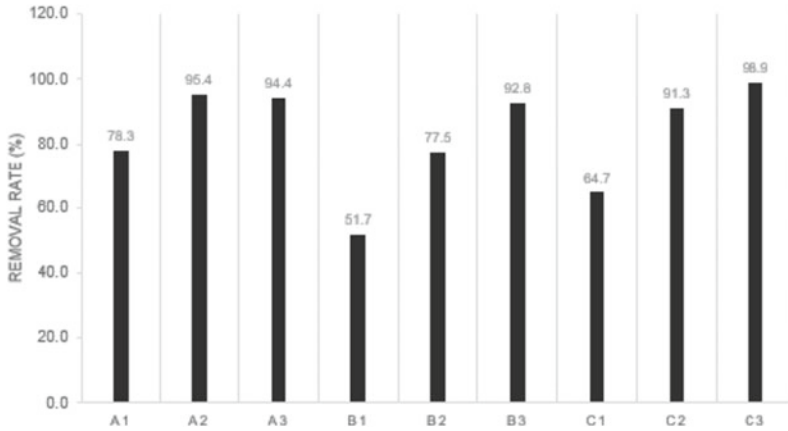


Fig. 4. COD Removal Rate for each set

comparing the control set to the vegetated sets, the control set gave the highest initial reduction of 78.3% to the vegetated sets of 51.7% and 64.7%. But for the final removal rates, all the column configurations show more than 93% reduction rate. Set C gave the highest reduction rate compared to Set A and Set B, but these two sets' reduction rate still considered high COD removal. Set C is the best treatment train system based on the three sets as it removes the highest amount of COD concentration in this column configuration consisting of *Cordyline Fruticosa* (CF). It is consistent on the studies by Ab. Aziz et al. (2020) mentioned that the reduction of COD was obtained because the plants underwent the process of photosynthesis. The photosynthesis activity increases the dissolve oxygen in water, this creating aerobic condition in wastewater in favour of aerobic bacterial activity to reduce COD contents. This can be indication that wastewater would have a lesser impact on the environment after being treated using bioretention system.

4 Conclusion and Recommendation

In conclusion, the objectives of this project were achieved. Even though the chemicals used for the synthetic water were limited, but the outcome of the experiment was satisfactory. Since there were several different sets of bioretention columns, it was expected that each set would give a different value of COD concentration reduction. It would be recommended that further study involve monitoring the performance of the treatment train system for a longer period of time to observe if the quality of effluent degrades over time. Aside from that, putting the treatment train system in place on a real steel industry would produce more convincing results as it would eliminate the usage of synthetic water and prove the system's performance on the real steel industry or factory. The installation of the treatment train was simple and

accessible. Finally, the study can examine other benefits of the treatment train system on a deeper level, such as the retention ability of the system.

Acknowledgements The research is funded by International Collaboration Research Fund Grant Cost Centre (015ME0-261) entitled “THE IMPACT OF URBAN WATERSHED TO HYDROLOGICAL PERFORMANCE WITH THE PRESENCE OF SUSTAINABLE STORMWATER MANAGEMENT SYSTEM”. Special thanks to Universiti Teknologi PETRONAS and River Engineering and Urban Drainage Research Center (REDAC), Higher Institution Centre of Excellence (HICoE) for Service for giving fully support of this project.

References

1. Brown RA, Line DE, Hunt WF (2012) LID treatment train: pervious concrete with subsurface storage in series with bioretention and care with seasonal high water tables. *J Environ Eng* 138(6):689–697
2. Krishnaveni R, Pramiladevi Y, Ramgopal RS (2013) Bioremediation of steel industrial effluents using soil microorganisms. *Int J Adv Biotechnol Res* 4(1):51–56
3. Liu C, Lu J, Liu J, Mehmood T, Chen W (2020) Effects of lead (Pb) in stormwater runoff on the microbial characteristics and organics removal in bioretention systems. *Chemosphere* 253:126721
4. Shafique M (2016) A review of the bioretention system for sustainable storm water management in urban areas. *Mater Geoenviron* 63(4):227–236
5. Singh RP, Zhao F, Ji Q, Saravanan J, Fu D (2019) Design and performance characterization of roadside bioretention systems. *Sustainability* 11(7):2040

Life Cycle Assessment of Utilization of Shredded Tire for Sustainable Road Embankment



Vera H. Loo , Wahidul K. Biswas , and Nicholas Z. S. Chin

Abstract This paper provides a life cycle assessment on the use of scrap tire used in subgrade for road embankment construction. The objective of this study is to compare energy consumption and greenhouse gas emission for two methods of constructing the fill embankment, a traditional method involving the filling with sand/soil materials and an alternative method utilizing the shredded tires. The replacement of shredded tires to soil by volume ranged from 10 to 50%. The life cycle assessment of scrapped tire is assessed. The result shows that the use of used car tire in embankment for soil is unlikely to offer environmental benefits due to the use of energy intensive tire recycling processes.

Keywords Life cycle assessment · sustainable · embankment

1 Introduction

Due to rapid growth in the usage of vehicles, 800 million scrap rubber tires are disposed of each year around the world, and it is expected to increase by about 2% annually [1]. The problem would become more severe due to the rapid growth in consumption of vehicles in developing countries. In Malaysia, rubber tires will end up disposed in the landfill site. Scrapped tires that were disposed will cause environmental problems such as mosquito breeding, occupied the landfill area, create fire hazards, etc. In a study regarding the products recycling desirability index, recycle of tire ranks number three after the car battery and polyethylene terephthalate (PET) bottle in Malaysia [2].

V. H. Loo (✉) · N. Z. S. Chin

Department of Civil and Construction Engineering, Curtin University Malaysia, Sarawak, Malaysia

e-mail: vera.loo@curtin.edu.my

W. K. Biswas

Sustainable Engineering Group, Curtin University, Perth, Australia

e-mail: w.biswas@curtin.edu.au

© Institute of Technology PETRONAS Sdn Bhd 2024

B. S. Mohammed et al. (eds.), *Proceedings of the International Conference on Emerging Smart Cities (ICESC2022)*, Lecture Notes in Civil Engineering 324,

https://doi.org/10.1007/978-981-99-1111-0_28

The research of recycling the scrapped tires was first carried out in the United States in early 1990s [3–5]. The application related to the use of scrapped tires for used as lightweight fill material in embankments and retaining structures. The standard practice for use of scrap tires in civil engineering application has been issues (ASTM D6270-98) in late 1998 [6]. According to U.S. Tire Manufacturers Association (USTMA), there was a billion scrap tires in stockpiles in the U.S. in 1990. However, through the efforts of recycling and reused, it was reported in 2018 over 81% of scrap tires are re-used in products such as tire-derived fuel, rubber modified asphalt and other products [7].

The use of tire chips is attractive of its characteristic such as low bulk density, high durability, non-biodegradable, low cost or free and available in the market. The objective of this study is to assess the energy consumption and greenhouse gas emission for fill embankment with traditional method involving the filling with soil materials and an alternative method utilizing the shredded tires in replacement of soil materials. The replacement will only focus on the subgrade of soil materials.

2 Performance of Soil Mixtures with Tire Chips

The engineering properties of mixtures of sand and tire chips had been studied by various researchers. The earliest published research investigated the feasibility of using tire chips mixed with soils as lightweight material in highway embankments [3]. The laboratory testing results showed that the rubber-sand with ratio of 38% or less exhibited excellent engineering properties such as easy to compact, low dry density, low compressibility and excellent drainage characteristics. The engineering properties of shear strength and permeability of shredded tires mixed with Ottawa sand, and a mixture of 50% sand and 50% shredded tires by volume, indicating that the use of shredded tires/Ottawa sand mixes as a lightweight fill material is very promising [4]. Several research [5, 8, 9] also showed that that soil containing shredded tires had higher strength than soil alone.

On the other hand, the test embankments of 1.8 m and 2.1 m high had been studied using the shredded tires [10, 11]. Two configurations of test embankment with side slopes of 1V:2H were carried out. One configuration was 0.91 m high large tire chip layer covered with sand layer and the other configuration is three repeated 0.3 m medium size tire chips covered with 0.3 m sand layers. The research showed that the performance of the embankment was better with the proper confinement of tire chips with topsoil [10]. Other test embankment [11] which used a 50/50 mixture of tire shreds and sand, by volume, showed that there no significant total and differential settlements. In addition, the environmental impact of the embankment on ground-water quality due to leaching of fill materials is within the maximum contaminant level for drinking water and there is no evidence of internal heat generation.

Comprehensive review [12] on different types of recycled waste tire-soil/sand mixtures to investigate the engineering properties such as compression and deformation behaviour, shearing properties, dynamic features, thermal/microstructural

characteristic, and the environmental concerns indicated that the re-utilization of recycled waste tire-soil/sand mixtures in geotechnical engineering is promising.

3 Characterization of the Fill Embankment

In this study, the design of the fill embankment is referring the standard drawings of Public Works Department [13] and schematically shown in Fig. 1. The material of the fill embankment to be compared is mixture of sand and shredded tires. The side slope of the embankment is 1V:2H.

Research indicated that the shear strength increases with a 10% of shredded tire by content [5]. Based on specification for embankments containing tire chips and sand/fine grained soils, the recommended ratio of chips to dry weight of rubber-sand/fine grained soils is 38% or less [3]. Other research showed that a mixture of 50% sand and 50% shredded tires by volume, indicating that the use of shredded tires/sand mixes as a lightweight fill material is very promising [4]. Therefore, the shredded scrap tires (SST) are to replace partially the subgrade of soil materials from 10 to 50% in volume. Three different types of tires mixes with suitable materials (SM) were evaluated. The first mix (M1) was a control set which consists of suitable materials. The second mix (M2), third mix (M3) and fourth mix will include the 10%, 30% and 50% of shredded scrap by volume, respectively. Assuming the bulk density of shredded scrap tires is estimated to be 500 kg/m³ while that for subgrade soils is about 1800 kg/m³. The mass of the shredded tires and soils are listed in Table 1.

For quantifying the environmental implications of the use of recycled tire in embankment, carbon footprint or GHG emissions and embodied energy consumption indicators have been considered in this research as the construction industries are responsible for almost 39% of global annual GHG emissions and approximately 36% of the total energy consumption [14].

Life Cycle Assessment (LCA) is an environmental management tool that has been extensively used to estimate carbon footprints and embodied energy consumption of construction sector.

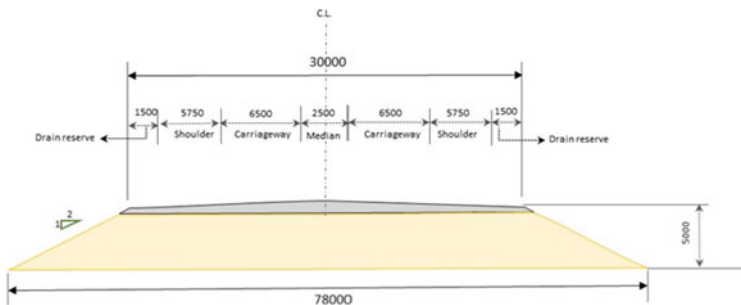


Fig. 1. Typical fill embankment cross section

Table 1. Mixture of suitable material and shredded scrap tires by volume

Mix number	Mix types	Quantity in kg/m ³	
		Suitable materials (SM) kg	Shredded scrap tires (SST) kg
M1	100 SM	1800	0
M2	90 SM + 10 ST	1620	50
M3	70 SM + 30 ST	1260	150
M4	50 SM + 50 ST	900	250

4 Life Cycle Assessment

In this study, LCA analyses are based on some hypotheses in the following:

1. All activities have been considered to be happened in Miri, Sarawak, Malaysia.
2. The soil in the adjacent location is suitable for use of construction of embankment.
3. Excavation of the soil and transport to the construction site. The distance is within 40 km.
4. Recycled shredded tire plant is assumed to located at Bintulu. The materials were assumed to have been transported for 200 km to the construction site.
5. Mixture of shredded tire materials and soils are carried on site.
6. Placement and spreading of soil mixture on site.
7. Compaction of soil mixture on site.

In this study, the environmental impacts (in particular greenhouse gas emissions and energy use) of embankment in Miri, Malaysia were assessed using a LCA tool, following four steps of ISO14040-2006 guidelines [15]: goal and scope, life cycle inventory, impact assessment and interpretation. The life cycle of an embankment in this analysis includes pre-construction, transportation, and construction stages. The environmental impacts associated with the use, demolition of embankment and its end-of-life activities (i.e. disposal, recycling) were excluded from this analysis.

The goal is to compare the carbon footprint and embodied energy of embankments with and without the use of shredded recycle tire. The functional unit, which is a basis for developing a life cycle inventory, is 1 m³ of embankment.

Life cycle inventory (LCI) was developed to determine the amount of inputs in the form of energy and material for pre-construction, transportation and construction stages for both conventional and shredded recycled tire based embankments, respectively. Data was validated by performing mass and energy balance for the functional unit and is presented in Table 2.

The energy consumption for shedding tire was based on the Yu Xin waste tire recycling granule equipment [16]. The tire is first cut into 100 mm pieces and then these pieces are further shredded into 10–15 mm granular size. The equipment consumes 300 kWh to shred 300 kg of used tire. The energy consumption for the construction of 1 m³ of embankment was based on Trani et al. [17]. About 36.35 MJ of diesel

Table 2. Life cycle inventory for transportation of embankment materials

Mix number	Soil (kg)	Shredded scrap tires (SST) kg	Transportation		
			Soil (tkm)	Recycled tyre (tkm)	Total (tkm)
M1	1800	0	72	0	72
M2	1620	50	64.8	10	74.8
M3	1260	150	50.4	30	80.4
M4	900	250	36	50	86

energy is used in excavator, wheel loader, vibratory soil compactor and medium sized road truck for producing 1 m³ of embankment.

Soil is excavated 40 km away from the construction site. The car tire shredding factory was in Bintulu in Sarawak, which is about 200 km away from Miri. The unit for transportation is tonne kilometre travelled or tkm. For example, the transportation of 1800 kg of soil from a distance of 40 km is 72 tkm. A truck of more than 16t was considered for transporting construction materials in this LCA.

The input data from LCI were entered into Simapro 9.4 LCA software [18]. Each input was linked to relevant emission database in the LCA software. For majority of the LCI input data, local LCA library databases were used to represent the Miri's situation. When the local database is absent in the software, a new library database was created by obtaining the information on material and energy from local industries or local reports and product datasheets. Sarawak electricity mix (i.e., hydro 85%, coal 6%, gas 7% and renewable energy 3% [19] was used to estimate the emission from the electricity use for used tire shredding. Since local emission databases are not available, eco-invent databases are used for emissions calculations.

Due to awareness of global warming, the main objective of this LCA study is to calculate the embodied energy consumption (MJ) and carbon footprint (kg of CO₂-e). The embodied energy consumption was calculated using cumulative energy demand method in the Simapro software, while IPCC 2013 GWP 100a V1.02 method which is also available in the software was used to calculate the carbon footprints of the embankment. Carbon footprint values are expressed over 20, 100 and 500-year time horizons to assist policy makers for making climate change decisions [20]. 100-year horizon for converting GHG emissions to CO₂ e- was used in this LCA, because this period has usually been considered as the reference for climate change policy [21]. Process flow charts were developed using a Simapro 9.4 LCA software to determine the breakdown of the GHG emissions and embodied energy consumption of all processes during the life cycle stages of 1 m³ of embankment. It also helps to identify the 'hotspot' causing the highest GHG emissions and energy consumption.

Some other impact categories such as toxicity and resource consumption are also important but they are outside the scope of this LCA hence the outcome of this study are only to facilitate decision making in developing strategies for lowering carbon footprint and embodied energy consumption in embankment construction works.

Finally, the results obtained from the Simapro 9.4 LCA software were used for the interpretation of the results.

The inputs used during the life cycle of embankment have been converted GHG emissions (e.g. CO₂, CH₄, N₂O), which were then converted to carbon dioxide-equivalent (CO₂ e-) using Eq. (1) to calculate carbon footprint (CFP) [22].

$$CFP(CO_2e-) = \sum_{i=1}^{i=N} \sum_{j=1}^{j=M} (I_i \times EF_{ij} \times F_j) \quad (1)$$

where, 'I' is the amount of an input

i: 1, 2, ..., N; type of inputs (e.g. cement, aggregate, sand, electricity etc.)

EF_{ij}: Emission factor; amount of emission of GHG type 'j' per kg of input of type 'i'.

F_j: F₁, F₂, ..., F_M; characterisation factors of GHGs (e.g. 1 for CO₂, 28 for CH₄, 265 for N₂O)

The cumulative energy demand (CED) method in the SimaPro software [18] was used. All inputs in the LCI have been multiplied by the corresponding energy consumption values (EE_i) by using Eq. (2) to determine the embodied energy consumption of embankments (EEC) [22].

$$EEC = \sum_{i=1}^{i=N} (I_i \times EE_i) \quad (2)$$

There are uncertainties associated with the quality of data (i.e. inputs and output, and the emission factors) that is used to determine carbon footprint and embodied energy consumption of concrete mixes. In this analysis, new databases for Miri situation were developed and therefore, it is crucial to ensure that these databases do not affect the quality of LCA results. Monte Carlo Simulation (MCS) was carried out for each of these data points to estimate these uncertainties. In addition, the prediction for the influence that a variable has on CFP and EEC of embankment mixes was estimated [23]. The simulation in an iterative process utilising an input value from a probability function to produce a distribution of all possible values for 1000 iterations and at 95% confidence level [24].

5 Results and Discussion

The study calculated cumulative energy demand or embodied energy in GJ (Table 3) and GHG emissions in tonne kg CO₂ e- for embankment constructed with and without recycled shredded tires.

Table 3 shows the total embodied energy of M1, M2, M3 and M4 mixes as 832, 1,004, 1,366 and 1,721 MJ respectively. The data indicates that the embodied energy consumption increased by 21%, 64% and 107%, respectively due to replacement of

Table 3. Carbon footprint and embodied energy consumption of M1-M4 mixes

Mix number	Soil	Shredded scrap tyre	Construction	Transport, lorry U	Total
Cumulative energy demand (MJ)					
M1	627	160	45	0	832
M2	556	234	45	169	1,004
M3	438	701	182	45	1,366
M4	313	1169	194	45	1,721
GWP (kg CO ₂ eq.)					
M1	42	10	3	0	55
M2	37	5	3	10	56
M3	29	16	11	3	59
M4	21	27	12	3	62

M1 to M2, M3 and M4. This is because of the fact that the shredding of tires is an energy intensive process. In the case of M4, tire alone accounted for the 68% of the embodied energy consumption (Fig. 2).

The values carbon footprints of M2, M3 and M4 are not as high as the embodied energy consumption. This is because 88% of the electricity which is considered for operating the waste tire recycling granule equipment in Bintulu Sarawak is generated from hydropower plants in Sarawak. While the carbon footprints of M2, M3 and M4 are 2%, 8% and 14% higher than M1, respectively (Table 3). In the case of M4, embodied energy consumption of scrapped tyre accounted for 68% of the total embodied energy consumption but carbon footprint accounted of that for 43% of the total carbon footprint (Fig. 2). At this stage, the only feasible way to make the recycled tyre-based embankment environmentally friendly is to improve the efficiency of the waste tire recycling granule equipment.

Research [25] showed that use of industrial by-products such as recycle concrete pavements, the energy consumption is higher than using the natural aggregates, which is due to high energy consumption to produce RCP. Other research [26] also shows that energy consumption of the using alternative construction material such as fly ash, crushed concrete waste and blast furnace is mainly during the pre-handling phase followed by transportation stage then the construction stage. This shows similar trend of energy consumption of pre-handling of this study.

Since the aforementioned LCA outputs were based on the newly created emission databases to represent Miri situation, an uncertainty analysis of these LCA results was carried out using MCS for 1000 iterations and 95% confidence level. Since both embodied energy consumption and carbon footprint present the same type of trends, MCS was carried out for carbon footprint values to assess the uncertainties associated with the quality of the inventory data to statistically validate the LCA outputs of the current analysis. Interestingly, there is no significant difference between calculated values and mean values, which confirms the statistical validity of LCA outputs as

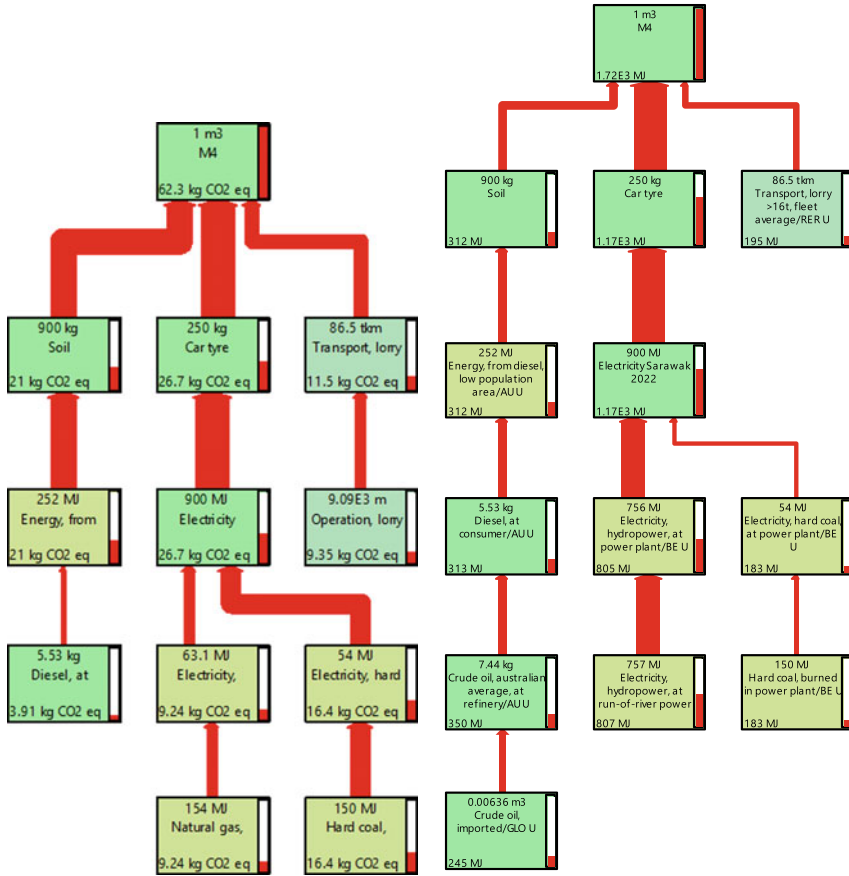


Fig. 2. Flow networks of M2 mixes

the CVs are around 5.5% for all these embankment mixes, which is statistically acceptable [27].

6 Conclusions

While the use of car tires in embankment construction could divert wastes from the landfill, there appears to be no carbon and energy saving benefits for most of the soil and recycled tire mixes due to the huge amount of energy used in shredding used tires. All mixes using recycled tires' both carbon footprint and the embodied energy consumption increased for replacing the conventional embankment using 100% soil. This research suggests that a significant energy efficiency improvement of the waste tire recycling equipment is needed to reduce both GHG emissions and

energy consumption. Although electricity that is generated in Sarawak is very clean compared to other states of Malaysia and Asian nations due to having hydropower contributing 88% to the Sarawak electricity, waste tire recycling plant is not going the take advantage of this clean energy sources due the higher amount of energy consumed by the recycling plant.

References

1. United Nations Conference on Trade and Development (UNCTAD) (1996) A statistical review of international trade in tyre and tyre-related rubber waste for the period 1990–1994. Papers on Commodity Resources, Trade and Environment No. 1. Geneva, UNCTAD
2. Sultan M et al (2022) Citation: critical materials determination as a complement to the product recycling desirability model for sustainability in Malaysia. *Appl Sci* 12:3456. <https://doi.org/10.3390/app12073456>
3. Ahmed I (1993) Laboratory Study on Properties of Rubber-Soils. Publication FHWA/IN/JHRP-93/04. Joint Highway Research Project, Indiana Department of Transportation and Purdue University, West Lafayette, Indiana
4. Masad E, Taha R, Ho C, Papagiannakis T (1996) Engineering properties of tire/soil mixtures as a lightweight fill material. *Geotech Test J* 19(3):297–304. <https://doi.org/10.1520/gtj10355j>
5. Foose GJ, Benson CH, Bosscher PJ (1996) Sand reinforced with shredded waste tires. *J Geotech Eng* 122(9):760–767. [https://doi.org/10.1061/\(asce\)0733-9410\(1996\)122:9\(760\)](https://doi.org/10.1061/(asce)0733-9410(1996)122:9(760))
6. ASTM D6270-98 (1998) Standard Practice for Use of Scrap Tires in Civil Engineering Applications. American Society for Testing and Materials
7. U.S. Tire Manufacturers Association: Sustainable Scrap Tire Markets. <https://www.ustires.org/sustainable-scrap-tire-markets>
8. Akbarimehr D, Eslami A, Aflaki E (2020) Geotechnical behaviour of clay soil mixed with rubber waste. *J Clean Prod* 271:122632. <https://doi.org/10.1016/j.jclepro.2020.122632>
9. Vinod JS, Sheikh MN, Mashiri S, Mastello D (2021) Laboratory investigations on the shear behaviour of sand-tyre derived aggregate mixtures. *Geotech Eng* 52(3):29–32
10. Bosscher PJ, Edil TB, Kuraoka S (1997) Design of highway embankments using tire chips. *J Geotech Geoenviron Eng* 123(4):295–304
11. Yoon S, Prezzi M, Siddiki NZ, Kim B (2006) Construction of a test embankment using a sand-tire shred mixture as fill material. *Waste Manage* 26(9):1033–1044. <https://doi.org/10.1016/j.wasman.2005.10.009>
12. Liu L, Cai G, Zhang J, Liu X, Liu K (2020) Evaluation of engineering properties and environmental effect of recycled waste tire-sand/soil in geotechnical engineering: a compressive review. *Renew Sustain Energy Rev* 126:109831. <https://doi.org/10.1016/j.rser.2020.109831>
13. Public Works Department Malaysia (1986) A Guide on Geometric Design of Roads
14. IEA (2019) Global Status Report for Buildings and Construction
15. ISO 14040 (2006) Environmental Management - Life Cycle Assessment - Principles and Framework. ISO, Geneva
16. Yuxi Waste Tires Recycling (2022) Waste tires crushing and separating line
17. Trani ML, Bossi B, Gangoles M, Casals M (2016) Predicting fuel energy consumption during earthworks. *J Clean Prod* 112:3798–3809. <https://doi.org/10.1016/j.jclepro.2015.08.027>
18. Pré Consultants (2021) SimaPro Database. The Netherlands
19. Pacudan R (2016) Road Map for Power Market Integration in the Brunei-Indonesia-Malaysia-Philippines (BIMP) Region
20. IPCC (2013) Climate Change 2013: the Physical Science Basis, Contribution of Working Group I to the Fifth Assessment Report (AR5) of the Intergovernmental Panel on Climate Change (IPCC)

21. Fearnside PM (2002) Why A 100-Year Time Horizon Should Be Used For Global Warming Mitigation Calculations
22. Fatimah YA, Biswas WK (2016) Remanufacturing as a means for achieving low-carbon SMEs in Indonesia. *Clean Technol Environ Policy* 18(8):2363–2379. <https://doi.org/10.1007/s10098-016-1148-5>
23. Clavreul J, Guyonnet D, Christensen TH (2012) Quantifying uncertainty in LCA-modelling of waste management systems. *Waste Manage* 32(12):2482–2495. <https://doi.org/10.1016/j.wasman.2012.07.008>
24. Goedkoop M, Oele M, Leijting J, Ponsioen T, Meijer E (2013) Introduction to LCA with SimaPro. PRé, The Netherlands
25. Chowdhury R, Apul D, Fry T (2010) A life cycle based environmental impacts assessment of construction materials used in road construction. *Resour Conserv Recycl* 54(4):250–255. <https://doi.org/10.1016/j.resconrec.2009.08.007>
26. Djadouni H, Trouzine H, Correia AG, da Silva Miranda TF (2019) Life cycle assessment of retaining wall backfilled with shredded tires. *Int J Life Cycle Assess* 24(3):581–589. <https://doi.org/10.1007/s11367-018-1475-3>
27. Mohammed F, Biswas WK, Yao H, Tadé M (2016) Identification of an environmentally friendly symbiotic process for the reuse of industrial byproduct – an LCA perspective. *J Clean Prod* 112:3376–3387. <https://doi.org/10.1016/J.JCLEPRO.2015.09.104>

Effect of Fire on High-Strength Fly-Ash-Based Geopolymer Concrete



Siti Nooriza Abd Razak, Nasir Shafiq, Laurent Guillaumat,
Vicky Kumar Lohana, Syed Ahmad Farhan,
and Farah Amira Ahmad Shafee

Abstract Fire resistance of geopolymer concrete is superior to that of ordinary Portland cement (OPC)-based concrete. However, vulnerability of geopolymer concrete when exposed to real fire events is an issue. In view of the issue, a comparative evaluation of the fire resistances of OPC-based and geopolymer concrete was performed. OPC-based and fly-ash (FA)-based geopolymer concrete specimens were prepared with a standard strength grade of 60 MPa. A laboratory-scale simulation of real fire events was conducted by exposing the specimens to fire at 200, 500 and 1000 °C for 2 h. Fire resistances of the specimens were evaluated by performing tests to determine mass loss and residual compressive strength and thermogravimetric analyses (TGA) before and after exposure to fire. Due to water evaporation, the OPC- based concrete incurred mass losses of 2.41, 4.45, and 7.7% when exposed to fire at 200, 500, and 1000 °C, respectively. Similarly, when exposed to fire at 200, 500, and 1000 °C,

S. N. A. Razak · N. Shafiq (✉) · V. K. Lohana · F. A. A. Shafee
Department of Civil and Environmental Engineering, Universiti Teknologi PETRONAS, Seri
Iskandar, Malaysia
e-mail: nasirshafiq@utp.edu.my

S. N. A. Razak
e-mail: siti_0008995@utp.edu.my

V. K. Lohana
e-mail: vicky_19000193@utp.edu.my

F. A. A. Shafee
e-mail: farah_17007585@utp.edu.my

S. N. A. Razak · L. Guillaumat
Laboratoire Angevin de Mécanique, Procédés et Innovation, École Nationale Supérieure d'Arts et
Métiers, 49035 Angers, France
e-mail: laurent.guillaumat@ensam.eu

N. Shafiq · S. A. Farhan
Institute of Self-Sustainable Building for Smart Living, Universiti Teknologi PETRONAS, 32610
Seri Iskandar, Malaysia
e-mail: syed.af_g02626@utp.edu.my

F. A. A. Shafee
School of Natural and Built Environment, University of South Australia, Adelaide 5001, Australia

the FA-based concrete had minor mass losses of 1.4, 1.96, and 2.59%, respectively. According to the TGA analysis, the weight loss of geopolymer concrete was slightly higher than that of OPC up to 400 °C due to evaporation of water from the sample. At higher temperatures, the total weight loss of OPC is 6.1% whereas geopolymer is 4.5%, indicating that geopolymer concrete was more chemically stable than OPC following exposure to high temperature fire.

Keywords fire resistance · fly ash · geopolymer concrete · mass loss · residual compressive strength · thermogravimetric analysis

1 Introduction

Green materials for civil engineering are still being researched and developed around the world, with a special focus on replacing partially or fully of those based on Ordinary Portland Cement (OPC) [1, 2]. As a result, it is crucial to improve both traditional natural resource extraction technologies and OPC-based concrete production technologies. The goal of these adjustments is to turn current cement plants into green concrete manufacturing facilities, such as geopolymers [3].

Geopolymers are environmentally friendly materials produced by the geopolymerisation chemical reaction, which happens when an aluminosilicate source is mixed with an aqueous solution. Geopolymer demonstrated exceptional durability as it can resist acid, sulphate, alkali-silica reaction, and fire as compared to the primary competitor OPC-based material. Moreover, geopolymer is more stable chemically and its production reduced 80% of CO₂ emission to the environment. As a result, geopolymer can be utilized as a green construction material with significant potential for sustainable development and as infill because of its superior durability and fire resistance [4].

Geopolymer which possess almost the same characteristic of OPC-based material, however, the vulnerability of its properties at certain condition remained to be explored such as resistance to fire at high temperature. Geopolymer known to be porous material and have high distributed pore network [Geo & OPC simulated fire]. Fly ash (FA) is abundantly generated all over the world and is rich in alumina and silica, with a low amount of calcium oxide, is often used in concrete as supplementary material. FA is cheap and easy to obtain than other raw material under the same cementitious material and using it brings environmental benefits by reducing resource, energy consumption and carbon dioxide emissions [5].

In modern days, it is vital to assess the fire endurance of the construction material to ensure the safety of life and property. The extent of cracking and spalling of a material after exposure to high temperature gives indication of fire endurance of the material.

Geopolymer materials have been developed as heat-resistant cement and concrete [6–8] that can be applied as fire-proof panels, refractory materials [9] and thermal insulators [10–12]. Application of geopolymer concrete as fire-resistant building materials entails investigating its micro-scale thermal performances, which are micro-structural or chemical stability, resistance to deformation, strength properties, and resistance to spalling when exposed to high temperatures [13].

Rickard et al. [14] investigated five different FA-based geopolymers at different Si/Al ratios of 2.0, 2.5 and 3.0 and found that reducing the amount of aluminate or silicate added by the activator solution improved the strength or retention after thermal exposure. Amorphous fly ash geopolymer with a reduced Si/Al ratio displayed excellent early compressive strength, which quickly deteriorated after the thermal exposure. When the geopolymers were fired, the hydrated phases that had been found in the 'as cured' geopolymers were eliminated. After burning, sodium-based feldspars were found in all samples. All the burnt geopolymers contained nepheline (NaAlSiO_4). After being exposed to fire, the peak intensity of the mullite and quartz phases decreased in all geopolymers. When geopolymers made from FA with a high Si/Al ratio in the glass were exposed to 1000 °C, they showed compressive strength gains and great thermal stability. Hosan et al. [15] discovered that class F FA-based geopolymers synthesized with potassium-based activators are more stable at high temperatures than their sodium-based equivalents, with higher residual compressive strengths, reduced mass losses, lower volumetric shrinkages, and lesser cracking damages. Razak et al. [16] discovered that, at the same temperature and time of fire exposure, FA-based geopolymer concrete suffered minor losses in mass and compressive strength in comparison to OPC-based concrete. The residual compressive strength of the FA-based concrete increased from 13 to 45% after being exposed to fire at 500 °C, but the OPC-based concrete was unable to maintain its compressive strength. SEM images revealed that the matrix of FA-based concrete after being exposed to fire was denser than that of the OPC-based concrete. Spectra of the FA-based concrete, which were generated by performing Fourier-transform infrared spectroscopy, revealed a small shift in wavelength. Findings of mechanical and microstructure analyses indicate that the FA-based concrete has a significantly high thermal stability and fire resistance, making it ideal for high thermal infrastructure applications.

A comparative evaluation of the fire resistances of OPC-based and geopolymer concrete was performed. OPC- and FA-based concrete specimens were prepared with a standard strength grade of 60 MPa. A laboratory-scale simulation of real fire events was conducted by exposing the specimens to fire at 200, 500 and 1000 °C for 2 h. Fire resistances of the specimens were evaluated by performing tests to determine mass loss and residual compressive strength and thermogravimetric analyses (TGA), before and after exposure to fire.

Table 1 Chemical compositions of ordinary Portland cement (OPC) and fly ash (FA)

Oxides (%)	SiO ₂	Al ₂ O ₃	Fe ₂ O ₃	CaO	SO ₃	K ₂ O	TiO ₂	SrO	P ₂ O ₅
OPC	20.06	4.93	2.86	63.94	3.67	–	–	–	–
FA	75.64	12.04	3.36	2.35	1.5	2.02	1.20	0.1	1.7

2 Materials and Methods

2.1 Materials

The OPC and FA Class F (ASTM C618 [17]) used as the raw material for the cement and geopolymer concrete specimens' production respectively. OPC was obtained from a local supplier in Angers, France. Fly ash was obtained from YTL Cement Marketing (Kuala Lumpur, Malaysia). Chemical compositions of OPC and FA, as shown in Table 1, were determined using an X-ray fluorescence spectrometer of model S8 TIGER, which was manufactured by Bruker AXS (Karlsruhe, Germany).

Coarse and fine aggregates were obtained from Les Quarry Site in Angers, France. Coarse aggregates of the size range 5–20 mm granulometric fraction were employed. In order to prepare the aggregates to be in a saturated surface-dry condition, they were washed to remove any dirt and dust, and then dried. Washed river sand of the size range of less than 5 mm granulometric fraction with a fineness modulus of 2.6 was employed as the fine aggregates. The sand was cleaned to remove any dirt and clay. Tap water was employed to prepare the OPC-based concrete, while sodium hydroxide and sodium silicate were employed to prepare the FA-based concrete.

Standard grade sodium silicate was prepared with a SiO₂/Na₂O weight ratio of 2.5 and a density of 1.39 g/mL at 25 °C. The sodium hydroxide was employed at the concentration of 10 M. Prior to preparing the specimens, the sodium hydroxide solution was prepared by dissolving sodium hydroxide pellets in distilled water for 24 h. 40 g of sodium hydroxide was dissolved in 1 L of water to achieve a 1 M concentration of sodium hydroxide. As a result, 400 g of sodium hydroxide pellets were dissolved in 1 L of water to prepare sodium hydroxide at the concentration of 10 M.

2.2 Casting and Curing

Table 2 shows the mix proportions of OPC- and FA-based concrete specimens. BS standard EN 206 was adopted to design the mixture for OPC concrete and Response surface methodology (RSM) software was used by applying certain parameters to design the FA-based geopolymer concrete. The concrete mixture was design to achieve standard high strength grade concrete specimen. All specimens were prepared in a VMI mixer. For mixing of the OPC-based specimens, fine and coarse

Table 2 Mix proportions of OPC- and FA-based concrete specimens

OPC-based concrete						
Mix	OPC (kg/m ³)	Water (kg/m ³)	Sand (kg/m ³)	Coarse aggregates (kg/m ³)		Superplasticizer (kg/m ³)
OPC	600	190	498	1162		4
FA-based concrete						
Mix	FA (kg/m ³)	Coarse aggregates (kg/m ³)	Sand (kg/m ³)	Sodium hydroxide (kg/m ³)	Sodium silicate (kg/m ³)	Water (kg/m ³)
GEO	460	1050	700	46	138	46

aggregates were mixed for 30 s. Half of the water was added and mixed for 1 min. Before adding OPC, the mixing was stopped for 8 min to allow the aggregates to absorb some water. Then, OPC was added, and mixing was continued for a minute until the mixture became homogeneous without segregation. For mixing of the FA-based specimens, the aggregates were mixed for 30 s prior to adding FA. Then, FA was added and mixed for a minute. Subsequently, an alkaline solution that contains sodium hydroxide and sodium silicate were added and mixed for 3 min until the mixture became homogeneous without segregation. The fresh concrete mixtures were casted into standard 100-mm stainless steel cube moulds and compacted with a vibrator. All specimens were cured at room temperature for 24 h prior to de-molding. The specimens were de-molded after 24 h and cured at room temperature until the day of testing.

2.3 Experimental Work

A total of twenty-four standard-sized 100-mm cube specimens of OPC- and FA-based concrete were prepared. A laboratory-scale fire test setup based on natural gas was developed to perform fire tests to investigate the fire resistance of the concrete specimens with exposure to fire at 200, 500 and 1000 °C for 2 hours. Prior to conducting the tests, the specimens were weighed to ensure that their density was consistent within the range of 2.3–2.5 kg per specimen. Fig. 1 shows the apparatus for the fire test setup. The distance between the fire torch and specimen was 200 mm. A K-type thermocouple was glued on the fire-exposed surface of the specimen. The thermocouple was connected to a data logger to record the temperature of the fire and ensure that the temperature was consistent for the experiment throughout the testing duration.

After cooling, visual observations were carried out to detect any cracking and spalling that were caused by the fire. Mass losses were determined by weighing the specimens prior to and after being exposed to fire. Compressive strength tests were

Fig. 1 Laboratory-scale fire test setup



performed in accordance with the method in EN 12390-4 [18] using a compressive testing machine of model RP 3000 TCT that was manufactured by 3R S.A.S (Montauban, France) to determine the residual compressive strength. An average of three specimens (3 OPC concrete specimens and 3 FA-based concrete specimens) were tested to ensure the consistency of the strength performance under compression.

3 Results and Discussion

3.1 Mass Loss and Residual Compressive Strength

Mass loss and residual compressive strength of the concrete specimens were determined before and after fire exposure. Fig. 2 displays the mass loss and residual compressive strength of OPC- and FA-based specimens at 200, 500, and 1000 °C. The mass loss increased as temperature was increased, while residual compressive strength reduced as temperature was increased. The main reason for the losses of mass and strength of the specimen is dehydration of water. Other than that, the losses also contribute from the cracks opening and spalling due to thermal stress differential within the concrete matrix. Subsequent to that, the compressive strength reduction also contributes from the cracks and spalling of specimens.

OPC control concrete specimen suffered high loss of mass and compressive strength after being exposed to fire as compared to FA-based geopolymer concrete specimen. OPC concrete suffered 2.41, 4.45 and 7.72% for exposure at 200, 500 and 1000 °C respectively as a result from water evaporation process during the

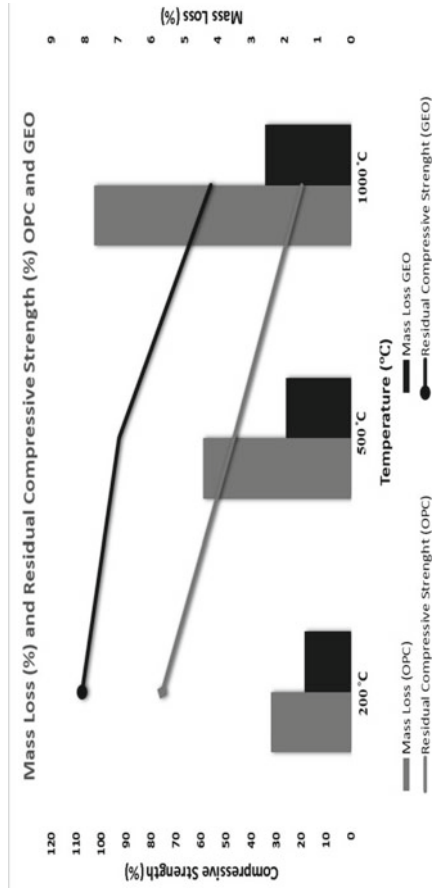


Fig. 2 Mass loss (%) and residual compressive strength (%) OPC and GEO

fire exposure. In contrast, FA-based geopolymer concrete suffered minor mass loss which is 1.4, 1.96 and 2.59% for exposure to 200, 500 and 1000 °C respectively. In geopolymer system, water only contribute to provide workability because the alkali is used as activator for binding the fly ash during geopolymerization reaction, hence, it significantly showed that geopolymer only suffered less dehydration from fire exposure.

It can be seen in the graph that OPC concrete specimen suffered high reduction of compressive strength after being exposed to fire at 200, 500 and 1000 °C. Contradict to that, FA-based geopolymer concrete specimen increased the compressive strength by 7.91% at 200 °C temperature exposure and gradually reduced the strength when further exposed to high temperature of 500 and 1000 °C. FA-based geopolymer concrete managed to maintained about 56.2% of strength when exposed to fire at 1000 °C compared to OPC which only managed to sustain 19.8% of residual strength at the same exposure level. High temperature caused decomposition of calcium silicates compound in OPC that contributes to the strength. At 200 °C exposure, OPC concrete remained 75.79% of strength while FA-based geopolymer concrete increased the strength to 107.91%. The increment of compressive strength is due to further geopolymerization reaction when exposed to fire, which is known as one alternative for geopolymer to enhance its strength when exposed to adequate heat. When exposed to 500 °C temperature, OPC concrete suffered more than 53% reduction of compressive strength and remained 46.93% of strength after exposure to fire, while FA-based geopolymer concrete remained 93.02% of compressive strength for the same level of exposure.

Exposure to fire leads to reduction in mass and compressive strength of concrete as fire is one of the dangerous elements that can degrade the service capability of material. From the graph, OPC concrete does not have adequate matrix integrity and stability to sustained high temperature while vice versa for FA-based geopolymer concrete where the strength increased at 200 °C and gradually suffered minor strength reduction at 500 and 1000 °C. This indicates that FA-based geopolymer concrete possess good matrix integrity and stability at high temperature exposure.

3.2 TGA Analysis for High Strength Concrete

TGA analysis was used in this study to analyze the thermal behavior of fly ash-based geopolymer concrete with the comparison of OPC. According to the TGA plot (Fig. 3), up to 400 °C, the weight loss of geopolymer concrete was slightly higher than that of OPC because evaporation of water took place from the sample. Above 400 °C, the weight loss of OPC samples is significant due to the rapid reduction of water and dehydration of C-S-H in the concrete. In addition, decomposition of calcium carbonate and portlandite was observed from 650 °C, which resulted in a sharp decrease in strength. Meanwhile, the geopolymer sample also experienced sluggish weight loss, but the weight loss was highest at temperatures above 600 °C due to dehydration of C-A-S-H in the geopolymer matrix. The dehydration of

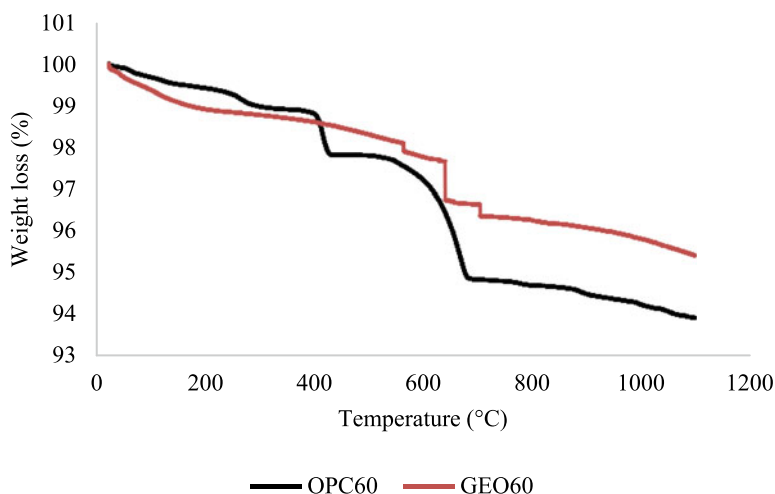


Fig. 3 TGA analysis of OPC and GEO

C-A-S-H causes a decrease in the strength of the geopolymer concrete. At higher temperature, the total weight loss of OPC is 6.1% while geopolymer is at 4.5% indicates that geopolymer concrete was chemically stable than OPC after exposure to high temperature fire.

4 Conclusion

Results revealed that the fire resistance of FA-based concrete is significantly higher as compared to OPC-based concrete. Specimens were exposed to fire at 200, 500 and 1000 °C to simulate real fire events. Mass losses of the OPC-based concrete were 2.41, 4.45 and 7.72 %, while those of the FA-based geopolymer concrete were 11.4, 1.96 and 2.59 %, after being exposed to fire at 200, 500 and 1000 °C, respectively, due to the dehydration of free water within the concrete. As a result, the FA-based concrete demonstrated a higher level of fire resistance when compared to the OPC-based concrete. Results on residual compressive strength reveal that the FA-based concrete demonstrated high stability and fire resistance. At 200 °C exposure, FA-based concrete demonstrated an increment in compressive strength by 7.91 % due to further geopolymerization reaction during firing. 56.2% of residual compressive strength was maintained for FA-based geopolymer concrete after exposure to 1000°C while OPC concrete managed to sustain 19.8% of residual strength after fire exposure as a result from complete dehydration. The weight loss of geopolymer concrete was slightly higher than that of OPC up to 400°C due to evaporation of water from the sample according to the TGA result. At higher temperatures, the total weight loss of

OPC is 6.1% whereas geopolymer is 4.5%, indicating that geopolymer concrete was more chemically stable than OPC following exposure to high temperature fire.

Acknowledgements The authors gratefully acknowledge École Nationale Supérieure d'Arts et Métiers, France and Universiti Teknologi PETRONAS, Malaysia for providing laboratory facilities and technical assistance.

References

1. Habert G, Ouellet-Plamondon C (2016) Recent update on the environmental impact of geopolymers. *RILEM Tech Lett* 1:17
2. Krishna RS, Mishra J, Zribi M, Adeniyi F, Saha S, Baklouti S, Shaikh FUA, Gökçe HS (2021) A review on developments of environmentally friendly geopolymer technology. *Materialia* 20:101212
3. Yahya Z, Abdullah MMAB, Mohd Ramli N, Burduhos-Nergis DD, Abd Razak R (2018) Influence of Kaolin in fly ash based geopolymer concrete: destructive and non-destructive testing. *IOP Conf Ser Mater Sci Eng* 374:012068
4. Duxson P, Fernández-Jiménez A, Provis JL, Lukey GC, Palomo A, Van Deventer JSJ (2007) Geopolymer technology: the current state of the art. *J Mater Sci* 42:2917–2933
5. Kong DLY, Sanjayan JG, Sagoe-Crentsil K (2007) Comparative performance of geopolymers made with metakaolin and fly ash after exposure to elevated temperatures. *Cem Concr Res* 37:1583–1589
6. Davidovits J (1991) Geopolymers: inorganic polymeric new materials. *J Therm Anal* 37:1633–1656
7. Davidovits J (1999) Fireproof geopolymeric cements. In *Proceedings of the 2nd International Conference Geopolymere*, Geopolymer Institute, Saint-Quentin, France, pp 165–169
8. Messina F, Ferone C, Colangelo F, Roviello G, Cioffi R (2018) Alkali activated waste fly ash as sustainable composite: influence of curing and pozzolanic admixtures on the early-age physico-mechanical properties and residual strength after exposure at elevated temperature. *Compos Part B Eng* 132:161–169
9. Perera DS, Trautman RL (2005) Geopolymers with the potential for use as refractory castables. *Adv Technol Mater Mater Process* 7:187–190
10. Rickard WDA, Vickers L, van Riessen A (2013) Performance of fibre reinforced, low density metakaolin geopolymers under simulated fire conditions. *Appl Clay Sci* 73:71–77
11. Rickard WDA, van Riessen A (2014) Performance of solid and cellular structured fly ash geopolymers exposed to a simulated fire. *Cem Concr Compos* 48:75–82
12. He J, Zhang J, Yu Y, Zhang G (2012) The strength and microstructure of two geopolymers derived from metakaolin and red mud-fly ash admixture: a comparative study. *Constr Build Mater* 30:80–91
13. Amran M, Huang SS, Debbarma S, Rashid RS (2022) Fire resistance of geopolymer concrete: a critical review. *Constr Build Mater* 324:126722
14. Rickard WDA, Temuujin J, van-Riessen A (2012) Thermal analysis of geopolymer pastes synthesized from five fly ashes of variable compositions. *J Non Cryst Solids* 358:1830–1839
15. Hosan A, Haque S, Shaikh F (2016) Compressive behaviour of sodium and potassium activators synthesized fly ash geopolymer at elevated temperatures: a comparative study. *J. Build. Eng.* 8:123–130
16. Razak SNA, Shafiq N, Guillaumat L, Farhan SA, Lohana VK (2022) Fire-exposed fly-ash-based geopolymer concrete: effects of burning temperature on mechanical and microstructural properties. *Materials* 15:1884

17. Suraneni P, Burris L, Shearer CR, Hooton RD (2021) ASTM C618 fly ash specification: comparison with other specifications, shortcomings, and solutions. *ACI Mater J* 118:157–167
18. European Standard (2019) Testing Hardened Concrete - Part 4: Compressive Strength - Specification for Testing Machines, EN 12390-4

Study on Correlation Among Roof Area, Reservoir Volume and Domestic Water Availability from Rainwater Harvesting in East Part of Surabaya



Umboro Lasminto, Satria Damarnegara, Bernadeta Elie, Rayhan Airlangga, Dina Permatasari, and Javier Aqilla

Abstract This research investigates the application of rainwater harvesting system as clean water source alternative in East Surabaya. The rainwater harvesting system performance is simulated to obtain the water availability for typical residential lot size in the study area. The water demand in this study is assumed as three scenarios. Reservoir volume is calculated based on available area for typical lot types in Indonesia. Daily and monthly rainfall data is used to simulate the rainwater harvesting system performance and to obtain the correlation between roof area, reservoir volume and water availability. Simulation results show that 90% water availability is achieved by the system for lower water demand of 20 l/person/day. The reservoir volume needed to hold water in annual, monthly, and daily simulations, respectively, is 15, 12 and 10.5 m³. The correlation between roof area and reservoir volume with water availability is also developed. The ratio between the volume of the reservoir used to hold water and the total water demand for one year is 34–51%. Even though the rainwater harvesting system could give a 90% water availability, there will be a deficit of water in dry season. Therefore, a large reservoir is needed to fulfil the water requirement in the dry season.

Keywords Rainwater Harvesting · Surabaya · Reservoir · Domestic · Mainstay Rainfall

U. Lasminto (✉) · S. Damarnegara · B. Elie · R. Airlangga · D. Permatasari
Department of Civil Engineering, Institut Teknologi Sepuluh Nopember, Kampus ITS, Sukolilo,
Surabaya 60111, Indonesia
e-mail: umboro@ce.its.ac.id

J. Aqilla
Department of Environmental Engineering, Institut Teknologi Sepuluh Nopember, Kampus ITS,
Sukolilo, Surabaya 60111, Indonesia

1 Introduction

Clean water availability is one main problem in the world. Clean water supply cannot keep up with its demand and lead to water scarcity. As a global problem, Indonesia is prone to water scarcity.

Data from Central Statistics Agency in 2018, only 74% of Indonesian population has access to clean water. The number is lower outside the metropolitan area. The critical water area is predicted to increase from 6% in 2000 to 9.6% in 2040 [1]. The main driven of water scarcity is the increasing demand due population growth. In the other hand, land use changes also impacted the water cycle. Land development usually increase surface water volume and decrease percolation for groundwater recharges. Indeed, freshwater volume for human consumption is very small compared to total volume of water on earth which make the problem more complex.

Rainwater harvesting (RWH) is one interesting option to mitigate water scarcity. Rainwater availability in rainy season is plentiful and can induce flood if not managed properly. RWH works by saving the excess rainwater in storage that can be used in case of water shortage. However, RWH application, especially in urban area, is limited by land availability. Several RWH application example are available in Africa, Australia, Europe, and America [2]. RWH performance in Australia is capable to reduce the potable water usage in range of 10 to 100% [3]. Another study in Queensland shows reduction of 31% in average for potable water usage [4]. A review about RWH in Malaysia [5] gives an overview of RWH application in tropical area. Indeed, a heavy rainfall in wet season is a potential source for RWH. The rainy day in Malaysia is around 138 days to 181 days per year which shows a great potential for RWH utilization. A local university hostel in Shah Alam, Malaysia could reduce treated water usage of 6500 m³ per year and economize up to RM 10,460 per year [6]. Several example of RWH system application are also found in Indonesia. Several RWH system is applied in Banda Aceh as source of clean water after the tsunami [7]. From three RWH system that installed, only one is found working well, even though the other two are not functioning because of non-technical issue. However, no quantified performance data is collected from these systems. Another study example in Denpasar investigates the RWH application for groundwater recharges [8]. In Semarang the RWH system is used as complementary water sources and found to be useful [9]. Indeed, to understand the RWH reliability in one specific site, investigation of its performance is needed.

In this paper, RWH system performance is analyzed in East Surabaya. RWH system parameter of roof area and reservoir volume is predicted using typical housing in the area. The roof area and reservoir requirement are calculated from available seasonal rainwater and domestic water usage. The water balance simulation is performed for several reservoir volume on annual, monthly, and daily basis. Similarly with roof area requirement. Each configuration reliability is assessed to understand its performance. The results of this study are expected to be a guide in determining the reservoir volume and roof area needed to meet domestic water needs from RWH system in East Surabaya.

2 The Material and Method

2.1 Rainwater Harvesting Concept

Rainwater harvesting is a technology for collecting rainwater obtained from building roofs, ground surfaces or roads to be used as a source of clean water [10]. Based on UNEP [11], there are several advantages in utilizing rainwater as an alternative source of clean water, including (1) the use of existing components such as roofs or gardens to minimize environmental impacts, (2) rainwater can be used as water reserves and reduce dependence on clean supply systems, and (3) rainwater harvesting is a simple technology so that it is easy to build according to needs. Rainwater harvesting is not only to fulfill some of the water but also to conserve water. There are 4 reasons rainwater harvesting is ecologically important for water conservation [12], namely:

1. Population development causes an increase in the need for water, increasing groundwater extraction. Excessive groundwater extraction will reduce groundwater reserves. Rainwater harvesting can reduce groundwater abstraction.
2. The rainy season and dry season greatly affect the fluctuation of water sources such as lakes, rivers, and underground water. Harvesting rainwater and storing it will help meet water needs in times of drought. Other water sources are usually located far from the home or community of users.
3. Availability of sufficient rainwater storage around the settlements will facilitate access to water sources so that it has a positive impact on health and strengthens the sense of ownership of users.
4. Rainwater quality is better than groundwater and surface water which have been polluted by industrial activities and human waste.

2.2 Rainwater Harvesting Components

The rainwater harvesting system consists of several components, namely the catchment area, conveyance system, filter, reservoir system, and pump [10].

- 1) *Catchment area*: a surface that serves to collect rainwater. The catchment area can collect more rainwater if it has a large enough area. The efficiency of the catchment area is determined based on the material used [13]. The material used is made of impermeable material. The catchment area material must also not contain toxins and materials that can reduce the quality of rainwater [11]. In general, catchment areas use anti-rust materials such as galvanized iron, aluminum, concrete, and fiberglass [14].
- 2) *Conveyance*: The drainage channel in the rainwater harvesting system consists of a collection channel or pipe that functions to drain rainwater from the catchment area to the reservoir system [15]. The collection channel must have the appropriate dimensions, slope, and installation so that it can accommodate maximum

water [10]. Indonesian standard for plumbing describes two types of drainage systems, namely gravity systems and pressurized systems. The gravity system is a drainage method that utilizes the force of gravity by adjusting the location and slope of the pipe. Meanwhile, the pressurized system uses a pump that works automatically to drain water [16]. Media that can be used as filters include silica sand, zeolite stone, activated carbon, and aquarium filter cotton [17].

- 3) *Filter*: Filtration is the process of separating solids and liquids. In the rainwater harvesting system, the filter functions to filter objects such as leaves, plastic, or twigs that flow with rainwater so that water quality is maintained [18].
- 4) *Reservoir*: The storage system (reservoir) is a component that functions to collect rainwater from the roof [19]. Reservoir based on its location consists of two types, namely reservoirs that are above ground and underground [18]. For storage with a small capacity, the reservoir can use bricks, rammed earth, or plastic sheets as the material. Reservoirs with larger capacities can utilize pottery, ferrocement, or polyethylene [20].
- 5) *Pump*: The pump is one of the components of the rainwater harvesting system that is needed to drain water if the rainwater storage area (reservoir) is located underground [18].

2.3 Clean Water Needs

Calculation of water needs is carried out using the number of occupants method based on the number of occupants and the number of average water usage requirements for each occupant according to the following equation.

$$B = D \times P \times T \quad (1)$$

Information:

B: total water requirement (liters)

D: water needs of one person in one day (liters/person/day)

P: number of occupants (person)

Q: period of use (days)

2.4 Calculation of Rainwater Harvesting

Rainwater harvesting depends on rainfall for its source. Therefore, the rainfall pattern analysis is important to understand its potential. The calculation of rainwater supply potential is performed to determine rainwater volume availability using equation as follows:

$$V = R \times A \times C \quad (2)$$

where:

V: volume of rainwater that can be accommodated (m^3)

R: rainfall (mm)

A: catchment area (m^2)

C: run-off coefficient

The run-off coefficient is determined based on the roof covering material.

2.5 Reservoir Capacity Calculation

Villarreal et al develop a computer model to quantify the potential of water saving from the rainwater collection scheme. In this study the performance model is assessed in terms of Water Saving Efficiency to determine the size of the storage [21]. Another study compared calculations using monthly and daily rain data to plan the tank size required for rainwater storage where it was found that calculations with monthly rain data resulted in an overestimated tank volume [22]. The detailed calculation of the need for rain harvesting water storage tanks was carried out by Santos et al. From the daily simulation results, it is found that the best saving ratio is 80% reliable [23]. A study conducted in 3 cities with different climatic conditions found that harvesting and storing rainwater made it possible to supply 75% of non-potable water demand [15].

Reservoir planning is carried out to determine the capacity of rainwater storage to meet daily water needs. Calculation of water availability in the reservoir according to the following equation:

$$I - O = \frac{dS}{dt} \quad (3)$$

Information

I: reservoir inflow (m^3 /time interval)

O: reservoir outflow (m^3 /time interval)

dS: change in reservoir capacity (m^3)

dt: time interval (day, month, or year)

2.6 Site Description

This research is conducted in East Surabaya especially in Sukolilo District. Land use in this area is dominated by residential area of 41%, conservation site of 39%, commercial area of 3%, public spaces of 11% and open spaces for the rest as described in land use map as seen in Fig. 1 [24]. The typical housing data is obtained from [25] Including land size, building size, number of restrooms, and number of occupants.

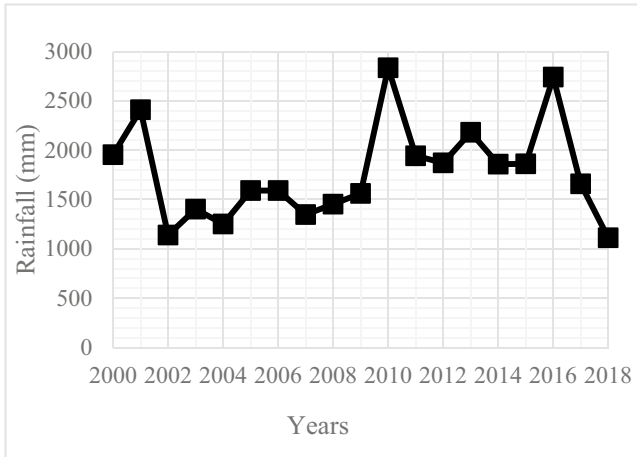


Fig. 1 Yearly rainfall data of Keputih Rainfall Station

The rainfall data is obtained from Keputih rainfall station for 18 years from 2000 to 2018.

2.7 Research Scenarios

Due to the limited availability of land in housing, the reservoir volume is determined based on available unused land area. Potential reservoir volume can be obtained from the available land area and reservoir depth. Meanwhile, the size of the land, buildings, and yard determine the area of land that can be used to build a reservoir. With the available land area, the reservoir volume is planned based on the selected depth of 1, 1.5, or 2 m. The maximum depth of the reservoir is planned to be 2-m because the groundwater conditions are quite high, so there will be no difficulty in making. In addition, a reservoir that is too deep causes the lift caused by water in the soil to be high, thus requiring a strong and expensive reservoir construction.

The water demand for secondary water uses such as washing, toilet flushing and watering plants in the simulation is varied from 20 L/person/day to 60 L/person/day. Two types of rainfall are used, the daily rainfall data and monthly rainfall data. The RWH performance is simulated based on scenario as shown in Table 1.

Table 1 Scenarios of Simulation

No	Scenarios		
	Rainfall data	Reservoir (M)depth	Water demand
1	Daily Rainfall data	1	20 L/person/day
			40 L/person/day
			60 L/person/day
		1,5	20 L/person/day
			40 L/person/day
			60 L/person/day
		2	20 L/person/day
			40 L/person/day
			60 L/person/day
2	Monthly Rainfall data	1	20 L/person/day
			40 L/person/day
			60 L/person/day
		1,5	20 L/person/day
			40 L/person/day
			60 L/person/day
		2	20 L/person/day
			40 L/person/day
			60 L/person/day

3 Result and Discussion

Housing located in the eastern part of Surabaya generally consists of 9 types, namely types 21, 36, 45, 54, 60, 70, 100, 120 and 180. The housing data used in this study are presented in Table 2. Each type of house has a land area with certain length and width.

Potential reservoir volume can be obtained from the available land area and reservoir depth. Meanwhile, the size of the land, buildings, and yard determine the area of land that can be used to build a reservoir. With the available land area, the reservoir volume is planned based on the selected depth of 1, 1.5, or 2 m. The maximum depth of the reservoir is planned to be 2-m because the groundwater conditions are quite high, so there will be no difficulty in making. In addition, a reservoir that is too deep causes the lift caused by water in the soil to be high, thus requiring a strong and expensive reservoir construction.

Where:

AH = Area of Houses (m²)

WH = Width of Houses (m)

WL = Width of Land (m)

Table 2 Data of Housing in Various Type

Data	Type of House								
	21	36	45	54	60	70	100	120	180
AH	21	36	45	54	60	70	100	120	180
AL	60	72	90	100	120	144	180	200	300
WH	6	6	6	7	7	8	9	10	12
LH	3.5	6	7.5	7.7	8.6	8.75	11.1	12	15
WL	6	6	6	7	7	8	9	10	12
LL	10	12	15	14	17	18	20	20	25
AH/AL	0.4	0.5	0.5	0.5	0.5	0.5	0.6	0.6	0.6
NR	1	2	2	3	3	4	4	5	5
NF	2	3	3	4	4	5	5	6	8
AR	4	5	6	7	8	10	12	14	20
AH/NF	10.5	12.0	15.0	13.5	15.0	14.0	20.0	20.0	22.5

NR = Number of Rest Room

AR = Land Area for Reservoir (m²)

AL = Area of Land (m²)

LH = Length of House (m)

LH = Length of House (m)

NF = Number of Family member

One of the rain stations located in the eastern part of Surabaya is the Keputih Rain Station. From this station, rain data can be used in this activity for 18 years of observation. The annual rain distribution recorded by the Keputih rain station is shown in Fig. 1. For 19 years of rain measurements at the Keputih Rain Station from 2000 to 2018, the minimum annual rainfall of 1112 mm occurred in 2018, the maximum annual rain of 2836 mm occurred in 2010, and the average annual rain was 1777 mm.

The results of the rain data consistency test for the Keputih Rain Station by describing the cumulative annual rainfall from 2000 to 2018, show no change in the measuring instrument so that what can be obtained can be concluded as consistent and can be used for analysis in this study.

The distribution of monthly rainfall for 18 years on average, the rainy season occurs from November to April, namely the months with high rainfall. Meanwhile, months with low rainfall or dry season occur from May to October.

The calculation of water availability with annual rainfall data is carried out by sorting the annual rainfall data from the highest to the lowest rainfall. Each rain that has been sorted is calculated as its mainstay. To provide water, 90% reliable rain was chosen which corresponds to 2002 data with a rainfall of 1140 mm as can be seen in Table 3.

The distribution of rainfall data in 2002 which corresponds to the reliability 90% can be seen in Fig. 2.

Table 3 Manstay Rain Calculatipn Using Annual Data

No	Years	R (mm)	P (%)
1	2010	2836	5.00
2	2016	2742	10.00
3	2001	2410	15.00
4	2013	2182	20.00
5	2000	1954	25.00
6	2011	1943	30.00
7	2012	1872	35.00
8	2015	1863	40.00
9	2014	1859	45.00
10	2017	1660	50.00
11	2006	1591	55.00
12	2005	1590	60.00
13	2009	1561	65.00
14	2008	1452	70.00
15	2003	1402	75.00
16	2007	1348	80.00
17	2004	1252	85.00
18	2002	1140	90.00
19	2018	1112	95.00

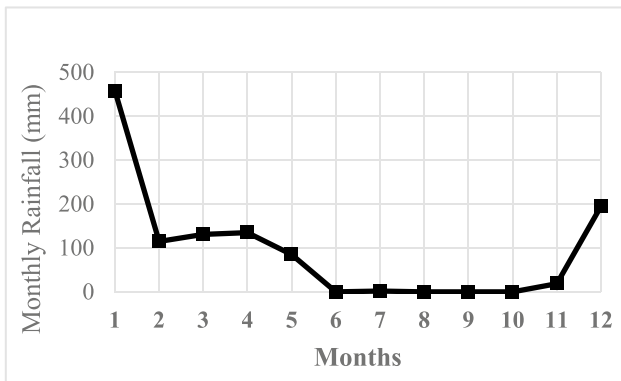


Fig. 2 Rainfall distribution of 2002 that equal reliability 90%

Calculation of water availability in the reservoir is calculated using Eq. 3, that the change in storage in the reservoir can be written:

$$dS = I.dt - O.dt \tag{4}$$

The change in reservoir dS is the difference between reservoirs S_2 and S_1 .

$$S_2 - S_1 = I.dt - O.dt \tag{5}$$

The storage volume S_2 can be written with the equation:

$$S_2 = S_1 + I.dt - O.dt \tag{6}$$

With the constraint S_2 is $0 < S_2 < Volume_{reservoir}$

Water supply is calculated by conducting reservoir simulations based on analysis of annual, monthly, and daily rainfall with different amounts of water requirements and reservoir depths. The maximum volume of rainwater inflow that enters the reservoir is as large as the available free space in the reservoir. The free space is obtained by subtracting the maximum volume of the reservoir from the previous storage volume. Even though there is high rainfall, the rainwater that can be accommodated is limited based on the volume of the reservoir.

From Fig. 3 for domestic water needs of 20 L/person/day, it shows that the adequacy of rainwater in the reservoir is still above 90%, both from the daily and monthly calculations. The daily calculation shows the percentage of water availability is greater than the monthly calculation. Meanwhile, for the water requirement of 40 L/house/day, the water adequacy decreased and further decreased for the water requirement of 60 L/person/day.

From the results of the calculations, it is found that rain to meet water needs with reliability 90% there are 6 months of unavailable water because of dry season. Therefore, to meet the lack of water supply for 6 months, a reservoir that can accommodate water is needed to meet water needs during that time. With this calculation method, the required reservoir volume is very large. For example, to meet the water demand

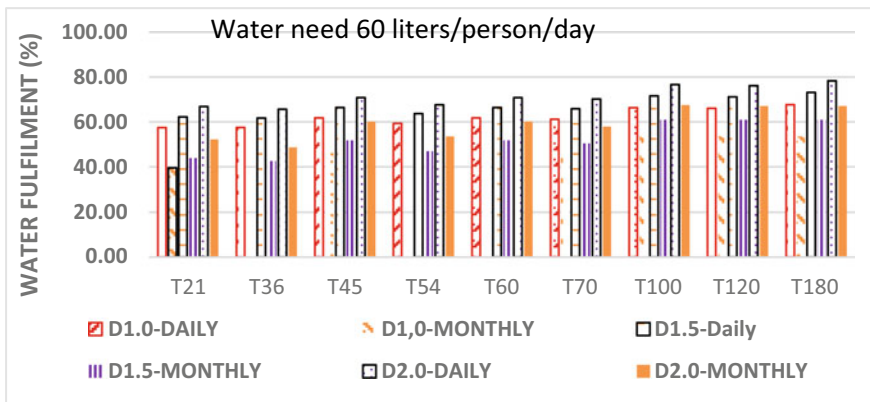


Fig. 3 Comparison of water fulfillment between daily and monthly rainfall calculation

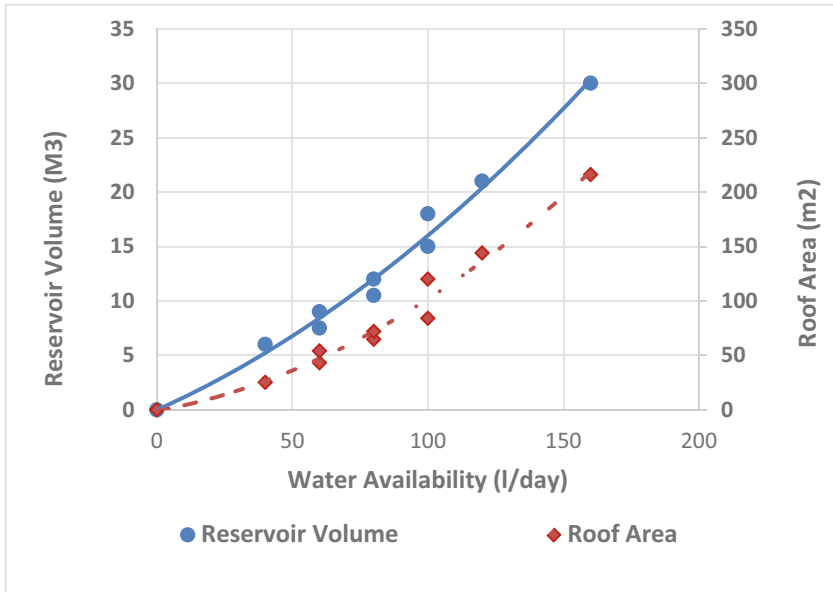


Fig. 4 Reservoir Volume and Roof Area Requirement for reliability 90%

of 4 people for 6 months with a demand of 20 L/person/day, a reservoir volume = 4 people × 20 L/person/day × 31 × 6 = 14,880 L = 15 m³.

Figure 4 shows the relationship between reservoir volume requirements (m³) compared to domestic water requirements (liters/family/day) for reliability 90%. This graph is obtained from the calculation of reliability 90% for various reservoir volumes and domestic water needs. From this graph can be obtained information on the volume of water storage needed to meet domestic water needs which are planned to be fulfilled by 90% for a year.

The relationship between the volume of the reservoir required to accommodate rainwater and water availability can be expressed by the equation:

$$RV = 0.0005W^2 + 0.1103W - 0.0516 \tag{7}$$

With:

RV = Reservoir volume (m³)

W = Water availability (liter/day)

Figure 4 also shows the relationship between the roof area needed to meet the water needs of rainwater and a reliable 90%. The relationship between the roof area required to capture rainwater and the water requirement which can be expressed by the equation:

$$RA = 0.0057W^2 + 0.4568W - 0.9593 \quad (8)$$

where:

RA = Roof area (m²)

W = Water availability (liter/day)

By comparing the volume of the reservoir used to hold water with the total volume of water demand for one year, the ratio of the required reservoir volume is 34–51% of the volume of water demand.

4 Conclusion

- a. For a reservoir size of 15 m³ the results of the annual simulation obtained that the water requirement of 20 l/person/day for 4 people is 90%, but when monthly and daily simulations are carried out, the increase is fulfilled to 96% for monthly simulations and 99% daily simulations. To meet the needs of 4 people with 20 L/person/day with a reliable volume of 90%, the reservoir volume needed to hold water in annual, monthly, and daily simulations, respectively, is 15, 12 and 10.5 m³. Simulation calculations with daily rainfall will provide detailed results compared to monthly or annual rainfall simulations. The smaller the time interval used in the reservoir routing simulation, the smaller the required reservoir volume.
- b. The relation between reservoir volume, RV (m³) required to accommodate rainwater and water availability, W (liter/day) can be expressed by the equation $RV = 0.0005W^2 + 0.1103W - 0.0516$.
- c. The relation between the roof area, RA (m²) required to capture rainwater with water availability, W (liter/day) can be expressed by the equation $RA = 0.0057W^2 + 0.4568W - 0.9593$.
- d. The ratio between the volume of the reservoir used to hold water and the total water demand for one year is 34–51%.

Acknowledgements We would like to thank Civil Engineering Department and Direktorat Riset dan Pengabdian Kepada Masyarakat of Institut Teknologi Sepuluh Nopember for supporting this research.

References

1. Harsoyo B (2010) Teknik pemanenan air hujan (rain water harvesting) sebagai alternatif upaya penyelamatan sumberdaya air di wilayah DKI Jakarta. *Jurnal Sains & Teknologi Modifikasi Cuaca* 11(2):29–39

2. Campisano A, Butler D, Ward S, Burns MJ, Friedler E, DeBusk K, Fisher-Jeffes LN, Ghisi E, Rahman A, Furumai H, Han M (2017) Urban rainwater harvesting systems: Research, implementation and future perspectives. *Water Res* 115:195–209. <https://doi.org/10.1016/j.watres.2017.02.056>
3. Burns MJ, Fletcher TD, Duncan HP, Hatt BE, Ladson AR, Walsh CJ (2015) The performance of rainwater tanks for stormwater retention and water supply at the household scale: an empirical study. *Hydrol Process* 29(1):152–160
4. Umapathi S, Chong MN, Sharma A (2012) Investigation and monitoring of twenty homes to understand mains water savings from mandated rainwater tanks in South East Queensland, Urban Water Security Research Alliance City East, QLD
5. Nor Hafizi M, Lani ZY, Syafiuddin A (2018) A review of rainwater harvesting in Malaysia: prospects and challenges. *Water* 10(4):506. <https://doi.org/10.3390/w10040506>
6. Hamid TB, Nordin B (2011) Green campus initiative: introducing RWH system in Kolej Perindu 3 UiTM Malaysia. In: 2011 3rd international symposium & exhibition in sustainable energy & environment (ISESEE)
7. Song J, Han M, Kim T-I, Song J-E (2009) Rainwater harvesting as a sustainable water supply option in Banda Aceh. *Desalination* 248(1–3):233–240
8. Sudiajeng L, Wiraga IW, Parwita IGL, Santosa G (2017) Domestic recharge wells for rainwater-harvesting in Denpasar City, Bali-Indonesia. *GEOMATE J* 13(36):50–57
9. Mukaromah H (2020) Rainwater harvesting as an alternative water source in Semarang, Indonesia: the problems and benefits
10. Abdulla FA, Al-Shareef AW (2009) Roof rainwater harvesting systems for household water supply in Jordan. *Desalination* 243(1–3):195–207
11. UNEP International Technology Center (2001) Rainwater Harvesting. Murdoch University of Western Australia
12. Worm J (2006) AD43E Rainwater harvesting for domestic use, Agromisa Foundation
13. Zabidi HA, Goh HW, Chang CK, Chan NW, Zakaria NA (2020) A review of roof and pond rainwater harvesting systems for water security: the design, performance and way forward. *Water* 12(11):3163
14. Amin MT, Han MY (2009) Water environmental and sanitation status in disaster relief of Pakistan's 2005 earthquake. *Desalination* 248(1–3):436–445
15. Mehrabadi MHR, Saghafian B, Fashi FH (2013) Assessment of residential rainwater harvesting efficiency for meeting non-potable water demands in three climate conditions. *Res Conserv Recycl* 73:86–93
16. Badan Standarisasi Nasional (2005) SNI 03-7065-2005 Tata cara perencanaan sistem plambing
17. Hadi W, et al (2014) Penggunaan unit slow sand filter, ozon generator dan rapid sand filter untuk meningkatkan kualitas air sumur dangkal menjadi air layak minum dengan parameter kekeruhan, Fe, dan Mn. *Jurnal Teknik ITS* 3(2):F256–F259
18. Yulistiyorini A (2011) Pemanenan Air Hujan Sebagai Alternatif Pengelolaan Sumber Daya Air Di Perkotaan. *Teknologi Dan Kejuruan: Jurnal Teknologi, Kejuruan Dan Pengajarannya* 34(1)
19. Prihadi LR, Yulistiyorini A, et al (2019) Desain Sistem Pemanenan Air Hujan Pada Rumah Hunian di Daerah Karst Kabupaten Malang. *Jurnal Manajemen Aset Infrastruktur & Fasilitas* 3(1)
20. Helmreich B, Horn H (2009) Opportunities in rainwater harvesting. *Desalination* 248(1–3):118–124
21. Villarreal EL, Dixon A (2005) Analysis of a rainwater collection system for domestic water supply in Ringdansen, Norrköping, Sweden. *Build Environ* 40(9):1174–1184
22. Imteaz MA, Adeboye OB, Rayburg S, Shanableh A (2012) Rainwater harvesting potential for southwest Nigeria using daily water balance model. *Res Cons Recycl* 62:51–55
23. Santos C, Taveira-Pinto F (2013) Analysis of different criteria to size rainwater storage tanks using detailed methods. *Res Cons Recycl* 71:1–6
24. Jihan JC (2014) Analisa Zona Perubahan Penggunaan Lahandi Kecamatan Sukolilo Surabaya Timurberbasis SIG
25. Hartini AS, Hermawan Y (2011) Modul Rumah Sehat

Criteria of Low Embodied Energy Material Selection for Sustainable Building Design



Yani Rahmawati, Rissa Syafutri, Ariessa K. Pratami,
Jatmika Adi Suryabrata, Christiono Utomo, and Aqsha

Abstract The high use of construction materials that have a massive value of Embodied Energy (EE) is one of the causes of Greenhouse Gas (GHG) emissions and they are still widely used in construction projects in Indonesia. This study was conducted to investigate the criteria of materials selection that have low embodied energy in supporting the realisation of sustainable building design. An extensive literature review was done to conclude the essential decision criteria for suitable construction materials, followed by a survey to confirm the criteria and identify possible alternatives for materials. Triangulation methodology was applied through qualitative and quantitative approaches. Safety and durability, maintainability, cost, life cycle, availability, and the process of installation/construction are found to be the criteria in the material selection.

Keywords Embodied Energy · Sustainable Construction · Construction Materials

1 Introduction

Embodied Energy (EE) produces CO² gas which is one of the biggest causes of greenhouse gas (GHG) emissions that hinder environmental sustainability [1]. The 2019 GHG emission inventory data shows that the manufacturing and construction sectors accounted for 21.46% of emissions, the third-highest overall percentage [2]. To prevent environmental degradation, it is necessary to maintain a low EE value [3]. With the understanding that the emission content in the EE value results in GHG

Y. Rahmawati (✉) · R. Syafutri · A. K. Pratami · J. A. Suryabrata
Department of Architecture and Planning, Universitas Gadjah Mada, Yogyakarta, Indonesia
e-mail: yani.rahmawati@ugm.ac.id

C. Utomo
Department of Civil Engineering, Institut Teknologi Sepuluh Nopember, Surabaya, Indonesia

Aqsha
Department of Bioenergy Engineering and Chemurgy, Institut Teknologi Bandung, Bandung, Indonesia

emissions and harms the environment, a study on this area is necessary. Although reducing CO² gas production in EE is an urgent matter for a better global environment, its implementation in Indonesia still requires intense efforts. Indonesia has committed to reducing the percentage rate of greenhouse gas emissions at the 15th Conference of Parties (COP) by a minimum of 26%. However, the reality of its application is still not significant. This can be seen from the percentage of EE in the production of materials, namely cement, bricks, and zinc roofing, which is often used as building materials in the construction sector [4]. The selection of suitable materials is needed to realise a sustainable built environment.

One of the approaches to significantly reduce the percentage of greenhouse gas emissions is the use of building materials that have a low value on EE [5]. An assessment of the building design to achieve optimal energy values and carbon emissions is essential [6]. Regarding this matter, [7] also found that the analysis of the EE in construction materials needs to be carried out in the decision-making process of materials selection to draw the potential negative impacts on the building and its surroundings. As confirmed that this process should be applied not only to new developments but also in the design process of revitalising old buildings, whereby the EE is also found in the buildings that experience retrofit [9]. With the matter of urbanisation still happening and raising, the consideration of EE in construction materials is necessary as the finding highlighted by [10] that the energy consumption by materials is increasing with the increasing number in the regional economic development. This study was conducted to find the critical criteria of low embodied energy material as well as the alternatives of the material.

2 Conceptual Background

Research on EE is developing, especially in construction materials since the issue of low energy and sustainable construction are currently getting critical. The emerging use and development of Building Information Modelling (BIM) in construction advances the method of analysing EE in materials. Some contemporary approaches have been developed, including the analysis of EE on the material supply [11] and the reduction of construction waste [12]. Previous studies also highlighted criteria that are needed to be considered to select materials that support the reduction of EE value through passive design on the use of materials [13–15].

Mathiyazhagan et al [14] investigated criteria for selecting materials that have potential impacts on the value of embodied energy and grouped them into the environmental, social, and economic. Inside the environmental scope, the contribution of the materials to the environment needs to be analysed, including the impacts of the mobility of the materials. During its transportation, materials capture the energy that increases the value of EE. Consideration use of recycled materials and prefabrication materials [12] is an effective strategy to reduce the EE value. The use of local materials is also an effective strategy that not only reduces the value of EE but also increases the value of social benefits. Despite the contribution to the environment,

strategy, and efforts in reducing the EE value by local or recycled materials and prefabricated materials may increase the economic value of its use [15]. Maintainability of the materials also needs to be considered to increase the economic value by reducing EE [16].

To reduce the EE value, management throughout the life cycle of materials is necessary to prevent negative impacts on the environment and increase the project's economic performance, especially in the use of the concept of green construction [17]. The EE value of a material is calculated based on the stages of its life cycle, which are divided into the cradle to site, cradle to gate, and cradle to grave. Throughout the stages, the materials experience the process of extraction, transportation, production, installation, and demolition. At the production stage, there are many changes in the shape of the material by the extraction and manufacturing processes so that it emits high emissions [18]. The EE value of each construction material depends on the number of stages and processes. Thus, the use of local materials, recycled materials, and prefabricated materials reduce the EE value by cutting the stages and duration of the process of transportation, production, and installation. Table 1 presents the criteria of materials selection for reducing the embodied carbon resulting from the literature study.

A review of previous studies found critical criteria for material selection that are supporting the sustainability of the built environment, especially in the effort of reducing the EE value captured by construction materials. The criteria can be qualitatively grouped into 6 criteria, which are durability and maintenance, health and safety, cost and benefit, life cycle, availability, and installation or construction.

3 Methodology

This study implemented the triangulation methodology that comprises both qualitative and quantitative approaches that were applied sequentially and simultaneously. Fig. 1 illustrates the application of the triangulation methodology. The study started with the development of a conceptual framework through grounded theory from literature review and observation to empirical condition. This first step produced the criteria of material selection that continued to be studied quantitatively through a survey by distributing questionnaires to project stakeholders. A design of a gallery located in West Java, Indonesia, was used as the research object to investigate and confirm selection criteria for material in the building. Fig. 2 illustrates the building design. Building's walls (both interior and exterior) were selected as a point of view since it was found that the wall has the biggest quantity in the building. Through this study, the Authors also investigated possible alternatives that may replace the current materials in terms of desired EE value.

The main goal of this study is to find critical criteria to select materials that contribute to sustainability through low EE value. A Scatter plot of mean and standard deviation was used to statistically analyse the data. The related method was used to investigate the importance of each criterion to be used in selecting materials, it was

Table 1 Criteria of Low Embodied Energy Materials

Criteria	Description	Reference
Durability & Maintenance	•The easiness of maintainability	[15]
	•energy saving during the process of extraction, fabrication, installation, and demolition	
Health & Safety Cost (cost & benefit)	•EE during the operational	[19–21]
	•Social benefits through the safety of installation and operation, no toxic	[11, 14]
	•The relation between embodied energy and cost in the material selection	[16, 22]
	•Cost and profit consideration	
	•The trade-off between the initial cost and maintenance cost in selecting materials	[23]
Material life cycle	•Green suppliers	[24, 25]
	•Prefabrication	[12]
	•Energy consumption during the process	[26]
	•Material management, green construction	[17]
	•Maintenance (period the materials experience retrofit process)	[9]
Availability	•Recycled materials, energy efficiency	[27, 28]
	•Optimising material supply (consideration of the availability of materials)	[29]
Installation/Construction	•Retrofit or revitalisation of materials from existing buildings	[8]
	•Recycled materials	[30]
	•Waste minimisation	[31]

also used to prioritise the criteria that can be used in the decision-making process of material selection in design. The result was then qualitatively analysed through focus group discussion with project stakeholders to synthesise the applicability of the result with the current empirical problem. Purposive sampling was used as a sampling technique to determine the potential respondents in both the survey and focus group discussion.

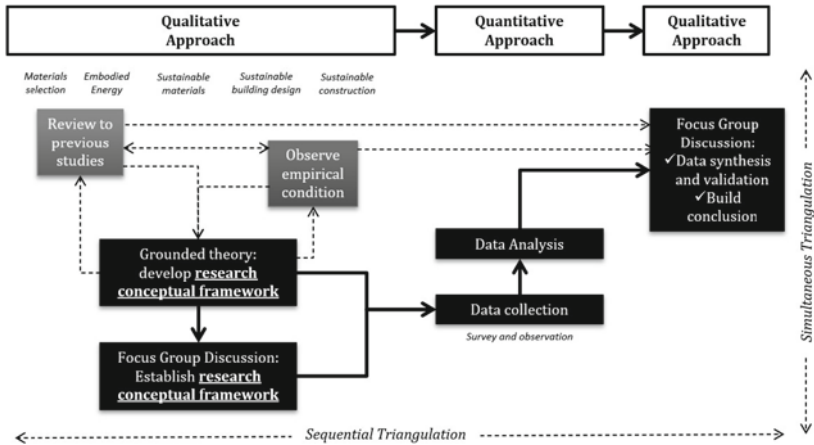


Fig. 1 Research Flow and Methodology

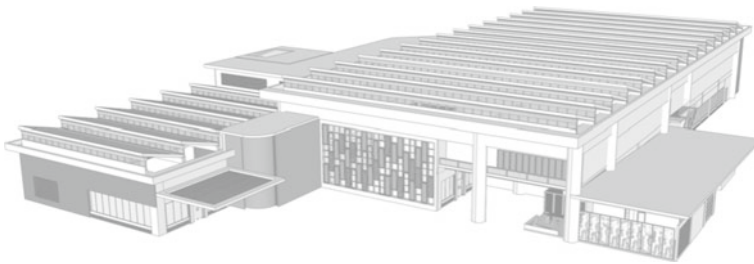


Fig. 2 Building Design (Sample of Study)

4 Result and Discussion

Six main criteria of material selection were found from the literature review and observation of the current empirical condition. This study takes place in Indonesia, particularly in West Java. The criteria were confirmed through a survey of 39 respondents of project stakeholders. Fig. 3 presents the background of the respondents. The respondents are classified into 2 groups, which are local respondents (from Indonesia) and overseas. There are 71.8% of respondents from Indonesia, 10.3% from Argentina and India, and also 2.6% from the UAE, Colombia and Brazil. Most respondents are architects and civil engineers.

The statistical results of the criteria based on the data received through the survey are presented in Table 2. The data were grouped into two categories, which are data from respondents located in Indonesia and outside Indonesia. Based on the analysis, the mean scores are in the range of 3,30 – 4,17 with a standard deviation below 1,00, it can be concluded that all the criteria are necessary to be considered in selecting materials that are able to reduce the EE value in the development of the building.

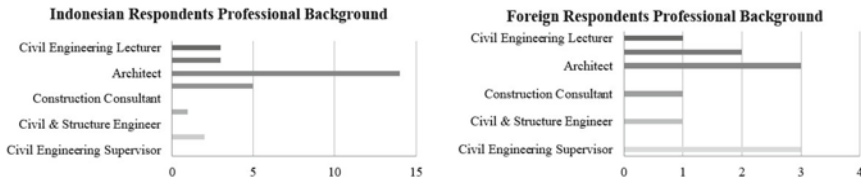


Fig. 3 The Professional Background of Respondents

Table 2 The result of the Survey on the Aspects of The Selection of Wall Materials

Category A: Analysis of Criteria (From Indonesian Respondents)			Category B: Analysis of Criteria (From non-Indonesian Respondents)		
Criteria	Mean	Std. Dev	Criteria	Mean	Std. Dev
Durability & Maintenance	4.17	0.60	Life Cycle of Materials	3.90	0.74
Health & Safety	4.17	0.60	Health & Safety	4.00	0.82
Cost	3.93	0.65	Installation/Construction	3.30	0.82
Availability	3.86	0.69	Durability & Maintenance	4.1	0.88
Installation/Construction	4.07	0.75	Cost	3.80	0.92
Life Cycle of Materials	3.93	0.75	Availability	4.00	0.94

To identify the level of importance of each criterion, the value of mean and standard deviation is mapped in a scatter plot, as presented in Fig. 4 and Fig. 5. Criteria with a higher score of mean and lower score of standard deviation has a higher importance value on the consideration. The related analysis technique was implemented in the related previous studies [32, 33].

Based on the scatter plot analysis, it can be highlighted that both categories of data (Indonesian respondents and non-Indonesian respondents) have different results. As highlighted in Table 2, the Life Cycles of Materials appeared as the most important criterion under category B, meanwhile, the related criterion falls into the last important criteria in category A. It can be justified that project stakeholders outside Indonesia are concerned about the process of the material, especially the number of stages that the materials have experienced before installation/construction. EE are captured by materials during the process from extraction until fabrication or installation. The utilisation of virgin materials contributes to higher EE value compared with the use of recycled materials since they need to go through some stages of the process and be transported from one process to another [15] before they are installed/constructed at the construction site. Thus, [12] suggested using prefabricated materials to cut or expedite the process and reduce the EE value during the production of materials. Recycled materials also can be considered to streamline the process and reduce the EE captured during the production process [30].

Under category A, two criteria appear as the most important criteria since both have a similar score. The criteria are durability and maintenance and also health and safety. From the perspective of respondents from Indonesia, both are important and

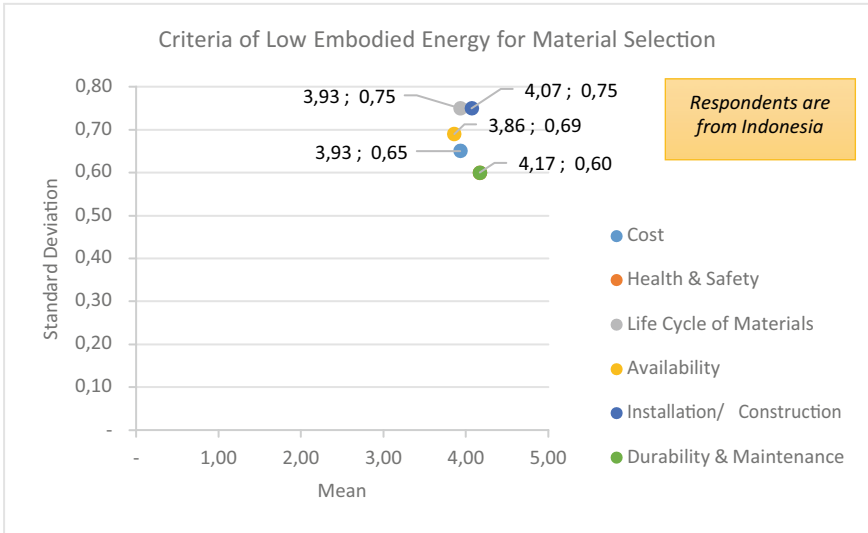


Fig. 4 Scatter Plot Analysis for Criteria of Material Selection (Indonesia)

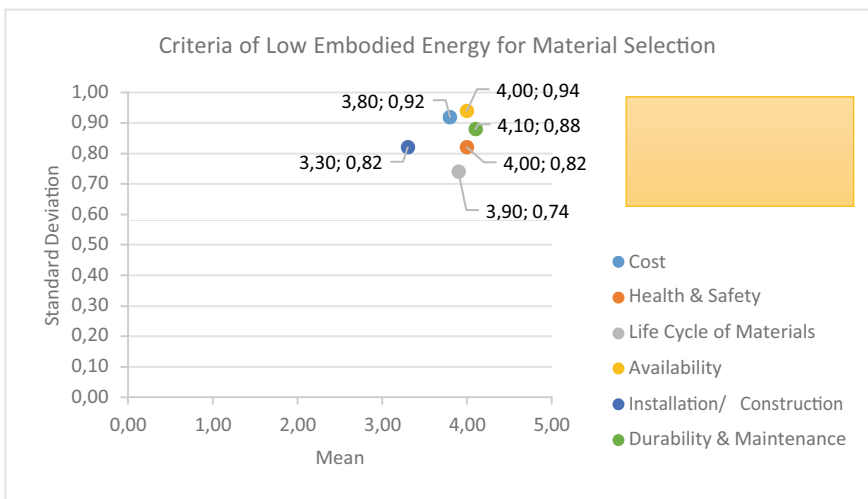


Fig. 5 Scatter Plot Analysis for Criteria of Material Selection (Outside Indonesia)

equal to be prioritised in selecting materials. It can be justified that these criteria reflect on the impact during the operation of the building as well as maintainability and constructability [11, 14], which are also related to the cost and benefits [16] that appear as the second important criteria in category A. These findings justified the background of why these three criteria appear as the top three criteria to be considered in category A. Meanwhile, the criteria related to cost and benefits appear as number

Table 3 Background of Respondents in FGD

Respondent	Experience	Role
Respondent 1	20 years	Owner
Respondent 2	6 years	Contractor
Respondent 3	8 years	Architect
Respondent 4	12 years	Green Building Consultant
Respondent 5	10 years	Green Building Consultant

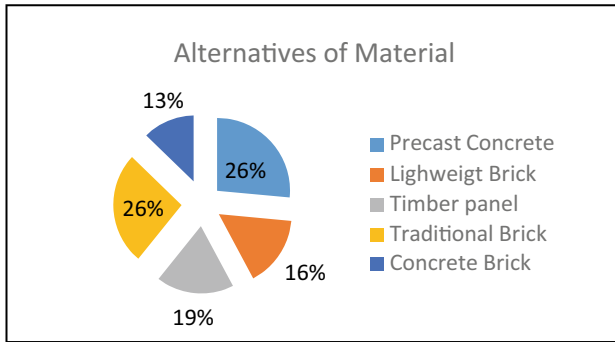


Fig. 6 Suitable Alternatives of Material

fourth in category B. It can be concluded that project stakeholders in Indonesia tend to select materials that have a negative contribution during operation compared with the process of materials and installation.

The result was then continued to be synthesised through Focus Group Discussion (FGD) by selected project stakeholders. The background of the respondents is presented in Table 3. Through FGD, it is confirmed that all criteria are valid to be used or considered in the decision-making process of selecting materials that will contribute to supporting the capture of EE value in the development and construction of the building, especially for the wall element. During FGD, it was also found that there are 5 alternative materials, as presented in Fig. 6, which are suitable with the criteria to be used as a strategy to reduce EE value through material selection.

5 Conclusion

Through the triangulation methodology, it was investigated that there are 6 main criteria to be considered in selecting materials that may reduce the EE value of development and construction, which are durability and maintenance, health and safety, cost, installation/construction, and also the life cycle of materials. Based on the study, it was also found the alternatives of materials that are related to the criteria, are precast concrete, traditional brick, timber panel, lightweight brick, and concrete

brick. The results that appeared in this study can be considered as a passive design strategy in reducing the value of EE captured during the development, construction, and operation of a building through the selection of low EE materials.

Acknowledgement The authors would like to thank the Indonesian Research Collaboration (RKI 2022), a collaboration between ITS, UGM, and ITB, for funding this research under contract no. 1564/UN1/DITLIT/Dit-Lit/PT.01.03/2022.

References

1. Metz B, et al (2007) IPCC AR4. Climate change 2007: mitigation, fourth assessment report of the intergovernmental panel on climate change
2. Indonesian ministry of energy and mineral resources: inventory of carbon emission (2020)
3. Indonesian ministry of public works, housing and settlement: PUPR ministerial regulation no 9 (2021)
4. Uda SAK (2021) Embodied energy and embodied carbon consumption analysis of 36- type simple house building materials. *TEKNIK* 42(2):160–168
5. Venkatarama Reddy VB (2009) Sustainable materials for low carbon buildings. *Int J Low Carbon Technol* 4:175e181
6. Agudelo LM, Mejía-Gutiérrez R, Nadeau JP, Pailhes J (2014) Life cycle analysis in preliminary design stages. In: Joint conference on mechanical, design engineering & advanced manufacturing, June 2014, Toulouse, France, pp 1–7. Hal-01066385
7. Alwan Z, Jones P (2014) The importance of embodied energy in carbon footprint assessment. *Struct Surv* 32(1):49–60
8. Hoxha V (2020) Measuring embodied CO2 emission in construction materials in Kosovo apartments. *Int J Build Pathol Adapt* 38(3):405–421
9. Forsythe P, Wilkinson S (2015) Measuring office fit-out changes to determine recurring embodied energy in building life cycle assessment. *Facilities* 33(3/4):262–274
10. Tang BJ, Gong PQ, Xiao YC, Wang HY (2017) Energy consumption flow and regional economic development: evidence from 25 economies. *J Model Manage* 12(19):96–118
11. Ahmadian FFA, Rashidi TH, Akbarnezhad A, Waller ST (2017) BIM-enabled sustainability assessment of material supply decisions. *Eng Constr Architect Manage* 24(4):668–695
12. Ahmadzadeh Amid, S., Noorzai E, Golabchi M (2022) Identifying factors affecting waste production throughout the construction project life cycle and proposing BIM-based solutions. *TQM J*
13. Udawatta N, Zuo J, Chiveralls K, Zillante G (2021) From green buildings to living buildings? Rating schemes and waste management practices in Australian educational buildings. *Eng Constr Archit Manag* 28(4):1278–1294
14. Mathiyazhagan K, Gnanavelbabu A, Lokesh Prabhuraj B (2019) A sustainable assessment model for material selection in construction industries perspective using hybrid MCDM approaches. *J Adv Manage Res* 16(2):234–259
15. AlKheder S, AlKandari D, AlYatama S (2022) Sustainable assessment criteria for airport runway material selection: a fuzzy analytical hierarchy approach. *Eng Constr Archit Manag* 29(8):3091–3113
16. Zeng R, Chini A, Ries R (2021) Innovative design for sustainability: Integrating embodied impacts and costs during the early design phase. *Eng Constr Archit Manag* 28(3):747–764
17. Onubi HO, Yusof N, Hassan AS (2020) Effects of green construction on project's economic performance. *J Financ Manag Prop Constr* 25(3):331–346

18. Hamida A, Alsudairi A, Alshaibani K, Alshamrani O (2021) Parametric study of the impact of building envelope systems on embodied and operational carbon of residential buildings. *Int J Build Pathol Adapt* 40(5):753–74
19. Tam VWY, Liu L, Le KN (2022) Modelling and quantitation of embodied, operational and mobile energies of buildings: a holistic review from 2012 to 2021. *Eng Constr Architect Manage*
20. K. Dixit M, H. Culp C, Lavy S, Fernandez-Solis J (2014) Recurrent embodied energy and its relationship with service life and life cycle energy: a review paper. *Facilities* 32(3/4):160–181
21. Peng Z, Deng W, Hong Y (2019) Materials consumption, indoor thermal comfort and associated energy flows of urban residential buildings: case studies from the cold climate zone of China. *Int J Build Pathol Adaptat* 37(5):579–596
22. Gounder S, Hasan A, Shrestha A, Elmualim A (2021) Barriers to the use of sustainable materials in Australian building projects. *Eng Constr Architect Manage* 30:189–209
23. Dabaieh M, Emami N, Heinonen JT, Marteinson B (2020) A life cycle assessment of a ‘minus carbon’ refugee house: global warming potential and sensitivity analysis. *Archnet-IJAR* 14(3):559–579
24. Liang R, Chong HY (2019) A hybrid group decision model for green supplier selection: a case study of megaprojects. *Eng Constr Architect Manage* 26(8):1712–1734
25. Rebane K, Reihan A (2016) Promoting building materials that have lower embodied carbon and energy in public procurements: Experience from Estonia. *Manag Environ Qual* 27(6):722–739
26. Oral NG, Özdeniz MB (2018) Embodied energy assessment of building materials used: case study northern Cyprus. *Open House Int* 43(3):22–32
27. Blackburne L, Gharehbaghi K, Hosseinian-Far A (2022) The knock-on effects of green buildings: high-rise construction design implications. *Int J Struct Integrity* 13(1):57–77
28. Jha NK (2022) Profitability, sustainability, and product development. In: Lawrence KD, Pai DR (ed) *Applications of management science (applications of management science, vol 21)*. Emerald Publishing Limited, Bingley, pp 67–84
29. Ismail Z-AB (2021) Hybrid intelligent vehicle system for managing construction supply chain in precast concrete building construction projects. *World J Eng* 18(4):538–546
30. Crowther P (2018) Re-valuing construction materials and components through design for disassembly. In: Crocker R, Saint C, Chen G, Tong Y (ed) *Unmaking waste in production and consumption: towards the circular economy*. Emerald Publishing Limited, Bingley, pp 309–321
31. Treloar GJ, Love PED, Faniran OO (2001) Improving the reliability of embodied energy methods for project life-cycle decision making. *Logist Inf Manag* 14(5/6):303–318
32. <https://doi.org/10.3390/su12229350>
33. <https://doi.org/10.3390/su11071911>

Improving the Quality of Agricultural Wastes for Solid Fuels Employing Torrefaction: A Case Study in Indonesia



Untoro Budi Surono, Mochamad Syamsiro, and Nugroho Agung Pambudi

Abstract Using biomass as a fuel has some limitations, including high moisture and volatile contents, low energy density, and easily degraded. Furthermore, torrefaction can be used as a pretreatment to reduce the weakness. The process is pyrolysis at low temperatures. Therefore, the aim of this study is to improve the quality of biomass using torrefaction. Three biomass samples were used: rice husk, cocoa pod shell, and sawdust. The results showed that rice husk has the lowest bulk density, while the highest is the cocoa pod shell. Sawdust possesses the highest mass yield, while the energy yield of cocoa husk is the highest. The torrefaction reduced the moisture and volatile contents, thereby increasing the fixed carbon and heating value. The results also showed that rice husk has the highest ash content before and after torrefaction. Furthermore, the samples changed from hydrophilic to hydrophobic with reduced reactivity. Also, the raw and torrefied rice husks had the highest residue after combustion, while the lowest was found in sawdust. Finally, the cocoa pod shell had the lowest combustion temperature, while the highest was found in the torrefied sawdust.

Keywords Biomass · cocoa pod husk · rice husk · saw dusk · torrefaction

U. B. Surono (✉) · M. Syamsiro
Department of Mechanical Engineering, Universitas Janabadra, Jalan T.R. Mataram 55-57,
Yogyakarta 55231, Indonesia
e-mail: untorobs@janabadra.ac.id

M. Syamsiro
e-mail: syamsiro@janabadra.ac.id

N. A. Pambudi
Department of Mechanical Engineering Education, Universitas Negeri Sebelas Maret, Jl. Ir.
Sutami 36A, Surakarta 57126, Indonesia
e-mail: agung.pambudi@staff.uns.ac.id

© Institute of Technology PETRONAS Sdn Bhd 2024
B. S. Mohammed et al. (eds.), *Proceedings of the International Conference on Emerging Smart Cities (ICESC2022)*, Lecture Notes in Civil Engineering 324,
https://doi.org/10.1007/978-981-99-1111-0_32

1 Introduction

Biomass is one of the renewable energy sources that potentially developed as a substitute for fossil fuels, considering that Indonesia is rich in biomass energy sources due to fertile natural soil, rainfall, and adequate sunlight. The sources come from agricultural products such as sugar cane plantation, corn, nuts, coconut, and palm, as well as byproducts of agricultural processes such as bagasse, rice husk, coconut shell, and palm shell. The sources can also be derived from the byproducts of wood, such as branches, twigs, and sawdust. In Indonesia, the state electricity company has been beginning to implement co-firing in coal-fired power plants by mixing biomass and coal since early 2020. The state-owned electricity company proposes to shift 114 existing coal-fired power plants to co-firing by 2024. There are 29 power plants owned by state electricity company that has undergone cofiring trials run process until the end of 2020 [1].

The advantages of biomass are renewable and environmentally friendly. The carbon dioxide emitted from its combustion is reabsorbed by the plants during photosynthesis, thereby reducing its impact on polluting the air and greenhouse emissions contributing to global warming [2–4]. Biomass energy from agricultural waste is also comparatively cheaper in raw materials. However, there are some inevitable weaknesses of biomass. It has high moisture and needs to be dried before being combusted. Therefore, they need to be used immediately after drying because it easily absorbs water [4, 5]. The fibrous nature of biomass makes it not to be easily crushed and ground into a powder [6, 7]. It is also decomposed by insects and microbes when stored for long periods [4].

Although biomass has great potential to suffice energy demands, the utilization to generate energy is still limited cause by costly and technological constraints. Torrefaction is a mild thermochemical process at relatively low temperatures range of 200–300 °C in an inert gas atmosphere [8]. The process is able to reduce the ratio of oxygen and hydrogen to carbon. The decrease in the oxygen-to-carbon ratio changes the properties of biomass from hydrophilic to hydrophobic [9, 10]. Torrefied biomass has a higher energy density than raw biomass [11]. During torrefaction, the fibrous structure of biomass is broken down through the decomposition of hemicellulose and cellulose. Thereby, torrefied biomass becomes a more homogeneous structure, brittle, and easy to grind [12]. Aside from all characteristics described, torrefaction reduces the biological activity, degradability, and combustion capacity [13]. The heating value gradually increases by releasing some mild volatile fractions, which mainly contain oxygen [14]. In general, biomass contains 1–3% moisture by weight after the torrefaction process [11]. Reducing transportation costs and preventing decomposition during storage are other advantages of torrefaction [15].

There are numerous studies about the torrefaction of many types of biomass wastes. Different from previous studies, this study compared the results of the torrefaction of three biomass wastes such as rice husk, cocoa pod shell, and sawdust. These wastes were chosen considering that they are abundantly available and have not been utilized widely for fuel. The biomasses have different initial properties. In this

research, the properties of biomass after the torrefaction process with respect to proximate analysis, calorific value, and hydrophilicity, as well as the thermogravimetric analysis, were investigated.

2 Materials and Methods

2.1 Materials

The feedstocks used in this study were cocoa pod shells, rice husks, and sawdust. Cocoa pod shell (CPS) was taken from a plantation in the Gunungkidul Regency, Yogyakarta, Indonesia. The moisture content of raw CPS is very high, so it needs to be dried under the sun for about 4 days after being chopped into small cuts of 0.5 cm thick and 2 cm long. The rice husk used in this study was acquired from rice mills, while the sawdust was obtained from a furniture company in Bantul, Yogyakarta, Indonesia. Sun drying for a day was performed on the rice husk and the sawdust to reduce the moisture content. Each sample was kept in plastic bags after drying to prevent changing the moisture content.

2.2 Torrefaction Process

The torrefaction of the samples was carried out in a batch-feeding reactor heated by an electrical heater. The reactor schematic is shown in Fig. 1, which is consisted of a furnace, tubular reactor, nitrogen gas cylinder, nitrogen gas regulator, temperature control, thermocouple, and data logger. The electrical heater made of Nichrome wire was used to heat the reactor, which was 46 cm in height and 13.8 cm in inside diameter. One thermocouple connected to the temperature control and one other was used to detect and keep the reactor at the torrefaction temperature. A rotameter was installed in the nitrogen gas line to measure the nitrogen gas flow rate.

The torrefaction process of each sample was started by entering each sample into the reactor. After be filled and closed, the reactor was connected to the nitrogen tank. The tubular reactor was put into the furnace once the desired torrefaction temperature setting was achieved. The temperature of the torrefaction process was set at 250 °C, and the holding time of 60 min. The biochar produced from the process was weighed and then put in an airtight plastic bag for further investigation.

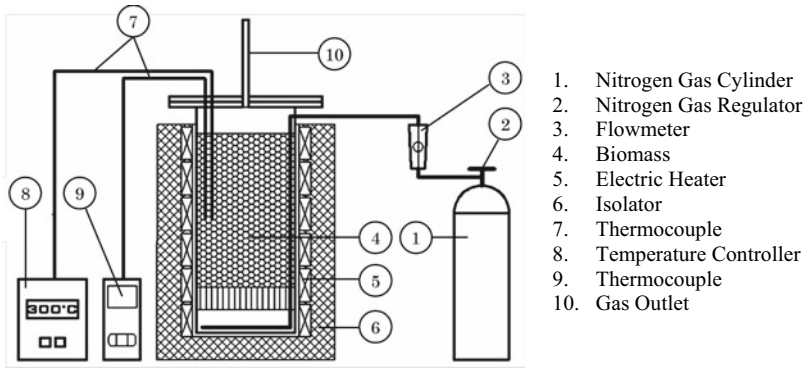


Fig. 1 A schematic of the biomass torrefaction system

2.3 Properties Experiment

The properties of the raw and torrefied samples were investigated for bulk density, heating value, hydrophobicity, and proximate analysis. The heating value and proximate analysis were conducted using the American Society for Testing of Materials (ASTM) standard. The calorific value was analyzed using ASTM D5865 by an adiabatic bomb calorimeter. The moisture, volatile, and ash contents were analyzed using ASTM D3173, ASTM D3175, and ASTM D3174, respectively. The fixed carbon content was determined by subtracting the volatile, moisture, and ash contents from the total dried biomass, while ASTM E-873–06 analyzed the bulk density. The sample was placed into a standard-size box and then dropped three times from a height of 150 mm for completely settle and refilling. Then the bulk density was calculated by divide the final weight of the biomass by the box volume.

The hydrophobicity test of the raw and torrefied sample was carried out by measuring the Equilibrium Moisture Content (EMC). Prior to the test, the sample was ground and then put in an oven at a temperature of 110 °C for 2 h. The sample (2 g) was loaded into a small cup and then put in the airtight container box at a constant relative humidity set at 75% by placing a saturated NaCl. The initial sample mass was weighed, and the increasing mass was measured daily for 4 days.

Thermogravimetric analysis (TGA) was carried out to determine the activation energy, ignition time, and combustion temperature employing a TGA Shimadzu 60. About 8 mg of sample was put in an alumina crucible and then heated at 110 °C for 1 h till the mass was constant. Then, the sample was heated from room temperature to 800 °C at a heating rate of 40 °C/min. The mass of the sample was measured and recorded to attain weight loss with increasing temperature.

Table 1 Properties of raw biomass

Properties	Cocoa pod shell	Saw dust	Rice husk
Bulk density	208.19	193.93	99.33
Proximate analysis			
Moisture (% wt, wb)	11.72	9.99	10.28
Volatile (% wt, db)	72.57	78.48	58.20
Fixed carbon (% wt, db)	9.23	7.98	7.59
Ash (% wt, db)	6.48	3.54	23.93
HHV (kJ/kg)	16.345	18.478	13.097

3 Results and Discussion

3.1 The Properties of Biomass Before Torrefaction

In this study, three types of biomass wastes (CPS, sawdust, and rice husks) were investigated. All the raw samples had comparable moisture and fixed carbon contents. The comparison of the raw sample's properties is shown in Table 1.

The rice husk had several disadvantages compared to cocoa pod shells and sawdust. At almost the same moisture content, the bulk density of rice husk is the lowest, whereas cocoa pod shells had the highest bulk density. The lowest the bulk density, the highest the transportation and storage costs. The rice husk also had the highest ash content, thereby producing higher residuals after combustion, while the sawdust had the lowest ash content. Table 1 shows that samples ranked in order of the heating values are rice husk, cocoa pod shell, and sawdust. It presents that there is a correlation between ash content and heating value. The highest the ash content, the lowest the heating value because ash is the incombustible part of fuel. The same correlation between ash content and the heating value of some biomass samples also was presented by Khan et al. [16]. Fuel with high ash content also increases the challenges in ash handling [1].

3.2 Color Change of the Torrefied Biomass

The three samples were subjected to torrefaction at 250 °C and a holding time of 60 min. The color change observed for each sample, as shown in Fig. 2, changed from dark brown to black. However, the cocoa pod shell produced darker biochar than the others, indicating that it has the highest carbon content.

Similar results were obtained in research conducted by Pimchuai et al. [17] involving rice husks, bagasse, sawdust, peanut husks and water hyacinth. Also, Gucho et al. [18] reported the same color change results in research involving beech and



Fig. 2 Comparison of biomass color before and after torrefaction

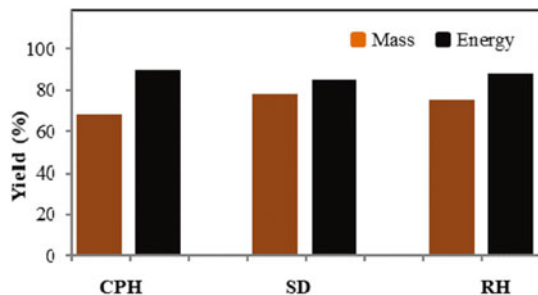
mischanthus wood. The discoloration resulted from biodegradation and evaporation of volatile matter in the biomass, thereby increasing its carbon content.

3.3 Mass and Energy Yield

During torrefaction, the moisture content in biomass evaporates first. The process also reduces mass because the components with low calorific values release too. High calorific value components, such as carbon, remain in the material. The three raw materials used in this research were torrefied at 250 °C and 60 min of holding time. Figure 3 compares the mass and energy yields of these materials.

Based on Fig. 3, sawdust had the highest mass yield, followed by rice husks and cocoa pod shells. It also means that the evaporated components in sawdust were the least compared with the others, which was possible because the particle size of sawdust was smaller. In general, the small particles, as possessed by sawdust, have a narrower gap between them, reducing heat conduction and interfering with releasing moisture and gas during the torrefaction process. However, the particle size of the cocoa pod shell is larger, and the gap between the particles is also larger.

Fig. 3 Mass and energy yields of torrefied biomass at temperature of 250 °C



Also, the energy yield of the three materials was the opposite of their mass yield. The highest energy yield (89.93%) was achieved by cocoa pods, followed by rice husks of 87.88% and sawdust of 85.16%. The difference in energy yield was affected by an increase in the heating value after torrefaction. The higher the caloric value, the greater the energy yield and the lower the mass yield.

3.4 Proximate and Heating Value Analyses

The torrefaction process changes the physical and thermal properties of the samples. Figure 4 compares the influence of torrefaction on the properties of the three types of biomass. The moisture content is the amount of water in the samples. The higher the moisture content, the lower the calorific value, the more heat loss in the combustion process, and the more tent to degrade by microorganisms. Based on Fig. 4a, cocoa pod shells had the highest moisture content of 11.72% before torrefaction compared with sawdust and rice husk, with almost 9.99% and 10.28%, respectively. After torrefaction, the rice husk had the lowest moisture content of 2.17%, while the cocoa pod shell had the highest of 5.94%. The reduce in the moisture content of the biomass indicates an increase in the quality of the biomass. The lower the moisture content, the easier the fuel to be ignited [19].

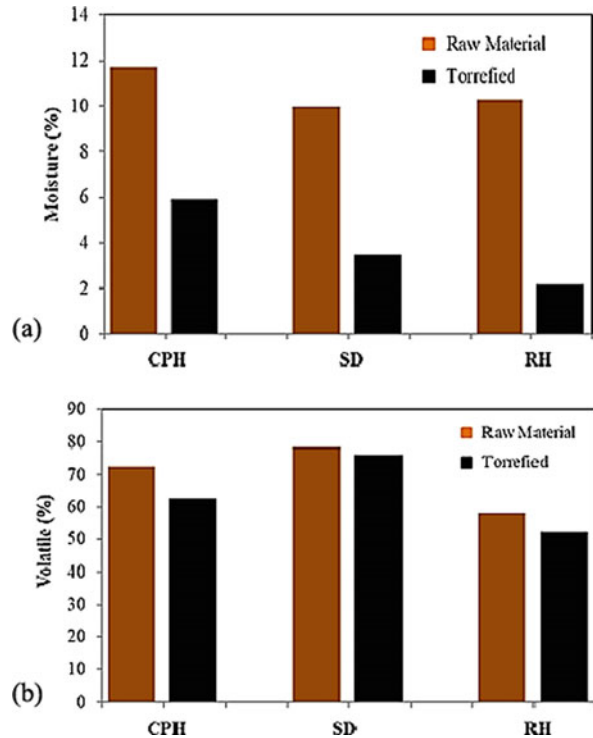
Besides reducing the moisture, torrefaction reduces the volatile components of the samples, although still relatively high after the process. The more volatile matter in the solid fuel, the easier it ignites because of its low ignition temperature. The fact is a major distinguishing factor between the charcoal produced through torrefaction and carbonization. Figure 4b shows that sawdust has the highest volatile matter before and after torrefaction, whereas rice husk has the lowest.

Figure 5a shows the comparison of fixed carbon content among the three materials before and after torrefaction. The highest carbon content in cocoa pod shell was 9.23%, while that of sawdust was 7.98%, and rice husk was 7.59%. The increase in the quality of the three biomasses is indicated by the increase in their fixed carbon content. The highest rise of fixed carbon content was found in sawdust, which was 107%, while cocoa pod shells and rice husk increased by 97% and 98%, respectively. Similar results have been obtained by authors Singh et al. [20] where the fixed carbon content of torrefied biomass increased significantly compared to raw pigeon pea stalk.

Figure 5a shows the comparison of fixed carbon content among the three materials before and after torrefaction. The highest carbon content in cocoa pod shell was 9.23%, while that of sawdust was 7.98%, and rice husk was 7.59%. The increase in the quality of the three biomasses is indicated by the increase in their fixed carbon content. The highest rise of fixed carbon content was found in sawdust, which was 107%, while cocoa pod shells and rice husk increased by 97% and 98%, respectively. Similar results have been obtained by authors Singh et al. [20] where the fixed carbon content of torrefied biomass increased significantly compared to raw pigeon pea stalk.

Ash is the solid inorganic residue obtained after the biomass has completely burnt [21]. The ash component of biomass does not play a part in energy production but

Fig. 4 Proximate analyses of raw and torrefied biomass
a Moisture content;
b Volatile content



causes problems such as fouling and slagging. Figure 5b shows that the ash content of cocoa pod and rice husks increased after torrefaction, while that of sawdust slightly decreased. The increase was due to the low moisture and volatile contents. Rice husk had the highest ash content, at 23.93% before and 30.39% after torrefactions. But the sawdust had the lowest ash content of 3.54% and slightly decreased to 3.74% after torrefactions.

Furthermore, the heating value is one of the critical parameters that indicate the quality of solid fuels and increasing the heating value was one of the goals of the torrefaction. There was an increase in the heating value of the three materials after torrefaction. The increase in heating value is related to the increase in fixed carbon content and reduced volatile matter [22]. Figure 6 shows that the calorific value of cocoa pod shells increased from 16,345 to 21,522 kJ/kg, an increase of 32.7%. The calorific value was the highest, followed by that of rice husk, which rose from 13,097 to 15,376 kJ/kg, an increase of 17.4%, and finally, an increase from 18,478 to 20,268 kJ/kg, in sawdust, representing 9.7% increment. Although the rise in the heating value of sawdust was the lowest, its actual heating value was higher than that of rice husk. In general, the lower the volatile matter in the biomass, the higher the fixed carbon and calorific value, as shown in Figs. 4b, 5a, and 6.

Fig. 5 Proximate analyses of raw and torrefied biomass
a Fixed carbon; **b** Ash content

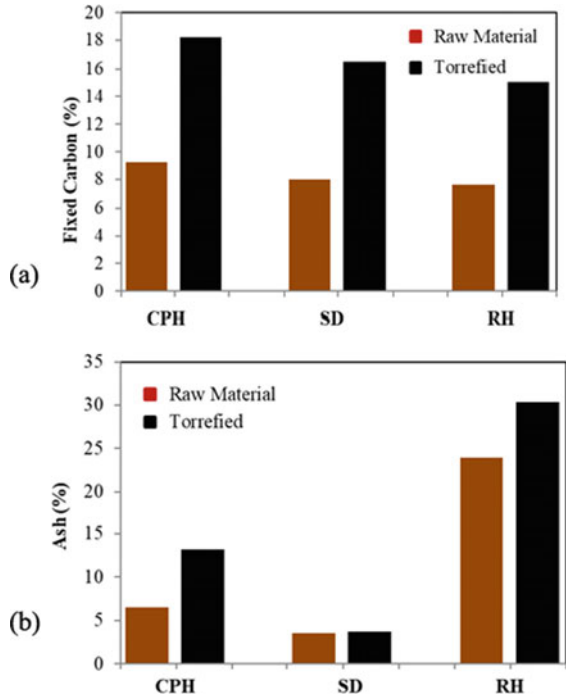
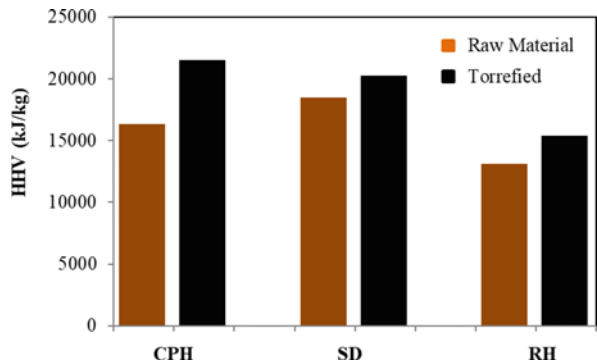


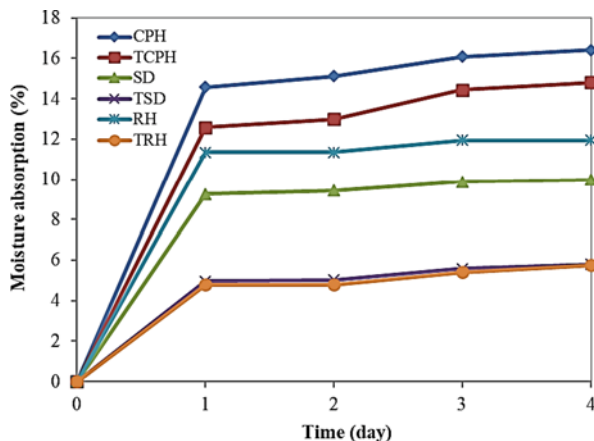
Fig. 6 Heating value of raw and torrefied biomass



3.5 Hydrophobicity

One of the limitations of using biomass is easily absorbed moisture from the air. Hence, the ability to absorb water poses challenges as it requires more time and space for drying. The phenomenon subsequently leads to a decrease in its heating value, making it easier for fungi to grow on it and increasing both the transportation and handling costs before burning [21]. Also, torrefaction process changes the hydrophilic characteristic of the biomass to hydrophobic [14].

Fig. 7 Hydrophobicity of raw and torrefied biomass



The hydrophobicity testing was conducted by placing 2 g of dry sample in a closed container where the humidity was maintained at 73 - 75% using a saturated solution of NaCl. Figure 7 shows the water absorption levels of the samples and the changes after torrefaction.

Based on the figure, sawdust had the lowest ability to absorb water at 9.98% before torrefaction, followed by rice husk at 11.95% and then the cocoa pod shells at 16.41%. Then after torrefaction, their ability to absorb moisture from the air reduced and those of sawdust and rice husk were almost the same, 5.80% and 5.76%, respectively, while the cocoa pod shell had the highest, which was 14.80%. The decrease in the ability to absorb moisture indicates an improvement in the quality of the three biomass.

Studies conducted by Supramono et al. [23], Li et al. [24] and Chen et al. [25], have already proven the increase in the hydrophobicity of biomass after torrefaction using corn stover, bagasse, bamboo, and cotton tree trunks, respectively. Based on those studies, the increase in the hydrophobicity of the biomass after torrefaction was a result of the reduction in the hemicellulose content. According to Supramono et al. [23], hemicellulose has many hydroxyl groups (-OH) which trigger biomass to become polar and easily to form hydrogen bonds with water molecules.

3.6 Thermogravimetry Analysis

Thermogravimetry and differential thermogravimetry curves are usually used to determine the combustion characteristics of solid fuels. The thermogravimetry curves describe mass reduction as a function of time or temperature. However, differential thermogravimetry represents the rate of mass reduction with temperature. Figure 8a and Fig. 8b illustrates the combustion process of the three biomass samples with the results obtained using a TGA Shimadzu 60 at a heating rate of 40 °C/min.

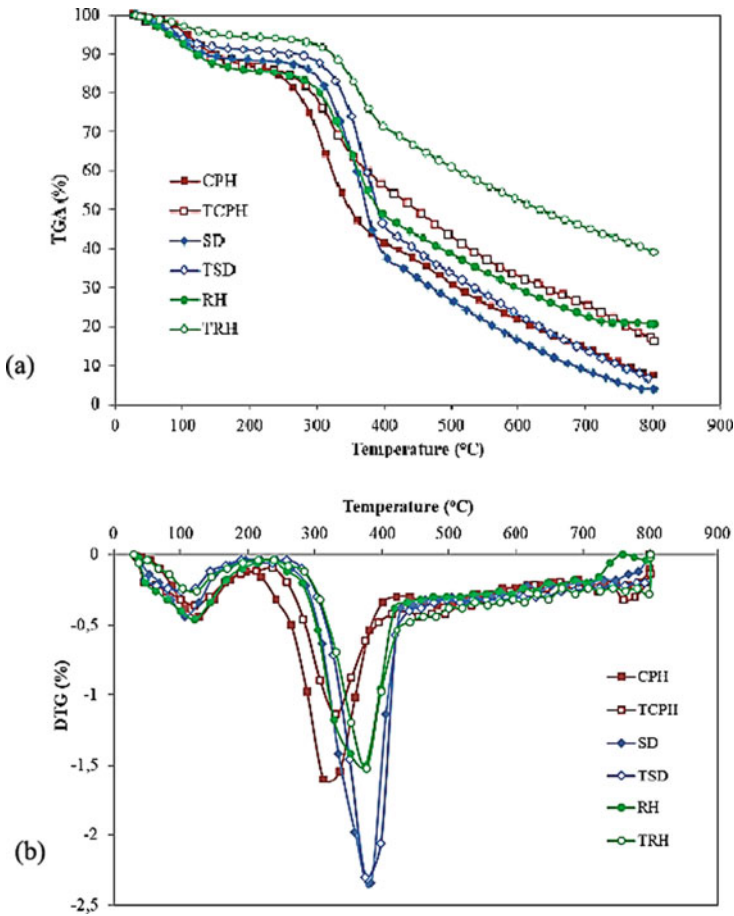


Fig. 8 Curve of raw and torrefied biomass at temperature of 250 °C **a** TG curve; **b** DTG curve

According to Fig. 8, the combustion process consisted of 3 stages - moisture evaporation, devolatilization, and carbon combustion. The evaporation stage is characterized by a rapid reduction in mass at the beginning of heating. Devolatilization is characterized by a rapid mass decline at the middle of the curve. A slow mass reduction represents the carbon combustion stage. These are consistent with the results of the studies conducted by Li et al. [26] and Jiang et al. [27]. All samples had the same combustion pattern. The evaporation stage initially occurred at the initial heating point up to about 150 °C. And the duration of this stage influenced the moisture. Figure 8a shows that the evaporation stage was shorter with torrefied biomass than the raw ones. The fact indicates that the moisture of the torrefied biomass is lower than the untreated ones.

Thermogravimetry and differential thermogravimetry curves are usually used to determine the combustion characteristics of solid fuels. The thermogravimetry curves

describe mass reduction as a function of time or temperature. However, differential thermogravimetry represents the rate of mass reduction with temperature. Figure 8a and Fig. 8b illustrates the combustion process of the three biomass samples with the results obtained using a TGA Shimadzu 60 at a heating rate of 40 °C/min.

Figure 8a shows the effect of volatile content on the profile of the combustion curve. The volatile evaporation and combustion stages of torrefied rice husk were shorter since they have the lowest volatile content. However, the second stage of sawdust was longer because sawdust has a more volatile content. In addition, the TGA curve shows the amount of solid residue left after the combustion is completed. According to Fig. 8b, the rice husk left a solid residue of 39.1%, while sawdust left 4.01% residue, all in the form of solid ash. The result is in accordance with the proximate analysis data shown in Fig. 5b, which shows that the rice husk had the highest ash content after the torrefaction process, while sawdust had the lowest.

Figure 8b shows that all samples in the differential thermogravimetry (DTG) curve have two peaks. The first is the peak of evaporation, and the second is that of volatile release. Also, the effects of moisture content and volatile matter on the samples are shown in Figs. 4a and 4b. The higher the moisture content, the higher the first peak of the DTG curve, and the higher the volatile content, the higher the second peak. Sawdust has the highest peak because, based on the proximate analysis data, it has the highest volatile content of all the biomass samples.

4 Conclusion

In conclusion, the rice husk has the lowest bulk density, while the cocoa pod shell has the highest. Also, the colour changed from light brown to dark brown and black after torrefaction. Furthermore, the sawdust had the highest mass yield, while cocoa pod shells produced the highest energy yield. By torrefaction, some of the improved biomass parameters are moisture and fixed carbon contents, calorific value, and hydrophobicity. The torrefaction process reduced the moisture and volatile contents of the biomass samples. At the same time, the samples increased their fixed carbon contents and calorific values. The rice husk also had the highest ash content before and after torrefaction. The ability of the three biomass samples to absorb water vapour from the air also decreased, thereby becoming hydrophobic. The three samples also undergone a decrease in reactivity. The raw and torrefied rice husks had the highest ash residue after combustion, while sawdust had trivial ash. Finally, the combustion temperature was raised between 20 to 30 °C, and the cocoa pod shell had the lowest combustion temperature, while sawdust had the highest combustion temperature.

References

1. Adhiguna P (2021) Indonesia's Biomass Cofiring Bet. Jakarta

2. Rentizelas AA, Li J (2016) Techno-economic and carbon emissions analysis of biomass torrefaction downstream in international bioenergy supply chains for co-firing. *Energy* 114:129–142. <https://doi.org/10.1016/j.energy.2016.07.159>
3. Miedema JH, Benders RMJ, Moll HC, Pierie F (2017) Renew, reduce or become more efficient? the climate contribution of biomass co-combustion in a coal-fired power plant. *Appl Energy* 187:873–885. <https://doi.org/10.1016/j.apenergy.2016.11.033>
4. Wilk M, Magdziarz A, Gajek M, Zajemska M, Jayaraman K (2017) Combustion and kinetic parameters estimation of torrefied pine, acacia and *Miscanthus giganteus* using experimental and modelling techniques. *Bioresour Technol* 243:304–314. <https://doi.org/10.1016/j.biortech.2017.06.116>
5. Wang L, Barta-Rajnai E, Skreiberg Ø, Khalil R, Czégény Z, Jakab E, Grønli M (2018) Effect of torrefaction on physicochemical characteristics and grindability of stem wood, stump and bark. *Appl Energy* 227:137–148. <https://doi.org/10.1016/j.apenergy.2017.07.024>
6. Wannapeera J, Fungtammasan B, Worasuwanarak N (2011) Effects of temperature and holding time during torrefaction on the pyrolysis behaviors of woody biomass. *J Anal Appl Pyrolysis* 92:99–105. <https://doi.org/10.1016/j.jaap.2011.04.010>
7. Thanapal SS, Annamalai K, Ansley RJ, Ranjan D (2016) Co-firing carbon dioxide-torrefied woody biomass with coal on emission characteristics. *Biomass Conv Biorefinery* 6:91–104. <https://doi.org/10.1007/s13399-015-0166-6>
8. Kai X, Meng Y, Yang T, Li B, Xing W (2019) Effect of torrefaction on rice straw physico-chemical characteristics and particulate matter emission behavior during combustion. *Bioresour Technol* 278:1–8. <https://doi.org/10.1016/j.biortech.2019.01.032>
9. Nhuchhen DR, Basu P, Acharya B (2016) Torrefaction of poplar in a continuous two-stage. Indirectly Heated Rotary Torrefaction. *Energy Fuels* 30:1027–1038. <https://doi.org/10.1021/acs.energyfuels.5b02288>
10. Zhang C, Ho S, Chen W, Xie Y, Liu Z (2018) Torrefaction performance and energy usage of biomass wastes and their correlations with torrefaction severity index. *Appl Energy* 220:598–604. <https://doi.org/10.1016/j.apenergy.2018.03.129>
11. Bergman PCA, Kiel JHA (2005) Torrefaction for biomass upgrading. In: *Energy research center, Netherlands*, pp 17–21
12. Ciolkosz D, Wallace R (2011) A review of torrefaction for bioenergy feedstock. *Biofuels Bioprod Biorefinery* 5:317–329. <https://doi.org/10.1002/bbb>
13. Rousset P, Davrieux F, Macedo L, Perré P (2011) Characterisation of the torrefaction of beech wood using NIRS: combined effects of temperature and duration. *Biomass Bioener* 35:1219–1226. <https://doi.org/10.1016/j.biombioe.2010.12.012>
14. Koppejan J, Sokhansanj S, Melin S, Madrali S (2012) Status overview of torrefaction technologies. *The Netherlands, Enschede*
15. Tumuluru JS, Sokhansanj S, Hess JR, Wright CT, Boradman RD (2011) A review on biomass torrefaction process and product properties for energy applications. *Ind Biotechnol* 7:384–401. <https://doi.org/10.1089/ind.2011.0014>
16. Khan AA, de Jong W, Jansens PJ, Spliethoff H (2009) Biomass combustion in fluidized bed boilers: Potential problems and remedies. *Fuel Process Technol* 90:21–50. <https://doi.org/10.1016/j.fuproc.2008.07.012>
17. Pimchuai A, Dutta A, Basu P (2010) Torrefaction of agriculture residue to enhance combustible properties. *Energy Fuel* 24:4638–4645. <https://doi.org/10.1021/ef901168f>
18. Gucho EM, Shahzad K, Bramer EA, Akhtar NA (2015) Experimental study on dry torrefaction of beech wood. *Energies* 8:3903–3923. <https://doi.org/10.3390/en8053903>
19. Bach Q, Skreiberg Ø (2016) Upgrading biomass fuels via wet torrefaction: a review and comparison with dry torrefaction. *Renew Sustain Energy Rev* 54:665–677. <https://doi.org/10.1016/j.rser.2015.10.014>
20. Singh R, Sarkar A, Chakraborty JP (2019) Effect of torrefaction on the physicochemical properties of pigeon pea stalk (*Cajanus cajan*) and estimation of kinetic parameters. *Renew Energy* 138:805–819. <https://doi.org/10.1016/j.renene.2019.02.022>

21. Basu P (2013) Biomass gasification, pyrolysis and torrefaction (practical design and theory). Academic Press, New York
22. Wilk M, Magdziarz A, Kalembe I (2015) Characterisation of renewable fuels' torrefaction process with different instrumental techniques. *Energy* 87:259–269. <https://doi.org/10.1016/j.energy.2015.04.073>
23. Supramono D, Devina YM, Tristantini D (2015) Effect of heating rate of torrefaction of sugarcane bagasse. *Int J Technol* 7:1084–1093
24. Li M, Li X, Bian J, Xu J, Yang S, Sun R (2015) Influence of temperature on bamboo torrefaction under carbon dioxide atmosphere. *Ind Crop Prod* 76:149–157. <https://doi.org/10.1016/j.indcrop.2015.04.060>
25. Chen D, Zheng Z, Fu K, Zeng Z, Wang J, Lu M (2015) Torrefaction of biomass stalk and its effect on the yield and quality of pyrolysis products. *Fuel* 159:27–32. <https://doi.org/10.1016/j.fuel.2015.06.078>
26. Li H, Xia S, Ma P (2016) Thermogravimetric investigation of the co-combustion between the pyrolysis oil distillation residue and lignite. *Bioresour Technol* 218:615–622. <https://doi.org/10.1016/j.biortech.2016.06.104>
27. Jiang X, Chen D, Ma Z, Yan J (2017) Models for the combustion of single solid fuel particles in fluidized beds: a review. *Renew Sustain Energy Rev* 68:410–431. <https://doi.org/10.1016/j.rser.2016.10.001>

Forecasting Longshore Sediment Transport on a Wave-Dominated Coast Using Various Wave Data Sources



Tania Edna Bhakty, Khusnul Setia Wardani, Nizar Achmad, Titiek Widyasari, and Gregorius Ranggawuni

Abstract Wave data is critical for calculating sediment transport, especially longshore sediment transport. However, wave measurement data is not always available in most areas of the Indonesian ocean, particularly on the Glagah-Congot Coast, Yogyakarta, Indonesia. Because of the breakwater construction, this coast is expected to experience unbalanced longshore sediment transport. Therefore, severe accretion and erosion occurred at certain locations on this coast. This study aims to look at how well ECMWF and ERDDAP wave data can be used to predict the transport of longshore sediment. Furthermore, the CERC equation is applied to calculate longshore sediment transport. These results compare to those of a previous computation utilizing Indian Ocean (JICA) wave data. The study's findings show that all wave data sources show the same trend of longshore sediment transport even though the values differ. Because the significant wave height is mostly from the south, sediment transport on this coast is primarily to the west.

Keywords Longshore sediment transport · ECMWF · ERDDAP

T. E. Bhakty · N. Achmad · T. Widyasari · G. Ranggawuni
Janabadra University, Yogyakarta, Indonesia
e-mail: tania@janabadra.ac.id

N. Achmad
e-mail: nizar_achmad@janabadra.ac.id

T. Widyasari
e-mail: titiekwidyasari@janabadra.ac.id

K. S. Wardani (✉)
National Research and Innovation Agency, Central Jakarta, Indonesia
e-mail: khus001@brin.go.id

1 Introduction

The Glagah-Congot Coast is located in Yogyakarta, Indonesia. Along this coast, there are several big infrastructures, such as Yogyakarta International Airport (YIA) and Tanjung Adikarto Fishing Port. Figure 1 shows the location of this study. This beach is flanked by River Serang and River Bogowonto as well. The wave field along the shore is characterized by swell waves, which are long and generally low waves. With a typical major the height of wave of 1.5 m and wave durations of roughly 10 s, these high-energetic waves are homogeneous in size, direction, and shape.. Furthermore, the net sediment transport comes from the east direction, especially in the dry season (east monsoon) [1]. At the mouths of the two rivers, sediment transport, which is called “longshore sediment transport,” causes problems. The construction of breakwaters on both sides of the Serang River influenced sedimentation on the east side, while erosion on the west side occurred due to a lack of sediment supply. The sedimentation in the river mouth’s navigation channel prevents the port from operating normally. The identical problem exists at the Bogowonto River’s mouth. A sand block blocks the river’s mouth. As soon as the rainy season arrived, the river flow unexpectedly increased, reaching levels that were close to the sand block. The hinterlands are inundated, and flooding occurs near the river’s mouth, putting the airport in jeopardy. To stabilize both sides of the mouth of the river, a double jetty can be constructed [2–8]. The Bogowonto double jetty is currently under construction and should be done by the middle of 2023.



Fig. 1 The location of the study

Longshore sediment transport is one of the most widely used methods in coastal engineering for analyzing the issues requiring the morphodynamic response of coastal areas. This method is also taken into account when designing the Bogowonto jetty and Glagah breakwater. In designing both the Glagah breakwater and Bogowonto jetty, they both used data from the project for Bali Beach Conservation (JICA, 1989). This is due to the difficulty in obtaining wave data. Satellite data is projected to be used as one way for planning coastal constructions.

The purpose of this study is to compare the results of forecasting longshore sediment transport using ECMWF (European Centre for Medium-Range Weather Forecasts) Reanalysis v5 wave data (ERA5), hereinafter referred to as “ERA-Interim,” and ERDDAP-Wavewatch data. Furthermore, the CERC equation is applied to calculate longshore sediment transport. These results compare to those of a previous computation utilizing Indian Ocean (JICA) wave data.

2 Data Collection and Technique

Previous study [1,9], the wave data obtained from wave statistics from the U.S. Navy Marines (USNMCAW) was subject to modification by JICA in 1989. This data consists of wave measurements from 1854 to 1974 using the vessel.

The wave rose data is depicted in Fig. 2 and the wave percentage information is shown in Table 1. Nowadays, climate change occurred in worldwide. Therefore, it is indicated that the wave condition has changed as well. As a result, in order to address the data shortage, we must seek out alternative wave data.

Many online wave data products, including ERA-Interim, ERDDAP-Wavewatch (NOAA), etc., offer satellite data. This data has been used in several studies [10–18], and the use of both data sources can generally be explained. This study aims to analyze longshore sediment transport using global reanalysis data from ERA-Interim and ERDDAP-Wavewatch data from the Administration of Oceanic and Atmospheric Resources.

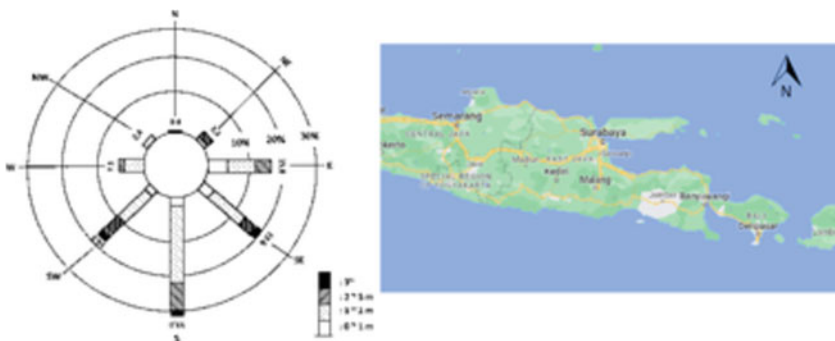


Fig. 2 Ocean of the Indian wave rose (South of Bali) [1]

Table 1 Ocean of the Indian wave rose (South of Bali) [1]

Wave Height	Wave Percentage (%)								
H (m)	N	NE	E	SE	S	SW	W	NW	Total
0-1	0,50	2,50	4,29	4,67	3,30	2,54	0,60	0,50	18,90
1-2	0,30	0,80	7,86	9,89	20,27	7,79	4,64	1,43	52,98
2-3	-	-	3,66	4,48	7,54	5,07	2,46	0,97	24,18
>3	-	-	-	0,56	1,89	1,50	-	-	3,95
Total	0,80	3,30	15,80	19,60	33,00	16,90	7,70	2,90	100,00

In this analysis, wave data from the ERA Interim and the ERDDAP-Wavewatch data from 2010 to 2020 were employed. According to the wave roses in Fig. 3 and the locations of the ERA Interim data, the main wave directions are from the southeast, south, and southwest. 7.9° latitude and 109.5° longitude were the coordinates used for the wave data analysis. Table 2 and Table 3 respectively display the ERA Interim and ERDDAP-Wavewatch data percentages of wave data occurrence.

Figure 4 illustrates the calculation of sediment transport, a simplified coastline layout, and wave direction based on earlier studies. JICA data are used to calculate the wave height, period, and probability with a 1:50 coastal slope. The average diameter of the sediment at Glagah-Congot beach is (d_{50}) 0.2–0.3 mm. Analyzing the longshore sediment transport along Glagah-Congot beach using the CERC equation [19].

$$S = p A H_0^2 C_o K_{rbr}^2 \text{Sin}(\alpha_{br}) \text{Cos}(\alpha_{br}) \tag{1}$$

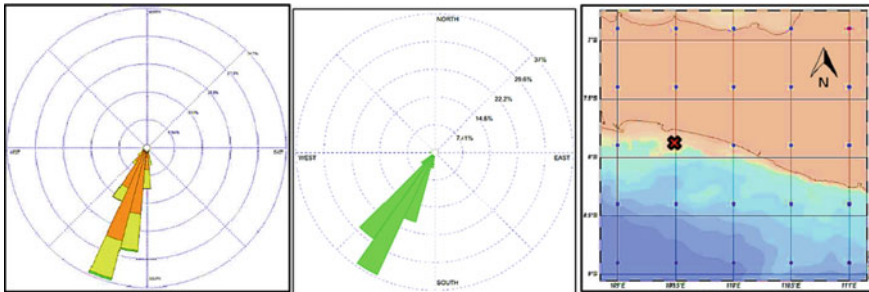


Fig. 3 ERA Interim and ERDDAP-Wavewatch data Wave Rose (2010–2020)

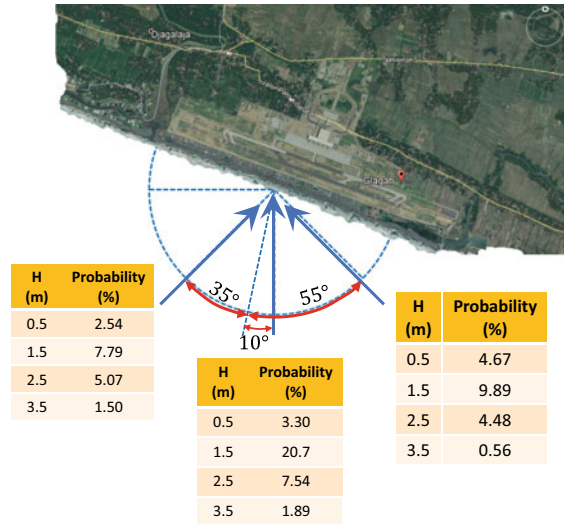
Table 2 Wave Percentage from the ERA Interim

Wave Height	Wave Period	Percentage (%)			
H	H ₀	T	SE	S	SW
0-1	0.5	7.0	0.000	0.209	0.000
1-2	1.5	9.0	3.364	60.807	2.332
2-3	2.5	11.0	2.513	27.897	1.873
>3	3.5	13.0	0.000	0.983	0.021
Total			5.877	89.897	4.226

Table 3 Wave Percentage from the ERDDAP-Wavewatch data

Wave Height		Wave Period		Percentage (%)		
H	H ₀	T	SE	S	SW	
0-1	0.5	7.0	0.000	0.000	0.000	0.000
1-2	1.5	9.0	0.042	0.014	0.002	0.002
2-3	2.5	11.0	0.022	0.011	0.008	0.008
>3	3.5	13.0	0.788	89.287	6.315	6.315
Total			0.852	89.312	6.325	

Fig. 4 Sediment transport calculation using the wave height and probability



where H_0 – significant deep water wave height, p – percentage of wave occurrence, S – longshore sediment transport, and A – CERC coefficient. K_{rbr} – refraction coefficient at breaking area, C_0 – deep water wave celerity, K_{rbr} – refraction coefficient at breaking area, α_{br} – angle of incoming wave at breaking area. We use a coefficient of $A = 0.44 \times 10^6$ in this calculation [19].

Finding the value of K_{rbr} leads one to calculate the incidence wave breaking angle (α_{br}), which is the first step in the estimation of sediment transport. To obtain the value of K_{rbr} , we use the relationship between deepwater wave steepness and the wave breaker height graph [19, 20].

3 The Result and the Discussion of the Research

The waves drive the majority of near-shore circulation and sediment transport in the surf zone and inner continental shelf [21]. Numerous investigations have been conducted on the south coast of Java by numerous institutions over the years. In the

preceding section, the calculations for the waves [9] and [1] were done using data from the Bali coast. The measurements were made by U.S. Navy Marines (USNMCAW) in the deep water in front of Bali’s coastline. Since there are no appreciable differences in the deep water conditions between the two locations, it may be considered that this deep water data is indicative of Glagah beach even though Bali is hundreds of kilometers away. Moreover, this data source only includes deep wave statistics that JICA (1989) has previously adjusted, which will restrict how in-depth the calculations are [22,23].

Using wave data from the Indian Ocean (JICA, 1989) and the CERC equation, the rate of sediment transport in the Glagah-Congot region can be approximated as follows: (see Table 4). Roughly 1.024 million m³/year is directed toward the west, and about 0.731 million m³/year is directed toward the east. The estimated net longshore sediment transport at Glagah-Congot is 0.29 million m³/year to the west based on this rate of sediment transport. It should be emphasized that the formula is still being developed, the wave information (wave height, direction, and event process) are erroneous, and this sediment transport estimate has minimal reliability [1].

Using the same method of calculation, the results of the calculations in Table 4 are used to compare the results of calculations using data from the ERA Interim and ERDDAP-Wavewatch data. Figure 5 shows that even though they have different values, ERA Interim and ERDDAP-Wavewatch data are considered to have the same trend. This is due to the assumption that each wave data calculation is different.

The South dominates the wave’s percentage of all data. A similar tendency is visible in both the ERA Interim and ERDDAP-Wavewatch data. Compared to [9] and [1], the eastward sediment transport of sediment is less. The distribution of wave percentage data for [9] and [1] is relatively uniform, with a wave percentage that has a value that is twice that of the waves in the South-East and South-West directions. The gap between ERA Interim and ERDDAP-Wavewatch data’s wave percentages, which have various data distributions, is the cause of the discrepancy.

Table 4 Sediment Transport at Glagah-Congot

Wave Directions in Deep Water	H_s (m)	Sediment Transport (10^3 m ³ /year)	Total Sediment Transport (10^3 m ³ /year)	Directions of Sediment Transport
South East	0.5	5.2		
	1.5	184.6		
	2.5	298.0		
	3.5	87.2		
			575	West
South	0.5	1.4		
	1.5	147.7		
	2.5	189.2		
	3.5	111.0		
			449.3	West
Transport of Total Sediment to the West			1024.3	West
South West	0.5	5.1		
	1.5	148.4		
	2.5	340.5		
	3.5	237.0		
			731.0	East
Transport of Total Sediment to the East			731.0	East
Net Transport			293.3	West

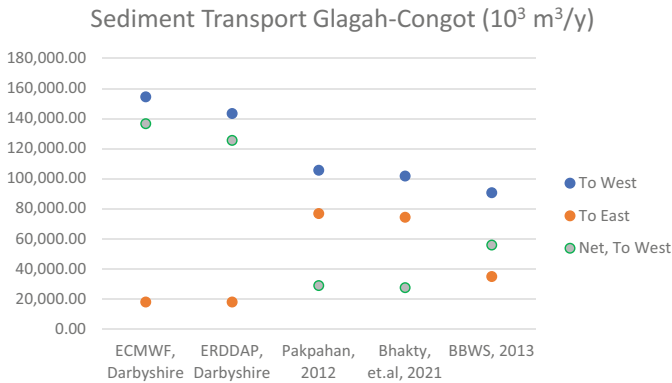


Fig. 5 Sediment Transport Glagah-Congot

The average number of waves that occur in the Southeast and Southwest is only 5%–7%, which is significantly less than the Southwest wave percentage. The results from ERA Interim and ERDDAP-Wavewatch data show very little eastward sediment transport, according to the schematic in Fig. 4.

The ERA Interim percentage was shown to be 25–30% lower in the southeast and southwest directions and approximately three times too high in the south direction when JICA percentage wave height data occurring from vessel observations was compared to ERA Interim data. Additionally, according to ERDDAP-Wavewatch data, the percentage of wave height data occurrences from the south is three times higher than those from JICA. The ERDDAP-Wavewatch data percentage wave height data occurrences, however, are 37% lower in the southwest and 4% lower in the southeast.

When it comes to transporting sediment, the ERA Interim wave data is higher than the ERDDAP-Wavewatch data. Because the significant wave height over the study area is underestimated more when the WAVE WATCH III model is forced by wave than when it is forced by wave from ERA Interim. This fits with the research results of [16].

According to research conducted by [17], ERA Interim Re-analysis Overall, the intermediate has greater temporal homogeneity than the NCEP Climate Forecast System Reanalysis, giving it a more credible model for simulating long-term processes. Therefore, care must be exercised while studying the highest percentiles. Moreover, using the initial conditions from the reanalysis, the assimilating forecast model’s ability to predict future observations is a very useful way to measure its success in this area [18].

4 Conclusion

This study assessed the accuracy of forecasting longshore sediment transport using ERA Interim and ERDDAP-Wavewatch data. The calculation findings from five research projects show the same trend, which is net sediment transfer to the west, based on Fig. 5. This pattern is in accordance with the field circumstances, where the mouth of the river on Yogyakarta's southern coast is unique in that it frequently turns west and the opening is closed by a sand block. Given that the JICA measuring year was quite old and less accurate, the use of satellite data can be taken into consideration. This is a result of climate change worldwide. Some of the effects of this change in the world's climate are a rise in sea level rise, an increase in wave height, an increase in average wind speed, and so on. In general, trends in sediment movement can be calculated using forecasting data from ERA Interim and ERDDAP- This study assessed the accuracy of forecasting longshore sediment transport using ERA Interim and ERDDAP-Wavewatch data. A crucial point to keep in mind is that field measurements must still be made in order to build a coastal structure.

References

1. Bhakty TE, Swasono AH, Yuwono N, Ghalizhan AF, Widayarsi T (2021) Determination of the length of Bogowonto double jetty as the river mouth stabilization. In: IOP conference series: earth and environmental science, vol 930, no 1
2. Oost AP et al (2012) Barrier island management: lessons from the past and directions for the future. *Ocean Coast Manag* 68:18–38
3. Saengsupavanich C (2019) Willingness to restore jetty-created erosion at a famous tourism beach. *Ocean Coast Manag* 178(April)
4. Promngam A, Charusrojthanadech N, Maleesee K, Yamamoto Y (2018) Effect of jetties in northern part of coastal change at Chumphon estuary. In: Proceedings of the international offshore polar engineering conference, vol 2018-June, pp 1379–1386
5. Martinez JO, Pilkey OH, Neal WJ (1990) Rapid formation of large coastal sand bodies after emplacement of Magdalena river jetties, northern Colombia. *Environ Geol Water Sci* 16(3):187–194
6. Sawaragi T, Kobune K (1970) Effect of jetties on water level fluctuation at a river mouth. *Coast. Eng. Japan* 13(1):153–159
7. Garel E, Sousa C, Ferreira Ó (2015) Sand bypass and updrift beach evolution after jetty construction at an ebb-tidal delta. *Estuar Coast Shelf Sci* 167:4–13
8. Van Rijn L. (2013) Erosion processes, no March, pp 1–33
9. Pakpahan IB (2014) Analisis transpor sedimen menyusur pantai dengan menggunakan metode grafis pada pelabuhan perikanan tanjung adikarta J Maroso 1(June 2013):7–14
10. Janssen P. (2000) Chapter 3 ECMWF wave modeling and satellite altimeter wave data. Elsevier *Oceanogr Ser* 63(C):35–56
11. Saket A, Etemad-Shahidi A, Moeini MH (2013) Evaluation of ECMWF wind data for wave hindcast in Chabahar zone. *J Coast Res* 65(65):380–385
12. Reikard G, Pinson P, Bidlot JR (2011) Forecasting ocean wave energy: te ECMWF wave model and time series methods. *Ocean Eng* 38(10):1089–1099
13. Lv X, Yuan D, Ma X, Tao J (2014) Wave characteristics analysis in Bohai Sea based on ECMWF wind field. *Ocean Eng* 91:159–171

14. Janssen PAEM, Hansen B, Bidlot JR (1997) Verification of the ECMWF wave forecasting system against buoy and altimeter data. *Weather Forecast* 12(4):763–784
15. Elkut AE, Taha MT, Abu Zed ABE, Eid FM, Abdallah AM (2021) Wind-wave hindcast using modified ECMWF ERA-Interim wind field in the Mediterranean Sea. *Estuar Coast Shelf Sci* 252(February):107267
16. Sangalugeme C, Luhunga P, Kijazi A, Kabelwa H (2018) Validation of operational WAVE-WATCH III wave model against satellite altimetry data over South West Indian ocean off-coast of Tanzania. *Appl Phys Res* 10(4):55
17. Stopa JE, Cheung KF (2014) Intercomparison of wind and wave data from the ECMWF reanalysis interim and the NCEP climate forecast system reanalysis. *Ocean Model* 75:65–83
18. Dee DP et al (2011) The ERA-Interim reanalysis: configuration and performance of the data assimilation system. *Q J R Meteorol Soc* 137(656):553–597
19. O. F. The and USACE, “SHORE PROTECTION MANUAL US Army Corps”, 4th ed. *Coast Eng* 1, vol 2, p 652
20. Goda Y (1970) On the arrangement of wave breaking indices. *Proc. Japan Soc. Civ. Eng.* 1970(180):39–49
21. Wright LD, Boon JD, Kim SC, List JH (1991) Modes of cross-shore sediment transport on the Shoreface of the middle Atlantic bight. *Mar Geol* 96(1–2):19–51
22. C. Report (2007) Indonesia : South Java flood control sector project Asian development bank, no November
23. BBWS Serayu Opak-TU Delft, “Project Yogya” (2016)

Literature Review on Covid-19 Pandemic Emergency Response



Afiqoh Akmalia Fahmi, Gustisia Rahmi Nastiti, Eko Setiawan,
and Arinda Soraya Putri

Abstract Covid-19 is a worldwide epidemic that has affected a number of countries. The purpose of this article is to disseminate information on the COVID-19 Pandemic Emergency Response. A Literature Review on the Emergency Response to the COVID-19 Pandemic was done to attain this purpose. Data from the CDC, Bioscience, Lancet, Nature, Oxford, NEJM, Cell, Science, Wiley, JAMA, BMJ, Elsevier, MedRxiv, MDPI, and Science Direct were obtained through a search process using the Google Scholar search engine with databases from CDC, Bioscience, Lancet, Nature, Oxford, NEJM, Cell, Science, Wiley, JAMA, BMJ, Elsevier, MedRxiv, MDPI, and According to the studies conducted, each government's emergency response to the COVID-19 Pandemic differs. Contact tracking, monitoring asymptomatic contacts, coordination, isolation, quarantine, limiting access in and out of the region, and arranging funds to aid the economy are among the measures adopted. The advantages of the COVID-19 Emergency Response Abroad should help improve the COVID-19 Emergency Response in Indonesia.

Keywords Literature Review · Coronavirus · COVID-19 · Emergency Response

1 Introduction

As of April 2020, there were more than 1,200,000 cases of COVID-19 worldwide, resulting in more than 67,000 fatalities [1]. Cures to stop this virus do not exist yet. In order to address the unanticipated spread of COVID-19 and attempt to lessen its negative social and physical effects, a methodical approach is needed at this time. Anxiety has spread throughout society as a result of the virus pandemic [2]. The authors are interested in performing this study since there hasn't been a literature

A. A. Fahmi · G. R. Nastiti · E. Setiawan (✉) · A. S. Putri
Department of Industrial Engineering, Universitas Muhammadiyah Surakarta, Surakarta, Jawa Tengah, Indonesia
e-mail: es268@ums.ac.id

© Institute of Technology PETRONAS Sdn Bhd 2024
B. S. Mohammed et al. (eds.), *Proceedings of the International Conference on Emerging Smart Cities (ICESC2022)*, Lecture Notes in Civil Engineering 324,
https://doi.org/10.1007/978-981-99-1111-0_34

review on the COVID-19 Pandemic Emergency Response up to May 2020. Findings on the emergency response to the COVID-19 pandemic up to this point are reviewed in this article to provide information. Researchers, the government, and healthcare professionals can use the findings of this review as a guide when initiating COVID-19 Pandemic Emergency Response activities and forming new habits around health protocols to stop the spread of this virus. It is necessary to unify the COVID-19 Pandemic Emergency Response System in order to simultaneously reduce the number of cases and the spread of this epidemic [3, 4].

The information gathered from the articles covers the COVID-19 Pandemic Emergency Response, from the virus's early 2020 emergence until May 2020. The systematic literature review approach, which adheres to the guidelines established in each procedure, is used to identify these data. It can be used to conduct reviews and identify articles systematically. It is envisaged that the identification results will contribute to the body of knowledge on the application of the SLR approach in identifying journals because the SLR method can eliminate subjective identification [5]. The goal of placing these numerous journals in different nations linked to COVID Emergency Response is to improve COVID-19 Emergency Response in Indonesia by taking steps to combat the COVID-19 Pandemic.

2 Method

The COVID-19 Pandemic Emergency Response undertaken by many nations is the subject of this study, both the international, national, and governmental emergency response. Then, based on the research topic, choose one or more research questions [6]. The Google Scholar literature search engine (<https://scholar.google.com>) was used for the search. Other literature databases, including the CDC, Bioscience, Lancet, Nature, Oxford, NEJM, Cell, Science, Wiley, JAMA, BMJ, Elsevier, MedRxiv, MDPI, and ScienceDirect, are available on the Google Scholar display for searching for journals or information regarding COVID-19. A Phase I Journal search using the keywords "COVID-19" OR "Covid-19" OR Coronavirus OR "Corona Virus" OR Coronaviruses OR "2019-nCoV" OR "Corona Virus" OR "Coronavirus". Phase II, which is the result of Phase I, journal searches using the keywords "Emergency Response" OR "People Under Surveillance" OR "Patient Under Surveillance" OR "Asymptomatic" [7]. The second stage is Review 1 to identify and analyze the journal output or the Exclusion Criteria. The results of a review will be selected again in review 2, where analysis will be carried out in terms of abstracts, keywords, and conclusions, as well as content analysis, called inclusion criteria. The remaining results in Review 2 will be analyzed in Review 3, which will explore in depth the contents of the writings in the study. Journal selection is made by assessing the quality of journals based on a list of Quality assessments (QA). The data collected will be analyzed to show the answers to the Research Questions or research questions.

3 Result

3.1 Search Process Result

Table 1 shows the Search Process Result in the journal database. The search process yielded 107 scientific articles. The search for scientific papers is followed by a review stage twice.

Table 2 shows the grouping by journal type. There are five types of journals, namely original research with 31 articles, review articles with nine articles, short reports with 42 articles, case studies with 16 articles, and methodologies with nine articles. The grouping of journal types aims to make it easier to see the kind of data or journal obtained through the search process. From the results of collection by journal type, the most presenting data on the COVID-19 Pandemic Emergency Response is the short report/letter because the researcher presents up-to-date research data so that the researcher makes the research concise and actual, as well as in-depth research. Will be directly asked to those who have a related knowledge concentration.

From the results of grouping by journal type, the most presenting data on the COVID-19 Pandemic Emergency Response is the short report/letter because the researcher presents up-to-date research data so that the researcher makes the research concise and actual as in-depth research. Will be directly asked to those who have a related knowledge concentration.

Table 1 Search Process Results

Search Stage		Stage 1	Review 1	Review 2	QA
Journal Article Database	BMJ	12	12	12	6
	Bio science	1	1	1	1
	Cell	1	1	1	1
	JAMA	5	5	5	4
	Journal of Hospital	3	3	3	3
	Lancet	14	14	11	7
	MDPI	1	1	1	1
	Nature	3	3	2	2
	NEJM	1	1	1	1
	Oxford	8	8	7	7
	Science Direct	52	47	40	30
	Science	1	1	1	0
	WHO	3	3	3	2
	TOTAL	107	101	90	67

Table 2 Grouping by Journal Type

No	Journal Type	Sub-Total
1	Original Research	31
2	Review Articles	9
3	Short reports/letter	42
4	Case studies	16
5	Methodologies	9
Total		107

3.2 Selection Results by Applying Inclusion and Exclusion Criteria

The search process results will be selected based on the exclusion and inclusion criteria. Exclusion criteria include journals related to “COVID-19 Pandemic Emergency Response”, journals published in the 2015–2020 range, journals that are by the formulation of the problem, are conferences or journals. Inclusion criteria include journals with abstracts related to COVID-19 Pandemic Emergency Response, journals with keywords that contain one of the keywords for COVID-19 Pandemic Emergency Response, and journals with shared paper content or formats. This process leaves 67 journals, and then a Quality Assessment is carried out.

3.3 Quality Assessment Result

Journals found will be assessed based on the following quality assessment criteria questions:

- 1) QA1: Does the journal provide information on Indonesia’s latest conditions regarding the COVID-19 pandemic emergency response?
- 2) QA2: Does the journal provide information on the international emergency response to the COVID-19 pandemic?
- 3) QA3: Does the journal include information on suggestions for changes to the emergency response to the COVID-19 pandemic?

Each journal will be given an answer score below for each of the questions above.

Y (Yes): for information and methods written in the journal.

N (Not): for information and methods not listed.

Table 3 shows the results of the Quality Assessment of 67 selected journal articles to show whether or not the data was used in this study. The results of the Quality Assessment show that from 67 journals, the information that can be used in this study are 63 journals.

Symbol description:

Table 3 Quality Assessment Results

Author	QA 1	QA 2	QA 3	Result
Chen et al., 2020	N	Y	Y	✓
Barret et al., 2020	N	Y	Y	✓
Driggin et al., 2020	N	Y	Y	✓
Zhu et al., 2020	N	Y	Y	✓
Jin et al., 2020	N	Y	Y	✓
Blomberg & Lauer, 2020	N	N	Y	✗
Fadel & Descatha, 2019	N	Y	Y	✓
Ebrahim et al., 2020	N	Y	Y	✓
S. Chen et al., 2020	N	Y	Y	✓
Krishnakumar & Rana, 2020	N	Y	Y	✓
Aluga, 2020 [9]	N	Y	Y	✓
Arain et al., 2020	N	Y	Y	✓
Holland et al., 2020	N	Y	Y	✓
Ekzayez et al., 2020 [10]	N	Y	Y	✓
Makurumidze, 2020	N	Y	Y	✓
Elachola et al., 2020	N	Y	Y	✓
Carinci, 2020	N	Y	Y	✓
Bedford et al., 2020	N	Y	Y	✓
Petersen et al., 2020	N	Y	Y	✓
Guan et al., 2020	N	Y	Y	✓
Kucharski et al., 2020	N	N	Y	✗
Lee et al., 2020	N	Y	Y	✓
Breidablik et al., 2020	N	Y	Y	✓
Turer et al., 2020	N	Y	Y	✓
Meghana et al., 2020	N	Y	Y	✓
Laskay et al., 2020	N	Y	Y	✓
Ha et al., 2020 [12]	N	Y	Y	✓
Hellewell et al., 2020	N	Y	Y	✓
Li et al., 2020	N	Y	Y	✓
Mouchtouri et al., 2020	N	Y	Y	✓
Cao et al., 2020	N	Y	Y	✓
Yan et al., 2020	N	Y	Y	✓
Lu et al., 2020	N	N	Y	✗
Hirschhorn et al., 2020	N	Y	Y	✓
Koo et al., 2020	N	Y	Y	✓
Pedersini et al., 2020	N	Y	Y	✓
Pan et al., 2020	N	Y	Y	✓

(continued)

Table 3 (continued)

Author	QA 1	QA 2	QA 3	Result
Hoefler et al., 2020	N	Y	Y	✓
Wee et al., 2020	N	Y	Y	✓
Razai et al., 2020	N	Y	Y	✓
Douglas et al., 2020	N	Y	Y	✓
Thomas et. al., 2020	N	Y	Y	✓
Ali et al., 2020	N	Y	Y	✓
Aruru et al., 2020	N	Y	Y	✓
Algaissi et al., 2020 [13]	N	Y	Y	✓
Kim et al., 2020	N	Y	Y	✓
World Health Organization (WHO)	N	Y	Y	✓
Gostin et al., 2020	N	Y	Y	✓
Watkins, 2020	N	X	Y	✗
Vimercati et al., 2020	N	Y	Y	✓
Kinner et al., 2020	N	Y	Y	✓
Patrikar et al., 2020	N	Y	Y	✓
Pandey et al., 2020	N	Y	Y	✓
Wang et al., 2020 [15]	N	Y	Y	✓
Djalante et al., 2020 [4]	Y	Y	Y	✓
Bachireddy et al., 2020	N	Y	Y	✓
Cheung et al., 2020	N	Y	Y	✓
World Health Organization (WHO)	N	Y	Y	✓
Wu et al., 2020	N	Y	Y	✓
Nguyen & Vu, 2020 [16]	N	Y	Y	✓
Balibrea et al., 2020	N	Y	Y	✓
Huang et al., 2020	N	Y	Y	✓
Bavel et al., 2020	N	Y	Y	✓
Kaplan et al., 2020	N	Y	Y	✓
Lepelletier et al., 2020	N	Y	Y	✓
Viswanath & Monga, 2020	N	Y	Y	✓
Goniewicz et al., 2020 [7]	N	Y	Y	✓

✓: For journals or data used in research. The journal was chosen because it has problems, approaches, and sufficient information for data selection.

4 Data Analysis

This stage answers the Research Question (RQ) and discusses the results of the types of handling and evaluation that emerged from the COVID-19 Pandemic Emergency Response.

RQ1: “What is the Current Condition of Emergency Response in Indonesia?” [4] is the only article containing information on emergency response in Indonesia. According to the article, the emergency response up to May 2020 is carried out by the national government, religious-based organizations, and communities.

After the initial reports of infection, Indonesia began to realize the turbidity of the situation. Since then, the National Government has issued various policies and actions to deal with COVID-19, including appointing 100 domestic public hospitals as Referral Hospitals on March 3, 2020. President Joko Widodo announced that Indonesia would carry out large-scale testing by conducting rapid detection tests on citizens. This test will use a recently developed test kit based on serology. Results will come out in 10–30 min, which is much faster than a PCR test. The National Disaster Management Agency (BNPB) has been assigned to work with the Ministry of Health to disseminate Covid-19 information through various media platforms, including SMS; Form a rapid response team; Provide logistics, materials, and health facilities; Supervise potential new cases of Covid-19; And in collaboration with the Indonesian National Armed Forces, the Indonesian National Police, and the Ministry of Health. The Minister of Finance has made six significant decisions, namely: (1) The decision to expand labour insurance (BPJS Tenaga Kerja) for job losses related to COVID-19, namely a 3-month cash transfer program where affected workers are entitled to Rp. 1 million per month, (2) A big push for banks to relax payments from certain business groups that are too risky to be excluded from the supply chain, such as Aviation, tourism, hotels, restaurants, shipping and transportation, (3) Through a counter-cyclical policy, the government decided to loosen fiscal policy by widening the 2020 State Budget deficit to around 2.5% of GDP from the original plan of 1.76% of GDP, (4) The choice to increase labor insurance (BPJS Tenaga Kerja) for job losses associated with COVID-19 is a 3-month cash support program under which impacted workers are eligible for Rp. 1,000,000 each month, (5) There has been a significant push for banks to loosen payment restrictions for several industry sectors, such as aviation, tourism, hotels, restaurants, shipping, and transportation, which are too dangerous to be excluded from supply chains, and (6) The administration chose to loosen fiscal policy through a counter-cycle approach, increasing the 2020 state budget deficit from the original plan of 1.76% of GDP to roughly 2.5% of GDP. The Indonesian Ulema Council (MUI) has issued Fatwa Number 14 of 2020, containing the implementation of worship in the COVID-19 pandemic situation to secure and prevent the spread of disease among Muslims. Digital Media has initiated information sharing and journalists and the media industry educated the public about COVID-19. This media movement aims to disseminate various educational content massively to combat the spread of the Coronavirus in Indonesia. Through this networked work, it is hoped that multiple important messages in controlling the spread of the Coronavirus

can be spread widely and quickly reach all levels of society. Communities, in the meantime, is expected to stay home, always wash their hands more, and practice social distancing.

The response, on the other hand, had several shortcomings: (1) Lack of data transparency may have led to the actual number of cases being underreported or a possible spread of the exact number of cases detected, but not the actual number of infections, which could go undetected due to, for example, lack of proper diagnosis. Such misinformation could seriously hinder future government responses. (2) Among testing kits developed, none has passed clinical trials without any clinical judgment of factual specification and sensitivity. Some reports indicate that other coronaviruses, or dengue fever, may give false positive results. (3) The current capacity of the health system is still below the ability to cope with the pandemic. (4) Various international mass media and foreign agencies outside Indonesia have even questioned the ability of Indonesian scientists and medical practitioners, as well as the existence of technical facilities and sufficient skills to detect and diagnose the disease. (5) Testing process runs very slowly because the Government is passive in conducting diagnostic testing. Health infrastructure, particularly health laboratories in Indonesia, has been identified as one of the weakest problems in the Indonesian health system. The spread of COVID-19 has exposed these health infrastructure gaps. (6) In the early phase of the outbreak, it was clear that the Government's scepticism and doubts, or even denial of the potential for a pandemic to occur in Indonesia, had a direct impact on the public awareness about the pandemic risks. This is coupled with relatively low awareness and training about the pandemic, although several socializations have been facilitated, for example, by the Ministry of Health. (7) Public perception of the risk of COVID-19 may be low despite the complex and rapid flow of information in recent times since January 2020. (8) The low risk perception of the virus, at least in the early stages, also creates an unfavourable response, which poses a big problem for the Government when deciding whether extreme measures should be taken to contain the spread of the virus or not. When schools closed nationwide, some families decided to leave for mass family vacations and return to their hometowns. WFH (work from home) as a relatively contemporary term is slowly coming in. (9) The process of self-isolation is also a new norm that almost never becomes a general reflection of Indonesia's sub-culture, which is different from Japan, for example. This is multiplied by the number of informal workers and the types of professions that do not allow one to work from home to earn a living. (10) Public misinformation and lack of intergovernmental communication trigger misleading interpretations through instant social media tools.

RQ2: “How is the Emergency Response that Has Been Carried Out in Abroad?”

Table 4 shows the Emergency Responses carried out in several countries the author has studied, including European countries, Australia, Singapore, the United States, Kenya, Syria, South Korea, Saudi Arabia, Japan, Taiwan, and Vietnam. However, the author only examines the advantages of Emergency Response in each country, and it has not been carried out in Indonesia.

Table 4 List of Scientific Articles along with emergency response policies

Authors	Advantages
[7] - Europe	Temporary closure of outside arrivals Counting fake news in a timely, transparent and fact-based manner
[8] - Singapore	Implement an earlier emergency response mechanism
[10] - Syria	IHD has initiated a project to establish 17 community-based isolation centers with a capacity of 1,400 beds which are expected to be ready in the first week
[11, 12] – South Korea	<ol style="list-style-type: none"> 1. The government utilizes digital technology through special applications, GPS, CCTV, and track records of credit card transactions in tracking and tracing to limit the spread of the COVID-19 virus 2. The K-walk-thru testing method is available in two chambers: negative and positive pressure chambers. Medical personnel will examine patients who are in separate booths. Through this method, the government can collect samples quickly and safely and reduce hospitals' burden 3. To reduce the risk of transmission to medical personnel, South Korea applies a “phone booth” method. Patients consult with doctors and nurses by telephone in separate rooms
[13] - UEA	<ol style="list-style-type: none"> 1. All international and domestic air travel, sporting events, and workplaces (except the security and health sector) are suspended 2. Digital health is rapidly being activated and used for several services, such as the “My Health” application, which allows people to seek medical help and receive medical prescriptions without the need to visit a health centre
[14] - Japan	<ol style="list-style-type: none"> 1. A complete contact survey should be carried out by the community health centre (Hokenjo), and identified patients should be reported to the prefectural government and isolated 2. The government is also strengthening travel bans to and from other countries 3. Preliminary guidance is effective in identifying truly infected patients and groups, preventing panicked people from rushing to the hospital for PCR testing 4. Puskesmas (Hokenjo) has deep expertise in conducting sick contact surveys, which have been established through tuberculosis management

(continued)

Table 4 (continued)

Authors	Advantages
[15] - Taiwan	<ol style="list-style-type: none"> 1. Taiwan’s well-resourced healthcare system and public emergency services don’t waste any time in putting 124 health protocols into practice, including border control from the air and sea, case identification (using new data and technology), quarantine of suspicious cases, proactive case finding, resource allocation (assessing and managing capacity), public assurance and education when combating misinformation, negotiations with other countries and territories, and formulation of policies on sc 2. The National Health Insurance Administration (NHIA) and the National Immigration Agency combine the patient’s last 14 days of travel history with information from their NHI identity card, enabling the government to monitor people who are at high risk due to recent travel activity in the impacted area. Those classified as high risk were electronically monitored via their mobile phones (while under home quarantine) 3. The NHIA database was enlarged to include information on patients from China, Hong Kong, and Macau’s most recent 14 days of travel 4. Foreigners can fill out a health declaration form by scanning a QR code that connects to an online form before leaving or upon arrival at the Taiwan airport thanks to the entry quarantine system, which has been put into place. The mobile health declaration card is then SMS-sent to a phone via a local telecom provider, enabling quicker and less-dangerous immigration clearance for them 5. The government declared that the patient’s travel history will be available to all Taiwanese hospitals, clinics, and pharmacies

Every nation in the COVID-19 Pandemic Emergency Response has its own system. Based on the technology employed, governmental rules, and health procedures, each nation has advantages—excellence in Digital Technology in Emergency Response in Taiwan, South Korea, and Saudi Arabia, for example. The nation keeps track of and keeps tabs on its inhabitants’ whereabouts using a citizen database and GPS. This can limit the outbreak’s immediate spread.

Before this virus spread, Singapore and Taiwan launched Emergency Response. The country expects an unexpected space because of its proximity to China. The security of its citizens and medical professionals is highly valued in Japan. Government regulations mandate that people examine their health at the Puskesmas as a first step in order to reduce the surge in patients in hospitals.

RQ3: What Are the Recommendations for Applying Methods, Techniques or Models for “COVID-19 Pandemic Emergency Response?”

The recommended action proposed by the researcher is based on a review of the studies. The object of handling groups these recommendations. Table 5 shows strategic guidance in the Covid-19 emergency response from various scientific article reviews. The results of the study got six recommendations in the Covid-19 Emergency Response.

Table 5 Recommended methods, techniques, or models in COVID-19 Emergency Response

No	Recommendation
1	Screening for symptoms such as fever and respiratory problems in the last 14 days after travelling outside the area with Digital Technology such as applications using Indonesian citizen databases, GPS, CCTV, track records of credit card transactions, and SMS services
2	The online clinic was created to facilitate patient triage. Free online consultations effectively ease the workload of medical personnel and enable early detection of potential cases
3	Require residents to first consult with officers at official COVID-19 call centres or visit local clinics or first-rate facilities
4	Make a policy to close entry access for foreign nationals. Policy making should be based on integrating resources, social mobilization, financial inputs, supply of medicines for vaccine development, and international cooperation
5	Early detection and rapid response to new clusters aimed at preventing the spread of infection by conducting contact tracing
6	All shopping centres are required to limit the number of shoppers at any given time and with a minimum social distancing requirement of 1.5 m

5 Conclusion

Based on the findings of the research, it has been determined that each nation's emergency response to the COVID-19 pandemic differs from the others. Contact tracing, managing asymptomatic contacts, coordination, isolation, quarantine, preventing entry into and out of certain locations, and setting aside money to support the economy are some of the measures adopted. The COVID-19 transmission prevention system, the COVID-19 protection system, the protection and control processes, and handling if exposed to COVID-19 are some of the aspects of the Emergency Response System that have been examined. It is anticipated that the benefits of the COVID-19 Emergency Response Overseas will help to improve the COVID-19 Emergency Response in Indonesia.

References

1. Spinazzè A, Cattaneo A, Cavallo DM (2020) COVID-19 Outbreak in Italy: protecting worker health and the response of the Italian industrial hygienists association. *Ann Work Expo Health* 64:559–564
2. Amirullah AK, Kartinah K (2020) Penanganan Kecemasan Pasien Survivor Covid-19 Intensive Care Unit: Literature Review. *Seminar Nasional Keperawatan Universitas Muhammadiyah Surakarta*, 8–15
3. Triandini E, Jayanatha S, Indrawan A, Werla Putra G, Iswara B (2019) Metode Systematic Literature Review untuk Identifikasi Platform dan Metode Pengembangan Sistem Informasi di Indonesia. *Indones J Inf Syst* 1:63
4. Djalante R et al (2020) Review and analysis of current responses to COVID-19 in Indonesia: period of January to March 2020. *Progr Dis Sci* 6:100091

5. Putri AS, Hisjam M (2019) Research development of sustainable supply chain management: a comparative study. In: AIP Conference Proceedings vol. 2097. American Institute of Physics Inc.
6. Wahono RS (2015) A systematic literature review of software defect prediction: research trends, datasets, methods and frameworks. *J Softw Eng* 1:1–6
7. Goniewicz K et al (2020) Current response and management decisions of the European union to the COVID-19 outbreak: a review. *Sustainability* 12:3838
8. Pathirathna R, Adikari P, Dias D, Gunathilake U (2020) Critical preparedness, readiness and response to COVID-19 pandemic: a narrative review. *J Admin Kesehatan Indones* 8:21
9. Aluga MA (2020) Coronavirus disease 2019 (COVID-19) in Kenya: preparedness, response and transmissibility. *J Microbiol Immunol Infect* 53:671–673
10. Ekzayez A et al (2020) COVID-19 response in northwest Syria: innovation and community engagement in a complex conflict. *J Public Health (Bangkok)* 42:504–509
11. Sari MI (2020) Kebijakan Korea Selatan dalam Meratakan Kurva COVID-19 tanpa Lockdown: Sebuah Pelajaran. The Habibie Centre
12. Ha K-M (2020) Emergency response to the outbreak of COVID-19: the Korean case. *Microbes Infect* 22:159–161
13. Algaissi AA, Alharbi NK, Hassanain M, Hashem AM (2020) Preparedness and response to COVID-19 in Saudi Arabia: building on MERS experience. *J Infect Public Health* 13:834–838
14. Okazawa M, Suzuki S (2020) Japanese tactics for suppressing COVID-19 spread. *Public Health* 186:6–7
15. Wang CJ, Ng CY, Brook RH (2020) Response to COVID-19 in Taiwan: big data analytics, new technology, and proactive testing. *JAMA - J Am Med Assoc* 323:1341–1342
16. Nguyen THD, Vu DC (2020) Summary of the COVID-19 outbreak in Vietnam – lessons and suggestions. *Travel Med Infect Dis* 37:101651

Investigation on the Properties of Reclaimed Asphalt Pavement Rejuvenated with Rubber Seed Oil



Nur Izzah Batrisyia Binti Mohd Yusof, Abdul Muhaimin Memon, and Muslich Hartadi Sutanto

Abstract Reclaimed asphalt pavement (RAP) lacks the volatility and became very hard over time due to aging effects. Rejuvenation is one of the methods used in the recycling of aged asphalt pavement to recover its original properties. The study aims to investigate the optimum RSO content to rejuvenate aged 60/70 grade binder and study their compatibility as well as microstructural properties of the binders. The conventional tests showed that the more RSO added, the softer the binder becomes. However, referring to the criteria limitations for both softening point and penetration tests for the 60/70 binder, an optimum percentage of RSO which is 3.25% has been determined. The storage stability test on the 0% and 3% RSO-rejuvenated samples show that the properties enhancement by RSO proves the compatibility of the binder. FTIR and GC–MS chemical characterization has shown important functional groups and chemical compounds that improve the volatility and soften the binder to its original properties. The responsible compounds recognized are palmitic acid, aromatics, oleic acid, oleamide, phthalic acid, disulfides, secondary amine, and aliphatic iodo-compound. Rejuvenation of RAP with RSO has had the bee structures, white spots, and peri-phase decreased while the perpetua phase increased through AFM surface analysis. AFM study concluded that the morphological properties of RAP has been altered by RSO rejuvenation.

Keywords Reclaimed asphalt pavement · Rejuvenator · Rubber seed oil · Bitumen · Morphology · Storage stability

N. I. B. B. M. Yusof (✉) · A. M. Memon · M. H. Sutanto
Department of Civil & Environmental Engineering, Universiti Teknologi PETRONAS, 32610
Perak, Malaysia
e-mail: nur_17008664@utp.edu.my

A. M. Memon
e-mail: abdul_22001390@utp.edu.my

M. H. Sutanto
e-mail: muslich.sutanto@utp.edu.my

1 Introduction

Asphalt being one of the components of refined fossil fuels, has been significantly contributing to the increasing demand of fossil fuel. The use of reclaimed asphalt pavement (RAP) is a highly recommended option to improve asphalt pavement quality over time which also reduce production cost, protects the environment from more wastes, and sustains land spaces [1]. RAP tends to have decreased maltenes and elasticity which makes the pavement more brittle and increases the risk of collapsing. RAP stiffness can be effectively reduced by using rejuvenators such as vegetable oils, *Jatropha curcas*, corn oils, and soybean oil compared to chemical-based rejuvenators [2–7]. On top of all, bio-based rejuvenators contribute a high portion to the enhancement of environment because waste biomass sources and waste construction materials are being reused instead of having to produce new ones. Rejuvenators used in other studies are either edible or requires huge consumption of resources. RSO is highly recommended to be used as a rejuvenating agent for RAP since studies lack in reporting the rejuvenating effects of RSO on the RAP binder. Hence, this study will investigate the rejuvenating effects of rubber seed oil (RSO) on the physiochemical and microstructural properties of RAP. Penetration and softening point tests were carried out to identify the RSO rejuvenation percentages which comply acceptable limits for 60/70 grade binder. The compatibility study of RSO rejuvenation with 60/70 grade RAP binder was investigated through storage stability test. FTIR will analyze the functional groups and chemical configuration of the RSO rejuvenated RAP. GC–MS will demonstrate the effects of every possible chemical configuration of binder. Lastly, AFM surface analysis will also be conducted to investigate the morphological features of RSO rejuvenated RAP.

2 Materials and Methods

2.1 Materials

Bitumen and RAP of grade 60/70 was obtained from reclaimed pavement quarry located in Taiping which has been sent to Sunway laboratory in Kampar for the bitumen extraction. The moisture content and asphalt content of the RAP were determined referring to ASTM C566 (2013) and AASHTO T308 procedures respectively. Recovered RAP aggregates were characterized for aggregate gradation, specific gravity, and water absorption, followed by the extraction of RAP binder using dichloromethane. RSO on the other hand was extracted from rubber seeds which were gathered from rubber plantation area. The rubber seeds were crushed and grinded to a fine diameter of 2-mm to provide the best condition for oil extraction. The rubber seed oil was extracted from the grinded rubber seed using Soxhlet extractor with n-Hexane as solvent. Then, to remove the solvent from the oil solution, the extracted oil and the solvent were separated using rotary evaporator.

2.2 Rejuvenation of RAP Binders Using RSO

RAP binder was poured into steel containers and the respective percentages of RSO were added into the bitumen. RSO and extracted aged bitumen from RAP were mixed using shear mixer with 135 °C control temperature for five minutes at the rate of 1000 rpm [8].

2.3 Conventional Tests on RAP Rejuvenated with RSO

To evaluate the most optimum percentage of RSO to rejuvenate aged binder from RAP, the standard penetration test was conducted on RAP with 0%, 1%, 2%, and 3% RSO. The target penetration value to be achieved by the most optimum percentage of RSO was 60 to 70 dmm. The softening point test was also conducted on all the samples to investigate the softening factor of rejuvenating RAP binders with RSO. Ring and ball apparatus was used for the tests where the samples were poured into the rings to a concaved surface and let to cool down at room temperature. The samples in the two rings were cooled down in a beaker with water and ice set at $5 \pm 1^\circ\text{C}$ with a magnetic stirrer to ensure uniform temperature distribution for 15 min. The temperature at which the samples touched the steel plate of the ring and ball apparatus was recorded as the softening point.

2.4 Storage Stability Test

The tendency of phase separation occurrence in the RSO-modified aged binder from RAP was determined through the storage stability test. The storage stability test was conducted on the controlled sample of aged binder with 0% RSO and the modified aged binder with 3% RSO. The samples were poured into aluminum tubes which were stored in the oven at $163 \pm 5^\circ\text{C}$ for 48 ± 1 h. The samples were then immediately kept in the freezer for 4 h at $-10 \pm 10^\circ\text{C}$. The aluminum toothbrush tubes should always be in vertical position. After freezing, the samples were cut into three parts and the softening point of the top and bottom parts of each sample were tested.

2.5 Chemical Characterization of RAP Rejuvenated with RSO

FTIR aims to study the chemical bonding and composition of rejuvenated RAP by vibrational mode. FTIR test was conducted through Attenuated Total Reflectance (ATR) method with varying infrared spectra using the available FTIR spectrometer.

FTIR test was conducted by radiation of infrared ranging from 4000 to 550 cm^{-1} [9]. PerkinElmer's Frontier FTIR Spectrometer was used for the chemical analysis. Gas Chromatography-Mass Spectrometry (GC-MS) chemical test was executed to determine the modified chemical content of the aged RAP bitumen which affects the physical properties of the mixture. Retention time can be measured from the baseline to peak and can be denoted as tR. The total height and area of the peaks indicate the concentration and molecular quantity respectively. Referring to the study by [8] which conducted GC-MS study on RAP rejuvenated by waste wood oil, an initial temperature of 40°C that is maintained for 2 min is used for chromatography analysis. Temperature was increased to 290°C with uniform increment of 4°C/min and kept for 20 min. Temperature of ion source was 260°C with transmission line of 280°C and 70 eV for electron beam energy was set. The carrier gas to be used is helium with flow rate of 1.2 mL/min [8].

2.6 Morphological Test on RAP Rejuvenated with RSO

Topographical and surface analysis of the RSO-rejuvenated aged binder were analyzed using Atomic Force Microscopy (AFM). Referring to the study by [10] which analyzed the morphological properties of binder rejuvenated by crude palm oil, the mode used was Phase Detection Mode (PDM) of Dynamic Force Mode (DFM) for scanning. A resonance frequency of $f = 149$ was used to scan the samples using sharp silicon tip with surface measurement of 8 μm by 8 μm . The nominal stiffness adopted was 40 N/m which was calibrated using thermal tune procedure as calibration sample.

3 Results and Discussion

3.1 Conventional Tests on RAP Rejuvenated by RSO

Rejuvenation by bio-based oil is expected to improve the softness of the aged binder and hence the softening point test was carried out. The result of the test is shown in Fig. 1 which proves that the softening point of the rejuvenated aged bitumen decreases as the percentage of RSO increases. The softening point test of 0% RSO-rejuvenated aged binder is the highest which exceeds the softening point range of 60/70 grade bitumen. The softening point range of 49 °C to 56 °C is satisfied when at least 0.75% RSO is added and at most 4.8% of RSO is added. The test shows that the higher the percentage of RSO added, the lower the softening point value. This consequently proves that rejuvenated aged binder has lowered viscosity and stiffness, and improved workability and low-temperature cracking resistance [11]. This properties of adding rejuvenator in aged binder is similarly proven by the standard penetration test.

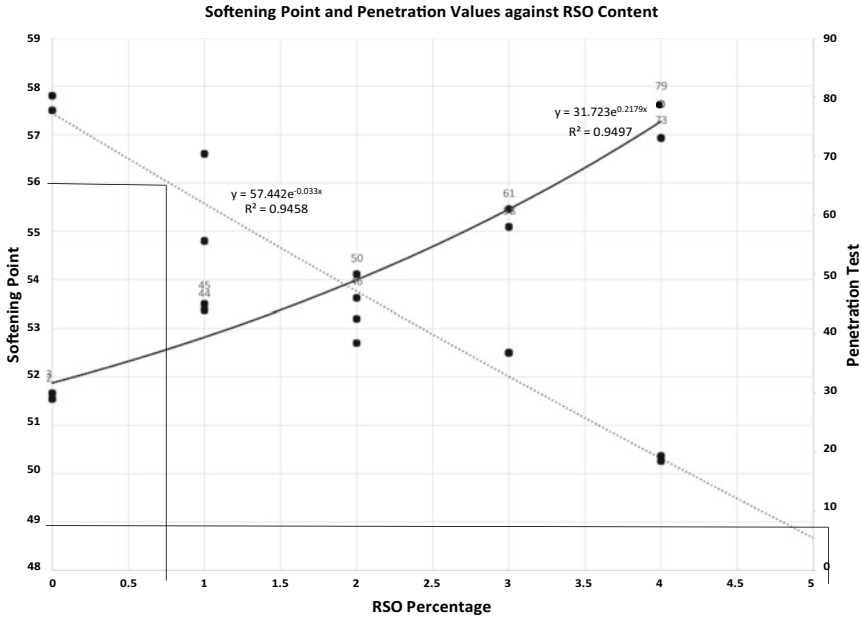


Fig. 1 Softening point and penetration test

The extracted aged binder is of the grade 60/70 which means the penetration value of the binder should be within the range of 60 to 70 dmm. However, penetration test on the unmodified aged binder found that the average penetration value is 29 dmm which is far very low from the acceptable range. Addition of RSO as rejuvenator has improved the softness of the aged binder by increasing the penetration value. To get the penetration value within the range of 60 to 70 dmm, by extrapolation, the RSO content should be between 2.9 to 3.6%. This can be clearly observed from Fig. 1. The increment in penetration value as the RSO content increases verifies that rejuvenating agent RSO significantly improves the softness of the aged binder.

3.2 Determination of Optimum RSO Content

Referring to Fig. 1, the RSO percentage range which successfully satisfy the acceptable softening point values is from 0.75% to 4.75% of rejuvenation whereas Fig. 2 shows that the acceptable range of penetration values can be achieved when the RSO percentage is from 2.9% until 3.6%. Hence, the RSO percentage range which satisfies both conditions are from 2.9% until 3.6%. The midpoint of these values was the average of the two which is 3.25%. RSO content of 3.25% was used as the optimum content for the study of morphological properties of RSO-rejuvenated aged binder recovered from RAP. Softening point test and penetration test on a sample

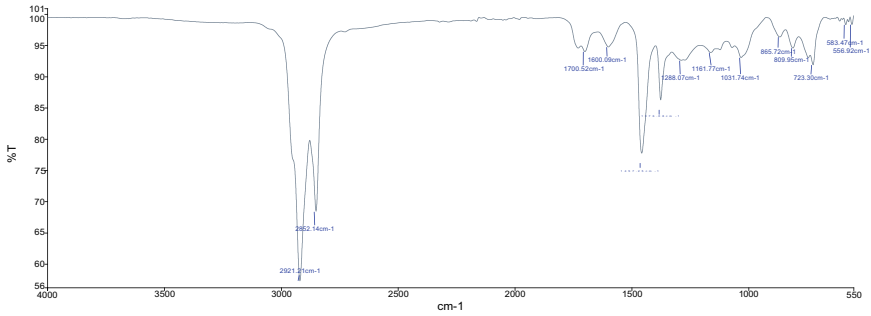


Fig. 2 FTIR spectrum on modified sample

of 3.25% RSO-rejuvenated aged binder were conducted to verify the estimation and the results were aligned with the hypothesis. As the RSO percentage increased to 3.25%, the average softening point value and penetration value observed were 52.2 °C and 63 dmm respectively. Both test results were within the criteria limitations which successfully verify the hypothesis.

3.3 Storage Stability Test

The difference limitations show that there is very slight to no tendency of phase separation between the rejuvenator and the bitumen. In this study, the test conducted to determine storage stability of rubber seed oil in aged bitumen of grade 60/70 from RAP is the softening point test. The test was conducted on the controlled sample with 0% rejuvenation and the highest rejuvenated sample which is the 3% RSO-rejuvenated sample because the highest modification will most possibly show the most obvious tendency of phase separation between RSO and the aged bitumen. The results of the softening point tests on both samples are shown in the Table 1. The difference in average softening point of the top and bottom parts of modified sample (3% RSO) is 0.8°C which meets the limitation criteria by EN 13,399:2010 which is < 5 units. The result portrays excellent compatibility of RSO in aged bitumen recovered from RAP and verifies the application of mixing parameters used.

Table 1 Storage stability test results

Samples	Controlled Sample		Modified Sample	
	Top	Bottom	Top	Bottom
Average Softening Point (°C)	62.7	65.9	53.2	54.0
Difference in Average Softening Point (°C)	3.2		0.8	

3.4 FTIR of RAP Rejuvenated with RSO

There were extreme peaks at the wavelength of range 2935–2915 and 2865–2845 cm^{-1} indicating the presence of methylene C-H both asymmetric and symmetric stretches and Olefinic with conjugated carbon–carbon double bond ($\text{C} = \text{C}$) at wavelength of 1600 cm^{-1} in controlled sample. Presence of carbonyl compound of carboxylic acid and aromatics are shown by a peak at wavelength of approximately 1700 cm^{-1} . Cyclohexane ring vibrations also present in both samples when there is a peak observed at wavenumber 1031 cm^{-1} . The peaks at approximately 1376 cm^{-1} is showing that there is also a presence of methyl C-H asymmetric and symmetric bends and alcohol and hydroxy compound of primary or secondary OH in-plane bend at wavenumber 1288 cm^{-1} . Lastly, there are weak peaks in the range of 890 cm^{-1} to 820 cm^{-1} in both samples which clarifies the existence of Peroxides of C-O-O- stretch. Optimum-modified sample independently shows a peak at wavenumber 583 cm^{-1} which is in the range of 705–570 cm^{-1} interpreting the presence of disulfides (C-S) stretch. The peaks at the wavenumbers in between 600–500 cm^{-1} assigns the existence of aliphatic iodo- compounds (C-I) stretch. Apart from that, there is also significantly observable peak at the wavenumber of 1162 cm^{-1} showing the presence of secondary amine (CN) stretch due to addition of RSO.

3.5 GC–MS of RAP Rejuvenated with RSO

Ten peaks were determined from the analysis and the detail of the chemical compounds at each retention time is outlined in Table 2. Six peaks in the retention time of 40.00 and above play the most important role in the mixture. This is because the other four peaks are coming from the solvent used which is n-hexane. At retention time of 40.667, the chemical compound found was n-Hexadecanoic acid which is equivalent to palmitic acid ($\text{C}_{16}\text{H}_{32}\text{O}_2$). This is aligned with the study by [12] which found 23.12% concentration of palmitic acid in rubber seeds oil through GC–MS characterization. In addition, there are a total of 37.37% area indicating the presence of oleic acid ($\text{C}_{18}\text{H}_{34}\text{O}_2$). The abundant existence of oleic acid is also mentioned by [12] where the GC–MS analysis on rubber seed oil found about 2.39% concentration. There is also a percentage area of 1.41 at the retention time indicating 9-octadecenamide ($\text{C}_{18}\text{H}_{35}\text{NO}$). Lastly, the chemical compound that is found in optimum-modified sample is phthalic acid with a percentage area of 4.70 ($\text{C}_8\text{H}_6\text{O}_4$).

Table 2 Chemical compounds in optimally modified sample

Compound name	Percentage Area (%)	Molecular Formula	Molar Mass (g/mol)
Palmitic acid	4.23	C16H32O2	256.40
Oleic acid	37.37	C18H34O2	282.47
Oleamide	1.41	C18H35NO	281.48
Phthalic acid	4.70	C8H6O4	166.13

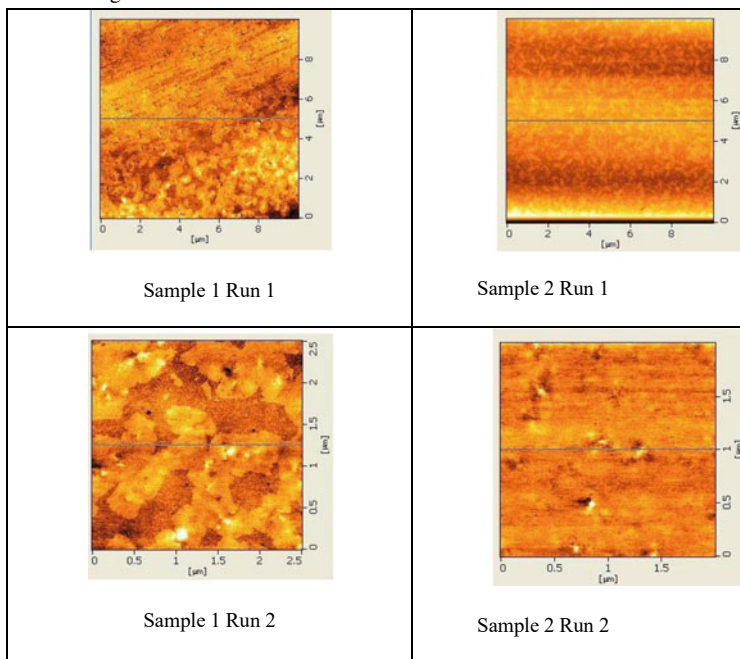
3.6 AFM on Aged Binder and Rejuvenated Binder

The results of Sample 1 seem inconsistent which may be because of long-term aging effects on the surface of the sample. The bottom side of the sample shows numerous bee structures which indicate asphaltenes due to increment of asphaltenes caused by aging. This is further proven by the image formed by Run 1 of Sample 2 which is the modified sample where observably, the frequency of bee structures has decreased significantly indicating reduced asphaltenes and aging effects. Run 2 of both samples shows clearer images which has been enlarged from run 1. The white spots indicating salphases are less observable in Sample 2. Not only that, but the presence of peri-phase on Sample 1 is more abundant than Sample 2. Peri-phase which surrounds the white spots and bee structures [12] indicates alteration of maltenes. However, increment of size of perpetua phase is shown by Sample 2 which indicates the solvent area of the sample [12] (Table 3).

4 Conclusions

This article summarizes the effects of rejuvenating reclaimed asphalt pavement (RAP) with 1%, 2%, 3%, and 3.25% of rubber seed oil (RSO).

- The results from conventional tests prove that adding RSO as rejuvenator successfully soften and improve the consistency of the binder. By interpolation, RSO content 3.25% would make the best rejuvenation of the binder. This hypothesis has been verified when the softening point and penetration values fall perfectly within the respective acceptable ranges.
- The compatibility of RSO in the reclaimed aged binder studied through storage stability test was clearly clarified when the difference of softening point between the top and bottom samples of 3% RSO-rejuvenated aged binder was less than 1.0°C.
- The chemical compounds and responsible functional groups found through GC-MS and FTIR respectively include phthalic acid, palmitic acid, oleic acid, oleamide, disulfides, secondary amine, aromatics, and aliphatic iodo- compounds.

Table 3 AFM images

- This rejuvenation of 60/70 RAP has reduced the bee structures, white spots, and peri-phase while increased perpetua phase of the sample. The study found out that rejuvenating 60/70 RAP with the optimum percentage of RSO has significantly modified the morphological properties of the binder.

Acknowledgements The authors acknowledge the facilities and financial sponsorship by Universiti Teknologi PETRONAS in terms of YUTP (Grant No. 015LC0-427).

References

1. Saeed SM et al (2021) Optimization of rubber seed oil content as bio-oil rejuvenator and total water content for cold recycled asphalt mixtures using response surface methodology. *Case Stud Constr Mater* 15:e00561. <https://doi.org/10.1016/j.cscm.2021.e00561>
2. Ji J et al (2017) Effectiveness of vegetable oils as rejuvenators for aged asphalt binders. *J Mater Civil Eng* 29(3):D4016003. [https://doi.org/10.1061/\(ASCE\)MT.1943-5533.0001769](https://doi.org/10.1061/(ASCE)MT.1943-5533.0001769)
3. Ahmad KA, Abdullah ME, Hassan NA, Usman N, Ambak K (2017) Investigating the feasibility of using jatropha curcas oil (JCO) as bio based rejuvenator in reclaimed asphalt pavement (RAP). *MATEC Web Conf* 103:09013. <https://doi.org/10.1051/mateconf/201710309013>

4. Ahmad KA et al (2018) Effect of bio based rejuvenator on mix design, energy consumption and GHG emission of high RAP mixture. *IOP Conf Ser Earth Environ Sci* 140:012086. <https://doi.org/10.1088/1755-1315/140/1/012086>
5. Ahmad T, Ahmad N, Jamal M, Badin G, Suleman M (2020) Investigation into possibility of rejuvenating aged asphalt binder using mustard oil. *Int J Pavement Eng* 23(6):1738–1753. <https://doi.org/10.1080/10298436.2020.1823388>
6. Rodrigues C, Capitão S, Picado-Santos L, Almeida A (2020) Full Recycling of Asphalt Concrete with Waste Cooking Oil as Rejuvenator and LDPE from Urban Waste as Binder Modifier. *Sustainability* 12(19):8222
7. Zhang D, Chen M, Wu S, Liu J, Amirghanian S (2017) Analysis of the relationships between waste cooking oil qualities and rejuvenated asphalt properties. *Materials* 10(5):508
8. Zaumanis M, Mallick RB, Poulikakos L, Frank R (2014) Influence of six rejuvenators on the performance properties of reclaimed asphalt pavement (RAP) binder and 100% recycled asphalt mixtures. *Constr Build Mater* 71:538–550. <https://doi.org/10.1016/j.conbuildmat.2014.08.073>
9. Santhanasamy R (2020) Investigation on the Mechanical and Morphological Properties of Regular and Irradiated Waste PET Modified Asphaltic Concrete Mixtures
10. Rafiq W et al (2021) Modeling and design optimization of reclaimed asphalt pavement containing crude palm oil using response surface methodology. *Constr Build Mater* 291:123288. <https://doi.org/10.1016/j.conbuildmat.2021.123288>
11. Nciri N, Shin T, Kim N, Caron A, Ismail HB, Cho N (2020) Towards the use of waste pig fat as a novel potential bio-based rejuvenator for recycled asphalt pavement. *Materials* 13(4):1002. <https://doi.org/10.3390/ma13041002>
12. Omowanie Joshua EAA (2018) Physico-chemical and GC-MS analysis of some selected plant seed oils castor neem and rubber seed oils. *FUW Trends Sci Technol J* 3(2):644–651

Environmental Impact Analysis on Dyes in Handwritten Batik



Etika Muslimah, Maharani Reynara, and Ratnanto Fitriadi

Abstract Batik Jambe Kusuma produces written and stamped batik using two types of synthetic dyes, namely indigosol and reactive dyes. The high level of batik demand using synthetic dyes materials has an impact on the environment. This study aims to calculate, analyze and compare the environmental impact of the use of synthetic dyes in batik production. Data processing uses the Life Cycle Assessment (LCA) method to compare the environmental impact due to the use of the two types of dyes. It was found that the indigosol material has a higher total impact than the reactive material, which is 78.8933 Pt, while the impact reactive material is 78.55291 Pt. This result shows that the production with indigosol dyes has more impact to the environment than reactive dyes. Recommendations for improvements to increase batik production by using reactive dyes because they are more environmental friendly.

Keywords Batik · Synthetic dyes · Impact environment

1 Introduction

The energy, raw materials, and waste treatment that follow production all contribute to the textile industry's unfavorable environmental records from a variety of perspectives. The textile industry, which includes batik, also has this issue [1]. Batik is an industry that has the potential to cause environmental damage. This is due to the use of chemicals in the production process and occurs in several places such as Indonesia and Malaysia. The effluents from the batik-making process are frequently laden with color and organic contaminants, and they must be properly treated before

E. Muslimah (✉) · M. Reynara
Departement of Industrial Engineering, Universitas Muhammadiyah Surakarta, Surakarta,
Indonesia
e-mail: etika.muslimah@ums.ac.id

R. Fitriadi
Center for Logistics and Industrial Optimization Studies, Universitas Muhammadiyah Surakarta,
Surakarta, Indonesia

© Institute of Technology PETRONAS Sdn Bhd 2024
B. S. Mohammed et al. (eds.), *Proceedings of the International Conference on Emerging Smart Cities (ICESC2022)*, Lecture Notes in Civil Engineering 324,
https://doi.org/10.1007/978-981-99-1111-0_36



Fig. 1 Handwritten and coloring batik processing

being released into the environment. It is well recognized that a strong demand for batik items will lead to increased production of wastewater with high COD values, making it one of Malaysia's primary sources of serious pollution [2]. Batik Jambe Kusuma is Small Medium Enterprises (SMEs) in Central Java, Indonesia which was initiated in 2010 produced of hand-written and stamped batik, that use synthetic dyes in coloring process. One of the most important batik processes is giving color to either the basic color or the polishing process (see Fig. 1).

Based on the observation, Batik Jambe Kusuma uses synthetic dyes in the coloring process. During the coloring process, sometimes Batik Jambe Kusuma uses two types of synthetic dyes, namely indigosol and reactive dyes. Consideration of using different dyes due to meet customer demand. Even though they have the same quality as the end result of the dyeing process, the use of indigosol synthetic dyes and reactive dyes has different compositions in the process of giving color to batik, which also affects the production costs. It is known that using of indigosol dye can be done within 1 day of processing by drying it in the sun, but batik production also often use alternative synthetic dyes such as reactive dyes, which can take at least 2 nights to process it. The owner of Batik Jambe Kusuma said that although it takes longer, using reactive dyes is cheaper than indigosol dyes. Indigosol has the advantage of a non-fading rate of 10% and has properties that do not fade easily, have an even and bright color, which is caused by the indigosol compound which is insoluble in water and becomes soluble after being reduced to become leuco-indigo and after leuco-indigo is absorbed into the fabric fibers, quickly oxidized again by oxygen in the air and becomes insoluble. While reactive dyestuffs are dyes that can react with cellulose or protein, have a small molecular weight, are soluble in water and have covalent bonds with fiber and can provide good color resistance properties against washing and sweating. Comparison of the properties of the two dyes in batik production, causes SMEs to add locking agents in the form of sulfuric acid and sodium nitrite to indigosol dyes and baking soda to reactive dyes. This material is useful for locking the color that optimisation the dye function and does not fade during the wax removing process.

Synthetic dyes are dyes used at temperatures that do not damage the wax, which include indigosol, naphthol, rapid, base, indanthreen, procion, and others. The tendency to use synthetic dyes is because the process is easier than natural dyes,

although on the other hand, the use of synthetic dyes creates environmental problems. River water that has been polluted by synthetic batik dye waste can seep into people's wells so that the quality of health in the community decreases [3]. If not managed properly, spilled dyes and chemicals that are discharged into the ground, public sewers and rivers are very harmful to the environment [4]. Environmental regulation has a positive impact on eco-efficiency in the short term and inhibitory effects in the long term so it is necessary to determine effective ways such as making technological and industrial innovations to increase environmental efficiency [5]. Generally, inefficient materials also cause negative impacts on the environment [6]. The use of synthetic dyes in batik production cannot be avoided by SMEs, because it is associated with production costs. This research is needed to recommend synthetic dyes that have a minimal impact on the environment.

2 Method

LCA is a technique for calculating a production process's environmental impact. The industrial process can be made more environmentally friendly by using LCA models. The aim and scope definition, inventory analysis, effect analysis, and interpretation are the four primary axes of the LCA approach, which is based on ISO 14040. It is envisaged that the LCA analysis will provide a more thorough understanding of the environmental impact of batik production [7]. LCA is recognized as a potential tool for evaluating the environmental impact of emerging technologies from cradle to grave and to facilitate decision making in policy making [8]. LCA approach can also be used to determine the environmental impact it causes and then take strategic steps to reduce the environmental impact, such as the clean production approach [9]. Based on a field study conducted at Batik Jambe Kusuma, information was obtained about the high level of demand, of course, very influential on environmental conditions, one of the causes is the use of synthetic dyes that have not been consistent without knowing the impact on the environment. Good production standards should pay attention to the safety and effects of the raw materials or materials used, in order to create harmony with the environment [10].

This research was conducted at the Batik Jambe Kusuma with the type of batik production using indigosol dyes and reactive dyes in batik process. Identify the materials needed during batik production process with LCA. Data collection was carried out by direct field studies and interviews with SMEs owners and workers to validate whether the data used were appropriate data. Production process of written batik has several stages, namely: written, first washing, first drying, coloring, second drying, wax removing, second washing and final drying. There is a slight difference in the process of using reactive dyes, where cotton fabrics that have gone through the second drying process must be left for at least 2 nights in order to get maximum color. Material requirements during the production process are: cloth, candles, diesel fuel, firewood, indigosol, sulfuric acid, sodium nitrite, water, starch, reactive dyes, baking soda.

The data that has been collected is then processed using Simapro 9.2 to analyze LCA of the production process that has been carried out. LCA is used with the aim of analyzing the environmental impact of the batik-making process and the input of raw materials that have the most significant environmental impact by taking an inventory of inputs and outputs based on a database using Simapro software [7]. Simapro software is used to collect, analyze, and monitor data for sustainable reporting, carbon and water footprints, product design, making environmental product declarations, and determining key performance [11]. LCA is particularly relevant to be used in the design of policies that focus on design for sustainability, sustainable consumer information, sustainable procurement and management of waste, minimization and prevention as well as sector-specific policies such as sustainable energy and food supply so that LCA is often applied to decision-making regarding action in the present or into the future [12]. LCA allows estimation of the cumulative environmental impact of all stages of the product life cycle [13]. LCA consists of 4 stages, namely: Goal and Scope, Life Cycle Inventory, Life Cycle Impact Assessment and Interpretation [14].

Goals and Scope, this stage is to determine the objectives and scope of the research to be carried out. The purpose of this study was to analyse the impact of the use of synthetic dyes on the production Batik Jambe Kusuma with a scope, namely the production of written batik using indigosol dyes and reactive dyes.

Life Cycle Inventory, this stage is the stage of determining what materials are needed in each batik process. The sequence of the production process for indigosol batik and reactive material batik relative the same as: batik, first washing, first drying, coloring, second drying, wax removing, second washing and last drying. Materials used for the batik process include: cloth, wax, indigosol and reactive as dyes and water for the process of wax removing and washing. The drying process is a process that does not require materials so that it does not have an impact on the environment.

Life Cycle Impact Assessment (LCIA), this stage is a calculation of the material that has been entered in the stage life cycle inventory. Measurement of the environmental impact of the manufacturing process using the Eco-Indicator 99 (H) method to determine the impact assessment in terms of human health, ecosystem quality and resources from the batik production process. Interpretation is the stage of processing and analyzing the results to draw conclusions and provide suggestions for improvements to the research.

3 Result and Discussion

Environmental impact calculation that is carried out after identifying raw dyes and making an inventory based on database using Simapro. The result of this calculation is output of 4 types of processing, namely: characterization, damage assessment, normalization and weights. Characterization is an assessment of the impacts of each required material on the environment.

Table 1 provides a summary of all damage assessments based on 11 aspects grouped into 3 groups, namely human health, ecosystem quality and resources that will be used as material for consideration in making decisions about efforts to improve environmental impacts.

The results of comparison calculations Characterization indigosol and reactive material in Table 1, shows the biggest impact for the category human health is on Respiratory inorganics in indigosol, which is 0.0004086 DALY. Respiratory inorganics are disturbed respiration caused by emission of dust, sulfur and nitrogen oxide into the air which is the impact of using indigosol. Category Ecosystem quality, the biggest impact is on Land use, which is 261.4869337 PAF*m2yr. Land use is the use of land on man-made systems impact on biodiversity. Dyes that are discharged into the environment have the greatest impact on the ecosystem around the batik industry. The third category, namely Resources has the greatest impact on fossil fuels which is 837.593089 MJ surplus, is an indicator of the depletion of fossil resources as the result of human actors who definitely choose best resources first then resources with lower quality requires more effort more to extract the remaining resources. The second analysis is comparing the total of damage assessment.

The following Table 2 gives a summary, a greater damage caused by indigosol both from human health, ecosystem quality and resources. Total category impact of human health is 0.000799 DALY which means the number of healthy years lost is 0.000799 years received by a person from the burden of disease caused by health problems and premature death, is caused by indigosol dyes. Second category, is ecosystem quality obtained a total of 288.254 PDF*m2yr, which means the potential loss of 288.254 species per m2 per year. These results were also mentioned in other research that using indigosol dye will produce colored liquid waste containing metal levels which over time will pollute the river flow and can damage the ecosystem in it [15]. As for the category resources obtained a total of 840.656 MJ surplus which means the amount of lost energy required to extract from a resource.

Table 1 Characterization of indigosol and reactive dyes

Impact category	Group	Unit	Indigosol	Reactive
Carcinogens	Human health	DALY	0,000,358	0,000,357
Resp. organics		DALY	1,63E-07	1,61E-07
Resp. inorganics		DALY	0,000,409	0,000,405
Climate change		DALY	3,24E-05	3,18E-05
Radiation		DALY	2,66E-08	2,15E-08
Ozone layer		DALY	5,85E-08	5,83E-08
Ecotoxicity	Ecosystem quality	PAF*m2yr	167,4428	166,0897
Acidification/ Eutrophication		PDF*m2yr	10,02,278	9,972,967
Land use		PDF*m2yr	261,4869	261,4052
Minerals	Resources	MJ surplus	3,062,906	2,951,251
Fossil fuels		MJ surplus	837,5931	833,9544

Table 2 Damage Assessment Total of indigosol and reactive dyes

Damage category	Unit	Indigosol	Reactive
Human Health	DALY	0.000799	0.000794
Ecosystem Quality	PDF*m2yr	288,254	287.9871
Resources	MJ surplus	840,656	836.9056

Normalization is a unit of all categories of the impact of the production process that has been equated (the result of this stage no units are used) in order to make it easier to compare them when doing analysis.

Based on the results of comparison normalization in Table 3 gives of summary of the impact on the category human health with indigosol batik has a greater on environmental impacts than reactive dyes. Indigosol containing trash from batik is extremely hazardous because it may have negative effects on health. These colors are extremely toxic and can lead to skin cancer in addition to other skin conditions [16].

Next analysis is the weighted impact that has been assessed by multiplying the category impact with weighting factors.

Based on the results of comparison calculations weight indigosol and reactive dyes in Table 4 shows the weighting for each impact. Indigosol has a greater total impact than reactive dyes, which is 78.8933 Pt and human health is the biggest impact that is equal to 36.4612 Pt. Based on its nature, indigosol can produce bright colors, but has a tendency towards pastel, faded or dull colors [17]. While the characteristics for these reactive dyes tend to have color properties that tend to be bright or bright even if only mixed with water [18]. The owners admitted that they used indigosol dyes more often than reactive ones and described the indigosol’s immobility rate of 10% so that the process was considered faster than reactive dyes which had a 50% impermeability rate. So based on the results of the calculation of the impact of indigosol dyes which is slightly larger than reactive material. Based on the nature of the two types of synthetic dyes, it can be concluded that the use of reactive dyes can be used as the main choice for dyes in the production process at Batik Jambe Kusuma. Reactive dyes cause minimal environmental impact, as well as more efficient production costs. Improvement to minimize environmental impact is replace synthetic dyes with natural dyes to consider environmentally friendly [19]. The other research said that combine the natural dyes and synthetic dyes for batik production, as is done in Malaysia that the combination is recommended to improve the environmental impact [20].

Table 3 Normalization of indigosol and reactive dyes

Damage category	Indigosol	Reactive
Human Health	0,091,153	0,090,597
Ecosystem Quality	0,050,387	0,05,034
Resources	0,111,387	0,11,089

Table 4 Weight of indigosol and reactive dyes

Damage category	Unit	Indigosol	Reactive
Human Health	Pt	36,4612	36,23,886
Ecosystem Quality	Pt	20,15,472	20,13,606
Resources	Pt	22,27,738	22,178
Total	Pt	78,8933	78,55,291

4 Conclusion

From the analysis and discussion that has been carried out, it can be concluded that for the two synthetic dyes it was found that indigosol dyes have a total impact on the environment of 78.8933 Pt which is greater than the reactive dyes, which is equal to 78.55291 Pt. The impact on human health is the biggest impact, namely 36.4612 Pt, when compared to the impact on the quality of ecosystems and resources. So the preference for reactive dyes is better.

It is undeniable that replacing synthetic dyes with natural dyes is the right step to reduce environmental impact, but various factors become obstacles for SMEs. The price is more expensive and the production time is longer. So after conducting this research, recommendations for improvement that can be used by looking at the current condition of SMEs are by increasing the production of batik using reactive dyes because it is more sustainable.

References

1. Yoshanti G, Dowaki K (2017) Batik life cycle assessment analysis (LCA) for improving batik small and medium enterprises (SMEs) sustainable production in Surakarta, Indonesia. In: Matsumoto M, Masui K, Fukushige S, Kondoh S (eds) *Sustainability Through Innovation in Product Life Cycle Design*. Springer Singapore, Singapore, pp 997–1008. https://doi.org/10.1007/978-981-10-0471-1_68
2. Yaacob MR, Ismail M, Zakaria MN, Zainol FA, Zain NFM (2015) Environmental awareness of batik entrepreneurs in Kelantan, Malaysia an early insight. *Int J Acad Res Bus Soc Sci* 5(4):338–347. <https://doi.org/10.6007/ijarbss/v5-i4/1576>
3. Alamsyah A (2018) Kerajinan Batik dan Pewarnaan Alami. *Endogami J Ilm Kaji Antropol* 1(2):136. <https://doi.org/10.14710/endogami.1.2.136-148>
4. Yaacob MR, Zain NFM (2021) Environmental awareness and perception on environmental management of entrepreneurs in batik industry in Kelantan, Malaysia. *J Trop Resour Sustain Sci (JTRSS)* 4(1):54–60. <https://doi.org/10.47253/jtrss.v4i1.574>
5. Li J, Cai C, Zhang F (2020) Assessment of ecological efficiency and environmental sustainability of the Minjiang-source in China. *Sustainability* 12(11):4783. <https://doi.org/10.3390/su12114783>
6. Muslimah E, Suparman S, Yanuwadi B, Riniwati H (2020) Using eco-efficiency to analyze environmental impact of the batik industry. <https://www.kansaiuniversityreports.com/article/using-eco-efficiency-to-analyze-environmental-impact-of-the-batik-industry>. Accessed 08 June 2020

7. Iqbal MN, Lestari SP, Yosafaat M, Mardianta KA (2021) Life cycle assessment approach to evaluation of environmental impact batik industry. *J Tek Kim dan Lingkung* 5(2):194–201
8. Moni SM (2019) Life cycle assessment of emerging technologies: a review. *J Indus Ecol* 24(1):52–63. <https://doi.org/10.1111/jiec.12965>
9. Sirait M (2018) Cleaner production options for reducing industrial waste: the case of batik industry in Malang, East Java-Indonesia. *IOP Conf Ser Earth Environ Sci* 106:012069. <https://doi.org/10.1088/1755-1315/106/1/012069>
10. Sumarata DNYF, Sukendar I (2019) Analisa Dampak Lingkungan Material dan Energi Proses pembuatan Batik menggunakan metode Life cycle Assessment (LCA) Studi Kasus : Batik Tobal Pekalongan. pp. 556–564
11. Widyanti F (2021) Analisis Ekoefisiensi Pemakaian Lilin Daur Ulang Pada Proses Produksi Batik di UKN Merak Manis Kampung Batik Laweyan
12. Verones F et al (2020) LC-IMPACT: A regionalized life cycle damage assessment method. *J Ind Ecol* 24(6):1201–1219. <https://doi.org/10.1111/jiec.13018>
13. Pesonen HL (2001) Environmental Management of Value Chains Promoting Life-cycle Thinking In Industrial Networks. Greenleaf Publishing, Finland
14. Sirait M (2020) Studi life cycle assessment produksi gula Tebu: Studi Kasus di Jawa Timur. *Rekayasa* 13(2):197–204. <https://doi.org/10.21107/rekayasa.v13i2.5915>
15. Desianna I, Putri CA, Yulianti I (2017) Selulosa Kulit Jagung sebagai Adsorben Logam Cromium (Cr) pada Limbah Cair Batik. *Unnes Phys. J.* 6(1):19–24
16. Riyanto EP (2018) Treatment of wastewater batik by electrochemical coagulation using aluminium (Al) electrodes. *IOP Conf Ser Mater Sci Eng* 299:012081. <https://doi.org/10.1088/1757-899X/299/1/012081>
17. Miranti DL, Prasetyaningtyas W (2020) Perbedaan Hasil Pencucian Kain Batik Sintetis Remazol Menggunakan Lerak dan Detergen. *TEKNOBUGA: Jurnal Teknologi Busana dan Boga* 8(1):17–24. <https://doi.org/10.15294/teknobuga.v8i1.21642>
18. Kusumawardhani B (2017) Identifikasi Dampak Material Pada Proses Produksi Batik Cap Terhadap Lingkungan dengan Menggunakan Software Simapro
19. Sunarjo WA, Setyanto RP, Suroso A (2022) Motives and green innovation performance in Indonesian small and medium enterprises Sme's Batik - a qualitative case study. *Qual. Access Success.* 23(186):17–24. <https://doi.org/10.47750/qas/23.186.10>
20. Ismail NW, Akhir NHM, Kaliappan SR, Said R (2019) The impact of innovation on firm performance in the Malaysian batik industry. *Int. J. Bus. Glob.* 23(1):1–25. <https://doi.org/10.1504/IJBG.2019.100784>

Effects of Change of Discretionary Trips & Activities, During COVID-19 Pandemic Towards Social & Mental Health



Rahayu Sulistyorini, Nur Shalin Abdi, Dimas B. E. Dharmowijoyo, and Liza EviantiTanjung

Abstract In order to analyse the complexity of travel behaviour, activity pattern study which is one of the human activity approaches which includes social science perspective has been implemented in this study to alleviate the limitations in traditional concept. Based on the multivariate analysis, only dining trips is significant towards social health. In addition, online shopping is found to impact both social and mental health model, while online grocery shopping is affecting mental health model only. In a nutshell, COVID-19 pandemic caused an activity-travel behavior changes specifically in out-of-home travel participations and in-home activities converging

R. Sulistyorini (✉)

Department of Infrastructure Engineering and Planning, Institut Teknologi Sumatera, Yogyakarta, Indonesia

e-mail: rahayu@itera.ac.id; rahayu.sulistyorini@eng.unila.ac.id

Department of Civil Engineering, Universitas Lampung, Bandar Lampung, Indonesia

N. S. Abdi · D. B. E. Dharmowijoyo · L. EviantiTanjung

Department of Civil and Environmental Engineering, Universiti Teknologi PETRONAS, Seri Iskandar, Malaysia

D. B. E. Dharmowijoyo

Institute of Transport and Infrastructure, Universiti Teknologi PETRONAS, Seri Iskandar, Malaysia

School of Planning and Policy Development, Institute Teknologi Bandung, Bandung, Indonesia

Department of Civil Engineering, Universitas Janabadra, Yogyakarta, Indonesia

D. B. E. Dharmowijoyo

e-mail: dimas.bayu@utp.edu.my

L. EviantiTanjung

e-mail: liza_19001673@utp.edu.my

L. EviantiTanjung

Department of Civil Engineering, Universitas Muhammadiyah Sumatera Utara, Medan, Indonesia

© Institute of Technology PETRONAS Sdn Bhd 2024

B. S. Mohammed et al. (eds.), *Proceedings of the International Conference on Emerging Smart Cities (ICESC2022)*, Lecture Notes in Civil Engineering 324,

https://doi.org/10.1007/978-981-99-1111-0_37

on socialising and discretionary purposes. For future work, it is suggested to incorporate individuals time-use diary over a time period in the dataset and evaluate health as three factor structure which are physical, social and mental health.

Keywords Travel behaviour during COVID-19 pandemic · Discretionary trips and online activities · Social and mental health

1 Introduction

As a measure to inhibit the spreading of COVID-19 cases, social distancing has been applied in many countries. The ‘lockdowns’ or travel restraints are the derivation of social distancing policy to succeed in the social distancing policy. The government of Malaysia imposed a full lockdown policy or Movement Control Order (MCO) on 16 March 2022 which was followed by implementation of many new standards to support MCO [1]. The MCO was prolonged and eased to a few stages in 2020 and 2021, including the Conditional Movement Control Order (CMCO) and Recovery Movement Control Order (RMCO).

Social health relates to individuals’ ability to engage and develop meaningful relationships with others [2] while mental health includes individuals’ social well-being, psychological and emotional [3]. Travel restrictions that implemented as a safety measure to promote social distancing in order to minimize health hazards caused by COVID-19 has estimated to give negative effects on individuals’ social and mental health as both variables’ definitions correlated with each other. Social distancing could undermine the social rhythm, by depriving individuals’ habitual coping responses with stress [4] as daily travel participation especially in socialising and discretionary trips are limited during the pandemic. Certain activities are considered to be more pleasurable, including socialising and recreation or leisure activities, which are deemed to have a positive impact on people’s everyday well-being [5] as cited [6]. The online activity participations covered in this study are work or school from home, online grocery shopping, online shopping, online meeting, food delivery and streaming movies. Meanwhile, this study also focuses on analysing travel participation in socialising and discretionary trips. Socialising trips are associated with trip purposely for social engagement with others such as visiting families, relatives or friends. While discretionary trips are trips for non-mandatory activities which can be re-scheduled at a high level of flexibility such as religion/civic services and hobbies.

During COVID-19 pandemic, travel is minimized mainly due to authority constraints (law enforcement such as lockdown and mobility restriction policies) and individuals’ perceived risk towards COVID-19. During COVID-19 pandemic, due to the authority constraint where there are limitations on travel due to the government’s restrictions, individuals cannot travel and participate in different activities on a given day which may affect their social and mental health. High perceived risks of COVID-19 also play a huge role in reducing travel and activity participation during the pandemic. Based on study conducted in Indonesia which investigates the

respondent attitudes and perspectives towards COVID-19, almost all of the respondents tended to have a strong perception towards COVID-19, with more than 96% of them thinking the pandemic is dangerous or extremely dangerous [7]. As a result, individuals will reduce daily travel frequency due to the fear of infection.

The application of social science in transportation field indicates an affirmation where transportation runs throughout a broader societal framework, including various approaches to impacts, costs and transportation modes. In traditional approaches of studying travel behaviour, travel is assumed to be a choice process. This is incorrect because in time–space-prisms, a circumstance in which travel is a fixed constraint, the choice element is eliminated. The traditional approach also assumes that all individuals engage in identical daily activities and travel. Therefore, the traditional concepts approach only valid to travel behaviour of homogeneous population groups [8] as cited in [9]. This concept disregards the fact that all individuals have different social and personal identities in social-cultural, geographical and economic aspects across time–space-prisms.

Activity pattern studies is more extensive because it takes account the demand for travel and activity participation as series of responses from social responsibility, biological needs, or the consequences due to the living environment itself [10]. In activity pattern studies which implemented in this study, activity and trips participation amid a time budget are translated to activity-travel pattern which used as the unit of analysis of activity-based models to investigate individuals' travel behaviour to alleviate the limitations in traditional concept.

The main weakness of the traditional approach is it does not provide relation between non-travel and travel context of ever day's life or the "secondary effects" on members of the household are not directly afflicted by the trip [10]. However, in the human activity approach, it recognizes household organization as a fundamental concept in understanding travel behaviour. It views travel in context of everyday household activity patterns, where each individual or group uses travel as a derived demand. It includes relation and linkages among members of the household, as well as explicit consideration of temporal, interpersonal and spatial constraints on travel and location options.

Over the past years, the advancement of transportation field introduced new extensive comprehensions in analysing the complexity of travel behaviour. The traditional approach which considered as one of the conventional models, pay only lip-service to the idea that travel is a derived demand and it fail to recognize the basic forces which generate travel and the numerous characteristics of travel, such as timing, duration of journey, mode, frequency, route selection and destination [11] as cited in [10]. Activity pattern study which is one of the human activity approaches, is considered more accurate in explaining individuals' travel behaviour compared to traditional approaches as the traditional approaches only recognize travel behaviour in mobility phenomena by considering only one-way trips. Therefore, in order to improve previous research related to topic, this study incorporates the activity pattern study to alleviate the weaknesses of the traditional approach. The data analysis method will include household and individual socio-demographic characteristics in order to recognize non-homogeneity of travel behaviour between individuals. It

will also include daily different individuals' travel pattern and activity participation during and before COVID-19 pandemic in Malaysia and health-related quality of life (QOL) questions which derived based on the Short-Form 36 (SF-36) to correlate effects of change of socialising and discretionary trips, and activities during COVID-19 pandemic on social and mental health.

Considering the recentness of COVID-19 pandemic, to the author's knowledge, there is only minimal amount of research study which relates travel pattern and activity participation changes due to the pandemic with social and mental health in Malaysia. Since socialising and discretionary trips tend to correlate on better well-being and social and mental health [12], the findings of this study may provide a better understandings and insight in establishing new policies on COVID-19 travel restrictions as transport and health are interrelated at many levels with transport directly and indirectly influencing health [13]. This study will investigate the effects of change of socialising and discretionary trips, and activities during COVID-19 pandemic on social and mental health, while incorporating the complexity of travel behaviour which is missing traditional approaches.

There are 2 objectives that set to be achieved for this study. Firstly, to correlate the effects of change of socializing and discretionary trips during COVID-19 pandemic on social and mental health using bivariate analysis. Secondly, to correlate the effects of change of socializing and discretionary trips, and activities during COVID-19 pandemic on social and mental health using multivariate analysis.

2 Literature Review

2.1 *Time–Space-Prism*

In time geography, Hägerstrand developed the time–space-prism which describes the theory in sociology and social-psychology into geography science. The time–space-prism encompasses the temporal and spatial potential for activity and travel participation within a time budget [14]. According to the time–space prism concept, an individual retains multiple characteristics in multiple dimensions, comprising personal, social, household and spatial dimensions [12]. Individual's multiple characteristics will interact within its multiple dimensions to form needs and constraints which will shape their everyday activity-travel participations. Since everyone has different daily needs and constraints, every individual's everyday decision-making process and activity-travel participations would be also different. This uniqueness justifies the reasoning on why every individual would have different daily time–space prisms with others. Hägerstrand recognised some constraints that may limit people's ability to travel and participate in activities [15]. Capability, coupling, and authority constraints are the three types of constraints identified by Hägerstrand. Capability constraints limits the individual's ability to participate in activity and travel in time–space-prism. As an example, our daily travel and activity participation are limited

as we need to spend a portion of our daily time budget to meet our physiological needs such as eating, sleep and personal care. Coupling constraints limit individuals' decisions due to the necessity to be in same location and time to engage with other individuals or materials. Authority constraints associate with limitations that are imposed by authorities who have control and influence over any given individuals.

Example of resources in time–space prism are travel mode options, money and built environment. The lack of or availability of these resources may also be linked to dissimilar activity-travel behavior [9]. Mobility poverty (such as demonstrated by fewer trips and trip chains and lower total travel time) and less discretionary trips, including for social engagement and visiting public amenities [16] are results from lacks resources in time–space prism which usually faced by individual with lower income. Human activity patterns represent the means by which people fulfil individual's desires and needs [17] as cited in [10]. Needs can be categorized into two groups. Firstly, subsistence needs (food, sleep, clothing, health care, shelter), plus activities which supply financial income to cover fundamental human needs [10]. Secondly, needs which included individually, socially and culturally defined needs. For example, activities that entails participation in a variety of social and recreational engagement such as out-of-home family dining trips and hobbies. Individuals' prisms and paths would be shaped by the interaction between constraints and needs due to personal and social identities in social-cultural, economic and geographical contexts across time–space prism. [9] and it is a fundamental concept to grasp in order to have a better comprehension of individual's daily activity-travel pattern.

2.2 Linkage Between Travel Behaviour and Social and Mental Health

In explaining the relation between travel behaviour and social and mental health, it is crucial to recognize the intermediate parameters involved within the particular causal effect relationship which proposed as shown in Fig. 1. In time–space-prism, individual's travel behaviour in travel and activity participation correlate with needs, constraints and availability of resources. Travel behaviour such as travel mode, number of trips chains and duration will affect well-being because while travelling as travelers are exposed to their surroundings environment which may stimulate emotional responses and lead to a particular mood [18]. As an example, different modes of transportation provide variety of travel experiences, levels of interaction with the outside environment and levels of physical activity. Therefore, their influence on individual's mood or emotions is likely to differ. Individuals who use public transport such as public bus in a metropolis city as travel mode during peak hours to a certain location, may exposed to road congestion whereby it is causing the individual to move at a slower speed, longer trip duration and increased vehicular queuing. As a result, he or she may experience negative emotions such as irritated or annoyed. If aggregated, and especially in the context of repetitive trips, such responses will

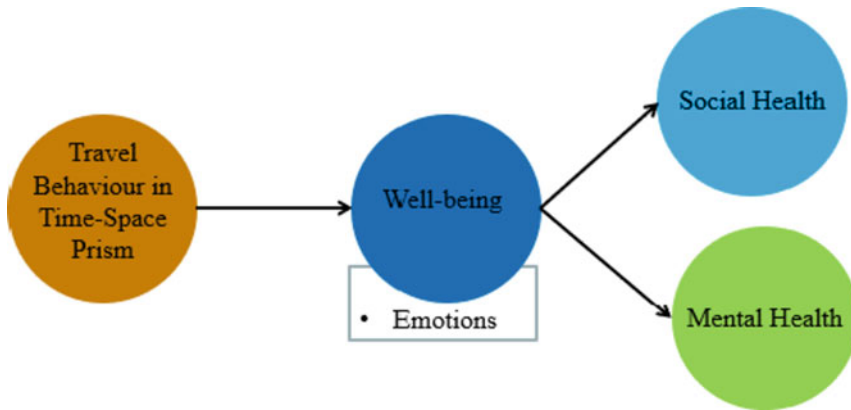


Fig. 1 Relation between travel behaviour in time–space prism and social and mental health

have negative impact on an individual’s social and mental health. During COVID-19 pandemic, the out-of-home activity restrictions are also found to influence individuals’ subjective well-being and consequently mental health, as some of the activities are essential to maintain or enhance their well-being [19] as cited in [7].

A person-centred analysis shown that in developing countries, individuals who have a more balanced life, with enough time spent for active leisure/travel, leisure activities, work/school and sleeping have better physical, mental, and social health [20] as cited in [9]. This shows that theoretically, in order to have a better social and mental health, individuals need to have more frequent leisure and social engagement associated with higher time spent and number of activities and trips which correlated to our social and well-being needs. In a study conducted to study the impact of people’s transportation-related social inclusion due to the duration of their activities, built environment, travel characteristics and socio demographics in Bandung, Indonesia, it reveals that individuals with higher social inclusion index are more likely to have longer time spent for out-of-home discretionary trips during weekday [12]. Higher social inclusion index may indicate a better social and mental health.

Several common approaches for evaluating health-related QOL have been developed. Among these methods, Short-Form 36 (SF-36) is one of the most commonly used generic health-related QOL measures and adopted by more than 110 countries [13]. The Short Form-36 was designed from the General Health Survey of the Medical Outcomes Study by Stewart and colleagues [21, 22] as cited in [13]. There are eight subscales that comprehended in SF-36 which are physical functioning (PF), bodily pain (BP), limitations on role functioning because of physical health (RP), mental health (MH), general health (GH), social functioning (SF), vitality (VT) and limitations on role functioning because of emotional problems (RE). These eight subscales are used as a health-related QOL to measure health, consist of physical, social and mental health.

2.3 Existing Studies Related to Travel Behaviour During COVID-19 Pandemic

According to a study that used instantaneous data from Taiwan's Taipei Metro System to investigate the effects of the COVID-19 outbreak on metro use, the effects of the COVID-19 is more significant during weekend compared weekday. From the analysis of the data, one COVID-19 case reduced metro use by 1.2% and 3.04% during weekdays and the weekends respectively [23]. From the analysis of daily ridership in metro station located near to leisure and entertainment areas, the recreational leisure trips decrease in both during weekend and weekdays. This is due to perceived factors of population whereby they intended to reduce their recreational leisure trips in response to the fear of infection [23].

In a study investigating activity-travel behavior change due to COVID-19 in Australia, it is shown that the outbreak distorted the respondents' out-of-home activities such as shopping, social activities, and dining trips by 76%, 80%, and 76%, respectively [24] as cited in [25]. In a study which aiming to examine the change in activities and associated travel during the beginning of COVID-19 pandemic in Indonesia, the results demonstrated 71.28% and 15.82% of the respondents reported their travel reductions as "very significant" and "significant," respectively [25]. Focusing on socialising and discretionary trips, result from the data analysis showing that sightseeing and dining trips also decreased from at least three times to once a week during the pandemic [25]. In addition, average number of social and shopping trips reduced substantially, from two to one and three to twice weekly [25].

In more extensive study conducted in Indonesia which investigates the effect of imposed experiences during the outbreak on travel behaviour changes during new-normal, most respondents from the online questionnaire irritated (4.19), dull (3.94), worried (3.81), tired (3.25) and annoyed (3.23) during the outbreak. This indicates most of the respondents have negative emotions due to the COVID-19 pandemic and this may affect their social and mental health. From the multinomial logistic regression of the data, the difference in frequency of travel during and before COVID-19 decreases for out-of-home activities with varied value of t-stat coefficients and thus, we can conclude that out-of-home dining trips, recreational trips and social trips decreases during the outbreak. All types of online in-home activity are significant with positive coefficient indicating its frequency increased during COVID-19 pandemic.

3 Methodology

This project will be investigating the relationship between change of socialising and discretionary trips, and activities during COVID-19 pandemic on social and mental health. The independent variables of this study which is the change of socialising and discretionary trips, and activities during COVID-19 pandemic, obtained from the survey conducted in the previous study entitled 'Survey on Effects of

COVID-19 Pandemic on Travel Behaviour in Malaysia’ datasets. The datasets consist of collected information on daily different individuals’ activity travel pattern and participation before and after COVID-19 pandemic in Malaysia.

In the data analysis, the Statistical Package for the Social Scientist (SPSS) software were used in carrying out the bivariate and multivariate analysis. Since the dependant variable, social and mental health are not quantitative elements, health-related quality of life (QOL) questions based on the Short-Form 36 (SF-36) was developed in the questionnaire design. Therefore, the state of social and mental health will be measured by carrying out factor score analysis incorporating the variables that are used to estimate mental and health indices as shown in Fig. 1. In the data analysis, analysis of variance (ANOVA) and linear regression were chosen to investigate the empirical relationship between change of socialising and discretionary trips, and activities during COVID-19 pandemic on social and mental health. The methodology flowchart is shown in Fig. 2.

Fig. 2 Health-related QOL with two-factor structure

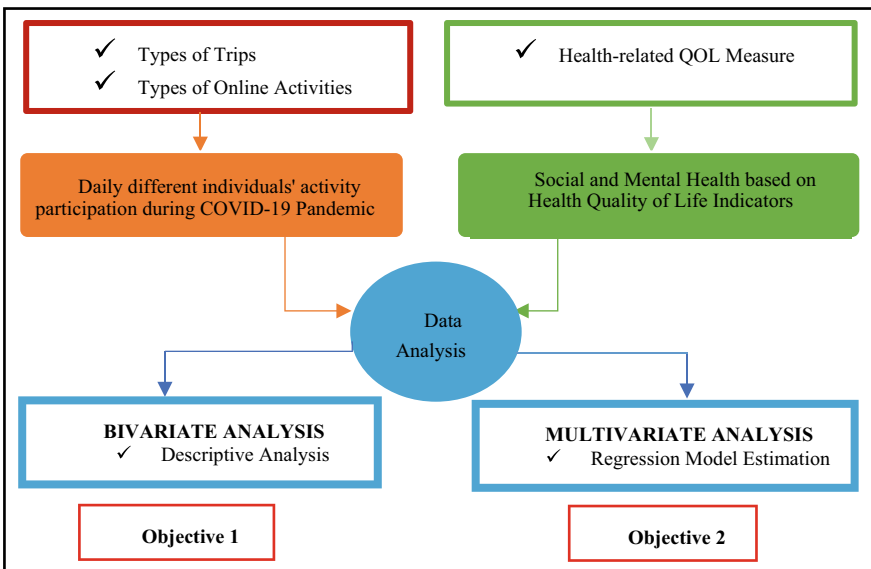
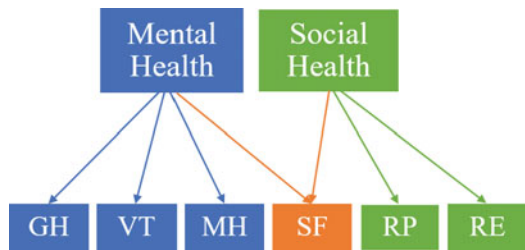


Fig. 3 Methodology Flowchart

3.1 ‘Survey on Effects of COVID-19 Pandemic on Travel Behaviour in Malaysia’ Dataset

The dataset was collected from November 2020 until June 2021. As shown in Tables 1, 2, 3 and 4, the survey was utilized to gather information about respondents’ individual and household socio-demographic and spatial characteristics which cover their personal characteristics and built environment. Besides, it also contained respondents’ activity travel behaviour, online activities comparison before and after COVID-19 pandemic (PKP, PKPB and PKPP) in weekdays and weekends based on a 7-point Likert scale, ranging from 1 (least frequent) to 7 (most frequent). The travel behaviour section covers their comparison of travel frequency, comparison of total number of daily trips, main purpose of travel and comparison of trip duration for the main purpose of travel. The data collected six categories of trip classifications, five of which are discretionary trips: grocery shopping, dining, socialising, sport and healthcare. Meanwhile, online activity participations covered in this survey are work or school from home, online grocery shopping, online shopping, online meeting, food delivery and streaming movies.

The respondents’ social and mental health were assessed using health-related quality of life (QOL) questions which derived from Short-Form 36 (SF-36). Social and mental health were assessed using a variety of category, including limitations on

Table 1 Questionnaire Contents – Section A

Socio-demographic and Spatial Characteristics	
Type of Data	Category
Individual sociodemographic information	Gender, Age, Highest level of education, Occupation, Occupation sector, Marital status
Household sociodemographic information	Household size, Household income, Number of cars owned by household, Number of motorcycles owned by household, State of residence, Postcode of residence
Journey to nearest amenity	Perceived time taken for journey to nearest city, nearest school, nearest grocery shop, nearest health clinic, nearest hospital, nearest mall

Table 2 Questionnaire Contents – Section B

Activity Travel Behaviour Comparison Before and After COVID-19 Pandemic			
• Comparison of travel frequency • Comparison of total number of daily trips	• Weekdays • Weekends	Time period	Type of trips
		• Before and after the COVID-19 pandemic (PKP and PKPB)	Work/school trips, Grocery shopping trips, Dining trips, Socialising trips, Sport/recreational trips, Healthcare trips
		• Before and after the COVID-19 pandemic (PKPP)	

Table 3 Questionnaire Contents – Section C

Online Activities Comparison Before and After COVID-19 Pandemic			
Comparison of weekly activity frequency	Activity	Time period	Purpose of Travelling
	<ul style="list-style-type: none"> • Work/study from home • Grocery e-shopping • E-shopping • E-meeting • Online delivery food/drinks • Streaming movies 	Before and after the COVID-19 pandemic (PKP and PKPB)	Work/school trips, Grocery shopping trips, Dining trips, Socialising trips,
		Before and after the COVID-19 pandemic (PKPP)	Sport/recreational trips, Healthcare trips, Others

Table 4 Questionnaire Contents – Section D

Health Before and After COVID-19 Pandemic		
Health-related Quality of Life (QOL) Questions	Time period	
<ul style="list-style-type: none"> • Weekdays • Weekends 	Before PKP	
	During PKP and PKPB	
	During PKPP	

role functioning due to physical health (RP), limitations on role functioning due to emotional problems (RE), social functioning (SF), general health (GH), bodily pain (BP), vitality (VT) and mental health (MH). Social health is defined by RP, SF and RE while mental health defined as BP, VT, GH, MH and SF. The survey’s responses in the health section were based on a 7-point Likert scale, with intensity levels ranging from 1 (none at all) to 7 (very intense). The social and mental health indexes were derived using factor score analysis with a varimax rotation of the specified categories which both dependent variables are defined based on the health-related quality of life (QOL) measures. Varimax rotation which is widely utilised when a factor is generated from the joint interaction of multidimensional data of the latent variables [26] as cited in [16]. The factor scores have mean of zero which are standardised variables within a range of -3 to 3 throughout the sample as a Z-score metric, fundamentally carrying identical data in a more compressed form [27] as cited in [16]. The least square method was used to obtain the factor scores using the Statistical Package for the Social Scientist (SPSS).

In this study, bivariate analysis is primarily used to investigate the relationship between two variables, namely independent variable: change of socialising and discretionary trips during COVID-19 pandemic, and dependant variables: social and mental health. Meanwhile, multivariate analysis is a more advanced form of statistical analysis technique when used when there are more than two independent variables in the data set which are change of socialising and discretionary trips during COVID-19 pandemic and online during COVID-19 pandemic, and dependant variable: social and mental health. The independent variables are obtained from ‘Survey on Effects of COVID-19 Pandemic on Travel Behaviour in Malaysia’ dataset. The comparison

covers the time period of before PKP/PKPB, during PKP/PKPB and during PKPP. The dependant variables involved in the analysis are social and mental health. Both variables are treated as separate variables, with a unique solution derived from factor score analysis for each of the variable. The method of analysis adopted in this study are Analysis of Variance (ANOVA) and simple linear regression model conducted using Statistical Package for the Social Scientist (SPSS). The summary of 'Survey on Effects of COVID-19 Pandemic on Travel Behaviour in Malaysia' dataset is shown in Tables 5 and 6.

Majority of the respondents are females (66.4%). Most of the respondents are in the age range of 23–45 years old (84.5%) where most of them have Degree as their highest level of education (48.6%). In terms of employment, the majority of respondents (59.3%) work full-time, with 69.1% of them not working in essential services. The monthly income distribution is dominated by respondents within 3001 to 7000 Ringgit Malaysia (32.6%). In relation of marital status, the majority of respondents (61.4%) are single and married (38.1%). The respondents are mainly from households with four to six members (57.3%), and they own one to two cars and motorcycles, with 83% and 56.4%, respectively.

Table 5 Respondents' socio-demographic and spatial characteristics, N = 438

Variables	Percentage	Variables	Percentage
Gender		Working in essential services	
Male	33.50	Not working in essential services	69.10
Female	66.40	Health services	5.70
Age		Banking and finance	4.10
< 22 years old	10.90	Food Supply and Services	3.70
23–45 years old	84.50	Internet and Communications	3.00
46–55 years old	3.90	Electricity	2.70
> 56 years old	0.70	Hospitality	1.80
Education		Retail	1.60
High School	6.60	Safety	1.40
Diploma	15.30	Fuels	1.10
Degree	48.60	Logistics	1.10
Master	21.20	Waste Management	1.10
Doctorate	8.20	Online Shop	0.90
Employment		Broadcaster	0.90
Full time	59.30	Transportation	0.70
Part time	3.40	Courier	0.70
Student	30.60	Water services	0.20
Housewife	2.50		
Not working	4.10		

Table 6 Respondents' socio-demographic and spatial characteristics, N = 438 (Continued)

Variables	Percentage	Variables	Percentage
Marital status		Household number	
Married	38.10	< 3	24.90
Single	61.40	4–6	57.30
Single Parents	0.50	8–9	11.90
Car numbers		> 10	5.70
0.00	6.90	Income (RM)	
1–2	83.00	< 3000	28.30
> 2	35.60	3001–7000	32.60
Motorcycle numbers		7001–10,000	17.30
0.00	32.00	> 10,000	21.70
1–2	56.40		
> 2	11.60		

4 Results and Discussion

4.1 Overall Social and Mental Health During PKP/PKPB and PKPP

Figure 4 shows the overall social and mental health during COVID-19 outbreak, specifically during PKP/PKPB and PKPP timeline. Individuals with high social and mental health refers to social and mental health score of greater than zero (>0). Low social and mental health, on the other hand, refers to those who have a social and mental health score of equal to or less than zero (<0). Since socialising and discretionary trips tend to correlate on better well-being and social and mental health [16], in general, higher number of socialising and discretionary trips will improve social and mental health. Since the change in comparison of social and mental health during PKP/PKPB and PKPP is statistically not significance (p value more than 0.1), this study will focus only on the timeline of PKP/PKPD to allow more critical analysis to be conducted on the dataset.

4.2 Descriptive Analysis of Social and Mental Health Based on Trip Comparison Before and After PKP/PKPB

Analysis of Variance (ANOVA) is used in this study to analyse the categorical factor of the independent variable and the continuous response of the dependant variable. For both social and mental health, the independent variable which is the travel frequency comparison before and after COVID-19 pandemic was categorized into three groups for each type of trip during weekdays and weekends. The categorization

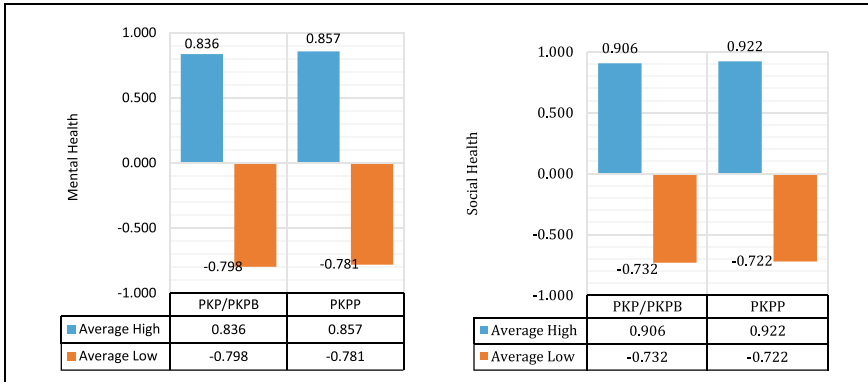


Fig. 4 Overall Social and Mental Health during COVID-19 Outbreak

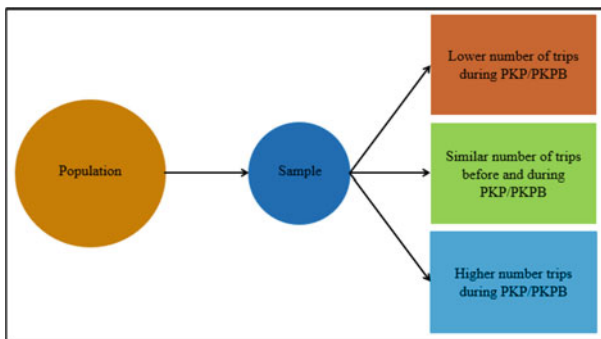


Fig. 5 One-Way-ANOVA – 3 independent groups based on trip frequency comparison before and after PKP/PKPB

of the groups is based on comparison of number of trips before and during the PKP/PKPB. The first group is those respondents who did lower number of trips during PKP/PKPB. Second group is those respondents who performed similar number of trips before and after PKP/PKPB. Last but not least is those individuals who did higher number trips during PKP/PKPB. The ANOVA was used to determine the range of values for the difference in means within each pair of the group which illustrated in Fig. 5.

4.2.1 Social and Mental Health During PKP/PKPB (Weekdays)

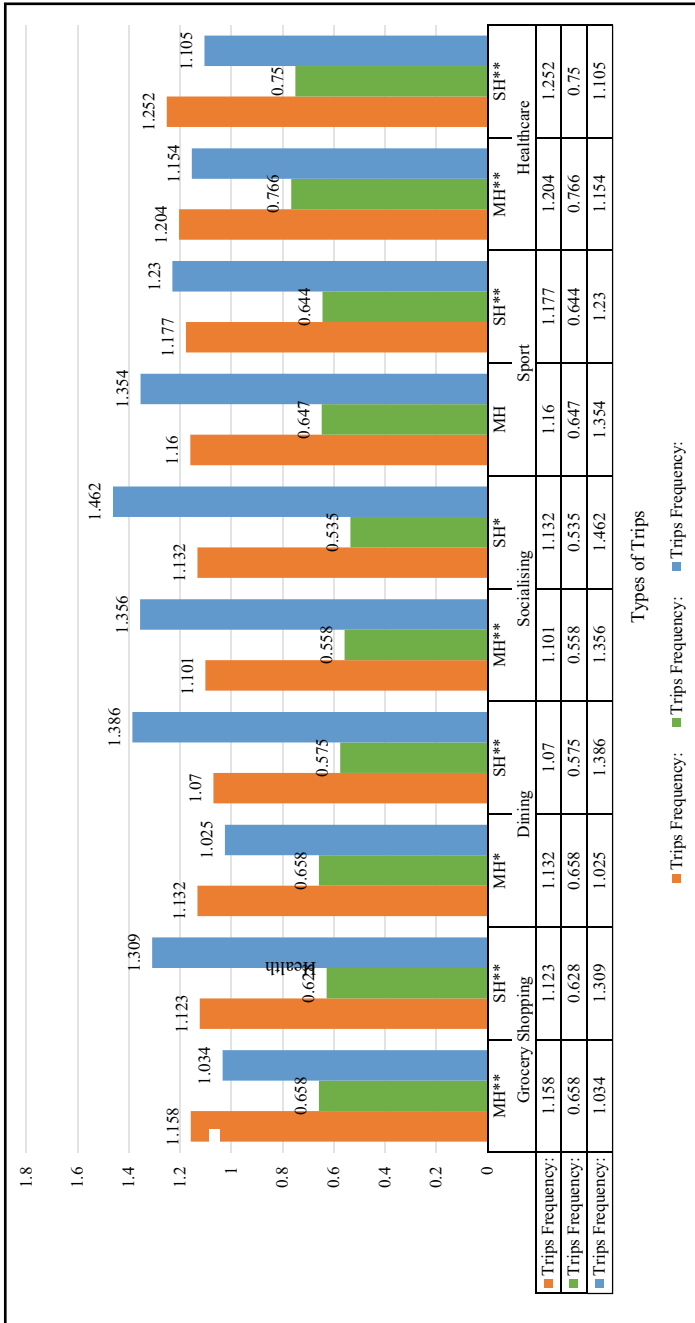
Based on Fig. 6, all types of trips: grocery shopping, dining, socialising, sport and healthcare performed during weekdays have significance correlation with social health based on the p values. The study shows that individuals who performed higher socialising and discretionary trips during weekdays, have a better social health

compared to those who do not. It is consistent with all types of trips except healthcare trips. Individuals who performed high number of healthcare trips tend to have poor health conditions which captured by the intermediate variables of social health which are limitations on role functioning due to physical health and emotional problems (RP and RE). Health is a constant limitation that limits activity-travel participation and characteristics, according to previous research related to this topic [28]. Since they have poor health conditions especially during the COVID-19 pandemic, it translates to additional capability constraints which limit the individual's ability to participate in daily activity and travel in time-space-prism. Therefore, lower number of trips for healthcare purposes will have higher social health score as the individual is assumed to be healthier. As shown in Fig. 6, individuals who performed higher weekdays healthcare trips have lower social health score compared to those who had less frequent weekdays healthcare trips with score of 1.105 and 1.252 respectively.

Individuals who performed higher weekdays socialising trips and dining trips during PKP/PKPB have the highest social health score with score of 1.462 and 1.386 respectively. This is due to the nature of the trip as socialising and dining trips strongly linked to higher social engagement in developing meaningful relationship with others resulting positive effects on social health. During the COVID-19 pandemic, perceived social isolation (lower social engagement) had a huge global impact, with significant emotional consequences for social health [29]. This is supported by this study where in the group pairs of Trip Frequency: Lower during PKP/PKPB, weekdays socialising and dining trips during PKP/PKPB have the lowest social health score which are 1.32 and 1.107 respectively as shown in Fig. 6.

Only weekdays grocery shopping, dining, socialising and healthcare trips have significance impact with mental health based on the p values. For mental health model, socialising trips have highest and lowest mental health within their travel frequency group pairs with score of 1.356 and 1.101 respectively. Weekdays sport trips have no significance impact towards mental health model. Sport trips tends to correspond to greater physical health as it involved with physical activity. However, when it comes to mental health, it does not establish a cause-and-effect relationship because there is not enough information to indicate that greater levels of depression and anxiety which related to mental health, are caused by a lack of physical activity [30]. [31] argued that the relationship works the other way around where the more depressed and anxious an individual becomes, the less likely they are to engage in physical activity and it is certainly supported in the case of depression, as depressed people are less likely to want to engage in physical activities. Moreover, [32] argued that although there is a substantial link between physical exercise and mental health, restoring physical activity through a short-term intervention does not necessarily improve mental health. This study supports these findings which shown in Fig. 6 where sport trips are statistically insignificant on mental health model.

During weekdays PKP/PKPD, individuals who had higher number of grocery shopping trips, dining trips, and healthcare trips had a lower mental health score than those who performed lower number of trips. Higher number of these trips means those individuals are most likely to have a more compact time-space-prism since they need to attend more trips (trades more of their time budget in time-space-prism)



Note: ** means very significance, $p < 0.05$, * means significance, $p < 0.1$

Fig. 6 Mean Square of Trips Frequency Comparison Within Groups on Social and Mental Health during PKP/PKPB (Weekdays)

in addition to mandatory activities such as work or school which are considered as primary activities during the weekdays. Besides, there is possibilities that their travel behaviour such as travel mode and duration of trips gives arise to negative well-being from their terrible travel experiences [18]. Since positive well-being is an important component of mental health [12], negative well-being will translate to poor mental health especially in the context of repetitive trips.

4.2.2 Social and Mental Health During PKP/PKPB (Weekends)

Based on Fig. 4, weekends sport and healthcare trips are significant towards social health. Meanwhile, only weekends healthcare trips that are significant towards mental health. While the other types of trips do not influence social and mental health as those relationships are insignificance based on the p values. Based on the overall activity travel participation between weekdays and weekends, it is concluded that socializing and discretionary trips during weekdays have stronger impact towards our social and mental health during COVID-19 pandemic. This suggests that most of the respondents may have spent higher amount of time for in-home activities which improves their social and mental health during the weekends thus reducing their out-of-home travel participation. This is highly the reasoning on whys the weekends socializing and discretionary trips are not significance towards social and mental health model. It follows the same trendline as another study which is based on the American Time Use Survey data, the estimated joint models found that individuals who engaged in less out-of-home activities were more likely to spend their leisure and personal time at home [33].

The imbalance between activity participation between weekdays and weekends is supported in other researches related to travel behaviour where individual will perform less travels or less size of activity space on weekends when they undertake other way around on weekdays [34] as cited in [6]. As a consequence, it will correspond to different state of weekdays and weekends social and mental health. Since this study does not support findings from previous research where the person trip rates during the weekends are marginally lower than those during the weekdays [35] and its purposes tend to be non-mandatory or discretionary (e.g., leisure and social) [36], as this findings only valid during the timeline before the COVID-19 pandemic. From the generic comparison, we can conclude that COVID-19 pandemic caused an activity-travel behavior change specifically in out-of-home activity travel participation which follows similar pattern from study conducted by in Indonesia [25].

5 Conclusion and Recommendations for Future Studies

5.1 Conclusion

In a nutshell, the effects of change of socialising and discretionary trips during COVID-19 pandemic on social and mental health in this study are vary depending on the trip purposes, which includes grocery shopping, dining, socialising, sport and healthcare, as well as whether the trips are made on weekdays or weekend. From the bivariate analysis, all of the weekday types of trips are statistically significance towards social health model. Only weekdays sport trips are not correlate to mental health model. Conversely, during weekends, only healthcare trips affecting social and mental health while sport trips fundamental to social health only. Based on the comparison of overall activity travel participation between weekdays and weekends, it is concluded that socialising and discretionary trips during weekdays have stronger impact towards our social and mental health during COVID-19 pandemic.

Based on the multivariate analysis, only dining trips is significant towards social health with coefficients 0.122 during weekdays and 0.174 during weekends. All types of trips are statistically insignificance in the mental health model. In this study, it is estimated that individuals have begun to look for ways to substitute their out-of-home activities with in-home activities. However, only online shopping has a statistically significant impact on both social and mental health with coefficient of 0.195 and 0.191 respectively. The reduced stress effects correlates to the increase of social and mental health state where our well-being acts as intermediate variable.

5.2 Recommendations

As for future works, several improvements can be implemented to improve the quality of research related to the project's topic. As recommendations to improve the quality of research related to the topic, the data analysis should use a more complex dataset such as individuals time-use diary over a time period as it provides a better understanding of individuals' daily time spent in activity participations with respect to time-space-prisms. Besides, it is essential to include other types of activities such as mandatory activities (e.g., work, school) to provide a more extensive analysis on how change in travel behaviour affects our health during COVID-19, specifically social and mental health. In the health-related quality of life (QOL) approaches, it is important to recognize health as three factor structure which are physical, social and mental health. By including physical health in the research, linkage between change in travel behaviour and overall health can be explored.

References

1. Fan V, Cheong R, MahWengKwai & Associates (2020) Malaysia: MCO, CMCO, RMCO, CMCO Again: Regulations and SOPs Movement Control Order (MCO)
2. Georgia T (2022) What is Social Health? Definitions, Examples and Tips on Improving Your Social Wellness, HIF Heal. Lifestyle Blog. <https://blog.hif.com.au/mental-health/what-is-social-health-definitions-examples-and-tips-on-improving-your-social-wellness>
3. U.S. Department of Health & Human (2020) Mental Health and Coping during the Coronavirus (COVID-19) Pandemic
4. Prakash J, Chatterjee K, Srivastava K (2020) Industrial impact of COVID-19 pandemic: mental health perspective. *Ind Psych J* 29(1):9. https://doi.org/10.4103/ipj.ipj_39_20
5. Kahneman D, Krueger AB, Schkade DA, Schwarz N, Stone AA (2004) A survey method for characterizing daily life experience: the day reconstruction method. *Science* 306(5702):1776–1780. <https://doi.org/10.1126/science.1103572>
6. Ramli MI, Dharmowijoyo DE (2018) Activity-travel behaviour, and daily and global well-being. *MATEC Web Conf.* 203:1–11. <https://doi.org/10.1051/mateconf/201820305004>
7. Rizki AM, Dharmowijoyo DBE, Balijepalli C, Joewono TB, Farda MM (2021) Travel-activity changes during new normal period: learning from the COVID-19 outbreak in Indonesia *Submitt. Transp.*
8. Senbil M, Kitamura R (2009) The optimal duration for a travel survey. *IATSS Res.* 33(2):54–61. [https://doi.org/10.1016/S0386-1112\(14\)60244-2](https://doi.org/10.1016/S0386-1112(14)60244-2)
9. Dharmowijoyo DBE (2016) The complexity and variability of individuals' activity-travel patterns in Indonesia
10. Fox M (1995) Transport planning and the human activity approach. *J Transp Geogr* 3(2):105–116. [https://doi.org/10.1016/0966-6923\(95\)00003-L](https://doi.org/10.1016/0966-6923(95)00003-L)
11. Burnett KP, Thrift NJ (1979) New approaches to travel behavior. *Behav. Travel demand Model.* London Croom Helm
12. Dharmowijoyo DBE, Joewono TB (2020) Mobility and health: the interaction of activity-travel patterns, overall well-being, transport-related social exclusion on health parameters. In: Sulaiman SA (ed) *Energy Efficiency in Mobility Systems*. Springer, Singapore, pp 53–83. https://doi.org/10.1007/978-981-15-0102-9_4
13. Zhang J (2013) Urban Forms and Health. Promotion: An Evaluation Based On Urban Forms And Health Health-Related Qol Indicators," *Proceeding 13th World Conf. Transp. Res.*, pp. 1–20, 2013.
14. Liao F (2019) Space – time prism bounds of activity programs : a goal-directed search in multi-state supernetworks. *Int J Geogr Inf Sci* 33(5):900–921. <https://doi.org/10.1080/13658816.2018.1563300>
15. Miller HJ (2005) What about people in geographic information science. *Re-present. Geogr. Inf. Syst.* 215–242 (2005)
16. Dharmowijoyo DBE, Susilo YO, Syabri I (2020) Time use and spatial influence on transport-related social exclusion, and mental and social health. *Travel Behav. Soc.* 21(June):24–36. <https://doi.org/10.1016/j.tbs.2020.05.006>
17. Fox M (1978) Transport planning and the human activity approach. *J Transp Geograph* 6923(95):3–8
18. van Wee B, Ettema D (2016) Travel behaviour and health: a conceptual model and research agenda. *J Transp Heal* 3(3):240–248. <https://doi.org/10.1016/j.jth.2016.07.003>
19. Ettema D, Gärling T, Olsson LE, Friman M (2010) Out-of-home activities, daily travel, and subjective well-being. *Transp. Res. Part A Policy Pract.* 44(9):723–732. <https://doi.org/10.1016/j.tra.2010.07.005>
20. Hunt E, McKay EA, Dahly DL, Fitzgerald AP, Perry IJ (2014) A person-centred analysis of the time-use, daily activities and health-related quality of life of Irish school-going late adolescents. *Qual Life Res* 24(6):1303–1315. <https://doi.org/10.1007/s11366-014-0863-9>
21. Ware JEJ, Sherbourne CD (1992) The MOS 36-item short-form health survey (SF-36). I. Conceptual framework and item selection. *Med Care* 30(6):473–483

22. McHorney CA, Ware JEJ, Raczek AE (1993) The MOS 36-item short-form health survey (SF-36): II. Psychometric and clinical tests of validity in measuring physical and mental health constructs. *Med Care* 31(3):247–263. <https://doi.org/10.1097/00005650-199303000-00006>
23. Chang H-H, Lee B, Yang F-A, Liou Y-Y (2021) Does COVID-19 affect metro use in Taipei? *J Transp Geogr* 91:102954. <https://doi.org/10.1016/j.jtrangeo.2021.102954>
24. Beck MJ, Hensher DA, Wei E (2020) Slowly coming out of COVID-19 restrictions in Australia: implications for working from home and commuting trips by car and public transport. *J Transp Geogr* 88:102846
25. Irawan MZ, Belgiawan PF, Joewono TB, Bastarianto FF, Rizki M, Ilahi A (2022) Exploring activity-travel behavior changes during the beginning of COVID-19 pandemic in Indonesia. *Transportation (Amst)* 49(2):529–553. <https://doi.org/10.1007/s11116-021-10185-5>
26. DiStefano C, Zhu M, Mindrila D (2009) Understanding and using factor scores: considerations for the applied researcher. *Pract. Assess. Res. Eval.* 14(1):20
27. Hair JF, Anderson RE, Tatham RL, William C (1998) *Black Multivariate Data Analysis*, Fifth ed. Prentice Hall, Englewood Cliffs
28. Ali M, Dharmowijoyo DBE, de Azevedo ARG, Fediuk R, Ahmad H, Salah B (2021) Time-use and spatio-temporal variables influence on physical activity intensity, physical and social health of travelers. *Sustainability* 13(21):12226
29. Pietrabissa G, Simpson SG (2020) Psychological consequences of social isolation during COVID-19 outbreak. *Front Psychol* 11:2201
30. Tyson P, Wilson K, Crone D, Brailsford R, Laws K (2010) Physical activity and mental health in a student population. *J Ment Heal* 19(6):492–499
31. Kroesen M, De Vos J (2020) Does active travel make people healthier, or are healthy people more inclined to travel actively? *J Transp Heal* 16:100844
32. Giuntella O, Hyde K, Saccardo S, Sadoff S (2021) Lifestyle and mental health disruptions during COVID-19. *Proc Natl Acad Sci* 118(9):e2016632118
33. Shabanpour R, Golshani N, Langerudi MF, Mohammadian A (2018) Planning in-home activities in the ADAPTS activity-based model: a joint model of activity type and duration. *Int J Urban Sci* 22(2):236–254. <https://doi.org/10.1080/12265934.2017.1313707>
34. Yamamoto T, Kitamura R (1999) An analysis of time allocation to in-home and out-of-home discretionary activities across working days and non-working days. *Transportation (Amst)* 26(2):231–250
35. Lockwood AM, Srinivasan S, Bhat CR (2005) Exploratory analysis of weekend activity patterns in the San Francisco Bay Area, California. *Transp Res Rec* 1926(1):70–78
36. Gim T-HT (2018) SEM application to the household travel survey on weekends versus weekdays: the case of Seoul, South Korea. *Eur Transp Res Rev* 10(1):1–16

Performance Border Gateway Protocol (BGP) on VLAN Network for Development Smart Hospitals



Ryan Ari Setyawan, Fatsyahrina Fitriastuti, and Agus Wari Yulianto

Abstract This research to analysis performace impelementation Border Gateway Protocol (BGP) for support infrastructure smart hospitals. BGP (Border Gateway Protocol) is a routing protocol used to exchange routing information between computers network. The performance of BGP is to map IP network table that points to the network reached between Autonomous Systems (AS). This study resulted in network optimization with a smaller response time of 39 ms when retrieving patient data. The method used is the analysis of quality of service. Testing using winbox as a simulation tool.

Keywords BGP · VLAN · Smart Hospitals · Quality of Service

1 Introduction

Smart hospital is one form of improving services for patients. One of them is an adequate internet network infrastructure. Internet usage is related to the performance of the protocol used [1]. The protocol that can be used is BGP. BPG is a form of protocol that can separate local networks and international networks [2, 3]. An Autonomous System (AS) is a network can be manage by a single organization. AS has two routing protocols: intra-AS routing and inter-AS routing protocol [3, 4]. BGP has been widely used to define routes data retrieval and have been utilized by stakeholders to direct traffic through certain paths and control the flow of information [5, 6]. With there is a separation of connection lines IIX (Indonesia Internet Exchange) and IX, It is expected that the connection that connects one ISP to another is on the Indonesia, then there is no need to use an external backbone line country. For this reason, this study tries to apply BGP to support the development of smart hospitals. Installing BGP on a VLAN network using Mikrotik. Mikrotik is a hardware and software that provides traffic management facilities, as well as other supporting

R. A. Setyawan (✉) · F. Fitriastuti · A. W. Yulianto
Departement of Informatics, Faculty of Engineering, Janabadra University, Yogyakarta, Indonesia
e-mail: ryan@janabadra.ac.id

© Institute of Technology PETRONAS Sdn Bhd 2024
B. S. Mohammed et al. (eds.), *Proceedings of the International Conference on Emerging Smart Cities (ICESC2022)*, Lecture Notes in Civil Engineering 324,
https://doi.org/10.1007/978-981-99-1111-0_38

facilities optimization in a network so that the network runs effectively, efficiently and stable [7, 8]. This research will also design BGP routing to separate data traffic used by a network network between the International network and IIX, and create network segments local to users with VLANs. The method used in this study is the quality of service [9]. Quality of service is used to measure internet network traffic, including response time [10, 11]. Quality of service is a method to determine the level of internet network service such as delay, latency, jitter and throughput [11, 12]. The research objective is to optimize internet performance by implementing routing BGP peer on Mikrotik to separate local and international connections, as well as how to implement Mikrotik VLAN. The tools used for testing are winbox. Winbox is a hardware device that is used to simulate the mikrotik network [13].

2 Materials and Method

2.1 Study Area

The study area is dr. Sardjito Hospital in Yogyakarta Indonesia, dr. Sardjito Hospital is a referral hospital for the Yogyakarta and Central Java, where patient care is the top priority. The hospital has a mission to provide excellent, patient-focused health services with a global market share. However, the increasing number of patients has hampered patient care a bit due to the response time in data collection. Internet network topology at dr. Sardjito with a simple topology uses unmanaged switches, the internet connection line is only an internet exchange line (international line), UTP cable as a transmission medium that connects network devices (Fig. 1) (Table 1).

2.2 Identify Problems Found

Based on the results of field observations with observations found problems:

1. There is a problem of user discomfort over the stored data because it can be accessed by other work units, because there is no IP Address grouping management for each work unit.
2. Less than optimal internet access, especially in retrieving patient data on other installation servers in collaboration with dr. Sardjito hospital, this is due to data retrieval via the global internet (internet exchange), thus requiring network optimization of path separation between local and international access.

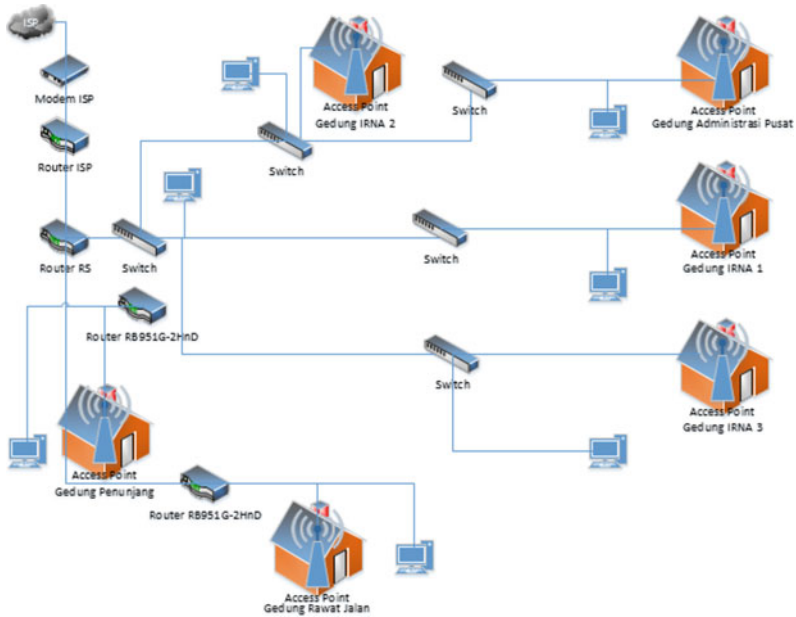


Fig. 1 Topology Internet Network in dr. Sardjito Hospital Existing computer network and its specifications in dr. Sardjito.

Table 1 Device Specification

Device	Qty	Unit
Modem	2	Huawei HG8245A
Cloud Core Router	1	CCR1009-7G-1C-15+
Cloud Core Router	1	CCR-1016 12G
RouterBoard Mikrotik	15	RB951G-2HnD
Switch Unmanaged	50	Allied Telesys AT-SFW716
Computer Client	600	PC
Access point	150	Ruckus & Unifi

2.3 Design New Topology

Dr. Sardjito Hospital already has a fiber optic network as the backbone. For that, create a new topology involving VLAN and BGP.

Figure 2. shows the ISP router connection flow, VLAN IX and VLAN IIX are created which are already connected to the Terabit BGP peer router as an ISP, then connected to a Hospital router where the router output in the form of VLANs is distributed through managed computer switches or work unit access points.

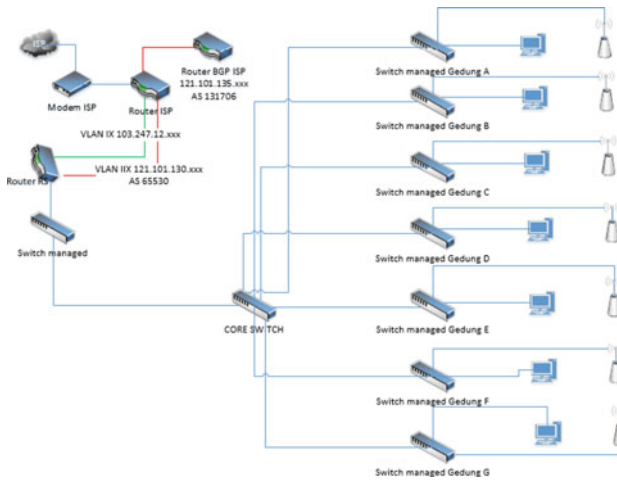


Fig. 2 Design New Topology Using VLAN and BGP

2.4 Configuration

The configuration carried out is the mikrotik configuration and checking the Mikrotik server through a personal computer.

Figure 3 show the interface layout, in order to make it easier for maintenance, ether1 and ether2 should be named according to the IP address that is set, the author gives ether1 a name with the name ether1_ISP_IX while ether2 with the name ether2_ISP_IIX. This Mikrotik router is configured graphically or using the CLI (Command Line Interface) command (Fig. 4).

for VLANs for local networks using the ether11 interface with the configuration, click the VLAN interface then click + in the name column, enter Satker1, the VLAN ID column is 750 while the interface column. For IP Configuration show Fig. 5.

Configuration BGP, ISP_IX router which has IP address 103.247.12.129 as gateway with dst-address 0.0.0/0. Next, configure the dst_address 121.101.135.33 which is the IP of the BGP peer router provided by the ISP, which is passed to the ISP_IIX gateway, which is 121.101.130.121 (Fig. 6).

3 Results

Testing with a ping test is carried out to test latency to the destination IP and traceroute to show the route traversed to the destination IP. This test compares between before and after using BGP Protocol (Figs. 7 and 8).

The response time for BGP testing can be shown in Table 2. response time needed to retrieve data from the server using the Postman application, which is an application

Fig. 3 Configuration Interface Ethernet

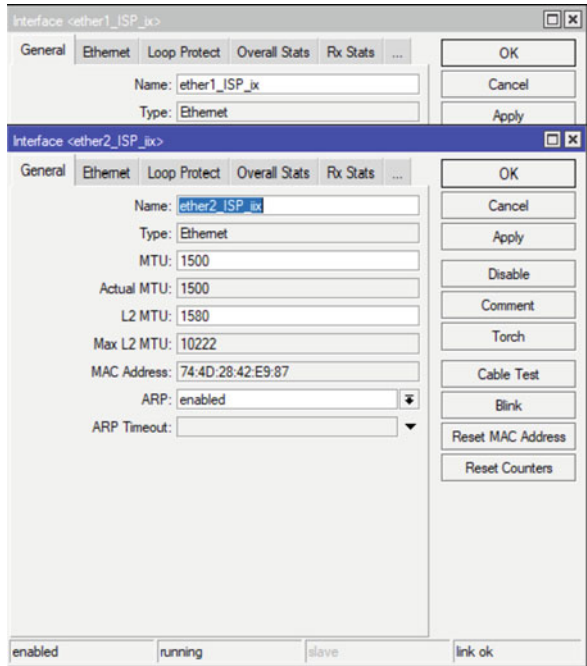


Fig. 4 Configuration VLAN

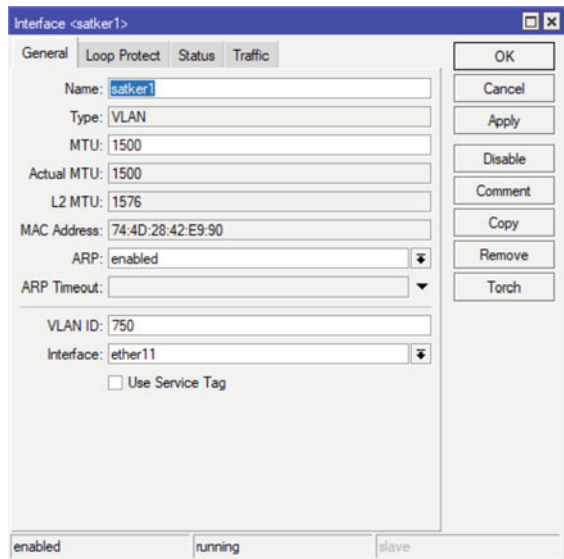
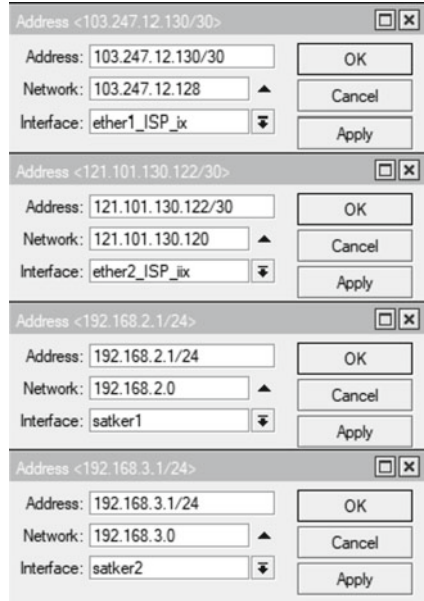


Fig. 5 IP Configuration



that functions as a REST CLIENT for REST API testing. Postman is used by API developers as a tool for testing APIs.

For QoS, Throughput measurement obtained an average value of 162 Kb/s, by calculating the number of bytes divided by the time span, and then the packet loss measurement is not found lost packets. while for delay, shown in Table 3.

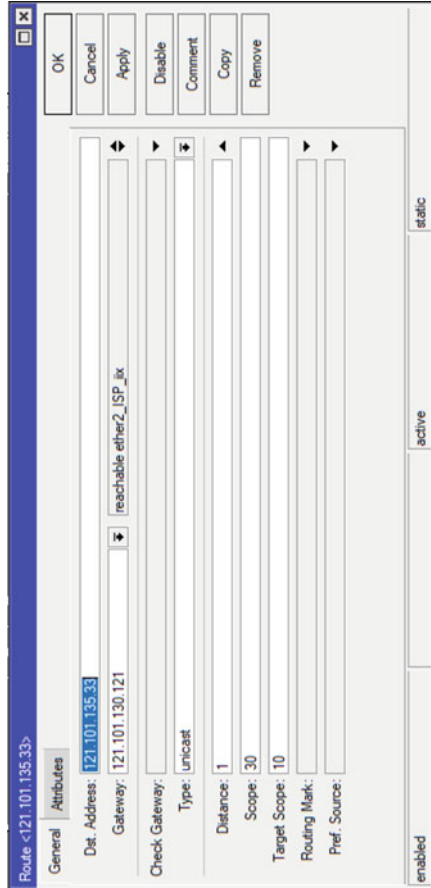
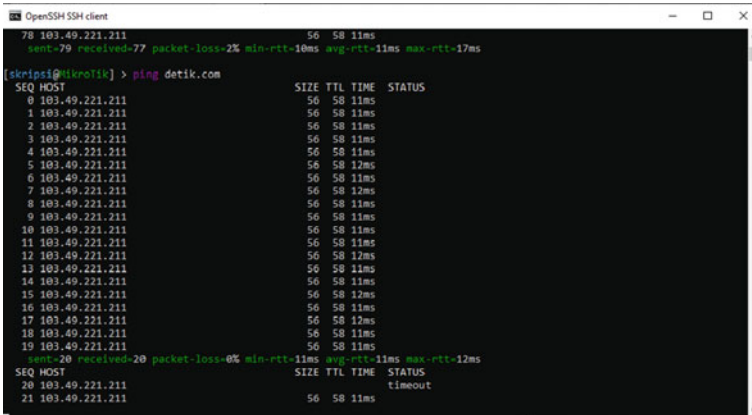


Fig. 6 BGP Peer Configuration



```
OpenSSH SSH client
78 103.49.221.211 56 58 11ms
sent=79 received=77 packet-loss=2% min-rtt=10ms avg-rtt=11ms max-rtt=17ms

[skripisi@nikro71k] > ping detik.com
SEQ HOST SIZE TTL TIME STATUS
0 103.49.221.211 56 58 11ms
1 103.49.221.211 56 58 11ms
2 103.49.221.211 56 58 11ms
3 103.49.221.211 56 58 11ms
4 103.49.221.211 56 58 11ms
5 103.49.221.211 56 58 12ms
6 103.49.221.211 56 58 11ms
7 103.49.221.211 56 58 12ms
8 103.49.221.211 56 58 11ms
9 103.49.221.211 56 58 11ms
10 103.49.221.211 56 58 11ms
11 103.49.221.211 56 58 11ms
12 103.49.221.211 56 58 12ms
13 103.49.221.211 56 58 11ms
14 103.49.221.211 56 58 11ms
15 103.49.221.211 56 58 12ms
16 103.49.221.211 56 58 11ms
17 103.49.221.211 56 58 12ms
18 103.49.221.211 56 58 11ms
19 103.49.221.211 56 58 11ms
sent=20 received=20 packet-loss=0% min-rtt=11ms avg-rtt=11ms max-rtt=12ms
SEQ HOST SIZE TTL TIME STATUS
20 103.49.221.211 timeout
21 103.49.221.211 56 58 11ms
```

Fig. 7 Latency Before Configuration BGP

```
OpenSSH-5.5p1 client
[serips@stros313] > ping detik.com
PING 103.49.221.211: 56 data bytes
0 103.49.221.211: 56 bytes from 103.49.221.211: icmp_seq=0 ttl=58 hrt=17ms
1 103.49.221.211: 56 bytes from 103.49.221.211: icmp_seq=1 ttl=58 hrt=11ms
2 103.49.221.211: 56 bytes from 103.49.221.211: icmp_seq=2 ttl=58 hrt=11ms
3 103.49.221.211: 56 bytes from 103.49.221.211: icmp_seq=3 ttl=58 hrt=11ms
4 103.49.221.211: 56 bytes from 103.49.221.211: icmp_seq=4 ttl=58 hrt=11ms
5 103.49.221.211: 56 bytes from 103.49.221.211: icmp_seq=5 ttl=58 hrt=11ms
6 103.49.221.211: 56 bytes from 103.49.221.211: icmp_seq=6 ttl=58 hrt=11ms
7 103.49.221.211: 56 bytes from 103.49.221.211: icmp_seq=7 ttl=58 hrt=11ms
8 103.49.221.211: 56 bytes from 103.49.221.211: icmp_seq=8 ttl=58 hrt=11ms
9 103.49.221.211: 56 bytes from 103.49.221.211: icmp_seq=9 ttl=58 hrt=11ms
10 103.49.221.211: 56 bytes from 103.49.221.211: icmp_seq=10 ttl=58 hrt=11ms
11 103.49.221.211: 56 bytes from 103.49.221.211: icmp_seq=11 ttl=58 hrt=11ms
```

Fig. 8 Latency After Configuration BGP

Table 2 Response Time

Server	Before	After
BPJS	118 ms	39 ms
SIRS	104 ms	80 ms
Sisrute	443 ms	139 ms

Table 3 Delay

	Total	Average
Delay	21.277162 ms	15.8666 ms
Jitter	21.28267 ms	15.87075 ms

4 Conclusion

Network optimization and internet performance by implementing peer BGP routing on Mikrotik to separate local and international connections as evidenced by the small response time in data collection on the BPJS server, and the application of Mikrotik VLAN as a segment between work units of dr. Sardjito Hospital succeeded with the proof of the PC client trial that he managed to get a DHCP IP according to the IP VLAN that was set on Mikrotik. So, Border Gateway Protocol using VLAN Network can for development smart hospital.

References

- Rodrigues VF, da Rosa R, Righi CA, da Costa R, Antunes S (2022) Smart hospitals and iot sensors: why is QoS essential here? *J Sens Actuator Netw* 11(3):33. <https://doi.org/10.3390/jsan11030033>
- Cheng M, Li Q, Lv J, Liu W, Wang J (2021) Multi-scale LSTM model for BGP anomaly classification. *IEEE Trans Serv Comput* 14(3):765–778. <https://doi.org/10.1109/TSC.2018.2824809>
- Zhao X, Band SS, Elnaffar S, Sookhak M, Mosavi A, Salwana E (2021) The implementation of border gateway protocol using software-defined networks: a systematic literature review. *IEEE Access* 9:112596–112606. <https://doi.org/10.1109/ACCESS.2021.3103241>
- Deng H, Li W, Agarwal DP (2002) Routing security in wireless ad hoc networks. *IEEE Commun Mag* 40(10):70–75. <https://doi.org/10.1109/MCOM.2002.1039859>
- Douzet F, Petiniaud L, Salamatian L, Limonier K, Salamatian K, Alchus T (2020) Measuring the fragmentation of the Internet: the case of the Border Gateway Protocol (BGP) during the Ukrainian Crisis. In: *International Conference on Cyber Conflict, CYCON*, vol. 2020-May, pp. 157–182. <https://doi.org/10.23919/CyCon49761.2020.9131726>.
- Chang LH, Sung CH, Chiu SY, Lin YW (2010) Design and realization of ad-hoc VoIP with embedded p-SIP server. *J Syst Softw* 83(12):2536–2555. <https://doi.org/10.1016/j.jss.2010.07.053>
- Tamil Nadu: The Secured OLSR Protocol for MANET
- A. I. Technology (2014) Efficient Secure Topology Control Protocol, vol. 61, no. 3 (2014)

9. Elbasheer MO, Aldegheisem A, Alrajeh N, Lloret J (2022) Video streaming adaptive QoS routing with resource reservation (VQoSRR) model for SDN networks. *Electronics* 11(8):1252. <https://doi.org/10.3390/electronics11081252>
10. El Brak S, Bouhorma M, Boudhir A (2012) VoIP over VANETs (VoVAN): a QoS measurements analysis of inter-vehicular voice communication in urban scenario. In: Proceedings of 2012 5th International Conference on New Technologies, Mobility and Security. NTMS 2012 Conference Workshop. <https://doi.org/10.1109/NTMS.2012.6208691>
11. Wang Q et al (2019) Enable advanced QoS-aware network slicing in 5G networks for slice-based media use cases. *IEEE Trans Broadcast* 65(2):444–453. <https://doi.org/10.1109/TBC.2019.2901402>
12. Barcel J, Bellalta B, Cano C, Sfairopoulou A (2008) Delay in Single-Hop Ad-Hoc
13. Zamros NA, Bahari A (2022) Wifi Security at Edu Hub. *Progr. Eng. App. Technol.* 3(1):571–579

Optimum Content of Matos as an Additive in the Application of Cement Soil Stabilization as a Cement Composite Soil Base Layer



Teguh Widodo, Nur Ayu Diana, and Arusmalem Ginting

Abstract The challenge of applying soil–cement stabilization as a soil–cement composite foundation layer (LFSKT) in Indonesia is to find quarry soil with a grain content of less than 35% passing filter no. (additive) to achieve the required strength. This paper presents a laboratory study’s results on adding Matos soil stabilizer additives to cement-free soil compressive strength. A series of laboratory tests based on the Indonesian National Standard was carried out on the soil–cement and soil–cement-mats mixture composition to determine the optimal Matos content. The cement content used was 6%, 8% and 10% of the dry weight of the soil grains, while the Matos content was 1%, 1.5% and 2% of the cement weight. The study’s results showed that the optimum Matos content of 1.5% occurred for all cement content in A-7-6 soil and 6% cement content in A-7-5 and A-4 soils.

Keywords Additives · matos grade · UCS

1 Introduction

Soil–cement stabilization is a combination of chemical and mechanical stabilization. Soil–cement is a mixture of soil, cement, and water that is compacted to form a new soil–cement material with solid and impermeable bonds [1, 2]. Stabilization mechanisms when soil mixing, water absorption, and ion exchange reactions, hydration processes, and pozzolanic reactions [3], soil and cement particles are bound to each

T. Widodo · N. A. Diana (✉) · A. Ginting
Departement of Civil Engineering, Universitas Janabadra, Jl. Tentara Rakyat Mataram 57,
Yogyakarta, Indonesia
e-mail: nurayu@janabadra.ac.id

T. Widodo
e-mail: teguh_widodo@janabadra.ac.id

A. Ginting
e-mail: aginting@janabadra.ac.id

other and group together to form soil–cement particles which [4]. Soil–cement has been widely used for foundations, slope and soil reinforcement, embankments, soil stabilization around tunnels, reservoir walls, pavement base layers, parking areas, road shoulders, and soil-columns. -cement [5, 6]. Soil cement is most widely used in stabilizing road subgrades or as an alternative material for road pavement base layers [2], and in Indonesia, it is referred to as the soil composite cement to the base layer.

Cement soil stabilization will work well with the proper moisture and cement content in well-graded sandy soils (A2, in the AASHTO classification) and low plasticity silt soils (A5) [2, 7]. Soil–cement has weaknesses, namely: 1) it is less flexible (brittle, brittle) and has a low peak load strain, so it is prone to cracking, mainly if used as a soil composite cement to the base layer, adding cement content in the soil [2]. On the one hand, it will increase the shear strength, but on the other hand, it will make the cement soil more brittle and 2) have poor performance on high plasticity clays (A7) [2, 7–9]. The challenge of applying soil–cement stabilization as a soil–cement composite base layer is to increase the free compressive strength and the value of the California Bearing Ratio, CBR, and increase the flexibility/ductility of the cement-soil, especially in high-plastic clay soils. Efforts to improve ductility and the performance of soil–cement stabilization on high plasticity clay soils have been investigated, including the everyday use of rice husk ash–cement [10], cement-fly ash [11], cement-lime in 1 stage of stabilization [3, 5, 12] and two stages of stabilization [7, 13]. Improvement of the gradation by adding sand to the A7 soil before cement stabilization also increases the cement-free soil compressive strength [14].

The application of soil–cement stabilization as an alternative material for road pavement base layers in Indonesia has several advantages, namely: 1) the use of local soil materials will reduce the use of stone and sand aggregates used in conventional and concrete pavements, making it environmentally friendly [15]; 2) the construction of road infrastructure for trans Sumatra, Kalimantan, Sulawesi, and Papua is faced with the problem of the availability of stone aggregates (Kalimantan and Papua) and the high cost of material transportation due to the unavailability of adequate road infrastructure. Using local materials/soil will reduce the cost of transportation of road materials.

In Indonesia, the application of soil–cement stabilization as a soil–cement composite base layer began in 1980 with varying degrees of success [16]. The maximum cement content used in stabilizing Indonesia's soil composite cement layer is 8%. If the 8% cement content of the soil composite cement layer does not meet the requirements, then an added material with a content of 2% of the weight of cement is used to reduce the cement content and increase the strength—compressive strength and durability of the resulting cement soil. The added material that can be used in the soil composite cement of the base layer is in the form of powder, which is a mixture of cementitious and non-polymer minerals which has the function of reducing cement content and increasing the compressive strength and durability of cementitious soils—generated [17].

The challenge of applying soil–cement stabilization in Indonesia is finding additives to increase the shear strength of the soil or increase the flexibility/ductility of compact cement soil so that it is easy and cheap to bring to the job site. Matos soil stabilizer is one of the additions in the form of light crystalline powder and small volume, making it easier and less costly to transport materials to the job site.

This research is a laboratory study of the effect of the addition of Matos soil stabilizer on the free compressive strength. This study aims to determine the optimal level of addition of Matos soil stabilizer to reduce the cement content to achieve the required cement-free soil compressive strength. The results of this study are expected to be used as an evaluation material for the application of the Interim Special Specification for Soil Composite Cement Base Layers, which regulates the use of additive materials of 2% of the cement weight.

2 Method

The study was conducted based on the Indonesian National Standard [18] and Soil Cement Laboratory Hand Book [19]. The research was divided into two stages. The research preparation stage is to test physical properties, including specific gravity test (SNI 03-1964-1990), water content (SNI 03-1965-1990), soil grain size analysis using a hydrometer (SNI 03-3423-1994), filter (SNI 03-1968-1990), liquid limit (SNI 03-1967-1990), and plastic limit (SNI 03-1966-1990) for a minimum of 5 (five) soil samples from various locations. The five soils were then classified according to the American Association of State Highway and Transportation Officials (AASHTO) and Unified Soil Classification System (USCS) classification systems and were selected as high plasticity clays (CL, USCS) or (A7, AASHTO) as test soil.

The main research stages include: 1) Light compaction test (SNI 03-1742-1989) original soil (cement 0%), soil + cement (4%, 6% and 8%), 2) Manufacture of free compression test specimens, unconfined compression test original soil sample (cement 0%), and soil sample + cement (4%, 6% and 8%) + Matos (1%, 1.5% and 2%), and 3) Free compression test (SNI 03-6887-2002) unsoaked and soaked conditions. The test object is compacted based on the results of the light compaction test. In the free compression test, the submerged condition of the free compression test object was immersed for 4 h before the test was carried out. The treatment period for each free compression specimen is seven days. Variations in cement content were 4%, 6%, and 8% of the dry weight of the soil, while the Matos content used was 1%, 1.5%, and 2% of the cement weight.

3 Results and Discussion

3.1 Physical Properties of Quarry Soil

Soil samples from three locations are 1. The road section of Jalan Kedang Ipil – Kota Bangun Kutai Kertanegara in the future is referred to as quarry 1, 2) Section of Jalan Rapak Lambur – Seroni Kutai Kertanegara in the future is referred to as quarry 2, and 3) Section of Road in Kenohan District, Kutai Kertanegara in the future referred to as quarry three was taken for laboratory studies. Physical properties, grain size distribution, and soil classification based on AASHTO and USCS soils from three quarries can be seen in Table 1, Fig. 1, and Fig. 2.

Table 1 Physical Properties of Quarry Soil

Laboratory Testing	Quarry 1	Quarry 2	Quarry 3
Plasticity Properties			
• Liquid limits, %	46	45	23
• Plastic limits, %	32,33	26,45	17,59
• Placticity Index, %	13,67	18,55	5,41
Grain Size Distribution			
• Gravel (G), %	1,94	0,86	2,6
• Sand (S), %	14,16	11,56	58,69
• Silt (M) dan Clay (C), %	83,91	87,91	38,72
Specific Gravity	2,56	2,55	2,63
Classification			
• AASHTO	A-7-5	A-7-6	A-4
• USCS	ML	CL	SC

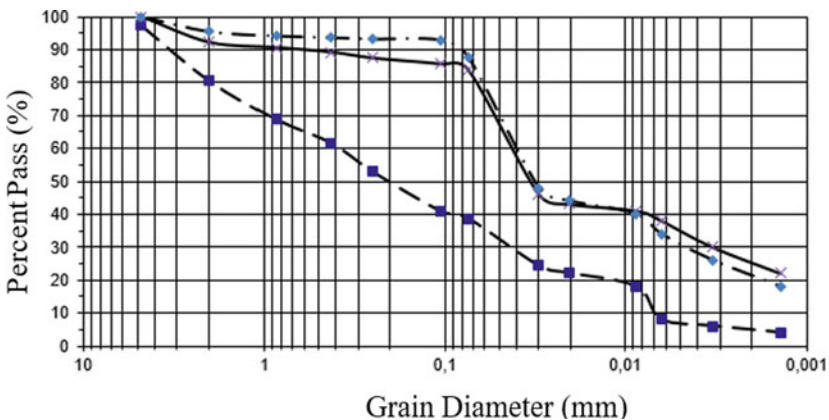


Fig. 1 Grain size distribution

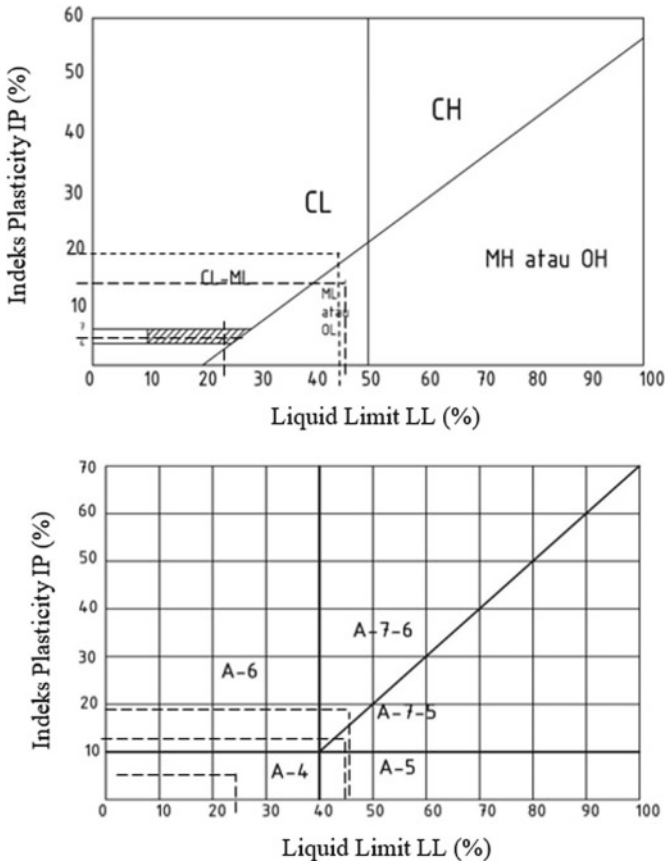


Fig. 2 Soil classification based on (a) USCS and (b) AASHTO

3.2 Compaction Test Results

The results of the compaction test can be seen in Table 2. Adding cement to the soil will cause the soil grains to slip more efficiently and be easier to compact, so maximum density is achieved at a lower optimum moisture content. Ease of compaction and the density of cement, which is greater than the specific gravity of soil grains, cause an increase in the maximum dry west value.

3.3 Free Compression Test Results

Figure 3 shows the 7-day-old unsubmerged UCS values for a) quarry 1 (A-7-5), b) quarry 2 (A-7-6), and c) quarry 3 (A-4). Stabilization of cement with levels up to

Table 2 Compaction Test Results

Mix Composition	Quarry 1		Quarry 2		Quarry 3	
	w _{opt} (%)	γ _{d maks} (g/cm ³)	w _{opt} (%)	γ _{d maks} (g/cm ³)	w _{opt} (%)	γ _{d maks} (g/cm ³)
Soil – cement 0%	21,4	1,48	19,10	1,53	13,8	1,62
Soil – cement 6%	19,3	1,52	16,9	1,58	12,2	1,72
Soil – cement 8%	18,4	1,53	16,4	1,61	12,3	1,77
Soil – cement 10%	17,1	1,56	15,1	1,59	11,7	1,75

10% in quarry one soil has not been able to reach the UCS value required in S.Kh. 2.5.4. of 20 kg/cm², the addition of 1.5% and 2% mats to 8% cement stabilization was able to increase the UCS value above the required UCS value (Fig. 3a). Adding Matos up to 2% in quarry two soil increased the cement stabilization performance. However, it could not reach the required UCS value (Fig. 3b). In quarry three soil, the required UCS can be achieved at 8% cement stabilization without adding mats or 6% cement with adding 1% mats (Fig. 3c). Mixed compositions required in S.Kh. 2.5.4. of 20 kg/cm² can be seen in Table 3.

The UCS value showed that the optimum Matos content in soil A-7-6 was 1.5% by weight of cement, while in soils A-7-5 and A-4, the optimum Matos content of 1.5% only occurred at the cement content of 6%. There was an increase in UCS value

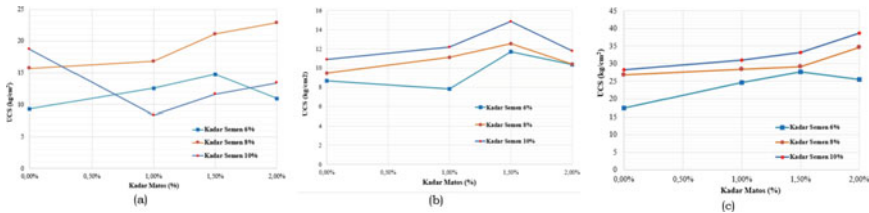


Fig. 3 Results of soil free compression test (a) Quarry 1 (b) Quarry 2 (c) Quarry 3

Table 3 Summary of Laboratory Mix Design

Soil	Mix Composition	
	cement %	Matos %
Quarry 1	8	1,5
Quarry 2	Does not reach UCS requirements	
Quarry 3	8	0
	6	1

at 8% and 10% cement content with the addition of 2% Matos content in A-7-5 and A-4 soils.

4 Conclusion

Soil classification according to AASHTO for quarry 1, quarry 2, and quarry 3 are A-7-5, A-7-6, and A-4, respectively, *while according to USCS, they are ML, CL, and SC.*

The addition of cement resulted in a decrease in the value of the optimum moisture content and an increase in the maximum dry volume weight.

The optimum Matos content of 1.5% occurred for all soil cement content in soil A-7-6 and 6% cement content in soil A-7-5 and A-4.

References

1. Anonymous (1995) Soil Cement Construction Hand Book, Portland Cement Assosiation, Illinois
2. Lim SM, Wijeyesekera, DC, Lim AJMS, Bakar IBH (June 2014) Critical review of innovative soil road stabilization techniques. Int J Eng Adv Technol (IJEAT) 3(5)
3. Todingrara' YT, Tjaronge MW, Harianto T, Ramli M (2017) Performance of laterite soil stabilized with lime and cement as a road foundation. Int J Appl Eng Res 12(14), 4699–4707 © Research India Publications. <http://www.ripublication.com>
4. Suksun H, Runlawan R, Avirut C, Yuttana R, Apichat S (2010) Analysis of strength development in cement-stabilized silty clay from microstructural considerations. Constr Build Mater 24, 2011–2021. www.elsevier.com/locate/conbuildmat
5. Okyay US, Dias D (2010) Use of Lime and Cement Treated Soils as Pile Supported Load Transfer Platform. Eng Geol 114
6. Khaled G, Assia I (2011) Stabilisation of Weathered Marls Using Lime or Cement, Pan-Am CGS Geotechnical Conference, 2011
7. Lucian C (2012) Effectiveness of two sequential mixing of lime -portland cement in stabilizing expansive soils. Int J Appl Sci Eng Res 1(6)
8. Gautreau GP, “Doc” Zhang Z, Wu Z (April 2009) Accelerated Loading Evaluation of Subbase Layers in Pavement Performance. Technical Report Louisiana Transportation Research Center, Los Angeles, April 2009
9. Rahman MM, Siddique A, Uddin MK (June 2012) Clay-Water/Cement Ratio is the Prime Parameter for Fine Grained Soil Improvement at High Water Content. DUET J 1(3):1–11. Dhaka University of Engineering & Technology, Gazipur, 3 June 2012 page 1–11
10. Aliyu MK, Abd Karim KT (April 2016) The effect of cement and rice husk ask on the compressive strength and leachability contaminated stabilized sedimment. ARPN J Eng Appl Sci 11(8), April 2016
11. Paul, GJ (2011) An Introduction to Soil Stabilization for Pavements, Continuing Education and Development, Inc. 9 Greyridge Farm Court Stony Point, NY
12. Mohammed K, dan Abdelkrim M (2014) Cement and Lime Mixture Stabilisazion of an Expansive Overconsolidated Clay, Applied Clay Science
13. Ruktiningsih R (2005) CBR Value of Ilite Clay Improvement with Lime and Portland Cement. International Seminar and Exhibition on Road Constructions (ISERC), vol. 3

14. dan Ekowati R WT (April 2004) Efektifitas Penambahan Pasir Semen dan Stabilizer pada Stabilisasi Tanah Lempung Ekspansif, *Jurnal Teknik* Vol 4 No 1 April 2014
15. Arif W, dan Sugeng W, Pengaruh Kadar Air dan Bahan Ikat Semen Terhadap Trend Keretakan Lapis Perkerasan Tanah Semen, *Konferensi Regional Teknik Jalan ke 13, Makassar, 2014*, halaman 1–17
16. Widiyanto. Arif (2005) Stabilisation Technology Implementation as the Way of Efficiency in The Road Betterment and Road Rehabilitation in Indonesia, *National Conference of Rekayasa Aplikasi dan Perancangan Industri (RAPI – IV)*, ISSN: 1412- 9612, Engineering Faculty Muhammadiyah University of Surakarta.
17. Anonymous, Spesifikasi Khusus Interim Seksi S.Kh. 2.5.4. Lapis Fondasi Semen Komposit Tanah, *Direktorat Jenderal Bina Marga Kementrian PUPR, Jakarta, 2010*
18. Anonymous (2002) *Metode, Spesifikasi dan Tata Cara Bagian 1 : Tanah, Longsor*, Badan Penelitian dan Pengembangan Departemen Permukiman dan Prasarana Wilayah, Jakarta
19. Anonymous (1992) *Soil Cement Laboratory Hand Book*, Portland Cement Assosiation, Illinois

IoT Implementation to Minimize the Vehicle Queue at the Traffic Lights Intersection



Fatsyahrina Fitriastuti, Ryan Ari Setyawan,
Muhammad Arif Ma'ruf Setiawan, and Jemmy Edwin Bororing

Abstract This study aims to minimize traffic jams that often occur at crossroads. Not all roads are congested with vehicles. Therefore, it is necessary to adjust the time duration for the traffic light according to the density of vehicles on a lane at the intersection. This system is based on IoT (Internet of Things) which refers to a network that connects various physical devices with different protocols. The Raspberry Pi 4 Model B functions as a controller to run the traffic light program. Infrared sensors are placed at several points to detect the queue length of vehicles and then become input to the system, then processed and converted into time duration. If the queue of vehicles is getting longer, then the duration of time for the green light will be even greater. Thus, vehicle users will be more comfortable driving because the time required at traffic lights becomes more efficient.

Keywords IoT · Traffic Light · Infrared Sensor · Raspberry

1 Introduction

Road congestion is a common problem in every city that requires serious handling. One source of traffic congestion is located at a crossroads because the number of vehicles on each lane is not the same but the duration of traffic light time is the same. This causes the queue of vehicles on a lane thereby reducing the comfort of

F. Fitriastuti (✉) · R. A. Setyawan · M. A. M. Setiawan · J. E. Bororing
Departement of Informatics, Faculty of Engineering, Janabadra University, Yogyakarta, Indonesia
e-mail: fitri@janabadra.ac.id

R. A. Setyawan
e-mail: ryan@janabadra.ac.id

M. A. M. Setiawan
e-mail: arifmaruf@student.janabadra.ac.id

J. E. Bororing
e-mail: jemmy@janabadra.ac.id

road users. IoT technology (Internet of Things) allows various objects to connect and communicate with each other. With IoT we can monitor and control various devices with different platforms more efficiently and effectively. The concept of IoT has been widely used in various sectors of life ranging from tourism, industry, transportation, hospitals, agriculture, and government [1]. Control of intelligent traffic lights is very important for efficient transportation systems. Most traffic lights are operated manually. The intelligent traffic light control system must be adjusted dynamically with real time traffic conditions [2]. “Internet of things (IoT) is a network of physical objects embedded with electronic, software, sensors and connectivity to enable them to achieve greater values and services by exchanging data with producers, operators and/or other connected devices. Various types of IoT implementation began to be developed in each region, for example the use of smart lamps with remote control [3]. Miratunisa and Budi (2018) succeeded in creating a traffic lights monitoring system that can monitor traffic congestion in real-time through a smartphone that has been carried out by this system using Nodemcu (ESP 8266 12E) which is equipped with IR sensors to show traffic congestion. To connect the internet, the system uses the ESP8266 12E WiFi in the Nodemcu chip. This will send a notification to users via smartphone. With this research, it is expected to increase the smooth running of the traffic jams so that the system can provide an efficient alternative route for users [4]. To reduce traffic density can be done by providing a priority scale of time duration based on the calculation of the number of vehicles. This is done by identifying SSID Vehicle Number Plate (Chip Wemos). But the weakness of this system is that it will not read new vehicles that are not or have not been paired with Wemos chip [5]. The purpose of the study is to design and build a prototype of IoT -based systems that can minimize vehicle queues at the crossroads of traffic lamps and make it easier for officers to adjust the duration of waiting for traffic lights based on the input obtained from the IR sensor. This system uses Raspberry PI 4 as a data processing center and functions as a controller to run a traffic light program.

2 Research Methodology

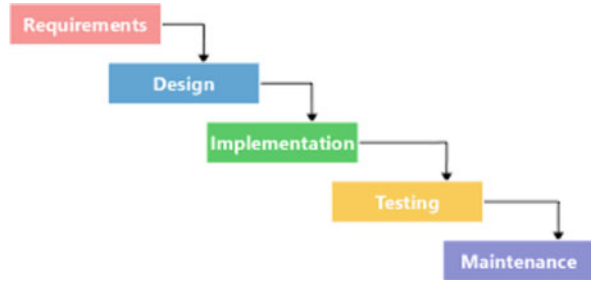
2.1 *Waterfall Method*

This research method adopts the waterfall method which is a system development method consisting of several stages. It defines several consecutive phases that should be completed one after another and it moves to the next phase only if the preceding phase is completely done [6] (Fig. 1).

1. Requirements

In the Requirement stage, two methods are used, namely field studies by directly reviewing the location used as a reference to designing prototypes, namely the intersection of the three Jetis Jetis Yogyakarta TR Roads to get data on traffic lights,

Fig. 1 Waterfall Approach
[6]



vehicle queues and duration of traffic lights. The next method is the literature study of hardware and software for the design of this system.

2. Design

At this stage the author designs prototype, namely by creating system architecture and preparing supporting tools and materials (Raspberry Pi 4, IR sensors, LEDs, web cameras, LDR and determining the software used to build this system (XAMPP, Sublime Text 3, Thonny Python, VNC Viewer, Windows OS, OS Raspbian).

3. Implementation

At the implementation stage this prototype assembly and web application creation. The assembly stage is the miniature assembly and its components, create software, connect Raspberry Pi 4 with IR, LED sensors, and light sensors, regulate the layout of IR sensors, coding programs on Raspberry using python language, coding programs for software to be used and connect Software with Raspberry Pi using API.

4. Testing

At this stage all units developed in the implementation stage are integrated into the system after the testing conducted by each unit. After the integration of the whole system is tested to check each failure or error.

5. Maintenance

The final stage in the waterfall model. Prototypes and software that are ready, run and maintenance. Maintenance is included in correcting errors that are not found in the previous step. Improving the implementation of system units and improving system services as new needs.

2.2 System Architecture

To design the prototype of the IoT -based system to minimize the queue of vehicles at the crossroads of traffic lights requires several supporting components such as in Fig. 2.

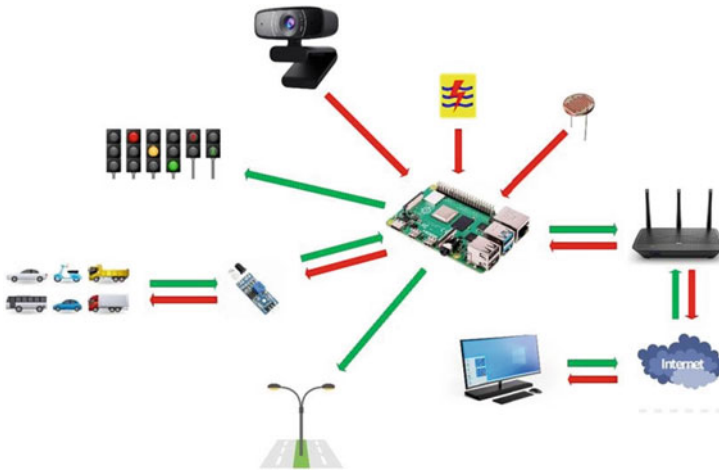


Fig. 2 Block Diagram Schematic

Figure 2 shows the IoT -based system diagram block which broadly explains that the IR sensor is installed at several points to detect vehicle queues at the traffic lights. If the IR sensor is installed at three points on each road. The IR sensor will detect whether the vehicle queue is at the first, second or third point when infrared light is blocked by objects. The IR sensor will send the data to the raspberry and then processed to be converted into the duration of the time the traffic lights turn on so that the path with the longest vehicle queue will get the duration of the time the green light is the longest.

3 Result and Discussion

3.1 *Prototype Hardware*

At this stage the prototype design of the traffic lights control system based on the vehicle queue includes designing the prototype of the road, the design of the sensor placement design and the duration of the traffic lights. Prototype design uses Sketchup and VISIO 2013 software (Fig. 3).

The design of the sensor placement is adjusted to the length of the road on the prototype and the average length of the car prototype size. Figure 4 is a sensor placement image based on crowded traffic conditions or not

Sensor placement based on traffic conditions refers to Fig. 4 as follows:

1. The length of the prototype road is 36.5 cm
2. The position of the sensor is adjusted to the length of the road.
3. Each sensor shows the condition of density that is quiet

Fig. 3 Design Traffic Lights

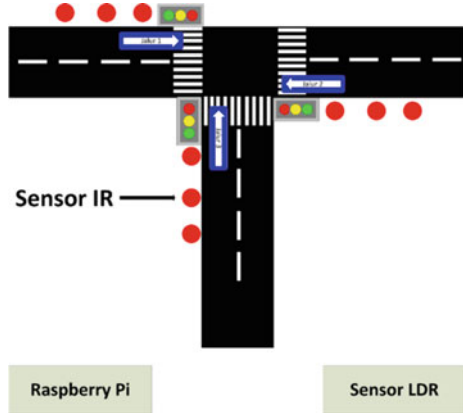
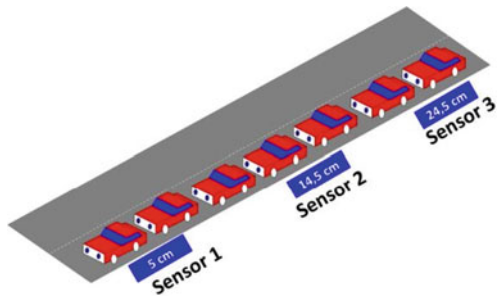


Fig. 4 Point of IR sensor placement



- 4. Conditions of density include light traffic, normal traffic or heavy traffic.
- 5. Sensor 1 is considered as a light traffic, placed in the position of 5 cm from the crossroads.
- 6. Sensor 2 is considered as a normal traffic, placed in the position of 14.5 cm from the road.
- 7. Sensor 3 is considered a heavy traffic, placed in a position 24.5 cm from the length of the road.

Furthermore, the traffic duration arrangement is adjusted to the traffic conditions. Table 1 is the duration of traffic lights based on the condition of density.

3.2 System Software

Software design is done by programming the Raspberry Pi computer with Python IDLE software. The software is provided by Aspberry Pi when Raspberry Pi has been installed in the operating system. This software makes it easy to develop Python programs using Raspberry Pi [7]

Table 1 Duration of traffic lights based on traffic conditions

Active sensor	Traffic Condition	Description
Sensor 1	Light traffic	If sensor 1 is active, it is considered a light traffic Every path that gets a light traffic will get a maximum green light duration for 15 s
Sensor 2	Normal traffic	If sensor 2 is active, it is considered a normal traffic Every path that gets a normal traffic will get a maximum green light duration for 25 s
Sensor 3	Heavy traffic	If sensor 3 is active, it is considered a heavy traffic Every path that gets a heavy traffic will get a maximum green light duration for 40 s
Inactive sensor	Empty path	If sensor 1, sensor 2, and sensor 3 are not active, it is considered as a 'empty path' condition. Every path that gets the 'empty path' condition will get a maximum green light duration for 5 s. So that the sensor on the next path can detect traffic conditions

Figure 5 is Diahram flow detection of traffic conditions. The explanation is:

1. The first process is the installation of all existing inputs/outputs or the introduction of 9 IR sensors installed on each line.
2. Raspberry Pi as the main controller regulates the condition of 'normal' traffic as an initial condition.
3. The system checks the green light on line 1.
4. If the lane 1 of the green light is on, the system will check the counter on the green light on line 1.
5. The system activates 3 IR sensors in Line 2 and the IR sensor on line 2 will carry out the vehicle detection process when the counter is on the green light on line 1 is complete.
6. The system is the process of detecting traffic conditions on lane 2 of the last vehicle detected by the IR sensor
7. The system disables the IR sensor on line 2.
8. Furthermore, the system checks the green light on line 2.
9. If on the line 2 the green light is on, the system will check the Counter on the green light on line 2.
10. The system activates 3 IR sensors in line 3 and the infrared sensor on line 3 will carry out the vehicle detection process when the counter is on the green light on the 2 line.
11. The system conducts a process of detecting traffic conditions in line 3 of the last vehicle detected by the IR sensor.
12. The system disables the IR sensor on line 3.
13. Furthermore, the system checks the green light on line 3.
14. If the 3 green light line is on, the system will check the Counter on the green light on line 3.

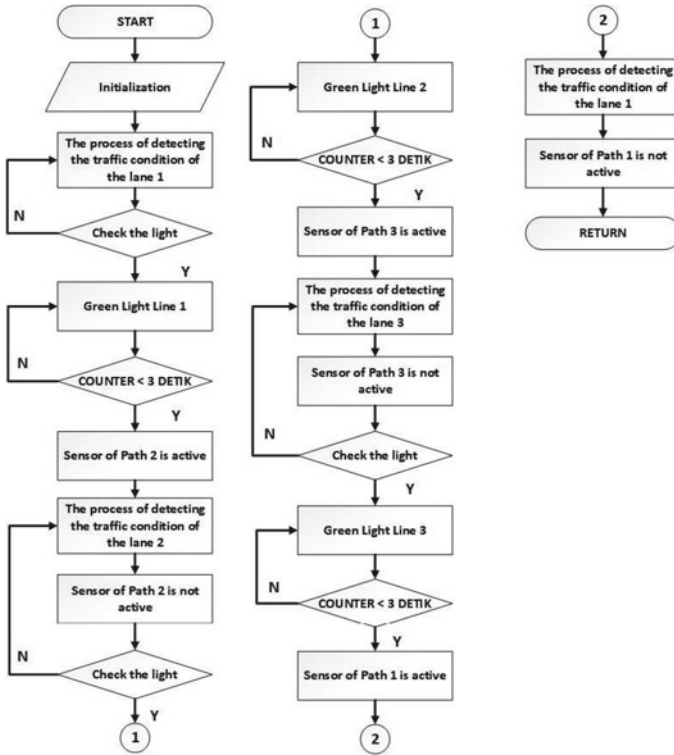


Fig. 5 Flow diagram detection of traffic condition

15. The system activates 3 IR sensors in line 1 and the IR sensor on line 1 will carry out the vehicle detection process when the counter is on the green light on line 3 is complete.
16. The system conducts a process of detecting traffic conditions on line 1 of the last vehicle detected by the IR sensor.
17. The system disables the IR sensor on line 1.
18. Return

3.3 Testing of System

After the design of the hardware and software is complete, followed by overall system testing. Figure 6 shows the prototype of the system that illustrates the intersection of the three on Jalan TR Mataram Jetis Yogyakarta, can be seen in each lane fitting 3 Sensor Ir. Sensor 1 shows 'light traffic', sensor 2 shows 'normal traffic' and sensor 3 shows 'heavy traffic'.



Fig. 6 Prototype Persimpangan tiga lampu lalu lintas

Table 2 shows that the system test results are in accordance with the design. In the system prototype trial, the car is placed on each lane. The sensor will detect the car as an object and the results are sent to Raspberry Pi to be processed. Furthermore, the system will conclude the traffic conditions displayed on the monitor include the results of the sensor reading, the duration of traffic lights, especially green and red, and traffic conditions.

The following explanation of the overall image and test table of trials.

1. When reading sensor A, sensor B, and sensor C is worth 0 or worth "0 0 0" then it is considered a sensor that does not detect vehicles, it is called 'empty traffic'. The duration of the green light on is 5 s.
2. When the reading of sensor A is worth 1 and sensor B is worth 0 and sensor C is worth 0 or worth "1 0 0" then it is called 'Light Traffic'. The duration of the green light is 10 s.
3. When the reading of sensor A is 1 and sensor B is 1 and the C sensor is worth 0 or worth "1 1 0" is called 'Normal Traffic'. The duration of the green light on is 25 s.
4. When reading sensor A is 1 and sensor B is worth 1 and sensor C is worth 1 or worth "1 1 1" called 'Heavy Traffic'. The duration of the green light is 40 s.
5. When reading sensor A is 0 and sensor B is worth 1 and sensor C is worth 0 or worth "0 1 0" is called 'Normal Traffic'. The duration of the green light on is 25 s.
6. When reading sensor A is 0 and sensor B is 0 and sensor C is worth 1 or worth "0 0 1" is called 'Heavy Traffic'. The duration of the green light on is 40 s.

Table 2 Data of System test results

No	Line	Sensor A	Sensor B	Sensor C	Traffic Condition	The duration of the lights (second)
1	1	0	0	0	Empty Traffic	5
2	1	1	0	0	Light Traffic	10
3	1	1	1	0	Normal Traffic	25
4	1	1	1	1	Heavy Traffic	40
5	1	0	1	0	Empty Traffic	5
6	1	0	0	1	Empty Traffic	5
7	1	1	0	1	Light Traffic	10
8	1	0	1	1	Empty Traffic	5
9	2	0	0	0	Empty Traffic	5
10	2	1	0	0	Light Traffic	10
11	2	1	1	0	Normal Traffic	25
12	2	1	1	1	Heavy Traffic	40
13	2	0	1	0	Empty Traffic	5
14	2	0	0	1	Empty Traffic	5
15	2	1	0	1	Light Traffic	10
16	2	0	1	1	Empty Traffic	5
17	3	0	0	0	Empty Traffic	5
18	3	1	0	0	Light Traffic	10
19	3	1	1	0	Normal Traffic	25
20	3	1	1	1	Heavy Traffic	40
21	3	0	1	0	Empty Traffic	5
22	3	0	0	1	Empty Traffic	5
23	3	1	0	1	Light Traffic	10
24	3	0	1	1	Empty Traffic	5

7. When the reading of sensor A is worth 1 and sensor B is 0 and the C sensor is worth 1 or worth “1 0 1” is called ‘Heavy Traffic’. The duration of the green light on is 40 s.
8. When reading sensor A is 0 and sensor B is worth 1 and sensor C is worth 1 or worth “0 1 1” is called ‘Heavy Traffic’. The duration of the green light on is 40 s.

From the overall system testing results it can be concluded that the more crowded the vehicle that is on the lane, the longer the duration of the green light and if the fewer vehicles are on the lane, the faster the duration of the green light.

4 Conclusion

This research has been successfully conducted with a waterfall research method which has systematic stages. This IoT -based system has been successfully designed and built in the form of prototype and combined with software. The device used is Raspberry Pi 4 as the main control of the system, the IR sensor used to detect the awareness queue at the crossroads. This system is also equipped with a monitoring camera to monitor traffic conditions and LDR to turn on the street lights automatically when the day is getting dark. System software is built by utilizing PHP programming languages, HTML5, CSS3, MySQL, Javascript and Bootstrap. After testing the system, it can be concluded that the implementation of IoT to minimize the queue of vehicles at the crossroads has been running according to the design. The system is able to detect traffic conditions in the form of light traffic, normal traffic and heavy traffic so that the duration of the green light can be arranged according to traffic conditions so as to reduce the queue of vehicles at the crossroads.

References

1. Haryanto E, Fitriastuti F, Setiyorini A, Haryanto EMON, Lukmanfiandy S (2022) Design and build remote watering system based on Internet of Things (IoT) (Case Study of Yogyakarta Code Tourism Park). IOP Conf Ser Earth Environ Sci 1030(1). <https://doi.org/10.1088/1755-1315/1030/1/012007>.
2. Wei H, Yao H, Zheng G, Li Z IntelliLight: a reinforcement learning approach for intelligent traffic light control. Proc ACM
3. *SIGKDD Int. Conf. Knowl. Discov. Data Min.*, pp. 2496–2505 (2018). <https://doi.org/10.1145/3219819.3220096>.
4. “Smarttraffic light,” p. 39 (2021). https://en.wikipedia.org/wiki/Smart_traffic_light
5. Miratunnisa GS, Budi AHS (2018) Traffic light monitoring system based on NodeMCU using Internet of Things. IOP Conf Ser Mater Sci Eng 384(1). <https://doi.org/10.1088/1757-899X/384/1/012024>.
6. Winardi S, Maulana SI, Wiwoho Mudjanarko S, Anindito B (September 2019) Determination of traffic lights duration by identification of vehicle numbers using IoT. Int J Comput Netw Secur Inf Syst, 6–12
7. Aroral HK (2021) Waterfall process operations in the fast-paced world: project management exploratory analysis. Int J Appl Bus Manag Stud 6(1):2021. http://www.ijabms.com/wp-content/uploads/2021/05/05_ARORAL_PB.pdf

Organic Matter Removal from Sanitary Landfill Leachate Through Chemical Oxidation



Nurfarizah Didi Binti Abdullah, Mohamed Hasnain Isa, Rozeana Hj Md Juani, Asmaal Muizz Salleh Bin Hj Mohammad Sultan, Zuliana Binti Hj Nayan, and Muhammad Raza Ul Mustafa

Abstract Advanced Oxidation Processes (AOPs) have been widely used for wastewater treatment. Persulfate (PS) activation through different pathways has attracted a lot of attention; due to the generation of sulfate radicals which have high oxidation potential. In this study, a series of laboratory-scale experiments were conducted on landfill leachate, using PS/Fe²⁺/H₂O₂ and PS/Fe²⁺/SO₃²⁻ systems. A statistical design of experiments was adopted using Design Expert 11 software. COD removal efficiency for both systems was evaluated and the optimum operating conditions were determined using Response Surface Methodology. The effects of the independent variables (pH, chemical doses, and reaction) on the removal of COD were studied. The optimised COD removal was 68% at pH 5 for PS/Fe²⁺/H₂O₂ system. Fe²⁺, H₂O₂, and PS doses were 1.95 mM, 0.05 mM, and 0.50 mM, respectively, with 10 min reaction time. 90% COD removal was obtained at pH 3.67, Fe²⁺ dose of 0.5 mM, SO₃²⁻ dose of 0.5 μM, and PS dose of 1.5 mM with 17 min reaction time for PS/Fe²⁺/SO₃²⁻ system.

N. D. B. Abdullah

Hengyi Industries Sdn Bhd, Jalan Ujong Sapuh, Pulau Muara Besar BT3328, Brunei Darussalam
e-mail: n.frzhabd@gmail.com

M. H. Isa (✉) · R. H. M. Juani · A. M. S. B. H. M. Sultan · Z. B. H. Nayan
Civil Engineering Programme Area, Universiti Teknologi Brunei, Tungku Highway,
Gadong BE1410, Brunei Darussalam
e-mail: mohamed.isa@utb.edu.bn

R. H. M. Juani
e-mail: rozeana.juani@utb.edu.bn

A. M. S. B. H. M. Sultan
e-mail: muizz.sultan@utb.edu.bn

Z. B. H. Nayan
e-mail: zuliana.nayan@utb.edu.bn

M. R. U. Mustafa
Department of Civil and Environmental Engineering, Universiti Teknologi PETRONAS, 32610,
Seri Iskandar, Perak Darul Ridzuan, Malaysia
e-mail: raza.mustafa@utp.edu.my

Keywords Advanced oxidation process · Persulfate · Landfill leachate

1 Introduction

1.1 Background

Landfilling is the most common method of solid waste disposal due to its ease and low cost. However, the disposal of solid wastes in landfills can cause serious environmental issues. These include problems such as the release of toxins, production of leachate, and the generation of greenhouse gases. Toxic substances and leachate may leach into surface and groundwater and contaminate the water sources. The release of greenhouse gas may further contribute to global warming. It was reported that approximately 95% of all MSW in the world were disposed of in landfills [9]. In the context of Brunei Darussalam, the Department of Environment, Parks and Recreation (JASTRe) estimated that 189,000 tonnes of solid wastes are being disposed yearly [3].

Leachate is a highly polluted wastewater generally characterised by high amount of COD, pH, ammoniacal nitrogen and heavy metals. It also has strong colour and unpleasant odour. Leachate is composed of the liquid that has entered the landfill from external sources (drainage, rainfall, groundwater, and water from underground springs) and that produced during biodegradation of the waste deposited in the landfill. The most important environmental aspects of landfill leachate are its impacts on the quality of surface water and groundwater.

Leachate can be treated using biological or physico-chemical methods. Conventional biological treatment processes have limited applications with regards to toxic and recalcitrant compounds in leachate [8]. Physico-chemical treatment processes, on the other hand, have issues related to cost, chemicals and sludge production.

The use of advanced oxidation processes (AOPs) in wastewater treatment has received increased attention of researchers [7]. Some of the benefits of using AOPs are: removes or reduces consumption of chemicals, less sludge production, involves lesser mechanical operations, easy to handle, user-friendly, operates at ambient temperature and pressure.

Sulfate radical ($\text{SO}_4^{\cdot-}$) has an oxidation potential comparable to that of $\cdot\text{OH}$ radical. In recent years, sulfate radical has attracted a lot of attention as a useful substance for chemical oxidation. It may even be preferred over $\cdot\text{OH}$ radical due to inability of the latter to oxidize ammonia [1]. Additionally, investigations have looked into the use of $\text{SO}_4^{\cdot-}$ in the destruction of non-biodegradable organic pollutants such dyes, insecticides, and antibiotics in the treatment of municipal wastewater [5]. To generate $\text{SO}_4^{\cdot-}$ radicals, persulfate can be activated through various approaches such as ultraviolet (UV) irradiation, heating as well as transition metals additions [10]. Among these approaches, the addition of transition metal to activate PS seems to be the most realistic way and the commonly used transition metals which act as

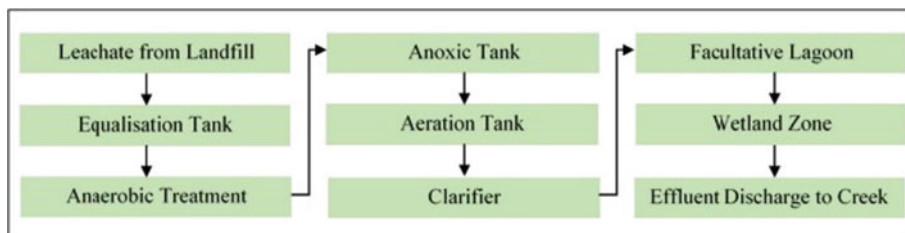


Fig. 1 Leachate treatment scheme at Sungai Paku Landfill

activators are Fe(II) and Fe(III). This is due to the metals being readily available in environmental media [5].

The activation of persulfate by the addition of transition metals and ligands such as Fe(III)/sulfite/persulfate system, have been researched on. However, there have not been studies specifically conducted on landfill leachate treatment. This study focuses on the application of Fe(II)/sulfite/persulfate and Fe(II)/H₂O₂/persulfate for COD removal from landfill leachate. There have not been many evaluations done on the performance of these systems, especially for landfill leachate.

2 Materials and Methods

2.1 Leachate Collection

Sungai Paku Landfill Site is an engineered landfill designed to receive 500 tons per day of solid waste. The total area of the landfill site is 110 hectares of which 16 hectares are allocated for waste disposal site. Whereas the remaining areas are for leachate treatment, buffer zones, internal roads, and other facilities. Figure 1 shows the leachate treatment scheme at the landfill. Leachate samples for the study were collected before the anoxic tank, transported to the laboratory and kept at 4°C until use.

2.2 Chemical Reagents

Sodium peroxydisulfate, Iron (II) sulfate heptahydrate, Hydrogen peroxide (30%) and Sodium sulfite were used for chemical oxidation. Since the treatments for the landfill leachate were to be conducted at different doses, stock solutions of each chemical were prepared. Required amounts of the stock solutions were added to the reaction mixtures to yield the desired concentration of the reactants. Sulfuric acid

(95–97%) and Sodium hydroxide were used for initial pH adjustment. All chemicals were obtained from Med Life Resources.

2.3 Experimental Procedure

Chemical oxidation experiments were conducted with 100 mL leachate samples in a 250 mL glass beaker with a magnetic stirrer. The pH of the samples was adjusted using 1 N sulphuric acid or sodium hydroxide. Chemical (iron(II) sulfate heptahydrate, sodium persulfate, etc.) were added from the stock solutions according to their desired concentrations. The reaction mixture was mixed with a magnetic stirrer according to the required reaction times.

2.4 Chemical Analysis

The pH of the samples was measured using a Waterproof pHTestr 30 portable pH meter. Chemical Oxygen Demand (COD) of the samples was determined using closed refluxed colorimetric method using a DR3900 spectrophotometer. The test for ammoniacal nitrogen was conducted using a DR3900 spectrophotometer.

2.5 Experimental Design and Analysis

Design Expert 13 software was used for statistical design of the experiments and process modelling. Response Surface Methodology (RSM) was used to optimize the operating variables used in the treatment of the landfill leachate. It helps to evaluate the effects of the variables involved in the treatment process and to determine the potential interactions between the variables [4, 2]. Range of each independent variable (i.e., pH, doses, and reaction time) was determined based on preliminary experiments and used to develop the Central Composite Design (CCD) for RSM. In this study, the effects of pH, chemical doses, and reaction time for each system on the dependent variables viz. COD concentration and COD removal efficiency were evaluated. The variables and their values used in this study are shown in Table 1.

Table 1 Variables and their values used for RSM

Chemicals	Values	
	PS/Fe ²⁺ /H ₂ O ₂	PS/Fe ²⁺ /SO ₃ ²⁻
Sodium Peroxodisulfate	5, 7, 9	3, 4, 5
Iron(II) Sulfate Heptahydrate	0.05, 1, 1.95 mM	1.5 μM, 0.5, 1 mM
Hydrogen Peroxide, 30%	0.05, 1, 1.95 mM	N/A
Sodium Sulfite	N/A	0.5, 1, 1.5 μM
Sulfuric Acid, 95–97%	0.05, 1, 1.95 mM	1, 1.5, 2 mM
Sodium Hydroxide	10, 30, 50 min	5, 15, 25 min

3 Results and Discussion

3.1 Leachate Characteristics

The partially treated leachate used in this study had the following characteristics: pH 6–8, COD 1000–4000 mg/L and ammoniacal nitrogen (NH₃-N) 700–1000 mg/L.

3.2 COD Removal – Response Surface Methodology (RSM)

For the evaluation of the impacts of each independent variable on the dependent variables, CCD with RSM was used to gain a better understanding of the interaction between the variables. 3D surface models based on the responses for each system were generated. Analysis of variance (ANOVA) was used to determine the significance of the model; p-values of less than 0.05 indicate that the terms are significant.

PS/Fe²⁺/H₂O₂ System. ANOVA results for COD removal efficiency using PS/Fe²⁺/H₂O₂ system are shown in Table 2. The model has an F-value of 2.44 which implies that it is significant. The final equation obtained in terms of actual factors is:

$$\begin{aligned}
 \text{COD Removal}(\%) = & +15.23647 + 1.53759 \text{ pH} + 5.88149 \text{ PS dosage} + \\
 & 23.98125 \text{ Fe(II) dosage} - 18.31317 \text{ H}_2\text{O}_2 \text{ dosage} + 1.06861 \text{ Reaction time} - \\
 & 1.31069 \text{ pH} \times \text{PS dosage} - 1.49293 \text{ pH} \times \text{Fe(II) dosage} + \\
 & 3.22957 \text{ PS dosage} \times \text{Fe(II) dosage} - 0.253569 \text{ Fe(II) dosage} \times \\
 & \text{Reaction time} + 0.369128 \text{ H}_2\text{O}_2 \text{ dosage} \times \text{Reaction time} - \\
 & 0.020333 \text{ Reaction time}^2
 \end{aligned}$$

(1)

Table 2 PS/Fe²⁺/H₂O₂ system ANOVA for COD removal efficiency

Source	Sum of Squares	df	Mean Square	F-value	p-value	
Model	8115.10	11	737.74	2.44	0.0216	significant
A-pH	217.98	1	217.98	0.7212	0.4014	
B-PS dosage	0.1248	1	0.1248	0.0004	0.9839	
C- Fe(II) dosage	2570.85	1	2570.85	8.51	0.0061	
D-H ₂ O ₂ dosage	1608.13	1	1608.13	5.32	0.0269	
E-Reaction time	17.45	1	17.45	0.0577	0.8115	
AB	198.45	1	198.45	0.6566	0.4231	
AC	257.47	1	257.47	0.8519	0.3622	
BC	271.85	1	271.85	0.8994	0.3493	
CE	742.76	1	742.76	2.46	0.1257	
DE	1574.03	1	1574.03	5.21	0.0285	
E ²	655.99	1	655.99	2.17	0.1494	
Residual	10,881.08	36	302.25			
Lack of Fit	9968.27	31	321.56	1.76	0.2760	not significant

The coefficient of determination (R^2) was 0.4272 for the fitted model. The low values of R^2 and adjusted R^2 may be caused by the different batch of samples taken. An adequate precision ratio is a ratio of the range of the predicted values at the design points to the average prediction error [6]. For this system, the adequate precision ratio was 8.1312. The desirable value of the ratio is more than 4.

The ANOVA results showed that Fe(II) and H₂O₂ are the main influencing factors that affect the performance of the treatment. Figure 2(a) presents an indicative 3D surface plot showing the effect of Fe²⁺ and pH on COD removal efficiency. The actual optimized COD removal was 68% at pH 5 for PS/Fe²⁺/H₂O₂ system. Fe²⁺, H₂O₂, and PS doses were 1.95 mM, 0.05 mM, and 0.50 mM, respectively, with 10 min reaction time.

PS/Fe²⁺/SO₃²⁻ System. Table 3 shows the ANOVA results for COD removal efficiency using PS/Fe²⁺/SO₃²⁻ system. The model is significant with an F-value of 11.12. The final equation obtained in terms of actual factors is:

$$\begin{aligned}
 \text{COD Removal}(\%) = & -414.16305 + 167.64981 \text{ pH} + \\
 & 53.0780 \text{ Fe(II) dosage} - 166.21299 \text{ Sulfite dosage} + \\
 & 204.08081 \text{ PS dosage} + 9.56819 \text{ Reaction time} - 8.69867 \text{ pH} \times \\
 & \text{Fe(II) dosage} - 0.851031 \text{ pH} \times \text{Reaction time} - 19.76316 \text{ pH}^2 + \\
 & 82.42738 \text{ Sulfite dosage}^2 - 67.53262 \text{ PS dosage}^2 - \\
 & 0.202982 \text{ Reaction time}^2
 \end{aligned} \quad (2)$$

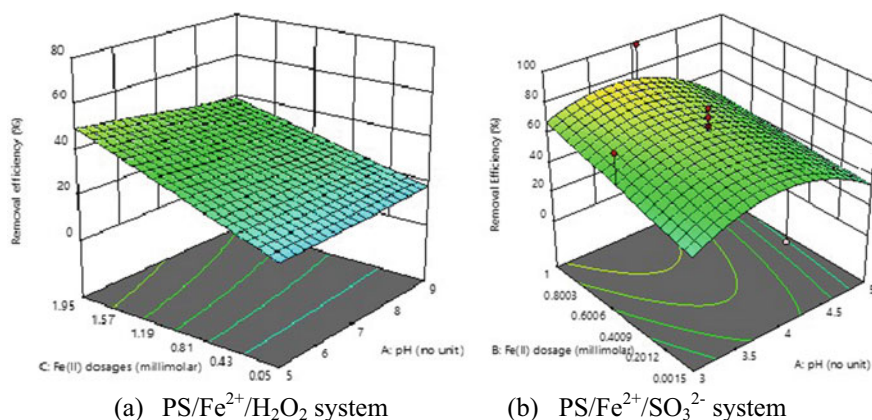


Fig. 2. 3D surface plot of COD removal efficiency as a function of Fe^{2+} dosage and pH

R^2 for the fitted model was 0.7727. Whereas adequate precision ratio obtained was 12.0195; it is desirable, and this model can be used for the design space.

Results obtained from ANOVA show that pH and Fe^{2+} doses are the main contributing factors to COD removal efficiency. Figure 2(b) presents an indicative 3D surface plot showing the effect of Fe^{2+} and pH on COD removal efficiency. 90% COD removal was obtained under optimized conditions of pH 3.67, Fe^{2+} dose of 0.5 mM, SO_3^{2-} dose of 0.5 μM , and PS dose of 1.5 mM with 17 min reaction time for $\text{PS}/\text{Fe}^{2+}/\text{SO}_3^{2-}$ system.

Table 3 $\text{PS}/\text{Fe}^{2+}/\text{SO}_3^{2-}$ system ANOVA for COD removal efficiency

Source	Sum of Squares	df	Mean Square	F-value	p-value	
Model	21,237.01	11	1930.64	11.12	< 0.0001	significant
A-pH	1951.85	1	1951.85	11.25	0.0019	
B-Fe(II) dosage	2832.86	1	2832.86	16.32	0.0003	
C-Sulfite dosage	15.68	1	15.68	0.0904	0.7655	
D-PS dosage	18.69	1	18.69	0.1077	0.7447	
E-Reaction time	18.89	1	18.89	0.1088	0.7434	
AB	603.52	1	603.52	3.48	0.0704	
AE	2317.61	1	2317.61	13.35	0.0008	
A^2	1021.33	1	1021.33	5.88	0.0204	
C^2	1110.39	1	1110.39	6.40	0.0159	
D^2	745.35	1	745.35	4.29	0.0455	
E^2	1077.37	1	1077.37	6.21	0.0175	
Residual	6247.78	36	173.55			
Lack of Fit	5183.21	31	167.20	0.7853	0.6997	not significant

3.3 Ammoniacal Nitrogen ($\text{NH}_3\text{-N}$) Removal

Under optimized conditions obtained for COD removal, both systems yielded similar removal of ammoniacal nitrogen. At $\text{NH}_3\text{-N}$ concentration of 936 mg/L, removal efficiency was 23.3 and 23.9% for $\text{PS/Fe}^{2+}/\text{H}_2\text{O}_2$ and $\text{PS/Fe}^{2+}/\text{SO}_3^{2-}$ systems, respectively.

4 Conclusions

In this research, the suitability of PS based chemical oxidation of leachate was studied. The effects of independent variables on the degradation of organic matter were examined. The results showed that both $\text{PS/Fe}^{2+}/\text{H}_2\text{O}_2$ and $\text{PS/Fe}^{2+}/\text{SO}_3^{2-}$ systems are capable of removing organic matter from landfill leachate; the latter being more effective. Under optimized conditions the COD removal efficiency was 68% and 90% using $\text{PS/Fe}^{2+}/\text{H}_2\text{O}_2$ and $\text{PS/Fe}^{2+}/\text{SO}_3^{2-}$ systems, respectively. Acidic conditions favored organic matter degradation. $\text{NH}_3\text{-N}$ removal was similar for both systems.

Acknowledgements The authors would like to thank Universiti Teknologi Brunei for the funding of the project under UTB Internal Grant, UTB/GSR/1/2019 (11).

References

1. Guerra-Rodriguez S, Rodroguex E, Narain Singh D, Rodriguez-Chueca J (2018) Assessment of sulphate radical-based oxidation processes for water and wastewater treatment: a review. *Water* 10(12):1828
2. Haneef T, Mustafa MR, Yusof KW, Isa MH, Bashir MJK, Ahmad M, Zafar M (2020) Removal of polycyclic aromatic hydrocarbons (PAHs) from produced water by ferrate (VI) oxidation. *Water* 12:3132
3. Hayat H (2020) Waging War on Plastic Waste. <https://borneobulletin.com.bn/waging-war-on-plastic-waste/#:~:text=Solid%20waste%20management%20was%20one,the%20highest%20in%20the%20region>. Accessed 10 Sept 2020
4. Heng GC, Isa MH, Lock SSM, Ng CA (2021) Process optimization of waste activated sludge in anaerobic digestion and biogas production by electrochemical pre-treatment using ruthenium oxide coated titanium electrodes. *Sustainability* 13(9). Article 4874
5. Liu Z, Guo Y, Shang R, Fang Z, Wu F, Wang Z (2016) A Triple system of Fe(III)/Sulfite/Persulfate: decolourisation and mineralisation of reactive brilliant red x-3b in aqueous solution at near-neutral pH values. *J Taiwan Inst Chem Eng* 68:162–168
6. Mahtab MS, Islam DT, Farooqi IH (2020) Optimisation of the process variables for landfill leachate treatment using Fenton based advanced oxidation technique. *Eng Sci Technol Int J* 24(2021):428–435
7. Mohajeri S, Hamidi AA, Isa MH, Zahed MA (2019) Landfill leachate treatment through electro-Fenton oxidation. *Pollution* 5(1):199–209

8. Singa PK, Isa MH, Lim JW, Ho YC, Krishnan S (2021) Photo-Fenton process for removal of polycyclic aromatic hydrocarbons from hazardous waste landfill leachate. *Int J Environ Sci Technol* 18(11):3515–3526
9. Tamru A, Chakma S (2015) Effects of landfilled MSW stabilisation stages on composition of landfill leachate: a review. *Int J Eng Res Technol (IJERT)* 4(3)
10. Xia X et al (2020) A review study on sulfate-radical-based advanced oxidation processes for domestic/industrial wastewater treatment: degradation, efficiency and mechanism. *J Front Chem* 8:592056

Infrastructure Efficiency

Construction Players' Awareness on the Use of Building Information Modelling (BIM) and Industrialized Building System (IBS) in Malaysian Construction Industry



Mohamad Zain Hashim, Idris Othman, Nur Syahirah M. Khalid, Siti Hafizan Hassan, and Muriatul Khusmah Musa

Abstract The Public Work Department's (JKR) strategic plan for 2020–2025 aims to implement BIM in 50% of projects, increasing by 10% annually. BIM promotes collaboration, while IBS represents prefabrication in Malaysia. Construction companies invest in BIM and IBS to meet client demands, gradually incorporating them into projects. Challenges arise due to the lack of standardized guidance and resistance to change. Businesses establish BIM units and training programs to address these issues. BIM facilitates technology adoption and changes in management practices. The government encourages BIM and IBS for sustainable construction. IBS provides cost and time savings, increased productivity, and higher quality output. A questionnaire survey examines awareness of BIM and IBS in Malaysia's construction industry. Most industry players are aware of IBS adoption (90.2%) and BIM use (80.4%), with positive responses on their benefits and challenges.

Keywords BIM · IBS · Construction industry · Construction waste minimization

M. Z. Hashim (✉) · N. S. M. Khalid · S. H. Hassan · M. K. Musa
School of Civil Engineering, Universiti Teknologi MARA, Cawangan Pulau Pinang, 13500,
Pematang Pauh, Pulau, Pinang, Malaysia
e-mail: mzain.hashim@uitm.edu.my

I. Othman
Department of Civil and Environment Engineering, Universiti Teknologi PETRONAS, 32610,
Seri Iskandar, Perak Darul Ridzuan, Malaysia
e-mail: idris_othman@utp.edu.my

© Institute of Technology PETRONAS Sdn Bhd 2024
B. S. Mohammed et al. (eds.), *Proceedings of the International Conference on Emerging Smart Cities (ICESC2022)*, Lecture Notes in Civil Engineering 324,
https://doi.org/10.1007/978-981-99-1111-0_42

1 Introduction

Malaysia's construction industry is currently under intense public pressure to improve efficiency, quality, and value. Even though the construction industry contributed only about 4.5 percent of Malaysia's Gross Domestic Product (GDP) in 2019, it was still an important component of the country's economic growth. There are several factors preventing Malaysia's construction industry from growing as quickly as it should, including its current level of quality, productivity, lack of safety, and over-reliance on unskilled foreign labor [1]. Thus, Malaysia's construction industry problems can be solved by implementing Building Information Modelling (BIM) and Industrialized Building Systems (IBS). The use of BIM as a design tool has transformed many aspects of the construction industry, including plan implementation, project execution, and facility management. According to Bryde [2], BIM is a suitable method for managing building projects, and project managers should use it. IBS, on the other hand, are types of construction processes that involve on-site application of techniques, products, materials, and a construction system, as well as prefabrication and on-site component installation. These components are designed to meet the needs of designers while also achieving the goal of high-quality construction. There are several advantages to using IBS, including less unskilled labor, less waste, fewer building materials, improved environmental and construction site cleanliness, and improved quality control. Furthermore, IBS offers benefits such as lower general construction costs, improved construction efficiency and productivity, reduced workplace health and safety concerns, and reduced reliance on foreign labor and skilled workers. The recent rapid increase in population has resulted in high demand for housing. According to Maryam [3], Malaysia would require 8,850,554 houses between 1995 and 2020, with an average of 1,790,820 units being built every ten years. To meet these demands, the construction industry must implement a quick method. Although most Malaysian construction companies are familiar with the BIM method, lack of guidance and government support, as well as a scarcity of well-trained employees, has prevented them from adopting the technology. Malaysian construction is thought to have taken longer to adapt to BIM than US construction, which bridged the gap within five years of implementing the technology there. While IBS has been around for over 40 years, the construction industry continues to use the traditional method, which has been shown to be dirty, unsafe, and inefficient. There are some issues with IBS that cause construction developers to prefer the traditional method. For example, Malaysia provides cheap foreign workers, which construction companies have used for decades and who are trained in traditional construction methods. As a result, in order to transition to IBS, the government must either establish a policy or impose a strict quota for IBS projects, or they may need to redefine the market with a mandatory quota program. Most small-scale contractors who work on small-scale projects are unwilling to switch to a mechanized system based on the IBS system. Therefore, the study is being conducted to determine the level of BIM and IBS adoption in the Malaysian construction industry and to investigate the benefits of both methods. Therefore, the purpose of this research is to determine the level of adoption of BIM

and IBS in the Malaysian construction industry, to investigate current awareness of it, and to investigate the benefits of BIM and IBS in the construction industry.

1.1 Building Information Modelling

BIM is a method that begins with the creation of an intelligent 3D model and continues throughout a project's lifecycle, enabling document management, coordination, and simulation (plan, design, build, operation and maintenance). BIM enables architects, engineers, and contractors to collaborate on coordinated models, which provides all parties with a better understanding of how their individual work fits into the overall project while also allowing them to work more efficiently. When an element in a model, is changed, every view is updated to reflect the new change in sections, elevations, and sheet views. The information in the model allows the user to make changes to their design before it is built. Realistic visualizations of BIM models can be used to obtain faster approvals in the field. Most importantly, a model's intelligence can be maintained throughout the construction process. BIM allows designers to gain insight into a design's constructability, allowing for greater efficiency and effectiveness during the construction phase, as well as improved future building operations and maintenance.

1.2 Industrialized Building System (IBS)

IBS is a building system in which structural components are manufactured in a factory, transported to the construction site, and assembled into a structure with minimal additional site work. Many government and private initiatives emphasize Industrialized Building Systems (IBS) or off-site production to improve the efficiency and quality of building and infrastructure development projects. Malaysia is one of the countries that has begun to recognize the advantages that IBS provides to the construction industry. Through the government's construction industry transformation plan (CITP) 2016–2020.

1.3 Level of Adoption of BIM and IBS in Malaysian Construction Industry

1.3.1 Building Information Modelling (BIM) Adoption

Although BIM implementation has many advantages, such as improving constructability and reducing conflict to provide better visualization, improving cost

estimation, and facilitating smooth coordination and information among parties in construction projects, adoption has been slow. Most construction industry players, according to Eastman [4], see BIM as a disruptive technology that transforms existing construction processes into new ones. As a result, BIM adoption is facing significant challenges from construction workers who are unwilling to change established traditional methods. BIM adoption challenges are classified into two types: technical and non-technical issues. According to Arayici [5], non-technical challenges are primarily focused on managing human resistance to change, explaining how BIM is superior to 2D drafting, and explaining the roles and responsibilities of various stakeholders in BIM. Technological upgrades, interoperability, compatibility, and complexity are among the technical issues addressed.

1.3.2 Industrialized Building System (IBS) Adoption

Today, IBS is increasingly being used in construction in Malaysia. Malaysia currently employs large panel systems, metal form systems, and modular systems for IBS systems. Despite the potential benefits of IBS, Malaysia's government believes its use is still low. The first IBS strategic plan was released in 2003, followed by two IBS "roadmaps," namely 2003–2010 and 2011–2015. Since then, it has been mandatory for government projects to include 70% or more IBS elements. However, the private sector has not widely adopted IBS. As a result, despite government efforts to implement an IBS system, the main issues remain unresolved. In some countries, such as Singapore, the advantages of IBS or prefabrication have been well documented. The IBS is then described as a complete construction process in which almost all of the component structures are manufactured at a location other than the main site. In this way, high-quality work can be accomplished while keeping project completion times to a minimum.

Based on the data from Malaysian Construction Institution and Development Board (CIDB), foreign workers make up 25% of Malaysia's total construction workforce. The levy on foreign workers in the manufacturing and construction industries has been raised from RM1,250 to RM2,500 in order to reduce over-reliance on low-skilled foreign labor [6]. Khalil [7] stated that, the implementation of IBS has been slow in Malaysia due to stakeholders' unwillingness to adopt the system because they are not convinced of its effectiveness. The government was expected to make IBS mandatory by 2020. Despite this, the move faces numerous challenges. According to a CIDB survey, despite the government's goal of increasing IBS use to 70%, companies were still about 15% behind in terms of implementation. The contractors believed the method was inefficient. This is due to the fact that, lifting and transporting prefabricated parts to the construction site would initially incur significant costs for the contractor.

2 Methodology

To collect data for this study, a questionnaire survey was administered to the local construction industry. The researcher focuses on construction workers in Malaysia to collect data. The questionnaire types were created using a one-to-five rating scale and respondents were asked to rate the answers provided. Aside from that, there were a few multiple-choice questions. The research questions were developed in response to the study's objective and a review of the literature. The questionnaire consists of seven parts, which are general information of the respondent, awareness of IBS and BIM, benefits of IBS and BIM, challenges faced by IBS and BIM also the perception of IBS and BIM in the Malaysian construction industry. All the data from the survey were tabulated and analyzed using Statistical Package for Social Science (SPSS).

3 Result

The demographic information for the respondents is shown in Table 1. Contractors accounted for 54.9 percent of respondents, consultants for 37.3 percent, and architecture firms accounted for 7.8 percent. 49% of respondents were from the central regions, 33.3 percent from the northern regions, and 11.98% from Peninsular Malaysia's southern region. On the other hand, only a small percentage of respondents (2%) were from Malaysia's East Coast and East Malaysia (3.9 percent). In terms of work experience, 47.1 percent had less than three years, 33.3 percent had three to five years, and 19.6 percent had five to ten years in the construction industry.

3.1 Awareness of the Adoption of Industrialized Building System (IBS) and Building Information Modelling (BIM) in the Malaysian Construction Industry

Table 2 shows respondents' concerns and awareness of IBS adoption. According to the findings, the vast majority of respondents (90.2 percent) were aware of IBS. Despite their knowledge of IBS, only 68.6 percent admitted to having exposure to the IBS system, with the remaining 31.4 percent having no knowledge of IBS. The vast majority of respondents (84.3 percent) were aware of the implementation of IBS in the construction industry, compared to only 15.7 percent who were not. According to the results, more than half of the respondents (56.9%) had experienced carrying out a project using the system, and 60.8 percent had previously attended the IBS introductory course.

Data were analyzed to determine whether the number of respondents who were aware of IBS adoption in the construction industry was equal to the number of respondents who were not aware of IBS adoption. The chi-square goodness of fit

Table 1 Respondents' Demographic Information

Respondents' classifications		Percentage (%)
Gender	Male	47.1%
	Female	52.9%
Zone	Northern Region	33.3%
	Central Region	49.0%
	Southern Region	11.8%
	Eastern Region	2.0%
	East Malaysia	3.9%
Company	Architect	7.8%
	Consultant	37.3%
	Contractor	54.9%
Qualification	Certificate/Diploma	9.8%
	Degree	86.3%
	Master/PhD	3.9%
Working experience	< 3 years	47.1%
	3 – 5 years	33.3%
	5 - 10 years	19.6%
	> 10 years	0.0%

Table 2 Responses on IBS adoption awareness

IBS adoption awareness	Yes	No
B1. Do you know about Industrialized Building System (IBS) system?	90.2%	9.8%
B2. Have you been disclosed on IBS system?	68.6%	31.4%
B3. Have you ever noticed IBS system being implemented, directly or indirectly?	84.3%	15.7%
B4. Have you ever carried out a project which using IBS system?	56.9%	43.1%
B5. Have you followed the IBS introductory course previously?	60.8%	39.2%

test was used to analyze the data. Table 3 shows that some variables rejected null hypotheses, $X^2(1) = 32.961(B1)$, $7.078(B2)$, and $24.020(B3)$, $p.05$. More than half of those polled were aware of IBS adoption in the construction industry. The null hypothesis in the Chi-Square goodness of fit test assumes that there is no significant difference between the observed and expected value.

Table 4 indicates that the use of BIM in the construction industry had led industry participants to seek BIM-related information. This is demonstrated by the fact that 80.4 percent of respondents said yes. However, 56.9% of respondents admitted to having insufficient exposure to the BIM system. Despite the fact that 52.9 percent of respondents said they had noticed the use of BIM in the construction industry, 47.1 percent of respondents said they had not. According to the findings, 35.3 percent of

Table 3 Chi-Square goodness of fit test on IBS adoption Awareness

	B1. Do you know about IBS system?	B2. Have you been disclosed on IBS system?	B3. Have you ever noticed IBS system being implemented, directly or indirectly?	B4. Have you ever carried out a project which using IBS system?	B5. Have you followed the IBS introductory course previously?
Chi-Square	32.961 ^a	7.078 ^a	24.020 ^a	0.961 ^a	2.373 ^a
df	1	1	1	1	1
Asymp. Sig	0.000	0.008	0.000	0.327	0.123

a. 0 cells (0.0%) have expected frequencies less than 5. The minimum expected cell frequency is 25.5 (Source: SPSS)

Table 4 Responses on BIM adoption awareness

BIM adoption awareness	Yes	No
C1. Do you know about Building Information Modelling (BIM) system?	80.4%	19.6%
C2. Have you been disclosed on BIM system?	43.1%	56.9%
C3. Have you ever noticed BIM system being implemented, directly or indirectly?	52.9%	47.1%
C4. Have you ever carried out a project which using BIM system?	35.3%	64.7%
C5. Have you followed the BIM introductory course previously?	45.1%	54.9%

Table 5 Chi-Square goodness of fit test BIM adoption Awareness

	C1. Do you know about BIM system?	C2. Have you been disclosed on BIM system?	C3. Have you ever noticed BIM system being implemented, directly or indirectly?	C4. Have you ever carried out a project which using BIM system?	C5. Have you followed the BIM introductory course previously?
Chi-Square	18.843 ^a	0.961 ^a	0.176 ^a	4.412 ^a	0.490 ^a
df	1	1	1	1	1
Asymp. Sig	0.000	0.327	0.674	0.036	0.484

a. 0 cells (0.0%) have expected frequencies less than 5. The minimum expected cell frequency is 25.5 (Source: SPSS)

project participants had started using BIM systems, while 64.7 percent had not. The answers to the final BIM question contradict the answers to the first.

Data were analyzed to determine whether the number of respondents who were aware of BIM adoption in the construction industry was equal to the number of respondents who were not aware of BIM adoption. The chi-square goodness of fit test was used to analyze the data. Table 5 shows that only one variable rejected null hypotheses, $X^2(1) = 18.843(C1)$, $p.05$. More than half of those polled were

aware of the use of BIM in the construction industry. The null hypothesis in the Chi-Square goodness of fit test assumes that there is no significant difference between the observed and expected value.

3.2 Respondents' Opinions on the Benefits of Industrialized Building System (IBS) and Building Information Modelling (BIM)

Table 6 displays some of the statements made by respondents on the advantages of using IBS and BIM in the construction industry. Despite the fact that some respondents had no knowledge of IBS and BIM systems, majority of them answered positively. This is reflected in a high mean value, with nearly all mean values greater than 4. The highest benefits chosen for the use of IBS were 'low labor dependence' ($M = 4.57$; $SD = 0.575$), 'shorter construction time' ($M = 4.57$; $SD = 0.640$), and 'optimal material usage and waste reduction' ($M = 4.51$; $SD = 0.644$). The findings also reveal that the benefits of using BIM as perceived by respondents were consistent with the use of IBS. The respondents had chosen 'reduces overall project duration' ($M = 4.47$; $SD = 0.612$), 'improve productivity and quantity take-off' ($M = 4.41$; $SD = 0.606$), and 'increases project delivery speed' ($M = 4.39$; $SD = 0.723$) as the benefits of using BIM. These results are supported by Bari's [8] findings that IBS construction can reduce overall costs, time, and manpower while producing higher-quality housing than traditional methods. IBS can also help with waste minimization and reduction, further emphasizing its economic benefits, while the reductions in overall manpower requirements at the construction sites may lead to less reliance on foreign labor.

3.3 Building Information System (BIM) and Industrialized Building System (IBS) Challenges Faced by Malaysian Construction Industry

Table 7 depicts the overall challenges in the use of BIM and IBS. The main challenge was to encourage the use of these two systems by small contractors. The highest mean score value of 4.65 demonstrates this. Thus, something needs to be done to increase the participation of small businesses in the use of this system. The findings are consistent with a study by Aizat [9] that identified human factors as the most difficult challenge in using BIM and IBS.

Table 6 Respondents' Opinions on The Benefits of IBS and BIM

	Mean	Std. Deviation
The benefits of Industrialized Building System (IBS)		
Low labor dependence	4.57	0.575
Shorter construction time	4.57	0.640
Optimum material usage and waste reduction	4.51	0.644
Increase of site safety and neatness	4.49	0.644
Lower weather impact to construction industry	4.37	0.799
Better finish product quality	4.33	0.931
Cost saving	3.94	1.121
The benefits of Building Information System (BIM)		
Reduces the overall project duration	4.47	0.612
Improves productivity and quantity take-off	4.41	0.606
Increases the speed of project delivery	4.39	0.723
Coordinate between Construction Phase	4.29	0.807
Clash detection and conflict resolution	4.18	0.793
Reduces overall project cost	4.14	0.849

Table 7 BIM and IBS challenges in construction industry

	Mean	Std. Deviation
Lack of involvement from small contractors	4.65	0.688
Lack of knowledge and exposure to IBS technology	4.53	0.758
Lack of knowledge on how to implement BIM	4.45	0.783
Steep learning curve to build up BIM expertise	4.43	0.671
Lack of demands for BIM	4.41	0.829
IBS as mass construction method	4.37	0.916

3.4 Respondents' Perceptions on the Use of IBS and BIM in the Construction Industry

Table 8 displays respondents' perceptions on the use of IBS and BIM in the construction industry. The vast majority of respondents acknowledged that using IBS and BIM could boost quality (M = 4.53: SD = 0.612), productivity, and overall work performance (M = 4.49: SD = 0.644). BIM can also help with decision-making (M = 4.45: SD = 0.610) and work efficiency (M = 4.41: SD = 0.698). Many respondents also agreed that the use of IBS and BIM would increase efficiency and effectiveness in construction work, as well as be extremely helpful in completing work quickly (M = 4.41: SD = 0.698). Intensive courses for industry players on IBS application are extremely beneficial in furthering IBS adoption in the construction industry [10].

Table 8 Respondents' Perceptions on the use of IBS and BIM in the construction industry

Respondents perception	Mean	Std. Deviation
I think using BIM and IBS improve quality of project delivery	4.53	0.612
I think using BIM and IBS increase productivity and work performance	4.49	0.644
I think using BIM and IBS provide help us make better decisions	4.45	0.610
Using BIM and IBS make it easier to do my job	4.43	0.700
I think using BIM and IBS enhances efficiency and effectiveness on the job	4.41	0.698
BIM and IBS system enables me to accomplish tasks more quickly	4.41	0.698
I find BIM and IBS easy also useful in my job	4.39	0.695
It is easy to use BIM and IBS to perform tasks on site	4.37	0.692
BIM and IBS are clear and understandable	4.35	0.658
I think that the advantages of using BIM and IBS outweigh the disadvantages	4.31	0.787
I think using BIM and IBS raise our chances to increase our profits	4.25	0.891

According to Jabar [11], it is critical to inform the community about the benefits of IBS as this will indirectly increase demand for IBS use. Some negative perceptions about the use of IBS must be addressed, including high construction costs, a lack of knowledge and exposure to IBS technology, and lack of IBS manufacturers.

4 Discussion

4.1 Benefits of BIM in the Malaysian Construction Industry

BIM technologies and methods are already having a positive impact on construction projects. BIM models can be used in the tender process to organize work details and product specifications. Tender document preparation becomes much more efficient and straightforward because it allows for a more precise understanding of the building process. BIM in construction allows for more effective planning and regulation. BIM helps to lower down the construction costs by reducing errors, changing materials quickly, and reducing construction time. Furthermore, advancements in technical systems, exteriors, and interiors can be reported in the BIM model, allowing for the updating of all business calculations as well as the tracking of installed materials and products within a single central database. BIM makes Facility Management and building operations more efficient by collecting data from all engineering systems. In addition, BIM provides numerous benefits to the building owner, developer, and other stakeholders. Buildings can be better understood with BIM, simulations on various scenarios can be performed, and visual aspects can be provided, as it contains energy

parameters that specify various cost indicators under various operating conditions. As a result, the financial risks associated with the processes of design, construction, and operation may be reduced. Apart from that, a variety of documentation packages can be issued to examine the parameters of any building, making the process of obtaining various approvals easier. A BIM-based design process can increase the value of project information while decreasing the effort required to create that information, resulting in a higher return on investment for the owner. BIM is used by facility managers during the operation and maintenance (O&M) stages of a building's life cycle for a variety of reasons, including warranty management, maintenance and service information, quality control, energy and space management assessment and monitoring, emergency management, and retrofit planning. The design and construction planning processes can be synchronized by using BIM. 4D modelling, in particular, allows construction stakeholders to visualize constructability, work sequencing, and project planning. Furthermore, most companies have used 4D models to identify and eliminate problems associated with off-site construction. BIM models in 4D and 5D have the potential to improve cost estimation and pricing, site planning, and safety management. To summarize, the benefits of BIM optimization include cost control or reduction, risk reduction (via the avoidance of rework due to clash detection), and increased construction quality due to better construction management, building quality, or having access to complete information during the construction period.

4.2 The Challenges of BIM in the Malaysian Construction Industry

Despite the numerous benefits that have resulted from using BIM, its adoption in Malaysia appears to be stagnant. Many organizations fear that the use of BIM will reduce production because it is difficult to understand and thus, disrupt the existing workflows. In addition, even though designers believed that the use of BIM would maximize benefits to owners and contractors, it is still risky. On top of that, there are also legal issues to resolve, such as who owns the design, who is responsible for maintaining the validity of the data during data entry, and who is responsible for any errors in the model. Many organizations believe that BIM implementation will alter their current business practices. The implementation of Information Technology (IT) could affect their business operations while lowering productivity. Shifting from fragmented to collaborative construction processes will harm project outcomes and client expectations. In reality, implementing BIM presents three challenges: legal issues (e.g., ownership, contracts, project management, and so on); technology (e.g., user-friendliness, software interoperability, cost, and so on); and organizational and business structure issues. As a result, in order for BIM to succeed in Malaysia, the government must overcome these obstacles.

4.3 Benefits of IBS in Malaysian Construction Industry

Data and information from previous IBS studies that have been analyzed show that there are many common indicator factors associated with the positive outcome of IBS construction. This indicates that the implementation of IBS in the construction industry has resulted in success. Some key points of the importance of the IBS implementation in Malaysia are as follows:

- Customer satisfaction with products and customer satisfaction with services,
- High reliability and quality of IBS design qualifications,
- Handling and managing many aspects of on-site construction challenges such as risk management, and quality assurance
- Efficient delivery time for designated projects
- Reduce waste materials and manpower required on-site
- Reduce operating costs that typically occur in typical construction projects

There are three main scopes towards sustainable construction, namely:

- Efficient resource management throughout the life cycle of the building,
- Cost estimates for construction phases in different time sets specifically consist of operation, maintenance, improvement and demolition, and
- Economic gains for local Small and Medium Enterprises (SMEs) are due to the consistent demand for resources for the construction of IBS components.

There are also studies stating that finance and reconcilable performance in obtaining high-quality building specifications are the two most influential drivers that will drive demand and supply for sustainable socioeconomic achievement for stakeholders [12].

4.4 The Challenges of IBS in the Malaysian Construction Industry

According to Tamrin [13], the implementation of IBS in the Malaysian construction sector is still quite low as compared to traditional methods in the construction industry. There are several factors contributing to this:

- **Costs and Return on Investment:** Large swings in housing demand, high interest rates, and low labor costs make large capital investments difficult to justify. Foreign workers are currently inexpensive in Malaysia, which is why contractors prefer the labor-intensive traditional construction method because it is much easier to lay off workers during slow periods of construction. According to previous experiences, IBS in Malaysia is more expensive than traditional construction due to stiff competition from traditional construction methods.

- **Manpower shortages:** For fully prefabricated construction systems, a high degree of precision is necessary. There is still a shortage of skilled workers in Malaysia following the implementation of IBS.
- **Lack of Incentive and Awareness:** Many architects and engineers are still unaware of the basic features of IBS, such as modular coordination, due to a lack of government incentives and promotion in the implementation of IBS.
- **The Practices:** There are many stakeholders in the construction industry because it is fragmented, diversified, and involves many stakeholders. The agreement is required during the planning stage when using IBS.

5 Conclusion

Overall, the study reveals that some Malaysian construction industry players were unfamiliar with IBS and BIM. Majority of the respondents had heard and learned about IBS and BIM, but were unaware of the technical aspects (i.e., how it works) and construction applications. Even though the respondents were unsure about IBS and BIM key benefits they believed that the implementation of these two methods in the construction industry could enhance construction sustainability. Thus, they enthusiastically supported the associated benefits. Finally, it can be concluded that due to their efficiency, IBS and BIM are in high demand in the construction industry. However, all construction players in the construction industry must be exposed and trained to become acquainted with the system, as many were unaware of the technical aspects. As a result, it is hoped that this study will assist decision-makers in developing encouraging policies and guidelines for IBS and BIM adoption.

Acknowledgements The authors would like to express their heartfelt gratitude to all participants for their responses and assistance in completing the survey. The authors would also like to thank the Ministry of Higher Education Malaysia for funding this research with the FRGS grant. YUTP grant reference (YUTP-FRG 1/2022 (015LC0-405)).

References

1. CIDB (2021) CIDB technical report publication no: 210 report on residential housing cost: a comparison between industrialised building system (IBS) and conventional system
2. Bryde D, Broquetas M, Volm JM (2013) The project benefits of building information modelling (BIM). *Int J Proj Manag* 31(7):971–980
3. Qays Oliewy M, Nasharudeen Mustapha K, Mohammad BS (2009) Advantages of industrialized building system in Malaysia, Student Conference Research and Development (SCORED) At Malaysia, no. January, pp 1–12
4. Eastman C, Teicholz P, Sacks R, Liston K (2008) *BIM Handbook: a guide to building information modeling for owners, managers, designers, engineers and contractors*, vol 12, no 3
5. Arayici Y, Egbu C, Coates P (2012) Building information modelling (Bim) implementation and remote construction projects: Issues, challenges, and critiques. *Electron J Inf Technol Constr* 17:75–92

6. Construction Industry Development Board (CIDB) (2016) MALAYSIA BIM-Report-2016.pdf
7. Khalil FDAA, Abd Aziz FNA, Hassim S, Jaafar MS (2016) A review on industrialised building system issues in Malaysia, MATEC Web of Conferences, vol 47, pp 0–3
8. Bari NAA, Abdullah NA, Yusuff R, Ismail N, Jaapar A (2012) Environmental awareness and benefits of industrialized building systems (IBS). *Procedia - Soc. Behav. Sci.* 50:392–404
9. Aizat K, Jamal A, Mohammad MF, Hashim N, Mohamed MR (2019) Challenges of building information modelling (BIM) from the Malaysian Architect's Perspective, MATEC Web of Conferences, vol 3, pp 0–4
10. Walter AS (2015) Perception on industrialised building system (IBS): a case study in Sabah
11. Iaili Jabar I, Ismail F, Aziz ARA (2015) Public Participation: Enhancing Public Perception towards IBS Implementation. *Procedia - Soc Behav Sci* 168:61–69
12. Hatem ZM, Alsamarraie MM, Flaih AY, Oda AM (2021) Barriers to the adoption of industrialized building system in Iraqi construction industry. *Zanco J Pure Appl Sci* 33(3)
13. Tamrin N, Nawi N, Nifa F (2017) Industrialised building system in construction projects: a study on readiness. *Soc Sci* 12(5):839–844

Experimental, Numerical and Field Investigations on the Hydraulics Performance of Stormwater Curb-Opening Inlets



Zahiraniza Mustaffa, Ebrahim Hamid Hussein Al-Qadami,
Aifaa Balqis Kamarul Zaman, and Syed Muzzamil Hussain Shah

Abstract Roadway drainage is designed to collect the stormwater and channel it to a proper drainage system such as the stormwater inlets to avoid flooding on the road. A common type of stormwater inlet is the curb-opening inlet. The efficiency of the curb-opening inlets remains as one of the major challenges that causes surface ponding on the pavements and disturb the traffic movement. This paper aims to assess the efficiency of a typical depressed curb-opening inlets used in Malaysia through experimental, numerical, and field investigations. The experiments were conducted for various flows in a fabricated full-scale halfway road model. Later, a three-dimensional (3D) numerical modelling was developed using FLOW-3D software to validate outcomes from the experiments. Furthermore, a field investigation was also conducted at a selected area within the university to further compare the results. Outcomes from these three approaches showed similar trend, whereby the efficiency of depressed curb-opening inlet decreases as the approaching flow increases. On the other hand, some difference was observed between the experimental and field results. This could have caused by the surface roughness of the actual road, which would have infiltrated into the ground, leaving less flows to be intercepted by the inlet.

Z. Mustaffa (✉) · A. B. K. Zaman
Department of Civil and Environmental Engineering, Universiti Teknologi PETRONAS, Seri
Iskandar, Malaysia
e-mail: zahiraniza@utp.edu.my

A. B. K. Zaman
e-mail: aifaabalqis@gmail.com

S. M. H. Shah
Interdisciplinary Research Center for Membranes and Water Security, King Fahd University of
Petroleum and Minerals, Dhahran, Saudi Arabia
e-mail: syed.shah@kfupm.edu.sa

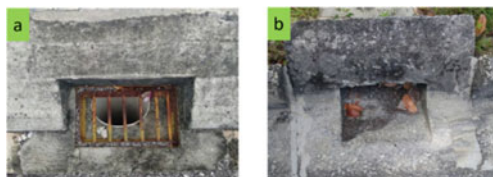
E. H. H. Al-Qadami
Eco Hydrology Technology Research Centre (Eco-Hytech), Faculty of Civil Engineering and
Built Environment, Universiti Tun Hussein Onn Malaysia, 86400 Parit Raja, Johor, Malaysia
e-mail: ebrahim@uthm.edu.my

Keywords Curb-opening inlet · Stormwater · Experiment · Numerical · Field investigation · Efficiency · Intercepted flow

1 Introduction

Malaysia is a tropical country that often subjected to high amount of stormwater throughout the year with yearly precipitation between 1801.6 mm to 4581.8 mm [19]. At the same time, the country is also well-known as a developing country that currently facing the phase of urbanization [2]. A lot of construction activities that involve concrete structures including roads in urban area for instance, has led to major replacement of permeable surfaces such as vegetated land with impermeable surfaces [31]. This has significantly reduced the natural infiltration and leading to the increase of excess runoff on the road. As a result, the existing road drainage system in Malaysia often found to exceed its designed capacity and become inefficient [31]. A phenomenon of water ponding and flash flood has become more common in Malaysia and as time goes by, it has turned out to be more severe than before. Therefore, it is very essential for every design of the urban road in Malaysia to serve dual functions efficiently. Stormwater inlet is the most important part that determines the efficiency and effectiveness of road drainage system in collecting and removing rainwater away from the road. There are several types of stormwater inlets practiced all around the world and each country may use different design standard in terms of patterns, sizes and configurations. In Malaysia, note that the stormwater inlet design standard is based on the Stormwater Management Manual for Malaysia (Manual Saliran Mesra Alam, MSMA) prepared by the Department of Irrigation and Drainage Malaysia [11]. Basically, there are four main types of stormwater inlets utilized for road drainage system and are defined as grate inlet, curb-opening inlet, slotted drain inlet and combination inlet. However, the most common curb inlets are the grate and curb-opening inlets, as shown in Fig. 1. Investigations on curb-opening inlets performance by means of experimental works are widely reported [7, 8, 17, 18, 28, 30]. Recently, lots of numerical works [10, 13, 15, 21, 26] and field works [14, 23], Mustafa et al., (2020) were reported specifically for stormwater grate inlet and very less for curb-opening inlets. In considering such gap and due to different design standard practice in Malaysia, this paper is to carry out experimental, numerical and field investigations by means of simulating the stormwater into a depressed curb-opening inlet which later gave overview on its efficiency. With that, this paper able to reveal the actual efficiency of the inlets through different mode of investigations thus able to provide a new guideline for Malaysia stormwater inlet design.

Fig. 1 Common road inlets used in Malaysia (a) Grate inlet, (b) Curb-opening inlet



2 Stormwater Inlets

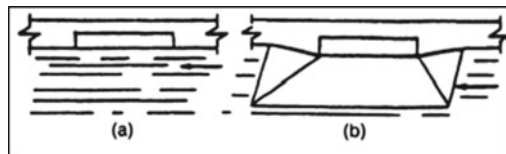
Stormwater inlet is a road drainage structure used to collect and convey the excess runoff from the road into the underground drainage system. Stormwater inlets are normally installed at the gutter section, roadside, paved medians and median ditches [8]. It is very essential to select a proper design and installation in order to avoid excess runoff from spread wider on the road. In order to design an efficient and effective stormwater inlet, it requires several considerations including the incoming flow, gutter flow, inlet capacity and spacing and etc. [12].

2.1 Curb-Opening Inlet

Curb-opening inlet, in some literature known as kerb inlet, is a vertical opening in the curb through which is covered by a top slab [22]. A curb-opening inlet is one of the most commonly used inlets that functions as a barrier by which runoff is guided and transferred to the opening inlet. There are two designs of the curb-opening inlet, namely undepressed and depressed inlets as shown in Fig. 2(a) and 2(b), respectively.

A depression of the inlet below the normal level of gutter, as shown in Fig. 2(b) increases the crossflow towards the opening. With that, the hydraulics performance of a curb-opening inlet will increase. The capacity of a curb-opening inlet, like any weir, depends upon the head and length of overfill. In the case of an undepressed curb-opening inlet as shown in Fig. 2(a), the head at the upstream end of the opening is the depth of flow in the gutter. Curb-opening inlets are useful in sag and on-grade situations because of their self-cleansing abilities and hydraulic efficiency. Most curb-opening inlets depend heavily upon an adjacent depression in the gutter for effective flow interception. Greater interception rates result in shorter and more economical inlet lengths. However, a large gutter depression can be unsafe for traffic flow and bicycle operation near the gutter line. Therefore, a compromise is in order when selecting an appropriate value for the gutter depression.

Fig. 2 Common road inlets used in Malaysia (a) Grate inlet, (b) Curb-opening inlet



2.2 Governing Equations of Curb-Opening Inlets

Along the way in bringing the flows into curb-opening inlet, there are three main road flows playing the roles. Flows known as approaching flows, Q_a travel into the inlet, then the flows over the inlet is sheared off into intercepted flows, Q_i and bypass flows, Q_b . Intercepted flow refers to flow that is successfully intercepted into the inlet while bypass flow is flow that fail to be intercepted by inlet and flowing downstream. Therefore, flows over a curb-opening inlet can be simply described as Eq. (1),

$$Q_a = Q_i + Q_b \quad (1)$$

On the other hand, the flow over curb-opening inlets can also be classified as either under weir or orifice flows. Weir flow refers to water that overflowing over the inlet. It consists of water that flows over the weir surface which is called crest and the overflowing sheet of water which is called as nappe. For curb-opening inlet that is under weir flow conditions, the interception capacity is expressed as Eqs. (2) and (3),

$$Q_{ic} = C_w(L_w + 1.8W)d^{1.5}, \text{ depressed} \quad (2)$$

$$Q_{ic} = C_wL_wd^{1.5}, \text{ undepressed} \quad (3)$$

where, Q_{ic} is interception capacity, C_w is weir coefficient, L is length of the curb-opening, W is lateral width of depression and d is depth at the curb. Meanwhile, orifice flow is referred to as water that flows over the inlet and water completely submerged the opening of the inlet. Orifice flow takes place when the water depth is high, and the inlet opening is fully covered or submerged by water. Under orifice flow condition, the interception capacity of curb-opening inlet could be expressed as Eqs. (4) and (5).

$$Q_{ic} = C_o h L_o (2g d_o)^{0.5}, \text{ depressed} \quad (4)$$

$$Q_{iw} = C_o A_g \left\{ 2g \left[d_i - \left(\frac{h}{2} \right) \right] \right\}^{0.5}, \text{ undepressed} \quad (5)$$

where, C_o is orifice coefficient (0.67), h is active head on the center of the orifice throat, L_o is length of orifice opening, A_g is clear area of opening, d_i is depth at lip of curb-opening and h is height of curb-opening. As for the curb-opening inlet efficiency, it could be computed using the given Eq. (6),

$$\eta = Q_i / Q_a \quad (6)$$

3 Methodology

A depressed curb-opening inlet used in Malaysia was selected in the analysis presented in this paper, details of which are shown in Fig. 3. The curb-opening inlet dimensions were 0.30 m length, 0.20 m width and 0.15 m height, while the outer curb dimensions were 0.6 m length, 0.2 m width and 0.35 height. The road surface immediately opposite of the curb was made depressed by 4% slope with lateral dimensions of 0.02 m and 0.05 m, respectively. Depression allows more flows to be captured, thus improving its performance. A wooden depressed curb-opening inlet was fabricated in the laboratory for experimental testing following the given dimensions, as shown in Fig. 4.

3.1 Experimental Modelling

A full scale of half roadway model was designed and constructed at the Hydraulics Laboratory of Universiti Teknologi PETRONAS (UTP), Malaysia as shown in Fig. 5(a). The model resembled a one-lane roadway typically used in Malaysia with a length of 6.0 m and width of 3.8 m. It was constructed with fixed slopes with longitudinal slope of 0.5%, cross slope of 2.5% and gutter slope of 4%. The surface of the roadway model was painted with sand of size 1.18 mm to simulate roughness similar to that of the road pavement. The depressed curb-opening inlet was placed in the middle section of the roadway model. Also, three tanks equipped with weirs were placed near to the roadway model labelled as supply, collection and bypass tanks as shown in Fig. 5(a). These tanks were used for discharge measurements of Q_a , Q_i and Q_b s, respectively. All tanks discharged waters into the sump tank and flows would then be re-circulated by the pump. Flows into the roadway model was controlled using a valve which regulated discharges up to 0.03 m³/s. A sketch showing different component of flows moving from upstream to the downstream of the roadway model was illustrated in Fig. 5(b). Q_a was measured using the rectangular weir and calculated by using the Eq. (7),

Fig. 3 Schematic views and dimensions of the depressed curb-opening inlet

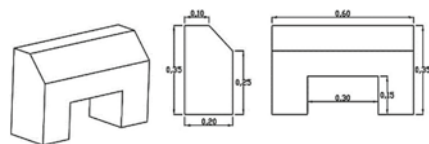
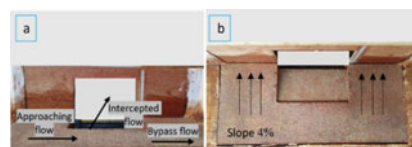


Fig. 4 Wooden depressed curb-opening inlets for experimental testing in the laboratory, (a) front view, (b) top view



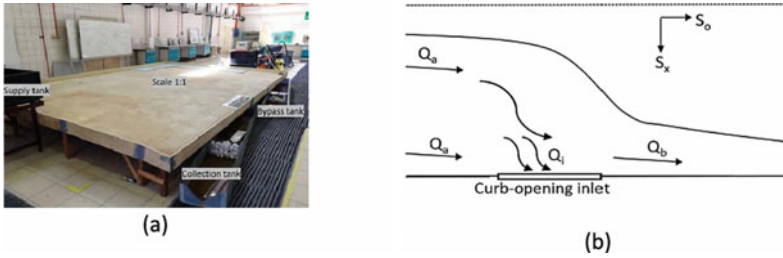


Fig. 5 Experimental set ups of half roadway model in the laboratory, (a) Full scale of half roadway model, (b) Sketch of flows onto the roadway model

$$Q_a = C_d \frac{2}{3} \sqrt{2g} L H^{3/2} \tag{7}$$

where C_d is the discharge coefficient, g is the gravity, L is the width of weir and H is the head of water above the crest. On the other hand, Q_i and Q_b were measured using the V-notch weir equation as described in Eq. (8),

$$Q_i = Q_b = C_d \frac{8}{15} \tan \frac{\theta}{2} \sqrt{2g} H^{5/2} \tag{8}$$

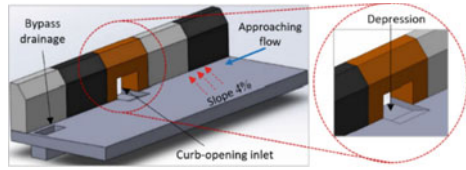
where, C_d is the discharge coefficient and H is head above the crest of the weir and θ is the angle of weir opening (90°).

3.2 Numerical Modelling

Simulations carried out in this study adapts theories of the computational fluid dynamics using a commercialised software called FLOW-3D. The software employs finite volume method and finite difference method to solve the equations of motion including continuity and momentum equations [3, 4]. In FLOW-3D, free surface flow is solved by volume of fluid (VOF) approach (Abdurrasheed et al., 2020, Mustafa et al., 2020), while the interaction between the solid and fluid is solved by Fractional Area Volume Obstacle Representation (FAVOR) solver [1], Al-Qadami et al., 2021). A 3D geometry model was first developed in SOLIDWORKS software for the depressed curb-opening inlet previously described in Fig. 3. Later, 3D geometry model was converted to stereolithography file (STL) format to be used in the FLOW-3D software; sample as shown in Fig. 6.

Meshing for the 3D geometry model was made using a non-confirming rectangular single block mesh system, having cell size of 0.008 m in the x-, y-, and z- directions with total cells number of 1,810,500 cells. The maximum adjacent size ratio was 1.0001 and the aspect ratios were 1.00003, 1.00743, and 1.00741 at the x-, y-, and z- directions, respectively. The cell size of 0.008 m was selected in compliance to

Fig. 6. 3D geometry model for depressed curb-opening inlet



the mesh sensitivity study. For the mesh sensitivity study, comparisons were made for three hydraulic parameters, namely velocity, Froude number (before the curb) and approaching flow. Once small difference was obtained among these parameters, the optimized cell size was selected to continue with the remaining simulations. In this analysis, Trail 2 was chosen based on the summary of the mesh sensitivity study shown in Table 1.

The boundary conditions were defined in accordance with the reality, with the inlet boundaries defined by the discharge and water depth, while two outlets (curb inlet point and drainage point) defined as stagnation pressure and zero fluid fraction. Free surface at the top boundary was also defined as stagnation pressure and zero fluid fraction as shown in Fig. 7. A total of two history probes were placed before and after the curb-opening inlet to aid in capturing flow parameters measurement such as velocity and dept as shown in Fig. 8. Three flux surfaces were also placed in three different locations including, before the inlet, at the inlet and at the bypass flow drain as shown in Fig. 8. The main function of flux surfaces is to measure the volume flow rates passing through with respect to time. In FLOW-3D outputs, the Froude number, velocities, water depth and specific hydraulic head were chosen to be calculated at each 0.01 s.

Table 1 Mesh independency study for depressed curb-opening inlet

Trail	Cell size (m)	Total cells number	Flow velocity (m/s)	Froude number	Approaching flow (m ³ /s)
1	0.010	920,160	0.601	0.698	0.0248
2	0.008	1,810,500	0.608	0.708	0.0250
3	0.006	4,263,300	0.700	0.709	0.0252

Fig. 7 Boundary conditions for the depressed curb-opening inlet

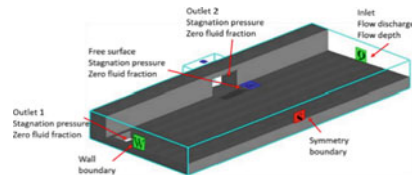
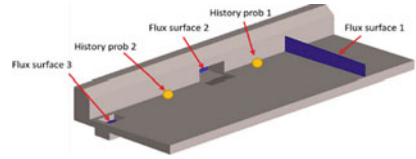


Fig. 8 Location of probes and flux surfaces



3.3 Field Investigation

An area was identified to carry out the field investigation for the depressed curb-opening inlet at UTP as shown in Fig. 9(b). The site was located closer to a lake as a source for water supply, as shown in Fig. 9(a). Water was pumped out from the lake and supplied into a tank which was equipped with a rectangular weir for discharge measurement. The tank was used to dampen the flow and later to discharge water onto the road in the form of sheet flows as shown in Fig. 10. Q_a released on the street would be moving downstream, part of which was intercepted into the depressed curb-opening inlet. Q_i were collected at the other end of the drain and measured using the common volumetric approach. Q_b was measured simply by subtracting Q_a and Q_i . Measurements were repeated for various Q_a by controlling the opening of the valve.

Fig. 9 Site location showing part of road with depressed curb-opening inlet, (a) site location, (b) depressed curb-opening inlet

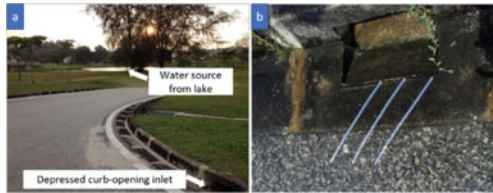


Fig. 10 Field investigation set up showing a rectangular weir tank placed at the site



4 Results and Discussion

4.1 Experimental Modelling

Discussion will be first given to the hydraulic efficiency of curb-opening inlets obtained from experimental investigation. Presented in Figs. 11 and 12 are scatter plots of approaching flow against efficiency relationship which provide overview on the actual capability of the curb in intercepting flows. At the range of approaching flow less than $\leq 0.001 \text{ m}^3/\text{s}$ as shown in Fig. 11, the results showed that the efficiency of curb-opening inlet was above 96%. Supposedly, the intercepted flow should have given 100% efficiency, however it was believed that due to the roughness of the roadway flume and low velocity, some portion of the approaching flows tend to be stagnant and remained on the roadway flume causing the minor losses and increasing trend of efficiency as the approaching flows increases.

Next, by looking at the behavior of curb-opening inlets at $Q_a \geq 0.001 \text{ m}^3/\text{s}$ as shown in Fig. 12, results showed that the inlet efficiency decreases with the increase of approaching flow. This results trend is similar to the works previously reported by [9, 16, 18, 24, 27, 29]. Such finding was believed to be significant in proving that every inlet design contained limitations in capturing flows. No single type of inlet can be considered the best [20]. It is able to capture approaching flows, but once it reaches the limitation to accept intercepted flows, deficiency will always be occurred. This is due to the fact that higher flow velocities produced during higher approaching flows causing the flow to gained higher inertia that let the water to be

Fig. 11 Approaching flow, Q_a against efficiency, η of curb-opening inlets at $Q_a \leq 0.001 \text{ m}^3/\text{s}$

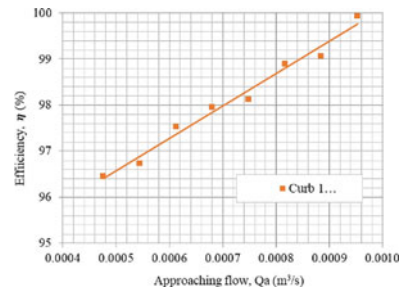
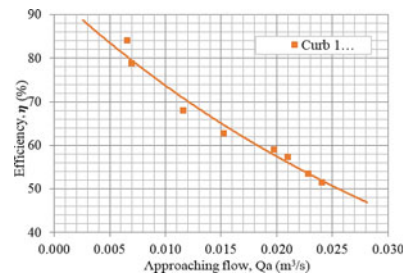


Fig. 12 Approaching flow, Q_a against efficiency, η of curb-opening inlet at $Q_a \geq 0.001 \text{ m}^3/\text{s}$

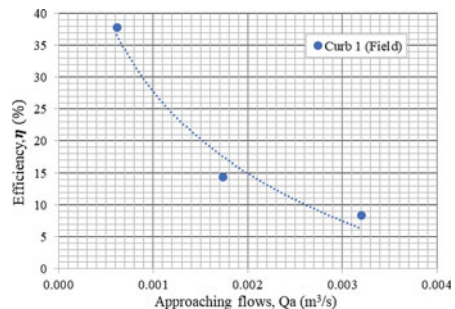


bypassed downstream instead of vertically intercept into the inlet by gravity. Next, discussion on efficiency of curb-opening inlet was furthered by taking an example at approaching flow, Q_a equal to $0.023 \text{ m}^3/\text{s}$. Results showed that the curb intercepted a flow amount of $0.01265 \text{ m}^3/\text{s}$ with 55% efficiency percentage. When compared the presented results with the previous findings reported by [31] that was related to a curb with same dimensions, it was observed that the curb efficiency was 46% only. The depression of the curb presented in this study was higher than the curb that was tested by [31], and this was the evident that allowed the tested curb to perform slightly higher with better efficiency. From there, it can be said that the higher the depression of a curb-opening inlet, the higher the efficiency. However, the need for deeper depression should be compromised to ensure efficiency requirement and relatively flat road to maintain the comfort of road users.

4.2 Field Investigation

A total of three runs at different approaching flows including 0.0006 , 0.0017 and $0.0032 \text{ m}^3/\text{s}$ were performed under the actual condition. Figure 13 illustrates the relationships between the approaching flow and curb efficiency. It was observed that the trend of efficiency plotted are similar to the results that obtained from the experimental runs (Fig. 12), at which the curb efficiency decreased with the increment of the amount of approaching flows. However, the efficiency of the curb that was tested in the field and under the actual conditions was low when compared with the efficiency of the curb that was tested in the laboratory. This was due to several reasons including, curb materials difference, surface friction coefficient, and back flow effects.

Fig. 13 Approaching flow, Q_a against efficiency, η of curb-opening inlet under varying flows



4.3 Numerical Modelling

A total of three cases (Case 1, 2 and 3) were simulated numerically using the art of computational fluid dynamics (CFD) at different approaching flows under the same setup used during the experimental runs. Tables 2 and 3 show the selected approaching flows and the results obtained from both numerical and experimental modelling, respectively.

4.3.1 Flow Discharge Comparison

Figures 14, 15 and 16 show the relationship between the three targeted discharges (Q_a , Q_i , and Q_b) with respect to time. Generally, it can be noticed that intercepted flow was bigger than the bypass flow in all cases as shown in Fig. 14. On the other hand, the highest intercepted flow was reported at Case 1 at which the highest approaching flow was existed, while the lowest intercepted flow was reported at Case 3. Besides, it was noticed that both intercepted and bypass flows decreased with the decrement of the approaching flow as shown in Figs. 15 and 16. In terms of curb efficiency, it was noticed that efficiency of the curb decreased with the increment of the approaching flow as shown in Fig. 17. For instance, the curb efficiency at Case 1 which was simulated at the highest approaching flow was the lowest with percentage value of 54%. On the other hand, 62% efficiency was reported for Case 3 at which the approaching flow was the lowest. This observation was in agreement with the experimental and field results.

Table 2 Numerical modelling results

Approaching flow (m ³ /s)	Intercepted flow (m ³ /s)	Bypass flow (m ³ /s)	Efficiency η %	Velocity before curb (m/s)	Velocity after curb (m/s)	Froude number before curb	Froude number after curb	Depth before curb (m)	Depth after curb (m)
Case 1, 0.025	0.014	0.011	54	0.608	0.228	0.707	0.292	0.063	0.071
Case 2, 0.021	0.012	0.009	58	0.517	0.235	0.692	0.327	0.058	0.064
Case 3, 0.016	0.010	0.006	62	0.460	0.207	0.651	0.304	0.051	0.053

Table 3 Experimental test results

Approaching flow (m ³ /s)	Intercepted flow (m ³ /s)	Bypass flow (m ³ /s)	Efficiency η %	Average water depth (m)	Velocity (m/s)	Froude number	Depth at curb (m)
0.024	0.012	0.010	51	0.075	0.226	0.263	0.074
0.021	0.012	0.008	57	0.073	0.203	0.239	0.066
0.015	0.010	0.005	63	0.07	0.155	0.187	0.067

Fig. 14 Variations of intercepted flow, Q_i and bypass flow, Q_b

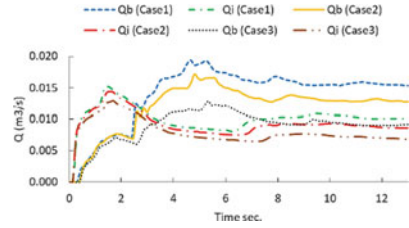


Fig. 15 Approaching flow and intercepted flow variation

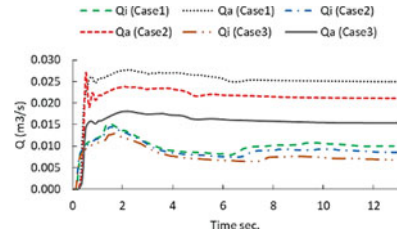


Fig. 16 Variations of approaching flow, Q_a and bypass flow, Q_b

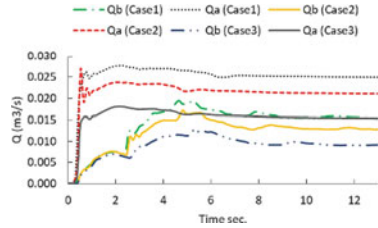
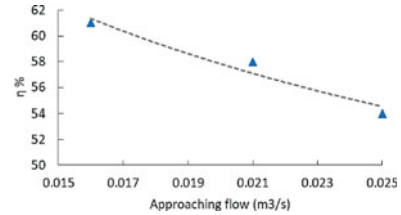


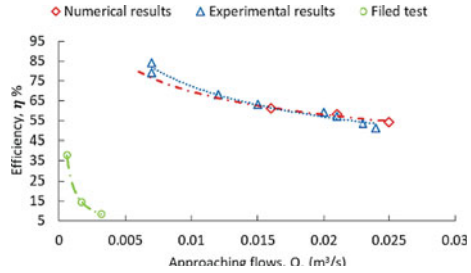
Fig. 17 Approaching flow, Q_a against efficiency, η at $Q_a \geq 0.001\text{m}^3/\text{s}$



4.4 Comparison Between Results

A comparison between experimental, numerical and field findings in terms of curb efficiency is presented in Fig. 18. Power fitting curves was developed for both experimental and numerical outcomes and a good agreement between both results was observed. Based on this agreement, it can be concluded that numerical modeling using computational fluid dynamics under the same conditions and framework used in this study can be used to investigate further on the curb efficiency under different conditions and designs. On the other hand, the inlet-opening curb efficiency obtained

Fig. 18 Comparison between all outcomes from the experimental, numerical and field investigations



from the filed runs was low when compared with experimental and numerical results. This was due to the effects of the back flow which were noticed in the experimental and numerical modelling. Besides, the difference in terms of surface friction between the road surface in the experimental and field investigations.

5 Conclusions

This paper has conducted several investigations which involved experimental, numerical and field investigations. According to the obtained results, it was observed that the curb inlet efficiency increased with the increment of the approaching flow (Q_a) when the Q_a was less than $0.001 m^3/s$. On the other hand, the curb efficiency decreased with the increment of the approaching flow (Q_a) when the Q_a more than $0.001 m^3/s$. This results trend was the same for all investigation approaches including the experimental, numerical and field investigations. A comparison between the obtained results was perform and it was noticed that a good agreement between the experimental and numerical investigations. However, there was some difference when experimental and numerical results were compared with the field tests.

References

1. Abdurrasheed S et al (2019) Modelling of flow parameters through subsurface drainage modules for application in BIOECODS. *Water* 11(9):1823
2. Ahmad AU, Ismail S, Jakada AH, Farouq IS, Muhammad AA, Mustapha UA, Muhammad A (2020) A heterogeneous relationships between urbanization, energy consumption, economic growth on environmental degradation: panel study of Malaysia and selected ASEAN+ 3 countries. *J Environ Treat Tech* 8(1):573–581
3. Al-Qadami EHH, Mustafa Z, Abdurrasheed AS, Khamaruzaman WY, Shah SMH, Malek M (2020) Numerical assessment on floating stability limits for static vehicle under partial submergence. *J Eng Sci Technol* 15(2):1384–1398
4. Al-Qadami EHH et al (2019) Numerical modelling of flow characteristics over sharp crested triangular hump. *Results Eng* 4:100052
5. Al-Qadami EHH, Mustafa Z, Martínez-Gomariz E, Yusof KW, Abdurrasheed AS, Shah SMH (2021) Numerical simulation to assess floating instability of small passenger vehicle under

- sub-critical flow. In: Mohammed BS, Shafiq N, Rahman M, Kutty, S, Mohamad H, Balogun AL, (eds) ICCOEE2020. ICCOEE 2021. LNCE, vol 132, pp 258–265. Springer, Singapore (2021). https://doi.org/10.1007/978-981-33-6311-3_30
6. American Society of Civil Engineer. Design and construction of urban stormwater management systems. In: American Society of Civil Engineers, Manuals and Reports on Engineering Practice (1992). <https://doi.org/10.1061/9780872628557>
 7. Bauer WJ, Woo D (1964) Hydraulic design of depressed curb-opening inlets. *Highway Res Rec* 58:158–164
 8. Brown SA, et al (2013) Hydraulic Engineering Circular No. 22, 3rd edn. Urban Drainage Design Manual. 3:478
 9. Burgi PH, Gober DE (1978). Hydraulic and safety characteristics of selected grate inlets. Transportation Research Board
 10. Carvalho RF, Leandro J, David LM, Martins R, Melo N (2011). Numerical research of the inflow into different gullies outlets. Urban Water Management: Challenges and Opportunities. In: 11th International Conference on Computing and Control for the Water Industry, CCWI 2011, 1, November 2014
 11. Department of Irrigation and Drainage-DID (2012). Government of Malaysia Department of Irrigation and Drainage Urban Stormwater Management Manual for Malaysia MSMA 2nd edn. <https://doi.org/10.1016/j.coldregions.2012.06.005>
 12. Despotovic J, Plavsic J, Stefanovic N, Pavlovic D (2005) Inefficiency of storm water inlets as a source of urban floods. *Water Sci Technol* 51(2):139–145. <https://doi.org/10.2166/wst.2005.0041>
 13. Djordjević S, Saul AJ, Tabor GR, Blanksby J, Galambos I, Sabtu N, Sailor G (2013) Experimental and numerical investigation of interactions between above and below ground drainage systems. *Water Sci Technol* 67(3):535–542. <https://doi.org/10.2166/wst.2012.570>
 14. Gómez M, Rabasseda GH, Russo B (2013) Experimental campaign to determine grated inlet clogging factors in an urban catchment of Barcelona. *Urban Water J* 10(1):50–61. <https://doi.org/10.1080/1573062X.2012.690435>
 15. Gómez M, Recasens J, Russo B, Martínez-Gomariz E (2016) Assessment of inlet efficiency through a 3D simulation: numerical and experimental comparison. *Water Sci Technol* 74(8):1926–1935. <https://doi.org/10.2166/wst.2016.326>
 16. Gómez M, Russo B (2010) Methodology to estimate hydraulic efficiency of drain inlets. *Proc Inst Civ Eng Water Manage* 164(2):81–90. <https://doi.org/10.1680/wama.900070>
 17. Guo J, Mackenzie K (2012). Hydraulic Efficiency of Grate and Curb-Opening inlets under clogging effect. Colorado, April
 18. Hammonds MA, Holley E (1995). Hydraulic Characteristics of Recessed Curb Inlets and Bridge Deck Drains (Vol. 7). The University of Texas at Austin
 19. Malaysia JP (2019). *Kompodium Perangkaan Alam Sekitar*
 20. John Hopkins University (1956). *The Design of Storm-Water Inlets*. Baltimore
 21. Lopes P, Leandro J, Carvalho RF, Russo B, Gómez M (2016) Assessment of the ability of a volume of fluid model to reproduce the efficiency of a continuous transverse gully with grate. *J Irrig Drain Eng* 142(10):1–9. [https://doi.org/10.1061/\(ASCE\)IR.1943-4774.0001058](https://doi.org/10.1061/(ASCE)IR.1943-4774.0001058)
 22. Mays LW (2011). *Water Resources Engineering* (2nd ed.). Wiley, Hoboken
 23. Mustafa Z, Meganathan SMP, Zaman ABK (2020) Efficiency of simple curb inlet design in Malaysia. *IOP Conf Ser Earth Environ Sci* 419:012093. <https://doi.org/10.1088/1755-1315/419/1/012093>
 24. Mustafa Z (2003). *An Experimental Investigation of The Hydraulics of Street Inlets*. University of Alberta
 25. Mustafa Z, Hamid Hussein Al-Qadami E, Muzzamil Hussain Shah S, Wan Yusof K (2020) Impact and mitigation strategies for flash floods occurrence towards vehicle instabilities. In: *Flood impact mitigation and resilience enhancement*. IntechOpen, 16 Dec 2020. <https://doi.org/10.5772/intechopen.92731>
 26. Rubinato M, Lee S, Martins R, Shucksmith JD (2018) Surface to sewer flow exchange through circular inlets during urban flood conditions. *J Hydroinf* 20(3):564–576. <https://doi.org/10.2166/hydro.2018.127>

27. Russo B, Gómez M, Tellez J (2013) Methodology to estimate the hydraulic efficiency of nontested continuous transverse grates. *J Irrig Drain Eng* 139(10):864–871. [https://doi.org/10.1061/\(ASCE\)IR.1943-4774.0000625](https://doi.org/10.1061/(ASCE)IR.1943-4774.0000625)
28. Schalla, FE (2016). Effects of flush slab supports on the hydraulic performance of curb inlets and an analysis of design equations. Austin
29. Spaliviero F, May RWP, Escarameia M (2000). Spacing of Road Gullies Hydraulic performance of BS EN 124 gully gratings and kerb inlets
30. Uyumaz A (1992) Discharge capacity for curb-opening inlets. *J Hydraul Eng* 118(7):1048–1051
31. Zaman ABK, Mustaffa Z, van Gelder P (2021) Probabilistic assessment for the capacity of grate-and curb-opening inlets during floods. *J Irrig Drain Eng* 147(11):4021048

Nonlinear Modeling and Analysis of Cold-Formed Steel Beam-Column Connection



Data Iranata, Djoko Irawan, and Muhammad Fauzan Akbari

Abstract In the moment resisting frame system, the cold-formed steel beam is designed to be able to deform inelastically and produce sufficient ductility. Therefore, it is necessary to design the detailing of the beam-column connection elements that can accommodate the ductility requirements of the structure. Previous studies have shown that the use of stiffeners can increase the ductility and energy dissipation of beams. In addition, there are studies showing that gusset plate elements can increase the initial stiffness of CFS connections and frames resulting in good ductility and energy dissipation. Therefore, this study will propose a connection design by evaluating the effect of several variations of beam stiffener configuration on the behaviour of the connection. This research is analytical in nature using finite element based Sub-Assemblage numerical modeling using Abaqus software. The analysed behaviour of the connection includes the rotational moment curve, moment capacity, and ductility, energy dissipation. The results of the analysis show that the stiffener configuration with the shape of X, which is represented by S8 specimen, produces optimal connection behavior from other configurations. The S8 specimen has the largest moment capacity of the other models, which is 37.10 kNm and increase 14.47% over the benchmark specimen, S1. The S8 specimen also has the greatest ductility compared to the other specimens, which is 4.04 and increase of 108.63% over the S1 specimen. Furthermore, the S8 specimen has the largest energy dissipation, which is 6.54 kNm-rad and increase of 37.69% over the S1 specimen.

Keywords Cold-formed steel · Beam-column connection · Nonlinear analysis · Finite element modeling

D. Iranata (✉) · D. Irawan · M. F. Akbari
Department of Civil Engineering, Institut Teknologi Sepuluh Nopember, Surabaya, Indonesia
e-mail: iranata80@gmail.com

© Institute of Technology PETRONAS Sdn Bhd 2024
B. S. Mohammed et al. (eds.), *Proceedings of the International Conference on Emerging Smart Cities (ICESC2022)*, Lecture Notes in Civil Engineering 324,
https://doi.org/10.1007/978-981-99-1111-0_44

1 Introduction

Cold-formed steel (CFS) is a type of steel made from thin steel plates (ranging between 0.4 and 6.4 mm) which are formed when cold with the help of a roll-forming machine [1]. The lightweight nature of the material offers convenience, speed in execution, and advantages in earthquake-resistant designs [2]. In addition, the advantage of cold rolled steel over other materials is its high strength-to-weight ratio [3]. However, because of its thin material, cold rolled steel elements are susceptible to local, distortional, and global buckling [3]. Another limitation is the low out-of-plane stiffness which causes cold rolled steel elements to have low ductility [4]. To design the CFS as a component of earthquake-resistant housing, the CFS elements should have sufficient ductility. In the moment resisting frame system, the beam is designed to be able to deform inelastically and produce sufficient ductility. Therefore, it is necessary to design the detailing of the beam-column connection elements that can accommodate the ductility requirements of the structure.

Several studies on the detailing of beam-column connection elements to optimize its capacity and behaviour have been carried out previously. Among them are optimizations carried out by adding gusset plate elements on the connections [5], as well as adding stiffeners on the beams [6]. Adding the gusset plate on the connection using the through plate was produce sufficient strength and ductility. An experimental study of the effect of horizontal-vertical stiffener on beam elements was carried out by [6], from the experimental results it was found that the use of stiffener had a significant effect on increasing moment capacity, ductility, and energy dissipation of the beam elements.

Based on this background, this paper proposes a connection design by evaluating the effect of several variations of beam stiffener configuration. From the several specimens that made and analysed for their behaviour, the connection that has the most optimum performance is proposed. The analysed behaviour of the connection includes moment capacity, ductility, and energy dissipation. This analytical study was performed using a finite element based numerical commercial software Abaqus.

2 Methodology

The research methodology consists of two stages. The first stage is to validate the numerical model with previous experimental research. This stage needs to be done to find out whether the input material used, the interaction between elements, boundary conditions, and the results of the numerical modeling show the same results as the experimental test, so that the modeling is validated. After the model has been validated, the next step is to model and analyse the connection specimens with several stiffener configurations.

2.1 Experimentally Validate FE Model

A finite element model is created by referring to the experimental tests carried out by [6]. The specimen used as validation is specimen A1, the configuration of the A1 specimen can be seen in Fig. 1. Because this study does not consider the presence of a slip mechanism and the behaviour of the bolt is assumed to be rigid, specimen A1 is chosen. The material used for each element of connection is S275, which the yield stress is 310 MPa. Young’ modulus and poisson ratio are 210 GPa and 0.33, respectively. The plastic stress–strain in Fig. 2 which is obtained from tensile test conducted by [7] is used in this study. Experiments were carried out by connecting the beam-column connection specimens to the reaction frame with bolts where the connection test set-up configuration can be seen in Fig. 3. The end of the beam is loaded with a cyclic load, where the cyclic load from the actuator is transferred by a hinge connection. The cyclic loading protocol refers to section S6.2 of AISC Seismic Provisions. Strain gauges, inclinometers, and LVDTs are installed at various points at the beam-column joints to measure stresses and deformations that occur. It was found that the failure pattern captured form the experimental test was dominated by flexural and local buckling, and the connection slip that occurred was small. The moment-rotation curve of specimen A1 can be seen in Fig. 4.

At the numerical modeling stage, 3D shell element using S8R element type, found in the Abaqus library, is used to model each element of the cold-formed steel connection. This model proves to be quite accurate in predicting the hysteretic

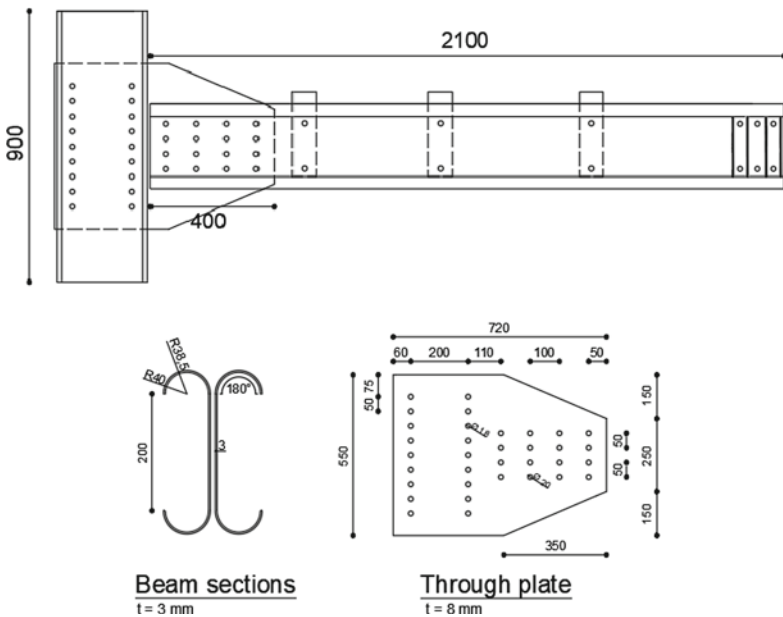


Fig. 1 Dimensions and configuration of specimen A1 [6]

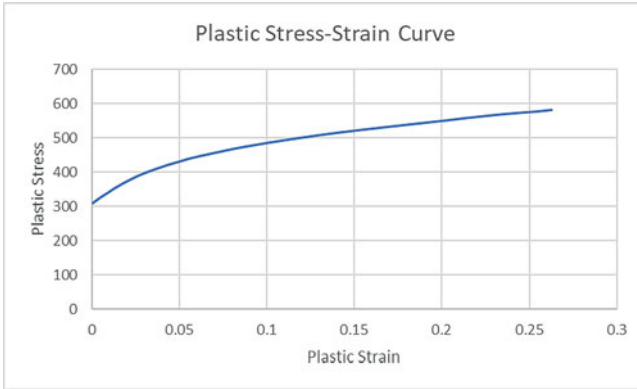


Fig. 2 The Stress-Strain Curve Used in The Model [7]

Fig. 3 Test Set-Up [6]

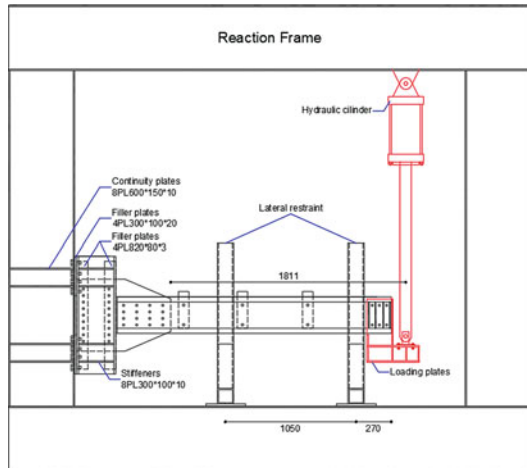
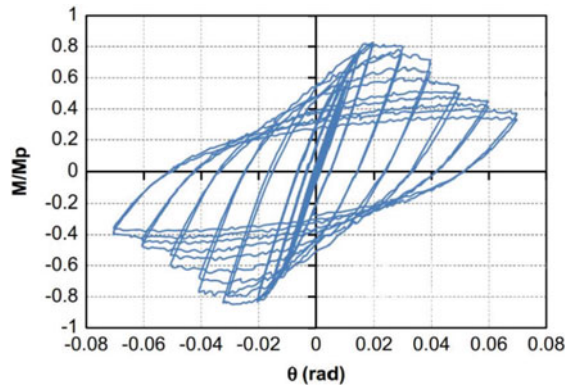


Fig. 4 Moment-Rotation Curve of Specimen A1 [6]



behaviour of the connection [8] and can capture the buckling failure that occurs [7]. After performing a mesh sensitivity analysis, the mesh size of 20×20 mm was chosen because it is computationally effective and quite accurate. The values of plastic stress-strain in Fig. 2 are digitized then the values are inputted into Abaqus. The combined hardening law is used as the material model since the reference connection undergoes plastic deformation due to cyclic loading. The point-based fastener is used to model each bolt. The bolt radius is defined using “physical radius” that will present the radius of bolt and simulate the interaction around the bolt hole. The bolt model using point-based fastener is chosen because it is more simple and computationally efficient than modeling the bolt as solid element, especially for cyclic loading. Boundary conditions of finite element model are defined as the experimental test setup by [6]. The stiffeners element is connected to the column and beam surface using “Tie” constraint. Infill plates connecting the two beams are modeled using tie constraint to couple the beams together in the U_x , U_y , U_z directions. The lateral bracing that prevents out-of-plane deformation is modeled using restrained deformation in the X-direction. To model the loading at the end of the beam, the nodes at the end of the beam are coupled to the section centroid using coupling constraint. To model the column support, the bottom of column is restrained in the U_x , U_y , and U_z directions, and the top of column is restrained in the U_x and U_y directions. The constrains and boundary conditions modelling in Abaqus can be seen in Fig. 5.

Geometrical imperfection needs to be considered in the finite element model because it is one of the factor that can affect the behaviour and can decrease the strength of the beam. The global buckling can be neglected because of the presence of lateral bracing and only local and distortional buckling mode of geometrical imperfection are considered. The magnitude values of local and distortional buckling geometrical imperfections for steel sheets which thickness less than or equal to 3 mm, recommended by [9], are $0.94 t$ and $0.34 t$, respectively. By performing an eigenvalue

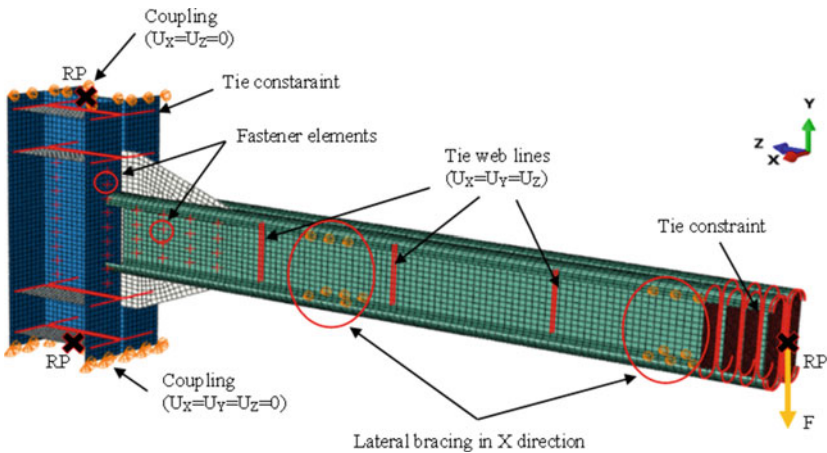


Fig. 5 Boundary Condition of Finite Element Model for Beam-Column Connection

buckling analysis, the first buckling mode can be obtained so the geometric imperfection of the local and distortional buckling can be defined. For monotonic analysis, it is carried out by providing a tip displacement load in the vertical direction (Y) which causes an asymmetrical displacement as shown in Fig. 6. For the cyclic analysis, the asymmetrical mode is obtained by combining the results of the monotonic analysis in the + Y and -Y directions.

Figure 7 shows the comparison between numerical and experimental results in the form of moment-rotation curve. The moment that occurs is normalized to the plastic moment of the beam (M_p), which the value of M_p is 75 kNm according to [6]. From Fig. 7 the numerical results show a good agreement with the experimental results. It can be seen in Fig. 8 that the shape of the deformation in the numerical model is close to the experimental results. This indicates that the model has successfully captured the rotational behaviour of the joint and is able to predict the deformation shape and location of local/distortional buckling.

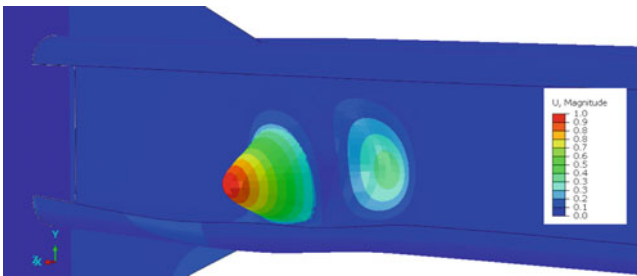


Fig. 6 Geometry Imperfection of Finite Element Model

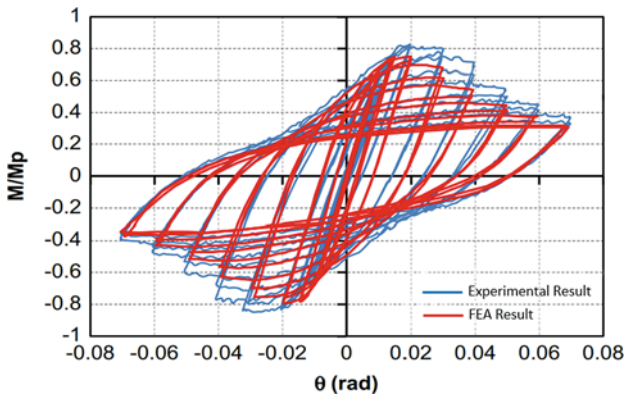


Fig. 7 Backbone Curve Comparison Between Numerical Models and Experimental Tests

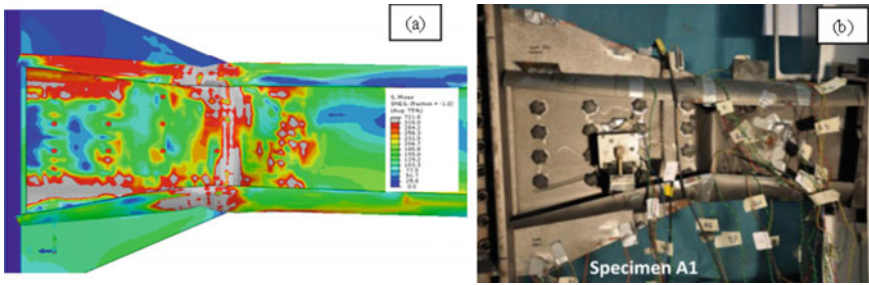


Fig. 8 Comparison of Failure Patterns (a) Numerical Model (b) Experimental Test

2.2 Design Parameters

The parameter investigated is the beam stiffener configuration at the cold-formed steel beam-column connection. In this study, there are eight connection specimens with different stiffener configurations. Where the determination of the location of the addition of stiffener is based on the pattern of connection damage being reviewed. In summary, the specimens used in this study can be seen in Table 1. Details of the cross sections of columns, beams and gusset plates can be seen in Fig. 9, stiffeners with a thickness of 3.2 mm are used, and bolts with a diameter of 18 mm are modeled as point-based fasteners, with rigid behaviour. Details of the S1 specimen which is the benchmark specimen can be seen in Fig. 10. Variations of beam stiffener configuration on other specimens can be seen in Fig. 11. The material used in each specimen element is S275 with an elastic modulus of 210 GPa, a Poisson ratio of 0.33, and a plastic stress–strain curve as shown in Fig. 2. The load applied to the connection is a cyclic load according to the loading protocol in AISC 341–16, cyclic loading can be seen in Fig. 12. Specimens were modeled as numerical modeling of the validation model. From each specimen, an analysis of the hysteresis behaviour of the connection will be carried out including moment capacity, ductility, and energy dissipation.

3 Analysis and Discussion

3.1 Moment-Rotation Curve

The moment-rotation hysteresis curve for each specimen can be seen in Fig. 13. This curve is obtained from the output of the Abaqus program in the form of moment and displacement reactions due to cyclic loading at the end of the beam. The moment taken is in front of the face of the column, more precisely in front of the gusset plate. Then the moment and displacement data are processed into a rotational moment curve. From the moment-rotation curve, 4 different zones can be observed based on

Table 1 CFS bolted moment frame beam-column connection specimens

Specimens	Column Sections	Beam Section	Gusset Plate Thickness (mm)	Stiffner Details
S1	Double Back-to-Back Lipped Channel 200 × 75 × 20 t = 3,2 mm	Double Back-to-Back Lipped Channel 150 × 65 × 20 t = 3,2 mm	6	Without stiffner
S2				2 vertical stiffners
S3				3 vertical stiffners
S4				3 vertical + 1 horizontal stiffners
S5				4 vertical stiffners
S6				5 vertical stiffners
S7				6 vertical stiffners
S8				3 vertical + 2 diagonal stiffners (X stiffners)

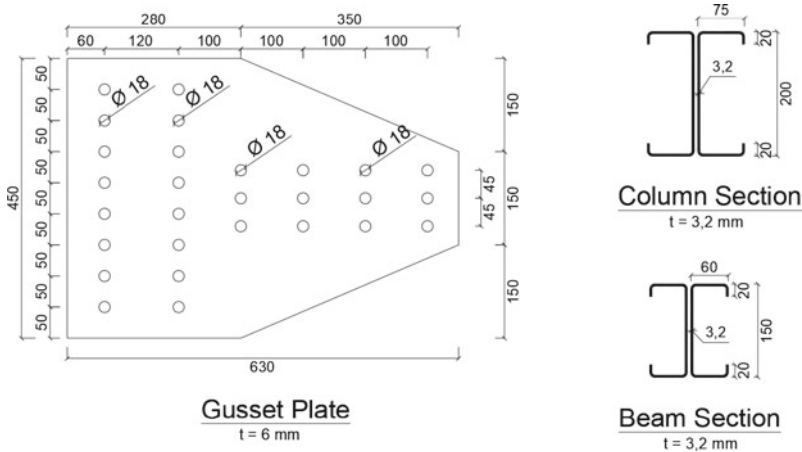


Fig. 9 Details of gusset plate, cross section of specimen column and beam

the behavior that can be identified, namely: (i) Elastic zone (A to B): in this zone the behavior of the connection is still elastic where the working stress has not yet reached its yield stress, which is 310 MPa. Points B and B- mark the end of the elastic phase and the start of the inelastic phase. (ii) Inelastic zone (B to C): In this phase, the beam melts where the stress has reached the yield stress. Points C and C- represent the maximum moment capacity of the connection. (iii) Post buckling zone (C to D): In this zone, a decrease in stiffness can be observed due to the initiation of buckling. Points D and D- represent 80% of the maximum moment of the connection. (iv) failure zone (D to E): in this zone connection failure occurs at points E and E-.

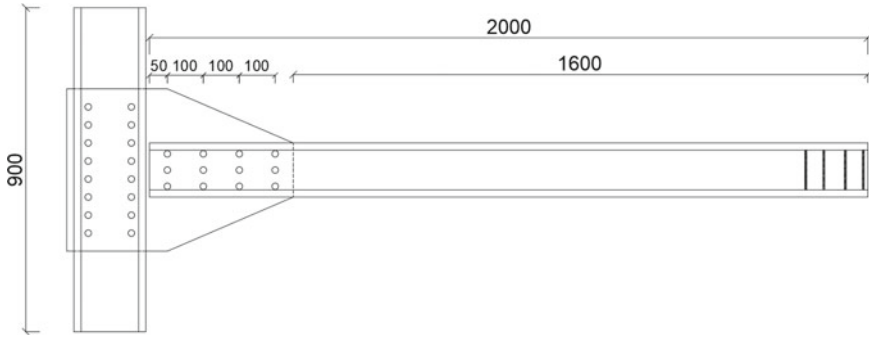


Fig. 10 Detail of specimen S1 (benchmark)

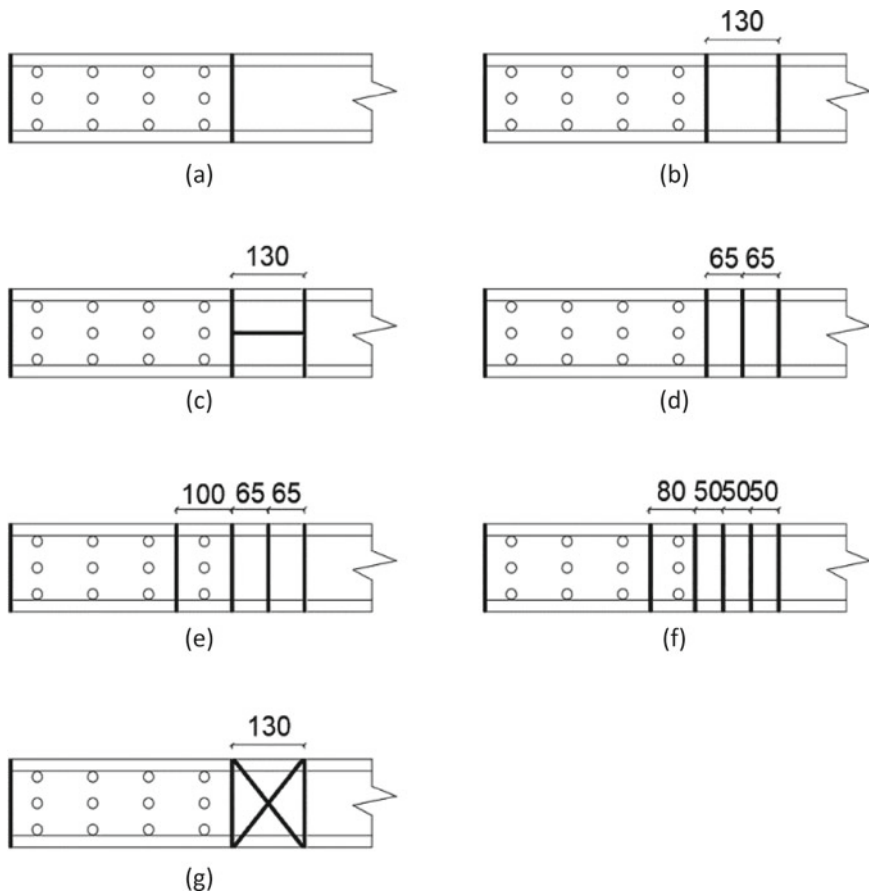


Fig. 11 Configuration of beam stiffener on specimen (a) S2, (b) S3, (c) S4, (d) S5, (e) S6, (f) S7, and (g) S8

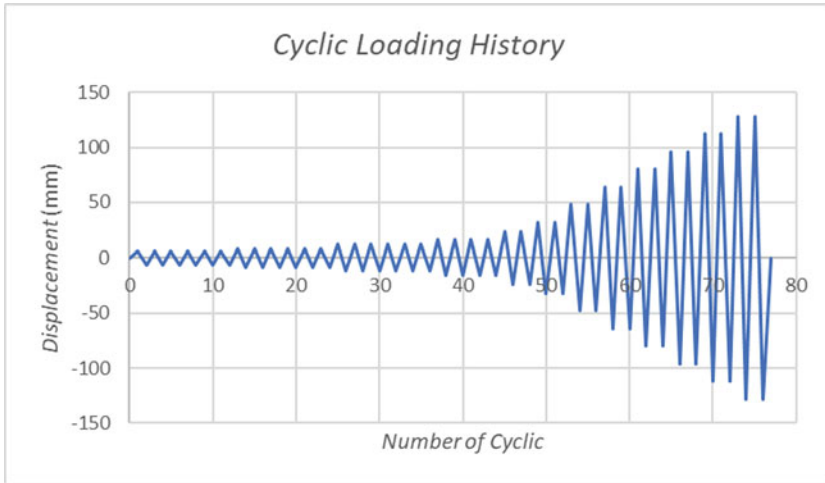


Fig. 12 Cyclic Loading Moment-Capacity

The moment capacity of each connection specimen can be obtained from the moment-rotation curve in Fig. 13 and the comparison of the moment capacities of each specimen can be seen in Fig. 14. It can be observed that the specimen S1 which is a specimen that has not been stiffened has the smallest capacity of the other six models, which is 32.41 kNm. Meanwhile, the S8 specimen has the largest moment capacity of the six other models, which is 37.10 kNm. The S8 specimen with the X stiffener configuration was able to provide a significant increase in moment capacity from the other five reinforced connection models, with an increase of 14.47% to the S1 specimen. This is because stiffener X contributes to resisting compression and tension on the beam during cyclic loading which has an effect on increasing the moment capacity at the connection. Meanwhile specimens S2, S3, S4, S5, S6, and S7 have relatively the same moment capacity of 33.6 kNm each; 34.46 kNm; 33.62 kNm; 34.83 kNm; 35.7 kNm, and 36.27 kNm. However, it can be observed in Fig. 14 that the difference in moment capacity of the eight specimens is not too large, so it can be concluded that the addition of stiffener to the beam does not provide a significant increase in moment capacity. However, increasing the moment capacity of the connection with stiffeners shows that stiffeners can increase the buckling resistance of the elements.

3.2 Ductility

The connection ductility can be determined by calculating the ratio of the rotational target (θ_t) to the rotation at first yielding (θ_y) from the moment-rotation curve of each connection specimen in Fig. 13. The yield rotation (θ_y) is determined when the

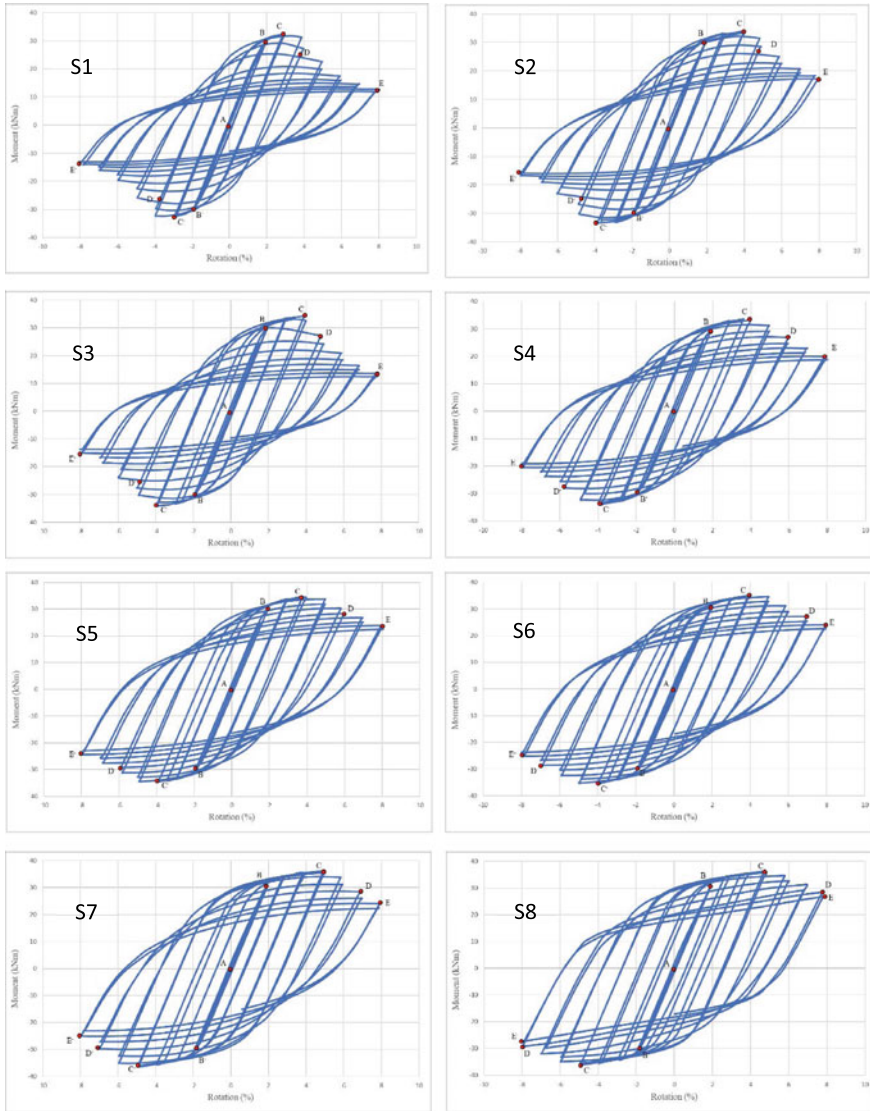


Fig. 13 Moment-Rotation Curve of Each Specimen

connection undergoes the first yielding at point B. The target rotation (θ_t) is determined based on the expected performance of the connection. It is generally assumed that the target rotation is the maximum rotation associated with the loss of strength from the maximum strength of the connection. In this study, the target rotation is defined as a rotation where the moment capacity of the connection decreases 20% (at point D) as recommended by AISC 341-16. The ductility of each connection

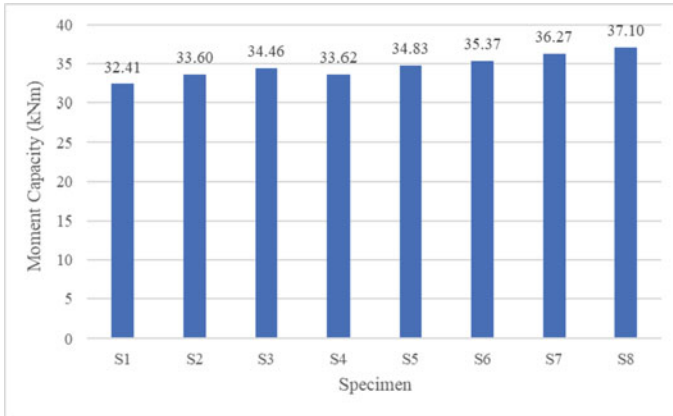


Fig. 14 Moment Capacity Value of Each Specimen

specimen can be seen in Fig. 15. It can be observed that the S1 specimen has the smallest ductility of the other six models, which is 1.93. Meanwhile, the S8 specimen has the greatest ductility of the seven other models, which is 4.04. The S8 specimen with X stiffener configuration was able to provide a significant increase in ductility from the other five reinforced connection models, with an increase of 108.63% to the S1 specimen. The high ductility value in the S8 specimen is the effect of stiffener X which contributes to resisting the compression and tension that occurs in the beam, so that local buckling in the flange and beam body can be delayed and the connection behaviour becomes more stable after the peak moment occurs as indicated by the rotation of the connection at moment 80% greater moment capacity when compared to other specimens. Meanwhile, it can be observed that the trend of the histogram graph in Fig. 15 is that the ductility value tends to increase with the increase in the number of stiffeners in the connection. This shows that the stiffener can delay local buckling in the beam so that the ductility value of the connection increases.

3.3 Energy Dissipation

The earthquake induces energy into the moment-resisting frame structure system where the energy is generally dissipated by the beam through plastic deformation. The energy dissipation of each connection specimen can be estimated by calculating the area of the moment-rotation curve of the connection. The energy dissipation of each connection specimen can be seen in Fig. 16. It can be observed that the S1 specimen has the smallest energy dissipation capacity of the other six models, which is 4.75 kNm-rad. Meanwhile, the S8 specimen has the largest energy dissipation capacity of the six other models, which is 6.54 kNm-rad. The S8 specimen with the X stiffener configuration was able to provide a significant increase in energy dissipation

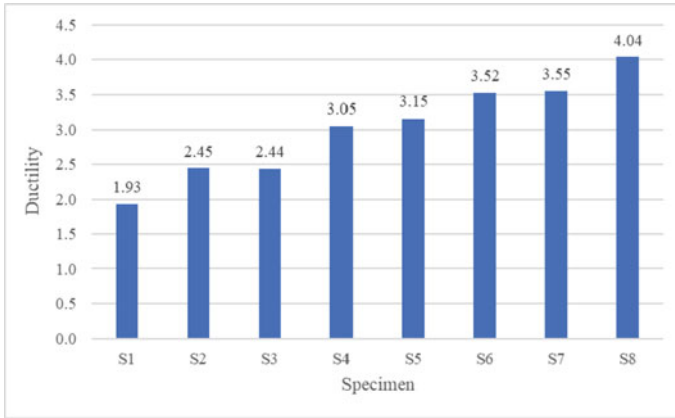


Fig. 15 Ductility comparison of each connection specimen

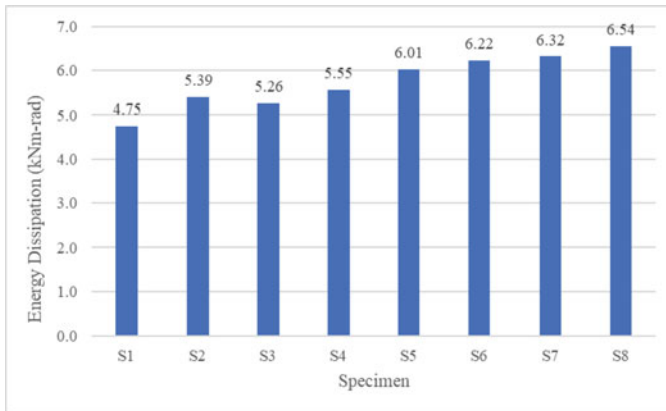


Fig. 16 Energy dissipation comparison of each connection specimen

compared to the other five reinforced connection models, with an increase of 37.69% for the S1 specimen. The use of stiffener X provides a more stable hysteresis behavior and a fatter curve due to the contribution of stiffener X in resisting compressive and tensile forces on the beam due to cyclic loading.

4 Conclusion

1. The stiffener configuration with the shape of X, which represented by S8 specimen, produces optimal connection behavior from other configurations. The S8 specimen has the largest moment capacity of the other six models, which is 37.10

kNm with an increase of 14.47% over the S1 specimen. The S8 specimen with X stiffener configuration can provide a significant increase in moment capacity from the other five connection models. The S8 specimen has the greatest ductility of the other six models, which is 4.04. The S8 specimen with X stiffener configuration was able to provide a significant increase in ductility from the other five reinforced connection models, with an increase of 108.63% to the S1 specimen. The S8 specimen has the largest energy dissipation capacity of the six other models, which is 6.54 kNm-rad. The S8 specimen with the X stiffener configuration was able to provide a significant increase in energy dissipation compared to the other five reinforced connection models, with an increase of 37.69% for the S1 specimen.

2. The addition of stiffener on the beam does not provide a significant increase in moment capacity. However, increasing the moment capacity of the connection with stiffeners shows that stiffeners can increase the buckling resistance of the elements. The ductility value tends to increase with the increase in the number of stiffeners in the joint. This shows that the stiffener can delay local buckling in the beam so that the ductility value of the joint increases. From the analysis results, the addition of stiffener produces a trend of increasing energy dissipation from the connection. In addition, the addition of a stiffener delays the buckling that occurs in the beam so that the connection behavior increases as the number of stiffeners installed increases.

Acknowledgement This research has been funded by Institut Teknologi Sepuluh Nopember, Surabaya, Indonesia

References

1. Vallabhy S, Ranjith S, Saravanan KR, Vairaprakash R, Rahul Gond M (2019) Buckling behaviour of cold formed steel sections. *Int Res J Eng Technol* 6(3):198–202. <https://www.irjet.net/archives/V6/i3/IRJET-V6I338.pdf>
2. Landolfo R (2001) Cold-formed steel structures in seismic area: research and applications. VIII Congresso de Construção Metálica e Mista, Guimarães, pp 3–22
3. Billah MM, Islam R, Bin A (2019) Cold formed steel structure: an overview. www.worldscientificnews.com
4. Bagheri Sabbagh A, Petkovski M, Pilakoutas K, Mirghaderi R (2011) Ductile moment-resisting frames using cold-formed steel sections: an analytical investigation. *J Constr Steel Res* 67(4):634–646. <https://doi.org/10.1016/j.jcsr.2010.11.016>.
5. Chen M, Huo J-H, Xing Y-W (2020) Seismic behavior of cold-formed steel frames with bolted moment connections. *J Struct Eng* 146(3):04019212. [https://doi.org/10.1061/\(asce\)st.1943-541x.0002538](https://doi.org/10.1061/(asce)st.1943-541x.0002538).
6. Bagheri Sabbagh A, Petkovski M, Pilakoutas K, Mirghaderi R (2012) Experimental work on cold-formed steel elements for earthquake resilient moment frame buildings. *Eng Struct* 42:371–386. <https://doi.org/10.1016/j.engstruct.2012.04.025>.
7. Bagheri Sabbagh A, Petkovski M, Pilakoutas K, Mirghaderi R (2013) Cyclic behaviour of bolted cold-formed steel moment connections: FE modelling including slip. *J Constr Steel Res* 80:100–108. <https://doi.org/10.1016/j.jcsr.2012.09.010>.

8. Foster P, Abdelal G, Lim JBP, Hajsadeghi M, McCrum D (2016) Finite element modelling of cyclic behaviour of cold-formed steel bolted moment-resisting connections. *J Constr Dev Countries* 21(1): 167–180. <https://doi.org/10.21315/jcdc2016.21.1.9>
9. Schafer, BW, Peköz T (1998) Computational modeling of cold-formed steel: characterizing geometric imperfections and residual stresses. *J Constr Steel Res* 47(3):193–210

Instrumented Pile Load Test Using Distributed Fibre Optic Sensor: Automation in Data Processing



Aizat Akmal A. Mohamad Beddelee, Hisham Mohamad, Bun Pin Tee, and Rini Asnida Abdullah

Abstract Distributed Optical Fibre Strain Sensing (DOFSS) instrumented pile load test yields a continuous strain profile along the pile shafts by Brillouin Optical Time Domain Analysis (BOTDA) technique, then further analyse to infer load transfer function (p-y curve) and shaft friction (t-z curve). The process of converting the raw DOFSS strain data to the meaningful pile load test report is however not that straightforward. It requires the process of trimming, positioning, flipping, averaging, curve fitting and other computations; often done manually and can result in inconsistency and interpretation errors of pile load performance. This paper aims to propose a standardised way of processing DOFSS data through an automated program incorporating the Finite Element Method (FEM). The developed algorithm was tested against several instrumented pile load tests with computational processing time in a matter of seconds. The interpretation of pile load-bearing capacity is compared between DOFSS and numerical analysis.

Keywords BOTDA · DOFSS · pile performance · data processing · FEM

A. A. A. M. Beddelee (✉) · H. Mohamad
Universiti Teknologi PETRONAS, Seri Iskandar, Malaysia
e-mail: aizat_18003476@utp.edu.my

H. Mohamad
e-mail: hisham.mohamad@utp.edu.my

B. P. Tee
Smart Sensing Technology Sdn Bhd, Shah Alam, Malaysia
e-mail: tee@smartsensing.com.my

R. A. Abdullah
Universiti Teknologi Malaysia, Skudai, Malaysia
e-mail: asnida@utm.edu.my

© Institute of Technology PETRONAS Sdn Bhd 2024
B. S. Mohammed et al. (eds.), *Proceedings of the International Conference on Emerging Smart Cities (ICESC2022)*, Lecture Notes in Civil Engineering 324,
https://doi.org/10.1007/978-981-99-1111-0_45

1 Introduction

Advancement of pile instrumentation has included the use of Distributed Optical Fibre Strain Sensor (DOFSS) using Brillouin Optical Time Domain Analysis (BOTDA) as an alternative tool to assess the load-carrying capacity of the piles. The need to employ such a sensor in the pile load test as structural complexity is a concern [1]. DOFSS offers various advantages utilizing it as opposed to conventional sensors, including continuous data along the pile length. Yet, the technology has not been fully commercialised worldwide, due to several factors and data processing is one of the major factors. Data processing of BOTDA is very challenging, in which may include the process of temperature compensation, trimming, positioning, smoothing and measurement error correction during data processing [2]. In the case of the pile, the geotechnical aspect needs to be considered together with the mentioned processes. The post data processing stage involves preparing the interested data sets for the analysis, i.e. pile load transfer mechanism (t - z and p - y curve). Hence, this whole complexity of data processing may lead to different interpreted results between DOFSS users. Recommendations on the consistency of pile load behaviour should be validated through numerical simulations, although, it may not be practical to perform to all DOFSS instrumented pile load tests as a routine checking.

1.1 Challenges in DOFSS Data Processing

Data acquired from the BOTDA is strenuous, and handling the data demands extensive data processing programs and processes. The concern arises by Mohamad [3], that the user will experience difficulty comprehending the outcome of the measurement while handling a wider measurement area with a number of the measurement point. Processing the raw data of fibre optic strain sensing is vital to appreciate the data for intended usage. As proven in the wide literature, the fibre optic data can provide information on the structural integrity/health of the measured structure, a great tool [4]. The data processing methods include (i) positioning [5, 6], (ii) trimming [2], (iii) averaging [7, 8], (iv) temperature compensation [9–11], measurement error correction [2], (v) denoising/smoothing/ filtering [12–14] and (vi) deconvolution [3]. Although there are significant numbers of publication on the BOTDA instrumented pile load test, the data processing processes of the raw field measurement was not reported in great detail due to complexity, uncertainty and overlap of the processes suited to the application to pile load test. The complexity needs high attention since it is significant to induce another error i.e. human error due to manual handling. The uncertainty is due to no parametric study of a suitable algorithm to choose suited the pile analysis and the overlap could happen in case of the compensation was pre-set by the analyser unit itself. In the current practice of the industry, the processing was done manually, and this practice consumed many resources, especially time. Manual processing of BOTDA raw strain data from the instrumented pile

test typically may take several days. Subsequently, there are issues of inconsistency and redundant terminology used to present the intended processing method. Thus, this study proposes to automate the process and standardise a systematic process.

Commercially available geotechnical modelling software such as Plaxis, ABAQUS and Rocscience 3 may be used to back analyse the pile shaft frictions or load transfer function. A few past works simulated the DOFSS instrumented pile load test using commercial software. A comprehensive soil parameter was fed into the software together with the structural geometry and loading intensity [15–18]. Doing this demands intensive data handling and professional supervision. The drawback of this practice is the issue of incomparable check and balance, suppose the checking is made from the same source of input, field BOTDA data. The software analysis output (derived from assumed soil reaction from the site investigation) cannot be compared to the back analysis of BOTDA data (derived from the actual site soil reaction from instrumented pile load test). This practice fails the objective to design a performance-based pile. Realistically the mentioned approach is not favourable to the BOTDA service provider/contractor as proven by the absence of post data processing in the test report. The root causes are the short reporting time demand by the client, time-consuming of the current approach, obtaining data from other parties such as site investigation contractor, software licensing cost ratio to the tool utilization and data integrity of third parties.

A tool to solve this issue is a great aid for BOTDA sensor deployment development. A simple numerical method using directly the spatially continuous fibre optic (FO) strain data from the pile load test activity to estimate the load-transfer curve as proposed by Pelecanos and Soga [19, 20], Pelecanos, Soga [21] is a great to be developed further. Adopting the Finite Element Modelling (FEM) had been proved reliable as a checking tool. Still, this approach needs further exploration in terms of utilization of concrete modulus of stiffness, element length definition for FEM and pile founding in tropical soil. This work aims to develop a practical tool using FEM utilizing field measured BOTDA data to check the load transfer of the BOTDA instrumented pile under axial loads.

2 Development of the Automated Program

The algorithm structure of the automated program started with the raw BOTDA data processing (as input) before the back analysis to get the field observed pile performance (p-y and t-z curve). There were a few algorithms published in the literature and practised in the instrumentation industry. The issues of complexity, inconsistency and pile integrity consideration make those algorithms need a revamp [3, 21–23]. As pile application was concerned the typical data processes presented in the earlier section are weighted accordingly. Trimming, positioning and averaging were the mandatory processes to be carried out. Compromising these processes induce difficulty to analyse the data. The temperature compensation process is considered optional since it is influenced by the monitoring period. While, the measurement error correction,

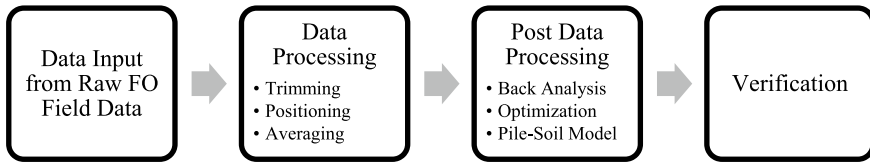


Fig. 1 Automated Program algorithm structure

denoising and deconvolution processes shall be excluded as those were micro impact to the pile application and not within the interest area of instrumentation engineering dealing with the mentioned issues of the available algorithm, and providing a systematic and clear algorithm, this study proposed an algorithm for the data processes as pictured as the following Fig. 1.

Later, the algorithm continues with post data processing which the pile performance is determined through FEM as proposed in the past study (see Sect. 2). The algorithm structure consists of a back analysis process, an optimization body and pile-soil modelling (see Fig. 1). The BOTDA strain data is back analysed to plot the load transfer of the pile and further used in the optimization body adopting the non-linear load transfer model as the objective function. The optimization body is expected to provide the parameters for the pile-soil model to get the finite element (FE) to observe the t-z curve. The t-z curves together with load and strain profile from field and FE are compared for verification. The development of the whole automated program was done in the MATLAB program.

2.1 Back Analysis of FO Field Data

The raw BOTDA data processing was made automated. The automated processed strain data is back-calculated to plot the t-z curve and mobilized load profile (p-y curve). The following are the equations adopted for back-calculation:

Axial force, F_a :

$$F_a = EA \cdot \varepsilon_a \quad (1)$$

Shaft friction, t :

$$t = \frac{1}{2\pi r} \frac{d}{dy} EA \cdot \varepsilon_a \quad (2)$$

Vertical displacement, u :

$$u = u_{y=0} + \int_0^y \varepsilon_a dy \quad (3)$$

E , A and r are the concrete stiffness, sectional area and radius of the pile. E is determined by assessing the top pile at least at one diameter (1D) depth. At this depth, the pile strain is not influenced by the soil [24, 25]. The strain reading at the said depth from all loading stages is plotted together with the best fit (trendline). The equation of the straight line is established and is used to back-calculate strain to get the E at each interest depth and loading stage. This approach better reflects the field measured data instead of assuming an E value for all interest layers as done by [19, 20, 26]. Moreover, this proposed approach is utilizing solely the BOTDA strain data in which the pile-based performance design is desired. ϵ_a is the average axial strain of the pile.

2.2 The Nonlinear Load Transfer Model

The plotted load transfer curve is optimized using the optimization algorithm. An objective function shall be established beforehand and the nonlinear load transfer model (t-z or q-z curve), Degradation and Hardening Hyperbolic Model (DHHM) by Pelecanos and Soga [26] is adopted. There are 4 parameters in DHHM that dominate different considerations of the curve as expressed in Eq. 4.

$$t = \frac{K_m z}{\sqrt[d]{1 + \left(\frac{K_m}{t_m} z\right)^{hd}}} \quad (4)$$

where K_m is the maximum stiffness for displacement at $z = 0$ (units: force / length³), t_m is the maximum value of shear stress, t (maximum only in the case of no hardening /softening, i.e., $h = 0$) (units: force/length²), d is unitless degradation parameter that governs the degradation of subgrade modulus, k , with displacement, z , and h is the unitless hardening parameter that mostly governs the model behaviour at large displacements, z . All four parameters shall be positive, and an optimization method is to be employed to obtain the optimum DHHM parameters from the measured load transfer curve. This model is the objective function for the optimization algorithm. The model is reasonably acceptable for vertically loaded piles. In fact, other possible load transfer models could be considered to be used to correspond to the specific condition.

2.3 Optimization Body

Levenberg–Marquardt Algorithm (LMA) is used to optimize the plot to an objective function (see Sect. 3.2). LMA is employed as it is an outperforms algorithm in solving a nonlinear problem. Despite LMA, other optimization schemes such as neural

networks and machine learning are possibly employed. Although, the mentioned schemes are computationally intensive, which demand big data, great hardware and time for development [19, 20]. Concerning current technology capability, research facility capacity, and research centre data pool, the said other optimization schemes could look into. The load transfer curve plotted from field measured DOFSS data is fitted to yield all the parameters, K_m , t_m , d , h , that are determined at the optimal set as the objective function is minimized; the t value is minimized at every z value at constraining of all parameters shall be positive.

2.4 Pile-Soil Model

The pile is modelled by a linear-elastic beam element and a series of nonlinear springs, representing the soil surrounding the pile body corresponding to each node. The standard Static Finite Element Formulation by Bathe [27] is the equation (Eq. 5) that satisfied the global equilibrium of the pile-soil problem [as cited in 21].

$$[K_p + K_s]\{U\} = \{F\} \quad (5)$$

The pile stiffness, K_p , is derived from the Euler–Bernoulli beam theory analysis using the stiffness method and forming the matrix. The analysis considers the displacement in vertical directions, horizontal directions and rotation at each node [28]. Subsequently, the soil stiffness matrix, K_s , is determined from a nonlinear load transfer curve detailed in the previous section. The K_m is the parameter that is to be a substitute into the global stiffness matrix as K_s in Eq. 5. The degree of freedom, U , of the model is determined by the loading condition of the pile, in this case, it is axial that only allowed vertical displacement degree of freedom. The externally applied load at the top of the pile, F , is the boundary condition of the global equilibrium matrix. The known parameters such as A , r , I and D are defined beforehand as input as well as the K_m from the optimization model. The computation of the model shall result in the vector of displacement along the pile.

2.5 The Element Length of FEM

The length of the element in the beam-spring model influences the analysis. The length is defined by the soil stratigraphy of the field. Theoretically, the load transfer of a pile is assessed by the soil layer defined from the soil investigation done on the field. This is the adopted design approach in practice, yet the soil layering might differ from the actual soil stratigraphy of the pile. This approach has also been adopted in the work by Pelecanos and Soga [19, 20], Pelecanos, Soga [21], assessing the pile performance from BOTDA data. Ironically, the work has not fully utilized the DOFSS main traits, continuous data. Exploiting this ability might give the pile

performance determination to a great extent and better accuracy of approximation (lessen the approximated input into the calculation).

Subsequently, the DOFSS contractor typically opted for the element length defined by the gradient of the plotted BOTDA strain profile observe at the field. This approach is meant to avoid the approximation error by the soil investigation. However, this approach is prone to be influenced by the spike increment/decrement of the strain contributed by the pile imperfection.

A possible approach is proposed by this work is to define the element length by an interval length e.g., at every 0.5 m. This proposal is worth to be considered as it utilises the continuous data from the BOTDA and it matches with the main intention of the work, to fully utilized the field measured BOTDA data to the fullest.

2.6 Model Computation Verification

The verification of the model plotted profile is performed by constitutively compares the vertical displacement, strain profile and load transfer profile to those plots from field measured data. The computed vertical displacement data from the finite element (FE) model is back analysed beforehand using equations Eqs. 1, 2 and 3. The verification is done constitutively, as long as the plot follows each other profile and direction. In the current constitutive comparison practice, there are no benchmark value/verification criteria to accept the comparison e.g., 10% difference [19–21]. Though, the validation attempt of the constitutive comparison done to the API (American Petroleum Institute) [29], is still subjective.

3 Application

The application was done to a test pile with a dimension of 900 mm in diameter and 32.5 m in length. The pile was cast by concrete grade 45 with at least 12 m casing length at initial depth. The pile is designed to take the load at 6500 kN up to 250% maximum working load. The soil stratigraphy is made up of 13 layers of soil and mostly weak soil before reaching the bedrock at a depth of 27 m. The bored pile is socketed into the sandstone beyond the depth of 27 m and the pile was designed to be an end-bearing pile. The groundwater table was at 3 m depth. The static load test through Maintain Load Test with three loading cycles (1st cycle: 100% working load, 2nd cycle: 200% working load and 3rd cycle: 250% working load), up to maximum loading at 16,260 kN with few load-unload steps. Two loops of fibre optic were installed into the pile on the X and Y axis, respectively. This makes there are four cables to be trimmed, positioned and averaged. The element length is defined by the gradient of the BOTDA strain profile from field observation. At least four (4) lengths or so-called soil layer.

4 Result and Discussion

Automation of data processing for the BOTDA instrumented pile load test was proposed in this study. The data has been processed according to the proposed algorithm. The processed raw strain data from BOTDA was back-calculated to plot the load-transfer curve of each layer of soil (Fig. 2). The top settlement is the LVDT reading during the pile load test. Layers 1 and 2 exhibit a soft and low ultimate strength. Only layers 3, 4 and base are stiff and great in ultimate strength. Each soil layer of the load-transfer curve was optimised by LMA treating the DHHM as the objective function. The optimization provides the model parameter as tabulated in Table 1.

Overall, the verification yielded a nearly matching plot, and the specific discussion of each plot is as follows. The FE calculated vertical displacement was plotted together with the field calculated as in Fig. 3(a). The plot shows that both lines are having a similar trend but with a maximum difference of 20%. Even so, this finding is considered acceptable, and the correction factor could be derived considering

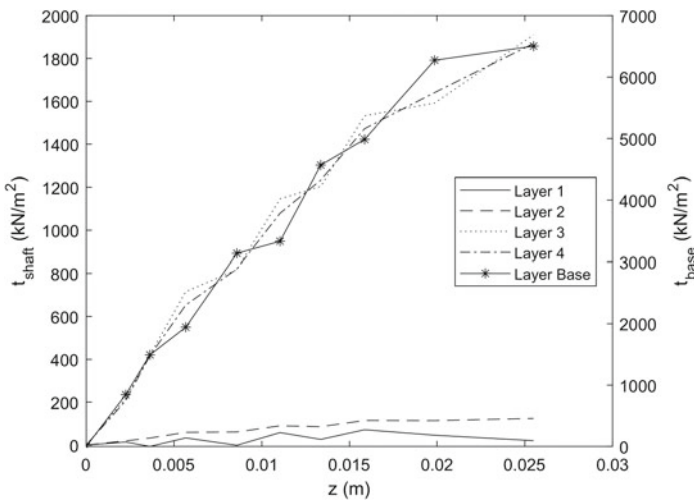


Fig. 2 Load-transfer curve of soil layers by back-calculation

Table 1 Model parameters of the load transfer curve

Layer	Depth (m)	k_m (kN/m ³)	t_m (kN/m ³)	d	h
1	1–12	2880	45	141.8	1
2	12–28.5	9480	149.1	1.9	1
3	28.5–30	91,320	1910.1	1101.7	1
4	30–32	90,670	1870	1091.1	1
Base	32	307,060	6503.1	3822.3	1

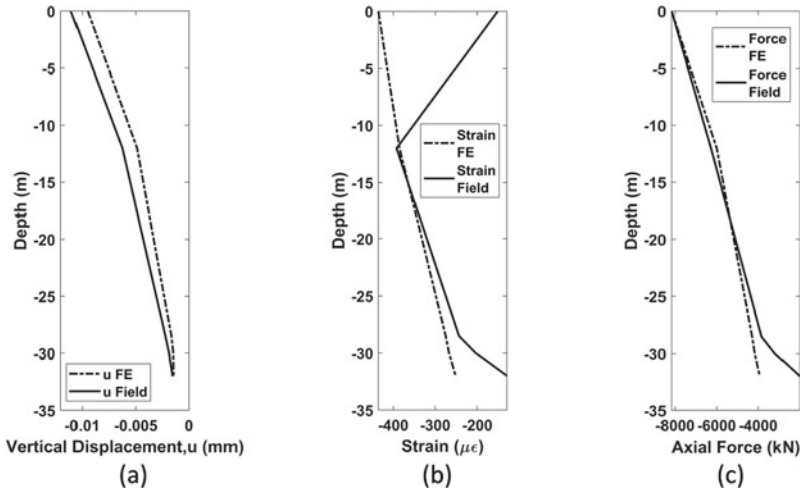


Fig. 3 Verification: **a** vertical displacement, **b** strain and **c** mobilise axial force profile

the difference which may be due to the mathematical approximation approach by the FEM. Indeed, the previous work was never reported, and it is significant to be highlighted.

The strain profile in Fig. 3(b) was the product of equation Eq. 3 and compared to the field measured strain. The top strain of both lines did not match probably due to (i) the usage of Eq. 1 to plot the strain FE that calculated the applied load on the top of the pile (the FEM boundary condition), (ii) the layering of the soil/beam-spring model and (iii) the strain field was influenced by the loading issue i.e., eccentricity.

In the axial force profile in Fig. 3(c), both lines were calculated by Eq. 1. Overall, the plots match one another. But, at the toe, the force from FE observes a much higher value at least double the field value ($-2017.3 \mu\text{m/m}$). Both issues in strain and axial force profile shall be explored further in the next publication. The automation of this process increases the computation time at 8.291 s elapsed time, multi-fold faster than current practice (a manual process). This is a great tool for the industry as processing work consumed hours even days.

5 Conclusion

This study developed an automated program with the algorithm structure that includes the data input from raw BOTDA strain data, proposed standard data processing, post data processing and verification, to cope with the above-mentioned issues. A few conclusions able to be drawn as such this study has proposed the standard data processing as pile instrumentation concern only includes trimming, positioning and averaging. The application of modulus of concrete stiffness specifically at interest

depth and loading stages reflect the actual pile configuration i.e., dimension and quality. Subsequently, the element length in the beam-spring model of FEM can be defined by the soil stratigraphy or gradient of the BOTDA strain profile but both have issues of the actuality of soil stratigraphy and the influence of pile imperfection, respectively. This work proposed the element length by an interval length and will be done in further publication. Overall verification for the application resulted in a nearly matching plot with a maximum 20% difference for vertical displacement profile from FE and field. As for strain profile and the axial force, the top strain and axial force at the toe from FE experience a significant difference in the field which needs further exploration.

Acknowledgements The authors of this paper wish to express their greatest gratitude to Universiti Teknologi PETRONAS, Smart Sensing Technology Sdn Bhd and Universiti Teknologi Malaysia for their support of this research work.

References

1. Federation of Piling Specialists (2006) Handbook of Pile Load testing. Federation of Piling Specialists: United Kingdom
2. Mei Y (2018) Error analysis for distributed fibre optic sensing technology based on Brillouin scattering, in Department of Engineering. University of Cambridge
3. Mohamad H (2018) Distributed Optical Fibre Strain Sensing of Geotechnical Structures, in Department of Engineering. University of Cambridge
4. Beddelee AAAM, Mohamad H, Tee BP (2022) Validation on laboratory simulated optical fibre sensor instrumented bored pile defect using 3D Finite Element Method. *J Civil Struct Health Monit* 12(5):991–1007
5. Ding Y, Wang P, Yu S (2015) A new method for deformation monitoring on H-pile in SMW based on BOTDA. *Measurement* 70:156–168
6. Fang Z, Su H, Ansari F (2021) Modal analysis of structures based on distributed measurement of dynamic strains with optical fibers. *Mech Syst Signal Process* 159:107835
7. Tee BP, et al (2017) Application of distributed fibre optic sensor in instrumented pile load test. *Dyn Pile Testing Sdn Bhd*
8. Tee BP, et al (2017) instrumented pile load tests on rock socketed piles with distributed fibre optic sensor. In: *PILE 2017, Bali, Indonesia*, pp H3-1–H3-7 (2017)
9. Pelecanos L, Soga K (2019) Innovative Structural Health Monitoring of reinforced concrete piles using distributed fibre optic sensing. In: *UKIERI concrete congress - concrete: the global builder, Jalandhar, Punjab, India*
10. Kechavarzi C et al (2019) Distributed fibre optic sensing for monitoring reinforced concrete piles. *Geotech Eng* 50:43–51
11. Dong-sheng X, Yin J, Liu H (2018) A new measurement approach for deflection monitoring of large-scale bored piles using distributed fiber sensing technology. *Measurement* 117:444–454
12. Kania JG, Sorensen KK, Fellenius BH (2020) Application of distributed fibre optic cables in piles. *Geotech Eng J SEAGS AGSSEA* 51(3):1–9
13. Feng C, Kadum J, Schneider T (2019) The state-of-the-art of brillouin distributed fiber sensing
14. Sun Y et al (2020) Distributed fiber optic sensing and data processing of axial loaded precast piles. *IEEE Access* 8:169136–169145
15. Zhang L, Wu Y (2015) Detection of defective piles using analysis tools. *EJGE* 20(14):6073–6082

16. Albuquerque PJR et al (2017) Behavioral evaluation of small-diameter defective and intact bored piles subjected to axial compression. *Soils Rocks* 40(2):109–121
17. Rui Y et al (2017) Integrity testing of pile cover using distributed fibre optic sensing. *Sensors* 17(12):2949
18. Zhong RY, Guo RC, Deng W (2018) Optical-fiber-based smart concrete thermal integrity profiling: an example of concrete shaft. *Adv Mater Sci Eng* 2018:8
19. Pelecanos L, Soga K (2017) The use of distributed fibre-optic strain data to develop finite element models for foundation piles. In: 6th international forum on opto-electronic sensor-based monitoring in geo-engineering, Nanjing, China (2017)
20. Pelecanos L, Soga K (2018) Development of load-transfer curves for axially-loaded piles using fibre-optic strain data, finite element analysis and optimisation
21. Pelecanos L et al (2018) Distributed fiber optic sensing of axially loaded bored piles. *J Geotech Geoenviron Eng* 144(3):04017122
22. Battista N, Kechavarzi C, Soga K (2016) Distributed fiber optic sensors for monitoring reinforced concrete piles using Brillouin scattering. In: Sixth European workshop on optical fibre sensors (EWOFS 2016), vol 9916. SPIE (2016)
23. Liu B, Zhang D, Xi P (2017) Mechanical behaviors of SD and CFA piles using BOTDA-based fiber optic sensor system: a comparative field test study. *Measurement* 104:253–262
24. Mohamad H, et al (2017) Investigation of shaft friction mechanisms of bored piles through distributed optical fibre strain sensing. In: 19th international conference on soil mechanics and geotechnical engineering, Seoul, South Korea
25. Fellenius BH (2001) From strain measurements to load in an instrumented pile. *Geotech News Mag* 19(1):25–28
26. Pelecanos L, Soga K (2017) Using distributed strain data to evaluate load-transfer curves for axially loaded piles. *J Geotech Geoenviron Eng*
27. Bathe KJ (1996) *Finite Element Procedures*, 1st edn. Prentice Hall, Englewood Cliffs
28. Hibbeler RC (2018) *Structural analysis*. In: T.K. Hwee TK (ed) SI Units, 8 edn. Pearson, Singapore
29. API (American Petroleum Institute) (2002) *Planning, designing and constructing fixed offshore platforms—Working stress design*. API RP 2A-WSD. Washington, DC.

Diagonal Shear Test on Indonesian Masonry Walls



Farisal Akbar Rofiussan, Ahmad Basshofi Habieb, Djoko Irawan,
and Budi Suswanto

Abstract Unreinforced or confined masonry is a common traditional method for housing construction, particularly in developing countries, thanks to its easy and low cost construction. However, it is well known that masonry performance against earthquake is poor, due to the low tensile and shear strength. The literatures on the shear properties of typical Indonesian masonry is limited. Therefore in this study, a diagonal shear test on Indonesian masonry wall was performed to investigate the shear strength. Brick units with dimension of $200 \times 100 \times 50$ mm and mortar with cement to sand ratio of 1:4 were used in this study. Such design is common in case of low rise Indonesian masonry housing. In addition, retrofitting method using bamboo is also proposed.

Keywords Indonesian masonry · diagonal shear test · experimental study · bamboo retrofitting

1 Introduction

Unreinforced or confined masonry are widely applied for low rise residential housing, particularly in developing countries, because it uses low cost materials and does not need skilled labour for construction. However, it is well known that the seismic performance of masonry structures is poor due the low shear strength and capacity [1–3].

One of experimental tests to evaluate the shear strength of masonry is diagonal shear test, as stated in ASTM E519. Many research have been performed to evaluate the masonry shear strength considering the local design and composition that often used in some countries. In Europe [4], a diagonal shear test on standard masonry was performed and resulted in the average shear strength about 1.678 MPa. In India [5], the test resulted in the average strength about 0.220 MPa.

F. A. Rofiussan · A. B. Habieb (✉) · D. Irawan · B. Suswanto
Civil Engineering Department, Institut Teknologi Sepuluh Nopember, Surabaya, Indonesia
e-mail: ahmad.basshofi@its.ac.id

© Institute of Technology PETRONAS Sdn Bhd 2024
B. S. Mohammed et al. (eds.), *Proceedings of the International Conference on Emerging Smart Cities (ICESC2022)*, Lecture Notes in Civil Engineering 324,
https://doi.org/10.1007/978-981-99-1111-0_46

However, there is a limited number of experimental reports regarding the diagonal shear test on Indonesian masonry. Some experimental parameters available in the literatures, mainly reported from Europe and India, may be not suitable for Indonesian context. Thus, it is important to conduct experimental tests on Indonesian masonry, particularly, when it becomes the structural elements of buildings.

When dealing with the practical design of low to medium rise building using confined masonry structure, it is often that the infilled masonry are not taken into account in the analyses. Only the frame structure that is analyzed in the numerical model. On the other hand, the infilled masonry itself can remarkably affect the seismic response of a building.

Considering the remarkable weakness of masonry structures, many researches on masonry retrofitting have been conducted. Researchers in [6–8] investigated the fiber reinforced polymer (FRP) reinforcement for masonry retrofitting. In [9, 10] fiber reinforced cementitious matrix (FRCM) is used for the masonry reinforcement. Those retrofitting method were found to be effective to improve the shear bearing capacity and the ductility of the masonry wall. [11] proposed an alternative for masonry retrofitting using PP bands for unreinforced masonry in rural area in Nepal. Such method is considered cheaper and easier because no special treatment or application is needed.

Another low cost method is using bamboo reinforcement as reported in [12]. After shaking table test, it is found that the bamboo reinforced masonry housing can stand longer than the unreinforced counterpart. The application of bamboo as structural reinforcement indeed has been proposed also for concrete reinforcement, as reported in [13–15]. In addition, bamboo material is considered sustainable because the growing rate of the plant is high and easy to find in rural areas.

In this study, masonry shear strength tests were performed to evaluate the mechanical properties of Indonesian masonry. In addition, retrofitting method using bamboo is also proposed.

2 Specimen Preparation and Testing Method

Two wall panels with dimension $1000 \times 1000 \times 100$ mm as shown in Fig. 1 were considered in this study. The thickness of the mortar joint is about 20 mm. The dimension of the brick unit is $200 \times 100 \times 50$ mm, see Fig. 2, and the mortar with cement to sand ratio of 1:4 is used. Such design is widely used in the construction of low rise housing in Indonesia.

The masonry shear strength test refers to ASTM E519. In general, this test aims to determine the capacity of the diagonal tensile force or shear strength of the masonry specimen by giving a compressive load from the diagonal direction. The diagonal shear test was performed when the masonry panel was 30 days old. During the mounting of the panels, they were restrained by double angle-steel frame and were mounted into the loading frame using electric hoist and lifting trolley (Fig. 3).

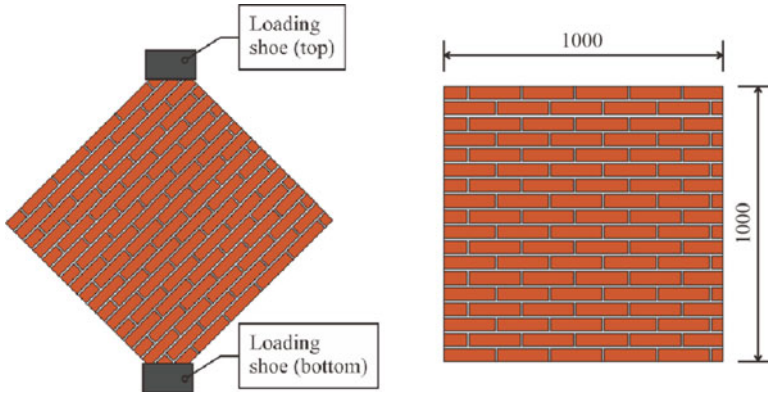


Fig. 1 Dimension of the masonry panel under study

Fig. 2 Dimension of common Indonesian brick unit

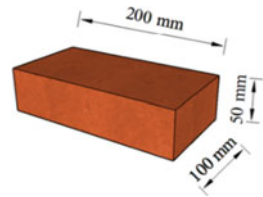


Fig. 3 Mounting of masonry panel into loading frame

During the diagonal shear test, three linear variable differential transformer (LVDTs) were used, as seen in Fig. 4. One was on the top of the specimen to monitor the vertical displacement, and two were used on the left and right angle of the panel to monitor the horizontal displacement where elongation was likely to happen.

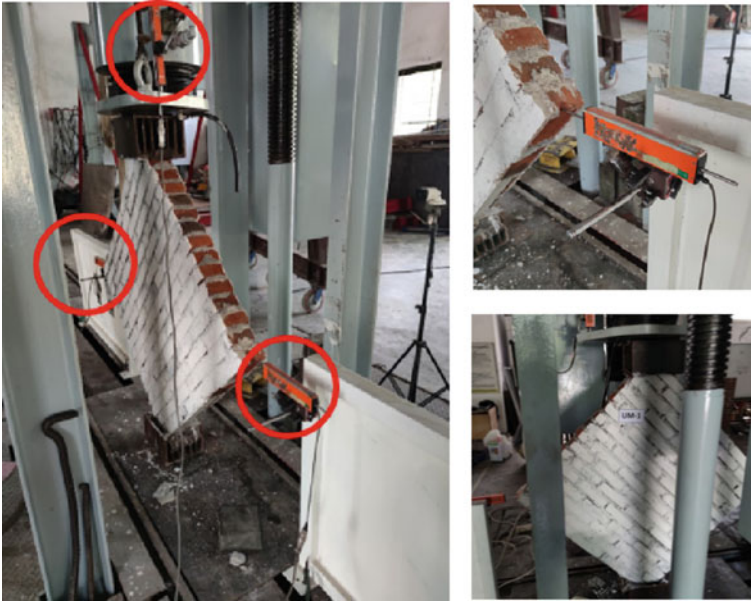


Fig. 4 Diagonal masonry panel in the loading frame with three LVDTs for displacement monitoring

3 Results

Figure 5 shows the crack patterns of the two masonry panels after the diagonal shear test. The two specimens present different crack patterns which may be caused by the lack of uniformity of the mortar mixing. The traditional mixing technique is applied in this study to represent the most construction method for residential housing. The force-vertical displacement curves of the two panels are depicted in Fig. 6.

As shown in Fig. 6, specimen UM-1 experienced crack when the load was about 16 kN, while specimen UM-2 cracked when the load is about 20 kN. According to

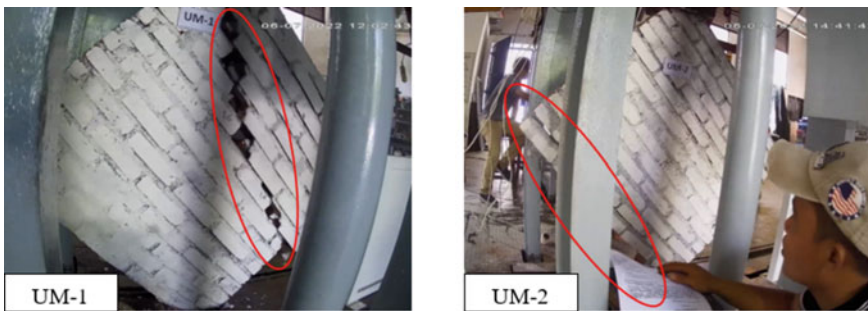


Fig. 5 Crack patterns of the two masonry panels

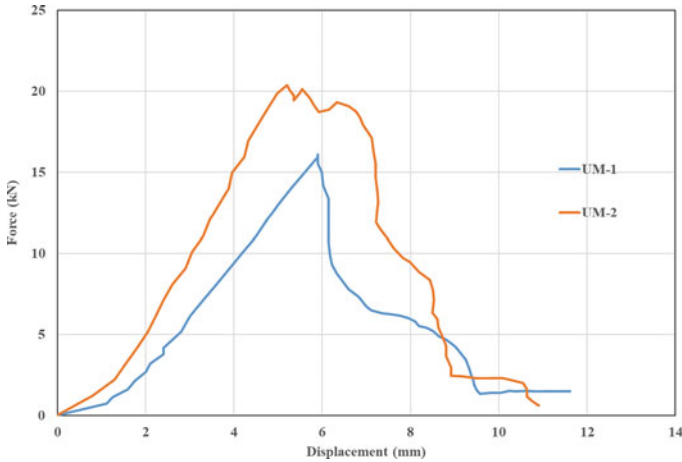


Fig. 6 Force-vertical displacement curves of two masonry panels under study

equation provided in ASTM E519, see Eq. 1 and 2, such values correspond to shear strength about 0.113 and 0.144 MPa, respectively. Where S_s is shear strength, P is crack load, A_n is netto area, w is width, h is height, and t is thickness of the panel.

$$S_s = 0.707 \frac{P}{A_n} \tag{1}$$

$$A_n = \left(\frac{w + h}{2} \right) \cdot t \tag{2}$$

Such shear strength values are significantly lower when compared to the standard specimens tested in Europe and India [4, 5]. A brittle behavior is shown by the two specimens. The masonry panels were instantaneously collapsed right after the cracks took place. Such behavior is unfavorable for life safety concept in earthquake resistant buildings. Hence, a retrofitting option can be adopted to improve the shear capacity and ductility of masonry wall.

4 Conclusion

Diagonal shear tests on Indonesian masonry were performed in this study. The specimens under study correspond to the common design of Indonesian low rise housing. The masonry panels used in this study had dimension of $1000 \times 1000 \times 100$ mm. Brick units with dimension of $200 \times 100 \times 50$ mm and mortar with cement to sand ratio of 1:4 was used in this study. Through diagonal shear test, it was found that the shear strengths of the two masonry walls under study are about 0.114 and 0.144 MPa,

respectively. Such values are considerably lower when compared to the standard specimens tested in Europe and India, which were about 1.678 and 0.220 MPa. Thus, the results of this experiments are important to be taken into account in the design of unreinforced or confined masonry, particularly in Indonesia.

Acknowledgements The authors would like to acknowledge the financial support received from the Institut Teknologi Sepuluh Nopember, Indonesia, for the experimental study.

References

1. Habieb AB, Milani G, Tavio T (2018) Two-step advanced numerical approach for the design of low-cost unbonded fiber reinforced elastomeric seismic isolation systems in new masonry buildings. *Eng Failure Anal* 90:380–396. <https://doi.org/10.1016/j.engfailanal.2018.04.002>
2. Habieb AB, Valente M, Milani G (2019) Base seismic isolation of a historical masonry church using fiber reinforced elastomeric isolators. *Soil Dyn Earthq Eng* 120:127–145. <https://doi.org/10.1016/j.soildyn.2019.01.022>
3. Tavio T, Milani F, Habieb AB, Milani G (2020) Seismic protection of unreinforced masonry buildings by means of low cost elastomeric isolation systems. *Int J Masonry Res Innov* 1(1):1. <https://doi.org/10.1504/IJMRI.2020.10029907>
4. Alecci V, Fagone M, Rotunno T, De Stefano M (2013) Shear strength of brick masonry walls assembled with different types of mortar. *Constr Build Mater* 40:1038–1045
5. Kadam SB, Singh Y, Li B (2014) Strengthening of unreinforced masonry using welded wire mesh and micro-concrete – behaviour under in-plane action. *Constr Build Mater* 54:247–257. <https://doi.org/10.1016/j.conbuildmat.2013.12.033>
6. Tumialan JG, Micelli F, Nanni DA (2001) Strengthening of masonry structures with FRP Composites. In: *Structures 2001*, pp 1–8
7. Carozzi FG, Poggi C, Bertolesi E, Milani G (2018) Ancient masonry arches and vaults strengthened with TRM, SRG and FRP composites: Experimental evaluation. *Compos Struct* 187:466–480. <https://doi.org/10.1016/j.compstruct.2017.12.075>
8. Grande E, Milani G, Sacco DE (2008) Modelling and analysis of FRP-strengthened masonry panels. *Eng Struct* 30(7):1842–1860
9. Lignola GP, Bilotta A, Ceroni F (2019) Assessment of the effect of FRCM materials on the behaviour of masonry walls by means of FE models. *Eng Struct* 184:145–157. <https://doi.org/10.1016/j.engstruct.2019.01.035>
10. Scacco J, Ghiassi B, Milani G, Lourenço DPB (2020) A fast modeling approach for numerical analysis of unreinforced and FRCM reinforced masonry walls under out-of-plane loading. *Compos Part B Eng* 180:107553
11. Shrestha H, Pradhan S, Guragain DR (2012) Experiences on retrofitting of low strength masonry buildings by different retrofitting techniques in Nepal. In: *15th World Conference on Earthquake Engineering*, Lisbon Port, no. January 2006
12. Meguro K, Soti R, Navaratnaraj S, Numada DM (2012) Dynamic testing of masonry houses retrofitted by bamboo band meshes. *J Japan Soc Civ Eng Ser A1 Struct Eng Earthq Eng* 68(4):I_760-I_765
13. Ghavami K (2005) Bamboo as reinforcement in structural concrete elements. *Cem Conc Compos* 27(6):637–649. <https://doi.org/10.1016/j.cemconcomp.2004.06.002>
14. Archila H, Kaminski S, Trujillo D, Escamilla EZ, Harries DKA (2018) Bamboo reinforced concrete: a critical review. *Mater Struct Constr* 51(4):1–18
15. Mali PR, Datta DD (2020) Experimental evaluation of bamboo reinforced concrete beams. *J Build Eng* 28:101071

Analysis of the Effect of Asbuton on Porous Asphalt Mixtures for Heavy Load Traffic



Sutoyo, Mochtar, and Prastyanto

Abstract The main problem of porous asphalt was clog up the pores that caused by the deformation of pavement under vehicular loading [19–21], and the creep of asphalt [22, 23], that is difficult to solve the pore blockage caused by vehicle loads and asphalt creep [24]. Porous asphalt requirements for heavy load traffic have not been determined, especially for Marshall stability values, permanent deformation (rutting) and void volume. For this reason, a certain gradation of a mixture of aggregate and high quality asphalt is required. Modification of asphalt with several types of additives to produce high quality asphalt will be carried out in this research. 60–70 penetration asphalt and PG-76 shell asphalt were used, with several additional materials, namely: cellulose fiber (Viatop), glass fiber and asbuton B-5/20. The best results were obtained from a combination of 60–70 penetration asphalt (3.5%) with B-5/20 asphalt (5%), which resulted in a Marshal stability value of 3200–4550 kg, flow = 5–7 mm, cavity volume = 9–10%, seepage (k) = 0.4–0.7 mm/s, AFD = 0.0% and contabro loss 8.43%. so that the influence of minerals and asphalt (asbuton) on the porous asphalt mixture will be analyzed.

Keywords Analyze · Asbuton B-5/20 · high Marshall stability · durable

1 Introduction

The main problem of porous asphalt was clog up the pores that caused by the deformation of pavement under vehicular loading [19–21], and the creep of asphalt [22, 23], that is difficult to solve the pore blockage caused by vehicle loads and asphalt creep

Sutoyo (✉)

Public Works Department of Highways of East Java Province, 167-Gayung Kebonsari Street, Surabaya, East Java Province, Indonesia
e-mail: toyosutoyo@yahoo.com

Mochtar · Prastyanto

Institute Technology Sepuluh Nopember Surabaya, ITS, ITS Sukolilo Campus, Surabaya 60111, Indonesia

© Institute of Technology PETRONAS Sdn Bhd 2024

B. S. Mohammed et al. (eds.), *Proceedings of the International Conference on Emerging Smart Cities (ICESC2022)*, Lecture Notes in Civil Engineering 324,
https://doi.org/10.1007/978-981-99-1111-0_47

555

[24]. Porous asphalt requirements for heavy load traffic have not been determined, especially for Marshall stability values, permanent deformation (rutting) and void volume. For this reason, a certain gradation of a mixture of aggregate and high quality asphalt is required. Precise aggregate grading can be done based on the stone-to-stone contact between the coarse aggregates, while high-quality asphalt can be produced by combining several additives with asphalt in the right proportions. Several references mention that porous asphalt is related to open gradation, high quality asphalt (modified) and fiber, as well as other additives. Modified asphalt is one of the main components of the porous asphalt mixture. Modified asphalt has excellent characteristics because it is made from a mixture of pure asphalt with polymer or plastomer materials and other materials for its workability. The use of modified asphalt (Esso and Shell), cellulose fiber and glass fiber, as well as other added materials are generally imported materials, resulting in dependence on large-scale use. This is a special consideration in planning if these materials are the main components in the porous asphalt mixture, whereas many studies related to local materials such as asbuton [14] are quite successful for asphalt mixtures, both as a binder. or as an additive to modified asphalt.

Utilization of asbuton as an added material is divided into 3 (three) types, namely pre-mixed, and others in the form of granules which are directly sent to pugmill in the mixing process at the Asphalt mixing plant (AMP). The types of granules in question are B-5/20 and B-50/30 which are in accordance with the technical specifications of the Directorate General of Highways 2018 revision-2. The notation B-5/20 means asphalt that has a penetration value of 0–5 (0.1 mm) and contains an asphalt content of about 20%. While B-50/30 means asphalt which has a penetration value of 40–50 (0.1 mm) and contains asphalt content of up to 30%. Each usage is limited to 2–3% for asbuton B-5/20, while asbuton B-50/30 can be up to 7–10%. These things will be used as a reference in this research. Of course, a different implementation method is needed from previous research in order to produce better properties.

Asbuton is a local material on the Indonesian island of Buton which consists of bitumen (asphalt) and minerals that have been mixed for thousands of years and even millions of years, [18]. It is possible that there are special characteristics of each material in Asbuton which strengthen the bond between the aggregates, thus producing additional strength in the Marshall stability value in the porous asphalt mixture. So that in its utilization it needs to be used together in large portions in an effort to improve the characteristics of the asphalt mixture for heavy-load traffic, including the porous asphalt mixture in this study.

To ascertain the effect and benefits of asbuton in the mixture, a more in-depth analysis is needed, especially the role of bitumen and its minerals in the mixture. By paying attention to the mineral content and asphalt of asbuton, it is hoped that the relationship between pure asphalt and asbuton, including the role of minerals, can produce a strong bond in asphalt mixtures, especially porous asphalt mixtures for heavy-load traffic. One of the indicators is the high melting point and adhesion, but in practice it can be done easily (workable). An appropriate mixing method is needed so that the characteristics of the oil asphalt are not disturbed, and asbuton can work effectively so that the role of asbuton in the mixture can be maximized.

2 Objective

Able to analyze the effect of asbuton B-5/20 as the best additive in porous asphalt mixtures for heavy traffic loads with the right method. With indicators: Marshall stability value above 3700 kg; seepage > 0.04 mm/s; loss of cantabro (CL) < 20%; and AFD < 0.3%.

3 Literature Review

3.1 Asphalt

The function of asphalt in a porous asphalt mixture is to support the bond between coarse aggregate grains, which will function as a very strong and durable bond. The asphalt mixture remains stable, so that the crushed stone does not shift when it receives dynamic loads from the repetition of heavy vehicles. The influence of the quality of asphalt in the mix is very important, to strengthen the shear resistance at high temperatures, over 60 °C and when subjected to repeated heavy vehicle loads. Asphalt with a high softening point value is required, so that it does not melt at the hottest temperature and does not clog the voids, and has a very strong bearing capacity. To meet these requirements, additional materials are needed [25] from the Department of Chemical Sciences, Faculty of Science, Tunku Abdul Rahman University, Malaysia.

Selected bitumen which has a softening point value above 60 °C is needed to support the mechanical bonds that occur between the coarse aggregate grains. In general, asphalt penetration 60–70 only has a softening point value of 48–51 °C, smaller than the temperature in the field which can reach temperatures up to 60 °C, therefore in this study the type of asphalt with a high softening point will be used, namely Asphalt Shell Cariphalte PG 76 (Softening Point 78 °C). Based on the manufacturer's certificate, the technical requirements are met, as in Table 1. From these data, if plotted on a graph of the correlation between temperature and viscosity values at a temperature of 135 °C and 170 °C, it can be interpolated to determine the temperature limits for mixing and compaction.

Table 1 Technical Specification for Asphalt Shell Cariphalte PG 76

Type of Testing	Units	Method	Specification	Test Results
Viscosity at 135 °C	Pa.s	SNI 7729-2011	Max 3,00	2,60
Viscosity at 170 °C	Pa.s	SNI 7729-2011	Max 0,80	0,51
Penetration at 25 °C	0,1 mm	SNI 2456-2011	40–70	50
Softening Point	°C	SNI 2434-2011	Reported	78
Elastic recovery, 10 cm	%	ASTM D6084	Min 75	80

The laboratory research, which will be used as a reference as the main criterion for porous asphalt mixtures for heavy overloaded traffic is a marshal stability value of at least 3700 kg with a maximum grain size of 1.5 in., and a void volume of 18–25% (NAPA 2003), Cantambro Abrasion Loss is a maximum of 20% dry (unaged), the maximum Asphalt Flow Down value is 0.3%. The main other requirement is a sufficient of voids for water to seep quickly, with a seepage coefficient of 0.04 mm/second, more than highest Indonesia rainfall value, 377 mm/day. Therefore, the seepage test was carried out, which will serve as a simulation that the surface water runs out when the rain stops.

A Penetration grade of 60–70 asphalt modify with the B-5/20 asbuton type is an alternative to use a binder for a porous asphalt mixture, as long as it meets the requirements, both technical and their application (workability). Ease of application means that it can easily mix with the aggregate evenly at a set temperature and does not agglomerate quickly during hauling, and easy to achieve design density by standard compaction. This requirement applies to all types of asphalt to be used in porous asphalt mixtures for heavy overloaded traffic. The choice of alternative use of added materials refers to the fulfillment of technical specifications, ease of implementation and adequacy of materials in the field, as well as the level of dependence on other parties during production, especially imported materials.

3.2 Additives

a. Cellulose Fiber

There are two types of fiber, namely natural fiber and synthetic fiber. Natural fibers are generally made from plants, stems, leaves, fruit. Meanwhile, synthetic fibers are made from chemicals that are able to provide functions as natural fibers. Some of the functions and properties of cellulose fiber are that it has a strong binding ability, has high tensile strength, is able to form networks, is not easily soluble in water, alkali and other organic solvents (Harsini and Susilowati 2010), so that the functions and properties of these fibers which is used in the porous asphalt mixture to strengthen the asphalt characteristics as required so that the porous asphalt function becomes stronger and more durable during the design service life.

In this research, the type of fiber used is cellulose fiber from the manufacturer with the product's name: VIATOP® 66 which is composed of 66% ARBOCEL ZZ 8/1 and 34% asphalt Penetration 50–70. ARBOCEL is a natural cellulose fiber with the characteristics as shown in Table 2 and Table 3. Viatop is a granular cellulose fiber product in packaged form which guarantees an even distribution of speed in the asphalt mixture so that it is more efficient and ensures the continuity of production of asphalt mixtures with uniform quality during production.

b. Glass Fibers

Table 2 Characteristics of ARBOCEL ZZ 8/1. Source: Business Unit Road Construction 73,494 Rosenberg (Germany)

Description	Value
Content of cellulose fiber as raw material	80% ± 5%
Average Fiber Length	1100 μ
Average Fiber Thickness	45 μ
pH value (5 g/100 ml)	7,5 ± 1

Table 3 Grain characteristics of cellulose fiber made from ARBOCEL ZZ 8/1. Source: Business Unit Road Construction 73,494 Rosenberg (Germany)

Description	Value
Bulk density	200–280 g/l
Weight loss after drying	Max.7%
Grains pass sieve no.4 (4.75 mm)	15–40%
Residual heating (850 °C, 4 h)	10–20%

This glass fiber comes from Korea in the form of pellets, with the characteristics as in Table 4. Recommendations from the manufacturer, that the effective mixture for porous asphalt mixtures is 1% by weight of the mixture.

c. Asbuton (Natural Asphalt from Buton Island, Indonesia)

Asbuton is natural asphalt in the form of bulk rock, in very large quantities, which is located on the island of Buton, Southeast Sulawesi, Indonesia. Currently, it is widely used as an additive in hot asphalt mixtures in relatively small amounts. Many studies related to the use of asbuton have been successful, but have not been utilized optimally, even now research is being conducted on the extraction of pure asbuton so that it can be utilized more. There are two types of asbuton based on their characteristics, namely Kabungka (B-5/20) and Lawele (B-50/30) which are currently used in the technical specifications of the Directorate General of Highways, Ministry for Public Works and Human Settlement 2018 revision-2. Where the utilization of hot mix asphalt is still limited, around 2–3% for asphalt type B-5/20, while type B-50/

Table 4 Characteristics of Glass Fiber

Description	Value
Color	Black
Shape	Rectangle
Length	10 mm
Width	3 mm
Density	2,53 g/cm ³
Melting point	300 °C
Humidity	<0,20%
Weight loss due to heating	<0,25%
Non-fibrous material	<1%

Table 5 Characteristics of a Asbuton (Bitumen). Source: Neni, Willy, Ismanto [14]

Characteristics	B-50/30	B-5/20	Unit
Bitumen content (%)	30,0	20,0	
Penetration (25 °C, 100 gr, 5 s)	36	4	0,1 mm
Softening point	59	101	°C
Ductility	>140	<140	cm
Solubility	99,6	-	% weight
Flash point	198	-	°C
Specific Gravity	1,037	1,046	-
Weight loss (TFO)	0,31	-	% weight
Penetration after TFO	94	-	% initial
Softening point after TFO	62	-	°C
Tensile Strength after TFO	>140	-	Cm

Table 6 Basic Components of Asbuton (Bitumen). Source: Neni, Willy, Ismanto [14]

Characteristics	B-50/30	B-5/20
Nitrogen bases (N), %	27,01	29,04
Acidaffins (A1), %	9,33	6,60
Acidaffins (A2), %	12,98	8,43
Paraffin (P) %	11,23	8,86
Malten Parameter	1,50	2,06
Nitrogen/ Paraffin, N/P)	2,41	3,28
Asphaltene	39,45	46,92

30 with a portion of 7–10%. The properties of the two types of asbuton are shown in Table 5, Table 6 and Table 7.

Table 7 Characteristics of a Asbuton (Minerals). Source: Neni, Willy, Ismanto [14]

Component	Value (%)	
	B-50/30	B-5/20
CaCO3	72,90	86,66
MgCO3	1,28	1,43
CaSO4	1,94	1,11
CaS	0,52	0,36
H2O	2,94	0,99
SiO2	17,07	5,64
Al2CO3+Fe2O3	2,31	1,52
LOI	1,05	0,96

4 Laboratory Research Activities

The research was conducted by 1 (one) gradation of porous aggregate for several types of asphalt and some additives, the stages of activities in the laboratory are as follows:

1. Design of porous asphalt grading with a maximum grain size of 1 in.
2. Calculate the asphalt content according to the design results of the porous asphalt gradation.
3. Make a variety of added materials for each type of asphalt.

4.1 Gradation Design

Based on previous research that the coarse fraction in the porous asphalt mixture is 75–85%. According to the VCADRC minimum value concept to determine the maximum density value of the coarse aggregate mixture, the total coarse fraction = 53% + 23% = 76%. The amount of fine aggregate and mineral asbuton is 19 + 5 = 24%, but after combined the amount of coarse fraction becomes 66.38% as shown in Table 8. The result of combining coarse and fine fractions is that the total fine aggregate (passed #4) is 33.62%. This shows that the medium fraction contains a lot of fine aggregate, so the precise fine aggregate calculation must be carried out carefully to provide the volume of voids in the porous asphalt mixture.

Table 8 Design Data for Porous Asphalt Mixture with a Maximum Grain of 1 cm

SIEVE	53,0	23,0	19,0	5,0	100,0
	CR-10-15	CR-5-10	CR-0-5	Asb-B5/20	Combined
1	100	100	100	100	100
3/4	96,86	100	100	100	98,34
1/2	41,39	98,23	100	100	68,58
3/8	12,87	92,7	100	100	52,36
#4	4,1	22,78	99,57	99,67	33,62
#8	2,64	2,64	72,47	94,21	22,58
#16	0	1,57	47,46	77,22	14,37
#30		1,38	32,93	55,21	10,28
#50		1,24	22,66	43,52	7,41
#100		1,06	14,89	19,05	4,44
#200		0,85	9,02	6,02	2,46

4.2 Calculation of Asphalt Content

Total surface are % passing (Table 8) multiple by surface area factor in Table 9 as detail below:

$$\frac{(100 \times 0,4 + (33,62 \times 0,4) + (22,58 \times 0,8) + (14,37 \times 1,6) + (10,28 \times 2,9) + (7,41 \times 6,2) + (4,44 \times 12,4) + (2,46 \times 33,0))}{100} = 3,063 \text{ m}^2$$

Asphalt content is obtained from the sum of the effective asphalt volume and the absorption of the aggregate to the asphalt. The effective asphalt volume is the surface area of aggregate according to the combined gradation multiplied by the asphalt film thickness of 10 microns. while the absorption of asphalt is a half of water absorption. According to this research the water absorption is 2,0%, so the value of asphalt absorption is $1/2 \times 2.0\% = 1.0\%$. The aggregate surface area is the result of multiplying the combined aggregate of each % passing the size of the sieve with a multiplier as shown in Table 9. From the calculation results obtained as follows:

- surface area per 1 kg of aggregate = $3.063 \text{ m}^2 = 3.063 \times 10 + 2 \text{ dm}^2$
- bitumen film thickness = $10 \mu = 10 \times 10^{-5} \text{ dm} = 10^{-4} \text{ dm}$
- asphalt volume = $3.063 \times 10 + 2 \times 10^{-4} \text{ dm}^3 = 3.063 \times 10^{-2} \text{ dm}^3 = 0.031 \text{ dm}^3 = 0.031 \text{ l}$.
- The weight of asphalt = asphalt volume multiplied by the specific gravity of asphalt = $\frac{0.031 \times 1.036 \text{ kg}}{\text{liters}} = 0,032 \text{ kg}$
- This value appoint that 0.032 kg of the effective asphalt in 1 kg of aggregate
- So that the effective asphalt content = $\frac{0.032}{(1+0.032)} \times 100\% = 3.076\%$.

Table 9 Multiplier of Surface Area in Units of ft2/lbs (m²/1 kg) Aggregate

% Sieve Passing	(mm)	Surface area factor ft ² /lb (m ² /kg)
11/2"	37,5	2 (0,4)
1"	25,4	
3/4"	19,1	
1/2"	12,7	
3/8"	9,5	
#4	4,75	2 (0,4)
#8	2,36	4 (0,8)
#16	1,18	8 (1,6)
#30	600 mikron	14 (2,9)
#50	300 mikron	30 (6,2)
#100	150 mikron	60 (12,4)
#200	75 mikron	160 (33,0)

Table 10 Matriculation of Experimental Variations in The Laboratory

Type of Asphalt	Added material (%)			Remarks
	Cellulose (Viatop)	Glass Fiber	Asbuton B-5/20	
Pertamina Asphalt Pen 60/70	-	0,5; 1,0	5,0	Mixing temperature 170–180 °C
Shell PG-76	0,3; 0,4; 0,5	-	-	Mixing temperature 190–198 °C

- Total asphalt content in the mixture is $3.076\% + 1\% = 4.076\%$ rounded up to 4,1%.

4.3 Added Materials (Additivies)

Variations of added materials can follow previous researchers, or recommendations from manufacturers for example for the value of cellulose fiber taken from 0.3–0.5% of the weight of the mixture, from the experimental results obtained a value of 0.4 which is the most suitable because it produces the highest marshal value. As for fiber glass from Korea, the manufacturer recommends using 1% of the total weight of the mixture. While the use of asbuton B-5/20 is 5% of the total weight of the mixture. On the basis of these circumstances, mixed type was carried out as shown in Table 10.

4.4 Laboratory Test Results

To compare the three types of additives, it was carried out using a 4-in. marshal test specimen. The characteristics of the mixture include Marshall stability, flow, density, voids in the mixture, seepage, Contambro loss (CL) and asphalt flow down (AFD). All test results are summarized in a report as listed in Table 11. Next, a 6 in. Marshall specimen with selected additives (asbuton B-5/20) will be used to make a porous asphalt mixture with a minimum Marshall stability of 3700 kg.

The other test conducted to combined of the asphalt (3,5%) and asbuton (5,0%) to produce a modified asphalt that are fulfill the requirements is penetration and softening point, that are as follow:

Penetration = 20 (0,1 mm) Softening point (SP) = > 100 °C, Ductility = < 10 cm

The manufacture of test objects for each type of test is carried out by heating asbuton at a temperature of 180 °C and asphalt at a temperature of 150 °C. By heating these materials, the properties of the mixture as mentioned above are obtained. Figure 1.a and Fig. 1.b. Illustration porous asphalt mixture with asbuton B-5/20.

Table 11 Characteristics of a porous asphalt mixture with various type and portion of additives

Component Material	MS (Kg)	Flow (mm)	Voids (%)	Seepage (mm/sec)	CL (%)	AFD (%)	Spec. Req.
Asphalt Pertamina Pen 60–70							
+Fiber 0,5%	828,7	3,05	15	0,189	-	-	
+Fiber 1,0%	892,4	3,00	13	0,206	9,5	0,01	ok
+Asb.B-5/20:5%	1147,4	4,00	12	0,165	8,4	0,00	ok
AspalShell PG-76:							
+Viatop 0,3%	866,9	3,00	14	0,274	-	-	
+Viatop 0,4%	1121,9	4,00	11	0,105	11,0	0,02	ok
+Viatop 0,5%	994,4	4,80	12	0,118	-	-	

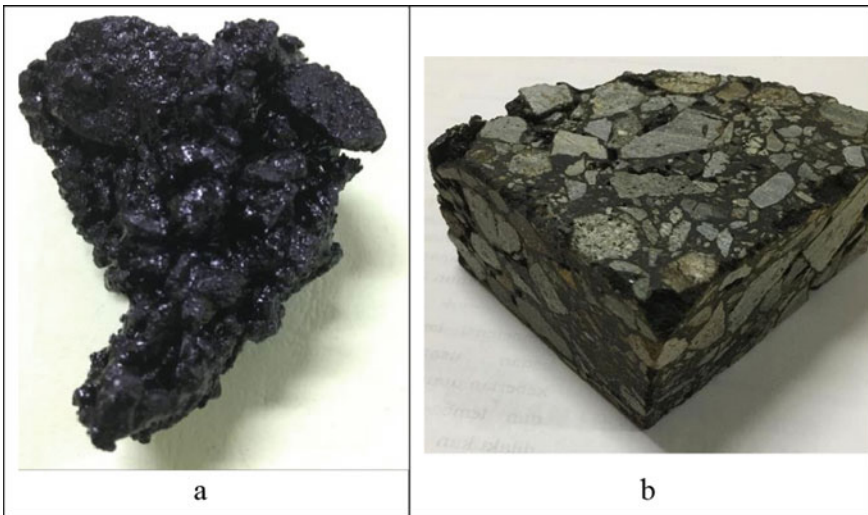


Fig. 1 a. Bulk mixture of porous asphalt with asbuton B-5/20. b. Solid mixture of porous asphalt with asbuton B-5/20

Explanation of experimental results and recommendations for selecting the type of additives, as follows:

1. All mixtures meet the requirements and there is no significant difference
2. In the case of asbuton as an additive, for the mixing and compaction temperatures under the other additives, it has almost the same Marshall stability value
3. Asbuton B-5/20 has a simple control in the homogeneity of the mixture, because it has the same grain size of minerals that pass through #8 retained #30
4. Utilization of local materials is maximized
5. There is no dependence on imported materials because there are sufficient enough as local deposits.
6. Asbuton B-5/20 was chosen as an additional material that can support the design of porous asphalt for heavy traffic loads.
7. There are several factories that produce asbuton granules that have a uniform asphalt content, both B-5/20 and B-5/20 types. So that the guarantee of the consistency of the asphalt content in the mixture can be achieved
8. Furthermore, a large sample of porous asphalt mixture which is equivalent to AC-Base is used, with a diameter of 6 in. (15.2 cm) and a thickness of 9.53 cm
9. Based on the calculation analysis of VCRDRC and VCAMIX, the best type of gradation of porous mixtures is as shown in Table 12.

Table 12 Matriculation of Experimental Variations in The Laboratory

Sieve	Lower Limit	Upper Limit	Comb. Grad	Grad. of Each Fraction	Grad. of Mix Extraction
% Pass The Sieve					
1 1/2	100,0	100,0	100,0	100,0	100,0
1	90,0	100,0	98,99	95,68	85,28
3/4	75,0	96,0	94,67	80,01	76,21
1/2	50,0	72,0	55,38	57,90	58,56
3/8	33,0	50,0	42,96	42,15	43,46
#4	18,0	32,0	31,18	22,08	28,88
#8	13,0	23,0	21,64	16,01	21,40
#16	9,0	17,0	13,89	10,70	15,89
#30	7,0	13,0	9,88	7,25	12,04
#50	4,0	9,0	7,07	4,91	9,00
#100	3,0	6,0	4,27	3,17	6,15
#200	2,0	4,0	2,38	2,08	3,69

4.5 Trial Steps

The gradation used is based on the analysis of VCRDRC and VCAMIX calculations, to get a design with stone on stone contact conditions (maximum interlock) and produce connected voids [4]. To prove that the cavities are interconnected, a seepage test is carried out, the test results show that the water actually permeates the entire surface of the porous mixture. While the indicators of high strength of the mixture are Marshall stability, minimum 3700 kg; maximum AFD value of 0.3% and maximum CL of 20% as an indication of the durability of the mixture.

4.6 Analysis of the Effect of Asbuton on Porous Asphalt Mixes

The combination of bitumen of asbuton B-5/20 and asphalt, with a composition of 3.5 (asphalt): 1.0 (bitumen of asbuton), then the combined softening point (SP) is as follows:

$$\begin{aligned} \text{SP of Asphalt} &= 51 \text{ } ^\circ\text{C}; \text{ SP of Asbuton} > 100 \text{ } ^\circ\text{C} \\ \text{SP of Combined} &= \frac{(3.5 \times 51 + 1 \times 101)}{4.5} = 62.1 \text{ } ^\circ\text{C}, \text{ that was different with laboratory} \\ &\text{result of } > 100 \text{ } ^\circ\text{C} \end{aligned}$$

Napa 1996, it is stated that for the assessment of the quality and durability of asphalt there are two indicators, namely the compatibility ratio and durability parameters by the certain formula, [17]). Based on data Table 6, the ratio of compatibility (RC) and durability parameters (K) can be determined by the formula:

$$RC = \frac{N}{P} = \frac{29.04}{8.86} = 3,28 \quad (1)$$

where,

The compatibility ratio is the suitability of the asphalt components, including the good category if the value is above 0.5.

RC = Ratio of compatibility

N = Basic component of Nitrogen P = Paraffin content

$$K = \frac{N + A1}{P + A2} = \frac{29.04 + 6.6}{8.86 + 8.43} = \frac{35.64}{17.29} = 2,06 \quad (2)$$

where,

Durability is included in the good category if the value is above 1.0. K = Durability

N = Basic component of Nitrogen P = Paraffin content

A1 = Acidafin 1

A2 = Acidafin 2

While for Asbuton B-50/30, the value of the variables are as follows: RC = 2.41

K = 1.50

Based on the indicator values above, asbuton B-5-20 is the best alternative to choose.

The mineral content of asbuton as shown in Table 7 is the basic ingredient for making cement, so if the material is combined with asphalt it will have a very strong adhesive strength. with the amount of mineral asbuton in the mixture of about 4% will provide a very large added strength to the porous asphalt mixture. The two ingredients in the asbuton in the mixture function as a binder which is equivalent to cement and asphalt. because its existence has long been mixed with asphalt in the asbuton. This study proves that a high Marshall stability value of 3200–4550 kg can be achieved, no creep occurs in the asphalt mixture as indicated by the AFD value = 0% at a temperature of 175 °C.

The mechanical-based gradation arrangement (interlock) will be stronger and more stable if it is supported by a strong modified asphalt. There is no settlement difference, no permanent deformation (rutting depth), and no creep in the asphalt mixture. Mechanical bonding in the coarse aggregate interlock and chemical bonding in modified asphalt are the main variables of porous asphalt mixtures for overloaded traffic. This study shows that the strongest modified asphalt is produced by both types of materials in asbuton, namely mineral and bitumen. The addition of adhesive strength is evidenced by the AFD value = 0.00% at a temperature of 175 °C and the cantabro loss value is 8.43% from the standard value of 20% for dry conditions without immersion.

This becomes one of the basis for the analysis that all parts of asbuton have a strong additional adhesion to the asphalt mixture, thus supporting the coarse aggregate fraction which is interlocked to produce a high value of Marshall stability in the porous asphalt mixture in this study.

5 Conclusion

Asbuton B-5/20 has an important role in porous asphalt mixtures, especially to support maximum interlock between coarse aggregates. Minerals and bitumen in asbuton have good adhesive strength properties, as evidenced by the Asphalt flow down (AFD) value = 0.00% at a temperature of 175 °C. In addition, the Marshaal stability value is very high, namely 3200–4550 kg and contabro loss = 8.43%, So it can be said that Asbuton B-5/20 is the best additive for porous asphalt mixtures for heavy traffic loads.

Acknowledgements On this occasion we feel helped by several parties in the implementation of this research, starting from the laboratory facilities. Laboratory technicians and discussion partners regarding the research I do. Therefore, I would like to express my gratitude to: Prof. Ir. Indrasurya

B Mochtar, M Sc PhD, as the main supervisor, Dr. Catur Arief Prastyanto, ST, M Eng, as a co supervisor, Ir. Edy Tambeng, MSi as Head of the Public Works Department of Highways of East Java Province and Other friends who provide support for this research. I really feel helped by this collaboration, so from the results of the laboratory we found many things that can improve in this research. I hope all parties involved are healthy and successful.

References

1. General Specifications Revision-2, for road and bridge works, Director General of Highways, Ministry for Public works and Human Settlement, 2018
2. Hot mix asphalt materials, mixture design, and construction, NAPA Education Foundation Lanham, Maryland 1996
3. Mochtar, Lectures (2008) Institute of Technology Sepuluh Nopember
4. Shreyas, Lavanya (2017) Comparison of flexible (Dense graded) & Porous (Open graded) asphalt surface course with stone dust as a filler in Marshal Mix design
5. Nashir (2013) Experimental study of porous asphalt mixture using polymer modified binder with polypropylene fiber stabilization
6. Ma Y, Chen X, Geng Y, Zhang X (2020) Effect of clogging on the permeability of porous asphalt pavement
7. Pradoto, Puri, Hadinata, Rahman, Az-Zuchruf (2019) Improving strength of porous asphalt: utilizing fly ash into nanomaterials in experimental approach
8. Oregon Department of Transport (ODOT), Pavement Services (2019) Porous Asphalt Concrete (PAC) is intended to be used for drainage or storm water infiltration. Do not design PAC for use in a travel lane. When PAC is used, ensure the design team is aware that PAC has a relatively high future maintenance and rehabilitation cost
9. Ghulam, Nariswari, Ariyanto, Gunawan (2017) Value of marshal stability using local materials. *J Potential* 19(1)
10. Yahya Abdurrohimi, Ary Setyawan, Suryoto (2017) Making job mix formulas for asphalt porous and evaluation of mixtures from application on environmental roads
11. Hasan (2016) Laboratory evaluation of modified porous asphalt mixtures
12. Anggraini, Saleh, Aquina (2014) Characteristics of mixed porous asphalt with Styrofoam substitution on 60/70 penetration asphalt
13. Arlia, Saleh, Anggraini (2014) Characteristics of porous asphalt mixture with Gondorukem substitution on 60/70 penetration asphalt
14. Neni, Ismanto, Willy (2005) Laboratory evaluation of lawele buton natural asphalt in asphalt concrete mixture
15. Fatoni, Afandi (2021) The effect of using Buton B5/20 asphalt with Madura local aggregate on hot mixed asphalt AC-WC towards Marshall characteristics. *J Civil Eng* 6(1)
16. Eisaa, Basiounya, Daloob (2020) Effect of adding glass fiber on the properties of asphalt mix. *Int J Pavement Res Technol*
17. Rostler FS, White RM (1962) Composition and changes in composition of highway asphalts, 85–100 penetration grade. *Assoc Asphalt Paving Technol* 31:35–89
18. Halimi, Mochtar, Altway (2014) A breakthrough in asphalt technology - cheaper bitumen extracted from “Asbuton”, the rock asphalt of Buton Island, Indonesia. *Int J Educ Res* 2(8):347–358
19. Mansour TN, Putman BJ (2013) The influence of aggregate gradation on the performance properties of porous asphalt mixtures
20. Suresha et al (2010b) Effect of aggregate gradations on properties of porous friction course mixes

21. Takahashi (2013) Comprehensive study on the porous asphalt effects on expressways in Japan: based on field data analysis in the last decade
22. Hamzah et al (2012) The effects of initial conditioning and ambient temperatures on abrasion loss and temperature change of porous asphalt
23. Ferguson B (2005) Porous pavement, e Book published 18 February 2005
24. Ling S et al (2021) Pore characteristics and permeability simulation of porous asphalt mixture in pouring semi-flexible pavement
25. Tinavallie G (2013) Improving the ductility and elastic recovery of bitumen - natural rubber latex blend

Assessment of an Eight-Story Hospital Building with Nonlinear Static Analysis



Fahmy Hermawan and Nicolas Kanisius Sianturi

Abstract The assessment of an existing eight-story reinforced concrete (RC) hospital building, built in 2011, was measured using Non-linear Static Analysis Procedures (NSAP). The research examines the performance of the building and its respond to the earthquake's magnitude increment, in accordance with SNI 1726:2019 [1]. The NSAP has been performed and tested using ETABS software, which uses incremental lateral forces, positioned at the performance points, to determine the level of performance during failure conditions under 3 distinct conditions, such as yield conditions, local failure conditions and global failure conditions. Performance-based seismic design regulates the RC performance, to prevent potential hazards and actual building response according to the applicable regulations. The NSAP analysis phase begins with specifying the performance objectives, identification of the existing design, and conduct assessment appropriately and finally resume the RC's performance accordingly. The analysis reveals the performance level condition at the RC's performance point, when it reaches the performance level both in X direction and Y direction the structure experiences local collapse which is considered as Collapse Prevention (CP) condition. The response of the structure indicates that the plastic hinges mechanism occurs both in the beam and the column as well at the 1st floor up to the roof floor. The structure is more ductile in the Y-direction compared to the X direction. The research has stated that the reinforced concrete structure possesses appropriate ductility, the failure condition is elastic in the collapse prevention category and meets the performance-based design criteria.

Keywords Nonlinear static procedure · pushover analysis · reinforced concrete

F. Hermawan · N. K. Sianturi (✉)
Civil Engineering Department, Universitas Trisakti, Jakarta, Indonesia
e-mail: nicolassius@gmail.com

F. Hermawan
e-mail: fahmy.hermawan@trisakti.ac.id

© Institute of Technology PETRONAS Sdn Bhd 2024
B. S. Mohammed et al. (eds.), *Proceedings of the International Conference on Emerging Smart Cities (ICESC2022)*, Lecture Notes in Civil Engineering 324,
https://doi.org/10.1007/978-981-99-1111-0_48

1 Introduction

Indonesia is a country prone to earthquakes with fairly high level of seismic activities, therefore the design and building's evaluation in Indonesia must be carried out with the right method and in accordance with the applicable regulations, in order to produce earthquake-resistant buildings. With the behavior of buildings that tend to deform inelastically when responding to earthquake magnitudes, as science develops in civil engineering, non-linear analysis methods are used to determine the behavior and performance of buildings when they pass their elastic capacity and to determine the mechanism of collapse that will occur. One of the non-linear analysis methods used to evaluate earthquake-resistant building structures is a non-linear static analysis or known as pushover analysis.

The non-linear static analysis procedure is carried out by providing a pattern of lateral static loads on a building with an increased magnitude until the building structure reaches the expected lateral displacement. Evaluation of building performance with non-linear static analysis procedure is carried out to determine the level of building performance and to obtain information related to structural components of buildings that are damaged or collapsed due to responding to earthquake magnitudes, so that reinforcement or assessment of these structural components can be carried out.

2 Literature Review

2.1 Building Performance

The level of building performance in responding to the magnitude of the earthquake that occurs, which is determined based on a combination of the performance level of structural components and non-structural components [2]. The general level of building performance can be seen in Table 1 [3].

Table 1 Building Performance Level

	Operational Level (1-A)	Immediate Occupancy Level (1-B)	Life Safety Level (3-C)	Collapse Prevention Level (5-D)
Level	Very Light	Light	Moderate	Severe
Description	The building continues to function normally as it was before the earthquake	The building remains safe to operate and requires only minor repairs where necessary	The stability of the building is maintained and the reduction in structural capacity is not significant	The building does not collapse but the capacity is very low, it is possible that there will be acceptable damage

2.2 Evaluation Procedure

Linear procedures are allowed for buildings with highly regular structural systems and meet the demand-capacity ratio (DCR) requirements, while nonlinear procedures can be used in building with highly irregular structural systems which the mass participation in the first variant is high, however if the mass participation in the first variant is low then dynamic linear procedures need to be considered. The results of the linear procedures can be very inaccurate when applied to buildings with highly irregular structural system, the magnitude and distribution of inelastic demands are indicated by DCRs. There are four particular irregular structure systems such as in-plane discontinuity irregularity, out-of-plane discontinuity irregularity, weak story and torsional strength [3].

$$DCR = \frac{QUD}{QCE}$$

QUD = Forced caused by gravity loads and earthquake forces

QCE = Expected strength of the component or element

General requirement for evaluation is analysis procedure, component gravity loads and load combination, mathematic modeling, configuration, multi directional seismic effect, p-delta effect, soil-structure interaction, overturning, diaphragm, continuity, structural walls and their anchorage, structures sharing common elements, building separation, verification of analysis assumptions.

There are four particular types of analysis procedure such as Linear Static Procedure (LSP), Linear Dynamic Procedure (LDP), Nonlinear Static Procedure (NSP) and Nonlinear Dynamic Procedure (NDP) can be seen in Table 2 [4].

Table 2 Analysis Procedures

Irregularities	Structural Characteristics ⁴		Linear Analysis		Nonlinear Analysis ⁵	
No	Structures with $T \leq 3.5T_a$		P	P	P	P
	Structures with $T \geq 3.5T_a$		NP	P	P	P
Yes	Only any of the irregularities defined in Sec 7.3.1.2		NP	P	P	P
	Irregularities defined in Sect. 7.3.1.1.1 or 7.3.1.1.2	$\mu_{strength}^2 < \mu_{max}^3$	NP	NP	P	P
		$\mu_{strength}^2 > \mu_{max}^3$			NP	P
	Irregularities defined in Sect. 7.3.1.1.3 or 7.3.1.1.4 w/DCRs ⁴ < min (3.0 and m)		P	P	P	P
Irregularities defined in Sect. 7.3.1.1.3 or 7.3.1.1.4 w/DCRs ⁴ > min (3.0 and m)	$\mu_{strength}^2 < \mu_{max}^3$	NP	NP	P	P	
	$\mu_{strength}^2 > \mu_{max}^3$			NP	P	

2.3 Nonlinear Static Procedure

Nonlinear Static Procedure (NSP) is a mathematical model that directly incorporates the nonlinear load deformation characteristics of each building component must apply a monotonically increasing lateral load that represents the inertial forces in the earthquake until the target displacement is exceeded. NSP can be performed using load-controlled procedure or displacement controlled [5].

Higher mode effects shall be considered significant if the shear in any story resulting from the modal analysis considering modes required to obtain 90% mass participation exceeds 130% of the corresponding story shear considering only the first mode response (Fig. 1).

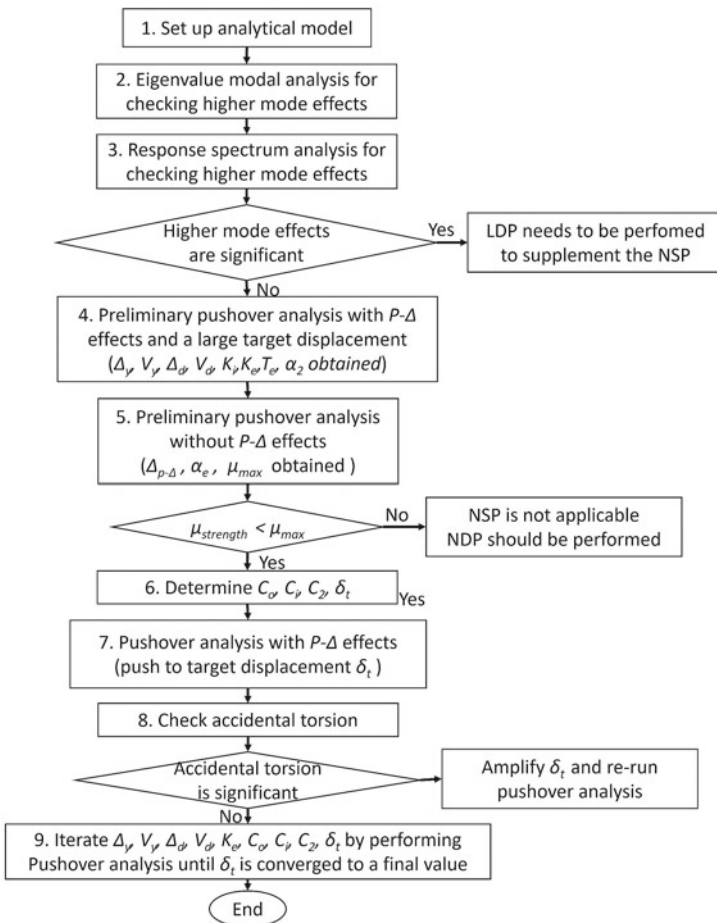


Fig. 1 Flowchart of NSP

Certain indicators need to be developed such as selection of control nodes, selection of earthquake force patterns, determination of the fundamental period, and application of analytical procedures must meet the requirements. The base shear force and the lateral displacement of the control node should be defined between 0–150% of the target displacement. Analytical model should be discretized to represent the force-deformation response at which plastic hinges occur and primary and secondary components should be designed in the model. However, NSP accuracy varies for various types of ground movement ensembles [6]. The post-disbursement behavior between X-direction and Y-direction is different which cannot be detected without performing a pushover analysis [7].

2.4 Building Data

A non-linear static analysis will be carried out using the ETABS program [8] to obtain the capacity of the structure, determine the displacement target (demand), and evaluate the performance of the building by referring to ASCE 41-13 and ASCE 41-17 regulations. The loading of buildings will use the SNI 1727: 2020 guidelines [9] (Tables 3 and 4).

Table 3 Building Data

Building Data	
Building Location	Makassar
Building Function	Hospital
Type of Building	Reinforced Concrete Structure
Number of Levels	8 Levels
Building Area	1820 m ² /floor
Building Height	33 m
Concrete Quality	fc' 30 MPa
Reinforcing Steel Quality	fy 420 MPa

Table 4 Structure Data

Fl.	Beam		Column	
	Main	Joist	Grid 1 & 11	Grid 2–10
	(mm ²)	(mm ²)	(mm ²)	(mm ²)
8	350 × 700	300 × 500	600 × 600	600 × 600
7	350 × 700	300 × 500	600 × 600	600 × 600
6	350 × 700	300 × 500	600 × 600	700 × 700
5	350 × 700	300 × 500	600 × 600	700 × 700
4	350 × 700	300 × 500	700 × 700	700 × 700
3	350 × 700	300 × 500	700 × 700	700 × 700
2	350 × 700	300 × 500	800 × 800	800 × 800
1	350 × 700	300 × 500	900 × 900	900 × 900
Floor plate thickness is 130 mm				

Effective Vibration Time

$$T_e = T_i \cdot \sqrt{\left(\frac{K_i}{K_e}\right)} \quad (1)$$

T_i : elastic fundamental period.

K_i : elastic lateral stiffness of the building in the direction of the earthquake being studied.

K_e : effective lateral stiffness of the building in the direction of the earthquake being studied.

Displacement Target

$$\delta_t = C_0 \cdot C_1 \cdot C_2 \cdot S_a \cdot \frac{T_e^2}{4\pi^2} \cdot g \quad (2)$$

S_a : spectral acceleration of the building in the effective fundamental period in the direction of the earthquake being studied.

g : gravitational acceleration

C_0 : modification factor to change the spectral displacement from a single degree of freedom (SDOF) system to a roof displacement in a multi degree of freedom (MDOF) system.

C_1 : modification factor for relating the magnitude of the maximum inelastic displacement to the displacement calculated from the linear elastic response.

C_2 : modification factor to show the pinching effect on the hysteresis shape, degradation of cyclic stiffness, and a decrease in the structure capacity when it reaches maximum displacement.

3 Study Results and Discussion

3.1 Structure Capacity

To obtain the capacity of the structure, in this analysis a reference point is determined which is placed at the center of the roof mass to monitor the increase in displacement and lateral forces. The structure capacity curve is obtained by reviewing the structure under conditions of first yielding, local collapse, and global collapse (Figs. 2, 3 and Table 5).

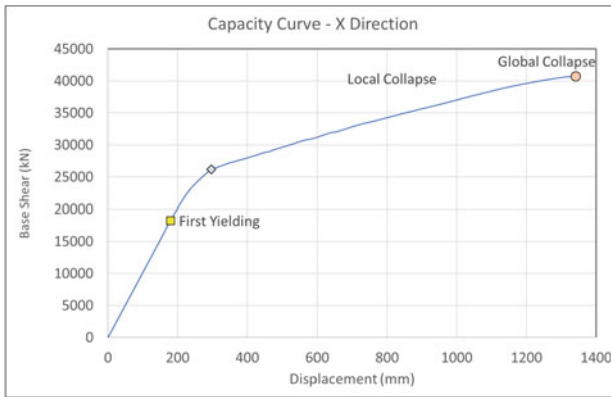


Fig. 2 X-Direction Structure Capacity Curve

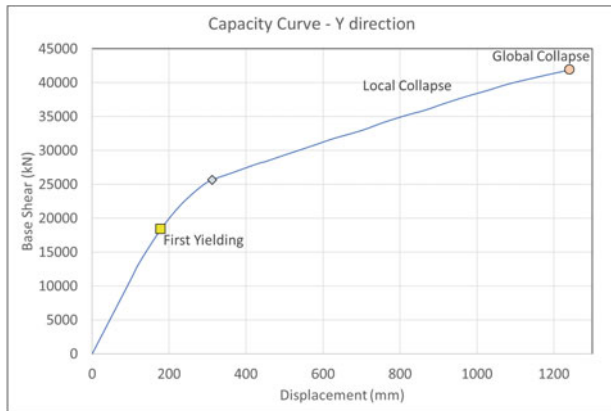


Fig. 3 Y-Direction Structure Capacity Curve

Table 5 Structural Condition Review

	First Yielding	Local Collapse	Global Collapse
X-direction			
Displacement (mm)	204.10	296.49	1342.5
Base Shear (kN)	20,747.96	26,126.97	40,676.12
Y-direction			
Displacement (mm)	149.67	312.25	1241.34
Base Shear (kN)	16,379.08	25,644.46	41,878.35

3.2 Displacement Target

Based on the results of the analysis, the parameters of the displacement target value are obtained as shown in Table 6 below.

Based on the table above, the magnitude of the displacement target value can be obtained as follows:

X-direction

$$\delta_t = 1.30 \times 1 \times 1 \times 0.28 \times 1.70^2/4\pi^2 \times 9806.65$$

$$\delta_t = 261.31 \text{ mm}$$

Y-direction

$$\delta_t = 1.30 \times 1 \times 1 \times 0.29 \times 1.64^2/4\pi^2 \times 9806.65$$

$$\delta_t = 251.88 \text{ mm}$$

Table 6 Displacement Target Parameters

Parameters	X-direction Value	Y-direction Value	
Δy	204.11	149.67	mm
V_y	20,747.96	16,379.08	kN
K_i	101,647.73	109,431.44	kN/m
K_e	101,647.73	109,431.44	kN/m
T_i	1.70	1.64	s
T_e	1.70	1.64	s
S_a	0.28	0.29	g
α	0.62	0.59	
$\mu_{Strength}$	1.69	2.22	
W	125,186.64	125,186.64	kN
C_m	1	1	
C_0	1.30	1.30	
C_1	1	1	
C_2	1	1	

3.3 Building Performance Evaluation

The lateral capacity of the frame structure increases with the increase in the capacity factor and the structural performance limit is affected by the increase in the number of stories which causes an increase in the risk of instability [10]. Based on the value of the displacement target that has been obtained and the condition of the structure being reviewed, in order to perform a safety check on the ultimate condition, the results can be summarized as follows.

Based on Table 7, is known that the value of the displacement target (demand) does not exceed the value of the displacement in local collapse conditions, therefore it can be stated that the structure performance for the evaluated both X-direction and Y-direction earthquake have met the safety requirements in the ultimate condition.

Based on the results of non-linear static analysis, it was found that in X-direction the structure went through 26 analysis steps until a sudden failure occurred at the 31th step as shown in Table 8 below while in Y-direction the structure went through several analysis steps until a sudden failure occurred at the 30th step as shown in Table 9 below.

With the X-direction displacement target value, $\delta t = 261.31$ mm, then based on the table above it can be seen that the X-direction displacement target was obtained before the analysis reached the 6th step. When the analysis reaches the 6th step where the

Table 7 Ultimate Condition Safety Check

Direction	Displacement (mm)	
	Displacement Target	Local Collapse Condition
X-direction	261.31	296.49
Y-direction	251.88	312.25

Table 8 X Earthquake Direction Analysis Results

Step	Monitored Displ (mm)	Base Force (kN)	A-IO	IO-LS	LS-CP	>CP	Total
0	-	0.000	3520	0	0	0	3520
1	50.000	5082.387	3520	0	0	0	3520
2	100.000	10,164.774	3520	0	0	0	3520
3	150.000	15,247.160	3520	0	0	0	3520
4	179.698	18,265.851	3520	0	0	0	3520
5	230.661	22,736.922	3520	0	0	0	3520
6	284.839	25,674.286	3520	0	0	0	3520
7	296.490	26,125.968	3518	0	0	2	3520
8	348.099	27,163.714	3492	0	0	28	3520
9	353.712	27,266.891	3492	0	0	28	3520
10	364.681	27,398.017	3492	0	0	28	3520

Table 9 Y Earthquake Direction Analysis Results

Step	Monitored Displ (mm)	Base Force (kN)	A-IO	IO-LS	LS-CP	>CP	Total
0	-	-	3520	0	0	0	3520
1	50.000	5,471.572	3520	0	0	0	3520
2	100.000	10,943.145	3520	0	0	0	3520
3	124.184	13,589.584	3520	0	0	0	3520
4	178.683	18,363.290	3520	0	0	0	3520
5	229.572	21,915.320	3520	0	0	0	3520
6	281.718	24,588.797	3520	0	0	0	3520
7	312.249	25,644.465	3512	0	0	8	3520
8	364.240	26,685.510	3492	0	0	28	3520
9	420.392	27,834.455	3476	6	0	38	3520
10	441.476	28,219.632	3446	16	0	58	3520

displacement value ($\delta = 284.83$ mm) has passed the X-direction displacement target, it is known that the structure performance enters the IO (Immediate Occupancy) performance level.

With the Y-direction displacement target value, $\delta t = 251.88$ mm, then based on the table above it can be seen that the Y-direction displacement target is before the analysis reaches the 6th step. When the analysis reaches the 6th step where the displacement value ($\delta = 281.71$ mm) has passed the Y-direction displacement target, it is known that the structure performance enters the IO (Immediate Occupancy) performance level.

4 Conclusion

The response of the structure indicates that the plastic hinges mechanism occurs both in the beam and the column as well. Upon reaching the performance point, in X-direction the structure response occurs the formation of plastic hinges starting from the 1st floor beams until they are distributed to the 4th floor and the ground floor columns, while in Y-direction the structure response occurs the formation of plastic hinges starting from the 1st floor beams until they are distributed to the 7th floor beams and columns. The structure is more ductile in the Y-direction compared to the X direction. The research has stated that the reinforced concrete structure possesses appropriate ductility, the failure condition is elastic in the collapse prevention category and meets the performance-based design criteria.

References

1. SNI 1726:2019 (2019) Tata cara perencanaan ketahanan gempa untuk struktur bangunan Gedung dan nongedung. Badan Standardisasi Nasional, Indonesia
2. ASCE 41-13 (2013) Seismic evaluation and retrofit of existing buildings. American Society of Civil Engineers, USA
3. ASCE 41-17 (2017) Seismic evaluation and retrofit of existing buildings. American Society of Civil Engineers, USA
4. LADBS. https://www.ladbs.org/docs/default-source/publications/information-bulletins/building-code/ib-p-bc-2020-148-procedures-for-the-application-of-asce-41-to-existing-buildings.pdf?sfvrsn=c44ff753_16. Accessed 16 Nov 2022
5. ODTU METU. <https://open.metu.edu.tr/handle/11511/15071>. Accessed 16 Nov 2022
6. Daei A, Poursha M (2021) On the accuracy of enhanced pushover procedures for seismic performance evaluation of code-conforming RC moment-resisting frame buildings subjected to pulse-like and non-pulse-like excitations. *Structures* 32:929–945
7. Dewobroto W (2005) Evaluasi kinerja struktur baja tahan gempa dengan analisa pushover. In: *Civil engineering national conference: sustainability construction & structural engineering based on professionalism*. Unika Soegijapranata, Indonesia
8. Prasetyo H et al (2020) Evaluasi kinerja struktur bangunan menggunakan pushover analysis dengan metode atc-40 dan fema 356. *Jurnal Pendidikan Teknik Sipil* 9(1):40–46
9. SNI 1727:2020 (2020) Beban desain minimum dan kriteria terkait untuk bangunan gedung dan struktur lain. Badan Standardisasi Nasional, Indonesia
10. Yahmi D et al (2017) Evaluation of behaviour factors of steel moment-resisting frames using standard pushover method. *Procedia Eng* 119:397–403

Consolidation Analysis Using Prefabricated Vertical Drain (PVD) and Preloading in the Phase I Belawan Reclamation Project with PLAXIS 2D and 3D



Gina Cynthia Raphita Hasibuan, Yunike Wulandari Br Tarigan, Roesyanto, and Rudianto Surbakti

Abstract Geotechnical experts play an important role in an infrastructure development plan in soil investigations and also in determining the condition of the soil in the phase I Belawan reclamation project along with analyzing soil mechanics, knowing the soil condition and the strength of the soil pavement layer at the port is essential for minimizing the occurrence of failures in the implementation of stockpiling in the Belawan reclamation project. This paper aims to analyze and compare the amount of consolidation settlement analytically using the Terzaghi 1 Dimension method, with the finite element method with modeling in PLAXIS 2D and 3D using coarse, very coarse, medium, fine, and very fine types with data settlement plate (S47) in the field and Analyze and compare the amount of consolidation settlement with the PLAXIS 2D and 3D finite element method with several types of fineness of the mesh with data settlement plate (S47) in the field. The amount of consolidation settlement using the analytical method using the 1-dimensional Terzaghi consolidation formula obtained a decrease of 7,012 m. The consolidation settlement with each mesh type using PLAXIS 2D obtained the following settlement data: very coarse = 7,114 m, coarse = 7,114 m, medium = 6,994 m, fine = 6,976 m, and very fine = 6,892 m. for PLAXIS 3D, very coarse = 5,682 m, coarse = 7,769 m, medium = 6,456 m, fine = 6,659 m, very fine = 6,938 m. The magnitude of the decrease that occurred in the field using the Settlement plate (S47) was 6,942 m.

Keywords Consolidation · Preloading · Prefabricated vertical drain · PLAXIS 2D · 3D

G. C. R. Hasibuan (✉) · Y. W. B. Tarigan · Roesyanto
Department of Civil Engineering, Faculty of Engineering, Universitas Sumatera Utara, Padang Bulan, Medan 20155, Indonesia
e-mail: gina.hasibuan@usu.ac.id

R. Surbakti
Politeknik Negeri Medan, Jl. Almamater No. 1, Padang Bulan, Medan Baru, Medan City, North Sumatra 20155, Indonesia

1 Introduction

Geotechnical experts play an important role in an infrastructure development plan whose duties and responsibilities are in carrying out primary surveys for soil investigations. They also serve to determine the condition of the soil in the phase I Belawan reclamation project along with analyzing soil mechanics, knowing the soil condition and the strength of the soil pavement layer at the port is very necessary for minimizing the occurrence of failures in the implementation of stockpiling in the Belawan reclamation project. Therefore, before the establishment of building construction, it is necessary to carry out an absolute soil investigation, namely to determine the natural condition of the soil layers in the port of Belawan, get examples of undisturbed and disturbed soil types, and determine the depth of each layer of soil (multilayer) until it reaches hard soil or also known as bore-log data that describes the soil conditions in the port. The results of the tests that have been carried out in the field after being checked are soft soil types, one of which is having a low bearing capacity so that it has the potential to cause losses in terms of increasingly expensive construction costs that threaten construction safety.

One solution for soil improvement techniques in the *phase I Belawan reclamation project* is the *Preloading* technique which combines with *Prefabricated Vertical Drain (PVD)*. This method was chosen because it is considered effective in accelerating soil consolidation as well as being able to reduce the total time required in the process of soil compaction by *preloading*. In this regard, PVD can also reduce the additional load required to achieve the desired soil density at the same time along with the application of temporary loads on the soil whose pressure will be equal to or greater than the design pressure. Soil stockpiling techniques combined with *preloading* with PVD (Prefabricated Vertical Drain) have great potential benefits to accelerate the consolidation process [1]. *Preloading* is a temporary load placed on a construction site that serves to optimize PVD performance and improve the bearing capacity of the subgrade where the construction will be erected. The simplest *preloading* is to use *embankment soil* [2]. PVD installation distance is generally greater than 1 meter, but according to (Fellenius, 2006 in [3], the PVD installation distance ranges between:

- For homogeneous clay: 1 to 1.6 m
- For silty clay: 1.2 to 1.8 m
- For coarser soils: 1.5 to 2 m

The first PVD installation pattern is the determination of the installation point which is usually used in certain patterns to facilitate implementation. In general, PVD is installed in a rectangular or triangular pattern. The area of influence of PVD work can be calculated by Eqs. (1) and (2) below:

$$D_e = 1,13 S \text{ (for square pattern)} \quad (1)$$

$$D_e = 1,05 S \text{ (for triangle pattern)} \quad (2)$$

where D_e is the equivalent diameter (after the cross-section is converted into a circle shape) and S is the space or distance between the PVDs. PVDs are usually installed on soft ground in a triangular or quadratic pattern with a typical distance of 1.2 to 3.5 m [4] which *Normally consolidated* is a state where the effective overburden stress is currently the largest (maximum) stress. That the land has experienced. Calculations to find the value of the *normally consolidated decrease* can be done using the ID Terzaghi method as in Eq. (3) below:

$$S_p = \frac{C_C \cdot H}{1 + e_0} \log \frac{P_0 + \Delta_p}{P_0} \quad (3)$$

With:

C_C : Soil compression index

P_0 : Effective overburden pressure

Δ_p : Additional vertical stress

e_0 : Pore number

H : Thickness of layer

S_p : primary decrease (Table 1).

Analysis of the calculation can be seen in Table 2 below.

Table 1 Material properties

Description	Unit	Material Properties						
		heap	Silty Clay 1	Fine Sand	Silty Clay 2	Silty Sand	Silty Clay 3	Clay
Model material		Mohr-Coulomb	Mohr-Coulomb	Mohr-Coulomb	Mohr-Coulomb	Mohr-Coulomb	Mohr-Coulomb	Mohr-Coulomb
Depth	meter	11,00-0,00	1,00-2,00	2,00-6,00	6,00-14,50	14,50-16,00	16,00-25,00	25,00 s/d 28,00
Drainage Type		drained	undrained	drained	undrained	drained	undrained	undrained
γ unsat	kN/m ³	13,95	7,3	6,3	6,2	7,3	6,5	6,2
γ sat	kN/m ³	18,50	15,71	15,71	15,71	15,71	17,00	18,00
E	kN/m ²	25,000	10,000	5,000	8000	5000	5000	2000
v (nu)	e	0,35	0,35	0,35	0,35	0,35	0,35	0,35
C	kN/m ²	42	6,0	6,5	6,0	6,0	6,5	6,5
ϕ (phi)	°	35,9	1	1	2	1	2	1,5
K	m/day	1	0,00,000,001	0,0005	0,00,000,001	0,000,005	0,00,000,001	0,000,005
Kx & Ky	m/day	1,E + 00	1,E-08	5,E-04	1,E-08	5,E-06	1,E-08	5,E-06
Kz	m/day	5,0,E-01	5,00,E-09	2,50,E-04	5,00,E-09	2,50,E-06	5,00,E-09	2,50,E-06
Layer Name	Preloading	1		2		3		4

Description	Unit	Material Properties				
		Sandy Clay	Silty Clay 4	Silty Clay 5	Silty	Silty Clay 6
Model material		Mohr-Coulomb	Mohr-Coulomb	Mohr-Coulomb	Mohr-Coulomb	Mohr-Coulomb
Depth	meter	28,00 s/d 32,00	32,00 s/d 41,00	41,00 s/d 44,00	44,00 s/d 46,00	46,00 s/d 60,00
Drainage Type		drained	undrained	undrained	undrained	undrained
γ unsat	kN/m ³	8,2	8,3	8,3	8,5	8,5
γ sat	kN/m ³	18,00	15,71	15,78	18,00	15,71
E	kN/m ²	2000	7000	7000	5000	8000
v (nu)	e	0,35	0,35	0,35	0,35	0,35
C	kN/m ²	6,5	6,5	6,0	6,0	6,5
ϕ (phi)	°	2	1	1	1	1
K	m/day	0,000,005	0,00,000,001	0,00,000,001	0,00,000,001	0,00,000,001
Kx & Ky	m/day	5,E-06	1,E-08	1,E-08	1,E-08	1,E-08
Kz	m/day	2,50,E-06	5,00,E-09	5,00,E-09	5,00,E-09	5,00,E-09
Layer Name	Preloading	7	8	9	10	11

Table 2 Analysis calculation results

heap phase	heap height (m)	Great Land Subsidence (m)				
		Silty Clay 1	Fine Sand	Silty Clay 2	Silty Sand	Silty Clay 3
Preloading 1	1	0,407	0,837	0,052	0,049	0,133
Preloading 2	0,3	0,108	0,184	0,015	0,014	0,040
Preloading 3	0,3	0,097	0,178	0,015	0,014	0,039
Preloading 4	0,11	0,039	0,067	0,006	0,007	0,016
Preloading 5	0,8	0,207	0,447	0,038	0,036	0,105
Preloading 6	1	0,246	0,562	0,048	0,046	0,136
Clay	Sandy Clay 4	Silty Clay 5	Silty	Silty Clay 6	Amount	
0,031	0,224	0,108	0,077	0,337	2,256	
0,009	0,067	0,032	0,025	0,143	0,637	
0,009	0,066	0,032	0,023	0,101	0,575	
0,004	0,027	0,013	0,009	0,039	0,227	
0,025	0,180	0,087	0,062	0,274	1,462	
0,033	0,233	0,113	0,081	0,357	1,855	
Total Drop (m)					7,012	

2 Results

2.1 Consolidation Calculations Using PLAXIS 2D

2.1.1 No Smear Zone Effect

Calculations and modeling on PLAXIS as shown in Figures 4.10 to 4.14 are as follows (Figs. 1, 2, 3, 4, 5 and 6):

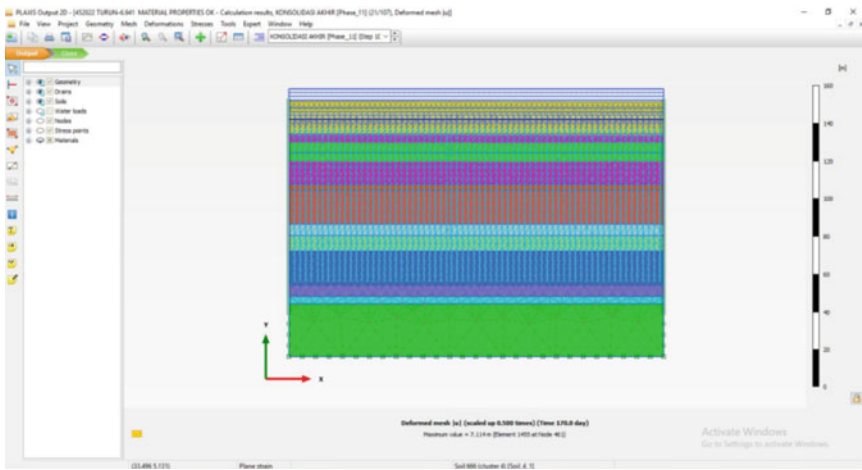


Fig. 1 Mesh fineness output results: very coarse

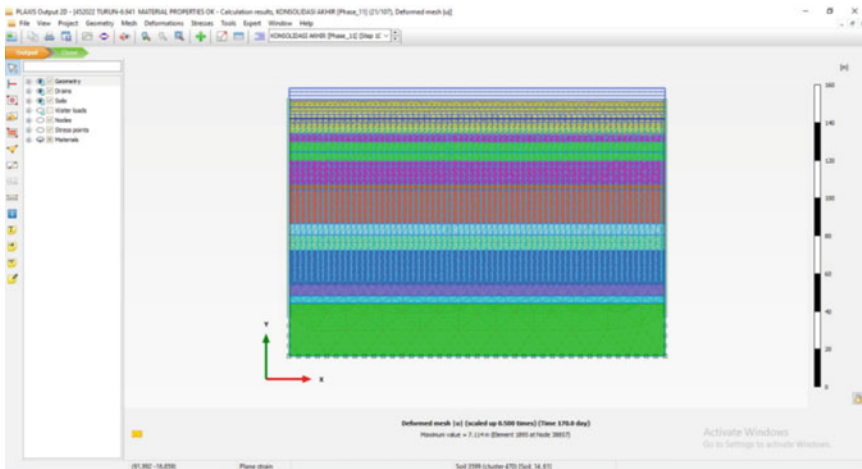


Fig. 2 Mesh fineness output results: coarse

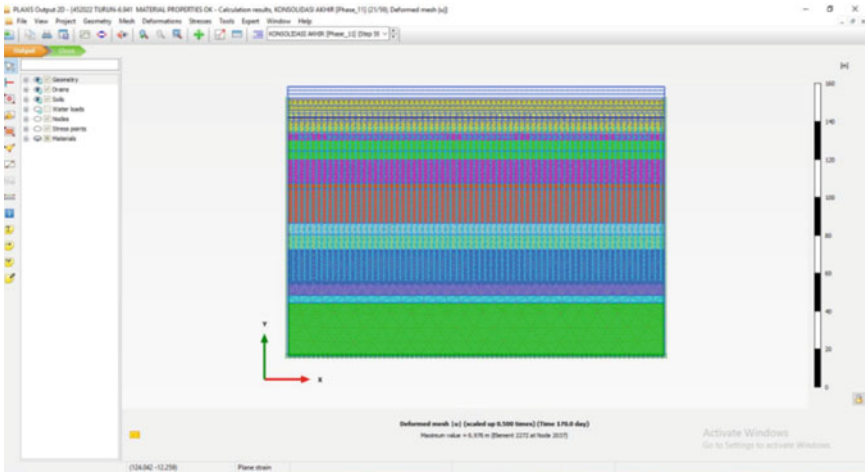


Fig. 3 Mesh fitness output results: fine

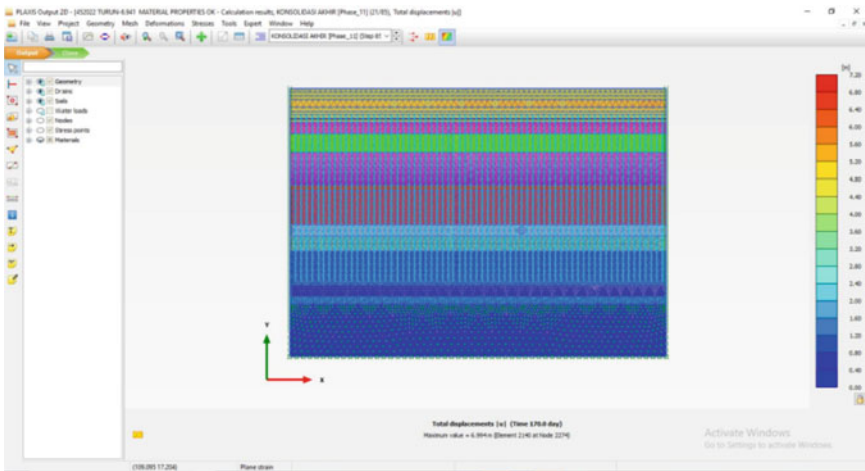


Fig. 4 Mesh fitness output results: medium

The results of the reduction in calculations using PLAXIS 2D from all stages and calculation processes are obtained as follows (Table 3):

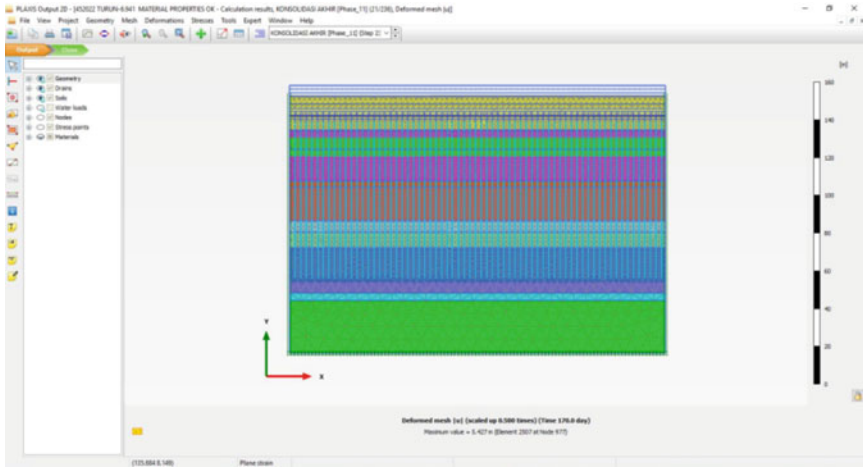


Fig. 5 Mesh fineness output results: very fine

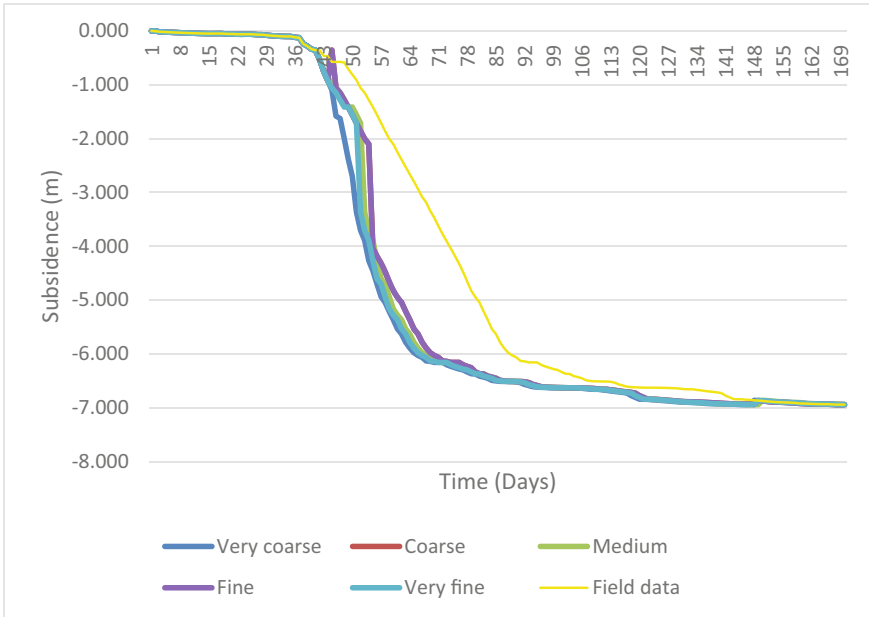


Fig. 6 Graph comparison of the decrease in fineness of very coarse, coarse, medium, fine, and very fine mesh

Table 3 Decreasing results of PLAXIS 2D analysis

PLAXIS 2D			
Mesh type	Decrease (m)	Element	Node
<i>very coarse</i>	7,114	1455	461
<i>coarse</i>	7,114	1895	38,857
<i>medium</i>	6,994	2140	2274
<i>fine</i>	6,976	2272	2037
<i>very fine</i>	6,892	3408	3055,5

2.2 Calculations with PLAXIS 3D

2.2.1 Smear zone Effect

According to [5] smear zone refers to a zone which is disturbed in soil by using a mandrel during PVD installation in which the mandrel's insertion in the PVD zone will reduce the soil k permeability. This method of PVD and Preloading to improve soil was similarly done in the runway of Kualanamu Airport in which the thickness of the soft soil is 11 m [6]. The calculation is carried out in several stages as shown in Figures 4.27 to 4.31 as follows (Figs. 7, 8, 9, 10, 11, 12, 13, 14, 15, 16, 17, 18 and Table 4):

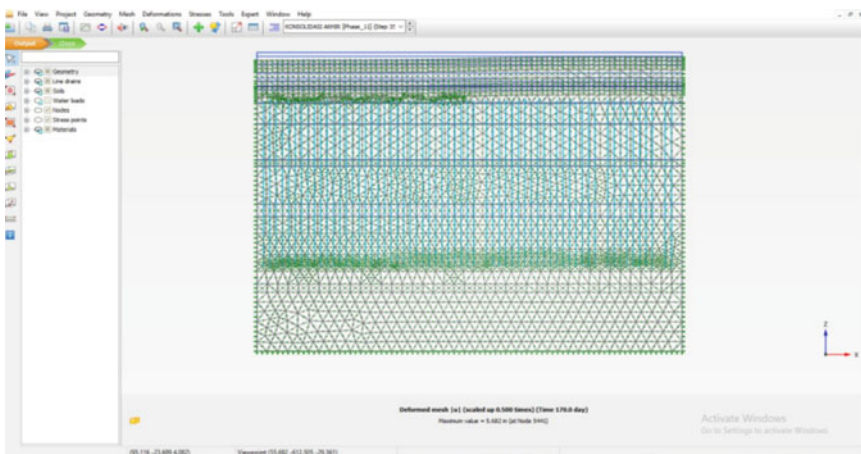


Fig. 7 Mesh fineness: very coarse

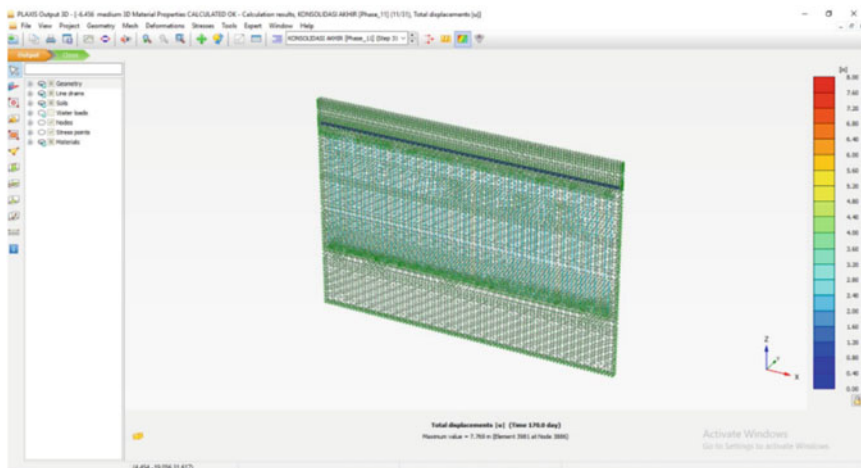


Fig. 8 Mesh fineness: coarse

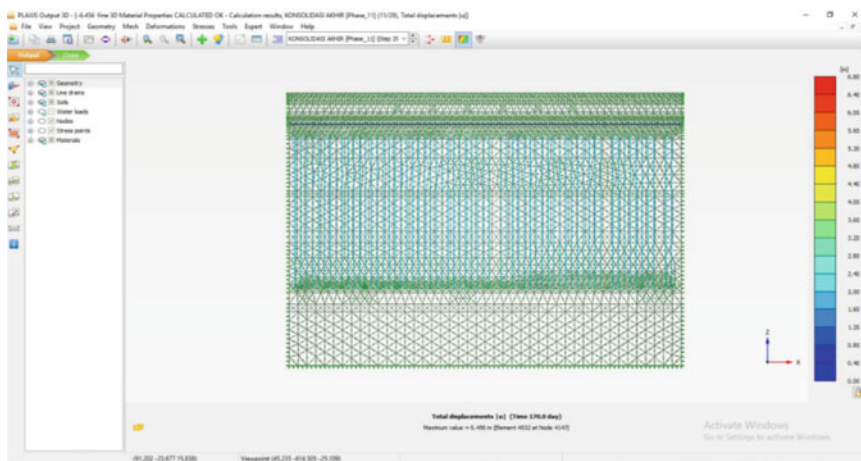


Fig. 9 Mesh fineness: medium

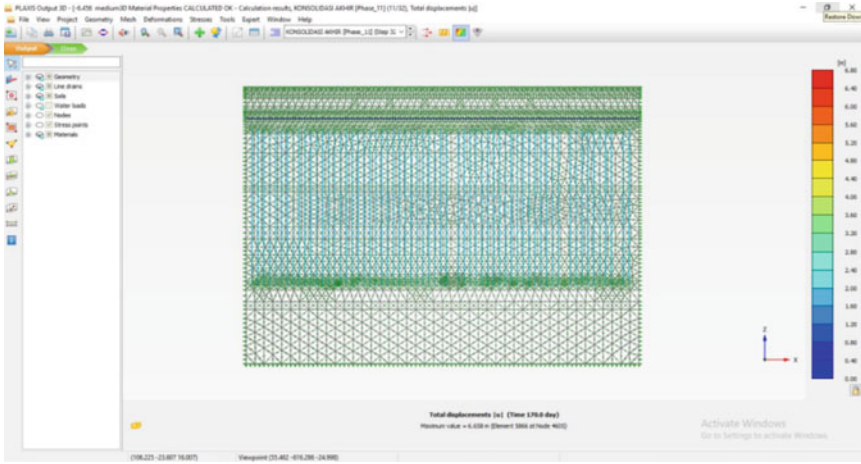


Fig. 10 Mesh fitness: fine

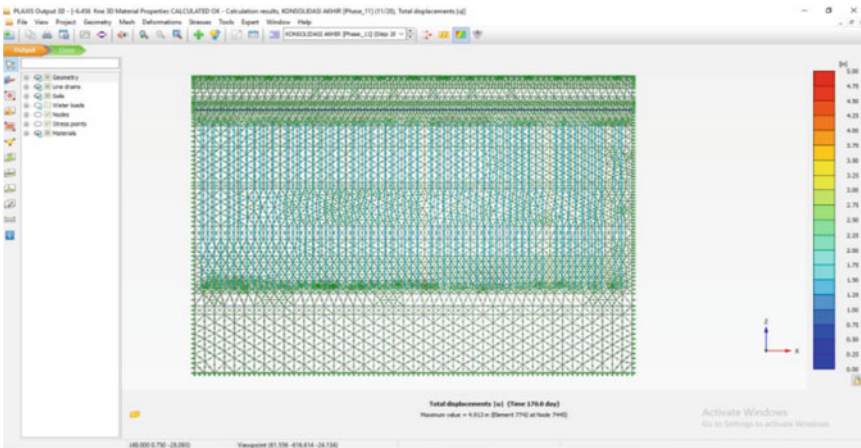


Fig. 11 Mesh fitness: very fine

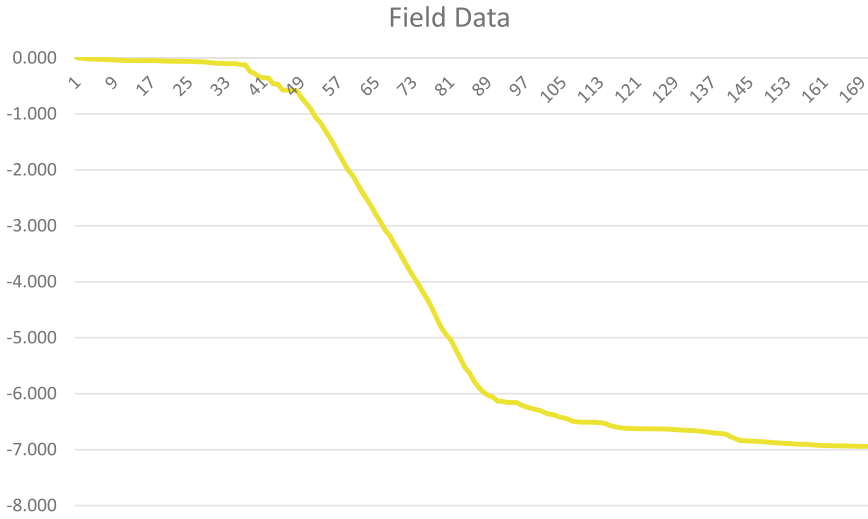


Fig. 12 Graph of field data decline

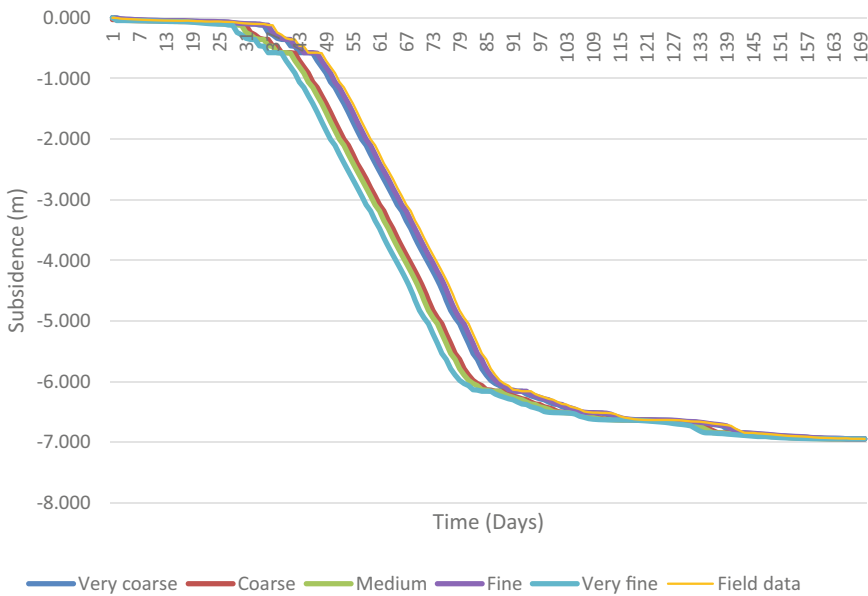


Fig. 13 Results of comparison of 3D PLAXIS data

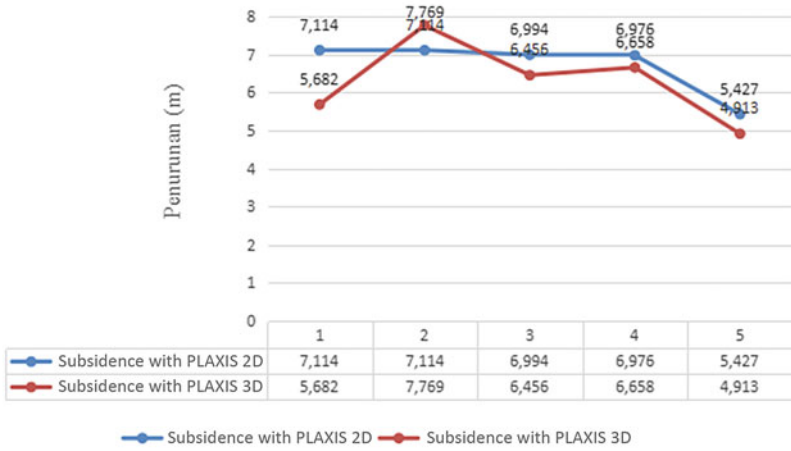


Fig. 14 Comparison results of 2D and 3D PLAXIS subsidence data

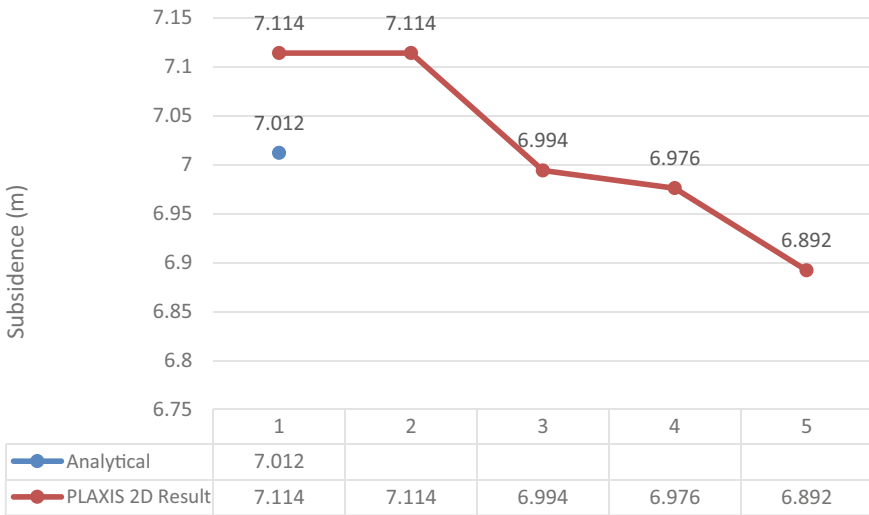


Fig. 15 Comparison results of Analytical Calculations with PLAXIS 2D results

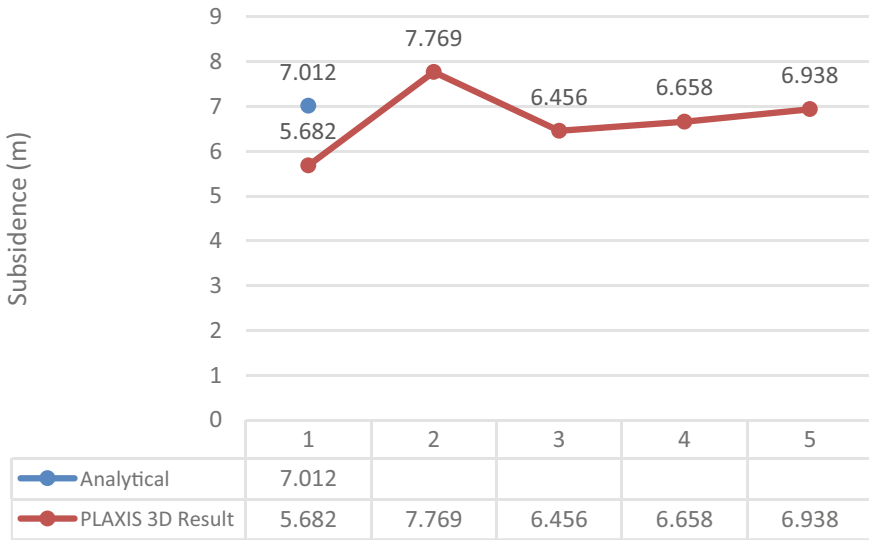


Fig. 16 Comparison of analytical data, field data, PLAXIS 2D and 3D

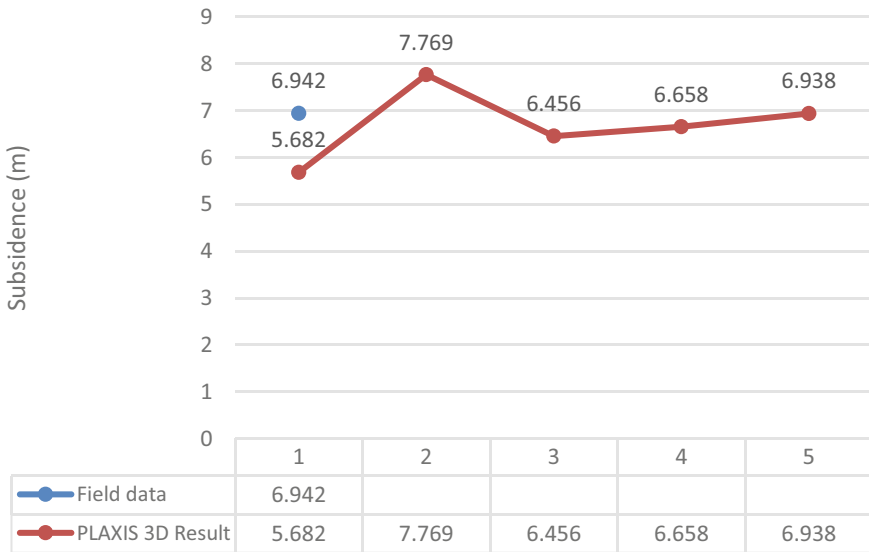


Fig. 17 Comparison of field data with PLAXIS 3D results

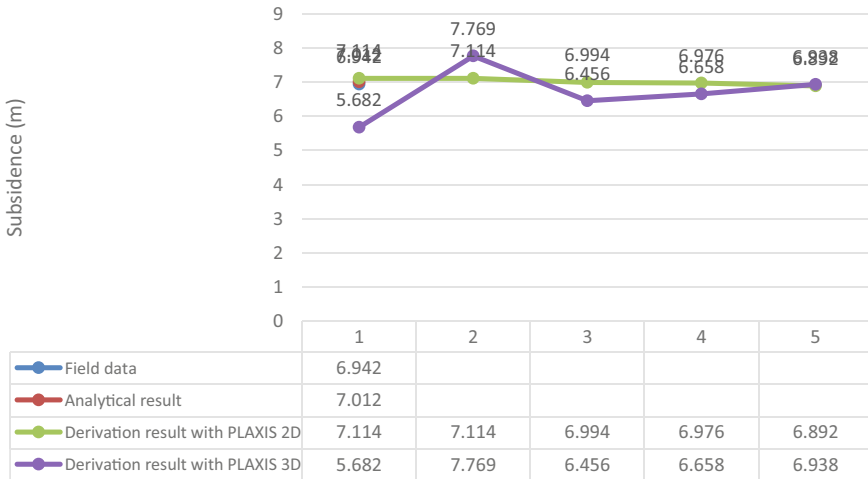


Fig. 18 Comparison results of field data reduction, analytical data, calculation results of PLAXIS 2D, and calculation results of PLAXIS 3D

Table 4 Derivation results using PLAXIS 3D

PLAXIS 3D			
Mesh type	Decrease (m)	Element	Node
<i>very coarse</i>	5,682	2608	5441
<i>coarse</i>	7,769	3981	3886
<i>medium</i>	6,456	4532	4147
<i>fine</i>	6,658	5866	4605
<i>very fine</i>	6,938	14,665	11,512,5

3 Conclusion

1. The magnitude of the consolidation settlement using the analytical method using the 1-dimensional Terzaghi consolidation formula obtained a decrease of 7,012 m. The consolidation settlement with each mesh type using PLAXIS 2D obtained the following settlement data: very coarse = 7,114 m, coarse = 7,114 m, medium = 6,994 m, fine = 6,976 m, and very fine = 6,892 m. For PLAXIS 3D, the results are very coarse = 5.682 m, coarse = 7.769 m, medium = 6.456 m, fine = 6.658 m, and very fine = 6.938 m. The magnitude of the decrease that occurred in the field using the Settlement plate (S47) was 6.942 m.
2. The results are close to the comparison of the magnitude of the settlement in the field using PLAXIS 2D and 3D modeling, respectively: fine mesh type with a drop size of 6.976 m with PLAXIS 2D. Meanwhile, with PLAXIS 3D modeling, a very fine mesh is obtained with a decrease of 6.938 m. From the calculation

results, modeling with PLAXIS 3D is proven to be more accurate than PLAXIS 2D.

References

1. Nasional BS (2017) Persyaratan Perancangan Geoteknik. BSI
2. Stapelfeldt T (2006) Preloading and Vertical Drains. http://www.wtkk.fi/Yksikot/Rakennus/Pohja/Preloading_and_vertical_drains.pdf
3. Hardiyatmo HC (2010) Mekanika Tanah. Jakarta: Gramedia Pustaka utama
4. Holtz RD (1987) Preloading with prefabricated vertical strip drains. *Geotext Geomembranes* 6(1–3):109–131. [https://doi.org/10.1016/0266-1144\(87\)90061-6](https://doi.org/10.1016/0266-1144(87)90061-6)
5. Iskandar R, Tarigan APM, Roesyanto APM (2018) A review on the characteristics of the smear zone: field data back calculation compared with laboratory testing. *Open Civil Eng J* 12(1):340–354. <https://doi.org/10.2174/1874149501812010340>
6. Roesyanto, Iskandar R, Silalahi SA, Fadliansyah (2018) Soil settlement analysis in soft soil by using preloading system and prefabricated vertical draining runway of Kualanamu Airport. In: IOP Conference Series: Materials Science and Engineering, vol. 309, no. 1, p. 012024. <https://doi.org/10.1088/1757-899X/309/1/012024>

Numerical Modeling of One-Way Reinforced Concrete Wall Panels with Openings Strengthened with Carbon Fiber Reinforced Polymer (CFRP)



M. J. Qaddura, L. W. Ean, B. S. Mohammed, and Cheng Yee Ng

Abstract The research reported in this paper is based on a comparative numerical analysis between the FE analysis conducted on RC walls by Lima et al. [1] and the physical experiment by Mohammed et al. [2]. Seventeen one-way RC walls with eccentric ($e = t/6$) were modeled. Several opening sizes were used (5%, 10%, 20%, and 30% of the concrete body total area). The results of the nonlinear analysis revealed that all walls with all possible CFRP configurations exhibited reduced deformation under load. The reduction percentage increases with opening size. On the other hand, the configuration of the CFRP affects the stress value and distribution, where CFRP sheets with 0° and 90° layout enhanced the maximum stress value by 5%. The strain value increased in areas far from the CFRP sheets and vice versa. The maximum strain occurred on the bottom corners of the openings, which explains the appearance of cracks in the concrete walls without CFRP.

Keywords Reinforced concrete (RC) wall · Carbon fiber reinforced polymer (CFRP) · Wall opening · Strengthening

M. J. Qaddura · L. W. Ean (✉)
Institute of Sustainable Energy, Universiti Tenaga Nasional, Jalan IKRAM-UNITEN, 43000
Kajang, Selangor, Malaysia
e-mail: Leewoen@uniten.edu.my

B. S. Mohammed · C. Y. Ng
Department of Civil and Environmental Engineering, Universiti Teknologi PETRONAS, 32610
Perak, Malaysia
e-mail: bashar.mohammed@utp.edu.my

C. Y. Ng
e-mail: chengyee.ng@utp.edu.my

1 Introduction

Walls are considered as important as beams and columns due to their ability to resist gravity loads [3–5]. Certain structural or functional requirements necessitate the provision of openings in the walls. Wall openings allow accessibility of the structure but affect the bearing capacity of the wall due to the extra stresses generated along the edges of the openings [6]. These stress concentrations along the edges of the openings facilitate the growth of cracks which impair the capacity of the walls [7, 8]. There are three types of openings, which are: (1) existing opening, (2) enlarged opening, and (3) new opening. In the past few years, researchers used to strengthen the edges of the openings with extra rebars on the stress areas [9], but new technologies are more effective in solving those issues by strengthening the concrete with Fiber Reinforced Polymer (FRP) [2, 10, 11]. Standard design codes developed procedures to design walls with opening, such as the Australian Standard AS3600 that instructed simplified procedures for one-way action walls, but the effect of opening can be neglected if the opening area is less than 10% of the wall and the height of the opening is less than 33% of the total height of the wall. The researchers found that the design codes have underestimated the load-bearing capacity of walls with two openings [12–14], and a significant increment of loads can be obtained if the wall is strengthened by externally bonded Carbon Fiber Reinforced Polymer (CFRP) sheets [1, 2, 15–18]. Mohammed et al. [2, 11] concluded that the different arrangement of CFRP on the one-way RC wall results in different load capacities. Two patterns of CFRP sheets were tested, 0° and 90° surrounding the four edges of the opening, and 45° sheets were placed on the corner of the opening. Thus, as recommended by Mohammed et al. [2], the latter arrangement is the best for walls with all opening sizes in terms of load bearing capacity enhancement, where the load bearing capacity of the wall with an opening is increased by decreasing the size of the opening. On the other hand, the study by Lima et al. [1] showed that 0° and 90° CFRP arrangement has a better enhancement on the load-bearing capacity of the wall than the 45° arrangement. Lima et al. [1] evaluated that the CFRP sheets are more effective to the load-bearing capacity of the one-way action wall panel with an opening when they used a combination of 0°, 90°, and 45° CFRP arrangements stacked on each other. In addition, the research is supported with numerical analysis using ABAQUS finite element solver and deployed a new design chart of designing a one-way RC wall with an opening strengthened by CFRP externally bonded without illustrating the reasons for that discrepancy between the two research. This study aims to verify the discrepancies between the two previous studies using a numerical analysis conducted by ANSYS finite element solver. Hence this will be achieved by establishing a finite element model for a one-way RC wall strengthened with CFRP based on existing experimental data.

2 Experimental and Results

2.1 Load–Deflection Curves

Figure 1. shows the nonlinear load versus deflection results of Mohammed et. al. [2] concrete walls with openings strengthened by CFRP that are modeled by ANSYS. Series 3, which has 90° and 0° CFRP layout, has a better load versus deflection than series 4, which has a 45° CFRP layout. However, series 4 has a higher failure load than series 3. Generally, the deflection against load is smaller when the RC wall has a smaller opening despite the CFRP layout. The leger in Fig. 1 has eight walls named as WO_{ij}, where *i* represents the opening size number (1, 2, 3, or 4) where the opening size is (5%, 10%, 20%, and 30% of total concrete area), and the *j* donates two letters (b or c) where b is related to the 90° and 0° CFRP layout and c for the 45° CFRP layout.

Table 1 shows the deformation on each wall. The comparison is applied by identifying the deformation at two loading stages for each wall; the first is the deformation at the failure load (late loading stage), according to Lima et al. [1] and Mohammed et al. [2], and the second is the deformation at the failure of the control specimens (early loading stage). The table shows where the location of the maximum deformation occurred. The maximum deformation location is in the middle of all the walls. Table 1 has the geometry of the walls and the openings. The last two columns of the table show the percentage of enhancement for each wall, where column 7 shows the rate of reduction in the deformation due to the CFRP strengthening at the failure load of the control specimens (early stage of loading), and column 8 identifies how the walls can deform without failing (late stage of loading). The comparison between the experimental result of Mohammed et al. [2] and the simulation result

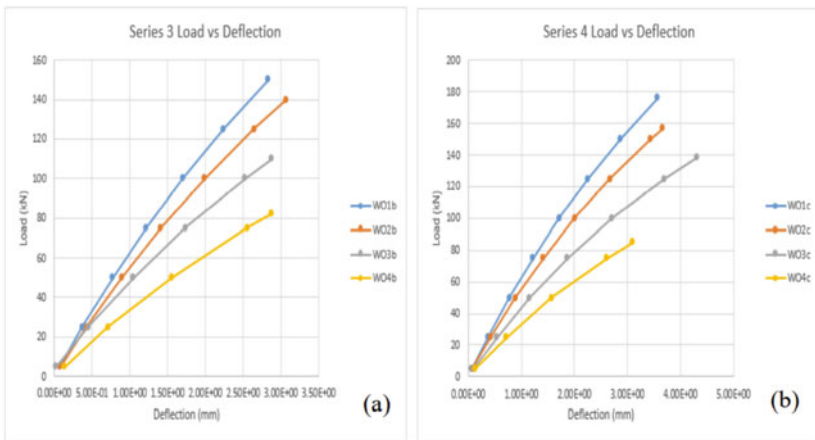


Fig. 1 Load vs. deflection of Mohammed et al. [2] series 3&4 each 25 Kn load step till failure load modeled by ANSYS

does not match in terms of load–deflection relationships. However, as expected, the simulation of the structural behavior, such as the deflection direction, maximum stress, and deflection location, is comparable to the concrete walls strengthened by CFRP sheets (at the middle) from the experimental results. According to Table 1, the CFRP sheets reduced the deformation at the failure load of the control panels, the percentage of enhancement is calculated at the failure load of the control panels, and the corresponding tested panels with CFRP that have the same opening size, the control panels are series two panels (WO1a, WO2a, WO3a, WO4a, and WO-NF). The deformation reduction percentage increased with the opening size, where series 3 have a higher deformation reduction than series four at an opening size of 5%, 10%, and 20% of the total concrete area. However, series 4 has a higher deformation reduction than series three at an opening size of 30% of the total concrete area. On the other hand, the result of load versus deflection of Lima et al. [1] panels was almost similar to the nonlinear analysis of this study, with a difference of less than 10% (see Fig. 2a&b). The best performance against load is WO-CF which conforms with the result conducted by Lima et al. [2]. However, the enhancement percentage of lateral deformation against axial eccentric load for each wall is presented in Table 1. Best deformation reduction at the control panel is found in WO-CF, which has the best performance among all the walls by Lima et al. [1]. Furthermore, the simulation of WO-CF stopped processing before the stated failure load (559 kN) by Lima et al. [1] was reached. The solver could not mathematically converge the outcomes; the last converged step was 107, corresponding to 535 kN, which shows that the model failure load is smaller than the assumed failure load.

2.2 Strain Distribution and Crack Pattern

Figure 3 shows the strain distribution on the tension side of each wall at failure load, including the control sample (without CFRP). The strain values increased at locations remote from the CRFP sheets and vice versa. The concrete panels' maximum total deformation and strain concentration are used to evaluate the crack pattern [9, 19]. The nonlinear study of the deflection behavior revealed that the largest deformation occurred in the center of the walls, as can be observed in Figs. 3 (a, c, and e) and the corresponding experimental results showing the actual cracks in Fig. 3 (b, d, and f), which are mostly horizontal due to the one-way support condition (supported on top and bottom). The maximum strain occurred on the bottom corners of the opening on all of the walls, which explains the appearance of cracks in the concrete walls without CFRP, and strain distribution on the middle area of the wall confirms the experiment result of Lima et al. [1] about the location and distribution of the horizontal cracks. Moreover, the strain concentrations on the opening's bottom corners are reduced in walls strengthened with CFRP; thus, fewer cracks appear in this area.

Table 1 Lateral deformation status of the walls

Designation	Max.Deflection Value at actual failure load (mm) (late loading stage)	Max.Deflection Value at control failure load (mm) (early loading stage)	Max. Def. Location (mm)	Hight of the wall (mm)	Opening Size (mm)	Difference with control load (%) (early loading stage)	Difference between col.2 and col.3 (%) (late loading stage)
Series 2							
WO1a	1.7132	-	400	800	170 × 95	-	-
WO2a	1.89	-	400	800	240 × 135	-	-
WO3a	2.1928	-	400	800	340 v 185	-	-
WO4a	2.5617	-	400	800	420 × 230	-	-
Series 3							
WO1b	2.8343	1.7027	400	800	170 × 95	0.61%	66.46%
WO2b	3.074	1.869	400	800	240 × 135	1.11%	64.47%
WO3b	2.8784	2.1638	400	800	340 × 185	1.32%	33.03%
WO4b	2.8725	2.49	400	800	420 × 230	2.80%	15.36%
Series 4							
WO1c	3.573	1.7113	400	800	170 × 95	0.111%	108.79%
WO2c	3.6624	1.8802	400	800	240 × 135	0.519%	94.79%
WO3c	4.3097	2.1899	400	800	340 × 185	0.132%	96.80%
WO4c	3.0998	2.479	400	800	420 × 230	3.228%	25.04%
Lima's walls							
WO-NF	6.362	-	600	1200	-	-	-
WO-AF	9.804	6.2446	600	1200	450 × 450	1.85%	57.00%
WO-DF	8.36	6.3189	600	1200	450 × 450	0.68%	32.30%
WO-WF	17.25	6.3097	600	1200	450 × 450	0.82%	173.39%
WO-CF	48	6.2064	600	1200	450 × 450	2.45%	673.40%

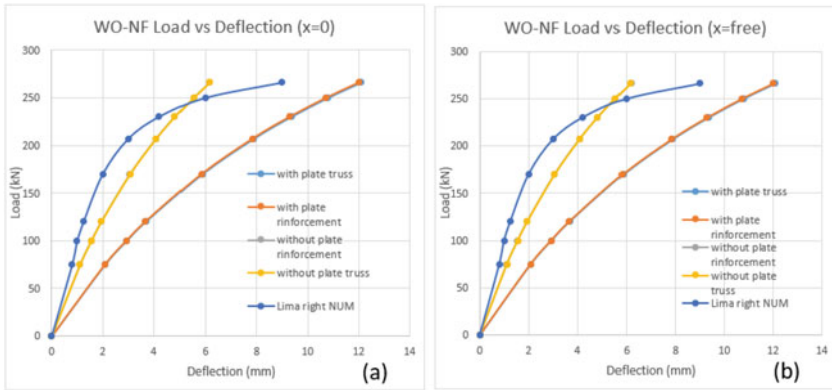


Fig. 2 Load vs deflection of WO-NF with several boundary conditions

2.3 Stress Distribution

Various techniques are available based on material failure (brittle, ductile..., etc.) to detect the stress concentration. The maximum principal stress approach is preferred for materials like concrete that exhibit brittle behavior. On the other hand, the walls of Mohammed et al. [2] were subjected to the Normal Stress technique to compare the results of the simulation and the experiment and support the findings of the nonlinear analysis. However, due to the absence of stress analysis results, the normal analysis was not applied to the walls of Lima et al. [1]. Figures 4 (a) to (q) show the stress distributions resulting from the nonlinear analysis. In contrast to the stress concentration distribution discovered by Lima et al. [1] and Mohammed et al. [2], who claimed that the maximum stress concentration was found at the edges of the openings, the maximum stress was found at various locations on the panel depending on the CFRP configuration of the wall. However, the concentration of the stress is higher at the opening’s upper edge of all Mohammed et al. [2] walls except for WO3c, which has the maximum stress value on the right side of the wall, and WO3a and WO4a, which have the maximum stress location on the bottom corners of the opening. The stress value decreased gradually from the opening edges towards the top and bottom sides. From Fig. 4, it is proved that the aspect ratio of the RC wall influences the stress concentration; the stress is concentrated at the corners of the opening when the aspect ratio equals one, as shown in the stress results of Lima et al. [1]. On the other hand, the stress concentration is redistributed on the upper edge of the openings and the right and left sides of the wall when the aspect ratio equals two, as shown in the stress results of Mohammed et al. [2]. Additionally, the CFRP sheets shift the maximum stress concentration location from the corners of the openings (in Fig. 4 WO3a and WO4a) to the upper edge of the openings (in Fig. 4 WO1b to WO4c except for WO3c). This stress concentration behavior occurred because of the CFRP effect on reducing the stress on the corners of the openings. Figure 5 shows the maximum stress value of each wall at 70 kN. Keeping in mind that the stress

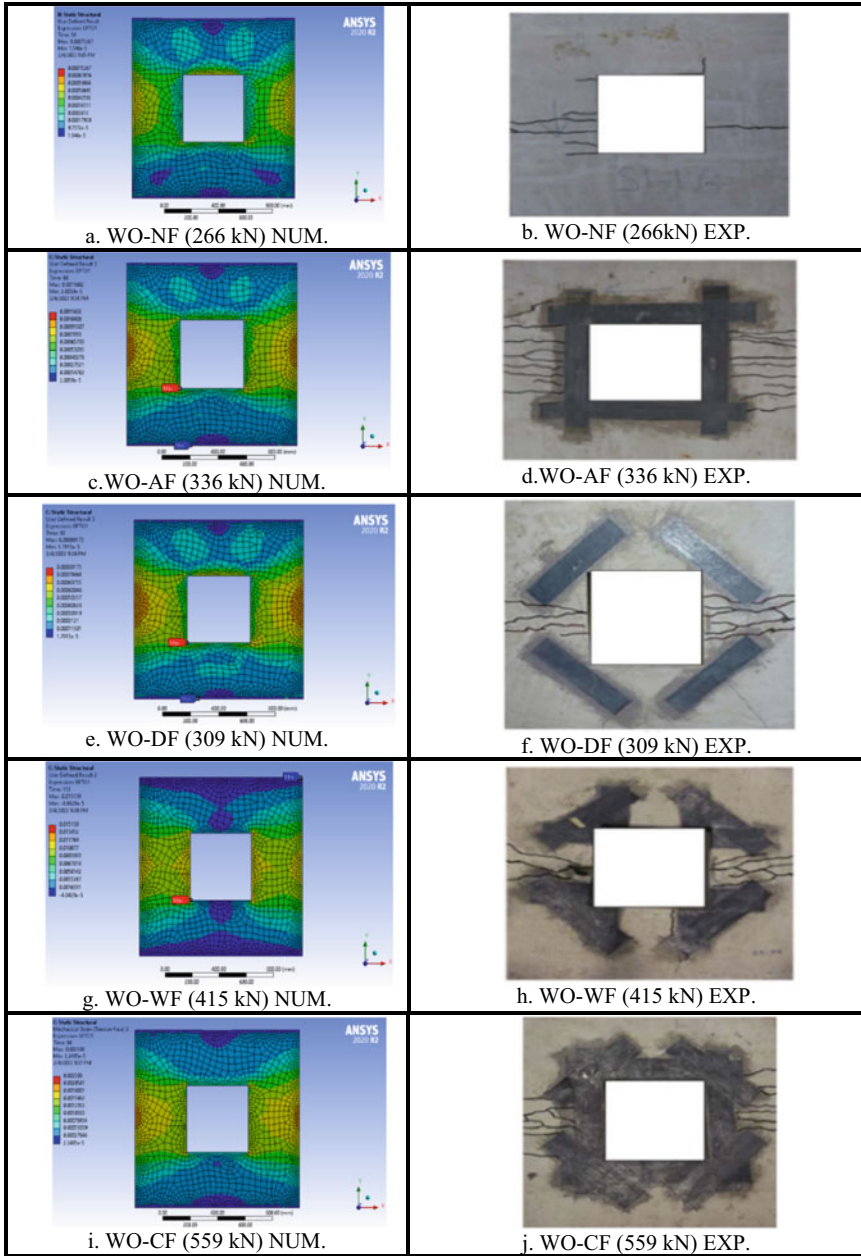


Fig. 3 Strain distribution and crack patterns

location is the same on all the walls, and the values presented are due to Mohammed et al. [2] walls only (series 2, series 3, and series 4 (WO1a to WO4c). The outcomes of Series 2 and 4 are almost similar due to the CFRP being positioned at a 45° on the corner of the openings. Because of this configuration, the upper edge of the wall is not reinforced, and the stress value is not reduced.

3 Conclusions

The conclusion of this study is based on comparative numerical analysis between the FE analysis conducted on RC walls by Lima et al. [1] and the physical experiment by Mohammed et al. [2].

1. Series 3, which has a CFRP layout of 90° along the sides of the openings, has a better load versus deflection than series 4, which has a 45° CFRP layout, which disagrees with the findings of Mohammed et al. [2] but agrees with the results of Lima et al. [1].
2. WO4c and WO1c (with a 90° layout) have the best deformation reduction at the early and late stages of loading, respectively, which disagree with the findings of Mohammed et al. [2].
3. WO-CF has the best deformation reduction at both stages of loading, which agrees with the result of Lima et al. [1].
4. The deflection against load is smaller when the RC wall has a smaller opening, irrespective of the CFRP layout.
5. The strain and deformation occurred at mid-height of all the walls, leading to the development of extra cracks in this area as established in both previous works considered.

It is recommended that different geometry, such as arc corners of the openings, should be studied, which may lead to better stress and strain distribution and fewer crack propagation.

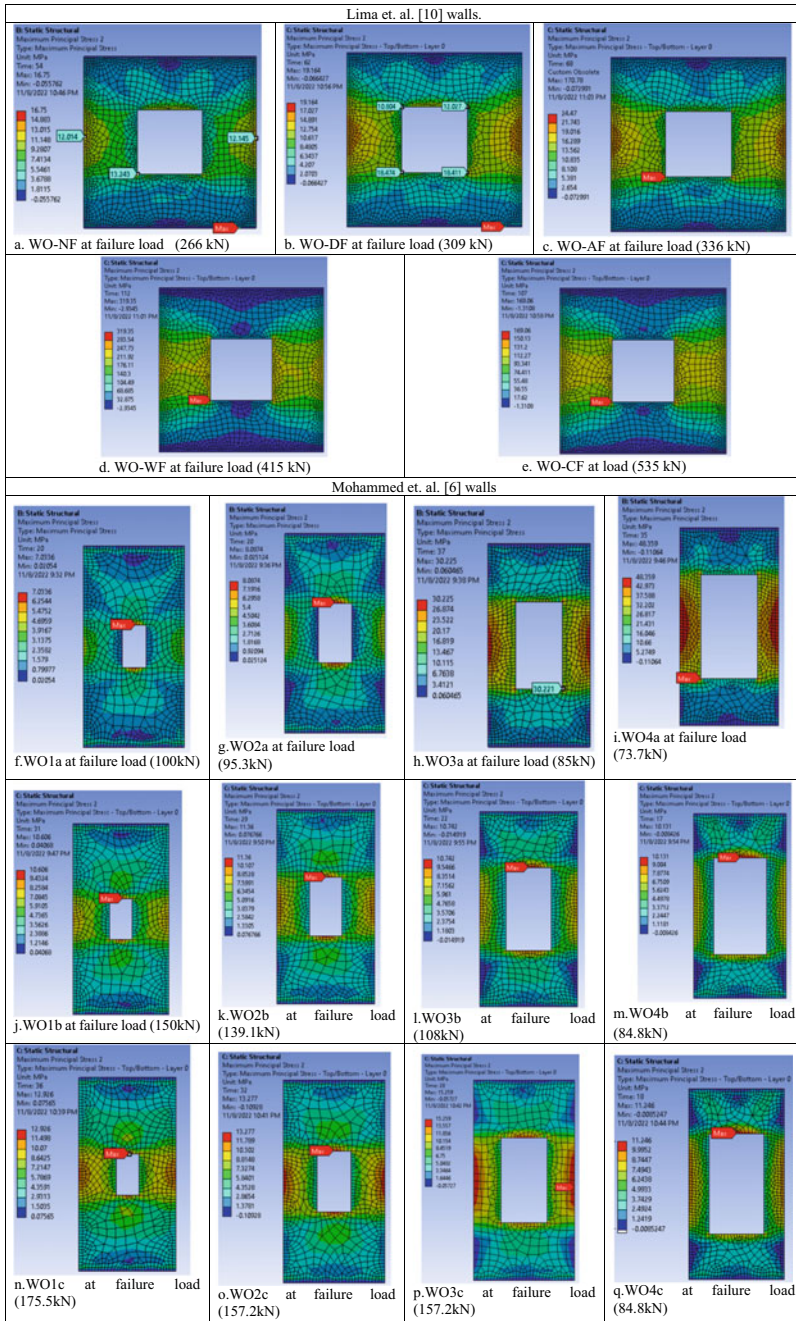


Fig. 4 Maximum values and locations of principal stresses

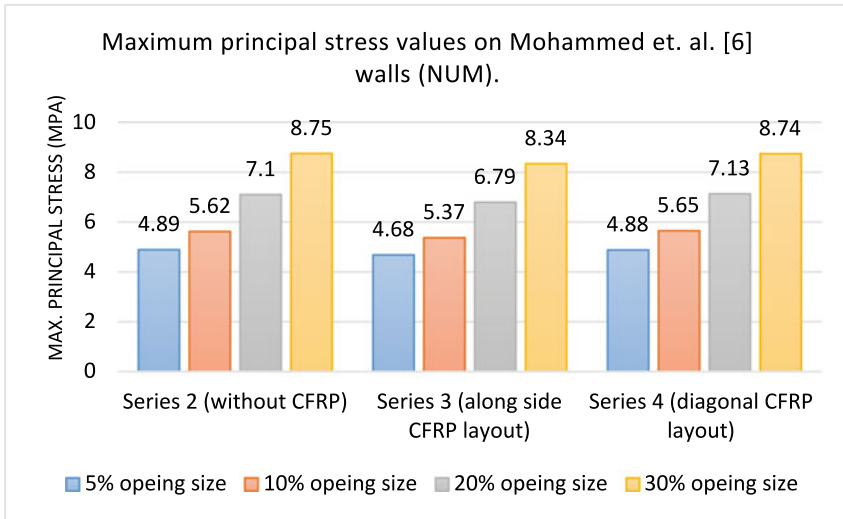


Fig. 5 Maximum principal stress value at 70 kN load for Mohammed et al. [2] walls

Acknowledgements The authors would like to acknowledge financial support from YUTP grant (015LC0-431) of Universiti Teknologi PETRONAS, and YCU Grant 2022 of University Tenaga Nasional, Malaysia. Grant code: 202210026YCU.

References

1. Lima M, Doh JH, Fragomeni S (2020) New design chart for CFRP strengthened RC walls with opening in one-way action. *Structures* 24:253–265
2. Mohammed BS, Ean LW, Malek MA (2013) One way RC wall panels with openings strengthened with CFRP. *Constr Build Mater* 40:575–583
3. Al-Fakih A, Wahab MMA, Mohammed BS, Liew MS, Wan Abdullah Zawawi NA, As'ad S (2020) Experimental study on axial compressive behavior of rubberized interlocking masonry walls. *J Build Eng* 29:101107
4. Al-Fakih A, et al. (2020) Characteristic compressive strength correlation of rubberized concrete interlocking masonry wall. *Structures* 26:169–184
5. Al-Fakih A, Mohammed BS, Wahab M, Liew M, Amran YM (2020) Flexural behavior of rubberized concrete interlocking masonry walls under out-of-plane load. *Constr Build Mater* 263:120661
6. Mohammed BS, Bakar BHA, Choong KK (2009) The effects of opening on the structural behavior of masonry wall subjected to compressive loading-strain variation. *Open Civil Eng J* 3(1)
7. Doh JH, Fragomeni S (2006) Ultimate load formula for reinforced concrete wall panels with openings. *Adv Struct Eng* 9(1):103–115
8. Al-Fakih A, Mohammed BS, Liew MS (2018) Behavior of the dry bed joint in the mortarless interlocking masonry system: an overview. *Civ Eng Res J* 4(5)
9. Saheb SM, Desayi P (1990) Ultimate strength of RC wall panels with openings. *J Struct Eng* 116(6):1565–1577

10. Aman SS, Mohammed BS, Wahab MA, Anwar A (2020) Performance of reinforced concrete slab with opening strengthened using CFRP. *Fibers* 8(4):25
11. Rahim NI, *et al.* (2020) Strengthening the structural behavior of web openings in RC deep beam using CFRP. *Materials* 13(12):2804
12. Robinson GP, Palmeri A, Austin SA (2013) Design methodologies for one way spanning eccentrically loaded minimally or centrally reinforced pre-cast RC panels. *Eng Struct* 56:1945–1956
13. Ho N-M, Doh J-H, Fragomeni S, Yang J, Yan K, Guerrieri M (2020) Prediction of axial load capacity of concrete walls with openings restrained on three sides. *Structures* 27:1860–1875 (2020)
14. Fragomeni S, Doh JH, Lee DJ (2012) Behavior of axially loaded concrete wall panels with openings: an experimental study. *Adv Struct Eng* 15(8):1345–1358
15. Lye HL, Mohammed BS, Liew MS, Wahab MMA, Al-Fakih A (2020) Bond behaviour of CFRP-strengthened ECC using response surface methodology (RSM). *Case Stud Constr Mater* 12
16. Mohammed BS, Ean LW, Hossain KMA (2011) CFRP composites for strengthening of reinforced concrete walls with openings. *Int J Eng Res Appl* 1(4):1841–1852
17. Mohammed, BS, Ean LW, Malek MA (2013) One way RC wall panels with openings strengthened with CFRP. *Constr Build Mater* 40:575–583
18. Al-Nini A, *et al.* (2020) Flexural behavior of double-skin steel tube beams filled with fiber-reinforced cementitious composite and strengthened with CFRP sheets. *Materials* 13(14):3064
19. Boyajian D, Zirakian T, Boyajian C, Chen S-E (2022) Experimental and statistical dry-fracture assessment of the CFRP-concrete interface bond. In: *Structures*, vol 36. Elsevier pp 580–588

The Effect of Transfer Function on Fatigue Life Determination in Spectral Fatigue Analysis



Arianta, Frengki Pardede, and Muhammad Sholeh

Abstract Fatigue life estimation is essential in the design phase and reassessment of structural strength. One fatigue analysis method is the spectral analysis which uses a wave spectrum in the frequency domain. This study conducted a spectral analysis on a three legs jacket structure with different transfer functions in determining fatigue life. API RP-2A recommends performing frequency selection from the wave data transfer function. The result of this study is that the fatigue life value from selecting the API RP-2A frequency is more conservative than the wave data transfer function. In the analysis process, the API RP-2A method is more efficient in terms of time and data storage.

Keywords spectral fatigue analysis · transfer function · fatigue life · wave response

1 Introduction

The fixed offshore platform structures receive various kinds of loading during their operation with wave loads which significantly affect the structure's integrity. The connection in the structure is a critical part of failure due to the stress concentration of the wave load. The stress concentration can be twice or more than the nominal stress on the member [1]. Stress cycles that repeatedly occur over a long time can cause cracks and lead to fatigue failure.

An essential step in the design stage is fatigue analysis. This analysis will estimate the life of a structure and compare it to the design life. Due to stress concentrations and the geometric effect of the type of joints, it is difficult to assess the fatigue life of tubular joints [2]. There are two methods of fatigue analysis deterministic and

Arianta (✉) · M. Sholeh
Civil Engineering, Universitas Pertamina, Jakarta, Indonesia
e-mail: arianta@universitaspertamina.ac.id

F. Pardede
PT. Singgar Mulia Engineering and Consultant, Jakarta, Indonesia

© Institute of Technology PETRONAS Sdn Bhd 2024
B. S. Mohammed et al. (eds.), *Proceedings of the International Conference on Emerging Smart Cities (ICESC2022)*, Lecture Notes in Civil Engineering 324,
https://doi.org/10.1007/978-981-99-1111-0_51

spectral analysis. The spectral analysis gives a more conservative fatigue life than deterministic analysis [1–3].

API RP 2A-WSD recommends estimating the stress range that caused the collapse by the spectral fatigue method. In spectral fatigue analysis, a transfer function shows the stress distribution at a specific spot of the structure per unit wave amplitude in the frequency domain. Defining a proper transfer function requires a frequency grid with the appropriate criteria. The transfer function is needed to evaluate the stress range value due to the wave and its importance in assessing fatigue failure.

2 Transfer Function

Ocean wave loads modeled as random waves will result in varying response structures. Each wave height with a difference in frequency or wave period will provide a varied loading. That way, the structure will undergo dynamic behavior, which can be described by a simple equation as follows:

$$M\ddot{u} + C\dot{u} + Ku = F_o \cos(\omega t) \quad (1)$$

The dynamic solution of Eq. 1 is as follows

$$(-M\omega^2 + iC\omega + K)u = F_o e^{i\omega t} \quad (2)$$

$$u(\omega t) = H(\omega) F_o e^{i\omega t} \quad (3)$$

where $H(\omega)$ is a transfer function that transfers the force to be a displacement to the structure. In spectral fatigue analysis, to obtain the displacement or stress response ($S_{xx}(f)$) of the structure, the water surface mean square spectral ($S_{\eta\eta}(f)$) is multiplied by the transfer function ($G(f)$).

$$S_{xx}(f) = |G(f)|^2 S_{\eta\eta}(f) \quad (4)$$

The transfer function produces a good structural response obtained from determining a frequency grid, especially in the natural frequency area of the structure, as seen in Fig. 1. It aims to get an accurate resonance peak, where the dynamic response can cause amplification in the structure's natural frequency area. Frequency selection to obtain the transfer function can refer to the following criteria:

- The lowest and highest frequencies are based on the frequency range contained in the wave scatter diagram.
- The wave frequencies around the peaks and valleys in the transfer function are selected to ensure the structure's response is well defined [4].

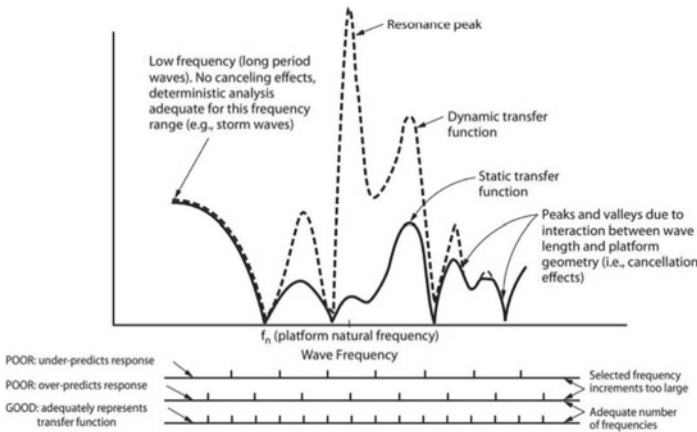


Fig. 1 Frequency selection for detailed analyses [5]

- Intermediate frequencies must be included to ensure the completeness of the form of the transfer function.
- The first three natural frequencies were selected, additional frequencies adjacent to natural frequencies (0.95fn, 0.98fn, 1.02fn, and 1.05fn), and frequencies at the center of damage [6].

3 Fatigue Life

Fatigue life is calculated based on Palmgren-Miner theory, and the API welded joint tubular (WJT) curve. Each stress range calculated from the spectral analysis results in a cycle to failure (N), and cumulated fatigue damage is obtained from Eq. 5.

$$D = \sum_{i=1}^k \frac{n_i}{N_i} \tag{5}$$

where k is the number of stress ranges considered; ni is the number of cycles applied at a particular stress range i; Ni is the allowable number of cycles under the stress range from API WJT curve.

Fatigue life in the connection components was obtained by dividing the platform’s service life by the maximum total damage of the 8 points reviewed. Joints are declared safe if the fatigue life value (tfat) obtained exceeds the minimum fatigue age value (treq).

$$t_{fat} = \frac{t_{service}}{D} \tag{6}$$

$$t_{req} = t_{service} \cdot SF \tag{7}$$

where SF is the safety factor.

4 Results and Discussion

The fixed offshore platform for the study is a three legs jacket structure with two different batters, 1:7 for leg A and 1:4 for leg B (Fig. 2). The water depth at the location of jacket platform is 31.55 m. The wave forces were analyzed omni-directionally with eight directions of incoming ocean waves, as in Fig. 3. Wave response analysis is carried out to determine the transfer function consisting of the base shear force and the overturning moment in the structure. The equivalent static load method is used to analyze the dynamic response of structures subjected to cyclical wave loads (inertia and hydrodynamic loads). The hydrodynamic load represents the actual force of the fluid calculated based on the Morison equation, and the inertia load is determined based on modal acceleration.

In the spectral fatigue analysis, the wave load is modeled as a random wave represented by a spectrum of wave energy. The wave spectrum used in the analysis is Jonswap, shallow to medium sea depths. The results of the wave response analysis are shown in Fig. 4.

The transfer function in Fig. 4 (case 1) is compared with the transfer function based on the criteria from the API RP-2A (case 2). The API RP-2A recommends fewer frequency grids according to the frequency selection discussed in the transfer function in this paper. The period range of 1 to 10 s is used to accommodate the area

Fig. 2 3D Model of Three Legs Fixed Jacket Platform

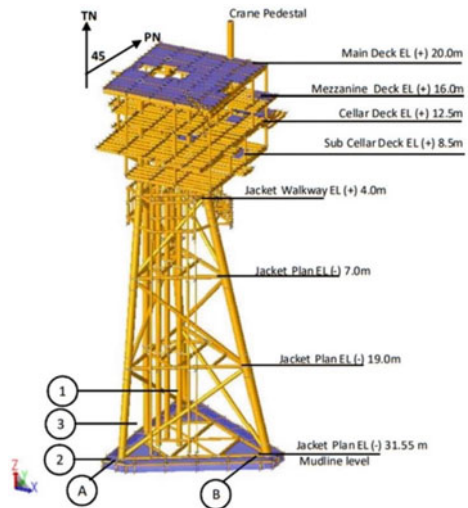


Fig. 3 Eight Directions of Wave Load

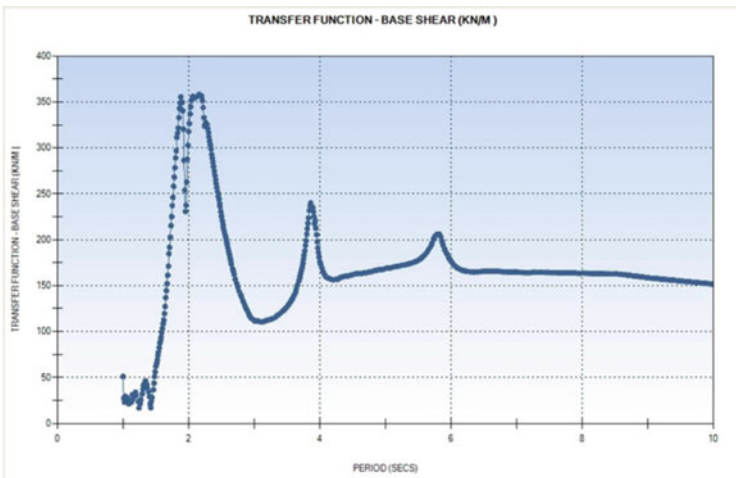
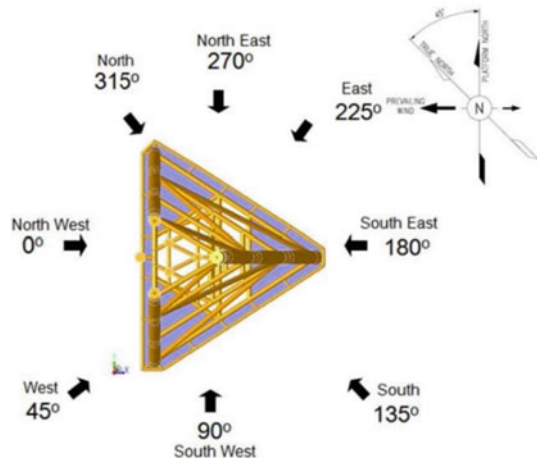


Fig. 4 Base shear transfer function at 0° direction

of the response spectrum based on the sea state/environmental conditions and the structure's dynamic characteristics. Based on environmental conditions, the wave period range is around 3–8 s, while the structure's dynamic characteristics are in the range of 1–3 s.

The frequency grid used for case 1 is from a frequency of 1 Hz or a period of 1 s to 0.1 Hz or 10 s with a delta of 0.01 s. For case 2, frequency grids are used with a minimum period of 1 s and a maximum period of 10 s with several wave periods selected based on API RP-2A. The results of the three natural frequencies obtained from the dynamic analysis can be seen in Table 1. The center of the damage period is 6.94 s (TCOD), obtained from the wave analysis. From Table 1 and the center of

damage period, the frequency value is based on the API RP-2A criteria, the frequency results can be seen in Table 2.

Furthermore, all the frequency in Table 2 is used as input into the fatigue analysis to obtain a new transfer function. The results of the transfer function in case 2 can be seen in Fig. 5. By using the scheme in API RP-2A, the number of frequencies in case 1 of which 901 frequencies can be reduced to 57 wave frequencies.

Figures 4 and 5 show that the first transfer function (case 1) with a very tight frequency grid has a relatively similar pattern to the second transfer function (case 2) with a less frequency grid. In the period range of 3 to 10 s, the first transfer function has a smoother shape than the second. Based on the results obtained, the first and second transfer functions have the same peak point of 359.588 kN/m in 2.14 s of period and a minimum value of 15.523 kN/m in 1.25 s of period. Fig. 6 shows a detailed comparison of the transfer function graph between case 1 and case 2.

Table 1 The first three periods (Tn) of the structure

Mode	Tn	A	B	C	D
		= 0.95Tn	= 0.98Tn	= 1.02Tn	= 1.05Tn
1	2.23	2.119	2.185	2.275	2.342
2	1.94	1.843	1.901	1.979	2.037
3	1.73	1.644	1.695	1.765	1.817

Table 2 Frequency selection based on API RP – 2A

Frequency	Periode	Wavelength	Wave Height	Wave Height Limitations	Remarks
Hz	Second	m	m	m	
0.14	6.95	75.35	3.75	3.75	T _{CO} D
0.43	2.30	8.25	0.41	0.41	1.05Tn1
0.45	2.23	7.76	0.39	0.39	Tn1
0.46	2.16	7.28	0.36	0.36	0.98Tn1
0.48	2.10	6.88	0.34	0.34	0.95Tn1
0.51	1.98	6.12	0.30	0.31	1.05Tn2
0.51	1.96	5.99	0.30	0.31	1.02Tn2
0.52	1.92	5.75	0.29	0.31	Tn2
0.53	1.88	5.51	0.27	0.31	0.98Tn2
0.55	1.82	5.17	0.26	0.31	0.95Tn2
0.56	1.78	4.94	0.25	0.31	1.05Tn3
0.57	1.74	4.72	0.24	0.31	1.02Tn3
0.59	1.70	4.51	0.22	0.31	Tn3
0.61	1.65	4.25	0.21	0.31	0.98Tn3
0.63	1.60	3.99	0.20	0.31	0.95Tn3

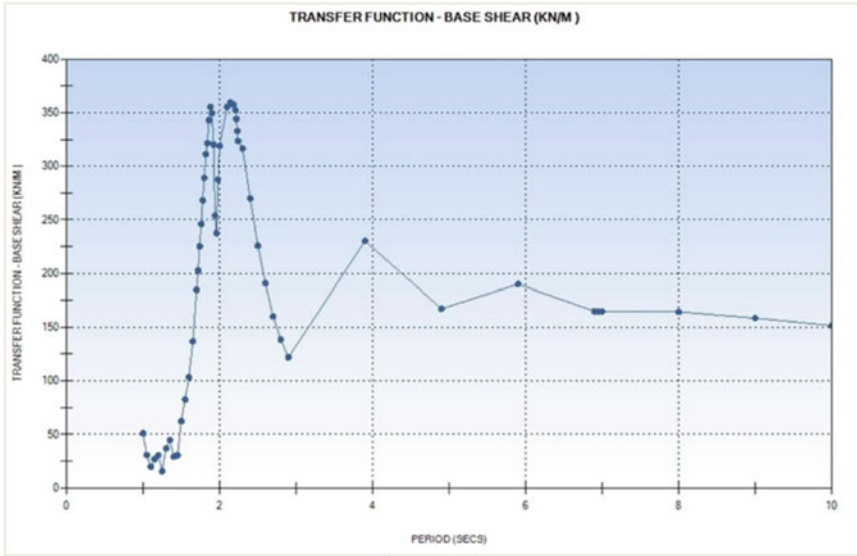


Fig. 5 Base shear transfer function at 0° direction (API RP-2A)

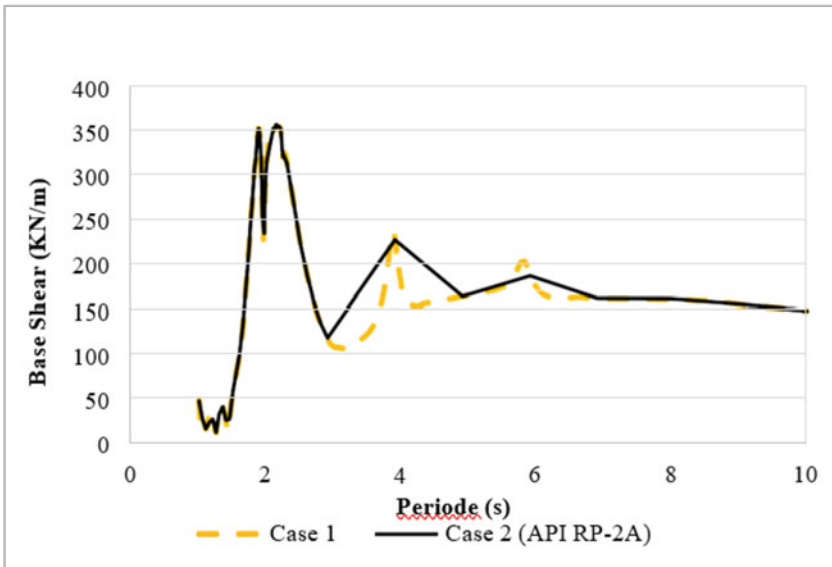


Fig. 6 Comparison transfer function

Table 3 Fatigue life comparison Case 1 and Case 2

Joint	Members	Type	Type	Case-1	Case-2	%
403L	403L - 503	Y	CHD	6562.937	5006.255	23.719
402L	402L - 502	T	CHD	77120.31	46423.39	39.804
401L	401L - 501	T	CHD	25638.37	20342.81	20.655
303L	365 - 303L	Y	Brc	35522.93	26268.85	26.051
302L	302L - 914	T	Brc	264309	182510.3	30.948
301L	301L - 320	Y	Brc	163796.4	119617.6	26.972
203L	237 - 203L	Y	Brc	714364.1	587972.8	17.693
202L	202L - 922	T	Brc	93213.45	69879.91	25.032
201L	201L - 241	Y	Brc	173493	157673.7	9.118
103L	103L - 153L	Y	CHD	90558.05	80427.59	11.187
102L	102L - 132L	T	CHD	312834.8	291536.9	6.808
101L	101L - 141L	T	CHD	366763.1	288655.8	21.296

The fatigue analysis results in Table 3 show that the fatigue life from case 1 has a greater fatigue life than in case 2, with an average difference of 21.61%. The difference is due to stress which results from the two transfer functions. The stress response depends on the area below the response density spectrum curve, resulting from the transfer function and the wave spectrum. Fig. 6 shows that the first transfer function (case 1) has a smaller area than the second one (case 2).

In terms of running time and data storage required, the transfer function with 57 wave frequencies (case 1) takes about 10 min and data of 500 MB for each wave direction. Meanwhile, the transfer function with 901 wave frequencies (case 2) takes about 360 min or 6 h to run with data of 5 GB. Thus, using the fewer frequency according to API RP-2A will provide an advantage in terms of time and save the data storage needed.

5 Conclusion

In this study, spectral analysis was used to determine the fatigue life of the 3 legs jacket structure. The load that affects the fatigue life is the wave load with eight directions. The transfer function obtained from wave analysis determines the fatigue life of the structure.

Two transfer function criteria are examined, the transfer function based on wave data (case 1) which produces 901 wave frequencies, with the transfer function based on API RP-2A (case 2) having 57 wave frequencies. The results are given that the fatigue life of API RP-2A is more conservative than case 1. In addition, API RP-2A is more efficient in terms of analysis time and large data storage with frequency selection.

References

1. Maddax NR, Wildenstein AW (1975) A spectral fatigue analysis for offshore structures. In: Proceedings of the Annual Offshore Technology Conference, pp 185–194
2. Rohith T, Jayalekshmi R (2017) Deterministic and spectral fatigue analysis of tubular joints of a jacket platform. *Int J Sci Eng Res* 8(11):149–158
3. Nallayarasu S, Goswami S, Manral J, Kotresh R (2010) Spectral fatigue analysis of jacket structure in Mumbai high field. *Int J Ocean Clim Syst* 1(3-4):209-221
4. Saadian R, Taheri A (2018) Fatigue damage analysis of an existing fixed offshore platform using spectral method for life extension. *J Mar Sci Technol* 23:877–887
5. API RP-2A (2014) Planning, Designing, and Constructing Fixed Offshore Platforms-Working Stress Desing. 22nd edn. American Petroleum Institute, Washington (2014)
6. Barltrop NDP, Adams AJ (1991) Dynamics of Fixed Marine Structures, 3rd edn. Butterworth-Heineman Ltd., Oxford

The Impact of Way Sekampung Dam Development on the Economy of the Community in Bumi Ratu, Indonesia



Ragil Arswindo, I. B. Ilham Malik, and Yudha Rahman

Abstract The purpose of this study was to examine the impact of the construction and development of a dam in Bumi Ratu Village, Pringsewu Regency, Lampung Province, Indonesia. Based on the theory, there are four variables used to measure the economic impact that occurs, namely Job Opportunities, Business Opportunities, Job changes, and Community Income. Based on the results of the analysis using inferential statistical analysis and descriptive analysis, it was found that the construction of the Way Sekampung dam has an impact on the economy in Bumi Ratu Village from four measurement variables. The construction of dams spurs economic growth by opening up job opportunities and increasing business opportunities, and another impact is a change in people's jobs and improving people's income. This research can eventually become a reference for the further development of the Way Sekampung Dam in Pringsewu Regency, Lampung Province, Indonesia.

Keywords Dam · Impact · Economic

1 Introduction

The dam is a water resource infrastructure with a high investment value in human life. Dam development can have a positive and negative impacts. The dam creates a positive impact on the economy by stimulating economic development, but the negative impact is a decrease in agricultural productivity [7].

R. Arswindo (✉) · I. B. I. Malik · Y. Rahman
Department of Urban and Regional Planning, Institut Teknologi Sumatera, South
Lampung 35365, Indonesia
e-mail: ragil.118220128@student.itera.ac.id

I. B. I. Malik
e-mail: ib.malik@pwk.itera.ac.id

Y. Rahman
e-mail: yudha.rahman@pwk.itera.ac.id

One of the infrastructure developments in Lampung Province is the Construction of the Way Sekampung Dam in Bumi Ratu Village, Pagelaran District, Pringsewu Regency. According to data from the Bumi Ratu government in 2020, Bumi Ratu Village has 2809 residents with a land area of 399 hectares, most of whom work as farmers. To get clean water, the people of Bumi Ratu village have not yet received piped network services, so they still use wells. Through descriptive analysis and inferential statistical analysis, the economic impact of the construction of the Way Sekampung Dam will be found and discussed.

2 Infrastructure Impact on Economic Development

Jafar M. (2007) states that infrastructure has a positive role in short-term economic growth through job opportunities in the construction sector, which will increase the efficiency and productivity of related sectors in the medium and long term [2]. Infrastructure is a solution needed by developing countries that want to encourage economic growth through reducing poverty, improving the quality of life, supporting the growth of economic centers, and increasing the mobility of goods and services as well as reducing the activities costs of domestic and foreign investors.

One study conducted in the USA by Munnell (1990) showed that infrastructure produces positive externalities, variables such as roads, schools, hospitals, drinking water facilities, gas, electricity, and other non-military infrastructure have a positive impact on output productivity [3]. These externalities are shown by increased productivity of the company without the company having to increase capital and labor inputs.

3 Research Methodology

3.1 Sampling Method

The data from this study were obtained through a questionnaire with the respondents being the people of Bumi Ratu village. The sampling technique in this study is cluster random sampling. According to Sugiyanto (2011), the ideal number of samples in a study is 50 to 500 samples so the number of samples used this time is 100 samples which are divided into 4 clusters with the proportion of each cluster by the number of residents of the cluster.

4 Analysis Method

First method used for this paper is Inferential statistics. [5] suggests that inferential statistics is a statistical technique used to analyse random sample data and the results can be applied to the population. Inferential statistical analysis was chosen because it can perform in-depth analysis so that conclusions can be drawn from a population. Steps used are:

- a. Hypothesis Testing the Mean Difference of Two Non-Independent Populations
- b. Determination of assumptions
- c. Determination of Hypothesis Statement
 - a. $H_0: \mu D \leq 0$, No Impact
 - b. $H_1: \mu D > 0$, Impacted
- d. Selection of Distribution of Sample Results and Determination of Critical Areas.
- e. Determination of Test Statistics
- f. Drawing Conclusions
 - 1) If the count is outside the “Critical Territory” → H_0 is accepted and H_1 is rejected
 - 2) If the count is in the “Critical Territory” → H_0 is rejected and H_1 is accepted

The second method is Population Proportion Hypothesis Test. The population proportion hypothesis test was conducted to determine whether or not there was an impact on the variables of nominal data types.

- a. Determination of assumptions
- b. Determination of Hypothesis Statement
- c. Selection of Distribution of Sample Results and Determination of Critical Area
- d. Determination of Test Statistics
- e. Conclusion
 - 1) Z is outside the “Critical Region”, then Hypothesis Zero is accepted and Hypothesis One is rejected.
 - 2) Z is in the “Critical Region”, then Hypothesis Zero is rejected and Hypothesis One is accepted.

Next method is Estimated Paired Mean Difference Interval. Test of the estimated interval of the paired mean difference was carried out to determine the description of the sampling distribution.

- a. Determining the Probability of Error = α , $\alpha = 0.05$
- b. Drawing Sampling Distribution by dividing into two Estimated average interval using distribution
- c. Creating Trust Intervals

Last method used is Descriptive analysis. A data analysis technique by describing or describing the data that has been collected as it is with the aim of concluding in general or generalizations [5].

5 Result and Discussion

The following is a synthesis of the impact of the construction of the Way Sekampung Dam on economic conditions consisting of 4 variables that have been previously analysed, namely, Job Opportunities, Business Opportunities, Job changes, and Community Income (Table 1):

The findings show that all the variables of economic assessed are affected by the construction of the Way Sekampung dam. Prasetyo and Firdaus (2009) stated that economic activity in Indonesia is still labor-intensive, while road infrastructure, electricity, and clean water have positive and significant impact on the economy [4]. Dam construction and development provides the community with job opportunities and the opportunity to open a business to fulfil the needs of the surrounding community and initially the workers.

Although the dam does not only have a direct economic impact on the Bumi Ratu village, pre-development activities such as road repairs increase the smooth distribution of goods and services, exchange of information, and other mobility. On a micro level, individual incomes and job changes have increased due to increased economic

Table 1 Result of Dam Development Impact on Economy in Bumi Ratu

Variable	Theory	Results
Job Opportunities	Infrastructure development triggers short and medium-term economic growth through job creation and increasing output productivity [2]	Job opportunities in Bumi Ratu Village were affected by the construction of the Way Sekampung dam. This is following the theory that the construction of dams provides jobs
Business Opportunities	Infrastructure development triggers short and medium-term economic growth through job creation and increasing output productivity [2]	The construction of the Way Sekampung Dam has an impact on business opportunities in Bumi Ratu Village. This shows that the development of dam infrastructure triggers an increase in community productivity
Job changes	One of the indicators of economic change as a form of impact from infrastructure development is employment [1]	Based on the findings and results of calculations, the people of the Bumi Ratu sub-district experienced a job change due to the construction of the Way Sekampung Dam. This is following the theory by Basrowi and Juairiyah
Community Income	Indicators of economic change as a form of impact from infrastructure development include income [1]	Income is one indicator of economic change in Bumi Ratu Village which is affected by the construction of the Way Sekampung Dam. By looking at the calculation results, it can be seen that the construction of the dam increases the income of the community

activity. Local economic growth has also increased in line with the growing investment climate driven by infrastructure development. Following the goal of infrastructure development, namely as an investment by the government, the Way Sekampung dam has succeeded in providing economic growth opportunities in Bumi Ratu Village. This is supported by the results of the analysis which show that after the construction of the dam, people's incomes increase, and people can adapt to new types of work without reducing productivity, thus absorbing labor.

6 Conclusion

This research aims to identify the impact of the construction of the Way Sekampung dam on the economic condition of the people of Bumi Ratu Village, Pagelaran District, Pringsewu Regency. After analysing the data obtained, the results show that the Way Sekampung dam has a positive on Bumi Ratu Village.

Positive changes created by dam development are job opportunities and business opportunities which encourage an increase in the income of the Bumi Ratu village community. Although the increase in income has not been felt evenly by the people of the Bumi Ratu village, the increase in community income has a positive impact on the local and regional economy. The increase in community income shows that the construction of dam infrastructure provides a positive externality to the place's economy. Positive changes in economic conditions due to the construction of dam infrastructure in the Bumi Ratu village are in accordance with Ja'far's (2007) opinion that infrastructure has a positive role in economic growth and supports increased efficiency and productivity of related sectors [2].

References

1. Juariyah S (2010) Analisis Kondisi Sosial Ekonomi Dan Tingkat Pendidikan Masyarakat Desa Srigading, Kecamatan Labuhan Maringgai, Kabupaten Lampung Timur. *Jurnal Ekonomi Dan Pendidikan*
2. Ja'far M (2007) *Infrastruktur Pro Rakyat, Strategi Investasi Infrastruktur Indonesia Abad 21*. Pustaka Toko Bangsa
3. Munnell AH, Cook LM (1990) How does public infrastructure affect regional economic performance? *New Engl Econ Rev* 11–33
4. Prasetyo RB, Firdaus M (2009) Pengaruh Infrastruktur Pada Pertumbuhan Ekonomi Wilayah Di Indonesia. *Jurnal Ekonomi dan Kebijakan Pembangunan* 2(2):222–236
5. Sugiyono (2015). *Metode Penelitian Kuantitatif Kualitatif dan R&D*, Bandung: Alfabeta
6. Suryono A (2010) *Dimensi-Dimensi Prima Teori Pembangunan*. Universitas Brawijaya Press, Malang
7. Wang P, Lassoie J, Morreale S (2013) A framework for social impact analysis of large dams: a case study of cascading dams on the Upper-Mekong River, China. *J Environ Manage* 117C:131-140. <https://doi.org/10.1016/j.jenvman.2012.12.045>

Gas Pipeline Stress Analysis Affected by Landslide Induced Soil Deformation



Kadek W. Ghaneswari, Rangga A. Sudisman, and Andri Mulia

Abstract The integrity of underground pipelines is critical in the gas transmission and distribution process. The effect of landslide-induced soil deformation on the stress development of an underground gas pipeline is discussed in this study. The finite element method is used to simulate soil deformation and determine its impact on pipeline stress. To represent a landslide condition on the field, soil strength parameters are reduced until the failure plane of the slope is formed. The results show that lowering the strength parameter to 15.7 kPa causes the stress in the pipe to exceed the allowable limit. To keep the stress on the pipe within the allowable stress limit, a recommendation for slope reinforcement using gabion walls at the slope's toe is made.

Keywords Finite element method · landslide-induced deformation · slope stability · underground pipeline

1 Introduction

Indonesia has a total length of 11,417.5 km of gas transmission and gas distribution pipelines that span various geographical and geological conditions [1]. Onshore gas pipelines are buried 1.5 to 2 m deep. Gas pipelines buried in landslide-prone areas will suddenly receive additional loads if a landslide occurs. Due to overstress, this incident may cause the pipeline to deform and fail. It may result in financial losses and danger to the surrounding community.

K. W. Ghaneswari · R. A. Sudisman (✉)
Faculty of Infrastructure Planning, Universitas Pertamina, Jakarta, Indonesia
e-mail: rangga.as@universitaspertamina.ac.id

K. W. Ghaneswari
e-mail: 104116001@student.universitaspertamina.ac.id

A. Mulia
PT. Nur Straits Engineering, Department of Engineering, Bandung, Indonesia

© Institute of Technology PETRONAS Sdn Bhd 2024
B. S. Mohammed et al. (eds.), *Proceedings of the International Conference on Emerging Smart Cities (ICESC2022)*, Lecture Notes in Civil Engineering 324,
https://doi.org/10.1007/978-981-99-1111-0_53

Unstable ground can induce landslides and pose a significant threat to buried pipelines since they can generate permanent ground displacement along or across the pipeline alignment [2]. Landslides and their effects on pipelines can occur in several ways depending on the landslide elevation relative to the buried pipelines. If the soil fails above a pipeline, it may cause impact loads. If the soil fails below a pipeline, it causes unintended spans. And if the soil fails on the ground crossed by a pipeline, it causes high compressive (or tensile) strains and pipeline buckling [3].

Soil loading acts in three general plan configurations: perpendicular to the pipeline (perpendicular), parallel to the pipeline alignment (parallel), or somewhere in between (oblique). Pipelines are frequently routed sub-parallel to slope contours in more mountainous terrain, either along ridge lines, valley bottoms, or via side hill cuts. Not all landslides that reach the pipeline result in pipe rupture. Some may only cause exposure, while others may result in bending or buckling [2].

When the driving loads reach the slope's maximum resistance, it begins to move or fails. This soil movement has the potential to significantly increase the load on the pipes. The response of the pipe is determined by the surrounding soil conditions, the geometrical condition of the slope, the characteristics of the pipe, and the pipe-soil interaction. Moving soil across a buried pipe causes displacement and stress on the pipe. The moving soil across or along a buried pipe should be simulated to analyze the pipeline's conditions and its hazardous potential.

This study aims to examine the displacement and stress of a pipeline caused by a landslide by using the Finite Element Method (FEM) simulation to determine the stress in the pipeline as well as the deformation of the pipeline and the soil around the pipe. This study also gives a mitigation recommendation to prevent the overstress of the pipeline due to a landslide.

2 Method

2.1 Preliminary Landslide Simulation

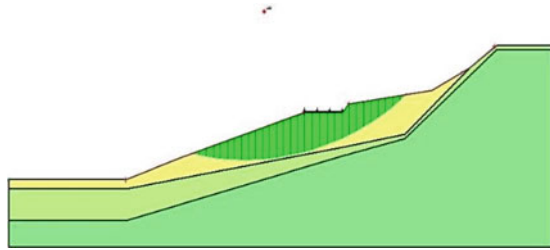
A 2-dimensional slope was modeled by using the Limit Equilibrium Method (LEM) as a preliminary design to obtain the critical soil strength at failure and the general slope failure. The preliminary design result from the LEM simulation was used as a reference in the FEM-based 2D Plane Strain model. There are several assumptions that have been made as part of the simulations, including: flow velocity and density are constant in time and space; trenching and backfilling are not included in the construction stage (in-place analysis); and frictional pipe-soil interaction follows the Coulomb friction law with a constant friction coefficient.

The slope was modeled using various models available in the GEOSLOPE software to obtain critical soil cohesion. It is noteworthy that the LEM solution was not necessarily an upper or lower bound, but it provided a factor safety value that was close to the exact solution for most slopes [4]. The LEM is combined with the

Table 1 Critical soil cohesion at failure

Method	Soil Cohesion (kPa)
Morgenstern-Price	18.55
Spencer	18.55
Janbu	18.92
Bishop	18.55
Ordinary	18.55

Fig. 1 Slope failure plane based on LEM analysis



strength reduction method to get the critical soil cohesion at failure. The method was conducted by progressively reducing the shear strength of the material to bring the slope to a state of critical equilibrium. The self-weight of the soil and road pavement on the slope was included in the applied loads on the 2D models for both LEM and FEM. Table 1 shows the soil cohesion result for the upper layer of soil when FS = 1 with various LEM models, and Fig. 1 shows the general slope failure.

The preliminary simulation value of 18.55 kPa in soil cohesion is then used as a reference in a FEM back calculation using ABAQUS. To obtain a more accurate result, the FEM is used. This is due to the LEM’s slope failure being limited to a circular or log spiral slope failure, whereas the FEM can provide a more realistic result of soil cohesion value and slope failure as it occurs on the real slope. An ABAQUS model was created using the 2D Plane Strain with CPE8ER (an 8-node biquadratic plane strain quadrilateral, reduce integration) element and a material modelled as elastic-perfectly plastic Mohr–Coulomb. As a result, with the slope failure plane shown in Fig. 2, the FEM soil cohesion value is greater than the LEM cohesion value of 20.4 kPa. The cohesion values were not significantly different, with less than a 10% difference. Figures 1 and 2 show that the FEM slope failure is similar to the LEM result but with a non-circular shape failure.

2.2 3-D Landslide-Pipe Model

Strength Reduction on Finite Element Method. A back calculation using the strength reduction method can be used to determine the approximate value of the pre-failure condition on a slope that has experienced a landslide. A Mohr–Coulomb

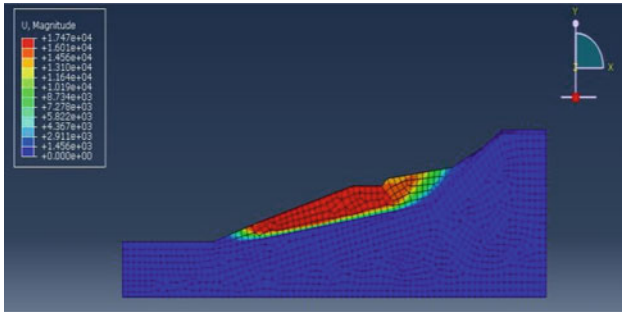


Fig. 2 Slope failure plane based on 2-D FEM analysis

elastic–plastic soil model is used in this study, while the pipe is assumed to be an elastic material. The soil strength is gradually reduced until the slope fails. The strength reduction method is used based on a case study done by Susila and Agrensa [5], which discusses the interaction between pipes and soil related to soil mass transfer by reviewing the displacement that occurs in three sizes of pipes buried on a slope; 16'' (1), 16'' (2), and 20''.

Soil Pipe Interaction. The soil pipe interaction is governed by the Coulomb Friction Law, with a constant friction coefficient throughout the model. FEM is used in which the soil is assumed to be an independent spring in three orthogonal directions, so that soil deformation in one direction has no effect on the interaction of pipe and soil in the other. A shell element represents the pipe, while a solid element represents the soil. The ABAQUS simulations used to study the soil pipe interaction begin with geostatic analysis to determine the initial stress and slope failure. ABAQUS will perform the analysis for the geostatic process and determine the equilibrium stress value between the gravity load and the restraint exerted on the soil [7].

Model Parameter and Geometry. According to the soil investigation report obtained after the landslide, the slope was modelled using a 3D deformable solid model comprised of three layers of soil. As shown in Fig. 3, the slope has a landslide width of 60 m. Throughout the model, landslide-prone slopes are assumed to have a consistent pattern of failure. An additional width of 30 m is added to both sides of the model to avoid the effect of restraints on the ends of the analyzed pipe. In this case study, the pipe buried on the slope is a 24'' diameter pipe buried 2 m underground and modelled as a 3D Shell.

The soil parameters used in the model are shown in Table 2. The soil cohesion of the first layer is a cohesion whose value is sought by using back calculation to obtain soil parameters at the initial conditions. These initial conditions are then used for analysis of soil interaction with pipes buried in it. The 24'' diameter pipe was modeled as an elastic material with the pipe specification shown in Table 3.

To improve the accuracy of the calculation in the sliding part, the meshing of the FEM model is made more detailed for the upper soil layer and the pipe buried

Fig. 3 3D model of slope and pipe

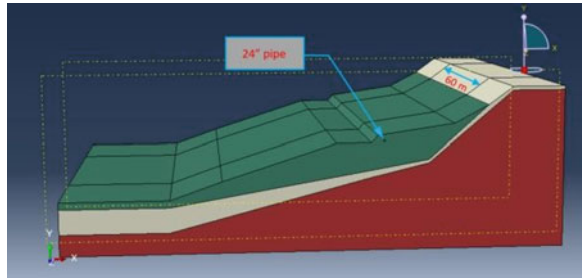


Table 2 Soil parameters

Soil Type	Weight Density (ton/m ³)	Elasticity Modulus (kPa)	Cohesion (kPa)	Friction Angle (°)	Poisson Ratio
Silty Clay	1.70	3,000	30	0	0.40
Medium Silty Clay	1.80	20,000	100	0	0.35
Stiff Silty Clay	1.85	25,000	150	0	0.35

Table 3 Pipe specification

Description	Specification
Pipe material	API-5L-X46
Outer diameter	24-inch (0.609 m)
Thickness	17.48 mm
Unit weight	7.8 ton/m ³
Elasticity modulus	2,056 × 10 ⁵ MPa
Ultimate stress	434.37 MPa
Yield stress (SMYS)	317.16 MPa
Poisson ratio	0.3
Internal pipe pressure	38 bars (3,800 kPa)

in it. The soil was modelled with element type C3D6 (A-6 linier node triangular prism), which allowed three translation degrees of freedom in the x, y, and z directions and yielded approximately 60,419 elements. The pipes were modelled with element type S4R (a 4-node doubly curved thin or thick shell, reduced integration, hourglass control, finite membrane strains) and quad free element control, yielding 4,008 elements. Figure 4 depicts the model meshing results.

The soil pipe interaction is defined as a tangential force and a normal force, with tangential behavior represented by a coefficient of friction of 0.3 and normal behavior defined as “hard contact”. To describe the contact that occurs between the pipe and the soil, the pipe and soil are given constraints in the form of embedded regions on the pipe and the soil around the pipe.

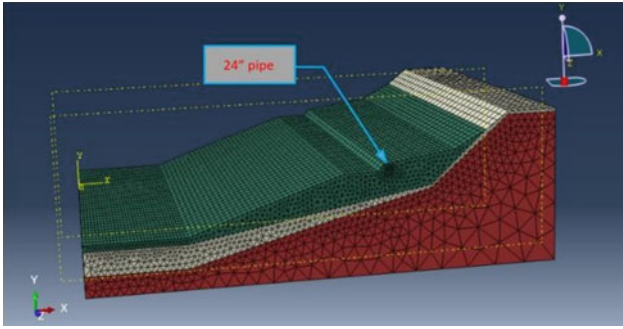


Fig. 4 Model meshing result

The calculation steps for this simulation are divided into four steps, consisting of one geostatic step and three static steps. First, geostatic step, or gravity loading, was defined by generating overburden pressure via gravity. However, soil displacement resulting from gravity loading was kept to a minimum until stress equilibrium was achieved. Second, in the first static step, the pipeline was inserted by activating the pipeline model into the soil mass without considering trenching and installation processes (in-place analysis). The second static step is to apply internal pressure of 3,800 kPa that occurs in the pipeline. The final static step is to reduce the strength parameter of the upper soil layer in order to obtain any potential soil movement.

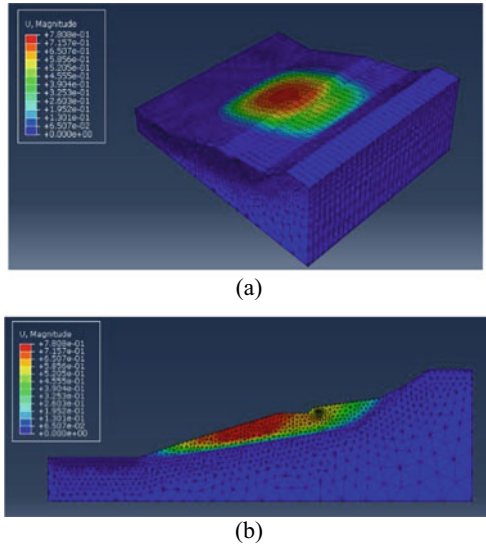
3 Result and Discussion

3.1 3-D Landslide-Pipe Simulation

The discussion of the study's findings focuses on the pipe-soil response and mitigation recommendations. The soil strength is reduced until the pipeline's stress reaches its allowable stress, which is 80% of its specified minimum yield strength. When the allowable stress of the pipeline was reached, the critical value of soil cohesion for the upper layer was 15.7 kPa. This value was smaller and more conservative than the results of the 2D Plane Strain simulation, which was 20.4 kPa. In a 2D plane strain model, soil is assumed to fail along the pipe's longitudinal axis. While there is a limited amount of soil failure in a 3D model, it also receives more restraint from both sides. This difference occurs as a result of an interaction between the failed and non-failed segments, as shown in Fig. 5.

During the final step of the calculation, the strength reduction factor was used to monitor the analysis progress, which can also be defined as a comparison between the existing shear strength of soils and the shear strength of soils at failure. The maximum soil deformation occurs in the slope, which has an effect on the soil around the pipe

Fig. 5 Soil deformation:
a 3-dimensional;
b 2-dimensional cross section

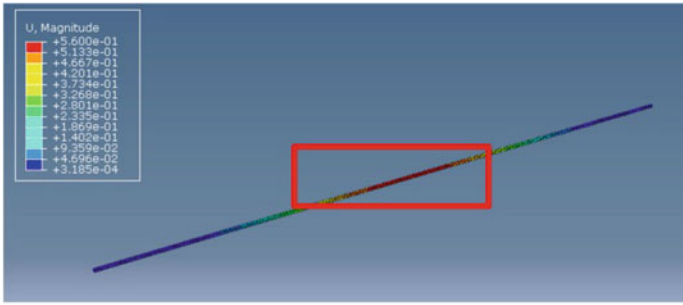


because the pipe position is in the slope plane failure, so the pipe is very likely to deform due to soil deformation.

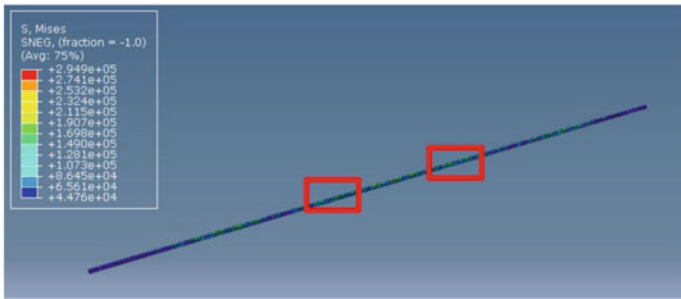
3.2 Pipe Stress Analysis

When the ground moves and collides with the pipe, the pipe will maintain its position due to its own weight and the restraint provided by stable soil. Because of soil deformation, the process of maintaining their position will increase pipeline stress. Figure 6 depicts the pipe deformation and pipe stress caused by soil deformation. The maximum pipe deformation is depicted in Fig. 6(a). It is in the slope failure plane, and the soil surrounding it was deformed during the slope stability analysis. Figure 6(b) depicts the maximum pipe stress location. They are positioned between the failing and stable soil segments. This occurs as a result of the pipe in the transition segment experiencing two events: maintaining its own position and moving with the soil.

Because the pipeline is located on a hill in a sparsely populated area, it is classified as a Class 1 pipe based on ASME B31.8–2003. This category is used to calculate the design factor of the pipe allowable stress, which is 0.8. The pipe allowable stress value is 253.73 MPa, which is the minimum requirement that should be met in this analysis. Figure 7 depicts the analysis’s findings, which show the relationship between soil movement and pipe stress. The stress on the pipe increases as the deformation increases. As we can see, the pipeline reaches its allowable stress when it is deformed by 43.6 cm due to soil deformation of 60.2 cm. The pipe may get overstressed due to 78 cm of soil deformation. The result also demonstrates that pipe



(a)

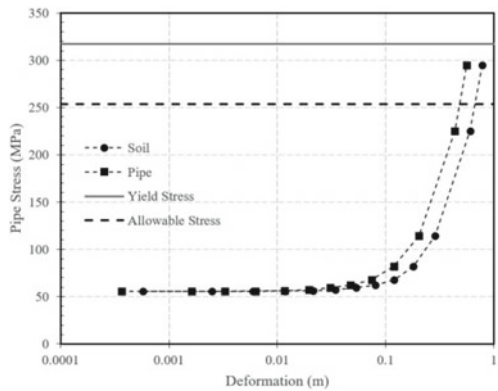


(b)

Fig. 6 **a** Location of maximum pipe deformation; **b** Location of maximum pipe stress

deformation is less than soil deformation due to the pipe's strength and restraints from stable soil on both sides.

Fig. 7
Deformation – Pipeline
Stress relation



3.3 Slope Reinforcement Analysis

Slope reinforcement is performed to keep the pipeline stress within allowable limits when the existing soil strength on the slope is reduced. Gabion was chosen as the slope reinforcement material to maintain slope stability. The gabion design plan is depicted in Fig. 8, with the toe of the slope backfilled up to one meter high to increase the bearing capacity of the soil beneath the gabion.

The stability was analyzed by comparing the slope safety factor to the overturning moment, sliding capacity, and bearing capacity. Each evaluation yielded a safety factor of 35.95 against overturning moments, 4.06 against sliding, and 30.75 against bearing capacity, indicating that the safety factor obtained met the minimum safety factor requirements. The slope reinforcement with gabion was also simulated, as shown in Fig. 9, to evaluate the pipeline condition after slope reinforcement.

After the slope is reinforced, soil deformation is reduced by 74%, pipeline deformation is reduced by 66%, and pipeline allowable stress is reduced by 58%. Figure 9

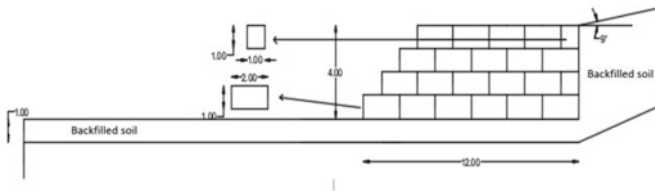
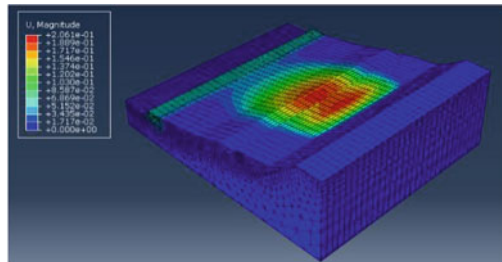
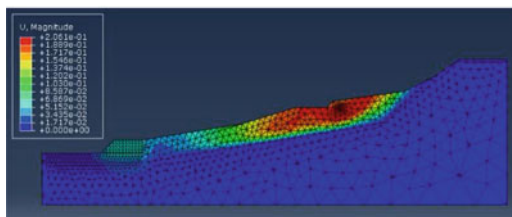


Fig. 8 Gabion reinforcement design

Fig. 9 Soil deformation after slope reinforcement:
a 3-dimensional;
b 2-dimensional cross section



(a)



(b)

shows how the slope failure plane has changed as a result of gabion slope reinforcement. This could happen because the gabion retains some of the soil on the toe and the pipe is kept in place to prevent soil movement from the top of the slope.

The dynamic loading effect on the slope stability after reinforcement also needs to be evaluated. It was carried out using the 2D Plane Strain model on ABAQUS. Slope stability is reviewed based on static and dynamic loads (pseudo-static analysis) in the form of earthquake loads. As a result, the slope safety factor with static loading shows a value of 1.4 and 1.2 under dynamic loading. The safety factor value after reinforcement shows that the slope stability meets the minimum requirement. As a result, the use of gabion walls as slope reinforcement is effective to prevent overstressing of the pipe.

4 Conclusion

Based on the results of the analysis, we can conclude that the Finite Element Method with ABAQUS can be used to simulate a landslide condition and its effect on a pipeline buried in a slope. If the slope's soil cohesion falls below 15.7 kPa and the soil deformation is greater than 0.78 m, the pipe becomes overstressed. Gabion reinforcement is intended to keep the pipe's allowable stress constant, preventing pipe overstress. The use of gabion walls is sufficient to reinforce the slope and prevent pipe overstressing due to static and dynamic load.

References

1. BPH Migas. <https://www.bphmigas.go.id>
2. Marinos V, Stoumpos G, Papathanassion G, Grendas N, Papouli D, Papazachos C (2016) Landslide geohazard for pipelines of natural gas transport. *Bul Geo Soc Greece* 50(2):845–864
3. Ferris G, Newton S, Porter M (2016) Vulnerability of burried pipelines to landslides. In: *Proceedings of the 2016 11th International Pipeline Conference*, pp 1–8. The American Society of Mechanical Engineers, Calgary
4. Wu S, Xiong L, Zhang S (2018) Strength reduction method for slope stability analysis based on a dual factoring strategy. *Int J Geomech* 18(10):04018123
5. Susila E, Agrensa F (2018) Behaviors of pipe-soil interaction on unstable slopes by finite element simulation. *J Tek Sip* 25(2):87–91
6. Popov VL (2010) *Contact Mechanics and Friction: Physical Principles and Applications*. Springer, Heidelberg
7. Guo P (2005) Numerical modeling of pipe-soil interaction under oblique loading. *J Geotech Geoenv Eng* 131(2):260–268
8. Farhadi B, Wong R C K (2014) Numerical modeling of pipe-soil interaction under tranverse condition. In: *Proceedings of the 2014 10th International Pipeline Conference*. The American Society of Mechanical Engineers, Calgary

Testing Using Bi-directional Method for Bored Pile on Clay Soil in Indonesia



Aksan Kawanda

Abstract Sei Alalak Curved Cable Stayed Bridge located at Banjarmasin, South Kalimantan is a replacement bridge located next to the previous bridge. Bored pile was chosen as its foundation with 1.8 m diameter and 70 m length design for 1350-ton ultimate capacity. The soil consists of medium to stiff clay along the pile length. Bi-directional load test was chosen over conventional load test considering the potentially damage in pile structure when using reaction system and cost when using the kentledge system. Vibrating wire strain gauge as its instrumentation installed at various level to get load transfer, skin friction distribution as well as t - z and q - z along the shaft. Result showed most of capacity borne by its shaft resistance under small displacement while the end bearing needs more displacement to fully mobilized.

Keywords Bi-directional load test · clay soil · vibrating wire strain gages (vwsg) · load–displacement · t - z · q - z .

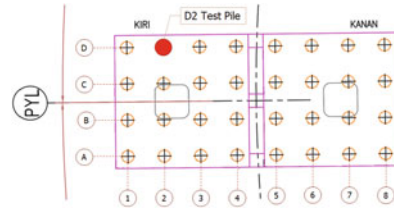
1 Introduction

Sei Alalak bridge is a curved cable stayed bridge with 141 m single span length. Bored pile with 1.8 m diameter and 70 m depth was chosen. There is (3) major structure: main pylon, counterweight and abutment as shown in Fig. 1. This paper will cover the pile test in pylon foundation. It was designed to have about 1350 tons ultimate capacity. Bi-directional load test chose to check the pile performance at pylon foundation. Since the construction site located in remote area, conventional static load test became more expensive and take longer time for set up and testing. Bi-directional load test method developed by Dr. Jorj O. (1984). This method required embedded calibrated hydraulic jack (cell) that will expand and push the pile upward and downward from its installation elevation. Pressure gauge use to measure the load

A. Kawanda (✉)
Universitas Trisakti, West Jakarta, Indonesia
e-mail: aksan.kawanda@trisakti.ac.id

© Institute of Technology PETRONAS Sdn Bhd 2024
B. S. Mohammed et al. (eds.), *Proceedings of the International Conference on Emerging Smart Cities (ICESC2022)*, Lecture Notes in Civil Engineering 324,
https://doi.org/10.1007/978-981-99-1111-0_54

Fig. 3 Foundation Layout



2.2 Soil Investigation

Soil investigation BH-5 conducted at west pylon to the depth of 100 m. Very soft clay layer found about 25 m below riverbed, followed with 5 m loose sand and 15 m medium to dense sand. Below this layer, stiff to very stiff clay found until the end of boring. Figure 4 showed the soil types, thickness and N_{SPT} value.

3 Bi-directional Static Axial Compressive Load Test

3.1 General

Bi-directional static axial load test conducted follows ASTM D8169/8169 M-18. In contrast to the classic axial compression loading applied with dead weight or reaction frame setups, the bi-directional load test is a high capacity sacrificial jack (cell) placed either near the foundation base or at mid-section elevations where the capacity found equal between upper and below cell. The bi-directional cell works in (2) directions, upward against the top portion side friction and self weight while downward against the end bearing and side friction. This will separating the upper and lower resistance components (Osterberg 1989). Figure 5 illustrate the schematics and basic instrumentation for a bi-directional load test. The upward and downward movement during the test was measured by tell-tale extensometer and collected by data-acquisition system. The cell placed at required depth at the pile shaft is expanded by pressurizing it through a hydraulic control system at the ground surface pushing the pile upward and downward at equal load. Since the cell was pre-calibrated, thus we can calculate the load by multiply the pressure with the specified calibration factor.

The bi-directional load test provides two direction of displacement curves: one showing the upward displacement of the pile above the cell versus the loading. This upward movement resisted by downward-acting skin friction plus the buoyant weight of the pile above the cell, while downward displacement below the cell, resisted by the end bearing plus any upward skin. Load test was terminated either the upper or below part of the cell already reach its ultimate capacity or the cell already reach its maximum load capacity or displacement capacity.

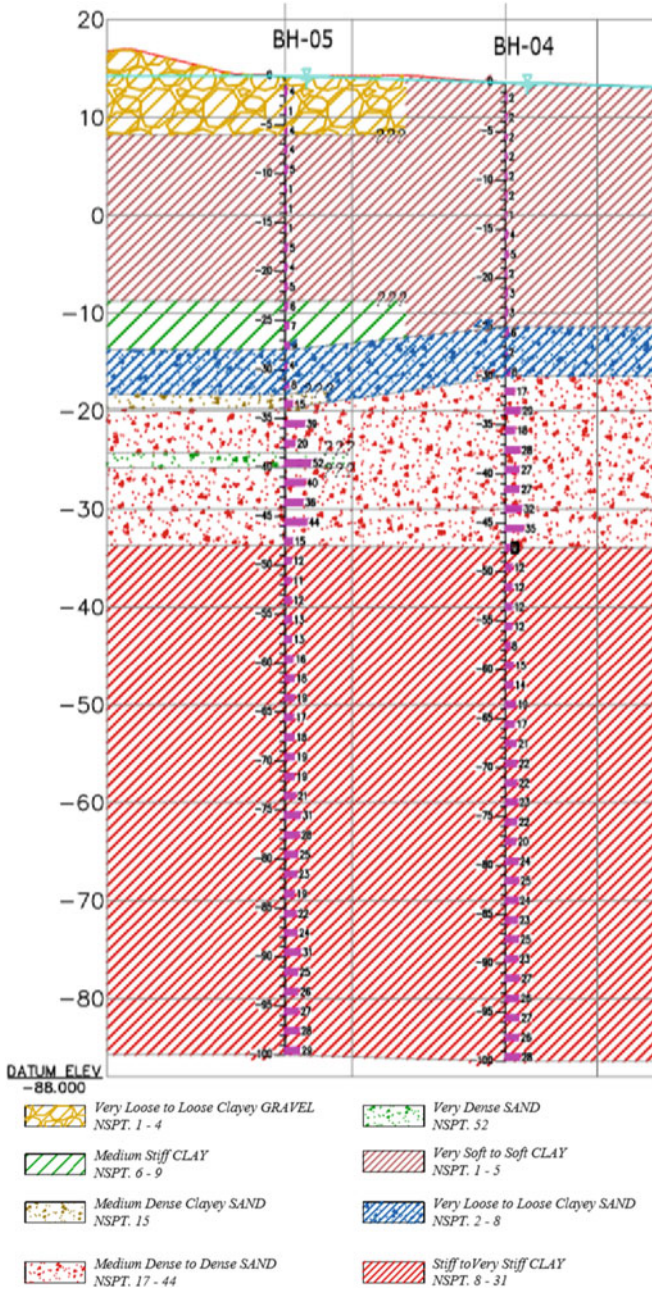


Fig. 4 Pylon Soil Investigation Data

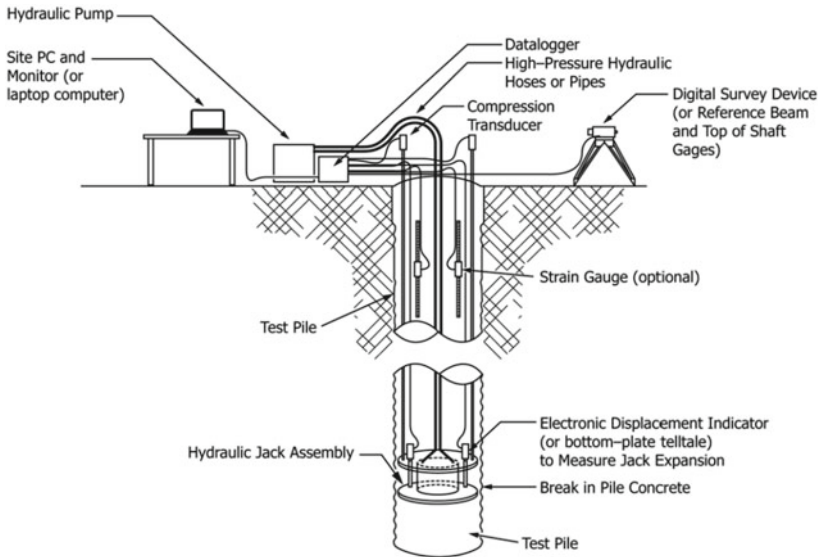


Fig. 5 Schematic of Bi-Directional Load Test (ASTM D8169/8169 M-18)

3.2 Equivalent Top Loaded Pile

Since the bi-directional load test only provide the upward and downward movement, this result needs to convert into top load movement. The first method was developed by Osterberg (1995). This original method converts upward-downward movement curve by select the similar movement at both curve and sum the load at each corresponded movement. This original method neglects the pile elastic compression. Then Schmertmann, 1998 modified the original method by adding the elastic compression using equation in Table 1 to the original movement method. Equation in Table 1 is for single cell configuration and referring to Fig. 6.

3.3 Cell Placements at Piles

In order to place the cell at equal capacity, static analysis (Reese & O’Neill, 1999) conducted with result shown in Fig. 7. Preliminary analysis shown that the cell can be placed at about 42 m below pile top where the upward friction estimated about 670 tons and pile weight about 118 tons against the downward friction of about 740 tons and 218 tons end-bearing. The cell intended to put at the level where the friction mainly as its major capacity.

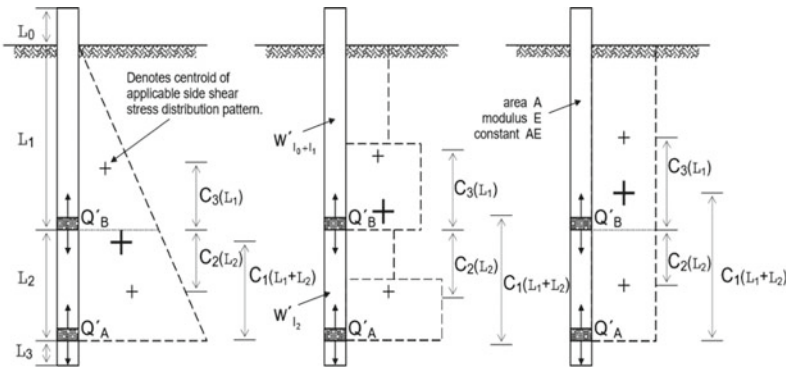


Fig. 6 Distance Load Factor for Calculate Elastic Compression

Table 1 Elastic compression for single cell (Q_a Only)

$C_1 = \frac{1}{3}$	$C_1 = C_1$	$C_1 = \frac{1}{2}$
$\delta_{(l_1+l_2)} = \frac{1}{3} \frac{Q_A(l_1+l_2)}{EA}$	$\delta_{(l_1+l_2)} = \frac{Q_A(l_1+l_2)}{EA}$	$\delta_{(l_1+l_2)} = \frac{1}{2} \frac{Q_A(l_1+l_2)}{EA}$

Where:

$C_{1,2,3}$ = Distance load factor

δ = Elastic compression

Q = Cell load

l = Segment length

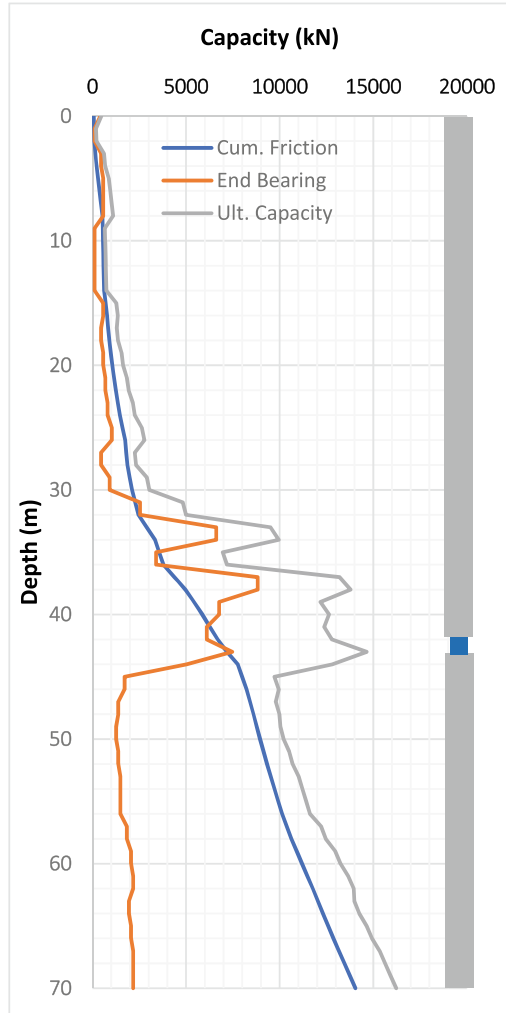
E = Pile elastic modulus

A = Pile area

3.4 Instrumentation with Vibrating Wire Strain Gauges (VWSG)

The vibrating wire strain gauge basic principle on measuring strain is by tensioned steel wire, when it's plucked, vibrates at a frequency proportional to the strain in wire. The gauge itself constructed so the wire held in tension between two end blocks and when electromagnet signal used to excite the wire, measuring the frequency is possible. The strain is then calculated by squaring the applying value and applying constant. Load at any location instrumented with VWSG later can easily calculated by using the modulus relation ($E = \sigma/\epsilon$) Where E is the modulus under certain load, σ is the pressure equal to load over area and ϵ is the measured strain. Five pair of VWSG installed at elevation (El.) +10.3 m, -19.7 m, -31.7 m, -43.7 m and -59.2 m; respectively, as shown in Fig. 8.

Fig. 7 Pile Capacity and Cell Location



4 Results

The test result showed maximum upward movement about 3.26 mm and downward movement at about 13.20 mm under 1350 tons load as shown in Fig. 9. Polynomial approach used to extrapolate the upward movement in order to get the equivalent top load and resulting in calculated settlement of about 16.53 mm at 1475 tons load (Fig. 10).

It is clearly shown from above result that capacity primarily borne by its friction. The instrumentation results also show the same, with calculated load transfer presented in Fig. 11 with the t-z and q-z curve in Fig. 12 and 13, respectively.

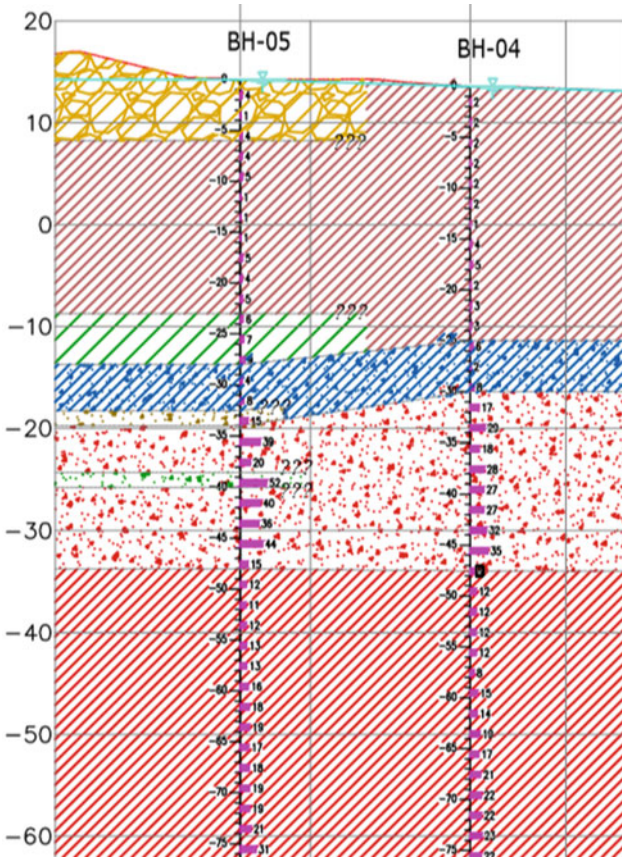
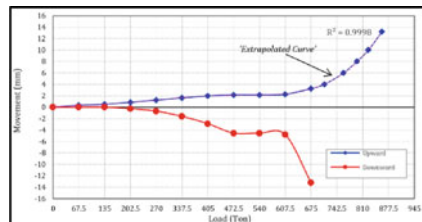


Fig. 8 VWSG's Location

Fig. 9 Downward & Upward Movement



The instrumentation showed that maximum mobilize skin friction are about 28 kPa at 0–30 m, 17.8 kPa at 30–42 m, 32.8 kPa at 42–54 m, and 49.4 kPa at 54–69.5 m with mobilized end bearing only about 50 kPa which is too small, but the cell stroke has already reached its limit.

Fig. 10 Equivalent Top Load Movement

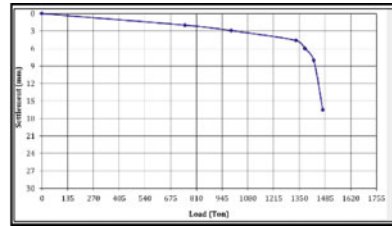


Fig. 11 Calculated Load Transfer from VWSG Measurement

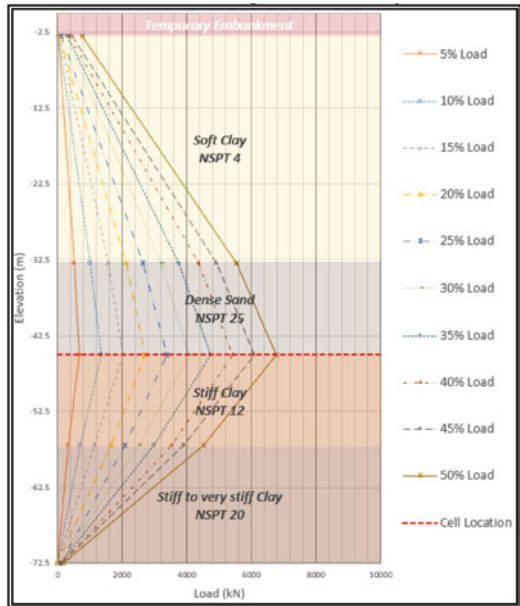


Fig. 12 t-z Curves

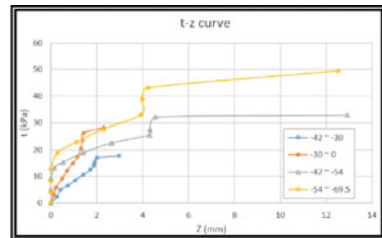
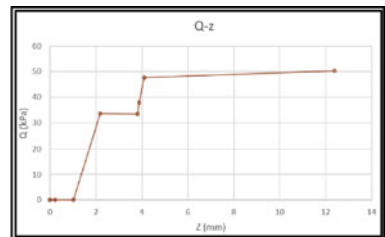


Fig. 13 q-z Curve



5 Summary

Bi-Directional load test should give good result when conducted properly with instrumentation. By considering the size of test, this method can save transportation cost especially in Indonesia with its thousand islands and of course the safety itself where no bulky construction onsite.

Test result for bored pile by bi-directional axial compression test with 1.8 diameter and 70.8 m effective length with 1475 tons load gave a total settlement of 16.5 mm. The results from instrumentation also shown that the mobilized unit friction was well comparable to estimated friction capacity by using Reese & O'Neill formula.

References

- ASTM D8169/D8169M-18, Standard Test Method for Deep Foundations under Bi-Directional Static Axial Compressive Loads, 2018.
- Geotech Efathama, D2 West Pylon Jembatan Sei Alalak Project axial compressive load test report, 2019.
- Osterberg JO (1984) A new simplified method for load testing drilled shafts. *Found Drill Mag* 23(6):9
- Osterberg J O (1998). The Osterberg load test method for bored and driven piles-the first ten years. In: *Proceedings of 7th International Conference and Exhibition on Piling and Deep Foundations*, Deep Foundation Institute, Vienna, Austria
- Schmertmann J H, Hayes J.A (1997). The Osterberg Cell and bored pile testing-A symbiosis. In: *Proceedings of 3rd International Geotechnical Engineering Conference Cairo Univ., Cairo, Egypt* pp 139–166
- SNI 8460:2017 Persyaratan Perancangan Geoteknik
- Woo S Y, Jeong S S, Moon I S, Lee J K (2006) Bearing Capacity analysis of large diameter drilled shafts by Osterberg-cell load test. In: *Proceedings of 2006 Korean Society of Civil Engineers Annual Conference, KSCE, Seoul* pp 1728–1732

Traditional Practices and Potential of Industrial Revolution 4.0 in the Construction Projects



I Gusti Agung Ayu Istri Lestari, I Gede Angga Diputera, Abdullah O. Baarimah, Wesam Salah Alaloul, Muhammad Ali Musarat, Aawag Mohsen Alawag, and Khalid Mhmoud Alzubi

Abstract The concept of Industrial Revolution (IR) 4.0 refers to the trend of digitization, automation, and use of information technology. Due to the unique environment of construction sites, the construction sector is currently lagging behind other industries when it comes to IR 4.0. Several research studies have made significant contributions to the use of IR 4.0 in construction projects. However, no scientometric research has been attempted to assess the holistic understanding of the current status of IR 4.0 applications. The purpose of this study is to conduct a bibliometric analysis of the present literature on IR 4.0 and its application in the construction sector. Automation, Blockchain, Digital Transformation, Digital Twin, Lean Construction, and Sustainability were found using keyword co-occurrence analysis to be the most IR 4.0 related topics implemented in the construction industry. In addition to that, it is

I. G. A. A. I. Lestari (✉) · I. G. A. Diputera · A. M. Alawag
Department of Civil Engineering, Universitas Mahasaraswati Denpasar, Denpasar, Bali, Indonesia
e-mail: gekistri82@unmas.ac.id

I. G. A. Diputera
e-mail: anggadiputera@unmas.ac.id

A. M. Alawag
e-mail: aawag_17006581@utp.edu.my

A. O. Baarimah · W. S. Alaloul · M. A. Musarat · K. M. Alzubi
Department of Civil and Environmental Engineering, Universiti Teknologi PETRONAS, Seri Iskandar, Malaysia
e-mail: abdullah_20000260@utp.edu.my

W. S. Alaloul
e-mail: wesam.alaloul@utp.edu.my

M. A. Musarat
e-mail: muhhammad_19000316@utp.edu.my

K. M. Alzubi
e-mail: khalid_20001254@utp.edu.my; alzoubi_khalid@bau.edu.jo

K. M. Alzubi
Civil Engineering Department, Albalqa Applied University, As-Salt, Jordan

recommended to develop more frameworks and strategies for enhancing the adoption of IR 4.0 in construction to enhance productivity and attain sustainable development. It is also found that adopting multiple emerging IR 4.0 technologies such as BIM, IoT, Blockchain, and Digital Twin in the construction industry will increase the advantages of IR 4.0. This study contributes to the field of the construction sector and IR 4.0 by assisting construction stakeholders and researchers to explore the current and future trends of IR 4.0.

Keywords IR 4.0, innovative technologies · construction 4.0 · projects · sustainable development · review · bibliometric analysis

1 Introduction

In the manufacturing industry, the adoption of a fully digital strategy has already led to more efficient production processes and better consumer satisfaction [1]. The “Fourth Industrial Revolution (IR 4.0)” is now being based upon the digital revolution, in which humans are connected through the digitization process, information transparency and connectivity [2, 3]. Technological advancement has discovered new ways to show off its prowess by fusing the boundaries between biological, digital, and physical things. When it comes to the term “IR 4.0”, the German government created the term and was first stated as “Industries 4.0” to the public, which is now used to describe a high-tech strategy referred to the development of “cyber-physical systems (CPSs) and dynamic data processes that use enormous volumes of data to drive smart machines” [4, 5]. Many different terms are used to describe IR 4.0, including “smart factory”, “smart manufacturing”, and “smart production” [1, 6]. The most recent technological advancements and innovations encouraged the emergence of IR 4.0, which promotes performance, conserves resources, and high-quality and adaptability of industrial systems [7, 8]. The revolution not only offers cutting-edge methods to support each industry component but also sustainability [9]. Hence, it is critical to evaluate operational, tactical, and strategic aspects influence on sustainability [10].

IR 4.0 refers to the trend of digitalization, and growing use of Information Technology (IT), which includes CPSs, cloud computing, Internet of Things (IoT), and cognitive computing [3, 11]. The primary contribution of IR 4.0 is the digitization of industrial operations in order to establish a flexible yet comprehensive production and new service network, as well as value-chain business strategies [12, 13]. Having been implemented in a variety of industries including manufacturing, software development and healthcare [14–16], IR 4.0 can improve the performance of the construction sector [17, 18]. In the construction industry, IR 4.0 has already fostered the adoption of numerous technologies, including sensor systems and intelligent machinery. Building information modeling (BIM) was one of the most significant technologies for a project’s digital information in terms of the creation and management of an asset’s digital information [19–21]. Furthermore, the IoT is compatible with CPS,

allowing humans to monitor processes in timely without physically being there, and has proven the abilities of the IR 4.0 vision chain [22, 23].

Understanding the level of the development of IR 4.0 technologies is crucial for maximizing the advantages of digitalization in the construction sector. Unfortunately, the construction is reluctant to implement the IR 4.0 technologies despite the advantages they offer [24, 25]. The construction industry has a few difficulties that lead to incompatibility. Oesterreich and Teuteberg [26] stated that the issue is exacerbated by complexity, culture, short-term thinking, supply chain fragmentation, and unpredictability. A project's degree of uncertainty is also determined by the unexpected environment that makes the project more complicated [27, 28]. Construction organizations with short-term thinking and supply chain fragmentation have limited options when the construction projects' short-term nature is a barrier to innovation [29, 30]. Thus, the effectiveness of IR 4.0 in construction, however, is far less well understood.

Various studies on applications of IR 4.0 in the construction industry have been conducted in recent years to investigate the numerous elements that play a role in the effective adoption of IR 4.0 technologies within the construction industry [3, 6–8, 17, 25]. However, no particular initiatives for stakeholders and practitioners to capitalize on the benefits of this shift in terms of quality and productivity increases have been developed. Academics, on the other hand, are employing scientometric analysis to identify new subjective problems in previous research [31–34]. In reality, there has been a shortage of attempts at scientometric analysis in all accessible research publications to investigate the comprehensive knowledge of the current state of applications of IR 4.0 in construction. To the best of the authors' knowledge, this is a unique bibliometric analysis study in the integration of the IR 4.0 within the construction projects. As a result, the purpose of this study is to undertake a bibliometric analysis of publications on the use of IR 4.0 technologies in the construction industry and to offer a view of the state of the research from August 2016 to August 2022. As a result, by evaluating Scopus database papers on IR 4.0 technologies in the construction sector, this analysis will also assist academics in making recommendations for future research.

2 Methodology

Academic articles related to the applications of IR 4.0 within the construction sector have been extracted from Scopus dataset to achieve the aims of this review. Scopus is a database that has been recommended by many academics as a comprehensive resource because it includes more scientific papers than any other database [35–37]. The keywords with the following query string were used: “(TITLE-ABS-KEY” (“Industrial Revolution* 4.0” OR “Industrial Revolution*” OR “IR 4.0” OR “Industry 4.0” OR “Fourth Industrial Revolution*” OR “4th Industrial Revolution”) AND (“Construction 4.0” OR “construction industry” OR “construction Project*” OR “construction management”))” to perform the literature search. Furthermore, the

time span was chosen from 2016 through August 2022. Initially, 404 were extracted, such as articles, conference papers, book chapters, and reviews. Following that, only documents available in articles and conference papers were included. This review included only English documents. Finally, 316 documents (165 articles and 153 conference papers) were selected and converted into an Excel spreadsheet for scientometric analysis.

Furthermore, once the selected documents were collected, scientometric analysis was performed. VOSviewer was used to construct the bibliometric networks in this study [38]. The acquired resources were analyzed utilizing journals, countries, and keywords. The sources mentioned above are widely acknowledged as the foundation of bibliometric analysis, allowing academics to easily and precisely comprehend the current state of research [39, 40]. The most important metrics comprised citations, number of documents, the average publication year, and average normalized citations [41].

3 Results and Discussions

3.1 Trend of Annual Publications

Figure 1 depicts the number of articles published each year that explore the application of IR 4.0 in the construction sector. The bibliometric analysis of 316 documents revealed, as illustrated in Fig. 2, that the publications were spread out between the years 2016 and August 2022.

The number of papers on the integration of IR 4.0 into the construction sector has gradually grown. Scholars are investigating the potential deployment of IR 4.0

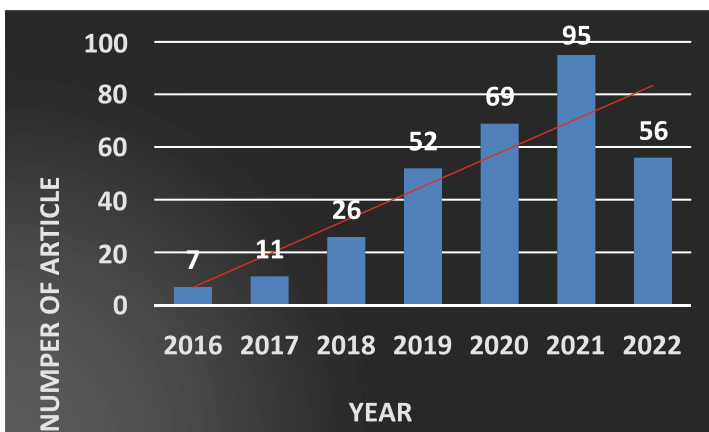


Fig. 1 Annual Publications Trend

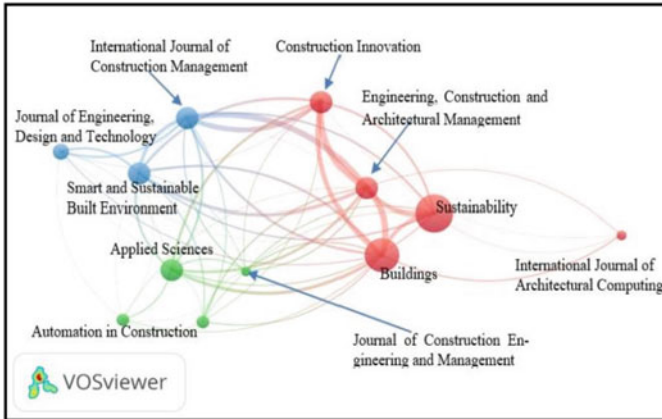


Fig. 2 Published Journals Network

in the construction industry, which is an intriguing fact. Furthermore, 2021 had the most publications, with 95 items released. Despite the fact that this evaluation only covers the first eight months of 2022, 56 papers have been recorded so far (despite the fact that 2022 is still ongoing), demonstrating a growing interest in studies on the application of IR 4.0 in the construction sector.

3.2 Published Journals Analysis

The VOSviewer was used to identify the sources that published articles regarding IR 4.0 applications in the construction sector, which are depicted in Fig. 2. A source’s min number of documents and citations was set at three and ten, respectively. 17 of the 166 journals satisfied the requirements. Moreover, A total of 17 of the 166 sources satisfied the thresholds. In addition, the leading 12 journals were interconnected as presented in Fig. 2. It is clear that the Sustainability node was significantly larger than the others and connected to the majority of them, showing that this journal was at the forefront of IR 4.0 in construction.

Table 1 provides extensive details regarding the published journals. It is possible to confirm that Sustainability has the most documents published in it and is the most influential journal (11 documents). Besides, it can be seen that “Automation in Construction” have the highest total citations (211) and average norm citations (4.2); reflecting its prominence and productivity in this field. It’s fascinating to point out again that “Automation in Construction” earns the greatest average normalized citations, followed closely by “International Journal of Construction Management” and “Smart and Sustainable Built Environment”. Furthermore, Other outstanding journals in this field, such as but are not limited to Buildings, Construction Innovation, Applied Sciences, and “Engineering, Construction and Architectural Management”.

Table 1 Details of top published journals

Source Journal	Documents	Total Link Strength	Total Citations	Avg. Norm Citations
Applied Sciences (Switzerland)	7	108	110	2.3
Automation in Construction	4	19	211	4.2
Buildings	11	194	97	1.5
Construction Innovation	7	178	41	1.2
Engineering, Construction and Architectural Management	7	242	75	1.7
IFIP Advances in Information And Communication Technology	4	41	42	0.7
International Journal of Architectural Computing	3	15	27	1.6
International Journal of Construction Management	7	176	59	3.8
Journal of Construction Engineering And Management	3	47	11	0.8
Journal of Engineering, Design And Technology	5	40	30	0.9
Smart and Sustainable Built Environment	7	125	116	3.3
Sustainability	12	113	41	0.6

3.3 Countries Network Analysis

If there is information available on leading countries in any study field, scholars will be able to work together on a specific research, projects, acquire funding, or disseminate findings of their research [42]. VOSviewer was used in this review to identify and rank the countries' contributions [38]. "The minimum numbers of documents and citations of a country were set at three and 20", respectively. As seen

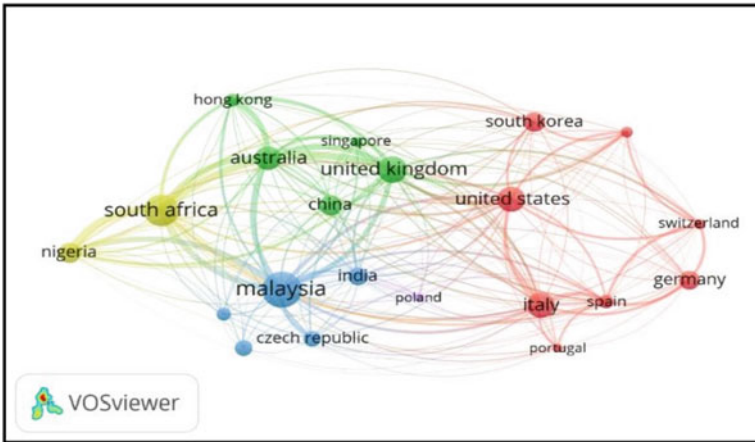


Fig. 3 Countries Network

in Fig. 3, only 21 out of the 58 countries met the condition. Figure 3 demonstrates how the countries were divided into four color-coded clusters, such as the South African and Nigeria research clusters. As shown in Fig. 3, Malaysia has the largest node, indicating that Malaysian academics have made considerable contributions to the literature concerning IR 4.0 in the construction sector.

Table 2 illustrates information on the network of countries with the most contribution levels regard to the subject. In terms of the total documents, it is evident that South Africa and Malaysia have a close relationship and rank first and second, respectively, in the research connected to IR 4.0 applications, followed by UK and USA.

Hong Kong, Poland, and Switzerland scored the highest average citations (15.3). Finally, academics from Switzerland ranked top, followed by academics from the UAE, with 5.7 and 4.6 average normalized citations, respectively, demonstrating that academics were extremely competitive and made considerable contributions to this subject.

3.4 Analysis of Keyword Co-occurrence

Keywords describe the main ideas of the current research, highlight the areas that have been looked into within certain topics, and help academics comprehend possible future research lines [43]. In this review, “The minimum number of occurrences of a keyword was set at five”.

As a result, 31 of 826 author keywords met the criteria, and Fig. 4 depicts the network of high-frequency keywords. Figure 4 depicts the research trend toward IR 4.0 technology for the construction sector.

Table 2 Details of top countries

Keywords	Documents	Total Link Strength	Total Citations	Avg. Citations	Avg. Pub. Year	Avg. Norm. Citations
Australia	23	2080	271	11.8	2020	2.1
China	16	257	103	6.4	2020	0.8
Czech Republic	10	343	91	9.1	2020	1.2
Germany	14	384	74	5.3	2019	0.5
Hong Kong	7	893	107	15.3	2021	3.4
India	13	356	40	3.1	2020	0.6
Indonesia	10	69	25	2.5	2020	0.3
Italy	25	975	295	11.8	2019	1.5
Malaysia	52	2326	395	7.6	2020	1.0
Nigeria	16	1532	146	9.1	2021	1.5
Poland	3	126	46	15.3	2019	2.1
Portugal	3	162	20	6.7	2020	0.9
Russian Federation	7	110	21	3.0	2020	0.4
Singapore	4	430	22	5.5	2022	2.0
South Africa	40	2899	304	7.6	2021	1.4
South Korea	15	293	35	2.3	2020	0.5
Spain	8	836	111	13.9	2021	2.7
Switzerland	4	498	61	15.3	2021	5.7
United Arab Emirates	5	397	55	11.0	2021	4.6
United Kingdom	28	2344	384	13.7	2020	2.7
United States	25	1104	164	6.6	2020	1.6
Russian Federation	7	110	21	3.0	2020	0.4
Singapore	4	430	22	5.5	2022	2.0
South Africa	40	2899	304	7.6	2021	1.4
South Korea	15	293	35	2.3	2020	0.5
Spain	8	836	111	13.9	2021	2.7
Switzerland	4	498	61	15.3	2021	5.7
United Arab Emirates	5	397	55	11.0	2021	4.6

(continued)

Table 2 (continued)

Keywords	Documents	Total Link Strength	Total Citations	Avg. Citations	Avg. Pub. Year	Avg. Norm. Citations
United Kingdom	28	2344	384	13.7	2020	2.7
United States	25	1104	164	6.6	2020	1.6

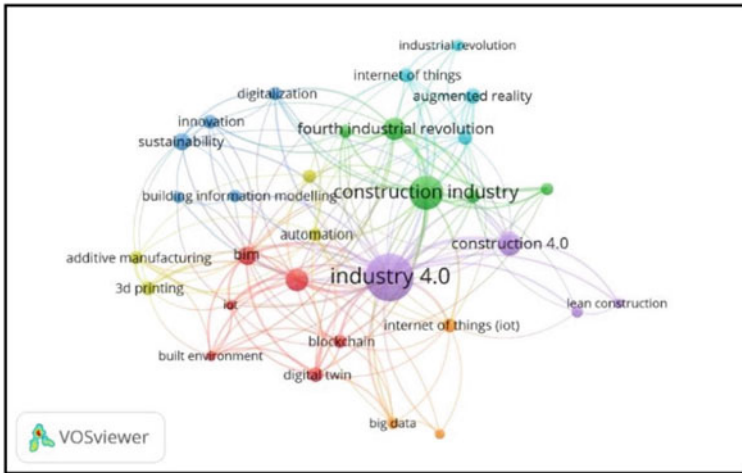


Fig. 4 Co-occurring Keywords Network

The fact that the keywords “Industry 4.0” and “Construction Industry” are the biggest nodes in this network is unsurprising considering that these phrases represent the domain’s backbone. Other keywords related to IR 4.0 and the construction industry include BIM, IoT, Automation, Blockchain, Digital Twin, Sustainability, and Lean Construction, indicating that phrases are frequently associated with IR 4.0 construction. Table 3 contains significant information on the frequency of terms, which corresponded to those in Fig. 4.

The phrases “Internet of Things,” “Digital Transformation,” “Building Information Modeling,” “Augmented Reality,” and “3D Printing” received the most citations. As demonstrated by the average publication year, certain keywords were popular recently. Articles related to Automation, Big Data, Blockchain, Construction 4.0, Digital, Transformation, Digital Twin, Digitalization, Lean Construction, and Sustainability were published in 2021, suggesting that such subjects have recently emerged as themes related to the applications of IR 4.0, and grabbed the interest of academics, may also offer future research opportunities. Furthermore, it is evident from Table 3 that Construction 4.0, BIM, and IoT are incorporated into the current research topic according to the frequency of the keywords. Therefore, it can be

Table 3 Top keywords co-occurrence

Keywords	Total Link Strength	Occurrence	Avg. Citations	Avg. Norm. Citations	Pub. Year
3D Printing	18	9	5.4	0.7	2020
Additive Manufacturing	14	8	8.5	0.9	2019
Augmented Reality	15	11	7.4	0.7	2020
Automation	18	7	4.9	0.8	2021
Big Data	14	6	3.8	0.7	2021
BIM	30	16	4.4	0.8	2020
Blockchain	18	8	3.8	0.9	2021
Building Information Modelling	87	27	11.8	1.5	2020
Built Environment	15	5	4.4	0.7	2020
Construction 4.0	31	25	4.2	1.2	2021
Construction Industry	72	81	9.6	1.7	2021
Construction Management	6	6	2.7	0.9	2020
Digital Transformation	18	8	19.0	2.3	2021
Digital Twin	24	10	7.3	1.4	2021
Digitalization	16	8	5.9	1.1	2021
Fourth Industrial Revolution	38	23	3.5	0.9	2021
Industrial Revolution 4.0	11	14	13.9	1.5	2020
Industry 4.0	119	103	9.6	1.3	2020
Innovation	13	9	3.7	0.9	2021
IoT	18	23	26.6	3.0	2020
Lean Construction	7	5	2.0	0.4	2021
Sustainability	15	13	4.3	0.6	2021

concluded that the incorporation of IR 4.0 applications is able to evaluate the impacts of various strategies on the projects' costs, quality, and productivity.

4 Conclusions

The current status of IR 4.0 applications construction primarily strives to produce guidelines necessary in order to capitalize on the benefits of this transition in terms of productivity and efficiency gains. To gain a comprehensive understanding of the present status of IR 4.0 applications in construction, the VOSviewer tool was employed to visualize the related studies. According to the findings, research in the field of applications of IR.

4.0 grew steadily in construction. In terms of scientific journals, Sustainability was named the most significant and leading journal. Malaysian researchers have made significant contributions to the literature on the adoption of IR 4.0 applications in construction. Automation, Blockchain, Digital Transformation, Digital Twin, Lean Construction, and Sustainability were found using keyword co-occurrence analysis to be the most IR 4.0 related topics implemented in construction. In addition to that, it is recommended to develop more frameworks and strategies for enhancing the adoption of IR 4.0 in construction to enhance productivity and attain sustainable development. It is also found that adopting multiple emerging technologies of IR 4.0 such as BIM, IoT, Blockchain, and Digital Twin in the construction industry will increase the advantages of IR 4.0. In terms of future research recommendations, it is suggested that more objective studies be conducted in order to develop frameworks for improving the adoption of IR 4.0 applications, which will result in improving construction productivity and achieving sustainable development. It is also advised to implement numerous developing IR 4.0 in construction in order to collaborate and establish synergies, such as BIM, IoT, Blockchain, and Digital Twin. These technologies will boost the competitiveness of construction projects and have a substantial influence on their progress and completion in terms of quality, on-time project delivery, and cost savings.

References

1. Osunsanmi TO, Aigbavboa C, Oke A (2018) Construction 4.0: the future of the construction industry in South Africa. *Int J Civil Environ Eng* 12(3):206–212. <https://doi.org/10.5281/zenodo.1315923>
2. Axelsson J, Fröberg J, Eriksson P (2019) Architecting systems-of-systems and their constituents: a case study applying Industry 4.0 in the construction domain. *Syst Eng* 22(6):455–470. <https://doi.org/10.1002/sys.21516>
3. Alaloul WS, Liew MS, Zawawi NAWA, Kennedy IB (2020) Industrial Revolution 4.0 in the construction industry: challenges and opportunities for stakeholders. *Ain Shams Eng J* 11(1):225–230. <https://doi.org/10.1016/j.asej.2019.08.010>
4. Strange R, Zucchella A (2017) Industry 4.0, global value chains and international business. *Multinatl Bus Rev* 25(3):174–184. <https://doi.org/10.1108/MBR-05-2017-0028>
5. Alaloul WS, Liew MS, Zawawi NAWA, Mohammed BS (2018) Industry revolution IR 4.0: future opportunities and challenges in construction industry. *MATEC Web of Conferences* 203:02010. <https://doi.org/10.1051/mateconf/201820302010>

6. Maskuriy R, Selamat A, Ali KN, Maresova P, Krejcar O (2019) Industry 4.0 for the construction industry—how ready is the industry? *Appl Sci* 9(14):2819. <https://doi.org/10.3390/app9142819>
7. Statsenko L, Samaraweera A, Bakhshi J, Chileshe N (2022) Construction 4.0 technologies and applications: a systematic literature review of trends and potential areas for development, *Construction Innovation* vol. ahead-of-p, no. ahead-of-print. <https://doi.org/10.1108/CI-07-2021-0135>.
8. Maskuriy R, Selamat A, Maresova P, Krejcar O, David OO (2019) Industry 4.0 for the construction industry: review of management perspective. *Economies* 7(3):68. <https://doi.org/10.3390/economies7030068>
9. Hidayatno A, Destyanto AR, Hulu CA (2019) Industry 4.0 technology implementation impact to industrial sustainable energy in Indonesia: a model conceptualization. *Energy Procedia* 156:227–233. <https://doi.org/10.1016/j.egypro.2018.11.133>
10. Cruz CO, Gaspar P, de Brito J (2019) On the concept of sustainable sustainability: an application to the Portuguese construction sector. *J Build Eng* 25:100836. <https://doi.org/10.1016/j.job.2019.100836>
11. Alaloul W S, Saad S, Qureshi A H (2021) Construction sector: IR 4.0 applications. In: Hussain, C M, Di Sia P Eds *Handbook of Smart Materials, Technologies, and Devices*, pp 1–50. Springer, Cham https://doi.org/10.1007/978-3-030-58675-1_36-1
12. Hallward-Driemeier M, Nayyar G (2017) *Trouble in the Making?: The Future of Manufacturing-led Development*. World Bank Publications, Washington
13. Liao Y, Deschamps F, Loures EDFR, Ramos LFP (2017) Past, present and future of Industry 4.0—a systematic literature review and research agenda proposal. *Int J Prod Res* 55(12):3609–3629. <https://doi.org/10.1080/00207543.2017.1308576>
14. Kumar A, Krishnamurthi R, Nayyar A, Sharma K, Grover V, Hossain E (2020) A novel smart healthcare design, simulation, and implementation using healthcare 4.0 processes. *IEEE Access* 8:118433–118471. <https://doi.org/10.1109/ACCESS.2020.3004790>
15. Frank AG, Dalenogare LS, Ayala NF (2019) Industry 4.0 technologies: implementation patterns in manufacturing companies. *Int J Prod Econ* 210:15–26. <https://doi.org/10.1016/j.ijpe.2019.01.004>
16. Baarimah S O, Baarimah A O (2021) PVT properties for Yemeni reservoirs using an intelligent approach. In: 2021 Third International Sustainability and Resilience Conference: Climate Change, pp 368–372 <https://doi.org/10.1109/IEEECONF53624.2021.9668185>
17. Demirkenen S, Tezel A (2021) Investigating major challenges for industry 4.0 adoption among construction companies. *Eng Constr Archit Manag* 29(3):1470–1503. <https://doi.org/10.1108/ECAM-12-2020-1059>
18. Alzubi K M, Alaloul W S, Al Salaheen M, Qureshi A H, Musarat, M A, Baarimah A O (2021) Automated monitoring for construction productivity recognition. In: 2021 Third International Sustainability and Resilience Conference: Climate Change, pp 489–494 <https://doi.org/10.1109/IEEECONF53624.2021.9668172>.
19. Baarimah AO et al (2021) A bibliometric analysis and review of building information modelling for post-disaster reconstruction. *Sustainability* 14(1):393. <https://doi.org/10.3390/su14010393>
20. Craveiro F, Duarte JP, Bartolo H, Bartolo PJ (2019) Additive manufacturing as an enabling technology for digital construction: a perspective on construction 4.0. *Autom Constr* 103:251–267. <https://doi.org/10.1016/j.autcon.2019.03.011>
21. Al-Ashmori YY, Othman I, Al-Aidrous A-HMH (2022) ‘Values, challenges, and critical success factors’ of building information modelling (BIM) in Malaysia: experts perspective. *Sustainability* 14(6):3192. <https://doi.org/10.3390/su14063192>
22. Magruk A (2015) The most important aspects of uncertainty in the internet of things field – context of smart buildings. *Procedia Eng* 122:220–227. <https://doi.org/10.1016/j.proeng.2015.10.028>
23. Alzubi K M, Salah Alaloul W, Al Salaheen M, Hannan Qureshi A, Musarat M A, Mohsen Alawag A (2022) Reviewing the applications of internet of things in construction projects In: 2022 International Conference on Decision Aid Sciences and Applications (DASA), pp 169–173 <https://doi.org/10.1109/DASA54658.2022.9765143>

24. Kor M, Yitmen I, Alizadehsalehi S (2023) An investigation for integration of deep learning and digital twins towards Construction 4.0. *Smart Sustain Built Environ* 12(3):461–487. <https://doi.org/10.1108/SASBE-08-2021-0148>
25. Das P, Perera S, Senaratne S, Osei-Kyei R (2022) Paving the way for industry 4.0 maturity of construction enterprises: a state of the art review. *Eng Constr Architectural Manag* vol. ahead-of-p, no. ahead-of-print <https://doi.org/10.1108/ECAM-11-2021-1001>
26. Oesterreich TD, Teuteberg F (2016) Understanding the implications of digitisation and automation in the context of Industry 4.0: a triangulation approach and elements of a research agenda for the construction industry. *Comput Ind* 83:121–139. <https://doi.org/10.1016/j.compind.2016.09.006>
27. Baarimah, A O, Alaloul W S, Liew M S (2022) Post-disaster Reconstruction Projects in Developing Countries: An Overview,” *Lecture Notes in Electrical Engineering*, vol 758 https://doi.org/10.1007/978-981-16-2183-3_88.
28. Al-Aidrous A-HMH, Rahmawati Y, Yusof KW, Baarimah AO, Alawag AM (2021) Review of industrialized buildings experience in Malaysia: an example of a developing country. *IOP Conference Series: Earth and Environmental Science* 682(1):12003. <https://doi.org/10.1088/1755-1315/682/1/012003>
29. Mohsen A, et al., (2021) Impact of the COVID-19 pandemic on construction industry in Malaysia. In: 2021 Third International Sustainability and Resilience Conference: Climate Change, pp 237–241 <https://doi.org/10.1109/IEEECONF53624.2021.9667984>.
30. Al-Aidrous A-H M H, Shafiq N, Mohammed B S, Al-ashmori Y Y, Baarimah A O, Al-masoodi A H H (2021) Investigation of the current innovative industrialized building systems (IBS) in Malaysia. In: 2021 Third International Sustainability and Resilience Conference: Climate Change, pp 382–387 <https://doi.org/10.1109/IEEECONF53624.2021.9668063>
31. Wu Z, Chen C, Cai Y, Lu C, Wang H, Yu T (2019) BIM-based visualization research in the construction industry: a network analysis. *Int J Environ Res Public Health* 16(18):3473. <https://doi.org/10.3390/ijerph16183473>
32. Sepasgozar SME, Hui FKP, Shirowzhan S, Foroozanfar M, Yang L, Aye L (2020) Lean practices using building information modeling (BIM) and digital twinning for sustainable construction. *Sustainability* 13(1):161. <https://doi.org/10.3390/su13010161>
33. Baarimah A O, Alaloul W S, Liew M S, Alawag A M, Musarat M A, Alzubi K M (2021) Current state of post-disaster reconstruction projects: a bibliometric analysis. In: 2021 International Conference on Decision Aid Sciences and Application (DASA), pp. 108–113. *IEEE*. <https://doi.org/10.1109/DASA53625.2021.9682326>.
34. H. Ghaleb, H. H. Alhajlah, A. A. Bin Abdullah, M. A. Kassem, and M. A. Al-Sharafi, “A Scientometric Analysis and Systematic Literature Review for Construction Project Complexity,” *Buildings*, vol. 12, no. 4, p. 482, Apr. 2022, doi: <https://doi.org/10.3390/buildings12040482>.
35. Zhao X, Zuo J, Wu G, Huang C (2019) A bibliometric review of green building research 2000–2016. *Archit Sci Rev* 62(1):74–88. <https://doi.org/10.1080/00038628.2018.1485548>
36. Aghaei Chadegani A. et al. (2013) A comparison between two main academic literature collections: web of science and scopus databases *Asian Soc Sci* 9(5), 18–26
37. Alaloul WS, Alzubi KM, Malkawi AB, Al Salaheen M, Musarat MA (2022) Productivity monitoring in building construction projects: a systematic review. *Eng Constr Architectural Manag* 29(7):2760–2785. <https://doi.org/10.1108/ECAM-03-2021-0211>
38. van Eck NJ, Waltman L (2010) Software survey: VOSviewer, a computer program for bibliometric mapping. *Scientometrics* 84(2):523–538. <https://doi.org/10.1007/s11192-009-0146-3>
39. Ren R, Hu W, Dong J, Sun B, Chen Y, Chen Z (2019) A systematic literature review of green and sustainable logistics: bibliometric analysis, research trend and knowledge taxonomy. *Int J Environ Res Public Health* 17(1):261. <https://doi.org/10.3390/ijerph17010261>
40. Baarimah A O, Alaloul W S, Liew M S, Al-Aidrous A-H M H Alawag A M, Musarat M A (2021) Integration of building information modeling (BIM) and value engineering in construction projects: a bibliometric analysis. In: 2021 Third International Sustainability and Resilience Conference: Climate Change, pp 362–367. <https://doi.org/10.1109/IEEECONF53624.2021.9668045>.

41. Jin R, Gao S, Cheshmehzangi A, Aboagye-Nimo E (2018) A holistic review of off-site construction literature published between 2008 and 2018. *J Clean Prod* 202:1202–1219. <https://doi.org/10.1016/j.jclepro.2018.08.195>
42. Hosseini MR, Martek I, Zavadskas EK, Aibinu AA, Arashpour M, Chileshe N (2018) Critical evaluation of off-site construction research: a scientometric analysis. *Autom Constr* 87:235–247. <https://doi.org/10.1016/j.autcon.2017.12.002>
43. Su H-N, Lee P-C (2010) Mapping knowledge structure by keyword co- occurrence: a first look at journal papers in technology foresight. *Scientometrics* 85(1):65–79. <https://doi.org/10.1007/s11192-010-0259-8>

Image Processing Applications in Construction Projects: Challenges and Opportunities



**Tjokorda Istri Praganingrum, Ni Luh Made Ayu Mirayani Pradnyadari,
Khalid Mhmoud Alzubi, Wesam Salah Alaloul, Marsail Al Salaheen,
Muhammad Ali Musarat, and Aawag Mohsen Alawag**

Abstract Image processing can be valuable in many aspects of the construction sector, including progress monitoring, material classification, resource tracking, and recognition. Massive images and videos are captured on construction sites regularly due to the growth of capturing devices, the accessibility of the Internet, and the increasing volume of storage databases, which has encouraged scholars to visually capture the different aspects and actual state of construction sites using image processing. Many researchers have conducted valuable attempts and developed a wide range of complicated methodologies for construction monitoring. Few studies, however, completely describe existing methodologies and introduce the challenges and opportunities for the implementation of image processing in the construction industry. As a result, this study focuses on the general technological path of many

T. I. Praganingrum (✉) · N. L. M. A. M. Pradnyadari
Department of Civil Engineering, Universitas Mahasaraswati, Denpasar, Bali, Indonesia
e-mail: praganingrum@unmas.ac.id

N. L. M. A. M. Pradnyadari
e-mail: mirayani2020@unmas.ac.id

K. M. Alzubi · W. S. Alaloul · M. Al Salaheen · M. A. Musarat · A. M. Alawag
Department of Civil and Environmental Engineering, Universiti Teknologi PETRONAS, Seri
Iskandar, Malaysia
e-mail: khalid_20001254@utp.edu.my; alzoubi_khalid@bau.edu.jo

W. S. Alaloul
e-mail: wesam.alaloul@utp.edu.my

M. Al Salaheen
e-mail: marsail_20001253@utp.edu.my; marsail.salaheen@bau.edu.jo

M. A. Musarat
e-mail: muhhammad_19000316@utp.edu.my

A. M. Alawag
e-mail: aawag_17006581@utp.edu.my

K. M. Alzubi · M. Al Salaheen
Civil Engineering Department, Albalqa Applied University, Salt, Jordan

applied image processing techniques and tools employed in the construction sector to help researchers select research methodologies and approaches. This is followed by a discussion of potential research directions.

Keywords Image processing · construction projects · progress monitoring · Resources tracking · Material classification

1 Introduction

The digital images captured at a construction site have increased dramatically in recent years. Furthermore, convenient, inexpensive, and quick access to these images sparked a wave of research into data collection and construction site monitoring [1, 2]. Videos and images allow project managers to monitor building sites more efficiently, enhance communication among stakeholders, and better track progress data [3, 4].

Many definitions have been proposed for image processing (IP). It is usually accepted that IP involves manipulating a digital image to generate a second image, while computer vision (CV) can extract the information from that image automatically [1, 2]. When discussing the adoption of IP in the construction industry, it is common to associate it with CV-based technologies and building information modelling (BIM), as illustrated in Fig. 1

The merging of IP and CV-based technologies promise to reduce traditional information gathering and report preparation time [2, 5]. This gives managers more time to focus on decision-making activities and to take corrective actions in real-time [5].

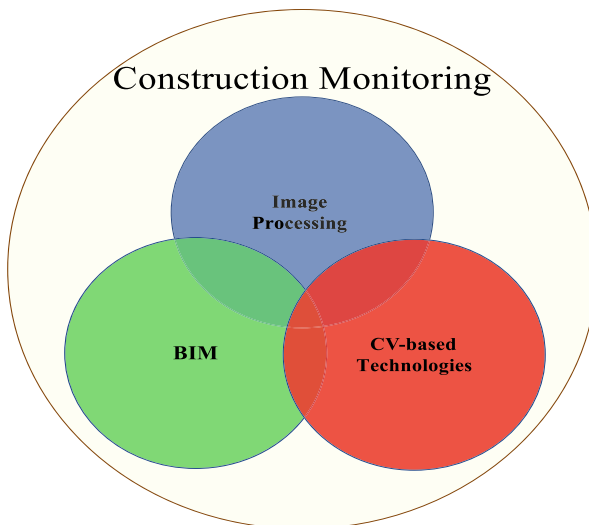


Fig. 1 Integration of monitoring technologies for construction monitoring

Construction managers rely on fast and accurate information to make successful decisions during the control process on the job site [5]. IP has increased the probability of construction site automation monitoring [6, 7].

IP studies have proved to be cost-effective and efficient for automated progress monitoring, resource tracking, and material classifications by extracting information directly from digital images [8–10]. This paper discussed the applications of IP in the construction industry, challenges it faces in adoption, and opportunities for more development. To achieve the objectives of this study, a review of the literature was conducted to select the relevant studies related to the applications of IP for monitoring construction projects.

2 Applications of IP in Construction

The applications of IP in the construction industry have increased dramatically recently among researchers due to the great improvement in specifications of capturing devices, ease of use of these devices (no high skills are required to capture images), high storage databases, and accessibility of the Internet [5–7]. The mechanism for reaping the benefits of IP in construction monitoring (CM) applications, applications of image processing regarded to construction progress monitoring (CPM), resources tracking (workers and machines), material classifications, productivity analysis, and structural element recognition are discussed in the next subsections.

2.1 The Mechanism of Image Processing in Construction Applications

The first aim of digital IP is to improve pictorial information for human interpretation, and the second is to process image data for transmission, representation, and storage for autonomous machine perception [2, 11]. The IP may be divided into low, medium, and high-level processes as shown in Fig. 2.

There are several procedures used for IP implementation in construction sites: image acquisition, general processing, feature extraction, object detection, and image segmentation [12].

2.2 Image Acquisition

Image capture can be done by various devices like digital cameras, smartphones, monocular cameras, surveillance cameras, unmanned ground vehicles (UGV), and

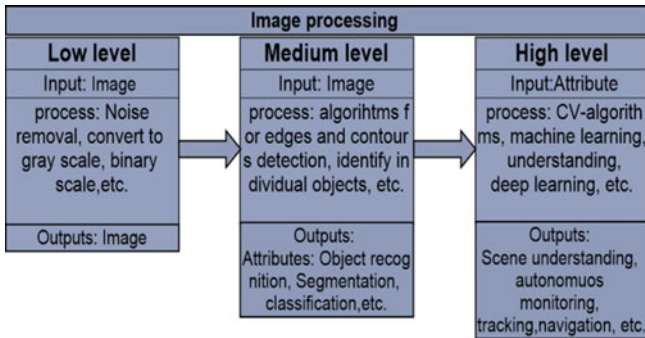


Fig. 2 Levels of image processing in construction

unmanned aerial vehicles (UAV) [6, 7]. The selected device for capturing has to be suitable for capturing images from the construction site because the construction sites have a uniquely dynamic environment where multiple machines and workers are working simultaneously, which causes occlusions and affects the captured scenes (for example, surveillance cameras fixed on construction sites are limited in view and could not cover the whole site) [6, 7]. It is also necessary to calibrate the selected device, which includes calculating the primary point location, radial distortions, and tangential distortions, which may be accomplished using a checkerboard or by utilising established camera calibration toolboxes [3, 4].

2.3 General Processing

Like image cropping, video clipping, key frame selection, and converting red, green, and blue (RGB) to other colour spaces (HIS, HSV, CIELAB, or grayscale) [12]. It is a vital phase in image and colour enhancement so that the end result is more appropriate than the original for certain applications. The goal of enhancement techniques is to draw attention to hidden elements or to highlight certain features of interest in an image [12].

2.4 Feature Extraction

Several techniques involve employing algorithms to detect features such as shapes, colours, and edges in images [12]. Extracting the needed features is critical to decreasing the number of resources without losing any significant information. Feature extraction is a stage in the dimensionality reduction process that involves reducing and sorting an initial collection of raw data into more manageable categories to simplify the subsequent processes [12].

2.5 *Object Detection*

Object detection is a part of image processing and computer vision that concerns itself with detecting instances of semantic items of a certain class (such as individuals, machines, construction elements, or equipment) in captured images and videos [12]. To produce meaningful results for object detection in construction, several algorithms typically use deep learning or machine learning to extract the required objects [12].

2.6 *Image Segmentation*

It is a technique used in digital IP to divide an image into various portions or regions, frequently according to the pixels' characteristics, and it might include separating background and foreground pixels or grouping regions of pixels based on shape similarity or colour [12].

2.7 *Progress Monitoring*

The state of CPM must be identified and corrected in real-time to prevent construction overruns (time and cost) [13, 14]. CPM is defined as the collection, recording, and reporting of progress information to prevent overruns and take corrective actions in real-time [5]. The traditional methods for progress monitoring need manual data collection from construction sites and schedules by construction engineers [5]. As a result, traditional techniques are time-consuming, expensive, and error-prone. To overcome these difficulties, IP and CV technologies were used to boost automation levels in CPM recently by several researchers [3, 4, 8, 10].

IP has increased the automation of CPM, overcome the limitations of manual observation and collected construction site information methods. Evaluation of progress monitoring can be achieved by comparing as-built and as-planned models [5, 15]. IP is used to collect and analyze the actual status of the construction sites by integrating image processing with CV-based tools and algorithms and with BIM. The automated CPM procedure includes: (a) capturing as-built from construction sites; (b) retrieving information from the collected data and captured images; and (c) estimating progress [5, 9, 16].

Several researchers have made a valuable contribution to automated CPM by adopting IP [4, 8, 16]. For instance, Deng et al., [8] proposed a method that combines IP with CV and BIM for automated progress monitoring of tiles. To train a tile classifier, support vector machines (SVMs) and feature extraction methods (local binary patterns (LBPs)) are used. The enhanced edge identification technique finds the boundaries of constructed tiles in the images provided. The boundary line coordinates are then transformed into a real-world coordinate system using the calibration

of the camera. Using information from room profile information from the BIM model and the camera location, the tiled area can be determined automatically. This model has a high accuracy of roughly 91.17 percent for tile categorization [8]. In addition to that, Hamledari et al., [4] used 2D digital images and a CV-based algorithm to find the current state of wall construction automatically. The proposed module recognised wall installation, plaster, and paint states, as well as studs and electrical outlets. Three databases of indoor building site images were used to validate the suggested technique. The model's good accuracy rates and quick performance allow it to be used at indoor sites and to provide information on the current status to future progress monitoring systems. The suggested technique has drawbacks such as its inability to recognise metallic boxes and the present state of partitions with restricted sight, its inability to evaluate a partially painted or plastered state, and its accuracy in poor shot scenes [4].

2.8 Resources Tracking

Tracking construction sites' resources is essential in many construction applications like productivity recognition, progress monitoring, and safety management. CV-based technologies have been adopted for tracking several resources on construction sites simultaneously using a network of cameras without the need for tags [17]. This feature makes vision tracking a cost-effective and time-efficient choice for crowded sites where a large number of resources must be tracked in a small area [17].

Several researchers have made valuable attempts for tracking resources (labours, cranes, dumper, loader, materials, etc.) using IP and CV-based technologies [17, 18]. For instance, Yang et al., [19] presented a comprehensive video camera tracking system for several workers, where machine learning is used in the tracking procedure. It employed kernel analysis to find statistically meaningful joint feature-spatial relationships, which were subsequently utilized to develop a construction worker appearance model. The tracking technique can track many workers in a given video sequence as shown in Fig. 3 [19]. Another study for tracking earthmoving equipment actions using support vector machine classifiers and spatio-temporal features was proposed by Golparvar et al., [20]. The testing findings showed average accuracies of 86.33 percent for excavator action identification and 98.33 percent for truck action recognition, respectively, indicating the potential for the suggested method's use for automated construction activity tracking and analysis [20].

2.9 Material Classification

Automatically monitoring construction sites using site image collections necessitates the recognition of semantic information such as construction materials [21, 22]. A valuable attempt for material classification has been presented by Dimitrov and

Fig. 3 Example for tracking construction workers by cameras, proposed by [19]



Golparvar [21], where a vision-based material classification system based on single images captured under unknown site lighting conditions and viewpoint was proposed as shown in Fig. 4 [21]. A database of 20 common building materials with more than 3000 images (about 150 images per category) was constructed and utilized for validation with an accuracy of (97.1%) was recorded [21].

Another study by Brilakis et al., [23] decomposed an image into colour, texture, and structure features using a series of content-based filters. Where an image was divided into cluster regions, using databases that were built and utilized to compare the feature signature of each cluster to develop material image classification. Also, Zuh and Brilakis [22] suggested machine learning algorithms for recognizing concrete material regions. To begin, the construction site image was segmented into regions using segmentation. After that, Artificial Neural Network (ANN) and Support Vector Machine (SVM) were used to classify visual characteristics based on texture and color. Experiment results showed that ANN performed better than SVM, with an average precision and recall of about 80%.

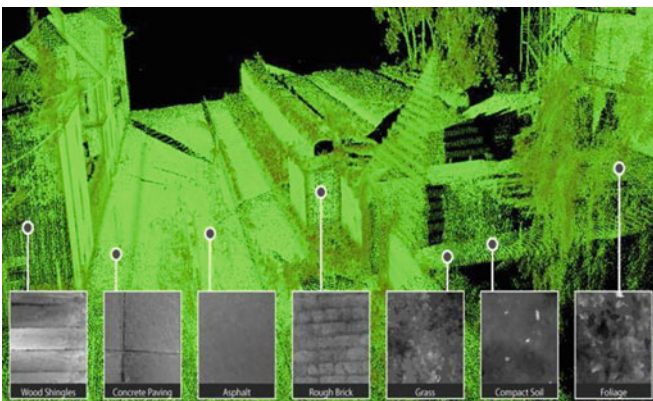


Fig. 4 Example for construction material classification and labelling proposed by [21]

Table 1 Examples for construction activities monitoring using image processing and CV-based technologies

Main objective	Input data	Adopted Process/algorithm/tools	Activity recognized/monitored	Accuracy	Reference
Automated progress monitoring using images and BIM	Images	SFM) and MVS algorithms, photogrammetric principles	Determine the quantity of performed work	99%	[1]
Localization and registration of images with BIM	Video	Augmented monocular SLAM, algorithm, Canny edge detector, BIM	Matching between the image frames and their corresponding	100%	[24]
			BIM views, to be used for indoor monitoring of construction		
Automated CV-based detection of components of underconstruction indoor partitions	Images	Canny edge detector, histogram of oriented gradients (HOG), k-means clustering algorithm, local binary patterns (LBP), SVM classifier	Detect electrical outlets, studs, and three states of walls' sheets	Around 90%	[4]
Tile alignment inspection using CV-based applications	Images	Adobe Photoshop CS4, Inspector2.1, FAST detector, Visual Basic	Alignments for tiles	-	[25]

The following table 1 represents some valuable research for monitoring and recognizing some activities in construction sites, in addition to the adopted tools and algorithms in each study.

3 Challenges and Opportunities for Adopting Image Processing in Construction

3.1 Challenges

Although the great development in capturing devices, high storage databases, and easy access to the Internet support image processing in construction, several challenges reduce the effectiveness and accuracy of IP applications in construction [5, 13, 26]. These challenges can be divided into two major groups: those related to the

adopted device and those related to the construction jobsite. The device challenges are mainly related to specifications of the captured device, distance of the device to the object (which change the scale of the tracked objects), angle of capturing (which change the scale of the tracked objects), images overlapping, device calibration, and image resolution [3, 5, 6]. While the challenge of construction job sites is related to the dynamic environment of the construction sites, occlusions, crowded job sites, lighting conditions, and weather [5, 26].

3.2 Opportunities

Despite researchers’ efforts, it has been observed that current studies did not encompass all complex construction sites and were based on a small sample of construction worker activities and machines separately [3, 5, 6]. To maximize the value of IP, future research may focus on monitoring the entire construction site, which would entail several people and machines operating at the same time [3, 5, 6]. It is also vital to develop the applications of IP and CV-based technologies through workshops, training, and conferences to keep current on knowledge and monitor technological trends, particularly in the field of IP and CV technologies. In addition to that, integrating IP, CV, and BIM together will increase the chance for more development of IP applications in the construction industry, and this will have a valuable and great impact on the development of construction and improve the chance of successful project completion [3, 5, 6].

Figure 5 depicts the conceptual framework in which the use of image processing in conjunction with CV and BIM will increase the efficiency of collecting and monitoring various elements of construction sites. This will result in increased construction productivity, improved safety monitoring, and effective decision-making. If these elements are improved in construction, it will lead to fewer errors, lower costs, taking timely corrective actions, and, ultimately, successful construction projects.

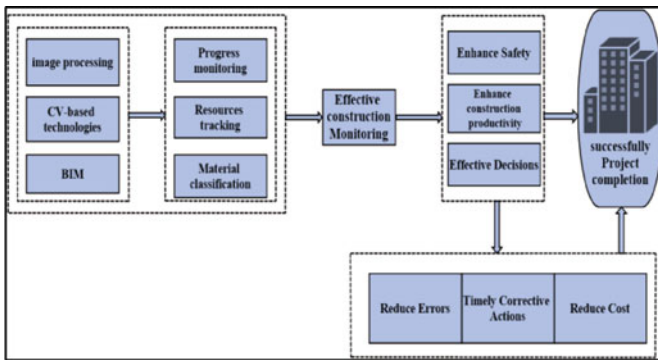


Fig. 5 Conceptual framework

4 Conclusions

The research focuses on several areas where IP may be applied in construction projects, in addition to challenges that IP adoption faces and opportunities for more improvement in the construction sector. The use of IP in construction raises the automation monitoring for several aspects of construction projects, such as progress monitoring, resource tracking, material classification, productivity analysis, and structural element recognition. which results in reducing and eliminating the limitations of traditional monitoring and collecting methods, enhancing the decision-making process, reducing errors, and improving timely corrective actions. All these items increase the chances of a successful project's completion.

Although the great development in capturing devices, high storage databases, and easy access to the Internet support IP in construction, there are several challenges that reduce the effectiveness and accuracy of image processing applications in construction. These challenges can be divided into two major groups: those related to the adopted device and those related to the construction jobsite. The device (camera) challenges are mainly related to specifications of the captured device, distance of the device to the object, angle of capturing, overlapping, device calibration, and image resolution. While the challenge of construction job sites is related to the dynamic environment of the construction sites, occlusions, crowded job sites, lighting conditions, and weather.

Acknowledgements The authors would like to thank Universiti Teknologi PETRONAS for the support provided in this research.

References

1. Mahami H, Nasirzadeh F, Hosseininaveh Ahmadabadian A, Nahavandi S (2019) Automated progress controlling and monitoring using daily site images and building information modelling. *Buildings* 9(3):70
2. Mostafa K, Hegazy T (2021) Review of image-based analysis and applications in construction. *Autom Constr* 122:103516. <https://doi.org/10.1016/j.autcon.2020.103516>
3. Alzubi KM, Alaloul WS, Al Salaheen M, Qureshi AH, Musarat MA, Baarimah AO (2021) Automated monitoring for construction productivity recognition. In: 2021 Third International Sustainability and Resilience Conference: Climate Change, 2021, pp 489–494
4. Hamledari H, McCabe B, Davari S (2017) Automated computer vision-based detection of components of under-construction indoor partitions. *Autom Constr* 74:78–94. <https://doi.org/10.1016/j.autcon.2016.11.009>
5. Alaloul WS, Alzubi KM, Malkawi AB, Al Salaheen M, Musarat MA (2021) Productivity monitoring in building construction projects: a systematic review. *Eng Constr Architect Manage* ahead-of-print, ahead-of-print. <https://doi.org/10.1108/ECAM-03-2021-0211>.
6. Alzubi KM, Alaloul WS, Malkawi AB, Al Salaheen M, Qureshi AH, Musarat MA (2022) Automated monitoring technologies and construction productivity enhancement: building projects case. *Ain Shams Eng J* 14:102042. <https://doi.org/10.1016/j.asej.2022.102042>.

7. Qureshi AH, Alaloul WS, Wing WK, Saad S, Alzubi KM, Musarat MA (2022) Factors affecting the implementation of automated progress monitoring of rebar using vision-based technologies. *Constr Innov* ahead-of-print. <https://doi.org/10.1108/CI-04-2022-0076>.
8. Deng H, Hong H, Luo D, Deng Y, Su C (2020) Automatic indoor construction process monitoring for tiles based on bim and computer vision. *J Constr Eng Manag* 146(1):04019095. [https://doi.org/10.1061/\(ASCE\)CO.1943-7862.0001744](https://doi.org/10.1061/(ASCE)CO.1943-7862.0001744)
9. Ekanayake B, Wong JK-W, Fini AAF, Smith P (2021) Computer vision-based interior construction progress monitoring: a literature review and future research directions. *Autom Constr* 127:103705. <https://doi.org/10.1016/j.autcon.2021.103705>
10. Golparvar-Fard M, Peña-Mora F, Savarese S (2015) Automated progress monitoring using unordered daily construction photographs and IFC-based building information models. *J Comput Civ Eng* 29(1):04014025. [https://doi.org/10.1061/\(ASCE\)CP.1943-5487.0000205](https://doi.org/10.1061/(ASCE)CP.1943-5487.0000205)
11. Teizer J (2015) Status quo and open challenges in vision-based sensing and tracking of temporary resources on infrastructure construction sites. *Adv Eng Inform* 29(2):225–238. <https://doi.org/10.1016/j.aei.2015.03.006>
12. Mathworks: Help Center (2022). <https://www.mathworks.com/support/search.html>. Accessed 02 Aug 2022
13. Alzubi KM, Alaloul WS, Qureshi AH (2022) Applications of cyber-physical systems in construction projects. In: *Cyber-Physical Systems in the Construction Sector*, CRC Press
14. Alzubi KM, Alaloul WS, Al Salaaheen M, Qureshi AH, Musarat MA, Alawag AM (2022) Reviewing the applications of internet of things in construction projects. In: *2022 International Conference on Decision Aid Sciences and Applications (DASA)*, pp 169–173. <https://doi.org/10.1109/DASA54658.2022.9765143>.
15. Qureshi AH, Alaloul WS, Wing WK, Saad S, Ammad S, Musarat MA (2022) Factors impacting the implementation process of automated construction progress monitoring. *Ain Shams Eng J* 13(6):101808. <https://doi.org/10.1016/j.asej.2022.101808>.
16. Bügler M, Ongunmakin G, Teizer J, Vela PA, Borrmann A (2014) A comprehensive methodology for vision-based progress and activity estimation of excavation processes for productivity assessment. In: *Proceedings of the 21st International Workshop: Intelligent Computing in Engineering (EG-ICE)*, Cardiff, Wales
17. Park M-W, Makhmalbaf A, Brilakis I (2011) Comparative study of vision tracking methods for tracking of construction site resources. *Autom Constr* 20(7):905–915
18. Gong J, Caldas CH (2011) An object recognition, tracking, and contextual reasoning-based video interpretation method for rapid productivity analysis of construction operations. *Autom Constr* 20(8):1211–1226. <https://doi.org/10.1016/j.autcon.2011.05.005>
19. Yang J, Arif O, Vela PA, Teizer J, Shi Z (2010) Tracking multiple workers on construction sites using video cameras. *Adv Eng Inform* 24(4):428–434. <https://doi.org/10.1016/j.aei.2010.06.008>
20. Golparvar-Fard M, Heydarian A, Niebles JC (2013) Vision-based action recognition of earth-moving equipment using spatio-temporal features and support vector machine classifiers. *Adv Eng Inform* 27(4):652–663. <https://doi.org/10.1016/j.aei.2013.09.001>
21. Dimitrov A, Golparvar-Fard M (2014) Vision-based material recognition for automated monitoring of construction progress and generating building information modeling for unordered site image collections. *Adv Eng Inform* 28(1):37–49. <https://doi.org/10.1016/j.aei.2013.11.002>
22. Zhu Z, Brilakis I (2010) Concrete column recognition in images and videos. *J Comput Civ Eng* 24(6):478–487
23. Brilakis IK, Soibelman L, Shinagawa Y (2006) Construction site image retrieval based on material cluster recognition. *Adv Eng Inform* 20(4):443–452. <https://doi.org/10.1016/j.aei.2006.03.001>
24. Asadi K, Ramshankar H, Noghabaei M, Han K (2019) Real-time image localization and registration with BIM using perspective alignment for indoor monitoring of construction. *J Comput Civ Eng* 33(5):04019031

25. Lin K-L, Fang J-L (2013) Applications of computer vision on tile alignment inspection. *Autom Constr* 35:562–567. <https://doi.org/10.1016/j.autcon.2013.01.009>
26. Qureshi AH, Alaloul WS, Manzoor B, Saad S, Alawag AM, Alzubi KM (2021) Implementation challenges of automated construction progress monitoring under industry 4.0 framework towards sustainable construction. In: 2021 Third International Sustainability and Resilience Conference: Climate Change, pp 322–326

Comparative Analysis of Vehicle Operating Cost Methods



(Cases Study: Medan-Binjai Toll Road)

Ridwan Anas, David Barry Hariganta, and Derry W. Nasution

Abstract In the life cycle cost analysis, retrenching the vehicle operational cost is estimated as a benefit due to an increase of road capacity and optimizing the life-cycle cost (LCC) is one strategic approach to achieve the sustainable infrastructure system. Vehicle operating cost is the cost related with ownership, operation, and ownership, and the cost of accumulation and vehicle insurance. With several types of VOC developing in the world, the purpose of this research is to analyse comparison of VOC between HDM 4, TRRL and other methods developed by the Indonesian Government. The results of this analysis indicates a significant difference towards the three model of estimation developed by the Indonesian Government or the one developed by the World Bank.

1 Introduction

Transportation must bring advantages as the fundamental function of it, which is to provide access to the people and play a significant role as a logistic function (Taking Raw Material; manufacture to consumer). Accordingly, improving the performance of transportation is accepted as a method to provide a better logistic system, reduce operation cost, and increase economic growth in one certain area. Increasing the road capacity will also increase the accessibility, reduce the travel time and transportation costs (Glen W.1998). Therefore, the need for transportation is inseparable from the development and the economic growth of a region (Anas, 2015).

The role and the function of the highway has several impacts towards sustainable issues, such as the environmental and economic matters [6]. In the life cycle cost analysis, retrenching the vehicle operational cost is estimated as a benefit due to an

R. Anas (✉) · D. B. Hariganta · D. W. Nasution
Department of Civil Engineering, Universitas Sumatera Utara, Medan, Indonesia
e-mail: ridwan.anas@usu.ac.id

D. W. Nasution
e-mail: derryns@usu.ac.id

increase of road capacity [12]. Optimizing the life-cycle cost (LCC) is one strategic approach to achieve the sustainable infrastructure system.

Linked to an investment in road infrastructure, the direct economic impact experienced by the users such as reducing the road users cost, consist of reducing the users' travel time, operating costs, and the accidents cost (Banister, 2000). Road user cost (RUC) is defined as the estimation of cost covered by the people as a consequence from traveling [7]. The cost of road users is a part of transportation costs, which consist of vehicle operational costs, cost of the time of travel, accidents, impacts to the environment and convenience [11].

The cost of the travel time and the vehicle operational cost are two major components of road user cost [5]. The cost of the time of travel is counted based on the opportunity lost from the road users caused by the increase amount of time for travel, meanwhile the cost of vehicle operation is the cost related with ownership, operation, and ownership, and the cost of accumulation and vehicle insurance. Respectively, each components of cost usually is elaborated separately and counted to acquire the entire vehicle operational cost [3].

2 Literature Review

2.1 Road User Cost (RUC)

Life Cycle Cost Analysis (LCCA) is a process to evaluate the economic value from one investment on transportation applying the principles of economy in estimating the indicators that affect (environment, economy, and social) to be a unit to be measured economically.

Generally, three basic components of the RUC must be estimated such as the vehicle operating cost, accident cost, the cost of the time of travel, and the emission cost [13]. RUC has been applied in several decision analysis aspects including planning, designing and preliminary engineering, and project construction.

2.2 An Overview of Vehicle Operational Cost (VOC) Models

Vehicle Operational Cost (VOC) is the major contribution towards the RUC [9]. The vehicle operational costs is a cost related with ownership, operational costs and vehicle maintenance, such as (ASHTO, 2003):

- Operating cost, includes: fuels costs, lubricants, tire and maintenance
- Ownership cost, includes: depreciation costs, tax, and administration expenditures

The model used in estimating the VOC can be categorized as empirical dan mechanical models. The mechanical model is formulated theoretically until it in

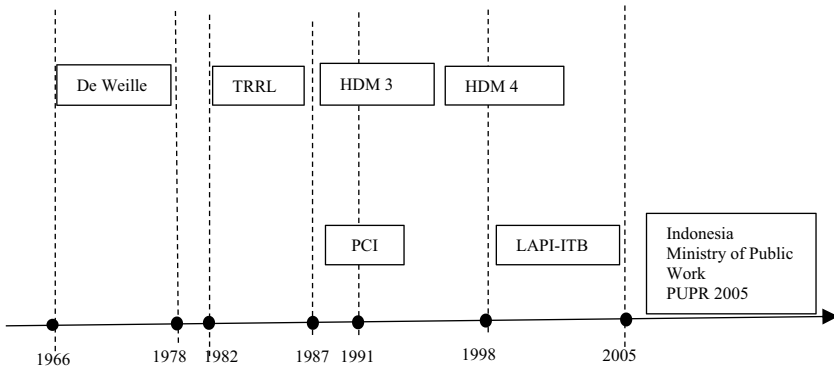


Fig. 1 The history and development of VOC Models

includes the major physical parameter according the elementary laws of physics/mechanic. Meanwhile the empirical model relies on the mathematical correlation towards the different parameter to create a model with a limited application towards the data input used in the development [1].

The basics of the VOC research derives from the De Weille (1966) study for the World Bank, known as the Highway Development and Management (HDM) program. On the other hand, the VOC estimated in Indonesia was initiated by Pacific International Consultant (1969), starting with the RED book AASHTO in 1977 furthermore upgraded by Texas Research and Development Foundation (TRDF) in 1982 (Fig. 1).

2.3 The Components of VOC

This section will explain the components from the vehicle operational costs, which includes:

1. The Cost of Fuel

The cost of fuel for the vehicle is calculated according to the fuel consumption for each type of vehicle each kilometre. The speed of the vehicle operation dominantly affect the fuel consumption level. The further adjustment to the fuel consumption level is calculated in order to measure the specific location such as the slope, curve, traffic jam, and the roughness of road surface [1].

2. The Costs of Oil

The cost is calculated for consuming oil in one operation of the type of vehicle for each kilometre gained. The quantity acquired from the multiplication of the results of oil consumption per kilometre with the price of oil per litre.

3. The Cost of Tire Consumption

The cost required for using tires within an operation of a certain type of vehicle is per kilometre gained. The prediction towards tire consumption is according to the mechanical model [1], with the estimation of a type of tire (lateral and normal conditions of the tire), by measuring the condition of road surface which are curve and road roughness.

4. The Cost of Spare Parts

The cost of spare parts is a cost required for purchasing spare parts in the operation of a certain type of vehicle for each kilometre gained. In the cost of spare parts, the age of the vehicle, road roughness and the acceleration change of the vehicle are measured.

5. The Cost of Maintenance

The Cost of Maintenance is the cost required for the maintenance in the operation of a certain type of vehicle for each kilometre gained. The quantity of the cost of maintenance for a certain type of vehicle is affected by the type of vehicle, the quantity of labour, and the calculation of the time of maintenance.

6. The Cost of Vehicle Crew

The cost of the vehicle crew is the cost spent by the owners of the vehicles to provide wages to the crews who operate a certain vehicle. The cost of the crew is counted for each kilometre gained which is affected by the amount of operational hours of the crew during a certain distance (each kilometre) of the vehicle.

7. The Cost of Vehicle Depreciation

The Cost of Depreciation occurs for calculating VOC which is caused by the reduction of the age of the vehicle's service due to the vehicle operation until the price or the vehicles depreciates.

8. The Cost of Capital Interest Rate

The Cost of Capital Interest is burdened to the owner of the vehicle while purchasing a new vehicle. An annual capital interest rate from the vehicle expressed as a fraction from the price of a new vehicle per kilometre gained every year (distance).

The methods which will be compared consists of several different component evaluated to the calculation of the vehicle operational cost. Each calculated component can be illustrated in the table below (Table 1).

In the third method calculation compared lists five similar components which are fuel consumption, lubricants, tire, spare parts, and the cost of maintenance. The methods of calculating the vehicle operation cost developed by the Indonesian Government (PUPR 2005) does not estimate the fix cost variables in estimating the Vehicle Operational Cost (VOC).

Table 1 Differences of the VOC method’s component

VOC		TRRL	HDM 4	PUPR 2005
Variable cost	Fuel Consumption	✓	✓	✓
	Oil Consumption	✓	✓	✓
	Tire Consumption	✓	✓	✓
	Spare Part Consumption	✓	✓	✓
Fixed cost	Cost of Vehicle Crew	✓	✓	-
	Depreciation	✓	✓	-
	Insurance	-	-	-
	Interest Rate	-	✓	-

3 Methodology

3.1 Representative Vehicles

The types of vehicles which will be used as a benchmark in the comparison of the VOC model is the small passenger car. The Toyota VIOS E is selected as the vehicle represented in the vehicle operational cost calculation with a vehicle type of a small passenger unit with the specification as listed below:

- The amount of axis: 2 unit
- The amount of tires: 4 unit
- Gross Vehicle Weight: 1.5 ton
- Fuel: liters of gasoline

3.2 Estimating the Vehicle Operational Cost

Estimating the vehicle operational cost uses the formula provided from each method. Estimating the cost acquired according to the similarities are mentioned below:

3.2.1 Fuel Consumption

The cost of fuel consumption is acquired with the similarities as mentioned below:

$$\text{TRRL; FL} = (53.4 + 499/V + 0.0058 V^2 + 1.594RS - 0.854F) \times 1.08$$

$$\text{HDM 4; Fuel Cost} = \sum_{k=1}^4 FC_k \times AADT_k \times \text{TypeCost}_k$$

$$\text{PUPR 2005; } B_i \text{BBMM}_{ij} = KBBM_i \times HBBM_j$$

The models developed estimate the parameter of the road geometric condition, the characteristics and the speed of the vehicle. For the TRRL and PUPR the speed and the ration from the power and the weight of the vehicle has already been considered,

meanwhile HDM 4 has already considered the effect of change of fuel acceleration and the machine efficiency factor towards consumption.

3.2.2 Oil Consumption

The Cost of Oil Consumption is calculated with the similarities as mentioned below:

TRRL; Oil Cost = 1.2 liter/1,000 km

HDM 4; $Oil\ Cost_{av} = \sum_{k=1}^4 Oil_k \times AADT_k \times Oil\ price_k$

PUPR 2005; $BO_i = KO_i \times HO_j$

Oil Consumption has been included in a model by HDM 4 and PUPR 2005, considering in this matter the oil that has evaporated due to contamination and the use of the vehicle oil.

3.2.3.1. Oil Consumption

The average cost of oil consumption can be calculated with the similarities as mentioned below:

TRRL; $TC = (-83 + 0,058R) \times 10^{-6} \times Tyre\ Price$

HDM 4; $TC_{av} = \sum_{k=1}^4 TC_{avk} \times Tyre\ cost_k$

PUPR 2005; $BB_i = KB_i \times HB_j / 1000$

The model developed by TRRL dan PUPR 2005 has already considered the road roughness level and the weight of the vehicle, while HDM 4 besides considering the roughness of the road surface and estimating the use of tire per 1000-km also considers the style that works on a tire.

3.2.3 Spare Parts Consumption

The cost of spare parts consumption can be acquired with the similarities as mentioned below:

TRRL; $PC = (-2.03 + 0.0018R) \times K \times 10^{-11} \times VP$

HDM 4; $LC = WAGECOST \times LH_{av}$

PUPR 2005; $BP_i = P_i \times HKB_j / 1000000$

The model developed considered the relative value of the cost of spare parts towards the price of a new vehicle or the spare part consumption and a duration of the maintenance work hours calculated from the function from the spare parts consumption and the amount of working hours for 1000 vehicle – km.

3.2.4 Maintenance Labour Hours

The cost of maintenance labour hours can be acquired with the similarities as mentioned below:

$$\begin{aligned} & \text{TRRL; LabourCost} = (851 - 0.078R) \text{ PC/VP} \\ & \text{HDM 4; LABOURCOST} = (K0lh \times [a0 \times \text{PCa1}] + K1lh) \times \text{WageCost} \\ & \text{PUPR 2005; BU}_i = \text{JP}_i \times \text{UTP}/1000 \end{aligned}$$

Maintenance labour hours are calculated as a function of the parts consumption. Labour wage rates are applied to the predicted number of labour hours to obtain labour costs.

4 Result

The Medan-Binjai Toll Road has a length of ± 17 km, and designed with a speed of 80–100 km/h, The data of the Medan-Binjai Toll Road Lane are mentioned below:

- Road roughness = 2.75 m/km
- The Width of the Lane = 3.5 m
- The Amount of Lanes = 2lane/direction
- Superelevation = 2%

VOC analysis uses a speed of 80 km/hour as a speed that represents. The VOC consists of two components which are an variable cost/running cost and fixed cost, in an analysis which will compare the quantity of the variable component cost for each method reviewed.

The table illustrated below can be seen with a comparison of the result of a variable cost estimation for the passing type of vehicle, towards each component (Table 2).

Calculating the vehicle cost can see the largest value acquired from the method developed by the Indonesian Government, where the largest component is the Maintenance Cost. Meanwhile, the most proper component for the model developed by HDM 4 and is the fuel consumption cost component.

Fixed cost is estimated by counting the costs of the vehicle crew members, the vehicle depreciation cost, the cost of the capital interest rate, and the cost of insurance within Rupiah’s per kilometre (Table 3).

From the table illustrated above, it could be determined that the model which has been developed by the Indonesian Government does not estimate the Fixed cost,

Table 2 Comparison Results for a variable cost for a speed of = 80 km/h (in Rupiah’s)

The Components of Cost	PUPR 2005	HDM 4	TRRL 1976
Fuel Consumption	618.09	668.82	805.52
Oil Consumption	14.89	27.40	51.00
Tire Consumption	13.64	21.66	39.78
Spare Parts Consumption	368.07	368.07	426.32
Maintenance Consumption	1,221.38	50.03	23.23
TOTAL	2,236.07	1,135.98	1,345.86

Table 3 Estimation of Fixed Cost

Components of Cost	PUPR 2005	HDM 4	TRRL 1976
Depreciation	-	4,928.64	2,336
Capital Interest Rate	-	191,03	
Total	-	5,119.67	1,345.86

meanwhile the largest value has been acquired from the model developed by HDM 4.

For the Medan-Binjai Toll Road, the VOC estimation value for the PUPR 2005 model amounts up to Rp. 38,013.21, HDM 4 is Rp. 105,568.64 and for the TRRL is Rp. 62,591.56.

5 Conclusion

VOC is the amount of cost spent by the vehicle owner for the operation, maintenance, and vehicle ownership. In estimating the VOC, the model developed estimates the parameter of the road geometrical condition, the characteristics of the vehicle, model-model and the speed of the vehicle.

The VOC consists of two major components which are the variable cost or the running cost and the fixed cost (standing cost or fixed cost). The components of the variable cost are: the cost of fuel consumption, the cost of oil, the cost of spare parts, the cost of maintenance, the cost of interest rate, and insurance costs.

From the results of analysis for the components from the variable cost, it is identified that for the model developed by HDM 4 and TRRL, that the cost of fuel consumption is the major component in contributing to the quantity value of VOC ($\pm 60\%$). The largest component cost from the PUPR 2005 model is the cost of maintenance which is $\pm 54\%$, while the cost of fuel consumption is $\pm 28\%$ of the total value of the variable cost.

For the components of the fixed cost, the model which has been developed by HDM 4 has estimated the quantity of depreciation and the capital interest rate and the model which has been developed by TRRL which only estimates the depreciation value. The fixed cost is not included in calculating the VOC, which has been developed by the Indonesian Government.

The benefit from one investment in the toll road is acquired from quantifying the retrenchment of the VOC after the operation of the toll road. The results of this analysis indicates a significant difference towards the three model of estimation developed by the Indonesian Government or the one developed by the World Bank.

References

1. Bein P (1993) Evaluation of state-of-the-art VOC models. *Road Transp. Res.* 2(3)
2. Bein P, Biggs DC (1993) Critique of Texas research and development foundation vehicle operating cost model. *Road Transp Res* 1395:114–121
3. Bennet CR, Greenwood ID (2003) HDM-4 calibration reference manual
4. International Study of Highway Development and Management Tools (ISOHDM)
5. Santos B, Picado-Santos L, Cavaleiro V, Neves J (2012) User costs in road life-cycle cost evaluation and optimization. *Research gate*
6. Choi J (2020) Road user costs for highway construction projects involving a lane closure. *Sustainability* 12(8):3084. <https://doi.org/10.3390/su12083084>
7. Daniels G, Stockton WR, Hundley R (2000) Estimating road user costs associated with highway construction projects: simplified method. *Transp Res Rec J Transp Res Board* 1732(1):70–79
8. Federal highway administration (2021) Calculating Road User Cost for Specific Sections of Highway for Use in Alternative Contracting Project, Tennessee Department of Transportation, p IV
9. Jenkins J, McAvoy D (2015) Evaluation of Traffic Flow Analysis and Road User Cost Tools Applied to Work Zones (FHWA/OH-2015/29). The Ohio Department of Transportation (ODOT)
11. National Cooperative Highway Research Program (NCHRP) (2012) Estimating the Effects of Pavement Condition on Vehicle Operating Costs, TRANSPORTATION RESEARCH BOARD, p3
12. Pentury C, Santoso I, Wibowo SS (2020) Kajian Sub model Biaya Operasi Kendaraan Pada Model HDM-4. *J Manumata* 6:46–52
13. US Department of Transportation (2021): Calculating Road User Cost for Specific Sections of Highway for Use in Alternative Contracting Project, Research Final Report from East Tennessee State University, p5.

Underwater Sill Layout for Efficient Sediment Deflection



Tania Edna Bhakty, Nur Yuwono, Bambang Triatmodjo,
and Ahmad Faramarz Ghalizhan

Abstract In ports with jetty-style berths, where the basins and navigation channel are placed in the surfzone, sedimentation problems are common. Installing an underwater sill (UWS) prevents the sedimentation of navigational channels and basins. The objective of this research is to investigate the influence of the UWS layout on the structure's capacity to redirect flow to the side. The three evaluated models (rectangular, trapezoidal, and curve) demonstrated that the UWS with a curve layout has a better capacity for deflecting flow away from the structure. This was indicated by the closeness of the exponent to the theoretical value, $n' \approx 1$.

Keywords deflect · UWS · layout

1 Introduction

Wind, waves, tides, and currents are important driving factors that affect sediment transport within the surf zone in the dynamic coastal zone [1, 2, 3]. Jetty-type berths that have been built in a surf zone will experience sedimentation problems caused by sediment transport [4, 5, 6, 7]. The weather and wave conditions have a significant impact on the jetty's operational time. Alternative solutions include constructing breakwaters to protect the port basin from waves and sedimentation problems caused by longshore sediment transport, relocating the port by extending the trestle out of the surf zone, performing maintenance dredging, and installing underwater sill (UWS)

T. E. Bhakty (✉)
Janabadra University, Yogyakarta, Indonesia
e-mail: tania@janabadra.ac.id

N. Yuwono · B. Triatmodjo
Universitas Gadjah Mada, Yogyakarta, Indonesia

A. F. Ghalizhan
Sepuluh Nopember Institute of Technology, Surabaya, Indonesia

© Institute of Technology PETRONAS Sdn Bhd 2024
B. S. Mohammed et al. (eds.), *Proceedings of the International Conference on Emerging Smart Cities (ICESC2022)*, Lecture Notes in Civil Engineering 324,
https://doi.org/10.1007/978-981-99-1111-0_58

around the basin and navigation channel to prevent sedimentation problems. UWS is also known as Submerged Dike (SD) [6].

In 1992, SD was implemented in the Japanese port of Kumamoto, while in 2000, UWS was adopted in the port of Semen Tuban, Indonesia [8]. According to the field survey, SD has prevented around 30% of the total deposition in the navigation channel at a height of 1 m above the bottom [9]. In Semen Tuban Port, the sedimentation in the port basin reduced from 1.0–1.70 m/year to approximately 0.40 m/year after the installation of UWS [10]. The installation of UWS as a solution to prevent sedimentation on both sides of the navigation channel and throughout the entire basin has shown to be quite advantageous. The effectiveness of the UWS construction must therefore be investigated in order to control the sedimentation current's pattern in the port basin.

2 The Research Method

The physical model research is conducted at Gadjah Mada University's Hydraulics Hydrology Laboratory. Determine UWS layout to have a better ability to divert the flow to the side of the structure is the aim of the research. The $24 \times 0.8 \times 1 \text{ m}^3$ "Arm-field" brand flume was used in this study. There is a tailgate in the upper section of the flume for adjusting the water level. An adequate pump must have a 15 l/s capacity to circulate flume current. To determine the pump's capacity, longshore current values in the range of 0.03–0.07 m/s are used. Using the fall velocity technique of sediment suspension, which has a fall velocity of 0.5–1.0 cm/s, the length of UWS is estimated (similar current). The water depth utilized in this experiment is $d = 0.5 \text{ m}$, and the discharge used is $Q = 9.914 \text{ l/s}$. The energy grade line is $I_e = 2.25 \times 10^{-7}$, the average velocity is $\bar{U} = 0.0198 \text{ m/s}$ in a section channel without a UWS structure, and $R_e = 4957 > 2000$ (turbulence).

The 10 mm acrylic is used to create the UWS model. The layout versions of the UWS that have been tested are rectangular, curved, and trapezoidal, with sizes $30 \times 400 \times h/d \text{ cm}^3$. Rectangular (UWS end is perpendicular 90°), trapezoidal (UWS end is inclined-approx. $40^\circ - 50^\circ$), and curved (semi-circular UWS end). The study plan is depicted in detail in Fig. 1. Acoustic Doppler Velocimeters (ADV) of the Micro ADV 16-MHz type are used to measure the velocity of current because they can read instantaneous current with an accuracy of up to 99% at a maximum rate of 50 data per second. Figure 1 and Fig. 2 show the detailed tested model.

Due to the field's use of trapezoidal-shaped UWS, the layout model of a trapezoidal UWS is used. In order to capture the current pattern phenomenon in the lower part of the UWS structure, the UWS structure's rectangular shape was chosen. In this structure, the upper layer current flows with the highest velocity, reduces near the UWS structure, and ultimately stops in the region where the UWS structure entirely blocks the area. As for picking a curved UWS, the goal is to achieve a streamline shape for the current pattern phenomenon surrounding the UWS structure. Along with the UWS pattern shapes, the height of UWS is also subject to measurement

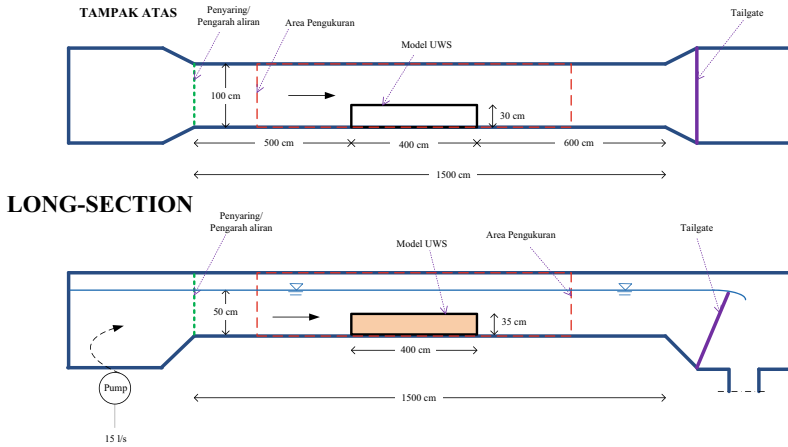


Fig. 1 Experimental plan in flume [6]

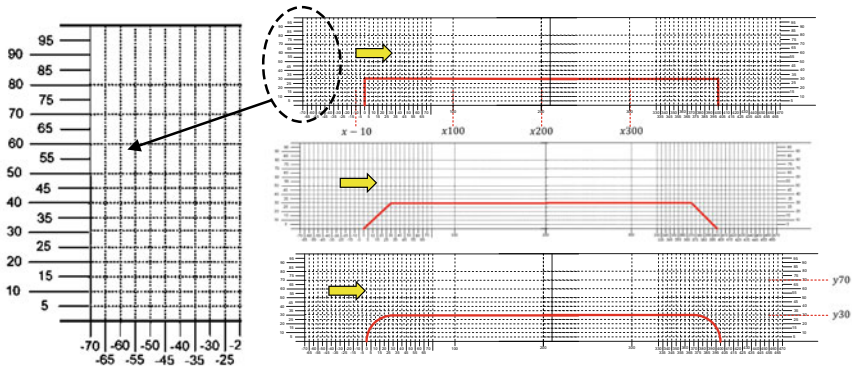


Fig. 2 Measurement point position [6]

fluctuation. If the UWS’s height is h and the water’s depth is d , then the possible values of h/d are 0.1, 0.2, 0.3, 0.4, 0.6, and 0.9.

The measurement grid on Fig. 2 was followed in the simulation of the model. For a layout model of a UWS structure with a certain value of h/d and coordinates, measurements are taken at depths of 0.05, 2.5, 5, 10, 15, 20, 30, and 40 cm (x, y). Each measurement point’s outcome is given a name based on the coordinates that were previously defined in accordance with the measurement site’s proximity to the bottom portion of the UWS structure that was used as the reference point.

3 The Result and the Discussion of the Research

3.1 Theoretical Velocity distribution and Effect of Underwater Sill Height

In prior research, it has been stated that the current velocity of non-UWS at z is analytically calculated using Eq. (1) [6]:

$$U_z = 5.75 V_* \log \frac{104z}{\delta} \tag{1}$$

In the paper, it is also stated that the UWS’s ability to deflect the current improves with increasing UWS. The UWS structure’s excessive height makes it less effective at diverting the current, which is necessary in the port basin to control sediment [6].

3.2 Flow Deflection as an Effect of the UWS Structure Layout

The discharge is the volume of fluid that moves through a stream in a given amount of time. Shear stress at the bottom and walls of the channel as well as the presence of a free surface cause the flow velocity for a given discharge rate to have a varied distribution as shown in Fig. 3:

From Fig. 3, if the discharge per unit width

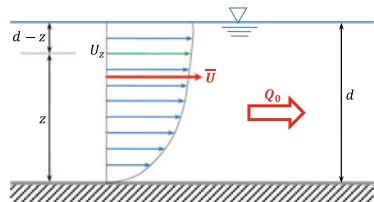
$$q = Q/B \tag{2}$$

where B is the width of the channel and the discharge has water depth from 0 to d , Eq. (1) becomes

$$q = \int_0^d U_z dz \tag{3}$$

Substitute Eq. (1) for Eq. (2),

Fig. 3 Velocity distribution without UWS



$$q = \int_0^d 5.75V_* \log\left(\frac{104}{\delta}z\right) dz \quad (4)$$

The solution to the integral Eq. (4) where the discharge through the channel width B is called Q_0 , then

$$Q_0 = B5.75V_*d \left(\log\left(\frac{104}{\delta}d\right) - 1 \right) \quad (5)$$

The presence of the UWS structure alters the flow distribution pattern in the channel. With reference to Fig. 4 and Eq. $q = Q/B$ (2, if the discharge that passes through the UWS structure has a height from h to d , then the discharge per unit width becomes:

$$q = \int_h^d U_z dz \quad (6)$$

Substitute Eq. $U_z = 5.75V_* \log\frac{104z}{\delta}$ (1 for equation $q = \int_0^d U_z dz$ (3,

$$q = \int_0^d 5.75V_* \log\left(\frac{104}{\delta}z\right) dz \quad (7)$$

The solution to the integral Eq. (7) where the discharge through the channel width B is called Q_1 , then

$$Q_1 = B5.75V_* \left[d \left(\log\left(\frac{104}{\delta}d\right) - 1 \right) - h \left(\log\left(\frac{104}{\delta}h\right) - 1 \right) \right] \quad (8)$$

In the case of flow with the UWS structure, dimensionless numbers are found by comparing the flow rate above the UWS structure Q_1 to the flow rate without the UWS structure Q_0 . This gives the equation a simplified:

$$\frac{Q_1}{Q_0} = 1 - \frac{h \left[\log\left(\frac{104}{\delta}h\right) \right]}{d \left[\log\left(\frac{104}{\delta}d\right) \right]} \quad (9)$$

Based on Eq. 1, then a graph is made as shown in Fig. 5

Following Fig. 4, Q_0 is the discharge obtained from the velocity measurement positioned before the UWS structure for all UWS layout models. Q_1 is the discharge obtained from the velocity measurement within the UWS structure.

Assuming $\left[\log\left(\frac{104}{\delta}h\right) \right] \approx \left[\log\left(\frac{104}{\delta}d\right) \right]$ at $h \geq 0.1d$ the equation is as follows:

$$\frac{Q_1}{Q_0} = 1 - \frac{h}{d} \quad (10)$$

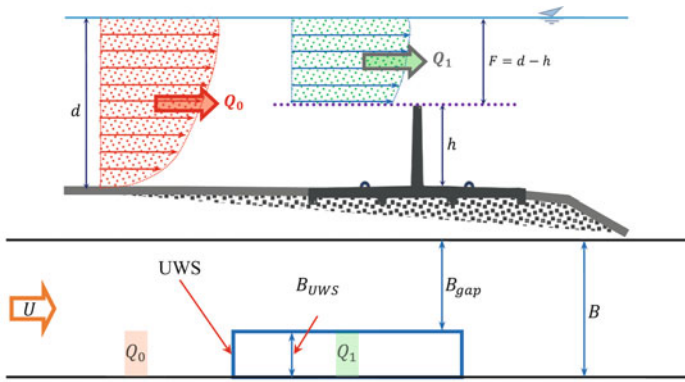
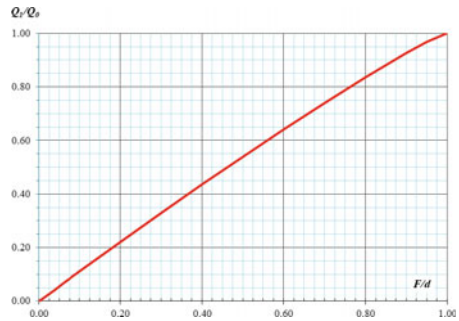


Fig. 4 Discharge through the UWS structure

Fig. 5 Q_1/Q_0 and F/d theoretical graph



If $h = d - F$, then $\frac{Q_1}{Q_0} = 1 - \left(\frac{d-F}{d}\right)$

$$\frac{Q_1}{Q_0} = \frac{F}{d} \tag{11}$$

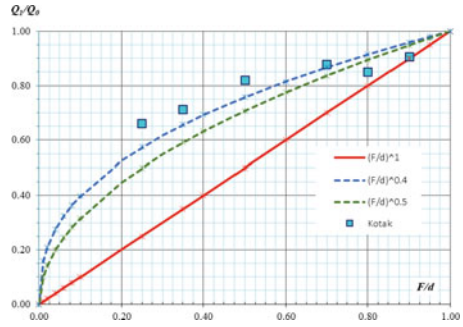
Equation (11) is approximated by the coefficient to the power of n' , when the effect of the UWS layout is taken into account, equation becomes

$$\frac{Q_1}{Q_0} = \left(\frac{F}{d}\right)^{n'} \tag{12}$$

This variation of the coefficient to the power of n' is determined based on the approximate value of the relation F/d and Q_1/Q_0 obtained from the velocity measurement for all UWS layout models.

Figure 6 depicts the rectangular UWS model measurement points plotted on the theoretical Q_1/Q_0 and $(F/d)^{n'}$ comparison graph. Measurements were taken at

Fig. 6 Q_1/Q_0 and F/d theoretical graph and rectangular UWS



$F/d \geq 0.25$, which means that the rectangular UWS was measured to a maximum height of $h = 0.75d$. The graph only applies to $B_{gap}/B = 0.67$.

To determine the degree (strength) of the correlation between the measurement data and the theoretical line, a correlation analysis of the measurement data against the theoretical line was performed. Correlation analysis of the measurement data against the theoretical line was performed. Correlation study on the theoretical line $(F/d)^n$ with $n' = 1, n' = 0.67, n' = 0.5$ dan $n' = 0.4$ is done in the rectangular UWS model. The maximum correlation value is on the theoretical line $(F/d)^{0.5}$ with a correlation value of $R_{xy} = 0.94$, according to the correlation analysis of the rectangular UWS model measurement data versus the theoretical line.

Trapezoidal UWS measurements are taken up to a height of $h = 0.9d$, with the goal of getting data trends from $h \approx 0$ to $h \approx d$ (Fig. 7). Correlation analysis was performed at the value of $F/d \geq 0.3$. In UWS planning in the field, the minimum height of the UWS commonly used is $h \geq 0.2d$. The correlation analysis between the measurement result and the theoretical line is for $(F/d)^{n'}$ with $n' = 1, n' = 0.91, n' = 0.8, n' = 0.67$ and $n' = 0.5$. The correlation analysis of the trapezoidal UWS model measurement data vs the theoretical line shows that the maximum correlation value is on the theoretical line $(F/d)^{0.67}$ with a correlation value of $R_{xy} = 0.90$.

The curved UWS measurements are collected up to a height of $h = 0.9d$ (Fig. 8). A correlation study was conducted using $F/d \geq 0.3$. The measurement result and theoretical line are correlated for $(F/d)^{n'}$ with $n' = 1, n' = 0.91, n' = 0.8$ and $n' = 0.67$. The maximum correlation value is on the theoretical line $(F/d)^{0.8}$ with a

Fig. 7 Q_1/Q_0 and F/d theoretical graph and trapezoidal UWS

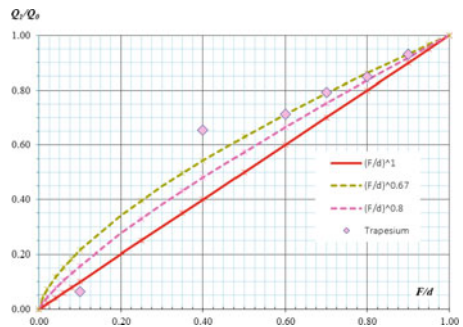


Fig. 8 Q_1/Q_0 and F/d theoretical graph and curved UWS

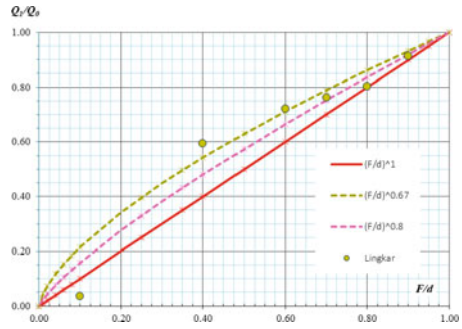


Table 1. n' for all UWS models.

UWS Model	n'	$(F/d)^{n'}$
Rectangular	$n' = 0.50$	$(F/d)^{0.50}$
Trapezoidal	$n' = 0.67$	$(F/d)^{0.67}$
Curved	$n' = 0.80$	$(F/d)^{0.80}$

correlation value of $R_{xy} = 0.93$, according to the correlation analysis of the curved UWS model measurement data vs. the theoretical line.

4 Conclusion

Theoretically, if the power value is $n' \approx 1$ then the measurement results are close to the theoretical value. For all UWS layout models with the same F/d value, on the theoretical line with a value of $n' = 1$ then the value of $F/d = Q_1/Q_0$. As for the theoretical line with $n' < 1$, then $F/d < Q_1/Q_0$. For the same F/d value, it may be claimed that the bigger the value of Q_1/Q_0 , the smaller the value of n' . The findings of the correlation study of the three UWS models are displayed in Table 1.

If the value of Q_1/Q_0 is getting bigger, then the discharge entering the UWS (Q_1) is also getting bigger, which means that the ability of the UWS to deflect the flow is getting lower. Table 1 shows that if the n values are sorted from the largest to the smallest, the largest n' value is the curved UWS model, then the Trapezoidal UWS model, and the smallest n' value is the Square UWS model. Comparing the curved UWS model to the trapezoidal UWS model and the rectangular UWS model, we can conclude that the curved UWS model is the most effective at flow deflection.

References

1. King EV, Conley DC, Masselink G, Leonardi N, McCarroll RJ, Scott T (2019) The impact of waves and tides on residual sand transport on a sediment-poor, energetic, and macrotidal continental shelf. *J Geophys Res: Oceans* 124(7):4974–5002
2. Fan R, Wei H, Zhao L, Zhao W, Jiang C, Nie H (2019) Identify the impacts of waves and tides to coastal suspended sediment concentration based on high-frequency acoustic observations. *Mar Geol* 408:154–164
3. Saengsupavanich C, Yun LS, Lee LH, Sanitwong-Na-Ayutthaya S (2022) Intertidal intercepted sediment at jetties along the Gulf of Thailand. *Front Mar Sci* 9:970592
4. Seymour RJ (2005) Longshore sediment transport. *Encycl Earth Sci Ser* 14:600
5. El-Asmar HM, White K (2002) Changes in coastal sediment transport processes due to construction of New Damietta Harbour, Nile Delta, Egypt. *Coast Eng* 46(2):127–138
6. Bhakty TE, Yuwono N, Triatmodjo B, Ghalizhan AF (2021) Effect of underwater sill height against flow patterns in order to reduce sedimentation in navigation channel and basins. *Lect. Notes Civ. Eng.* 132(1):232–240
7. Irie I, Hidayat R, Morimoto K, Ono N (2002) Study of siltation protection in Asian Ports. In: *Proceedings of the International Offshore and Polar Engineering Conference*
8. Irie I, Ono N, Morimoto K, Takeuchi N, Hidayat R (2003) Cross section of submerged dike for efficient siltation protection. In: *Coastal Engineering*, pp 1733–1743
9. Tsuruya H, Murakami K, Irie I (1990) Report of the Port and Harbour Research Institute
10. Ono N, Irie I, Hidayat KR Protection of siltation experience the regent, no 2

Efficiency of Infrastructure Planning of Retaining Wall as Flood Control in Bangin River Pecatu Badung Bali



Anak Agung Ratu Ritaka Wangsa, I Made Nada, and Ida Bagus Suryatmaja

Abstract A problem often caused by floods is the destructive power of water. Retaining wall construction is one of the flood prevention efforts. The purpose of this study is to identify the problem of flooding in Bangin River in Pecatu Badung Bali in order to take appropriate measures against flooding. B. Ability to plan retaining walls. When planning a retaining wall structure, some analysis of hydrology, hydraulics, and building safety in consideration of economic aspects. The methods used in this study are quantitative methods, namely direct observation and field measurements. Then, recalculations are made based on the design flood discharges at different times for the planning of flood barriers. The design flood discharge results are 15.47 m³/s in Q1, 49.74 m³/s in Q2 and 65.89 m³/s in Q5. The results of the HEC-RAS modeling, the critical depth value at the discharge of the 2- year return period is 1.54 m, the 5-year return period is 1.80 m, the 10-year return period is 1.93 m, the 25-year return period is 2.06 m. and the 50-year return period is 2.04 m. The design height of the retaining wall is 2,91 m above the riverbed. Safety analysis of retaining wall structures calculated based on normal and seismic building stability, bearing capacity it was determined that the design met the requirements due to soil, reinforcement, and foundation correspondences.

Keywords infrastructure · retaining wall · flood · rivers

1 Introduction

A watershed is an area of ridges and hills that act as a barrier through which rainfall is absorbed and flows through tributaries into the main river [1]. High human need to meet basic needs leads to high risk of land use change due to watershed development activities. One of the possible consequences is a reduction in upstream catchment

A. A. R. R. Wangsa (✉) · I. Nada · I. B. Suryatmaja
Program Studi Teknik Sipil, Fakultas Teknik, Universitas Mahasaraswati Denpasar, Kota
Denpasar, Indonesia
e-mail: ritaka2020@unmas.ac.id

© Institute of Technology PETRONAS Sdn Bhd 2024
B. S. Mohammed et al. (eds.), *Proceedings of the International Conference on Emerging Smart Cities (ICESC2022)*, Lecture Notes in Civil Engineering 324,
https://doi.org/10.1007/978-981-99-1111-0_59

area (infiltration) and an increase in runoff coefficient values that greatly increase the risk of flooding. Floods generally have an energy-intensive flood component that can have an impact such as damage to buildings around the river and causing material and social losses [2].

Badung Regency is the regent of Bali. Badung regency has great potential to be a commodity and source of foreign currency earnings for the government from various sectors and efforts to develop and promote the world of tourism and other industries are now being undertaken by companies of all kinds. increasingly implemented. Pecatu, one of his industrial areas in Badung regency, has a great influence on the water cycle and has a great impact on the drainage system. This is due to increasing urbanization leading to changes in land use. A drainage system is defined as a set of water structures designed to reduce or remove excess water from an area or land so that the land can be used optimally.

The Bangin River is a type of ephemeral river that carries water only during the rainy season. This flow type is almost the same as the temporary flow type, except that the water type is not necessarily abundant during the rainy season. Since there are buildings around the Bangin River that flood during the rainy season, it is necessary to renovate the buildings by creating backrests and the results of design flood calculations.

Design flood discharge is the maximum discharge planned for a river or natural waterway with a specified return period that can pass without endangering the environment or the stability of the river. Among other things, determines the design discharge rate at various return times for the design of flood barriers [3].

2 Flood Retaining Wall Infrastructure

Seawall means a river control building constructed with certain technical requirements to protect the area around a river from runoff of river water. Flood barriers are usually constructed of suitable materials such as compacted earth, masonry, brick masonry, concrete masonry and steel piles. The design flood discharge from the flood control project is used for the technical dimensions of the height of the flood barrier. Determination of design flood discharge according to economic aspects and protected area conditions [3].

2.1 Technical Factors and Costs at River Boundaries

The following engineering factors should be considered when determining the seawall direction [4]:

1. To minimize costs, flood barriers will be constructed as straight as possible to conform to terrain, existing boundaries, existing building fixtures, and river bends.
2. The distance between the flood barrier and the river bank (river bank) should be wide enough to accommodate the planned flood flow. Embankments Standard distances to river banks depend on local conditions. The recommended distance for seawalls from river banks is 10–25 m in urban areas and 25 m or more in rural areas.
3. Consideration should be given to the potential for hydraulic improvement of rivers by installing drainage channels in areas of extreme meandering, as drainage channels can shorten or straighten flood barriers.
4. To protect the floodplain from inundation by the dam, flood barriers can be erected to the left and right of the inflow to the area of influence of the dam.

2.2 River Technique

To assess the river impact of building a flood barrier, the following steps should be taken [5]:

1. Review of proposed flood barrier plans and identification of areas where lateral erosion rates and downstream meandering may damage flood barriers.
2. Presumed linear options to minimize levee erosion management costs. Consideration of constraints such as land use, availability of erosion control costs, and cost of placing flood barriers with greater spacing than specified above.
3. Embankment Conditions and Design Flood Calculations Select the correct hydraulic foundation and roughness for hydraulic calculations.
4. Compare channel velocity with and without flood barriers against design flood discharge. If the velocity change is less than 30%, the effect of cliff erosion and sediment transport is negligible. If this change is between 30 and 50%, it will affect sediment transport, cliff erosion, and stability of the river under consideration. Large terrain changes occur when the speed change exceeds 50%. In this case, adjust the position of the flood barrier. If the position of the flood barrier cannot be adjusted, river management and erosion control measures are required.

2.3 Hydraulic Analysis

The purpose of hydraulic analysis is to describe the profile of flood levels along the river under consideration. The resulting water level profile serves as the basis for determining the height of embankments or flood barriers [6].

1. Analysis with Assumed Permanent Flow Conditions

If the floodplain reservoir is very small and the flood inflow hydrograph does not stay in the reservoir long enough, then an analysis with the assumption that the flow

conditions are persistent and non-uniform (steady non-uniform flow) is acceptable (submersion). To calculate the water level profile, the Army Corps of Engineers, USA developed the computer model HEC-2 to use. The HEC-2 model is described in detail in a manual written. It can be used to calculate water levels as an alternative to the slope method discussed.

2. Analysis with Assumption of Non-Permanent Flow Conditions

Calculating peak water levels in floodplains with large reservoirs requires dynamic routing or non-permanent flow analysis, resulting in significantly reduced flood peaks. Computer models used for dynamic routing include 1-D and DWOPER, MIKE-11 and network.

3. Manning Roughness Coefficient

To determine the magnitude of the Manning roughness coefficient, the following factors should be considered:

- a. Different roughness coefficients are used for river basins and floodplain areas.
- b. Different roughness coefficients along grooves of different sizes.
- c. The potential influence on the future development of floodplain areas on the magnitude of the roughness coefficient should be taken into account.
- d. Coefficient of roughness can be calculated with certainty based on measurements of discharge and water level.
- e. The roughness coefficient is affected by changes in the shape of the riverbed or the growth rate of plants.

4. Other Considerations in Hydraulic Analysis.

Factors to consider when performing a hydraulic analysis include:

- a. Potential changes in river morphology, including natural and man-made erosion and degradation.
- b. Obstacles to current or future river flow are like bridges.

2.4 Geotechnical

To ensure the stable performance of flood barriers, the following criteria can be considered [7]:

- a. Flood barriers and foundations must be strong and not excessively deformed under the influence of various loads that may occur during construction or service life, including seismic loads.
- b. Seepage from flood barriers and foundations should be controlled to prevent excessive uplift, plumbing, instability, delamination and erosion.
- c. The height of protection must be sufficient to prevent overflow (runoff) in the event of flooding.
- d. The height of the flood retaining wall should be exceeded for the possibility of settlement.

- e. The slope of the seawall is designed to resist erosion during normal river flow, rain, and floods.

1. Implementation.

The following measures are being considered to ensure the repair of flood barriers:

- a. Implementation of foundation repairs.
- b. Use of stockpile materials
- c. Gradient control
- d. Control of moisture content
- e. Density control
- f. Installation of seepage and piping control facilities

4. Geotechnical Technical Planning Factors

During the engineering design of dams and flood barriers, several factors of the following geotechnical aspects should be considered:

a. Field geological conditions

Determining the foundation material on which the building will be based, including the type and extent of foundation restoration required, can also incorporate the type of foundation material into the engineering design of the flood barrier.

b. Seismic Area

Whether the location is located in an area that has the potential to be seismically active or not, so that it can determine the type or flood-retaining building used.

c.. Available Construction Materials

The technical planning of the embankment can use the best materials that come from the nearest place.

d. Economy

The technical planning of the building must be able to provide a balance between economy, use, safety, and the environment.

3. Stability

A slope of 1 V: 2 H is very suitable for a well-compacted homogeneous flood barrier built on a masonry foundation that meets the requirements according to the stability map. For retaining walls greater than 3 meters in height and in poor ground conditions, a stability analysis should be performed to determine the slope of the slope. Provides flood barrier loading conditions for static stability analysis and material strength parameters and minimum values to avoid damage to the dam. The selection of the safety factor is detailed. Provides a method for estimating the liquefaction potential of loose cohesive subsoils and assessing the stability of flood barriers against earthquakes increase.

4. Settlement and Seepage

Provides procedures for calculating settlement of flood barriers and foundations and planning appropriate mitigation measures in the event of excessive settlement. The calculated settlement along the top of the flood barrier shall not exceed $0.05 H$ where H is the height of the flood barrier from the height of the foundation [8].

Provides a method for estimating leachate flow and controlling excess leachate flow through the main body and underside of flood barriers to do.

2.5 Guard Height (Freeboard)

Protective heights are provided to prevent seawall overflow due to [9]:

1. Run and make waves.
2. Can't at the outer bend of the canal.
3. Possibility of subsidence or damage to the top of the seawall.
4. Local water level fluctuations are caused by local disturbances (e.g. banana plantations in floodplains).
5. Factors affecting the water level of the main river.

An additional protection height of 0.3 meters is recommended along critical areas where there is a high risk to life and property in the event of a flood retaining wall failure. If the height of the flood barrier exceeds 3.5 meters, an additional collection height of 0.3 meters will be added.

3 Research Methods

The method used in this study is a quantitative method that calculates the design rainfall and design flood discharge by performing engineering analysis based on the identification and measurement results at the site.

The types of data used in this study are primary and secondary data. Primary data were obtained by identifying, measuring and recording the condition of the Bangin River. Secondary data required maximum rainfall data for an average of eight years from 2012 to 2019. Rainfall data were collected from the rain station closest to the work site, namely Ungasan rainfall station in Kuta district, Regency Badung. and collected at the Udayana University rainwater station.

The following data collection tools were used in this study:

1. Meter as a flow measuring instrument
2. Camera as a document in the field.
3. Data processing with MS Excel.

4 Results and Discussion

4.1 Field Identification Results

Based on the results of field identification, the Tukad Bangin Watershed has an area of 1.33 km² with a river length of 1.24 km. This river has a bottom width of 5 m.

The site location is in the south with coordinates -8.812260, 115.116510 covering an area of 3000 m² will be rehabilitated as a building next to the Bangin River. The location of this bangin river has the following boundaries (Fig. 1):

1. North side: Puri Laundry (Community House)
2. East side: Buana Sari street
3. South side: Jian House
4. West side: vacant land

4.2 Recapitulation of Design Rainfall Calculation Results

1. Recapitulation of the results of the design rainfall using the log Pearson type III method from a return period of 1 to 1000 years by converting the data series into logarithmic form.

Fig. 1 Site Location



No.	Kala Ulang	Hujan Rancangan Metode Log Pearson	UJI SMIRNOV KOLMOGOROF	
	(Tahun)	(mm/hr)	$\Delta_{max} < \Delta_{kritis}$	
1	1,01	123,50	Delta Maximum, (Δ_{max})	13,04
2	1,25	221,54	Derajat Signifikansi, (α)	
3	2,00	293,72	Delta Kritis, (Δ_{kritis})	
4	5,00	371,97	HIPOTESA	
5	10,00	413,94	UJI CHI S	
6	20,00	445,86	X²	
7	25,00	455,08	Chi - Square hitung	
8	50,00	451,10	Chi - Square kr	
9	100,00	499,95	Derajat Be	
10	200,00	518,00	Deraja	
11	1000,00	545,56	H	

Fig. 2 Recapitulation of Design Rainfall Calculation Results

- The recapitulation of this examination is intended to determine the truth of the hypothesis of the frequency distribution suitability test. With the examination of the Smirnov Kolmogorof test, the results obtained Delta Maximum (max) of 13.04%, Degree of Significance (α) of 5% and Delta Critical (Critical) of 47%, then the results of the examination are declared accepted because the results of $max < Critical$.
- The recapitulation of the examination of the Chi Square Test is intended to determine the truth of the hypothesis of the frequency distribution suitability test. With the examination of the Chi Square Test in the table above, the results of the examination are declared accepted because the results of $X^2_{count} < X^2_{cr}$.

4.3 Flood Discharge Recapitulation Design of the HSS Nakayasu Method

The analysis is carried out in the form of the Nakayasu HSS which consists of curve segments obtained from the Bangin River watershed analysis (Fig. 3).

4.4 Nakayasu Synthetic Unit Hydrograph Recap

The graph shows the maximum discharge of 92.57 m³/sec in the Bangin River Basin (Fig. 4).

4.5 Channel Capacity Evaluation

The calculation of the evaluation of the discharge capacity of the existing canal is carried out to determine the fulfillment of the discharge of the existing channel to the design flood discharge. From the results of the calculation table above, in the Bangin River watershed, the discharge capacity of the existing channel throughout the return period of the channel does not meet the design flood discharge, there will be flooding. Thus, planning and modeling of HEC-RAS is then carried out to determine the condition of the discharge capacity and water level profile in the existing canal (Figs. 5 and 6).

4.6 Cross Section

Planning at the stage of the shoal with a slope of 1.00, height 2.91 m, stone thickness of 1.00 m shrinking upwards with a size of 0.30 m is the same as the detailed planning of the ledge in Figs. 7, 8, and 9.

No.	Waktu (jam)	Ordinat HSS (Qt) (m ³ /det/mm)	Debit Banjir Rancangan							
			Q _{1.01 th} (m ³ /dt)	Q _{2 th} (m ³ /dt)	Q _{5 th} (m ³ /dt)	Q _{10 th} (m ³ /dt)	Q _{20 th} (m ³ /dt)	Q _{25 th} (m ³ /dt)	Q _{50 th} (m ³ /dt)	Q _{100 th} (m ³ /dt)
1	0,00	0,00	0,00	0,00	0,00	0,00	0,00	0,00	0,00	0,00
2	0,50	0,47	15,47	49,74	65,89	74,61	81,27	83,19	82,36	92,57
3	1,00	0,12	8,14	26,16	34,66	39,25	42,75	43,76	43,32	48,70
4	1,50	0,05	4,46	17,56	23,27	26,35	28,69	29,37	29,08	32,69
5	2,00	0,02	4,10	13,17	17,44	19,75	21,51	22,02	21,80	24,51
6	2,50	0,01	3,26	10,49	13,90	15,74	17,14	17,55	17,38	19,53
7	3,00	0,00	2,73	8,77	11,62	13,16	14,33	14,67	14,53	16,33
8	3,50	0,00	2,37	7,60	10,07	11,41	12,42	12,72	12,59	14,15
9	4,00	0,00	2,10	6,76	8,96	10,15	11,05	11,21	11,20	12,59
10	4,50	0,00	1,91	6,13	8,12	9,20	10,02	10,26	10,15	11,41
11	5,00	0,00	1,75	5,64	7,47	8,45	9,21	9,43	9,33	10,49
12	5,50	0,00	0,55	1,77	2,35	2,66	2,90	2,97	2,94	3,30
13	6,00	0,00	0,22	0,72	0,96	1,08	1,18	1,21	1,20	1,35
14	6,50	0,00	0,10	0,32	0,42	0,48	0,52	0,53	0,53	0,59
15	7,00	0,00	0,04	0,14	0,19	0,21	0,23	0,23	0,23	0,26
16	7,50	0,00	0,02	0,06	0,08	0,09	0,10	0,10	0,10	0,11
17	8,00	0,00	0,01	0,03	0,04	0,04	0,04	0,05	0,04	0,05
18	8,50	0,00	0,00	0,01	0,02	0,02	0,02	0,02	0,02	0,02
19	9,00	0,00	0,00	0,01	0,01	0,01	0,01	0,01	0,01	0,01
20	9,50	0,00	0,00	0,00	0,00	0,00	0,00	0,00	0,00	0,00
21	10,00	0,00	0,00	0,00	0,00	0,00	0,00	0,00	0,00	0,00
22	10,50	0,00	0,00	0,00	0,00	0,00	0,00	0,00	0,00	0,00
23	11,00	0,00	0,00	0,00	0,00	0,00	0,00	0,00	0,00	0,00
24	11,50	0,00	0,00	0,00	0,00	0,00	0,00	0,00	0,00	0,00
25	12,00	0,00	0,00	0,00	0,00	0,00	0,00	0,00	0,00	0,00
26	12,50	0,00	0,00	0,00	0,00	0,00	0,00	0,00	0,00	0,00
27	13,00	0,00	0,00	0,00	0,00	0,00	0,00	0,00	0,00	0,00
28	13,50	0,00	0,00	0,00	0,00	0,00	0,00	0,00	0,00	0,00
29	14,00	0,00	0,00	0,00	0,00	0,00	0,00	0,00	0,00	0,00
30	14,50	0,00	0,00	0,00	0,00	0,00	0,00	0,00	0,00	0,00
31	15,00	0,00	0,00	0,00	0,00	0,00	0,00	0,00	0,00	0,00
32	15,50	0,00	0,00	0,00	0,00	0,00	0,00	0,00	0,00	0,00
33	16,00	0,00	0,00	0,00	0,00	0,00	0,00	0,00	0,00	0,00
34	16,50	0,00	0,00	0,00	0,00	0,00	0,00	0,00	0,00	0,00
35	17,00	0,00	0,00	0,00	0,00	0,00	0,00	0,00	0,00	0,00
36	17,50	0,00	0,00	0,00	0,00	0,00	0,00	0,00	0,00	0,00
37	18,00	0,00	0,00	0,00	0,00	0,00	0,00	0,00	0,00	0,00
38	18,50	0,00	0,00	0,00	0,00	0,00	0,00	0,00	0,00	0,00
39	19,00	0,00	0,00	0,00	0,00	0,00	0,00	0,00	0,00	0,00
40	19,50	0,00	0,00	0,00	0,00	0,00	0,00	0,00	0,00	0,00
41	20,00	0,00	0,00	0,00	0,00	0,00	0,00	0,00	0,00	0,00
42	20,50	0,00	0,00	0,00	0,00	0,00	0,00	0,00	0,00	0,00
43	21,00	0,00	0,00	0,00	0,00	0,00	0,00	0,00	0,00	0,00
44	21,50	0,00	0,00	0,00	0,00	0,00	0,00	0,00	0,00	0,00
45	22,00	0,00	0,00	0,00	0,00	0,00	0,00	0,00	0,00	0,00
46	22,50	0,00	0,00	0,00	0,00	0,00	0,00	0,00	0,00	0,00
47	23,00	0,00	0,00	0,00	0,00	0,00	0,00	0,00	0,00	0,00
48	23,50	0,00	0,00	0,00	0,00	0,00	0,00	0,00	0,00	0,00
49	24,00	0,00	0,00	0,00	0,00	0,00	0,00	0,00	0,00	0,00
Q maksimum (m ³ /dt)			15,47	49,74	65,89	74,61	81,27	83,19	82,36	92,57

Fig. 3 Flood Discharge Recapitulation Design of the HSS Nakayasu Method

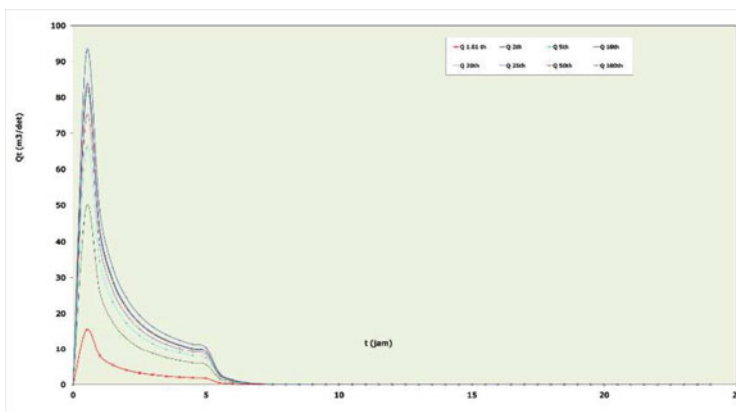


Fig. 4 Nakayasu Synthetic Unit Hydrograph Recap

No	Ruas Sungai	Q	B	q	h	l	n ₁	P ₁	n ₂ = n ₃	P ₂	n ₄	A	P	R	V	F	Q hitung	
		(m ³ /dt)	(m)	(m ³ /dt)	(m)			(m)	(m)	(m)	(m)	(m ²)	(m)	(m)	(m/dt)	(m ³ /dt)		
1	Tukad Bangin																	
	- Q 1,01th	15,47	5,00	3,09	0,778	0,02000	0,030	5,00	0,030	2,200	0,030	4,494	7,200	0,624	3,443	1,25	15,47	
	- Q 2th	49,74	5,00	9,95	1,538	0,02000	0,030	5,00	0,030	4,349	0,030	10,053	9,349	1,075	4,948	1,27	49,74	
	- Q 5th	65,89	5,00	13,18	1,804	0,02000	0,030	5,00	0,030	5,103	0,030	12,276	10,103	1,215	5,368	1,28	65,89	
	- Q 10th	74,61	5,00	14,92	1,935	0,02000	0,030	5,00	0,030	5,473	0,030	13,418	10,473	1,281	5,561	1,28	74,61	
	- Q 20th	81,27	5,00	16,25	2,030	0,02000	0,030	5,00	0,030	5,740	0,030	14,267	10,740	1,328	5,696	1,28	81,27	
	- Q 25th	83,19	5,00	16,64	2,056	0,02000	0,030	5,00	0,030	5,816	0,030	14,509	10,816	1,341	5,734	1,28	83,19	
	- Q 50th	82,36	5,00	16,47	2,045	0,02000	0,030	5,00	0,030	5,783	0,030	14,405	10,783	1,336	5,718	1,28	82,36	
	- Q 100th	92,57	5,00	18,51	2,182	0,02000	0,030	5,00	0,030	6,172	0,030	15,671	11,172	1,403	5,907	1,28	92,57	

Fig. 5 Channel Capacity Evaluation

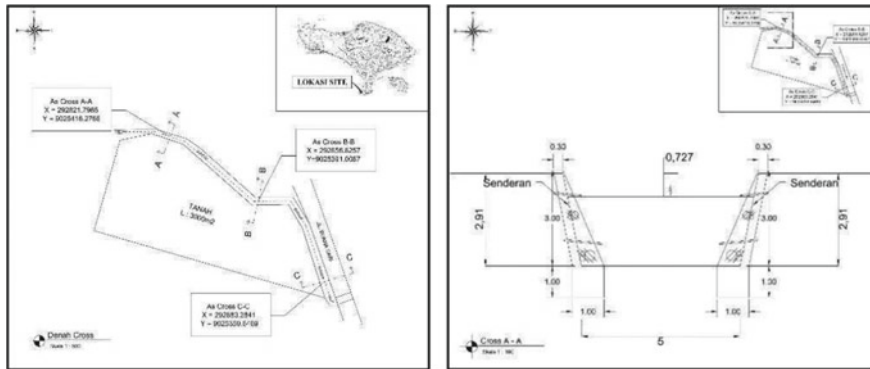


Fig. 6 Cross Section

4.7 Flood Retaining Wall Detail Design

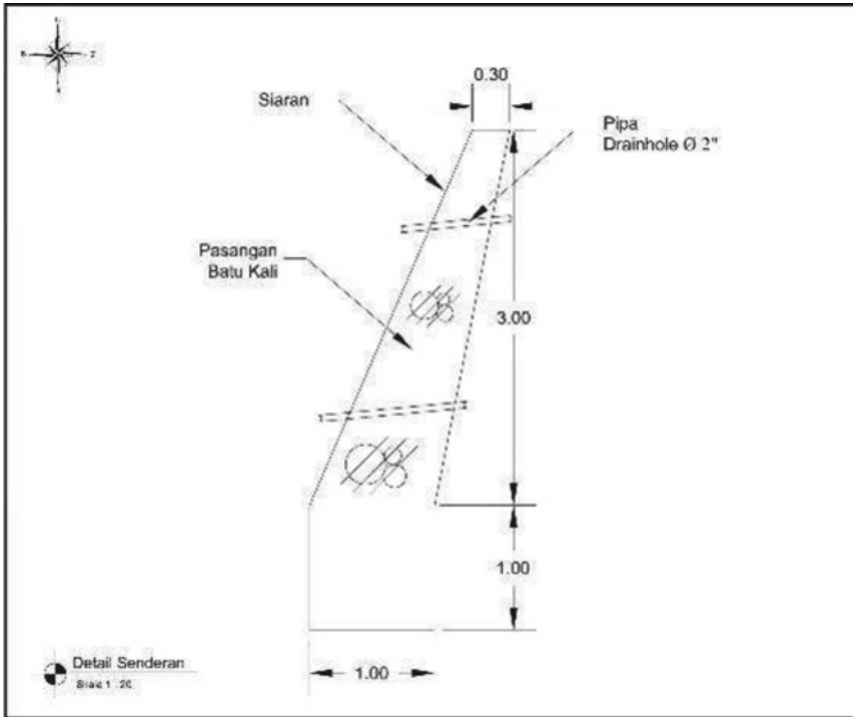


Fig. 7 Flood Retaining Wall Detail Design

4.8 Calculation Result of Design Flood Discharge

Fig. 8 Calculation Result of Design Flood Discharge

No.	Kala Ulang (Tahun)	Debit Banjir Rancangan (m ³ /dt)	h (m)
1	1,01	15,47	0,78
2	2,00	49,74	1,54
3	5,00	65,89	1,80
4	10,00	74,61	1,93
5	20,00	81,27	2,03
6	25,00	83,19	2,06
7	50,00	82,36	2,04
8	100,00	92,57	2,18

4.9 HEC-RAS Modeling Result

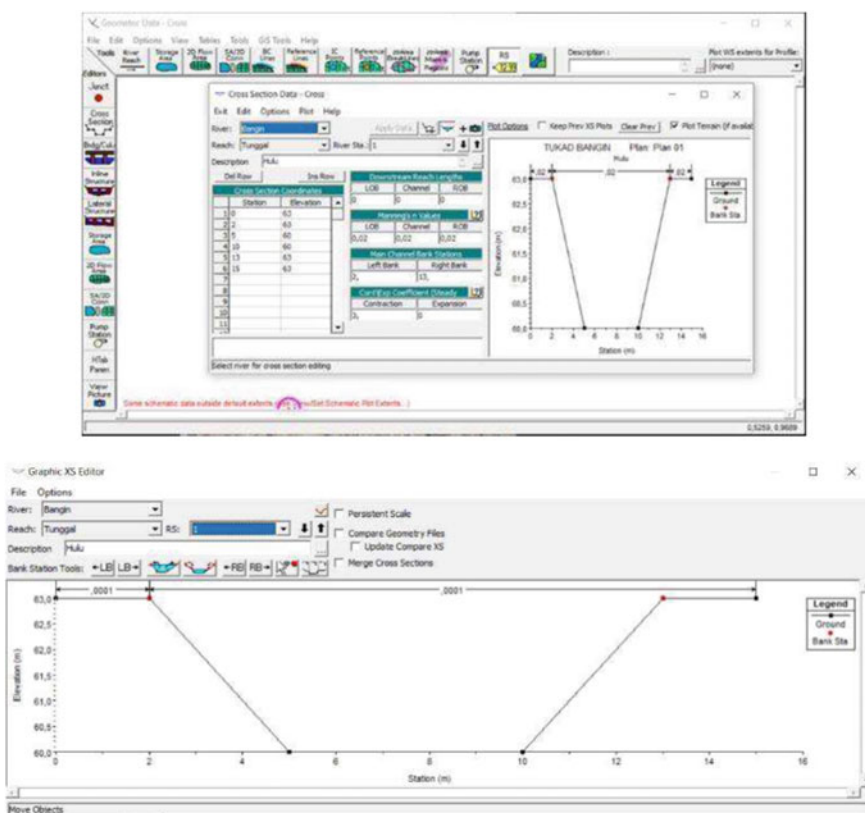


Fig. 9 HEC-RAS Modeling Results

5 Conclusions and Suggestions

The design flood discharge results are 15.47 m³/s in Q1, 49.74 m³/s in Q2 and 65.89 m³/s in Q5. The results of the HEC-RAS modeling, the critical depth value at the discharge of the 2-year return period is 1.54 m, the 5-year return period is 1.80 m, the 10-year return period is 1.93 m, the 25-year return period is 2.06 m and the 50-year return period is 2.04 m. The design height of the retaining wall is 2,91 m above the riverbed. So that with the HEC-RAS modeling can control the height of the flood protection plan in the field.

Suggestions that can be given are from the results of hydrological analysis depending on the accuracy and completeness of hydroclimatological data, so that the availability and condition of data recording equipment and recording accuracy need to be considered as well as possible. The use of water must be balanced with environmental care, especially the river area to keep it clean.

References

1. Asdak C (1995) Hidrologi dan Pengolahan Daerah Aliran Sungai. Gajah Mada University Press
2. Soemarto CD (1995) Ir. B.I.E. DIPL.H. Hidrologi Teknik Edisi Ke-2
3. Syarifudin, A., et al. (2017). Hidrologi Terapan. Andi: Yogyakarta Erlangga: Jakarta
4. Hardiyatmo HC (2003) Mekanika Tanah II. Gajah Mada University Press 91(5):1–398
5. Sosrodarsono S (1984). Perbaikan dan Pengaturan Sungai. Jakarta Pusat: P.T. Pradnya Paramita
6. Kodoatie R., dan Syarief R (2013) Pengelolaan Sumber daya Air Terpadu. Andi: Yogyakarta
7. Chow VT (1985) Hidrolika Saluran Terbuka (Open Channel Hydraulics). Jakarta: Erlangga
8. Badan Standarisasi Nasional B S (2017). SNI 8460: 2017 Persyaratan Perancangan Geoteknik. Jakarta: Badan Standarisasi Nasional
9. Kodoatie RJ (2012) Tata Ruang Air Tanah. Andi: Yogyakarta
10. Suripin (2001) Pelestarian Sumber Daya Tanah dan Air. Andi Offset: Yogyakarta

Impact of Changes in SNI 1726 and SNI 2847 on Reinforcing Steel Weight of High-Rise Reinforced Concrete Buildings in Jakarta



Suradjin Sutjipto, Indrawati Sumeru, and Sherrica Augustin Sucipto

Abstract Updates to the Indonesian seismic design code (SNI 1726) and the reinforced concrete design code (SNI 2847) have been implemented in practice simultaneously. Under these new codes, seismic loads increase significantly, especially for high-rise buildings in many areas of Indonesia, and the design requirements for concrete reinforcement become much more stringent. Therefore, it is predicted by the construction industry that there will be a significant increase in the need for reinforcing steel. By using a 32-story reinforced concrete case study building with a special moment resisting frame system as its lateral force resisting system, this paper presents a comparison of the design reinforcing steel weight when the building is designed based on a combination of SNI 1726:2012 and SNI 2847:2013, and when it is designed using a combination of SNI 1726:2019 and SNI 2847:2019. This study shows that although the increase in seismic load is significant, the increase in reinforcing steel is much lower, and the result can then be a reference of the increase in design reinforcement based on the latest codes.

Keywords SNI 1726 · SNI 2847 · reinforcing steel weight · high-rise

1 Introduction

In order to minimize the impact that occur on structures due to earthquakes and as a country dominated by many earthquake-prone areas, Indonesia regularly updates its building codes. Two new building codes were issued by the Indonesian National Standardization Body (BSN) in 2019: the seismic design code, SNI 1726:2019 [1], updating SNI 1726:2012 [2]; and the reinforced concrete design code, SNI 2847:2019 [3], renewing SNI 2847:2013 [4]. With the application of the 2017 seismic map [5] into SNI 1726:2019, the seismic loads for high-rise buildings increase significantly

S. Sutjipto (✉) · I. Sumeru · S. A. Sucipto
Civil Engineering Department, Trisakti University, Jakarta, Indonesia
e-mail: suradjin@trisakti.ac.id

© Institute of Technology PETRONAS Sdn Bhd 2024
B. S. Mohammed et al. (eds.), *Proceedings of the International Conference on Emerging Smart Cities (ICESC2022)*, Lecture Notes in Civil Engineering 324,
https://doi.org/10.1007/978-981-99-1111-0_60

in most parts of Indonesia [6]. Meanwhile, the requirements of confinement reinforcement for columns with high compressive axial loads are much stricter in SNI 2847:2019.

Most of stakeholders in the construction industry certainly want to know how far the impact of the changes of the two new design codes on their projects. This paper is intended to answer that question, especially for high-rise buildings that are thought to be the most affected by the changes.

It should note that SNI 1726:2012 and SNI 1726:2019 adopted ASCE 7-10 [7] and ASCE 7-16 [8], with modifications for Indonesian conditions, including the development of its seismic maps. While SNI 2847:2013 and SNI 2847:2019 adopted identically ACI 318 M-11 [9] and ACI 318 M-14 [10].

There are 2 reasons why the city of Jakarta was chosen as the location of this study. Firstly, as the capital city of the nation, Jakarta has become a benchmark for the high-rise building construction industry in Indonesia. Secondly, in terms of seismic design, Jakarta is in a moderate seismicity area without anomalies in its medium and soft soil site classes design response spectra [11].

The study was conducted using a simple methodology. On a case study building, comprehensive analysis and design were performed based on a combination of SNI 1726:2012 and SNI 2847:2013 as well as a combination of SNI 1726:2019 and SNI 2847:2019 following standard design procedures [12–14]. The resulting reinforcing steel weights from those designs were then compared.

For the purpose of obtaining more accurate and reliable results, the study utilized ETABS to analyze and design beams and columns, SAFE to analyze and design slabs, and CSiDetail to detail all reinforcement and to produce bills of quantities (BOQ).

2 Case Study Building

As a case study building, the study used a 32-story reinforced concrete office building, which is considered to represent a high-rise building, located in Jakarta on an SE (soft soil) site class area. Figure 1 shows that the building has a typical simple, regular, and symmetrical floor plan comprising of 3 by 5 bays spanning 8 m each, with a total area of 960 m² (24 m × 40 m). The frame elevation sections and the 3D view of the analytical model are shown in Fig. 2. The typical floor height is 3.5 m, and therefore, the total height of the building is 112 m. The building uses a special moment frame system with a fixed base assumption for all frames, both in the long and short directions of the building. This framing system is indicated to be more ductile and requires less seismic loads than other structural system in the code [15].

Table 1 lists the dimensions and specified compressive strength of concrete (f'_c) of all structural elements of the case study building. Deformed bars with a specified yield stress (f_y) of 420 MPa (BjTS 420B) are used for all longitudinal and transverse reinforcement.

Fig. 1 Case study building typical floor plan

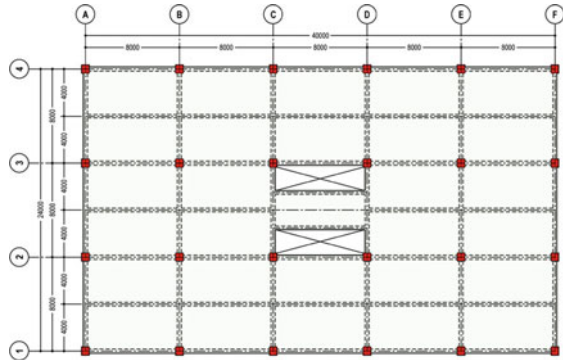
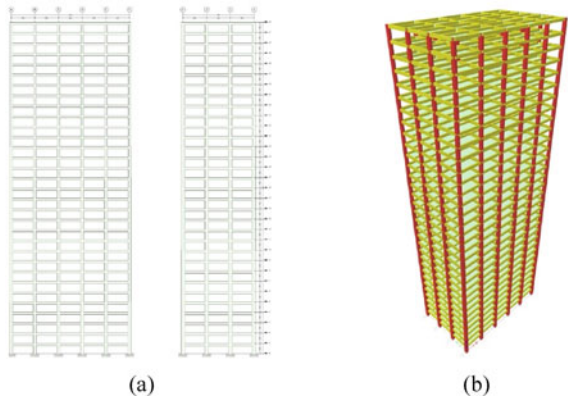


Fig. 2 Frame elevation section in the long and short directions (a) and the 3D model (b)



3 Gravity Loading

All gravity loads applied to the case study building are shown in Table 2. It is important to note that the structural analysis program automatically calculates the self-weights of all structural elements with a unit weight of 24 kN/m^3 , therefore, the dead loads listed in the Table 2 are superimposed dead loads.

The live loads used in this study comply with the latest Indonesian loading code, SNI 1727:2020 [16], whose values are the same as the previous code, SNI 1727:2013 [17]. Note that SNI 1727:2013 and SNI 1727:2020 adopted identically ASCE 7–10 and ASCE 7–16, respectively.

Table 1 Dimensions and concrete specified compressive strength of the structural elements

Structural elements	Level		Direction	Height (mm)	Width (mm)	f'_c (MPa)
Slabs	<u>21–32</u>			120	–	<u>30</u>
	<u>11–20</u>					<u>35</u>
	01–10					40
Beams	21–32	<u>Secondary</u>		<u>500</u>	<u>300</u>	30
		Frame	<u>Long</u>	<u>700</u>	<u>400</u>	
			Short	750	450	
	11–20	<u>Secondary</u>		<u>500</u>	<u>300</u>	35
		Frame	<u>Long</u>	<u>750</u>	<u>450</u>	
			Short	800	450	
	01–10	<u>Secondary</u>		<u>500</u>	<u>300</u>	40
		Frame	<u>Long</u>	<u>750</u>	<u>450</u>	
			Short	800	450	
Columns	21–32			1,000	700	35
	<u>18–20</u>			<u>1,100</u>	<u>800</u>	40
	11–17			1,100	900	45
	<u>06–10</u>			<u>1,150</u>	<u>900</u>	
	01–05			1,150	950	

Table 2 Case study building gravity loads

	Loads		
Dead	Finishes, Ceiling & MEP	1.50	kN/m ²
	Facade	0.60	kN/m ²
Live	Roof	0.96	kN/m ²
	Office	2.40	kN/m ²
	Partitions	0.72	kN/m ²

4 Seismic Loading

Tables 3, 4 and 5 present the determination of seismic loads for the case study building in a systematic and step-by-step manner based on SNI 1726:2012 and SNI 1726:2019 where each number can be compared at each step.

Based on the given location coordinates and soil site class, all of the design response spectrum parameters in Table 3 were obtained from the Indonesian Design Spectra web applications: namely <http://rsa.ciptakarya.pu.go.id/2010/> [18] for SNI 1726:2012, and <http://rsa.ciptakarya.pu.go.id/2021/> [19] for SNI 1726:2019. The two design response spectra were then plotted together in one chart in Fig. 3 to illustrate the differences.

Table 3 Design response spectra of SNI 1726:2012 and SNI 1726:2019

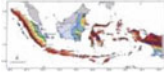
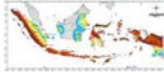
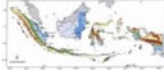

	SNI 1726:2012	SNI 1726:2019
Latitude / Longitude	-6.191° / 106.786°	
Site class	SE (soft soil)	
Seismic map for short period		
Seismic map for long period		
S_{DS} (g)	0.607	0.670
Ratio of $S_{DS\ 2019}$ to $S_{DS\ 2012}$	1.104	
S_{D1} (g)	0.560	0.634
Ratio of $S_{D1\ 2019}$ to $S_{D1\ 2012}$	1.133	
T_0 (sec.)	0.184	0.189
T_s (sec.)	0.922	0.946

Table 4 Case study building fundamental period at service and ultimate levels

Level	Fundamental period (second)		
Service	$T1 = Tx = 3.723$	$T2 = Ty = 3.583$	$T3 = Tz = 3.108$
Ultimate (MCE _R)	$T1 = Tx = 4.478$	$T2 = Ty = 4.228$	$T3 = Tz = 3.732$

For determining seismic loads and for member design purposes, 2 sets of analyzes were performed applying the proper stiffness modifiers for service level and ultimate level (MCER) conditions. Table 4 and Fig. 4 present the results of the dynamic analysis of the case study building in the form of fundamental periods and mode shapes. The first and second modes are translation, and the third mode is rotation, indicating that the building has good and ideal behavior.

Table 5 shows the calculations of the seismic response coefficients (C_s) and the design seismic base shears (V_{Design}) of the case study building based on SNI 1726:2012 and SNI 1726:2019. For comparison, the seismic response coefficients (C_s) of the two codes are plotted together in Fig. 5. It can be seen that the case study building fundamental periods at service level, ultimate level and based on $C_u T_a$ are greater than T_s , so that the governing seismic response coefficient is $C_s = S_{D1}/(T(R/I_e))$, with $T = T_{1\ Service\ Level}$ (the smallest of the three). However, since this C_s is smaller than $C_{s\ min}$, then $C_{s\ min}$ is the one that determines the design seismic base shears (V_{Design}).

From the last row of Table 5, it can be seen that the design seismic base shear of SNI 1726:2019 is approximately 30% higher than that of SNI 1726:2012.

Figure 6 presents seismic story shears and lateral forces from the dynamic analysis of the case study building based on SNI 1726:2012 and 2019, respectively. All values of SNI 1726:2019 appear to be around 30% higher than those of SNI 1726:2012. Besides, it seems that the story shears in the X and Y directions almost coincide.

Table 5 Case study building design base shear based on SNI 1726:2012 and SNI 1726:2019

		SNI 1726:2012	SNI 1726:2019
Approximate period		Table 15	Table 18
C_t		0.0466	
X		0.9	
h_n	(m)	112	
T_a	(sec.)	3.256	
Coeff. of upper limit		Table 14	Table 17
$C_u (S_{D1} > 0.4)$		1.4	
$C_u T_a$	(sec.)	4.558	
Risk Category		II	
I_e		1.0	
Seismic Design Category (SDC)		D	
Lateral Force Resisting System		Special RC Moment Frames	
R		8	
$C_s = SD1/(T(R/I_e))$		0.0188	0.0213
$C_s \min = 0.044 S_{DS} I_e$		0.0267 > 0.010	0.0295 > 0.010
W	(kN)	299,632	
V	(kN)	8,008	8,839
Scaling provision		Section 7.9.4.1	Section 7.9.1.4.1
Scale factor		0.85	1.00
V_{Design}	(kN)	6,807	8,839
Ratio of V_{Design} 2019 to V_{Design} 2012		1.298	

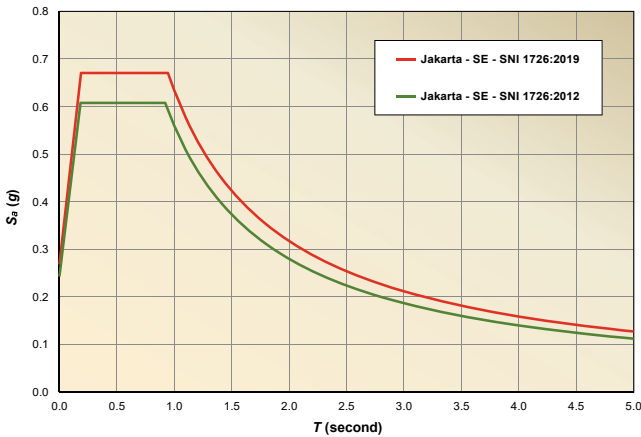


Fig. 3 Design response spectra of SNI 1726:2012 and SNI 1726:2019

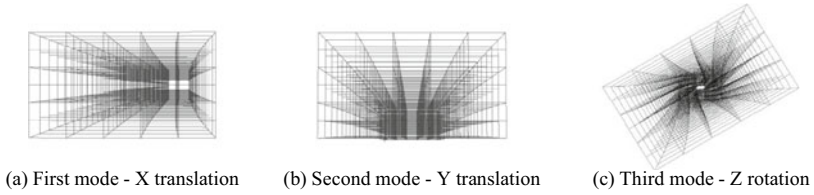


Fig. 4 Case study building mode shapes

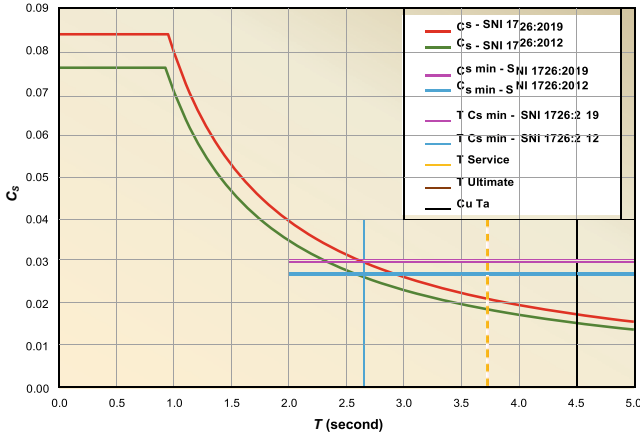


Fig. 5 Seismic response coefficients based on SNI 1726:2012 and SNI 1726:2019

This is because: first, the lateral stiffnesses of the building in the X and Y directions are nearly the same, as indicated from the first and second periods of the building being so close; and second, their base shears are scaled to the same value in both directions based on the building first period.

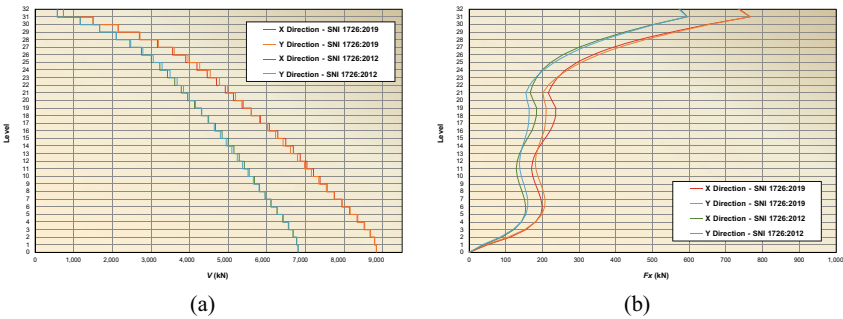


Fig. 6 Seismic story shears (a) and lateral forces (b) based on SNI 1726:2012 and SNI 1726:2019

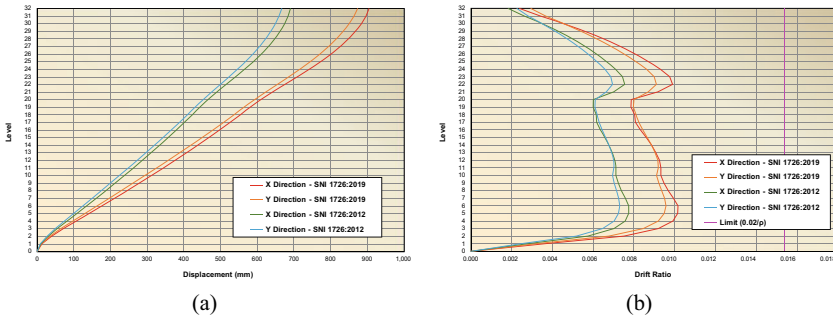


Fig. 7 Story displacement (a) and drift ratios (b) based on SNI 1726:2012 and SNI 1726:2019

Figure 7 shows the story displacements and story drift ratios resulting from the analysis, due to the applied seismic loads of the two codes. Note that all values have been multiplied by the deflection amplification factor $Cd = 5.5$. The story displacements based on SNI 1726:2019 looks about 30% greater than the story displacements based on SNI 1726:2012, which corresponds to the increment of the seismic loads. From the chart in Fig. 7(b), it can be seen that the resulting story drift ratios based on SNI 1726:2019 are still far below the limit allowed by the code.

5 Design Reinforcement Results

This study assumes that all slabs and secondary beams only carry gravity loads. Although there is a new chapter in SNI 2847:2019 (Chapter 12), concerning the function of the slab as a diaphragm that distributes seismic forces to the lateral force resisting system, since all frames in both directions in this case study building are assigned as lateral force resisting systems, then the chord and collector forces will be very small and sufficient to be resisted by trimmer bars and slab reinforcement. Thus, there is no change in the reinforcement of slabs and secondary beams based on SNI 2847:2013 and 2019.

The longitudinal and transverse reinforcement of the case study building frame beams are designed based on Chapter 21 of SNI 2847:2013 and Chapter 18 of SNI 2847:2019 for special moment frame beams. An example of a comparison of the resulting longitudinal and transverse reinforcement of the frame beams in L3 is shown in Fig. 8. Obviously, the rise of seismic loads in the new code causes the reinforcement to increase. The longitudinal reinforcement in frame beams typically increases by 2 bars in SNI 2847:2019, while transverse reinforcement increases by 1 leg or requires closer spacing in SNI 2847:2019 although the confinement requirements that generally control the design are the same between SNI 2847:2019 and SNI 2847:2013.

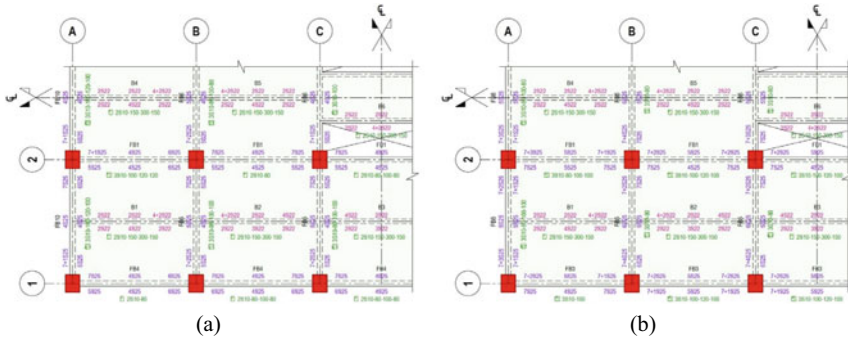


Fig. 8 Comparison of longitudinal and transverse reinforcement of secondary beams and frame beams in L3 based on SNI 2847:2013 (a) and SNI 2847:2019 (b)

CODE		2013		2019	
LEVEL		1			
SIZE (H x W)		1150 x 950		1150 x 950	
VERTICAL REINFORCEMENT		22 S29		22 S36	
TIES	ZONE A	6 + 5 S16 - 100		7 + 6 S16 - 100	
	ZONE B	6 + 5 S16 - 100		7 + 6 S16 - 100	
	ZONE C	6 + 5 S16 - 150		7 + 6 S16 - 150	
	ZONE D	6 + 5 S16 - 100	7 + 6 S16 - 100		
Lo		1150	1150		

Fig. 9 Comparison of longitudinal and transverse reinforcement of a column in L1 based on SNI 2847:2013 and SNI 2847:2019

All columns of this case study building meet the requirements of strong-column-weak-beam and beam-column joint shear. Their longitudinal and transverse reinforcement are designed to comply with Chapter 21 of SNI 2847:2013 and Chapter 18 of SNI 2847:2019 for special moment frame columns. In this case study building, many columns in the lower stories carry an axial compression exceeding $0.3 A_g f'_c$, thus the confinement requirements of Section 18.7.5.2(f) and equation (c) in Table 18.7.5.4 of SNI 2847:2019 apply. Figure 9 shows the comparison of longitudinal and transverse reinforcement of a column in L1 based on SNI 2847:2013 and 2019. Due to the seismic loads in the new code the longitudinal reinforcement increases significantly. Meanwhile, due to the confinement requirements, the transverse reinforcement needs to be added 1 leg in each direction.

6 Comparison of Reinforcing Steel Weight

Table 6 summarizes the bills of quantities of reinforcing steel in the case study building based on the combination of SNI 1726:2012/2847:2013 and SNI 1726:2019/2847:2019. The table also presents the ratio of the reinforcing steel weight to

the concrete volume (S/C ratio) for each structural element as commonly used in the Indonesian construction industry. Figure 10 shows the comparison graphically. It should be noted that the calculations of reinforcing steel weights in slabs, secondary beams, frame beams and columns already include their development lengths, standard hooks and lap splices.

It is clear that based on the two new codes, SNI 1726:2019 and SNI 2847:2019, the weight of reinforcing steel in the frame beams increases by 23.92% and in the columns increases by 8.95%. However, if taken into account for all frames of the lateral force resisting system, the increase is 15.68%, and for the overall structure, it is only 11.40%.

Table 6 Bills of quantities of the case study building based on SNI 1726:2012/2847:2013 and SNI 1726:2019/2847:2019

Structural elements	Concrete volume m ³	SNI 1726:2012/2847:2013		SNI 1726:2019/2847:2019		Ratio of 2019/2013
		Steel weight	S/C Ratio	Steel weight	S/C Ratio	
		kg	kg/m ³	kg	kg/m ³	
Slabs	3,686	330,948	90	330,948	90	1.0000
Secondary beams	614	101,380	165	101,380	165	1.0000
Frame beams	3,238	517,655	160	641,492	198	1.2392
Columns	2,403	633,659	264	690,356	287	1.0895
Lateral force resisting system	5,641	1,151,314	204	1,331,848	236	1.1568
Overall	9,941	1,583,643	159	1,764,177	177	1.1140

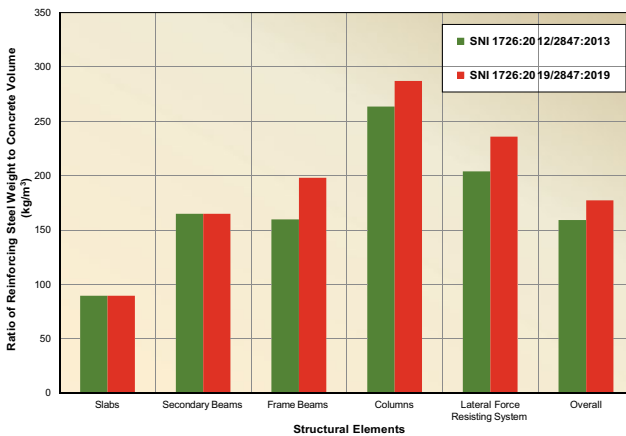


Fig. 10 Comparison of S/C ratio for each structural element based on SNI 1726:2012/2847:2013 and SNI 1726:2019/2847:2019

7 Conclusion

This study shows that:

- The design seismic load based on SNI 1726:2019 is approximately 30% higher than that based on SNI 1726:2012 for a given case study building location in Jakarta.
- For the overall structure of the case study building, the reinforcing steel weight increases 11.40%. The major increment occurs in frame beams, followed by columns as a result of the new reinforcement detailing requirements in SNI 2847:2019 that apply for many columns in lower stories having axial compression exceeding $0.3 A_g f'_c$.

References

1. SNI 1726:2019 (2019) Tata cara perencanaan ketahanan gempa untuk struktur bangunan gedung dan non gedung. Badan Standardisasi Nasional, Jakarta
2. SNI 1726:2012 (2012) Tata cara perencanaan ketahanan gempa untuk struktur bangunan gedung dan non gedung. Badan Standardisasi Nasional, Jakarta
3. SNI 2847:2019 (2019) Persyaratan beton struktural untuk bangunan gedung dan penjelasan. Badan Standardisasi Nasional, Jakarta
4. SNI 2847:2013 (2013) Persyaratan beton struktural untuk bangunan gedung. Badan Standardisasi Nasional, Jakarta
5. Pusat Studi Gempa Nasional (2017) Peta Sumber dan Bahaya Gempa Indonesia Tahun 2017. Pusat Litbang Perumahan dan Pemukiman - BPP - PUPR, Bandung
6. Sutjipto S, Sumeru I (2019) Comparison of the RSNI 1726:2018 and the SNI 1726:2012 design response spectra of 17 major cities in Indonesia. In: Prasetijo J et al (eds) 1st international conference of construction, infrastructure, and materials, IOP conference series: MSE, vol 650, 012032. IOP Science, Jakarta
7. ASCE/SEI 7-10 (2010) Minimum design loads for buildings and other structures. American Society of Civil Engineers, Reston
8. ASCE/SEI 7-16 (2017) Minimum design loads and associated criteria for buildings and other structures. American Society of Civil Engineers, Reston
9. ACI 318M-11 (2011) Building code requirements for structural concrete. American Concrete Institute, Farmington Hills
10. ACI 318M-14 (2015) Building code requirements for structural concrete. American Concrete Institute, Farmington Hills
11. Sutjipto S, Sumeru I (2021) Anomaly phenomena on the new Indonesian Seismic Code SNI 1726:2019 design response spectra. In: Mohammed BS et al (eds) 6th international conference on civil, offshore and environmental engineering 2020. LNCE, vol 132. Springer, Singapore, pp 375–384
12. Fanella DA (2018) Structural load determination - 2018 IBC and ASCE/SEI 7–16. International Code Council, Washington DC
13. Fanella DA (2007) Seismic detailing of concrete buildings, 2nd edn. Portland Cement Association, Skokie
14. Fanella DA (2016) Reinforced concrete structures - analysis and design, 2nd edn. International Code Council, Washington DC

15. Sutjipto S, Sumeru I (2022) Seismic design load comparison of reinforced concrete special moment frame and dual systems based on SNI 1726:2019. In: Lie HA et al (eds) The second international conference of construction, infrastructure, and materials. LNCE, vol 216. Springer, Singapore, pp 231–237
16. SNI 1727:2020 (2020) Beban desain minimum dan kriteria terkait untuk bangunan gedung dan struktur lain. Badan Standardisasi Nasional, Jakarta
17. SNI 1727:2013 (2013) Beban minimum untuk perancangan bangunan gedung dan struktur lain. Badan Standardisasi Nasional, Jakarta
18. RSA 2010. <http://rsa.ciptakarya.pu.go.id/2010/>. Accessed 05 July 2022
19. RSA 2021. <http://rsa.ciptakarya.pu.go.id/2021/>. Accessed 05 July 2022

Effective Mixing Lag Time of Two Phase Lime-Cement Stabilization on High Plasticity Clay



Teguh Widodo and Nur Ayu Diana

Abstract The use of soil–cement as pavement base material is one solution to the limitations of split rock in an area. The challenge of soil–cement use in Indonesia is how to increase the soil–cement strength to achieve requirements as a pavement material, especially in high-plasticity clay soils. One method of increasing soil–cement strength is to mix the soil with lime before it is mixed with cement and compacted. The mixing lag time must be sufficient so that the soil–lime chemical reaction runs well at once, but short enough to speed up the process of application. This paper presents the results of a laboratory study of the effect of mixing lag time on the UCS values of soil- cement-lime material. A series of physical properties, compaction and unconfined compression test according to SNI were performed on the untreated soil, and soil–lime-cement sample that prepared in mixing lag time 0, 2, 4 and 24 h. Lime content used is 2%, 6% and 10%, while the cement content is 10% of the soil dry weight. Grain size analysis and atterberg limit test performed to describe flocculation process and soil lime chemical reaction. The results of the study showed that the UCS value of sample prepared at 2 h and 4 h time-lag are 1/3 – 2/5 times UCS value of sample prepared at 24 h. The effective mixing lag time to provide sufficient soil–lime chemical reaction process is 24 h.

Keywords Chemical reaction · mixing lag time · UCS

T. Widodo (✉) · N. A. Diana
Departement of Civil Engineering, Janabadra Univercity Yogyakarta, Jl. Tentara Rakyat Mataram
57, Yogyakarta, Indonesia
e-mail: teguh_widodo@janabadra.ac.id

N. A. Diana
e-mail: nurayu@janabadra.ac.id

© Institute of Technology PETRONAS Sdn Bhd 2024
B. S. Mohammed et al. (eds.), *Proceedings of the International Conference on Emerging Smart Cities (ICESC2022)*, Lecture Notes in Civil Engineering 324,
https://doi.org/10.1007/978-981-99-1111-0_61

1 Introduction

Some of the Merauke – Tanah Merah sections were built in 2018 use soil–cement as pavement base material for substitute rock aggregate that must be imported from Sulawesi [1]. The use of soil–cement as pavement base material in Indonesia has varying degree of success [2]. Soil–cement material is pulvylized soil smaller than 4.75 mm and cement that mix omogenously and compacted at optimum water content [3, 4]. The process of water absorption, ion exchange, hydration and cement pozzolanic reaction cause particles bonds formed soil–cement material with larger particles, solid, strength, and is water-resistant [4–5]. Some technical advantage soil–cement pavement base material are: 1) soil–cement is solid material causes a wider spread of wheel load pressure on subgrade compared to granular split rock material, 2) soil–cement elastic strain is 2–3% or 10 times the concrete elastic strain gives plastic deformation is achieved in higher subgrade strain compared to concrete used on rigid pavement. The use of local soil materials also provides environmental benefits and saves material transportation costs.

Dry cement particles contain crystals $3\text{CaO}\cdot\text{SiO}_2$, $4\text{CaO}\cdot\text{SiO}_4$, $3\text{CaO}\cdot\text{Al}_2\text{O}_3$ and solid materials in the form of $4\text{CaO}\cdot\text{Al}_2\text{O}_3\text{Fe}_2\text{O}_3$. When cement is added to the soil, calcium Ca^{++} ions are released through hydrolysis and ion exchange on the surface of clay particles resulting the clay particles clump and better soil consistency. The main reaction related to strength is the hydration of $3\text{CaO}\cdot\text{SiO}_2$ and $2\text{CaO}\cdot\text{SiO}_2$ consisting of calcium silicate and through the hydration of hydrates such as calcium silicates and aluminate are formed causes hardening process. Hydration process produse calcium hydroxide that react with the soil (pozzolanic reaction) resulting strengthening the bonds between particles [5]. As a result of the hydration process and pozzolanic reaction soil and cement particles are bound together and clustere to form larger soil–cement particles [6].

The soil–cement strength is influenced by: soil type, cement content, density, and water content [7–10]. Low plasticity silt, (A5, under AASHTO classification) and low plasticity clay soil (A6) produces hight strength soill-cement [4, 11]. High plasticity clay A7 produces poor strength soil–cement in submerge condition caused by: 1) clay has very small particles so that it has a large particles surface area, it takes a greater cement to cover the perticles surface area, and 2) clay has clay minerals that absorb water, the surface of particles that are not closed cement paste will absorb water [4, 8, 9, 11]. Soil–cement stabilization in high-plasticity clays also has high sensitivity to water and low unconfined compressive strength in soaked conditions.

Surface soil in the form of high plasticity clay is often found in Indonesia, therefore the challenge of using soil–cement as pavement material in Indonesia is how to increase soil–cement strength to achieve requirements as pavement material, especially in high-plasticity clay soils. Addition of rice husk ash [12], fly ash [13], lime [5, 6, 13–15] and sand [16] in soil–cement mixtures to improve soil–cement strength according to the requirements as pavement material have been studied. Addition of lime in 2 stages of stabilization has also been studied [11, 17].

Lime were produces from limestone which were burned at high temperatures: $\text{CaCO}_3 \rightarrow \text{CaO} + \text{CO}_2$. Blackout of lime, CaO using H₂O produces powder (dry) or thick liquid (wet): $\text{CaO} + \text{H}_2\text{O} \rightarrow \text{Ca(OH)}_2$. Lime will harden if it reacts with water. This property is caused by the occurrence of compounds with SiO₂, Al₂O₃ and others. Soil–lime mix results in a pozzolanic reaction, reduce plasticity index and flocculation into larger aggregate thereby reduce the particle surface area. The two phase lime-cement soil stabilization with time lag between lime and cement addition give time to soil–lime chemical reaction process formed lime-soil material that had low plasticity, large particle thereby reduce cement needed to cover particle surface area and increases strength of soil–lime-cement material.

The 24-h time lag of two phase stabilization lime-cement on high plasticity clay resulting UCSsoaked value of 2.63 times UCSsoaked soil–cement-lime without a lag time [18]. The 7 day lag time increase BCR values and reduce swelling of high cement content samples (6%, 8% and 10%) [17]. The 4 h time lag increases maximum elastic strain as well as unconfined compressive strength low cement content samples (2%, 4% and 6%) [11].

This paper presents the results of a laboratory study of the effect of the time lag between addition of lime and cement to the unconfined compressive strength and water sensitivity value, on expansive clay. This study aims to determine the minimum time lag of mixing lime and cement to produce soil–cement strength according to the requirements as pavement material.

2 Method

The research was carry out based on Indonesian National Standards [19] and divided into two stages. The reseach preparation stage aims to choose test material soil. The physical properties testing, includes: specific gravity test (SNI 03–1964-1990), water content (SNI 03–1965-1990), soil grain size analysis using a hydrometer (SNI 03–3423-1994), and sieve (SNI 03–1968-1990), liquid limit (SNI 03–1967-1990), and plastic limit (SNI 03–1966-1990) performed to classified five soil samples from various locations according to the American Association of State Highway and Transportation Official classification system (AASHTO) and the Unified Soil Classification System (USCS). The soil which clasified as high plasticity clays (CL, USCS) or (A7, AASHTO) are choose as material test.

The main research stage are: 1) Proctor standard compaction test (SNI 03–1742-1989) of untreated soil, cemenet stablezed soil and lime-cement stabilized soil, 2) liquid limit test (SNI 03–1967-1990), plastic limit (SNI 03–1966-1990), grain size analysis using a hydrometer (SNI 03–3423-1994), and sieve (SNI 03–1968-1990) of lime stabilized soil aims to study decrease of the plasticity index value and flocculation process at the end of 0, 2, 4, and 24 h curing time, and 3) unconfined compression test (SNI 03–6887-2002) of unsoaked and soaked 7 days curing time sample that compacted at maximum dry density and optimum moisture content. The cement content used is 10% while lime content are 2%, 6% and 10%.

Table 1 Physical and mechanical properties of *untreated* soil

Test	Value
Atterberg Limit Liquid Limit, % Plastic Limit, % Plasticity Index, %	71.2 23.16 48.04
Grain Size Distribution Gravel (G), % Sand (S), % Silt (M) and Clay (C), %	0 5.32 94.68
Specific Gravity	2.53
Soil Classification AASHTO USCS	A7-6 CH
Unconfined Compression Strength UCS Unsoaked kg/m ² UCSsoaked kg/m ²	1.98 failure

3 Result and Discussion

3.1 *Physical and Mechanical Properties of Untreated Soil*

The soil sample from KM9 Wates Evenue which classified as high plasticity clays (CL, USCS) or (A7, AASHTO) are choose as material test soil. The physical properties test and grain size distribution of the soil can be seen in Table 1. Soil has a fine grain content of 94.68%, 5.32% sand and 0% gravel. Based on the USCS classification the soil was high-plasticity clay, CH, whereas according to the AASHTO classification the soil was included in the A7-6.

3.2 *Effect of Lime and Cement on Optimum Moisture Content and Maximum Dry Dencity*

The standard proctor compaction test results of untreated soil, cement treated soil, and lime-cement treated soil can be seen in Table 2. Compaction test results show that the addition of lime and cement makes the soil easier to compact and has an optimum moisture content lower than the untreated soil and has a greater maximum dry weight. The addition of cement and lime has resulted in soil granules moving more easily between the grains when compacted to obtain a higher particle density level at lower water content.

Table 2 The standard proctor compaction test results

Composition	wopt(%)	γd max (g/cm ³)
Untreated Soil	25.2	1.34
Lime 2% - Cement 10% Treated Soil	25.5	1.36
Lime 6% - Cement 10% Treated Soil	23.9	1.37
Lime 10% - Cement 10% Treated Soil	23.15	1.42

3.3 Effect of Mixing Time Lag on Granular Content > 0.075 mm and Plasticity Index

The soils-lime chemical reaction resulted pozzolanic reaction and flokulation of aggregate into a large aggregate and decreased plasticity index, therefore percentage of aggregate > 0.075 mm and decrease plasticity index can be used to describe the effectiveness of soil–lime reaction at the time lag of 2 h, 4 h and 24 h. Figure 1 shows increase of time lag will increase percentage of aggregate > 0.075 mm. Percentage of aggregate > 0.075 mm at a time lag of 2 h and 4 h is much smaller when compared with a 24-h that describe the flokulation process of soil grains into a larger grain is not maximized.

The plasticity index decrease as seen in Fig. 2 also shows that the soil-chalk reaction process is not maximized at a time lag of 2 h and 4 h. The plasticity index of untreated soil 48.04% decrease to 20.72% (after 2 h time lag after soil- lime mixing) and 19.60% (4 h) is more due to the change in the physical properties of the soil after mixed by lime 10%. Soil aggregate more easily slip each other so the lower liquid limit is obtained. On the other hand the addition of lime will reduce the clay particle per unit volume of soil, reduce the cohesion and increase the plastic limit.

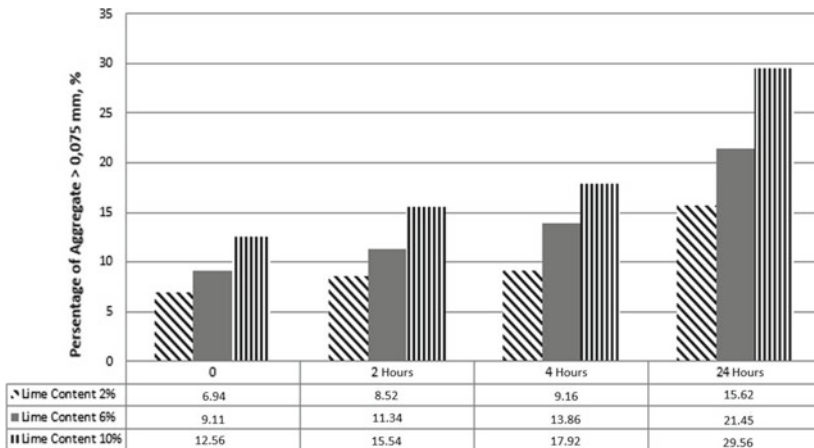


Fig. 1 Effect of mixing time lag againt percentage of aggregate > 0,075 mm

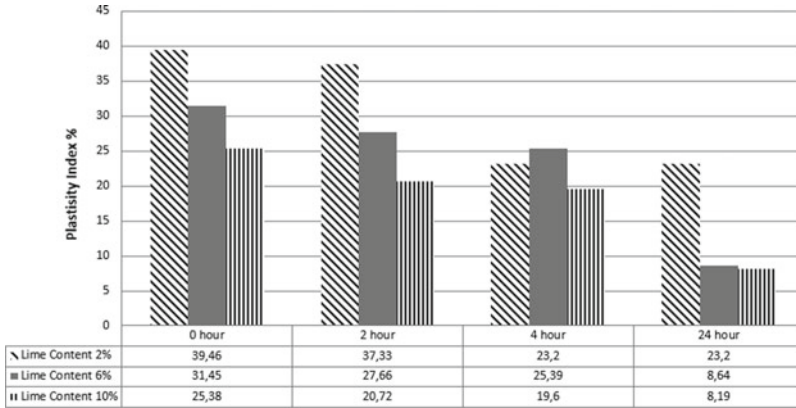


Fig. 2 Effect of mixing time lag against plasticity index

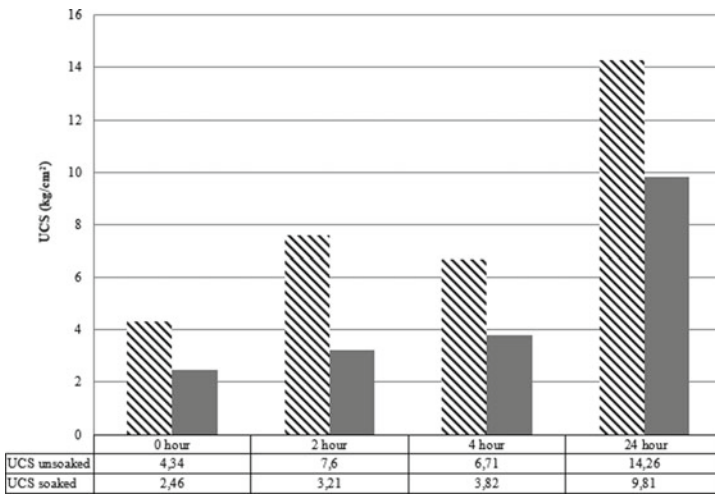


Fig. 3 Effect of mixing time lag against unconfined compression test

Effectiveness of soil–lime chemical reaction at 24-h time lag is illustrated by decrease in the plasticity index by addition of 10% lime from 19.6% at 4-h time lag to 8.19% at 24 h time lag and increase in the percentage of aggregate > 0.075 mm from 19.92% at 4 h time lag to 29.56% at 24 h time lag. Figure 1 and Fig. 2 show that the effectiveness of soil–lime chemical reaction at 24-h time lag occurs in lime addition of 2%, 6% and 10%. The increase in the percentage of grains > 0.075 mm and the decrease in the plasticity index that occurs at intervals of 2 h and 4 h is more due to changes in physical properties due to a mixture of two materials with different physical properties. Grains size analysis and atterberg limits at the time lag 2 h, 4 h

and 24 h showed that the greater of lime additions the greater percentage of grain size > 0.075 mm and the smaller the plasticity index value.

3.4 Effect of Mixing Time Lag on UCS Value

Unconfined compression test was carried out on treated soil by 10% lime and 10% cement with a time lag of mixing 2 h, 4 h and 24 h to determine the effect of the time lag of mixing on unconfined compressive strength, UCS value (Fig. 3). Effectiveness of soil–lime chemical reaction illustrated by increase of UCS_{unsoaked} value of lime-cement treated soil with 24-h time lag is 2 times UCS_{unsoaked} value with 4 h time lag while UCS_{soaked} value is 2.5 times.

Soil–lime chemical reactions when mixing soil lime at the first phase will decrease of plasticity index, pozzolanization and flocculate into larger grains, thereby reducing the surface area of the grains before mixing cement in the two phase of stabilisations [5, 7, 15]. At the interval of mixing time of 2 h and 3 h the increase in UCS value was not maximal because the process of flocculation and lime-soil reaction described by the plasticity index were still at an initial level and not yet maximal. Increased density (Table 1) between grains due to soil grains is more easily compacted when mixed with lime and cement, also resulting in increased UCS values.

4 Conclusion

1. The flocculation process and lime-soil chemical reaction has not been effective at the soil–lime mixing time lag of 2 h and 4 h.
2. The value of UCS unsoaked and UCS soaked at soil–lime mixing time lag of 2 h and 4 h one-third to half times the value of UCS submerged and UCS is submerged at intervals of 24 h.
3. Minimum time lag between soil–lime mixing and soil–lime-cement mixing to produce a effective strength increase of soil–lime-cement material is 24 h.

References

1. Marbun OH, Asniaty AM, Hutagalung D (2020) Pelaksanaan Pekerjaan Lapis Fondasi Semen Komposit Tanah pad Ruas Jalan Merauke-Tanah Merah, Jurnal HPJI, vol 6(1), pp 43-50 Januari
2. Arif W, Sugeng W (2014) Pengaruh Kadar Air dan Bahan Ikat Semen Terhadap Trend Kere-takan Lapis Perkerasan Tanah Semen, Konferensi Regional Teknik Jalan ke 13, Makassar, halaman , pp 1–17
3. Anonim, Soil Cement Construction Hand Book, Portland Cement Assosiation, Illinois (1995)
4. Lim SM, Wijeyesekera DC, Lim, AJMS, Bakar IBH. (June 2014) Critical review of innovative soil road stabilization techniques. Inter J Eng. Adv Technol (IJEAT), 3(5)

5. Todingrara' YT, Tjaronge MW, Harianto T, Ramli M (2017) Performance of laterite soil Stabilized with Lime and Cement as a Road Foundation. *Inter J Appli Eng Res* 12(14), 4699–4707 © Research India Publications. <http://www.ripublication.com>
6. Okyay US, Dias D (2010) Use of lime and cement treated soils as pile supported load transfer Platform *Eng Geol* 114
7. Suksun H, Runlawan R, Avirut C, Yuttana R, Apichat S (2010) Analysis of strength development in cement-stabilized silty clay from microstructural considerations. *Const Build Mater* 24, 2011–2021. <http://www.elsevier.com/locate/conbuildmat>
8. Anonim, Soil Cement Laboratory Hand Book, Portland Cement Assosiation, Illinois (1992)
9. Gautreau GP, Zhang ZD, Wu Z (April 2009) Accelerated Loading Evaluation of Subbase Layers in Pavement Performance. Technical Report Louisiana Transportation Research Center, Los Angeles,
10. Rahman MM, Siddique A, Uddin MK (2012) Clay-water/cement ratio is the prime parameter for fine grained soil improvement at high water content. *DUET J* 1(3), 1–11
11. Arif W (2005) Stabilisation Technology implementation as the way of efficiency in the road betterment and road rehabilitation in Indonesia. In: National Conference of Rekayasa Aplikasi dan Perancangan Industri (RAPI – IV), Engineering Faculty Muhammadiyah University of Surakarta, ISSN: 1412- 9612
12. Lucian C (2012) Effectiveness of two sequential mixing of lime -Portland cement in stabilizing expansive soils. *Int J Appli Sci Eng Res* 1(6)
13. Aliyu MK, Karim ATA (2016) The effect of cement and rice husk ask on the compressive strength and leachability contaminated stabilized sedimment. *ARPN J Eng Appli Sci* 11(8)
14. Kumar MA, Prasaja Raju GVR (2009) Use of lime cement stabilized pavement construction. *Indian J Eng Mater Sci* 16, 269–276
15. Gharib1 M, Saba H, Barazesh A (2012) The effect of additives on clay soil properties using cement and lime. *Inter J Basic Sci Appli Res* 1 (3) 66–78
16. Goli N, Abid S (Desember 2015) Stabilization of clayed soil using lime and cement. In: *Indian Geotechnical Conference*
17. dan Ekowati R WT (April 2014) Efektifitas Penambahan Pasir Semen dan Stabilizer pada Stabilisasi Tanah Lempung Ekspansif, *Jurnal Teknik*, vol. 4(1)
18. Ruktiningsih R (2005) CBR value of Ilite clay improvement with lime and Portland cement. In: *International Seminar and Exhibition on Road Constructions (ISERC)*, vol 3
19. Widodo T, Yasir M (2018) Effectiveness of 2 phase stabilization lime- cement on high plasticity clay. *J Phys Conf. Ser.* 1175, 1st International Conference on Advance and Scientific Innovation 23–24 April
20. Anonim, Metode, Spesifikasi dan Tata Cara Bagian 1 : Tanah, Longsoran, Badan Penelitian dan Pengembangan Departemen Permukiman dan Prasarana Wilayah, Jakarta (2002)

The Thermal Comfort of Sangkring Art Space Yogyakarta



Rini Hidayati, Martha Karerinna Anugerah, and Fadhilla Tri Nugrahaini

Abstract Thermal comfort is one factor that affects the level of human comfort when carrying out activities and interacting. Human needs comfortable thermal conditions for carrying out activities indoors. Sangkring Art Space one of the galleries in Yogyakarta makes efforts to maximize natural airflow mechanism building. This study aims to determine the condition of thermal comfort and analyze the effect of natural airflow on the thermal comfort of Sangkring Art Space buildings. The method used in this study is a quantitative method by observing and measuring temperature, humidity and wind speed. Based on observation and measurement data, PMV (Predicted Mean Vote) and PPD (Pre-dicted Percentage Dissatisfied) calculations were carried out using the CBE Thermal Comfort Tool ASHRAE-55 to obtain a value scale that describes the thermal comfort conditions of visitors or users of the Sangkring Art Room. The results showed that Sangkring Art Space did not meet the standards for natural airflow and thermal comfort. Factors that cause it namely the speed of motion of air in space, location and shape of the ve building conditions and surrounding environment.

Keywords Thermal comfort · Natural airflow · Sangkring art space

1 Introduction

Architecture is a field of study that creates a space for human activities according to their needs. In designing a space, it is necessary to pay attention to many factors that can affect the level of user comfort. Comfort in a room can be defined as a condition that provides a feeling of comfort and pleasure for users in carrying out their activities [1]. One of the factors affecting the level of human comfort when carrying out activities and interacting with their physical environment is thermal

R. Hidayati (✉) · M. K. Anugerah · F. T. Nugrahaini
Architecture Department, Universitas Muhammadiyah, Engineering Faculty, Surakarta, Indonesia
e-mail: rh215@ums.ac.id

© Institute of Technology PETRONAS Sdn Bhd 2024
B. S. Mohammed et al. (eds.), *Proceedings of the International Conference on Emerging Smart Cities (ICESC2022)*, Lecture Notes in Civil Engineering 324,
https://doi.org/10.1007/978-981-99-1111-0_62

727

comfort [2]. Thermal comfort creates a balance between human body temperature (37 °C) and the temperature of the surrounding environment [1].

According to Lee and Chang, most people spend more time (more than 90%) on indoor activities, so good airspeed is needed to produce a comfortable space for activities [3]. Indonesia has a humid tropical climate with relatively high air temperatures and humidity. Scorching and long solar radiation is crucial in creating thermal comfort, especially the quality factor of natural lighting in buildings. The quality of living as one of the factors affecting thermal comfort needs to be maximized. One way is by providing air circulation into the building. The airflow naturally gives a comfortable and healthy feeling to its users.

Yogyakarta city is a city of arts and culture. This will make Art Space an alternative to art galleries [4]. Sangkring Art Space is one of the art gallery buildings that make efforts to maximize the natural lighting factor in the building. However, there are indications that the art gallery building gives a feeling of thermal discomfort to visitors, characterized by visitors feeling hot and sweaty. In addition, there are fans that indicates that thermal comfort is not achieved in some spaces. This study aims to determine the thermal condition and the influence of natural airflow on the thermal comfort of the building. In addition, an analysis of the aspects that affect natural ventilation.

2 Literature Review

2.1 *Natural Airflow*

Natural airflow is the process of air exchange in the building through the help of open building elements. Good air circulation in the building can provide thermal comfort for users or occupants because it accelerates evaporation on the skin's surface [5]. Good air circulation in optimizing natural livelihoods can be achieved by analyzing the arrival of wind direction accompanied by considerations of the macroclimate (wind from Southeast to Southwest) and microclimate (weather, existing conditions, surrounding environment, etc.).

2.2 *Thermal Comfort*

Thermal comfort is a state of mind satisfied with the thermal environment. This condition needs to be controlled to ensure the comfort and health of occupants as well as the proper functioning of sensitive equipment in sensitive in spaces [6]. Human physical comfort in buildings is dominated by thermal comfort, including air temperature, humidity, and airflow speed [7]. Based on the thermal comfort standards

of the International Standard Organization [8], thermal comfort is influenced by the following factors:

2.3 Air Temperature

Indoors, the average radiant temperature can vary from point to point. In most cases only a rough approximation such as the average room surface temperature can be achieved [9]. Temperature is a quantity that expresses the degree of cold heat of an object, and the device used to measure temperature is a thermometer. Based on (SNI 03–6572-2001), thermal comfort standards for the tropics are divided into:

- Comfortable cool, between effective temperatures of 20.5°–22.8 °C;
- Optimum comfort, between effective temperatures of 22.8°–25.8 °C ;
- Comfortable warm, between effective temperatures of 25.8°–27.1°C

Air Humidity

Air humidity is moisture contained in the air. The humidity limit in humid tropics to achieve comfort is $40\% < RH < 60\%$ with casual activities, light, and layers of clothing [10].

Wind Speed

Wind speed is the speed of the airflow moving horizontally at two meters above the ground, and the optimal wind speed to achieve thermal comfort is $0.6 < V < 1.5$ m/s [10].

Radiation Temperature (MRT)

Radiation temperature is the heat generated by the radiation of an object that emits heat. The magnitude of the radiation temperature can be assumed to be the same as the air temperature. Still, for more accurate results in determining the PMV (thermal comfort) scale, it must be calculated in more detail.

Activity or Type of Activity

The type of activity affects the human body's metabolic rate (Metabolic Rate), which varies because it depends on the activity it carries out.

Types of Clothing (Clothing Insulation)

The type of clothing worn will affect the heat exchange between the body and the surrounding environment because clothing can inhibit the release of heat from the body to the surrounding environment, so the type of clothing determines a person's comfort level.

Fanger, define thermal comfort as a condition or feeling of pleasure and satisfaction that a person feels in the face of his thermal environment and to find out the indication of the level of thermal comfort of a domain with the perception of the level of comfort that a person feels; it is necessary to have a scale of calculation of thermal comfort parameters.

3 Research Method

The method used in this research is a quantitative method with the following stages, (1) Determining the variables of thermal comfort aspects through literature studies, (2) Observing and determining measurement points. The points are determined in the area that is the location of visitors in observing the object of the exhibition, (3) Field data collection through visitor interviews, observation of ambient conditions, measurement of thermal comfort aspects using hygro-thermometer and anemometer, (4) Analyzing data using thermal comfort parameters: PMV (Predicted Mean Vote) and PPD (Predicted Percentage Dissatisfied). Finally discuss the results of the analysis.

4 Result and Discussion

4.1 *Building Existing Condition*

Sangkring Art Space is an art gallery building established in 2007 in Bantul Regency, Yogyakarta. The building is a creative and experimental space for artists and art activists to share, respect differences, and emphasize unity in art. Sangkring Art Space consists of 2 floors with an area of each floor $\pm 38 \text{ m} \times 15.34 \text{ m}$. Sangkring Art Space only has a single door as an entry and exit lane with access to the 2nd floor using stairs. There is 1 fan on the 1st floor and 4 fans on the 2nd floor (Figs. 1 and 2).

4.2 *Measurement Results*

Observations and measurements of factors affecting thermal comfort (temperature, humidity, and wind speed) were carried out on the 1st and 2nd floors totaling 16 measuring points, with each floor eight measuring points and the distance between points 2 m-3 m. Figure 3. Observations and measurements of temperature, humidity, and wind speed are carried out for three days during the day and evening at 1 PM and 4 PM. Observations are made when the room operates as a showroom so that there is activity by visitors and supporting tools for thermal comfort such as the fan turn on and off condition to see the effect on the heating of the space. As a support for the data results, interviews were conducted with several visitors to find out from the perspective of space users about the thermal comfort of Sangkring Art Space (Figs. 3 and 4).

Fig. 1 First Floor Interior Sangkring Art Space

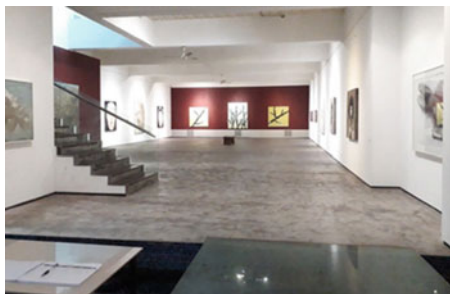


Fig. 2 Second Floor Interior

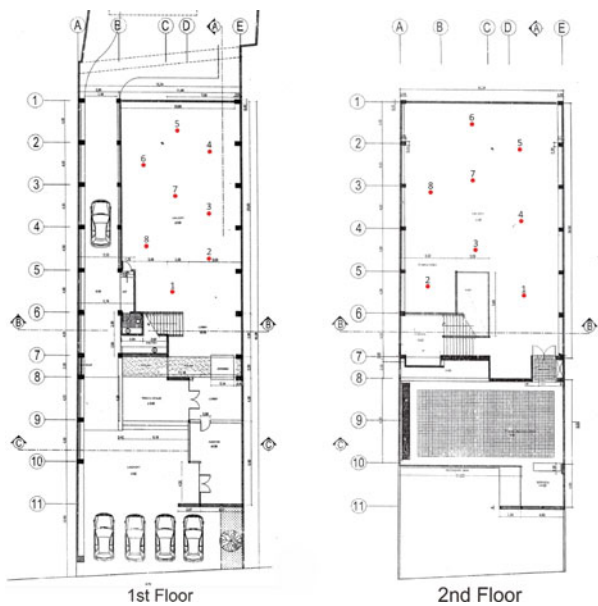
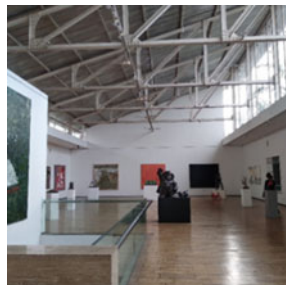


Fig. 3 Measuring Point Plan

Fig. 4 PMV and PPD Calculation with Comfort Calculator (CBE Thermal Comfort Tool for ASHRAE-55)

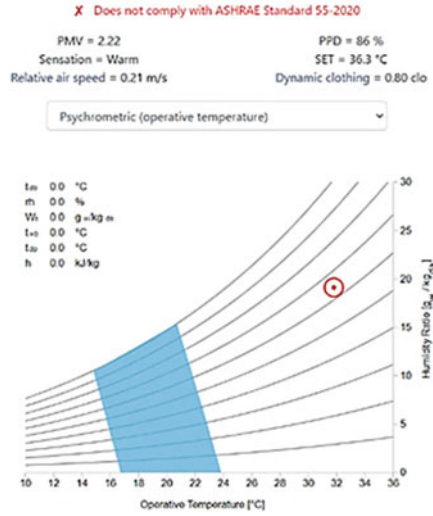


Fig. 5 Ventilation on the 1st floor



Fig. 6 Ventilation inlet on 2nd floor



The result of the thermal condition of the room with the fan state on is that the highest average temperature occurs during the day on the 2nd floor (30.98 °C). The lowest occurs in the afternoon on the 1st floor (29.5 °C), then the highest average humidity occurs in the afternoon on the 2nd floor (70.1%), and the lowest occurs during the day on the 2nd floor (63.8%). While the highest average wind speed occurs in the afternoon on the 2nd floor (0.054 m / sec), and the lowest occurs during the

Fig. 7 Vent the door and hole above the pond (1st Floor)



Fig. 8 Eastside vent door in the 2nd Floor

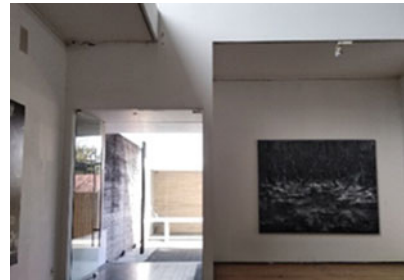
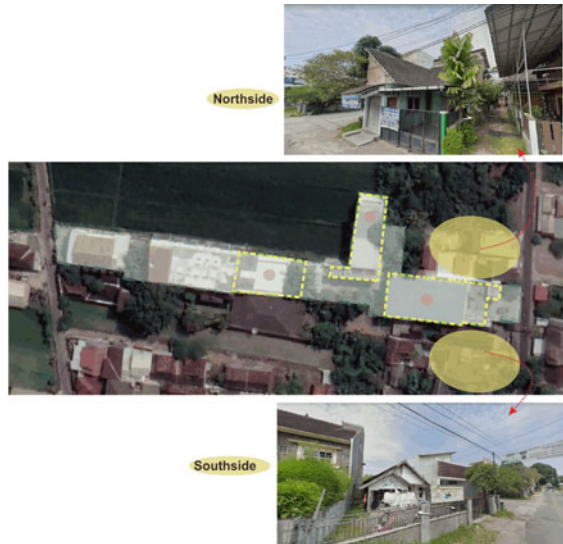


Fig. 9 Building environment conditions



day on the 1st floor (0 m / sec), due to the number of fans that affect the size of the airspeed, temperature, and room humidity (Figs. 5, 6, 7, 8, 9 and 10).

The measurements room with the fan off obtained the highest average temperature results during the day on the 2nd floor (31.8 °C). The lowest occurred in the afternoon



Fig. 10 South side building

on the 1st floor (29.7 °C), then the highest average humidity result happened in the afternoon on the 2nd floor (69.5%), and the lowest occurred during the day on the 2nd floor (64.2%). Meanwhile, the airspeed at each measurement time produces 0 m / sec due to the absence of an opening medium that can maximize the natural airflow of entering the building.

To corroborate the thermal comfort results based on temperature, humidity, and airspeed measurements, PMV and PPD calculations were carried out and interviews with several visitors to the artwork showroom. Based on observational data, PMV and PPD calculations were carried out through the CBE Thermal Comfort Tool for ASHRAE-55 to obtain a value scale that describes the thermal comfort conditions of visitors or users of the Sangkring Art Space space.

During the three days of observation, from noon to evening, interviews were conducted with 50 visitors, resulting in 0 visitors feeling cold, 11 people feeling cool, 39 people feeling hot, 22% feeling cool, and 78% feeling hot. Cool air results in the space are primarily due to the influence of climatic factors of the surrounding environment, weather, and artificial lighting devices in the form of fans.

From the PMV and PPD calculation tables above and the results of visitor interviews, it can be concluded that the condition of the Sangkring Art Space room with the fan turn on and off has the same result, which is uncomfortable or not by the standards of thermal comfort of the space and users. Here is one of the calculations to determine PMV and PPD using data on the average results of room measurements with the fan off during the day on the 2nd floor as the highest temperature.

4.3 Discussion

The natural thermal comfort of the Sangkring Art Space building is not optimal, causing the thermal conditions in the space to be uncomfortable. Here are some aspects that can affect thermal comfort in buildings.

a. Buildings Orientation Towards the Sun

The orientation of the building is the main factor in determining the amount of solar radiation that the building will receive. The Sangkring Art Space building has made efforts to achieve thermal comfort with the orientation of the shorter side of the building as an East-facing façade and the long side of the building facing North and South so that the heat radiation received by the building becomes less.

b. Buildings Orientation Toward the Wind

The microclimate based on the results of wind measurements comes from the South-west and South-West directions. Sangkring Art Space building responds to the direction the wind is coming by placing the longest side of the building on the South side but with minimal ventilation. Good ventilation is affected by free air speed, the orientation and shape of ventilation to the direction of the coming wind, the area of ventilation holes, barriers in the room, the distance between the inlet and the outlet, and the conditions of the surrounding environment.

- 1) The speed of motion of air in space should be even and sufficient, with the optimal limit for thermal comfort being 1.5 m/s [5]. Sangkring Art Space building does not meet the requirements for the optimal limit of airspeed in the space (produces a maximum average rate of 0.054 m/s).
- 2) The location and shape of the vents.

The location and shape of the vents can support the occurrence of cross ventilation in buildings. The best position is positioned by the outlet more elevated than the inlet, and the shape of the vent is adjusted to the direction of coming air because it can affect the direction and speed of air movement [5]. Sangkring Art Space building does not apply this concept, the location of the inlet and outlet are facing each other, and the shape of the opening is only in the form of an air gap between the roof and the glass, doors, and air grille (exhaust fan) so that the natural airflow in the space is not optimal.

- 3) Ventilation area

The ventilation area can help the process of air circulation as an air path to enter the building so that the natural life that enters the building can be maximized. The minimum area of air openings or vents is 60%–80% of the façade area or 20% of the space area. In the Sangkring Art Space building, the air vent area does not reach the minimum requirement because the openings are only in the form of doors, grilles, and air gaps.

Table 1 Calculation of PMV and PPD

Calculation Results according to <i>Thermal Comfort Tool</i>				
Observation Time		Fan On	Fan Off	Information
Noon	1st Floor	PMV: 1.88 PPD: 71%	PMV: 2.04 PPD: 78%	Not Appropriate/Uncomfortable
	2nd Floor	PMV: 1.85 PPD: 69%	PMV: 2.22 PPD: 86%	Not Appropriate/Uncomfortable
Evening	1st Floor	PMV: 1.95 PPD: 74%	PMV: 1.76 PPD: 65%	Not Appropriate/Uncomfortable
	2nd Floor	PMV: 1.79 PPD: 66%	PMV: 1.95 PPD: 74%	Not Appropriate/Uncomfortable

Table 2 Results of Influence Data from Weather and microclimate

Observation Time		Temperature (°C)	Humidity (%)	Airspeed	Ket
Noon	1st Floor	29,8	73,6	0	BMKG: - thick cloudy -31 th C -70% -winds 10 km/h from the Southwest
	2nd Floor	31,7	68,3	0	
Evening	1st Floor	28,96	74,5	0	BMKG: -cloudy -25 °C -80% -winds 20 km/h from the Southwest
	2nd Floor	28,8	77,1	0	

4) Building conditions and surrounding environment.

The environmental conditions around the site are one of the factors that can affect the natural airflow. Buildings on the South side of Sangkring Art Space are crowded together, making it difficult for free air circulation to enter the building. In addition, the outer wall south of the Sangkring Art Space building is as high as the roof, so the wind is blocked by the wall and cannot optimally enter the building.

(Source: googlearth)

There is green land to the west and north of the site, so it has little influence on the temperature of the 1st-floor room due to the presence of an air grille on the West side. The effect of these circumstances can be seen in Table 2. The results of measuring the thermal comfort factor without the help of a fan show that the temperature of the 1st floor during the day and evening is lower than the 2nd floor with higher humidity.

iii. Weather and microclimate

Weather and microclimate influence thermal comfort in buildings, including air temperature, air humidity, wind speed, and direction. Based on data from the Meteorology, Climatology, and Geophysics Agency (BMKG) of Bantul Regency and data

from the measurement of thermal comfort factors in the Sangkring Art Space building on November 24, 2021, the following results were obtained:

5 Conclusion

The natural life of the Sangkring Art Space Yogyakarta building still does not meet thermal comfort standards. Based on the measurement results, the highest air speed is 0.054 m/s from the optimal airspeed standard of 1.5 m/s. Natural airflow significantly affects the thermal comfort of Sangkring Art Space. Table 1 shows the difference from the PMV results, which is quite large; namely, the results of the pmv scale of the space with the fan off show a scale of 2.22. The results of the PMV scale of the room with the fan turn on show a scale of 1.85 so that the airspeed in space can provide a difference in the PMV scale up to 0.37.

Thermal comfort in Sangkring Art Space buildings has not reached the thermal comfort standard. The measurement results show the results of the study exceeding the optimal limits of thermal comfort standards. The natural airflow and thermal comfort of the Sangkring Art Space building are influenced by several aspects, namely the orientation of the building to the sun and wind, free air speed, the location and shape of ventilation or openings, ventilation area, building conditions, and the surrounding environment, as well as weather and microclimate factors.

References

1. Karyono TH (2001) Penelitian Kenyamanan Termis Di Jakarta Sebagai Acuan Suhu Nyaman Manusia Indonesia. *Jurnal Teknik Arsitektur DIMENSI* 29(1):24–33
2. Rilatupa J (2008) Aspek Kenyamanan Termal Pada Pengkondisian Ruang Dalam. *Jurnal Sains Dan Teknologi EMAS* 18(3):191–198
3. Chang SL (2000) Indoor and outdoor air quality investigation at schools in Hongkong. *PERGAMON J. Chemosphere* 41(09) 113
4. Burhn K Art and Youth Culture of the Post Reformasi Era: Social engagement, Alternative expression, and the Public Sphere in Yogyakarta (Ohio University). Retrieved from http://rave.ohiolink.edu/etdc/view?acc_num=ohiou1364899327.
5. Latifah SMNL (2015) Fisika Bangunan 1. Griya Kreasi, Penebar Swadaya Group, Jakarta
6. Bradshaw V (2006) *The Building Environment : Active and Passive Control System*, 3rd edn. John Wiley and Sons Inc., New York
7. Baharuddin MT (2013) Analisis Kenyamanan dan Lingkungan Termal pada Ruang Kuliah dengan Ventilasi Alami (Studi Kasus: Kampus II Fakultas Teknik Unhas Gowa). *Semesta Arsitektur Nusantara SAN 2*. Malang: San 111213
8. International Standard Organization, ISO Standard 7730 : Moderate thermal environments (2003)
9. Nicol F, Humphreys M, Roaf S (2012) *Adaptive Thermal Comfort : Principles and Practice*. Routledge, New York
10. Fanger P (1970) *Thermal Comfort*. McGraw-Hill Book Company, United States

Challenges and Recommendations for Offshore Monopod Platform Installation



Khairan Syuhada Binti Kassim

Abstract The design of a monopod structure is to suit shallow water depth with minimal platform facilities. This is for the platform to be less than 600MT, either the jacket or the topside portion. To reduce the cost of offshore installation, the design of the jacket or the topside may also require less tonnage derrick crane barge capacity. Hence, there are many optimized designs currently in the market. However, the risk during offshore installation can be very high, which can cause many challenges. This paper explains some of the challenges of installing a monopod, including the recommendations for the future design of monopods.

Keywords Offshore · Monopod · Challenges

1 Introduction

Offshore oil and gas platforms in Malaysia include various water depths depending on the field's location, ranging from typically 10 m to 100 m water depth. Some designs are more suitable for shallower water depths, such as 10 m to 30 m, while some can be suitable for typically 70 m to 100 m water depth. There are few designs of monopod structures such as single caisson, tarpon with guyed wires, or caisson with braced members as per Fig. 1. Under extreme weather conditions, wired guys provide stability to a monopod platform [1]. The facilities on the topside shall be minimal as the substructure may not be able to withstand high loads.

El-Reedy [2] provided a practical guide for conventional and advanced techniques applicable to designing, construction, installation, inspection, repairing, strengthening, maintaining, and rehabilitation of fixed offshore platforms suiting all operational environments and conditions. The selection of the appropriate offshore structure was discussed from a techno-economic point of view, considering all factors,

K. S. B. Kassim (✉)

Project Delivery and Technology, PETRONAS, Level 33, Tower 3, KLCC, Kuala Lumpur, Malaysia

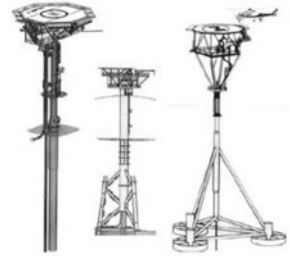
e-mail: khairan_syuhada@petronas.com

© Institute of Technology PETRONAS Sdn Bhd 2024

B. S. Mohammed et al. (eds.), *Proceedings of the International Conference on Emerging Smart Cities (ICESC2022)*, Lecture Notes in Civil Engineering 324,

https://doi.org/10.1007/978-981-99-1111-0_63

Fig. 1 Typical monopod designs for shallow water [1]



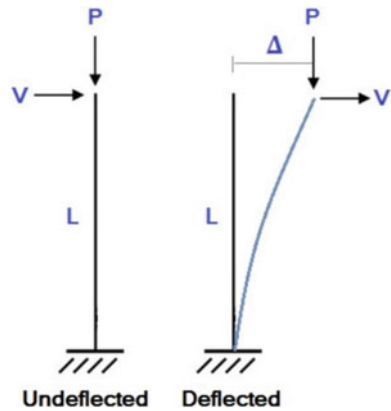
parameters and constraints that control the resultant design alternatives at each design stage Gardner [3] introduced the latest scientific and engineering developments in the field of tubular steel structures. Various keys and emerging subjects concerning the hollow structural sections such as special applications and case studies, static and fatigue behavior of connections/joints, earthquakes and dynamic response, and fire resistance were covered. Reddy and Swamidas [4] examined the engineering ideas and offshore drilling platforms used for oil and gas exploration and production. A clear demonstration of both the theory and application of the relevant procedures of structure, fluid, and geotechnical mechanics to offshore structures was presented. A global description of the environmental forces that include those due to wave, wind, current, tides, earthquakes, ice floe/sheet action, and limit ice-load on Arctic structures was offered. The emphasized analytical principles comprehend the various issues that need to be considered in the analysis and design of an offshore structure. A detailed overview of the various structures used in the offshore environment and the preliminary costing factors that influence the site choice was highlighted.

In light of all aforementioned studies this paper explains some of the challenges of installing a monopod, including the recommendations for the future design of monopods.

2 Challenges of Monopod Installation

One of the significant challenges of a monopod is the issue of P-Delta. P-Delta is the significant secondary moment due to a deflected structure depicted generally, as shown in Fig. 2. P-Delta analysis is required to be performed against linear analysis as it caters to the no-linearities [5]. For a monopod, having a single main pile holding the substructures together can be a challenge during offshore installation. For not-so-shallow water depths such as 70 m to 100 m, the main pile may be slanting due to unsupported length from mudline to platform sea deck impacted by weather and ocean current. It will be difficult to control the slanting if the Center of Gravity (COG) is not at the center of the main pile. As it is a single pile, it can be easily affected by other structures connected to it. To install the main pile with high accuracy and minimal tooling is also a challenge to avoid the levelness being out of tolerance.

Fig. 2 Deflected vs. non-deflected structure [5]



Another major challenge is when the on-bottom stability. A typical platform design will have a mudmat that functions to prevent offshore structures from sinking into soft soil on the seabed [6]. Figure 3 illustrates the samples of mudmats. However, the monopod design does not obtain this mudmat as the substructure’s base. Hence, on-bottom stability issues, including possible slanting/deflection of the platform, can be a result of this. To correct a slant on the base of the platform with minimal facilities on the installation vessel creates a challenge for the installer. An underwater diving intervention is needed to mitigate the leveling and slanting issues. Saturation divers are not usually mobbed for typical platform installation campaigns.

For topside installation, COG on the topside needs to be in the center within COG envelope as the topside is only placed at one leg. Due to this, if the COG is not exactly at the center of the leg, it can cause the monopod leg to slant at the angle of the topside COG. Furthermore, any movement to the leg or if the crane on the main work barge does not have heave compensation; it will be very difficult to place the topside onto the leg. It is difficult to operate offshore hydraulic cranes due to large inertia and sway issues if heave compensation and anti-sway control approaches are not available [7]. Figure 3 shows a sample of offshore lift operations. Once the topside is placed onto the leg, the main work barge is still connected to the structure. To avoid safety issues, both the topside needs to be secured in place and the crane to release its connection. These activities risk workers at the site, and the ‘As Low As Reasonably Practicable’ (ALARP) approach should be in place [8] (Fig. 4)

Installing the main caisson/monopod leg is crucial to be performed during a good weather window. Hence, the offshore installation campaign must be planned during the non-monsoon period. The utilized Main Work Barge has its weather limitation criteria as well the work itself must be done according to the weather limitation (i.e., Hs 1.5 m) that has been studied. To reduce the criteria, there are monopods that have been installed by jack-up Mobile Offshore Drilling Units [9].

Leveling a monopod, especially a braced type, is another challenge as there are not many structures that can be depended on to perform the leveling. To avoid leveling issues, the monopod leg cum pile must be installed in a controlled manner with



Fig. 3 Mudmat for jacket structure

Fig. 4 Offshore crane operation [7]



the assistance of an outrigger frame on the main work barge to achieve verticality requirements resulting in compliance with level tolerance. As a contingency, the design must account for the leveling technique upfront, including mobilizing the right equipment to perform the leveling. Some of the leveling methods include using a jack, mobilizing a leveling tool, or using the pre-install trunnion for lifting method. Figure 5 shows a picture of offshore pile lifting using ILT.



Fig. 5 Pile lifting & handling [10]

A quality issue on the weldment between the topside and main caisson will be massive if the structures are still moving. A lot of repairs need to be conducted, and this prolongs the condition of the platform at the stage where it is still yet to be completed. The main pile needs to remain stable to place and weld the topside.

3 Challenges of Monopod Installation

The design of monopods is recommended for shallower water depths, for example, 50 m and below. This is because when a single substructure component is involved, the sub-structure has which is prone to slant at the angle of the most weight has less degrees of freedom. The process of installing various facilities means the whole duration depends on the weather at the site. Although good weather windows can be obtained outside of monsoon season, severe weather in between the installation without the structure yet to be properly secured can cause difficulty for the installer to correct what the weather has impacted at the site. A non-linear analysis or P-Delta analysis to be run for pre-service conditions, i.e., during the course of installation. The design of the main caisson should consider the deflection issue, as mentioned. High strength, bigger size and/or higher thickness material shall be utilized as per study and analysis.

The accuracy of soil data is critical to ensure main pile/caisson verticality and target penetration are achievable. Soil investigation is to be performed at the proposed platform location. For a brace monopod, a good mudmat structure design will be able to ensure on-bottom stability, especially during the early phases of installation. Prior to installation, the seabed profile should be ensured to be flat as well. Other than this, proper removal of any existing debris should be done upfront to avoid any hiccups during the offshore installation activity.

The COG of the structure is to be ensured at the center of the monopod. If any pre-installed items can cause the shift in COG, it is recommended to install the facility/

Table 1 Dynamic amplification factors

Weight (ton)	Offshore (DAF)	Inshore (DAF)
<100	1.30	1.15
100–1000	1.20	1.10
1000–2500	1.15	1.05
<2500	1.10	1.05

equipment later at offshore. A monopod is highly sensitive to any shift of COG that can cause the structure to slant.

Should the design of the platform still be new, there are many lessons learned yet to be known. With this, minimal equipment mobilization can create a handicap for the installer when faced with many issues. As an example, without air and saturation diving spread, various underwater intervention is not an option. To find these divers for urgent mobilization is not an option due to their availability, including many inspections and audits prior to mobilization.

The leveling method must be considered during design to avoid any hiccup in correcting the levelness issues at offshore. Since the platform is a monopod, the leveling will be quite difficult. Hence, the design should already decide which method is best for performing the leveling at the site.

Main Work Barge shall also be equipped with a heave-compensated crane that embeds Dynamic Amplitude Frequency (DAF) into its crane load chart. For small structures and offshore lifts, the DAF is as per Table 1 [11]. A higher crange capacity will be able to assist should a major lifting require to be performed due to any issue. However, this comes with the price of mobilizing such a vessel. Hence, the risk of a new design can cause a higher cost than intended.

It is highly recommended that a monopod installation be closely vetted by following the qualifications of each personnel, especially the key personnel such as the field engineers, crane operators, barge foreman, and marine captains. A similar installation experience will be a plus point as these personnel will be able to anticipate the issues and recommend the way forward should a similar issue prevail.

It is recommended that the experienced designer to be mobilized at offshore as well. Immediate intervention is required if any issues prevail. Together, the solution can be revealed, avoiding any delay and cost incurred.

4 Conclusion

All in all, the design of a monopod needs to consider the installation method, including the risks involved to the workers, facilities to install, and the existing facilities nearby the location. These installation parameters must be considered and studied early during the FEED engineering phase. The final product depends on the quality of work during the installation period. Hence, good work performance during

installation can ensure the integrity of the structure and ensure that it will last the facility's lifespan.

Acknowledgements This technical paper is made possible through the collaboration and support by colleagues in PD&T either in line Department of Construction Installation (DCI) of Construction and De-commissioning Delivery (CDD) of Group Project Delivery (GPD) and from the Project Management Team (PMT) including Group Technical Solution (GTS). The project is made successful by the Offshore Installation Contractor and Contract Owner, Malaysia Petroleum Management (MPM).

References

1. Jamaluddin MA (2014) M. S. Response of Monopod Platform Under Extreme Wave In Malaysian Water. June: ResearchGate
2. El-Reedy M (2012) Offshore structures: design, construction and maintenance, 1st ed. Gulf Professional Publishing Co. Massachusetts: Elsevier Applied Science
3. Gardner L (2012) Tubular structures XIV. In: Proceedings of the 14th international symposium on tubular structures, (ISTS' 14), Imperial College London, CRC Press
4. Reddy D, Swamidas A (2013) Essentials of offshore structures: framed and gravity platforms, 1st edn. The CRC Press, New York
5. Comino P. SkyCiv. Retrieved from What os P-Delta Analysis? <https://skyciv.com/education/p-delta-analysis-and-p-delta-effects/>. Accessed 29 Apr 2016
6. Yarrarapu SK (2015) Mudmat role in offshore drilling operations. *Int J Eng Manage Res* 5(4):57–59 (2015)
7. Filippo Sanfilippo HZ (2014) An effective heave compensation and anti-sway control approach for offshore hydraulic crane operations. In: IEEE international conference on mechatronics and automation (ICMA), Tianjin, China
8. Jones-Lee M (2011) ALARP—What does it really mean? *Reliability Eng Syst Saf* 96(8):877–882
9. McRae LD (1994) Installation of Monopod Production Structures Using Jackup MODU's. IADC/SPE Drilling Conference. OnePetro
10. STATS Group (2021). <https://www.statsgroup.com/products-services/repair-maintenance/pile-lifting-handling>
11. Tahan BD (2005) Handbook of Offshore Engineering. ScienceDirect

Infill-Walls Interaction on Steel Moment Resisting Frame Due to Lateral Forces



I Ketut Diartama Kubon Tubuh, I Gede Gegiranang Wiryadi,
I Putu Agus Putra Wirawan, I Kadek Aditya Setyawan,
and I Made Laksana Wira Saputra

Abstract Infill-walls are often used as partition for most low-rise buildings building structure and are usually considered as non-structural components. However, infill-walls can interact and affect its frame structure behavior due to lateral loads. Studies that had been done mostly using reinforced concrete as structure frame. Regarding to this matter, analysis is performed by creating ten models of three and five-stories steel moment resisting frame which contain infill-walls considered as loads only (M3Open & M5Open) , infill-walls with stiffened openings in centric position (M3Hole-strut, M3Hole-shell, M5Hole-strut, & M5Hole-shell), and full infill-walls (M3Full-strut, M3Full-shell, M5Full-strut, & M5Full-shell). Infill-walls that its stiffness is considered on are modeled as diagonal strut and shell elements. Each structure models then are analyzed to obtain elastic story displacement and inter-story drift. Results show that story displacements plot of strut-modeled cross section area of infill-walls with hole need to be reduced by 0.4 to approach shell-modeled plot. Meanwhile, no need to modify strut for full infill-walls.

Keywords Infilled-frame · centric stiffened opening · strut · property modifier · story displacement

I. K. D. K. Tubuh (✉) · I. G. G. Wiryadi · I. P. A. P. Wirawan · I. K. A. Setyawan ·
I. M. L. W. Saputra
Department of Civil Engineering, Universitas Mahasaraswati Denpasar, Kota Denpasar, Indonesia
e-mail: diartamakubon@unmas.ac.id

I. G. G. Wiryadi
e-mail: gegiranangwiryadi@unmas.ac.id

I. P. A. P. Wirawan
e-mail: agusputrawirawan2020@unmas.ac.id

© Institute of Technology PETRONAS Sdn Bhd 2024
B. S. Mohammed et al. (eds.), *Proceedings of the International Conference on Emerging Smart Cities (ICESC2022)*, Lecture Notes in Civil Engineering 324,
https://doi.org/10.1007/978-981-99-1111-0_64

1 Introduction

Infill-walls are one of the important parts of a building which are often used as partitions separating rooms inside or as outer cover of buildings on reinforced concrete structures and steel structures, especially for low rise and medium rise buildings. In structure building designing process, infill-walls are usually considered as non-structural components. This is the reason structure is generally designed as an open frame and infill-walls are just considered as loads to the structure. But infill-walls tend to interact with its frame structure when major lateral load works on [3]. Infill-walls that have large area will have a large enough inertia to make structure stiffer. Although do not stiffen structure significantly like other lateral stiffening method such as shear wall, bracing, enlarging structure elements dimension, infill-walls can act reducing and or retarding collapsing process due to gravity loads also lateral loads [5].

Infill-walls is basically modeled as shell elements and its frame structure as frame elements. Connections between frame and shell has been studied and considered as gap elements [4]. While infilled frame receives lateral loads, infill-walls will develop a diagonal strut mechanism. This make infill-walls can be modeled as frame element of diagonal strut in simpler way. Considering infill-walls as diagonal strut is also the way to do nonlinear static analysis of infilled frame because strut frame elements can be assigned with plastic hinges. There are many researchers that studied to calculate strut width such as Mainstone [10] and Paulay and Priestly [6]. However, their formulas only calculated strut width for full infill-walls without openings.

Although there are openings, infilled frame has been tested and proofed that are stiffer than open frame [9]. Unstiffened infilled frame specimen always experience crack on the corner of the openings that makes it need to be strengthened with lintel frame [12]. Asteris et al. [8] proposed reduction factor of strut width calculation for infill-walls with unstiffened opening only. Sigmund and Penava [11], Sukrawa and Budiwati [13], and Wirawan et al. [7] has proposed formula to calculate strut width of stiffened opening infill-walls, but the frame was made from reinforced concrete. Therefore, needs to be studied on how stiffened opening infill-walls affect on steel moment frame behavior.

2 Methodology

2.1 Modeling Infill-Walls as Shell Elements

The shell element is a type of area object used to model the behavior of membrane, plates, and shells in three-dimensional planes and structures. Infill frame with shell element modeling is done by modeling the frame structure as a frame element and the infill-walls as a shell element. Relationship between infill-walls and the frame structure modeled in the form of link or gap elements contained in the study by Dorji

and Thambiratnam [4]. The gap strength formula was made as follows:

$$K_g = 0.0378E_i t_i + 347 \tag{1}$$

K_g is the gap stiffness which affected by elasticity modulus (E_i) and thickness (t_i) of infill-walls masonry.

2.2 Modeling Infill-Walls as Diagonal Strut

Infill-walls receives the lateral force exerted by the surrounding frame, where the infill wall will act as an equivalent diagonal strut. The effect of alternating lateral loads due to the earthquake can be overcome by the formation of a diagonal strut in the other direction which is also under compression. Mechanical properties sought by this method are based on nonlinear failure conditions and at the same time the resistance or nominal strength of the equivalent compression diagonal is obtained [3].

Dimensions for the strut are diagonal length, width, and thickness of the infill-walls. Diagonal length of the strut is measured from corner to corner of infill-walls and the thickness is the infill-walls thickness itself. Based on the equation of Paulay and Priestley [6], full infill-walls strut width is calculated using the following equation.

$$W_{ds} = \frac{d}{4} \tag{2}$$

From Eq. (2) can be seen that diagonal strut width (W_{ds}) is one-fourth of diagonal length of infill-walls. Wirawan et al. [7] has developed formula to calculate strut width of stiffened opening infill-walls on reinforced concrete frame which is shown in equation below.

$$W_{co} = \frac{d}{4 \tan \phi} Cc \tag{3}$$

$$Cc = 1.2022r^2 - 2.0953r + 1.045 \tag{4}$$

Equation (3) calculates strut width considering diagonal strut angle measured from horizontal line and infill-walls' strength coefficient (Cc) which is taking opening area percentage (r) into account.

2.3 Structure Models

This study is reviewing a steel structure building with functions as an office building with a special moment resisting frame structural system. The building consists of two variations number of floors which are 5-stories and 3-stories building with four transverse portals with a distance between the portals of 6 m. The elongated portal has 6 number of spans with a span length of 6 m, with a height of 3.5 m on each floor and a wall thickness is 12 cm. Typical plan of building and portals can be seen on Fig. 1.

From variation number of floor and infill-walls consideration, ten structure models were created which are M3Open, M5Open, M3Hole-strut, M3Hole-shell, M5Hole-strut, M5Hole-shell, M3Full-strut, M3Full-shell, M5Full-strut, and M5Full-shell. The M3Open and M5Open model is a structure models with open frame system so that infill-walls are considered as loads only. This model is analyzed to obtain dimensions with stress ratios that meet the requirements for steel. The behavior of this model will be compared with eight other models of infilled frame. Infilled frame models are models whose geometry, dimensions, and structural elements are identical to open frame model. M3Hole-strut, M3Hole-shell, M5Hole-strut, and M5Hole-shell are models with stiffened opening infill-walls. Openings area are taken 30% relative of full infill-walls area. While the rests are models with full infill-walls on the steel frame structure. Layout plan for infill-walls placement on frame structure is shown on Fig. 2.

From Fig. 2 can be seen black solid lines indicates where infill-walls to be placed. Other nonsolid lines are assumed filled with non-infill-walls such as glass claddings or partition boards. All infill-walls then will be modeled using shell elements and diagonal strut.

Steel specification that is used in these models has quality of BJ37. According to SNI 03-1729-2002 [1], BJ37 has yield and ultimate stress of 240 and 370 MPa. Infill-walls material is Autoclaved Aerated Concrete (AAC) lightweight bricks that has properties of compressive stress, elasticity modulus, and weight per unit volume as 2,97 MPa, 1633,5 MPa, and 5,96 kN/m³ respectively [16]. Gravity loads that work on the structure are from dead loads referring to PPIUG 1983 [15] and live loads referring to SNI 1727:2020. Lateral loads are from earthquake loads which is calculated using SNI 1726:2019 [2] standard.

3 Results

3.1 Structure Elements Dimension

Dimension of steel section are calculated according to SNI 1729:2020 and being chosen based on optimum demand per capacity ratio. Dimensions of steel frames for 3-stories and 5-stories building are shown in Table 1.

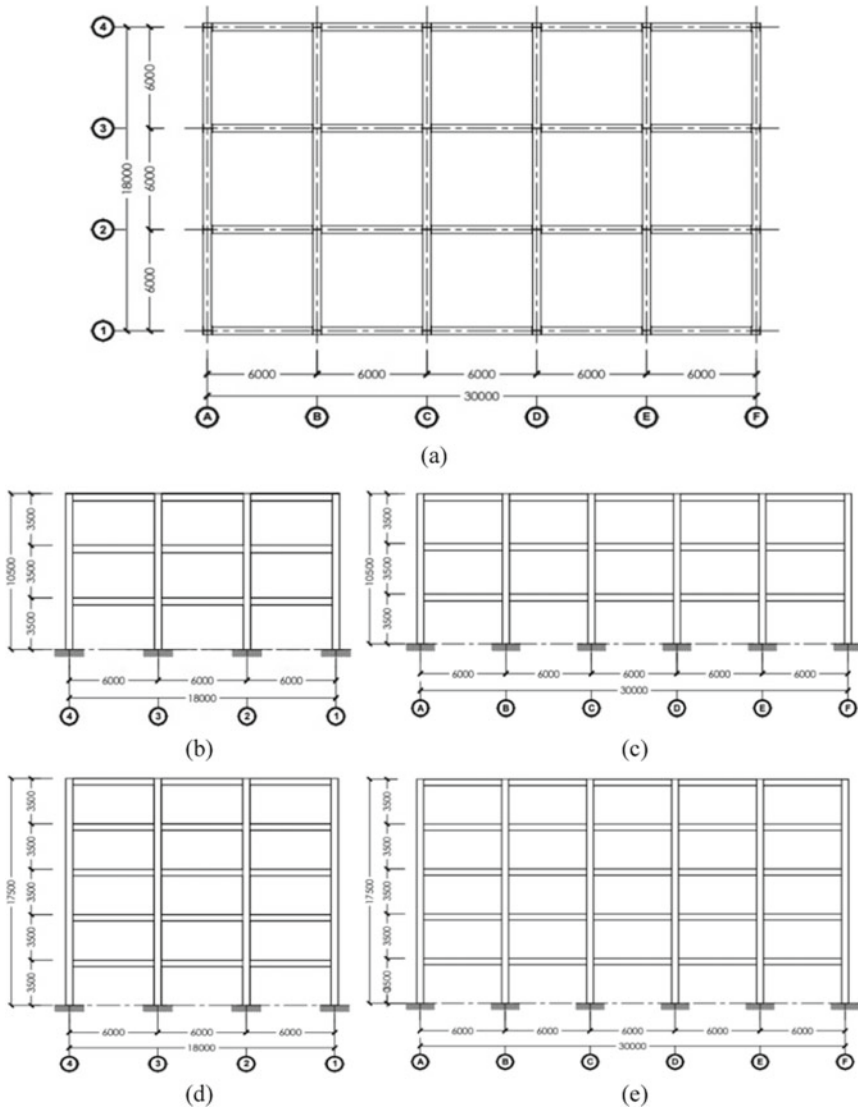


Fig. 1 Plan and sections of building. (a) Typical plan of each floor, (b) Cross section of 3-stories building, (c) Long section of 3-stories building, (d) Cross section of 5-stories building, (e) Long section of 5-stories building

Steel section that used in this study are according to ArcelorMittal Japan section database. Strut width for full infill-walls and infill-walls with opening are 1737 and 1562 mm. Calculated gap stiffness for infill-walls of 12 cm thickness is 7757 N/m.

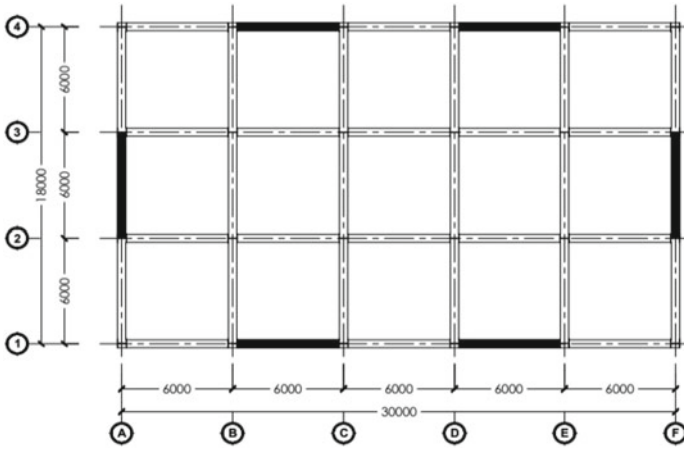


Fig. 2 Infill-walls placement layout plan

Table 1 Dimension of steel section frames

Story	Columns	Primary Beams	Secondary Beams
3-stories building			
3	H 300 × 300 × 12 × 10	H 250 × 125 × 6 × 9	H 200 × 100 × 5.5 × 8
2	H 350 × 350 × 12 × 19	H 300 × 200 × 8 × 12	H 200 × 100 × 5.5 × 8
1	H 350 × 350 × 12 × 19	H 300 × 200 × 8 × 12	H 200 × 100 × 5.5 × 8
5-stories building			
5	H 350 × 350 × 12 × 19	H 250 × 125 × 6 × 9	H 200 × 100 × 5.5 × 8
4	H 350 × 350 × 12 × 19	H 300 × 200 × 8 × 12	H 200 × 100 × 5.5 × 8
3	H 350 × 350 × 12 × 19	H 300 × 200 × 8 × 12	H 200 × 100 × 5.5 × 8
2	H 350 × 350 × 12 × 19	H 300 × 200 × 8 × 12	H 200 × 100 × 5.5 × 8
1	H 350 × 350 × 12 × 19	H 300 × 200 × 8 × 12	H 200 × 100 × 5.5 × 8

3.2 Story Displacement

Story displacement of all models are observed at portal F for X-direction and at portal 4 for Y-direction of earthquake loads. Story displacement is calculated using load combination dead, live, and earthquake added linearly which the plot can be seen on Figs. 3 and 4.

From Figs. 3 and 4, can be observed model which infill-walls are just considered as loads only (M3Open and M5Open) have the largest displacement. It is happened because infill-walls stiffness contribution is not taken into considerations to frame structure. Full infill-walls models, which are modeled as shell elements (M3Full-shell, M5Full-shell) and modeled as diagonal strut (M3Full-strut, M5Full-strut) have

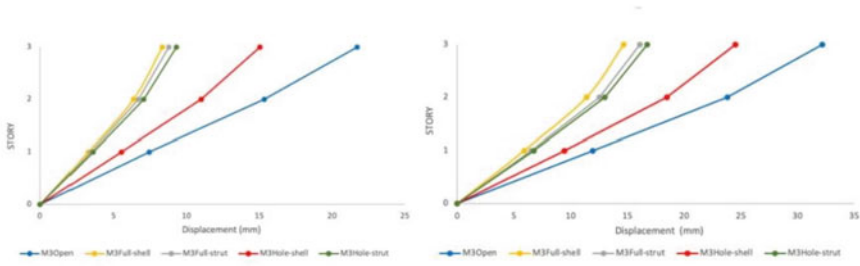


Fig. 3 Story displacement of 3-stories building in X (left) and Y (right) direction

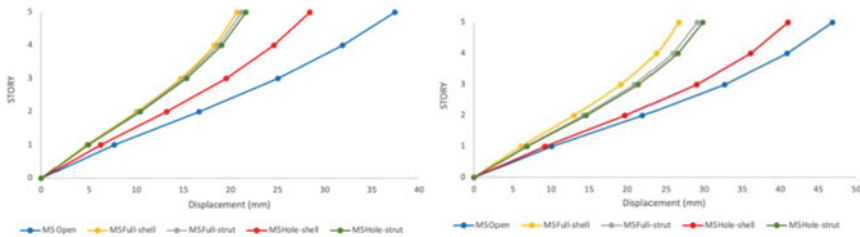


Fig. 4 Story displacement of 5-stories building in X (left) and Y (right) direction

plot curve that are close to each other. Curves may seem inaccurately close, but infill-walls masonry material has high nonlinearity.

Meanwhile, infill-walls with stiffened openings models which are modeled as diagonal strut (M3Hole-strut, M5Hole-strut) have large deviation of story displacement to shell elements modeled (M3Hole-shell, M5Hole-shell) infilled frame. This means, formula that used to calculate strut width which is obtained from experimental and analytical analysis on reinforced concrete frame structure cannot be applied on steel frame structure. Then, that strut width formula needs to be modified to get curve plots are closer to each other. Modification is done by simply reducing strut width to make strut modeled infilled frame story displacements larger until approach shell modeled curve. Reduction factor for cross section area of strut is taken 0.4 by trial-and-error process. After modified, story displacement changed curve can be seen on Figs. 5 and 6.

From new curve plot shown by Figs. 5 and 6, it can be seen curve of strut modeled of infill-walls with stiffened opening are very close to shell modeled curve.

For overall analysis results, infill-walls can contribute stiffness to steel frame structure. Infilled frame with full infill-walls that are modeled with both shell elements and diagonal strut are the stiffest with the smallest story displacement. Infill-walls with opening models still can contribute its stiffness to frame structure which are shown by their story displacements are smaller than models without considering infill-walls stiffness contribution.

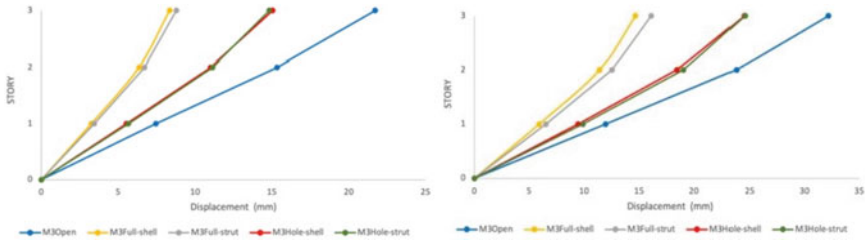


Fig. 5 Story displacement of 3-stories building in X (left) and Y (right) direction with modified strut for stiffened opening infill-walls model

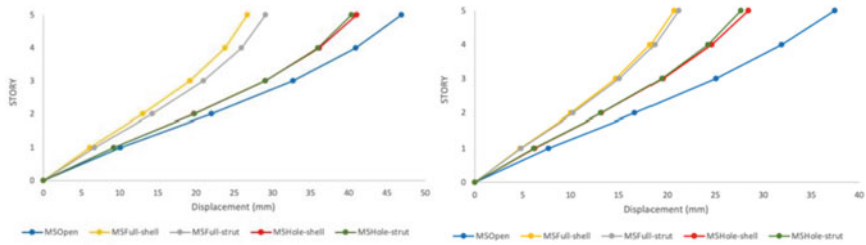


Fig. 6 Story displacement of 5-stories building in X (left) and Y (right) direction with modified strut for stiffened opening infill-walls model

4 Conclusion

From this study can be conclude that formula to calculate strut width of infill-walls with stiffened opening proposed by Wirawan et al. [7] needs to be multiplied by 0.4 on steel frame structure. It can be proofed that considering infill-walls stiffness contribution can make frame structure stiffer even if there is an opening.

References

1. BSN (2002) Tata Cara Perencanaan Struktur Baja Untuk Bangunan Gedung. 215
2. BSN (2019) Tata Cara Perencanaan Ketahanan Gempa Untuk Struktur Bangunan Gedung dan Non Gedung, 254
3. Dewobroto W (2005) Evaluasi Kinerja Struktur Baja Tahan Gempa dengan Analisa Pushover. Seminar Bidang Kajian 28. http://blog.ub.ac.id/bagoestif/files/2010/03/wiryanto_di_soegijaprana.pdf
4. Dorji J, Thambiratnam DP (2009) Modelling and analysis of infilled frame structures under seismic loads. *Open Constr Build Technol J* 3(2):119–126. <https://doi.org/10.2174/1874836800903020119>
5. Giri IBD, Susila IGA, Suprpto FH (2016) Perilaku Dan Kinerja Struktur Rangka Baja Dengan Dinding Pengisi Dan Tanpa Dinding Pengisi 22(2):184–206

6. Paulay T, Priestley MJ (1992) *Seismic design of reinforced concrete and masonry buildings*. Wiley, New York
7. Wirawan IPAP, Tubuh IKDK, Wiryadi IGG (2022) Studi Analitikal Perilaku Dan Kinerja Struktur Rangka Dinding Pengisi Dengan Bukaannya Sentris 11:49–56
8. Asteris GP, Giannopoulos IP, Chrysostomou CZ (2012) Modeling of infilled frames with openings. *Open Constr Build Technol J* 6(Suppl 1):81–91. <https://doi.org/10.2174/1874836801206010081>
9. Kakaletsis DJ, Karayannis CG (2009) Experimental investigation of infilled reinforced concrete frames with openings. *ACI Struct J* 106(2):132–141. <https://doi.org/10.14359/56351>
10. Mainstone R (1971) The influence of bounding frame on the racking stiffness and strength of brick walls. In: *Proceedings of the 2nd international brick masonry conference*
11. Sigmund V, Penava D (2014) Influence of openings, with and without confinement, on cyclic response of infilled R-C frames—an experimental study. *J Earthq Eng* 18(1):113–146. <https://doi.org/10.1080/13632469.2013.817362>
12. Sukrawa M (2015) Earthquake response of RC infilled frame with wall openings in low-rise hotel buildings. *Procedia Eng* 125:933–939. <https://doi.org/10.1016/j.proeng.2015.11.118>
13. Sukrawa M, Budiwati IAM (2019) Analysis and design methods for infilled frames with confined openings. *Int J Technol* 126–136. <https://doi.org/10.14716/ijtech.v10i2.2467>
14. BSN (2020) *Beban desain minimum dan kriteria terkait untuk bangunan gedung dan struktur lain (SNI 1727:2020)*. Badan Standardisasi Nasional, Jakarta
15. DPMB (1983) *Peraturan Pembebanan Indonesia untuk Gedung*. Yayasan Lembaga Penyelidikan Masalah Bangunan, Bandung
16. Tjahjanto HH, Imran I (2009) Kajian Performance Struktur Portal Beton Bertulang dengan Dinding Pengisi. in *Seminar dan Pameran HAKI*
17. BSN (2020) *Spesifikasi untuk bangunan gedung baja struktural (SNI 1729:2020)*. Badan Standardisasi Nasional, Jakarta

Making the Strategic Disaster Mitigation in Building Foundations: A Case Study Pandak II Public Health Center



Widya Kartika, Buddewi Sukindrawati, and Sarju

Abstract The soil conditions are mostly sandy and the groundwater level is shallow in Bantul Regency. Work of excavation construction is easy to landslides makes a hazard to workers. For this reason, comprehensive efforts are needed to reduce the risk of landslides that can endanger workers by carrying out mitigation activities. The case study was taken at Pandak II Public Health Center. This research aims to analyze the disaster mitigation of foundation work which previously had a design plan but different in the real conditions. Data analysis was carried out by reviewing real conditions and redesigning planning drawings that had previously been reviewed in the literature study and implementation methods that were in accordance with shallow groundwater levels so that the implementation of foundation work could be carried out safely and avoided landslides. Building foundation disaster mitigation is carried out with structural mitigation in the form of making a redesign of infrastructure drawings (redesign) as a driver of minimizing the impact of damage to building construction. Furthermore, non- structural mitigation with emergency planning if the building that has been built nearby will collapse due to the foundation in which the soil has been dug up beside the foundation.

1 Introduction

Pandak II Public Health Center construction project activities for additional rooms are used to provide health service facilities. Construction projects are built with a complex technology, it is considerably significant to ensure project quality and safety under the construction time, cost and other constraints (1). Construction is often characterized by a diversity of contracted works that demand various participants, many of whom are also simultaneously burdened by activities in their other dealings (2). Management function is the main key to success management of a project (3). It

W. Kartika (✉) · B. Sukindrawati · Sarju
Program Studi Teknik Sipil, Fakultas Teknik, Universitas Janabadra, Jl. Tentara Rakyat Mataram
No. 58, Yogyakarta 55231, Indonesia
e-mail: widya.kartika@janabadra.ac.id

© Institute of Technology PETRONAS Sdn Bhd 2024
B. S. Mohammed et al. (eds.), *Proceedings of the International Conference on Emerging Smart Cities (ICESC2022)*, Lecture Notes in Civil Engineering 324,
https://doi.org/10.1007/978-981-99-1111-0_65

is the responsibility of the construction team, including the client, architect/engineer, contractor, construction manager, subcontractor and suppliers, to ensure that each project is completed without injuries or recorded accidents (4).

As deep as 0.5 m, excavation work is carried out and then the groundwater level and the sandy soil is high so that when the foundation is excavated. However, in many cases, in such countries located in arid and semi-arid regions, groundwater mineralization (GWM) processes are not sufficiently taken into account in the study of groundwater (5). The position or condition of the soil on the right and left of the excavated landslides (high shear value). This can be dangerous to surrounding buildings and workers doing the excavation. The pile of soil above can collapse suddenly on the workers below it (6).

The application of mitigation in the world of education can be applied starting with the inclusion of disaster mitigation materials in the curriculum. The existence of disaster mitigation material in the curriculum makes students are required to learn and understand about the disaster. But the learning should be packaged in the form of learning that is close to the daily lives of students.

Mitigation disaster can applied with starting inclusion of disaster mitigation materials in the curriculum.

2 Research Methods

See Fig. 1.

3 Results and Discussion

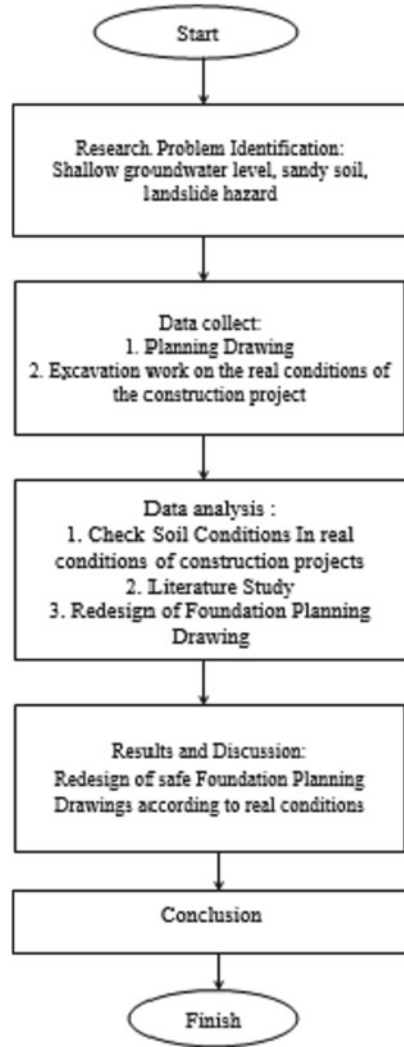
The following real situation.

The design plan used a footplat foundation with a cyclop foundation underneath. The real condition in Fig. 2 shows that the groundwater level in Bantul Regency is shallow. The excavation was carried out to a depth of 0.5 m and ground water had emerged. Besides that, the soil conditions tend to be sandy so there is a lot of sand next to the excavation walls of landslides.

Above Fig. 3 is a plan drawing that shows detailed drawings of the footplat foundation and cyclop foundation that have not been protected by concrete buis.

Steps to disaster mitigate of building foundations by carrying out structural mitigation in the form of making a redesign of infrastructure drawings (redesign) as a point of minimizing the impact of damage to building construction and non-structural mitigation is by emergency planning if the finished building nearby will collapse due to partially embedded foundations when work of excavated beside the foundation. Figure 4 shows a redesign of the footplate foundation and the cyclop foundation that has been given concrete buis. Figure 5 shows the process of excavating soil for foundation work carried out quickly assisted by a water pump (dewatering), water

Fig. 1 Research flow chart



pumps when the foundation excavation work is carried out according to plan. When the water decreases or recedes, a pair of white stones (mixture of 1 PC: 3 PS) can be added for the cyclop foundation. Because the soil conditions in the real are sandy, there is a lot of soil around the excavation walls. This is because the shear angle in sandy soil is very small. The internal shear angle is the angle formed from the relationship between the normal stress and the shear stress in the soil or rock material. The internal shear angle is the fracture angle formed when a material is subjected to a stress or force against it that exceeds the shear stress (7). The greater the shear angle in a material, the more resistant the material will be to the external stresses

Fig. 2 Excavation conditions (Source Widya Kartika 2021)

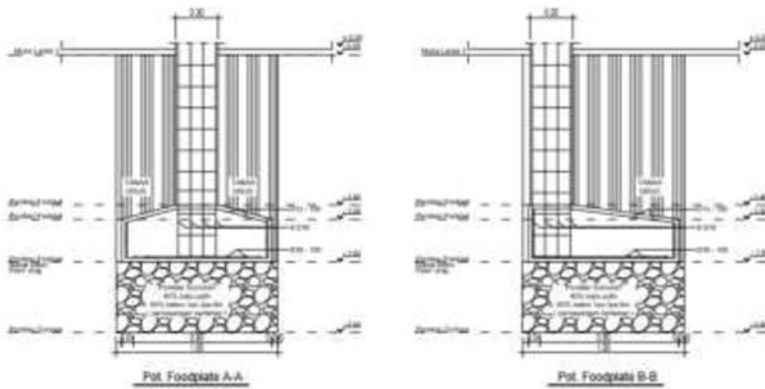


Fig. 3 Footplat foundation plan drawing details (Source Widya Kartika 2021)

imposed on it. The value of the internal shear angle (ϕ) is also related to the density level of a type of soil, which can be seen in Table 1.

Therefore to avoid landslides around the excavation, a concrete buis is needed that will protect the cyclop and footplat foundations from landslides around the soil, so that the excavation work can be carried out as needed, according to the plan and workers are protected from the risk of being buried by the excavation walls. Figure 6 shows the implementation of the footplat foundation after dewatering is carried out.

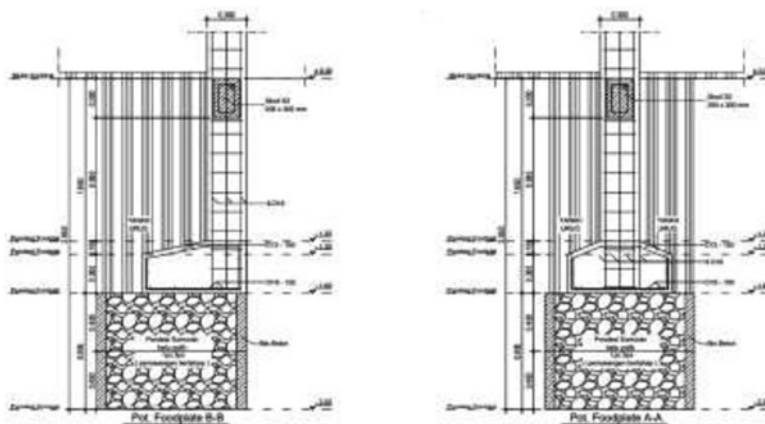


Fig. 4 Footplat foundation redesign drawing (*Source* Widya Kartika 2021)

Fig. 5 Dewatering process
(*Source* Widya Kartika 2021)



Fig. 6 Footplat foundation work after dewatering
(Source Widya Kartika 2021)



Table 1 Magnitude of the Angle of Shear in Soil

Density level	Internal shear angle (ϕ)
Very loose	<30
Loose	30–35
Almost solid	35–40
Solid	40–45
Very solid	>45

(Source Bowles JE, 1989)

4 Conclusion

Steps are taken on the plan drawings that do not match the real conditions of the construction project by redesigning the drawings that are adapted to real conditions and building safety factors are also considered.

Building foundation disaster mitigation is carried out with structural mitigation in the form of making a redesign of infrastructure drawings (redesign) as a driver of minimizing the impact of damage to building construction. Furthermore, non-structural mitigation with emergency planning if the building that has been built nearby will collapse due to the foundation in which the soil has been dug up beside the foundation.

References

1. Luong DL, Tran DH, Nguyen PT (2021) Optimizing multi-mode time-cost-quality trade-off of construction project using opposition multiple objective difference evolution. *Int J Constr Manag* 21(3):271–83. <https://doi.org/10.1080/15623599.2018.1526630>
2. Dasović B, Galić M, Klanšek U (2020) A survey on integration of optimization and project management tools for sustainable construction scheduling. *Sustain* 12(8)
3. Kartika et al (2020). <https://e-journal.janabadra.ac.id/index.php/TS/article/view/1266>
4. Buniya MK, Othman I, Sunindijo RY, Kineber AF, Mussi E, Ahmad H (2021) Barriers to safety program implementation in the construction industry. *Ain Shams Eng J* 12(1):65–72. <https://doi.org/10.1016/j.asej.2020.08.002>
5. Kulmatov RA, Adilov SA, Khasanov S (2020) Evaluation of the spatial and temporal changes in groundwater level and mineralization in agricultural lands under climate change in the Syrdarya province, Uzbekistan. *IOP Conf Ser Earth Environ Sci* 614(1)
6. Kartika W, Sukindrawati B (2021) Analisa Visual Keselamatan Kerja Pada Pekerja Konstruksi Galian Tanah. *Agregat* 6(1):525–531
7. 336 AC (1993) Suggested analysis and design procedures for combined footings and mats.1993;88 (Reapproved 2002)

Analysis of Runoff Discharge on Kaliurang Road Drainage Channels KM 6.5 – 7 Using SWMM 5.2 Model



Titiek Widyasari, Nizar Achmad, Tania Edna Bhakty,
and Ardha Candra Perdana

Abstract Overflow in the highway drainage channel is a malfunction of the drainage function on Kaliurang road KM 6.5 - 7. A good drainage system is very necessary, so it is necessary to evaluate the drainage function on Kaliurang road KM 6.5 – 7 using the SWMM 5.2 model so that it can function optimally. The goal of the study was figure out the runoff discharge so that the drainage capacity could be evaluated and the highway could work as well as possible. SWMM model analysis to determine runoff discharge in each of the sub catchment area (DTA). The total runoff is an accumulation of draft rains with 2, 5 and 10-year re-periods. The largest runoff discharge in J7 is 0.728 m³/s at 2-year re-period, 0.729 m³/s at 5-year re-period, 0.73 m³/s at 10-year re-period. The simulation results obtained the largest runoff discharge in J7 because it is an accumulation of J6 and the catch from DTA 7 is the most extensive, which is 2.1 ha. SWMM 5.2 simulation results for link capacity analysis for existing channels, can be seen on channels SAL 6 and SAL 9 cannot receive runoff discharge from rain in 2, 5 and 10-years re-period. SAL 4 almost overflowed to receive rainwater runoff in a 10-year re-period. It is necessary to redesign the drainage channel to obtain the ideal channel size for SAL 4, SAL 6 and SAL 9.

Keywords Runoff discharge · Drainage · SWMM 5.2

T. Widyasari (✉) · N. Achmad · T. E. Bhakty · A. C. Perdana
Janabadra University, Yogyakarta, Indonesia
e-mail: titiekwidyasari@janabadra.ac.id

N. Achmad
e-mail: nizar_achmad@janabadra.ac.id

T. E. Bhakty
e-mail: tania@janabadra.ac.id

A. C. Perdana
e-mail: candraperdanaa@gmail.com

1 Introduction

Rain causes inundation or flooding in various cities which is a routine problem that occurs every year. Urban population growth in general exceeds the ability to provide urban facilities and infrastructure so that problems such as urban drainage problems will arise [1]. Drainage channels are water buildings that have an important function to channel excess water that is on the surface. A good drainage channel is a channel that can hold excess water and reduce the potential for inundation or flooding during the rainy season [2].

Highways as part of transportation play a very important role in realizing the process of human movement or movement of goods smoothly and are able to show good performance in operation [3]. A highway drainage system is a surface drainage that holds rain runoff caught in a highway area. The form of the highway drainage system is artificial drainage that serves to channel water from the road surface and the surrounding area to the nearest river body. Problems that occur in the drainage system are caused by sedimentation, clogged garbage, and reduction of infiltration areas due to development.

Kaliurang road is a state-owned arterial road with an oversight status under the Central Java and Yogyakarta Public Works Office. The drainage channel on Kaliurang road KM 6.5 - 7 Depok, Sleman Regency, cannot accommodate rainwater runoff properly resulting in overflows around the Kaliurang road area. Overflow in the highway drainage channel is a malfunction of the road drainage function that can interfere with the function of the highway. The overflow of drainage channels that occurred on Kaliurang road KM 6.5 - 7 resulted in disrupted traffic and inundated shops on the side of the highway [4].

The development of science and technology in the development of hydraulic building design is very rapid, there are several models that aim to facilitate the calculation of the design of a channel network system to collect runoff discharge in the form of a computer application program (*software*). The evolving model of drainage system design is the Storm Water Management Model (SWMM) developed by the United States - Environmental Protection Agency (EPA) [5]. The SWMM program is a runoff modeling as a solution to help evaluate and plan urban drainage systems [2].

Because a good drainage system is very necessary, it is necessary to evaluate the drainage function on Kaliurang road KM 6.5 – 7 using the SWMM 5.2 model so that it can function optimally. The design rain analysis uses the frequency analysis method, the results of which are used to calculate the amount of rain intensity. The purpose of the study was to determine the runoff discharge to evaluate the drainage capacity so that the function of the highway runs optimally.

2 The Research Method

The research used rain data in station Gemawang Sleman Regency, because of the closest position of the location, while the drainage channel reviewed was 628 m. Rain data used was annual maximum series data from 2010 – 2020. Regional maps and topographic data are taken from *Google Earth*. Drainage network and drainage channel data on Kaliurang road KM 6 – 7.5 can be seen on Fig. 1 dan Table 1.

Data on sub catchment areas and land use accommodated in drainage channels on Kaliurang road KM 6 – 7.5 can be seen in Table 2. SWMM 5.2 is a dynamic rain-to-runoff discharge simulation model used for simulation of single or long-term (sustainable) events of the quantity and quality of runoff from primarily urban areas. SWMM runoff components operate on catchment pools that receive rain and produce runoff.

SWMM model analysis to determine runoff discharge in each of the sub catchment area (DTA) with 2, 5 and 10-year return period (re-period). The total runoff is the accumulation of rainfall design and the calculation of rain intensity using the Mononobe equation can be seen in Table 3, the rain time is simulated for 15 min obtained from the concentration time, and the channel slope is 0,016.

3 The Result and the Discussion of the Research

The Storm Water Management Model (SWMM) is a dynamic runoff rainfall simulation model used for single-event or long-term (sustainable) simulation of the quantity and quality of runoff from primarily urban areas. SWMM runoff components operate on sub catchment pools of areas that receive rainfall and produce runoff and pollutant loads. The routing section of the SWMM transports this runoff through pipelines, channels, storage/processing devices, pumps, and regulators [5]. SWMM was first released in 1971 and has undergone some major improvements since then, and continues to be used widely worldwide for planning, analysis, and design related to stormwater runoff, combined sewers, sanitary sewers, and other drainage systems in urban areas, with many applications in non-urban areas as well [6].

3.1 SWMM Node Inflow Analysis Results

The inflow node is intended to determine the incoming discharge at each point of the drainage channel node, where the flow load received from the sub catchment and the previous channel simulates the occurrence of rain for 15 min according to the concentration time calculated using the Kirpich formula. Node inflows were analyzed with 2, 5 and 10-years re-period.



Fig. 1 Drainage network on Kaliurang road KM 6,5 – 7

Table 1 Drainage channels data on Kaliurang road KM 6,5 – 7

Conduit Code	Channel Type	Location	Junction		Elevation (m)		Length (m)	Shape	Measure (m)		Roughness Manning (n)
			Start	End	Start	End			Depth (H)	Width (B)	
SAL 1	Main channel	Jl. Kaliurang	J1	J3	178	177	101	RECT CLOSED	0,8	0,6	0,025
SAL 2	Secondary channel	Jl. Jurungsari II	J2	J3	179	177	109	RECT CLOSED	0,5	0,6	0,025
GG	Main channel (culverts)	Jl. Kaliurang	J3	J5	177	177	5	RECT CLOSED	0,8	0,6	0,025
SAL 3	Secondary channel	Jl. Jurungsari II	J4	J5	180	177	215	RECT CLOSED	0,7	0,5	0,025
SAL 4	Main channel	Jl. Kaliurang	J5	J7	177	172	250	RECT CLOSED	0,8	0,6	0,025
SAL 5	Secondary channel	Jl. Kayen I	J6	J7	178	172	295	RECT OPEN	0,4	0,7	0,025
SAL 6	Main channel	Jl. Kaliurang	J7	J10	172	169	252	RECT CLOSED	0,8	0,6	0,025
SAL 7	Tertiary channel	ST. Sato Paulus	J8	J10	171	169	116	RECT OPEN	0,8	0,6	0,025
SAL 8	Secondary channel	Jl. Timor-timur	J9	J10	171	169	144	RECT OPEN	0,5	0,6	0,025
SAL 9	Main channel	Jl. Kaliurang	J10	OUT1	169	168	20	RECT CLOSED	0,8	0,6	0,025

Table 2 Sub catchment area and land use data

No	Sub catchment Area	Area A (ha)	L0 1/2 width (m)	% Slope (slope of the land)	n0 (impermeable)	% - impervious	n0 (permeable)
					roughness coefficient N-impervious		roughness coefficient N-perv
1	DTA 1	0,55	22,7	1%	0,013	50%	0,2
2	DTA 2	0,55	22,7	1%	0,013	50%	0,2
3	DTA 3	0,35	12	1%	0,013	50%	0,2
4	DTA 4	0,8	14	1%	0,013	40%	0,2
5	DTA 5	1,1	25	1%	0,013	60%	0,2
6	DTA 6	0,81	40	1%	0,013	70%	0,2
7	DTA 7	2,1	78	1%	0,013	40%	0,2
8	DTA 8	1,43	52	1%	0,013	50%	0,2
9	DTA 9	0,2	8	1%	0,013	50%	0,2
Total		7,89					

Table 3 Rainfall design and rain intensity

No	Return Period (re-period)	Rainfall design (mm)	Rain Intensity (mm/hour)
1	2	100,38	87,69
2	5	146,72	123,17
3	10	174,19	152,17

Table 4 SWMM 5.2 simulation runoff results in junction

Junction	Runoff Discharge (m ³ /s)			Junction	Runoff Discharge (m ³ /s)		
	Re-Period				Re-Period		
	2-year	5-year	10-year		2-year	5-year	10-year
J1	0,079	0,126	0,157	J6	0,268	0,423	0,521
J2	0,079	0,126	0,156	J7	0,728	0,729	0,73
J3	0,158	0,252	0,312	J8	0,22	0,357	0,446
J4	0,054	0,088	0,11	J9	0,029	0,046	0,057
J5	0,369	0,583	0,718	J10	0,712	0,726	0,731

Maximum flow is debit maximal that enters or passes junction from the flow load on the sub catchment runoff and the previous channel. The simulation results obtained runoff discharge in junction in Table 4. The largest runoff discharge in J7 is 0,728 m³/s at 2-year re-period, 0,729 m³/s at 5-year re-period, 0,73 m³/s at 10-year re-period, as it is an accumulation of J6 and the most extensive catch of DTA 7 is 2.1 ha.

3.2 SWMM Link Capacity Analysis Results

Analysis of link capacity with 2-year re-periode seen in Fig. 2. Channels SAL 6 and SAL 9 are already unable to receive runoff discharge from rain in the 2-year re-period. Link capacity analysis with a 5-year re-period can be seen Fig. 3 that channels SAL 6 and SAL 9 are no longer able to receive runoff discharge from the 5-year re-period of rain, while channel SAL 4 has become affected because channels SAL 6 and SAL 9 are no longer able to receive runoff discharge. Analysis link capacity with 10-year re-period, in Fig. 4 it can be seen that channels SAL 6 and SAL 9 are not able to receive runoff discharge from rain with 10-year re-period, while channel SAL 4 is almost overflowing due to channels SAL 6 and SAL 9 already unable to receive rainwater runoff. Redesign needs to be done to get the ideal channel size to channels SAL 4, SAL 6 and SAL 9. The water level profile in the cross section of the channel and knowing the capacity of the drainage channel was carried out a simulation of the

modeling of the drainage channel profile, so that an evaluation can be carried out to find the channel that needs further handling.

Fig. 2 Link capacity 2-year re-period

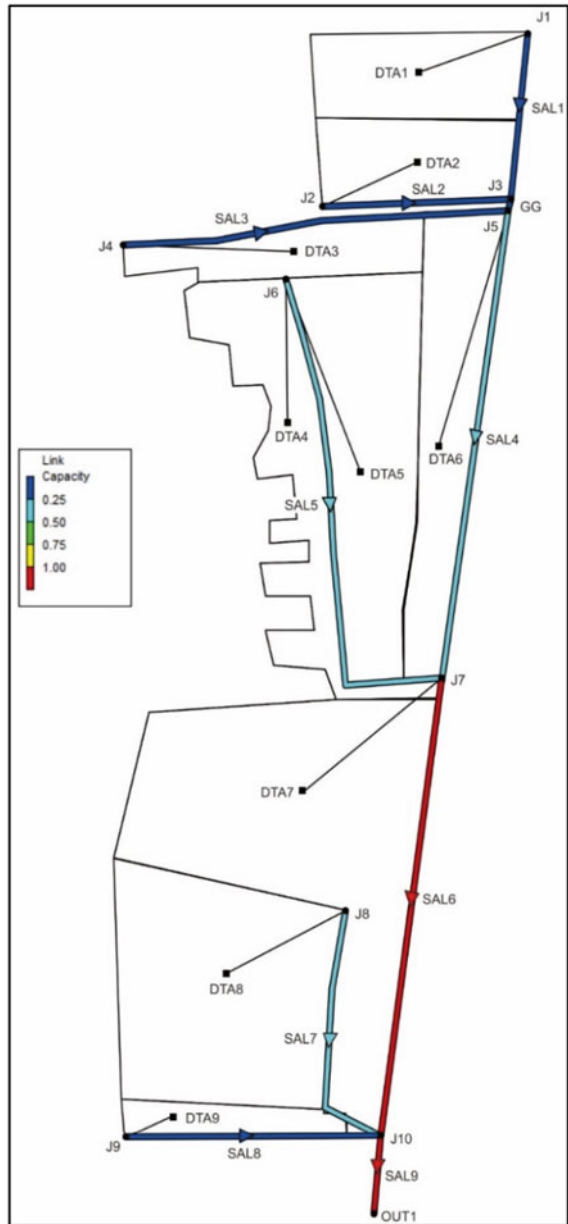


Fig. 3 Link capacity 5-year re-period

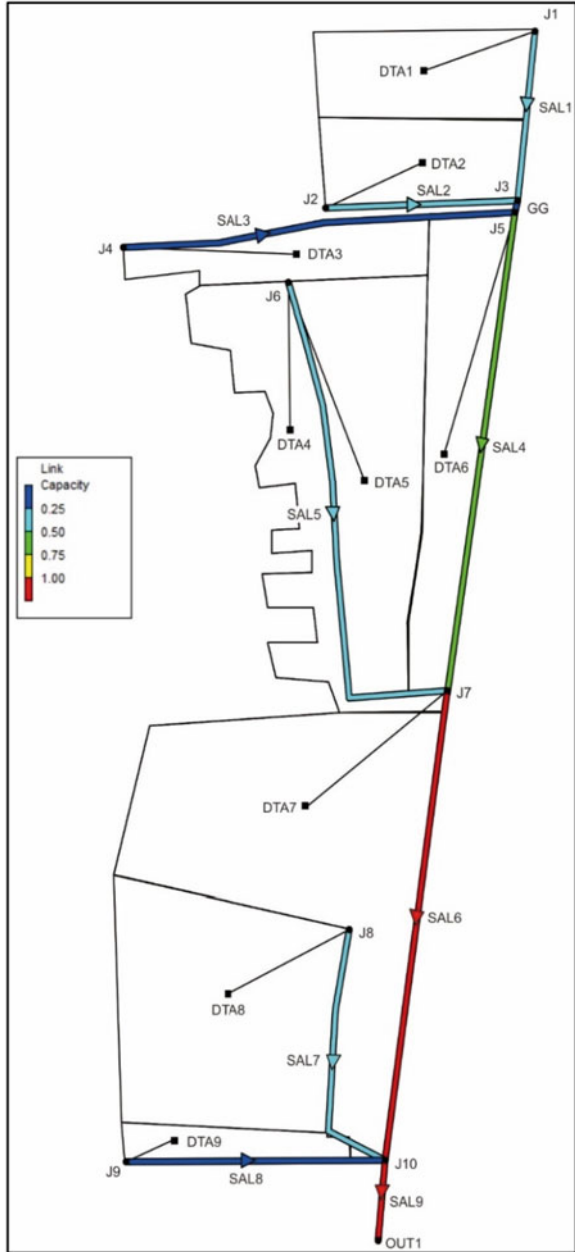
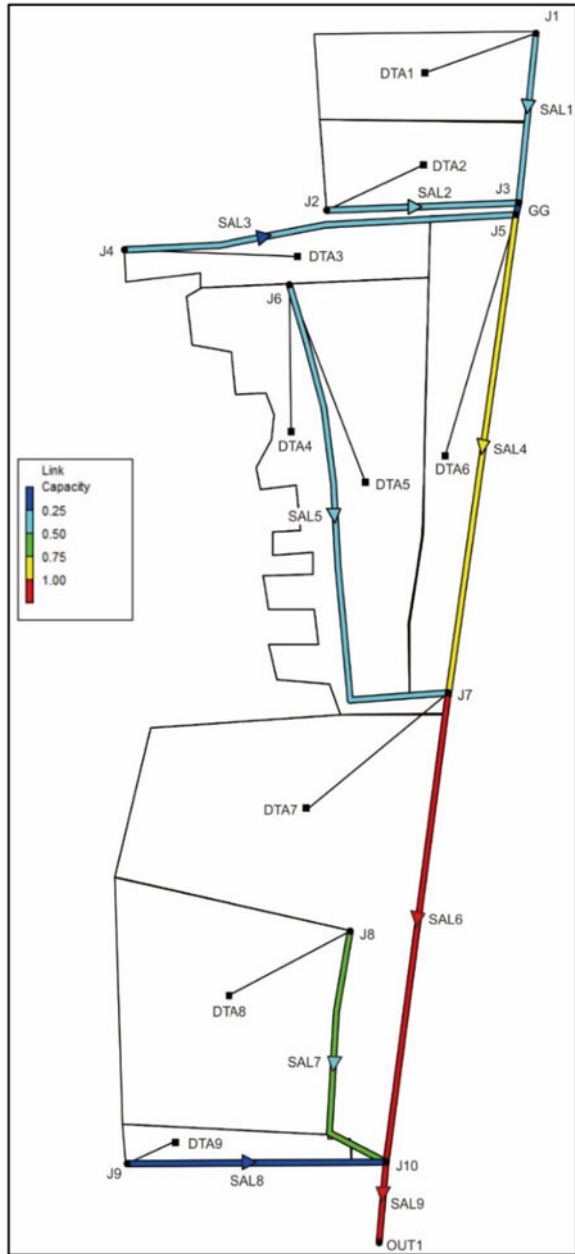


Fig. 4 Link capacity
10-year re-period



4 Conclusion

The largest runoff discharge in J7 is 0.728 m³/s at 2-year re-period, 0.729 m³/s at 5-year re-period, 0.73 m³/s at 10-year re-period. The simulation results obtained the largest runoff discharge in J7 because it is an accumulation of J6 and the catch from DTA 7 is the most extensive area, which is 2.1 ha.

SWMM 5.2 simulation results for analysis link capacity for existing channels on channels SAL 6 and SAL 9 were not able to receive runoff discharge from rains on 2, 5 and 10-years re-period. There is a channel SAL 4 almost overflowing to receive rainwater runoff in a 10-year re-period. The results of this research can be used to redesign drainage channels to obtain the right channel size for SAL 4, SAL 6 and SAL 9.

References

1. Musa R, Ashad H (2022) Sistem Informasi Geografis (SIG) pada Jaringan Drainase Kota Watampone. *Jurnal Konstruksi: teKNik, infraSTRUKtur, dan SaIns* 1(7):40–48
2. Kartiko L, Santoso DR, Waspodo B (2018) analisis kapasitas saluran drainase menggunakan program SWMM 5.1 di perumahan Tasmania Bogor, Jawa Barat (Drainage Channel Capacity Evaluation Using SWMM 5.1 in Tasmania Residence Bogor, West Java)
3. Yunianta A, Setiadji BH (2022) Sistem drainase jalan raya yang berkelanjutan. *Tohar Media*
4. Widyasari T, Achmad N, Pradipta DA (2021) Redesign saluran drainase jalan kaliurang km. 6, 5–7. *Rancang Bangun Teknik Sipil* 8(1): 6
5. al Amin MB (2020) Pemodelan sistem drainase perkotaan menggunakan SWMM. Deepublish
6. Rossman L (2022) Storm water management model user's manual version. www.epa.gov/water-research

The Comparison of the Effect of Activity Space on Health Performance (Physical and Mental Health) Between Malaysia City and Indonesia City



Tjokorda, Joan Rona Justin, Dimas B. E. Dharmowijoyo,
Nindy Cahyo Kresnanto, and Liza Evianti Tanjung

Abstract As the human population getting higher, people demand for more facilities to satisfy their daily needs. In order to fulfil their needs, people need to travel. More facilities will result in more mobility requirement by people and at the same time more travels will be done. The travel pattern of people can be best illustrated by using the space–time prism as it takes into account the distance and time of the travels performed to the required location. Increasing travels might affect the health performances of people in various condition. Several health variables such as general health, physical functioning, social functioning, etc. need to be considered while studying the effect of activity space towards health performances. The results of the study might differ or remain the same if it is conducted in two or more different places. Therefore, this paper aims to compare the effect of activity space (measured

Tjokorda (✉)

Department of Civil Engineering, Universitas Mahasarawati, Denpasar, Indonesia
e-mail: tjokorda@springer.com

J. R. Justin · D. B. E. Dharmowijoyo · L. E. Tanjung

Department of Civil and Environmental Engineering, Universiti Teknologi Petronas, Seri Iskandar, Malaysia
e-mail: joan.rhona_25506@utp.edu.my

D. B. E. Dharmowijoyo

e-mail: dimas.bayu@utp.edu.my

L. E. Tanjung

e-mail: liza_19001673@utp.edu.my

D. B. E. Dharmowijoyo

Institute of Transport and Infrastructure, Universiti Teknologi Petronas, Seri Iskandar, Malaysia
School of Planning and Policy Development, Institute Teknologi Bandung, Bandung, Indonesia

D. B. E. Dharmowijoyo · N. C. Kresnanto

Department of Civil Engineering, Universitas Janabadra, Yogyakarta, Indonesia
e-mail: nindy_ck@janabadra.ac.id

L. E. Tanjung

Department of Civil Engineering, Universitas Muhammadiyah Sumatera Utara, Medan, Indonesia

© Institute of Technology PETRONAS Sdn Bhd 2024

775

B. S. Mohammed et al. (eds.), *Proceedings of the International Conference on Emerging Smart Cities (ICESC2022)*, Lecture Notes in Civil Engineering 324,
https://doi.org/10.1007/978-981-99-1111-0_67

by using Euclidian distance method) on health performances (physical health and mental health) between Seri Iskandar, Perak, Malaysia and Yogyakarta, Indonesia. It is found that there is no difference in the comparison of the effect of activity space on the health performances between Malaysia and Indonesia. By conducting this study, it is expected that the outcome of the study can provide engineers and planners the information and guidance to design optimized built environment based on human travel behavior by prioritizing their health performance in each location.

Keywords Time–space prism · Time-use diary · Daily experience · Activity satisfaction · Physical health · Mental health · Bandung · Indonesia · Seri Iskandar · Malaysia

1 Introduction

The study on space–time prism is made to learn how the prism reflect the human activity pattern by considering the activities locations and time of travel. The shape of the space–time prism is affected by the individuals' constraints, needs and resources they are facing while performing their travel within stipulated time. (Hägerstrand 1970) (Schönfelder and Kay W Axhausen 2003) (Dharmowijoyo, Susilo, and Karlström 2014, 2016), (Miller 2017), and (Liu, Susilo, and Dharmowijoyo 2018) showed that people's daily activities and travels are a result of interaction between constraints, needs and resources. (Hägerstrand 1970) and (Miller 2017) confirmed the three types of constraints that can shape how people do their activities and travels throughout time and space.

The constraints are capability constraints, coupling constraints and authority constraints. Capability constraints is a constraint that limit an individual to do other activity since he restricts his time to meet his basic needs like sleep, eating and personal care. Meanwhile coupling constraint is a constraint that made the individual to interact with another human or objects where he need to spend his time to achieve both essential functions. Authority constraints is a constraint that the authority made to limit the access for the individual to be at the specific space. As example, a bank can only be access during working hour (Schwanen, Kwan, and Ren 2008). Resources on the other hand are defined as the money and transportation mode that will be required to perform the activity space. Needs is described as the reason or desire for the activity space to be performed such as for grocery shopping, working, eating, etc. (Chapin 1974).

How people do their activities and travels in space dimension can be shown by activity space (Hägerstrand 1970). Activity space measures the spread, the area, or the distances among activity locations visited by individuals on given days. There are two anchors that are supposed to limit the size of activity space. Those anchors are the location of home and workplace (Schönfelder and Kay W. Axhausen 2003). Anchors are defined as the places that people stay longer due to commitments to do the activities in the places.

Some researchers have argued the effects of activity space on health. People's activities and travels are believed to correlate with their health conditions (Dharmowijoyo and Joewono 2020; van Wee and Ettema 2016). Activity space might show the correlations of people's commitments to do various activities and travels in space scale towards their health conditions. People who commit to do walking and cycling in reaching some destinations might only visit activity locations near their anchors. However, the commitments to do some out-of-home activities farther from their anchors might make individuals depend on public or private transportation more often. Commitments to visit more activity locations on given day farther from the anchors might also urge people to choose their own cars that might correlate with various health conditions.

Some studies on activity space and health performances might focus on how health become a part of capability constraints and affecting activity space (Zhang 2013). This study tries to do other way around, which is studying how the effects of activity space as representations of people's commitments to do various activities and travels in space dimension affect their health performances. The understanding might be able to show how we do activities and travels in space dimension can be used to infer our health conditions.

In addition, this study will also comprise on the comparison of the activity space effects towards health performances between Seri Iskandar, Perak, Malaysia and Yogyakarta, Indonesia. Even though these two countries are located nearer to each other, the comparison between the results are remain unknown. Assumption that the outcome might be the same are high since the countries share the same cultures and locations. This study will answer the query by the end of the study period. Understanding the comparisons of activity space between Malaysia and Indonesia might provide insight the effects of built environment (including transportation infrastructure and land use shape) and daily activity-travel patterns on the differences of activity spaces. More structured land use shape, less compact built environment, high dependency on transport networks and better income conditions are hypothesised to correlate on higher activity space of travellers in Malaysia than travellers in Indonesia. However, more structured work arrangements might make Malaysian travellers to have lower activity space during weekdays than Indonesia travellers, but expand their activity space on Saturday and Sunday due to off days. However, six working days and spending longer time at home on Sunday might make Indonesia travellers to have lower activity space on Saturday and Sunday than Malaysian travellers.

2 Literature Review

2.1 *Space Time Prism*

Space–time prism is used to illustrate individuals’ daily activities based on space and time. The shape of the space–time prism is influenced by the individuals’ constraints, needs and resources they are having during or while planning for their travel within stipulated time. The constraints that limiting individuals travel are divided into three categories which are capability constraint, coupling constraint and authority constraint (Hägerstrand 1970). Since every individual has different day-to-day constraints, needs, and resources, the space–time prism might differ every day.

Time geography is proposed by Torsten Hägerstrand in the mid-1960s. It is an ecological theory demonstrating a person’s activities and trips during a given period, by creating a continuous path through space and time. This trajectory also shaped by the three space–time constraints. This theory also used to classify the flexibility and fixity of the activities based on the individuals’ space and time.

Activity must be done in a particular space and space here represents the locations travelled by the individuals. Activity space is strongly related to the anchors or pegs of the locations where the individuals spend most of their time at (Miller 2017). Activities with fixed timing have more consistent travel pattern whereas leisure activities with flexible timing have less consistent travel pattern (Schwanen et al. 2008).

2.2 *Activity Space Measurements*

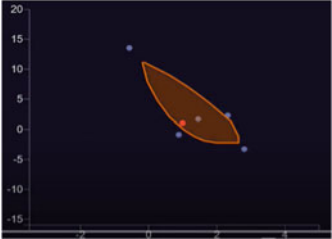
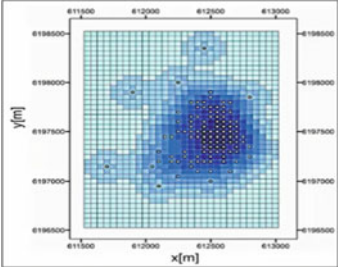
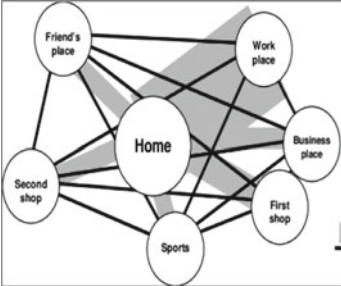
There are five activity space measurements that were studied to identify which measurement to be used in this project. The descriptions have been tabulated in Table 1 for better understanding. The descriptions are based on the survey made by (Schönfelder and Kay W Axhausen 2003).

2.3 *Health Parameters and Variables*

There are total of three factors of health structure as shown in Fig. 3 (Zhang 2013). For this study, only two health parameters to be considered which are physical health and mental health. The figure shows how these two health parameters are related to each other which prompt the needs to include the eight variables into this study.

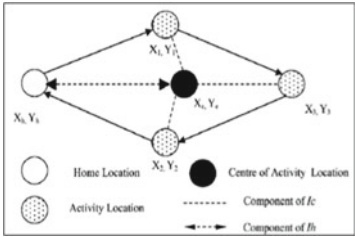
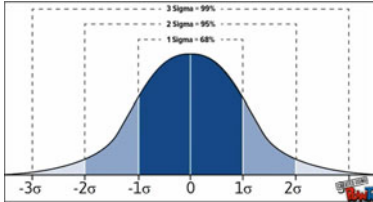
The eight chosen variables from the health-related quality of life (QOL) will represent the two health parameters (Ware and Sherbourne 1992). The description of each variables is as the following table.

Table 1 Activity space measurements (Schönfelder and Kay W Axhausen 2003)

Method	Description
<p>Confidence Ellipse</p> 	<ul style="list-style-type: none"> · Measuring the observed activity space directly to home location · Measure the dispersion area of visited locations · Unit in area · Disadvantages · An area may overgeneralize the activity space size by its geometric rigidity · Means that huge area that is not visited might be included
<p>Kernel Density</p> 	<ul style="list-style-type: none"> · Measure activity space directly to home location · Unit in area · Measure the number of cells times area of cell for only the most visited activity locations on a given period · Disadvantages · Ignores the spread of the out-of-home activity locations · Means that the locations that are visited while going to the main location are ignored <p>For example, a student from UTP want to go to Billion (main location) but she also visited KFC, Secret Recipe and Tesco before arriving Billion. But the measured area is only from UTP directly to Billion excluding the three locations</p>
<p>Spanning Tree</p> 	<ul style="list-style-type: none"> · Measuring the observed activity space directly to home location · Unit in length · Disadvantages · It ignores the spread of the out-of-home activity locations · Means that the locations that are visited while going to the main location are ignored <p>For example, a student from UTP want to go to Billion (main location) but she also visited KFC, Secret Recipe and Tesco before arriving Billion. But the measured area is only from UTP directly to Billion excluding the three locations</p>

(continued)

Table 1 (continued)

Method	Description
<p data-bbox="147 231 323 284">Euclidian Distance (I_c and I_h)</p>  <p data-bbox="154 442 509 518"> Home Location Centre of Activity Location Activity Location Component of I_c Component of I_h </p>	<ul style="list-style-type: none"> · The I_c and I_h are complement to each other to describe the out-of-home activity locations distribution · Unit in length · Measurement will cover an individual's potential action space near the visited action space · Advantages · I_c will reduce the overgeneralization of the activity space size by finding the centre of activities locations · Means that the centre of Vanessa's activity location will be observed and used to find the I_c and I_h · Disadvantages · Take direct straight distance by coordinates · Interpretation of the value can be complicated to distinguish between number of locations and distance travelled <p data-bbox="612 732 1029 813">For example, 20 km can be interpret as 5 locations with 2 km distance each or can be 3 locations with 3.19 km distance each</p>
<p data-bbox="147 813 323 843">Standard Distance</p> 	<ul style="list-style-type: none"> · Indicates the extent of the dispersion of action spaces · Defined as the quadratic mean of distance between each location and mean center · Number of locations visited will be lower as the distance increase, due to time taken to reach the location · Advantages · Explain the real measurement of activity space and the dispersion of activity locations · Take real road distance travelled · A larger standard distance indicates a wider dispersion of activity locations on a given day · Easily distinguish between number of locations and distance travelled · x-axes represent the distance and y-axes represent number of locations · Disadvantages <p data-bbox="612 1349 1029 1478">The real distance travelled might differ as a person might encounter problem such as miss the entrance or junction to their whereabouts, or problem in finding parking, which cause them to travel further</p>

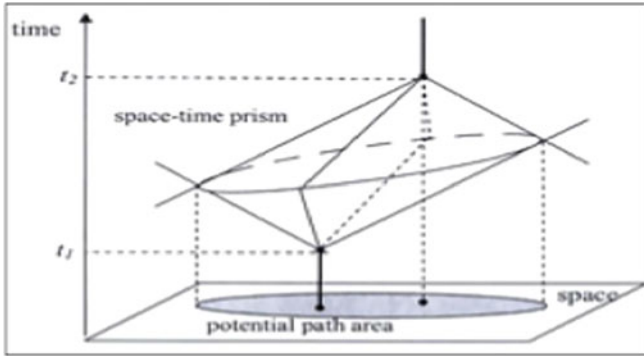


Fig. 1 Space–time prism (Hägerstrand 1970)

Fig. 2 Example of space–time path among activity stations (Miller 2017)

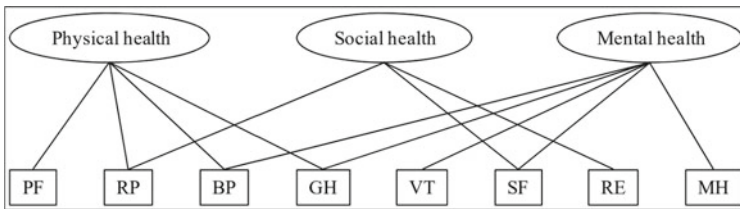
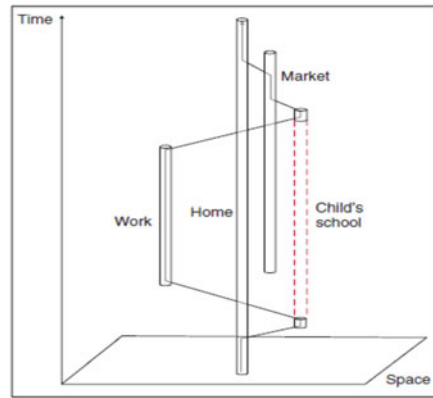
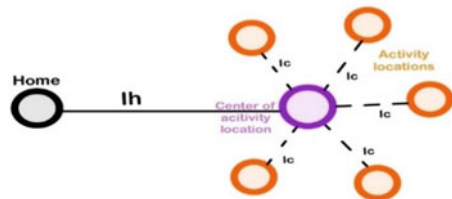
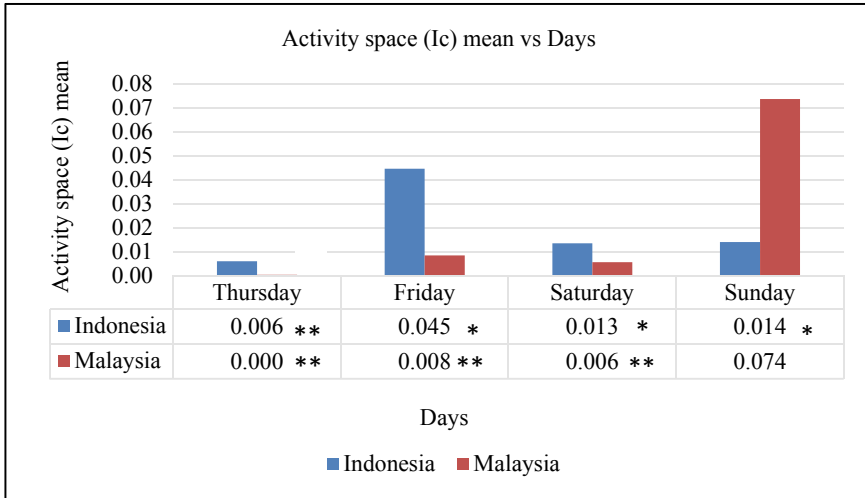


Fig. 3 Three-factors of health structure (Zhang 2013)

Fig. 4 Components of I_c and I_h





(*) Indicates the mean are significantly different from the opposite group with p-value < 0.05.
 (**) Indicates the mean are significantly different from the opposite group with p-value < 0.01.

Fig. 5 Activity space (Ic) mean vs Days graph

3 Data Extracted from Dataset of Seri Iskandar and Yogyakarta

There are two sources of datasets used in this study which are from Seri Iskandar (Malaysia) and Yogyakarta (Indonesia) datasets. The data in Malaysia’s dataset was collected for five days consecutively (Wednesday to Sunday), and involves 143 individual respondents. For Indonesia, the dataset was collected for four days consecutively (Thursday to Sunday), and involves 400 individual respondents.

Both datasets are using the same questionnaires and the respondents are assisted by the surveyor in order to ease the survey process. There are two types of surveys that were conducted to respondents, which are Diary Survey and Lifestyle Survey. All the questionnaires are correlated with the activity space (Ic and Ih) and health parameters (physical and mental health). In these surveys, the data is categorized into three distinct groups of data, which are activity-travel diary, and well-being and health data.

For the activity-travel diary, respondents were required to records the duration of time used by respondents on different categories of activities. Each activity was recorded in 15-min intervals for 24 h and is repeated for five (Malaysia) and four (Indonesia) consecutive days. Therefore, 96 divisions of time per day were recorded by each respondent. The only activity that will be observed in this study is out-home

activity which can be categorized into out-home mandatory, out-home maintenance, and out-home leisure.

Out-home mandatory is defined as activities that require the respondent to be spatially and temporally fixed in specific location with the objective to fulfil basic needs such as sleeping, eating, and studying. Out-home maintenance is activities that satisfy the individual's demands for biological and physiological needs such as health check-ups and housekeeping. Out-home leisure is activities that satisfy the individual's demands for cultural and physiological needs such as listening to music, reading and watching movies. Out-home activities were observed in this study because this activity will give a huge effect towards the activity space of the individuals.

For the well-being and health data, respondents were asked to answer questionnaires regarding their well-being and health status. The questionnaires are based on the health variables as shown in the Table 2. For this study, the health condition of each respondent is evaluated in two categories which are physical health and mental health. Table 3 shows the summary design of the survey for both Malaysia and Indonesia.

4 Descriptive Analysis Result from Descriptive and ANOVA Analysis

4.1 Analysis of Activity Space Measurements (I_c and I_h)

Figure below show the components of activity space measurements, I_c and I_h . I_c represents the distance of activity locations to the centre of activity location. I_h is the distance of centre of activity location to the home location.

Based on the p-value in Table 4, several data are statistically significant where the p-values are lower than 0.05. As can be seen from the ANOVA analysis, the I_c of Malaysians and Indonesians are significantly different on Thursday and Sunday. Indonesians tend to have higher I_c than Malaysians on Thursday meanwhile Malaysians tend to have higher I_c than Indonesians on Sunday. This means Indonesians has more disperse activity locations than Malaysians on Thursday, whereas Malaysians has more disperse activity locations on than Indonesia on Sunday. ANOVA analysis of I_h shows significant differences on Friday, Saturday and Sunday. This can be observed where Malaysians tend to have higher I_h compared to Indonesians on Thursday, Friday and Saturday. This means Malaysians travel farther from their home location than Indonesian on Friday, Saturday and Sunday.

The previous result is strengthened by separating the I_c and I_h of Malaysia and Indonesians into weekdays and weekend. From the ANOVA analysis in Table 5, there is significant difference for I_c on weekend where Malaysians tend to have more disperse activity locations than Indonesians on weekend. For I_h , there is significant

Table 2 Health variables based on QOL (Ware and Sherbourne 1992)

Variable	Description
Physical Functioning (PF)	Vigorous activities, such as running, lifting heavy objects, participating in strenuous sports
	Moderate activities, such as moving a table, pushing a vacuum cleaner, bowling, or playing golf
	Lifting or carrying groceries
	Climbing several flights of stairs
	Climbing one flight of stairs
	Bending, kneeling, or stooping
	Walking more than a mile (a kilometer in Japanese version)
	Walking several blocks (about several hundred meters in Japanese version)
	Walking one block (about one hundred meters in Japanese version)
	Bathing or dressing yourself
Limitation on Role Functioning because of Physical Health (RP)	Cut down the amount of time you spent on work or other activities
	Accomplished less than you would like
	Were limited in the kind of work or other activities
	Had difficulty performing the work or other activities (for example, it took extra effort)
Bodily Pain (BP)	How much bodily pain have you had during the past 4 weeks?
	During the past 4 weeks, how much did pain interfere with your normal work (including both work outside the home and housework)?
General Health (GH)	In general, would you say your health is? (Excellent, very good, good, fair, poor)
	I seem to get sick a little easier than other people
	I am as healthy as anybody I know
	I expect my health to get worse
	My health is excellent
Vitality (VT)	Did you feel full of pep?
	Did you have a lot of energy?
	Did you feel worn out?
	Did you feel tired?

(continued)

Table 2 (continued)

Variable	Description
Social Functioning (SF)	During the past 4 weeks, to what extent has your physical health or emotional problems interfered with your normal social activities with family, friends, neighbors, or groups?
	During the past 4 weeks, how much of the time has your physical health or emotional problems interfered with your social activities (like visiting with friends, relatives, etc.)?
Limitations on Role Functioning because of Emotional Problems (RE)	Cut down the amount of time you spent on work or other activities
	Accomplished less than you would like
	Did not do work or other activities as carefully as usual
Mental Health (MH)	Have you been a very nervous person?
	Have you felt so down in the dumps that nothing could cheer you up?
	Have you felt calm and peaceful?
	Have you felt downhearted and blue?
	Have you been a happy person?

Table 3 The design of survey

Data Type	Characteristics of Data
Activity-travel diary	Location visited with coordinate
	Type of activities
	Time for out-home mandatory activities
	Time for out-home maintenance activities
	Time for out-home leisure activities
Well-being and health	Question based on QOL in Table 2
	Physical functioning (PF)
	Limitation on role functioning because of physical health (RP)
	Bodily pain (BP)
	General Health (GH)
	Vitality (VT)
	Social functioning (SF)
	Limitation on role functioning because of emotional problems (RE)
Mental health (MH)	

Table 4 Daily Ic and Ih ANOVA analysis

Activity space	Days	Daily Ic and Ih ANOVA analysis			
		F critical	F value	Significance value	p-value (<0.05 is significant)
Ic	Thursday	25.687	16.665	0.05	0.000**
	Friday	1.189	0.390	0.05	0.533
	Saturday	4.793	2.510	0.05	0.114
	Sunday	35.855	8.784	0.05	0.003**
Ih	Thursday	0.030	0.013	0.05	0.910
	Friday	21.056	5.914	0.05	0.015*
	Saturday	93.573	24.165	0.05	0.000**
	Sunday	50.422	15.313	0.05	0.000**

(*) Indicates the mean are significantly different from the opposite group with p-value < 0.05.

(**) Indicates the mean are significantly different from the opposite group with p-value < 0.01.

Table 5 Ic and Ih (weekday and weekend) ANOVA analysis

Activity space	Days	Ic and Ih (Weekday and Weekend) ANOVA analysis			
		F critical	F value	Significance value	p-value (<0.05 is significant)
Ic	Weekday	1.330	0.519	0.05	0.471
	Weekend	27.232	6.051	0.05	0.014*
Ih	Weekday	2.763	0.760	0.05	0.000**
	Weekend	86.856	24.231	0.05	0.384

(*) Indicates the mean are significantly different from the opposite group with p-value < 0.05.

(**) Indicates the mean are significantly different from the opposite group with p-value < 0.01.

difference between Malaysians and Indonesians on weekdays where Malaysians tend to travel farther from their home on weekdays compared to Indonesians.

4.2 Analysis of Out-Home Activities

Referring to Table 6, Malaysians and Indonesians have significantly difference out-home mandatory activities from Thursday to Sunday. As can be seen in Fig. 9 Malaysians tend to spend more time for out-home mandatory activities than Indonesians on Thursday and Friday. On the other hand, Indonesians spend more time for out-home mandatory activities than Malaysians on Saturday and Sunday. For out-home maintenance, there are significant differences found for the whole four days.

Table 6. Out-home activities ANOVA analysis.

Out-home activities	Days	Out-home activities ANOVA analysis			
		F critical	F value	Significance value	p-value (<0.05 is significant)
Out-home mandatory	Thursday	25.533	12.245	0.05	0.001*
	Friday	49.388	16.525	0.05	0.000**
	Saturday	3.837	31.823	0.05	0.000**
	Sunday	14.063	50.021	0.05	0.000**
Out-home maintenance	Thursday	114.936	60.863	0.05	0.000**
	Friday	40.559	27.397	0.05	0.000**
	Saturday	16.012	36.815	0.05	0.000**
	Sunday	10.530	18.887	0.05	0.000**
Out-home leisure	Thursday	11.838	24.537	0.05	0.000**
	Friday	29.059	45.730	0.05	0.000**
	Saturday	49.509	6.001	0.05	0.015*
	Sunday	31.176	0.414	0.05	0.520

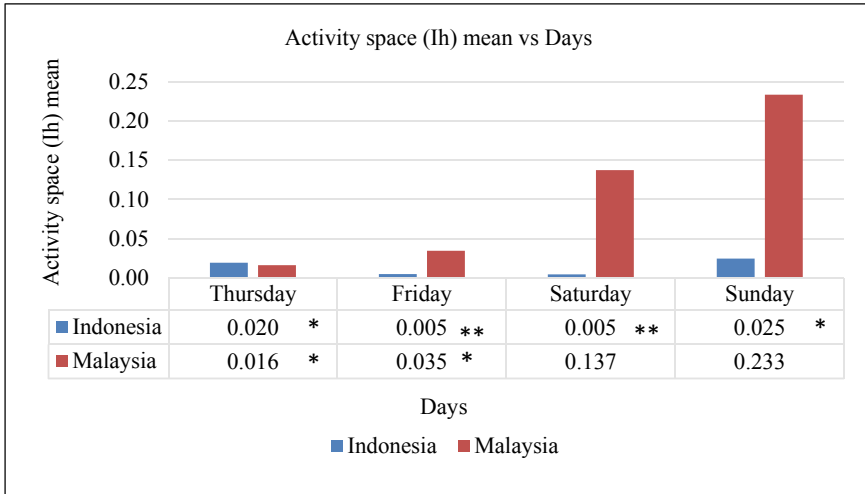
(*) Indicates the mean are significantly different from the opposite group with p-value < 0.05.

(**) Indicates the mean are significantly different from the opposite group with p-value < 0.01.

This can be observed in Fig. 10 where Indonesians tend to spend more time for out-home maintenance activities compared to Malaysian for the whole four days. For out-home leisure activities, the differences are significant on Thursday, Friday, and Saturday. This is shown in Fig. 11 where Indonesians tend to spend more time for out-home leisure than Malaysians on weekdays. In contrast, Malaysians tend to spend more out-home leisure activities than Indonesian on Saturday.

4.3 Analysis of Health Parameters (Physical Health and Mental Health)

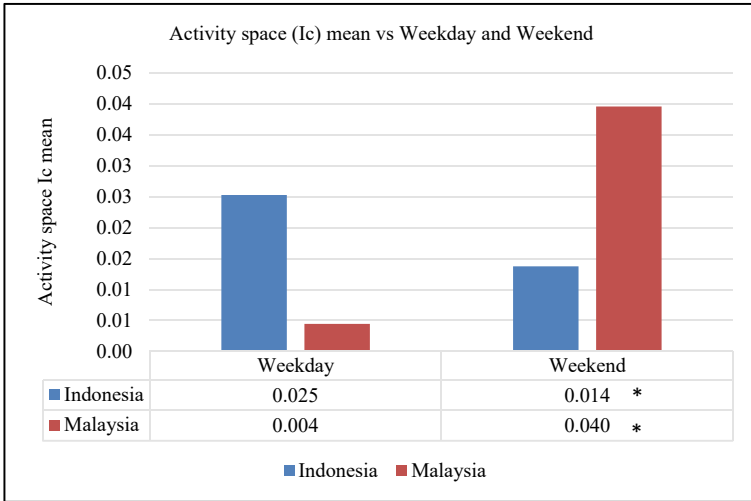
From Fig. 12, there are small differences between Malaysia and Indonesia health parameters. It is shown that for low physical health and mental health, Malaysia has lower mean than Indonesia. Same goes to high physical health and mental health, Malaysia also has lower mean compared to Indonesia. This can be due to different mode of transportation used in their daily life. Since Malaysian people tend to travel further from their home than Indonesia people as illustrated in Fig. 6, they most like will use motorized vehicles such as their own private vehicles or other kind of public transportation. Plus, Malaysian people tend to spend most of their time for



(*) Indicates the mean are significantly different from the opposite group with p-value < 0.05.
 (**) Indicates the mean are significantly different from the opposite group with p-value < 0.01.

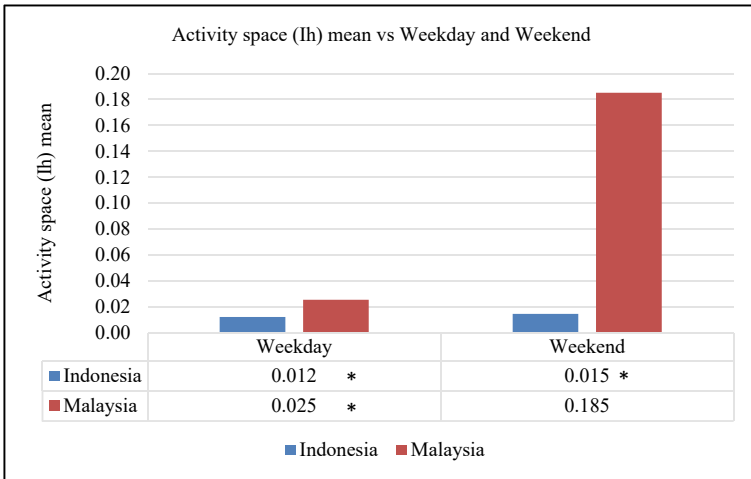
Fig. 6 Activity space (Ih) mean vs Days graph

out-home mandatory such as working and studying compared to Indonesia people which reduce their time to exercise during weekday. Hence, these causes affecting the physical health of Malaysia to be lower than Indonesia. Since Malaysian tend to use motorized vehicles more than Indonesia, the air pollution produced by vehicles is higher in Malaysia and will directly reduce the mental health in Malaysia. However, based on the observation made in Table 7, there is no significant difference for both physical health and mental health between Malaysia and Indonesia where the p-values are higher than 0.05.



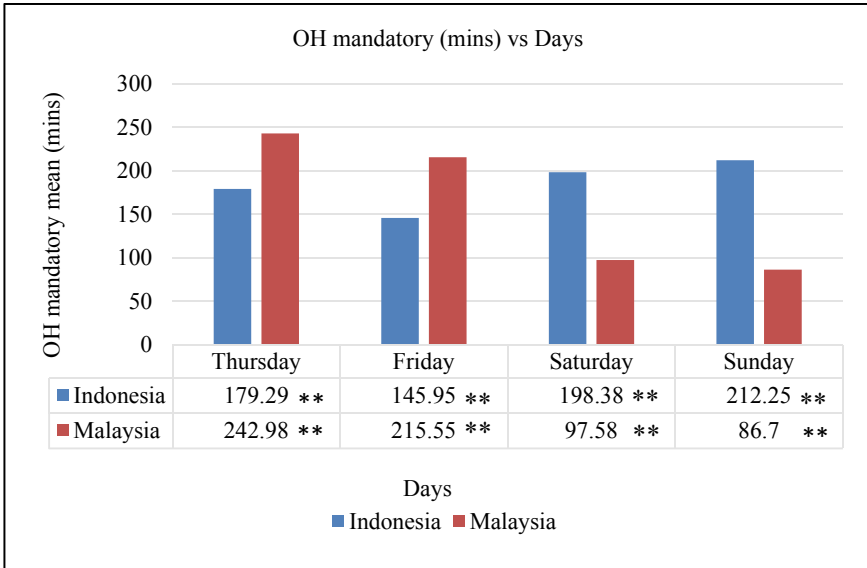
(*) Indicates the mean are significantly different from the opposite group with p-value < 0.05.
 (**) Indicates the mean are significantly different from the opposite group with p-value < 0.01.

Fig. 7 Activity space (Ic) mean vs Weekday and Weekend graph



(*) Indicates the mean are significantly different from the opposite group with p-value < 0.05.
 (**) Indicates the mean are significantly different from the opposite group with p-value < 0.01.

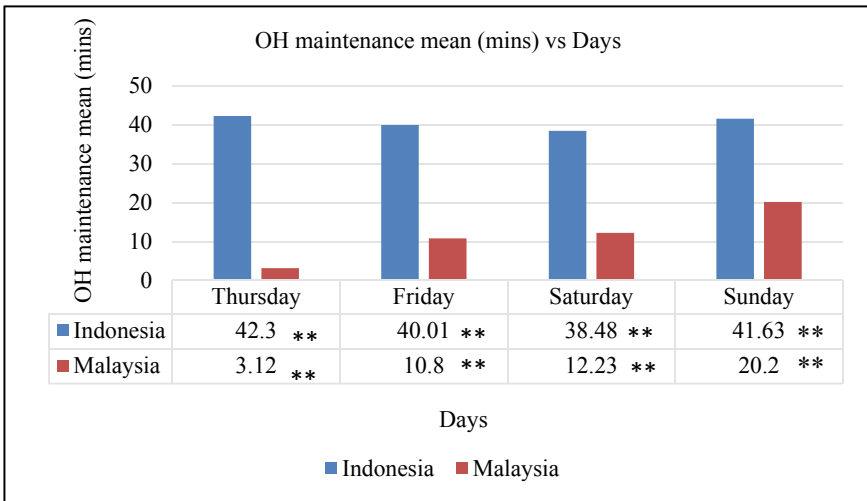
Fig. 8 Activity space (Ih) mean vs Weekday and Weekend graph



(*) Indicates the mean are significantly different from the opposite group with p-value < 0.05.

(**) Indicates the mean are significantly different from the opposite group with p-value < 0.01.

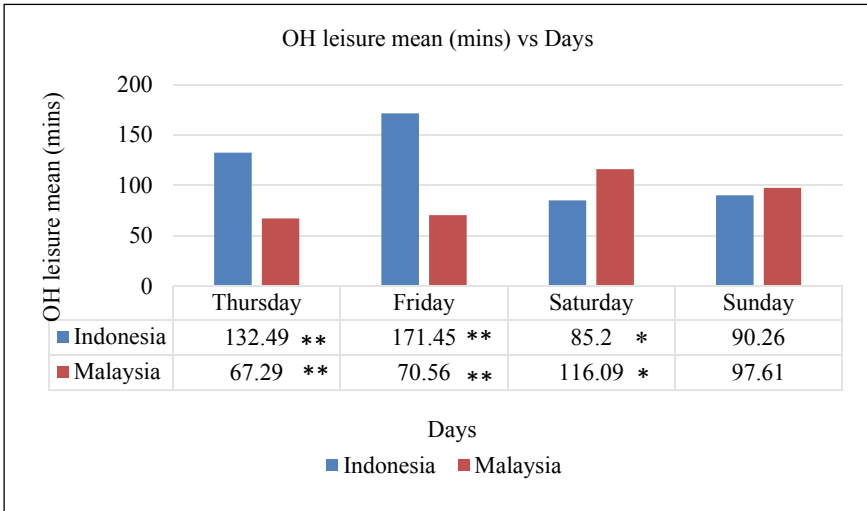
Fig. 9 Out-home mandatory (mins) vs Days graph



(*) Indicates the mean are significantly different from the opposite group with p-value < 0.05.

(**) Indicates the mean are significantly different from the opposite group with p-value < 0.01.

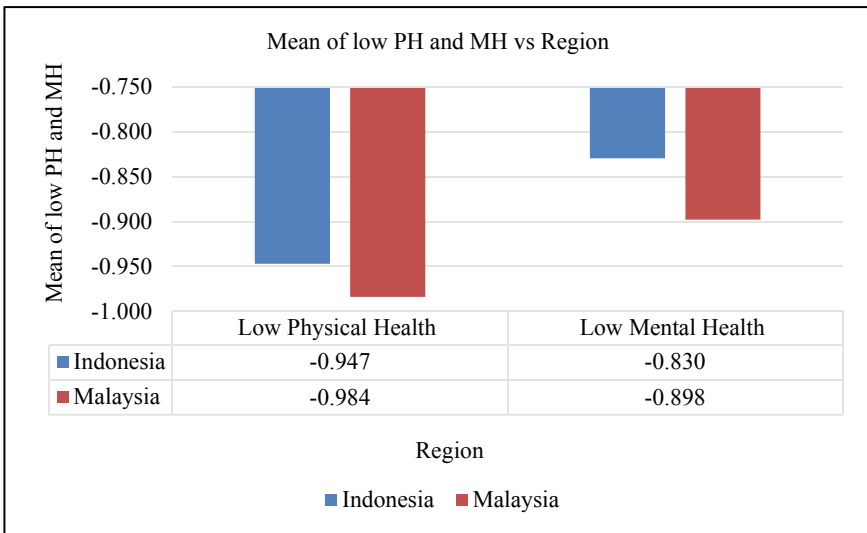
Fig. 10 Out-home maintenance (mins) vs Days graph



(*) Indicates the mean are significantly different from the opposite group with p-value < 0.05.

(**) Indicates the mean are significantly different from the opposite group with p-value < 0.01.

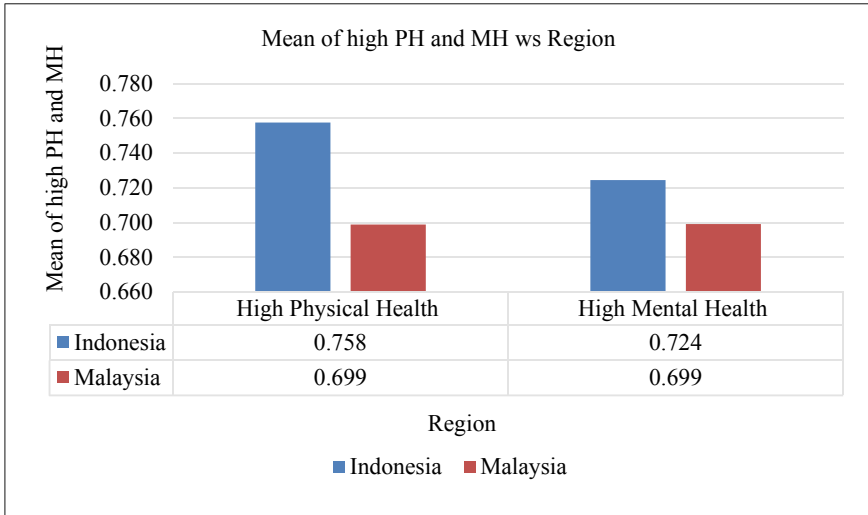
Fig. 11 Out-home leisure (mins) vs Days graph



(*) Indicates the mean are significantly different from the opposite group with p-value < 0.05.

(**) Indicates the mean are significantly different from the opposite group with p-value < 0.01.

Fig. 12 Mean of low PH and MH vs Region graph



(*) Indicates the mean are significantly different from the opposite group with p-value < 0.05.
 (**) Indicates the mean are significantly different from the opposite group with p-value < 0.01.

Fig. 13 Mean of high PH and MH vs Region graph

Table 7 Health parameters ANOVA analysis

Health parameters	Health parameters ANOVA analysis			
	F critical	F value	Significance value	p-value (<0.05 is significant)
Low Physical health	8.689	0.151	0.05	0.698
High Physical health	0.008	0.945	0.05	0.332
Low Mental health	0.033	0.464	0.05	0.496
High Mental health	1.329	0.101	0.05	0.751

(*) Indicates the mean are significantly different from the opposite group with p-value < 0.05.
 (**) Indicates the mean are significantly different from the opposite group with p-value < 0.01.

5 Conclusion

In conclusion, comparison on the effect of activity space (Ic and Ih) on health performnace (physical health and mental health) between Malaysia and Indonesia have been done successfully. Even though most of the activity space measurements are significantly different, however there is no significant difference on Malaysians' and Indonesians' health condition.

From the differences observed in the activity space between Malaysians and Indonesians, there are several suggestions made to increase the activity space as high activity space correlate with high health conditions. The first suggestion is to increase the income for Indonesians so that they have the opportunity to travel further and spend time with their families or friends for vacations or for doing outdoor activities that require higher expenses such as scuba diving, paragliding, and hiking. Next suggestion is to improve the public transportation system to allow Indonesians travel further in a group of their family member or friends.

For future works, it is recommended that the results obtained from this paper are analyzed alongside with in-home activities and social health. People who have high in-home activities might also have higher or lower health conditions that should be taken into considerations. Social health is recommended to be included as well. This is because people with high physical and mental health, might have lower or higher social health. These recommendations can increase the accuracy of the study and more importantly by considering all the major health parameters which are physical health, mental health and social health.

Furthermore, it is recommended to have the similarities and differences compared before proceeding with the analysis for both locations not only in term of cultural and distance towards each other, but also in term of their built environment such as the respondents' ages and professions. This is because Bandar Seri Iskandar, Malaysia tends to be comprised of high professions such as teachers, lecturers and businessman. Plus, high population of students are observed by referring to the numbers of universities located in Bandar Seri Iskandar. This might affect the results where the activity space of Malaysians tends to be higher in weekend when compared with Yogyakarta, Indonesia which tends to have variations of professions.

References

- Chapin FS (1974) Human activity patterns in the city: things people do in time and in space. Wiley
- Dharmowijoyo DBE, Joewono TB (2020) Mobility and health: the interaction of activity-travel patterns, overall well-being, transport-related social exclusion on health parameters. *Energy Effi Mobility Syst* 53–83. https://doi.org/10.1007/978-981-15-0102-9_4
- Dharmowijoyo DBE, Susilo YO, Karlström A (2014) Day-to-day interpersonal and intrapersonal variability of individuals' activity spaces in a developing country. *Environ Plann B Plann Des* 41(6):1063–1076. <https://doi.org/10.1068/b130067p>
- Dharmowijoyo DBE, Susilo YO, Karlström A (2016) Relationships among discretionary activity duration, its travel time spent and activity space indices in the Jakarta metropolitan area, Indonesia. *J Transp Geogr* 54:148–160
- Hägerstrand T (1970) What about people in regional science? By Torsten H/Igerstrand *. *Pap Reg Sci* 66:1–6. <https://doi.org/10.1111/j.1435-5597.1970.tb01464.x>
- Liu C, Susilo YO, Dharmowijoyo DBE (2018) Investigating intra-household interactions between individuals' time and space constraints. *J Transp Geogr* 73:108–119. <https://doi.org/10.1016/j.jtrangeo.2018.10.015>
- Miller HJ (2017) Time geography and space-time prism. *Int Encyclopedia Geography* 1–19. <https://doi.org/10.1002/9781118786352.wbieg0431>

- Schönfelder S, Axhausen KW (2003) Activity spaces: measures of social exclusion? *Transp Policy* 10(4):273–286. <https://doi.org/10.1016/j.tranpol.2003.07.002>
- Schwanen T, Kwan MP, Ren F (2008) How fixed is fixed? Gendered rigidity of space-time constraints and geographies of everyday activities. *Geoforum* 39. <https://doi.org/10.1016/j.geoforum.2008.09.002>
- Ware JE Jr, Sherbourne CD (1992) The MOS 36-item short-form health survey (SF-36). I. Conceptual framework and item selection. *Med Care* 30(6):473–483
- van Wee B, Ettema D (2016) Travel behaviour and health: a conceptual model and research agenda. *J Transp Health* 3(3):240–248. <https://doi.org/10.1016/j.jth.2016.07.003>
- Zhang J (2013) Urban forms and health. promotion: an evaluation based on urban forms and health health-related qol indicators. In: *Proceeding of the 13th world conference on transportation research*, pp 1–20